τ-Charm Physics at *BES-III*

Editor-in-Chief:
Kuang-Ta Chao and Yifang Wang

Editors:
Shan Jin, Hai-Bo Li, Jian-Ping Ma,
Ya-Jun Mao, Cong-Feng Qiao, Bing-Song Zou

Authors

A. A[1], B. B[2], C. .C[3] ....

[1] *Institute of High Energy Physics, Beijing 100049, People's Republic of China*

[2] *Peking University, Beijing 100871, People's Republic of China*

[3] *Tsinghua University, Beijing 100084, People's Republic of China*

Working Group and Conveners

This book presents a review of the physics opportunities at the *BES-III* experiment at BEPCII, at Institute of High Energy Physics. The results are from the following working groups with the conveners named.

Part One: The BESIII experiment and its physics
Conveners: Jian-Ping Ma, Ya-Jun Mao;
Part Two: Hadron production
Conveners: Xiao-Yuan Li, Yuan-Ning Gao;
Part Three: Light hadron physics
Conveners: Bing-Song Zou, Xiao-Yan Shen;
Part Four: Charmonium Physics
Conveners: Cong-Feng Qiao, Changzheng Yuan;
Part Five: Charm Physics
Conveners Zhi-Zhong Xing, Hai-Bo Li;
Part Six: Tau Physics
Conveners: Toni Pich, Changzheng Yuan;
Part Seven: Comparison with other facilities and future prospects
Conveners: Cai-Dian Lu, Shan Jin.

Preliminary Schedule of *BES-III* Physics Book– Three Stages

- First Stage: Now - 28 March 2006
  Framework established.
- Second Stage: May, 2006
  Key points ready and theoretical review done.
- The Third Stage: End of 2006
  All experimental and theoretical work finished.

During those periods, we are going to organize a τ-Charm workshop June 2006 in China. Phone conferences may be also possible if some intensive discussions are needed. Thanks!

Abstract

Hadron spectroscopy and Charm physics are becoming more exciting, this revival interesting has been driven by experimental reports of the narrow D_{sJ} states, $X(3872)$, $X(3940)$, $Y(3940)$ and the newest unexpected $Y(4260)$ from B factories and other related experiments, the proton-antiproton threshold enhancement and $X(1835)$ observed at BESII also attracted people's attention. In the meanwhile, MIMD Lattice Calculation (MILC) and High Precision QCD (HPQCD) collaborations predicted $f_{D^+} = 201 \pm 3 \pm 17$ MeV, CLEO-c collaboration also reported the result $f_{D^+} = 223 \pm 16 \pm 8$ MeV. The two results agree well within the errors of about 8% for each. It will challenge the theoretical prediction and provide important tests of the predictive powers of lattice QCD.

The *BES-III* at BEPCII under construction in Beijing can accumulate 10×10^9 J/ψ, 3×10^9 $\psi(2S)$, 30 million $D\overline{D}$ or 2 million $D_S^+ D_S^-$-pairs per running year, respectively, when it is turned to run at resonances in 2007. Coupled with what is available at CLEO-c, *BES-III* will make it possible for the first time to study in detail the light hadron spectroscopy in the decays of charmonium states and the charmed mesons. In addition, about 90 million $D\overline{D}$ pairs will be collected at BESIII in three years at $\psi(3770)$ peak. Many high precision measurements, including CKM matrix elements related to Charm weak decays, decay constants f_{D^+} (f_{D_S}), Dalitz decays of D meson and absolute decay branching fraction and so on, will be achieved. *BES-III* analyses are likely to be essential in deciding if some intriguing signals in particular in D decays are actually due to New Physics or not. With modern techniques and unprecedented high statistical data sample, Searching for rare D, Charmonium and tau decays will be possible, such as lepton number and flavor violated decays, invisible decays. The study of τ- Charm physics could reveal or indicate the possible presence of New Physics in the low energy region.

This physics book will give detail discussions on τ-Charm physics in the next few years, both theoretical and experimental studies will be covered. Extensive review of the more recent theoretical developments and experimental techniques will be given. Some intense discussions on the following physics topics will be especially addressed: possible innovation on Partial Wave Analysis (PWA), theoretical and experimental techniques on Dalitz plot analysis in D decays, analysis tools to extract the absolute branching

fraction, decay constants, form factors, CP parameters and parameters in $D^0\overline{D}^0$ Oscillations. The motivation of tau lepton physics near the threshold will be also studied so that a plan can be made at *BES-III*.

Contents

Abstract **vii**

I The *BES-III* experiment and its physics **1**

1 Physics goal of *BES-III* **3**

2 The *BES-III* detector and offline software **5**

3 Analysis tools **7**
3.1 Particle Identification . . . 7
3.2 Kinematic Fitting and Vertex Fitting . . . 7
3.3 Luminosity Measurement at BESIII . . . 7
3.4 Monte Carlo Generators . . . 7
3.5 Partial Wave Analysis . . . 7
3.6 Dalitz-plot Analysis Formalism . . . 7
3.6.1 Barrier Factor B_L . . . 9
3.6.2 Angular Distributions . . . 9
3.6.3 Dynamical Function T_R . . . 11
3.6.4 Breit-Wigner Formulation . . . 11
3.6.5 K-matrix Formalism . . . 11
3.6.6 Flatté Formalism . . . 13
3.6.7 Branching Ratios from Dalitz Fits . . . 13

II Hadron production **21**

4 Physics Processes **23**

5 Hadron Production and Fregmentation **25**

6 R values **27**

7 QCD studies at $\sqrt{s} = 2 - 5$ GeV **29**

8 Production cross sections of $D^0\overline{D}^{(*)0}$ and $D_S^+ D_S^{(*)-}$ (?) **31**

9 Measurements of Parameters of Charmonium Resonances 33
9.1 Introduction . . . 33
9.2 Key points of precise measurements . . . 34
9.3 An example for measuring $\psi(2S)$ and $\psi(3770)$ parameters . . . 35
9.4 Measurements of the parameters of $\psi(2S)$, $\psi(3770)$ and other resonances with BES-III at BEPC-II . . . 40
9.5 Summary . . . 44

III Light hadron physics 47

10 Overview of light hadron physics 49

11 Physics of soft pions and lightest scalars at BES-III 53
11.1 Partially conserved vector current (PCAC) and soft pions . . . 53
11.1.1 PCAC . . . 53
11.1.2 Adler' theorem with one soft pion . . . 53
11.1.3 Linear σ model and the chiral shielding . . . 56
11.1.4 Why there should exist a σ resonance . . . 58
11.2 Go beyond the Breit–Wigner description of a broad resonance . . . 59
11.2.1 How to describe a light and broad resonance . . . 60
11.2.2 The σ and κ poles in BESII experiments . . . 61
11.2.3 Universality of pole location . . . 61
11.3 Final state theorem and Omnés solution . . . 62
11.3.1 Final state theorem . . . 62
11.3.2 $D^+ \to K^-\pi^+ l\nu_l$ decays . . . 63
11.3.3 $D^+ \to K^-\pi^+\pi^+$ decays . . . 63
11.3.4 The Omnés solution . . . 64
11.3.5 More on final state interactions in the $J/\Psi \to \omega\pi\pi$ process . . . 65
11.4 On the nature of the lightest scalar resonances . . . 67

12 Meson spectrum 69
12.1 Introduction . . . 69
12.2 Conventional meson spectrum . . . 69
12.3 Glueball spectrum . . . 71
12.3.1 Glueball signatures . . . 73
12.3.2 Glueball candidates . . . 77
12.4 Hybrid Mesons, multiquarks and molecular states . . . 88
12.4.1 Hybrid Mesons . . . 89
12.4.2 Multiquarks . . . 102
12.4.3 Molecular states . . . 109

13 Baryon spectrum 111
13.1 Outstanding problems in Baryon Spectroscopy . . . 111
13.2 Baryon Spectroscopy at BESI and BESII . . . 113
13.3 Prospects for baryon spectroscopy at BESIII . . . 118

14 Hunting for glueballs, multiquark states and hybrids at BESIII/BEPCII 123
14.1 Introduction . . . 123
14.2 Search for glueballs . . . 123
14.2.1 Scalar glueball . . . 124
14.2.2 Pseudoscalar glueball . . . 124
14.2.3 Tensor glueball . . . 124
14.3 Search for the hybrid states . . . 124
14.4 Search for the multi-quark states . . . 124
14.5 Some examples on searching for glueballs, hybrids and multi-quark states . 125
14.5.1 The tensor glueball candidate in $J/\psi \to \gamma\eta\eta$ and $\gamma\eta\eta'$ . . . 125
14.5.2 Inclusive photon spectrum . . . 132
14.5.3 Simulation of $X(1835)$ in J/ψ radiative and hadronic decays . . . 133

15 Two-photon physics 139
15.1 Introduction . . . 139
15.2 Experimental status of two-photon processes . . . 141
15.3 Measurement of two-photon processes at the BESIII . . . 142

IV Charmonium Physics 157

16 Theoretical Frameworks of Charmonium Physics 159
16.1 Non-Relativistic QCD effective theory . . . 159
16.1.1 NRQCD effective theory . . . 159
16.1.2 Inclusive Charmonium Annihilation Decays . . . 161
16.2 pNRQCD and its applications . . . 164
16.2.1 Introduction . . . 164
16.2.2 Scales and EFTs . . . 164
16.2.3 pNRQCD . . . 165
16.2.4 Applications . . . 166
16.2.5 QCD potentials . . . 167
16.2.6 Precision determination of Standard Model parameters . . . 168
16.2.7 Spectra . . . 169
16.2.8 Transitions . . . 171
16.2.9 Inclusive Decays . . . 171
16.2.10 Baryons with two or more heavy quarks . . . 171
16.2.11 Gluelump Spectrum and exotic states . . . 172
16.2.12 Outlook . . . 172

17 Charmonium Spectroscopy 175
17.1 Introduction . . . 175
17.2 Conventional charmonium states . . . 177
17.2.1 Spectrum . . . 177
17.3 EM Couplings . . . 180
17.3.1 e^+e^- widths of 1^{--} states . . . 180
17.3.2 EM Transitions Between Charmonium States . . . 181

17.3.3 Two-photon couplings . . . 185
17.3.4 Strong Decays . . . 186
17.3.5 Additional $\psi(3770)$ and $\psi(4415)$ topics. . . . 189
17.4 Novel states incorporating a $c\bar{c}$ subsystem . . . 189
17.4.1 Charm Molecules . . . 189
17.4.2 Charmonium Hybrids . . . 191

18 Charmonium Inclusive Decays **201**
18.1 Theoretical Review . . . 201
18.2 Leptonic and other EM Decays . . . 201
18.2.1 Introduction . . . 201
18.2.2 Weak coupling regime . . . 202
18.2.3 Final discussion . . . 207
18.3 Inclusive Radiative Decays . . . 207
18.3.1 Introduction . . . 207
18.3.2 The photon spectrum . . . 208
18.3.3 Extraction of $\alpha_s(M_{J/\psi})$ . . . 213
18.3.4 Learning about the nature of J/ψ and $\psi(2S)$ . . . 215
18.3.5 Conclusions . . . 216

19 Charmonium transition **217**
19.1 Hadronic transitions . . . 217
19.1.1 QCD Multipole Expansion . . . 217
19.1.2 Hadronic Transitions Between $\boldsymbol{S}$-Wave Quarkonia . . . 218
19.1.3 $\boldsymbol{\pi\pi}$ Transitions of $\boldsymbol{D}$-Wave Charmonium . . . 222
19.1.4 Studying the $\boldsymbol{h_c}$ State . . . 224
19.1.5 $\boldsymbol{\pi\pi}$ Transitions of $\boldsymbol{P}$-Wave Quarkonia . . . 227
19.1.6 Summary . . . 230
19.2 Radiative transition . . . 230
19.2.1 Introduction . . . 230
19.2.2 $M1$ transition . . . 231
19.2.3 $E1$ Transition . . . 236
19.3 Channels for study . . . 237
19.3.1 Introduction . . . 237
19.3.2 Radiative transitions . . . 238
19.3.3 Hadronic transitions . . . 241
19.3.4 Discussions and conclusions . . . 254

20 Radiative decays **255**
20.1 Introduction . . . 255
20.2 Radiative decays of vector charmonia . . . 255
20.3 Radiative decays of pseudoscalar charmonia . . . 257
20.4 Radiative decays of P-wave charmonia . . . 257
20.5 Discussions and conclusions . . . 258

21 Hadronic decays **259**
21.1 $\rho - \pi$ puzzle . . . 259
21.1.1 Introduction . . . 259
21.1.2 Review of theoretical works on $\rho\pi$ puzzle . . . 260
21.1.3 Evaluation of ratio of J/ψ to ψ' decay . . . 272
21.1.4 Comment on the $\rho\pi$ puzzle . . . 275
21.1.5 Summary . . . 278
21.2 $\psi(3770)$ non-$D\overline{D}$ decays . . . 278
21.2.1 Introduction . . . 278
21.2.2 S-D mixing and mixing angle $\theta_{\rm mix}$ . . . 279
21.2.3 Electromagnetic transitions . . . 280
21.2.4 Hadronic transition . . . 282
21.2.5 Light hadron decays . . . 285
21.2.6 Studies of inclusive decays . . . 289
21.2.7 Summary . . . 292
21.3 Baryonic decays . . . 292
21.3.1 Introduction . . . 293
21.3.2 Theoretical Framework . . . 294
21.3.3 Two-body decays . . . 302
21.3.4 Three-body decays . . . 309
21.3.5 Multi-body and Semi-inclusive decay . . . 322
21.3.6 Special topics . . . 325
21.3.7 Summary and discussion . . . 334
21.4 Rare and forbidden charmonium decays . . . 335
21.4.1 Weak Decays of Charmonium . . . 335
21.4.2 Search for the invisible decays of Quarkonium . . . 339
21.4.3 Search for C or P violating processes in J/ψ decays . . . 344
21.4.4 Lepton flavor violating processes in decays of J/ψ . . . 346

22 Miscellaneous **349**
22.1 Bell Inequalities in High Energy Physics . . . 349

V Charm Physics **391**

23 D Tag Reconstruction Efficiencies and Rates **395**
23.1 The Tag Reconstruction . . . 395
23.2 Beam constrained mass . . . 396
23.3 Multiple Counting . . . 397
23.3.1 Mass plots fitting . . . 398

24 Leptonic, semileptonic $D(D_S)$ decays and CKM matrix **401**
24.1 Leptonic Decays . . . 401
24.1.1 Theoretical Review . . . 401
24.1.2 Decay Constants . . . 404
24.1.3 Measurements Leptonic Decays at BESIII . . . 406

24.2 Semileptonic Decays . . . 414
24.2.1 Theoretical Review . . . 414
24.2.2 Exclusive Semileptonic Decays . . . 425
24.2.3 Inclusive Semileptonic Decays . . . 434
24.3 Combined Results and Impact on CKM Measurements . . . 440

25 Hadronic $D(D_S)$ decays **441**
25.1 Present Status and Implication for QCD . . . 441
25.2 Theoretical Review . . . 442
25.2.1 The Effective Weak Hamiltonian . . . 442
25.2.2 Factorization and First Generation Theoretical Technologies . . . 443
25.2.3 The $1/N_C$ ansatz . . . 445
25.2.4 Treatment with QCD sum rules . . . 445
25.2.5 Modern Developments . . . 446
25.2.6 Symmetry Analysis . . . 447
25.3 Two-Body Decays . . . 448
25.3.1 Kinematics and Topologies of Amplitudes . . . 449
25.3.2 $D \to PP$, $D \to PV$ and $D \to VV$ Decays . . . 449
25.3.3 $D \to SP$ Decays . . . 452
25.3.4 $D \to AP$ Decays . . . 457
25.3.5 $D \to TP$ Decays . . . 459
25.3.6 Other Decay Modes . . . 460
25.4 Three-Body Decays . . . 460
25.4.1 Kinematics and Dalitz Plot . . . 460
25.4.2 Resonant Three-Body Decays . . . 463
25.4.3 Nonresonant Three-Body Decays . . . 463
25.4.4 Beyond Three-Body Decays . . . 464

26 Charm baryon production and decays **467**
26.1 Introduction . . . 467
26.2 Production of charmed baryons at BESIII . . . 468
26.3 Spectroscopy . . . 468
26.4 Strong decays . . . 473
26.4.1 Strong decays of s-wave charmed baryons . . . 473
26.4.2 Strong decays of p-wave charmed baryons . . . 475
26.5 Lifetimes . . . 477
26.6 Hadronic weak decays . . . 484
26.6.1 Quark-diagram scheme . . . 485
26.6.2 Dynamical model calculation . . . 486
26.6.3 Discussions . . . 490
26.6.4 Charm-flavor-conserving weak decays . . . 495
26.7 Semileptonic decays . . . 495
26.8 Electromagnetic and Weak Radiative decays . . . 496
26.8.1 Electromagnetic decays . . . 497
26.8.2 Weak radiative decays . . . 499

27 $D^0 - \overline{D}^0$ Mixing **503**
27.1 Theoretical Review . . . 504
27.1.1 Oscillation Formalism: the Phenomenology . . . 504
27.1.2 Standard Model Predictions for Oscillation Parameters . . . 506
27.1.3 Time-dependent Rate for Incoherent D Decays . . . 510
27.2 Experimental Review . . . 512
27.2.1 Semileptonic Decays . . . 512
27.2.2 Hadronic Final States . . . 514
27.2.3 D^0 Decays to CP Eigenstates . . . 518
27.2.4 Dalitz Plots . . . 520
27.3 Measurements on $\psi(3770)$ peak . . . 525
27.3.1 Mixing Rate: R_M . . . 528
27.3.2 Doubly Cabibbo Suppressed Rate and Strong Phase $\cos\delta_{K\pi}$ . . . 529
27.3.3 The Comprehensive Quantum Correlation Analysis . . . 531

28 CP and T Violation **533**
28.1 CP Violation in $D^0 - \overline{D}^0$ Mixing . . . 536
28.2 CP Violation in Decay . . . 537
28.3 CP Violation in the Interference of Decays with and without Mixing . . . 538
28.4 Rate of the CP Violation in the Coherent $D^0\overline{D}^0$ Pair . . . 540
28.5 CP Violation on Dalitz Plots . . . 541
28.5.1 with Flavor Tag . . . 541
28.5.2 with CP Tag . . . 541
28.6 T Violation . . . 541

29 Rare and Forbidden Charm Decays **545**
29.1 Introduction . . . 545
29.2 The rare charm decays in the SM . . . 546
29.2.1 Radiative charm decays . . . 546
29.2.2 GIM Suppressed Decays . . . 547
29.3 New Physics Analysis . . . 550
29.3.1 R-parity conserving SUSY . . . 550
29.3.2 R-parity violating SUSY . . . 552
29.3.3 Large Extra Dimensions . . . 553
29.4 Summary . . . 554

VI τ Physics **575**

30 τ mass near threshold **577**

31 Leptonic τ decays **579**

32 Hadronic τ decays **581**

33 Search for CP Violation in τ decays **583**

34 Study of the Lorentz structure in the Tau Lepton Decays **585**
34.1 Michel parameters . . . 585
34.2 Anomalous tenzor coupling . . . 586
34.3 Measurement of Michel parameters and search for the anomaluos tenzor coupling . . . 587
34.4 Summary . . . 590

VII Comparison with other facilities and future prospects **595**

35 τ-Charm physics at B factories **597**

36 Opportunities of τ-Charm physics at Super-B factories **599**

37 Do we need a Super-Charm factories **601**
Acknowledgements . . . 610

A Statistics in HEP data analysis **611**
A.1 Parameter estimation . . . 611
A.1.1 Estimators for mean and variance . . . 612
A.1.2 The method of maximum likelihood(ML) . . . 613
A.1.3 The method of least squares(LS) . . . 618
A.2 Interval estimation, confidence interval and upper limit . . . 621
A.2.1 Frequentist confidence interval . . . 621
A.2.2 Bayesian confidence interval . . . 628
A.3 Tests of hypotheses . . . 630
A.3.1 Goodness-of-fit test . . . 630
A.3.2 Statistical significance of signal . . . 633

List of Figures

9.1 (a) The distribution of the event vertex in z; (b) the efficiencies versus the nominal c.m. energies. 36
9.2 The hadronic cross sections versus the nominal c.m. energies (see text). . . 37
9.3 The observed cross sections versus the nominal c.m. energies. 37
9.4 The observed cross sections versus the nominal c.m. energies. 41
9.5 The observed cross sections versus the nominal c.m. energies. 42

11.1 Dalitz plot and $\pi^+\pi^-$ invariant mass spectrum in $J/\Psi \to \omega\pi\pi$ decays [25]. 59
11.2 Fit results of $\psi(2S) \to \pi^+\pi^- J/\psi$ (P.K.U. ansatz). Dots with error bars are data and the histograms are the fit results. (a) and (b) are the $\pi^+\pi^-$ invariant mass, (c) and (d) the cosine of the σ polar angle in the lab frame, and (e) and (f) the cosine of the π^+ polar angle in the σ rest frame. (From Ref. [33]) 62
11.3 The comparison between the scalar form factor and the scalar amplitude extracted from BES $J/\Psi \to \omega\pi\pi$ process. Data are from Ref. [42]. 66

12.1 The mass spectrum of glueballs in the pure $SU(3)$ gauge theory. The masses are given both in terms of r_0 ($r_0^{-1} = 410\,\mathrm{MeV}$) and in GeV. The height of each colored box indicates the statistical uncertainty of the mass. 72
12.2 (a) The K^+K^- invariant mass distribution for $J/\psi \to K^+K^-\pi^+\pi^-$. (b) The $\pi^+\pi^-$ invariant mass for events selected within ± 15 MeV/c^2 of the ϕ. 78
12.3 (a) The K^+K^- invariant mass distribution for $J/\psi \to K^+K^-K^+K^-$. (b) The K^+K^- invariant mass for events selected within ± 15 MeV/c^2 of the ϕ. 78
12.4 Invariant mass spectrum of $\pi^+\pi^-$ and the Dalitz plot for $J/\psi \to \gamma\pi^+\pi^-$, where the lightly and dark shaded histograms in the upper panel correspond to $J/\psi \to \pi^+\pi^-\pi^0$ and other estimated backgrounds, respectively. 80
12.5 Invariant mass spectrum of $\pi^0\pi^0$ and the Dalitz plot for $J/\psi \to \gamma\pi^0\pi^0$, where the shaded histogram in the upper panel corresponds to the estimated backgrounds. 80
12.6 The $\pi^+\pi^-$ invariant mass distribution from $J/\psi \to \gamma\pi^+\pi^-$. The crosses are data, the full histogram shows the PWA fit projection, and the shaded histogram corresponds to the background. 81
12.7 Invariant mass spectra of a) K^+K^-, b) $K^0_SK^0_S$ for $J/\psi \to \gamma K\bar{K}$ events, where the shaded histogra correspond to the estimated background contributions. 82
12.8 K^+K^- invariant mass spectrum in $J/\psi \to \omega K^+K^-$. The crosses are data and the histogram is PWA fit projection. 84

12.9 (a) The $K^+K^-\pi^+\pi^-\pi^0$ invariant mass distribution for the $J/\psi \to \gamma\omega\phi$ candidate events. The dashed curve indicates the acceptance varying with the $\omega\phi$ invariant mass. (b) Dalitz plot. 85
12.10(a) The $2(\pi^+\pi^-\pi^0)$ invariant mass distribution for candidate events. The dashed curve is the phase space invariant mass distribution, and the dotted curve shows the acceptance versus the $\omega\omega$ invariant mass. (b) The Dalitz plot. (c) The shaded histogram is the background. 87
12.11(a) The near threshold $M_{p\bar{p}} - 2m_p$ distribution for the $\gamma p\bar{p}$ event sample. The dashed curve is the background function described in the text. The dotted curve indicates how the acceptance varies with $p\bar{p}$ invariant mass; the dashed curve shows the fitted background function. (b) The $M_{p\bar{p}} - 2m_p$ distribution with events weighted by q_0/q. 103
12.12Invariant mass distributions for selected $J/\psi \to \gamma\pi^+\pi^-\eta'(\eta' \to \pi^+\pi^-\eta, \eta \to \gamma\gamma)$ candidate events. (a) The invariant mass distribution of $\gamma\gamma$ pairs. (b) The $\pi^+\pi^-\eta$ invariant mass distribution. (c) The $\pi^+\pi^-\eta'$ invariant mass distributions; the open histogram is data and the shaded histogram is $J/\psi \to \gamma\pi^+\pi^-\eta'$ phase-space MC events (with arbitrary normalization). . . 104
12.13Invariant mass distributions for the selected $J/\psi \to \gamma\pi^+\pi^-\eta'(\eta' \to \gamma\rho)$ candidate events, (a) The invariant mass distribution for $\gamma\gamma$ pairs. (b) The $\gamma\pi^+\pi^-$ invariant mass distribution. (c) The $\pi^+\pi^-\eta'$ invariant mass distributions: the open histogram is data and the shaded histogram is from $J/\psi \to \gamma\pi^+\pi^-\eta'$ phase-space MC events (with arbitrary normalization). . 105
12.14The $\pi^+\pi^-\eta'$ invariant mass distribution for selected events from both the $J/\psi \to \gamma\pi^+\pi^-\eta'(\eta' \to \pi^+\pi^-\eta, \eta \to \gamma\gamma)$ and $J/\psi \to \gamma\pi^+\pi^-\eta'(\eta' \to \gamma\rho)$ analyses. The bottom panel shows the fit (solid curve) to the data (points with error bars); the dashed curve indicates the background function. . . . 106
12.15(a) The points with error bars indicate the measured $p\bar{\Lambda}$ mass spectrum; the shaded histogram indicates phase space MC events (arbitrary normalization). (b) The Dalitz plot for the selected event sample. (c) A fit (solid line) to the data. The dotted curve indicates the Breit-Wigner signal and the dashed curve the phase space 'background'. (d) The $\cos\theta_p$ distribution under the enhancement, the points are data and the histogram is the MC (normalized to data) 108
12.16(a) The $\gamma\gamma$ invariant mass distribution. (b) The Dalitz plot for $K^+K^-\pi^0$ candidate events. (c) The K^+K^- invariant mass distribution for $K^+K^-\pi^0$ candidate events; the solid histogram is data and the shaded histogram is the background (normalized to data). (d) The K^+K^- invariant mass distribution for the π^0 mass sideband events (not normalized). 110

13.1 Various pictures for internal quark-gluon structure of baryons: (a) $3q$, (b) $3qg$ hybrid, (c) diquark, d) meson-baryon state, (e) pentaquark with diquark clusters. 111
13.2 $\bar{p}N^*$, $\bar{\Lambda}\Lambda^*$, $\bar{\Sigma}\Sigma^*$ and $\bar{\Xi}\Xi^*$ production from e^+e^- collision through ψ meson. 113
13.3 left: $\gamma\gamma$ invariant mass for $J/\psi \to \bar{p}p\gamma\gamma$; right: $p\eta$ invariant mass spectrum for $J/\psi \to \bar{p}p\eta$. BESI data 114

13.4 $p\pi^0$ invariant mass spectrum for $J/\psi \to \bar{p}p\pi^0$ from BESI (left) and preliminary BESII data (right) . . . 115
13.5 The $p\pi^-$ and $\bar{p}\pi^+$ invariant mass spectra for $J/\psi \to p\pi^-\bar{n}$ (left) and $\bar{p}\pi^+n$ (middle), compared with phase space distribution; And data divided by Monte Carlo phase space vs $p\pi$ invariant mass for $J/\psi \to \bar{p}\pi^-\bar{n}$ (solid circle) and $J/\psi \to \bar{p}\pi^+n$ (open square). . . . 115
13.6 pK (left) and $K\Lambda$ (middle) invariant mass spectra for $J/\psi \to pK^-\bar{\Lambda}$+c.c., compared with phase space distribution; right: Dalitz plot for $J/\psi \to pK^-\bar{\Lambda}$+c.c. . . . 116
13.7 $\bar{\Sigma}\pi$ (left) and $\Lambda\pi$ (right) invariant mass spectrum for $J/\psi \to \Lambda\bar{\Sigma}^+\pi^-$ (up) and $J/\psi \to \Lambda\bar{\Sigma}^-\pi^+$ (down), respectively. Preliminary BESII data [266] . . 117
13.8 Data corrected by MC simulated efficiency and phase space versus $p\pi^-$ (or $\bar{p}\pi^+$) and $\bar{n}\pi^-$ (or $n\pi^+$) invariant mass for $\psi' \to p\bar{n}\pi^- + c.c.$ candidate events [268]. . . . 120
13.9 Predicted Λ^*,Σ^*,Ξ^* mass spectra (solid line) by the classical 3q quark model [269, 230] and the predicted lowest $1/2^-$ Λ^*,Σ^*,Ξ^* states (dashed line) with pentaquark configuration [238], compared with observed states (box). . . . 121

14.1 The $\eta\eta$ invariant mass spectrum in $J/\psi \to \gamma\eta\eta \to 5\gamma$. The generated signals and backgrounds are normarized to $10^{10}J/\psi$ events and are added incoherently. . . . 127
14.2 The $\eta\eta$ invariant mass spectrum in $J/\psi \to \gamma\eta\eta \to 5\gamma 2(\pi^+\pi^-)$. The generated signals and backgrounds are normarized to $10^{10}J/\psi$ events and are added incoherently. . . . 127
14.3 Fit result after adding all resonances together. $(J/\psi \to \gamma\eta\eta, \eta \to \gamma\gamma, \eta \to \gamma\gamma$ channel) . . . 128
14.4 Fit result after adding all resonances together.$(J/\psi \to \gamma\eta\eta, \eta \to \pi^+\pi^-\pi^0, \eta \to \pi^+\pi^-\pi^0$ channel) . . . 128
14.5 Fit result after adding all resonances together. $(J/\psi \to \gamma\eta\eta, \eta \to \gamma\gamma, \eta \to \gamma\gamma$ channel) . . . 129
14.6 Fit result after adding all resonances together.$(J/\psi \to \gamma\eta\eta, \eta \to \pi^+\pi^-\pi^0, \eta \to \pi^+\pi^-\pi^0$ channel) . . . 129
14.7 The $\eta\eta$ invariant mass spectrum in $J/\psi \to \gamma\eta\eta' \to 5\gamma\pi^+\pi^-$. The generated signals and backgrounds are normarized to $10^{10}J/\psi$ events and are added incoherently. . . . 131
14.8 The $\eta\eta$ invariant mass spectrum in $J/\psi \to \gamma\eta\eta' \to 5\gamma\pi^+\pi^-$. The generated signals and backgrounds are normarized to $10^{10}J/\psi$ events and are added incoherently. . . . 131
14.9 The inclusive photon spectrum in J/ψ radiative decays. . . . 132
14.10The $\eta'\pi^+\pi^-$ invariant mass for $J/\psi \to \gamma\eta'\pi^+\pi^-$. The generated signals and backgrounds are normarized to $3\times10^9 J/\psi$ events and are added incoherently. 134
14.11The $\eta'\pi^+\pi^-$ invariant mass for $J/\psi \to \omega\eta'\pi^+\pi^-$. The generated signals and backgrounds are normarized to $3\times10^9 J/\psi$ events and are added incoherently. 134
14.12The $\eta'\pi^+\pi^-$ invariant mass for $J/\psi \to \phi\eta'\pi^+\pi^-$. The generated signals and backgrounds are normarized to $3\times10^9 J/\psi$ events and are added incoherently. 135

14.13The $\eta\pi^0$ invariant mass spectrum for $J/\psi \to \rho\eta\pi^0$. The generated signals and backgrounds are normarized to $6 \times 10^9 J/\psi$ events and are added incoherently. 136

14.14Left: Invariant mass spectrum of $\eta\pi^0$. The blue shaded histogram shows the contribution from $a_2(1320)$. Right: The scan curves for the mass and width of $a_2(1320)$. 136

14.15Left: Invariant mass spectrum of $\eta\pi^0$. The blue shaded histogram shows the contribution from $1^{-+}(1390)$. Right: The scan curves for the mass and width of $1^{-+}(1390)$. 137

15.1 The values of cross-section of pion pair production. 140

15.2 Feynman diagrams for hadron pair production. The contribution from diagram b) enhanced by poles of intermediate photons. 140

15.3 Kinematics of two-photon process. 141

17.1 Predicted and observed spectrum of charmonium states (Table 17.2). The solid lines are experiment for reasonably well-established charmonium states, and the particle labels give the actual 2006 PDG masses in MeV rather than the usual rounded PDG mass labels. The broken lines are theory (NR model left, GI right). In the theoretical spectra, spin triplet levels are dashed and spin singlets are dotted. The DD open-charm threshold at 3.73 GeV is also shown. 179

17.2 Predicted radiative partial width for the E1 transition $\psi(3770) \to \gamma\chi_2$ as a function of the 2^3S_1-$^3D_1$ mixing angle θ. 183

18.1 Prediction for the $\Upsilon(1S)$ decay rate to e^+e^-. We work in the RS' scheme. Figure from Ref. [176]. 203

18.2 Prediction for the $\eta_b(1S)$ decay rate to two photons. We work in the RS' scheme. Figure from Ref. [176]. 203

18.3 The spin ratio as the function of the renormalization scale ν in LO≡LL (dotted line), NLO (short-dashed line), NNLO (long-dashed line), NLL (dot-dashed line), and NNLL (solid line) approximation for the bottomonium ground state with $\nu_h = m_b$. For the NNLL result the band reflects the errors due to $\alpha_s(M_Z) = 0.118 \pm 0.003$. Figure from Ref. [179]. 205

18.4 The spin ratio as the function of the renormalization scale ν in LO≡LL (dotted line), NLO (short-dashed line), NNLO (long-dashed line), NLL (dot-dashed line), and NNLL (solid line) approximation for the charmonium ground state with $\nu_h = m_c$. For the NNLL result the lower (yellow) band reflects the errors due to $\alpha_s(M_Z) = 0.118 \pm 0.003$. The upper (green) band represents the experimental error of the ratio where the central value is given by the horizontal solid line. Figure from Ref. [179]. 206

18.5 Direct contributions in the weak coupling regime. The solid green line corresponds to the calculation for the central region at NLO, which should be reliable up to $z \lesssim 0.7$. The blue dot-dashed line corresponds to the calculation for the upper end-point region, which is expected to provide a reasonable model for $0.7 \lesssim z \lesssim 0.9$. The red dashed line is the curve obtained by merging. 212

18.6 The red dashed line corresponds to the direct contributions (merging), the blue dot-dashed line to the fragmentation contributions (v scaling for $O_8(^3S_1)$) and the solid green line is the total. 214

18.7 The red dashed line corresponds to the direct contributions (merging), the blue dot-dashed line to the fragmentation contributions (lattice, nrqcd algorithm, for $O_8(^3S_1)$) and the solid green line is the total. 214

18.8 The red dashed line corresponds to the direct contributions (central region), the blue dot-dashed line to the fragmentation contributions (v scaling for $O_8(^3S_1)$) and the solid green line is the total. 214

18.9 The red dashed line corresponds to the direct contributions (central region), the blue dot-dashed line to the fragmentation contributions (lattice, nrqcd algorithm, for $O_8(^3S_1)$) and the solid green line is the total. 215

19.1 Diagram for a typical hadronic transition in the single-channel approach. 218

19.2 Charmonium spectroscopy below the open charm threshold. 238

19.3 Radiative transitions between charmonium states below the open charm threshold. 241

19.4 Hadronic transitions of ψ' to other charmonium states. 242

19.5 Hadronic transitions of η_c' to other charmonium states. 245

19.6 Hadronic transitions of $h_c(^1P_1)$ to other charmonium states. 247

19.7 Hadronic transitions of χ_{c2} to other charmonium states. 249

19.8 Hadronic transitions of χ_{c1} to other charmonium states. 251

19.9 Hadronic transitions of χ_{c0} to other charmonium states. 253

20.1 Radiative decays of vector charmonium state into light hadrons. 256

21.1 The ratio $R_{\psi(3770)/\psi(3686)}$ of the scaled leptonic widths as a function of mixing angle $\theta_{\rm mix}$, where the dashed lines show the $\pm 1\sigma$ intervals of the measured quantities. 281

21.2 The distributions of the invariant masses of (a) $\pi^+\pi^-\pi^+\pi^-$, (b) $K^+K^-\pi^+\pi^-$, (c) $p\bar{p}\pi^+\pi^-$ and (d) $\pi^+\pi^-\pi^+\pi^-\pi^+\pi^-$ combinations, where the charged particles are coming from the $\chi_{cJ(J=0,1,2)}$ decays. 283

21.3 The ratio $R_{\psi(3770)/\psi(3686)}(J/\psi\pi^+\pi^-)$ of the partial widths as a function of the ratio $\left|\frac{c_2}{c_1}\right|$, where the dashed lines show the $\pm 1\sigma$ intervals of the measured quantities. 285

21.4 The distributions of the ratio $R = E_{\rm measure}/E_{\rm cm}$ and the invariant masses of $\gamma\gamma$ combinations, where the (a), (b), (c) and (d) show the R for the combinations of $\pi^+\pi^-\pi^+\pi^-$, $K^+K^-\pi^+\pi^-$, $p\bar{p}\pi^+\pi^-$ and $3(\pi^+\pi^-)$, respectively; while the (e), (f), (g) and (h) show the invariant masses of $\gamma\gamma$ combinations for the final states of $2(\pi^+\pi^-)\pi^0$, $K^+K^-\pi^+\pi^-\pi^0$, $p\bar{p}\pi^+\pi^-\pi^0$ and $3(\pi^+\pi^-)\pi^0$, respectively. 289

21.5 The observed cross sections versus the nominal c.m. energies. 291

21.6 The lowest-order Feynman graphs for J/ψ or $\psi(2S)$ (left) and η_c or χ_{cJ} decays into a baryon-antibaryon pair. 295

21.7 Helicity configurations in the creation of a light $q\bar{q}$ pair (left) and for a leading-twist parton–proton transition (right). 296

21.8 Baryon-antibaryon nonet. The J^P of this nonet is either 0^- or 1^-. The three circles in the figure indicate the following three states: $(n\overline{n}-p\overline{p})/\sqrt{2}$, $(n\overline{n}+p\overline{p}-2\Lambda\overline{\Lambda})/\sqrt{6}$, and $(n\overline{n}+p\overline{p}+\Lambda\overline{\Lambda})/\sqrt{3}$. 310

21.9 The definition of the angles for $\Lambda, \bar{\Lambda}, p, \bar{p}, \pi^+$ and π^- in helicity system. . . 328

21.10 The $\vec{a}\cdot\vec{b}$ distribution, where the solid line is M.C. simulation and the crosses with error bars are data. 329

21.11 The distribution in the angle θ between the π^+ and the π^- as predicted by Quantum Mechanics (solid line), and if a "hidden" Λ polarization measurement is done before the decay (dashed line). The shaded area gives the domain where the inequality is satisfied. 330

21.12 *The demonstration of $J/\psi \to \phi\eta$ or $\phi\eta'$, the ϕ, which is reconstructed in the K^+K^- decay mode, and can be used to tag the invisible decays of the missing particles.* 341

21.13 (a) The m_{KK} distribution for candidate events. The arrows on the plot indicate the signal region of ϕ candidates. (b) P_{miss} distribution for the events with $1.005 < m_{KK} < 1.035$ GeV/c^2 in (a). The means of the missing momenta for $J/\psi \to \phi\eta$ and $J/\psi \to \phi\eta'$ are located around 1.32 and 1.20 GeV/c, respectively, as indicated by the two arrows. 342

21.14 The P_{miss} distribution for candidate events. The data (black crosses) are compared to the total fit results. The dotted curve is the projection of η signal component, and the dashed curve is the projection of η' signal component, and the solid curve is the total likelihood fit result. 343

22.1 The best fit to the experimental measurement [586]. The two points with error bars correspond to time difference $\Delta t = 0$ and $\Delta t = 1.2\tau_s$. The solid line represents the QM prediction. 354

22.2 The experiment result of the violation of inequality [587]. The horizontal axis refers to Δt and the vertical axis to the S. The LHVTs limit of 2 is shown by the solid line. 355

22.3 The violation degree of the Bell inequalities (the dashed line for EI type and the solid line for CHSH type) in terms of the entanglement. Here, for the sake of transparency, we make a coordinator exchange, the $C = 1 - x^2$. The magnitudes of *VD* less than zero means the broken of the BIs. 358

23.1 Beam constrained mass distribution for the tags of $D^0 \to K^-\pi^+$ and $D^0 \to K^-\pi^+\pi^0$. The red curves show the sum of signal and background functions. The blue curves indicate the background fits. 398

24.1 The Feynman diagram for $D^+ \to l^+\nu_\ell$ 402
24.2 Summary of theoretical predictions and experimental data for f_{D^+} 403
24.3 The beam constraint masses for the singly tagged $\bar{D}^-$ modes: (a) $K^+\pi^-\pi^-$, (b) $K^0\pi^-$, (c) $K^-K^+\pi^-$ and (d) $K^+\pi^-\pi^-\pi^0$. 410
24.4 The fitted beam constraint masses for the singly tagged $\bar{D}s^-$ 411
24.5 the candidate muon momentum for (a) $D^+ \to \mu^+\nu_\mu$ and (b) $D_s^+ \to \mu^+\nu_\mu$. 412
24.6 The MM^2_{miss} distribution of the muon candidates on the recoil-side of the four D^- tag modes $K^+\pi^-\pi^-$, $K^+K^-\pi^-$, $K^0_S\pi^-$ and $K^+\pi^-\pi^-\pi^0$ (about $800pb^{-1}$ sample). 412
24.7 The M^2_{miss} distribution of the muon candidates on the recoil-side of the three D_s^- tag modes $\phi\pi^-$ (about 10 fb^{-1} sample). 413
24.8 Feynman diagram of semileptonic D decay 415
24.9 The beam constraint masses of the $Kn\pi$ combinations for the singly tagged $\bar{D}^0$ modes: (a) $K^+\pi^-$, (b) $K^+\pi^-\pi^0$, (c) $K^+\pi^-\pi^-\pi^+$ and (d) $K^0\pi^+\pi^-$. . . . 429
24.10The U_{miss} distribution of the candidates for the semileptonic decay $D^0 \to K^-e^+\nu_e$. 430
24.11The U_{miss} distribution of the candidates for the semileptonic decay $D^0 \to \pi^-e^+\nu_e$, where the $D^0 \to K^-e^+\nu_e$ events have been misidentified as $D^0 \to \pi^-e^+\nu_e$, since the K^- has been allowed to be misidentified as a π^-, see the peak B. 430
24.12The beam constraint masses of the $Kn\pi$ combinations for the singly tagged $\bar{D}$ modes: (a) $\bar{D}^0 \to K^+\pi^-$, (b) $\bar{D}^0 \to K^+\pi^-\pi^0$, (c) $\bar{D}^0 \to K^+\pi^-\pi^-\pi^+$ and (d) $D^- \to K^+\pi^-\pi^-$. 437
24.13The fitted beam constraint masses for $Kn\pi$ combinations of the events in which one electron is observed in the system recoiling against the tagged $\bar{D}$: (a), (a') $\bar{D}^0 \to K^+\pi^-$; (b), (b') $\bar{D}^0 \to K^+\pi^-\pi^0$; (c), (c') $\bar{D}^0 \to K^+\pi^-\pi^-\pi^+$ and (d), (d') $D^- \to K^+\pi^-\pi^-$, where (a), (b), (c) and (d) are for the right-sign events, while (a'), (b'), (c') and (d') are for the wrong-sign events. 438

26.1 Charmed baryons and some of their orbital excitations [4]. 470
26.2 Contributions to nonleptonic decay rates of charmed baryons from four-quark operators: (a) c-quark decay, (b) W-exchange, (c) destructive Pauli interference and (d) constructive interference. 479
26.3 Quark diagrams for charmed baryon decays 485
26.4 Pole diagrams for charmed baryon decay $\mathcal{B}_i \to \mathcal{B}_f + M$. 488
26.5 Chiral loop contribution to the E2 amplitude of $\Sigma_c^* \to \Lambda_c\gamma$. 498
26.6 W-exchange diagrams contributing to the quark-quark bremsstrahlung process $c + \bar{u} \to s + \bar{d} + \gamma$. The W-annihilation type diagrams are not shown here. 500

27.1 Standard Model box diagrams of flavor-changing neutral currents contributing to $D^0 - \overline{D}^0$ mixing at the quark level. 506

27.2 A hadron-level diagram of a long-distance physics contribution to $D^0 - \overline{D}^0$ mixing. 508

27.3 Standard Model predictions for $|x|$ (open triangles) and $|y|$ (open squares). Horizontal line references are tabulated in Table 4 in Ref. [260]. 509

27.4 New Physics predictions for $|x|$. Horizontal line references are tabulated in Table 5 in Ref. [260]. 510

27.5 *(a)* ΔM *distribution for right-sign* $D^0 \to K^- l^+ \nu$ *candidate decays; (b) wrong-sign* $D^0 \to K^+ l^- \overline{\nu}$ *decays, from Belle using 253* fb^{-1} *of data [267]. The wrong-sign plot shows no visible signal above background.* 513

27.6 *The distribution for (a) Right-sign* $M_{K\pi}$ *with* $0 < Q < 20$ *MeV, (b) Right-sign Q with 1.81* $GeV/c^2 < M_{K\pi} < 1.91$ GeV/c^2*, (c) Wrong-sign* $M_{K\pi}$ *with* $5.3 < Q < 6.5$ *MeV, and (d) Wrong-sign Q with* $1.845 < m_{K\pi} < 1.885$ GeV/c^2*. Note that the wrong-sign plots are shown for a* 3σ *signal interval in Q and* $MK\pi$*, respectively. Superimposed on the data (points with error bars) are projections of the* $M_{K\pi} - Q$ *fit. The results are from Belle experiment with 400* fb^{-1} *of data.* 517

27.7 *Left: wrong-sign* $D^0 \to K^+\pi^-$ *decay-time distribution and fit projections. Right: 95% C.L. region for* x'^2*,* y'*. From Belle using 400* fb^{-1} *of data [277].* 518

27.8 *Dalitz plot and one-dimensional projection onto* $m^2_{K\pi^0}$ *for CF decays (left) and DCS decays (right). The shaded histograms in the lower plots are projections of the Dalitz plots above them, with error bars superimposed. The data are from BaBar with 230* fb^{-1}*.* 519

27.9 *Decay time distributions for CF* $D^0 \to K^-\pi^+$ *(upper left),* $D^0 \to K^+K^-$ *(upper right),* $D^0 \to \pi^+\pi^-$ *(lower left), and* $D^0 \to K^+K^-$ *selected without using a* D^{*0} *tag (lower right), from BaBar using 91* fb^{-1} *of data [290]. The higtograms are fit results superimposed on the data (dotted histograms). The shaded histograms is the portion of the sample assigned by the fit to the background. The points presented below the histograms are the difference between data and dit divided by the statistical error with error bars of unit length.* 521

27.10 *Dalitz plot (lower right) and projections (lower left, upper plots) for* $D^0 \to K^0_S\,\pi^+\pi^-$ *decays, from CLEO using 9.0* fb^{-1} *of data.[292]* 523

29.1 One-loop diagrams inducing the $c \to u\gamma$ 546

29.2 - Two-loop diagrams for the $c \to u\gamma$ 547

29.3 Dilepton mass distribution for $D^+ \to \pi^+ e^+ e^-$. The dashed (solid) line is the short-distance (total) SM contribution. The dot-dashed line is the R-parity violating contribution. 548

29.4 Long distance contributions to $D^0 \to \ell^+\ell^-$. 549

29.5 Long distance contributions to $D^+ \to \pi^+\ell^+\ell^-$. 549

29.6 A typical contribution to $c \to u$ FCNC transitions in the MSSM. The cross denotes one mass insertion $(\delta^u_{12})_{\lambda\lambda'}$ and λ, λ' are helicity labels. 551

29.7 Dilepton mass distributions for $D^0 \to \rho^0 e^+ e^-$ in the mass insertion approximation of MSSM. The SM prediction (solid curve) is provided for reference and the MSSM curves refer to (i) $M_{\tilde{g}} = M_{\tilde{q}} = 250$ GeV, (ii) $M_{\tilde{g}} = 2M_{\tilde{q}} = 500$ GeV, (iii) $M_{\tilde{g}} = M_{\tilde{q}} = 1000$ GeV and (iv) $M_{\tilde{g}} = M_{\tilde{q}}/2 = 250$ GeV. . . . 552

34.1 The shapes of polynomial functions h for the Michel parametrisation of tau decays. . . . 586
34.2 The deviation of the spectrum of leptons from tau decays from the Standard model prediction. Dashed line: for the non-zero value of the anomaluos tenzor coupling. Solid line: for $\rho \neq 0.75$. . . . 588
34.3 Left: the muon hypothesis pull for the electron candidate. Right: the electron hypothesis pull for the muon candidate. The selection cuts were +3 for the electron candidate and -3 for the muon candidate. . . . 589
34.4 Left: the number of hits in muon chambers associated with the muon candidates. Right: the relative electromagnetic energy deposition E/P in the EMC for the electron candidates. The selection cuts were: $N_{HIT} \geq 3$ for muons and $E/P > 0.8$ for electrons. . . . 590
34.5 The momentum spectra of the selected muon (left) and electron (right) candidates. The statistics corresponds to 5 fb^{-1}. . . . 591

A.1 Construction of the confidence belt 622

List of Tables

3.1 Blatt-Weisskopf barrier factors. 9

3.2 Angular distributions for each J, L, l for *unpolarized* initial states where θ is the angle between particles a and c in the rest frame of resonance r, $\sqrt{1+\zeta^2}$ is a relativistic correction with $\zeta^2 = E_r^2/m_{ab}^2 - 1$, and $E_r = (m_R^2 + m_{ab}^2 - m_c^2)/2m_R$. 10

3.3 Angular distributions for $J \neq 0, L \neq 0, l$ for *polarized* initial states where $\cos\theta$ is the angle between particles a and c in the rest frame of resonance r, $\gamma = E_r/m_{ab}$, and $E_r = (m_R^2+m_{ab}^2-m_c^2)/2m_R$. F_λ denotes the fraction of the initial state in helicity state λ. For unpolarized initial states setting F_λ=1 recovers the angular distributions obtained from the Zemach formalism shown in 3.2. 10

9.1 The measured $\psi(3770)$ and $\psi(2S)$ parameters, where M is the mass, $\Gamma^{\rm tot}$ the total width [$\Gamma^{\rm tot} = \Gamma_0$ for $\psi(3770)$], Γ^{ee} the partial leptonic width and ΔM the measured mass difference of the $\psi(3770)$ and the $\psi(2S)$. 39

9.2 The input and measured $\psi(2S)$ parameters, where M is the mass, $\Gamma^{\rm tot}$ the total width and Γ^{ee} the partial leptonic width, where the "input" means the value of the parameter set in the Monte Carlo simulation and the "measured" means the measured value of the parameters from the Monte Carlo simulation. 42

9.3 The input and measured $\psi(3770)$ parameters, where M is the mass, $\Gamma^{\rm tot}$ the total width [$\Gamma^{\rm tot} = \Gamma_0$ for $\psi(3770)$] and Γ^{ee} the partial leptonic width, where the "input" means the value of the parameter set in the Monte Carlo simulation and the "measured" means the measured value of the parameters from the Monte Carlo simulation. 42

9.4 The input and measured $R_{\rm uds}$ values in the resonance region from 3.65 to 3.88 GeV. 42

9.5 The input and measured branching fraction for $\psi(3770) \to {\rm non} - D\bar{D}$, where the "input" means the value of the parameter set in the Monte Carlo simulation and the "measured" means the measured value of the parameters from the Monte Carlo simulation. 43

12.1 Quark model classification for some of those low-lying $q\bar{q}$ states. f' and f denote the octet-singlet mixings. It should be noted that the nature of $f_0(1710)$ and $f_0(1370)$ is still under debating. 71

12.2 The final glueball spectrum in physical units. In column 2, the first error is the statistical uncertainty coming from the continuum extrapolation, the second one is the 1% uncertainty resulting from the approximate anisotropy. In column 3, the first error comes from the combined uncertainty of $r_0 M_G$, the second from the uncertainty of $r_0^{-1} = 410(20)\,\mathrm{MeV}$ 73
12.3 Results of $f_0(1710)$ from different experiments before BES2 era. 83
12.4 Decay widths of the 1^{-+} hybrid meson from the two flux tube model. . . . 90
12.5 2^{-+} Isovector Hybrid Decay Modes from Ref. [201]. 91
12.6 1^{-+} Isovector Hybrid Decay Modes from Ref. [201]. 92
12.7 1^{--} Isovector Hybrid Decay Modes from Ref. [201]. 93
12.8 2^{+-} Isovector Hybrid Decay Modes from Ref. [201]. 94
12.9 0^{-+} Isovector Hybrid Decay Modes from Ref. [201]. 94
12.101^{+-} Isovector Hybrid Decay Modes from Ref. [201]. 95
12.110^{+-} Isovector Hybrid Decay Modes from Ref. [201]. 95
12.121^{++} Isovector Hybrid Decay Modes from Ref. [201]. 96
12.13Isoscalar Hybrid Decay Modes from Ref. [201]. 97
12.14$s\bar{s}$ Hybrid Decay Modes from Ref. [201]. 98
12.15$c\bar{c}$ Hybrid Decay Modes from Ref. [201]. 99
12.16Comparison of the decay widths of the 1^{-+} hybrid meson from the flux tube model and QCD sum rule approach. 100
12.17Previous experiments searching for the 1^{-+} hybrid meson. 101

13.1 Measured J/ψ decay branching ratios (BR$\times 10^3$) for channels involving baryon anti-baryon and meson(s) [67, 264] 120

14.1 The masses and widths of the input resonances 125
14.2 Mass resolutions and efficiencies for $J/\psi \to \gamma\eta\eta$ 126
14.3 Input and output comparison of mass, width and branching ratio in the simulation. Here, the masses and widths of $f_0(2100)$ and $f_2(2150)$ are fixed. ($J/\psi \to \gamma\eta\eta, \eta \to \pi^+\pi^-\pi^0, \eta \to \pi^+\pi^-\pi^0$ channel) 129
14.4 Mass resolutions and efficiencies for $J/\psi \to \gamma\eta\eta'$ 130
14.5 $J/\psi \to \phi X$ and its background channels 135

16.1 Different recent determinations of $\overline{m}_b(\overline{m}_b)$ and $\overline{m}_c(\overline{m}_c)$ in the $\overline{\mathrm{MS}}$ scheme from the bottomonium and the charmonium systems. The displayed results either use direct determinations or non-relativistic sum rules. Here and in the text, the * indicates that the theoretical input is only partially complete at that order. 169
16.2 Different perturbative determinations of the B_c mass compared with the experimental value and a recent lattice determination. 170

17.1 Experimental spectrum of reasonably well established "conventional" $c\bar{c}$ states. This table gives the usual quark model multiplet and spectroscopic assignment for each state and the PDG label for the state, followed by their masses and widths. Partner states that are expected theoretically but not yet identified experimentally are indicated by a dash. 177

17.2 Theoretical predictions for the spectrum of $c\bar{c}$ states in a nonrelativistic potential model (NR) and the Godfrey-Isgur relativized potential model (GI). (This table is abstracted from Ref.[95].) 194
17.3 Predictions of a nonrelativistic $c\bar{c}$ potential model for e^+e^- partial widths, together with current (2006) PDG experimental values [448]. 195
17.4 E1 radiative transitions of the low-lying narrow $c\bar{c}$ states in the NR and GI potential models, abstracted from Ref.[95]. The masses are taken from Table 17.2; experimental masses were used (rounded "input" column) if known, otherwise, theoretical values were assumed. 196
17.5 E1 radiative transitions of the broader 1^{--} charmonium states above 4 GeV in the NR and GI quark models (evaluated as in Table 17.4). 197
17.6 Theoretical E1 radiative partial widths of the $\psi(4040)$ and $\psi(4160)$ into $C = (+)$ 2P $c\bar{c}$ states, recalculated in the NR model with masses suggested by the new XYZ states. 198
17.7 Theoretical and experimental M1 radiative partial widths of the ψ and ψ', neglecting recoil effects. 198
17.8 Theoretical ($^3P_0$ model) open-flavor strong decay amplitudes and widths of the four 1^{--} charmonium states above 3.73 GeV most easily accessible at BES (abstracted from Ref.[95]). Multiamplitude decay channels are indicated by boldface. 199

19.1 The determined $|C_1|^2$ and the predicted rates $\Gamma(\Upsilon' \to \Upsilon\ \pi\pi)$, $\Gamma(\Upsilon'' \to \Upsilon\ \pi\pi)$, and $\Gamma(\Upsilon'' \to \Upsilon'\ \pi\pi)$ (in keV) in the Cornell model and the BGT model. The corresponding updated experimental values of the transition rates quoted from Ref. [4] are also listed for comparison. 221
19.2 The predicted transition rate $\Gamma(\psi(3770) \to J/\psi + \pi^+ + \pi^-)$ (in keV) in the Cornell model and the CK model with the updated input data (19.16). 223
19.3 Predictions for the numbers of events in the exclusive detection of the process (19.53) in the CK potential model using the η_c decay modes shown in (19.56)−(19.64) at BES II, BES III, and CLEO-c. The accumulated numbers of the ψ' events are taken to be 1.4×10^7 for BES II, 10^8 for BES III, and 3×10^7 for CLEO-c. The detection efficiency is taken to be 10% for BES II, and 15% for BES III and CLEO-c. 229

20.1 Branching fractions of ψ' radiative decays, only modes observed are listed, for a complete list of al the measurements, refer to PDG [309]. 256
20.2 calculated branching fractions of $\chi_{cJ} \to \gamma V$ from Ref. [363], in unit of $\times 10^{-6}$. 258

21.1 Predictions and measurements for Q_{VP} in unit of 1% for all VP final states. The value for $\rho\pi$ and $K^{*0}\overline{K}^0 + c.c.$ from Ref. [364] were used as input. The theoretical parameter $x = 0.64$ is due to results of Ref. [365] and the experimental results come from Refs. [325, 326, 498, 366]. 265
21.2 Comparison of predictions [395] and measurements [343] for the branching ratios (10^{-5}) for ψ' decays. The upper limits are presented at 90% C.L. . . 271

21.3 Experimental data on the branching fractions for J/ψ and ψ' decays through virtual photon and to lower mass charmonium states used in this analysis. Most of the data are taken from PDG [343], except for $\mathcal{B}(J/\psi, \psi' \to \gamma^* \to$ hadrons), which are calculated by the product $R \cdot \mathcal{B}(J/\psi, \psi' \to \mu^+\mu^-)$, with $R = 2.28 \pm 0.04$ [400]. In estimating the errors of the sums, the correlations between the channels are considered [401]. 273

21.4 Branching fractions for ψ' and J/ψ decays, and Q_h values are also calculated. For $\psi' \to \pi^+\pi^-$, K^+K^- decays, the results are the weighted average of measurements from CLEO [321] and BES [402], while for $J/\psi \to \pi^+\pi^-\pi^0$, the result is the weighted average of measurements from BES [319] and BABAR [320]. Except for values with †, all others from PDG [343]. . . 274

21.5 The input and measured branching fraction for $\psi(3770) \to \text{non} - D\bar{D}$, where the "input" means the value of the parameter set in the Monte Carlo simulation and the "measured" means the measured value of the parameters from the Monte Carlo simulation. 290

21.6 Amplitude parametrization forms for decays of the J/ψ into a pair of octet baryons (phase space is not included). General expressions in terms of singlet A, as well as symmetric and antisymmetric charge-breaking (D, F) and mass-breaking terms (D', F'). 299

21.7 The values of n_{eff} and k for some kinds of the J/ψ and ψ' decay modes . . 301

21.8 Experiment results of η_c decays into baryon-contained final state. The upper limits are given at 90% confidence level. $\mathcal{B}_{\eta_c \to X} = \mathcal{B}_{J/\psi,\psi' \to \gamma\eta_c,\ \eta_c \to X} / \mathcal{B}_{J/\psi,\psi' \to \gamma\eta_c}$ and the values of $\mathcal{B}_{J/\psi,\psi' \to \gamma\eta_c}$ are from PDG06 [448]; the values with $\star$ are for $\psi' \to \gamma\eta_c$ while the other for $J/\psi \to \gamma\eta_c$. 302

21.9 Comparison of theoretical and experimental branching ratios for various χ_{cJ} decays into pairs of light hadrons 303

21.10 Experimental data [448] of two-body baryonic decays for the J/ψ and ψ'. The Q_h and κ_h defined in Eq. (21.58) and (21.63) respectively, are also listed. The upper limits are given at 90% C.L. 305

21.11 The results of two-body octet baryonic final state on the reduced branching ratio $\tilde{\mathcal{B}}$ are compared with the parametrization of the squared amplitude described in the text. The numbers in the parentheses are the calculated results with fitted parameters given in Table 21.12 for $\phi = -90°$. 305

21.12 Fit results for two-body baryonic decay. The parametrization forms and data are give in Table 21.11. The $\star$ indicate the phase value is fixed in the fit. 306

21.13 Comparison between theoretical evaluation [446] and experimental data [448] (or refer to Table 21.10). Here the branching fractions are transformed into decay widths by using $\Gamma_{J/\psi} = (93.4 \pm 2.1)$ keV [448]. $\mathcal{R} \equiv \Gamma_{B\bar{B}}/\Gamma_{p\bar{p}}$. 307

21.14 Angular distribution parameter α for $J/\psi \to B\bar{B}$ decays. They are assumed to be the form of $dN/d\cos\theta \propto 1 + \alpha\cos^2\theta$. 307

21.15 Quantum numbers of baryon-antibaryon nonet with $J^P = 0^-$ or 1^-. I is isospin, I_3 is the third component of I, $\mathcal{S}$ is the strangeness and Q is the charge of the state. The column "symbol" gives nomenclature of the 0^- and 1^- states for easy reference in the Letter. 310

21.16Decay modes containing baryon-antibaryon nonets in charmonium decays. The first J^P is for the accompanying particle while the second for the baryon-antibaryon resonance. 311

21.17Color-magnetic interaction energy of $q^3\overline{q}^3$ eigen-states in common quark model, and the conjugates states are not included. The subscript numbers indicate the detail configurations as explained in Ref. [534]. Here the state is denoted by symbol $|2S(tot)+1, D_f \otimes D_f\rangle$ which is the synthetic state constructed by states such as $|D_{cs}(tot), D_c(tot), 2S(tot)+1; D_f(tot)\rangle$ (refer to Ref. [534] or discussion in the text). 315

21.18The allowed states of the total system in the configuration $(q^3)-(\overline{q}^3)$ and the mass splitting (Table III of Ref. [534]). 316

21.19The allowed states of the total system in the configuration $(q^2\overline{q})$-$(q\overline{q}^2)$ and the mass splitting (Table V of Ref. [534]). 317

21.20Branching ratios of three body decays involving baryons at charmonium region. Most of results from PDG06 [448], except for χ_{cJ} decays, which from CLEOc [533]. The upper limits are given at 90% C.L. and $Q_h = \mathcal{B}_{\psi'\to h}/\mathcal{B}_{J/\psi\to h}$ is also given for possible final states. The numbers in parentheses are the "reduced" branching fraction defined as $\tilde{\mathcal{B}} = \mathcal{B}/PSF_3$, where PSF_3 is the phase space factor for there-body decay (the exact definition and calculation formula of PSF_3 could be found in Appendix **??**, Eq. (**??**)). The unity of PSF_3 is 10^1 and 10^{-1} for the J/ψ and ψ' decays respectively. 320

21.21Experiment searching for exclusive baryonic decay at ψ'' [499]. Listed are the cross section upper limit including the systematic error (90% C.L.), and the branching ratio upper limit including the systematic error (90% C.L.). 321

21.22Decays of η_c and η_c' into $N\overline{N}+$ pions, according to the statistical mode or the constant-matrix-element (phase-space) model. [Each allowed $N\overline{N}$ charge state occurs with half the probability tabulated under "specific charge states."] The first of each pair of entries is for η_c, the second is for η_c'. 323

21.23Summary of J/ψ SU(2) and SU(3) forbidden decay modes measured. . . . 325

21.24*Branching ratios of $\psi \to PP$ decays from reference [606] in the Standard Model. The transition mode, $\Delta C = \Delta S = +1$, corresponds to Cabibbo-allowed decay modes, while $\Delta C = +1$, $\Delta S = 0$ corresponds to Cabibbo-suppressed decay modes.* 337

21.25*Branching ratios of $\psi \to PV$ decays from reference [606] in the Standard Model. The transition mode, $\Delta C = \Delta S = +1$, corresponds to Cabibbo-allowed decay modes, while $\Delta C = +1$, $\Delta S = 0$ corresponds to Cabibbo-suppressed decay modes.* 338

21.26 *$\psi(2S)$ and J/ψ decay modes which can be used to study the invisible decays of J/ψ, χ_{c0}, χ_{c1}, χ_{c2}, $\eta_c(1S)$ and $\eta_c(2S)$. The branching fractions are listed from PDG [619]. For each mode, a "tagging topology" is given, which is the set of visible in the detector's acceptance. In each case the tagging topology has a well-defined kinematics. The produced number of events are the expected events in 3 billions $\psi(2S)$ (10 billions J/ψ) data set, in which we did not consider the decay rate of the tagging particles.* 340

21.27 *The numbers used in the calculations of the ratios in Eq. (21.99), where n^{η}_{UL} ($n^{\eta'}_{UL}$) is the upper limit of the signal events at the 90% confidence level, ϵ_η ($\epsilon_{\eta'}$) is the selection efficiency, $n^{\eta}_{\gamma\gamma}$ ($n^{\eta'}_{\gamma\gamma}$) is the number of the events of $J/\psi \to \phi\eta(\eta')$, $\phi \to K^+K^-$, $\eta(\eta') \to \gamma\gamma$, $\epsilon^{\eta}_{\gamma\gamma}$ ($\epsilon^{\eta'}_{\gamma\gamma}$) is its selection efficiency. σ^{stat}_{η} ($\sigma^{stat}_{\eta'}$) is the relative statistical error and σ^{sys}_{η} ($\sigma^{sys}_{\eta'}$) is the relative statistical error of $n^{\eta}_{\gamma\gamma}$ ($n^{\eta'}_{\gamma\gamma}$), σ_η ($\sigma_{\eta'}$) is the total relative error.* . . 344

21.28 *J/ψ decay modes which can be used to study the invisible decays of η, η', ρ, ω and ϕ. The branching fractions are listed from PDG [619]. For each mode, a "tagging topology" is given, which is the set of visible in the detector's acceptance. In each case the tagging topology has a well-defined kinematics. The produced number of events are the expected events in 10 billions J/ψ data set at BES-III, in which we already considered the decay rate of the tagging particles.* 345

24.1 Predicted D^+ and D_s decay rates and branching fractions assuming $f_D = f_{D_s} = 200$ MeV, $|V_{cd}| = 0.21$ and $|V_{cs}| = 0.97$. 407

24.2 The previous measured f_D. 408

24.3 The previous measured f_{D_s}. 408

24.4 The expected errors of f_{D^+} and $f_{D_s^+}$ in the BESIII measurement with $20fb^{-1}$ data. 414

24.5 Form factors of $F_+^{D\pi}(0)$ and $F_+^{DK}(0)$. 417

24.6 Branching ratios of $D^0 \to \pi^-\ell^+\nu$ and $D^0 \to K^-\ell^+\nu$. 418

24.7 Branching ratios of D and D_s^+ to η, η', K transition channels. 419

24.8 Form factors of $D \to V$ transitions. 421

24.9 Comparison of r_V and r_2 with experimental data. 422

24.10 Ratios of the polarized decay widthes and total branching ratios of $D \to V\ell^+\nu$ decays. 423

24.11 Form factors of $D_{(s)} \to S\ell^+\nu$ decays. 424

24.12 Summary of the measured branching fractions for $D^0 \to K^-e^+\nu_e$ from different experiments, where 'absolute' means that the branching fraction is made absolutely. 426

24.13 Summary of the measured branching fractions for $D^0 \to \pi^-e^+\nu_e$ from different experiments, where 'absolute' means that the branching fraction is made absolutely. 427

24.14 Expected relative statistical error of $\mathcal{B}(D^0 \to K^-e^+\nu_e)$ and $\mathcal{B}(D^0 \to \pi^-e^+\nu_e)$ on BESIII. 431

24.15 The errors of in the determination of the form factor $|f_+^{K(\pi)}(0)|$ with 20 fb^{-1} $\psi(3770)$ data on BESIII. 432

24.16The errors of in the determination of $|V_{cs(d)}|$ with 20 fb^{-1} $\psi(3770)$ data on BESIII. . . . 433

24.17Summary of the measured branching fractions for $D^0 \to Xe^+\nu_e$ from different experiments, where ^{N} means that the measurement has not been used in average by PDG. . . . 435

24.18Summary of the measured branching fractions for $D^+ \to Xe^+\nu_e$ from different experiments, where ^{N} means that the measurement has not been used in average by PDG. . . . 436

24.19Summary of the measured branching fractions for $D^0 \to X\mu^+\nu_\mu$ from different experiments. . . . 436

25.1 *Predicted branching ratios for $D \to PP$ (in 10^{-2}). Most decay modes involving a neutral K meson are given as K^0_S in PDG06 instead of $\overline{K}^0$ in PDG04 which are presented here as well.* . . . 453

25.2 *Predicted branching ratios for $D \to PV$ (in 10^{-2}). Most decay modes involving a neutral K meson are given as K^0_S in PDG06 instead of $\overline{K}^0$ in PDG04 which are presented here as well.* . . . 454

25.2 *(continued) Predicted branching ratios for $D \to PV$ (in 10^{-2}). Most decay modes involving a neutral K meson are given as K^0_S in PDG06 instead of $\overline{K}^0$ in PDG04 which are presented here as well.* . . . 455

25.3 *Experimental branching ratios of various $D \to SP$ decays measured by ARGUS, E687, E691, E791, CLEO, FOCUS and BaBar. For simplicity and convenience, The mass identification for $f_0(980)$, $a_0(980)$ and $K^*_0(1430)$ have been dropped.* . . . 456

25.4 *Branching ratios for various $D \to SP$ decays. Experimental results are taken from Table 25.3.* . . . 458

25.5 *Branching ratios for $D \to Ka_1(1260)$ and $D \to Kb_1(1235)$. Most decay modes involving a neutral K meson are given as K^0_S in PDG06 instead of $\overline{K}^0$ in PDG04 which are presented here as well.* . . . 459

25.6 *Branching ratios of $D \to K_1(1270)\pi$ and $D \to K_1(1400)\pi$ calculated for various $K_{1A} - K_{1B}$ mixing angles.* . . . 461

25.7 *Experimental branching ratios of various $D \to TP$ decays measured by BaBar, CLEO, E791, FOCUS and PDG06. For simplicity and convenience, we have dropped the mass identification for $f_2(1270)$, $a_2(1320)$ and $K^*_2(1430)$.* . . . 461

25.8 *Branching ratios for various $D \to TP$ decays. Experimental results are taken from Table 25.7.* . . . 462

25.9 *Branching ratios (in %) for nonresonant 3-body D decays in various models. Most decay modes involving a neutral K meson are given as K^0_S in PDG06 instead of $\overline{K}^0$ in PDG04 which are presented here as well.* . . . 465

26.1 *The p-wave charmed baryons and their quantum numbers, where S_ℓ (J_ℓ) is the total spin (angular momentum) of the two light quarks. The quantum number in the subscript labels J_ℓ. The quantum number in parentheses is referred to the spin of the baryon. In the quark model, the upper (lower) four multiplets have even (odd) orbital wave functions under the permutation of the two light quarks. That is, L_ℓ for the former is referred to the orbital angular momentum between the diquark and the charmed quark, while L_ℓ for the latter is the orbital angular momentum between the two light quarks. The explicit quark model wave functions for p-wave charmed baryons can be found in [157].* 469
26.2 Mass spectra and decay widths (in units of MeV) of charmed baryons. Experimental values are taken from the Particle Data Group [4] except $\Lambda_c(2880)$, $\Lambda_c(2940)$, $\Xi_c(2980)^{+,0}$, $\Xi_c(3077)^{+,0}$ and $\Omega_c(2768)$ for which we use the most recent available BaBar and Belle measurements. 471
26.3 Decay widths (in units of MeV) of s-wave charmed baryons. Theoretical predictions of [178] are taken from Table IV of [179]. 474
26.4 Same as Table 26.3 except for p-wave charmed baryons [163]. 475
26.5 Various contributions to the decay rates (in units of 10^{-12} GeV) of charmed baryons. The charmed meson wavefunction at the origin squared $|\psi^D(0)|^2$ is taken to be $\frac{1}{12} f_D^2 m_D$. Experimental values are taken from [4]. 482
26.6 Branching ratios of Cabibbo-allowed $\mathcal{B}_c \to \mathcal{B} + P$ decays in various models. Results of [209, 213, 212] have been normalized using the current world averages of charmed baryon lifetimes [4]. Branching ratios cited from [225] are for $\phi_{\eta-\eta'} = -23^\circ$ and $r = 1.4$. 489
26.7 The predicted asymmetry parameter α for Cabibbo-allowed $\mathcal{B}_c \to \mathcal{B} + P$ decays in various models. Results cited from [225] are for $\phi_{\eta-\eta'} = -23^\circ$ and $r = 1.4$ 490
26.8 Branching ratios of Cabibbo-allowed $\mathcal{B}_c \to \mathcal{B} + V$ decays in various models. The experimental value denoted by the superscript $*$ is the branching ratio relative to $\Xi_c^+ \to \Xi^-\pi^+\pi^+$. 491
26.9 Branching ratios and decay asymmetries (in parentheses) of Cabibbo-allowed $\mathcal{B}_c \to \mathcal{B}(3/2^+) + P(V)$ decays in various models. Experimental values denoted by the superscript $*$ are the branching ratios relative to $\Xi_c^+ \to \Xi^-\pi^+\pi^+$. The model calculations of Xu and Kamal are done in two different schemes [230]. 492
26.10 Predicted semileptonic decay rates (in units of $10^{10} s^{-1}$) and decay asymmetries (second entry) in various models. Dipole q^2 dependence for form factors is assumed whenever the form-factor momentum dependence is not calculated in the model. Predictions of [238] are obtained in the non-relativistic quark model and the MIT bag model (in parentheses). 496
26.11 Electromagnetic decay rates (in units of keV) of charmed baryons. 499

27.1 *Summary of Charm experiments nowadays with different techniques, luminosity, charm production cross section and ratio of signal to noise.* 512
27.2 *Results for R_M in D^0 semileptonic decays from PDG2006.* 514

27.3 *Results for R_{WS} and A_D in $D^0 \to K^+\pi^-$, if one assumes that there is no mixing and CP violation in DCSD decay.* . . . 516
27.4 *Limits on x'^2 and y', both 95% C.L. for the case where CP violation is allowed and the case where it is not allowed.* . . . 516
27.5 Summary of y_{CP}results. . . . 520
27.6 *Limits on mixing and CP violation parameters from a t-dependent fit to the $D^0 \to K^0_S\,\pi^+\pi^-$ Dalitz plot, from CLEO using 9.0 fb^{-1}.[291] The errors are statistical, experimental systematic, and modelling systematic, respectively.* 524
27.7 *The sensitivity for R_M measurements at BESIII with different decay modes with 4 years' run at BESPCII* . . . 529

28.1 *Measurements of CP violating asymmetries, A_{CP} (or A_T) in Charm decays. BaBar compares D^+ versus D^- rates. The CLEO results are obtained using a Dalitz plot analysis. CDF uses the decay of $D^{*+} \to D^0\pi^+$ as a flavor tag, and FOCUS uses triple product correlations to measure T violation.*535
28.2 *Estimate of the number of fully reconstructed semileptonic tagged events with CP-eigenstates in one year running time at BESIII.* . . . 540
28.3 *Summary of CP violation measurements at BES-III* . . . 543

29.1 Standard Model predictions and current experimental limits for the branching fractions due to short and long distance contributions for various rare D meson decays. . . . 550
29.2 *Current and projected 90%-CL upper limits on rare D^+ decay modes at BES-III with 20 fb^{-1} data at $\psi(3770)$ peak. We assume the selection efficiencies for all modes are 35%.* . . . 555
29.3 *Current and projected 90%-CL upper limits on rare D^0 decay modes at BES-III with 20 fb^{-1} data at $\psi(3770)$ peak.* . . . 556

37.1 Hadronic D, D^+, D_s^+ Decays . . . 602
37.2 Exclusive Semileptonic Decays . . . 603
37.3 Inclusive Semileptonic Decays . . . 603
37.4 Leptonic Decays . . . 604
37.5 Rare Decays . . . 605
37.6 Charm Mixing . . . 606
37.7 CP and T Violation . . . 606
37.8 Λ_c . . . 606
37.9 CKM Impact . . . 607

A.1 Area of the tails α outside $\pm\delta$ from the mean of a Gaussian distribution. . 623
A.2 Q_γ for $k = 1, 2, 3$ corresponding to a coverage probability $\gamma = 1 - \alpha$ in the large data sample limit. . . . 624
A.3 Lower and upper (one-sided) limits for the mean s of a Poisson variable given n observed events in the absence of background, for CL of 90% and 95% . . . 625
A.4 Unified confidence interval $[s_1, s_2]$ for a mean s of a Poisson variable given n observed events in the absence of background, for CL of 90% and 95% . 627

A.5 *Statistical Significance S and correlated p−value*. 635

Part I

The *BES-III* Experiment and Its Physics

Conveners: Jian-Ping Ma, Ya-Jun Mao

Chapter 1

Physics Goal of *BES-III*

Conveners: Jian-Ping Ma

Chapter 2

The *BES-III* detector and offline software

Chapter 3

Analysis tools

3.1 Particle Identification

3.2 Kinematic Fitting and Vertex Fitting

3.3 Luminosity Measurement at BESIII

3.4 Monte Carlo Generators

3.5 Partial Wave Analysis

3.6 Dalitz-plot Analysis Formalism[1]

Originally the primary application of Dalitz-plot analyses was to determine the spin and parity of light mesons. Recently Dalitz-plot analyses have emerged as a powerful tool in the study of D and B mesons.

Charm meson decay dynamics have been studied extensively over the last decade. Recent studies of multi-body decays of charm mesons probe a variety of physics including doubly-Cabibbo suppressed decays[1][2][3], searches for CP violation[2][4][5][6][7], T violation[8], D^0–$\overline{D}^0$ mixing[9][10], the properties of established light mesons[11][12][13][14], the properties of $\pi\pi$[1][13][15], $K\pi$[16][17], and KK [18] S-wave states, and the dynamics of four-body final states[19][20].

Recently B meson decay dynamics have been studied. Multi-body decays of B mesons also probe a variety of physics including, charmless B-decays[21] [**?**][23][24][25], measurements of the Cabibbo-Kobayashi-Maskawa (CKM) angle γ/ϕ_3 [26][27][28][29][30], searches for direct CP violation[23] [24][31], charm spectroscopy[32][33], the properties of established light mesons [21][24][25], the properties of KK[21][25] and $K\pi$[21][23][24] S-wave, and the three-body production of baryons[**?**][34]. Time-dependent Dalitz-plot (TD) analyses have been used to determine the CKM angle α/ϕ_2 with $B \to \pi^+\pi^-\pi^0$[35] and to resolve the two-fold ambiguity in the CKM angle β/ϕ_1 with $B \to D\pi^0, D \to K^0_S\pi^+\pi^-$[36][37].

[1] By David Asner

A TD analysis of $B^0 \to D^{*\pm}K^0\pi^\mp$[38] is sensitive γ/ϕ_3. Future studies could improve sensitivity to new physics in TD analyses of $b \to s$ penguin decays[25].

Additionally, partial wave analyses have been used to study the dynamics of charmonium decays to hadrons, following the formalism presented in Refs.[39][40], in radiative decays[41][42][43][44] and in decays to all hadronic final states[45][46][47][48]. Multi-body decays of charmonium to all hadronic final states can be analyzed with the Dalitz-plot analysis technique. Studies of the $\pi\pi$, $K\pi$ and KK S-wave in charmonium decays probe most of the phase space accessible in B decays. Thus Dalitz-plot analyses of charmonia could lead to reduced systematic errors in many B analyses.

Weak nonleptonic decays of B and charm mesons are expected to proceed dominantly through resonant two-body decays in several theoretical models[218]; see Ref.[50] for a review of resonance phenomenology. These amplitudes are typically calculated with the Dalitz plot analysis technique[51], which uses the mininum number of independent observable quantities. For three-body decay of a spin-0 particle to all pseudo-scalar final states, $D, B \to abc$, the decay rate[52] is

$$\Gamma = \frac{1}{(2\pi)^3 32\sqrt{s^3}} \left|\mathcal{M}\right|^2 dm_{ab}^2 dm_{bc}^2, \tag{3.1}$$

where m_{ij} is the invariant mass of $i-j$ and the coefficient of the amplitude includes all kinematic factors. The scatter plot in m_{ab}^2 versus m_{bc}^2 is called a Dalitz plot. If $\left|\mathcal{M}\right|^2$ is constant the allowed region of the plot will be populated uniformly with events. Any variation in $\left|\mathcal{M}\right|^2$ over the Dalitz plot is due to dynamical rather than kinematical effects. It is straightforward to extend the formalism beyond three-body final states. For N-body final states, phase space has dimension $3N-7$. Other cases of interest include one vector particle or a fermion/anti-femion pair (e.g. $B \to D^*\pi\pi$, $B \to \Lambda_c p\pi$, $B \to K\ell\ell$) in the final state. For the former case phase space has dimension $3N-5$ and for the latter two $3N-4$.

The amplitude of the process, $R \to rc, r \to ab$ where R is a D, B, or $q\bar{q}$ meson and a,b,c are pseudo-scalars, is given by

$$\begin{aligned} \mathcal{M}_r(J, L, l, m_{ab}, m_{bc}) &= \textstyle\sum_\lambda \left\langle ab|r_\lambda\right\rangle T_r(m_{ab}) \left\langle cr_\lambda|R_J\right\rangle \\ &= Z(J, L, l, \vec{p}, \vec{q}) B_L^R(|\vec{p}|) B_L^r(|\vec{q}|) T_r(m_{ab}), \end{aligned} \tag{3.2}$$

where the sum is over the helicity states λ of the intermediate resonance particle r, a and b are the daughter particles of the resonance r, c is the spectator particle, J is the total angular momentum of R, L is the orbital angular momentum between r and c, l is the orbital angular momentum between a and b equivalent to the spin of r, $\vec{p}$ and $\vec{q}$ are the momentum of c and a, respectively, in the r rest frame, Z describes the angular distribution of final state particles, B_L^R and B_L^r are the barrier factors for the production of rc and ab, respectively, with angular momentum L, and T_r is the dynamical function describing the resonance r. The amplitude for modeling the Dalitz plot is a phenomenological object. Differences in the parametrizations of Z, B_L and T_r, as well as the set of resonances r, complicate the comparison of results from different experiments.

Usually the resonances are modeled with a Breit-Wigner although some more recent analyses have used the K-matrix formalism[53][54][55] with the P-vector approximation[56] to describe the $\pi\pi$ S-wave.

The nonresonant (NR) contribution $D \to abc$ is parameterized as constant (S-wave) with no variation in magnitude or phase across the Dalitz plot. The available phase space is much greater for B decay and the nonresonant contribution to $B \to abc$ requires a more sophisticated parametrization. Theoretical models of the NR amplitude[57][58] [59][60] do not reproduce the distibutions observed in the data. Experimentally, several parametrizations have been used[21][25].

3.6.1 Barrier Factor B_L

The maximum angular momentum L in a strong decay is limited by the linear momentum $\vec{q}$. Decay particles moving slowly with an impact parameter (meson radius) d of order 1 fm have difficulty generating sufficient angular momentum to conserve the spin of the resonance. The Blatt-Weisskopf[61][62] functions B_L, given in **??**, weight the reaction amplitudes to account for this spin-dependent effect. These functions are normalized to give $B_L = 1$ for $z = (|\vec{q}|\, d)^2 = 1$. Another common formulation B'_L, also in **??**, is normalized to give $B'_L = 1$ for $z = z_0 = (|\vec{q}_0|\, d)^2$ where q_0 is the value of q when $m_{ab} = m_r$.

L	$B_L(q)$	$B'_L(q, q_0)$
0	1	1
1	$\sqrt{\frac{2z}{1+z}}$	$\sqrt{\frac{1+z_0}{1+z}}$
2	$\sqrt{\frac{13z^2}{(z-3)^2+9z}}$	$\sqrt{\frac{(z_0-3)^2+9z_0}{(z-3)^2+9z}}$
where $z = (\|\vec{q}\|\, d)^2$ and $z_0 = (\|\vec{q}_0\|\, d)^2$		

Table 3.1: Blatt-Weisskopf barrier factors.

3.6.2 Angular Distributions

The tensor or Zemach formalism[272][64] and the helicity formalism[65][64] yield identical descriptions of the angular distributions for the decay process $R \to rc, r \to ab$ for reactions where a, b and c are spin-0 and the initial state is unpolarized. In this scenario, the angular distributions for $J = 0, 1, 2$ are given in 3.2. For polarized initial states, the helicity formalism[65] is used to determine the distinct angular distribution for each helicity state $|\lambda|$. The angular distributions for $J = 1, 2$ for a polarized initial are given in 3.3. The sign of the helicity cannot be determined from the Dalitz plot alone when a, b and c are spin-0. For final state particles with non-zero spin (e.g. radiative charmonium decays), the helicity formalism is required.

For the decays of pseudoscalars to three pseudoscalars the formalism simplifies considerably as the angular distribution Z depends only on the spin l of resonance r. Since $J = 0$ and $L = l$ only the first three rows of 3.2 are required.

$J \to l + L$	Angular Distribution
$0 \to 0+0$	uniform
$0 \to 1+1$	$(1+\zeta^2)\cos^2\theta$
$0 \to 2+2$	$(\zeta^2+\frac{3}{2})^2(\cos^2\theta-1/3)^2$
$1 \to 0+1$	uniform
$1 \to 1+0$	$1+\zeta^2\cos^2\theta$
$1 \to 1+1$	$\sin^2\theta$
$1 \to 1+2$	$1+(3+4\zeta^2)\cos^2\theta$
$1 \to 2+1$	$(1+\zeta^2)[1+3\cos^2\theta+9\zeta^2(\cos^2\theta-1/3)^2]$
$1 \to 2+2$	$(1+\zeta^2)\cos^2\theta\sin^2\theta$
$2 \to 0+2$	uniform
$2 \to 1+1$	$3+(1+4\zeta^2)\cos^2\theta$
$2 \to 1+2$	$\sin^2\theta$
$2 \to 2+0$	$1+\frac{\zeta^2}{3}+\zeta^2\cos^2\theta+\zeta^4(\cos^2\theta-1/3)^2$
$2 \to 2+1$	$1+\frac{\zeta^2}{9}+(\frac{\zeta^2}{3}-1)\cos^2\theta-\zeta^2(\cos^2\theta-1/3)^2$
$2 \to 2+2$	$1+\frac{\zeta^2}{9}+(\frac{\zeta^2}{3}-1)\cos^2\theta+\frac{(16\zeta^4+21\zeta^2+9)(\cos^2\theta-1/3)^2}{3}$

Table 3.2: Angular distributions for each J, L, l for *unpolarized* initial states where θ is the angle between particles a and c in the rest frame of resonance r, $\sqrt{1+\zeta^2}$ is a relativistic correction with $\zeta^2 = E_r^2/m_{ab}^2 - 1$, and $E_r = (m_R^2 + m_{ab}^2 - m_c^2)/2m_R$.

$J \to l + L$	Angular Distribution
$1 \to 1+0$	$F_0\gamma^2\cos^2\theta + F_1\sin^2\theta$
$1 \to 1+1$	$F_1\sin^2\theta$
$1 \to 1+2$	$F_0(2\gamma/3)^2\cos^2\theta + F_1(1/9)\sin^2\theta$
$1 \to 2+1$	$2F_0\gamma^4(\cos^2\theta - 1/3)^2$
	$+F_1\gamma^2[2/9+2/3\cos^2\theta-2(\cos^2\theta - 1/3)^2]$
$1 \to 2+2$	$F_1\gamma^2\cos^2\theta\sin^2\theta$
$2 \to 1+1$	$F_0(2\gamma^2/3)\cos^2\theta^2 + F_1(1/2)\sin^2\theta$
$2 \to 1+2$	$F_1\sin^2\theta$
$2 \to 2+0$	$F_0(4\gamma^4/3 + 4\gamma^2/3 + 1/3)(\cos^2\theta-1/3)^2$
	$+F_1\gamma^2[4/9 + 4/3\cos^2\theta - 4(\cos^2\theta-1/3)^2]$
	$+F_2[8/9 - 4/3\cos^2\theta + (\cos^2\theta-1/3)^2]$
$2 \to 2+1$	$F_1\gamma^2[1/9+1/3\cos^2\theta - (\cos^2\theta-1/3)^2]$
	$+F_2[8/9 - 4/3\cos^2\theta + (\cos^2\theta-1/3)^2]$
$2 \to 2+2$	$3F_0(4\gamma^2/9-1/9)^2(\cos^2\theta-1/3)^2$
	$+F_1\gamma^2[1/9+4/3-(\cos^2\theta-1/3)^2]/9$
	$+F_2[8/9-4/3\cos^2\theta + (\cos^2\theta-1/3)^2]/9$

Table 3.3: Angular distributions for $J \neq 0, L \neq 0, l$ for *polarized* initial states where $\cos\theta$ is the angle between particles a and c in the rest frame of resonance r, $\gamma = E_r/m_{ab}$, and $E_r = (m_R^2 + m_{ab}^2 - m_c^2)/2m_R$. F_λ denotes the fraction of the initial state in helicity state λ. For unpolarized initial states setting F_λ=1 recovers the angular distributions obtained from the Zemach formalism shown in 3.2.

3.6.3 Dynamical Function T_R

The dynamical function T_r is derived from the S-matrix formalism. In general, the amplitude that a final state f couples to an initial state i $S_{fi} = \langle f|S|i\rangle$, where the scattering operator S is unitary and satisfies $SS^\dagger = S^\dagger S = I$. The transition operator $\hat{T}$ is defined by separating the probability that $f = i$ yielding,

$$S = I + 2iT = I + 2i\left\{\rho\right\}^{1/2}\hat{T}\left\{\rho\right\}^{1/2}, \tag{3.3}$$

where I is the identity operator, $\hat{T}$ is Lorentz invariant transition operator, ρ is the diagonal phase space matrix where $\rho_{ii} = 2q_i/m$ and q_i is the momentum of a in the r rest frame for decay channel i. In the single channel S-wave scenario $S = e^{2i\delta}$ satisfies unitarity and implies

$$\hat{T} = \frac{1}{\rho}e^{i\delta}\sin\delta. \tag{3.4}$$

There are three common formulations of the dynamical function. The Breit-Wigner formalism is the simplest formulation - the first term in a Taylor expansion about a T matrix pole. The K-matrix formalism[53] is more general (allowing more than one T matrix pole and coupled channels while preserving unitarity). The Flatté distribution[66] is used to parameterize resonances near threshold and is equivalent to a one-pole, two-channel K-matrix.

3.6.4 Breit-Wigner Formulation

The common formulation of a Breit-Wigner resonance decaying to spin-0 particles a and b is

$$T_r(m_{ab}) = \frac{1}{m_r^2 - m_{ab}^2 - im_r\Gamma_{ab}(q)} \tag{3.5}$$

where the "mass dependent" width Γ is

$$\Gamma = \Gamma_r\left(\frac{q}{q_r}\right)^{2L+1}\left(\frac{m_r}{m_{ab}}\right)B'_L(q,q_0)^2 \tag{3.6}$$

where $B'_L(q,q_0)$ is the Blatt-Weisskopf barrier factor from 3.1. A Breit-Wigner parametrization best describes isolated, non-overlapping resonances far from the threshold of additional decay channels. For the ρ and $\rho(1450)$ a more complex parametrization as suggested by Gounaris-Sakarai[67] is often used [23][28][30][35].

Unitarity can be violated when the dynamical function is parameterized as the sum of two or more overlapping Breit-Wigners. The proximity of a threshold to the resonance shape distorts the line shape from a simple Breit-Wigner. This scenario is described by the Flatté formula and is discussed below.

3.6.5 K-matrix Formalism

The T matrix can be described as

$$\hat{T} = (I - i\hat{K}\rho)^{-1}\hat{K}, \tag{3.7}$$

where $\hat{K}$ is the Lorentz invariant K-matrix describing the scattering process and ρ is the phase space factor.

Resonances appear as a sum of poles in the K-matrix

$$\hat{K}_{ij} = \sum_{\alpha} \frac{\sqrt{m_\alpha \Gamma_{\alpha i}(m) m_\alpha \Gamma_{\alpha j}(m)}}{(m_\alpha^2 - m^2)\sqrt{\rho_i \rho_j}}. \tag{3.8}$$

The K-matrix is real by construction thus the associated T-matrix respects unitarity.

For the special case of a single channel, single pole we obtain

$$K = \frac{m_0 \Gamma(m)}{m_0^2 - m^2} \tag{3.9}$$

and

$$T = K(1 - iK)^{-1} = \frac{m_0 \Gamma(m)}{m_0^2 - m^2 - i m_0 \Gamma(m)} \tag{3.10}$$

which is the relativistic Breit-Wigner formula. For the special case of a single channel, two poles we have

$$K = \frac{m_\alpha \Gamma_\alpha(m)}{m_\alpha^2 - m^2} + \frac{m_\beta \Gamma_\beta(m)}{m_\beta^2 - m^2} \tag{3.11}$$

and in the limit that m_α and m_β are far apart relative to the widths we can approximate the T matrix as the sum of two Breit-Wigners, $T(K_\alpha + K_\beta) \approx T(K_\alpha) + T(K_\beta)$,

$$T \approx \frac{m_\alpha \Gamma_\alpha(m)}{m_\alpha^2 - m^2 - i m_\alpha \Gamma_\alpha(m)} + \frac{m_\beta \Gamma_\beta(m)}{m_\beta^2 - m^2 - i m_\beta \Gamma_\beta(m)}. \tag{3.12}$$

In the case of two nearby resonances 3.12 is not valid and exceeds unity (and hence T violates unitarity).

This formulation, which applies to S-channel production in two-body scattering $ab \to cd$, can be generalized to describe the production of resonances in processes, such as the decay of charm mesons. The key assumption here is that the two-body system described by the K-matrix does *not* interact with the rest of the final state[56]. The quality of this assumption varies with the production process and is appropriate for scattering experiments like $\pi^- p \to \pi^0 \pi^0 n$, radiative decays such as $\phi, J/\psi \to \gamma\pi\pi$ and semileptonic decays such as $D \to K\pi\ell\nu$. This assumption may be of limited validity for production processes such as $p\overline{p} \to \pi\pi\pi$ or $D \to \pi\pi\pi$. In these scenarios the two-body Lorentz invariant amplitude, $\hat{F}$, is given as

$$\hat{F}_i = (I - i\hat{K}\rho)^{-1}_{ij} \hat{P}_j = (\hat{T}\hat{K}^{-1})_{ij} \hat{P}_j \tag{3.13}$$

where P is the production vector which parameterizes the resonance production in the open channels.

For the $\pi\pi$ S-wave, a common formulation of the K-matrix[55][13][30] is

$$K_{ij}(s) = \left\{ \sum_{\alpha} \frac{g_i^{(\alpha)} g_j^{(\alpha)}}{m_\alpha^2 - s} + f_{ij}^{sc} \frac{1 - s_0^{sc}}{s - s_0^{sc}} \right\} \times \frac{s - s_A/2m_\pi^2}{(s - s_{A0})(1 - s_{A0})}. \tag{3.14}$$

The factor $g_i^{(\alpha)}$ is the real coupling constant of the K-matrix pole m_α to meson channel i; the parameters f_{ij}^{sc} and s_0^{sc} describe a smooth part of the K-matrix elements; the multiplicative factor $\frac{s-s_A/2m_\pi^2}{(s-s_{A0})(1-s_{A0})}$ suppresses a false kinematical singularity near the $\pi\pi$ threshold - the Adler zero; and the number 1 has units GeV^2.

The production vector, with $i=1$ denoting $\pi\pi$, is

$$P_j(s) = \left\{ \sum_\alpha \frac{\beta_\alpha g_j^{(\alpha)}}{m_\alpha^2 - s} + f_{1j}^{pr} \frac{1-s_0^{pr}}{s-s_0^{pr}} \right\} \times \frac{s-s_A/2m_\pi^2}{(s-s_{A0})(1-s_{A0})}, \tag{3.15}$$

where the free parameters of the Dalitz plot fit are the complex production couplings β_α, and the production vector background parameters f_{1j}^{pr} and s_0^{pr}. All other parameters are fixed by scattering experiments. Ref. [54] describes the $\pi\pi$ scattering data with a 4 pole, 2 channel ($\pi\pi$, KK) model while Ref. [55] describes the scattering data with 5 pole, 5 channel ($\pi\pi$, KK, $\eta\eta$, $\eta'\eta'$ and 4π) model. The former has been implemented by CLEO[6] and the latter by FOCUS[13] and BaBar[30]. In both cases only the $\pi\pi$ channel was analyzed. A more complete coupled channel analysis would simultaneously fit all final states accessible by rescattering.

3.6.6 Flatté Formalism

The scenario where another channel opens close to the resonance position can be described by the Flatté formulation

$$\hat{T}(m_{ab}) = \frac{1}{m_r^2 - m_{ab}^2 - i(\rho_1 g_1^2 + \rho_2 g_2^2)}, \quad g_1^2 + g_2^2 = m_r \Gamma_r. \tag{3.16}$$

This situation occurs in the $\pi\pi$ S-wave where the $f_0(980)$ is near the $K\overline{K}$ threshold and in the $\pi\eta$ channel where the $a_0(980)$ also lies near $K\overline{K}$ threshold. For the $a_0(980)$ resonance the relevant coupling constants are $g_1 = g_{\pi\eta}$ and $g_2 = g_{KK}$ and the phase space terms are $\rho_1 = \rho_{\pi\eta}$ and $\rho_2 = \rho_{KK}$ where

$$\rho_{ab} = \sqrt{\left(1 - (\frac{m_a - m_b}{m_{ab}})^2\right)\left(1 + (\frac{m_a - m_b}{m_{ab}})^2\right)} \tag{3.17}$$

For the $f_0(980)$ the relevant coupling constants are $g_1 = g_{\pi\pi}$ and $g_2 = g_{KK}$ and the phase space terms are $\rho_1 = \rho_{\pi\pi}$ and $\rho_2 = \rho_{KK}$. The charged and neutral K channels are usually assumed to have the same coupling constant but separate phase space factors due to $m_{K^+} \neq m_{K^0}$ resulting in

$$\rho_{KK} = \frac{1}{2}\left(\sqrt{1 - \left(\frac{2m_{K^\pm}}{m_{KK}}\right)^2} + \sqrt{1 - \left(\frac{2m_{K^0}}{m_{KK}}\right)^2} \right). \tag{3.18}$$

3.6.7 Branching Ratios from Dalitz Fits

The fit to the Dalitz plot distribution using either the Breit-Wigner or the K-matrix formalism factorizes into a resonant contribution to the amplitude $\mathcal{M}_j$ and a complex

coefficient, $a_j e^{i\delta_j}$, where a_j and δ_j are real. The definition of a rate of a single process, given a set of amplitudes a_j and phases δ_j is the square of the relevant matrix element (see 3.1). In this spirit, the fit fraction is usually defined as the integral over the Dalitz plot (m_{ab} vs m_{bc}) of a single amplitude squared divided by the integral over the Dalitz plot of the square of the coherent sum of all amplitudes,

$$\text{Fit Fraction}_j = \frac{\int \left| a_j e^{i\delta_j} \mathcal{M}_j \right|^2 dm_{ab}^2 dm_{bc}^2}{\int \left| \sum_k a_k e^{i\delta_k} \mathcal{M}_k \right|^2 dm_{ab}^2 dm_{bc}^2} \tag{3.19}$$

where $\mathcal{M}_j$ is defined by 3.2 and described in Ref.[4]. The sum of the fit fractions for all components will in general not be unity due to interference.

It should be noted that, when the K-matrix description in 3.13 is used to describe a wave (e.g. $\pi\pi$ S-wave) then $\mathcal{M}_j$ refers to the entire wave. In these circumstances, it may not be straightforward to separate it into a sum of individual resonances unless these are narrow and well separated, in which case 3.12 can be used.

Reconstruction Efficiency

The efficiency for reconstructing an event as a function of position on the Dalitz plot is in general non-uniform.

Describe the efficiency parametrizations used at CLEO

Typically, a signal Monte Carlo sample generated with a uniform distribution in phase space is used to determine the efficiency. The variation in efficiency across the Dalitz plot varies with experiment and decay mode. Most recent analyses utilize a full GEANT[68] detector simulation.

Finite detector resolution can usually be safely neglected as most resonances are comparatively broad. Notable exceptions where detector resolution effects must be modeled are $\phi \to K^+K^-$, $\omega \to \pi^+\pi^-$, and $a_0 \to \eta\pi^0$. One approach is to convolve the resolution function in the Dalitz-plot variables m_{ab}^2, m_{bc}^2 with the function that parameterizes the resonant amplitudes. In high statistics data samples resolution effects near the phase space boundary typically contribute to a poor goodness of fit. The momenta of a,b and c *can* be recalculated with a R mass constraint. This forces the kinematical boundaries of the Dalitz plot to be strictly respected. If the three-body mass is not constrained, then the efficiency (and the parametrization of background) may also depend on the reconstructed mass. In fits to multi-body decays of charmonia and bottomonia it is not appropriate to constrain the mass due to the finite natural width of the parent.

Background Parametrization

The contribution of background to the charm and B samples varies by experiment and final state. The background naturally falls into five categories: (i) purely combinatoric background containing no resonances, (ii) combinatoric background containing intermediate resonances, such as a real K^{*-} or ρ, plus additional random particles, (iii) final states containing identical particles as in $D^0 \to K_S^0\pi^0$ background to $D^0 \to \pi^+\pi^-\pi^0$ and $B \to D\pi$ background to $B \to K\pi\pi$, (iv) mistagged decays such as a real $\overline{D}^0$ or $\overline{B}^0$ incor-

rectly identified as D^0 or B^0 and (v) particle misidentification of the decay products such as $D^+ \to \pi^-\pi^+\pi^+$ or $D_s^+ \to K^-K^+\pi^+$ reconstructed as $D^+ \to K^-\pi^+\pi^+$.

The contribution from combinatoric background with intermediate resonances is distinct from the resonances in the signal because the former do *not* interfere with the latter since they are not from true resonances. Additionally, processes such as $\psi' \to \gamma\chi_{c2} \to \gamma(\gamma J/\psi) \to \gamma\gamma(\pi\pi)$ and $\psi' \to \pi^0 J/\psi, J/\psi \to \pi\pi$, do *not* interfere since electromagnetic and hadronic transitions proceed on different time scales. Similarly, $D^0 \to \rho\pi$ and $D^0 \to K_S^0\pi^0$ do not interfere since strong and weak transitions proceed on different time scales. The usual identification tag of the initial particle as a D^0 or a $\overline{D}^0$ is the charge of the distinctive slow pion in the decay sequence $D^{*+} \to D^0\pi_s^+$ or $D^{*-} \to \overline{D}^0\pi_s^-$. Another possibility is the identification or "tagging" of one of the D mesons from $\psi(3770) \to D^0\overline{D}^0$ as is done for B mesons from $\Upsilon(4S)$. The mistagged background is subtle and may be mistakenly enumerated in the *signal* fraction determined by a D^0 mass fit. Mistagged decays contain true $\overline{D}^0$'s or $\overline{B}^0$'s and so the resonances in the mistagged sample exhibit interference on the Dalitz plot.

Bibliography

[1] H. Muramatsu *et al.* (CLEO Collab.), Phys. Rev. Lett. **89**, 251802 (2002) [Erratum-ibid. **90**, 059901 (2003)]

[2] G. Brandenburg *et al.* (CLEO Collab.), Phys. Rev. Lett. **87**, 071802 (2001)

[3] J. M. Link *et al.* (FOCUS Collab.), Phys. Lett. B **601**, 10 (2004)

[4] S. Kopp *et al.* (CLEO Collab.), Phys. Rev. D **63**, 092001 (2001)

[5] D. M. Asner *et al.* (CLEO Collab.), Phys. Rev. D **70**, 091101 (2004)

[6] D. Cronin-Hennessy *et al.* (CLEO Collab.), Phys. Rev. D **72**, 031102 (2005)

[7] B. Aubert *et al.* (BABAR Collab.), Phys. Rev. D **71**, 091101 (2005)

[8] J. M. Link *et al.* (FOCUS Collab.), Phys. Lett. B **622**, 239 (2005)

[9] D. M. Asner (CLEO Collab.), Phys. Rev. D **72**, 012001 (2005)

[10] See the Note on D^0–$\overline{D}^0$ Mixing by D. Asner in the Review; Dalitz plot analysis of the wrong sign rate $D^0 \to K^+\pi^-\pi^0$[2] is a candidate processes

[11] P. L. Frabetti *et al.* (E687 Collab.), Phys. Lett. B **407**, 79 (1997)

[12] E. M. Aitala *et al.* (E791 Collab.), Phys. Rev. Lett. **86**, 765 (2001)

[13] J. M. Link *et al.* (FOCUS Collab.), Phys. Lett. B **585**, 200 (2004)

[14] P. Rubin *et al.* (CLEO Collab.), Phys. Rev. Lett. **93**, 111801 (2004)

[15] E. M. Aitala *et al.* (E791 Collab.), Phys. Rev. Lett. **86**, 770 (2001)

[16] E. M. Aitala *et al.* (E791 Collab.), Phys. Rev. Lett. **89**, 121801 (2002)

[17] E. M. Aitala *et al.* (E791 Collab.), submitted to Phys. Rev. D, arXiv:hep-ex/0507099 - submitted to Phys. Rev. D

[18] B. Aubert *et al.* (BABAR Collab.), Phys. Rev. D **72**, 052008 (2005)

[19] J. M. Link *et al.* (FOCUS Collab.), Phys. Lett. B **575**, 190 (2003)

[20] J. M. Link *et al.* (FOCUS Collab.), Phys. Lett. B **610**, 225 (2005)

[21] A. Garmash *et al.* (Belle Collab.), Phys. Rev. D **71**, 092003 (2005)

[22] M. Z. Wang *et al.*, Phys. Lett. B **617**, 141 (2005)

[23] B. Aubert *et al.* (BABAR Collab.), arXiv:hep-ex/0408073

[24] B. Aubert *et al.* (BABAR Collab.), submitted to Phys. Rev. D, arXiv:hep-ex/0507004

[25] B. Aubert *et al.* (BABAR Collab.), arXiv:hep-ex/0507094

[26] A. Poluektov *et al.* (Belle Collab.), Phys. Rev. D **70**, 072003 (2004)

[27] K. Abe *et al.* (Belle Collab.), arXiv:hep-ex/0411049

[28] K. Abe *et al.* (Belle Collab.), arXiv:hep-ex/0504013

[29] B. Aubert *et al.* (BABAR Collab.), Phys. Rev. Lett. **95**, 121802 (2005)

[30] B. Aubert *et al.* (BABAR Collab.), arXiv:hep-ex/0507101

[31] A. Garmash, arXiv:hep-ex/0505048; A. Garmash, arXiv:hep-ex/0510059;

[32] K. Abe *et al.* (Belle Collab.), Phys. Rev. D **69**, 112002 (2004)

[33] K. Abe *et al.* (Belle Collab.), arXiv:hep-ex/0412072

[34] K. Abe *et al.* (Belle Collab.), arXiv:hep-ex/0409005

[35] B. Aubert *et al.* (BABAR Collab.), arXiv:hep-ex/0408099

[36] A. Bondar, T. Gershon and P. Krokovny, Phys. Lett. B **624**, 1 (2005)

[37] K. Abe *et al.* (Belle Collab.), arXiv:hep-ex/0507065

[38] B. Aubert *et al.* (BABAR Collab.), submitted to Phys. Rev. Lett., arXiv:hep-ex/0412040

[39] B. S. Zou and D. V. Bugg, Eur. Phys. J. A **16**, 537 (2003)

[40] S. Dulat and B. S. Zou, Eur. Phys. J. A **26**, 125 (2005)

[41] J. Z. Bai *et al.* (BES Collab.), Phys. Rev. D **68**, 052003 (2003)

[42] J. Z. Bai *et al.* (BES Collab.), Phys. Lett. B **476**, 25 (2000)

[43] J. Z. Bai *et al.* (BES Collab.), Phys. Lett. B **472**, 207 (2000)

[44] J. Z. Bai *et al.* (BES Collab.), Phys. Lett. B **472**, 200 (2000)

[45] M. Ablikim *et al.* (BES Collab.), Phys. Rev. D **72**, 092002 (2005)

[46] M. Ablikim *et al.* (BES Collab.), Phys. Lett. B **619**, 247 (2005)

[47] M. Ablikim *et al.* (BES Collab.), Phys. Lett. B **598**, 149 (2004)

[48] M. Ablikim *et al.* (BES Collab.), Phys. Lett. B **603**, 138 (2004)

[49] M Bauer, B. Stech and M. Wirbel, Z. Phys. C **34**, 103 (1987); P. Bedaque, A. Das and V.S. Mathur, Phys. Rev. D **49**, 269 (1994); L.-L. Chau and H.-Y. Cheng, Phys. Rev. D **36**, 137 (1987); K. Terasaki, Int. J. Mod. Phys. A **10**, 3207 (1995); F. Buccella, M. Lusignoli and A. Pugliese, Phys. Lett. B **379**, 249 (1996)

[50] J. D. Jackson, Nuovo Cim. **34**, 1644 (1964)

[51] R. H. Dalitz, *Phil. Mag.* **44**, 1068 (1953)

[52] See the note on Kinematics revised by J. D. Jackson in this *Review*

[53] S.U. Chung *et al.*, Ann. Physik. **4**, 404 (1995)

[54] K. L. Au, D. Morgan and M. R. Pennington, Phys. Rev. D **35**, 1633 (1987)

[55] V. V. Anisovich and A. V. Sarantsev, Eur. Phys. J. A **16**, 229 (2003)

[56] I. J. R. Aitchison, Nucl. Phys. **A 189**, 417 (1972)

[57] S. Fajfer, R. J. Oakes and T. N. Pham, Phys. Rev. D **60**, 054029 (1999)

[58] H. Y. Cheng and K. C. Yang, Phys. Rev. D **66**, 054015 (2002)

[59] S. Fajfer, T. N. Pham and A. Prapotnik, Phys. Rev. D **70**, 034033 (2004)

[60] H. Y. Cheng, C. K. Chua and A. Soni, arXiv:hep-ph/0506268

[61] J. Blatt and V. Weisskopf, *Theoretical Nuclear Physics*, New York: John Wiley & Sons (1952)

[62] F. von Hippel and C. Quigg, Phys. Rev. D **5**, 624, (1972)

[63] C. Zemach, Phys. Rev. B **133**, 1201 (1964); C. Zemach, Phys. Rev. B **140**, 97 (1965)

[64] V. Filippini, A. Fontana and A. Rotondi, Phys. Rev. D **51**, 2247 (1995)

[65] M. Jacob and G. C. Wick, Annals Phys. **7**, 404 (1959) [Annals Phys. **281**, 774 (2000)]; S. U. Chung, Phys. Rev. D **48**, 1225, (1993); J. D. Richman, CALT-68-1148

[66] S. M. Flatté, Phys. Lett. B **63**, 224 (1976)

[67] G. J. Gounaris and J. J. Sakarai, Phys. Rev. Lett. **21** 244, (1968)

[68] R. Brun *et al.*, GEANT 3.15, CERN Report No. DD/EE/84-1 (1987); R. Brun *et al.*, GEANT 3.21, CERN Program Library Long Writeup W5013 (1993), unpublished; S. Agostinelli *et al.* (GEANT4 Collab.), Nucl. Instrum. Meth. A **506**, 250 (2003)

Part II

e^+e^- Collision at $\sqrt{s} = 2 - 5$ GeV

Conveners: Xiao-Yuan Li, Yuan-Ning Gao
Authors: A. A, B .B, ...

Chapter 4

Physics Processes

Chapter 5

Hadron Production and Fregmentation

Chapter 6

R values

Chapter 7

QCD studies at $\sqrt{s} = 2 - 5$ GeV

Chapter 8

Production cross sections of $D^0\overline{D}^{(*)0}$ and $D_S^+ D_S^{(*)-}$ (?)

Chapter 9

Measurements of Parameters of Charmonium Resonances[1]

9.1 Introduction

The resonances of 1^{--} quarkonium family are generally described by the parameters which are the mass M, the total width $\Gamma_{\rm t}$, the hadronic width $\Gamma_{\rm h}$, and the leptonic width $\Gamma_{\rm ee}$ of the resonances. These parameters describe the shape of a resonance Breit-Wigner cross section for the formation and subsequent decay of the $q\bar{q}$ resonance produced in the e^+e^- annihilation. There are 6 different 1^{--} charmonium resonances established, which can directly be produced in e^+e^- annihilation in the energy region between 3.0 and 4.5 GeV. These are J/ψ, $\psi(2S)$, $\psi(3770)$, $\psi(4040)$, $\psi(4160)$ and $\psi(4415)$, which are interpreted as the 1^3S_1, 2^3S_1, 1^3D_1-dominant , 3^3S_1, 4^3S_1-dominant and 5^3S_1 of $c\bar{c}$ charmonium states[1], respectively. Based on the well measured resonance parameters of J/ψ and $\psi(2S)$, the charmonium models can predict the masses, the total widths and the leptonic widths of other charmonium states.

Additional to the above 6 conversational charmonium resonances, there is another 1^{--} resonance named Y(4260) discovered by BaBar experiment in searching their ISR (Initial State Radiation) return products of e^+e^- annihilation. In addition to the interpretation of this new state, however, there are still arguments about the interpretation of the most of the charmonium states based on various theoretical models and suggestions. For example, F.E. Close and P.R. Page [2] suggested that $\psi(4040)$ and $\psi(4160)$ are strong mixtures of ground state hybrid charmonium at the center-of-mass energy $E_{\rm cm} \sim 4.1$ GeV and the $\psi(3S)$ of conventional charmonium. The interpretation of the charmonium states from all of the theoretical arguments should be based on the measured resonance parameters and their decay products. To clarify this situation, one needs to more precisely measure the resonance parameters of the resonances and study the final states of their decays. Another example for needing to more precisely measure the parameters is for the understanding of the nature of the $\psi(3770)$ resonance. At present the $\psi(3770)$ is assigned to be a mixture of 1^3D_1 and 2^3S_1 (or the mixture of $^3D_1$ and $^3S_1$ waves) based on the measured leptonic width. However, there are still open questions for $\psi(3770)$ production and decays.

[1]By Gabg Rong and Da-Hua Zhang

According to QCD more than 97% of the $\psi(3770)$ decays into $D\bar{D}$ ($D^0\bar{D}^0$ and D^+D^-) final states. However, BES Collaboration recently measured the branching fraction for $\psi(3770) \to \text{non}-D\bar{D}$ to be $B[\psi(3770) \to \text{non}-D\bar{D}] = (16.4 \pm 7.3 \pm 4.2)\%$ [418] and $B[\psi(3770) \to \text{non}-D\bar{D}] = (14.5 \pm 1.7 \pm 5.8)\%$ [4], which were obtained by analyzing different data samples with different analysis methods. Both the measured branching fractions are larger than 3% as expected by QCD. If the branching fraction is really significantly larger than 3%, there may be something new. To uncover this puzzle, one needs to more accurately measure the resonance parameters of the $\psi(3770)$ and more carefully analyze the line-shapes of the resonance formation and subsequent decays in the inclusive hadronic decay mode, in the inclusive J/ψ decay mode and in some other exclusive decays modes.

In the energy region between 3.0 and 4.5 GeV, there may be some other 1^{--} states, such as hybrid charmonium, glueball, molecular and 4-quark states additional to the conventional charmonium states. To understand the nature of the charmonium states well and search for the 1^{--} hybrid charmonium, glueball, molecular and 4-quark states in the energy region and test various theoretical models, more precise measurements of the resonance parameters and careful analysis of the line-shapes of the resonances production and decays in different modes are crucial.

9.2 Key points of precise measurements

The parameters of the resonances can directly be measured by analyzing the energy dependence of the cross sections for the resonance production in e^+e^- annihilation. These parameters can also be measured in charm production experiments like $p\bar{p}$ annihilation [5].

MARK-I [6][7], FRAG [8], FRAM [9] DASP [10], MARK-II [11], DELCO [12], BES [13] and BES-II [14][418] experiments previously measured the parameters of the resonances produced in the e^+e^- annihilation, and E760 [5] measured the masses and the total widths of J/ψ and $\psi(2S)$ in $p\bar{p}$ annihilation by analyzing the cross section scan data.

Examining the analysis of the cross section scan data from these experiments, we find that there were some problems with dealing with the experimental data to extract the resonance parameters. First, no e^+e^- experiment considered the effects of photon vacuum porlarization corrections for the continuum hadron production on the total and leptonic widths of the resonances except the recent BES-II data analysis for measuring the resonance parameters of $\psi(2S)$ and $\psi(3770)$ [418]. If not considering this effect in data reduction, the measured total width of the $\psi(2S)$ resonance would be reduced by about 40 keV [418], while the leptonic width of the $\psi(2S)$ resonance would be increased by about 4%. Moreover, most experiments assumed that the detection efficency for observation of inclusive hadronic events as a function of the center-of-mass energy of the e^+e^- annihilation almost is a stright line. This assumption would systematicly increase the measured leptonic width of the resonance. In addition, no experiment considered the effects of the possible interference between the two amplitudes of continuum hadron production and the resonance hadronic decays in the e^+e^- experiment. This effect may also systematicly shift the measured resonance parameters significantly.

To more precisely measure the resonance parameters, we should carefully and ac-

curantely estimate the detection efficencies for observation of inclusive hadronic events at different center-of-mass energies; we should consider the photon vacuum polarization corrections for the continuum hadron production in the resonance region; we should study/consider possible interference between the continuum hadron production and the electronmagnetic decays of the resonances. Moreover, we should choice a better method to deal with the inital state radiative (ISR) and photon vacuum polarization corrections in analysis of the cross section scan data.

To more precisely estimate the detection efficencies for observation of inclusive hadronic events at different center-of-mass energies, we need a Monte Carlo generator in which the ISR and photon vacuum polarization corrections are biult in. This generator should include not only all of the charmonium production and decays, but also all sub-processes of the charmonium states production and decays. It also should include the possible interference between the two amplitudes of the continuum and the resonances. Especially, it should simulate the line-shapes of the narrow resonances exactly. Recently, Dahua Zhang et al [15] developed one of such generators, which was used in measurements of the resonance parameters of $\psi(3770)$ and $\psi(2S)$ and branching fractions for $\psi(3770) \to D^0\bar{D}^0, D^+D^-$ and $\psi(3770) \to \text{non}-D\bar{D}$ [418] [4]. This generator is being developed for the aim of the precise measurements of the resonance parameters and search for the new 1^{--} states with BES-III detector at BEPC-II collider.

9.3 An example for measuring $\psi(2S)$ and $\psi(3770)$ parameters

Among the 6 resonaces which can directly be produced in the e^+e^- annihilation in the energy region from 3.0 to 4.5 GeV, the locations of the $\psi(2S)$ and $\psi(3770)$ are closest each other. To get more reliable measured parameters of the two resonances, it had better to measure the parameters of the two resonaces simultaneously with the same data sets. These make measuring the parameters of the two resonances more difficult than measuring the parameters of one resonance only in experiment. In this section, we take **"Measurements of the parameters of the $\psi(2S)$ and $\psi(3770)$ resonaces"** performed with BES-II at BEPC as an example to discuss how to measure the parameters of the two resonance simultaneously. The methods for measuring the parameters of 1^{--} resonances in the more complicate case are similar. The data sets used in the measurements of the parameters were taken in March, 2003. The total integerated luminosity of the data sets is about ~ 5 pb^{-1} collected in the range from 3.66 to 3.88 GeV.

The parameters of $\psi(3770)$ and $\psi(3686)$ resonances can be extracted from a fit to the observed hadronic cross sections. The observed hadronic cross section is determined by

$$\sigma_{\rm had}^{\rm obs} = \frac{N_{\rm had}^{\rm obs}}{L\ \epsilon_{\rm had}\ \epsilon_{\rm had}^{\rm trig}}, \tag{9.1}$$

where $N_{\rm had}^{\rm obs}$ is the number of the observed hadronic events, L is the integrated luminosity, $\epsilon_{\rm had}$ is the efficiency for the detection of inclusive hadronic events and $\epsilon_{\rm had}^{\rm trig}$ is the trigger efficiency for collecting hadronic events in online data acquisition system. The hadronic

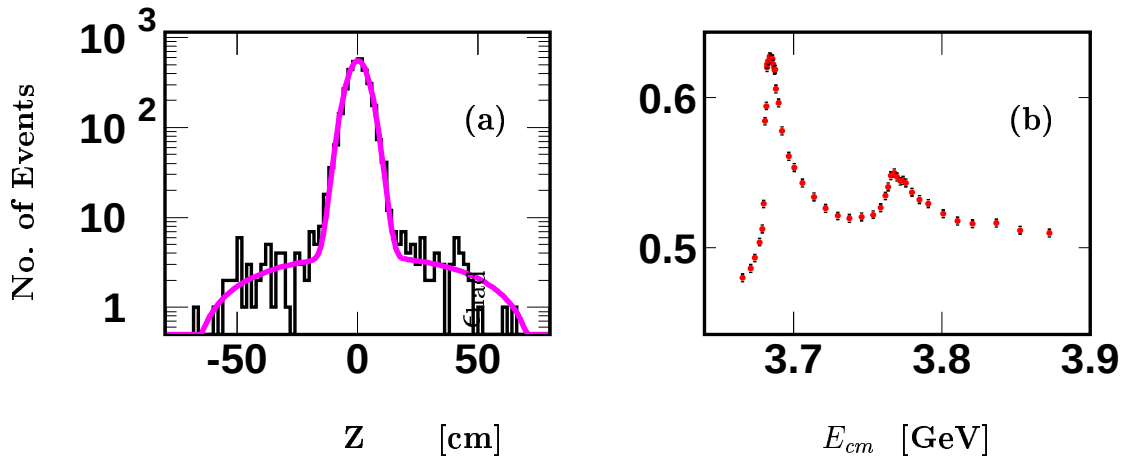

Figure 9.1: (a) The distribution of the event vertex in z; (b) the efficiencies versus the nominal c.m. energies.

events are required to have more than 2 good charged tracks. Each of the charged tracks is required to have well-measured momenta and to satisfy selection criteria as described in Ref [4]. To separate some beam-gas associated background events and cosmic rays background events from the hadronic events we calculated the event vertex in the beam line direction. Fig. 9.1(a) shows the distribution of the event vertex of the accepted events. Using a Gaussian function to describe the hadronic events plus a second order polynomial for the background to fit the distribution, we obtain the number, $N_{\rm had}^{\rm zfit}$, of the candidates for the hadronic events. This number of candidates for hadronic events contains contaminations from some background sources such as $e^+e^- \to \tau^+\tau^-$, $e^+e^- \to (\gamma)e^+e^-$, $e^+e^- \to (\gamma)\mu^+\mu^-$, and two-photon processes. The number of background events, $N_{\rm b}$, due to these processes can be estimated by means of a Monte Carlo simulation [4]. Subtracting $N_{\rm b}$ from $N_{\rm had}^{\rm zfit}$ yields the number of the observed hadronic events, $N_{\rm had}^{\rm obs}$. The systematic uncertainty in measuring the produced hadronic events due to the hadronic event selection criteria is estimated to be $\sim 2.5\%$ [4]. The integrated luminosities of the data sets are determined using large-angle Bhabha scattering events as described in Ref [4]. The systematic uncertainty in the measured luminosities is estimated to be $\sim 1.8\%$ [4]. The detection efficiency for hadronic events is determined via a special Monte Carlo generator [15] in which the radiative corrections to α^2 order are taken into account. These generated events are simulated with the GEANT3-based Monte Carlo simulation package [16]. The systematic uncertainty in the efficiencies due to the generator is estimated to be $\sim 2.0\%$ ($\sim 0.7\%$) [4] for reconstruction of the hadronic events from $\psi(3770)$ and $\psi(2S)$ decays (from continuum hadrons). Fig. 9.1(b) shows the Monte Carlo efficiencies for the detection of hadronic events produced at the different nominal c.m. energies. The trigger efficiencies are measured to be $\epsilon_{\rm trig} = (100.0^{+0.0}_{-0.5})\%$ for both the $e^+e^- \to (\gamma)e^+e^-$ and $e^+e^- \to$ *hadrons* events [4].

The observed cross section for $D^0\bar{D}^0$ (or D^+D^-) production is determined by

$$\sigma^{\rm obs}_{D^0\bar{D}^0({\rm or}\ D^+D^-)} = \frac{N_{D^0_{\rm tag}}({\rm or}\ N_{D^+_{\rm tag}})}{2 \times L \times B \times \epsilon}, \qquad (9.2)$$

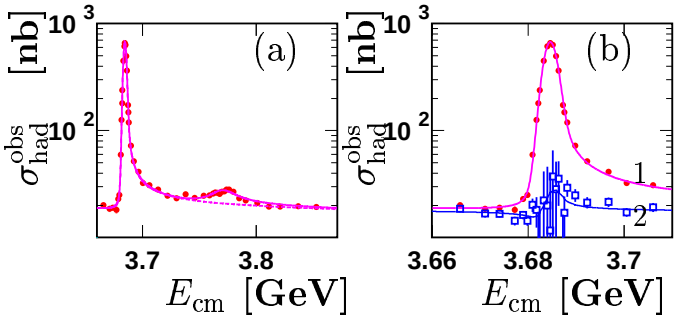

Figure 9.2: The hadronic cross sections versus the nominal c.m. energies (see text).

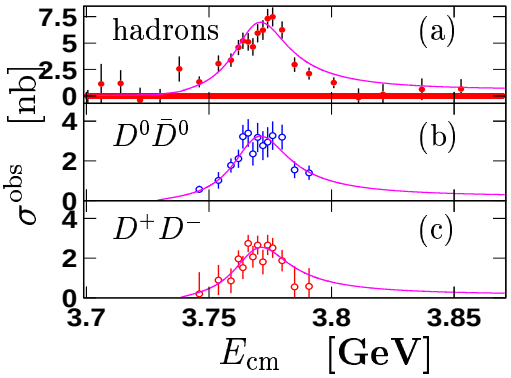

Figure 9.3: The observed cross sections versus the nominal c.m. energies.

where $N_{D^0_{\rm tag}}$ (or $N_{D^+_{\rm tag}}$) is the reconstructed D^0 (or D^+) events obtained by analyzing the invariant mass spectra of $K^\mp\pi^\pm$ and $K^\mp\pi^\pm\pi^\pm\pi^\mp$ (or $K^\mp\pi^\pm\pi^\pm$) as discussed in detail in Ref. [17]; B is the branching fraction for the decay mode in question, and ϵ is the efficiency for reconstruction of this decay mode.

Figure 9.2 shows the observed cross sections (points with error) for inclusive hadronic event production, while Fig. 9.3(b) and 9.3(c), respectively, display the observed cross sections (circles with error) for $D^0\bar{D}^0$ and D^+D^- production. The error bars represent the combined statistical and point-to-point systematic uncertainties including the statistical uncertainties in the luminosity and the efficiencies for the detection of Bhabha events, hadronic events and singly tagged D events.

The determination of the parameters of the resonances is accomplished by simultaneously fitting the observed cross sections for $\psi(2S)$, $\psi(3770)$, $D^0\bar{D}^0$ and D^+D^- to functions that describe the combined $\psi(2S)$, $\psi(3770)$ resonance shapes, the tail of J/ψ resonance and the non-resonant hadronic background, as well as the partial $\psi(3770)$ resonance shapes for $\psi(3770)\to D^0\bar{D}^0$ and $\psi(3770)\to D^+D^-$. The functions are corrected for the radiative corrections [18, 19]. For J/ψ and $\psi(2S)$, we take Breit-Wigner function

$$\sigma^{\rm B}(s^{'}) = \frac{12\pi\Gamma^{ee}\Gamma^{h}}{(s'-M^2)^2+(\Gamma^{\rm tot}M)^2}, \tag{9.3}$$

to describe their production for $s'=s(1-x)$, where x is a parameter related to the total energy of the emitted photons and $\sqrt{s}$ is the nominal c.m. energy; M and $\Gamma^{\rm tot}$

are, respectively, the masses and total widths of the resonances, and Γ^{ee} and Γ^{h} are the partial widths to the e^+e^- final state and to the inclusive hadronic final states, respectively. Assuming that there are no other new structures and effects, we use a pure p-wave Born order Breit-Wigner function with energy-dependent total widths to describe the $\psi(3770)$ production and the $D\bar{D}$ ($D^0\bar{D}^0$ and D^+D^-) production from the $\psi(3770)$ decays. The $\psi(3770)$ resonance shape is taken as

$$\sigma^{\rm B}_{\psi(3770)}(s^{'}) = \frac{12\pi\Gamma^{ee}_{\psi(3770)}\Gamma^{\rm tot}_{\psi(3770)}(s^{'})}{(s^{'}-M^2_{\psi(3770)})^2+[M_{\psi(3770)}\Gamma^{\rm tot}_{\psi(3770)}(s^{'})]^2}, \tag{9.4}$$

while the $D\bar{D}$ resonance shapes are taken as

$$\sigma^{\rm B}_{D\bar{D}}(s^{'}) = \frac{12\pi\Gamma^{ee}_{\psi(3770)}\Gamma_{D\bar{D}}(s^{'})}{(s^{'}-M^2_{\psi(3770)})^2+[M_{\psi(3770)}\Gamma^{\rm tot}_{\psi(3770)}(s^{'})]^2}, \tag{9.5}$$

where $M_{\psi(3770)}$ and $\Gamma^{ee}_{\psi(3770)}$ are the mass and leptonic width of the $\psi(3770)$ resonance, respectively; $\Gamma_{D\bar{D}}$ is the partial width of $\psi(3770)$ decay into $D\bar{D}$; $\Gamma^{\rm tot}_{\psi(3770)}(s^{'})$ and $\Gamma_{D\bar{D}}(s^{'})$ are chosen to be energy dependent defined as

$$\Gamma^{\rm tot}_{\psi(3770)}(s^{'}) = \Gamma_{D^0\bar{D}^0}(s^{'}) + \Gamma_{D^+D^-}(s^{'}) + \Gamma_{{\rm non}-D\bar{D}}(s^{'}), \tag{9.6}$$

where

$$\Gamma_{D^0\bar{D}^0}(s^{'}) = \Gamma_0\ \theta_{00}\frac{(p_{D^0})^3}{(p^0_{D^0})^3}\frac{1+(rp^0_{D^0})^2}{1+(rp_{D^0})^2}B_{00}, \tag{9.7}$$

$$\Gamma_{D^+D^-}(s^{'}) = \Gamma_0\ \theta_{+-}\frac{(p_{D^+})^3}{(p^0_{D^+})^3}\frac{1+(rp^0_{D^+})^2}{1+(rp_{D^+})^2}B_{+-}, \tag{9.8}$$

and

$$\Gamma_{{\rm non}-D\bar{D}}(s^{'}) = \Gamma_0\ \left[1-B_{00}-B_{+-}\right], \tag{9.9}$$

where p^0_D and p_D are the momenta of the D mesons produced at the peak of $\psi(3770)$ and at the actual c.m. energy $\sqrt{s^{'}}$, respectively; Γ_0 is the total width of the $\psi(3770)$ at its peak, $B_{00}=B(\psi(3770)\to D^0\bar{D}^0)$ and $B_{+-}=B(\psi(3770)\to D^+D^-)$ are the branching fractions for $\psi(3770)\to D^0\bar{D}^0$ and $\psi(3770)\to D^+D^-$, respectively, r is the interaction radius of the $c\bar{c}$, θ_{00} and θ_{+-} are the step functions to account for the thresholds of the $D^0\bar{D}^0$ and D^+D^- production, respectively. In the fit we take Γ_0, B_{00}, B_{+-} and r as free parameters.

The non-resonant background shape is taken as

$$\begin{aligned}\sigma^{nrsnt}_h(s) &= \int_0^\infty ds'' G(s,s'')\int_0^1 dx \frac{R_{uds}(s')\sigma^B_{\mu^+\mu^-}(s')}{|1-\Pi(s')|^2}F(x,s)\\ &+f_{D\bar{D}}\left[(\frac{p_{D^0}}{E_{D^0}})^3\theta_{00}+(\frac{p_{D^+}}{E_{D^+}})^3\theta_{+-}\right]\sigma^B_{\mu^+\mu^-}(s),\end{aligned} \tag{9.10}$$

where $F(x,s)$ is the sampling function [18], $1/|1-\Pi(s(1-x))|^2$ is the vacuum polarization correction function [19] including the contributions from all 1^{--} resonances, the

Table 9.1: The measured $\psi(3770)$ and $\psi(2S)$ parameters, where M is the mass, $\Gamma^{\rm tot}$ the total width [$\Gamma^{\rm tot} = \Gamma_0$ for $\psi(3770)$], Γ^{ee} the partial leptonic width and ΔM the measured mass difference of the $\psi(3770)$ and the $\psi(2S)$.

Res.	M (MeV)	$\Gamma^{\rm tot}$ (MeV)	Γ^{ee} (eV)	ΔM (MeV)
$\psi(3770)$	$3772.2 \pm 0.7 \pm 0.3$	$26.9 \pm 2.4 \pm 0.3$	$251 \pm 26 \pm 11$	
$\psi(2S)$	$3685.5 \pm 0.0 \pm 0.3$	$0.331 \pm 0.058 \pm 0.002$	$2330 \pm 36 \pm 110$	86.7 ± 0.7

QED continuum hadron spectrum as well as the contributions from the lepton pairs (e^+e^-, $\mu^+\mu^-$ and $\tau^+\tau^-$) [15]; $\sigma^B_{\mu^+\mu^-}(s)$ is the Born cross section for $e^+e^- \to \mu^+\mu^-$, E_{D^0} and E_{D^+} are the energies of D^0 and D^+ mesons produced at the nominal energy $\sqrt{s}$, $f_{D\bar{D}}$ is a parameter to be fitted, and $R_{uds}(s')$ is the R value for the light hadron production through one photon annihilation directly. In the fit we take $R_{uds}(s')$ as a free parameter, assuming that the value is independent of the energy; we fix the J/ψ resonance parameters at the values given by PDG [21]. We also consider the effects of the BEPC energy spread on the calculation of the expected cross sections in the fit. $G(s, s'')$ in Eq. (10) is the Gaussian function to describe the c.m. energy distribution of the BEPC machine.

Figure 9.2(a) shows the observed cross sections with the fit to the data, where the solid line shows the fit to the data and the dashed line represents the contributions from J/ψ, $\psi(2S)$ and continuum hadron production. To examine the contribution from the vacuum polarization corrections to the Born hadronic cross section due to one photon annihilation directly, we subtract the contributions of $\psi(2S)$ and $\psi(3770)$ as well as J/ψ from the observed cross sections to yield the expected cross sections of the continuum hadron production corrected with the radiative effects, which is given by Eq. (10). The squares with error in Fig. 9.2(b) show the yielded-expected cross sections, where the errors are the originally absolute errors of the totally observed cross sections as shown in Fig. 9.2(a). The blue line (line 2) in Fig. 9.2(b) shows the fit to the expected cross sections of the continuum hadron production corrected for the radiative effects as given in Eq. (10). Fig. 9.3(a) shows the observed cross sections for the inclusive hadronic event production, where the contributions from J/ψ and $\psi(2S)$ radiative tails as well as the continuum hadron production are removed. Fig. 9.3(b) and Fig. 9.3(c) display the observed cross sections for $D^0\bar{D}^0$ and D^+D^- production with the fits to the data, respectively. The results from this fit are summarized in table 9.1, where the first error is statistical and second systematic. From the fit we obtain the R_{uds} in the region between 3.660 and 3.872 GeV to be

$$R_{uds} = 2.262 \pm 0.054 \pm 0.109,$$

where the errors are, respectively, statistical and the systematic. The fit yields the non-$D\bar{D}$ branching fraction of $\psi(3770)$ decay to be

$$B(\psi(3770) \to {\rm non} - D\bar{D}) = (16.4 \pm 7.3 \pm 4.2)\%.$$

This fit gives $\chi^2/{\rm n.o.f} = 65.4/64 = 1.02$.

The continuum background shape affects the measured total and leptonic widths of

the resonances from the line-shape analysis. If we take

$$\sigma_h^{nrsnt}(s) = h\,\sigma^B_{\mu^+\mu^-}(s) + f_{D\bar{D}}\times \left[(\tfrac{p_{D^0}}{E_{D^0}})^3\theta_{00} + (\tfrac{p_{D^+}}{E_{D^+}})^3\theta_{+-}\right]\sigma^B_{\mu^+\mu^-}(s), \quad (9.11)$$

in fitting the data (where h is a free parameter in the fit), we would obtain $\Gamma^{\rm tot}_{\psi(2S)} = 290 \pm 59 \pm 5$ keV, $\Gamma^{ee}_{\psi(2S)} = 2.378 \pm 0.036 \pm 0.103$ keV, $\Gamma^{\rm tot}_{\psi(3770)} = 27.3 \pm 2.5 \pm 1.1$ MeV and $\Gamma^{ee}_{\psi(3770)} = 256 \pm 27 \pm 13$ eV, and almost unchanged measurements of the resonance masses. This fit yields χ^2/n.o.f $= 75.3/64 = 1.18$. This indicates that the vacuum polarization corrections to the Born order cross sections for the continuum hadron production can not be ignored when precisely measuring the resonance parameters of the narrow resonances like J/ψ and $\psi(2S)$ as well as $\Upsilon(1S)$ etc. in e^+e^- cross section scan experiments. Ignoring the effects of the vacuum polarization corrections on the continuum hadron production cross sections in the analysis of the cross section scan data taken in the $\psi(2S)$ resonance region would decrease the $\psi(2S)$ total width by about 40 keV.

9.4 Measurements of the parameters of $\psi(2S)$, $\psi(3770)$ and other resonances with BES-III at BEPC-II

As we mentioned before, precisely measuring the parameters of the 1^{--} charmonium resonance is important in the understanding of the dynamics of the charmonium resonance production in e^+e^- annihilation. Before clarifying the situation of the understanding the exact natures of the $\psi(4040)$ and $\psi(4160)$, one has to precisely and accurately measure the parameters of the resonances. At present, one still does not understand why $\psi(3770)$ decays to non-$D\bar{D}$ with a such large branching fraction. To uncover this "puzzle", one has to more precisely measure the parameters of $\psi(3770)$ as well as $\psi(2S)$ resonances. In this section, we will mainly discuss how well we can measure the branching fraction of $\psi(3770)$ decay and measure the parameters of $\psi(3770)$ resonance with BES-III at BEPC-II.

According to our experiences with analysis of the cross section scan data to measure the parameters of $\psi(3770)$ [418][22] and $\psi(2S)$ resonances [418], to measure the branching fraction for $\psi(3770) \to {\rm non}-D\bar{D}$ [418, 4], and to measure the R values in the range from 3.65 to 3.88 GeV [23] [4], we expect that the total systematic uncertainty of the observed cross section for inclusive hadronic event production can be reduced to the level of $\sim 2.5\%$ in the range from 3.50 to 3.88 GeV with the BES-III at BEPC-II. In this case, one should consider to collect the data with statistical uncertainty of $\sim 1.5\%$ in the measurements of the total cross section. Assuming that there are only two resonances of $\psi(2S)$ and $\psi(3770)$ plus the continuum hadron production in the range from 3.65 to 3.88 GeV, we did a Monte Carlo simulation to study how well we can measure the parameters of the $\psi(2S)$ and $\psi(3770)$ resonances and the branching fraction for $\psi(3770) \to {\rm non}-D\bar{D}$. The events were generated at the 49 different energy points at which we collected cross section scan data with BES-II detector in March, 2003. The total integrated luminosity of the data is about 60 pb^{-1}. Following the same procedure as that we used to deal with the cross section scan data as discussed in section 3, we obtain the parameters of the $\psi(2S)$ and $\psi(3770)$ resonances and the branching fraction for $\psi(3770) \to {\rm non}-D\bar{D}$.

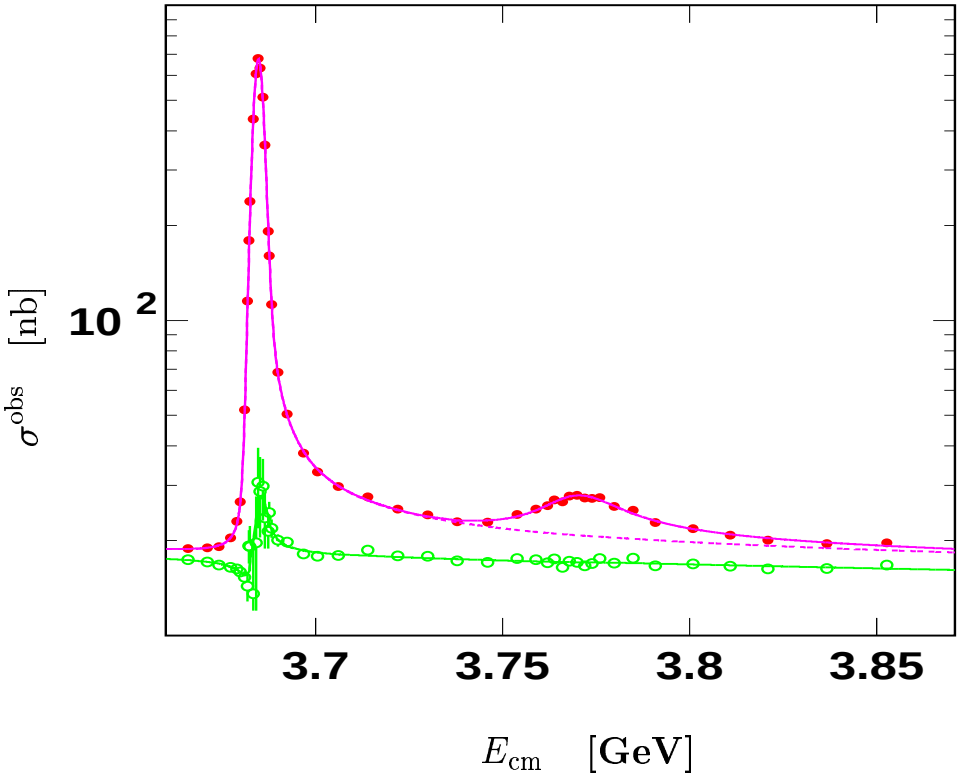

Figure 9.4: The observed cross sections versus the nominal c.m. energies.

Figure 9.4 shows the observed cross section as a function of the center-of-mass energy, where the dot with error show the cross section for inclusive hadronic event production; the circle with error represents the cross section for continuum hadron production with considering the ISR and photon vacuum polarization corrections; the red (green) solid line gives the best fit to the observed cross sections for inclusive hadronic event production (for the continuum hadronic event production); while the red dashed line shows the total contributions from the continuum hadronic event production, $\psi(2S)$ production and J/ψ production. Table 9.2 and 9.3 summarize, respectively, the results on measurement of the parameters of $\psi(2S)$ and $\psi(3770)$ resonances, where the errors are statistical and systematic, respectively. As a comparison, we also list the values of the parameters set in the Monte Carlo simulation. The measured $R_{\rm uds}$ value ("measured") along with the set $R_{\rm uds}$ value ("input") are listed in Table 9.4, where the errors are statistical and systematic errors, respectively.

In table 9.2, the "non-rsnc BCK shape" means which non-resonant background shape, as given in Eq. (10) and Eq. (11), is taken in the data reduction. From the Monte Carlo simulation, we find that the total width of the $\psi(2S)$ resonance is reduced by $\sim 20\%$ and the partial leptonic width is increased by $\sim 4\%$ if we do not consider the effect of the photon vacuum polarization corrections on the continuum hadron production in the data reduction.

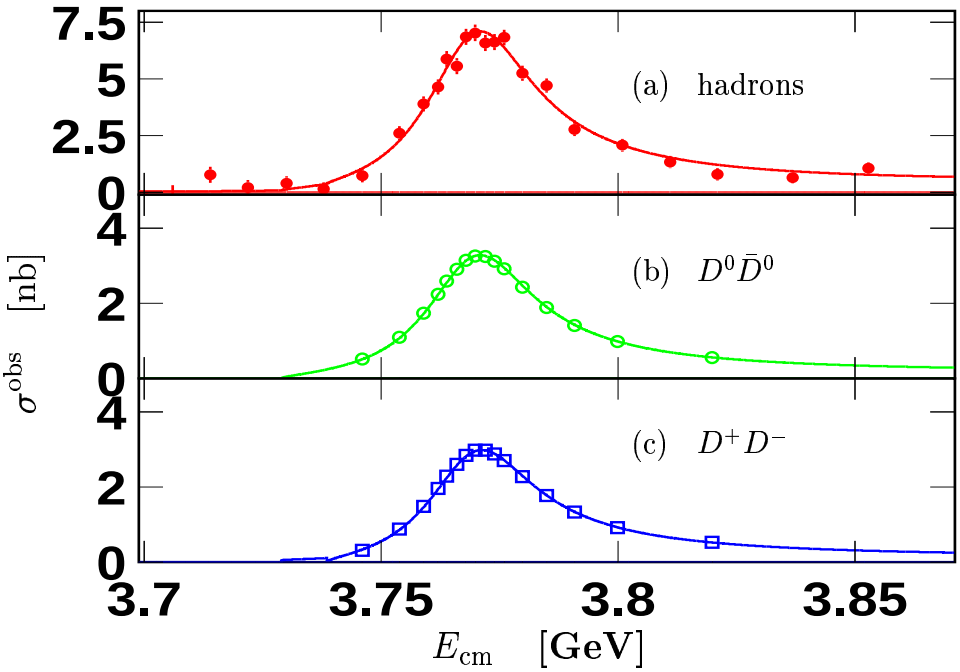

Figure 9.5: The observed cross sections versus the nominal c.m. energies.

Table 9.2: The input and measured $\psi(2S)$ parameters, where M is the mass, $\Gamma^{\rm tot}$ the total width and Γ^{ee} the partial leptonic width, where the "input" means the value of the parameter set in the Monte Carlo simulation and the "measured" means the measured value of the parameters from the Monte Carlo simulation.

input or measured	M (MeV)	$\Gamma^{\rm tot}$ (keV)	Γ^{ee} (keV)	non-rsnc BCK shape
input	3686.09	337	2.33	–
measured	$3686.08 \pm 0.01 \pm \Delta_{\rm sys}$	$349.6 \pm 13.0 \pm \Delta_{\rm sys}$	$2.33 \pm 0.01 \pm \Delta_{\rm sys}$	Eq. (10)
measured	$3686.06 \pm 0.01 \pm \Delta_{\rm sys}$	$289.1 \pm 11.0 \pm \Delta_{\rm sys}$	$2.42 \pm 0.01 \pm \Delta_{\rm sys}$	Eq. (11)

Table 9.3: The input and measured $\psi(3770)$ parameters, where M is the mass, $\Gamma^{\rm tot}$ the total width [$\Gamma^{\rm tot} = \Gamma_0$ for $\psi(3770)$] and Γ^{ee} the partial leptonic width, where the "input" means the value of the parameter set in the Monte Carlo simulation and the "measured" means the measured value of the parameters from the Monte Carlo simulation.

input/measured	M (MeV)	$\Gamma^{\rm tot}$ (MeV)	Γ^{ee} (eV)
input	3772.3	26.9	251
measured	$3772.1 \pm 0.2 \pm \Delta_{\rm sys}$	$26.8 \pm 0.5 \pm \Delta_{\rm sys}$	$255 \pm 7 \pm \Delta_{\rm sys}$

Table 9.4: The input and measured $R_{\rm uds}$ values in the resonance region from 3.65 to 3.88 GeV.

$R_{\rm uds}$ [measured]	$R_{\rm uds}$ [input]
$2.254 \pm 0.012 \pm 0.056$	2.260

Table 9.5: The input and measured branching fraction for $\psi(3770) \to \text{non} - D\bar{D}$, where the "input" means the value of the parameter set in the Monte Carlo simulation and the "measured" means the measured value of the parameters from the Monte Carlo simulation.

input/measured	$B(\psi(3770) \to D\bar{D})$ [%]	$B(\psi(3770) \to \text{non} - D\bar{D})$ [%]
input	90%	10%
measured	$88.8 \pm 2.4 \pm 2.0$	$11.2 \pm 2.4 \pm 2.0$

Figure 9.5(b) and Fig. 9.5(c) show the observed cross sections for $D^0\bar{D}^0$ and D^+D^- production with the best fits to the data, respectively. The observed cross sections for the decays $\psi(3770) \to$ hadrons is displayed in Fig. 9.5(c). The fit yields the branching fractions for $\psi(3770) \to D\bar{D}$ and $\psi(3770) \to \text{non}-D\bar{D}$, which are summarized in table 9.5 along with the branching fractions set in the Monte Carlo simulation. The errors listed in the table are the statistical and systematic, respectively. The fit also gives the measured branching fractions for $\psi(3770) \to D^0\bar{D}^0$ and $\psi(3770) \to D^+D^-$ to be

$$B[\psi(3770) \to D^0\bar{D}^0] = (46.3 \pm 1.3 \pm 1.0)\%,$$

and

$$B[\psi(3770) \to D^+D^-] = (42.5 \pm 1.2 \pm 0.9)\%,$$

which are corresponding to the set values of the branching fractions of $B[\psi(3770) \to D^0\bar{D}^0] = 46.8\%$ and $B[\psi(3770) \to D^+D^-] = 43.2\%$ in the Monet Carlo simulation, respectively.

From analyzing the Monte Carlo sample generated at the 49 energy points, we notice that the line-shape of the observed cross sections are changed in smooth. However, if there are some other states except the $\psi(2S)$ and $\psi(3770)$ in the energy region, the observed cross sections would be changed away from the expectation (as shown by the lines in the Fig. 9.4 and Fig. 9.5). These provide us a method to search for the new 1^{--} states in the energy region from 3.0 to 4.5 GeV.

For the measurements of the parameters of the resonances in the energy region from 3.87 to 4.50 GeV, the method of the data analysis is the same as that used in the measurements of the parameters of the $\psi(2S)$ and $\psi(3770)$ resonances. However, since the locations of the $\psi(4040)$, $\psi(4160)$ and $Y(4260)$ resonances are close to each other, we should consider the possible interference among the $\psi(4040)$, $\psi(4160)$ and $Y(4260)$ [2] amplitudes in data reduction to extract the parameters. To get reliable parameters of the resonances, we should use the point-to-point detection efficiencies to determine the observed cross sections for inclusive hadronic event production, instead of using the almost straight line detection efficiency curve as that used in determination of the observed cross sections in most previous e^+e^- experiments. We should also select a better formalism to deal with the ISR correction for the data taken in the resonance region in data reduction. Keeping these points in mind together with these discussed in section 2 and section 3, we can more precisely and accurately measure the parameters of the resonances in the higher energy region. We can also precisely and accurately measure the parameter of J/ψ resonance with taking all of these considerations.

[2] At present, the leptonic width of the $Y(4260)$ resonance is not measured.

9.5 Summary

To understand the dynamics of the charmonium resonance production in e^+e^- annihilation, we need to precisely measure the parameters of the charmonium resonance in the energy region from 3.0 to 4.5 GeV. At present, the most available measurements on the parameters of the 1^{--} charmonium resonance may be biased since the most e^+e^- experiments did not consider the effects of the photon vacuum polarization corrections on the continuum hadron production cross section, did not consider the possible interference between the continuum hadron amplitude and the resonance amplitude, and most experiments used almost straight line detection efficiency curve to determine the observed cross sections for the resonance subsequent decays. For these reasons, we should re-measure the parameters of the resonances with the coming BES-III detector at BEPC-II collider. These measurements can help to clarify the arguments about the interpretation of the $\psi(4040)$ and $\psi(4160)$ states. Precision measurements of the parameters of $\psi(2S)$ and $\psi(3770)$ would help to uncover the puzzle of the non-$D\bar{D}$ decays of $\psi(3770)$. Careful analysis of the line-shape of the observed cross sections for inclusive hadronic event production, $D\bar{D}$ (including D^* and D_S^+) production, and some other exclusive final states (such as $J/\psi\pi\pi$, $J/\psi\eta$, $J/\psi\eta'$, $J/\psi\omega$, ϕK^+K^-, $\phi\pi^+\pi^-$, $\chi_{cJ}\rho$, $\chi_{cJ}\omega$), and inclusive final states ($J/\psi X$, ηX, $\eta' X$ ...) production at different energies in the range from 3.7 to 4.5 GeV provide us the opportunity to search for the new states additional to the conventional charmonium resonances. These can well be done with the coming BES-III detector at BEPC-II collider.

Bibliography

[1] Yi-Bing Ding, Kuang-Ta Zhao and Dan-Hua Qin, Phys Rev. D **51** (1995) 5064.

[2] F.E. Close and P.R. Page, Phys. Lett. B **366** (1996) 323.

[3] BES Collaboration, M. Ablikim *et al.*, Phys. Rev. Lett., 97, 121801 (2006).

[4] BES Collaboration, M. Ablikim *et al.*, Phys. Lett., B641, 145 (2006).

[5] E760 Collaboration, T.A. Armstrong *et al.*, Phys Rev. D **47** (1993) 772.

[6] M. Boyaski et al., Phys. Rev. Lett., 34, 1357(1975)

[7] MARK-I Collaboration, P.A. Rapidis *et al.*

[8] R. Baldini Celio et al., Phys. Lett. B58, 471(1975)

[9] B. Esposito et al., Lett. Nuovo Cim., 14 73(1975)

[10] R. Brandelik et al., Z. Phys., Cl, 233(1997).

[11] MARK-II Collaboration, R.H. Schindler *et al.*, Phys Rev. D **21** (1980) 2716.

[12] DELCO Collaboration, W. Bacino *et al.*, Phys. Rev. Letts. **40** 671 (1978).

[13] BES Collaboration, J.Z. Bai *et al.*, Phys. Lett. **B 355** 374 (1995).

[14] BES Collaboration, J.Z. Bai *et al.*, Phys. Lett. **B 550** 24 (2002).

[15] D.H. Zhang, G. Rong, and J.C. Chen, Phys Rev. D **74** (2006) 054012.

[16] M. Ablikim *et al.* (BES Collaboration), physics/0503001, submitted to Nucl. Instr. and Meth. A.

[17] J.Z. Bai *et al.* (BES Collaboration), Phys. Lett. **B 603** 130 (2004).

[18] E. A. Kuraev and V. S. Fadin, Yad Fiz. **41**, 377 (1985); [Sov. J. Nucl. Phys. **41**, 466 (1985).]

[19] F.A. Berends and G.J. Komen, Phys. Lett. **B 63** 432 (1976); Andrej B. Arbuzov, Eduard A. Kuraev *et al.*, JHEP10 006 (1997).

[20] M. Ablikim *et al.* (BES Collaboration), Nucl. Phys. **B 727** 395 (2005).

[21] S. Eidelman *et al.* (Particle Data Group), Phys. Lett. **B 592** 1(2004).

[22] BES Collaboration, M. Ablikim *et al.*, hep-ex/0612056.

[23] BES Collaboration, M. Ablikim *et al.*, Phys. Rev. Lett., 97, 262001 (2006).

Part III

Light Hadron Physics

Conveners: Xiaoyan Shen, Bingsong Zou

Authors: Vladimir Bytev, Ying Chen, Hong-Ying Jin, Shan Jin, Xiaoyan Shen, Qiang Zhao, Alexey Zhemchugov, Hanqing Zheng, Shi-Lin Zhu, Bingsong Zou, Ning Wu

Chapter 10

Overview of light hadron physics

Hadron spectroscopy has been a major platform for probing many dynamic aspects of strong interactions in the non-perturbative regime. It also bridges fundamental approaches such as lattice QCD calculations with phenomenological studies such as quark model, QCD sum rules, etc., from which insights into the non-pQCD phenomena can be gained.

Quarks, as basic building blocks for hadrons, are bound together by the color force generated by gluon exchanges to form color-singlet hadrons, and the underlying dynamics are described by the widely-tested QCD Lagrangian [1]:

$$\begin{aligned}\mathcal{L} &= i\sum_i \bar{q}_i(x)[\partial_\mu - ig_s\sum_a \frac{1}{2}\lambda^a A^a_\mu(x)]\gamma^\mu q_i(x) \\ &\quad -\frac{1}{4}\sum_a F^a_{\mu\nu}(x)F^{\mu\nu a}(x) - \sum_i \bar{q}_i(x)m_i q_i(x)\ ,\end{aligned} \tag{10.1}$$

where g_s is the strong coupling constant, and i is the flavor index for quark $q_i(x)$, which is a Dirac spinor and a three dimensional vector in color space. λ^a denotes the 3×3 Gell-Mann matrices with $a = 1, \ldots, 8$. Thus, a $q\bar{q}$ pair is the minimum number of quark and antiquark to form a color-singlet meson, while qqq is the minimum to form a color-singlet baryon.

Note that QCD quark-gluon interaction conserves flavor, and the interaction strength is flavor-independent. The only dependence on flavor in the QCD Lagrangian is thus through the quark-mass terms.

In the light quark sector, i.e. u, d and s, the mass difference is relatively small, $m_d - m_u \simeq 3$ MeV and $m_s - m_d = 150$ MeV. Therefore, the strong interactions have an approximate global SU(3) flavor symmetry, and quarks (antiquarks) are assigned to representation $\mathbf{3}$ ($\bar{\mathbf{3}}$). Mesons made of $q\bar{q}$ are then irreducible representations given by the following product decomposition:

$$\mathbf{3}\otimes\bar{\mathbf{3}} = \mathbf{1} + \mathbf{8}\ , \tag{10.2}$$

and baryons are:

$$\mathbf{3}\otimes\mathbf{3}\otimes\mathbf{3} = \mathbf{1}_a + \mathbf{8}_\lambda + \mathbf{8}_\rho + \mathbf{10}_s, \tag{10.3}$$

where the subscripts a, s, λ and ρ denote antisymmetry, symmetry, and two mixed symmtries for the two-body substates within the three-quark system.

The SU(3) flavor symmetry implies the existence of flavor nonets with the same J^P but difference charges in the meson spectrum. For example, there are 8 pseudoscalars with masses below 500 MeV and one at about 1 GeV, i.e., π^0, $\pi^\pm$, K^0, $\bar{K}^0$, $K^\pm$, η, and η'. These states together are identified as the 0^- flavor nonet in the meson spectrum.

Similarly, for the lowest-mass baryons, one would expect the existence of a flavor singlet, octet and decuplet. Comparing with the baryon spectrum for the low-lying states, one identifies eight baryons for the octet with $J^P = 1/2^+$: $p(uud)$, $n(udd)$, $\Sigma^+(uus)$, $\Sigma^0(uds)$, $\Sigma^-(dds)$, $\Lambda(uds)$, $\Xi^0(uss)$, and $\Xi^-(dss)$, of which the masses are in a range of $0.9 \sim 1.3$ GeV, and 10 states for the decuplet with $J^P = 3/2^+$: $\Delta^{++}(uuu)$, $\Delta^+(uud)$, $\Delta^0(udd)$, $\Delta^-(ddd)$, $\Sigma^+(uus)$, $\Sigma^0(uds)$, $\Sigma^-(dds)$, $\Xi^0(uss)$, $\Xi^-(dss)$, and $\Omega^-(sss)$ in a range of $1.2 \sim 1.7$ GeV. The flavor singlet baryon with $1/2^+$ has a higher mass arising from the spatial and spin degrees of freedom.

By relating the SU(3) flavor symmetry breaking to the mass term in the QCD Lagrangian, a premier evidence for the validity of the quark model solution is that the hadrons within an SU(3) flavor multiplet will differ in mass linearly due to the presence of different number of s ($\bar{s}$) in the hadrons. Namely, one has

$$\begin{aligned} \Omega^-(1672) - \Xi(1530) &\simeq \Xi(1530) - \Sigma(1385) \\ &\simeq \Sigma(1385) - \Delta(1232) \\ \phi(1020) - K^*(890) &\simeq K^*(890) - \rho(770) \ . \end{aligned} \tag{10.4}$$

A compact expression is given by the Gell-Mann-Okubo mass relation:

$$\Sigma + 3\Lambda = 2(N + \Xi) \ . \tag{10.5}$$

In brief, there are hypotheses made for the naive quark model [2, 363] as required by QCD: i) Chiral symmetry spontaneous breaking leads to the presence of massive constituent quarks within a hadron as an effective degrees of freedom. ii) Hadrons can be viewed as a quark system in which the gluon fields generate effective potentials that depend on the positions and spins of the massive quarks.

These two hypotheses make the non-relativistic treatment an inspiring approach at leading order. Meanwhile, since the quarks are such massive objects compared to the QCD scale, the creation of constituent quark pairs will be suppressed. Thus, the low-lying states would be $q\bar{q}$ for meson and qqq for baryon. By treating the gluon fields as effective potentials the hadron wavefunction will only depend on quark variables.

Based on those simple hypotheses and accommodating the color, flavor, spin, and spatial degrees of freedom in the wavefunction solutions for the quark binding system, quark model provides an efficient and evidently successful classification for a large number of hadrons observed in experiment [4].

In the light hadron sector, the nonrelativistic approach of the naive quark model unavoidably suffers the problem that the excitation energies of the resonances are comparable to the constituent masses, and thus makes the nonrelativistic approach questionable. Although it is still unclear why such a nonrelativistic model works so well for the light flavor

quark system consisting of u, d and s, there is no doubt of its extensive empirical successes. Various investigations are making progress on providing a firm basis for the quark model phenomenology, and it is believed to be a good approximation for non-perturbative QCD. For instance, the progress on lattice QCD is providing evidence for the effective degrees of freedom known as constituent quarks inside the nucleon.

Applications of various phenomenologies to the study of hadron spectroscopy can be also found in the literature, such as semirelativistic flux-tube model [5, 6], instanton model [7], Goldstone boson exchange model [8], and diquark model [9] etc. Masses of the non-strange P-wave baryons are also examined by a mass operator analysis in large N_c QCD [10]. On the other hand, attempts to the development of a relativistic version have been made since early 70's [11]. QCD-inspired approaches for the understanding of the dynamics for hadron EM and strong decays and hadron-hadron interactions are also extensively explored in the literature. Generally, those approaches distinguish themselves by taking into account different ingredients in the quark interactions and thus shed a light on some aspects of non-perturbative QCD (see Ref. [12] for a recent review). An ultimate prescription for the non-perturbative QCD dynamics in the light quark sector may rely on future lattice QCD studies.

Chapter 11

Physics of soft pions and lightest scalars at BES-III

A brief introduction to the physics related to the soft pions, light scalar mesons and final state theorem for BES-III experiments is given.

11.1 Partially conserved vector current (PCAC) and soft pions

11.1.1 PCAC

Strong interaction physics is described by Quantum Chromodynamics (QCD). In QCD $\bar{\psi}\psi$ has vacuum quantum number and contains non-vanishing vacuum expectation value: $< \bar{\psi}\psi > \neq 0$. As a consequence the pseudo-Goldstone bosons, π^a, couples to the axial current, $< 0|A^a_\mu|\pi^a > \neq 0$. If isospin is a good quantum number then,

$$< 0|A^a_\mu|\pi^b >= f_\pi \delta^{ab} p_\mu \ , \tag{11.1}$$

where $f_\pi = 93$MeV is the π decay constant, determined from $\pi \to l\nu$ decay. For on-shell pion Eq. (11.1) becomes

$$< 0|\partial^\mu A^a_\mu|\pi^b >= f_\pi \delta^{ab} m^2_\pi \ , \ \text{ or } \ < 0|\partial^\mu A^a_\mu|\pi^b >= f_\pi m^2_\pi < 0|\phi^a|\pi^b > \ . \tag{11.2}$$

Generalize to the operator form, we have

$$\partial^\mu A^a_\mu = f_\pi m^2_\pi \phi^a \ . \tag{11.3}$$

This is the celebrated form of Partial Conservation of Axial Current (PCAC) [13]. The most important application of PCAC may be the derivation of various soft pion theorems. In the following we briefly discuss a few of them.

11.1.2 Adler' theorem with one soft pion

Adler's theorem: *In order to calculate any strong interaction matrix element with one soft pion: $i \to f + \pi$, it only needs to consider the process without the pion, $i \to f$, and inserts*

the pion in any of the external lines, using derivative coupling theory. A diagramatic explanation to the Adler's theorem is given in the following:

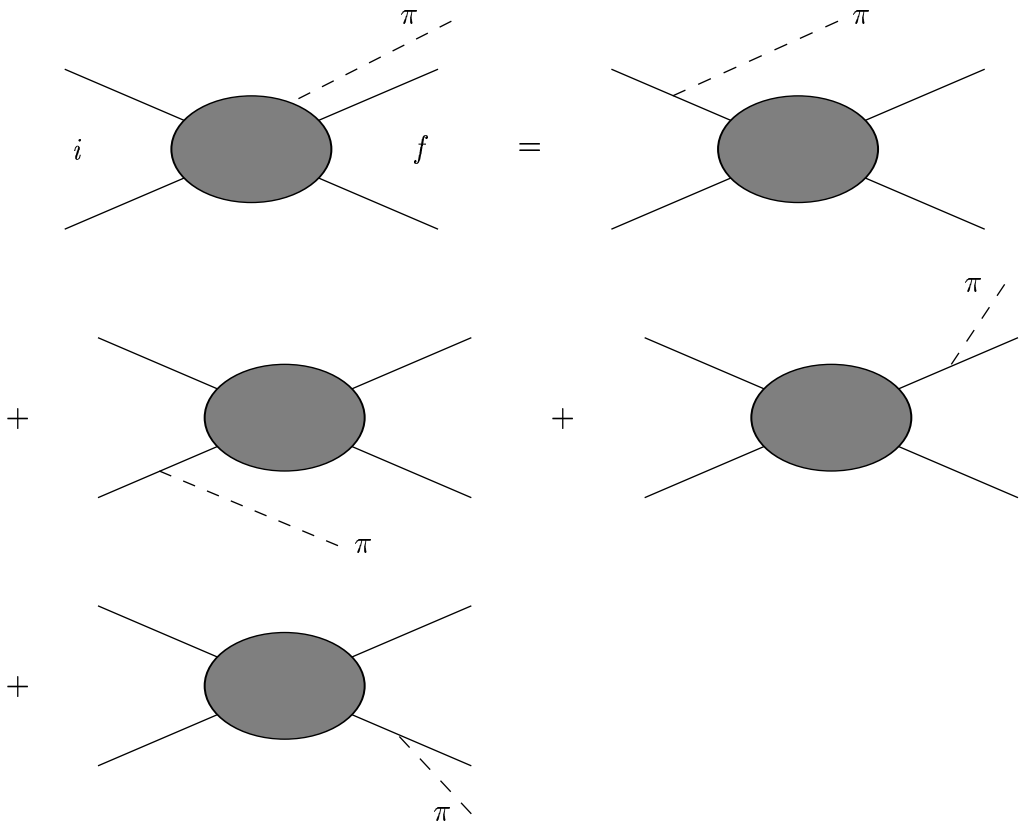

Notice that the theorem as stated above is only exact when each 4-component of the pion momentum $k_\pi^\mu \to 0$ simultaneously (π off-shell). In reality it means any quantity $k \cdot p$ with p any momentum involved in the process $i \to f + \pi$ can be considered as a small quantity. A simple proof of the theorem follows [14]:

According to the reduction formula the S matrix element of the process $i \to f + \pi$ can be associated with PCAC as follows,

$$S_{f\pi,i} \propto -i(k^2 - m_\pi^2) < f|\pi|i >= im_\pi^2 < f|\pi|i >= \frac{-k_\mu}{f_\pi} < f|A_\mu|i > \ . \tag{11.4}$$

In above the first relation comes from the LSZ reduction formula the first equality is due to soft pion momentum, the second equality is due to PCAC. When $k_\mu \to 0$ the above expression does not vanish in general. This is clearly seen from the following diagram (taking $NN \to NN\pi$ process for example),

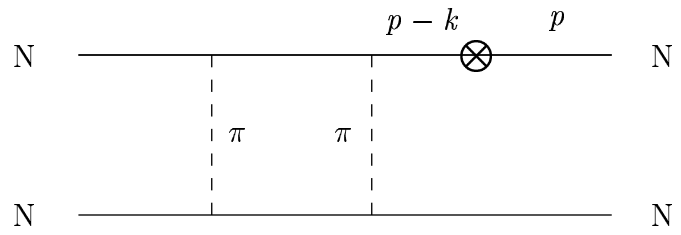

when $p - k \to p \to$ on shell, there appears a pole in the above diagram. But for the diagram below, no additional pole would appear when $k_\mu \to 0$,

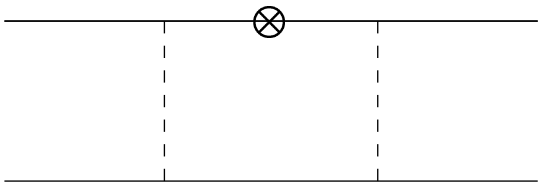

since from Landau's rule the singularity structure of this diagram (when $k_\mu \to 0$) is the same as



and there is no pole for the latter. Hence we demonstrated the theorem.

An important application of the soft pion theorem is to $\pi\pi \to \pi\pi$ scatterings. Because there is no 3π coupling, so

$$T(p_1, p_2, p_3 \to 0, p_4) = 0 \ . \tag{11.5}$$

Using Mandelstam variables, when $p_3 \to 0$, one has $s = (p_1 + p_2)^2 = m_\pi^2$, $t = (p_1 - p_3)^2 = m_\pi^2$, $u = (p_1 - p_4)^2 = m_\pi^2$, we find the Adler zero of $\pi\pi$ scattering corresponds to $s = t = u = m_\pi^2$. This zero is not far from $\pi\pi$ scattering threshold. Hence the threshold parameters of $\pi\pi$ scatterings are suppressed due to the existence of this T matrix zero.

An important process in J/Ψ physics on which soft pion theorem applies is the $\Psi' \to J/\Psi\pi\pi$ process. The decay branching ratio of $\Psi'(3685)$ into J/Ψ and light hadrons is $(55.7 \pm 2.6)\%$ [15]. In which $\mathrm{Br}(\Psi' \to J/\Psi\ \pi^+\pi^-) = (30.5 \pm 1.6)\%$, $\mathrm{Br}(\Psi' \to J/\Psi\ \pi^0\pi^0) = (18.2 \pm 1.2)\%$. Therefore the $\Psi' \to J/\Psi\pi\pi$ process is an important channel for Ψ' decay. The transition amplitude of $\Psi' \to J/\Psi\pi\pi$ is

$$M = < \Psi\pi\pi|\Psi' > = < P, \epsilon; p_{1a}, p_{2b}|P', \epsilon' > \ . \tag{11.6}$$

Using PCAC one can obtain, after some algebra manipulation [16],

$$\begin{aligned} < \Psi\pi\pi|\Psi' > &= -(p_1^2 - m_\pi^2)(p_2^2 - m_\pi^2)(\phi^a\phi^b) \\ &= f_\pi^{-2} p_1^\mu p_2^\nu (\overline{A}_\mu^a \overline{A}_\nu^b) - i f_\pi^{-1}(p_1^2 + p_2^2 - m_\pi^2) < \Psi|\tilde{\Sigma}^{ab}|\Psi' > , \end{aligned} \quad (11.7)$$

where $\overline{A}$ means that the pion pole part of the axial vector current, A, has been subtracted. In above both the first term inside the small bracket and the second term with inner product (the Sigma term) are regular functions when $p_\mu \to 0$ [16]. Apparently one sees from the above formula that when $p_1^\mu \to 0$ and p_2 on-shell or vice versa, $M \to 0$. That is the Adler zero condition.

11.1.3 Linear σ model and the chiral shielding

In history the σ meson was firstly introduced in association with the $SU(2) \times SU(2)$ linear σ model, in an attempt to describe the spontaneous breaking of chiral symmetry. The model has the advantage of a natural realization of PCAC and current algebra. In the linear sigma model lagrangian there are iso-triplet (π_1, π_2, π_3) fields and a scalar iso-singlet σ field [17]:

$$\begin{aligned} \mathcal{L} &= \mathcal{L}_s + c\sigma \ , \\ \mathcal{L}_s &= \frac{1}{2}[(\partial_\mu\sigma)^2 + (\partial_\mu\pi)^2] - \frac{m^2}{2}[\sigma^2 + \pi^2] - \frac{\lambda}{4}[\sigma^2 + \pi^2]^2 \ . \end{aligned} \quad (11.8)$$

The last term of the first equation indicates that chiral symmetry is not exact, $c = f_\pi m_\pi^2$ is a small quantity. If c=0 then the lagrangian is invariant under the following $SU_L(2) \times SU_R(2)$ chiral rotations:

$$\begin{aligned} &\vec{\pi} \to \vec{\pi} + \vec{\alpha} \times \vec{\pi} - \vec{\beta}\sigma \ , \\ &\sigma \to \sigma + \vec{\beta} \cdot \vec{\pi} \ . \end{aligned} \quad (11.9)$$

When $m^2 < 0$, chiral symmetry is spontaneously broken, the minimum of the effective potential is taken at $< \sigma >= f_\pi$, and we can redefine another scalar field with vanishing vacuum expectation value s,

$$\sigma = s + f_\pi \ , \quad < s >= 0 \ . \quad (11.10)$$

The new lagrangian expressed in terms of the shifted field is

$$\mathcal{L} = \frac{1}{2}[(\partial_\mu\pi)^2 - {m_\pi}^2\pi^2] + \frac{1}{2}[(\partial_\mu s)^2 - {m_\sigma}^2 s^2] - \lambda f_\pi s(s^2 + \pi^2) - \frac{\lambda}{4}[s^2 + \pi^2]^2 \ . \quad (11.11)$$

In above we have

$${m_\sigma}^2 = m_\pi^2 + 2\lambda f_\pi^2 \ . \quad (11.12)$$

Also we get the $\sigma\pi\pi$ coupling constant,

$$g_{\sigma\pi\pi} = \frac{m_\sigma^2 - m_\pi^2}{f_\pi} = 2\lambda f_\pi \ . \quad (11.13)$$

the coupling constant $g_{\sigma\pi\pi}$ is proportional to the mass square of the σ meson and hence the interaction becomes very strong when taking the large m_σ limit. Therefore there does not exist a trivial decoupling limit when $m_\sigma \to \infty$. As a consequence, the decay width of $\sigma \to \pi\pi$ (in the chiral limit) at tree level is proportional to the m_σ^3:

$$\Gamma(\sigma \to \pi\pi) \;=\; \frac{3m_\sigma^3}{32\pi f_\pi^2}\sqrt{1-\frac{4m_\pi^2}{m_\sigma^2}}\;. \tag{11.14}$$

From this formula one sees that when $m_\sigma = 600MeV$, $\Gamma_\sigma \simeq 660$MeV, i.e., a large width already exceeds the mass. The appearance of a large width indicates the failure of perturbation calculation and also that a Breit–Wigner description of resonances fails since the latter is only a narrow width approximation [18]. The $\pi\pi$ scattering amplitudes at tree level can be calculated using linear sigma model. See the following figure:

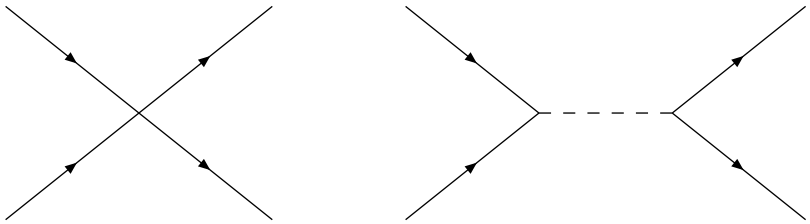

(a) (b)

First-order Feynman graphs for $\pi\pi$ scatterings in linear σ model, one has to take the crossed channel diagrams into account as well.

One sees that there are only two type of diagrams, corresponding to a) 4π contact interaction, and b) σ exchange diagram, respectively. One gets,

$$\begin{aligned} T^{I=0}(s,t,u) &= 3A(s,t,u) + A(t,u,s) + A(u,s,t)\;,\\ T^{I=1}(s,t,u) &= A(t,u,s) - A(u,s,t)\;,\\ T^{I=2}(s,t,u) &= A(t,u,s) + A(u,s,t)\;, \end{aligned} \tag{11.15}$$

where

$$A(s,t,u) = -2\lambda(1+\frac{2\lambda v^2}{s-{m_\sigma}^2}) = -\frac{{m_\sigma}^2-{m_\pi}^2}{s-{m_\sigma}^2}\frac{s-{m_\pi}^2}{{f_\pi}^2}\;. \tag{11.16}$$

In above, the first term on the *r.h.s.* of the first equality corresponds to the background contact $\lambda\phi^4$ interaction. To preserve the boundedness from below of vacuum energy, λ must be positive and hence $\lambda\phi^4$ contact interaction is repulsive. The second term is from the σ pole and provides an attractive force at low energies. The explicit calculation confirms the conclusion obtained in the end of Sec. 11.1.2: the two terms in Eq. (11.16) cancel almost exactly at threshold, which is within expectation from the low energy soft pion theorem.

The partial wave projection to the full amplitude is,

$$T_J^I(s) = \frac{1}{32\pi(s-4m_\pi^2)} \int_{4m_\pi^2-s}^{0} dt\, P_J(1+\frac{2t}{s-4m_\pi^2}) T^I(s,t,u) \ . \tag{11.17}$$

From Eq. (11.16) one gets partial wave amplitude T_J^I as follows,

$$\begin{aligned} T_0^0 &= \frac{\lambda}{16\pi}\left(\frac{3(m_\sigma^2-m_\pi^2)}{m_\sigma^2-s} + \frac{2(m_\sigma^2-m_\pi^2)\log[\frac{m_\sigma^2+s-4m_\pi^2}{m_\sigma^2}]}{s-4m_\pi^2} - 5\right) \ , \\ T_0^2 &= -\frac{\lambda}{8\pi}\left(1 - \frac{2\lambda v^2}{s-4m_\pi^2}\log[\frac{m_\sigma^2+s-4m_\pi^2}{m_\sigma^2}]\right) \ , \\ T_1^1 &= \frac{\lambda^2 v^2(16m_\pi^2-4s-2(4m_\pi^2-2m_\sigma^2-s)\log[\frac{m_\sigma^2+s-4m_\pi^2}{m_\sigma^2}])}{8\pi(s-4m_\pi^2)^2} \ . \end{aligned} \tag{11.18}$$

It is not very easy to see immediately the T matrix zero from the above partial wave amplitudes. Taking the $m_\sigma \to \infty$ limit while keeping λ fixed, we find the zero are located at $s = m_\pi^2/2$, $4m_\pi^2$ and $2m_\pi^2$ for IJ=00, 11 and 20 partial waves, respectively. The positions of these zeros also receive small corrections at higher orders. In the limit $m_\sigma \to \infty$ and f_π fixed partial wave amplitudes from Eq. (11.18) now looks like

$$T_0^0 = \frac{2s-m_\pi^2}{32\pi f_\pi^2} \ , \ T_0^2 = \frac{2m_\pi^2-s}{32\pi f_\pi^2} \ , \ T_1^1 = \frac{s-4m_\pi^2}{96\pi f_\pi^2} \ , \tag{11.19}$$

which agree with the lowest order results from chiral perturbation theory, and are in fact predictions from current algebra.

The lesson we learn from above is that it is very difficult to distinguish the σ pole contribution (if there is) from experiments, since the background contribution cancels σ's contribution near threshold, as dictated by the soft pion theorem. In the language of Ref. [19] this is called 'chiral shielding'. Furthermore, the σ meson has a large width which makes it difficult to be distinguished from background contributions.

11.1.4 Why there should exist a σ resonance

The chiral shielding of σ is probably known since the invention of the linear σ model. It implies, in one aspect, the cancelation between a positive σ contribution and a negative background contribution to the $\pi\pi$ scattering phase shift. This fact led many physicists to argue the possible existence of the σ resonance [20, 21]. On the other side, since no firm evidences for the σ meson had been found experimentally, it was thought that the σ meson is not necessary for describing chiral symmetry breaking and the non-linear realization of chiral symmetry was invented, from which chiral perturbation theory was constructed [22]. The latter is found to be very successful in studying low energy strong interaction physics without referring to the σ meson. Indeed the chiral cancelation mechanism in the linear realization only provides at most a self-consistent description to the data and was insufficient to provide a solid proof on the existence of the σ pole. However, the background contribution from nearby left hand cut can be estimated using chiral perturbation theory

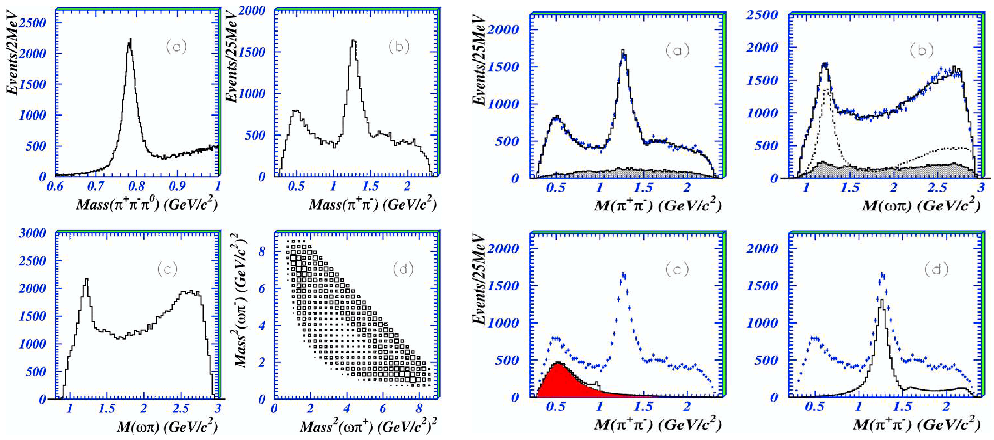

Figure 11.1: Dalitz plot and $\pi^+\pi^-$ invariant mass spectrum in $J/\Psi \to \omega\pi\pi$ decays [25].

either. It is found that the background contribution to the $\pi\pi$ scattering phase shift is negative. Hence it proves that the σ pole is essential to adjust chiral perturbation theory to experiments [23].

The existence of the σ pole has been reported in production experiments [24, 25]. In Ref. [24], from a sample of 1172 ± 61 $D^- \to \pi^-\pi^+\pi^+$ decay (the ration $\Gamma(D^+ \to \pi^-\pi^+\pi^+)/\Gamma(D^+ \to K^-\pi^+\pi^+)$ is about 3%) strong evidence for the existence of a scalar resonance is found with mass and width $M = 478^{+24}_{-23} \pm 17$MeV, $\Gamma = 324^{+42}_{-40} \pm 21$MeV, which corresponds to a pole mass $M = 489$MeV, $\Gamma = 346$MeV. Furthermore, it is found that the broad scalar resonance accounts approximately half of all decays. The two results from the BES collaboration [25] and the E791 collaboration [24] look somewhat different, reflecting the uncertainties in parameterizing a light and broad resonance.

11.2 Go beyond the Breit–Wigner description of a broad resonance

In production experiments evidences from different processes have shown evidences for the σ meson. However, since the σ pole has a large width it is difficult to separate it unambiguously from background contributions. In phase shift analysis, it was pointed out that crossing symmetry plays a very important role and hence is being used in determining the pole location [26]. The mass and width are found to be $m_\sigma = 470 \pm 50$MeV and $\Gamma_\sigma = 570 \pm 50$MeV, respectively, which is in good agreement with the Roy equation determination to the σ pole: $m_\sigma = 441^{+16}_{-8}$MeV and $\Gamma_\sigma = 544^{+18}_{-25}$MeV [27]. The existence of such light and broad resonance requires one to pay more attention to the issue on how to parameterize a broad resonance.

11.2.1 How to describe a light and broad resonance

For a broad resonance as the σ meson, its lineshape mass can be drastically different from its pole mass location [28]. One may write down a simple form of a resonance propagator,

$$\triangle(s) = \frac{1}{s - M^2 + iM\Gamma(s)} \ , \tag{11.20}$$

where $\Gamma(s)$ is the momentum dependent width being proportional to the square of the coupling constant, g^2 and also proportional to the phase space factor, ρ. In Eq. (11.20) M is a mass parameter (the lineshape mass), when $\sqrt{s} = M$ the real part of the propagator vanishes. The pole mass of the resonance, denoted as m_{pole}, however, is defined as the zero of the denominator of $\triangle(s)$:

$$m_{pole}^2 - M^2 + iM\Gamma(m_{pole}^2) = 0 \ . \tag{11.21}$$

The complex root of this equation locates on the un-physical sheet[1] as dictated by micro-causality requirement. Apparently, m_{pole} is usually complex. It may be further written as $m_{pole} \equiv m - i\Gamma/2$. It is easily understood that m and Γ can be totally different from M and $\Gamma(M^2)$, respectively, when the coupling constant g is large. Taking the σ resonance for example, one estimation gives $m_{pole} \simeq 450$MeV, but the lineshape mass can easily reach 1GeV. The latter in general is not a good definition of a broad resonance, because when the coupling strength becomes strong the real part of the self-energy may contain a non-negligible s dependence [20]. One of the frequently used simple parametrization form of the σ meson is

$$\triangle(s) = \frac{1}{s - M^2 + i\rho(s)G} \ , \tag{11.22}$$

where G is a constant to be fixed by the fit. Nevertheless as pointed out in Ref. [29] Eq. (11.22) does not describe one pole only, rather, it contains an additional virtual pole for equal mass scatterings or an additional resonance pole for unequal mass scatterings. These additional poles locate in the small $|s|$ region and should not exist if we trust chiral perturbation theory predictions in the small $|s|$ region. The spurious pole(s) hidden in Eq. (11.22) may be simply subtracted out and the Eq. (11.22) can be simply rewritten as,

$$\triangle(s) = \frac{1}{s - M^2 + i\rho(s)sG} \ . \tag{11.23}$$

This equation, though very simple, depicts very well the smooth but steady rise of low energy $\pi\pi$ phase shift in the IJ=00 channel, which is named as "red dragon" by Minkowski and Ochs [30]. A frequently used parametrization form found in the literature introduces an exponential form-factor aiming at suppressing a resonance contribution at large momentum separation (See for example, Ref. [31, 20]) and it looks like,

$$\Gamma(s) = \alpha(2s - m_\pi^2)\frac{\sqrt{s - 4m_\pi^2}}{\sqrt{s}} e^{-(s-M_r^2)/4\beta^2} \ , \tag{11.24}$$

[1] The kinematic factor, ρ is of square root cut structure when the resonance couples to two massive particles. The un-physical sheet is reached by changing the sign of ρ.

where α and β are free parameters and M_r is the resonance's mass. Other parametrization forms can also be found in the literature [32]. BES experiment [25] tested both Eq. (11.23) and Eq. (11.24). Despite that different parameterizations look quite different, the experiment, at its current level, is not able to distinguish the fit quality of different parameterizations. On the other side there exist some ambiguities in association with the description of a broad resonance. There are only a few certain general rules when one tries to write down its propagator: firstly, chiral suppression of the σ coupling to pion fields at low energies has to be taken into account; secondly, spurious singularities hidden in the propagator, if there are any, have to lie very far away from the physical region and hence may be considered as purely background contributions; thirdly, the propagator must obey real analyticity. The latter means $\Delta(s-i\epsilon) = \Delta(s+i\epsilon)^*$. Beside these it is not known how to clearly separate the background contributions from a broad pole contribution. There exist some freedoms to absorb part of the background contributions into the σ propagator and vice versa. Hence the differences between two parameterizations only reflect the different definition of background contributions. Nevertheless, the σ pole location itself is a physical quantity and should not in principle depend on the parametrization form used.

11.2.2 The σ and κ poles in BESII experiments

From $J/\Psi \to \omega\pi^+\pi^-$ [25] process the BESII collaboration has found evidence for the existence of σ. See Fig. 11.1, the pole mass and width are found to be $m_\sigma = 541 \pm 39$MeV, $\Gamma_\sigma = 504 \pm 84$MeV. Different parameterizations are tested in the analysis. Nevertheless, within the current experimental precision and the lack of knowledge on production vertex, it is still difficult to distinguish the quality between different parametrization forms.

In an early study the $\Psi' \to J/\Psi\,\pi^+\pi^-$ process is investigated by BES collaboration and it is found that the data can be well described without assuming the existence of σ at all. However, the σ pole, if exist in $J/\Psi \to \omega\pi\pi$ process, has also to occur in $\Psi' \to J/\Psi\,\pi^+\pi^-$ as well. In Ref. [33], this process is re-investigated and it is found that the data can be described by the cancelation between the sigma pole and a negative background, which is in agreement with the picture as given in section 11.1.3. More importantly the sigma pole location determined, though with large uncertainties, is found to be stable and consistent with the result given in Ref. [25], in agreement with the concept of pole universality discussed in section 11.2.3. See Fig. 11.2 for illustration.

11.2.3 Universality of pole location

Another elementary property in particle physics is that for a certain resonance, its pole location is unique, no matter in which process it appears. This is certainly as it should be, otherwise it will become a total mess, if different pole positions emerge in different processes. Nevertheless the mathematical proof is more involved than the simple intuition. In the following we present a simplified proof for illustration, taking elastic $\pi\pi \to \pi\pi$ scattering for example. Assuming there is a resonance in the channel I,J. Then the question is, in any process $i \to (\pi\pi)_{IJ} + f$, whether there exists the same pole and whether the pole location is the same as that in the elastic process $\pi\pi \to \pi\pi$?

The answer to the above question is yes and a simplified proof follows: considering

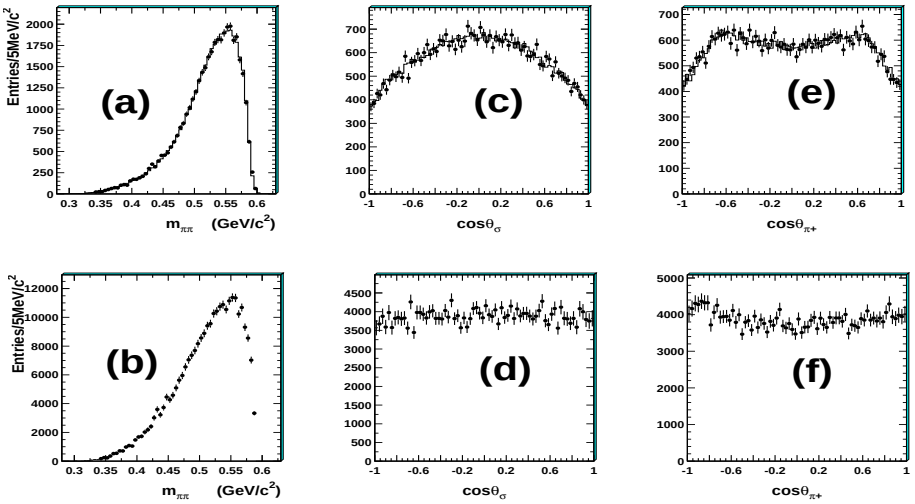

Figure 11.2: Fit results of $\psi(2S) \to \pi^+\pi^- J/\psi$ (P.K.U. ansatz). Dots with error bars are data and the histograms are the fit results. (a) and (b) are the $\pi^+\pi^-$ invariant mass, (c) and (d) the cosine of the σ polar angle in the lab frame, and (e) and (f) the cosine of the π^+ polar angle in the σ rest frame. (From Ref. [33])

any process $i \to f + (\pi\pi)_{IJ}$, depicted by the transition amplitude $A(s_1, s_2, \cdots, s_n)$, where $s_i = (p_{i_1} + p_{i_2})^2$ are generalized Mandelstam variables, the square of the sum of two arbitrary momenta of any in and out state particles. Especially we define $s_1 = (p_{\pi_1} + p_{\pi_2})^2$. Amplitude A as a real analytic function of complex variable s_1, i.e.,

$$A(s_1^*, s_2 \cdots, s_n) = A^*(s_1, s_2 \cdots, s_n) \tag{11.25}$$

can be proved to maintain the following property, using Cutkosky rule:

$$\begin{aligned} &\text{disc } A(s_1, s_2 \cdots, s_n) = A(s_1, s_2 \cdots, s_n) - A(s_1^*, s_2 \cdots, s_n) \\ &= 2iA(s_1, s_2 \cdots, s_n)\rho_{\pi\pi}(s_1)T^*_{\pi\pi\to\pi\pi}(s_1) \ . \end{aligned} \tag{11.26}$$

Further using $T^*(s_1) = T^{II}(s_1) = T(s_1)/S(s_1)$ and simple deduction leads to,

$$A^{II}(s_1, \cdots) = A^*(s_1, \cdots) = A(s_1, \cdots)/S(s_1) \ , \tag{11.27}$$

where $S(s_1)$ is the single channel S matrix for $\pi\pi$ elastic scatterings. From Eq. (11.27) one sees that any matrix element A contains the same poles as those appeared in $\pi\pi$ elastic scattering, on the second sheet of s_1 variable.

11.3 Final state theorem and Omnés solution

11.3.1 Final state theorem

Assuming there exist a group of eigenstates of strong interaction and total angular momentum J (J is a good quantum number), $|1>, |2>, ..., |n>$. The strong interaction

S matrix is of diagonal form $S_0 = diag(e^{2i\delta_1}, \cdots, e^{2i\delta_n})$. Now introducing the "weak" interaction and the S matrix elements are no longer diagonal. The non-diagonal elements are assumed weak, $i\Sigma \propto O(\epsilon)$. In the zero-th order approximation, $S = S_0$. In first order approximation

$$S = S_0 + i\Sigma \ . \tag{11.28}$$

Unitarity requires $SS^+ = S^+S = 1$, or

$$1 \simeq S_0^+ S_0 + i(\Sigma S_0^+ - S_0\Sigma^+) + O(\epsilon^2) \ . \tag{11.29}$$

This leads to $\Sigma S_0^+ = S_0\Sigma^+$. From time reversal invariance $\Sigma_{mn} = \Sigma_{nm}$ we get

$$\Sigma_{mn} = |\Sigma_{mn}|e^{i(\delta_n+\delta_m)} \ . \tag{11.30}$$

For a "weak" two body final state amplitude,we have $A_{i\to f} = |A_{i\to f}|e^{i\delta_f}$ where δ_f is the phase shift of the two body final state interaction. This is called the Watson's theorem for final state interaction [34]. Examples are $\gamma\gamma \to 2\pi$, $K_s \to 2\pi$, $\Sigma^- \to n\pi^-$ and $\Lambda^0 \to \pi N$, etc..

11.3.2 $D^+ \to K^-\pi^+ l\nu_l$ decays

An important process in future BESIII experiments for which the final state theorem applies is $D^+ \to K^-\pi^+ l\nu_l$. Since the leptons are spectator for strong interactions, the strong phase generated from πK rescattering, when the invariant mass of πK system is less than the $\pi\eta'$ threshold, are exactly the same as the one appeared in πK elastic scatterings, according to the final state theorem. The $D^+ \to K^-\pi^+ l\nu_l$ process is p wave dominant ($D^+ \to \bar{K}^{*0} l\nu_l$). However the Focus Collaboration found evidence for a small, even spin $K\pi$ amplitude that interferes with the dominant $\bar{K}^{*0}$ component [35]. The data can be described by $\bar{K}^{*0}$ interference with either a constant amplitude or a broad spin 0 resonance. So a careful reanalysis at BESIII to extract the s wave component and the phase is very important to further investigate the κ pole problem. The final state theorem is also confirmed in Ref. [36]. Edera and Pennington gave a review on the related experimental analyses in Ref. [37].

11.3.3 $D^+ \to K^-\pi^+\pi^+$ decays

In Ref. [38], an isobar model is used to parameterize the partial wave amplitude. In this model, the decay amplitude $\mathcal{A}$ is described by a sum of quasi two-body terms $D \to R + k$, $R \to i + j$, in each of the three channels $k = 1, 2, 3$:

$$\mathcal{A} = d_0 e^{i\delta_0} + \sum_{n=1}^{N} d_n e^{i\delta_n} \ \frac{F_{_R}(p, r_{_R}, J)}{m_{R_n}^2 - s_{ij} - i m_{R_n}\Gamma_{R_n}(s_{ij})} \times F_{_D}(q, r_{_D}, J) \ M_J(p, q) \ ,$$

where s_{ij} is the squared invariant mass of the ij system. J is the spin, m_{R_n} the mass and $\Gamma_{R_n}(s_{ij})$ the width of each of the N resonances R_n in the decay process. $F_{_R}$ and $F_{_D}$ are form factors, with effective radius parameters $r_{_R}$ and $r_{_D}$, for all R_n and for the parent D meson, respectively. p and q are momenta of i and k, respectively, in the ij

rest frame. $M_J(p,q)$ is a factor introduced to describe spin conservation in the decay. For more detailed discussions on these expressions one is referred to Ref. [24]. The complex coefficients $d_n e^{i\delta_n}$ $(n = 0, N)$ are determined by the D decay dynamics and are parameters estimated by a fit to the data. The first, non-resonant (NR) term describes direct decay to $i + j + k$ with no intermediate resonance, and d_0 and δ_0 are assumed to be independent of s_{ij}. For $D^+ \to K^-\pi_a^+\pi_b^+$ decays $\mathcal{A}$ is Bose-symmetrized with respect to interchange of π_a^+ and π_b^+. In Ref. [38] it is noticed that the NR term was small, and that a further term, parameterized as a new $J = 0$ resonance $\kappa(800)$ with $m_R = (797 \pm 19 \pm 43)$MeV and $\Gamma_R = (410 \pm 43 \pm 87)$MeV, gave a much better description of the data.

Apparently the above parametrization forms are not satisfactory for the purpose of exploring wide and broad resonance and for testing final state phases. In Ref. [39] an improved approach to the above analysis is presented using a generalized isobar picture of two body interactions. While higher $K\pi$ waves are described by sums of known resonances, the s-wave amplitude and phase are determined bin-by-bin in $K\pi$ mass. The phase variation is found not to be that of $K^-\pi^+$ elastic scattering obtained from LASS Collaboration [40]. The applicability of Watson theorem in the 3 body hadronic decay is examined in Ref. [39]. In the 3 body D decays, $K^-\pi^+$ forms both isospin 1/2 and 3/2 components. It is not clear, however, how to estimate the $I = \frac{3}{2}$ component in s-wave. In the literature it is often assumed using the simple quark spectator model of D decay to $K\pi\pi$ that the $K\pi$ system has only $I = 1/2$. However, it is found that if $I = \frac{1}{2}$ dominates, then the Watson theorem does not describe these data well. This question is re-examined in Ref. [37]. It is suggested that in $D \to K\pi\pi$ decays there exists a different mixture of $I = 1/2$ and $I = 3/2$ s-wave interactions than in elastic scattering. Applying Watson's theorem to this generalized isobar model allows one to estimate the $I = 3/2$ $K\pi$ s-wave component, and it is found to be larger than in hadronic scattering or semi-leptonic processes.

Another very interesting process in future BESIII experiment is $\Psi' \to J/\Psi\pi\pi$. It is a three body final state. But due to the color transparency argument, it is a very good approximation to neglect the final state interaction between J/Ψ and the pions at all. Hence the problem is reduced to a two body final state. The kinematics constrains the two π system to be solely elastic and hence the $\Psi' \to J/\Psi\,\pi\pi$ channel provides another good opportunity to extract the final state phase of s wave $\pi\pi$ interactions. However, in this channel the phase is obtained by interference between s and d waves and the latter is very small. So high statistics is needed which is expected to be accomplishable by BESIII experiments. The measured phase shift difference $\delta_0^0 - \delta_0^2$ will be an important complimentary to other determinations, since it covers the energy region around 500MeV, which are not covered by previous experiments.

Precision experiments also urges more theoretical investigations on the 3-body final state interactions, like for example the $D \to K\pi\pi$ process. Corrections to Watson theorem in 3 body decays are discussed theoretically in Ref. [41].

11.3.4 The Omnés solution

Consider a pion formfactor, or a formfactor like quantity, $A(s)$ which is analytic functions on the entire cut s plane. Neglecting the inelasticity effect and assuming single channel

unitarity relation holds on the entire physical region: $4m_\pi^2 < s < \infty$. The spectral function of the form-factor satisfies

$$\mathrm{Im}A = \rho A T^* \ , \tag{11.31}$$

where T is the $\pi\pi$ (partial wave) scattering amplitude. The Eq. (11.31) has a simple solution, called the Omnés solution:

$$A(s+i\epsilon) = P_n(s)\exp\{\frac{s}{\pi}\int_{4m_\pi^2}^{\infty}\frac{\delta_\pi(s')ds'}{s'(s'-s-i\epsilon)}\} \ , \tag{11.32}$$

where $P_n(s)$ is a (real analytic) polynomial, representing the possible zeros of $A(s)$ on the complex s plane, and δ_π is the $\pi\pi$ scattering phase shift.

The simplest way to prove Eq. (11.32) may be the following: Firstly, from Eq. (11.31) to make analytic continuation of $A(s)$ we get the following relation

$$A(s-i\epsilon) = A^{II}(s+i\epsilon) = A(s+i\epsilon)/S \ . \tag{11.33}$$

Next we remove all possible zeros of on the complex plane by dividing a polynomial: $A \to A/P_n(s)$. Then $\log(A/P_n(s))$ is also analytic on the entire cut plane and obeys a simple dispersion relation:

$$\begin{aligned}
&\log(A/P_n(s)) = \frac{1}{2\pi i}\int_C \frac{\log(A(s')/P_n(s'))}{s'-s}ds' \\
&= \frac{1}{2\pi i}\int_{\infty}^{4m_\pi^2}\frac{\log(A(s'-i\epsilon)/P_n(s'))}{s'-s}ds' + \frac{1}{2\pi i}\int_{4m_\pi^2}^{\infty}\frac{\log(A(s'+i\epsilon)/P_n(s'))}{s'-s}ds' \\
&= \frac{1}{2\pi i}\int_{4m_\pi^2}^{\infty}\frac{\log(A(s'+i\epsilon)/A(s'-i\epsilon))}{s'-s}ds' = \frac{1}{2\pi i}\int_{4m_\pi^2}^{\infty}\frac{\log(S(s'))}{s'-s}ds' \\
&= \frac{1}{\pi}\int_{4m_\pi^2}^{\infty}\frac{\delta_\pi(s')}{s'-s}ds' \ ,
\end{aligned} \tag{11.34}$$

which reproduces Eq. (11.32).

11.3.5 More on final state interactions in the $J/\Psi \to \omega\pi\pi$ process

The final state phases in $J/\Psi \to \omega\pi\pi$ process is also discussed [42]. The final state is three body and complicated pattern of final state interaction is involved. Nevertheless the $\omega\pi$ two body interaction may be subtracted using a suitable parametrization (the generalized isobar model). In the low invariant mass region of $\pi\pi$ system the 4π final state interaction is negligible. Hence the remaining part of the decay amplitude characterizing the $\pi\pi$ final state interactions, denoted as A_0, may be related to Watson theorem which fixes the final state phase:

$$A_0(s) = |A_0(s)|e^{i\delta_\pi} \ , \tag{11.35}$$

which is similar to the scalar form factor

$$F_0(s) = |F_0(s)|e^{i\delta_\pi} \ . \tag{11.36}$$

That means the ratio $R(s) = A_0(s)/F_0(s)$ is real when $s < 4M_K^2$. Furthermore, since the σ pole both in A_0 and F_0 cancel each other and the cut in R is distant (starting from $4M_K^2$), R has to be a slowly varying function, at least at low energies (i.e., when $s << 4M_K^2$). This can be seen immediately if one writes down a dispersion relation of R with one subtraction,

$$R(s) = R_0 + R_1 s + \frac{(s-4M_K^2)^2}{\pi}\int_{4M_K^2} \frac{\mathrm{Im}R(t)}{(t-4M_K^2)^2(t-s)} \ . \tag{11.37}$$

The scalar form factor can be determined from theory side [43]. The ration R is plotted in Fig. 11.3 where one sees that R does not show any curvature like structure, hence the integral in Eq. (11.37) is small and $R \simeq R_0 + R_1 s$. Furthermore, the scalar amplitude may be parameterized as $A_0(s) = R_0(1 - s/s_0)F_0(s)$ and $s_0 \simeq 1.65\mathrm{GeV}^2$ [44]. On the other side, J/Ψ decays to $\omega\pi\pi$, $\omega K\bar{K}$, $\phi\pi\pi$ and $\phi K\bar{K}$ are studied in Ref. [45], using an assumption that $A_0/F_0 \simeq const.$ The observed energy dependence as shown in Fig. 11.3 seems to suggest that the final state interaction between ω and π and also 3 body final state interaction can be safely removed. This conclusion seems to disagree with the conclusion reported from E791 $D \to K\pi\pi$ decays (bare in mind that they are different processes). Hence it would be interesting that the future BESIII experiments and related theoretical studies can improve the understanding on the issue of three body final state interactions.

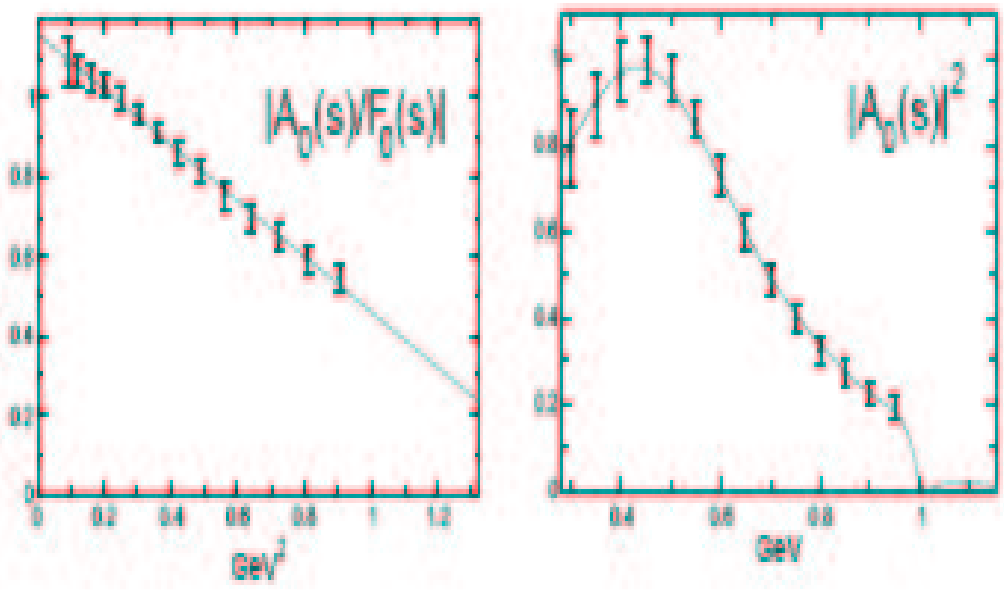

Figure 11.3: The comparison between the scalar form factor and the scalar amplitude extracted from BES $J/\Psi \to \omega\pi\pi$ process. Data are from Ref. [42].

11.4 On the nature of the lightest scalar resonances

Physics related to the lightest scalar resonances, σ, κ, $f_0(980)$ and $a_0(980)$ has attracted much interests in the past. Except σ, among these resonances there exists another broad resonance κ with the pole location $M_\kappa = 721 \pm 19 \pm 43$MeV, $\Gamma_\kappa = 584 \pm 43 \pm 87$MeV, [46] and $M_\kappa = 878 \pm 23^{+64}_{-55}$MeV, $\Gamma_\kappa = 499 \pm 52^{+55}_{-87}$MeV, [47] to be compared with a recent phase shift analysis based on LASS [40] data: $M_\kappa = 694 \pm 53$MeV, $\Gamma_\kappa = 606 \pm 59$MeV [48], and the Roy–Steiner equation analysis [49]: $M_\kappa = 658 \pm 13$MeV, $\Gamma_\kappa = 557 \pm 24$MeV. A first interesting question concerning these scalars is whether they consist of the lowest scalar octets, and if the answer is yes, how to explain the the large difference between their masses and widths. A widely accepted understanding to such question has not been emerged yet, but the key must be related to a proper treatment to the strong interaction dynamics especially respecting unitarity. Large $SU_f(3)$ breaking effects must be taken into account as well. First of all, it should be stressed that a naive quark model description to the lightest scalar meson can not be successful. As emphasized by Törnqvist [50], this is simply because in naive quark models chiral symmetry is absent but is crucial for scalars. Indeed, if the 'σ' resonance really has something to do with the σ particle in the linear σ model, Eq. (11.11), then from Eq. (11.9) it is realized that the σ is the chiral partner of the pion fields. The latter is a collective excitation – the would be goldstone boson. Hence the σ must share many properties of the pion fields, and we know that it is very difficult to understand the pion field in terms of simple quark models.

The κ meson contains s quark component and a_0 not. In the naive $\bar{q}q$ picture this would indicate a heavier κ than a_0. In a phenomenological approach, Jaffe relates the unusual properties of the light scalar mesons to the assumption that the lightest scalar mesons are mainly composed of $(qq)(\bar{q}\bar{q})$ [51]. With this he observed that the spectrum of the flavor nonet is inverted as compared to a standard $q\bar{q}$ nonet, and contains a light isospin singlet, a strange doublet, and a heavy triplet plus singlet with hidden strangeness. This picture agrees well with the observed spectrum of a light σ, a strange κ, and the heavier $a_0(980)$ and $f_0(980)$. It also explained why the $a_0(980)$ and $f_0(980)$ strongly couple to $K\bar{K}$ and $\pi\eta$. Nevertheless, the large width of σ and κ are still waiting for an explanation in this approach. On the other side, the mass splitting between the σ and $a_0(980)$ may also be explained by the instanton effects [52] and are investigated in the literature [53].

The $\gamma\gamma \to \pi^+\pi^-,\ \pi^0\pi^0$ process has been studied in Ref. [54] using a dispersive calculation and the decay width $\Gamma(\sigma \to 2\gamma)$ is extracted. The result is compared with quark model calculations with different assumptions on the content of the sigma meson and indicates that the extracted σ coupling to two photons are very different from the gluonium or even tetra quark description to the σ resonance.

In Ref. [55], the QCD spectral sum rules (QSSR) calculations based on different proposals ($\bar{q}q$, $\bar{q}\bar{q}qq$ and gluonium) are performed and discussed. It is found that, in the I=1 and I=1/2 channel the unusual wrong splitting between the mass of $a_0(980)$ and κ and also the width of $a_0(980)$ can be understood from QSSR within a $\bar{q}q$ assignment. Nevertheless the large width of κ can not be explained both using $\bar{q}q$ and $\bar{q}\bar{q}qq$ picture. In the I=0 channel the important role of QCD trace anomaly was emphasized based on which the observed spectrum of σ and $f_0(980)$ can be explained as a maximal mixing between

a low lying gluonium and a conventional $\bar{q}q$ state, based on analysis to the BES data of $J/\Psi \to \phi\pi\pi$, $\omega\pi\pi$, $f_0K^+K^-$ and other other experimental information. Furthermore with the aid of experimental information on OZI violating $J/\Psi \to \phi\pi\pi$, $D_s \to 3\pi$ decays and especially $J/\Psi \to \gamma S$ it is found that most of the vacuum scalars below 2GeV contain large gluonium component except the $f_0(1370)$ state.

The lattice study of the vacuum scalar have also been performed, and it suggests the existence of a low-lying sigma [56]. It is pointed out that the physics content of the σ, i.e., a tetraquark, a hybrid with the glue ball or the $q\bar{q}$ collective state, is obscure: The disconnected diagram gives the dominant contribution [56]. Investigations have also been made based on lagrangian models at meson or quark levels. In Ref. [57] the lightest scalars are depicted as a nonet with a complicated structure. Near the center they are $(qq)_{\bar{3}}(\bar{q}\bar{q})_3$ in S-wave, with some $\bar{q}q$ in P-wave, but further out they rearrange as $(q\bar{q})_1(q\bar{q})_1$ and finally as meson-meson states. In Ref. [58], a review is given to the studies on lightest scalars based on a couple channel model of potential scatterings. The potential contains a confining part of harmonic oscillator type as well as a $^3P_0$ transition potential characterizing the phase transition from a $\bar{q}q$ pair to a meson pair. In such a model calculation T matrix zeros are found to be close to those predicted by current algebra. Reasonable fit results are found on phase shifts, using only a small set of parameters and the σ and κ resonances are predicted dynamically. Variations of Padé approximations to χPT amplitudes are also studied in the literature to explore the nature of the lightest scalars which are generated dynamically [59].

The substructure of the $f_0(980)$ resonance is also a long standing issue. Even its small peak width may be explained as the Flatté effect, which means, manifests itself as a narrow peak, the $f_0(980)$ may contain a large decay width [60]. One interpretation of the quark content of $f_0(980)$ is that it is mainly of $\bar{s}s$ component while another explanation is that it is a $K\bar{K}$ molecule. The latter would require

$$\frac{\Gamma(\phi \to f_0\gamma)}{\Gamma(\phi \to a_0\gamma)} \sim 1 \ . \tag{11.38}$$

Nevertheless the recent KLOE results indicates [61]

$$\frac{\Gamma(\phi \to f_0\gamma)}{\Gamma(\phi \to a_0\gamma)} = 6.1 \pm 0.6 \ . \tag{11.39}$$

If on the other side they are explained as $q\bar{q}$ states then it can not explain the large branching ratio ($\geq 10^{-4}$). Another interpretation to the lightest resonances is that they are $qq\bar{q}\bar{q}$ states. In such a scheme the mass relations are explained [62] without considering the large widths and strong interaction corrections. In Ref. [63] some decay modes of these resonances are estimated using both $q\bar{q}$ and $qq\bar{q}\bar{q}$ picture and it was found that neither picture could give the correct branching ratio.

To conclude, the nature of the lightest scalars remains to be mysterious. The future BESIII experiments will be greatly welcomed since it can provide helpful information in understanding the strong interaction physics at low energies.

Acknowledgement: I would like to thank Gang Li and Ning Wu for helpful discussions in understanding related BESII experimental results. I also thank Bingsong Zou and HaiBo Li for a careful reading of the manuscript and helpful discussions.

Chapter 12

Meson spectrum

12.1 Introduction

The ultimate goal of studying the hadron spectroscopy is to learn the dynamics for the constituent interactions. As we know that in the light hadron sector due to the failure of perturbation expansion for QCD, the course towards such an ultimate goal will rely on either phenomenological approaches or lattice QCD (LQCD) calculations. In the past decade the LQCD has experienced drastic improvements along with the fast development of computing resources. But there still exist a lot of technical difficulties in the simulation of a fully non-perturbative QCD process, e.g. so far, an unquenched calculation is still unavailable. In contrast, the development of phenomenologies has marked the whole course of modern sciences, especially, in the study of hadron spectroscopy (see Ref. [64] and references therein). Experimental data will provide necessary constraints on the parameters introduced to the theory.

Focussing on the meson spectroscopy in this subsection, we shall learn how to construct a $q\bar{q}$ meson in the quark model [4, 64]. It is also known that apart from the conventional $q\bar{q}$ mesons, the non-Abelian property of QCD also allows the possible existence of bound states which are made of gluons, i.e. the so-called "glueball", and/or a gluon continuum. Furthermore, it is also possible to form multiquark mesons, such as $qq\bar{q}\bar{q}$, and the so-called "hybrid" which contains both $q\bar{q}$ and gluon (g) as its constituents, $q\bar{q}g$. All these unconventional states, if exist, will enrich greatly the meson spectrum and shed light on the dynamics of strong QCD scenario. Thus, searching for those unconventional mesons in experiment has been a topical subject in modern intermediate high-energy physics [65, 66].

12.2 Conventional meson spectrum

For conventional $q\bar{q}$ meson, a phenomenological study is, on the one hand, to find an empirically efficient way to describe the meson spectrum, and on the other hand keep some general properties from QCD (see the general remarks on the quark model). In the quark model framework, to study the meson spectrum is to construct the Hamiltonian

for a color-singlet $q\bar{q}$ system:

$$H = \int d\mathbf{x} \sum_i q_i^\dagger(\mathbf{x})\beta\left(m_i - \frac{\Delta}{2m_i}\right) q_i(\mathbf{x}) + \frac{1}{2}\int d\mathbf{x}d\mathbf{y} V_0(\mathbf{x}-\mathbf{y}) \sum_{ija} q_i^\dagger(\mathbf{x})\frac{\lambda^a}{2} q_i(\mathbf{x}) q_j^\dagger(\mathbf{y})\frac{\lambda^a}{2} q_j(\mathbf{y}) \ , \tag{12.1}$$

where i and j are flavor indices, and λ^a is the Gell-Mann Matrices for the SU(3)-color interactions; $V_0(\mathbf{x}-\mathbf{y})$ is a central potential, i.e. only depends on $|(\mathbf{x}-\mathbf{y})|$. Note that this Hamiltonian is independent of flavor as required by QCD. Also, one can see that a particular assumption for the form of the potential V_0 can reflect the QCD properties such as one-gluon-exchange Coulomb approximation, $V_0(\mathbf{x}) = \alpha_s/|\mathbf{x}|$, and confinement potentials.

The potential part of the Hamiltonian operating on a color-singlet $q\bar{q}$, $|(q\bar{q})_{\mathbf{1}}\rangle$, gives

$$\langle(q\bar{q})_{\mathbf{1}}|\hat{V}|(q\bar{q})_{\mathbf{1}}\rangle = -\frac{4}{3}V_0 \ , \tag{12.2}$$

where $\hat{V}$ denotes the second term of Eq. (12.1). Therefore, one can simplify the Hamiltonian for a color-singlet $q_i\bar{q}_j$ system to be:

$$H = \frac{\mathbf{p}_x^2}{2m_i} + \frac{\mathbf{p}_y^2}{2m_j} - \frac{4}{3}V_0(\mathbf{x}-\mathbf{y}) \ , \tag{12.3}$$

where $\mathbf{p}_x$ ($\mathbf{p}_y$) and $\mathbf{x}$ ($\mathbf{y}$) are the momentum and position of quark i (j), respectively.

In the center-of-mass frame, the Hamiltonian can be written as

$$H = \frac{\mathbf{P}^2}{2M} + \frac{\mathbf{p}^2}{2m} + V(\mathbf{r}) \ , \tag{12.4}$$

where $\mathbf{P} = \mathbf{p}_x + \mathbf{p}_y$ is the c.m. momentum of the $q\bar{q}$ system; and $\mathbf{r} = \mathbf{x} - \mathbf{y}$ and $\mathbf{p} = (\mathbf{p}_x - \mathbf{p}_y)/2$ are the relative distance and momentum between these two quarks; $M \equiv m_i + m_j$ and $m \equiv m_i m_j/M$ are the total and reduced masses. As $V(\mathbf{r})$ is assumed to be spin-independent, Eq. (12.3) is invariant under separate orbital and spin rotations. By defining the radial quantum number N, orbital angular momentum L, and total spin $S = 0, 1$, one can express the eigenstate of Eq. (12.3) (including the spin wavefunctions) as $N^{2S+1}L_J$ with the total angular momentum $J = L$ for $S = 0$ or $J = |L-1|,\ L,\ L+1$ for $S = 1$. With an explicit form of $V(\mathbf{r})$, one in principle will be able to produce a $q\bar{q}$ spectrum to compare with the experimental data. For instance, the ground state will correspond to $N = 1, L = 0$ with $S = 0$ or 1, i.e. a spin singlet 1^1S_0 and a spin triplet 1^3S_0. In the charmonium spectrum, – a suitable example for spin-independent potential quark model, one can identify $\eta_c(2980)$ and $J/\psi(3097)$. In Table 12.2, a classification for some of the low-lying mesons in the light quark sector are listed [67].

There are also spin-dependent forces between the quarks which result in fine and hyperfine structures in the hadron spectroscopy. In fact, without the spin-dependent forces, the spectrum obtained from the Hamiltonian of Eq. (12.3) cannot match the pattern observed in experiment. On the other hand, the relativistic effects will break the invariance of Hamiltonian under separate orbital and spin rotations. Therefore, it is natural to introduce spin-dependent forces which are phenomenologically analogous to those in hydrogen atom.

Table 12.1: Quark model classification for some of those low-lying $q\bar{q}$ states. f' and f denote the octet-singlet mixings. It should be noted that the nature of $f_0(1710)$ and $f_0(1370)$ is still under debating.

		$I=1$	$I=1/2$	$I=0$	$I=0$
$N^{2S+1}L_J$	J^{PC}	$u\bar{d}, d\bar{u}, (d\bar{d}-u\bar{u})/\sqrt{2}$	$u\bar{s}, s\bar{u}, d\bar{s}, s\bar{d}$	f'	f
1^1S_0	0^{-+}	π	K	η	η'
1^3S_1	1^{--}	$\rho(770)$	$K^*(892)$	$\phi(1020)$	$\omega(782)$
1^1P_1	1^{+-}	$b_1(1235)$	K_{1B}	$h_1(1380)$	$h_1(1170)$
1^3P_0	0^{++}	$a_0(1450)$	$K_0^*(1430)$	$f_0(1710)$	$f_0(1370)$
...					

It is attributed to De Rujula, Georgi and Glashow who illustrated that the spin-dependent forces in the quark potential are originated from the short-range QCD one-gluon-exchange (OGE) [1]. In a nonrelativistic expansion, in addition to a colored Coulomb type potential, the OGE leads to the Breit-Fermi interaction:

$$H_{BF} = k\alpha_s \sum_{i<j} S_{ij} \ , \tag{12.5}$$

where $k = -4/3$ and $-2/3$ are for a $q\bar{q}$ singlet and $q\bar{q}$ in $\bar{\mathbf{3}}$, respectively; and

$$\begin{aligned} S_{ij} \ = \ & \frac{1}{|\mathbf{r}|} - \frac{1}{2m_i m_j}\left(\frac{\mathbf{p}_i\cdot\mathbf{p}_j}{|\mathbf{r}|} + \frac{\mathbf{r}\cdot(\mathbf{r}\cdot\mathbf{p}_i)\mathbf{p}_j}{|\mathbf{r}|^3}\right) - \frac{\pi}{2}\delta(\mathbf{r})\left(\frac{1}{m_i^2}+\frac{1}{m_j^2}+\frac{16\mathbf{S}_i\cdot\mathbf{S}_j}{3m_i m_j}\right) \\ & -\frac{1}{2|\mathbf{r}|^3}\left\{\frac{1}{m_i^2}(\mathbf{r}\times\mathbf{p}_i)\cdot\mathbf{S}_i - \frac{1}{m_j^2}(\mathbf{r}\times\mathbf{p}_j)\cdot\mathbf{S}_j\right. \\ & \left. +\frac{1}{m_i m_j}\left[2(\mathbf{r}\times\mathbf{p}_i)\cdot\mathbf{S}_j - 2(\mathbf{r}\times\mathbf{p}_j)\cdot\mathbf{S}_i - 2\mathbf{S}_i\cdot\mathbf{S}_j + 6\frac{(\mathbf{S}_i\cdot\mathbf{r})(\mathbf{S}_j\cdot\mathbf{r})}{|\mathbf{r}|^2}\right]\right\} \end{aligned} \tag{12.6}$$

Although it is still questionable to apply the OGE picture in the hadron spectrum, their results turn to be in a good agreement with the experimental observations.

We do not review the Goldstone boson exchange model developed in the past decade, but refer readers to recent reviews [8] for details. A review of constituent quark model approaches for $q\bar{q}$ system can be found in Ref. [64].

12.3 Glueball spectrum

Glueballs are bound states of at least 2 or 3 gluons in a color singlet due to the non-Abelian property of QCD:

$$\begin{aligned} gg: \quad & \mathbf{8}\otimes\mathbf{8} \quad = \mathbf{1}+\mathbf{8}+\ldots \\ ggg: \quad & \mathbf{8}\otimes\mathbf{8}\otimes\mathbf{8} \quad = (\mathbf{8}\otimes\mathbf{8})_{\mathbf{8}}\otimes\mathbf{8} = \mathbf{1}+\ldots, \end{aligned} \tag{12.7}$$

where the charge conjugation is $C=+$ for gg states and $C=-$ for ggg states. Assuming that gluons inside glueballs are massive, for the gg, with the orbital angular momentum

$L = 0$, states of 0^{++} and 2^{++} can be formed, and 0^{++} is the groundstate glueball. For ggg, the lowest states are 0^{-+}, 1^{--} and 3^{--}.

Both gg and ggg can form states of which the quantum numbers cannot be produced by the $q\bar{q}$ quark model states. Such states, called "oddballs", will be "smoking gun" in the search for glueball candidates for which, however, experimental evidence is still unavailable. Possible quantum numbers for oddballs are: 0^{--}, 0^{+-}, 1^{-+}, 2^{+-}, 3^{-+}.... However, for gg states, if the gluons inside are massless, $J =$ odd states will be forbidden by Yang's theorem [67] though they may exist in ggg sector.

There is no explicit correlations between the gg and ggg ground state masses though the 0^{++} is expected to be lighter than the 0^{-+}. Theoretical predictions for the glueball masses vary significantly among different approaches.

Early phenomenologies find rather light masses for the scalar glueball, e.g. $M(0^{++}) = 0.65 \sim 1.21$ GeV in the bag model [69, 70, 71], and $M(0^{++}) = 1.15$ GeV in a potential model [72]. Other QCD-based approaches produce larger masses for the scalar such as $M(0^{++}) = 1.52$ GeV in a flux-tube model [73], and $M(0^{++}) \simeq 1.5$ GeV in QCD sum rule calculations [74, 301, 76, 77, 78, 79, 80].

In the last twenty years, extensive numerical studies have been carried out to calculate the glueball spectrum in LQCD. Although earliest LQCD predictions [81, 82] for the glueball masses vary significantly, nowadays, the predictions for several lightest glueballs converge to similar mass region despite of the various approaches being used [83, 84, 85, 352]. The lowest glueball state is the $J^{PC} = 0^{++}$ state (scalar) which has a mass about $1.5 \sim 1.7$ GeV, and the mass ratios of the tensor and psuedoscalar to the scalar is about 1.4 and 1.5, respectively. The newest results [352] of the glueball spectrum from larger and finer lattice are listed in Table 12.3 and Figure 12.1.

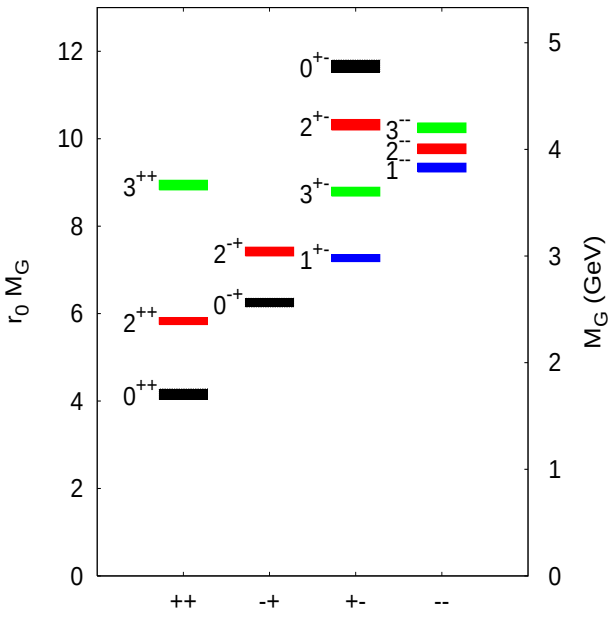

Figure 12.1: The mass spectrum of glueballs in the pure $SU(3)$ gauge theory. The masses are given both in terms of r_0 ($r_0^{-1} = 410$ MeV) and in GeV. The height of each colored box indicates the statistical uncertainty of the mass.

Table 12.2: The final glueball spectrum in physical units. In column 2, the first error is the statistical uncertainty coming from the continuum extrapolation, the second one is the 1% uncertainty resulting from the approximate anisotropy. In column 3, the first error comes from the combined uncertainty of $r_0 M_G$, the second from the uncertainty of $r_0^{-1} = 410(20)$ MeV

J^{PC}	$r_0 M_G$	M_G (MeV)
0^{++}	4.16(11)(4)	1710(50)(80)
2^{++}	5.83(5)(6)	2390(30)(120)
0^{-+}	6.25(6)(6)	2560(35)(120)
1^{+-}	7.27(4)(7)	2980(30)(140)
2^{-+}	7.42(7)(7)	3040(40)(150)
3^{+-}	8.79(3)(9)	3600(40)(170)
3^{++}	8.94(6)(9)	3670(50)(180)
1^{--}	9.34(4)(9)	3830(40)(190)
2^{--}	9.77(4)(10)	4010(45)(200)
3^{--}	10.25(4))(10)	4200(45)(200)
2^{+-}	10.32(7)(10)	4230(50)(200)
0^{+-}	11.66(7)(12)	4780(60)(230)

The calculations of the glueball spectrum are mostly from quenched lattice QCD. Therefore, it is still an open question, *How large the systematic uncertainty of the quenched approximation would be?* A recent preliminary analysis of the scalar glueball mass based on the MILC dynamical gauge configuration [87] shows that the scalar glueball mass of the dynamic lattice simulation does not change much [87].

12.3.1 Glueball signatures

Taking the spectrum of the $q\bar{q}$ nonet of pseudoscalar (0^-) and vector (1^-) as a reference, the scalar nonet should lie in the mass range of 1∼2 GeV [64, 65, 66]. Established states $a_0(1450)$ and $K_0^*(1430)$ in this mass region can be naturally assigned as the $I = 1$ and $I = 1/2$ multiplets, respectively, and thus bring the issue about the $I = 0$ multiplets for the scalar nonet to attention. For $I = 0$, there are more than two states reported in the literature [88, 89, 90, 91, 92], namely, $f_0(1370)$, $f_0(1500)$, $f_0(1710)$, $f_0(1790)(?)$, $f_0(1810)(?)$. This could be a signal for the existence of scalars beyond conventional quark model classifications such as glueball, hybrid or multiquark states.

There also exists another scalar nonet below 1 GeV, i.e. $f_0(980)$, $a_0(980)$, $\sigma(600)$, and $\kappa(800)$, which are candidates for multiquark or molecule states [93, 94]. Details about this are discussed in Chapter XXX.

The up-to-date LQCD result [84, 85, 352] makes the mass region between 1 - 2 GeV extremely interesting for the search for the groundstate scalar glueball ($J^{PC} = 0^{++}$), in particular, due to the observation of more than two f_0 states with similar masses ($f_0(1370)$, $f_0(1500)$ and $f_0(1710)$) [95]. However, since the glueball properties are not expected to

drastically different from the conventional $q\bar{q}$ mesons, one will be encountered with the difficulty of distinguishing the scalar glueball from conventional $q\bar{q}$ states. Nonetheless, more than two f_0 states with similar masses imply that mixings of the pure gluonic scalar (glueball) with nearby $q\bar{q}$ nonet can occur [96, 97, 98, 99, 100, 101, 102, 79]. This greatly complicates the efforts of identifying the scalar glueball in both experiment and theory. In contrast, signals for oddballs will be decisive evidence for the existence of glueballs. Unfortunately, so far concrete experimental identification of oddballs is still unavailable.

Theoretical expectations for a glueball with conventional quantum numbers have been widely explored in the literature [65]. Although in most cases they are not sufficient for distincting a glueball candidate from conventional $q\bar{q}$ states, they are still useful for providing a guidance for further efforts. We list some of those expectations as a brief review:

1). Flavor-blindness of glueball decays

This character leads to the prediction of the flavor-singlet glueball decay branching ratio fraction:

$$\frac{1}{P.S.}\Gamma(G \to \pi\pi : K\bar{K} : \eta_8\eta_8 : \eta_1\eta_8 : \eta_1\eta_1) = 3 : 4 : 1 : 0 : 1 \ , \tag{12.8}$$

where P.S. denotes the phase space factor, and η_1 and η_8 are the $I = 0$ flavor singlet and octet of the SU(3) nonet. It can be shown that this relation holds for $\pi\pi : K\bar{K} : \eta\eta : \eta\eta' : \eta'\eta'$ after taking into account the singlet-octet mixing:

$$\begin{aligned} \eta &= \eta_8 \cos\theta - \eta_1 \sin\theta \\ \eta' &= \eta_8 \sin\theta + \eta_1 \cos\theta. \end{aligned} \tag{12.9}$$

The most significant feature for a pure glueball decays to PP is the vanishing branching ratio for $G \to \eta\eta'$. However, an observed vanishing ratio for $X \to \eta\eta'$ does not necessarily lead to the conclusion that $X = G$ since interferences between different components in a $q\bar{q}$ state can also lead to vanishing $\eta\eta'$ branching ratio [96, 97, 98].

2). Glueball couplings to $\gamma\gamma$

Since glue is charge neutral, glueball production in $\gamma\gamma$ collision is suppressed. Similarly, their decays into $\gamma\gamma$ should also be suppressed. Therefore, one would expect that a glueball candidate should have small decay branching ratio to $\gamma\gamma$. However, again, a small branching ratio for $X \to \gamma\gamma$ does not necessarily lead to the conclusion that X is a glueball due to interferences from possible mixed components. For instance, in Ref. [103], it is shown that the branching ratio fractions for $f_0^i \to \gamma\gamma$, where $i = 1, 2, 3$ denotes $f_0(1710)$, $f_0(1500)$, and $f_0(1370)$, respectively, are found to be $f_0^1 : f_0^2 : f_0^3 \simeq 1 : 2 : 12$ with larger $\gamma\gamma$ couplings for $f_0(1500)$ than $f_0(1370)$ of which the $q\bar{q}$ component is strongly favored.

Alternatively, the scalar's $q\bar{q}$ component can be probed in e^+e^- annihilation via two virtual photon intermediate states. VEPP and DAΦNE have access to the production of scalars in $1\sim 2$ GeV, while the BEPC will be accessible to heavier scalar search at about

3 GeV [104].

3). Glueball production in heavy quarkonium radiative decays

The J/ψ radiative decay is a gluon rich process and ideal for the search for glueballs as the intermediate resonance in $J/\psi \to \gamma G \to \gamma +$ all. It gives access to all isoscalar states with charge conjugation $C = +$ and forbids all $C = -$ states. Those allowed quantum numbers include the low-lying glueballs and hybrids for which the production phase space are generally large enough. Thus, a systematic study of J/ψ radiative decays with high statistics at BESIII will be extremely important for clarifying some long-standing puzzles.

Information about the intermediate resonances is obtained by measuring their hadronic or radiative decays. Two measures were proposed in the literature to quantify the gluonic contents of the resonances. "Stickiness",

$$S = \frac{\Gamma(J/\psi \to \gamma X) \times P.S.(X \to \gamma\gamma)}{\Gamma(X \to \gamma\gamma) \times P.S.(J/\psi \to \gamma X)} \tag{12.10}$$

defined by Chanowitz [105], is designed to measure the color-to-electric-charge ratio with the phase space factored out, and maximize the effects from the glue dominance inside a glueball. If X is a glueball, one would expect that its production is favored in J/ψ radiative decays, while its decays into $\gamma\gamma$ are strongly suppressed. Therefore, a glueball should have large stickiness in comparison with a $q\bar{q}$ state.

Cakir and Farrar [106] propose another quantitative measure of the gluonic content of a resonance by calculating its branching ratio to gluons, i.e. $b_{R\to gg}$. This quantity can be related to the production b.r. of resonance R in heavy quarkonium radiative decays. Its value is in a range of $b_{R\to gg} = O(\alpha_s^2) \simeq 0.1 - 0.2$ for a $q\bar{q}$ state, and ~ 1 for a glueball. Interestingly, for most of the well-established $q\bar{q}$ states $b_{R\to gg}$ is found rather small, while for the scalar glueball candidates $f_0(1500)$ and $f_0(1710)$ the value is rather large, in particular for $f_0(1710)$ [103].

These two measures, however, still cannot provide unambiguous evidence for glueballs. The "stickiness" works in a world that glueball and $q\bar{q}$ must not have mixings (quenched approximation in LQCD), i.e. for pure glueballs. In case that glueball-$q\bar{q}$ mixing occurs (unquenched), the complicated interferences from glueball and $q\bar{q}$ components can violate the expectation of large stickiness corresponding to glueball states. In this sense, the scheme of Ref. [106, 103] seems to be more sensible because it directly measures the coupling of a resonance to gluons.

4). Chiral suppression

Another criteria pointed out by Carlson [107] and recently developed by Chanowitz [108] is the chiral suppression mechanism for $J = 0$ glueballs. Due to the fact that in pQCD the amplitude is proportional to the current quark mass in the final states, the $J = 0$ glueballs will have larger couplings into e.g. $K\bar{K}$ rather than $\pi\pi$. For $J \neq 0$, the decay amplitude is flavor symmetric. Combined with the quenched LQCD prediction, it places $f_0(1710)$ as a gluon-dominant state while $f_0(1500)$ dominated by the $s\bar{s}$ [99]. However, because of the complexity of the gluon hadronization and unclear $G - q\bar{q}$ mixings, the

observation of relatively larger b.r. to $K\bar{K}$ for a candidate does not necessarily lead to its being a glueball [109, 110].

5). Charmonium hadronic decays

The Charmonium hadronic decays has great advantages of performing a systematic analysis of light hadrons, i.e. both meson and baryon. For instance, the SU(3) flavor symmetry breakings can be investigated by decays of $J/\psi \to VP, VS, VT$; $\chi_{cJ} \to VV$, PP, SS; $\eta_c \to VV$, PP, etc. Nonetheless, the decays of $J/\psi \to Vf_1$ also give access to the axial vectors, $f_1(1285)$ and $f_1(1420)$. An important issue here is to study the properties of the final state mesons and look for evidence for exotics, such as $f_0(980)$ and $a_0(980)$ as four quark states [93] or $K\bar{K}$ molecules; scalar glueball in $f_0(1370)$, $f_0(1500)$, and $f_0(1710)$; and hybrids. Specifically, by recoiling ω and ϕ in $J/\psi \to \omega X$ and ϕX, one can gain information about the flavor components of resonance X. Since ω and ϕ are ideally mixed, i.e. $|\omega\rangle = |u\bar{u} + d\bar{d}\rangle/\sqrt{2}$ and $|\phi\rangle = |s\bar{s}\rangle$, the flavor contents of resonance X can be probed based on the OZI rule [342]. However, it should cautioned that so far the role played by the empirical OZI rule has not been fully understood at the charmonium energy region. For the recoiling process of two light mesons, possible large OZI violations were found in QCD-inspired calculations [112, 113, 114]. Dynamical studies of the possible OZI rule violations should be carried out, which may be essentially important for understanding the nature of many final state mesons [98, 115, 116, 117].

6). Other glueball-favored processes

The glueball signals are also searched in other reactions, such as $p\bar{p}$ annihilation, and central collisions of $pp \to ppG$. In $p\bar{p}$ reaction, due to the competition of the quark and antiquark rearrangement to form the $q\bar{q}$ meson, identification of glueball signals will be contaminated. Similarly, competitions from the $q\bar{q}$ production in pp central collisions will mix with any possible signals of the glueballs.

It is proposed by Close and Kirk [118] that in the pp central collisions, the production of the S-wave resonances (e.g. 0^{++} and 2^{++} glueball made of vector gluons, or S-wave tetraquark states or $K\bar{K}$ molecules) will be favored the small recoiled transverse momentum difference ($\mathrm{d}P_T$) of the final state protons, while the $q\bar{q}$ production will favor the larger $\mathrm{d}P_T$ region ($\mathrm{d}P_T \geq O(\Lambda_{QCD})$). Therefore, different kinematic regions serve as a production filter for the S-wave resonances. Following this, experimental analysis at WA102 [119] indeed reveals a clear azimuthal dependence as a function of J^{PC} and P_T at the proton vertices, and scalars appear to divide into two classes: $f_0(980)$, $f_0(1500)$ and $f_0(1710)$ strongly peak at small ϕ angle (corresponding to small $\mathrm{d}P_T$) and $f_0(1370)$ at large ϕ.

The above criteria individually cannot provide indisputable evidence for a glueball candidate with conventional quantum numbers, especially for the scalar glueball. However, putting all together the above expectations and criteria for a glueball candidate one might still be able to place a bound on the glueball and $q\bar{q}$ contents of a state, and gain some insights into the complex issue of strong QCD. In fact, due to the limit of quenched approximation applied by the present LQCD calculations, the effects arising from an un-

quenched approach need to be investigated in detail. Phenomenological progress towards this direction was proposed by Tornqvist [120] who emphasized the difference between bare states (quark model bound states that do not decay) and dressed ones (physical states that decay to hadrons). In the scalar case, Boglione and Pennington [121] showed that a pure glue or $q\bar{q}$ state (e.g. unquenched bare state studied by LQCD) is so different from the dressed hadrons that reliable calculations of the hadron properties are crucial for extracting the scalars and make sense of experiment.

12.3.2 Glueball candidates

Scalar glueball candidates

In the mass region of $1 \sim 2$ GeV, the abundance of isoscalar scalars, i.e. $f_0(1370)$, $f_0(1500)$, and $f_0(1710)$ ($f_0(1790)$ and $f_0(1810)$ need to be confirmed in further experiment), makes them natural scalar glueball candidates. As follows, we shall brief the experimental information for these states and examine the theoretical expectations of their natures. Controversies will be addressed.

1). $f_0(1370)$

The $f_0(1370)$ turns to be broader than $f_0(1500)$ and $f_0(1710)$, and strongly coupled to $\pi\pi$. Its decays into $K\bar{K}$ were also observed by Crystal Barrel in $p\bar{p}$ annihilation [88], and then confirmed by WA102 in pp scattering [89] in the production channels for $\pi\pi$, $K\bar{K}$ and $\eta\eta$. Meanwhile, its absence in $\eta\eta'$ implies that its configuration is mainly $q\bar{q}$. Taking into account the large ratio of $BR_{f_0(1370)\to\pi\pi}/BR_{f_0(1370)\to K\bar{K}} = 2.17 \pm 0.9$ [89], $f_0(1370)$ can be assigned as an $n\bar{n}$ candidate of $q\bar{q}$ scalar.

The new data from BESII 5.8×10^7 J/ψ events also presented the observation of $f_0(1370)$ in $J/\psi \to \phi\pi^+\pi^-$ [90] .

Fig. 12.2(a) shows the K^+K^- invariant mass distribution for $J/\psi \to K^+K^-\pi^+\pi^-$ from BESII data. The ϕ signal is clearly seen. The $\pi^+\pi^-$ invariant mass spectrum which recoils against ϕ is shown in Fig. 12.2(b), which exhibits a clear bump at around 1370 MeV/c^2, in addition to a strong $f_0(980)$ peak.

No significant $f_0(1370)$ is observed in $J/\psi \to \phi K^+K^-$ [90], ωK^+K^- [91] and $\omega\pi^+\pi^-$ [122].

Figs. 12.3(a) and (b) show the ϕ signal and K^+K^- invariant mass recoiling against ϕ for $J/\psi \to K^+K^-K^+K^-$.

A partial wave analysis (PWA) is performed to $J/\psi \to \phi\pi^+\pi^-$ and ϕK^+K^-. Amplitudes are fitted to relativistic tensor expressions which are documented in Ref. [123]. The full angular dependence of decays of the ϕ and $\pi^+\pi^-$ or K^+K^- resonances is fitted, including correlations between them. The line-shape of the ϕ is not fitted, because the ϕ is much narrower than the experimental resolution. The $\phi\pi^+\pi^-$ and ϕK^+K^- data are fitted simultaneously, constraining resonance masses and widths to be the same in both sets of data. The PWA results show that the peak at around 1370 MeV/c^2 in the $\pi^+\pi^-$ invariant mass spectrum in Fig. 12.2(b) comes from a dominant $f_0(1370)$ interfering with $f_2(1270)$ and a smaller $f_0(1500)$. The $\phi K\bar{K}$ data contain a strong peak due to $f_2'(1525)$.

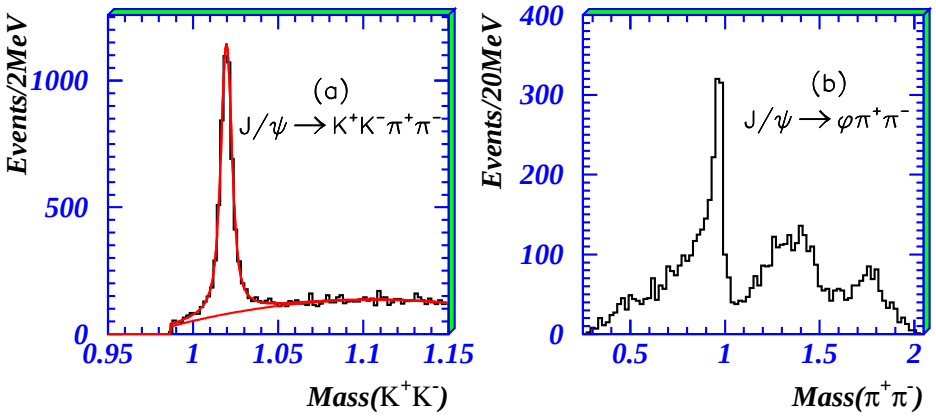

Figure 12.2: (a) The K^+K^- invariant mass distribution for $J/\psi \to K^+K^-\pi^+\pi^-$. (b) The $\pi^+\pi^-$ invariant mass for events selected within ± 15 MeV/c^2 of the ϕ.

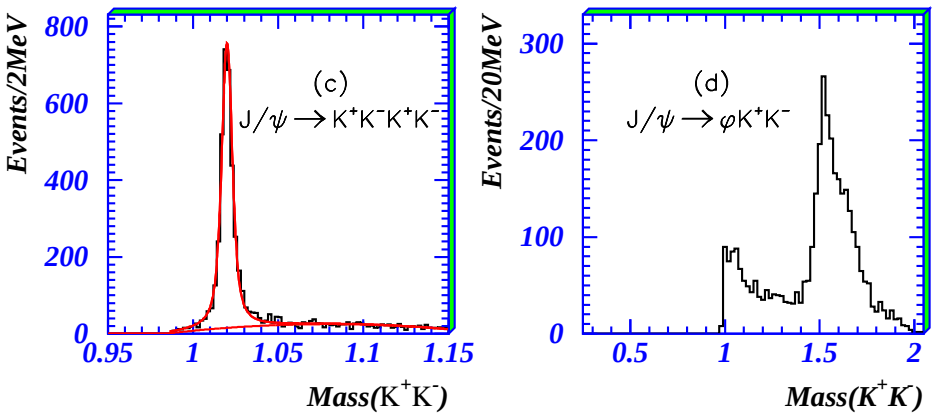

Figure 12.3: (a) The K^+K^- invariant mass distribution for $J/\psi \to K^+K^-K^+K^-$. (b) The K^+K^- invariant mass for events selected within ± 15 MeV/c^2 of the ϕ.

A shoulder on its upper side may be fitted by interference between $f_0(1500)$ and $f_0(1710)$. The mass and width of $f_0(1370)$ are determined to be: $M = 1350 \pm 50$ MeV/c^2 and $\Gamma = 265 \pm 40$ MeV/c^2.

The absence of $f_0(1370)$ in $J/\psi \to \omega\pi\pi$ suggests that the branching ratio for $J/\psi \to \phi f_0(1370)$ is larger than that for $J/\psi \to \omega f_0(1370)$. This certainly raised concerns about the $f_0(1370)$ configurations since one would expect that $f_0(1370)$ of $n\bar{n}$ is more likely to recoil against ω instead of ϕ due to the application of the OZI rule.

2). $f_0(1500)$

The $f_0(1500)$ was observed in many experiments, such as pion induced reaction $\pi^- p$, $p\bar{p}$ annihilation [124, 125], pp central collisions [126, 127] and J/ψ radiative decays [128, 129]. Most of the data on $f_0(1500)$ was from Crystal Barrel collaboration, who resolved two scalar states in this mass region, and determined its decay branching ratios to a number of final states, including $\pi^0\pi^0$, $\eta\eta$, $\eta\eta'$, $K_L K_L$ and $4\pi^0$, using $p\bar{p}$ annihilation at rest. It is also observed that in glueball suppressed processes of $\gamma\gamma$ collision to $K_s K_s$ and $\pi^+\pi^-$, $f_0(1500)$ is absent. All of these favor $f_0(1500)$ being a non-$q\bar{q}$ state.

J/ψ radiative decays have been suggested as promising modes for glueball searches. If $f_0(1500)$ is a scalar glueball, it should be copiously produced in J/ψ radiative decays. The $J/\psi \to \gamma\pi^+\pi^-$ process was analyzed previously in the Mark III [130], DM2 [131] and BES I [132] experiments, in which there was evidence for $f_2(1270)$ and an additional $f_2(1720)$. However, the high mass shoulder of the $f_2(1270)$, at about 1.45 GeV/c^2, was unsettled. A revised amplitude analysis of Mark III data assigned the shoulder to be a scalar at $\sim$ 1.43 GeV/c^2, and, in addition, found the peak at $\sim$ 1.7 GeV/c^2 to be scalar rather than tensor [133]. The $J/\psi \to \gamma\pi^0\pi^0$ process was also studied by the Crystal Ball [134] and BES I experiments [135], but no partial wave analysis has yet been performed on this channel.

Recently, BES reported the results on J/ψ radiative decays to $\pi^+\pi^-$ and $\pi^0\pi^0$ based on a sample of 58M J/ψ events taken with the BES II detector [136]. Fig. 12.4 shows the $\pi^+\pi^-$ mass spectrum for the selected events, together with the corresponding background distributions and the Dalitz plot. There is a strong $\rho^0(770)$ peak mainly due to background from $J/\psi \to \rho^0\pi^0$. A strong $f_2(1270)$ signal, a shoulder on the high mass side of the $f_2(1270)$, an enhancement at $\sim$ 1.7 GeV/c^2, and a peak at $\sim$ 2.1 GeV/c^2 are clearly visible. The lightly shaded histogram in Fig. 12.4 corresponds to the dominant background $J/\psi \to \pi^+\pi^-\pi^0$. The other backgrounds are shown as the dark shaded histogram in Fig. 12.4. Fig. 12.5 shows the $\pi^0\pi^0$ mass spectrum and the Dalitz plot. The shaded histogram corresponds to the sum of estimated backgrounds determined using PDG branching ratios [67]. In general, the $\pi^+\pi^-$ and $\pi^0\pi^0$ mass spectra exhibit similar structures above 1.0 GeV/c^2.

Partial wave analyses (PWA) are carried out using the relativistic covariant tensor amplitude method in the 1.0 to 2.3 GeV/c^2 $\pi\pi$ mass range. There are conspicuous peaks due to the $f_2(1270)$ and two 0^{++} states in the 1.45 and 1.75 GeV/c^2 mass regions. The first 0^{++} state has a mass of $1466 \pm 6 \pm 20$ MeV/c^2, a width of $108^{+14}_{-11} \pm 25$ MeV/c^2, and a branching fraction $\mathcal{B}(J/\psi \to \gamma f_0(1500) \to \gamma\pi^+\pi^-) = (0.67 \pm 0.02 \pm 0.30) \times 10^{-4}$, which is considered as $f_0(1500)$. Spin 0 is strongly preferred over spin 2. Fig. 12.6 shows the

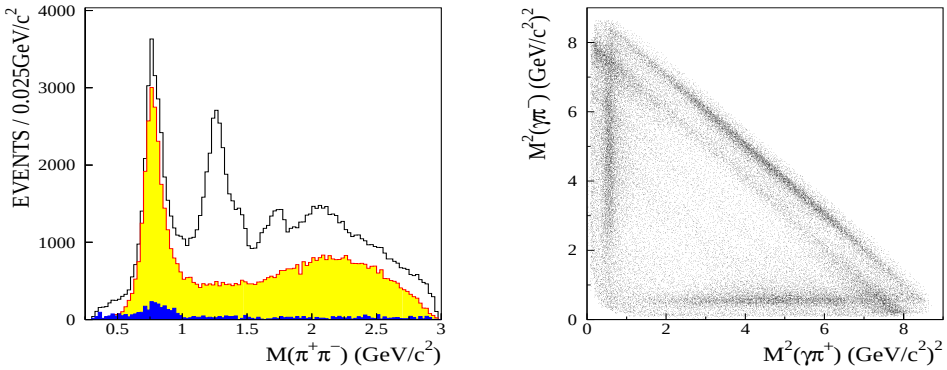

Figure 12.4: Invariant mass spectrum of $\pi^+\pi^-$ and the Dalitz plot for $J/\psi \to \gamma\pi^+\pi^-$, where the lightly and dark shaded histograms in the upper panel correspond to $J/\psi \to \pi^+\pi^-\pi^0$ and other estimated backgrounds, respectively.

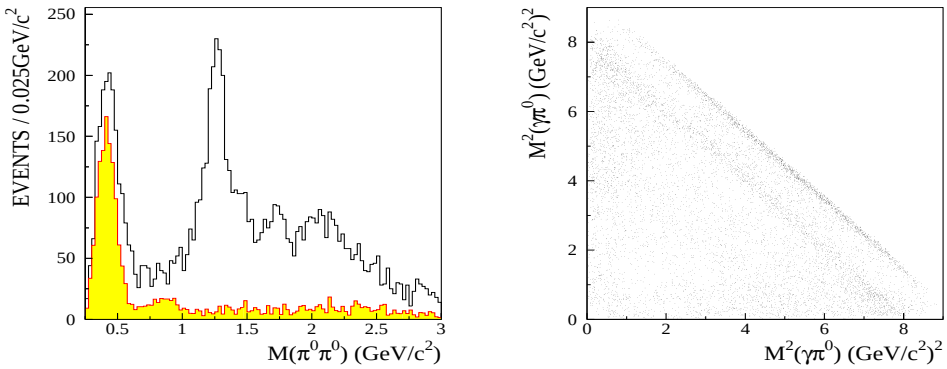

Figure 12.5: Invariant mass spectrum of $\pi^0\pi^0$ and the Dalitz plot for $J/\psi \to \gamma\pi^0\pi^0$, where the shaded histogram in the upper panel corresponds to the estimated backgrounds.

$\pi^+\pi^-$ and $\pi^0\pi^0$ invariant mass distributions from $J/\psi \to \gamma\pi^+\pi^-$ and $\gamma\pi^0\pi^0$, where, the corsses are data and the histogram shows the PWA fit projection.

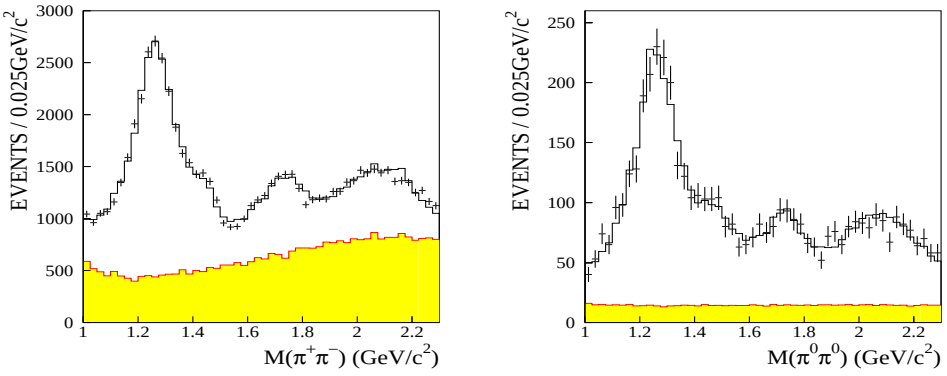

Figure 12.6: The $\pi^+\pi^-$ invariant mass distribution from $J/\psi \to \gamma\pi^+\pi^-$. The crosses are data, the full histogram shows the PWA fit projection, and the shaded histogram corresponds to the background.

In contrast to the $f_0(1370)$, the $f_0(1500)$ is not directly observed in J/ψ hadronic decays, such as $J/\psi \to \phi K\bar{K}$, $\omega K\bar{K}$, $\phi\pi\pi$, $\omega\pi\pi$ at BES [90, 91]. In most of the above production channels, the $f_0(1500)$ turns to have larger branching ratio to $\pi\pi$ than $K\bar{K}$. However, the recent data for $B^+ \to K^+K\bar{K}$ and $K^+\pi\pi$ [137] suggest a 0^{++} scalar at 1.5 GeV with larger branching ratio to $K\bar{K}$ than $\pi\pi$.

Searching for $f_0(1500)$ in more decay modes and studying its spin-parity are crucial in clarifying the nature of $f_0(1500)$.

3). $f_0(1710)$

The $f_0(1710)$ is a main competitor of $f_0(1500)$ for being the lightest 0^{++} glueball candidate due to its large production rate in gluon rich processes, such as J/ψ radiative decays, pp central production etc., and the predictions of lattice QCD. However, there has been a long history of uncertainty about the properties of the $f_0(1710)$. Table 12.3.2 [67] lists the results of $f_0(1710)$ from different experiments before BES2 era. Apparently, different experiments gave different masses, widths and spin-parities. The latest analysis of MarkIII $J/\psi \to \gamma K\bar{K}$ data by Dunwoodie [133] favors $J^P = 0^+$ over an earlier assignment of 2^+, the latest central production data of WA76 and WA102 ($pp \to p(K\bar{K})p$) favor 0^+ [138, 139] and BESI $J/\psi \to \gamma 4\pi$ data also favor 0^+ [129]. The spin-parity of $f_0(1710)$ in the observed processes is crucial in clarifying whether $f_0(1710)$ is a $q\bar{q}$ or non-$q\bar{q}$ state. If $J = 0$, then the $f_0(1710)$ and $f_0(1500)$ might represent the glueball and the $q\bar{q}$ state, or more likely each is a mixture of both. However, if $J = 2$, it will be difficult to assign a glueball status to $f_2(1710)$, since that would be at odds with all current lattice gauge calculations.

To study the structure at around 1.7 GeV/c^2, partial wave analyses (PWA) of $J/\psi \to \gamma K\bar{K}$, $\gamma\pi\pi$, $\omega\pi^+\pi^-$, ωK^+K^-, $\phi\pi^+\pi^-$ and ϕK^+K^- are carried out, based on 5.8×10^7 J/ψ events collected at BES2.

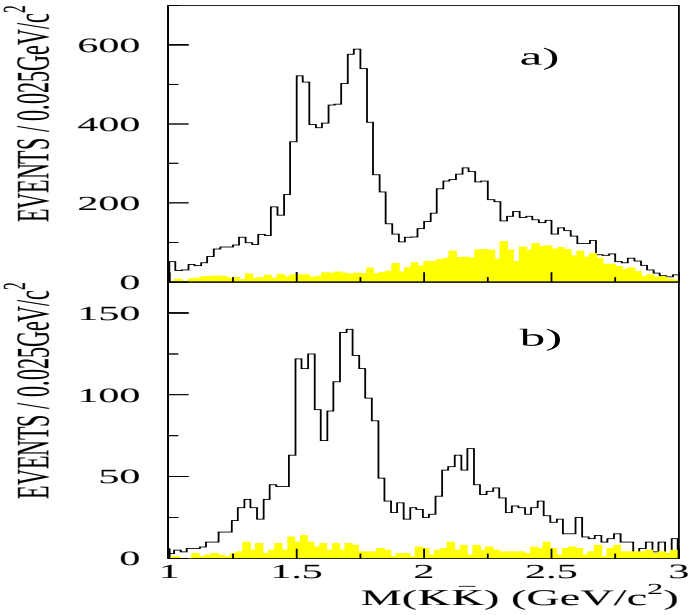

Figure 12.7: Invariant mass spectra of a) K^+K^-, b) $K^0_SK^0_S$ for $J/\psi \to \gamma K\bar{K}$ events, where the shaded histogra correspond to the estimated background contributions.

Fig. 12.7 shows the K^+K^- and $K^0_SK^0_S$ mass spectra for the selected $J/\psi \to \gamma K\bar{K}$ events, together with the corresponding background distributions. These two mass spectra agree closely below 2.0 GeV. The resonant structure in the mass regions of 1.7 GeV/c^2 is very clearly visible in both decay modes, in addition to the strong $f_2'(1525)$.

The partial wave analyses, using relativistic covariant tensor amplitudes constructed from Lorentz-invariant combinations of the 4-vectors and the photon polarization for J/ψ initial states with helicity ± 1, is carried out in the $K\bar{K}$ mass below 2.0 GeV. Both bin-by-bin and global fits are performed and the consistent results are obtained. The analyses show that spin 0 is strong preferred over spin 2 for the resonance at around 1.7 GeV/c^2. The $f_0(1710)$ peaks at a mass of $1740 \pm 4^{+10}_{-25}$ MeV/c^2 with a width of 166^{+5+15}_{-8-10} MeV/c^2.

For $J/\psi \to \omega K^+K^-$, the K^+K^- invariant mass shows a conspicuous signal for $f_0(1710)$, as is shown in Fig. 12.3.2. The partial wave analysis determines its mass and width to be: $M = 1738 \pm 30$ MeV/c^2, $\Gamma = 125 \pm 20$ MeV/c^2.

In the $\pi^+\pi^-$ invariant mass spectrum which recoils against ϕ, shown in Fig. 12.2, a peak at around 1.79GeV/c^2 is evident. No peak in this region is seen in $J/\psi \to \phi K^+K^-$ channel. A simultaneous PWA fit to $J/\psi \to \phi K^+K^-$ and $\phi\pi^+\pi^-$ shows that this peak has a mass and width of $M = 1790^{+40}_{-30}$ MeV/c^2 and $\Gamma = 270^{+60}_{-30}$ MeV/c^2; spin 0 is preferred over spin 2. This state, $f_0(1790)$, is distinct from $f_0(1710)$, seen in $J/\psi \to \gamma K^+K^-$ and ωK^+K^- channels, because of its different mass, width and decay or production branching fractions to $\pi\pi$ and KK from those of $f_0(1710)$.

For $J/\psi \to \gamma\pi\pi$, the production of a 0^{++} is also observed in 1.7 GeV/c^2 mass region. Its mass and width are $1765^{+4}_{-3} \pm 13$ MeV/c^2 and $145 \pm 8 \pm 69$ MeV/c^2. This 0^{++} state may be $f_0(1710)$ which is observed in $J/\psi \to \gamma K\bar{K}$ and ωK^+K^-, or may be $f_0(1790)$ which is shown in $J/\psi \to \phi\pi^+\pi^-$, or may also be a superposition of $f_0(1710)$ and $f_0(1790)$.

More recently, BES reported the observation of an enhancement near threshold in the

Table 12.3: Results of $f_0(1710)$ from different experiments before BES2 era.

Process	Collaboration	M(MeV)	Γ(MeV)	J^{PC}
$J/\psi \to \gamma\eta\eta$	C. B.(82)	1640 ± 50	200^{+100}_{-70}	2^{++}
$\pi^- p \to K^0_S K^0_S n$	BNL(82)	1771^{+77}_{-53}	200^{+156}_{-9}	0^{++}
$\pi^- N \to K^0_S K^0_S n$	FNAL(84)	1742 ± 15	57 ± 38	—
$\pi^- p \to \eta\eta N$	GAMS(86)	1755 ± 8	< 50	0^{++}
$J/\psi \to \gamma K^+ K^-$	MARK3(87)	1720 ± 14	130 ± 20	2^{++}
$J/\psi \to \gamma K^+ K^-$	DM2(88)	1707 ± 10	166 ± 33	—
$pp \to p(K^+K^-)p$ $\to p(K^0_S K^0_S)p$	WA76(89)	1713 ± 10 1706 ± 10	181 ± 30 104 ± 30	2^{++}
$J/\psi \to \gamma K\bar{K}$	MARK3(91)	1710 ± 20	186 ± 30	0^{++}
$p\bar{p} \to \pi^0\eta\eta$	E760(93)	1748 ± 10	264 ± 25	$even^{++}$
$J/\psi \to \gamma 4\pi$	MARK3 data D. Bugg(95)	1750 ± 15	160 ± 40	0^{++}
$J/\psi \to \gamma K\bar{K}$	MARK3 data Dunwoodie	1704^{+16}_{-23}	124^{+52}_{-44}	0^{++}
$pp \to p(K\bar{K})p$	WA102(99)	1730 ± 15	100 ± 25	0^{++}
$J/\psi \to \gamma 4\pi$	BES(2000)	1740^{+20}_{-25}	135^{+40}_{-25}	0^{++}

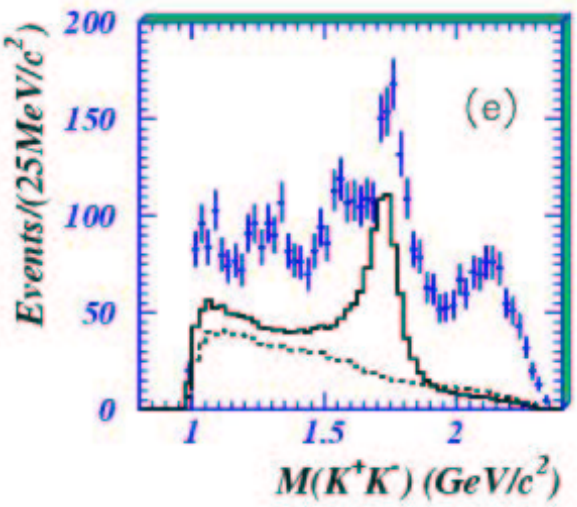

Figure 12.8: K^+K^- invariant mass spectrum in $J/\psi \to \omega K^+K^-$. The crosses are data and the histogram is PWA fit projection.

$\omega\phi$ invariant mass spectrum from the OZI suppressed decays of $J/\psi \to \gamma\omega\phi$ [140], based on a sample of 5.8×10^7 J/ψ events collected with the BESII detector. Fig. 12.9(a) shows the $K^+K^-\pi^+\pi^-\pi^0$ invariant mass distribution for events with K^+K^- invariant mass within the nominal ϕ mass range ($|m_{K^+K^-} - m_\phi| < 15$ MeV/c^2) and the $\pi^+\pi^-\pi^0$ mass within the ω mass range ($|m_{\pi^+\pi^-\pi^0} - m_\omega| < 30$ MeV/c^2), and a structure peaked near $\omega\phi$ threshold is observed. The peak is also evident as a band along the upper right-hand edge of the Dalitz plot in Fig. 12.9(b). No evidence of an enhancement near $\omega\phi$ threshold is observed from the sideband events of ω and ϕ. And the study from inclusive and exclusive Monte-Carlo shows that the $\omega\phi$ threshold enhancement is not from backgrounds.

The significance of the $\omega\phi$ threshold enhancement is more than 10σ. From a partial wave analysis with covariant helicity coupling amplitudes, the spin-parity of the $X = 0^{++}$ with an $\mathcal{S}$-wave $\omega\phi$ system is favored. The mass and width of the enhancement are determined to be $M = 1812^{+19}_{-26}$ (stat) $\pm$ 18 (syst) MeV/c^2 and $\Gamma = 105 \pm 20$ (stat) $\pm$ 28 (syst) MeV/c^2, and the product branching fraction is $\mathcal{B}(J/\psi \to \gamma X) \cdot \mathcal{B}(X \to \omega\phi) = (2.61 \pm 0.27$ (stat) $\pm$ 0.65 (syst)) $\times 10^{-4}$. The mass and width of this state are not compatible with any known scalars listed in the Particle Data Group (PDG) [67].

These states, if confirmed, may raise tremendous interests in the study of their natures [141, 142, 143, 144, 145, 146]. It will also raise essential questions about their production mechanism in the J/ψ hadronic and radiative decays [146].

In additional to the above, recent analyses suggest the existence of a broad scalar $f_0(1200-1600)$ with a half width 500-900 GeV [147, 148]. Nonetheless, the sign of such a broad state leads to a rearrangement of the scalar nonets, where $\sigma(600)$ and $\kappa(800)$ are no longer physical states. In contrast to those two nonets, above/below 1 GeV, the new nonets are arranged to be: i) $f_0(980)$, $f_0(1300)$, $a_0(980)$, $K_0(1415)$ for the $q\bar{q}$ with radial quantum number $n = 1$; and ii) $f_0(1500)$, $f_0(1750)$, $a_0(1520)$, $K_0(1820)$ for $n = 2$. The broad $f_0(1200-1600)$ is then regarded as the descendant of the scalar glueball.

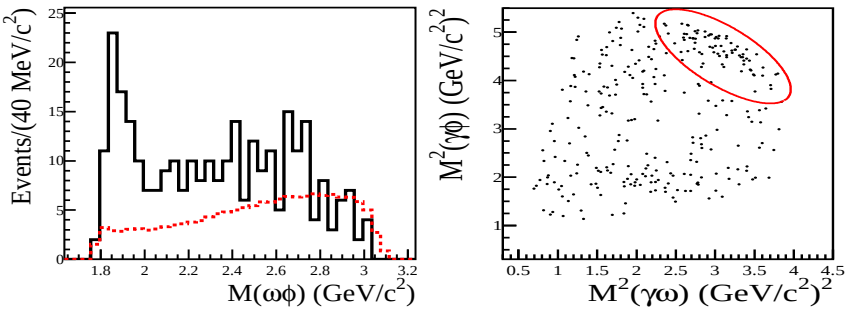

Figure 12.9: (a) The $K^+K^-\pi^+\pi^-\pi^0$ invariant mass distribution for the $J/\psi \to \gamma\omega\phi$ candidate events. The dashed curve indicates the acceptance varying with the $\omega\phi$ invariant mass. (b) Dalitz plot.

The light-meson spectroscopy of scalar states in the mass range of 1-2 GeV/c^2, which has long been a source of controversy, is still very complicated. Overlapping states interfere with each other differently in different production and decay channels. Therefore more experimental data are needed to clarify the properties of these scalar states.

In brief, at the energies of 1$\sim$2 GeV, at least three isoscalar scalars, $f_0(1370)$, $f_0(1500)$ and $f_0(1710)$, are established in experiment. However, there appear quite unexpected behaviors of these states in different processes, which raises a lot of questions about their nature. Those questions include: What are the constituent structures of these scalars? Is any one of these scalars a glueball state? Is the glueball a pure state? What does the present experimental information tell us about the scalar production and decay mechanisms? ...

Pseudoscalar glueball candidates

In PDG [67], five 0^{-+} states above 1 GeV are included in the particle lists: $\eta(1295)$, $\eta(1405)$, $\eta(1475)$, $\eta(1760)$, and $\eta(2225)$. The former three are well established by various experimental observations (see review by Amsler and Masoni [67]), while the latter two states need further confirmation.

Signals for $\eta(1295)$ were observed in $\pi^- p$ [149, 150, 151], $\bar{p}p$ annihilation [152, 153, 154], and J/ψ radiative decays [155] in the $\eta\pi\pi$ spectrum either via $a_0(980)\pi$ or directly coupled to $\eta\pi\pi$. There is no clear signal for $\eta(1295)$ in $K\bar{K}\pi$ which could be a hint for its non-strange $q\bar{q}$ nature.

Historically, there was only one pseudoscalar, the so-called $E/\iota(1440)$, observed in $p\bar{p}$ annihilation [156] and J/ψ radiative decays [157, 158, 159]. After 90's, more and more observations revealed the existence of two resonance structures around 1.45 GeV in $a_0(980)\pi$, $K\bar{K}\pi$ and $K^*\bar{K}$ spectra [160, 149, 161, 155, 162, 163, 164]. It shows that a lower state $\eta(1405)$ has large couplings to $a_0(980)\pi$ and $K\bar{K}\pi$, while a high mass state $\eta(1475)$ favors $K^*\bar{K}$. The $\eta(1405)$ was also confirmed by MARKIII [165], Crystal Barrel [166] and DM2 [159] in its decays into $\eta\pi\pi$ in either J/ψ radiative decays or $\bar{p}p$ annihilations.

In contrast, although $\eta(1475)$ was observed in $K\bar{K}\pi$ ($K^*\bar{K}$) [160, 149, 161, 155, 162, 163, 164], its signals were not seen in $\eta\pi\pi$. Nonetheless, the study of $K\bar{K}\pi$ and $\eta\pi\pi$ channels in $\gamma\gamma$ collisions [167] showed that $\eta(1475)$ appeared in $K\bar{K}\pi$, but not in $\eta\pi\pi$,

while $\eta(1405)$ escaped from both channels.

A reasonable assignment of those three states, $\eta(1295)$, $\eta(1405)$ and $\eta(1475)$, was proposed by Close and Kirk [168], and Barnes *et al.* [169]. It was suggested that $\eta(1295)$ be the radial excitation of η'. Due to its degeneracy with the $\pi(1300)$, $\eta(1295)$ should be dominantly $n\bar{n}$ and hence strongly coupled to $\eta\pi\pi$ (it has not been seen in $K\bar{K}\pi$). As a result, its $I = 0$ partner should be mainly $s\bar{s}$ due to the ideal mixing. Notice that $\eta(1405)$ was not seen in $\gamma\gamma$ while $\eta(1475)$ appears in $K\bar{K}\pi$ but $\eta\pi\pi$. This observation leads to the identification of $\eta(1475)$ being a $s\bar{s}$ state, while $\eta(1405)$ a 0^{-+} glueball candidate [168, 169, 103].

The above classification was questioned by E. Klempt who pointed out that the absence of $\eta(1295)$ in $\gamma\gamma$ collision made it hard to assign it as a $q\bar{q}$ state [170]. Applying the quark model approach by Barnes *et al.* [169], Klempt showed that those three η resonances are presumably due to only one state. The wavefunction overlap in the initial and final state may give rise to different invariant mass distributions in $\eta^* \to a_0(980)\pi$, $\sigma\eta$ and $K^*\bar{K}$, thus, result in different peak positions which may have been interpreted as signals for different states. In this scheme, $\eta(1440)$ exists as the radial excitation of η in the range from 1.3 to 1.5 GeV, while that for η' will be assigned to $\eta(1760)$.

To clarify the nature of those η resonances, higher-statistics search in $\gamma\gamma$ collision and J/ψ radiative decays are strongly urged. In the recent analysis from BES experiment [**?**], $\eta(1295)$ is observed in $J/\psi \to \gamma\eta(1295) \to \gamma\rho$, but absent in $J/\psi \to \gamma(\gamma\phi)$. Meanwhile, another state $\eta(1424)$ is seen in $J/\psi \to \gamma X$ with $X \to \gamma\rho$, and again absent in its decays into $\gamma\phi$. This seems to favor the interpretation by Klempt; but still cannot be concluded.

The $\eta(1760)$ was reported by the MARK III collaboration in J/ψ radiative decays and was found to decay to $\omega\omega$ [172] and $\rho\rho$ [173]. It was also observed by the DM2 collaboration in J/ψ radiative decays in the $\rho\rho$ decay mode with a mass of $M = 1760 \pm 11$ MeV/c^2 and a width of $\Gamma = 60 \pm 16$ MeV/c^2 [174] and in the $\omega\omega$ decay mode [175]. The BESI experiment reported its $\eta\pi^+\pi^-$ decay with a mass of $M = 1760 \pm 35$ MeV/c^2, but without a determination of its width [176]. Also, possible pseudoscalar production at threshold in the $\phi\phi$ mode has been observed in $\pi^- p$ scattering [177]. The $\eta(1760)$ was suggested to be a 3^1S_0 pseudoscalar $q\bar{q}$ meson, but some authors suggest a mixture of glueball and $q\bar{q}$ or a hybrid [178, 179]. Recently, in Ref. [180], it was argued that the pseudoscalar glueball may be in the 1.5 to 1.9 GeV/c^2 mass region, and that it also has Vector Vector decay modes.

The decay channel $J/\psi \to \gamma\omega\omega$, $\omega \to \pi^+\pi^-\pi^0$ is analyzed by BESII, using a sample of 5.8×10^7 J/ψ events [181]. The histogram of Fig. 12.10(a) shows the $2(\pi^+\pi^-\pi^0)$ invariant mass distribution of events with both $\pi^+\pi^-\pi^0$ masses within the ω range ($|m_{\pi^+\pi^-\pi^0} - m_\omega| < 40$ MeV/c^2). The $\omega\omega$ invariant mass distribution peaks at 1.76 GeV/c^2, just above the $\omega\omega$ threshold. The phase space distribution and the acceptance versus $\omega\omega$ invariant mass are also shown in the figure. The corresponding Dalitz plot is shown in Fig. 12.10(b). The shaded histogram in Fig. 12.10(c) is the background.

Analysis of angular correlations indicates that the $\omega\omega$ system below 2 GeV/c^2 is predominantly pseudoscalar. A partial wave analysis confirms the predominant pseudoscalar structure, together with small 0^{++} and 2^{++} contributions, and yields a pseudoscalar mass $M = 1744 \pm 10$ (stat) ± 15 (syst) MeV/c^2, a width $\Gamma = 244^{+24}_{-21}$ (stat) ± 25 (syst) MeV/c^2, and a product branching fraction $\mathrm{Br}(J/\psi \to \gamma\eta(1760)) \cdot \mathrm{Br}(\eta(1760) \to \omega\omega) = (1.98 \pm$

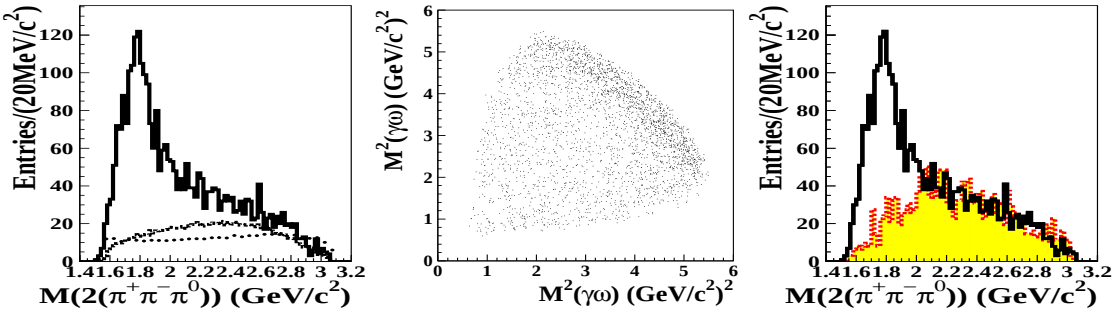

Figure 12.10: (a) The $2(\pi^+\pi^-\pi^0)$ invariant mass distribution for candidate events. The dashed curve is the phase space invariant mass distribution, and the dotted curve shows the acceptance versus the $\omega\omega$ invariant mass. (b) The Dalitz plot. (c) The shaded histogram is the background.

0.08 (stat) $\pm$ 0.32 (syst)) $\times$ 10^{-3}. The $\eta(1760)$ observed here is broader than the one listed in PDG [67].

To identify the pseudoscalar glueball and clarify the pseudoscalar spectrum, the further study of $\eta(1295)$, $\eta(1405)$, $\eta(1475)$, $\eta(1760)$ and high mass 0^{-+} states are urged with large statistics data.

Tensor glueball candidates

Lattice QCD predicted 2^{++} tensor glueball as the second lowest state with a mass around 2.3 GeV, which makes it interesting to search for this state at the mass region of around 2.3 GeV in experiment.

Mark III first presented signals for a narrow state ($\Gamma \sim 20$ MeV), so-called $\xi(2230)$, at 2.2 GeV in $J/\psi \to \gamma K^+K^-$ [182], and later in $\gamma K_s^0 K_s^0$ [183]. However, there was no clear signal seen at DM2 in the same channels [184]. In hadron scattering experiments, GAMS Collaboration found a structure at $m = 2220 \pm 10$ MeV with a width of $\Gamma \sim 80$ MeV in $\pi^- p \to \eta\eta' n$ interactions at 38 GeV and 100 GeV, in the $\eta\eta'$ invariant mass spectrum [185], while the LASS group reported a structure at 2.2 GeV in the invariant mass of $K_s^0 K_s^0$ in $K^- p \to K_s^0 K_s^0 \Lambda$ [186].

Further evidence for this state was from BES-I with $\sim 8 \times 10^6$ J/ψ events. A structure was reported in $\pi^+\pi^-$, K^+K^-, $K_s^0K_s^0$, $p\bar{p}$, and $\pi^0\pi^0$ [187, 188]. In addition, stringent limits have been placed on the two-photon coupling of the $\xi(2230)$ by the CLEO collaboration in the reactions $\gamma\gamma \to K_sK_s$ [189] and $\gamma\gamma \to \pi^+\pi^-$ [190]. The copious production of $\xi(2230)$ in J/ψ radiative decays, the narrow width and a small two-photon width of $\xi(2230)$ suggest it be the lightest tensor glueball candidate. However, $\xi(2230)$ was not seen in the inclusive γ spectrum by Crystal Ball collaboration [191] and $p\bar{p}$ annihilations to $K_s^0K_s^0$ [192], $\eta\eta$ and $\pi^0\pi^0$ [193].

.....

.....

12.4 Hybrid Mesons, multiquarks and molecular states

According to the constituent quark model (CQM), mesons and baryons are composed of $q\bar{q}$ and qqq respectively. CQM provides a convenient framework in the classification of hadrons. Most of experimentally observed hadron states fit into this scheme quite neatly. Any states beyond CQM are labelled as "non-conventional" hadrons.

However, CQM is only a phenomenological model. It's not derived from the underlying theory of the strong interaction—Quantum Chromodynamics (QCD). Hence the CQM spectrum is not necessarily the same as the physical spectrum in QCD, which remains ambiguous and elusive after decades of intensive theoretical and experimental exploration. No one is able to either prove or exclude the existence of these non-conventional states rigorously since nobody can solve the confinement issue in QCD now.

Hadron physicists generally take a modest and practical attitude. If one supposes these non-conventional states exist, then the important issues are: (1) How to determine their characteristic quantum numbers and estimate their masses, production cross-section and decay widths reliably? (2) How and in which channels to dig out the signal from backgrounds and identify them experimentally?

There are three classes of "non-conventional" hadrons. The first class are mesons with "exotic" J^{PC} quantum numbers. The possible angular momentum, parity and charge conjugation parity of a neutral $q\bar{q}$ meson are $J^{PC} = 0^{++}, 0^{-+}, 1^{++}, 1^{--}, 1^{+-}, \cdots$. In other words, a $q\bar{q}$ meson can never have $J^{PC} = 0^{--}, 0^{+-}, 1^{-+}, 2^{+-}, 3^{-+}, \cdots$. Any state with these "exotic" quantum numbers is clearly beyond CQM. We want to emphasize they are "exotic" only in the context of CQM. One can construct color-singlet local operators to verify that these quantum numbers are allowed in QCD. "Exotic" quantum numbers provide a powerful method for the experimental search of these "non-conventional" states. In contrast, a qqq baryon in CQM exhausts all possible J^P, i.e., $J^P = \frac{1}{2}^{\pm}, \frac{3}{2}^{\pm}, \frac{5}{2}^{\pm}, \cdots$.

The second class are hadrons with exotic flavor content. One typical example is the Θ^+ pentaquark. It was discovered in K^+n channel with the quark content $uudd\bar{s}$. Such a state is clearly beyond CQM. Exotic flavor content is also an asset in the experimental search of them.

The third class are hadrons which have ordinary quantum numbers but do not easily fit into CQM. Let's take the $J^{PC} = 0^{++}$ scalar mesons as an example. Below 2 GeV, we have $\sigma, f_0(980), f_0(1370), f_0(1500), f_0(1710), f_0(1790), f_0(1810)$. Within CQM there are only two scalars within this mass range if we ignore the radial excitations. With radial excitations, CQM could accommodate four scalars at most. Clearly there is serious overpopulation of the scalar spectrum. If all the above states are genuine, the quark content of some of them is not $q\bar{q}$. Overpopulation of the spectrum provides another useful window in the experimental search of non-conventional states.

Glueballs are hadrons composed of gluons. Quenched lattice QCD simulation suggests the scalar glueball is the lightest. Its mass is around $(1.5 \sim 1.7)$ GeV. Glueballs with the other quantum numbers are high-lying. In the large N_c limit, glueballs decouple from the conventional $q\bar{q}$ mesons [194]. Moreover, one gluon splits into two gluons freely in this limit. Hence the number of the gluon field inside glueballs is indefinite when $N_c \to \infty$. In the real world with $N_c = 3$, glueballs mix with nearby $q\bar{q}$ mesons with the same quantum numbers, which renders the experimental identification of scalar glueballs very difficult.

Reviews of glueballs can be found in the previous chapters. In the following we discuss the other non-conventional hadrons according to their underlying quark gluon structure.

12.4.1 Hybrid Mesons

Theoretical models for hybrid mesons

a). Large N_C expansion

Hybrid mesons are composed of a pair of $q\bar{q}$ and one explicit gluon field G. In the large N_c limit, the amplitude of creating a hybrid meson from the vacuum has the same N_c order as that of creating a $q\bar{q}$ meson [195]. If kinematics and other conservation laws allow, the production cross section of hybrid mesons is expected to be roughly the same as that of ordinary mesons. At least it's not suppressed in the large N_c limit. In the same limit, hybrid mesons and ordinary mesons mix freely if they carry the same quantum numbers. Hence, the identification of hybrid mesons is very difficult unless they have exotic quantum numbers. That's why so many efforts have been devoted to the search of the 1^{-+} hybrid meson.

b). Flux tube model

The flux model is obtained intuitively in the strong coupling limit of lattice QCD [196, 197]. In this picture a meson is described as a pair of quark-antiquark linked by a color flux tube. The quarks move adiabatically in an effective potential generated by the flux tube dynamics. The orbital angular momentum along the flux tube is zero. The flux tube can also rotate along its axis. When the flux tube is in its ground state, the excitation of the quark-antiquark degree of freedom yields the conventional meson spectrum.

The hybrid mesons are defined as excitations of the color flux tube. The lowest-lying exotic hybrid meson is predicted to be with the quantum number $j^{PC} = 1^{-+}$ and a mass around 1.9 GeV [197], which is quite consistent with the prediction of the lattice QCD. The decay of a meson is triggered by breaking the flux tube in the flux tube model [196]. A quark-antiquark pair is assumed to be created with spin $S_{q\bar{q}} = 1$ and, orbital angular momentum $L_{q\bar{q}} = 1$ and total angular momentum $J_{q\bar{q}} = 0$. This process is called " $^3P_0$ pair creation". By the conservation of spin, a state with spin $S = 0$ can not decay into two $S = 0$ states [198]. The quark aniti-quark pair inside the lowest-lying 1^{-+} hybrid are the spin singlet in the flux tube model. Therefore it can not decay into a pair of spin zero mesons, such as $\pi\pi$,$\pi\eta$. Besides, when a flux tube is broken into two flux tubes (two mesons), since the relative coordinate of the two final flux tubes (the line connects the centers of the two flux tubes) is parallel to the original one (denoted as $\mathbf{r}$), the two final mesons cannot absorb the unit of string angular momentum about the $\mathbf{r}$ axis [196, 198] via their relative orbital angular momentum. Therefore the 1^{-+} hybrid (with one excited phonon polarized along the flux tube) cannot decay into two ground states, such as $\pi\pi$,$\pi\eta$ and $\pi\rho\cdots$. The preferential decay modes are those with one excited meson, such as $b_1\pi$, $f_1\pi\cdots$. This selection rule can be violated when the two final ground states have different spatial wave functions (i.e. they have different spatial size). One calculation shows that

	$b_1\pi$	$\rho\pi$	$f_1\pi$	$\eta(1295)\pi$	K^*K
PSS(MeV)	24	9	5	2	0.8
IKP(MeV)	59	8	14	1	0.4

Table 12.4: Decay widths of the 1^{-+} hybrid meson from the two flux tube model.

the partial width of $1^{-+} \to \rho\pi$ can be large and compatible with $\pi_1(1600)$ being a hybrid if the π shrinks to a point [199].

The original flux tube model (IKP model) was modified by introducing a new decay vertex. The vertex is constructed by using the heavy quark expansion of the Coulomb gauge QCD Hamiltonian to identify relevant operator [200, 201]. This new model (PSS model) extends the selection rule of IKP. PSS states that the decay amplitude of a hybrid meson vanishes when the daughter mesons are identical. This means that not only are the S+S-wave final states forbidden but also are the P+P-wave final states. The preferred channels are S+P-wave pairs. The prediction of the partial width of the 1^{-+} hybrid meson for each channel is also different as shown in Table 12.4 [201].

where the mass of the 1^{-+} hybrid is set to be 1.6 GeV. It should be noticed that the width of $\rho\pi$ is bigger than that of $f_1\pi$ in PSS. An extensive study of the decay patterns of the hybrid mesons with other quantum numbers in the flux tube model are collected in table 24.5 - table 12.15 , which are taken from Ref. [201].

c). QCD sum rules

The mass and decay width of the 1^{-+} hybrid meson has been studied using QCD sum rules. Within this framework, one considers a two-point correlator

$$\Pi_{\mu\nu}(q^2) = i \int \mathrm{d}^4x\, \mathrm{e}^{iqx} \langle 0|T\{j_\mu(x), j_\nu^+(0)\}|0\rangle \tag{12.11}$$

where $j_\mu(x) = \bar{q}(x)T^a\gamma_\nu igG^a_{\mu\nu}q(x)$ is the interpolating current for the 1^{-+} isospin vector hybrid meson.

The spectral density $\rho_v(s) = \frac{1}{\pi}\mathbf{Im}\Pi_v(s)$ can be expressed in terms of the hybrid meson observables like its mass etc:

$$\frac{1}{\pi}\mathbf{Im}\Pi_v(s) = \sum_R M_R^6 f_R^2 \delta\left(s - M_R^2\right) + \text{QCD continuum}, \tag{12.12}$$

It can also be related to the correlator $\Pi_v(q^2)$ at the scale $-q^2$ via the dispersion relation

$$\Pi_{v,s}(q^2) = (q^2)^n \int_0^\infty ds \frac{\rho_v(s)}{s^n(s-q^2)} + \sum_{k=0}^{n-1} a_k (q^2)^k, \tag{12.13}$$

where the a_k are appropriate subtraction constants.

After invoking the Borel transformation to enhance the lowest-lying resonance in the spectral density, we have the QCD sum rules

$$R_k(\tau, s_0) = \int^{s_0} s^k \mathrm{e}^{-s\tau} \rho_v(s) \mathrm{d}s \;;\; k = 0, 1, 2, \ldots \tag{12.14}$$

Table 12.5: 2^{-+} Isovector Hybrid Decay Modes from Ref. [201].

			alt	high mass	standard	IKP	reduced
2^{-+}	$\rho\pi$	P	9	16	13	12	57
	K^*K	P	1	5	2	1	17
	$\rho\omega$	P	0	0	0	0	20
	$f_2(1270)\pi$	S	19	10	9	14	
		D	.1	.2	.05	11	
	$f_1(1285)\pi$	D	.1	.3	.06	Ø	
	$f_0(1370)\pi$	D	.02	.08	.01	.6	
	$b_1(1235)\pi$	D	Ø	Ø	Ø	20	
	$a_2(1320)\eta$	S	–	7	–	–	
		D	–	.01	–	–	
	$a_1(1260)\eta$	D	0	.05	0	0	
	$a_0(1450)\eta$	D	–	0	–	–	
	$K_2^*(1430)K$	S	–	11	–	–	
		D	–	0	–	–	
	$K_1(1270)K$	D	0	.01	0	.02	
	$K_0^*(1430)K$	D	–	0	–	–	
	$K_1(1410)K$	D	–	0	–	–	
	$\rho_1 450)\pi$	P	.8	12	3	2	
	$K^*(1410)K$	P	–	1	–	–	
	Γ		30	63	27	59	

Table 12.6: 1^{-+} Isovector Hybrid Decay Modes from Ref. [201].

			alt	high mass	standard	IKP	reduced
1^{-+}	$\eta\pi$	P	0	.02	.02	.02	99
	$\eta'\pi$	P	0	.01	.01	0	30
	$\rho\pi$	P	9	16	13	12	57
	K^*K	P	1	5	2	1	17
	$\rho\omega$	P	0	0	0	0	13
	$f_2(1270)\pi$	D	.2	.5	.1	Ø	
	$f_1(1285)\pi$	S	18	10	9	14	
		D	.06	.2	.04	7	
	$b_1(1235)\pi$	S	78	40	37	51	
		D	2	3	1	11	
	$a_2(1320)\eta$	D	–	.02	–	–	
	$a_1(1260)\eta$	S	5	7	3	8	
		D	0	.01	0	.01	
	$K_2^*(1430)K$	D	–	0	–	–	
	$K_1(1270)K$	S	4	7	2	6	
		D	0	.2	0	.04	
	$K_1(1410)K$	S	–	33	–	–	
		D	–	0	–	–	
	$\pi(1300)\eta$	P	–	5	–	–	
	$\eta_u(1295)\pi$	P	3	27	11	8	
	$K(1460)K$	P	–	.8	–	–	
	$\rho(1450)\pi$	P	.8	12	3	2	
	$K^*(1410)K$	P	–	1	–	–	
	Γ		121	168	81	117	

Table 12.7: 1^{--} Isovector Hybrid Decay Modes from Ref. [201].

			alt	high mass	standard	IKP	reduced
1^{--}	$\omega\pi$	P	9	16	13	12	57
	$\rho\eta$	P	4	9	6	4	30
	$\rho\eta^{'}$	P	.1	1	.2	.1	1
	K^*K	P	3	9	5	3	34
	$a_2(1320)\pi$	D	.5	2	.3	16	
	$a_1(1260)\pi$	S	78	41	37	51	
		D	.4	.8	.2	11	
	$h_1(1170)\pi$	S			Ø		
		D			Ø		
	$b_1(1235)\eta$	S			Ø		
		D			Ø		
	$K_2^*(1430)K$	D	–	0	–	–	
	$K_1(1270)K$	S	6	12	4	11	
		D	0	.01	0	0	
	$K_1(1400)K$	S	–	17	–	–	
		D	–	0	–	–	
	$\omega(1420)\pi$	P	1	14	4	4	
	$K^*(1410)K$	P	–	3	–	–	
	Γ		103	121	70	112	

where the quantity R_k represents the QCD prediction, and s_0 is the threshold parameter.

The sum rules for 1^{-+} hybrid meson were obtained by various authors. The prediction for the hybrid mass is sensitive to the threshold s_0. The sum rule in the leading order of α_s expansion is unstable. When the next to leading order correction is included, the sum rule becomes more stable. It predicts the upper bound of 1^{-+} hybrid mass is 2.0 GeV [202].

The decay widths of the 1^{-+} hybrid can be obtained by considering the three-point correlator

$$\Pi(p,q) = i\int \mathrm{d}^4x\mathrm{d}^4y\,\mathrm{e}^{ipx+iqy}\langle 0|T\{j_A(x)j_B(y)j_\mu(0)\}|0\rangle, \tag{12.15}$$

where $j_A(x)$ and $j_B(y)$ are operators which annihilate the final states A and B respectively.

When A and B are two pseudoscalars, $\Pi(p,q) = F_1(p+q)_\mu + F_2(p-q)_\mu$. Only F_2 is relevant to the process $1^{-+} \to AB$ and vanishes at the leading order [203]. At the next leading order, it was estimated [204]: $\Gamma(1^{-+} \to \pi\eta') \sim 3$MeV, $\Gamma(1^{-+} \to \pi\eta) \sim 0.3$MeV, which was quite consistent with the prediction from the flux tube model.

However, the channel $\pi\rho$ is not narrow from QCD sum rules approach. By using the three-point function at the symmetric point, the width of $1^{-+} \to \pi\rho$ was predicted in the region 250-600 MeV [204, 205]. Later, it was pointed out that the calculation at the symmetric point receives large contamination from the high resonances and continnuum contribution [206]. By using the light-cone QCD sum rules and the double Borel transformation, the width is reduced to be 40 ± 20 MeV [206]. The similar channel K^*K is suppressed by the kinematic space. The channel $f_1\pi$ is very broad (~ 100 MeV) in QCD

Table 12.8: 2^{+-} Isovector Hybrid Decay Modes from Ref. [201].

			alt	high mass	standard	IKP	reduced
2^{+-}	$\omega\pi$	D	.5	1	1	1	4
	$\rho\eta$	D	.1	.6	.2	.1	1
	$\rho\eta'$	D	0	.02	0	0	0
	K^*K	D	.04	.2	.08	.04	.6
	$a_2(1320)\pi$	P	.7	.9	.4	130	
		F	0	.02	0	.2	
	$a_1(1260)\pi$	P	3	4	2	45	
		F	.01	.02	0	.3	
	$h_1(1170)\pi$	P	2	2	1	69	
		F	.01	.03	.01	.5	
	$b_1(1235)\eta$	P	.02	.5	.01	.8	
		F	0	0	0	0	
	$K_2^*(1430)K$	P	–	.04	–	–	
		F	–	0	–	–	
	$K_1(1270)K$	P	0	.03	0	.6	
		F	0	0	0	0	
	$K_1(1400)K$	P	–	.3	–	–	
		F	–	0	–	–	
	$\pi(1300)\pi$	D	.08	1	.2	.2	
	$\omega(1420)\pi$	D	.02	.4	.04	.04	
	$K^*(1410)K$	D	–	.01	–	–	
	Γ		7	11	5	248	

Table 12.9: 0^{-+} Isovector Hybrid Decay Modes from Ref. [201].

			alt	high mass	standard	IKP	reduced
0^{-+}	$\rho\pi$	P	37	63	51	47	230
	K^*K	P	5	18	10	5	69
	$\rho\omega$	P			Ø		
	$f_2(1270)\pi$	D	1	3	.6	8	
	$f_0(1370)\pi$	S	62	40	30	62	
	$a_2(1320)\eta$	D	–	.1	–	–	
	$a_0(1450)\eta$	S	–	4	–	–	
	$K_2^*(1430)K$	D	–	.02	–	–	
	$K_0^*(1430)K$	S	–	44	–	–	
	$\rho(1450)\pi$	P	3	47	10	10	
	$K^*(1410)K$	P	–	5	–	–	
	Γ		108	224	102	132	

Table 12.10: 1^{+-} Isovector Hybrid Decay Modes from Ref. [201].

			alt	high mass	standard	IKP	reduced
1^{+-}	$\omega\pi$	S	23	19	26	38	118
		D	.3	.8	.4	.3	2
	$\rho\eta$	S	15	21	25	22	118
		D	.07	.3	.1	.06	.6
	$\rho\eta^{'}$	S	3	8	5	4	25
		D	0	.01	0	0	0
	K^*K	S	27	52	47	36	339
		D	.02	.1	.04	.02	.3
	$a_2(1320)\pi$	P	19	26	10	49	
		F	0	.02	0	.1	
	$a_1(1260)\pi$	P	9	10	5	29	
	$a_0(1450)\pi$	P	3	6	1	26	
	$h_1(1170)\pi$	P	Ø	Ø	Ø	95	
	$b_1(1235)\eta$	P	Ø	Ø	Ø	1	
	$K_2^*(1430)K$	P	–	1	–	–	
		F	–	0	–	–	
	$K_1(1270)K$	P	.04	.6	.02	5	
	$K_0^*(1430)K$	P	–	.4	–	–	
	$K_1(1400)K$	P	–	.4	–	–	
	$\omega(1420)\pi$	S	16	82	58	79	
		D	.01	.2	.02	.02	
	$K^*(1410)K$	S	–	110	–	–	
		D	–	.01	–	–	
	Γ		115	338	177	384	

Table 12.11: 0^{+-} Isovector Hybrid Decay Modes from Ref. [201].

			alt	high mass	standard	IKP	reduced
0^{+-}	$a_1(1260)\pi$	P	Ø	Ø	Ø	309	
	$h_1(1170)\pi$	P	47	45	24	37	
	$b_1(1235)\eta$	P	.6	12	.4	.3	
	$K_1(1270)K$	P	.7	10	.4	7	
	$K_1(1400)K$	P	–	1	–	–	
	$\pi(1300)\pi$	S	60	246	222	312	
	$K(1460)K$	S	–	115	–	–	
	Γ		108	429	247	665	

Table 12.12: 1^{++} Isovector Hybrid Decay Modes from Ref. [201].

			alt	high mass	standard	IKP	reduced
1^{++}	$\rho\pi$	S	23	19	26	38	116
		D	1	3	2	1	8
	K^*K	S	14	26	24	18	170
		D	.04	.3	.09	.04	.6
	$\rho\omega$	S	0	0	0	0	47
		D	0	0	0	0	.03
	$f_2(1270)\pi$	P	4	5	2	75	
		F	.01	.03	0	.3	
	$f_1(1285)\pi$	P	7	9	4	62	
	$f_0(1370)\pi$	P	Ø	Ø	Ø	4	
	$b_1(1235)\pi$	P	Ø	Ø	Ø		
	$a_2(1320)\eta$	P	–	.9	–	–	
		F	–	0	–	–	
	$a_1(1260)\eta$	P	.2	3	.09	1	
	$a_0(1450)\eta$	P	–	Ø	–	–	
	$K_2^*(1430)K$	P	–	.4	–	–	
		F	–	0	–	–	
	$K_1(1270)K$	P	.07	1	.05	1	
	$K_0^*(1430)K$	P	–	0	–	–	
	$K_1(1400)K$	P	–	.7	–	–	
	$\rho(1450)\pi$	S	14	80	50	66	
		D	.02	.6	.05	.04	
	$K^*(1410)K$	S	–	55	–	–	
		D	–	.01	–	–	
	Γ		63	204	108	269	

Table 12.13: Isoscalar Hybrid Decay Modes from Ref. [201].

			alt	high mass	standard	IKP	reduced
2^{-+}	K^*K	P	1	5	2	1	17
	$a_2(1320)\pi$	S	52	31	25	45	
		D	.2	.6	.1	22	
	$a_1(1260)\pi$	D	.5	1	.3	Ø	
	$a_0(1450)\pi$	D	.02	.1	.01	.6	
	$f_2(1270)\eta$	S	–	8	–	–	
		D	–	.02	–	–	
	$f_1(1285)\eta$	D	–	.02	–	–	
	$f_0(1370)\eta$	D	–	0	–	–	
	$K_2^*(1430)K$	S	–	11	–	–	
		D	–	0	–	–	
		G	–	0	–	–	
	$K_1(1270)K$	D	0	.01	0	0	
	$K_0^*(1430)K$	D	–	0	–	–	
	$K_1(1400)K$	D	–	0	–	–	
	$K^*(1410)K$	P	–	1	–	–	
	Γ		54	58	27	69	
1^{-+}	$\eta^{'}\eta$	P	0	0	0	0	10
	K^*K	P	1	5	2	1	17
	$a_2(1320)\pi$	D	.4	1	.2	Ø	
	$a_1(1260)\pi$	S	59	30	28	38	
		D	.3	.6	.2	34	
	$f_2(1270)\eta$	D	–	.05	–	–	
	$f_1(1285)\eta$	S	–	8	–	–	
		D	–	.01	–	–	
	$K_2^*(1430)K$	D	–	0	–	–	
	$K_1(1270)K$	S	4	7	2	7	
		D	0	.2	0	0	
	$K_1(1400)K$	S	–	33	–	–	
		D	–	0	–	–	
	$\pi(1300)\pi$	P	8	65	27	27	
	$\eta_u(1295)\eta$	P	–	6	–	–	
	$K(1460)K$	P	–	.8	–	–	
	$K^*(1410)K$	P	–	1	–	–	
	Γ		73	158	59	107	
0^{-+}	K^*K	P	5	18	10	5	69
	$a_2(1320)\pi$	D	2	6	1	16	
	$a_0(1450)\pi$	S	145	114	70	175	
	$f_2(1270)\eta$	D	–	.2	–	–	
	$f_0(1370)\eta$	S	–	23	–	–	
	$K_2^*(1430)K$	D	–	.02	–	–	
	$K_0^*(1430)K$	S	–	44	–	–	
	$K^*(1410)K$	P		5			
	Γ		152	210	81	196	
1^{--}	$\rho\pi$	P	28	47	38	35	172
	$\omega\eta$	P	3	9	6	4	29
	$\omega\eta^{'}$	P	.1	1	.2	.3	.8
	K^*K	P	3	9	5	3	35
	$b_1(1235)\pi$	S	Ø	Ø	Ø		

Table 12.14: $s\bar{s}$ Hybrid Decay Modes from Ref. [201].

			alt	high mass	standard	IKP	reduced
2^{-+}	K^*K	P	6	13	11	8	82
	$K_2^*(1430)K$	S	28	29	21	44	
		D	.03	.5	.02	1	
	$K_1(1270)K$	D	.2	.5	.1	10	
	$K_0^*(1430)K$	D	.02	.3	.01	.2	
	$K_1(1400)K$	D	.06	.5	.03	.6	
	$f_2^{'}(1525)\eta$	S	–	20	–	–	
		D	–	.2	–	–	
	$f_1(1510)\eta$	D	–	.03	–	–	
	$f_0(1370)\eta$	D	.01	.08	0	.1	
	$K^*(1410)K$	P	2	27	6	5	
	Γ		36	91	38	69	
1^{-+}	$\eta^{'}\eta$	P	0	0	0	0	44
	K^*K	P	6	13	11	8	82
	$K_2^*(1430)K$	D	.07	1	.04	Ø	
	$K_1(1270)K$	S	14	10	11	14	
		D	3	8	2	21	
	$K_1(1400)K$	D	83	76	61	121	
		D	.03	.2	.02	.4	
	$f_2^{'}(1525)\eta$	D	–	.04	–	–	
	$f_1(1510)\eta$	S	–	21	–	–	
		D	–	.02	–	–	
	$K(1460)K$	P	1	45	4	3	
	$\eta_s(1490)\eta$	P	–	15	–	–	
	$K^*(1410)K$	P	2	27	6	5	
	Γ		109	216	95	172	
0^{-+}	K^*K	P	26	52	46	33	330
	$K_2^*(1430)K$	D	.4	6	.2	1	
	$K_0^*(1430)K$	S	113	117	83	174	
	$f_2^{'}(1525)\eta$	D	–	.2	–	–	
	$f_0(1370)\eta$	S	72	105	64	109	
	$K^*(1410)K$	P	7	110	22	18	
	Γ		218	390	215	335	
1^{--}	K^*K	P	13	26	23	16	165
	$\phi\eta$	P	2	19	11	3	89
	$\phi\eta^{'}$	P	.01	2	.1	.02	.5
	$K_2^*(1430)K$	D	.1	2	.07	2	
	$K_1(1270)K$	S	23	16	18	24	
		D	.2	.6	.1	2	
	$K_1(1400)K$	S	43	40	32	63	
		D	.1	.6	.04	.7	
	$h_1(1380)\eta$	S			Ø		
		D			Ø		
		D	.07	.6	.04	.3	
	$K^*(1410)K$	P	3	55	11	9	
	Γ		84	155	95	120	
2^{+-}	K^*K	D	1	3	2	1	13
	$\phi\eta$	D	.06	.8	.3	.08	2
	$\phi\eta^{'}$	D	.0	.0	.0	.0	.0

Table 12.15: $c\bar{c}$ Hybrid Decay Modes from Ref. [201].

			alt	high mass	standard	IKP	reduced
2^{-+}	D^*D	P	.5	.1	.8	4	19
	$D^{**}(2^+)D$	S	–	9	–	–	
		D	–	.2	–	–	
	$D^{**}(1^+_L)D$	D	–	.2	–	–	
	$D^{**}(0^+)D$	D	–	.2	–	–	
	$D^{**}(1^+_H)D$	D	–	.2	–	–	
	Γ		.5	10	.8	4	
1^{-+}	D^*D	P	.5	.1	.8	4	19
	$D^{**}(2^+)D$	D	–	.5	–	–	
	$D^{**}(1^+_L)D$	S	–	1.2	–	–	
		D	–	2.5	–	–	
	$D^{**}(1^+_H)D$	S	–	25	–	–	
		D	–	0	–	–	
	Γ		.5	29	.8	4	
0^{-+}	D^*D	P	2	.3	3	16	76
	$D^{**}(2^+)D$	D	–	2.5	–	–	
	$D^{**}(0^+)D$	S	–	25	–	–	
	Γ		2	28	3	16	
1^{--}	D^*D	P	1	.2	1.5	8	38
	$D^{**}(2^+)D$	D	–	1	–	–	
	$D^{**}(1^+_L)D$	S	–	7	–	–	
		D	–	.3	–	–	
	$D^{**}(1^+_H)D$	S	–	10	–	–	
		D	–	.2	–	–	
	Γ		1	19	1.5	8	
2^{+-}	D^*D	D	.2	.2	.3	1	7
	$D^{**}(2^+)D$	P	–	.5	–	–	
		F	–	.02	–	–	
	$D^{**}(1^+_L)D$	P	–	0	–	–	
		F	–	0	–	–	
	$D^{**}(1^+_H)$D	P	–	3	–	–	
		F	–	0	–	–	
	Γ		.2	4	.3	1	
1^{+-}	D^*D	S	.3	.1	.5	8	12
		D	.1	.1	.1	.5	4
	$D^{**}(2^+)D$	P	–	13	–	–	
		F	–	.01	–	–	
	$D^{**}(1^+_L)D$	P	–	2	–	–	
	$D^{**}(0^+)D$	P	–	8	–	–	
	$D^{**}(1^+_H)D$	P	–	2.5	–	–	
	Γ		.4	26	.6	8.5	
0^{+-}	$D^{**}(1^+_L)D$	P	–	25	–	–	
	$D^{**}(1^+_H)D$	P	–	15	–	–	
	Γ		–	40	–	–	
1^{++}	D^*D	S	.2	.1	.3	1	6
		D	.2	.2	.3	.3	8
	$D^{**}(2^+)D$	P	–	5	–	–	
		F	–	.03	–	–	

	QCDSR	Flux Tube Model	PDG ($\pi_1(1600)$)
$b_1\pi$(MeV)	unstable	40 ± 20	seen
$f_1\pi$ (MeV)	100	10 ± 5	seen
$\rho\pi$(MeV)	40 ± 20	9	seen
K^*K (MeV)	8	0.6	no
$\eta'\pi$ (MeV)	3	small	seen
$\eta\pi$ (MeV)	0.3	small	no

Table 12.16: Comparison of the decay widths of the 1^{-+} hybrid meson from the flux tube model and QCD sum rule approach.

sum rules.

It is interesting to compare the prediction of the QCD sum rules with that of the flux tube model, although the bases of these two approaches are contradictory. The first one is based on the α_s expansion while the second one is based on the strong coupling expansion.

From Table 12.16, the decay patterns from these two approaches are very similar although the partial decay width for each channel is quite different:

$$\Gamma(f_1\pi) > \Gamma(\rho\pi) > \Gamma(K^*K) > \Gamma(\eta'\pi) > \Gamma(\eta\pi). \tag{12.16}$$

d). Comments

It's important to note that the gluon inside the hybrid meson can easily split into a pair of $q\bar{q}$. Therefore tetraquarks can always have the same quantum numbers as the hybrid mesons, including the exotic ones. Discovery of hadron candidates with $J^{PC} = 1^{-+}$ does not ensure it's an exotic hybrid meson. One has to exclude the tetraquark possibility based on its mass, decay width and decay pattern *etc.* This argument holds for $\pi_1(1400)$ and $\pi_1(1600)$.

The flux tube model predicts hybrid mesons prefer decaying into a pair of mesons with L=1 and L=0. Heavy hybrid mesons tend to decay into one P-wave heavy meson and one pseudoscalar meson according to a light-cone QCD sum rule calculation [207]. A lattice QCD simulation suggests the string breaking mechanism may play an important role for the decays of the hybrid heavy quarkonium [208]. When the string between the heavy quark and anti-quark breaks, new light mesons are created. In other words, the preferred final states are one heavy quarkonium plus light mesons. However, readers should be very cautious of these so-called "selection rules". None of them has been tested by experiments because none of the 1^{-+} hybrid candidates has been established unambiguously.

Signatures of the hybrid mesons

Hybrid mesons are color-singlet mixture of constituent quarks and gluons, such as $q\bar{q}g$ bound states. The evidence of the existence of the hybrid mesons is also a direct proof of the existence of the gluonic degree of freedom and the validity of QCD. The conventional wisdom is that it would be more fruitful to search for the low lying hybrid mesons

with exotic quantum numbers than to search for glueballs. Hybrids have the additional attraction that, unlike glueballs, they span complete flavour nonets and hence provide many possibilities for experimental detection. In addition, the lightest hybrid multiplet includes at least one J^{PC} exotics.

In searching for hybrids, there are two ways to distinguish them from conventional states. One approach is to look for an access of observed states over the number predicted by the quark model. The drawback to this method is that it depends on a good understanding of hadron spectroscopy in a mass region that is still rather murky. At present, the phenomenological models have not been tested to the extent experimentally so that a given state can be reliably ruled out as a conventional meson. The situation is further muddied by expected mixing between conventional $q\bar{q}$ states and hybrids with the same J^{PC} quantum numbers. The other approach is to search for the states with quantum numbers that cannot be accommodated in the quark model. The discovery of exotic quantum numbers would be definite evidence of something new.

From the theoretical estimation, we know that $\Gamma(J/\psi \to MH) > \Gamma(J/\psi \to MM') > \Gamma(J/\psi \to MG)$, where M stands for ordinary $q\bar{q}$ meson, G stands for a glueball and H stands for a hybrid. Therefore, the J/ψ hadronic decay to hybrid states will have relatively large branching ratios and is an ideal place to study hybrid states and to search for exotic states.

Some previous experiments have searched for the 1^{-+} hybrid state $\pi_1(1400)$. Table 12.4.1 shows the list of the experiments searching for 1^{-+} resonances in $\eta\pi$ final states. All the experiments listed in Table 12.4.1 observed a clear forward-backward asymmetry and all of them except NICE suggested or claimed the evidence of an exotic $J^{PC} = 1^{-+}$ resonance. Of them, VES and E852 gave consistent results. From Crystal Barrels results on $\bar{p}d \to \eta\pi^-\pi^0 p$, the Dalitz plot is dominated by $\rho^- \to \pi^-\pi^0$ and there is a clear $\eta\pi$ P-wave which interferes with it. The fit to the Dalitz plot is improved when $\pi_1(1400)$ is included and the mass and width of $\pi_1(1400)$ are quite consistent with those from E852 experiment. E852 also found the evidence of another 1^{-+} exotic $\pi_1(1600)$, decaying to $\rho\pi$ in $\pi^- p \to \pi^-\pi^+\pi^- p$ reaction, with the mass and width being 1593 ± 8 MeV/c^2 and 168 ± 20 MeV/c^2. Tentative evidence was put forward by the VES collaboration in $\eta'\pi$ from $\pi^- N \to \pi^-\eta' N$ process. VES saw a broad but resonant P_+ wave near this mass. However the phase motion is not distinctive.

Exps.	Lab.	Reaction	p_{beam} (GeV/c)	Year
NICE	IHEP	$\pi^- p \to \eta\pi^0 n$	40	1981
GAMS	CERN	$\pi^- p \to \eta\pi^0 n$	100	1988
BENKEI	KEK	$\pi^- p \to \eta\pi^- p$	6.3	1993
VES	IHEP	$\pi^- N \to \eta\pi^- X$	37	1993
E852	BNL	$\pi^- p \to \eta\pi^- p$	18	1997

Table 12.17: Previous experiments searching for the 1^{-+} hybrid meson.

12.4.2 Multiquarks

When N ($N \geq 4$) quarks/antiquarks are confined within a single MIT bag, a multiquark state is formed. The color structure within a multiquark state is complicated and not unique. It always has a component which is the product of two (or more) color-singlet hadrons. Special mechanism is needed to prevent the multiquark to fall apart easily and become extremely broad when it lies above threshold.

There are several well-known multiquark candidates. The first one is the H dibaryons suggested by Jaffe decades ago [209]. The on-going doubly-strange hypernuclei experiments have pushed its binding energy to be less than several MeV. Its existence is very dubious now. Jaffe also suggested that the low-lying scalar nonet are also tetraquarks because of their low mass and special mass pattern [303]. The third one is the fading Θ^+ pentaquark. Interested readers may consult the review paper [211].

The multiquark states are expected to have very broad width since they can easily fall apart into mesons and/or baryons if their masses are above the sum of the masses of the hadrons in the final states. Here the sum of the masses of the hadrons are called as the mass threshold of the hadrons. The multiquark states may be only experimentally observable near the mass thresholds - either below or just above the mass thresholds, otherwise, the widths of multiquark states might be too wide to be observed experimentally. The J/ψ meson has been playing a unique role for searches for new hadrons and studies of light hadron spectroscopy. Recently, a number of new structures have been observed in J/ψ decays. These include strong near-threshold mass enhancements in the $p\bar{p}$ invariant mass spectrum from $J/\psi \to \gamma p\bar{p}$ decays [312], the $p\bar{\Lambda}$ and the $K^-\bar{\Lambda}$ mass spectra in $J/\psi \to pK^-\bar{\Lambda}$ decays [213], the $\omega\phi$ mass spectrum in the double-OZI suppressed decay $J/\psi \to \gamma\omega\phi$ [140], and two new resonances, the $X(1835)$, in $J/\psi \to \gamma\pi^+\pi^-\eta'$ decays [214] as well as a very broad 1^{--} resonant structure in the invariant mass spectrum of K^+K^- in the channel $J/\psi \to K^+K^-\pi^0$. All these new structures have the possibility coming from multiquark states.

1. Observation of a strong near-threshold mass enhancement in the $p\bar{p}$ invariant mass spectrum

The BES Collaboration observed an anomalous strong enhancement near the $p\bar{p}$ mass threshold in $J/\psi \to \gamma p\bar{p}$ decays [312]. It can be fit with an S- or P- wave Breit-Winger resonance function. In the case of S-wave fit, the mass is $1859^{+3}_{-10}{}^{+5}_{-0.5}\mathrm{MeV}/c^2$ and the width is smaller than 30 MeV/c^2 at 90% C.L.(Fig. 12.11).

It is interesting to notice that such a strong mass threshold enhancement is neither observed in $p\bar{p}$ cross section measurements, nor in B decays [215] or in $\Upsilon \to \gamma p\bar{p}$ decays [216], i.e., so far it is uniquely observed in $J/\psi \to \gamma p\bar{p}$ decays.

This surprising experimental observation has stimulated a number of theoretical speculations [217, 218, 219, 220, 221, 222], and among the various theoretical interpretations of the $p\bar{p}$ mass threshold enhancement, the most intriguing is that of a $p\bar{p}$ bound state, sometimes called *baryonium* [217, 223, 220], which has been the subject of many experimental searches [224].

It is worth noting that if the observed $p\bar{p}$ mass enhancement is due to a resonance,

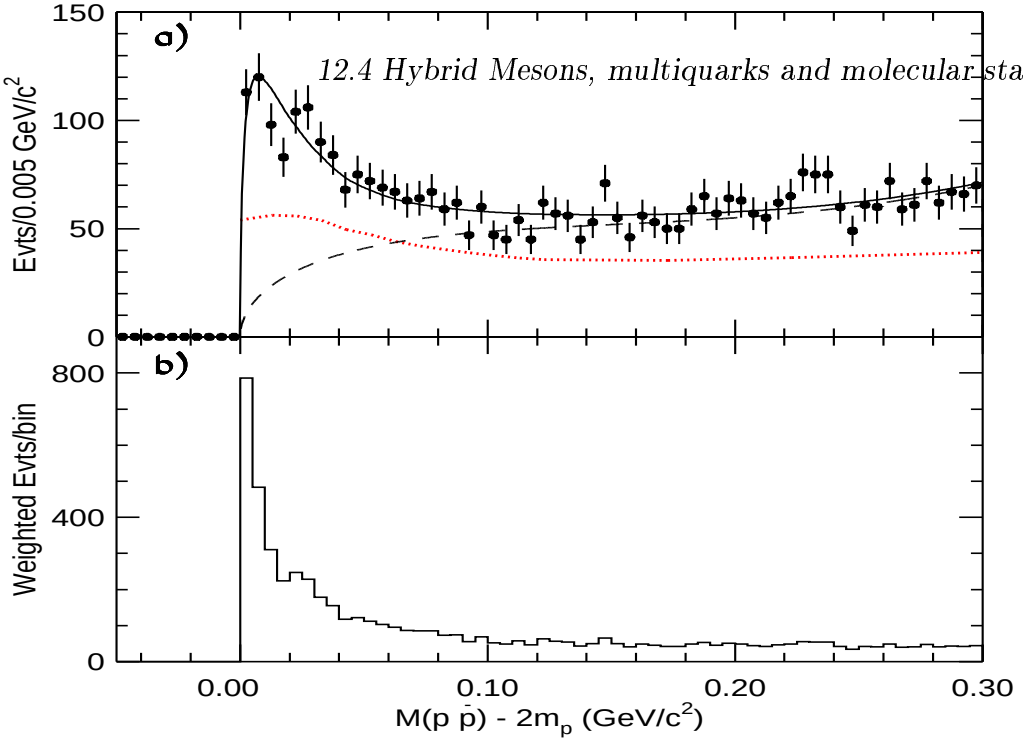

Figure 12.11: (a) The near threshold $M_{p\bar{p}} - 2m_p$ distribution for the $\gamma p\bar{p}$ event sample. The dashed curve is the background function described in the text. The dotted curve indicates how the acceptance varies with $p\bar{p}$ invariant mass; the dashed curve shows the fitted background function. (b) The $M_{p\bar{p}} - 2m_p$ distribution with events weighted by q_0/q.

the decay branching fraction (BF) to $p\bar{p}$ is larger than expected for a conventional $q\bar{q}$ meson. From Ref. [312], $B(J/\psi \to \gamma X) \cdot B(X \to p\bar{p}) = (7.0 \pm 0.4(stat)^{+1.9}_{-0.8}(syst)) \times 10^{-5}$. Measurements of the inclusive photon spectrum in J/ψ decays by the Crystal Ball group limit the radiative production rate of a narrow resonance around 1.85 GeV/c^2 to below 2×10^{-3} (an esitmate from Ref. [191]). Thus, a resonance that produces the observed enhancement would have a BF to $p\bar{p}$ that is larger than 4%, which would be the *largest* $p\bar{p}$ BF for all known mesons [67]. Since decays to $p\bar{p}$ are kinematically possible only for a small portion of the high-mass tail of the resonance and have very limited phase space, a large $p\bar{p}$ branching fraction implies an unusually strong coupling to $p\bar{p}$, as expected for a $p\bar{p}$ bound state.

2. Observation of X(1835) in $J/\psi \to \gamma\pi^+\pi^-\eta'$

The baryonium interpretation of the $p\bar{p}$ mass enhancement requires a new resonance with a mass around 1.85 GeV/c^2 and it would be supported by the observation of the resonance in other decay channels. Possible decay modes for a $p\bar{p}$ bound state, suggested in Ref. [219, 220], include $\pi^+\pi^-\eta'$.

The analysis of $J/\psi \to \gamma\pi^+\pi^-\eta'$ is described in detail in Ref. [214]. For the $J/\psi \to \gamma\pi^+\pi^-\eta'(\eta' \to \pi^+\pi^-\eta, \eta \to \gamma\gamma)$ channel, Figure 19.62(b) shows the $\pi^+\pi^-\eta$ invariant mass distribution , where a clear η' signal is visible. The $\pi^+\pi^-\eta'$ invariant mass spectrum

for the selected events is shown in Fig. 19.62(c), where a peak at a mass around 1835 MeV/c^2 is observed. For the $J/\psi \to \gamma\pi^+\pi^-\eta'(\eta' \to \gamma\rho)$ channel, the $\gamma\pi^+\pi^-$ invariant mass distribution shows an η' signal (Fig. 12.13(b)). For this channel there is also a distinct peak near 1835 MeV/c^2 in the $\pi^+\pi^-\eta'$ invariant mass spectrum (Fig. 12.13(c)).

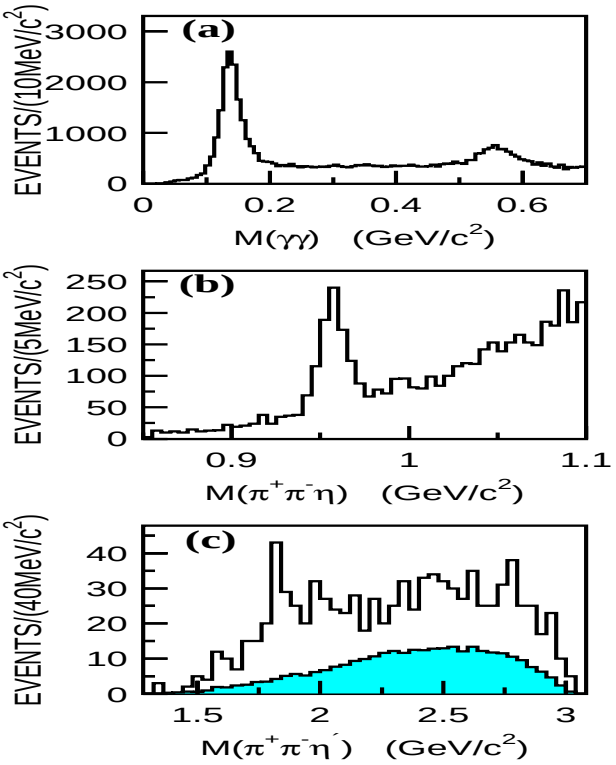

Figure 12.12: Invariant mass distributions for selected $J/\psi \to \gamma\pi^+\pi^-\eta'(\eta' \to \pi^+\pi^-\eta, \eta \to \gamma\gamma)$ candidate events. (a) The invariant mass distribution of $\gamma\gamma$ pairs. (b) The $\pi^+\pi^-\eta$ invariant mass distribution. (c) The $\pi^+\pi^-\eta'$ invariant mass distributions; the open histogram is data and the shaded histogram is $J/\psi \to \gamma\pi^+\pi^-\eta'$ phase-space MC events (with arbitrary normalization).

The combined spectrum (the sum of the histograms in Figs. 19.62(c) and 12.13(c))) is fitted with a Breit-Wigner (BW) function convolved with a Gaussian mass resolution function (with $\sigma = 13$ MeV/c^2) to represent the $X(1835)$ signal plus a smooth polynomial background function. The mass and width obtained from the fit (shown in the bottom panel of Fig. 12.14) are $M = 1833.7 \pm 6.1$ MeV/c^2 and $\Gamma = 67.7 \pm 20.3$ MeV/c^2. The signal yield from the fit is 264 ± 54 events with a confidence level 45.5% ($\chi^2/d.o.f. = 57.6/57$) and $-2\ln L = 58.4$. A fit to the mass spectrum without a BW signal function returns $-2\ln L = 126.5$. The change in $-2\ln L$ with $\Delta(d.o.f.) = 3$ corresponds to a statistical significance of 7.7 σ for the signal.

Using MC-determined selection efficiencies of 3.72% and 4.85% for the $\eta' \to \pi^+\pi^-\eta$ and $\eta' \to \gamma\rho$ modes, respectively, we determine a product BF of

$$B(J/\psi \to \gamma X(1835)) \cdot B(X(1835) \to \pi^+\pi^-\eta') = (2.2 \pm 0.4) \times 10^{-4}.$$

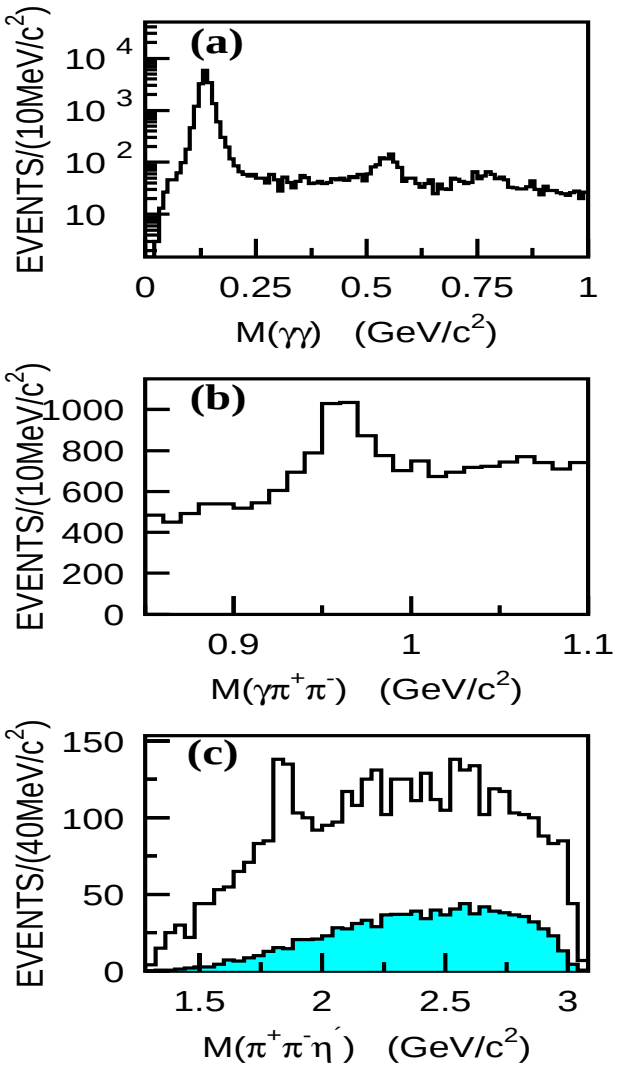

Figure 12.13: Invariant mass distributions for the selected $J/\psi \to \gamma\pi^+\pi^-\eta'(\eta' \to \gamma\rho)$ candidate events, (a) The invariant mass distribution for $\gamma\gamma$ pairs. (b) The $\gamma\pi^+\pi^-$ invariant mass distribution. (c) The $\pi^+\pi^-\eta'$ invariant mass distributions: the open histogram is data and the shaded histogram is from $J/\psi \to \gamma\pi^+\pi^-\eta'$ phase-space MC events (with arbitrary normalization).

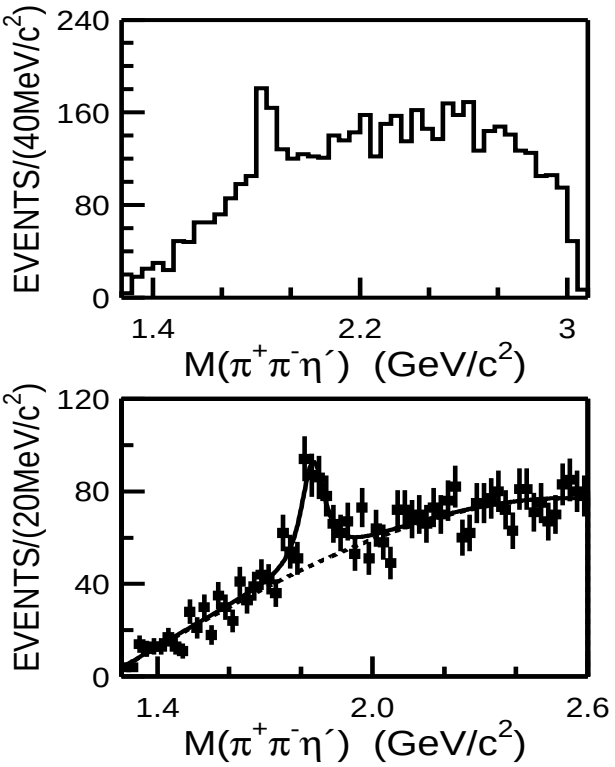

Figure 12.14: The $\pi^+\pi^-\eta'$ invariant mass distribution for selected events from both the $J/\psi \to \gamma\pi^+\pi^-\eta'(\eta' \to \pi^+\pi^-\eta, \eta \to \gamma\gamma)$ and $J/\psi \to \gamma\pi^+\pi^-\eta'(\eta' \to \gamma\rho)$ analyses. The bottom panel shows the fit (solid curve) to the data (points with error bars); the dashed curve indicates the background function.

The mass and width of the $X(1835)$ are not compatible with any known meson resonance [67]. We examined the possibility that the $X(1835)$ is responsible for the $p\bar{p}$ mass threshold enhancement observed in radiative $J/\psi \to \gamma p\bar{p}$ decays [312]. It has been pointed out that the S-wave BW function used for the fit in Ref. [312] should be modified to include the effect of final-state-interactions (FSI) on the shape of the $p\bar{p}$ mass spectrum [221, 222]. Redoing the S-wave BW fit to the $p\bar{p}$ invariant mass spectrum of Ref. [312] including the zero Isospin, S-wave FSI factor of Ref. [222], yields a mass $M = 1831 \pm 7$ MeV/c^2 and a width $\Gamma < 153$ MeV/c^2 (at the 90% C.L.); these values are in good agreement with the mass and width of $X(1835)$ reported here. Moreover, according to Ref. [220], the $\pi\pi\eta'$ decay mode is expected to be strong for a $p\bar{p}$ bound state. Thus, the $X(1835)$ resonance is a prime candidate for the source of the $p\bar{p}$ mass threshold enhancement in $J/\psi \to \gamma p\bar{p}$ process. In this case, the J^{PC} and I^G of the $X(1835)$ could only be 0^{-+} and 0^+, which can be tested in future experiments. Also in this context, the relative $p\bar{p}$ decay strength is quite strong: $B(X \to p\bar{p})/B(X \to \pi^+\pi^-\eta') \sim 1/3$ [The product BF determined from the fit that includes FSI effects on the $p\bar{p}$ mass spectrum is within the systematic errors of the result reported in Ref. [312].]. Since decays to $p\bar{p}$ are kinematically allowed only for a small portion of the high-mass tail of the resonance and have very limited phase space, the large $p\bar{p}$ branching fraction implies an unusually strong coupling to $p\bar{p}$, as expected for a $p\bar{p}$ bound state [223, 225]. However, other possible interpretations of the $X(1835)$ that have no relation to the $p\bar{p}$ mass threshold enhancement are not excluded.

3. Observation of $p\bar{\Lambda}$ mass threshold enhancement in $J/\psi \to pK^-\bar{\Lambda}$

The detailed analysis is described in Ref. [213]. The $p\bar{\Lambda}$ invariant mass spectrum for the selected events is shown in Fig. 12.15(a), where an enhancement is evident near the mass threshold. No corresponding structure is seen in a sample of $J/\psi \to pK^-\bar{\Lambda}$ MC events generated with a uniform phase space distribution. The $pK^-\bar{\Lambda}$ Dalitz plot is shown in Fig. 12.15(b). In addition to bands for the well established $\Lambda^*(1520)$ and $\Lambda^*(1690)$, there is a significant N^* band near the $K^-\bar{\Lambda}$ mass threshold, and a $p\bar{\Lambda}$ mass enhancement, isolated from the Λ^* and N^* bands, in the right-upper part of the Dalitz plot.

This enhancement can be fit with an acceptance weighted S-wave Breit-Wigner function, together with a function describing the phase space contribution, as shown in Fig. 12.15(c). The fit gives a peak mass of $m = 2075 \pm 12$ MeV and a width $\Gamma = 90 \pm 35$ MeV. The enhancement deviates from the shape of the phase space contribution with a statistical significance of about 7σ.

The fit yields $N_{res} = 238 \pm 57$ signal events, corresponding to a branching ratio

$$BR(J/\psi \to K^-X)BR(X \to p\bar{\Lambda}) = (5.9 \pm 1.4) \times 10^{-5}.$$

Searching for the same enhancement in $K\pi$ and $K\pi\pi$ modes in the $J/\psi, \psi' \to KK\pi, KK\pi\pi$ processes would help to confirm the presence of this anomalous peak and understand its nature, and in particular distinguish whether it is from a conventional K^* meson, a possible multi-quark state, or a resonance in the baryon-antibaryon interaction. If its decay widths to $K\pi$ and $K\pi\pi$ modes are much smaller than to $p\bar{\Lambda}$ modes, the interpretation as conventional K^* meson would be disfavored.

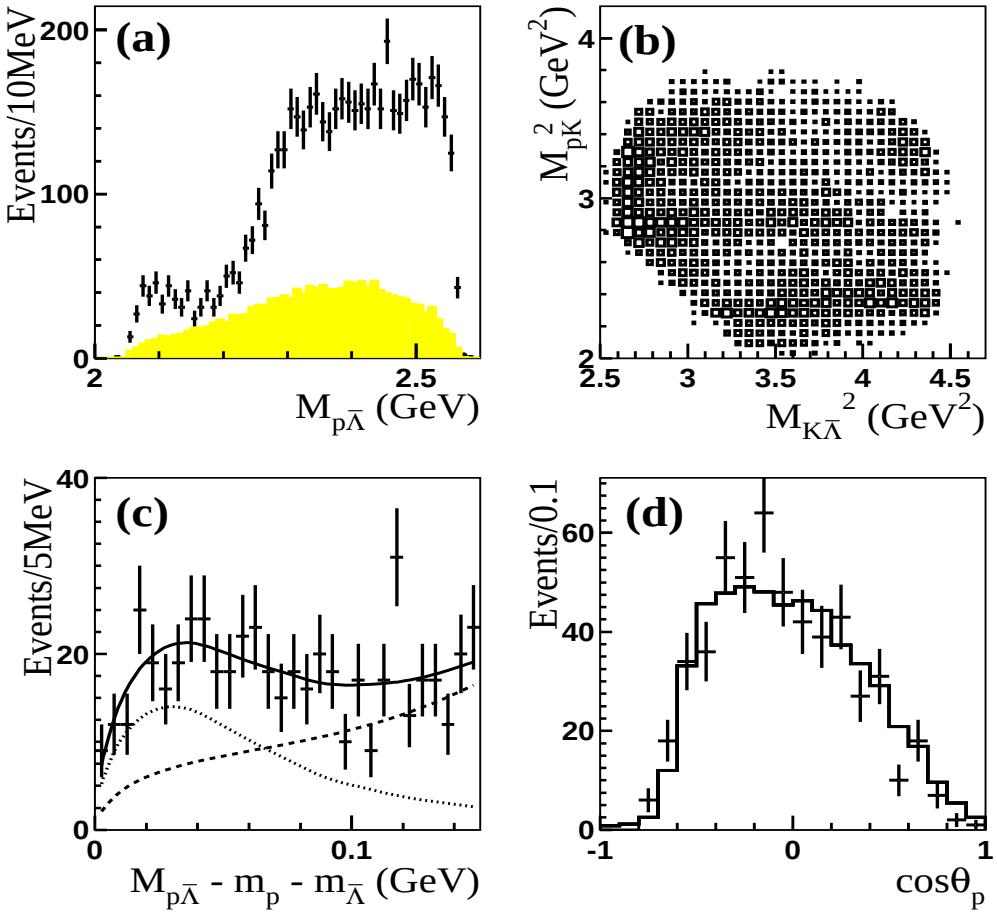

Figure 12.15: (a) The points with error bars indicate the measured $p\bar{\Lambda}$ mass spectrum; the shaded histogram indicates phase space MC events (arbitrary normalization). (b) The Dalitz plot for the selected event sample. (c) A fit (solid line) to the data. The dotted curve indicates the Breit-Wigner signal and the dashed curve the phase space 'background'. (d) The $\cos\theta_p$ distribution under the enhancement, the points are data and the histogram is the MC (normalized to data)

4. Observation of $K^-\bar{\Lambda}$ mass threshold enhancement in $J/\psi \to pK^-\bar{\Lambda}$

In the above Dalitz plot (Fig. 12.15(b)), a clear band, is observed near the $K^-\bar{\Lambda}$ mass threshold. We have performed very preliminary partial wave analysis (PWA) and obtained: The mass of this threshold structure N_X^* is in the range of 1500 MeV to 1650 MeV, the width is about 70 MeV to 110 MeV and its spin-parity favors $1/2^-$. In particular, it has a braching ratio $B(J/\psi \to \overline{p}N_X^*)B(N_X^* \to K^-\bar{\Lambda})$ larger than 2×10^{-4}.

Considering the mass of N_X^* is below or very close to $K^-\bar{\Lambda}$ threshold, i.e., the phase space producing $K^-\bar{\Lambda}$ final state is very small, the large branching ratio to $K^-\bar{\Lambda}$ indicates N_X^* has very strong coupling to $K^-\bar{\Lambda}$, suggesting that it could be the $K^-\bar{\Lambda}$ resonant state predicted by chiral SU(3) quark model[561].

5. Observation of a broad 1^{--} resonant structure in the K^+K^- mass spectrum in $J/\psi \to K^+K^-\pi^0$

A broad peak is observed at low K^+K^- invariant mass in $J/\psi \to K^+K^-\pi^0$ decays, detailed analysis is described in Ref. [227].

The Dalitz plot for the selected 10631 events is shown in Fig. 12.16(b), where a broad K^+K^- band is evident in addition to the $K^*(892)$ and $K^*(1410)$ signals. This band corresponds to the broad peak observed around 1.5 GeV/c^2 in the K^+K^- invariant mass projection shown in Fig. 12.16(c).

A partial wave analysis shows that the J^{PC} of this structure is 1^{--}. Its pole position is determined to be (1576^{+49+98}_{-55-91}) MeV/c^2 - $i(409^{+11+32}_{-12-67})$ MeV/c^2, and the branching ratio is $B(J/\psi \to X\pi^0) \cdot B(X \to K^+K^-) = (8.5 \pm 0.6^{+2.7}_{-3.6}) \times 10^{-4}$, where the first errors are statistical and the second are systematic. These parameters are not compatible with any known meson resonances [67].

To understand the nature of the broad 1^{--} peak, it is important to search for a similar structure in $J/\psi \to K_S K^\pm \pi^\mp$ decays to determine its isospin. It is also intriguing to search for $K^*K, KK\pi$ decay modes. In the mass region of the X, there are several other 1^{--} states, such as the $\rho(1450)$ and $\rho(1700)$, but the width of the X is much broader than the widths of these other mesons. This may be an indication that the X has a different nature than these other mesons. For example, very broad widths are expected for multiquark states [228].

12.4.3 Molecular states

Molecular states are bound states of two (or more) color-singlet hadrons. In other words, there are two (or more) MIT bags. Color-singlet hadrons are exchanged between these bags to produce the attractive force. Very often pions mediate the long-range interaction. There have been speculations of $f_0(980)$ being a $K\bar{K}$ molecule since it's only 10 MeV below $K\bar{K}$ threshold [229]. $\Lambda(1405)$ is sometimes postulated as a KN molecule.

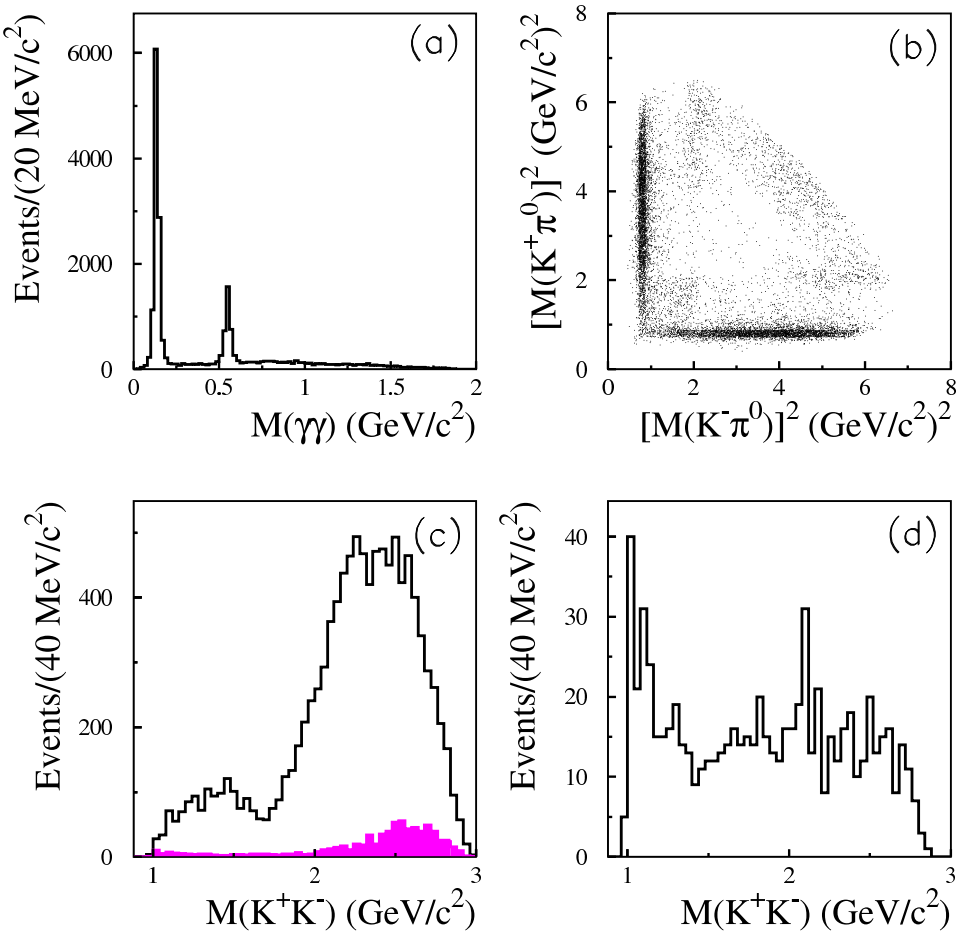

Figure 12.16: (a) The $\gamma\gamma$ invariant mass distribution. (b) The Dalitz plot for $K^+K^-\pi^0$ candidate events. (c) The K^+K^- invariant mass distribution for $K^+K^-\pi^0$ candidate events; the solid histogram is data and the shaded histogram is the background (normalized to data). (d) The K^+K^- invariant mass distribution for the π^0 mass sideband events (not normalized).

Chapter 13

Baryon spectrum

13.1 Outstanding problems in Baryon Spectroscopy

Our present knowledge on baryon spectroscopy is still in its infancy [67]. Many fundamental issues in baryon spectroscopy are still not well understood [230].

On theoretical side, an unsolved fundamental problem is: what are effective degrees of freedom for describing the internal structure of baryons? Several pictures based on various effective degrees of freedom are shown in Fig.29.2.1.

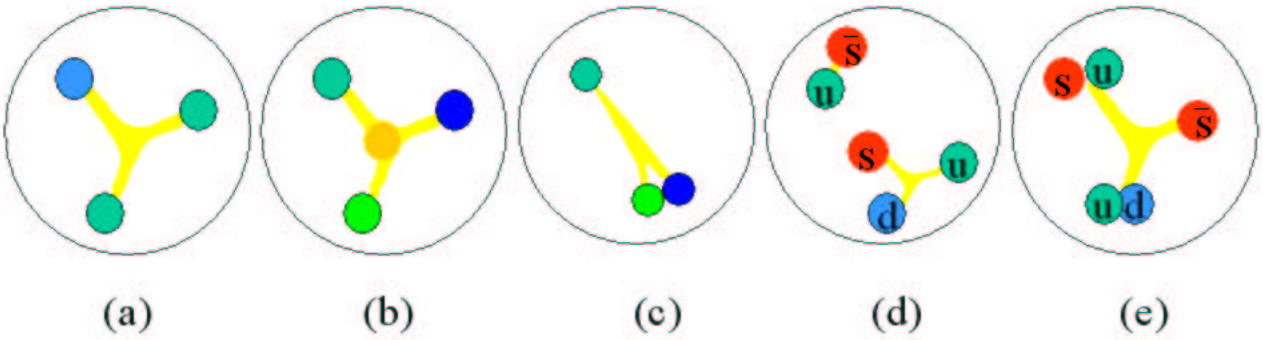

Figure 13.1: Various pictures for internal quark-gluon structure of baryons: (a) $3q$, (b) $3qg$ hybrid, (c) diquark, d) meson-baryon state, (e) pentaquark with diquark clusters.

The classical simple 3q constituent quark model as shown by Fig.29.2.1(a) has been very successful in explaining the static properties, such as mass and magnetic moment, of the spatial ground states of the flavor SU(3) octet and decuplet baryons. Its predicted Ω baryon with mass around 1670 MeV was discovered by later experiments. However its predictions for the spatial excited baryons failed badly. In the simple 3q constituent quark model, the lowest spatial excited baryon is expected to be a (uud) N^* state with one quark in orbital angular momentum $L = 1$ state, and hence should have negative parity. Experimentally [67], the lowest negative parity N^* resonance is found to be $N^*(1535)$, which is heavier than two other spatial excited baryons : $\Lambda^*(1405)$ and $N^*(1440)$. In the classical 3q constituent quark model, the $\Lambda^*(1405)$ with spin-parity $1/2^-$ is supposed to be a (uds) baryon with one quark in orbital angular momentum $L = 1$ state and about

130 MeV heavier than its N^* partner $N^*(1535)$; the $N^*(1440)$ with spin-parity $1/2^+$ is supposed to be a (uud) state with one quark in radial $n = 1$ excited state and should be heavier than the $L = 1$ excited (uud) state $N^*(1535)$, noting the fact that for a simple harmonic oscillator potential the state energy is $(2n + L + 3/2)\hbar\omega$. So for these three lowest spatial excited baryons, the classical quark model picture is already failed.

The second outstanding problem in the classical 3q quark model is that in many of its forms it predicts a substantial number of 'missing N^* states' around 2 GeV/c^2, which have not so far been observed [230]. Since the more number of effective degrees of freedom the more predicted number of excited states, the 'missing N^* states' problem is argued in favor of the diquark picture as shown in Fig.29.2.1(c) which has less degree of freedom and predicts less N^* states [231]. But it is only successful for very limited aspects. Moreover, non-observation of these 'missing N^* states' does not necessarily mean that they do not exist. They may have weak coupling to πN and γN, hence can hardly produced by presently available πN and γN experiments [230]. Other production processes should be explored.

The third outstanding problem for the classical 3q quark model is that from deep inelastic scattering and Drell-Yan experiments the number of $\bar{d}$ is found to be more than the number of $\bar{u}$ by 0.12 in the proton [232]. This is argued in favor of a mixture of the meson-baryon states as shown by Fig.29.2.1(d). With this picture, the excess of $\bar{d}$ over $\bar{u}$ in the proton is explained by a mixture of $n\pi^+$ with the π^+ composed of $u\bar{d}$ [233]; the $N^*(1535)$ and $\Lambda^*(1405)$ are ascribed as quasi-bound states of $K\Sigma$ and $\bar{K}N$, respectively [234]. However the mixture of the pentaquark components with diquark clusters as shown by Fig.29.2.1(e) can also explain these properties [235, 236, 237, 238].

Another unsolved fundamental problem is: even if we know the effective degrees of freedom in the baryon, how to deal with the interaction between them? In most fields of physics, in general, two-body force dominates and three-body force is regarded as a residual interaction. In QCD, however, the three-body force among three quarks is expected to be a "primary" force reflecting the $SU(3)_c$ gauge symmetry and this is strongly supported by a recent lattice calculation[239]. An earlier constituent quark model calculation[240] also suggested that the three quark potential is directly responsible for the structure and properties of baryons. It's much more complicated to deal with the three-body force than the usual two body force. Furthermore, the center of the Y-shape gluon field could act as an additional degree of freedom to vibrate so that the baryon behaves as a $gqqq$ hybrid as shown by Fig.29.2.1(b). Fortunately, the gluonic excitation energy is found to be about 1 GeV in the typical hadronic scale, which is relatively large compared with the excitation energy of the quark origin [241]. This large gluonic excitation energy justifies the great success of the simple 3q quark model for the baryons in spatial ground states.

On the other hand, the three-body Y-shape gluon field interaction is obtained in quenched approximation [239]; some people believe that the effective interaction field between the constituent quarks should be meson field instead of the gluon field [242]. To make things more complicated, mesons may exist in baryons not only in the form of virtual field but also in the form of real particle [234, 243]; furthermore there may exist genuine pentaquark states [244, 245, 246]. So for a baryon state around 2 GeV, it could be a mixture of all five configurations shown in Fig.29.2.1.

On experimental side, our present knowledge of baryon spectroscopy came almost

entirely from partial-wave analyses of πN total, elastic, and charge-exchange scattering data of more than twenty years ago [67]. Only recently, a new generation of experiments on N^* physics with electromagnetic probes has been started at new facilities such as CEBAF at JLAB, ELSA at Bonn, GRAAL at Grenoble and SPRING8 at JASRI. Some nice results have been produced [247, 248, 249]. However, a problem for these experiments is that above 1.8 GeV there are too many broad resonances with various possible quantum numbers overlapping with each other and it is very difficult to disentangle them. Moreover resonances with weak couplings to πN and γN will not show up in these experiments.

13.2 Baryon Spectroscopy at BESI and BESII

Joining the new effort on studying the excited nucleons, N^* baryons, BES started a baryon resonance program [250] at Beijing Electron-Positron Collider (BEPC). The J/ψ and ψ' experiments at BES provide an excellent place for studying excited nucleons and hyperons – N^*, Λ^*, Σ^* and Ξ^* resonances [251]. The corresponding Feynman graph for the production of these excited nucleons and hyperons is shown in Fig. 13.2 where ψ represents either J/ψ or ψ'.

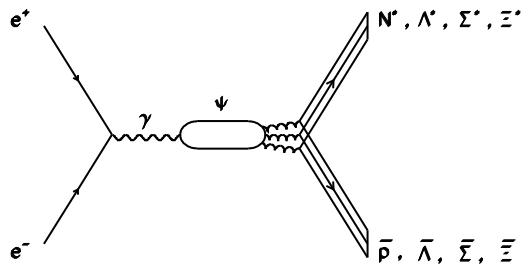

Figure 13.2: $\bar{p}N^*$, $\bar{\Lambda}\Lambda^*$, $\bar{\Sigma}\Sigma^*$ and $\bar{\Xi}\Xi^*$ production from e^+e^- collision through ψ meson.

Comparing with other facilities, our baryon program has advantages in at least three obvious aspects:

(1) We have pure isospin 1/2 πN and $\pi\pi N$ systems from $J/\psi \to \bar{N}N\pi$ and $\bar{N}N\pi\pi$ processes due to isospin conservation, while πN and $\pi\pi N$ systems from πN and γN experiments are mixture of isospin 1/2 and 3/2, and suffer difficulty on the isospin decomposition;

(2) ψ mesons decay to baryon-antibaryon pairs through three or more gluons. It is a favorable place for producing hybrid (qqqg) baryons, and for looking for some "missing" N^* resonances which have weak coupling to both πN and γN, but stronger coupling to g^3N;

(3) Not only N^*, Λ^*, Σ^* baryons, but also Ξ^* baryons with two strange quarks can be studied. Many QCD-inspired models [240, 252] are expected to be more reliable for baryons with two strange quarks due to their heavier quark mass. More than thirty Ξ^* resonances are predicted where only two such states are well established by experiments. The theory is totally not challenged due to lack of data.

BES started data-taking in 1989 and was upgraded in 1998. The upgraded BES is named BESII while the previous one is called BESI. BESI collected 7.8 million J/ψ events

and 3.7 million ψ' events. BESII has collected 58 million J/ψ events and 14 million ψ' events.

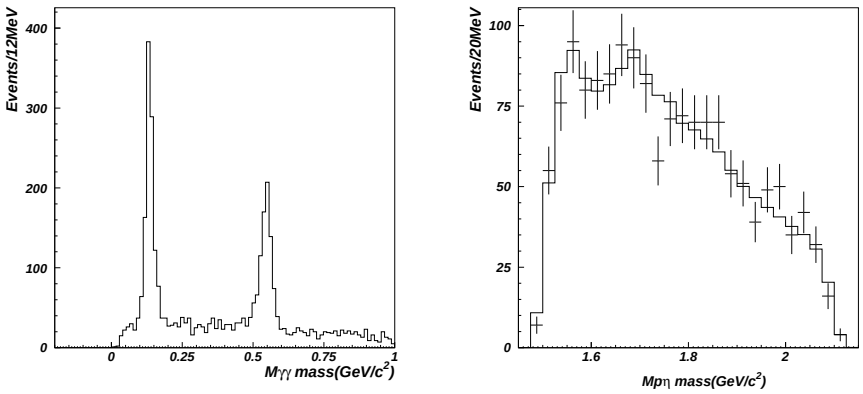

Figure 13.3: left: $\gamma\gamma$ invariant mass for $J/\psi \to \bar{p}p\gamma\gamma$; right: $p\eta$ invariant mass spectrum for $J/\psi \to \bar{p}p\eta$. BESI data

Based on 7.8 million J/ψ events collected at BESI from 1990 to 1991, the events for $J/\psi \to \bar{p}p\pi^0$ and $\bar{p}p\eta$ have been selected and reconstructed with π^0 and η detected in their $\gamma\gamma$ decay mode [250]. The invariant mass of $\gamma\gamma$ is shown in Fig. 29.2.1 (left) with two clear peaks corresponding to π^0 and η. The $p\eta$ invariant mass spectrum is shown in Fig. 29.2.1 (right) with two peaks at 1540 and 1650 MeV. Partial wave analysis has been performed for the $J/\psi \to \bar{p}p\eta$ channel [250] using the effective Lagrangian approach [253, 254] with Rarita-Schwinger formalism [255, 256, 257, 258] and the extended automatic Feynman Diagram Calculation (FDC) package [259]. There is a definite requirement for a $J^P = \frac{1}{2}^-$ component at $M = 1530 \pm 10$ MeV with $\Gamma = 95 \pm 25$ MeV near the ηN threshold. In addition, there is an obvious resonance around 1650 MeV with $J^P = \frac{1}{2}^-$ preferred, $M = 1647 \pm 20$ MeV and $\Gamma = 145^{+80}_{-45}$ MeV. These two N^* resonances are believed to be the two well established states, $S_{11}(1535)$ and $S_{11}(1650)$, respectively. In the higher $p\eta(\bar{p}\eta)$ mass region, there is an evidence for a structure around 1800 MeV; with BESI statistics one cannot determine its quantum numbers. The $p\pi^0$ invariant mass spectrum from $J/\psi \to p\bar{p}\pi^0$ is shown in Fig. 13.4 with two clear peaks around 1500 and 1670 MeV, and some weak structure around 2 GeV.

With 58 million new J/ψ events collected by BESII of improved detecting efficiency, one order of magnitude more reconstructed events can be obtained for each channel. Results for J/ψ to $p\bar{p}\pi^0$, $p\bar{n}\pi^- + c.c.$, $pK^-\bar{\Lambda} + c.c.$ and $\Lambda\bar{\Sigma}\pi$+c.c. channels are shown in Figs.13.4,13.5,13.6,13.7, respectively. These are typical channels for studying N^*, Λ^* and Σ^* resonances.

For $J/\psi \to p\bar{p}\pi^0$ channel, the $N\pi$ invariant mass spectrum looks similar to the BESI data as shown in Fig.13.4, but with much higher statistics.

For $J/\psi \to p\bar{n}\pi^-$ channel, proton and π^- are detected. With some cuts of backgrounds, the missing mass spectrum shows a very clean peak for the missing antineutron. In the $p\pi^-$ invariant mass spectrum as shown in Fig.13.5 (left), besides two well known N^* peaks at 1500 and 1670 MeV, there are two new clear N^* peaks around 1360 and 2030

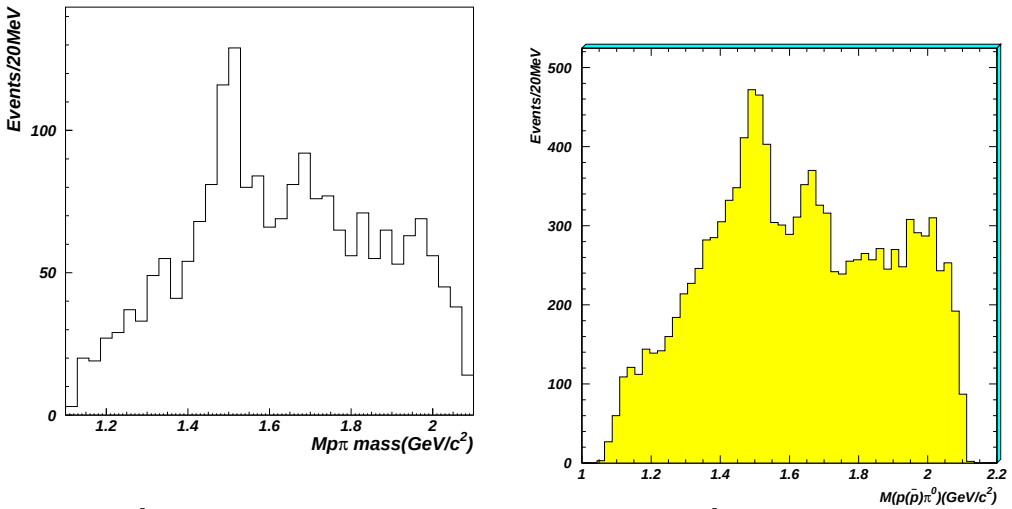

Figure 13.4: $p\pi^0$ invariant mass spectrum for $J/\psi \to \bar{p}p\pi^0$ from BESI (left) and preliminary BESII data (right)

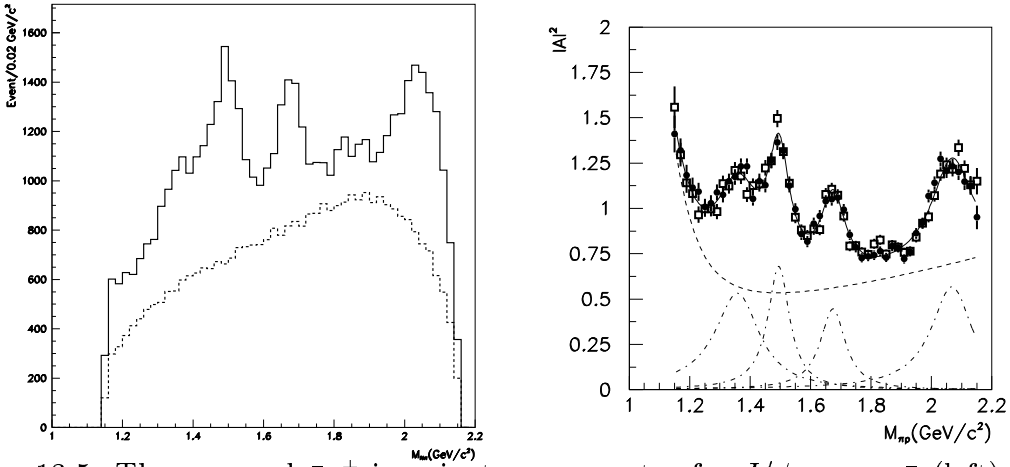

Figure 13.5: The $p\pi^-$ and $\bar{p}\pi^+$ invariant mass spectra for $J/\psi \to p\pi^-\bar{n}$ (left) and $\bar{p}\pi^+n$ (middle), compared with phase space distribution; And data divided by Monte Carlo phase space vs $p\pi$ invariant mass for $J/\psi \to \bar{p}\pi^-\bar{n}$ (solid circle) and $J/\psi \to \bar{p}\pi^+n$ (open square).

MeV. Its charge conjugate channel $\bar{p}\pi^+ n$ gives very similar results as shown in Fig.13.5 (middle).

To investigate the behavior of the amplitude squared as a function of invariant mass, one should remove the phase space factor and efficiency factor from the invariant mass distribution by dividing the data by Monte Carlo phase space times the detection efficiency. The results are shown in Fig. 13.5 (right). At low $p\pi$ invariant mass, the tail from nucleon pole term, expected from theoretical considerations [260, 261], is clearly seen. There are clearly four peaks around 1360 MeV, 1500 MeV, 1670 MeV and 2065 MeV. Note that the well known first resonance peak ($\Delta(1232)$) in πN and γN scattering data does not show up here due to the isospin filter effect of our J/ψ decay. While the two peaks around 1500 MeV and 1670 MeV correspond to the well known second and third resonance peaks observed in πN and γN scattering data, the two peaks around 1360 MeV and 2065 MeV have never been observed in πN invariant mass spectra before. The one around 1360 MeV should be from $N^*(1440)$ MeV which has a pole around 1360 MeV [67, 262, 263] and which is usually buried by the strong Δ peak in πN and γN experiments; the other one around 2065 MeV may be due to the long sought "missing" N^* resonance(s). For the decay $J/\psi \to \bar{N}N^*(2065)$, the orbital angular momentum of $L = 0$ is much preferred due to the suppression of the centrifugal barrier factor for $L \geq 1$. For $L = 0$, the spin-parity of $N^*(2065)$ is limited to be $1/2+$ and $3/2+$. This may be the reason that the $N^*(2065)$ shows up as a peak in J/ψ decays while no peak shows up for πN invariant mass spectra in πN and γN production processes which allow all $1/2\pm$, $3/2\pm$, $5/2\pm$ and $7/2\pm$ N^* resonances around 2.05 GeV to overlap and interfere with each other there. A simple Breit-Wigner fit [264] gives the mass and width for the $N^*(1440)$ peak as $1358 \pm 6 \pm 16$ MeV and $179 \pm 26 \pm 50$ MeV, and for the new N^* peak above 2 GeV as $2068 \pm 3^{+15}_{-40}$ MeV and $165 \pm 14 \pm 40$ MeV, respectively. A partial wave analysis indicates that the $N^*(2065)$ peak contains both spin-parity $1/2+$ and $3/2+$ components [264].

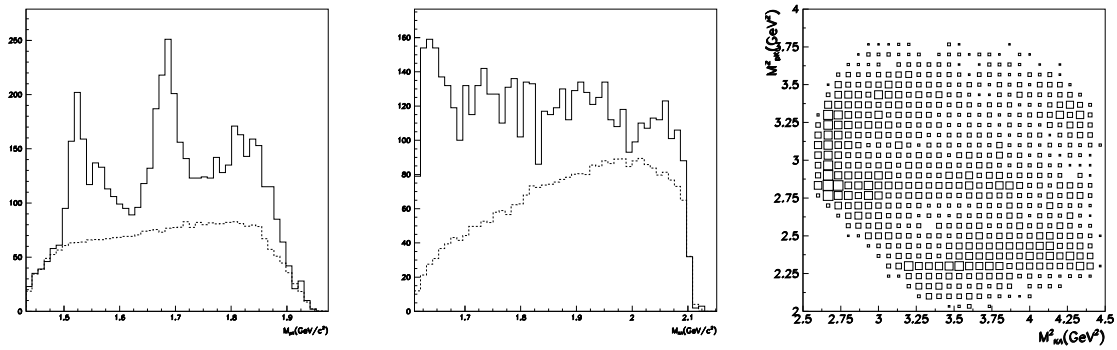

Figure 13.6: pK (left) and $K\Lambda$ (middle) invariant mass spectra for $J/\psi \to pK^-\bar{\Lambda}$+c.c., compared with phase space distribution; right: Dalitz plot for $J/\psi \to pK^-\bar{\Lambda}$+c.c.

For $J/\psi \to pK^-\bar{\Lambda}$ and $\bar{p}K^+\Lambda$ channels [265], there are clear Λ^* peaks at 1.52 GeV, 1.69 GeV and 1.8 GeV in pK invariant mass spectrum, and N^* peaks near $K\Lambda$ threshold, 1.9 GeV and 2.05 GeV for $K\Lambda$ invariant mass spectrum. The SAPHIR experiment at ELSA[248] also observed a N^* peak around 1.9 GeV for $K\Lambda$ invariant mass spectrum from

photo-production. The N^* peak near $K\Lambda$ threshold is most probably due to $N^*(1535)$ which was found to have large coupling to $K\Lambda$ [243]. The N^* peak at 2.05 GeV is compatible with that observed in $N\bar{N}\pi$ channels. The spin-parity $3/2^+$ is found preferred for this $N^*(2050)$ to reproduce the Dalitz plot.

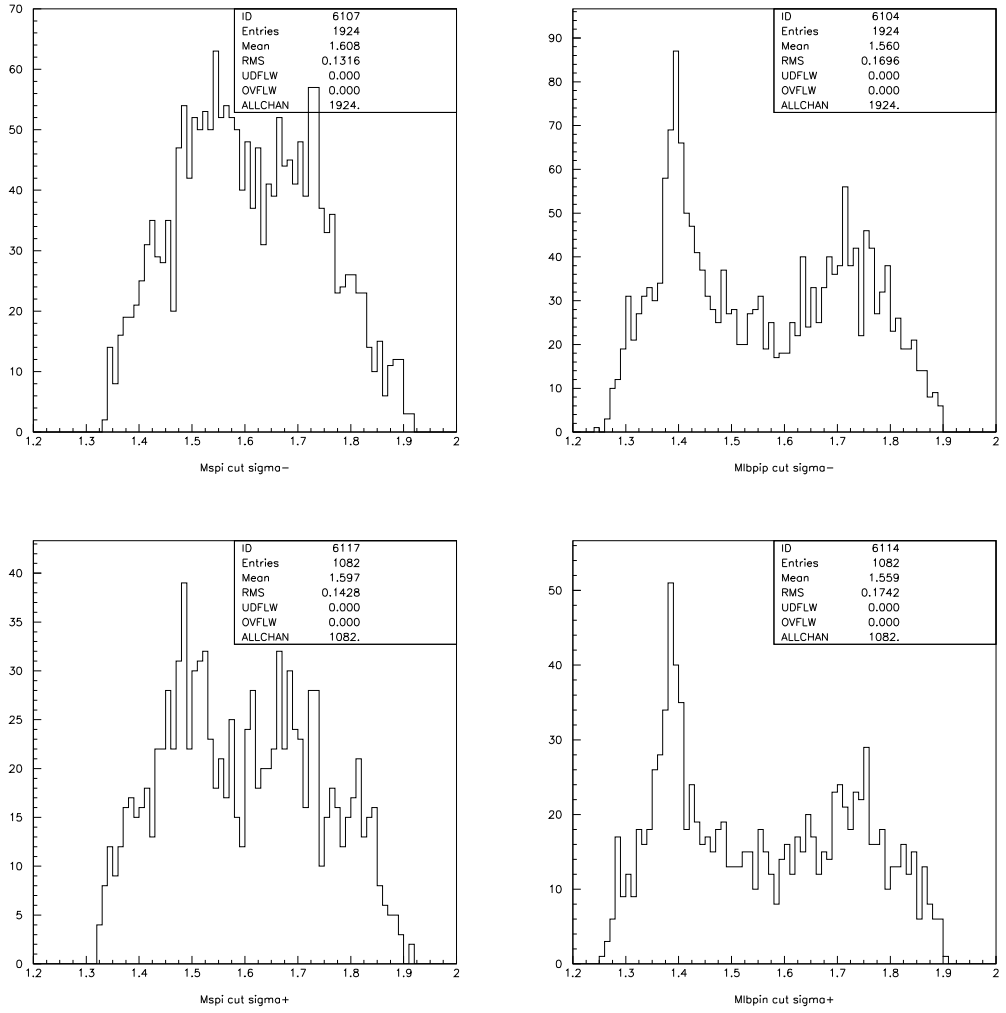

Figure 13.7: $\bar{\Sigma}\pi$ (left) and $\Lambda\pi$ (right) invariant mass spectrum for $J/\psi \to \Lambda\bar{\Sigma}^+\pi^-$ (up) and $J/\psi \to \Lambda\bar{\Sigma}^-\pi^+$ (down), respectively. Preliminary BESII data [266]

For $J/\psi \to \Lambda\Sigma\pi$ channels [266], it seems also Λ^* peaks at 1.52 GeV, 1.69 GeV and 1.8 GeV in $\Sigma\pi$ invariant mass spectra, similar to those in the $pK\Lambda$ channel, although less clear. In $\Lambda\pi$ invariant mass spectra, there is a very clear peak around 1.385 GeV corresponding to the well-established $\Sigma(1385)$ resonance and there is also another Σ^* peak around 1.72 GeV.

In order to get more useful information about properties of the baryon resonances involved, such as their J^{PC} quantum numbers, mass, width, production and decay rates, etc., partial wave analysis (PWA) is necessary.

The basic procedure for our partial wave analysis is the standard maximum likelihood method:

(1) construct amplitudes A_i for each i-th possible partial waves;

(2) from linear combination of these partial wave amplitudes, get the total transition probability for each event as $w = |\sum_i c_i A_i|^2$ with c_i as free parameters to be determined by fitting data;

(3) maximize the following likelihood function L to get c_i parameters as well as mass and width parameters for the resonances.

$$L = \prod_{n=1}^{N} \frac{w_{data}}{\int w_{MC}}, \tag{13.1}$$

where N is the number of reconstructed data events and w_{data}, w_{MC} are evaluated for data and Monte Carlo events, respectively.

For the construction of partial wave amplitudes, we assume the effective Lagrangian approach[253, 254] with Rarita-Schwinger formalism[255, 256, 257]. In this approach, there are three basic elements for constructing amplitudes: particle spin wave functions, propagators and effective vertex couplings; the amplitude can be written out by Feynman rules for tree diagrams.

For example, for $J/\psi \to \bar{N}N^*(3/2+) \to \bar{N}(k_1, s_1)N(k_2, s_2)\pi(k_3)$, the amplitude can be constructed as

$$A_{3/2+} = \bar{u}(k_2, s_2)k_{2\mu}P^{\mu\nu}_{3/2}(c_1 g_{\nu\lambda} + c_2 k_{1\nu}\gamma_\lambda + c_3 k_{1\nu}k_{1\lambda})\gamma_5 v(k_1, s_1)\psi^\lambda \tag{13.2}$$

where $u(k_2, s_2)$ and $v(k_1, s_1)$ are 1/2-spinor wave functions for N and $\bar{N}$, respectively; ψ^λ the spin-1 wave function,/i.e., polarization vector, for J/ψ. The c_1, c_2 and c_3 terms correspond to three possible couplings for the $J/\psi \to \bar{N}N^*(3/2+)$ vertex. The c_1, c_2 and c_3 can be taken as constant parameters or with some smooth vertex form factors in them if necessary. The spin 3/2 propagator $P^{\mu\nu}_{3/2}$ for $N^*(3/2^+)$ is

$$P^{\mu\nu}_{3/2} = \frac{\gamma \cdot p + M_{N*}}{M^2_{N*} - p^2 - iM_{N*}\Gamma_{N*}} \left[g^{\mu\nu} - \frac{1}{3}\gamma^\mu\gamma^\nu - \frac{2p^\mu p^\nu}{3M^2_{N*}} + \frac{p^\mu\gamma^\nu - p^\nu\gamma^\mu}{3M_{N*}} \right] \tag{13.3}$$

with $p = k_2 + k_3$. Other partial wave amplitudes can be constructed similarly[255, 258].

13.3 Prospects for baryon spectroscopy at BESIII

Recently, empirical indications for a positive strangeness magnetic moment and positive strangeness radius of the proton suggest that the 5-quark components in baryons may be largely in colored diquark cluster configurations rather than mainly in "meson cloud" configurations or in the form of a sea of quark-antiquark pairs [235, 236]. The diquark cluster picture also gives a natural explanation for the excess of $\bar{d}$ over $\bar{u}$ in the proton with a mixture of $[ud][ud]\bar{d}$ component in the proton. More precise measurements and analyses of the strange form factors are needed to examine the relative importance of the meson-cloud components and $q^2q^2\bar{q}$ components in the proton.

For excited baryons, the excitation energy for a spatial excitation could be larger than to drag out a $q\bar{q}$ pair from gluon field with the q to form diquark cluster with a valence quark. Hence the 5-quark components could be dominant for some excited baryons.

The diquark cluster picture for the 5-quark components in baryons also gives a natural explanation for the longstanding mass-reverse problem of $N^*(1535)$, $N^*(1440)$ and $\Lambda^*(1405)$ resonances as well as the unusual decay pattern of the $N^*(1535)$ resonance with a large $|[ud][us]\bar{s}>$ component [235, 237].

The diquark cluster picture predicts the existence of the SU(3) partners of the $N^*(1535)$ and $\Lambda^*(1405)$,/i.e., an additional Λ^* $1/2^-$ around 1570 MeV, a triplet Σ^* $1/2^-$ around 1360 MeV and a doublet Ξ^* $1/2^-$ around 1520 MeV [238]. There is indeed evidence for all of them in the data of J/ψ decays at BES. Fig. 13.6 (left) shows the pK invariant mass spectrum for $J/\psi \to pK^-\bar{\Lambda}$+c.c. and Fig. 13.7 (right) $\Lambda\pi$ invariant mass spectrum for $J/\psi \to \Lambda\bar{\Sigma}^+\pi^-$ from BES [266]. In the pK invariant mass spectrum, under the narrow $\Lambda^*(1520)$ $3/2^-$ peak, there is a quite obvious broader peak around 1570 MeV. Preliminary partial wave analysis [267] gave its spin-parity as $1/2^-$. This $\Lambda^*(1570)$ $1/2^-$ resonance fits in the new scheme for the $1/2^-$ SU(3) baryon nonet very well. In the $\Lambda\pi$ invariant mass spectrum, under the $\Sigma^*(1385)$ $3/2^+$ peak, there is also a broader peak around 1360 MeV. No partial wave analysis has been performed for this channel yet. But there is a good reason to reckon that there may be $1/2^-$ component underneath the $\Sigma^*(1385)$ $3/2^+$ peak.

According to PDG [67], the branching ratios for $J/\psi \to \bar{\Sigma}^-\Sigma^*(1385)^+$ and $J/\psi \to \bar{\Xi}^+\Xi^*(1530)^-$ are $(3.1\pm0.5)\times10^{-4}$ and $(5.9\pm1.5)\times10^{-4}$, respectively. These two processes are SU(3) breaking decays since Σ and Ξ belong to SU(3) $1/2^+$ octet while $\Sigma^*(1385)$ and $\Xi^*(1530)$ belong to SU(3) $3/2^+$ decuplet. Comparing with the similar SU(3) breaking decay $J/\psi \to \bar{p}\Delta^+$ with branching ratio of less than 1×10^{-4} and the SU(3) conserved decay $J/\psi \to \bar{p}N^*(1535)^+$ with branching ratio of $(10 \pm 3) \times 10^{-4}$, the branching ratios for $J/\psi \to \bar{\Sigma}^-\Sigma^*(1385)^+$ and $J/\psi \to \bar{\Xi}^+\Xi^*(1530)^-$ are puzzling too high. A possible explanation for this puzzling phenomena is that there were substantial components of $1/2^-$ under the $3/2^+$ peaks but the two branching ratios were obtained by assuming pure $3/2^+$ contribution. This possibility should be easily checked with the high statistics BESIII data in near future.

With two order of magnitude more statistics at BESIII, plenty important channels for baryon spectroscopy can be studied from both J/ψ and ψ' decays. The ψ' data will significantly extend the mass range for the study of baryon spectroscopy. For example, for $\psi' \to p\bar{n}\pi^- + c.c.$ events collected at BESII [268], there are obvious structures for $M_{N\pi} > 2$ GeV in the $N\pi$ invariant mass spectra as shown in Fig. 13.8. However due to low statistics at BESII, no conclusive information can be drawn for the N^* resonances with mass above 2 GeV from ψ' decays [268, 270]. With BESIII statistics, determination of properties for these high mass N^* resonances can be done. More importantly, plenty "missing" Λ^*,Σ^* and Ξ^* hyperon resonances are expected to be produced and observed by high statistics BESIII J/ψ and ψ' data. Fig. 13.9 shows the Predicted Λ^*,Σ^*,Ξ^* mass spectra (solid line) by the classical 3q quark model [269, 230] and the predicted lowest $1/2^-$ Λ^*,Σ^*,Ξ^* states (dashed line) with pentaquark configuration [238], compared with observed states (box). The classical 3q quark model [269] predicts more than 30 Ξ^* resonant states between 1.78 and 2.35 GeV as shown in Fig.13.9. None of them

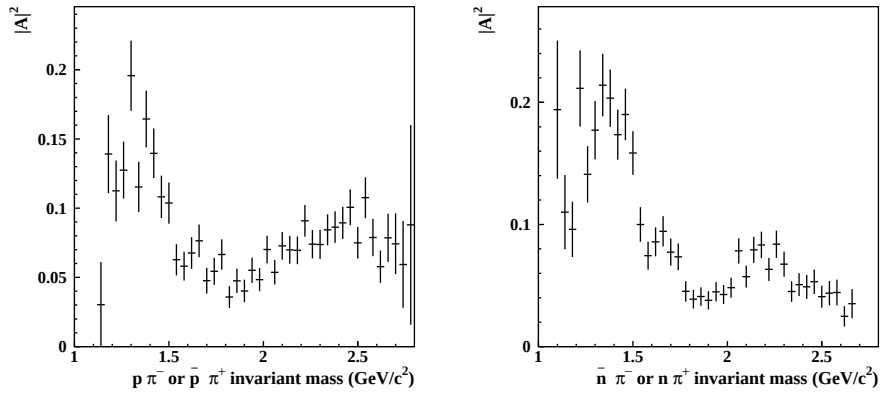

Figure 13.8: Data corrected by MC simulated efficiency and phase space versus $p\pi^-$ (or $\bar{p}\pi^+$) and $\bar{n}\pi^-$ (or $n\pi^+$) invariant mass for $\psi' \to p\bar{n}\pi^- + c.c.$ candidate events [268].

have been established yet. These Ξ^* states cannot be produced by J/ψ decays due to limited phase space, but all can be produced by ψ' decays. The BESIII ψ' data will enable us to complete the Λ^*, Σ^* and Ξ^* spectrum and examine various pictures for their internal structures, such as simple 3q quark structure and more complicated structure with pentaquark components dominated.

Table 13.1: Measured J/ψ decay branching ratios (BR$\times 10^3$) for channels involving baryon anti-baryon and meson(s) [67, 264]

$p\bar{n}\pi^-$	$p\bar{p}\pi^0$	$p\bar{p}\pi^+\pi^-$	$p\bar{p}\eta$	$p\bar{p}\eta'$	$p\bar{p}\omega$
2.4 ± 0.2	1.1 ± 0.1	6.0 ± 0.5	2.1 ± 0.2	0.9 ± 0.4	1.3 ± 0.3
$\Lambda\bar{\Sigma}^-\pi^+$	$pK^-\bar{\Lambda}$	$pK^-\bar{\Sigma}^0$	$\bar{p}p\phi$	$\Delta(1232)^{++}\bar{p}\pi^-$	$pK^-\bar{\Sigma}(1385)^0$
1.1 ± 0.1	0.9 ± 0.2	0.3 ± 0.1	0.045 ± 0.015	1.6 ± 0.5	0.51 ± 0.32

The measured J/ψ decay branching ratios for channels involving baryon anti-baryon plus meson(s) are listed in Table 13.1. With 10^{10} J/ψ events, all these channels will get enough statistics for partial wave analysis. Among these channels, the $\Sigma\bar{\Lambda}\pi + c.c.$ channels should have high priority for pinning down the lowest $1/2^-$ Σ^* and Λ^* as well as other higher excited Σ^* and Λ^* states. Another very important channel is $K^-\Lambda\bar{\Xi}^+ + c.c.$ which is the best channel for finding the lowest $1/2^-$ Ξ^* resonance and many other "missing" Ξ^* states with $\Xi^* \to K\Lambda$. This channel should be rather easy to be reconstructed by BESIII. One can select events containing K^- and Λ with $\Lambda \to p\pi^-$, then from missing mass spectrum of $K^-\Lambda$ one should easily identify the very narrow $\bar{\Xi}^+$ peak.

For 10^9 ψ' events, the $K^-\Lambda\bar{\Xi}^+ + c.c.$ and $p\bar{p}\phi$ channels should have high priority. These two channels are strongly limited by phase space in J/ψ decays. From ψ' decays, the phase space is much increased. The $K^-\Lambda\bar{\Xi}^+ + c.c.$ channel should allow us to discover many "missing" Ξ^* resonances, while the $p\bar{p}\phi$ channel should allow us to find those N^* resonances with large coupling to $N\phi$ and hence large 5-quark components.

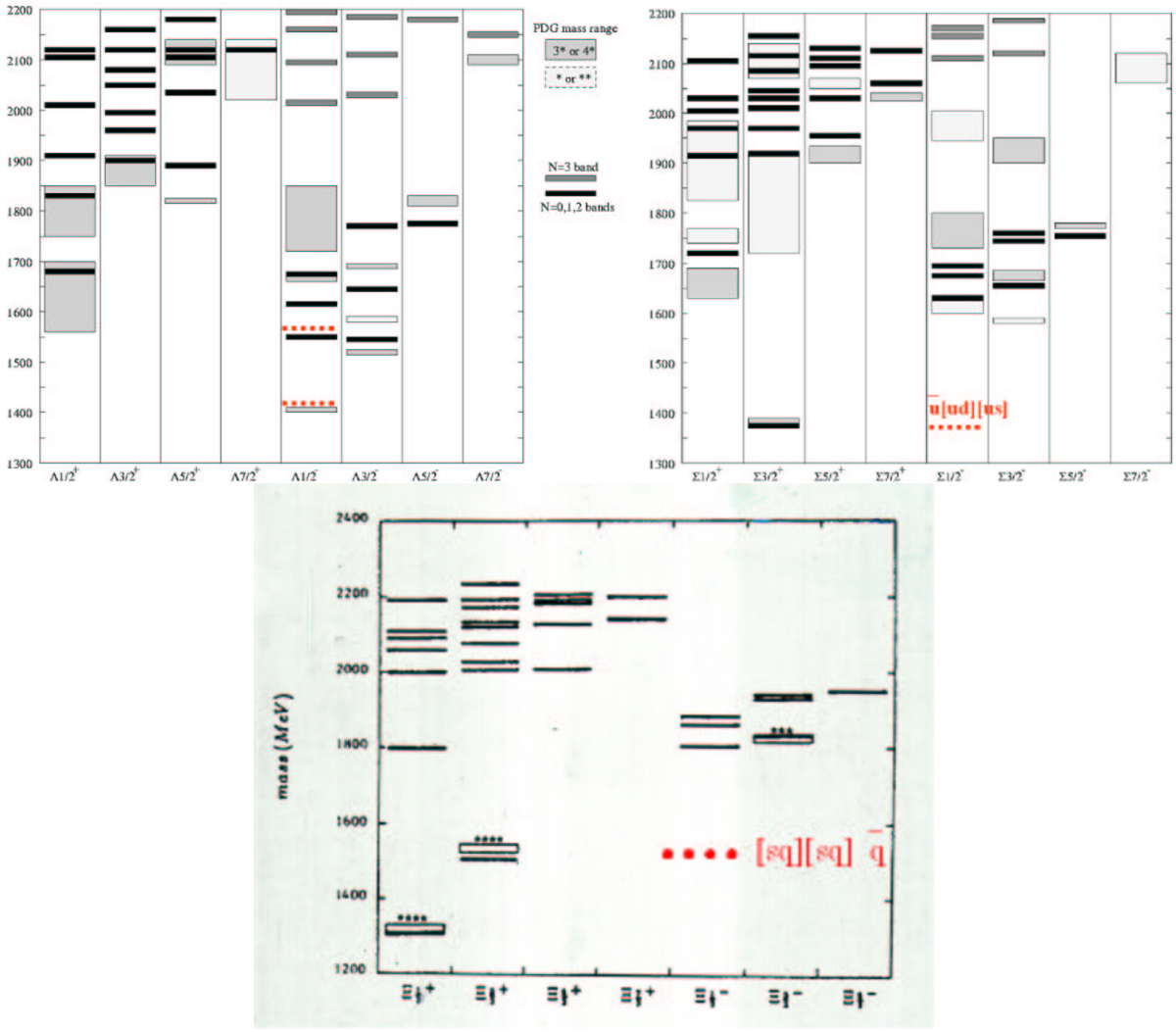

Figure 13.9: Predicted Λ^*,Σ^*,Ξ^* mass spectra (solid line) by the classical 3q quark model [269, 230] and the predicted lowest $1/2^-$ Λ^*,Σ^*,Ξ^* states (dashed line) with pentaquark configuration [238], compared with observed states (box).

After analyzing the easier 3-body final states, 4-body and 5-body channels should also be investigated. Among them, $\Delta(1232)^{++}\bar{p}\pi^-$ in $p\bar{p}\pi^+\pi^-$ and $\Delta(1232)^{++}\bar{\Sigma}^-K^-$ in $p\bar{\Sigma}^-\pi^+K^-$ are very good channels for finding "missing" $\bar{\Delta}^{*--}$ decaying to $\bar{p}\pi^-$ and $\bar{\Sigma}^-K^-$, respectively. The spectrum of isospin 3/2 Δ^{++*} resonances is of special interest since it is the most experimentally accessible system composed of 3 identical valence quarks. Recently, the lowest $1/2^-$ baryon decuplet is proposed to contain large vector-meson-baryon molecular components [271]. In the new scheme, the $\Xi^*(1950)$ is predicted to be $1/2-$ resonance with large coupling to ΛK^*. The $\psi' \to \bar{\Xi}\Lambda K^*$ will provide a very good place to look for "missing" Ξ^* with large coupling to ΛK^*.

In summary, BESIII data can play a very important role in studying excited nucleons and hyperons, i.e., N^*, Λ^*, Σ^*, Ξ^* and Δ^{*++} resonances.

Chapter 14

Hunting for glueballs, multiquark states and hybrids at BESIII/BEPCII

14.1 Introduction

With the double-ring design, the peak luminosity of BEPCII will reach the luminosity of $10^{33}\ cm^{-2}s^{-1}$ at the center of mass energy around $\psi(3770)$ peak. Then, the luminosity at J/ψ peak will be about 60% of that at $\psi(3770)$ peak. If assuming the average luminosity is half of the peak luminosity and the effective running time for data accumulation is around 10^7 s each year, the expected J/ψ events for one year's running is about 10 billion, taking into account the 3400 nb peak cross section for J/ψ production. This is a huge data sample. On the other hand, the new BESIII detector consists of a drift chamber (MDC) which has a small cell structure filled with a helium-based gas, an electromagnetic calorimeter (EMC) made of CsI(Tl) crystals, time-of-flight counters (TOF) for particle identification made of plastic scintillators, a muon system made of Resistive Plate Chambers (RPC) and a super conducting magnet. The designed single wire spatial resolution, dE/dx resolution and momentum resolution for the MDC are 130μm, 6% and 0.5 % $\sqrt{1+p^2}$ (p in GeV/c), respectively. The time resolution for TOF is $\sigma_{TOF} = 100$ ps for Bhabha events and the energy resolution for photons is $\sigma_E/E \simeq 2.5\ \% /\sqrt{E}$ (E in GeV) in EMC. The huge J/ψ data sample taken with BESIII, a detector having much better performance, make the systematic study of the light hadron spectroscopy possible and make the search for the new hadron states, eg. glueballs, hydrids and multi-quark states possible.

14.2 Search for glueballs

Glueballs are considered to be copiously produced in radiative J/ψ decays. The inclusive photon spectrum from radiative J/ψ decays can be used to search for the new states, especially when these states have a relatively big production rate in radiative J/ψ decays. Therefore the inclusive photon spectrum provides an ideal laboratory in searching for

glueballs.

The study of the exclusive J/ψ radiative and hadronic decays, as well as two-photon processes would also provide improtant information for the identification of the glueballs. As suggested by F. Close, the decays of $J/\psi \to \gamma\gamma\rho$ and $\gamma\gamma\phi$ can act as a flavor filter and therefore can be used to tag the flavor of the mesons.

14.2.1 Scalar glueball

As briefly summarized in Section 3.3.2, at the energies of 1$\sim$2 GeV, the existence of at least three isoscalar scalars, $f_0(1370)$, $f_0(1500)$ and $f_0(1710)$, is no longer questioned by the elementary particle physics community. However their origins remain a mystry. Recently, two new scalars, $f_0(1790)$ and $f_0(1810)$, were reported by BESII and are calling for the comfirmation.

Using a high statistics J/ψ data taken with a high performance detector, the confirmation of the new states with the determination of their quantum numbers via PWA, the determination of their masses, widths and decay branching ratios, as well as the systematic study of $f_0(1370)$, $f_0(1500)$ and $f_0(1710)$ from the radiative and hadrnic decays to PP (P denotes the pseudoscalar meson), VV (V denotes the vector meson), *etc* is necessary and possible. This helps to clarify the situation of the scalars. In addition, the study of these states in the high statistics two-photon data will be crucial in determining their gluonic content through the determination of their two-photon couplings.

14.2.2 Pseudoscalar glueball

Five pseudoscalar states above 1 GeV, $\eta(1295)$, $\eta(1405)$, $\eta(1475)$, $\eta(1760)$, and $\eta(2225)$ are listed in the PDG [67]. Of which, some are well established, while some need further confirmation. The nature of these states is still controversal, as is discussed in Section 3.3.3. With BESIII data, the decays of $J/\psi \to \gamma\eta\pi\pi$, $\gamma\eta'\pi\pi$, $\gamma K\bar{K}\pi$, γVV *etc* and their corresponding hadronic decays can be investigated, which helps to identify the pseudoscalar glueballs and understand the pseudoscalar spectrum eventually.

14.2.3 Tensor glueball

Jin S. will write this part.

14.3 Search for the hybrid states

The dominant decay modes of the hybrid states, obtained in flux-tube model, are listed in table 24.5-table 12.15, which give the guidance in searching for the hybrid states.

14.4 Search for the multi-quark states

The multiquark states are expected to have very broad width and therefore they may be only experimentally observable near the mass thresholds.

14.5 Some examples on searching for glueballs, hybrids and multi-quark states

14.5.1 The tensor glueball candidate in $J/\psi \to \gamma\eta\eta$ and $\gamma\eta\eta'$

We study $J/\psi \to \gamma\eta\eta$ and $\gamma\eta\eta'$ decays to investigate the sensitivity of 2^{++} glueball candidate $f_J(2220)$ at BESIII, with η decaying to $\gamma\gamma$ or $\pi^+\pi^-\pi^0$ and η' to $\eta\pi^+\pi^-$. The full Monte-Carlo simulation is based on GEANT4 and BESIII design.

The final states of the examined channels include 5 photons or 5 photons together with multi-prong charged pions. In the event selection, all the candidate events are required to satisfy following common selection criteria for charged tracks and photons: 1). all the charged tracks are required to be within the polar angle region $|\cos\theta| < 0.93$ and have the point of the closest approach of the track to the beam axis be within 1 cm of the beam axis and within 5 cm from the center of the interaction region along the beam line; 2). the total net charge being zero is required; 3). each candidate photon is required to have an energy deposit in the EMC greater than 40 MeV, to be isolated from charged tracks by more than 20° in both $x-y$ and $r-z$ planes and the angle between two photons be greater than 7°. The η is reconstructed through the decays $\eta \to \gamma\gamma$ or $\eta \to \pi^+\pi^-\pi^0$, and the η' is reconstructed from $\eta' \to \eta\pi^+\pi^-$, $\eta \to \gamma\gamma$. A four-constraint (4C) energy-momentum conservation kinematic fit is subjected to the hypothesis of each decay modes. When the number of photons in an event exceeds the minimum, all combinations are tried, and the combination with the smallest χ^2 is retained.

a). $J/\psi \to \gamma\eta\eta$

In the simulation of $J/\psi \to \gamma\eta\eta$, we have included the possible processes, such as $J/\psi \to \gamma f_0(1500)$, $\gamma f_0(1710)$, $\gamma f_2(1910)$, $\gamma f_0(2100)$, $\gamma f_2(2100)$ and $\gamma f_J(2220)$. The input masses and widths of the resonances are listed in table 14.5.1, which are taken from PDG [67].

Table 14.1: The masses and widths of the input resonances

	$f_0(1500)$	$f_0(1710)$	$f_2(1910)$	$f_0(2100)$	$f_2(2150)$	$f_J(2220)$
Mass(MeV/c^2)	1507.0	1714.0	1915.0	2103.0	2156.0	2231.0
Width((MeV/c^2)	109.0	140.0	163.0	206.0	167.0	23.0

From PDG[67], the following branching fractions can be obtained as:

$$Br(J/\psi \to \gamma f_0(1500))Br(f_0(1500) \to \eta\eta) = 1.84 \times 10^{-5}$$

$$Br(J/\psi \to \gamma f_0(1710))Br(f_0(1710) \to \eta\eta) = 2.88 \times 10^{-5}.$$

The other branching ratios which are not listed in PDG are assumed to be:

$$Br(J/\psi \to \gamma f_2(1910))Br(f_2(1910) \to \eta\eta) \sim 1 \times 10^{-5}$$

$$Br(J/\psi \to \gamma f_0(2100))Br(f_0(2100) \to \eta\eta) \sim 1 \times 10^{-5}$$
$$Br(J/\psi \to \gamma f_2(2150))Br(f_2(2150) \to \eta\eta) \sim 1 \times 10^{-5}$$
$$Br(J/\psi \to \gamma f_J(2220))Br(f_J(2220) \to \eta\eta) \sim 1 \times 10^{-5}.$$

The $|M_{\gamma\gamma} - M_\eta| < 0.035$ GeV/c^2 or $|M_{\pi^+\pi^-\pi^0} - M_\eta| < 0.030$ GeV/c^2 are further required for $J/\psi \to \gamma\eta\eta$, $\eta \to \gamma\gamma$ or $\eta \to \pi^+\pi^-\pi^0$ respectively. Table 14.5.1 lists the mass resolutions and efficiencies in each resonance region for both cases after above selection criteria. For the case of $\eta \to \pi^+\pi^-\pi^0$, there are charged pions in the final states and therefore the mass resolution is better than that in the $\eta \to \gamma\gamma$ case where there are only neutral tracks. However, the selection efficiency is very low.

Table 14.2: Mass resolutions and efficiencies for $J/\psi \to \gamma\eta\eta$

process	η decay mode	mass resolution (MeV/c^2)	efficiency(%)
$J/\psi \to \gamma f_0(1500) \to \gamma\eta\eta$	$\eta \to \gamma\gamma$	18.4 ± 0.2	25.7
	$\eta \to \pi^+\pi^-\pi^0$	10.9 ± 0.4	1.56
$J/\psi \to \gamma f_0(1710) \to \gamma\eta\eta$	$\eta \to \gamma\gamma$	20.1 ± 0.2	25.9
	$\eta \to \pi^+\pi^-\pi^0$	9.7 ± 0.6	1.71
$J/\psi \to \gamma f_2(1910) \to \gamma\eta\eta$	$\eta \to \gamma\gamma$	21.3 ± 0.3	25.9
	$\eta \to \pi^+\pi^-\pi^0$	10.7 ± 0.5	1.73
$J/\psi \to \gamma f_0(2100) \to \gamma\eta\eta$	$\eta \to \gamma\gamma$	22.0 ± 0.2	26.5
	$\eta \to \pi^+\pi^-\pi^0$	10.5 ± 0.4	1.37
$J/\psi \to \gamma f_2(2150) \to \gamma\eta\eta$	$\eta \to \gamma\gamma$	22.2 ± 0.2	26.5
	$\eta \to \pi^+\pi^-\pi^0$	9.8 ± 0.4	1.44
$J/\psi \to \gamma f_J(2230) \to \gamma\eta\eta$	$\eta \to \gamma\gamma$	22.8 ± 0.3	26.7
	$\eta \to \pi^+\pi^-\pi^0$	11.0 ± 0.3	2.09

The main backgrounds of $J/\psi \to \gamma\eta\eta \to 5\gamma$ come from $J/\psi \to \omega\eta, \omega \to \gamma\pi^0$ and $J/\psi \to \gamma\eta, \eta \to \pi^0\pi^0\pi^0$. However, they accumulate in the high mass region of the $\eta\eta$ invariant mass spectrum.

Fig. 14.5.1 shows the $\eta\eta$ invariant mass spectrum for the incoherent sum of the generated signals and backgrounds in both η decaying into 2γ case when assuming the above mentioned branching fractions. The generated signal and background events are normarized to 10^{10} total J/ψ number.

For $J/\psi \to \gamma\eta\eta \to 5\gamma 2(\pi^+\pi^-)$, the main contamination to the $\eta\eta$ spectrum is from $J/\psi \to 2(\pi^+\pi^-)3\pi^0$. The $\eta\eta$ invariant mass spectrum for the incoherent sum of the generated signals and backgrounds in η decaying into $\pi^+\pi^-\pi^0$ case is shown in Fig. 14.5.1. The generated signal and background events are normarized to 10^{10} total J/ψ number.

The $f_J(2220)$ is significantly seen in either η decaying to $2gamma$ or $\pi^+\pi^-\pi^0$ cases. The Breit-Wigner fit to the $\eta\eta$ invariant mass spectra tells us that the statistical significance of $f_J(2220)$ is larger than 7σ in both cases.

If assuming the branching ratios of $J/\psi \to \gamma f_J(2220), f_J(2220) \to \eta\eta$ to be 0.5×10^{-5} and $J/\psi \to \gamma f_J(2150), f_J(2150) \to \eta\eta$ to be 1×10^{-5}, then the statistical significance of $f_J(2220)$ is larger than 7σ for $\eta \to 2\gamma$ and $\eta \to \pi^+\pi^-\pi^0$ The $\eta\eta$ invariant mass spectra

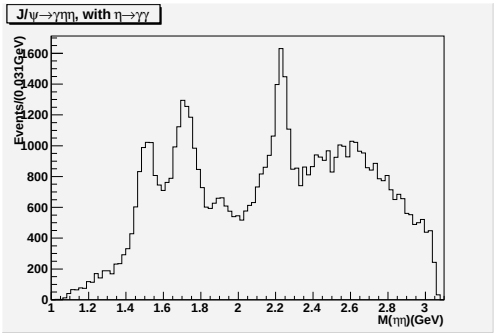

Figure 14.1: The $\eta\eta$ invariant mass spectrum in $J/\psi \to \gamma\eta\eta \to 5\gamma$. The generated signals and backgrounds are normarized to $10^{10} J/\psi$ events and are added incoherently.

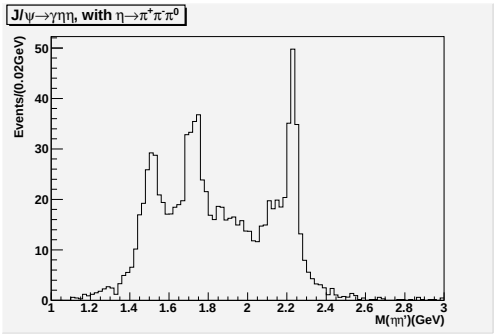

Figure 14.2: The $\eta\eta$ invariant mass spectrum in $J/\psi \to \gamma\eta\eta \to 5\gamma 2(\pi^+\pi^-)$. The generated signals and backgrounds are normarized to $10^{10} J/\psi$ events and are added incoherently.

are shown in Fig. 14.3 for $\eta \to 2\gamma$ and Fig. 14.4 for $\eta \to \pi^+\pi^-\pi^0$, respectively. If assuming the branching ratios of $J/\psi \to \gamma f_J(2220), f_J(2220) \to \eta\eta$ to be 0.5×10^{-6} and $J/\psi \to \gamma f_2(2150), f_2(2150) \to \eta\eta$ to be 3×10^{-5}, then the statistical significance of $f_J(2220)$ is larger than 7σ for $\eta \to 2\gamma$ and 4.3σ for $\eta \to \pi^+\pi^-\pi^0$ The $\eta\eta$ invariant mass spectra are shown in Figs. 14.5 and 14.6, respectively.

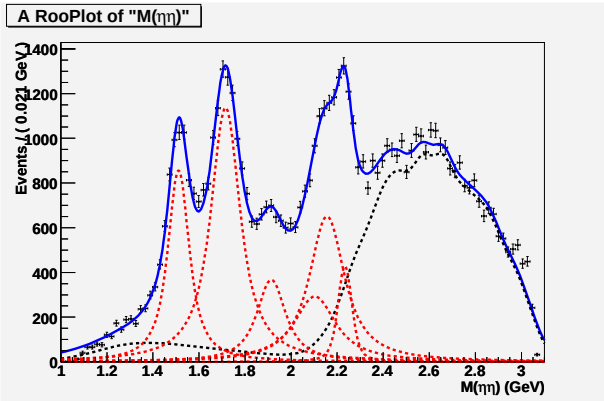

Figure 14.3: Fit result after adding all resonances together. ($J/\psi \to \gamma\eta\eta, \eta \to \gamma\gamma, \eta \to \gamma\gamma$ channel)

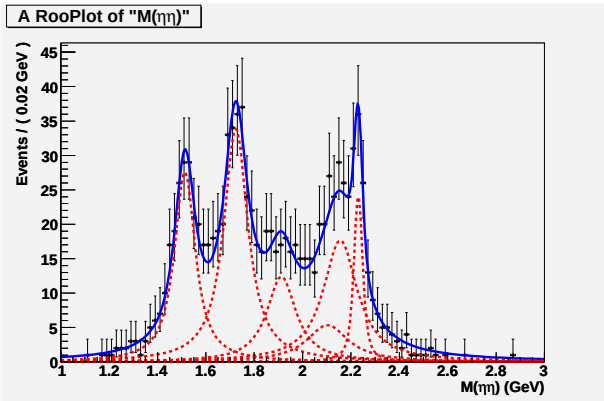

Figure 14.4: Fit result after adding all resonances together.($J/\psi \to \gamma\eta\eta, \eta \to \pi^+\pi^-\pi^0, \eta \to \pi^+\pi^-\pi^0$ channel)

Table 14.3 shows the comparison of the input resonances' masses, widths and branching ratios with those obtained from the fit, when the branching ratios of $J/\psi \to \gamma f_J(2220)$, $f_J(2220) \to \eta\eta$ is assumed to be 0.5×10^{-5} and $J/\psi \to \gamma f_2(2150)$, $f_2(2150) \to \eta\eta$ to be 1×10^{-5}. The fit results are consistent with the input values.

From the simulation, one can see that if the branching ratio of $f_J(2220)$ is big enough compared with its nearby resonance, e.g. $f_2(2150)$, the $f_J(2220)$ can be clearly seen in the mass spectrum, as shown in Figs. 14.5.1, 14.5.1, 14.3, 14.4. While if $f_J(2220) \to \eta\eta$ to be 0.5×10^{-6} and $J/\psi \to \gamma f_2(2150), f_2(2150) \to \eta\eta$ to be 3×10^{-5}, then the broad $f_2(2150)$ may mess up the observation of $f_J(2220)$, as are shown in Figs. 14.5 and 14.6.

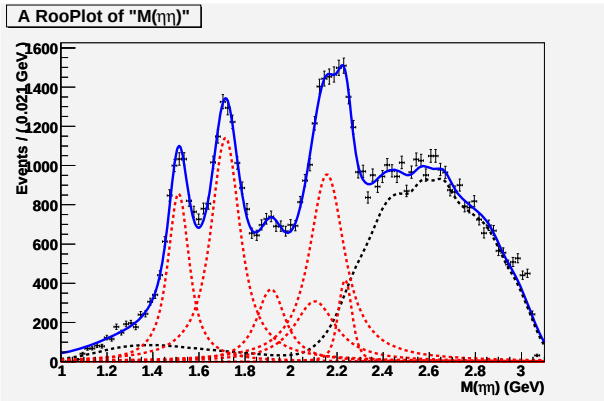

Figure 14.5: Fit result after adding all resonances together. ($J/\psi \to \gamma\eta\eta, \eta \to \gamma\gamma, \eta \to \gamma\gamma$ channel)

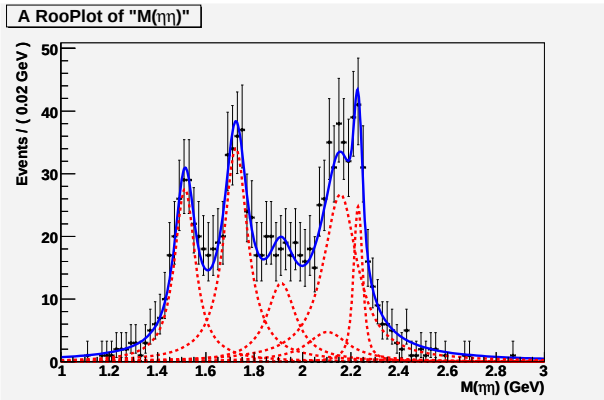

Figure 14.6: Fit result after adding all resonances together.($J/\psi \to \gamma\eta\eta, \eta \to \pi^+\pi^-\pi^0, \eta \to \pi^+\pi^-\pi^0$ channel)

	Mass(MeV)		Width(MeV)		Branching ratio($\times 10^{-7}$)	
	input	fit	input	fit	input	fit
$f_0(1500)$	1507.0	1512.8 ± 3.8	109.0	97.4 ± 8.2	14.43	14.67 ± 0.94
$f_0(1710)$	1714.0	1723.8 ± 3.5	140.0	117.2 ± 10.4	22.58	22.75 ± 1.47
$f_2(1910)$	1915.0	1912.2 ± 1.1	163.0	143.8 ± 8.2	7.8	7.98 ± 0.93
$f_0(2100)$	2103.0	fixed	206.0	fixed	7.8	6.59 ± 2.62
$f_2(2150)$	2156.0	fixed	167.0	fixed	7.8	7.98 ± 2.72
$f_J(2220)$	2231.1	2230.8 ± 2.7	23.0	27.6 ± 7.2	3.9	4.57 ± 0.71

Table 14.3: Input and output comparison of mass, width and branching ratio in the simulation. Here, the masses and widths of $f_0(2100)$ and $f_2(2150)$ are fixed. ($J/\psi \to \gamma\eta\eta, \eta \to \pi^+\pi^-\pi^0, \eta \to \pi^+\pi^-\pi^0$ channel)

In this case, a partial wave analysis (PWA), which determines the contribution of each component with certain spin-parity, will be needed to distinguish $f_J(2220)$ from $f_2(2150)$.

b). $J/\psi \to \gamma\eta\eta'$

According to some theoretical calculations, $f_J(2220)$ may have a big decay branching fraction to $\eta\eta'$. Therefore we performed a full Monte-Carlo simulation to investigate the sensitivity of the observation of $f_J(2220)$ in this decay. Here, only the case with the η' being reconstructed through $\eta' \to \eta\pi^+\pi^-$ and the η through $\eta \to \gamma\gamma$ is considered. Thus, there are 5 phtons and one $\pi^+\pi^-$ pairs in the final states. To reconstruct η and η', $|M_{\gamma\gamma} - M_\eta| < 0.035$ GeV/c^2 and $|M_{\pi^+\pi^-\eta} - M_{\eta'}| < 0.040$ GeV/c^2 are further required. The resonances included in the simulation are taken as the same as those in $J/\psi \to \gamma\eta\eta$ process. Table 14.5.1 lists the mass resolutions and efficiencies in each resonance region for $J/\psi \to \gamma\eta\eta'$.

Table 14.4: Mass resolutions and efficiencies for $J/\psi \to \gamma\eta\eta'$

process	mass resolution (MeV/c^2)	efficiency(%)
$J/\psi \to \gamma f_0(1500) \to \gamma\eta\eta'$	14.2 ± 0.4	4.5
$J/\psi \to \gamma f_0(1710) \to \gamma\eta\eta'$	16.7 ± 0.5	4.8
$J/\psi \to \gamma f_2(1910) \to \gamma\eta\eta'$	17.2 ± 0.4	4.9
$J/\psi \to \gamma f_0(2100) \to \gamma\eta\eta'$	18.6 ± 0.4	5.6
$J/\psi \to \gamma f_2(2150) \to \gamma\eta\eta'$	18.1 ± 0.4	5.7
$J/\psi \to \gamma f_J(2220) \to \gamma\eta\eta'$	19.0 ± 0.5	6.1

The main backgrounds of $J/\psi \to \gamma\eta\eta' \to 5\gamma\pi^+\pi^-$ may come from $J/\psi \to \omega\eta, \omega \to \pi^+\pi^-\pi^0$, $\eta \to \gamma\gamma$, $J/\psi \to \omega\pi^0$, $\omega \to \pi^+\pi^-\pi^0$ and $J/\psi \to \omega\eta', \omega \to \pi^+\pi^-\pi^0, \eta \to \gamma\gamma$.

According to PDG [67],

$$Br(J/\psi \to \gamma f_0(1500))Br(f_0(1500) \to \eta\eta') \sim 1.8 \times 10^{-5}$$

$$Br(J/\psi \to \gamma f_0(1710))Br(f_0(1710) \to \eta\eta') \sim 1.8 \times 10^{-5}$$

. The other branching ratios which are not listed in PDG are assumed as:

$$Br(J/\psi \to \gamma f_2(1910))Br(f_2(1910) \to \eta\eta') \sim 1 \times 10^{-5}$$

$$Br(J/\psi \to \gamma f_0(2100))Br(f_0(2100) \to \eta\eta') \sim 1 \times 10^{-5}$$

$$Br(J/\psi \to \gamma f_2(2150))Br(f_2(2150) \to \eta\eta') \sim 1 \times 10^{-5}$$

$$Br(J/\psi \to \gamma f_J(2220))Br(f_J(2220) \to \eta\eta') \sim 1 \times 10^{-5}.$$

Fig. 14.5.1 shows the $\eta\eta'$ invariant mass spectrum for the incoherent sum of the generated signals and backgrounds, with the assumption of the branching ratios listed above. The generated signal and background events are normarized to 10^{10} total J/ψ number. The background level in 2220 MeV/c^2 region is very low and the $f_J(2220)$ signal can be clearly seen.

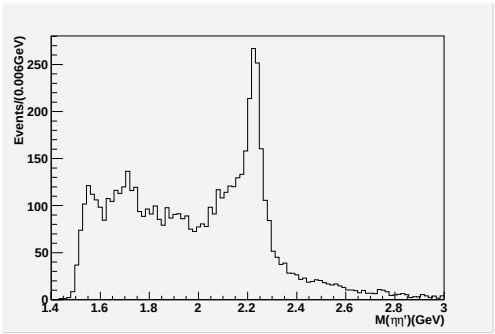

Figure 14.7: The $\eta\eta$ invariant mass spectrum in $J/\psi \to \gamma\eta\eta' \to 5\gamma\pi^+\pi^-$. The generated signals and backgrounds are normarized to $10^{10} J/\psi$ events and are added incoherently.

If assuming the branching ratios are:

$$Br(J/\psi \to \gamma f_2(2150))Br(f_2(2150) \to \eta\eta') \sim 3 \times 10^{-5}$$

$$Br(J/\psi \to \gamma f_J(2220))Br(f_J(2220) \to \eta\eta') \sim 1 \times 10^{-6},$$

the $\eta\eta'$ invariant mass spectrum for the incoherent sum of the generated signals and backgrounds is shown in Fig. 14.5.1.

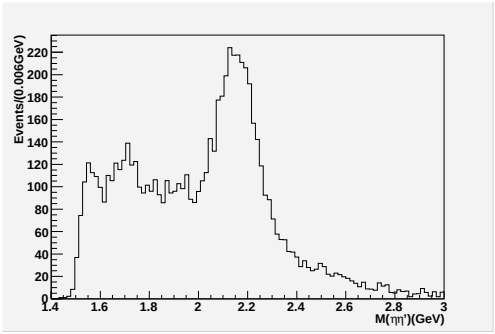

Figure 14.8: The $\eta\eta$ invariant mass spectrum in $J/\psi \to \gamma\eta\eta' \to 5\gamma\pi^+\pi^-$. The generated signals and backgrounds are normarized to $10^{10} J/\psi$ events and are added incoherently.

Using full Monte-Carlo simulation, the decays of $J/\psi \to \gamma\eta\eta$ and $\gamma\eta\eta'$ are studied based on the design of BESIII. From the simulation one can see that the sensitivity of searching for the tensor glueball $f_J(2220)$ at BESIII not only depends on the production rate of $f_J(2220)$ in J/ψ radiative decays and its decay branching ratios to the examined final states, but also depends on the production and decay branching ratios of the nearby resonances. For example, if the branching ratio of $f_J(2220)$ is big enough compared with that from its nearby resonance, e.g. $f_2(2150)$, the $f_J(2220)$ can be clearly seen in the mass spectrum. While if $f_J(2220) \to \eta\eta$ to be 0.5×10^{-6} and $J/\psi \to \gamma f_2(2150)$, $f_2(2150) \to \eta\eta$ to be 3×10^{-5}, then the broad $f_2(2150)$ may mess up the observation of $f_J(2220)$ from the mass spectrum. In this case, a partial wave analysis is needed. Therefore, to finally identify a glueball experimentally, the PWA is needed.

14.5.2 Inclusive photon spectrum

The inclusive photon spectrum from radiative J/ψ decays can be used to search for the new states, especially when these states have a relatively big production rate in radiative J/ψ decays. Glueballs are considered to be copiously produced in radiative J/ψ decays. Therefore the inclusive photon spectrum provides an ideal laboratory in searching for glueballs.

The Crystal Ball experiment once presented the inclusive photon spectrum from radiative J/ψ decays, where the η, η' and the peak at around 1440 MeV/c^2 are clearly seen [191]. However no clear signal for $J/\psi \to \gamma f_J(2220)$ is observed and no numerical upper limit on inclusive $f_J(2220)$ production in radiative J/ψ decays is set because of the uncertainties in the photon efficiency as a function of energy.

A Monte-Carlo study of inclusive radiative J/ψ decays at BESIII is performed. For the selected events, the charged tracks are required to be within the polar angle region $|\cos\theta| < 0.93$ and to come from the interaction point. The total net charge of the charged tracks being zero is required. The candidate photon is required to have an energy deposit in the EMC greater than 40 MeV and have the polar and azimuthal angle between the candidate photon and the charged track greater than 20°. In order to reject the photons from π^0 decays, it is required that the invariant mass spectrum of any photon pairs $m_{\gamma\gamma}$ should be greater than 0.2 GeV/c^2. Photon pairs with invariant mass between 0.5 and 0.7 GeV/c^2 are considered to be η candidates and are removed too.

Fig. 14.5.2 shows the Monte-Carlo study of inclusive radiative J/ψ decays at BESIII, based on a sample of xxxx J/ψ events. Here, the branching ratio of $J/\psi \to \gamma f_J(2220)$ is assumed to be $Br(J/\psi \to \gamma f_J(2220)) = 2.5 \times 10^{-3}$.

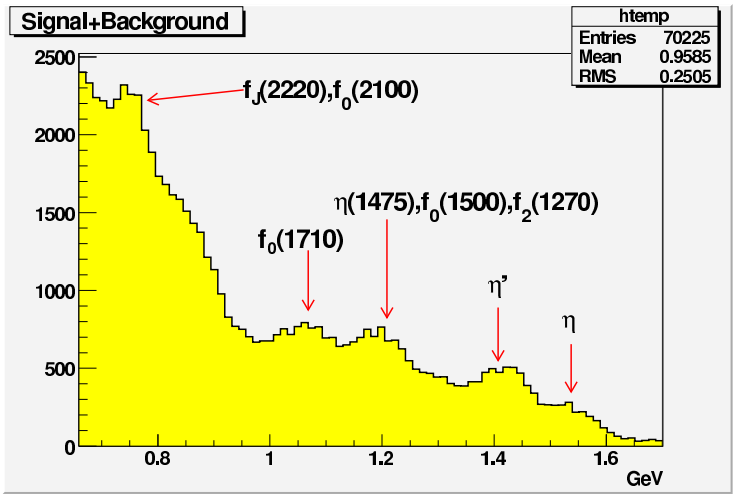

Figure 14.9: The inclusive photon spectrum in J/ψ radiative decays.

14.5.3 Simulation of $X(1835)$ in J/ψ radiative and hadronic decays

Recently, anomalous enhancements near threshold in the invariant mass spectra of $p\bar{p}$ and $pK\bar{\Lambda}$ pairs were observed in $J/\psi \to \gamma p\bar{p}$ [312] and $J/\psi \to pK\bar{\Lambda}$ [213]decays, respectively, by the BESII experiment. These surprising experimental observations stimulated many theoretical speculations. Later, $X(1835)$ was observed in $J/\psi \to \gamma X(1835)$, $(X(1835) \to \eta'\pi^+\pi^-)$ [214]. The mass and width of the X(1835) are not compatible with any known meson resonance. The production of $X(1835)$ in J/ψ hadronic decays, together with its production in J/ψ radiative decay provide improtant information in clarifying the nature of $X(1835)$.

Here, we analyze the production of $X(1835)$ in $J/\psi \to \gamma X(1835)$, $J/\psi \to \omega X(1835)$ and $J/\psi \to \phi X(1835)$, with $(X(1835) \to \eta'\pi^+\pi^-)$, based on BESIII design.

$J/\psi \to \gamma X(1835)$

In the simulation, we only focus on the decay mode of $X(1835) \to \eta'\pi^+\pi^-$ with $\eta' \to \eta\pi^+\pi^-$ and $\eta \to \gamma\gamma$. Therefore, the final states include $3\gamma 2(\pi^+\pi^-)$. The main backgrounds come from $J/\psi \to \eta'\pi^+\pi^-\pi^0$, $\omega\eta'$, $b_1\pi$ and $\phi f_2'$, in which $J/\psi \to \eta'\pi^+\pi^-\pi^0$ is the dominant background.

The good charged tracks are selected by requiring that they are within the polar angle region $|\cos\theta| < 0.93$ and within the vertex region of r_{xy}¡1 cm and $|z|$ <5 cm. The number of good charged tracks being 4 and the totle net charge being zero are required. Each candidate photon is required to have an energy deposit in the EMC greater than 40 MeV, to be isolated from charged tracks by more than 20° in both $x-y$ and $r-z$ planes and the angle between two photons be greater than 7°. Finally, the four charged tracks and photons in the event are kinematically fitted using four energy and momentum conservation constraints (4C) under the $J/\psi \to 3\gamma 2(\pi^+\pi^-)$ hypothesis. The fit is repeated using all permutations and the combination with the best fit to $3\gamma 2(\pi^+\pi^-)$ is retained. In order to further suppress the backgrounds and improve the mass resolution, a 5C kinematic fit is imposed to constrain the invariant mass of 2 photons to the η mass. The η' is selected by requiring $|m_{\eta\pi^+\pi^-} - m'_\eta| < 0.04$ GeV/c^2.

About 108553 $J/\psi \to \gamma X(1835)$, $X(1835) \to \eta'\pi^+\pi^-$, $\eta' \to \eta\pi^+\pi^-$ and $\eta \to \gamma\gamma$ signal events are generated and simulated to pass through above cut creteria. According to the branching ratio obtained in reference [214], the 108553 events are equivalent to 3×10^9 total J/ψ number. We also generated the background events from above mentioned background channels and normarized the background events to the same J/ψ total number.

The mass resolution for the $\eta'\pi^+\pi^-$ mass at 1835 MeV/c^2 is about 3 MeV/c^2 and the selection effficiency is 9

Fig. 14.5.3 shows the invariant mass spectrum of $\eta'\pi^+\pi^-$ for the $J/\psi \to \gamma X(1835)$, $X(1835) \to \eta'\pi^+\pi^-$ signal events and background events after above cut criteria. Compared with BESII results, the background level at BESIII is much lower.

The fit with a Breit-Wigner signal and a second order polynomial yields consistent mass, width and branching fractions of $X(1835)$ with the input parameters.

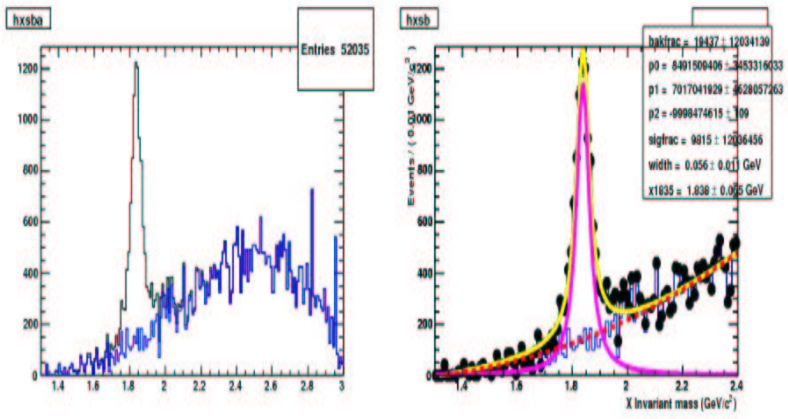

Figure 14.10: The $\eta'\pi^+\pi^-$ invariant mass for $J/\psi \to \gamma\eta'\pi^+\pi^-$. The generated signals and backgrounds are normarized to $3 \times 10^9 J/\psi$ events and are added incoherently.

$J/\psi \to \omega X(1835)$

The $J/\psi \to \omega X(1835)$ events are generated with ω decaying into $\pi^+\pi^-\pi^0$ and $X(1835)$ to $\eta'\pi^+\pi^-$. The final states include 4γ and $3(\pi^+\pi^-)$. The possible background channels are $J/\psi \to \omega K_s K\pi$, $KK4\pi$, $\phi 4\pi$, $\phi K^\star K$, $\omega K^\star K$, and $\pi^0 6\pi$.

The selection of the good charged tracks and photons are similar to those in $J/\psi \to \gamma X(1835)$. Here, the events with six good charged tracks and at least four good photon are retained. The 4C kinematic fit is applied to $J/\psi \to 4\gamma 3(\pi^+\pi^-)$.

After the final cut, the selection efficiency for $J/\psi \to \omega X(1835)$, $\omega \to \pi^+\pi^-\pi^0$, $X(1835) \to \eta'\pi^+\pi^-$, and $\eta' \to \eta\pi^+\pi^-$ is about 2.4

Fig. 14.5.3 shows the invariant mass spectrum of $\eta'\pi^+\pi^-$ for the $J/\psi \to \omega X(1835)$, $\omega \to \pi^+\pi^-\pi^0$, $X(1835) \to \eta'\pi^+\pi^-$ signal and background events.

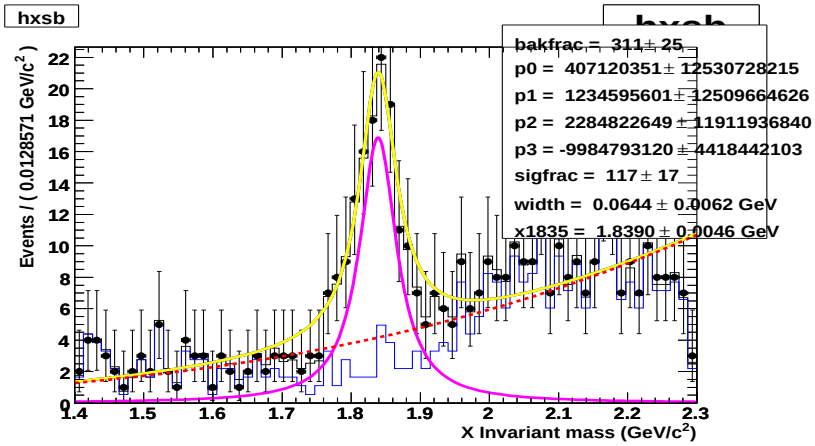

Figure 14.11: The $\eta'\pi^+\pi^-$ invariant mass for $J/\psi \to \omega\eta'\pi^+\pi^-$. The generated signals and backgrounds are normarized to $3 \times 10^9 J/\psi$ events and are added incoherently.

$J/\psi \to \phi X(1835)$

For $J/\psi \to \phi X(1835)$, $\phi \to K^+K^-$ and $\eta' \to \eta\pi^+\pi^-$, the final states include 2 photons, 2 kaons and 4 charged pions. The generated signal and background events after passing through the event selection are listed in table 14.5, where one can see that the background level is very low. The invariant mass spectrum of $\eta'\pi^+\pi^-$ for the $J/\psi \to \phi X(1835)$, $\phi \to K^+K^-$, $X(1835) \to \eta'\pi^+\pi^-$ for signal and background events are shown in Fig. 14.5.3, where the $X(1835)$ is almost free of the backgrounds. The selection effciency for the channel is about xxx and the mass resolution at 1835 MeV/c^2 is about xxx MeV/c^2.

Table 14.5: $J/\psi \to \phi X$ and its background channels

	$\phi X(1835)$	$KK4\pi$	$\omega K_s K\pi$	$\phi f_2'$	$\phi 4\pi$	$\omega K^\star K$	$\pi^0 6\pi$
Entries	169318	54798	89891	79874	45959	90866	127540
$N_{ch} = 6$	21272	15611	15025	1254	11405	26310	48359
$N_{\pi^+} = 2$ $N_{\pi^-} = 2$	18024	13021	1036	1063	9266	2224	516
$N_{K^+} = 1$ $N_{K^-} = 1$	17492	12409	184	1031	8972	175	9
Vertex	5434	3816	18	464	2671	91	8
4C-fit	2369	206	2	42	156	0	0
5C-fit	1914	0	0	3	1	0	0
Scale	1914	0	0	8	86	0	0

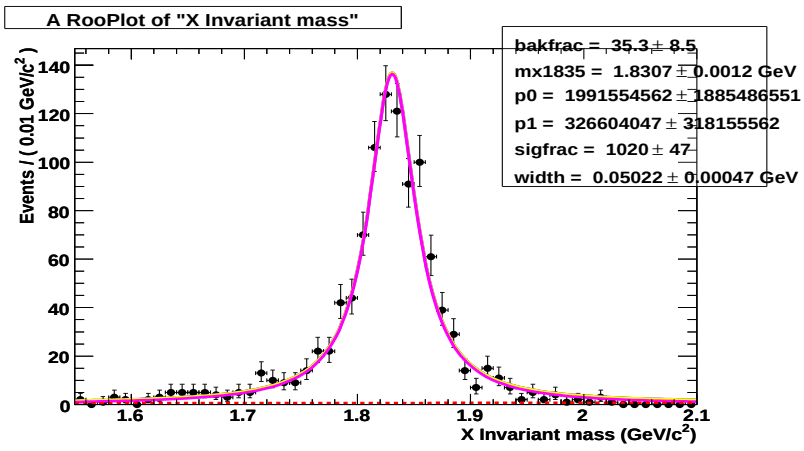

Figure 14.12: The $\eta'\pi^+\pi^-$ invariant mass for $J/\psi \to \phi\eta'\pi^+\pi^-$. The generated signals and backgrounds are normarized to $3 \times 10^9 J/\psi$ events and are added incoherently.

1^{-+} exotic state in $J/\psi \to \rho\eta\pi^0$

The decays of $J/\psi \to \rho\eta\pi^0$ are studied to search for 1^{-+} exotic state. Totally $6\times10^9 J/\psi \to \rho\eta\pi^0$ Monte-Carlo events are generated from a fast simulation of BESIII detector. In the simulation, the possible $a_2(1320), 1^{-+}X(1390), a_0(980)$ and $1^{-+}X(2300)$, resonances, as well as the background events are included. Fig. 14.5.3 shows the invariant mass spectrum of $\eta\pi^0$ for the selected events, where the included $a_0(980)$ and $1^{-+}X(2300)$ are clearly seen, while $a_2(1320), 1^{-+}X(1390)$ are merged together because of the similar masses and broad widths. A partial wave analysis (PWA) is applied to this channel. After PWA, the $a_2(1320)$ and $1^{-+}X(1390)$ can be well distinguished, because the angular distributions of $a_2(1320)$ and $1^{-+}X(1390)$ are very different due to their different spin-parities. Their contributions and the mass and width scan curves are plotted in Fig. 14.14 and Fig. 14.15. The minimum in the scan curve gives the mass or width of this resonance.

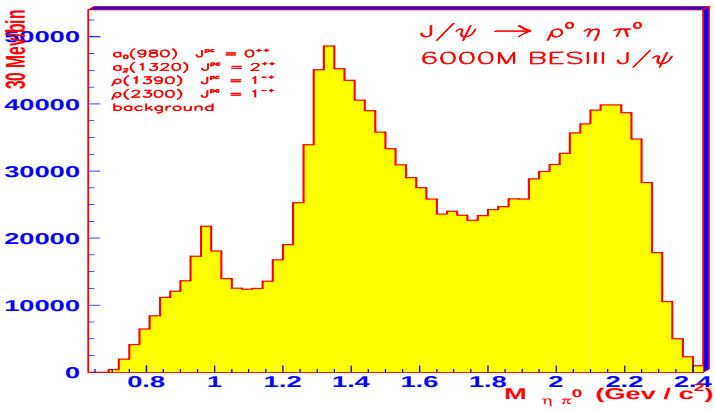

Figure 14.13: The $\eta\pi^0$ invariant mass spectrum for $J/\psi \to \rho\eta\pi^0$. The generated signals and backgrounds are normarized to $6 \times 10^9 J/\psi$ events and are added incoherently.

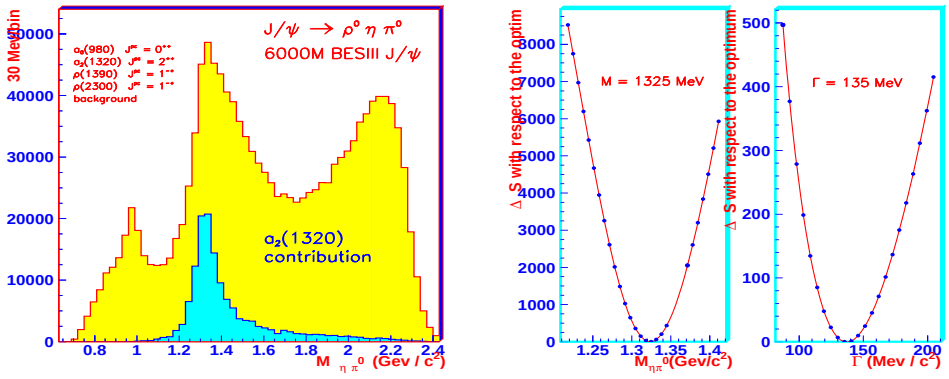

Figure 14.14: Left: Invariant mass spectrum of $\eta\pi^0$. The blue shaded histogram shows the contribution from $a_2(1320)$. Right: The scan curves for the mass and width of $a_2(1320)$.

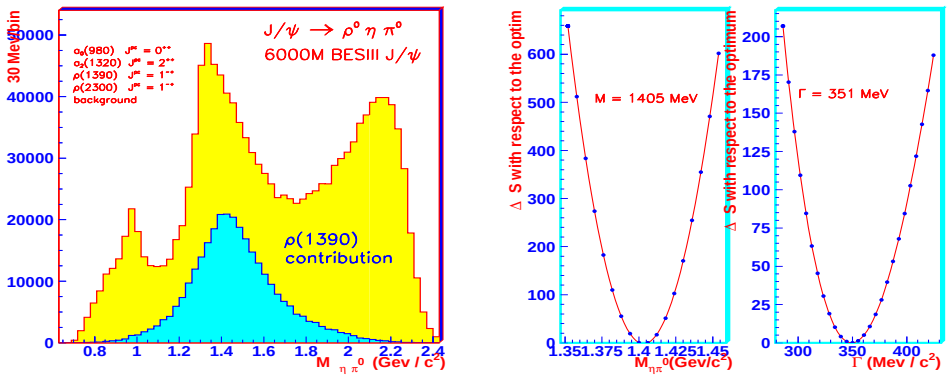

Figure 14.15: Left: Invariant mass spectrum of $\eta\pi^0$. The blue shaded histogram shows the contribution from $1^{-+}(1390)$. Right: The scan curves for the mass and width of $1^{-+}(1390)$.

From this Monte Carlo study, one can see that the partial wave analysis is able to separate components which have different spin-parities but at the same mass, when the statistics is enough and the resolution of the detector is good. With a large statistics, it is also possible to measure the phase motion and so give a more convincing evidence for the existence of a resonance.

Chapter 15

Two-photon physics

[1]

15.1 Introduction

The two-photon processes were always very interesting for physicists due to fascinating opportunity to study conversion of pure photons to matter (leptons, hadrons). Original calculation of such processes has been developed in work [272], and the first detailed consideration of possible application of these process was done by two independent groups [273, 274].

The two-gamma process can be obtained on electron-positron or electron-electron colliders:

$$e^{\pm} + e^{-} \to e^{\pm} + e^{-} + \gamma + \gamma \to e^{\pm} + e^{-} + X$$

where X describes any final state. Note, that intermediate photons here can be not only virtual, but almost real, which gives the possibility to study processes of type $\gamma\gamma \to X$.

The very interesting feature of this process is that its cross-section slowly rises with the energy and becomes comparable with annihilation channel at $\sqrt{s}/2 \approx 1$ GeV, see fig. 15.1, [275]. For example, the cross section of $\pi^+\pi^-$ pair production in annihilation channel is proportional to the α^2/q^2, where q is the virtuality of intermediate photon, and though the two photon process has the additional factor α^2 it has the logarithmical reinforcement and increases with the energies of initial particles logarithmically [276]:

$$\sigma_{e^{\pm}e^{-}\to e^{\pm}e^{-}h} = \frac{\alpha^4}{18\pi^2 m_\pi^2} \ln\frac{s m_\rho^2}{m_e^2 m_\pi^2} \ln\frac{s m_\rho^6}{m_e^6 m_\pi^2} \left(\ln\frac{s}{m_\pi^2}\right)^2$$

The reason is that the cross-section of two-photon process has an enhancement when the virtualities of intermediate photons come to zero (see fig. 15.2) They are almost real and from kinematical restrictions are emitted along initial particle directions (fig. 15.3). As a consequence one can split the cross-section of two gamma process in two different parts: one part is connected with emission of two real photon by initial particles and the other part is final state production by two photons:

$$\sigma_{e^{\pm}+e^{-}\to e^{\pm}+e^{-}X} = \sigma_{e^{\pm}+e^{-}\to e^{\pm}+e^{-}\gamma\gamma} \quad \sigma_{\gamma\gamma\to X}$$

[1] By V. Bytev and A. Zhemchugov

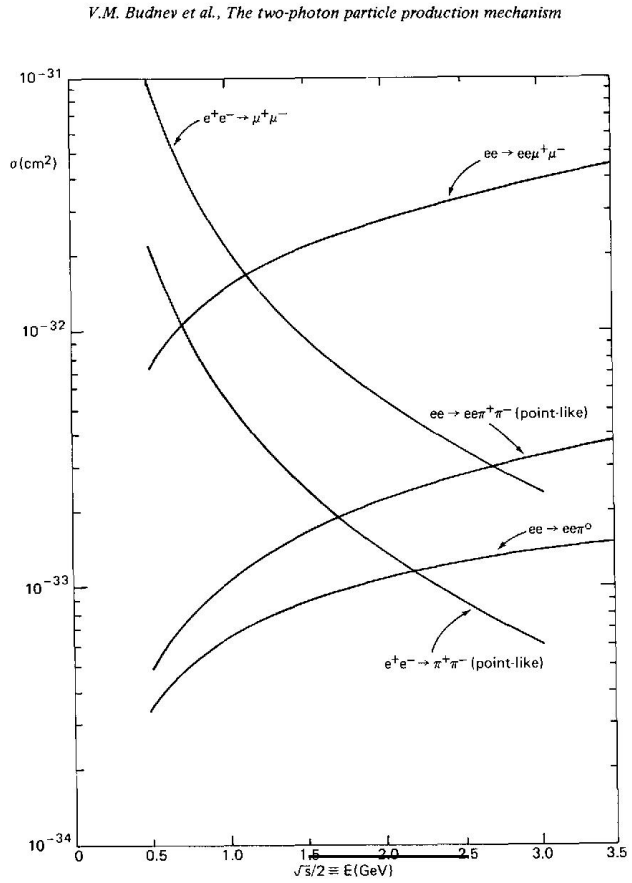

Figure 15.1: The values of cross-section of pion pair production.

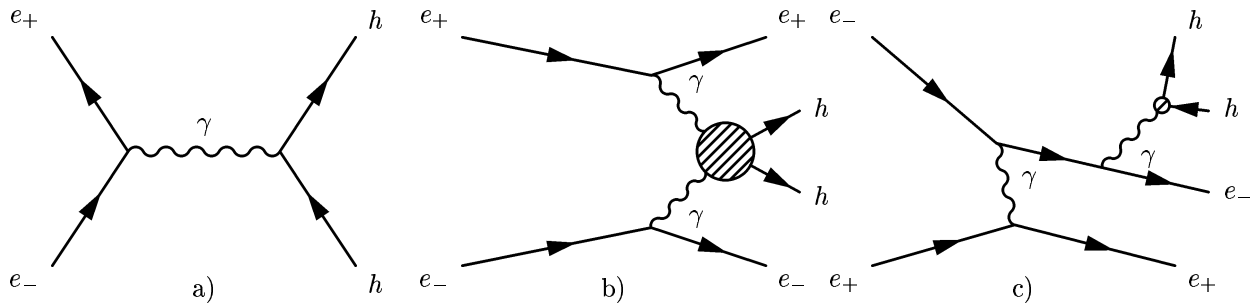

Figure 15.2: Feynman diagrams for hadron pair production. The contribution from diagram b) enhanced by poles of intermediate photons.

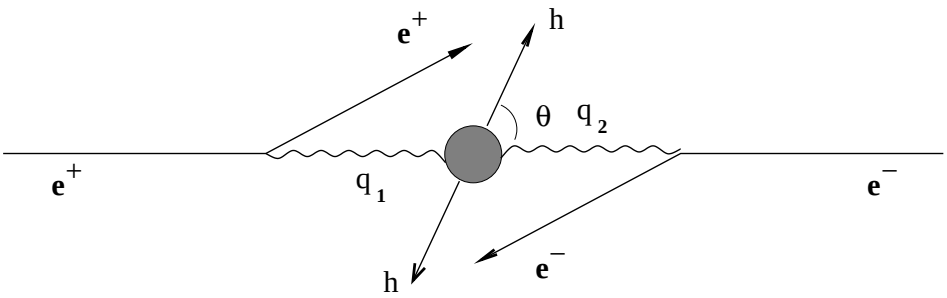

Figure 15.3: Kinematics of two-photon process.

Here, the first part can be easily calculated exactly in frames of QED. So, from experiment one can directly measure cross-section of lepton or hadron production by two photons. This approximation for cross-section is called Equivalent Photon Approximation (EPA).

Of course, events with big virtuality of an intermediate photon are present as well, but they are much more rare, since there is no q^2 pole enhancement. They are called "single-tag" (one photon with nonzero virtuality q^2) and can be used for study resonance production by off-shell photons.

Not any final state can be obtained in two-photon processes. Since two photons have even C parity only states with C=+1 are possible.

15.2 Experimental status of two-photon processes

For the theoretical reviews the original papers are [273, 274], recent can be found in the paper [277]. Last experimental summary one can find in paper [278].

The lepton production in two-photon processes can readily be calculated in frames of QED. It does not make any interest for new physics, however it can be considered as precise test of QED predictions at large c.m.s. energies, where the radiative corrections become essential. At the BESIII energies, lepton production by two photons is not interesting, and should be taken into account as a significant contribution to the background only.

Much more interesting are the two photon processes with hadron final state. In the last years a lot of experiments with single-tag photon were made, mainly to measure hadron structure function F_2^γ at the energies much higher than BESIII ones. Also at high energies $\gamma\gamma \to jet$ or $\gamma\gamma \to 2jet$ processes have been studied, p_T distributions of inclusive π production and also cross-sections of charm and beauty production in two-photon interaction have been measured.

In the energy range reachable by BESIII hadron production by two photons have been studied by several experiments.

At the MARK-II experiment [279] the $\pi^+\pi^-$ pair production was observed with the invariant mass of pair $0.35 - 1.6$ Gev and data on $f_2(1270)$ and $f_0(1010)$ were obtained. Also they measured the width of decay $\eta'(958)$ to the photons [280].

The Crystal Ball collaboration considered the process of $\pi^0\pi^0$ [281] from threshold up to the 2 Gev of invariant pair mass. They measured width of $f_2(1270)$ and $f_0(975)$.

At the invariant mass in the range 1.5 and 5.0 Gev the CLEO II collaboration detected pairs of charged pion and kaon. Their data show the 40% discrepancy from LO QCD

predictions [188].

Collaboration CELLO measured $\pi^+\pi^-$ pair production at the energy range $0.75 - 1.9$ Gev [283].

The Belle collaboration reports on $f0(980)$ observation in $\gamma\gamma \to \pi^+\pi^-$ channel [284] but form of resonance is distinct from Breit-Wigner one and the width is much lower than the PDG value. The authors of the paper [285] argue that this effect can be explained by destructive interference with background.

Neutral pion pair production by two photons has been measured by the Crystal Ball collaboration [281]. This is the only measurement available now. The process of $\gamma\gamma \to \pi^0\pi^0$ is the very crucial test of ChPT [286]. The key feature is that this process appears only in one-loop calculation in ChPT and some theoretical predictions contradict with the Crystall Ball data. Also it can be used for 2-loop contribution estimation and determination of higher-order renormalization constants. Due to very high luminosity of BEPCII it should be possible to obtain new and more precise data of neutral pion pair production on BESIII.

In the intermediate region $0.5 < W < 2$ GeV in exclusive hadronic processes one can measure resonant structures. In $\pi\pi$ final state the only clear resonance is $f_2(1270)$. The scalar resonances like $f_0(400 - 1200)$, $f0(980)$, $f0(1370)$, $f0(1500)$, $f0(1710)$ are not well established and some authors doubt in its existence [287]. On BESIII experiment higher statistics can be obtained at the same anglular acceptance as at (for example) Belle experiment. By combining data from different channels $\pi^0\pi^0$, $\pi^+\pi^-$ it will be possible to separate the contribution of states with definite spin into total cross-section. The accurate measurement of this channel can provide the possibility of glueballs observation (or non-observation at some level of accuracy).

Search for events with large hadron multiplicity in final state is also interesting. As an example, one can search for the three pions with invariant mass below 2 Gev. The ARGUS collaboration obtained data which revealed clear a2(1370) resonance but did not observe pseudoscalar resonance $\pi_2(1300)$ and any significant enhancement in the invariant mass of pions at $\pi_2(1670)$ [288]. However, this measurementcontradicts to the data from the Crystal Ball [289] and CELLO [290] experiments. BESIII can possibly shed light on this puzzle.

Single-tag data (when one of the photons is considerably off-shell) can be possibly measured by BESIII, however the cross section is much lower than for two photon processes with real photons. Having measured this, one can estimate hadronic structure function at small q^2.

The total cross-section can be possibly measured by BESIII as well, but this strongly depends on the angular acceptance of the detector.

15.3 Measurement of two-photon processes at the BESIII

to be delivered by A.Z.

Bibliography

[1] A. De Rujula, H. Georgi and S.L. Glashow, Phys. Rev. D **12**, 147 (1975).

[2] N. Isgur and G. Karl, Phys. Lett. **72B**, 109 (1977); N. Isgur and G. Karl, Phys. Rev. D**18**, 4187 (1978); *ibid* D 19, 2653 (1979); Erratum **23**, 817 (1981); *ibid* D**20**, 1191 (1979).

[3] K.-T. Chao, N. Isgur and G. Karl, Phys. Rev. D **23**, 155 (1981).

[4] F.E. Close, *Introduction to quarks and partons* (Academic Press 1978).

[5] J. Carlson, J.B. Kogut and V.B. Pandharipande, Phys. Rev. D **28**, 2807 (1983).

[6] R. Sartor and F. Stancu, Phys. Rev. D **31**, 128 (1985); *ibid.* **33**, 727 (1986); F. Stancu and Stassart, Phys. Rev. D **41**, 916 (1990); Phys. Lett. B **269**, 243 (1991).

[7] W.H. Blask *et al.*, Z. Phys. A **337**, 327 (1990); E.V. Shuryak and J.L. Rosner, Phys. Lett. B **218**, 72 (1989); A. Dorokhov and N.I. Kochelev, Sov. J. Nucl. Phys. **52**, 135 (1990); D. Klabucar, Phys. Rev. D **49**, 1506 (1994).

[8] L. Y. Glozman and D. O. Riska, Phys. Rept. **268**, 263 (1996).

[9] M. Anselmino, E. Predazzi, S. Ekelin, S. Fredriksson, and D.B. Lichtenberg, Rev. Mod. Phys. **65**, 1199 (1993).

[10] C.E. Carlson *et al.*, Phys. Lett. B **438**, 327 (1998); Phys. Rev. D **59**, 114008 (1999).

[11] R.P. Feynman, M. Kislinger, and F. Ravndal, Phys. Rev. D **3**, 2706 (1971); F. Ravndal, Phys. Rev. D **4**, 1466 (1971); L.A. Copley, G. Karl, and E. Obryk, Phys. Rev. D **4**, 2844 (1971); R.G. Lipes, Phys. Rev. D **5**, 2849 (1972); S. Godfrey and N. Isgur, Phys. Rev. D **32**, 189 (1985); S. Capstick and N. Isgur, Phys. Rev. D **34**, 2809 (1986); F.E. Close and Z.-P. Li, Phys. Rev. D **42**, 2194 (1990); Z.-P. Li and F.E. Close, Phys. Rev. D **42**, 2207 (1990); S. Capstick and B.D. Keister, Phys. Rev. D **51**, 3598 (1995).

[12] S. Capstick and W. Roberts, Prog. Part. Nucl. Phys. **45**, 5241 (2000).

[13] Y. Nambu and G. Jona-Lasinio, Phys. Rev. **122**(1961)345;
K. C. Chou, JETP 12(1961)492.

[14] S. Coleman, *Aspects of Symmetry*, Cambridge University Press 1985.

[15] S. Eidelman et al. (The Particle Data Group), Phys. Lett. **B592**(2004)1.

[16] L. S. Brown and R. N. Cahn, Phys. Rev. Lett. **35** (1975)1.

[17] A theoretical review on linear σ model can be found in, B. W. Lee, *Chiral Dynamics*.

[18] See for example, C. S. Gao and J. Y. Zeng, *Lectures on Particle Physics and Nuclear Physics*, High Education Press, Beijing, 1990(in chinese).

[19] N. N. Achasov, A. V. Kiselev and G. N. Shestakov, Talk given at e+ e- Collisions from phi to psi, Novosibirsk, Russia, 27 Feb - 2 Mar 2006; hep-ph/0605126.

[20] N. A. Törnqvist, Zeit. Phys. **C68**(1995)647.

[21] R. Kaminski, L. Leśniak and J.-P. Maillet, Phys. Rev. **D50**(1994)3154;
N. N. Achasov and G. N. Shestakov, Phys. Rev. **D49**(1994)5779;
M. Ishida, S. Ishida and T. Ishida, Prog. Theor. Phys. **99**(1998)1031.

[22] J. Gasser and H. Leutwyler, Annals Phys.158:142,1984.

[23] Z. G. Xiao and H. Q. Zheng, Nucl. Phys. **A695**(2001)273.

[24] E. M. Aitala et al., Phys. Rev. Lett. **86**(2001)770.

[25] M. Ablikim et al. (The BESII Collaboration), Phys. Lett. **B598**(2004)149; J. Z. Bai et al., High Energy Phys. Nucl. Phys. **28**(2004)215.

[26] Z. Y. Zhou et. al., JHEP0502(2005)43.

[27] I. Caprini, G. Colangelo and H. Leutwyler, Phys. Rev. Lett. **96**(2006)132001.

[28] L. Y. Xiao, H. Q. Zheng, Z. Y. Zhou, *Lightest scalars as chiral partners of the Nambu-Goldstone bosons* Invited talk given at 13th International Conference in QCD (QCD 06), Montpellier, France, 3-7 Jul 2006. hep-ph/0609009.

[29] H. Q. Zheng *et al.*, Nucl. Phys. **A733**(2004)235.

[30] P. Minkowski, W. Ochs, *Talk given at Workshop on Hadron Spectroscopy (WHS 99), Rome, Italy, 8-12 Mar 1999. In *Frascati 1999, Hadron spectroscopy* 245-255*; hep-ph/9905250.

[31] B.S. Zou and D.V. Bugg, Phys. Rev. D48 (1993) R3948.

[32] See for example, N. N. Achasov and A. V. Kiselev, Phys. Rev. **D73**(2006)054029;
L. O. Arantes and M. R. Robilotta, Phys. Rev. **D73**(2006)034028.

[33] M. Ablikim et al. (The BESII Collaboration), Phys. Lett. **B**, to appear (hep-ex/0610023).

[34] K. M. Watson, Phys. Rev. **88** (1952) 1163.

[35] J. M. Link *et al.*, (The FOCUS Collaboration), Phys. Lett. **B535** (2002)43.

[36] J. M. Link *et al.*, (The FOCUS Collaboration), Phys.Lett. B621 (2005)72.

[37] L. Edera, M. R. Pennington Phys. Lett. **B623**(2005)55.

[38] E. M. Aitala et al., Phys. Rev. Lett. **89**(2002)121801.

[39] B. Meadows, hep-ex/0506040; to appear in proceedings of Moriond QCD 2005, La Thuile, March 2005.

[40] D. Aston et al. (LASS Collaboration), Nucl. Phys. **B296**(1988)493.

[41] I. Caprini, Phys. Lett. **B638**(2006)468 and reference therein; A. V. Anisovich and V. V. Anisovich, Phys. Lett. **B**345(1995)321.

[42] D. V. Bugg, hep-ph/0608081.

[43] B. Ananthanarayan, I. Caprini, G. Colangelo, J. Gasser, H. Leutwyler, Phys. Lett. **B602**(2004)218.

[44] H. Leutwyler, talk given at QCHS VII, Ponta Delgada, Azores, Portugal, September 2 - 7, 2006.

[45] T. A. Lahde, Ulf-G. Meissner, Phys. Rev. **D74**(2006)034021.

[46] E. M. Aitala et al. (E791 Collaboration), Phys. Rev. Lett. **89**, 121801(2002).

[47] M. Ablikim et al. (BES Collaboration), Phys. Lett. **B633**(2006)681.

[48] Z. Y. Zhou and H. Q. Zheng, Nucl. Phys. **A755**(2006)212.

[49] S. Descotes-Genon, B. Moussallam, hep-ph/0607133.

[50] N. A. Törnqvist, Talk given at International Europhysics Conference on High-Energy Physics (EPS-HEP 99), Tampere, Finland, 15-21 Jul 1999; hep-ph/9910443.

[51] R. L. Jaffe, Phys. Rev. **D15**(1977)267;
M. G. Alford and R. L. Jaffe, Nucl. Phys. **B578**(2000)367.

[52] G. 't Hooft, Phys. Rep. **142**(1986)357.

[53] N. A. Tornqvist, hep-ph/0606041;
Y. B. Dai and Y. L. Wu, Eur. Phys. J. **C39**(2005)S1;
T. Schafer, Phys. Rev. D68(2003)114017;
M. Napsuciale, S. Rodriguez, Int. J. Mod. Phys. **A16**(2001)3011.

[54] M. R. Pennington, Phys. Rev. Lett. 97, 011601 (2006).

[55] S. Narison, Phys. Rev. **D73**(2006)114024.

[56] T. Kunihiro, talk given at "New Forntiers in QCD: exotic hadrons and hadronic matter", November 20 – December 8, 2006, Kyoto, Japan. http://www2.yukawa.kyoto-u.ac.jp/ ykis06/

[57] F. E. Close and N. A. Tornqvist, J. Phys. G28(2002)R249.

[58] E. van Beveren, D. V. Bugg, F. Kleefeld and G. Rupp, hep-ph/0606022.

[59] J. A. Oller, E. Oset, J. R. Pelaez, Phys. Rev. **D59**(1999)074001, Erratum-ibid. **D60**(1999)099906; J. Peláez, Phys. Rev. Lett. **92**(2004)102001.

[60] V. V. Anisovich, D. Bugg, A. V. Sarentsev and B. S. Zou, Phys. Rev. **D50**(1994)972.

[61] A. Aloisio et al., Phys. Lett. **B537**(2002)21; A. Aloisio et al., Phys. Lett. **B536**(2002)209.

[62] L. Maiani, F. Piccinini, A. D. Polosa and V. Riquer, Phys. Rev. Lett. **93**(2004)212002.

[63] D. V. Bugg, Eur. Phys. J. **C47**(2006)57.

[64] S. Godfrey and J. Napolitano, Rev. Mod. Phys. **71**, 1411 (1999).

[65] F. E. Close and N. A. Tornqvist, J. Phys. G **28**, R249 (2002)

[66] C. Amsler and N.A. Törnqvist, Phys. Rep. **389**, 61 (2004).

[67] W.-M. Yao *et al.* (Particle Data Group), J. Phys. G: Nucl. Part. Phys. **33**, 1(2006).

[68] C.N. Yang, Phys. Rev. **77**, 242 (1950).

[69] C.E. Carlson, T.H. Hansson and C. Peterson, Phys. Rev. D **30**, 1594 (1984).

[70] J.F. Donoghue, K. Johnson and B. Li, Phys. Lett. B **99**, 416 (1981).

[71] M. Chanowitz and S. Sharpe, Nucl. Phys. B **222**, 211 (1983).

[72] J.M. Cornwall and A. Soni, Phys. Lett. B **120**, 431 (1983).

[73] N. Isgur and J. Paton, Phys. Lett. **124B**, 247 (1983); Phys. Rev. D **31**, 2910 (1985).

[74] V.A. Novikov, M.A. Shifman, and V.I. Zakharov, Nucl. Phys. B**165**, 67 (1980).

[75] M.A. Shifman, A.I. Vainshtein, and V.I. Zakharov, Nucl. Phys. B**147**, 385 (1979)

[76] J.L. Latorre *et al.*, Phys. Lett. **147B**, 169 (1984).

[77] S. Narison, Phys. Lett. B **509**, 312 (1998).

[78] L. S. Kisslinger, J. Gardner and C. Vanderstraeten, Phys. Lett. B **410**, 1 (1997).

[79] F. Giacosa, T. Gutsche, V. E. Lyubovitskij and A. Faessler, Phys. Rev. D **72**, 094006 (2005) [arXiv:hep-ph/0509247].

[80] T. Huang, H. Jin, and A. Zhang, Phys. Rev. D **59**, 034026 (1999).

[81] K. Ishikawa, M. Teper and G. Schierholz, Phys. Lett. **116B**, 429 (1982); C. Michael and I. Teasdale, Nucl. Phys. B **215**, 433 (1983); H.W. Hamber and V.M. Heller, Phys. Rev. D 29, 928 (1984).

[82] P. De Forcrand *et al.*, Phys. Lett. **B152**, 107 (1985); A. Patel *et al.*, Phys. Rev. Lett. **57**, 1288 (1986).

[83] C. Michael and M. Teper, Nucl. Phys. **B314**, 347 (1989).

[84] C. Morningstar and M. Peardon, Phys. Rev. D **56**, 4043 (1997); Phys. Rev. **D60**, 034509 (1999).

[85] G. Bali *et al.*, UKQCD Collaboration, Phys. Lett. **B 309**, 378 (1993).

[86] Y. Chen *et al.*, Phys. Rev. D **73**, 014516 (2006).

[87] A. Irving *et al*, PoS(Lat2005)027

[88] A. Abele *et al.*, [Crystal Barrel Collaboration], Phys. Lett. B**385**, 425 (1996).

[89] D. Barberis *et al.*, [WA102 Collaboration], Phys. Lett. B **479**, 59 (2000).

[90] M. Ablikim *et al.* [BES Collaboration], Phys. Lett. B **607**, 243 (2005) [arXiv:hep-ex/0411001].

[91] M. Ablikim *et al.* [BES Collaboration], Phys. Lett. B **603**, 138 (2004) [arXiv:hep-ex/0409007].

[92] M. Ablikim *et al.* [BES Collaboration], Phys. Rev. Lett., **96**, 162002 (2006) [arXiv:hep-ex/0602031].

[93] R.L. Jaffe, Phys. Rev. D**15**, 267 (1977); *ibid*, D**15**, 281 (1977).

[94] R.L. Jaffe and F.E. Low, Phys. Rev. D**19**, 2105 (1979).

[95] D.V. Bugg, Phys. Rept. **397**, 257 (2004).

[96] F.E. Close and C. Amsler, Phys. Lett. B **353**, 385 (1995); Phys. Rev. **D53**, 295 (1996).

[97] F.E. Close and A. Kirk, Phys. Lett. B **483**, 345 (2000).

[98] F.E. Close and Q. Zhao, Phys. Rev. D **71**, 094022 (2005).

[99] W. Lee and D. Weingarten, Nucl. Phys. B, Proc. Suppl.**53**, 236 (1997); Phys. Rev. D **61**, 014015 (1999).

[100] H. Y. Cheng, C. K. Chua and K. F. Liu, Phys. Rev. D **74**, 094005 (2006) [arXiv:hep-ph/0607206].

[101] D. M. Li, H. Yu and Q. X. Shen, Commun. Theor. Phys. **34**, 507 (2000); Eur. Phys. J. C **19**, 529 (2001).

[102] X. G. He, X. Q. Li, X. Liu and X. Q. Zeng, Phys. Rev. D **73**, 114026 (2006)

[103] F.E. Close, G.R. Farrar, and Z. Li, Phys. Rev. D **55**, 5749 (1997).

[104] S.J. Brodsky, A.S. Goldhaber and J. Lee, Phys. Rev. Lett. **91**, 112001 (2003).

[105] M. Chanowitz, in *Proceeding of the VI International Workshop on Photon-Photon Collisions, 1984*, edited by R. Lander (World Scientific, Singapore, 1985), pp4.

[106] M.B. Cakir and G.R. Farrar, Phys. Rev. D **50**, 3268 (1994).

[107] C. E. Carlson, J. J. Coyne, P. M. Fishbane, F. Gross and S. Meshkov, Phys. Lett. B **99**, 353 (1981).

[108] M. Chanowitz, Phys. Rev. Lett. **95**, 172001 (2005) [arXiv:hep-ph/0506125].

[109] K. T. Chao, X. G. He and J. P. Ma, arXiv:hep-ph/0512327.

[110] Z. F. Zhang and H. Y. Jin, arXiv:hep-ph/0511252.

[111] S. Okubo, Phys. Lett. **5**, 1975 (1963); G. Zweig, in *Development in the Quark Theory of Hadrons*, edited by D.B. Lichtenberg and S.P. Rosen (Hadronic Press, Massachusetts, 1980); J. Iizuka, Prog. Theor. Phys. Suppl. **37**, 38 (1966).

[112] P. Geiger and N. Isgur, Phys. Rev. D **47**, 5050 (1993).

[113] H.J. Lipkin and B.S. Zou, Phys. Rev. D **53**, 6693 (1996).

[114] X.Q. Li, D.V. Bugg, and B.S. Zou, Phys. Rev. D **55**, 1421 (1997).

[115] Q. Zhao, B. S. Zou and Z. B. Ma, Phys. Lett. B **631**, 22 (2005) [arXiv:hep-ph/0508088].

[116] Q. Zhao, Phys. Rev. D **72**, 074001 (2005) [arXiv:hep-ph/0508086].

[117] Q. Zhao, Phys. Lett. B **636**, 197 (2006) [arXiv:hep-ph/0602216].

[118] F.E. Close and A. Kirk, Phys. Lett. B 397, 333 (1997).

[119] D. Barberis *et al.* [WA102 Collaboration], Phys. Lett. B **397**, 339 (1997).

[120] N.A. Tornqvist, Acta Phys. Pol. **B 16**, 503 (1985); Z. Phys. C **68**, 647 (1995).

[121] M. Boglione and M.R. Pennington, Phys. Rev. Lett. **79**, 1998 (1997); M.R. Pennington, hep-ph/9811276.

[122] M. Ablikim *et al.* [BES Collaboration], Phys. Lett. B **598**, 149 (2004) [arXiv:hep-ex/0406038].

[123] B. S. Zou and D. V. Bugg, Euro. Phys. J. **A16** (2003) 537

[124] Amsler, C., et al., [CBR collaboration], Phys. Lett. **B340** (1994) 259, Phys. Lett., B355 (1995) 425

[125] Abele, A., et al., [CBR collaboration], Phys. Lett. **B380** (1996) 453, Phys. Lett. B385 (1996) 425, Nucl. Phys. **A609** (1996) 562

[126] Antinori, F., et al., [WA91 collaboration], Phys. Lett. **B353** (1995) 589

[127] Arberis, D., et al., [WA102 collaboration], Phys. Lett. **B413** (1997) 217

[128] Bugg, D., et al., Phys. Lett. **B353** (1995) 378

[129] Bai, J. Z., et al., [BES collaboration], Phys. Lett. **B472** (2000)207

[130] R. M. Baltrusaitis et al., [MARKIII Collaboration], Phys. Rev. D **35**, 2077 (1987)

[131] J. E. Augustin et at., [DM2 Collaboration], Zeit. Phys. C **36**, 369 (1987).

[132] J. Z. Bai et at., [BES Collaboration], Phys. Rev. Lett. **76** 3502 (1996).

[133] W. Dunwoodie, *Hadron Spectroscopy*, AIP Conf. Proc. No. 432 (AIP. Melville, NY, 1997), p. 753.

[134] L. Köpke, N. Wermes, Phys. Rep. **174**, 67 (1989).

[135] J. Z. Bai et al., [BES Collaboration], Phys. Rev. Lett. **81**, 1179 (1998).

[136] M. Ablikim et al., [BES Collaboration], Phys. Lett. **B 642**, 441 (2006).

[137] A. Garmash et al., Belle Collaboration, Phys. Rev. **D 71**, 092003 (2005).

[138] B. French *et al.*, [WA76 Collaboration], Phys. Lett. **B214** (1999) 213.

[139] D. Barberis *et al.*, [WA102 Collaboration], Phys. Lett. **B453** (1999) 305 and 316;

[140] M. Ablikim et al., [BES Collaboration], Phys. Rev. Lett. **96**, 162002 (2006)

[141] P. Bicudo, S.R. Cotanch, F.J. Llanes-Estrada, and D.G. Robertson, hep-ph/0602172.

[142] D.V. Bugg, hep-ph/0603018.

[143] K.T. Chao, hep-ph/0602190.

[144] X. G. He, X. Q. Li, X. Liu and X. Q. Zeng, arXiv:hep-ph/0604141.

[145] B.A. Li, hep-ph/0602072.

[146] Q. Zhao and B.S. Zou, hep-ph/0606196.

[147] V.V. Anisovich, hep-ph/0510409.

[148] P. Minkowsky and W. Ochs, Eur. Phys. J. C **9**, 283 (1999).

[149] T. Adams *et al.*, Phys. Rev. Lett. **87**, 041801 (2001).

[150] S. Fukui *et al.*, Phys. Lett. B **267**, 293 (1991).

[151] J.J. Manak *et al.*, Phys. Rev. D **62**, 012003 (2000).

[152] A. Abele *et al.*, Phys. Rev. D **57**, 3860 (1998).

[153] A.V. Anisovich, Nucl. Phys. A **690**, 567 (2001).

[154] C. Amsler *et al.*, Euro. Phys. J. C **33**, 23 (2004).

[155] J.E. Augustin *et al.*, Phys. Rev. D **46**, 1951 (1992).

[156] P.H. Baillon *et al.*, NC 50A, 393(1967).

[157] D.L. Scharre *et al.*, Phys. Lett. **97B**, 329 (1980).

[158] C. Edwards *et al.*, Phys. Rev. Lett. **49**, 259 (1982); *ibid*, **50**, 219 (1982).

[159] J.E. Augustin *et al.*, Phys. Rev. D **42**, 10(1990).

[160] M.G. Rath *et al.*, Phys. Rev. D **40**, 693 (1989).

[161] Z. Bai *et al.*, Phys. Rev. Lett. **65**, 2507 (1990).

[162] A Bertin *et al.*, Phys. Lett. B**361**, 187 (1997); *ibid* **400**, 226 (1997).

[163] C. Cicalo *et al.*, Phys. Lett. B**462**, 453 (1999).

[164] F. Nichitiu *et al.*, Phys. Lett. B **545**, 261 (2002).

[165] T. Bolton *et al.*, Phys. Rev. Lett. **69**, 1328 (1992).

[166] C. Amsler *et al.*, Phys. Lett. B **358**, 389 (1995).

[167] M. Acciarri *et al.*, Phys. Lett. B**501**, 1 (2001).

[168] F.E. Close and A. Kirk, Phys. Lett. B **397**, 333 (1997).

[169] T. Barnes, F.E. Close, P.R. Page and E.E. Swanson, Phys. Rev D. 4157 (1997).

[170] E. Klempt, hep-ph/0409148.

[171] J.Z. Bai *et al.* [BES Collaboration], Phys. Lett. B**594**, 47 (2004).

[172] R. M. Baltrusaitis et al. (MARKIII Collaboration), Phys. Rev. Lett. **55**, 1723 (1985).

[173] R. M. Baltrusaitis et al. (MARKIII Collaboration), Phys. Rev. D **33**, 1222 (1986).

[174] D. Bisello et al. (DM2 Collaboration), Phys. Rev. D **39**, 701 (1989).

[175] D. Bisello et al. (DM2 Collaboration), Phys. Lett. B **192**, 239 (1987).

[176] J. Z. Bai et al. (BES Collaboration), Phys. Lett. B **446**, 356 (1999).

[177] A. Etkin et al., Phys. Rev. Lett. **40**, 422 (1978).

[178] P. R. Page, X. Q. Li, Eur. Phys. J. C1, **579** (1998).

[179] N. Wu et al, Chin. Phys. **10**, 611 (2001); /hep-ph/0011338.

[180] B. A. Li, hep-ph/0510093 (2005).

[181] M. Ablikim et at., BES Collaboration, Phys. Rev. **D 73**, 112007 (2006)

[182] K. Einsweiler, SLAC-PUB-4279 (1983).

[183] R.M. Baltrusaitis *et al.*, Phys. Rev. Lett. **56**, 107 (1985).

[184] J.E. Augustin *et al.*, Phys. Rev. Lett. **60**, 2238 (1988).

[185] D. Alde *et al.*, Phys. Lett. **177B**, 120 (1986).

[186] D. Aston *et al.*, Phys. Lett. B **201**, 169 (1988).

[187] J.Z. Bai *et al.* [BES Collaboration], Phys. Rev. Lett. bf 76, 3502 (1996).

[188] J.Z. Bai *et al.* [BES Collaboration], Phys. Rev. Lett. **81**, 1179 (1998).

[189] Godang R., et at., CLEO collaboration, Phys. Rev. Lett., 79, 3829 (1997)

[190] Alam M. S., et at., CLEO collaboration, Phys. Rev. Lett., 81, 3328 (1998)

[191] L. Kopke and N. Wermes, Phys. Rep. 174 (1989) 67

[192] C. Evangelista *et al.* [JETSET Collaboration], Phys. Rev. D **56**, 3803 (1997).

[193] K.K. Seth, Proceedings of XXXI Rencontres de Moriond, Les Arcs, 1997, edited by J. Tren Thanh Van (Edidtions Frontieres, Paris), p599.

[194] E. Witten, Nucl. Phys. B 169 (1979) 57.

[195] T. D. Cohen, Phys. Lett. B 427 (1998) 348.

[196] N. Isgur, R. Kokoski and J. Paton, Phys. Rev. Lett. 54 (1985) 869.

[197] N. Isgur and J. Paton, Phys. Rev. **D31** (1985) 2910.

[198] F. E. Close and P. R. Page, Nucl. Phys. **B443** (1995) 233.

[199] F. E. Close, J. J. Dudek, Phys. Rev. **D70** (2004) 094015.

[200] E. S. Swanson and A. P. Szczepaniak. Phys. Rev. **D56** (1997) 5692.

[201] P. R. Page, E. S. Swanson and A. P. Szczepaniak. Phys. Rev. **D59** (1999) 034016.

[202] H. Y. Jin, J. G. Korner and T. G. Steele, Phys. Rev. **D67** (2003) 014025.

[203] J. Govaerts *et al.*, Phys. Rev. Lett**53** (1984) 2207.

[204] J. I. Latorre, P. Pascual and S. Narison, Z. Phys. **C37**(1987) 347.

[205] S. Narison, QCD Spectral Sum Rules, Lecture Notes in Physics, Vol. 26, P368.

[206] S.-L. Zhu, Phys. Rev. **D60** (1999) 097502.

[207] S.-L. Zhu, Phys. Rev. D 60 (1999) 014008.

[208] G. S. Bali, Phys. Rev. D 71 (2005) 114513.

[209] R. L. Jaffe, Phys. Rev. Lett. 38 (1977) 195.

[210] R. L. Jaffe, Phys. Rev. D 15 (1977) 267.

[211] S.-L. Zhu, Int. J. Mod. Phys. A 19 (2004) 3439.

[212] BES Collaboration, J.Z. Bai/et al., Phys. Rev. Lett. **91**, 022001 (2003).

[213] BES Collaboration, M. Ablikim/et al., Phys. Rev. Lett. **93**, 112002 (2004).

[214] BES Collaboration, M. Ablikim/et al., Phys. Rev. Lett. **95**, 262001 (2005).

[215]

[216]

[217] A. Datta, P.J. O'Donnell, Phys. Lett. **B567**, 273 (2003); M.L. Yan/et al., hep-ph/0405087; B. Loiseau, S. Wycech, hep-ph/0502127.

[218] J. Ellis, Y. Frishman and M. Karliner, Phys. Lett. **B566**, 201 (2003); J.L. Rosner, Phys. Rev. D **68**, 014004 (2003).

[219] C.S. Gao and S.L. Zhu, Commun. Theor. Phys. 42, 844 (2004), hep-ph/0308205.

[220] G.J. Ding and M.L. Yan, Phys. Rev. C **72**, 015208 (2005).

[221] B.S. Zou and H.C. Chiang, Phys. Rev. D **69**, 034004 (2003).

[222] A. Sibirtsev/et al., Phys. Rev. D **71**, 054010 (2005).

[223] I.S. Shapiro, Phys. Rept. **35**, 129 (1978); C.B. Dover, M. Goldhaber, Phys. Rev. D **15**, 1997 (1977).

[224] For recent reviews of this subject, see E. Klempt *et al.*, Phys. Rep. **368**, 119 (2002) and J-M. Richard, Nucl. Phys. Proc. Suppl. **86**, 361 (2000).

[225] S.L. Zhu and C.S. Gao, hep-ph/0507050.

[226] F. Huang and Z.Y. Zhang, Phys.Rev C **72**, 024003 (2005), nucl-th/0507025.

[227] BES Collaboration, M. Ablikim/et al., Phys. Rev. Lett. **97**, 142002 (2006).

[228]

[229] J. Weinstein, N. Isgur, Phys. Rev. D 41 (1990) 2236

[230] S.Capstick and W.Robert, *Prog. Part. Nucl. Phys.* **45**, S241 (2000).

[231] K.F.Liu and C.W.Wong, *Phys. Rev.* **D28** (1983), 170.

[232] G.T.Garvey, J.C.Peng, Prog. Part. Nucl. Phys. 47 (2001) 203, and references therein.

[233] J.P.Speth and A.W.Thomas, Adv. Nucl. Phys. 24 (1997) 93, and references therein.

[234] N.Kaiser, P.B.Siegel and W.Weise, Phys. Lett. **B362**, 23 (1995); N.Kaiser, T.Waas and W.Weise, Nucl. Phys. **A612**, 297 (1997).

[235] B.S.Zou, nucl-th/0610062, Nucl. Phys. A (in press) and reference therein.

[236] B. S. Zou and D. O. Riska, Phys. Rev. Lett. 95 (1005) 072001; C. S. An, B. S. Zou and D. O. Riska, Phys. Rev. C73 (2006) 035207.

[237] B.C. Liu and B.S. Zou, Phys. Rev. Lett. **96**, 042002 (2006)

[238] A.Zhang et al., hep-ph/0403210, High Energy Phys. Nucl. Phys. **29**, 250 (2005).

[239] T.T.Takahashi et al., *Phys. Rev. Lett.* **86**, 18 (2001); *Phys. Rev.* **D65**, 114509 (2002).

[240] S.Capstick and N.Isgur, *Phys. Rev.* **D34**, 2809 (1986).

[241] T.T.Takahashi et al., *Nucl. Phys.* **A721**, 926 (2003).

[242] A.Manohar and H.Georgi, *Nucl. Phys.* **B234**, 189 (1984); L.Ya.Glozman and D.O.Riska, *Phys. Rep.* **268**, 1 (1996).

[243] E.Oset et al., *Int. J. Mod. Phys.* **A18**, 387 (2003).

[244] T. Nakano et. al., *Phys. Rev. Lett.* **91**, 012002 (2003); V.V. Barmin et. al., *Phys. Atom. Nucl.* **66**, 1715 (2003); S. Stepanyan et. al., *Phys. Rev. Lett.* **91**, 252001 (2003); J. Barth et. al., *Phys. Lett.* **B572**, 127 (2003); A.Airapetian et al., *Phys. Lett.* **B585**, 213 (2004).

[245] H.J.Lipkin, *Phys. Lett.* **B195**, 484 (1987); D. Diakonov, V. Petnov and M. Polyakov, *Z. Phys.* **A359**, 305 (1997); S.L.Zhu, *Phys. Rev. Lett.* **91**, 232002 (2003).

[246] For a recent review see e.g. E.Klempt, hep-ph/0404270.

[247] M. Ripani et al., *Phys. Rev. Lett.* **91**, 022002 (2003).

[248] M.Q.Tran/et al., *Phys. Lett.* **B445**, 20 (1998); T.Mart and C.Bennhold, *Phys. Rev.* **C61**, 012201 (2000).

[249] Y. Assafiri et al., Phys. Rev. Lett. **90**, 222001 (2003).

[250] BES Collaboration, J.Z.Bai et al., Phys. Lett. **B510**, 75 (2001); BES Collaboration, H.B.Li et al., Nucl. Phys. **A675**, 189c (2000); BES Collaboration, B.S.Zou et al., /Excited Nucleons and Hadronic Structure, Proc. of NSTAR2000 Conf. at JLab, Feb 2000. Eds. V.Burkert et al., World Scientific (2001) p.155.

[251] B.S.Zou, Nucl. Phys. **A684**, 330 (2001); Nucl. Phys. **A675**, 167 (2000).

[252] L.Glozman, W.Plessas, K.Varga and R.Wagenbrunn, Phys. Rev. **D58**, 094030 (1998).

[253] M.Benmerrouche, N.C.Mukhopadhyay and J.F.Zhang, Phys. Rev. Lett. 77, 4716 (1996); Phys. Rev. D51, 3237 (1995).

[254] M.G.Olsson and E.T.Osypowski, Nucl. Phys. B87, 399 (1975); Phys. Rev. D17, 174 (1978); M.G.Olsson et al., *ibid.* 17, 2938 (1978).

[255] W.Rarita and J.Schwinger, Phys. Rev. **60**, 61 (1941).

[256] C.Fronsdal, Nuovo Cimento Suppl. **9**, 416 (1958); R.E.Behrends and C.Fronsdal, Phys. Rev. **106**, 345 (1957).

[257] S.U.Chung,/Spin Formalisms, CERN Yellow Report 71-8 (1971); Phys. Rev. **D48**, 1225 (1993); J.J.Zhu and T.N.Ruan, Communi. Theor. Phys. **32**, 293, 435 (1999).

[258] W.H.Liang, P.N.Shen, J.X.Wang and B.S.Zou, J. Phys. **G28** (2002) 333.

[259] J.X.Wang, Comput. Phys. Commun. **77**, 263 (1993).

[260] R. Sinha and S. Okubo, Phys. Rev. D30 (1984) 2333.

[261] W.H.Liang, P.N.Shen, B.S.Zou and A.Faessler, Euro. Phys. J. A21 (2004) 487.

[262] R.A. Arndt et al., Phys.Rev.C69, 035213 (2004); M.Manley, talk at NSTAR2004, Grenoble, March 2004.

[263] T.P.Vrana, S.A.Dytman and T.S.H.Lee, Phys. Rep. 328 (2000) 181.

[264] BES Collaboration, Phys. Rev. Lett. 97 (2006) 062001.

[265] H.X.Yang et al., (BES Collaboration), Int. J. Mod. Phys. A20 (2005) 1985; BES Collaboration, Phys. Rev. Lett. 93 (2004) 112002.

[266] B.S.Zou (for BES Collaboration),/Proc. of the Workshop on the Physics of Excited Nucleons (NSTAR2004), Grenoble, France, March 2004. Eds. J.P.Bocquet et al., World Scientific (2004) p.271.

[267] H.X.Yang, IHEP Ph.D thesis (2001).

[268] BES Collaboration, Phys.Rev. D74 (2006) 012004.

[269] S. Capstick and N. Isgur, Phys. Rev. D34 (1986) 2809.

[270] BES Collaboration, Phys.Rev. D71 (2005) 072006.

[271] J.J.Xie and B.S.Zou, nucl-th/0701021.

[272] F. Calogero, C. Zemach, Phys. Rev. 120 (1960) 1860

[273] V. E. Balakin, V. M. Budnev and I. F. Ginzburg, Pisma Zh. Eksp. Teor. Fiz. **11** (1970) 559.

[274] S. J. Brodsky, T. Kinoshita and H. Terazawa, Phys. Rev. Lett. **25** (1970) 972.

[275] V. M. Budnev, I. F. Ginzburg, G. V. Meledin and V. G. Serbo, Phys. Rept. **15** (1974) 181.

[276] V. M. Budnev, I. F. Ginzburg, Phys. Lett. **37B** (1971) 320.

[277] M. R. Pennington hep-ph 0311299, hep-ph 0511146

[278] M. R. Whalley, J. Phys. G: Nucl. Part. Phys. 27 (2001) A1-121

[279] J. Boyer et. al. Phys. Rev. D42 (1990), 1350

[280] F. Butler et. al. Phys. Rev. D42 (1990), 1368

[281] H. Marsiske et. al. Phys. Rev. D41 (1990), 3324

[282] J. Dominick et. al, Phys. Rev. D50 (1994), 3027

[283] H. J. Behrend et. al. Z. Phys. C56 (1992), 381

[284] T. Mori et. al. in Proceedings of the International Simposium on Hadron Spectroscopy Chiral Symmetry and relativistic Description of Bound Systems, Tokio, 2003 edited by S. Ishida, K. Takamashi, T. Tsuru, S. Y. Tsai, M. Ishida, T. Komada (KEK Proceedings 2003-7) p. 159

[285] N.N. Achasov, G.N. Shestakov, Yadernaya Fizika, 2006, Vol. 69, No. 9, pp. 15451556,hep-ph/0506046

[286] L. Miani, Proc. Workshop on Physics and Detectors for DAFNE (1991) 719

[287] M.R. Pennington hep-ph/0509265
P. Minkowski, W. Ochs, Eur. Phys. J. C9 (1999) 283, hep-ph/9811518
W. Ochs hep-ph/0311144

[288] H. Albrecht et. al. Z. Phys. C74 (1997) 469

[289] D. Antreasyan et. al. Z. Phys. C48 (1990) 561

[290] H. J. Behrend et. al. Z. Phys. C46 (1990) 583

[291] L. Lonnblad et. al., hep-ph/9512371

[292] G. Schuler hep-ph/9710506

[293] F.A. Berends, P.H. Daverveld, R. Kleiss, Nucl. Phys. B253 (1985) 421, Comput. Phys. Commun. 40 (1986) 271,285,309

[294] F.L. Kinde, "charm production in two-photon physics", RX-1224 (LEIDEN) (1988) thesis

Part IV

Charmonium Physics

Cong-Feng Qiao, Changzheng Yuan.
Authors: A. A, B. B, ...

Chapter 16

Theoretical Frameworks of Charmonium Physics

16.1 Non-Relativistic QCD effective theory

Charmonia are bound states of the $c\bar{c}$ pair by the strong interaction. The charm quark mass m_c is so large that the motion of the charm quark inside the bound state is slow and charmonium can be approximately regarded as a non-relativistic bound state. $v^2 \sim 0.3$ for charmonia and 0.1 for bottomnia by potential model calculations or by Lattice simulation, where v is the relative velocity between the c and $\bar{c}$. For a small value of v, there are several distinct energy scales in charmonium. The 3-momentum is order $m_c v$. The binding energy is order $m_c v^2$. Numerically, they are around 800 MeV and 500 MeV, respectively. In the limit of $v^2 \ll 1$, those energy scales satisfy a hierarchy relation $m_c \gg m_c v \gg m_c v^2$, with which the effects at energy scale m_c can be integrated out explicitly. The resultant theory, when it is expressed as a Pauli two-component field theory, is just the *nonrelativistic QCD* (NRQCD) effective theory[198, 2, 271]. NRQCD is equivalent to the full QCD but it simplifies QCD by taking a nonrelativistic expansion and by reducing the number of the energy scales. Essentially, NRQCD can be regarded as an effective theory which expands the full QCD in powers of v. It turns out to be very useful in dealing with charmonium relevant processes such as spectroscopies, annihilation decays, and inclusive productions. Starting from NRQCD, one may integrate out further the effects at energy scale $m_c v$ and obtain an effective theory contains only energy scale $m_c v^2$, called as *potential NRQCD* (pNRQCD)[272, 201, 202], which will be reviewed in the next subsection.

16.1.1 NRQCD effective theory

QCD fully describes the strong interactions of the quarks and gluons. QCD lagrangian for heavy quark is given by:

$$\mathcal{L} \;=\; \bar{\Psi}(x)\,(\,i\;\not{D}^{\mu} - m_c\,)\Psi(x)\;, \tag{16.1}$$

where $iD^{\mu} = i\partial^{\mu} + gA^{a\mu}T^{a}$ is the covariant derivative. It looks simple but it turns out to be complicated. As a relativistic quantum field theory, it describes heavy quark and antiquark together and quantum effects from all energy scales. It can be simplified

in the nonrelativistic limit $v \ll 1$. First, in this limit, the heavy quark pair creation and annihilation effects is suppressed. The quark and the antiquark are decouple. All relativistic effects can be expanded as power series of v. Second, those quantum effects arising from high energy scales m or above are perturbatively calculable since QCD is a theory with asymptotical freedom. This can be done by taking the hard cut-off energy scale Λ less than m_c. Quantum effects above Λ can be expressed as contributions from a sum of certain local operators in powers of v since in this region the internal particle are far off-shell and can only propagate in a short distance which is less than $1/m_c$. Consequently, taking $\Lambda < m_c$, adding certain local operators in the lagrangian, and making expansion in terms of v, one obtain an effective theory. It reproduces the results of the full QCD at low energy scale. The coefficients of those local operators are called as the Wilson short distance coefficients which can be calculated by matching the QCD full theory and that of the effective theory.

In NRQCD effective theory, the quark and the antiquark fields are described by the two component Pauli field instead of the Dirac four component field in QCD. Up to order v^4, the NRQCD effective lagrangian reads[198, 2, 271]

$$\mathcal{L}_{\rm NRQCD} \;=\; \mathcal{L}_l \,+\, \mathcal{L}_0 \,+\, \delta\mathcal{L}\,, \tag{16.2}$$

where $\mathcal{L}_l$ is the usual lagrangian that describes gluons and light quarks;

$$\mathcal{L}_0 \;=\; \psi^\dagger\left(iD_0 + \frac{\mathbf{D}^2}{2m_c}\right)\psi \,+\, \chi^\dagger\left(iD_0 + \frac{\mathbf{D}^2}{2m_c}\right)\chi \tag{16.3}$$

is the leading order NRQCD effective lagrangian; and

$$\begin{aligned}\delta\mathcal{L} \;=\; & \frac{c_1}{8m_c^3}\,\psi^\dagger\,(\mathbf{D}^2)^2\psi \,+\, \frac{c_2}{8m_c^2}\,\psi^\dagger\, g(\,\mathbf{D}\cdot\mathbf{E} - \mathbf{E}\cdot\mathbf{D}\,)\psi \,+\, \frac{c_3}{2m_c}\,\psi^\dagger\, g\boldsymbol{\sigma}\cdot\mathbf{B}\,\psi \\ & + i\frac{c_4}{8m_c^2}\,\psi^\dagger\, g\,\boldsymbol{\sigma}\cdot(\mathbf{D}\times\mathbf{E} - \mathbf{E}\times\mathbf{D})\,\psi \,+\, \text{charge conjugate terms}\end{aligned} \tag{16.4}$$

are v^2 correction terms to $\mathcal{L}_0$. Here ψ and χ are the Pauli spinor fields of quark and antiquark, respectively, Gauge invariance implies that gluon field appear in the lagrangian always only through the gauge-covariant derivatives iD_0, $i\mathbf{D}$ and the QCD field strength $\mathbf{E}$, $\mathbf{B}$.

In $\mathcal{L}_0$, both the iD_0 term and the $\mathbf{D}^2/2m_c$ term contribute to the same order of the quarkonium energy. In QED, taking Coulomb gauge and neglecting $\mathbf{A}$ field, variation to the $\mathcal{L}_0$ gives to the Schødinger equation of the hydragon atom. An explicit spin symmetry at leading order in v follows from absent of the Pauli matrix σ^i in $\mathcal{L}_0$. This implies that at leading order the states J/ψ and η_c are degenerate and the states $\chi_{c0}, \chi_{c1}, \chi_{c2}$, and h_c are also degenerate. This symmetry is violated after including the next leading order corrections since the spin dependent term with σ^i appearing in $\delta\mathcal{L}$. The velocity scaling rule[198, 2, 271] can be used to count the relative importance of each term in $\delta\mathcal{L}$. Those Wilson short-distance coefficients c_i's has been calculated in pQCD. They can be expanded as power series of α_s at energy scale m_c. Other coefficients can be determined by matching the full QCD and the NRQCD effective theory. Some relationships between these coefficients follows from the reparameterization invariance[7, 8, 9, 273, 10, 11, 12]. Especially, the coefficient of the kinetic energy term in $\mathcal{L}_0$ is free of renormalization.

16.1.2 Inclusive Charmonium Annihilation Decays

An important decay mode of charmonium is the annihilation decay, in which the $c\bar{c}$ pair annihilates into a light quark antiquark pairs or gluons, or photon(s). These light partons eventually form light hadrons by hadronization. The inclusive process that $c\bar{c}$ annihilate into all light hadrons is infrared safety and hence perturbatively calculable although the hadronization process is infrared sensitive. When a $c\bar{c}$ pair annihilates, the total energy $2m_c$ is released. Thus it occurs at distance of $1/(2m_c)$. The typical size of a charmonium state is order of $1/(m_c v)$. Thus in the limit of $v \ll 1$, the effects happened at these two distinct distance scales are separated well. NRQCD factorization formula[271] provide a systematic method to analysis the annihilation decay rates. In the formula, the annihilation decay rate is factorized into a sum of the products of the short-distance effects and the long-distance matrix elements[271]:

$$\Gamma(H) \;=\; \frac{1}{2M_H} \sum_{mn} \frac{C_{mn}(\mu)}{m_c^{d_{mn}-N-1}} \langle H|\mathcal{O}_{mn}|H\rangle^{(\mu)} \;, \tag{16.5}$$

where M_H is the mass of the charmonium state H and d_{mn} is the mass dimension of the operator $\mathcal{O}_{mn}$. The matrix elements $\langle H|\mathcal{O}_{mn}|H\rangle$ are expectation values in the quarkonium state H of local 4-fermion operators that have the structure

$$\mathcal{O}_{mn} \;=\; \psi^\dagger \mathcal{K}'^\dagger_m \chi\; \chi^\dagger \mathcal{K}_n \psi \;, \tag{16.6}$$

where $\mathcal{K}_n$ and $\mathcal{K}'^\dagger_m$ are products of a color matrix (1 or T^a), a spin matrix, and a polynomial in the gauge covariant derivative $\mathbf{D}$. In NRQCD factorization formula, the quantum number of the state H is not necessarily the same with that of the operator O. When H and Q hold the same quantum number, H decays via the leading Fock space. Otherwise, H decays via the higher Fock space with electric or magnetic transition. It differs from the conventional color-singlet model in which the H decays only via the leading Fock space. The relative importance of each matrix element can be estimated by the velocity scaling rule[271]. Suppose E and M be the total number of the electric and magnetic transitions; D the derivative number contain in the operator O, then the matrix element $\langle H|\mathcal{O}_{mn}|H\rangle$ scales like $v^{3+D+E+3M/2}$. This rule can be used to estimate the order of magnitude of the NRQCD matrix elements.

To reduce the number of the NRQCD matrix elements, some comments can be given below:

(1) In the electromagnetic annihilation decay mode, the $c\bar{c}$ pair annihilates to the vacuum. Thus one needs to insert a vacuum state $|0\rangle\langle 0|$ between those two two-fermion operators. It corresponds to take the vacuum saturation approximation, in which the NRQCD matrix elements are proportional to the square of the wavefunctions at the origin for $S-$wave and its derivative for $P-$wave and so on. The approximation validates up to order v^4[271].

(2) In charmonium, the relativistic correction is large. The Gramm-Kapustin relation[206] relates the leading order matrix elements to the relativistic correction ones. However, the pole mass enter into the relation so that some ambiguities are involved.

(3) With pNRQCD, the color-octet matrix elements are related to the corresponding color-singlet one by some universal factor which are state and flavor independent[272, 201, 202]. This will be reviewed in detail in the next subsection.

Thus to certain order of v, there are only a few independent long-distance matrix elements are involved. They are nonperturbative in nature. They may be determined by fitting experimental data, by Lattice simulation, or by pNRQCD. This feature makes NRQCD factorization formula is useful in analyzing the inclusive or eletromagnetic charmonium annihilation decays.

The short-distance coefficients for annihilation decay rates $C_{mn}(\mu)$ can be expanded as a power series of $\alpha_s(\mu)$. They can be determined by matching perturbative calculations of $c\bar{c}$ scattering amplitudes. For annihilation decays, $\mu \sim m$. The μ dependence in the short-distance coefficients cancel that in the matrix elements. A general matching prescription is the threshold expansion method[14].

Below we list the applications of the NRQCD factorization formula to the inclusive annihilation decays of the J/ψ, ψ', η_c, χ_{cJ}.

J/ψ, ψ' decay

The J/ψ and ψ' can decay to light hadrons proceeds via the annihilation of the c and $\bar{c}$. The annihilation decay dominates the J/ψ decay rate, while it account for 15% of the ψ' decay rate since hadron and the electro-magnetic transitions govern ψ' decays. In the NRQCD factorization formula[**?**], the inclusive decay rate of J/ψ reads:

$$\begin{aligned}\Gamma(J/\psi \to l.h.) &= \left(\frac{20(\pi^2-9)\alpha_s^3}{243m_c^2} + \frac{16\pi\alpha^2}{27m_c^2}\right)\langle \mathcal{O}_1(^3S_1)\rangle_{J/\psi} + \frac{5\pi\alpha_s^2}{6m_c^2}\langle \mathcal{O}_8(^1S_0)\rangle_{J/\psi} \\ &+ \frac{19\pi\alpha_s^2}{6m_c^2}\langle \mathcal{O}_8(^3P_0)\rangle_{J/\psi} + \frac{\pi\alpha_s^2}{m_c^2}\langle \mathcal{O}_8(^3S_1)\rangle_{J/\psi} + \ldots . \qquad (16.7)\end{aligned}$$

where $\alpha_s = \alpha_s(m_c)$. The matrix elements are expectation values in the J/ψ of local gauge-invariant NRQCD operators that measure the inclusive probability of finding a $c\bar{c}$ in the J/ψ at the same point and in the color and angular-momentum state specified. The same expression of the decay rate hold for ψ' once the state J/ψ is substituted by the ψ'. Those specific local four-fermion operators are listed below:

$$\begin{aligned}&\mathcal{O}_1(^3S_1) = \psi^\dagger \boldsymbol{\sigma}\chi\,\chi^\dagger\boldsymbol{\sigma}\psi, \psi, \qquad && \mathcal{O}_8(^1S_0) = \psi^\dagger \mathrm{T}^a\chi\,\chi^\dagger\mathrm{T}^a\psi, \\ &\mathcal{O}_8(^3P_0) = \psi^\dagger \mathrm{T}^a\mathbf{D}\cdot\boldsymbol{\sigma}\chi\,\chi^\dagger\mathrm{T}^a\mathbf{D}\psi, && \mathcal{O}_8(^3S_1) = \psi^\dagger \mathrm{T}^a\boldsymbol{\sigma}\cdot\boldsymbol{\sigma}\chi\,\chi^\dagger\mathrm{T}^a\boldsymbol{\sigma}\psi, \quad (16.8)\end{aligned}$$

The matrix element of the $c\bar{c}_1(^3S_1)$ term in (**??**) is proportional to the square of the wavefunction at the origin and scales as v^3. Its coefficient includes a term of order α_s^3 from $c\bar{c} \to ggg$ and a term of order α^2 from the electromagnetic annihilation process $c\bar{c} \to \gamma^* \to q\bar{q}$. The color-octet terms in (**??**) represent contributions from higher Fock states. Their matrix elements scale like v^6, v^7 and v^7, respectively. Their coefficients are all of order α_s^2 and come from $c\bar{c} \to gg$ for the $c\bar{c}_8(^1S_0)$ and $c\bar{c}_8(^3P_0)$ terms and from $c\bar{c} \to g^* \to q\bar{q}$ for the $c\bar{c}_8(^3S_1)$ term. Note that the coefficients of the color-octet matrix elements are two orders of magnitude larger than that of $\langle \mathcal{O}_1(^3S_1)\rangle_{J/\psi}$, which suggests that the higher Fock states may play a more important role in annihilation decays than is commonly believed.

η_c decay

The η_c is the ground state of the charmonium states. It can decay only via annihilation of the $c\bar{c}$. NRQCD factorization formula for $\eta_c \to$ light hadrons decay rate reads:

$$\Gamma(\eta_c \to l.h.) = \frac{\pi C_F}{N_c m_c^2}\alpha_s^2(2m_c)\left\{1 + \left[\left(\frac{\pi^2}{4} - 5\right)C_F + \left(\frac{199}{18} - \frac{13\pi^2}{24}\right)C_A - \frac{8}{9}n_f\right]\frac{\alpha_s}{\pi}\right\}\langle \mathcal{O}_1(^1S_0)\rangle_{\eta_c} + \cdots . \quad (16.9)$$

Comparing with the J/ψ, the decay width of η_c is much larger because $c\bar{c}$ can annihilate into two gluons and the short distance coefficients is order α_s^2 at the leading order. Also in the case of $J\psi$, there is an additional suppression factor $\pi^2 - 9$ in the short distance coefficient of $c\bar{c} \to ggg$

The η_c have also electromagnetic decay $\eta_c \to \gamma\gamma$. NRQCD factorization formula can also apply for $\eta_c \to \gamma\gamma$. An interesting quantity is the ratio of the decay rate for $\eta_c \to$ light hadrons to that for the $\eta_c \to \gamma\gamma$, the inverse branching fraction, denoted by R. It is relatively easy to be measured in experiments. In R, the NRQCD matrix element cancel up to order v^4, the relativistic corrections also cancel at the leading order of α_s. This leaves R almost a pure short-distance number. In principle, R may be calculated precisely in pQCD. However, one find that the radiative correction to R is quite large and R is sensitive to the choice of the renormalization scale μ. *e.g.*, when μ varies from $2m_c$ to $0.5m_c$, R varies by factor 5 for the next leading order result. Bodwin and Chen show that the most important corrections arise from the bubble diagram. After the bubble diagrams are resumed, a result which is insensitive to μ is obtained, which is in agreement with the experimental results. This quantity is expected to be measured accurately at BES III.

P-wave χ_{cJ} decay

An interesting application of the NRQCD factorization formula is the charmonium $P-$wave annihilation. The decay rate was calculated by Barbieri[**?**, **?**] to the next-leading order of α_s in the color-singlet model. It was found that there were infrared divergences in the expression of the short distance coefficients, which arise from the process $\chi_{cJ} \to q\bar{q}g$. This implies that the long-distance effects enter into the short-distance coefficients and the conventional color-singlet model fails. The problem is nicely solved in the NRQCD factorization framework, in which the decay rates are given by:

$$\Gamma(\chi_{cJ} \to l.h.) = A_J \langle \mathcal{O}_1(^3P_J)\rangle_{\chi_{cJ}} + B\langle \mathcal{O}_8(^3S_1)\rangle_{\chi_{cJ}} \quad (16.10)$$

$$\Gamma(h_c \to l.h.) = C\langle \mathcal{O}_1(^1P_1)\rangle_{\chi_{h_c}} + B\langle \mathcal{O}_8(^3S_1)\rangle_{\chi_{h_c}} \quad (16.11)$$

$$\mathcal{O}_1(^3S_1) = \psi^\dagger \boldsymbol{\sigma}\chi\,\chi^\dagger\boldsymbol{\sigma}\psi, \psi, \qquad \mathcal{O}_8(^1S_0) = \psi^\dagger \mathrm{T}^a\chi\,\chi^\dagger\mathrm{T}^a\psi,$$
$$\mathcal{O}_1(^3P_1) = \psi^\dagger \mathrm{T}^a\mathbf{D}\times\boldsymbol{\sigma}\chi\,\chi^\dagger\mathrm{T}^a\mathbf{D}\times\boldsymbol{\sigma}\psi, \qquad \mathcal{O}_1(^3P_2) = \psi^\dagger \mathrm{T}^a\sigma^{(i}D^{j)}\chi\,\chi^\dagger\mathrm{T}^a\sigma^{(i}D^{j)}\psi, \quad (16.12)$$

16.2 pNRQCD and its applications

16.2.1 Introduction

The J/Ψ discovery in 1974 had great impact on the development of the theory of strong interactions and the Standard Model. Systems made by two heavy quarks occupy still today a prominent place [267] in our investigation of the QCD dynamics within and beyond the Standard Model. They are multi-scale systems probing all the energy regimes of QCD, from the hard region, where an expansion in the coupling constant is legitimate, to the low energy region, where nonperturbative effects dominate. Heavy quark-antiquark states are thus an ideal and to some extent unique laboratory where our understanding of nonperturbative QCD and its interplay with perturbative QCD may be tested in a controlled framework. In correspondence with the hierarchy of energy scales in quarkonia, a hierarchy of nonrelativistic effective field theries (NR EFT) may be constructed, each one with less degrees of freedom left dynamical and thus simpler. Some of these physical scales are large and may be treated in perturbation theory. These features make two heavy quark systems accessible inside QCD.

Here we will focus on the lowest energy EFT, called pNRQCD [272, 201], that can be constructed for heavy quarkonium. We will give a brief introduction to the main concepts underlying this new EFT and discuss a wide range of applications. The focus and the main interest is clearly on charmonium physics, but results obtained in bottomonium physics are also discussed for their potential interest and impact on charmonium physics. Due to the simplicity of pNRQCD several model independent predictions become possible. Therefore, on one hand the progress in our understanding of NREFTs [202] makes it possible to move beyond phenomenological models and to provide a systematic description from QCD of all aspects of heavy-quarkonium physics. On the other hand, the recent progress (coming from B-factories, CLEO, Fermilab and BES) in the measurement of several heavy-quarkonium observables makes it meaningful to address the problem of their precise theoretical determination.

In this situation BESIII offers a unique opportunity to advance our understanding of strong interactions and our control of some parameters of the Standard Model.

16.2.2 Scales and EFTs

The description of hadrons containing two heavy quarks is a rather challenging problem, which adds to the complications of the bound state in field theory those coming from a nonperturbative QCD low-energy dynamics. A simplification is provided by the non-relativistic nature suggested by the large mass of the heavy quarks and manifest in the spectrum pattern. Systems made by two heavy quarks are characterized by three energy scales, hierarchically ordered by the heavy quark velocity in the center of mass frame $v \ll 1$: the mass m (hard scale), the momentum transfer mv (soft scale), which is proportional to the inverse of the typical size of the system r, and the binding energy mv^2 (ultrasoft scale), which is proportional to the inverse of the typical time of the system. In bottomonium $v^2 \sim 0.1$, in charmonium $v^2 \sim 0.3$. In perturbation theory $v \sim \alpha_s$. Feynman diagrams will get contributions from all momentum regions associated with these

scales. Since these momentum regions depend on α_s, each Feynman diagram contributes to a given observable with a series in α_s and a non trivial counting. For energy scales close to $\Lambda_{\rm QCD}$, the scale at which nonperturbative effects become dominant, perturbation theory breaks down and one has to rely on nonperturbative methods. Regardless of this, the non-relativistic hierarchy $m \gg mv \gg mv^2$ will persist also below the $\Lambda_{\rm QCD}$ threshold.

The wide span of energy scales involved makes also a lattice calculation in full QCD extremely challenging. We may, however, take advantage of the existence of a hierarchy of scales by substituting QCD with simpler but equivalent EFTs. Lower energy EFTs may be constructed by systematically integrating out modes associated to energy scales not relevant for the two quark system. Such integration is made in a matching procedure that enforces the equivalence between QCD and the EFT at any given order of the expansion in v. Any prediction of the EFT is therefore a prediction of QCD with an error of the size of the neglected order in v. By integrating out the hard modes one obtains Nonrelativistic QCD [198] (cf. the contribution by ... in the BES Yellow Book). In such EFT soft and ultrasoft scales are left dynamical and still their mixing complicates calculations and power counting. In the last few years the problem of systematically treating the remaining dynamical scales in an EFT framework has been addressed by several groups [20] and has now reached a good level of understanding. We give here an introduction to the simplest EFT you can write down for two heavy quark systems, where only ultrasoft degrees of freedom remain dynamical. This is potential NRQCD[272, 201] [1].

16.2.3 pNRQCD

pNRQCD [272, 201, 202] is the EFT for two heavy quark systems that follows from NRQCD by integrating out the soft scale mv. Here the role of the potentials and the quantum mechanical nature of the problem are realized in the fact that the Schrödinger equation appears as zero order problem for the two quark states. We may distinguish two situations: 1) weakly coupled pNRQCD when $mv \gg \Lambda_{\rm QCD}$, where the matching from NRQCD to pNRQCD may be performed in perturbation theory; 2) strongly coupled pNRQCD when $mv \sim \Lambda_{\rm QCD}$, where the matching has to be nonperturbative. Recalling that $r^{-1} \sim mv$, these two situations correspond to systems with inverse typical radius smaller than or of the same order as $\Lambda_{\rm QCD}$.

Weakly coupled pNRQCD

The effective degrees of freedom that remain dynamical are: low energy $Q\bar{Q}$ states (that can be decomposed into a singlet and an octet field under colour transformations) with energy of order $\Lambda_{\rm QCD}, mv^2$ and momentum $\mathbf{p}$ of order mv, plus low energy (ultrasoft) gluons with energy and momentum of order $\Lambda_{\rm QCD}, mv^2$. All the gluon fields are multipole expanded (i.e. expanded in the quark-antiquark distance r). The Lagrangian is then given by terms of the type

$$\frac{c_k(m,\mu)}{m^k} \times V_n(r\mu', r\mu) \times O_n(\mu', mv^2, \Lambda_{\rm QCD})\; r^n. \tag{16.13}$$

[1] for an alternative and equivalent EFT (in the case in which $\Lambda_{\rm QCD}$ is the smallest scale) see [21].

where the matching coefficients c_k are inherited from NRQCD and contain the logs in the quark masses, while the pNRQCD potential matching coefficients V_n encode the non-analytic behaviour in r. At leading order in the multipole expansion, the singlet sector of the Lagrangian gives rise to equations of motion of the Schrödinger type. Each term in the pNRQCD Lagrangian has a definite power counting. The bulk of the interaction is carried by potential-like terms, nut non-potential interactions, associated with the propagation of low energy degrees of freedom are present as well. These retardation (or non-potential) effects start at the next-to-leading order (NLO) in the multipole expansion and are systematically encoded in the theory and typically related to nonperturbative effects [201]. There is a systematic procedure to calcolate corrections in v to physical observables: higher order perturbative (bound state) calculations in this framework become viable. In particular the EFT can be used for a very efficient resummation of large logs (typically logs of the ratio of energy and momentum scales) using the renormalization group (RG) adapted to the case of correlated scales [22, 21]; Poincaré invariance is not lost, but shows up in some exact relations among the matching coefficients [23]. The renormalon subtraction may be implemented systematically obtaining $\alpha_{\rm s}$ perturbative series better behaved and allowing a factorization of the genuine QCD nonperturbative effects.

Strongly coupled pNRQCD

In this case the matching to pNRQCD is nonperturbative. Away from threshold (precisely when heavy-light meson pair and heavy hybrids develop a mass gap of order $\Lambda_{\rm QCD}$ with respect to the energy of the $Q\bar{Q}$ pair), the quarkonium singlet field S remains as the only low energy dynamical degree of freedom in the pNRQCD Lagrangian (if no ultrasoft pions are considered), which reads [169, 27, 202]:

$$L_{\rm pNRQCD} = {\rm Tr}\left\{ {\rm S}^\dagger \left(i\partial_0 - \frac{\mathbf{p}^2}{2m} - V_S(r) \right) {\rm S} \right\}. \tag{16.14}$$

The matching potential $V_S(r)$ is a series in the expansion in the inverse of the quark masses: static, $1/m$ and $1/m^2$ terms have been calculated, see [169, 27]. They involve NRQCD matching coefficients and low energy nonperturbative parts given in terms of Wilson loops and field strengths insertions in the Wilson loop. In this regime we recover the quark potential singlet model from pNRQCD. However the potentials are calculated from QCD in the formal nonperturbative matching procedure. An actual evaluation of the low energy part requires lattice evaluation [24] or QCD vacuum models calculations [25].

16.2.4 Applications

It is important to establish when $\Lambda_{\rm QCD}$ sets in, i.e. when we have to resort to nonperturbative methods. For low-lying resonances, it is reasonable, although not proved, to assume $mv^2 \gtrsim \Lambda_{\rm QCD}$. The system is weakly coupled and we may rely on perturbation theory, for instance, to calculate the potential. The theoretical challenge here is performing higher-order calculations and the goal is precision physics. For high-lying resonances,

we assume $mv \sim \Lambda_{\rm QCD}$. The system is strongly coupled and the potential must be determined non-perturbatively, for instance, on the lattice. The theoretical challenge here is providing a consistent framework where to perform lattice calculations and the progress is measured by the advance in lattice computations.

For what concerns systems close or above the open flavor threshold, a complete and satisfactory understanding of the dynamics has not been achieved so far. Hence, the study of these systems is on a less secure ground than the study of states below threshold. Although in some cases one may develop an EFT owing to special dynamical conditions (as for the $X(3872)$ interpreted as a loosely bound $D^0\,\bar{D}^{*\,0} + \bar{D}^0\,D^{*\,0}$ molecule), the study of these systems largely relies on phenomenological models. The major theoretical challenge here is to interpret the new states in the charmonium region discovered at the B-factories in the last years.

16.2.5 QCD potentials

pNRQCD allows us to properly define the QCD potentials and give a well defined procedure to properly calculate them. In this modern description the potentials are matching coefficients of the EFT and as such depend on the scale of the matching. In weakly coupled pNRQCD the soft scale is bigger than $\Lambda_{\rm QCD}$ and so the singlet and octet potentials have to be calculated in the perturbative matching. In [28] a determination of the singlet potential at three loops leading log has been obtained inside the EFT which gives the way to deal with the well known infrared singularity arising in the potential at this order. From this, $\alpha_{\rm s}$ in the V regularization can be obtained, showing at this order and for this regularization a dependence on the infrared behaviour of the theory. The finite terms in the singlet static potential at three loops are not yet known but has been estimated [31]. Recently also the logarithmic contribution at four loops has been calculated [34]. The three loop renormalization group improved calculation of the static singlet potential has been compared to the lattice calculation and found in good agreement up to about 0.25 fm [29]. The static octet potential is known at two loops [32] and again agrees well with the lattice data [33].

At a scale μ such that $mv \sim \Lambda_{\rm QCD} \gg \mu \gg mv^2$, confinement sets in and the potentials become admixture of perturbative terms, inherited from NRQCD, which encode high-energy contributions, and non-perturbative objects. Strongly coupled pNRQCD gives us the general form of the potentials obtained in the nonperturbative matching to QCD in the form of Wilson loops and Wilson loop chromoelectric and chromomagnetic field strengths insertions [169, 27], very well suited for lattice calculations. These will be in general acomplex valued functions. The real part controls the spectrum and the imaginary part controls the decays.

The real part of the potential has been one of the first quantities to be calculated on the lattice (for a review see [24]). In the last year, there has been some remarkable progress. In [36], the $1/m$ potential has been calculated for the first time. The existence of this potential was first pointed out in the pNRQCD framework [169]. A $1/m$ potential is typically missing in potential model calculations. The lattice result shows that the potential has a $1/r$ behaviour, which, in the charmonium case, is of the same size as the $1/r$ Coulomb tail of the static potential and, in the bottomonium one, is about 25%.

Therefore, if the $1/m$ potential has to be considered part of the leading-order quarkonium potential together with the static one, as the pNRQCD power counting suggests and the lattice seems to show, then the leading-order quarkonium potential would be, somewhat surprisingly, a flavor-dependent function. In [37], spin-dependent potentials have been calculated with unprecedented precision. In the long range, they show, for the first time, deviations from the flux-tube picture of chromoelectric confinement [35]. The knowledge of the potentials in pNRQCD could provide an alternative to the direct determination of the spectrum in NRQCD lattice simulations: the quarkonium masses would be determined by solving the Schrödinger equation with the lattice potentials. The approach may present some advantages: the leading-order pNRQCD Lagrangian, differently from the NRQCD one, is renormalizable, the potentials are determined once for ever for all quarkonia, and the solution of the Schrödinger equation provides also the quarkonium wave functions, which enter in many quarkonium observables: decay widths, transitions, production cross-sections. The existence of a power counting inside the EFT selects the leading and the subleading terms in quantum-mechanical perturbation theory. Moreover, the quantum mechanical divergences (typically encountered in perturbative calculations involving iterations of the potentials, as in the case of the iterations of spin delta potentials) are absorbed by NRQCD matching coefficients. Since a factorization between the hard (in the NRQCD matching coefficients) and soft scales (in the Wilson loops or nonlocal gluon correlators) is realized and since the low energy objects are only glue dependent, confinement investigations, on the lattice and in QCD vacuum models become feasible [**?**, 35].

The potentials evaluated on the lattice once used in the Schrödinger equation produce the spectrum. The calculations involve only QCD parameters (at some scale and in some scheme).

16.2.6 Precision determination of Standard Model parameters

c and b mass extraction

The lowest heavy quarkonium states are suitable systems to extract a precise determination of the mass of the heavy quarks b and c. Perturbative determinations of the $\Upsilon(1S)$ and J/ψ masses have been used to extract the b and c masses. The main uncertainty in these determinations comes from nonperturbative nonpotential contributions (local and nonlocal condensates) together with possible effects due to subleading renormalons. These determinations are competitive with those coming from different systems and different approaches (for the b mass see e.g. [73]). We report some recent determinations in Tab. 16.2.6.

A recent analysis performed by the QWG [267] and based on all the previous determinations indicates that at the moment the mass extraction from heavy quarkonium involves an error of about 50 MeV both for the bottom (1% error) and in the charm (4% error) mass. It would be very important to be able to further reduce the error on the heavy quark masses.

reference	order	$\overline{m}_b(\overline{m}_b)$ (GeV)
[171]	NNNLO*	$4.210 \pm 0.090 \pm 0.025$
[172]	NNLO +charm	$4.190 \pm 0.020 \pm 0.025$
[77]	NNLO	4.24 ± 0.10
[76]	NNNLO*	4.346 ± 0.070
[173]	NNNLO*	4.20 ± 0.04
[79]	NNNLO*	4.241 ± 0.070
[180]	NNLL*	4.19 ± 0.06
reference	order	$\overline{m}_c(\overline{m}_c)$ (GeV)
[170]	NNLO	1.24 ± 0.020
[77]	NNLO	1.19 ± 0.11

Table 16.1: Different recent determinations of $\overline{m}_b(\overline{m}_b)$ and $\overline{m}_c(\overline{m}_c)$ in the $\overline{\rm MS}$ scheme from the bottomonium and the charmonium systems. The displayed results either use direct determinations or non-relativistic sum rules. Here and in the text, the * indicates that the theoretical input is only partially complete at that order.

Determinations of $\alpha_{\rm s}$.

Heavy quarkonia leptonic and non-leptonic inclusive and radiative decays may provide means to extract α_s. The present PDG determination of α_s from bottomonium pulls down the global α_s average noticeably [267]. Recently, using the most recent CLEO data on radiative $\Upsilon(1S)$ decays and dealing with the octet contributions within weakly coupled pNRQCD, a new determination of $\alpha_{\rm s}(M_{\Upsilon(1S)}) = 0.184^{+0.014}_{-0.013}$ has been obtained [72], which corresponds to $\alpha_{\rm s}(M_Z) = 0.119^{+0.006}_{-0.005}$ in agreement with the central value of the PDG and with competitive errors. A similar extraction of $\alpha_{\rm s}$ from the inclusive photon spectrum for radiative J/Ψ decays may be possible (cf. the contribution by ... in the BES Yellow Book).

Top-antitop production near threshold at ILC.

In [180, 81] the total cross section for top quark pair production close to threshold in e+e- annihilation is investigated at NNLL in the weakly coupled EFT. Here we see how the summation of the large logarithms in the ratio of the energy scales significantly reduces the scale dependence. Studies like these will make feasible a precise extractions of the strong coupling, the top mass and the top width at a future ILC.

16.2.7 Spectra

We will consider separately systems with a small interquark radius (low-lying states) and systems with a radius comparable or bigger than the confinement scale $\Lambda_{\rm QCD}^{-1}$ (high-lying states). It is difficult to say to which group a specific resonance may belong, since there are no direct measurements of the interquark radius. Electric dipole transitions or quarkonium dissociation in a medium, once a well founded theory treatment of such

processes will be given, may give a clear cut procedure. At the moment one uses the typical EFT approaches assuming that a particular scales hierarchy holds and checking then a posteriori that the prediction and the error estimated inside such framework are consistent with the data.

Low-lying $Q\bar{Q}$ states are assumed to realize the hierarchy: $m \gg mv \gg mv^2 \gtrsim \Lambda_{\rm QCD}$, where mv is the typical scale of the inverse distance between the heavy quark and antiquark and mv^2 the typical scale of the binding energy. At a scale μ such that $mv \gg \mu \gg mv^2$ the effective degrees of freedom are $Q\bar{Q}$ states (in color singlet and octet configurations), low-energy gluons and light quarks.

B_c mass (MeV)				
[71] (expt)	[70] (lattice)	[69] (NNLO)	[170] (NNLO)	[172] (NNLO)
$6287 \pm 4.8 \pm 1.1$	$6304 \pm 12^{+12}_{-0}$	6326(29)	6324(22)	6307(17)

Table 16.2: Different perturbative determinations of the B_c mass compared with the experimental value and a recent lattice determination.

Once the heavy quark masses are known, one may use them to extract other quarkonium ground-state observables. The B_c mass has been calculated at NNLO in [69, 170, 172], see Table 16.2. These values agree well with the unquenched lattice determination of [70], which shows that the B_c mass is not very sensitive to non-perturbative effects. This is confirmed by a recent measurement of the B_c in the channel $B_c \to J/\psi\,\pi$ by the CDF collaboration at the Tevatron; they obtain with 360 pb^{-1} of data $M_{B_c} = 6285.7 \pm 5.3 \pm 1.2$ MeV [71], while the latest available figure based on 1.1 fb^{-1} of data is $M_{B_c} = 6276.5 \pm 4.0 \pm 2.7$ MeV (see http://www-cdf.fnal.gov/physics/new/bottom/060525.blessed-bc-mass/).

The bottomonium and charmonium ground-state hyperfine splitting has been calculated at NLL in [178]. Combining it with the measured $\Upsilon(1S)$ mass, this determination provides a quite precise prediction for the η_b mass: $M_{\eta_b} = 9421 \pm 10^{+9}_{-8}$ MeV, where the first error is an estimate of the theoretical uncertainty and the second one reflects the uncertainty in $\alpha_{\rm s}$. Note that the discovery of the η_b may provide a very competitive source of $\alpha_{\rm s}$ at the bottom mass scale with a projected error at the M_Z scale of about 0.003. Similarly, in [83], the hyperfine splitting of the B_c was calculated at NLL accuracy: $M_{B_c^*} - M_{B_c} = 65 \pm 24^{+19}_{-16}$ MeV.

High-lying $Q\bar{Q}$ states are assumed to realize the hierarchy: $m \gg mv \sim \Lambda_{\rm QCD} \gg mv^2$. A first question is where the transition from low-lying to high-lying takes place. This is not obvious, because we cannot measure directly mv. Therefore, the answer can only be indirect and, so far, there is no clear agreement in the literature. A weak-coupling treatment for the lowest-lying bottomonium states ($n = 1$, $n = 2$ and also for the $\Upsilon(3S)$) appears to give positive results for the masses at NNLO in [170] and at N^{3}LO* in [174]. The result is more ambiguous for the fine splittings of the bottomonium $1P$ levels in the NLO analysis of [43] and positive only for the $\Upsilon(1S)$ state in the N^{3}LO* analysis of [175].

Masses of high-lying quarkonia may be accessed by lattice calculations.

16.2.8 Transitions

Allowed magnetic dipole transitions between charmonium and bottomonium ground states have been considered at NNLO in [269, 60]. The results are: $\Gamma(J/\psi \to \gamma\,\eta_c) = (1.5 \pm 1.0)$ keV and $\Gamma(\Upsilon(1S) \to \gamma\,\eta_b) = (k_\gamma/39\ \mathrm{MeV})^3\ (2.50 \pm 0.25)$ eV, where the errors account for uncertainties (which are large in the charmonium case) coming from higher-order corrections. The width $\Gamma(J/\psi \to \gamma\,\eta_c)$ is consistent with [61]. Concerning $\Gamma(\Upsilon(1S) \to \gamma\,\eta_b)$, a photon energy $k_\gamma = 39$ MeV corresponds to a η_b mass of 9421 MeV.

In the weak-coupling regime, the magnetic-dipole hindered transition $\Upsilon(2S) \to \gamma\,\eta_b$ at leading order [269] does not agree with the experimental upper bound [276], while the ratios for different n of the radiative decay widths $\Gamma(\Upsilon(nS) \to \gamma\,X)$ are better consistent with the data if $\Upsilon(1S)$ is assumed to be a weakly-coupled bound state and $\Upsilon(2S)$ and $\Upsilon(3S)$ strongly coupled ones [230].

The radiative transition $\Upsilon(1S) \to \gamma\,X$ has been considered in [219, 197]. The agreement with the CLEO data of [195] is very satisfactory (cf. the contribution by .... in this BES Yellow Book).

16.2.9 Inclusive Decays

The imaginary part of the potential provides the NRQCD decay matrix elements in pNRQCD.

For excited states, they typically factorize in a part, which is the wave function in the origin squared (or its derivatives), and in a part which contains gluon tensor-field correlators [55, 205, 56, 57]. This drastically reduces the number of non-perturbative parameters needed; in pNRQCD, these are wave functions at the origin and universal gluon tensor-field correlators, which can be calculated on the lattice. Another approach may consist in determining the correlators on one set of data (e.g. in the charmonium sector) and use them to make predictions for another (e.g. in the bottomonium sector). Following this line in [55, 58], at NLO in $\alpha_{\rm s}$, but at leading order in the velocity expansion, it was predicted $\Gamma_{\rm had}(\chi_{b0}(2P))/\Gamma_{\rm had}(\chi_{b2}(2P)) \approx 4.0$ and $\Gamma_{\rm had}(\chi_{b1}(2P))/\ \Gamma_{\rm had}(\chi_{b2}(2P)) \approx 0.50$. Both determinations turned out to be consistent, within large errors, with the CLEO III data [267].

For the lowest resonances, inclusive decay widths are given in weakly coupled pNRQCD by a convolution of perturbative corrections and nonlocal nonperturbative correlators. The perturbative calculation embodies large contributions and requires large logs resummation. The ratio of electromagnetic decay widths was calculated for the ground state of charmonium and bottomonium at NNLL order in [179]. In particular, they report: $\Gamma(\eta_b \to \gamma\gamma)/\Gamma(\Upsilon(1S) \to e^+e^-) = 0.502 \pm 0.068 \pm 0.014$, which is a very stable result with respect to scale variation. A partial NNLL* order analysis of the absolute width of $\Upsilon(1S) \to e^+e^-$ can be found in [176].

16.2.10 Baryons with two or more heavy quarks

The SELEX collaboration at Fermilab reported evidence of five resonances that may possibly be identified with doubly charmed baryons [44]. Although these findings have

not been confirmed by other experiments (notably by FOCUS, BELLE and BABAR) they have triggered a renewed theoretical interest in doubly heavy baryon systems.

Low-lying QQq states are assumed to realize the hierarchy: $m \gg mv \gg \Lambda_{\rm QCD}$, where mv is the typical inverse distance between the two heavy quarks and $\Lambda_{\rm QCD}$ is the typical inverse distance between the centre-of-mass of the two heavy quarks and the light quark. At a scale μ such that $mv \gg \mu \gg \Lambda_{\rm QCD}$ the effective degrees of freedom are QQ states (in color antitriplet and sextet configurations), low-energy gluons and light quarks. The most suitable EFT at that scale is a combination of pNRQCD and HQET [45, 46]. The hyperfine splittings of the doubly heavy baryon lowest states have been calculated at NLO in $\alpha_{\rm s}$ and at LO in $\Lambda_{\rm QCD}/m$ by relating them to the hyperfine splittings of the D and B mesons (this method was first proposed in [47]). In [45], the obtained values are: $M_{\Xi^*_{cc}} - M_{\Xi_{cc}} = 120 \pm 40$ MeV and $M_{\Xi^*_{bb}} - M_{\Xi_{bb}} = 34 \pm 4$ MeV, which are consistent with the quenched lattice determinations of [48, 49, 50, 51]. Chiral corrections to the doubly heavy baryon masses, strong decay widths and electromagnetic decay widths have been considered in [52].

Also low-lying QQQ baryons can be studied in a weak coupling framework. Three quark states can combine in four color configurations: a singlet, two octets and a decuplet, which lead to a rather rich dynamics [45]. Masses of various QQQ ground states have been calculated with a variational method in [53]: since baryons made of three heavy quarks have not been discovered so far, it may be important for future searches to remark that the baryon masses turn our to be lower than those generally obtained in strong coupling analyses. For QQQ baryons with a typical distance of the order $\Lambda_{\rm QCD}$ inverse, the form of the static, $1/m$ and spin dependent nonperturbative potentials have been obtained in pNRQCD [45]. Up to now only the static potential has been evaluated on the lattice [24, 67].

16.2.11 Gluelump Spectrum and exotic states

The gluelumps are states formed by a gluon and two hravy quarks in a octet configuration at small interquark distance [85] . The mass of such nonperturbative objects are typically measured on the lattice. The tower of hybrids static energies [84] reduces to the gluelump masses for small interquark distances. In pNRQCD [201, 33] the full structure of the gluelump spectrum has been studied, obtaining model independent predictions on the shape, the pattern, the degeneracy and the multiplet structure of the hybrid static energies for small $Q\bar{Q}$ distances that well match and interpret the existing lattice data. These studies may be important both to elucidate the confinement mechanism (the gluelump masses control the behaviour of the nonperturbative glue correlators appearing in the spectrum and in the decays) and in relation to the exotic states recently observed at the B-factories. The $Y(4260)$ in the charmonium sector may be identified with an hybrid state inside such picture [86].

16.2.12 Outlook

pNRQCD makes possible to investigate a wide range of heavy quarkonium observables in a controlled and systematic fashion and therefore it makes possible to learn about one of

the most elusive sectors of the Standard Model: low-energy QCD. Among the most interesting and open theory challenges there are: the construction of an EFT close to threshold to understand the new exotic states, the taming of quarkonium production and the development of an EFT approach to quarkonium suppression in media and quarkonium-nuclei interaction.

The many new data coming in the last few years from B-Factories, CLEO, BES, HERA and the Tevatron experiment have given us glimpses of interesting physics to be explored. With the new theory tools discussed here and with the impressive number of produced and detected charmonium states, BES-III will make the difference in this field allowing to carry on important investigation inside the Standard Model and beyond the Standard Model (see [267] Chapter Beyond the Standard Model and [87]).

Chapter 17

Charmonium Spectroscopy

17.1 Introduction

Historically [88, 89, 90, 91, 92, 93] charmonium has played an important rôle in the study of the strong interaction, including the search for exotica, and in the development of our understanding of the forces between quarks. The spectrum of relatively narrow charmonium states that cannot decay into open-charm modes is experimentally very clear; this has made it possible to precisely measure the masses of states that in the quark model are identified with N,L multiplets, and in addition the effects of the weaker spin-dependent forces (spin-spin, spin-orbit and tensor) in splitting these multiplets into states of definite S and J can also be quantified. Not only are the effects of the Breit-Fermi Hamiltonian (which is due to one gluon exchange, "OGE") evident in the spectrum, but the Lorentz nature of the confining interaction itself has also been established (as scalar rather than timelike vector).

In future studies of charmonium spectroscopy at BES it should be possible to discover many charmonium states that are expected theoretically but have not yet been observed. Some of the as yet unknown states are expected to be very narrow resonances. In addition one can presumably identify novel exotica that are currently unknown or poorly understood, such as charm molecules and charmonium hybrids. Our understanding of the known charmonium states can be greatly improved through more precise measurements of transitions involving these states, including both radiative and strong couplings. These studies have the potential to greatly improve our understanding of strong decays in particular. In this section we will review the current status of our understanding of charmonium and closely related systems, and will discuss some ways in which BES can contribute to our understanding of QCD through future experimental studies of charmonium.

The areas we will consider in particular are as follows:

I. Conventional charmonium

a. spectrum

b. EM couplings

b.1. e^+e^- widths of 1^{--} states
b.2. EM transitions between charmonium states
b.3. $\gamma\gamma$ widths

c. strong decays
c.1. annihilation decays
c.2. open-flavor strong decays

II. Novel states incorporating a $c\bar{c}$ subsystem

a. charm molecules

b. charmonium hybrids

17.2 Conventional charmonium states

17.2.1 Spectrum

The spectrum of the known "conventional" charmonium states, by which we mean states that appear to be in relatively good agreement with the predictions of simple $c\bar{c}$ potential models, is summarized in Table 17.1. The table, which is abstracted from the 2006 PDG [448], gives the usual quark model N,L multiplet assignment, the quark model spectroscopic assignment, the PDG name, and the mass and width of each state.

Mult.	Spec.	Expt. state	Mass [MeV]	Width [MeV]
1S	1^3S_1	$J/\psi(1S)$	3096.916 ± 0.011	0.0934 ± 0.0021
	1^1S_0	$\eta_c(1S)$	2980.4 ± 1.2	25.5 ± 3.4
1P	1^3P_2	$\chi_{c2}(1P)$	3556.20 ± 0.09	2.06 ± 0.12
	1^3P_1	$\chi_{c1}(1P)$	3510.66 ± 0.07	0.89 ± 0.05
	1^3P_0	$\chi_{c0}(1P)$	3414.76 ± 0.35	10.4 ± 0.7
	1^1P_1	$h_c(1P)$	3525.93 ± 0.27	< 1
2S	2^3S_1	$\psi(2S)$	3686.093 ± 0.034	0.337 ± 0.013
	2^1S_0	$\eta_c(2S)$	3638 ± 4	14 ± 7
1D	1^3D_3	-		
	1^3D_2	-		
	1^3D_1	$\psi(3770)$	3771.1 ± 2.4	23.0 ± 2.7
	1^1D_2	-		
2P	2^3P_2	$\chi_{c2}(2P)$	$3929 \pm 5 \pm 2$	$29 \pm 10 \pm 2$
	2^3P_1	-		
	2^3P_0	-		
	2^1P_1	-		
3S	3^3S_1	$\psi(4040)$	4039 ± 1	80 ± 10
	3^1S_0	-		
2D	2^3D_3	-		
	2^3D_2	-		
	2^3D_1	$\psi(4160)$	4153 ± 3	103 ± 8
	2^1D_2	-		
4S	4^3S_1	$\psi(4415)$	4421 ± 4	62 ± 20
	4^1S_0	-		

Table 17.1: Experimental spectrum of reasonably well established "conventional" $c\bar{c}$ states. This table gives the usual quark model multiplet and spectroscopic assignment for each state and the PDG label for the state, followed by their masses and widths. Partner states that are expected theoretically but not yet identified experimentally are indicated by a dash.

This spectrum of states can be described surprisingly well using a simple $c\bar{c}$ potential model. In these models one typically assumes a zeroth-order (spin-independent) potential that combines a OGE color Coulomb term and a linear confining interaction,

$$V_0^{(c\bar{c})}(r) = -\frac{4}{3}\frac{\alpha_s}{r} + br. \tag{17.1}$$

This is augmented by the spin-dependent Breit-Fermi Hamiltonian due to OGE, and an inverted spin-orbit term that arises from the (assumed) scalar nature of the confining interaction,

$$V_{spin-dep} = \frac{32\pi\alpha_s}{9m_c^2}\,\vec{\mathrm{S}}_c \cdot \vec{\mathrm{S}}_{\bar{c}}\,\delta(\vec{x}\,) + \frac{1}{m_c^2}\left[\left(\frac{2\alpha_s}{r^3} - \frac{b}{2r}\right)\vec{\mathrm{L}}\cdot\vec{\mathrm{S}} + \frac{4\alpha_s}{r^3}\,\mathrm{T}\right]. \tag{17.2}$$

Two examples of the spectra predicted by this type of model, a fully nonrelativistic potential model "NR" and the relativized Godfrey-Isgur model [96] "GI" are shown in Fig.17.1. (Here and in much of our discussion of charmonia we will refer to the $c\bar{c}$ potential model of Ref.[95], since potential models give predictions for many of the observed properties of charmonium resonances. Much of the original literature is also cited in this reference, and should be reviewed for a more complete discussion. We also note that several excellent and very extensive reviews of charmonia have appeared [97, 98, 267, 100, 101, 102, 103] which discuss recent developments in the field in detail.)

The experimental and theoretical masses (in the two models of Table 17.2) are shown in Fig. 17.1. Evidently there is reasonably good agreement between the current experimental spectrum and the potential model predictions. Comparison between the nonrelativistic and relativized models shows some discrepancies, notably in the scales of 2P and 3P multiplet splittings and in the positions of the higher-L multiplets. The immediate experimental tasks suggested by this spectrum are the identification of the remaining 2P states, the 3P states and the higher-L levels. Identification of the remaining 2P states (those with C=(+)) can be carried out at BES using E1 radiative transitions from the higher 1^{--} levels $\psi(4040)$ and $\psi(4160)$). Identification of the 3P levels will be more complicated because hybrid charmonia are expected at similar masses; we shall see that this may be possible using $\psi(4415)$ radiative transitions. Finally, the important problem of the identification of the higher-L states is a difficult problem. It may be possible to identify one such state, the $^3\mathrm{F}_2$ $c\bar{c}$, in radiative transitions from the $\psi(4160)$. Experimentally accessing the other higher-L $c\bar{c}$ states is an unsolved problem.

It is also possible to predict the spectrum of charmonia, especially the lowest-lying states in each sector of state space, using lattice gauge theory (LGT); for some recent references see Refs.[104, 105, 106, 107]. This approach is very attractive in that it does not require the assumptions of potential models, and can in addition be applied to the study of novel states such as the $\mathrm{J^{PC}}$-exotic charmonium hybrids, where potential models are of unknown accuracy. To date the results of LGT for the charmonium spectrum are very similar to the predictions of potential models for the lighter states, which are experimentally well established. Current LGT predictions for the more controversial higher-mass states unfortunately have rather large errors (100 MeV is typical at present), so they cannot yet

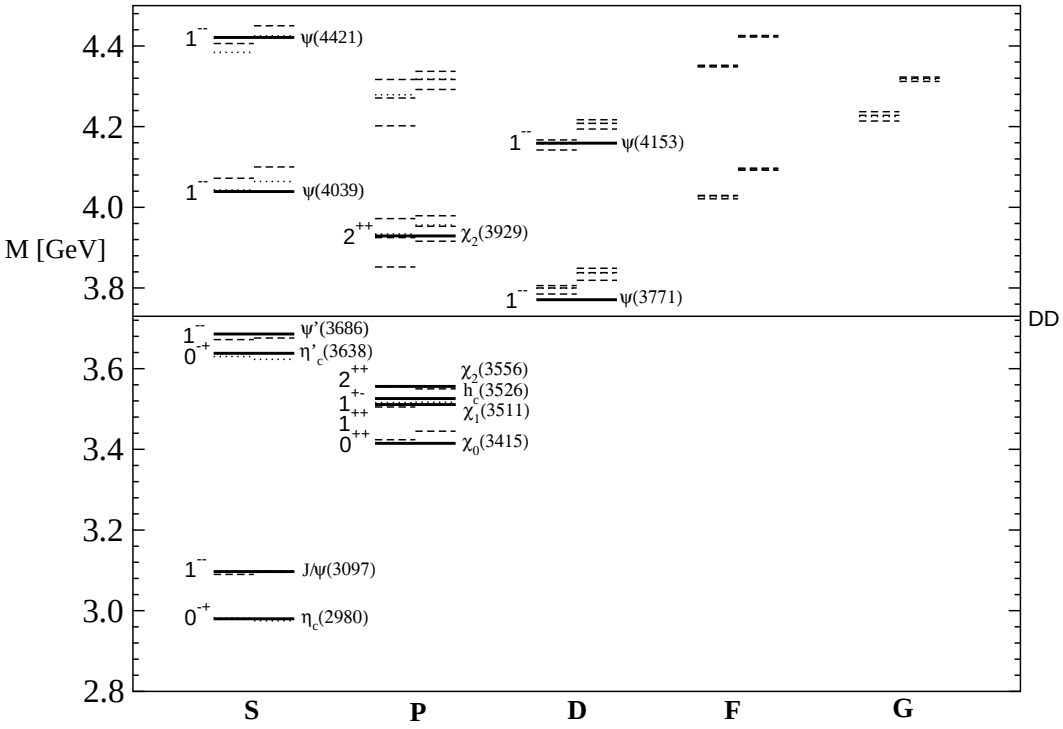

Figure 17.1: Predicted and observed spectrum of charmonium states (Table 17.2). The solid lines are experiment for reasonably well-established charmonium states, and the particle labels give the actual 2006 PDG masses in MeV rather than the usual rounded PDG mass labels. The broken lines are theory (NR model left, GI right). In the theoretical spectra, spin triplet levels are dashed and spin singlets are dotted. The DD open-charm threshold at 3.73 GeV is also shown.

usefully be compared to experimental candidates or potential model calculations. Future LGT calculations of the charmonium spectrum should be very interesting in this regard. One very interesting question that LGT can hopefully address will be the importance of quenching (the effect of closed $q\bar{q}$ loops on the spectrum and couplings of charmonia). The closely related question of the importance of closed virtual continuum channels on the properties of heavy quarkonia and hadrons more generally is a very important and controversial issue.

17.3 EM Couplings

17.3.1 e^+e^- widths of 1^{--} states

Leptonic partial widths are immediately accessible at e^+e^- machines, and they provide interesting (and currently rather puzzling) information regarding the wavefunctions of 1^{--} charmonium states. In the nonrelativistic limit of an S-wave quarkonium system the coupling to e^+e^- through a virtual photon involves the wavefunction at contact (the van Royen - Weisskopf formula); for an S-wave $c\bar{c}$ system this partial width is given by [108],

$$\Gamma_{c\bar{c}}^{e^+e^-}({}^3\mathrm{S}_1) = \frac{16}{9}\,\alpha^2\,\frac{|\psi(0)|^2}{\mathrm{M}_{c\bar{c}}^2} \tag{17.3}$$

where the radial wavefunction is normalized to $\int_0^\infty r^2 dr\,|\psi(r)|^2 = 1$. for relativistic bound states the annihilation is nonlocal, so a nonvanishing e^+e^- coupling of D-wave (and higher-L 1^{--} states) is also predicted. This width at leading nonrelativistic order is proportional to the Lth derivative of the $Q\bar{Q}$ wavefunction at contact, and for D-wave $c\bar{c}$ states is given by

$$\Gamma_{c\bar{c}}^{e^+e^-}({}^3\mathrm{D}_1) = \frac{50}{9}\,\alpha^2\,\frac{|\psi''(0)|^2}{\mathrm{M}_{c\bar{c}}^2 m_c^4}. \tag{17.4}$$

This is typically much smaller than the leptonic widths of ${}^3\mathrm{S}_1$ states. Evaluating these widths using the nonrelativistic quark model wavefunctions described here gives the results quoted in Table 17.3.1.

Note that the agreement between the model and experiment is not especially good. This overestimate of the J/ψ leptonic width by roughly a factor of two seems to be a common difficulty in naive potential models, and may in part be due to the use of the nonrelativistic "wavefunction at contact" approximation for this decay rate. Non-valence components in the charmonium states, such as $c\bar{c}g$ or D meson pairs from decay loops, may also contribute to this inaccuracy. Concerns have also been expressed that the leading-order QCD radiative corrections may be large [109], which could significantly reduce the overall scale of the leptonic widths. Of course the leading-order pQCD corrections are prescription-dependent, so it is not clear that this claim is reliable. In any case it is evident that a simple change of scale alone will not resolve the discrepancies in Table 17.3.1, since the nominally D-wave states $\psi(3770)$ and $\psi(4160)$ both have much larger couplings that would be expected for pure D-wave states.

The large experimental leptonic widths of the $\psi(3770)$ and $\psi(4160)$ relative to predictions for pure D-wave $c\bar{c}$ states (see Table 17.3.1) may be due to admixtures of S-wave $c\bar{c}$

components [110, 500]. As we shall discuss in the next section, these mixing angles can be estimated through measurements of the E1 radiative decay rates $\psi(3770) \to \gamma\chi_2$ and (with more difficulty) $\psi(4160) \to \gamma\chi_2$ and $\gamma\chi_2{}'$, since these transitions are very sensitive to the presence of S-wave $c\bar{c}$ components. Radiative width ratios such as $\Gamma(\psi(3770) \to \gamma\chi_2)/\Gamma(\psi(3770) \to \gamma\chi_1)$ and the leptonic width ratio $\Gamma(\psi(3770) \to e^+e^-)/\Gamma(\psi' \to e^+e^-)$ provide two independent tests of S-D mixing.

At BES, in addition to testing the existing measurements of the leptonic widths of the vector states cited in Table 17.3.1, it will also be very important to determine the leptonic widths of new 1^{--} hybrid candidates such as the Y(4260) (to be discussed in the section on hybrid charmonia). It has widely been anticipated that 1^{--} hybrids should have suppressed leptonic widths relative to conventional S-wave 1^{--} vector quarkonia; this may indeed be the case for the Y(4260), since it is not apparent in the existing R measurements.

17.3.2 EM Transitions Between Charmonium States

E1 radiative transitions

Radiative transitions are a very interesting feature of charmonium physics. They are quite straightforward to evaluate in $c\bar{c}$ potential models, and (with sufficient statistics) provide a route from the initial 1^{--} states produced in e^+e^- annihilation to C = (+) charmonia.

The largest rates are for E1 (electric dipole) transitions, which in the nonrelativistic quark model involve a simple matrix element of $\vec{x}$. The results we will quote here use the expression

$$\Gamma_{\rm E1}({\rm n}\,^{2{\rm S}+1}{\rm L}_{\rm J} \to {\rm n}'\,^{2{\rm S}'+1}{\rm L}'_{\rm J'} + \gamma) = \frac{4}{3}\, e_c^2\, \alpha\, {\rm E}_\gamma^3\, \frac{{\rm E}_f^{(c\bar{c})}}{{\rm M}_i^{(c\bar{c})}}\, C_{fi}\, \delta_{\rm SS'}\, |\, \langle {\rm n}'\,^{2{\rm S}'+1}{\rm L}'_{\rm J'} |\, r\, |\, {\rm n}\,^{2{\rm S}+1}{\rm L}_{\rm J} \rangle\, |^2 \tag{17.5}$$

where $e_c = 2/3$ is the c-quark charge in units of $|e|$, α is the fine-structure constant, $\rm E_\gamma$ is the photon's energy, and the angular matrix element C_{fi} is

$$C_{fi} = \max({\rm L},\ {\rm L}')(2{\rm J}'+1) \left\{ \begin{array}{ccc} {\rm L}' & {\rm J}' & {\rm S} \\ {\rm J} & {\rm L} & 1 \end{array} \right\}^2 . \tag{17.6}$$

This is the formula quoted by Ref.[112], except for our inclusion of a relativistic phase space factor. (We note in passing that it is also possible to evaluate these E1 transition rates using LGT; preliminary results of this work have been presented by Dudek [270].) We evaluate the matrix elements $\langle n'^{2{\rm S}'+1}{\rm L}'_{\rm J'} |\, r\, | n^{2{\rm S}+1}{\rm L}_{\rm J} \rangle$ using the nonrelativistic Schrödinger wavefunctions obtained in the model described in the previous section.

Several very interesting features of E1 radiative transitions are evident in Tables 17.4,17.5. First, the 1P $\to$ 1S (Table 17.4) transitions are in very reasonable agreement with experiment. It is notable that the predicted radiative partial width for $h_c \to \gamma\eta_c$ is especially

large, which would be an interesting measurement provided that an entry channel for the h_c can be identified at BES.

The theoretical rates for the 2S $\rightarrow$ 1P transitions (Table 17.4) appear too large by about a factor of two, although the relativized model of Godfrey and Isgur [96] does not share this difficulty. We note in passing that apparent good agreement between a pure-$c\bar{c}$ charmonium potential model and experiment may actually be spurious; decay loop effects will contribute two-meson continuum components to all these charmonium resonances, which may significantly modify the predicted radiative transition rates.

E1 radiative transitions from the higher-mass charmonium states are especially interesting. The 1^3D_1 candidate $\psi(3770)$ (Table 17.4) is predicted to have large partial widths to $\gamma\chi_1$ and $\gamma\chi_0$ (with branching fractions of 0.5% and 1.7% respectively), but the branching fraction to $\gamma\chi_2$ is predicted to be only about $2 \cdot 10^{-4}$. This small number however follows from the assumption that the $\psi(3770)$ is a pure $^3D_1$ state; if there is a significant admixture of S-wave basis states in the $\psi(3770)$,

$$|\psi(3770)\rangle = \cos(\theta)\,|^3D_1\rangle + \sin(\theta)\,|2^3S_1\rangle \tag{17.7}$$

one typically finds a much larger radiative width to $\gamma\chi_2$ [115, 110, 500]. (See Fig. 17.2. The sign of the mixing angle θ depends on the convention for the normalization of the $^3D_1$ and 2^3S_1 basis states; note for example in Fig.1 of Ref.[500] that a zero $\psi(3770) \rightarrow \gamma\chi_2$ width requires a small negative mixing angle, whereas with our conventions it would be positive.) Since the coupling of the $\psi(3770)$ to e^+e^- suggests a significant 2^3S_1 component, a measurement of this radiative partial width at BES will be especially useful as an independent test of the presence of this amplitude in the $\psi(3770)$ wavefunction.

We note in passing that if the dominant mechanism of $^3D_1$ - 2^3S_1 basis state mixing in the $\psi(3686)$ and $\psi(3770)$ is through virtual charm meson decay loops such as DD, DD* and D*D*, the assumption of a $2 \otimes 2$ orthogonal mixing matrix as in Eq.17.7 is incorrect. In this case the $\langle^3D_1|\psi(3686)\rangle$ and $\langle 2^3S_1|\psi(3770)\rangle$ overlaps will no longer be simply related, and radiative transition amplitudes will also receive contributions due to photon emission from the two-meson continua.

Next we consider radiative decays of the higher-mass vectors $\psi(4040)$ and $\psi(4160)$. As is evident in Table 17.5, if the $\psi(4040)$ is dominantly a 3^3S_1 state as we assume here, it should have very small E1 radiative widths to the triplet members of the 1P multiplet, with branching fractions of at most about 10^{-6}. Since other components of the $\psi(4040)$ state vector (for example $^3D_1$ or charmed meson continua) may lead to significant radiative couplings to 1P states, it will be very interesting for BES to search for these radiative modes. The radiative widths of the $\psi(4040)$ to the controversial 2P triplet states are predicted to be much larger, with branching fractions of up to $\sim 10^{-3}$. Since the 2P states should have large strong branching fractions to DD (χ_0 and χ_2) and DD* (χ_1 and χ_2) [95], it may be possible to identify these states in the DD and DD* invariant mass distributions of the decays $\psi(4040) \rightarrow \gamma$DD and γDD*.

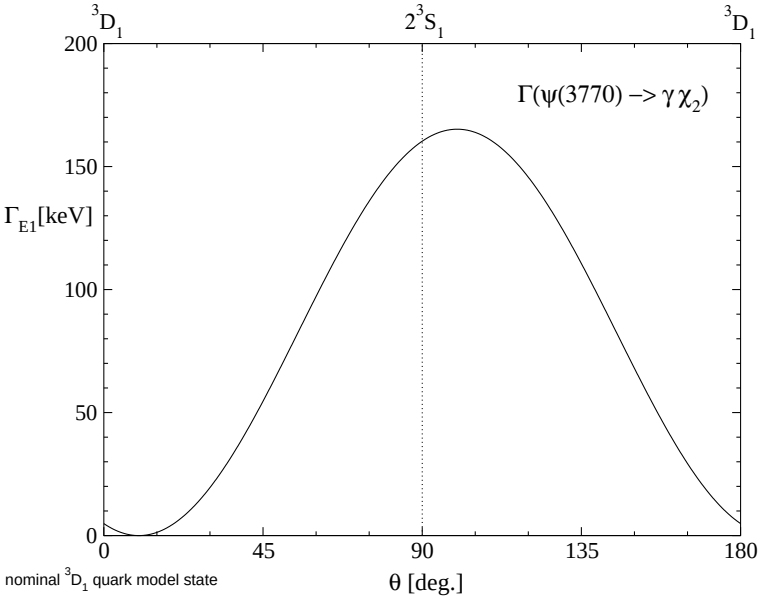

Figure 17.2: Predicted radiative partial width for the E1 transition $\psi(3770) \to \gamma\chi_2$ as a function of the 2^3S_1-$^3D_1$ mixing angle θ.

Radiative decays of the $\psi(4160)$ share certain features with the decays of both the $\psi(3770)$ and the $\psi(4040)$. First, the coupling to the 2P multiplet is again predicted to be much stronger than to the 1P multiplet, so radiative decays of the $\psi(4160)$ can be used to search for 2P states. The branching fraction to the 2^3P_0 χ_0 state in particular may be as large as $\sim 0.5\%$ if it is at ≈ 3850 MeV. Second, just as for the $\psi(3770)$ a strong suppression of decays to all $^3P_2$ "χ_2" states is predicted, but this follows from the assumption that the $\psi(4160)$ is a pure D-wave $c\bar{c}$ state; with an S-wave $\psi(4160)$ admixture, which is required to explain the $\psi(4160)$ leptonic width, the coupling to $^3P_2$ states may be much larger; this should be searched for at BES. Finally, an interesting feature of D-wave $c\bar{c}$ E1 decays is that one may reach the currently unknown 1F $c\bar{c}$ multiplet (specifically the state $^3F_2$); $\psi(4160)$ decays to γDD should be appropriate for this. Unfortunately, the $^3F_2$ state is expected to be rather broad [95].

Accessing the new states near 3.9 GeV through E1 transitions

The $\psi(4040)$ and $\psi(4160)$ can be used as 1^{--} entry states for the study of the new XYZ states near 3.9 GeV. As shown in Table 17.6, both these states are expected to have relatively large E1 branching fractions into the 2P $c\bar{c}$ multiplet, $\psi(4040, 4160) \to \gamma\chi'_J$. (These E1 partial widths were calculated as in Table 17.5 and Ref.[95], but the final masses were lowered to 3929 MeV and 3940 MeV to accommodate the new XYZ resonances as 2P candidates.) Note that these lower masses give significantly larger E1 partial widths than in Table 17.5. Evidently, studies of E1 transitions from the $\psi(4040)$ and $\psi(4160)$ at BES should allow the identification of the 2P resonances through their hadronic decays. In this approach one would study the invariant mass and angular distributions of the final charmed mesons in the processes $e^+e^- \to \psi(4040, 4160) \to \gamma$DD and γDD*.

M1 radiative transitions

M1 transitions between charmonium states in pure $c\bar{c}$ models result from photon emission through the $H_I = -\vec{\mu} \cdot \vec{B}$ magnetic moment interaction of the c quark (and antiquark), and as such are suppressed relative to E1 transitions by the small factor of $1/m_c$ in the magnetic moment operator. The M1 transition amplitude is proportional to the matrix element of the spin operator, with a spatial factor that (without recoil corrections) is simply the matrix element of unity. M1 transitions are therefore nonzero only between states with the same $\mathrm{L}_{c\bar{c}}$ (and different $\mathrm{S}_{c\bar{c}}$, since the C-parity must change). If we assumed a spin-independent zeroth-order potential and neglect recoil effects, M1 transitions between different radial multiplets would vanish because the $\mathrm{n}^3\mathrm{S}_1$ and $\mathrm{n}'^1\mathrm{S}_0$ states have orthogonal spatial wavefunctions. One such transition is actually observed in charmonium, $\psi' \to \gamma\eta_c$, which must be due in part to the nonorthogonal ψ' and η_c spatial wavefunctions and final meson recoil effects.

The formula for M1 decay rates analogous to the E1 formula used in the previous section is

$$\Gamma_{\mathrm{M1}}(\mathrm{n}\,^{2\mathrm{S}+1}\mathrm{L}_{\mathrm{J}} \to \mathrm{n}'\,^{2\mathrm{S}'+1}\mathrm{L}'_{\mathrm{J}'} + \gamma) = \frac{4}{3}\, e_c^2\, \frac{\alpha}{m_c^2}\, \mathrm{E}_\gamma^3\, \frac{\mathrm{E}_f^{(c\bar{c})}}{\mathrm{M}_i^{(c\bar{c})}}\, \frac{2\mathrm{J}'+1}{2\mathrm{L}+1}\, \delta_{\mathrm{LL}'}\, \delta_{\mathrm{S,S}'\pm 1}$$
$$\cdot |\, \langle \mathrm{n}'\,^{2\mathrm{S}'+1}\mathrm{L}'_{\mathrm{J}'} |\, \mathrm{n}\,^{2\mathrm{S}+1}\mathrm{L}_{\mathrm{J}} \rangle\, |^2 \ . \qquad (17.8)$$

Evaluating this formula for transitions from the ψ and ψ' gives the results shown in Table 17.7. A more detailed study of M1 radiative decay rates, incorporating recoil corrections (which are numerically important for transitions between multiplets such as $2\mathrm{S} \to 1\mathrm{S}$) appears in Ref.[95].

An even larger discrepancy between experiment and theory is evident in the "hindered" M1 transition $\psi' \to \gamma\eta_c$. Since this rate is only nonzero due to recoil effects (not included here) and corrections to the naively orthogonal 1S and 2S $c\bar{c}$ wavefunctions, the discrepancy is perhaps less surprising than that found in the allowed $1\mathrm{S} \to 1\mathrm{S}$ $\psi \to \gamma\eta_c$ transition rate. In any case this is another example of an M1 transition rate in charmonium in which experiment and theory are clearly in disagreement. Since the experimental rate is again only about 4σ from zero, it would be very useful to improve the accuracy of this measurement at BES.

A well-known problem is evident in the decay rate $\mathrm{J}/\psi \to \gamma\eta_c$, which is that the predicted rate in the nonrelativistic potential model is about a factor of 2-3 larger than experiment. Since this rate only involves the charm quark magnetic moment, and hence only its mass, this discrepancy is a surprise. The relativized Godfrey-Isgur model [96] predicts a somewhat smaller rate of 2.4 keV, which is still about a factor of two larger than experiment. Since the errors are rather large, it would clearly be very interesting to improve the experimental accuracy of this surprising partial width. If this discrepancy is confirmed, it may be an indication that pure-$c\bar{c}$ models are a rather inaccurate description of charmonium, and that other components of the state vector such as two-meson continua make comparable important contributions to the M1 transition amplitudes. In view of

the inaccuracy of the theoretical 1S M1 transition rate, it would also be interesting to test the 2S transition rate $\psi' \to \gamma\eta_c'$ experimentally. Unfortunately, this rate is predicted to be a rather small 0.21 keV in the nonrelativistic $c\bar{c}$ model.

An even larger discrepancy between experiment and theory is evident in the "hindered" M1 transition $\psi' \to \gamma\eta_c$. Since this rate is only nonzero due to recoil effects (not included here) and corrections to the naively orthogonal 1S and 2S $c\bar{c}$ wavefunctions, the discrepancy is perhaps less surprising than that found in the allowed 1S $\to$ 1S $\psi \to \gamma\eta_c$ transition rate. In any case this is another example of an M1 transition rate in charmonium in which experiment and theory are clearly in disagreement. Since the experimental rate is again only about 4σ from zero, it would be very useful to improve the accuracy of this measurement and to search for the other M1 transitions at BES.

M1 decays between charmonium resonances have only been observed between S-wave states. The rates between orbitally excited states are typically predicted to be quite small, due to the small splittings within excited-L multiplets. They are large enough however to be observable given narrow initial states and large event samples. For example, a hypothetical $^1D_2$ $c\bar{c}$ assignment for the X(3872) could be tested through a search for its M1 decay to $\gamma\psi(3770)$, which would have a partial width of about 1.2 keV in the nonrelativistic potential model. The h_c decay $h_c \to \gamma\chi_0$ has similar phase space, and is predicted to have a partial width of 0.8 keV. In contrast, the smaller phase space of the M1 transition from the higher-mass χ_2 state leads to an expected partial width for $\chi_2 \to \gamma h_c$ of only about 60 eV.

17.3.3 Two-photon couplings

Although BES will not have adequate $\sqrt{s}$ to usefully exploit two-photon production of charmonium resonances, this has been a useful technique at higher-energy e^+e^- facilities, which we briefly mention here in the interest of completeness. This subject has been reviewed elsewhere [116].

Two-photon resonance production involves the reaction $e^+e^- \to e^+e^-R$, $R \to f$, where R is a C = (+) meson resonance and f is the exclusive final state observed. This process proceeds dominantly through the two-photon coupling of the resonance, $e^+e^- \to e^+e^-\gamma\gamma$, $\gamma\gamma \to R$, and hence implicitly gives the two-photon partial width $\Gamma_{\gamma\gamma}(R)$ times the branching fraction $B(R \to f)$. One may also consider the case of one or both photons significantly off mass shell $q_\gamma^2 \neq 0$, which gives the generalized widths $\Gamma_{\gamma^*\gamma}(R)$ and $\Gamma_{\gamma^*\gamma^*}(R)$. The interesting question for off-shell widths is whether they are given by a vector dominance formula with the mass of the relevant vector, in this case the J/ψ.

In the limit of large quark mass (and hence a zero-range charm quark propagator) the two-photon width of an S-wave charmonium state is proportional to the wavefunction at contact squared. In this approximation, higher-L states are produced with amplitudes proportional to the Lth derivative of the wavefunction at contact [117, 118]. (In practice the attractively simple contact approximation appears marginal at best at the $c\bar{c}$ mass

scale.) Both the η_c and $\eta_c{}'$ have been seen in two-photon collisions; the $\gamma\gamma$ width of the η_c is approximately 7 keV, comparable to quark model expectations. Two-photon production of the η_c' has been observed by CLEO-c [119], but the $\eta_c{}' \to \gamma\gamma$ partial width is not known because experimentally one measures the $\gamma\gamma$ width times the branching fraction to an exclusive final state, and the $\eta_c{}'$ absolute branching fractions are not known.

Higher-L $c\bar{c}$ two-photon widths are suppressed by the mass of the charm quark, and therefore are not very well established; only the P-wave χ_0 and χ_2 states and the $2^3\mathrm{P}_2$ candidate $\chi_2(3929)$ have been observed. The theoretical ratio of P-wave $\gamma\gamma$ widths within a multiplet (such as 1P or 2P) in the large quark mass limit is $\Gamma_{\gamma\gamma}(^3\mathrm{P}_0)/\Gamma_{\gamma\gamma}(^3\mathrm{P}_2) = 15/4$, however this may be modified significantly by QCD radiative corrections and finite quark mass effects. Nonrelativistically the $\gamma\gamma$ state produced by the $^3\mathrm{P}_2$ should be pure helicity two; relativisitic corrections are expected to give rise to a small helicity-zero $\gamma\gamma$ component as well. Although one can in principle produce higher-L $c\bar{c}$ states in $\gamma\gamma$ collisions, in practice these rates fall rapidly with increasing L for $c\bar{c}$ and heavier $Q\bar{Q}$ systems. As an example, the two-photon width of a hypothetical $^1\mathrm{D}_2(3840)$ $c\bar{c}$ state is predicted to be only 20 eV [116].

17.3.4 Strong Decays

Annihilation Decays

Charmonium states that are below their open-charm decay threshold (all states below $2m_D = 3.73$ GeV, and in addition the lightest 2^{-+} and 2^{--} 1D states) must decay through annihilation of the $c\bar{c}$ pair. The total widths in these decays have traditionally been described as annihilation into gluons, using the corresponding formulas for positronium annihilation into photons but with α_s vertices and combinatoric color factors.

These calculations are dubious for several reasons. First, the assumption of free gluons final states and pQCD dynamics is presumably a bad approximation, since the actual glueball spectrum has widely spaced discrete levels and a mass gap that is about half as large as charmonium itself. Second, when higher-order pQCD radiative corrections are incorporated, it is often found that they are so large as to make the numerical predictions clearly unreliable. Finally, the use of positronium formulas is a nonrelativistic approximation, which is not well justified for the charmonium system.

Despite these many caveats these pQCD predictions for charmonium annihilation total widths remain interesting as rough guidelines, and some of the qualitative predictions do seem to be satisfied. For example, since α_s is not large at the $c\bar{c}$ mass scale one expects that the annihilation decay widths of negative C-parity charmonia (which must decay into at least three gluons) should be rather smaller than the decay widths of similar positive C-parity charmonia (which can decay into two gluons). Inspection of the total widths of well established $c\bar{c}$ states below 3.73 GeV in Table 17.1 shows that this guideline is indeed

well satisfied.

Similar positronium annihilation rate formulas for other states can be adapted to give strong (gluonic and $q\bar{q}g$) total annihilation width estimates for other heavy quarkonia. These lead to the expectation that the two as yet unknown D-wave $c\bar{c}$ states h_{c2} (2^{-+} $^1D_2$) and ψ_2 (2^{--} $^3D_2$) should be quite narrow, with strong annihilation widths of perhaps ~ 1 MeV [120]. These predictions of very narrow widths make the discovery of the h_{c2} and ψ_2 two of the most important outstanding experimental goals of charmonium spectroscopy. We note in passing that their 1D partner state ψ_3 (3^{--} $^3D_3$) should have a comparably small total width; it can decay to DD, but the L=3 angular momentum barrier should make this a narrow state as well.

Discovery of these narrow states may be feasible at BES. Production of the three narrow 1D $c\bar{c}$ states may be possible using E1 radiative transitions from the appropriate 2P $c\bar{c}$ states; once formed, these narrow 1D states may then be detected through their large E1 branching fractions to the 1P $c\bar{c}$ multiplet. (Ref.[95] gives E1 radiative partial width estimates for all these transitions.)

Open-flavor Strong Decays

BES should be able to make some especially interesting contributions in this area.

It is well known from the phenomenology of even the lightest hadrons that the dominant strong decays of mesons are those that do not involve the annihilation of the valence $q\bar{q}$ pair. It was this observation, in the context of the decays of the $\phi(1020)$, that led Zweig to the suggestion of strange quarks. (Specifically, he suggested that the dominance of the $\phi(1020)$ decay mode KK over $\rho\pi$ could be understood if the $\phi(1020)$ contained a valence $s\bar{s}$ pair that could not easily annihilate, which is now known as the OZI rule. This assumption would explain why the KK transition ($s\bar{s} \to (s\bar{n})(n\bar{s})$, where $n = u, d$) dominates the transition to $\rho\pi$ ($s\bar{s} \to (n\bar{n}')(n'\bar{n})$), although KK has very little phase space.

Although these open-flavor decay modes are usually the dominant strong decay amplitudes when allowed by phase space, they remain surprisingly poorly understood. The approach normally used by theorists to model these decays is to assume pair production of a $q\bar{q}$ pair from the vacuum with 0^{++} (vacuum) quantum numbers, with a dimensionless amplitude γ that is independent of the initial state and the flavor of the $q\bar{q}$ pair. This is now known as the $^3P_0$ model, and originally suggested by Micu in 1968 [121] (pre-QCD), and was subsequently developed for explicit quark model wavefunctions by the Orsay group of LeYaouanc *et al.* [122]. The well-known flux-tube decay model of Kokoski and Isgur [123] is actually a variant of this model with some spatial modulation assumed for the $q\bar{q}$ pair production amplitude. A description in terms of Feynman diagrams and a comparison with OGE and other pair production amplitudes was given by Ackleh *et al.* [124]. This $^3P_0$ model has now been applied very extensively to most sectors of hadron Hilbert space, including charmonia [125, 126, 120, 95]. Ref.[95] gives numerical predictions

for the decay amplitudes and strong branching fractions of all charmonia expected to the mass of the $\psi(4415)$. These predictions are especially interesting because the $^3P_0$ model is only a simple phenomenological description, and may be inaccurate in practice. Since the many theoretical predictions of the preferred strong decay modes of many hadrons, including light and strange mesons [96, 127, 128], baryons, including suggestions for finding the "missing" baryons [129, 130], and hybrid mesons [131, 132] all rely on this specific decay model, it is evidently very important to test its accuracy in describing strong decays in an experimentally relatively clear sector such as charmonium.

Of course one can easily construct other models for strong decay amplitudes, and it is interesting that in their early studies of charmonium the Cornell group [133] used such an alternative model. In particular they assumed that these strong decays were a result of the linear confining interaction, which gave rise to $q\bar{q}$ pair production from the initial $c\bar{c}$ system with a $\gamma_0 \otimes \gamma_0$ nonlocal interaction and a linear br kernel between the vertices. (This choice of $\gamma_0 \otimes \gamma_0$ was motivated by the belief current in the 1970s that confinement acted as a timelike vector interaction rather than a Lorentz scalar, which is the more usual assumption at present.) Several recent charmonium papers also assume this timelike vector decay model [134, 135]. An alternative model with an $I \otimes I$ linear scalar confining interaction was developed and applied to light quarks by Ackleh *et al.* [124], but has not yet been applied to charmonium.

It will be very interesting to use charmonium decays at BES to test these strong decay models. The most sensitive tests involve the determination of amplitude *ratios*, which require studies of open-flavor decays into final states that have more than one amplitude. These relative amplitude phases are typically very sensitive to the assumed quantum numbers of the $q\bar{q}$ pair produced during the decay, whereas simple branching fractions and partial widths are affected by common features such as the available phase space. For the decays of the most easily accessible 1^{--} charmonia, studies of relative decay amplitude phases requires final states consisting of a pair of open-charm vectors, the "VV modes", since the PsPs and PsV modes involve single amplitudes (respectively $^1P_1$ and $^3P_1$). Thus PsPs and PsV final states do not allow measurements of the relative phases of strong decay amplitudes, whereas in the decay $1^{--} \to VV$ there are three amplitudes present, $^1P_1$, $^5P_1$ and $^5F_1$. The $^3P_0$ model predicts very characteristic ratios for these decay amplitudes, depending on whether the initial 1^{--} $c\bar{c}$ is an S-wave ($^3S_1$) or a D-wave ($^3D_1$) state. For an S-wave one finds $^5P_1/^1P_1 = -2\sqrt{5}$ and $^5F_1 = 0$, whereas for a D-wave one finds $^5P_1/^1P_1 = -1/\sqrt{5}$ and $^5F_1 \neq 0$ (both sets of results are independent of the radial wavefunction). There is some evidence that the physical states $\psi(4040)$ and $\psi(4160)$ may be strongly mixed linear combinations of S- and D-wave basis states, which will instead give a weighted set of decay amplitudes. Of course an experimental study of the decays of these vector states should begin with a simple scan in energy of the exclusive cross sections for e^+e^- into the various open-charm final states, to establish whether the individual resonances contributions can be clearly separated. Some preliminary studies of exclusive open-charm cross sections have recently been carried out at CLEO-c.

Unfortunately, the corresponding predictions for the open-flavor decay amplitudes of

these charmonium states using other strong decay models, such as the timelike vector model assumed by the Cornell group [133], have not yet been published. It will be a very important exercise for theorists to evaluate the strong decay predictions of this model for comparison both with future BES data and with the predictions of the $^3P_0$ model shown here.

17.3.5 Additional $\psi(3770)$ and $\psi(4415)$ topics.

Another very interesting question that can be addressed using the $\psi(3770)$ is the strength of the coupling of orbitally excited $c\bar{c}$ states to $p\bar{p}$. This is a very important question for the future PANDA experiment [137] at GSI, which plans to use $p\bar{p}$ annihilation to produce excited $c\bar{c}$ and charmonium hybrids. At present we have the intriguing experimental observation that the L=1 $c\bar{c}$ χ_J states couple much more strongly to $p\bar{p}$ than the L=0 J/ψ, but whether this trend continues to L=2 is an open question. BES can easily answer this question through a high-statistics search for $\psi(3770) \to p\bar{p}$. Charmonium decays to final states including a $p\bar{p}$ pair, such as $\Psi \to p\bar{p}$ and $\Psi \to p\bar{p}m$ (where Ψ is a generic charmonium or charmonium hybrid resonance and m is a light meson) are also very interesting in this regard, and can be used to estimate the associated production cross section for $p\bar{p} \to m\Psi$ (see Refs.[138, 139]); this reaction in particular will be used by PANDA to search for J^{PC}-exotic charmonium hybrids.

Finally, the highest-mass $c\bar{c}$ state known at present is the 1^{--} $\psi(4415)$, which is usually given a 4^3S_1 assignment. Nothing is currently known about its exclusive decay modes. (The PDG [448] says that the $\psi(4415)$ decays dominantly to "hadrons", which is not especially surprising.) Calculations of the decay branching fractions of a 4^3S_1 $c\bar{c}$ $\psi(4415)$ in the $^3P_0$ model [95] predict that the largest mode should be the unusual DD_1 (the narrow D_1), and in pure D-wave rather than S-wave! It would clearly be a very interesting test of strong decay models to measure the strong decay amplitudes and branching fractions of this state. There is also an "industrial" application of the $\psi(4415)$ [95, 140]; by running on the high mass tail of this resonance, one can expect a relatively large branching fraction into the enigmatic $D_{s0}(2317)$, which is otherwise difficult to produce with useful statistics. A study of interesting decays such as the radiative branching fraction of the $D_{s0}(2317)$ into γD_s^* could then be carried out at BES; this would be valuable in determining the relative size of the $c\bar{s}$ and DK components of the $D_{s0}(2317)$.

17.4 Novel states incorporating a $c\bar{c}$ subsystem

17.4.1 Charm Molecules

Molecules are weakly bound states of more than one hadron, of which by far the best known examples are nuclei and hypernuclei. There are also speculations that certain unusual hadrons may also be similar weakly bound states of mesons, such as the $f_0(980)$ and $a_0(980)$ "KKbar-molecule" candidates. One of the earliest suggestions for a mesonic molecule in the charm sector pertains to the $\psi(4040)$; it was suggested by Voloshin *et al.* [141] that this state might be a D^*D^* molecule, because the mass is close to the mass

of two D^* mesons, and this state couples very strongly to D^*D^* final states. (See also Refs.[142, 143].) It has since been realized that this D^*D^* dominance is also expected for a conventional 3^3S_1 $c\bar{c}$ charmonium state [125, 95].

The obvious characteristics of molecules are that they should have masses just below the sum of the masses of their constituent hadrons (to within a nuclear physics scale binding energy of perhaps *ca.* 10 MeV, and that they should decay strongly to their constituents (if allowed by width effects) or to final states that those constituents would naturally couple strongly to. Their most plausible quantum numbers are those of an S-wave constituent pair, since the residual binding forces between color-singlet hadrons are relatively weak and short relative to forces between quarks and gluons. (This argues against the $\psi(4040)$ being a D^*D^* molecule, since the binding forces would be competing against a P-wave angular momentum barrier.)

Rather remarkably, a very strong candidate for a charmed meson molecule was identified in recent years in B-meson decays, the X(3872). This state was originally identified by Belle [144] in the final state $J/\psi\pi^+\pi^-$, where the mass distribution of the $\pi^+\pi^-$ system is consistent with, and believed to be dominantly due to, a ρ^0.

The mass and width (still only known as an upper limit) for this state are

$$\mathrm{M(X(3872))} = \ 3871.2 \pm 0.5 \ \ \mathrm{MeV}, \tag{17.9}$$

$$\Gamma\mathrm{(X(3872))} \ < \ 2.3 \ \mathrm{MeV}, \ 90\% \ c.l. \tag{17.10}$$

There is now clear evidence from the decay angular distribution that the J^{PC} quantum numbers are 1^{++} [145]. Comparison with the spectrum of expected $c\bar{c}$ states in Fig.17.1 shows that no 1^{++} $c\bar{c}$ state is expected near this mass, although one could clearly consider a low-mass 2^3P_1 χ_1' state as a possibility. This and other $c\bar{c}$ possibilities were initially considered, and the combined mass and narrow width of the X(3872) were found to be inconsistent with any $c\bar{c}$ assignment [120].

The proximity of the X(3872) to the mass of a (neutral) D^0D^{*0} pair (at an almost identical 3871.2 ± 0.6 MeV) immediately suggested that this state might be a weakly bound D^0D^{*0} molecule (see for example Refs.[146, 147, 148]). (A binding energy of *ca.* 1 MeV is allowed by the current experimental mass errors.) Note that this DD^* molecule would have a much smaller charged D^+D^{*-}, D^-D^{*+} component, since this basis state has a mass of 3879.3 ± 0.6 MeV, and hence is at a much higher mass on the scale of a bound state with only 1 MeV binding.

Although the residual "nuclear" forces that can lead to the formation of hadronic molecules are usually not well understood, in this case there is less ambiguity; the longest-ranged force, which should be the most important for a weakly bound system, is one pion exchange. Since the strength of the required $D^*D\pi$ coupling can be inferred from the partial width for $D^* \to D\pi$, it is straightforward to calculate the effective DD^* interaction due to one pion exchange. (There is however some ambiguity in the treatment of the short-range truncation of this force.) Studies of one pion exchange forces in the DD^*

system by Tornqvist [146] and Swanson [148] showed that the 1^{++} state experienced the strongest binding forces from one pion exchange, and that they were numerically just strong enough to (perhaps) form a DD* bound state.

One especially striking prediction of the (neutral D) D^0D^{*0} molecule model is that one should observe comparable strength $J/\psi\omega$ and $J/\psi\rho^0$ decay modes [148] (see also Ref.[149]), due to the maximal isospin breaking present in the initial state. This prediction appears to have been confirmed by the evidence from Belle for the ω in the 3π mode X(3872)$\rightarrow J/\psi\pi^+\pi^-\pi^0$ [150]. The 3π invariant mass peaks at the highest mass, as expected for a virtual ω, and the ratio of 2π to 3π branching fractions is close to unity,

$$\frac{\Gamma(\mathrm{X}(3872) \rightarrow J/\psi\pi^+\pi^-\pi^0)}{\Gamma(\mathrm{X}(3872) \rightarrow J/\psi\pi^+\pi^-)} = 1.0 \pm 0.4 \pm 0.3, \tag{17.11}$$

as predicted by Swanson in the DD* model.

There is also evidence from Belle for the radiative transition X(3872)$\rightarrow \gamma\ J/\psi$ [150], with the width ratio

$$\frac{\Gamma(\mathrm{X}(3872) \rightarrow \gamma\ J/\psi)}{\Gamma(\mathrm{X}(3872) \rightarrow J/\psi\pi^+\pi^-)} = 0.14 \pm 0.05, \tag{17.12}$$

which should be useful in testing the details of different models of the X(3872).

There are several interesting studies of charm molecules that might be possible at BES. Detection of this 1^{++} state at all at an e^+e^- facility is nontrivial, but may be feasible through E1 decays of the $\psi(4040)$ and $\psi(4160)$. (Both will couple to the X(3872) through it's $c\bar{c}$ component.) If the X(3872) can be studied, a measurement of the total width of the X(3872) would be very interesting, since the current upper limit is not far above the estimate Swanson gives in the DD* molecule model [148, 101]. Measurements of the branching fractions of the X(3872) into the various final states predicted by the molecule model would then be very interesting, especially the ratios of different isospin modes such as J/$\psi\omega$ versus J/$\psi\rho^0$.

Given that the X(3872) does appear likely as a DD* molecule, it is of interest to search for other molecules that are predicted assuming similar interactions between charmed mesons. Swanson [101] notes that one attractive possibility is a 0^{++} D*D* molecule, which could be produced in $\psi(4160)$ E1 decays and observed in the J/$\psi\omega$ final state.

17.4.2 Charmonium Hybrids

The discovery of charmonium hybrids may be the most exciting goal of the current and near future studies of the charmonium system. These states should be accessible at BES.

Hybrids are hadrons in which the gluonic degree of freedom has been excited. The nature of this gluonic excitation is not well understood at present, and has been described

by various models, including valence gluon models such as the bag model and nonperturbative systems such as the flux tube model. To date most theoretical studies have considered hybrid mesons ($q\bar{q}$ with a gluonic excitation) and hybrid baryons (qqq with a gluonic excitation). Although the models differ in detail regarding their predictions for the spectrum of hybrids, there is general agreement that hybrid mesons have the very attractive feature of including states with J^{PC}-exotic quantum numbers. These are the quantum numbers $J^{PC} = 0^{--}$ and the series $0^{+-}, 1^{-+}, 2^{+-}, 3^{-+}, \ldots$, which are forbidden to conventional $q\bar{q}$ systems, but can all be formed from hybrid basis states. The search for resonances with exotic quantum numbers is therefore a principal goal of searches for hybrid mesons. Hybrids basis states also span all the conventional $q\bar{q}$ J^{PC} quantum numbers, and should give rise to a rich overpopulation of the experimental spectrum relative to the expectations of the naive $q\bar{q}$ quark model.

In view of the current uncertainty regarding the nature of hybrids in models, the predictions of LGT studies are correspondingly very important. The most recent studies of charmonium hybrids suggest a mass scale for the lightest exotic charmonium hybrid, which probably has $J^{PC} = 1^{-+}$, of approximately 4.4 GeV (see for example Refs.[270, 151, 152, 153, 154, 155]). In the flux tube model, which in comparison anticipates the lightest charmonium hybrid multiplet near 4.2 GeV [156], this lightest hybrid multiplet is predicted to contain three exotic and five nonexotic hybrid states, including both a 1^{-+} exotic and a 1^{--} nonexotic.

The prediction of hybrids in this approximate mass region, including a nonexotic 1^{--} state, is especially interesting in view of the recent discovery of the Y(4260). This remarkable new state was reported by BaBar in initial state radiation (ISR) in the reaction $e^+e^- \to \gamma_{ISR} J/\psi\pi^+\pi^-$ [157], and has been confirmed by CLEO-c [159] and Belle [160] in the same process. There may also be evidence for an enhancement in $J/\psi\pi^+\pi^-$ near 4.26 GeV in the decay B$\to$K$J/\psi\pi^+\pi^-$ (in both neutral and negative B/K charge states) [161]. The mass and width reported for the Y(4260) by BaBar [157] are

$$\mathrm{M} = 4259 \pm 8\,^{+2}_{-6}\ \mathrm{MeV}, \tag{17.13}$$

$$\Gamma = 88 \pm 23\,^{+6}_{-4}\ \mathrm{MeV}, \tag{17.14}$$

with consistent results from CLEO-c, but a somewhat higher mass and larger width from Belle.

The ISR production mechanism tells us that this state must be 1^{--}, but it cannot be a conventional $c\bar{c}$ state because the 1^{--} states in this mass region are well established from earlier e^+e^- annihilation experiments. (The Y(4260) is bracketed by the $2^3\mathrm{D}_1$ $\psi(4160)$ and the $4^3\mathrm{S}_1$ $\psi(4415)$, which have masses that are in excellent agreement with the expectations of $c\bar{c}$ potential models.)

The Y(4260) (if a real resonance) evidently represents "overpopulation" of the expected quark potential model spectrum of 1^{--} $c\bar{c}$ states. In addition, as most models

of hybrids have a vanishing $c\bar{c}$ wavefunction at contact, it has long been speculated that they would have small e^+e^- widths, and thus make rather weak contributions to R. This overpopulation of the spectrum and the fact that there is no enhancement visible in R near this mass has led to suggestions that this state may be a charmonium hybrid [162].

Another indication that the Y(4260) may be a charmonium hybrid follows from a LGT study by the UKQCD group [163] of the strong decay couplings of exotic $b\bar{b}$ hybrids. This LGT study found strikingly large couplings of $b\bar{b}$ hybrids to closed flavor modes (specifically to $\chi_b S$, where S is a light scalar isoscalar meson that would decay to $\pi\pi$). This is sufficiently similar to the BaBar observation of the Y(4260) in the single closed-charm mode $J/\psi\pi^+\pi^-$ to be cited as additional possible evidence for a hybrid interpretation.

The unusual $J/\psi\pi^+\pi^-$ mode and the UKQCD study suggest searches of any other accessible closed-charm modes with 1^{--} quantum numbers, such as $J/\psi\eta$, $J/\psi\eta'$, $\chi_J\omega$ and so forth. Ideally the light system should have quantum numbers thought to couple strongly to pure glue, such as 0^{++} and 0^{-+}.

In specific decay models, notably the flux-tube decay model [131], theorists have long anticipated that the dominant open-flavor decay modes of hybrids would be a meson pair with one internal S-wave (for charmonium hybrids, D, D*, D_s, D_s^*) and one internal P-wave (such as D_J and D_{sJ}). In the case of the Y(4260) this suggests dominance of the decay mode $DD_1(2430)$. This broad D_1 has a width of *ca.* 400 MeV, and decays to D$^*\pi$, so this suggests a search for evidence of the Y(4260) in DD$^*\pi$. Since this is a prediction of a decay model in an untested regime (hybrids), one should be cautious and search the more familiar two-body modes DD, DD*, D*D*, D_sD_s, $D_sD_s^*$ and $D_s^*D_s^*$ for evidence of the Y(4260) as well. If there is evidence of a large $DD_1(2430)$ signal, the Y(4260) would then be quite convincing as a hybrid having properties predicted by the flux tube model. If it appears in some of these open charm modes such as DD* and $D_sD_s^*$ at rates comparable to or larger than $J/\psi\pi^+\pi^-$, one might claim a hybrid but speculate that the flux tube decay model was inaccurate in predicting hybrid decay modes. Finally, if the Y(4260) does not appear in any other mode, one might be skeptical about whether the $J/\psi\pi^+\pi^-$ signal is due to a resonance at all; there are nonresonant possibilities, such as production of DD_1 in $e^+e^- \to DD_1$ followed by an inelastic FSI that produces a broad $J/\psi\pi^+\pi^-$ enhancement due to the (very broadened) onset of $DD_1(2430)$ threshold events (which would appear near 4.3 GeV).

In any case since it is clear from the reported mass that the Y(4260) is not a conventional $c\bar{c}$ state, it will be very important to establish the properties of this signal through the accumulation of better statistics. This applies even more strongly to the more recently reported state at 4350 MeV [164], which has been claimed in an analogous closed-flavor mode, $\psi'\pi\pi$.

Mult.	State	Input mass (NR model)	Theor. mass NR	Theor. mass GI
1S	$J/\psi(1^3S_1)$	3097	3090	3098
	$\eta_c(1^1S_0)$	2979	2982	2975
2S	$\psi'(2^3S_1)$	3686	3672	3676
	$\eta_c'(2^1S_0)$	3638	3630	3623
3S	$\psi(3^3S_1)$	4040	4072	4100
	$\eta_c(3^1S_0)$		4043	4064
4S	$\psi(4^3S_1)$	4415	4406	4450
	$\eta_c(4^1S_0)$		4384	4425
1P	$\chi_2(1^3P_2)$	3556	3556	3550
	$\chi_1(1^3P_1)$	3511	3505	3510
	$\chi_0(1^3P_0)$	3415	3424	3445
	$h_c(1^1P_1)$		3516	3517
2P	$\chi_2(2^3P_2)$		3972	3979
	$\chi_1(2^3P_1)$		3925	3953
	$\chi_0(2^3P_0)$		3852	3916
	$h_c(2^1P_1)$		3934	3956
3P	$\chi_2(3^3P_2)$		4317	4337
	$\chi_1(3^3P_1)$		4271	4317
	$\chi_0(3^3P_0)$		4202	4292
	$h_c(3^1P_1)$		4279	4318
1D	$\psi_3(1^3D_3)$		3806	3849
	$\psi_2(1^3D_2)$		3800	3838
	$\psi(1^3D_1)$	3770	3785	3819
	$\eta_{c2}(1^1D_2)$		3799	3837
2D	$\psi_3(2^3D_3)$		4167	4217
	$\psi_2(2^3D_2)$		4158	4208
	$\psi(2^3D_1)$	4159	4142	4194
	$\eta_{c2}(2^1D_2)$		4158	4208
1F	$\chi_4(1^3F_4)$		4021	4095
	$\chi_3(1^3F_3)$		4029	4097
	$\chi_2(1^3F_2)$		4029	4092
	$h_{c3}(1^1F_3)$		4026	4094
2F	$\chi_4(2^3F_4)$		4348	4425
	$\chi_3(2^3F_3)$		4352	4426
	$\chi_2(2^3F_2)$		4351	4422
	$h_{c3}(2^1F_3)$		4350	4424
1G	$\psi_5(1^3G_5)$		4214	4312
	$\psi_4(1^3G_4)$		4228	4320
	$\psi_3(1^3G_3)$		4237	4323
	$\eta_{c4}(1^1G_4)$		4225	4317

Table 17.2: Theoretical predictions for the spectrum of $c\bar{c}$ states in a nonrelativistic potential model (NR) and the Godfrey-Isgur relativized potential model (GI). (This table is abstracted from Ref.[95].)

State	Asst.	$\Gamma^{e^+e^-}_{thy.}$ (keV)	$\Gamma^{e^+e^-}_{expt.}$ (keV)
J/ψ	$1\,^3S_1$	12.13	$5.55 \pm 0.14 \pm 0.02$
ψ'	$2\,^3S_1$	5.03	2.48 ± 0.06
$\psi(3770)$	1^3D_1	0.056	$0.242\,^{+0.027}_{-0.024}$
$\psi(4040)$	$3\,^3S_1$	3.48	0.86 ± 0.07
$\psi(4160)$	2^3D_1	0.096	0.83 ± 0.07
$\psi(4415)$	$4\,^3S_1$	2.63	0.58 ± 0.07

Table 17.3: Predictions of a nonrelativistic $c\bar{c}$ potential model for e^+e^- partial widths, together with current (2006) PDG experimental values [448].

Initial meson	Multiplets	Final meson	E_γ (MeV) NR	GI	Γ_{thy} (keV) NR	GI	Γ_{expt} (keV)
χ_2	$1P \to 1S$	J/ψ	429.	429.	424.	313.	426. ± 51.
χ_1	$1P \to 1S$	J/ψ	390.	389.	314.	239.	291. ± 48.
χ_0	$1P \to 1S$	J/ψ	303.	303.	152.	114.	119. ± 19.
h_c	$1P \to 1S$	η_c	504.	496.	498.	352.	
ψ'	$2S \to 1P$	χ_2	128.	128.	38.	24.	27. ± 4.
		χ_1	171.	171.	54.	29.	27. ± 3.
		χ_0	261.	261.	63.	26.	27. ± 3.
η_c'	$2S \to 1P$	h_c	111.	119.	49.	36.	
$\psi_3(1^3D_3)$	$1D \to 1P$	χ_2	242.	282.	272.	296.	
$\psi_2(1^3D_2)$		χ_2	236.	272.	64.	66.	
		χ_1	278.	314.	307.	268.	
$\psi(3770)$		χ_2	208.	208.	4.9	3.3	< 21 (90% *c.l.*) [114]
		χ_1	250.	251.	125.	77.	70 ± 17 [114]
		χ_0	338.	338.	403.	213.	172 ± 30 [114]
$h_{c2}(1^1D_2)$		h_c	264.	307.	339.	344.	

Table 17.4: E1 radiative transitions of the low-lying narrow $c\bar{c}$ states in the NR and GI potential models, abstracted from Ref.[95]. The masses are taken from Table 17.2; experimental masses were used (rounded "input" column) if known, otherwise, theoretical values were assumed.

Initial meson	Transition	Final meson	E_γ (MeV) NR	GI	Γ_{thy} (keV) NR	GI	Γ_{expt} (keV)
$\psi(4040)$	$3S \to 2P$	χ_2'	67.	119.	14.	48.	
		χ_1'	113.	145.	39.	43.	
		χ_0'	184.	180.	54.	22.	
	$\to 1P$	χ_2	455.	508.	0.70	12.7	
		χ_1	494.	547.	0.53	0.85	
		χ_0	577.	628.	0.27	0.63	
$\psi(4160)$	$2D \to 2P$	χ_2'	183.	210.	5.9	6.3	
		χ_1'	227.	234.	168.	114.	
		χ_0'	296.	269.	483.	191.	
	$\to 1P$	χ_2	559.	590.	0.79	0.027	
		χ_1	598.	628.	14.	3.4	
		χ_0	677.	707.	27.	35.	
	$\to 1F$	$\chi_2(1^3F_2)$	128.	101.	51.	17.	
$\psi(4415)$	$4S \to 3P$	$\chi_2(3^3P_2)$	97.	112.	68.	66.	
		$\chi_1(3^3P_1)$	142.	131.	126.	54.	
		$\chi_0(3^3P_0)$	208.	155.	0.003	25.	
	$\to 2P$	χ_2'	421.	446.	0.62	15.	
		χ_1'	423.	469.	0.49	0.92	
		χ_0'	527.	502.	0.24	0.39	
	$\to 1P$	χ_2	775.	804.	0.61	5.2	
		χ_1	811.	841.	0.41	0.53	
		χ_0	887.	915.	0.18	0.13	

Table 17.5: E1 radiative transitions of the broader 1^{--} charmonium states above 4 GeV in the NR and GI quark models (evaluated as in Table 17.4).

Initial State	Final State	E1 Width (keV)	E1 B.F.
$\psi(4040)$	$\chi_2'(3929)$	56.	$0.7 \cdot 10^{-3}$
	$\chi_1'(3940)$	25.	$0.3 \cdot 10^{-3}$
	$\chi_0'(3940)$	8.3	$0.1 \cdot 10^{-3}$
$\psi(4160)$	$\chi_2'(3929)$	9.9	$0.1 \cdot 10^{-3}$
	$\chi_1'(3940)$	129.	$1.3 \cdot 10^{-3}$
	$\chi_0'(3940)$	172.	$1.7 \cdot 10^{-3}$

Table 17.6: Theoretical E1 radiative partial widths of the $\psi(4040)$ and $\psi(4160)$ into $C = (+)$ 2P $c\bar{c}$ states, recalculated in the NR model with masses suggested by the new XYZ states.

Initial meson	Final meson	$\Gamma_{thy.}$ (keV)	$\Gamma_{expt.}$ (keV)
J/ψ	η_c	2.9	1.2 ± 0.3
ψ'	η_c'	0.21	
ψ'	η_c	4.6	0.8 ± 0.2
η_c'	J/ψ	7.9	

Table 17.7: Theoretical and experimental M1 radiative partial widths of the ψ and ψ', neglecting recoil effects.

Table 17.8: Theoretical ($^3P_0$ model) open-flavor strong decay amplitudes and widths of the four 1^{--} charmonium states above 3.73 GeV most easily accessible at BES (abstracted from Ref.[95]). Multiamplitude decay channels are indicated by boldface.

Meson	State	Mode	Γ_{thy} [Γ_{expt}] (MeV)	Amps. ($GeV^{-1/2}$)
$\psi(3770)$	1^3D_1	DD	43 [23.0 ± 2.7]	$^1P_1 = +0.1668$
$\psi(4040)$	3^3S_1	DD	0.1	$^1P_1 = -0.0052$
		DD^*	33	$^3P_1 = -0.0954$
		$\mathbf{D^*D^*}$	33	$^1P_1 = +0.0338$
				$^5P_1 = -0.1510$
				$^5F_1 = 0$
		D_sD_s	7.8	$^1P_1 = +0.0518$
		total	74 [80 ± 10]	
$\psi(4160)$	2^3D_1	DD	16	$^1P_1 = -0.0522$
		DD^*	0.4	$^3P_1 = +0.0085$
		$\mathbf{D^*D^*}$	35	$^1P_1 = +0.0489$
				$^5P_1 = -0.0219$
				$^5F_1 = -0.0845$
		D_sD_s	8.0	$^1P_1 = -0.0427$
		$D_sD_s^*$	14	$^3P_1 = +0.0733$
		total	74 [103 ± 8]	
$\psi(4415)$	4^3S_1	DD	0.4	$^1P_1 = +0.0066$
		DD^*	2.3	$^3P_1 = +0.0177$
		$\mathbf{D^*D^*}$	16	$^1P_1 = -0.0109$
				$^5P_1 = +0.0487$
				$^5F_1 = 0$
		$\mathbf{DD_1}$	31	$^3S_1 = 0$
				$^3D_1 = +0.0933$
		$\mathbf{DD_1'}$	1.0	$^3S_1 = +0.0168$
				$^3D_1 = 0$
		DD_2^*	23	$^5D_1 = -0.0881$
		$\mathbf{D^*D_0^*}$	0.0	$^3S_1 = -8.7 \cdot 10^{-4}$
			0	$^3D_1 = 0$
		D_sD_s	1.3	$^1P_1 = -0.0135$
		$D_sD_s^*$	2.6	$^3P_1 = +0.0212$
		$\mathbf{D_s^*D_s^*}$	0.7	$^1P_1 = +0.0027$
				$^5P_1 = -0.0119$
				$^5F_1 = 0$
		total	78 [62 ± 20]	

Chapter 18

Charmonium Inclusive Decays

18.1 Theoretical Review

18.2 Leptonic and other EM Decays

18.2.1 Introduction

The use of effective field theories allows to tackle the computation of heavy quarkonium observables directly from QCD. The effective field theories available for the study of these systems are NRQCD [198, 166] and pNRQCD [167, 201, 169]. They profit from the fact that a dimensionless variable (the relative velocity between the quark and antiquark), $v \ll 1$, appears and that the mass, m_Q, of the heavy quark is much larger than $\Lambda_{\rm QCD}$. Therefore, a bunch of inequalities between the different physical scales appearing in the system show up and effective field theories are specially suitable to take profit of them. The most obvious inequalities we have are $m_Q \gg m_Q v \gg m_Q v^2$ and $m_Q \gg \Lambda_{\rm QCD}$, though some others may arise in some specific cases as we will discuss next.

Trying to get a further understanding on the dynamics of the heavy quarkonium one can distinguish between the weak and strong coupling regime. In short, we will denote by weak coupling regime the situation where the soft scale, $m_Q v$, is much larger than $\Lambda_{\rm QCD}$ and the strong coupling regime the situation when $m_Q v \sim \Lambda_{\rm QCD}$. To discern to which regime each bottomonium and charmonium state belongs to is one of main open questions in heavy quarkonium physics. Whereas there is certain consensus that the bottomonium ground state belongs to the weak coupling regime [170, 171, 172, 173, 174, 175]. The situation is not that clear for higher excitations of bottomonium and for charmonium. There are different claims by different groups. To illustrate the point, we can find the evaluations in Refs. [170, 172] where they perform a weak coupling analysis for the first two states of charmonium and for the first three states of bottomonium claiming that a reasonable description can be obtained with perturbation theory. On the other hand there is the analysis of Ref. [175], where they claim that no convergence is found in the perturbative series for these states. It should be mentioned that different renormalon subtraction schemes has been used in both approaches. It would be welcome to see how things work out in other schemes. Another point that should be stressed is that these analysis mainly focussed on the determination of the heavy quarkonium spectrum.

However, if a given state belongs to the weak or strong coupling regime should also be reflected in other observables of these states. In particular this should happen for the inclusive electromagnetic decays, being among the cleanest observables one can think of. However, the situation for the inclusive electromagnetic decays is quite less clear. The convergence of the perturbative series is much worse than in the spectrum (actually this has some side effects in finite order computation of heavy quarkonium sum rules). A detailed discussion can be found in Ref. [176]. Note that this bad convergence also affects to the bottomonium ground state, not to mention higher excitations or charmonium. Therefore, before making clear cut statements upon whether one state belongs to the weak or strong coupling regime the situation of the inclusive electromagnetic decay widths should be clarified.

Another aspect that should be mentioned is that finite order theoretical evaluations of the inclusive electromagnetic decay widths appear to be very scale dependent. At this respect the use of renormalization group techniques [177] have shown itself to be a convenient tool to reduce the scale dependence of bottomonium and charmonium observables [178, 179, 180, 176].

In the next section we elaborate in somewhat more detail upon the above discussion.

18.2.2 Weak coupling regime

In the weak coupling regime the inclusive electromagnetic decay widths read

$$\Gamma(\Upsilon(nS)\to e^+e^-) = 16\pi\,\frac{C_A}{3}\left[\frac{\alpha_{EM}\,e_Q}{M_{\Upsilon(nS)}}\right]^2 \left|\phi_n^{(s=1)}(\mathbf{0})\right|^2 \left\{c_1 - d_1\frac{M_{\Upsilon(nS)}-2m_Q}{6m_Q}\right\}^2 ; \quad (18.1)$$

$$\Gamma(\eta_b(nS)\to \gamma\gamma) = 16\pi\,C_A\left[\frac{\alpha_{EM}\,e_Q^2}{M_{\eta_b(nS)}}\right]^2 \left|\phi_n^{(s=0)}(\mathbf{0})\right|^2 \left\{c_0 - d_0\frac{M_{\eta_b(nS)}-2m_Q}{6m_Q}\right\}^2 . \quad (18.2)$$

The coefficients $c_{0,1}$ are known with two loop accuracy [181, 182, 183, 184, 185]. $d_0 = d_1 = 1$ at lowest order. The wave function corrections are also known with two-loop accuracy. The corrections to the wave function at the origin are obtained by taking the residue of the Green function at the position of the poles

$$\left|\phi_n^{(s)}(\mathbf{0})\right|^2 = \left|\phi_n^{(0)}(\mathbf{0})\right|^2\left(1+\delta\phi_n^{(s)}\right) = \operatorname*{Res}_{E=E_n} G_s(\mathbf{0},\mathbf{0};E)\,, \quad (18.3)$$

where the LO wave function is given by

$$\left|\phi_n^{(0)}(\mathbf{0})\right|^2 = \frac{1}{\pi}\left(\frac{m_Q C_F\alpha_s}{2n}\right)^3 . \quad (18.4)$$

The corrections to $\delta\phi_n^{(s)}$ produced by δV have been calculated with NNLO accuracy [186, 187] in the direct matching scheme. One can also obtain them in the dimensional regularized $\overline{\rm MS}$ scheme with NNLL accuracy by incorporating the renormalization group improved matching coefficients [176]. Also a partial evaluation of the matching coefficients at NNLL is available [180, 176], see also [188, 177, 189]. Therefore, the complete NNLO

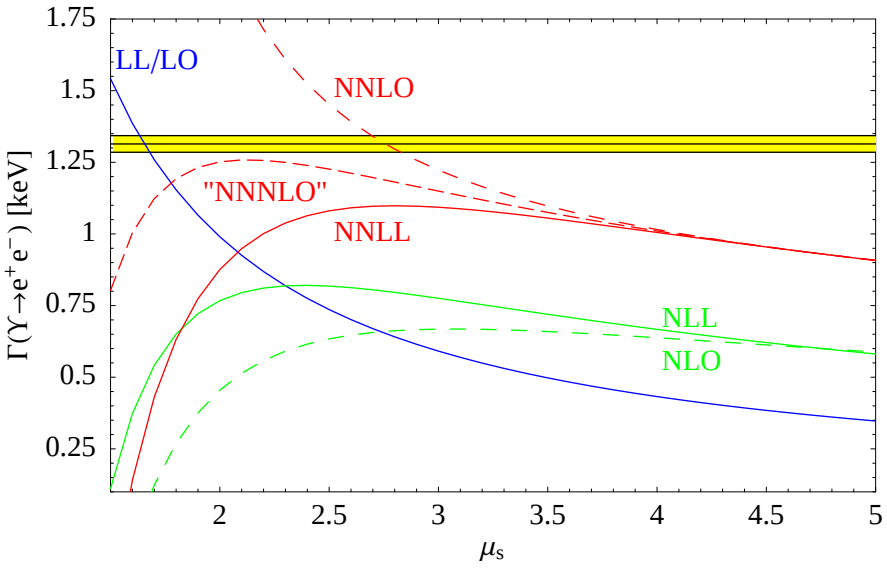

Figure 18.1: Prediction for the $\Upsilon(1S)$ decay rate to e^+e^-. We work in the RS' scheme. Figure from Ref. [176].

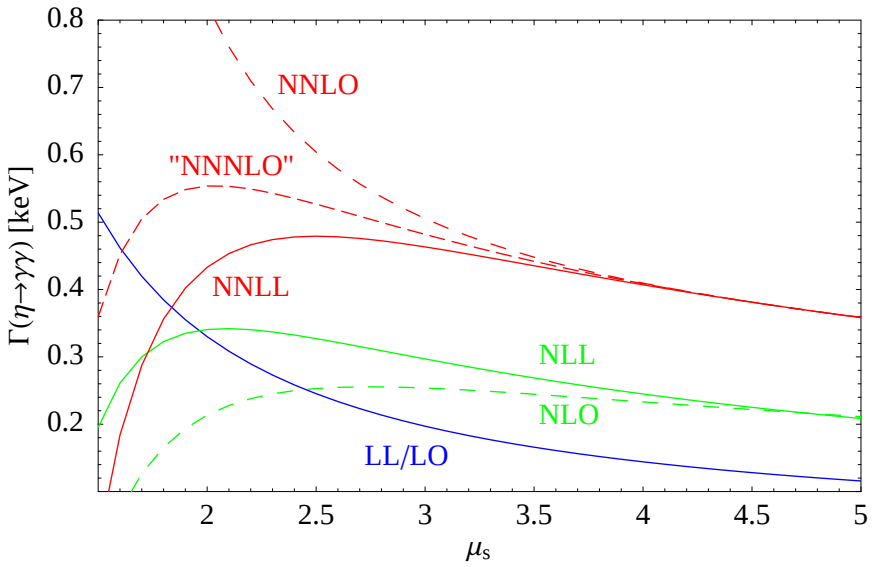

Figure 18.2: Prediction for the $\eta_b(1S)$ decay rate to two photons. We work in the RS' scheme. Figure from Ref. [176].

result for the decay is at present available as well as a partial evaluation with NNLL accuracy. One may try then to apply these results to charmonium and bottomonium decay widths.

The results for the vector and pseudoscalar bottomonium ground state decay can be found in Figs. 18.1 and 18.2 respectively. One problem is the large magnitude of the two loop correction to the matching coefficient of the electromagnetic current. This is

puzzling from the theoretical point of view, since the hard scale should be perturbative in nature. On the other hand one may argue that the result for the matching coefficient is scheme dependent and that a better convergence is expected for the full result where the scheme dependence disappears. This is actually not so as we show in Figs. 18.1 and 18.2, which we take from Ref. [176]. One can discuss whether the charm quark mass is large enough but the convergence problem also appears in the case of bottomonium. This may point out to the fact that this convergence problem is fake. One may try to introduce renormalization group techniques. This significantly diminishes the scale dependence of the theoretical prediction and improves the convergence of the series, yet, the absolute magnitude of the correction is large. From the numerical analysis, we find that the NNLL corrections are huge, especially for the $\eta_b(1S) \to \gamma\gamma$ decay. The result we obtain for this decay is compatible with the number obtained in Ref. [179]. This is somewhat reassuring, since in that reference the ratio of the spin-one spin-zero decay was considered, which was much more scale independent, as well as more convergent (yet still large) than for each of the decays themselves. This agreement can be traced back to the fact that, for the spin-one decay, for which we can compare with experiment, we find that the NNLL result improves the agreement with the data. Overall, the resummation of logarithms always significantly improves over the NNLO result, the scale dependence greatly improves, as well as the convergence of the series. On the other hand the problem of lack of convergence of the perturbative series is not really solved by the resummation of logarithms and it remains as an open issue. Due to the lack of convergence no numbers or errors are given. In this respect we can not avoid to mention that, whereas the perturbative series in non-relativistic sum rules is sign-alternating, is not sign-alternating for the electromagnetic decays. Finally, we would also like to remark the strong scale dependence that we observe at low scales, which we believe to have the same origin than the one observed in $t\bar{t}$ production near threshold in Ref. [176].

One may argue that maybe considering the ratio between spin one and spin zero decays one may get a better convergence (moreover for the renormalization group result we do not have the complete expression at NNLL but we do for the ratio [179]). Actually this is so as we can see for the bottomonium but for charmonium physics the magnitude of the corrections is still very large. One may wonder whether there are renormalon effects here [190].

For bottomonium, the logarithmic expansion shows nice convergence and stability (c.f. Fig. 18.3) despite the presence of ultrasoft contributions with α_s normalized at a rather low scale ν^2/m_b. At the same time, the perturbative corrections are important and reduce the leading order result by approximately 41%. For illustration, at the scale of minimal sensitivity, $\nu = 1.295$ GeV, we have the following series:

$$\mathcal{R}_b = \frac{\Gamma(\Upsilon(1S) \to e^+e^-)}{\Gamma(\eta_b(1S) \to \gamma\gamma)} = \frac{1}{3Q_b^2}\left(1 - 0.302 - 0.111\right) . \tag{18.5}$$

In contrast, the fixed-order expansion blows up at the scale of the inverse Bohr radius.

For the charmonium, the NNLO approximation becomes negative at an intermediate scale between $\alpha_s m_c$ and m_c (c.f. Fig. 18.4) and the use of the NRG is mandatory to get a sensible perturbative approximation. The NNLL approximation has good stability against the scale variation but the logarithmic expansion does not converge well. This is

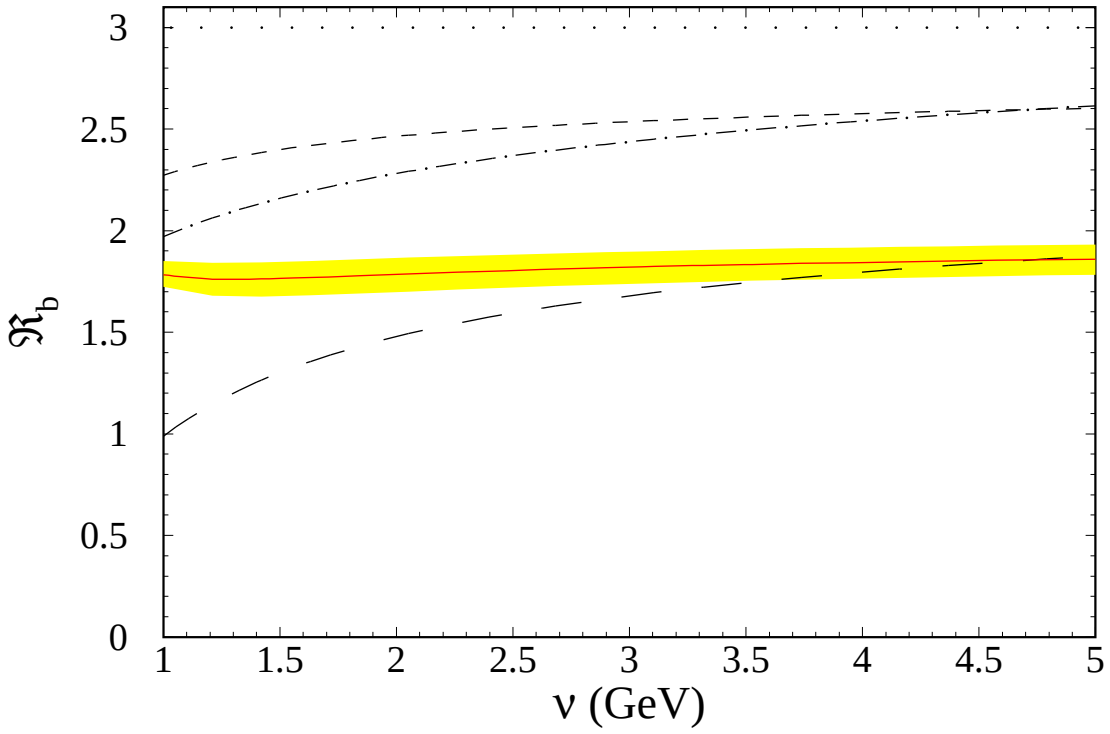

Figure 18.3: The spin ratio as the function of the renormalization scale ν in LO≡LL (dotted line), NLO (short-dashed line), NNLO (long-dashed line), NLL (dot-dashed line), and NNLL (solid line) approximation for the bottomonium ground state with $\nu_h = m_b$. For the NNLL result the band reflects the errors due to $\alpha_s(M_Z) = 0.118 \pm 0.003$. Figure from Ref. [179].

the main factor that limits the theoretical accuracy since the nonperturbative contribution is expected to be under control. For illustration, at the scale of minimal sensitivity, $\nu = 0.645$ GeV, we obtain

$$\mathcal{R}_c = \frac{\Gamma(J/\Psi(1S) \to e^+e^-)}{\Gamma(\eta_c(1S) \to \gamma\gamma)} = \frac{1}{3Q_c^2}\,(1 - 0.513 - 0.326)\ . \tag{18.6}$$

The central value of our NNLL result is 2σ below the experimental value. The discrepancy may be explained by the large higher order contributions. This should not be surprising because of the rather large value of α_s at the inverse Bohr radius of charmonium. For the charmonium hyperfine splitting, however, the logarithmic expansion converges well and the prediction of the renormalization group is in perfect agreement with the experimental data [178]. Thus one can try to improve the convergence of the series for the production/annihilation rates by accurately taking into account the renormalon-related contributions. One point to note is that with a potential model evaluation of the wave function correction, the sign of the NNLO term is reversed in the charmonium case [185].

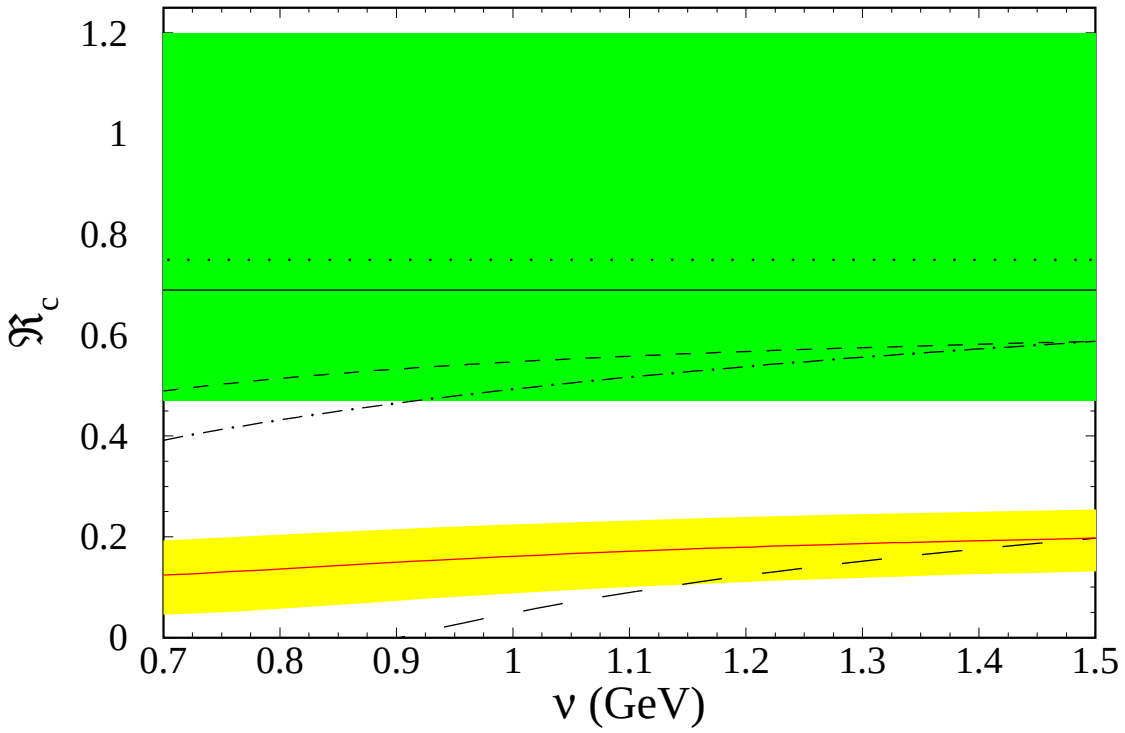

Figure 18.4: The spin ratio as the function of the renormalization scale ν in LO≡LL (dotted line), NLO (short-dashed line), NNLO (long-dashed line), NLL (dot-dashed line), and NNLL (solid line) approximation for the charmonium ground state with $\nu_h = m_c$. For the NNLL result the lower (yellow) band reflects the errors due to $\alpha_s(M_Z) = 0.118 \pm 0.003$. The upper (green) band represents the experimental error of the ratio where the central value is given by the horizontal solid line. Figure from Ref. [179].

This is very interesting since, actually, one can also see that the main effects of higher order effects in the static potential is to make it to agree with the lattice potential and therefore with the standard parameterizations of the non-perturbative potential like Cornell, etc... At the same time the subtraction of the pole mass renormalon from the perturbative static potential makes explicit that the potential is steeper and closer to lattice and phenomenological potential models [47]. Therefore, the incorporation of higher order effects from the static potential may improve the agreement with experiment, and it may look foreseeable to obtain a description of the ground state charmonium with mainly perturbative ingredients. However, how to match the hard coefficient with the perturbative potential is challenging since the logs of the potential get entangled with those of the hard matching coefficient. In any case, if we estimate the theoretical uncertainty as the difference of the NNLL and the NLL result at the soft scale $\alpha_s m_c$, the theoretical and experimental values agree within the error bars.

18.2.3 Final discussion

In order to unambiguously determine which bottomonium and charmonium states belong to the weak or strong coupling regime it is necessary to understand the lack of convergence of the perturbative series for the inclusive electromagnetic decays. At this respect understanding the following points would be of great help:

- A complete NNLL computation would be most welcome to have a better estimate of the theoretical uncertanties.
- A complete NNNLO computation would be most welcome to have a better estimate of the theoretical uncertanties. Moreover it would help to asses the importance of the resummation of logarithms.
- Estimate of the non-perturbative corrections. They also depend on the same chromoelectric gluonic correlator than the $\Upsilon(1S)$ mass.
- Rearrangement (renormalon-based?) of the perturbative series.

Finally also note that a renormalization group analysis for non-relativistic charmonium sum rules remains to be done. On this respect there are new R measurements in the precharmonium region with BES at BEPC and just above the charm threshold with CLEO at CESR. These provide important input to the determinations of the charm quark mass.

18.3 Inclusive Radiative Decays

18.3.1 Introduction

Inclusive radiative decays of heavy quarkonium systems to light hadrons have been a subject of investigation since the early days of QCD [192, 193]. It was thought for some time that a reliable extraction of $\alpha_{\rm s}$ was possible from the inclusive γgg decay normalized

to the inclusive ggg decay. However, when the experimental data became available for J/ψ [194], it turned out that the photon spectrum, and in particular the upper end-point region of it, appeared to be poorly described by the theory. The situation was slightly better for the $\Upsilon(1S)$ [195], where, at least, good agreement with QCD was found in the central region [196]. In fact, the whole photon spectrum for the $\Upsilon(1S)$ is now well understood thanks to a number of theoretical advances which have taken place in recent years (see [197] and references therein). Here we will mainly translate in a critical way these advances to the case of the J/ψ.

We will stay in the effective theory framework of Non-relativistic QCD (NRQCD) [198, 271] and Potential NRQCD (pNRQCD) [272, 201], and our terminology will follows that of [202]. Let us remind the reader that heavy quarkonium systems enjoy the hierarchies of scales $m \gg mv \gg mv^2$ and $m \gg \Lambda_{\rm QCD}$, where m is the heavy quark mass, $v \ll 1$ the relative velocity of the heavy quarks and $\Lambda_{\rm QCD}$ a typical hadronic scale. States fulfilling $\Lambda_{\rm QCD} \lesssim mv^2$ are said to be in the weak coupling regime (the binding is essentially due to a Coulomb-like potential) whereas states fulfilling $\Lambda_{\rm QCD} \gg mv^2$ are said to be in the strong Coupling regime (the binding is due to a confining potential). States below the open flavor threshold and not too deep are expected to be in the strong coupling regime whereas deep states are expected to be in the weak coupling one. States above (or very close to) the open flavor threshold are not expected to be in either regime.

18.3.2 The photon spectrum

The contributions to the decay width can be split into direct (^{dir}) and fragmentation (^{frag})

$$\frac{d\Gamma}{dz} = \frac{d\Gamma^{dir}}{dz} + \frac{d\Gamma^{frag}}{dz} \tag{18.7}$$

We will call direct contributions to those in which the observed photon is emitted from the heavy quarks and fragmentation contributions to those in which it is emitted from the decay products (light quarks). This splitting is correct at the order we are working but should be refined at higher orders. $z \in [0,1]$ is defined as $z = 2E_\gamma/M$, M being the heavy quarkonium mass.

Direct Contributions

The starting point is the QCD formula [203]

$$\frac{d\Gamma}{dz} = z\frac{M}{16\pi^2}{\rm Im}T(z) \qquad T(z) = -i\int d^4x e^{-iq\cdot x}\,\langle V_Q(nS)|T\{J_\mu(x)J_\nu(0)\}|V_Q(nS)\rangle\,\eta_\perp^{\mu\nu} \tag{18.8}$$

where $J_\mu(x)$ is the electromagnetic current for heavy quarks in QCD and we have restricted ourselves to $^3S_1$ states. q is the photon momentum, which in the rest frame of the heavy quarkonium is $q = (q_+, q_-, q_\perp) = (zM, 0, 0)$, $q_\pm = q^0 \pm q^3$. Different approximations to this formula are necessary for the central ($z \sim 0.5$), lower end-point ($z \to 0$) and upper end-point ($z \to 1$) regions.

1. The central region

For z away from the lower and upper end-points (0 and 1 respectively), no further scale is introduced beyond those inherent of the non-relativistic system. The integration of the scale m in the time ordered product of currents in (18.8) leads to local NRQCD operators with matching coefficients which depend on m and z. At leading order one obtains

$$\frac{1}{\Gamma_0}\frac{d\Gamma_{\rm LO}}{dz} = \frac{2-z}{z} + \frac{z(1-z)}{(2-z)^2} + 2\frac{1-z}{z^2}\ln(1-z) - 2\frac{(1-z)^2}{(2-z)^3}\ln(1-z), \qquad (18.9)$$

where

$$\Gamma_0 = \frac{32}{27}\alpha\alpha_s^2 e_Q^2 \frac{\langle V_Q(nS)|\mathcal{O}_1(^3S_1)|V_Q(nS)\rangle}{m^2}, \qquad (18.10)$$

and e_Q is the charge of the heavy quark. The α_s correction to this rate was calculated numerically in Ref. [204] for the bottomonium case. A reasonable estimate for charmonium maybe obtained by multiplying it by $\alpha_{\rm s}(2m_c)/\alpha_{\rm s}(2m_b)$. The expression corresponding to (18.10) in pNRQCD is obtained at lowest order by just making the substitution

$$\langle V_Q(nS)|\mathcal{O}_1(^3S_1)|V_Q(nS)\rangle \;=\; \frac{N_c}{2\pi}|R_{n0}(0)|^2, \qquad (18.11)$$

where $R_{n0}(0)$ is the radial wave function at the origin. The final result coincides with the one of the early QCD calculations [192, 193]. The NLO contribution in the weak coupling regime reads [271],

$$\frac{d\Gamma_{\rm NLO}}{dz} = C'_{\mathbf{1}}\left(^3S_1\right)\frac{\langle V_Q(nS)|\mathcal{P}_1(^3S_1)|V_Q(nS)\rangle}{m^4} \qquad (18.12)$$

ant it is v^2 suppressed with respect to (18.9). The new matrix element above can be written in terms of the original one [205]

$$\frac{\langle V_Q(nS)|\mathcal{P}_1(^3S_1)|V_Q(nS)\rangle}{m^4} = \left(\frac{M-2m-\mathcal{E}_1/m}{m}\right)\frac{\langle V_Q(nS)|\mathcal{O}_1(^3S_1)|V_Q(nS)\rangle}{m^2}\left(1+\mathcal{O}\left(v^2\right)\right) \qquad (18.13)$$

In the weak coupling regime $\mathcal{E}_1/m$ is absent [206], but in the strong coupling regime it must be kept ($\mathcal{E}_1 \sim \Lambda^2_{\rm QCD}$ is a bound state independent non-perturbative parameter) . The matching coefficient can be extracted from an early calculation [207] (see also [208]). It reads

$$C'_{\mathbf{1}}\left(^3S_1\right) = -\frac{16}{27}\alpha\alpha_s^2 e_Q^2\left(\left(F_B(z)+\frac{1}{2}F_W(z)\right)\frac{1}{2}+\frac{1}{\Gamma_0}\frac{d\Gamma_{\rm LO}}{dz}\right) \qquad (18.14)$$

where $F_B(z)$ and $F_W(z)$ are defined in ref. [208][1].

In the weak coupling regime the contributions of color octet operators start at order v^4. Furthermore, away of the upper end-point region, the lowest order color octet

[1] The last term in (18.14) was missing in [197], see footnote 4 of [209].

contribution identically vanishes [210]. Hence there is no $1/\alpha_s$ enhancement in the central region and we can safely neglect these contributions in this case. However, in the strong coupling regime the color octet contributions may become order v^2 and should be kept at NLO.

Then in the weak coupling regime (if we use the counting $\alpha_s(m) \sim v^2$, $\alpha_s(m\alpha_s) \sim v$) the complete NLO ($v^2$ suppressed) contribution consists of the α_s correction to (18.9), the relativistic corrections in (18.12) and the corrections to the wave function at the origin up to order $\alpha_s^2(m\alpha_s)$ [211, 212]. Using $m = m_c = 1.6\,GeV$, $M = 3.1\,GeV$, $\alpha_s(2m_c) = 0.23$ and $\alpha_s(m\alpha_s) = 0.4$ we obtain the solid green curve in Fig. 18.5.

2. The lower end-point region

   For $z \to 0$, the emitted low energy photon can only produce transitions within the non-relativistic bound state without destroying it. Hence the direct low energy photon emission takes place in two steps: (i) the photon is emitted (dominantly by dipole electric and magnetic transitions) and (ii) the remaining (off-shell) bound state is annihilated into light hadrons. For z very close to zero it has a suppression $\sim z^3$ with respect to Γ_0 (see [213, 214] for a recent analysis of this region in QED). Hence, at some point the direct photon emission is overtaken by the fragmentation contributions $\bar{Q}Q \to ggg \to gg\bar{q}q\gamma$ [215, 210]. In practise this is expected to happen somewhere between $0.2 \lesssim z \lesssim 0.4$, namely much before than the z^3 behavior of the very low energy direct photon emission can be observed, and hence we shall neglect the latter in the following.

3. The upper end-point region

   In this region the standard NRQCD factorization is not applicable [203]. This is due to the fact that small scales induced by the kinematics enter the problem and have an interplay with the bound state dynamics. In order to study this region, one has to take into account collinear degrees of freedom in addition to those of NRQCD. This can be done using Soft-Collinear Effective Theory (SCET) [216, 217] as it has been described in [218, 219]. This region has only been considered in the weak coupling regime, which we will restrict our discussion to. The color octet contributions are only suppressed by v^2 or by $1-z$. Since their matching coefficients are enhanced by $1/\alpha_s(m)$, they become as important as the color singlet contributions if we count $\alpha_s(m) \sim v^2 \sim 1-z$. The formula one may use for the semi-inclusive width in the end-point region, which was successful for the bottomonium case, reads

$$\frac{d\Gamma^e}{dz} = \frac{d\Gamma^e_{CS}}{dz} + \frac{d\Gamma^e_{CO}}{dz} \tag{18.15}$$

   where CS and CO stand for color singlet and color octet contributions respectively.

   For the color singlet contribution one may use the expression with the Sudakov resummed coefficient in ref. [220]

$$\frac{1}{\Gamma_0}\frac{d\Gamma^e_{CS}}{dz} = \Theta(M-2mz)\frac{8z}{9}\sum_{n\ \text{odd}}\left\{\frac{1}{f^{(n)}_{5/2}}\left[\gamma^{(n)}_+ r(\mu_c)^{2\lambda^{(n)}_+/\beta_0} - \gamma^{(n)}_- r(\mu_c)^{2\lambda^{(n)}_-/\beta_0}\right]^2 +\right.$$

$$+\frac{3f_{3/2}^{(n)}}{8[f_{5/2}^{(n)}]^2}\frac{{\gamma_{gq}^{(n)}}^2}{\Delta^2}\left[r(\mu_c)^{2\lambda_+^{(n)}/\beta_0}-r(\mu_c)^{2\lambda_-^{(n)}/\beta_0}\right]^2\Bigg\} \tag{18.16}$$

where the definitions for the different functions appearing in (18.16) can be found in [220, 197].

For the color octet contributions we use

$$\frac{d\Gamma_{CO}^e}{dz}=\alpha_s(\mu_u)\,\alpha_s(\mu_h)\,e_Q^2\left(\frac{16M\alpha}{9m^4}\right)\int_z^{\frac{M}{2m}}C(x-z)S_{S+P}(x)dx \tag{18.17}$$

$\mu_u \sim mv^2$ and $\mu_h \sim m$ are the ultrasoft and hard scales respectively. $C(x-z)$ contains the Sudakov resummations of ref. [218]. The (tree level) matching coefficients (up to a global factor) and the various shape functions are encoded in $S_{S+P}(x)$. See [197] for a precise definition of these objects.

We would like to comment on the validity of the formulas above. This is limited by the perturbative treatment of the collinear and ultrasoft gluons. For the collinear gluons, entering in the jet functions, we have $1GeV \lesssim M\sqrt{1-z}$, which for J/ψ implies $z \lesssim 0.9$. The formalism is not reliable beyond that point. For the ultrasoft gluons, entering in the shape functions ($S_{S+P}(x)$), we have $1GeV \lesssim M(1-z)$, which implies $z \lesssim 0.7$. Hence, due to the latter, we do not really have a reliable QCD description of the upper end-point region for charmonium. However, for the bottomonium system, the shape function above turns out to describe very well the data even in the far end-point region, where it is not supposed to be reliable either. In view of this, we believe that the formulas above may provide a reasonable model for the description of the region $0.7 \lesssim z \lesssim 0.9$. The outcome is the blue dot-dashed curve of Fig. 18.5 (the flattening of the curve for $z > 0.85$ is an artifact, see footnote 2 of Ref. [197])

4. Merging the central and upper end-point regions

   As we have seen, different approximations are necessary in the central and upper end-point regions. It is then not obvious how the results for the central and for the upper end-point regions must be combined in order to get a reliable description of the whole spectrum. When the results of the central region are used in the upper end-point region, one misses certain Sudakov and Coulomb resummations which are necessary because the softer scales $M\sqrt{1-z}$ and $M(1-z)$ become relevant. Conversely, when results for the end-point region are used in the central region, one misses non-trivial functions of z, which are approximated by their end-point ($z \sim 1$) behavior. In [197] the following merging formula was proposed, which works reasonably well for bottomonium,

$$\frac{1}{\Gamma_0}\frac{d\Gamma^{dir}}{dz}=\frac{1}{\Gamma_0}\frac{d\Gamma^c}{dz}+\left(\frac{1}{\Gamma_0}\frac{d\Gamma^e}{dz}-\frac{1}{\Gamma_0}\frac{d\Gamma^e}{dz}\bigg|_c\right) \tag{18.18}$$

   $|_c$ means the expansion of the end-point formulas when z approaches the central region. This expansion must be carried out at the same level of accuracy as the one we use for the formulas in the central region.

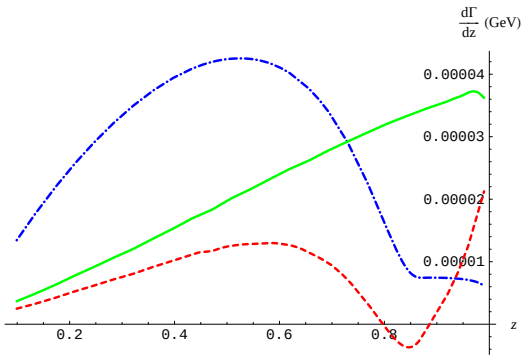

Figure 18.5: Direct contributions in the weak coupling regime. The solid green line corresponds to the calculation for the central region at NLO, which should be reliable up to $z \lesssim 0.7$. The blue dot-dashed line corresponds to the calculation for the upper end-point region, which is expected to provide a reasonable model for $0.7 \lesssim z \lesssim 0.9$. The red dashed line is the curve obtained by merging.

Putting all the ingredients together in formula (18.18) we obtain the red dashed line in Fig. 18.5 for the direct contributions to the photon spectrum. Note that a deep is generated for $0.8 \lesssim z \lesssim 0.9$ which makes the decay width negative. This happens in the region $0.7 \lesssim z$ where the calculation of the shape function is not reliable. A deep was also generated in the $\Upsilon(1S)$ case, but the effect was not so dramatic there [197]. We conclude that, unlike in the $\Upsilon(1S)$ case, the limitations in the theoretical description of the end point region make the merging procedure deliver an unsatisfactory description of this end point region for J/ψ. Clearly, further work is required to understand better the end-point region, in particular a description assuming J/ψ in the strong coupling regime would be desirable. For the present analysis, one should only use the outcome of the merging procedure for $z < 0.7$, if at all. Indeed, an alternative way to proceed would be to ignore the end-point region and only try to describe data in the central region with the QCD formulas for this region given above.

Fragmentation contributions

The fragmentation contributions can be written as

$$\frac{d\Gamma^{\rm frag}}{dz} = \sum_{a=q,\bar{q},g} \int_z^1 \frac{dx}{x} C_a(x) D_{a\gamma}\left(\frac{z}{x}, M\right), \tag{18.19}$$

where C_a represents the partonic kernels and $D_{a\gamma}$ represents the fragmentation functions. The partonic kernels can again be expanded in powers of v [210]

$$C_a = \sum_{\mathcal{Q}} \hat{C}_a[\mathcal{Q}] \frac{\langle J/\psi|\mathcal{Q}|J/\psi\rangle}{m^{d_{\mathcal{Q}}-1}} \tag{18.20}$$

where $\mathcal{Q}$ stands for NRQCD operators, $\hat{C}_a[\mathcal{Q}]$ for their matching coefficients, and $d_{\mathcal{Q}}$ for their dimension. The leading order term in v is the color singlet rate to produce three gluons ($\mathcal{Q} = \mathcal{O}_1(^3S_1)$). The color octet contributions have a $1/\alpha_s$ enhancement. In the weak

coupling regime, which we will assume in the following, they are v^4 suppressed, but one should keep in mind that in the strong coupling regime they may become order v^2. Then the color singlet fragmentation contribution is of order $\alpha_s^3 D_{g\to\gamma}$ and the color octet fragmentation are of order $v^4\alpha_s^2 D_{g\to\gamma}$ ($\mathcal{Q} = O_8(^1S_0)$, $O_8(^3P_J)$) or $v^4\alpha_s^2 D_{q\to\gamma}$ ($\mathcal{Q} = O_8(^3S_1)$). We can use, as before, the counting $v^2 \sim \alpha_s$ to compare the relative importance of the different contributions. The existing models for the fragmentation functions [221] show us that $D_{q\to\gamma}$ is much larger than $D_{g\to\gamma}$. This causes the $v^4\alpha_s^2 D_{q\to\gamma}$ of the $O_8(^3S_1)$ contribution to dominate in front of the singlet $\alpha_s^3 D_{g\to\gamma}$ and the octet $v^4\alpha_s^2 D_{g\to\gamma}$ contributions. Moreover, the α_s corrections to the singlet rate will produce terms of order $\alpha_s^4 D_{q\to\gamma}$, that is of the same order as the octet $O_8(^3S_1)$ contribution, which are unknown. This results in a large theoretical uncertainty in the fragmentation contributions, which would be greatly reduced if the leading order calculation of $\hat{C}_q[O_1(^3S_1]$ (this requires a tree level four body decay calculation plus a three body phase space integral) was known.

For the quark fragmentation function we will use the LEP measurement [222] and for the gluon fragmentation function the model [223]. These are the same choices as in [219]. For the $O_8(^1S_0)$ and $O_8(^3P_0)$ matrix elements we will use our estimates in [224]

$$\left\langle J/\psi|O_8(^1S_0)|J/\psi\right\rangle\Big|_{\mu=M} \sim 0.0012\,GeV^3 \tag{18.21}$$

$$\left\langle J/\psi|O_8(^3P_0)|J/\psi\right\rangle\Big|_{\mu=M} \sim 0.0028\,GeV^5 \tag{18.22}$$

The estimate for $\langle J/\psi|O_8(^1S_0)|J/\psi\rangle$ is compatible with the lattice results [225] (nrqcd and Coulomb algorithms). For the $O_8(^3S_1)$ matrix element the same lattice calculation gives

$$\left\langle J/\psi|O_8(^3S_1)|J/\psi\right\rangle_{\rm nrqcd} = 0.0005\,GeV^3 \qquad \left\langle J/\psi|O_8(^3S_1)|J/\psi\right\rangle_{\rm coulomb} = 0.0002\,GeV^3 \tag{18.23}$$

which is much smaller than using the NRQCD v scaling

$$\left\langle J/\psi|O_8(^3S_1)|J/\psi\right\rangle \sim v^4\left\langle J/\psi|O_1(^3S_1)|J/\psi\right\rangle \sim 0.05\,GeV^3 \tag{18.24}$$

with $v^2 \sim 0.3$. With the choices above we obtain the blue dot-dashed curves in Fig. 18.6 (v scaling) and Fig. 18.7 (lattice, nrqcd algorithm) for the fragmentation contributions. These curves turns out to be very sensitive to the value assigned to $\langle J/\psi|O_8(^3S_1)|J/\psi\rangle$. When we put together direct (red dashed curve in Figs. 18.6 and 18.7) and fragmentation contributions we obtain the solid green curves in Fig. 18.6 and 18.7, if the merging formula is used, and Fig. 18.8 and 18.9, if only the central region is taken into account. The shape of this curve in Fig. 18.6 is in qualitative agreement with the early Mark II results for $0.4 \lesssim z \lesssim 0.7$ [194].

18.3.3 Extraction of $\alpha_{\rm s}(M_{J/\psi})$

As mentioned in the introduction, $\alpha_{\rm s}(M_{J/\psi})$ can in principle be extracted from the ratio $\Gamma(J/\psi \to \gamma_{\rm direct}X)$ over $\Gamma_{\rm strong}(J/\psi \to X)$, X stands for light hadrons, $\gamma_{\rm direct}$ for photons produced from the heavy quarks and Γ_{strong} for subtracting from Γ the decays mediated by a virtual photon. This maybe done in an analogous way as it has been recently carried out for bottomonia in [226]. In order to obtain $\Gamma(J/\psi \to \gamma_{\rm direct}X)$ it is important to have

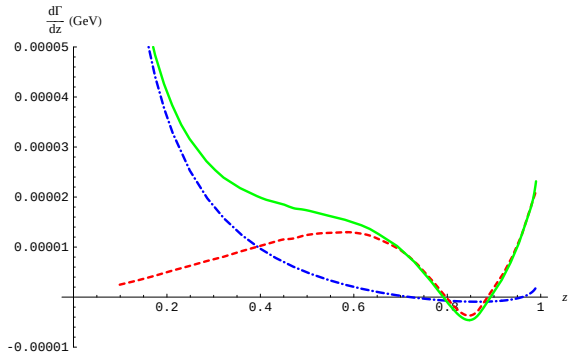

Figure 18.6: The red dashed line corresponds to the direct contributions (merging), the blue dot-dashed line to the fragmentation contributions (v scaling for $O_8(^3S_1)$) and the solid green line is the total.

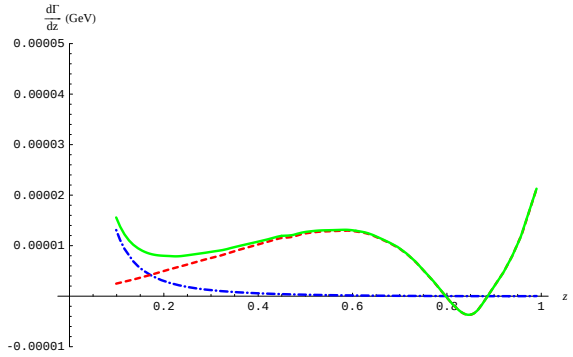

Figure 18.7: The red dashed line corresponds to the direct contributions (merging), the blue dot-dashed line to the fragmentation contributions (lattice, nrqcd algorithm, for $O_8(^3S_1)$) and the solid green line is the total.

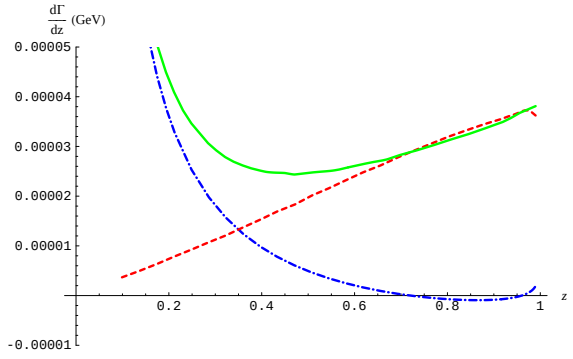

Figure 18.8: The red dashed line corresponds to the direct contributions (central region), the blue dot-dashed line to the fragmentation contributions (v scaling for $O_8(^3S_1)$) and the solid green line is the total.

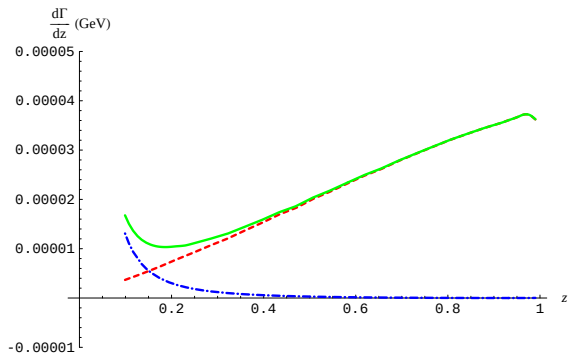

Figure 18.9: The red dashed line corresponds to the direct contributions (central region), the blue dot-dashed line to the fragmentation contributions (lattice, nrqcd algorithm, for $O_8(^3S_1)$) and the solid green line is the total.

a good QCD description of the photon spectrum since one should be able to disentangle fragmentation contributions from direct ones. This may be done by restricting the fit to data of the QCD expression for direct contributions to the upper end-point region and the part of the central region where fragmentation contributions are negligible. As we have seen in the previous section, we do not have at the moment a good QCD description of the upper end point region for J/ψ and hence a model, like the one in [227](see also [228]), might be unavoidable. This expression is then used to interpolate data to small z and hence to be able to obtain the full inclusive width for direct photons. Then $\alpha_s(M_{J/\psi})$ may be extracted from

$$R_\gamma \equiv \frac{\Gamma(J/\psi \to \gamma_{\rm direct}\, X)}{\Gamma_{\rm strong}(J/\psi \to X)} = \frac{36}{5}\frac{e_c^2\alpha}{\alpha_s}\left(1 + \mathcal{O}(\alpha_s) + \mathcal{O}(\frac{v^4}{\alpha_s(m)}) + \cdots\right) \quad (18.25)$$

where $e_c^2 = 4/9$, the $\mathcal{O}(v^2)$ cancel in the ratio, and $\cdots$ stand for higher order contributions. In the extraction of α_s from bottomonium of [226], $\mathcal{O}(\alpha_s(m))$ corrections were taken into account but not $\mathcal{O}(\frac{v^4}{\alpha_s})$ which are of the same order if $\alpha_s(m) \sim v^2$ and in practise turn out to be very important. These have been included in [229].

18.3.4 Learning about the nature of J/ψ and $\psi(2S)$

It has recently been shown that if two heavy quarkonium states are in the strong coupling regime then the ratio of their total photon spectrum in the central region is predictable from QCD at NLO [230]. If the spectrum of both J/ψ and $\psi(2S)$ is measured and fits well with the strong coupling regime formula, it would indicate that both J/ψ and $\psi(2S)$ are in the strong coupling regime. Unfortunately, if it does not, we will not be able to learn much, because it may be due to the fact that J/ψ is in the weak coupling regime or to the fact that $\psi(2S)$ is too close to the open flavor threshold for the strong coupling regime to hold for it (or to both).

18.3.5 Conclusions

A new measurement of the inclusive photon spectrum for radiative J/ψ decays would be of great interest since it has only been measured before by the Mark II collaboration more than 25 years ago. The theoretical progress which has occurred since may allow, among other things, for a sensible extraction of $\alpha_s(M_{J/\psi})$. The additional measurement of the photon spectrum for $\psi(2S)$ might shed some light on the nature of these states. No theoretical analysis are available for other states like η_cs or χ_cs. Experimental measurements would definitively trigger them.

Chapter 19

Charmonium transition

19.1 Hadronic transitions

19.1.1 QCD Multipole Expansion

Hadronic transitions are important decay modes of heavy quarkonia (bound states of heavy quarks Q and $\bar{Q}$). For instance, the branching ratio for $\psi' \to J/\psi + \pi + \pi$ is approximately 50%. In general, let us consider the hadronic transitions

$$\Phi_I \to \Phi_F + h \tag{19.1}$$

in which Φ_I, Φ_F and h stand for the initial state quarkonium, the final state quarkonium, and the emitted light hadron(s), respectively.

In the $c\bar{c}$ and $b\bar{b}$ systems, the typical mass difference $M_{\Phi_I} - M_{\Phi_F}$ is around a few hundred MeV, so that the typical momentum of the light hadron(s) h is low. In this section, we consider only the single-channel approach (For coupled-channel approach, see Refs. [231, 232] and references therein). Then the light hadron(s) h are converted from the gluons emitted by Q or $\bar{Q}$ in the transition. So the typical momentum of the emitted gluons is also low, and thus perturbative QCD does not work in these processes. Certain nonperturbative approaches are thus needed for studying hadronic transitions. *QCD multipole expansion* (QCDME) is a feasible approach to hadronic transitions.

Due to the nonrelativistic nature, the heavy quarkonia $n^\sigma L_J$ [labelled by the principal quantum number n, the orbital angular momentum L, the total angular momentum J, and the spin multiplicity σ ($\sigma = 1$ or 3)], can be calculated by solving the Schrödinger equation with a given potential model. The typical radius $a = \sqrt{\langle r^2 \rangle}$ of the $c\bar{c}$ and $b\bar{b}$ quarkonia obtained in this way is of the order of 10^{-1} fm. For soft gluon emissions with the gluon momentum k satisfying $ak < 1$, ak can be a good expansion parameter, i.e., we can expand the gluon fields in powers of ak. This is the so-called *QCD multipole expansion* (QCDME). In classical electrodynamics, the coefficient of the $(ak)^l$ term in the multipole expansion contains a factor $\dfrac{1}{(2l+1)!!}$. Hence multipole expansion actually works better than what is expected by simply estimating the size of $(ak)^l$. Thus QCDME works for

hadronic transitions. Note that the convergence of QCDME does not depend on the value of the QCD coupling constant g_s. Therefore QCDME is a feasible approach to the soft gluon emissions in hadronic transitions (19.1).

QCDME has been studied by many authors [233, 234, 235, 236, 174, 238]. The gauge invariant formulation is given in Ref. [174]. For a systematic review of this kind the theory and its applications to hadronic transitions, see Ref. [232]. In this expansion, the general formula for the S matrix element between the initial state $|I\rangle$ and the final state $|F\rangle$ in the single-channel approach has been given in Ref. [238], which is

$$\langle F|S|I\rangle = -i2\pi\delta(E_F+\omega_F-E_I)\left\langle F\left|H_2\frac{1}{E_I-H_{QCD}^{(0)}+i\partial_0-H_1}H_2\cdots H_2\frac{1}{E_I-H_{QCD}^{(0)}+i\partial_0-H_1}H_2\right|I\right\rangle$$

where ω_F is the energy of the emitted gluons;

$$H_{QCD}^{(0)} = \int \Psi^\dagger(x_1,t)\Psi(x_1,t)\hat{H}\Psi^\dagger(x_2,t)\Psi(x_2,t)d^3x_1d^3x_2 \tag{19.3}$$

with

$$\hat{H}\equiv -\frac{1}{2m_Q}(\partial_1^2+\partial_2^2+V_1(|\boldsymbol{x}_1-\boldsymbol{x}_2|)+\sum_{a=1}^{8}\frac{\lambda_a}{2}\frac{\bar{\lambda}_a}{2}V_2(|\boldsymbol{x}_1-\boldsymbol{x}_2|)+2m_Q, \tag{19.4}$$

and

$$\begin{aligned} &H_{QCD}^{(1)} = H_1+H_2,\\ &H_1\equiv Q_aA_0^a(\boldsymbol{X},t), \qquad H_2\equiv -\boldsymbol{d}_a\cdot\boldsymbol{E}^a(\boldsymbol{X},t)-\boldsymbol{m}_a\cdot\boldsymbol{B}^a(\boldsymbol{X},t)+\cdots, \end{aligned} \tag{19.5}$$

in which

$$Q_a\equiv g_E\int\Psi^\dagger(\boldsymbol{x},t)\frac{\lambda_a}{2}\Psi(\boldsymbol{x},t)d^3x, \tag{19.6}$$

$$\boldsymbol{d}_a\equiv g_E\int(\boldsymbol{x}-\boldsymbol{X})\Psi^\dagger(\boldsymbol{x},t)\frac{\lambda_a}{2}\Psi(\boldsymbol{x},t)d^3x, \tag{19.7}$$

$$\boldsymbol{m}_a\equiv \frac{g_M}{2}\int(\boldsymbol{x}-\boldsymbol{X})\times\Psi^\dagger(\boldsymbol{x},t)\boldsymbol{\gamma}\frac{\lambda_a}{2}\Psi(\boldsymbol{x},t)d^3x \tag{19.8}$$

are the color charge, color-electric dipole moment, and color-magnetic dipole moment of the $Q\bar{Q}$ system, respectively. Eq. (19.2) is the basis of the study of hadronic transitions in QCDME. Explicit evaluation of the S matrix elements in various cases will be presented in the following sections.

19.1.2 Hadronic Transitions Between *S*-Wave Quarkonia

In the single-channel approach, the amplitude of hadronic transitions (19.1) is diagrammatically shown in FIG. 1.

Figure 19.1: Diagram for a typical hadronic transition in the single-channel approach.

In Fig. 19.1, there are two complicated vertices: namely, the vertex of *multipole gluon emissions* (**MGE**) from the heavy quarks and the vertex of *hadronization* (**H**) describing the conversion of the emitted gluons into light hadron(s). The **MGE** vertex is at the scale of the heavy quarkonium, and it depends on the property of the heavy quarkonia. The **H** vertex is at the scale of the light hadron(s), and is independent of the heavy quarkonia. In the following, we shall treat them separately. To illustrate how Eq. (S) works, we take the $\pi\pi$ and η transitions between S-wave quarkonia as examples.

$\pi\pi$ Transitions

Consider the transition $n_I^3S_1 \to n_F^3S_1 + \pi + \pi$. These processes are dominated by double electric-dipole transitions (E1E1). The transition amplitude can be obtained from (19.2). With certain algebra, we obtain [238, 174, 239]

$$\mathcal{M}_{E1E1} = i\frac{g_E^2}{6}\left\langle \Phi_F h \left| \overline{\boldsymbol{x}}\cdot\boldsymbol{E}\frac{1}{E_I - H_{QCD}^{(0)} - iD_0}\overline{\boldsymbol{x}}\cdot\boldsymbol{E}\right| \Phi_I \right\rangle, \tag{19.9}$$

where $\overline{\boldsymbol{x}}$ is the separation between Q and $\bar{Q}$, and $(D_0)_{bc} \equiv \delta_{bc}\partial_0 - g_s f_{abc}A_0^a$. Let us insert a complete set of intermediate states with the principal quantum number K and the orbital angular momentum L. Then Eq. (19.9) can be written as

$$\mathcal{M}_{E1E1} = i\frac{g_E^2}{6}\sum_{KLK'L'}\left\langle \Phi_F h\left|\overline{\boldsymbol{x}}\cdot\boldsymbol{E}\right|KL\right\rangle\left\langle KL\left|\frac{1}{E_I - H_{QCD}^{(0)} - iD_0}\right|K'L'\right\rangle\left\langle K'L'\left|\overline{\boldsymbol{x}}\cdot\boldsymbol{E}\right|\Phi_I\right\rangle \tag{19.10}$$

According to the angular momentum selection rule, the intermediate states must have $L = L' = 1$. The intermediate states in the hadronic transition are the states after the emission of the first gluon and before the emission of the second gluon shown in FIG. 1, i.e. they are states with a gluon and a color-octet $Q\bar{Q}$. There is strong interaction between the gluon and $Q\bar{Q}$ since they all carry colors. Thus these states are the so-called hybrid states. It is difficult to calculate the hybrid state from the first principles of QCD. So we shall take a reasonable model for it. The model should *reasonably reflect the main properties of the hybrid states* and should *contain as few unknown parameters as possible* in order not to affect the predictive power of the theory. There is a quark confining string (QCS) model [240] satisfying these requirements (Another possible model is the MIT bag model for the hybrid states. Hadronic transitions with the MIT bag model as the model for the intermediate states has been studied in Ref. [241], and the predictions are shown to be very close to those in the QCS model if the same data are taken as inputs. Thus the predictions are not sensitive to the model for the intermediate states.). With the QCS model describing the intermediate states, the transition amplitude (19.10) becomes [239]

$$\mathcal{M}_{E1E1} = i\frac{g_E^2}{6}\sum_{KL}\frac{\langle\Phi_F|\bar{x}_k|KL\rangle\langle KL|\bar{x}_l|\Phi_I\rangle}{E_I - E_{KL}}\langle\pi\pi|E_k^aE_l^a|0\rangle, \tag{19.11}$$

where E_{KL} is the energy eigenvalue of the intermediate vibrational state $|KL\rangle$. We see that, in this approach, the transition amplitude contains two factors: namely, the heavy quark **MGE** factor (the summation) and the **H** factor $\langle\pi\pi|E_k^aE_l^a|0\rangle$. The first

factor concerns the properties of the heavy quarkonia which can be calculated for a given potential model. The second factor at the scale of light hadrons is highly nonperturbative. So far, there is no reliable way of calculating this **H** factor from the first principles of QCD. Therefore we take a phenomenological approach based on an analysis of the structure of this matrix element using PCAC and soft pion technique in Ref. [242]. In the center-of-mass frame, the two pion momenta q_1 and q_2 are the only independent variables describing this matrix element. According Ref. [242], we can write this matrix element as [239]

$$\frac{g_E^2}{6}\langle\pi_\alpha(q_1)\pi_\beta(q_2)|E_k^a E_l^a|0\rangle = \frac{\delta_{\alpha\beta}}{\sqrt{(2\omega_1)(2\omega_2)}}\left[C_1\delta_{kl}q_1^\mu q_{2\mu} + C_2\left(q_{1k}q_{2l}+q_{1l}q_{2k}-\frac{2}{3}\delta_{kl}\boldsymbol{q}_1\cdot\boldsymbol{q}_2\right)\right] \quad (19.12)$$

where C_1 and C_2 are two unknown constants. In the rest frame of Φ_I (the center-of-mass frame), for a given $\pi\pi$ invariant mass $M_{\pi\pi}$, the C_1 term is isotropic (S-wave), while the C_2 term is angular dependent (D-wave). In the nonrelativistic single-channel approach, the **MGE** factor in (19.11) is proportional to δ_{kl} due to orbital angular momentum conservation. So that only the C_1 term contributes to the S-state to S-state transitions. In this case, the $n_I^3S_1 \to n_F^3S_1 + \pi + \pi$ transition rate can be expressed as [239]

$$\Gamma(n_I^3S_1 \to n_F^3S_1\ \pi\ \pi) = |C_1|^2 G |f^{111}_{n_I 0 n_F 0}|^2, \quad (19.13)$$

where

$$f^{LP_IP_F}_{n_Il_In_Fl_F} \equiv \sum_K \frac{\int R_F(r) r^{P_F} R^*_{KL}(r) r^2 dr \int R^*_{KL}(r') r'^{P_I} R_I(r') r'^2 dr'}{M_I - E_{KL}}, \quad (19.14)$$

and the phase-space factor G is [239]

$$G \equiv \frac{3}{4}\frac{M_{\Phi_F}}{M_{\Phi_I}}\pi^3 \int K\sqrt{1-\frac{4m_\pi^2}{M_{\pi\pi}^2}}(M_{\pi\pi}^2 - 2m_\pi^2)^2\, dM_{\pi\pi}^2, \quad (19.15)$$

$$K \equiv \frac{\sqrt{(M_{\Phi_I}+M_{\Phi_F})^2 - M_{\pi\pi}^2}\sqrt{(M_{\Phi_I}-M_{\Phi_F})^2 - M_{\pi\pi}^2}}{2M_{\Phi_I}}.$$

In (19.14), R_I, R_F, and R_{KL} are radial wave functions of the initial, final, and intermediate vibrational states, and they can be calculated from the Schrödinger equation with a given potential model.

Now there is only one overall unknown constant C_1 left in this transition amplitude, and it can be determined by taking a well-measured hadronic transition rate as an input. So far, the best measured S-state to S-state $\pi\pi$ transition rate is $\Gamma(\psi' \to J/\psi\ \pi\pi)$. The updated experimental value is (Here we take the world averaged value of the total width of ψ' given in Ref. [4]) [4]

$$\Gamma_{\rm tot}(\psi') = 277 \pm 22\ {\rm keV},$$
$$B(\psi' \to J/\psi\ \pi^+\pi^-) = (31.8 \pm 0.6)\%, \qquad B(\psi' \to J/\psi\ \pi^0\pi^0) = (16.46 \pm 0.35)\% \quad (19.16)$$

Taking (19.16) as an input to determine C_1, we can predict all the S-state to S-state $\pi\pi$ transitions rates in the Υ system. Since the amplitude (19.14) depends on the

Table 19.1: The determined $|C_1|^2$ and the predicted rates $\Gamma(\Upsilon' \to \Upsilon\ \pi\pi)$, $\Gamma(\Upsilon'' \to \Upsilon\ \pi\pi)$, and $\Gamma(\Upsilon'' \to \Upsilon'\ \pi\pi)$ (in keV) in the Cornell model and the BGT model. The corresponding updated experimental values of the transition rates quoted from Ref. [4] are also listed for comparison.

	Cornell	BGT	Expt.
$\|C_1\|^2$	83.4×10^{-6}	67.8×10^{-6}	
$\Gamma(\Upsilon' \to \Upsilon\pi\pi)$ (keV)	8.6	7.8	8.89 ± 1.17
$\Gamma(\Upsilon'' \to \Upsilon\pi\pi)$ (keV)	0.44	1.2	1.33 ± 0.22
$\Gamma(\Upsilon'' \to \Upsilon'\pi\pi)$ (keV)	0.78	0.53	0.98 ± 0.28

potential model, the determined value of $|C_1|$ is model dependent. Here we take the Cornell Coulomb plus linear potential model [244] and the Buchmüller-Grunberg-Tye (BGT) potential model [245] as examples to show the determined $|C_1|$ and the predicted rates of $\Upsilon' \to \Upsilon\ \pi\pi$, $\Upsilon'' \to \Upsilon\ \pi\pi$, and $\Upsilon'' \to \Upsilon'\ \pi\pi$. The results are listed in TABLE I. We see that the predicted rates in the BGT model are close to the experimental values.

Note that the phase space factor G in $\Upsilon'' \to \Upsilon\ \pi\pi$ is much larger than that in $\Upsilon' \to \Upsilon\ \pi\pi$, $G(\Upsilon'' \to \Upsilon\ \pi\pi)/G(\Upsilon' \to \Upsilon\ \pi\pi) = 33$. So one may naively expect that $\Gamma(\Upsilon'' \to \Upsilon\ \pi\pi) > \Gamma(\Upsilon' \to \Upsilon\ \pi\pi)$. However, as we see from the experimental values in TABLE I that $\Gamma(\Upsilon'' \to \Upsilon\ \pi\pi)/\Gamma(\Upsilon' \to \Upsilon\ \pi\pi) \approx 1.33/8.89 = 0.15$. The reason why our predictions for this ratio is close to the experimental value is that the contributions from various intermediate states to the overlapping integrals in the summation in f^{111}_{3010} [cf. Eq. (19.14)] *drastically cancel* each other due to the fact that the Υ'' wave function contains two nodes. This is a *characteristic* of this kind of intermediate state models (QCS or bag model).

Improved theoretical study of these processes in a systematic relativistic coupled-channel theory is expected since ψ' and Υ'' are close the the open flavor thresholds.

Recently, the η_c' state was found experimentally with the mass $M_{\eta_c'} = 3.638 \pm 0.004$ GeV [4]. It will be interesting to measure the hadronic transition $\eta_c' \to \eta_c\pi\pi$ at BES III. A very crude estimate of the transition rate was made in Ref. [202] by only estimating the phase space in the single-channel approach. Since η_c' lies very close to the $c\bar{c}$ threshold, a more sophisticated theoretical study of this transition taking into account the coupled-channel and relativistic corrections is expected.

η Transitions

The transitions $n^3_I S_1 \to n^3_F S_1 + \eta$ are contributed by E1M2 and M1M1 transitions, and is dominated by the E1M2 transition. The transition amplitude is

$$\mathcal{M}_{E1M2} = -\frac{i}{2m_Q}\frac{g_E g_M}{6}\sum_{KL}\frac{\langle\Phi_F|\bar{x}_k|KL\rangle\langle KL|S_l\bar{x}_m|\Phi_I\rangle + \langle\Phi_F|S_l\bar{x}_m|KL\rangle\langle KL|\bar{x}_k|\Phi_I\rangle}{E_I - E_{KL}}\langle\eta|E^a_k\partial_m B^a_l|0\rangle \quad (19.17)$$

where $\boldsymbol{S}$ is the total spin of the quarkonium. The **MGE** matrix element is proportional to δ_{km}. Similar to the idea in (19.12), we can phenomenologically parameterize the **H** factor according to its Lorentz structure as [247]

$$\frac{g_E g_M}{6}\langle\eta(q)|E^a_k\partial_k B^a_l|0\rangle = i(2\pi)^{3/2}\ C_3\ q_l, \quad (19.18)$$

in which the phenomenological constant can be determined by taking the data [4]

$$\Gamma_{\rm tot}(\psi') = 277 \pm 22 \text{ keV},, \qquad B(\psi' \to J/\psi\ \eta) = (3.09 \pm 0.08)\% \tag{19.19}$$

as input, and so we can predict the rates for $\Upsilon' \to \Upsilon\ \eta$ and $\Upsilon'' \to \Upsilon\ \eta$. This is equivalent to

$$\Gamma(\Upsilon(n_I^3S_1) \to \Upsilon\ \eta) = \frac{\left|\dfrac{f^{111}_{n_I010}(b\bar{b})}{m_b}\right|^2}{\left|\dfrac{f^{111}_{2010}(c\bar{c})}{m_c}\right|^2} \frac{|\boldsymbol{q}(b\bar{b})|^3}{|\boldsymbol{q}(c\bar{c})|^3} \Gamma(\psi' \to J/\psi\ \eta). \tag{19.20}$$

where $\boldsymbol{q}(b\bar{b})$ and $\boldsymbol{q}(c\bar{c})$ are the momenta of η in $\Upsilon(n_I^3S_1) \to \Upsilon\ \eta$ and $\psi' \to J/\psi\ \eta$, respectively. Taking the BGT model as an example to calculate the ratio of transition amplitudes in (19.20), we obtained

$$\Gamma(\Upsilon' \to \Upsilon\ \eta) = 0.022 \text{ keV}, \qquad \Gamma(\Upsilon'' \to \Upsilon\ \eta) = 0.011 \text{ keV}. \tag{19.21}$$

These are consistent with the present experimental bounds [4]

$$\Gamma(\Upsilon' \to \Upsilon\ \eta) < 0.064 \text{ keV}, \qquad \Gamma(\Upsilon'' \to \Upsilon\ \eta) < 0.045 \text{ keV}. \tag{19.22}$$

We can also compare the ratios $R' \equiv \Gamma(\Upsilon' \to \Upsilon\ \eta)/\Gamma(\psi' \to J/\psi\ \eta)$ and $R'' \equiv \Gamma(\Upsilon'' \to \Upsilon\ \eta)/\Gamma(\psi' \to J/\psi\ \eta)$ with the recent experimental measurements. Recently BES has obtained an accurate measurement of $\Gamma(\psi' \to J/\psi\ \eta)$ and $\Gamma(\psi' \to J/\psi\ \pi^0)$ [248]. With the new BES data and the bounds on $\Gamma(\Upsilon' \to \Upsilon\ \eta)$ and $\Gamma(\Upsilon'' \to \Upsilon\ \eta)$ [4], the experimental bounds on R' and R'' are [248]

$$R'|_{expt} < 0.0061, \qquad R''|_{expt} < 0.0043. \tag{19.23}$$

Taking the BGT model to calculate the ratios R' and R'', we obtain

$$R'|_{BGT} = 0.0025, \qquad R''|_{BGT} = 0.0013. \tag{19.24}$$

These are consistent with the experimental bounds (19.23). BES III can further improve the measurements of $\Gamma(\psi' \to J/\psi\ \eta)$ and $\Gamma(\psi' \to J/\psi\ \pi^0)$.

19.1.3 $\pi\pi$ Transitions of D-Wave Charmonium

$\psi(3770)$ (or ψ'') is essentially the $1D$ state of the charmonium. The measured leptonic width of $\psi(3770)$ is (0.24 ± 0.06) keV [4]. If we simply regard $\psi(3770)$ as a pure $1D$ state of charmonium, the predicted leptonic width will be smaller than the experimental value by an order of magnitude. Therefore people consider $\psi(3770)$ as a mixture of charmonium states, i.e., the observed ψ' and $\psi(3770)$ states are [249, 250, 251].

$$\begin{aligned} \psi' &= \psi(2S)\cos\theta + \psi(1D)\sin\theta, \\ \psi(3770) &= -\psi(2S)\sin\theta + \psi(1D)\cos\theta. \end{aligned} \tag{19.25}$$

The mixing angle θ can be determined phenomenologically by fitting the ratio of the leptonic width of ψ' and $\psi(3770)$. The leptonic widths of $\psi(2S)$ and $\psi(1D)$ are proportional to the wave function at the origin $\psi_{2S}(0)$ and the second derivative of the wave function at the origin $\frac{5}{\sqrt{2}}\frac{d^2\psi_{1D}(0)/dr^2}{2m_c^2}$, respectively. Therefore the determination of θ depends on the potential model. Here we take two potential models as examples, namely the Cornell model [244] and an improved QCD motivated potential model by Chen and Kuang (CK) [252] which leads to more successful phenomenological results. The determined values of θ are

$$\begin{aligned} &\text{Cornell}: \quad \theta = -10^\circ, \\ &\text{CK}: \quad \theta = -12^\circ. \end{aligned} \tag{19.26}$$

Since $\psi(3770)$ lies above the $D\bar{D}$ threshold, it is usually believed that $\psi(3770)$ mainly decays into the open channel $D\bar{D}$. However, the measured cross section $\sigma(e^+e^- \to \psi(3770) \to D\bar{D}) = 5.0 \pm 0.5$ nb [253] is smaller than the measured direct production cross section $\sigma(e^+e^- \to \psi(3770)) = 7.5 \pm 0.8$ nb [255, 254]. People have been searching for non-$D\bar{D}$ decays of $\psi(3770)$. In 2005, BES detected the hadronic transition $\psi(3770) \to J/\psi\,\pi\pi$ [256],and later CLEO-c also detected this transition [257]. This is the first experimentally discovered non-$D\bar{D}$ decay mode of $\psi(3770)$. People are searching for more non-$D\bar{D}$ decay channels.

Theoretical study of the transition $\psi(3770) \to J/\psi\,\pi\pi$ were given much earlier [249, 250]. This transition is dominated by E1E1 gluon emission. The transition rate is [249]

$$\Gamma\big(\psi(3770) \to J/\psi\,\pi\pi\big) = |C_1|^2\left[\sin^2\theta\; G(\psi')\;|f_{2010}^{111}(\psi')|^2 + \frac{4}{15}\left|\frac{C_2}{C_1}\right|^2 \cos^2\theta\; H(\psi'')\;|f_{1210}^{111}(\psi'')|^2\right] \tag{19.27}$$

This rate depends on the value of C_2/C_1 and the potential model (through the amplitudes f_{2010}^{111}, f_{1210}^{111}). We take the Cornell model [244] and the CK model [252] as examples. Taking the possible range for the parameter [249]

$$1 \le C_2/C_1 \le 3, \tag{19.28}$$

we obtain the values of $\Gamma\big(\psi(3770) \to J/\psi + \pi^+ + \pi^-\big)$ listed in TABLE II. Note that S-D

Table 19.2: The predicted transition rate $\Gamma(\psi(3770) \to J/\psi + \pi^+ + \pi^-)$ (in keV) in the Cornell model and the CK model with the updated input data (19.16).

Model	$\Gamma(\psi(3770) \to J/\psi\;\pi^+\pi^-)$ (keV)
Cornell	26 – 139
CK	32 – 147

mixing only affects a few percent of the rate, so that the rate is essentially $\Gamma(\psi(1D) \to J/\psi\;\pi^+\pi^-)$.

The BES measured branching ratio of $\Gamma(\psi(3770) \to J/\psi + \pi^+ + \pi^-)$ based on 27.7 pb^{-1} data of $\psi(3770)$ is [256]

$$B\big(\psi(3770) \to J/\psi + \pi^+ + \pi^-\big) = (0.34 \pm 0.14 \pm 0.09)\%. \tag{19.29}$$

With the total width [4]

$$\Gamma_{tot}\big(\psi(3770)\big) = 23.0 \pm 2.7 \text{ MeV}, \tag{19.30}$$

the partial width is [256]

$$\Gamma_{BES}\big(\psi(3770) \to J/\psi + \pi^+ + \pi^-\big) = 80 \pm 32 \pm 21 \text{ keV}. \tag{19.31}$$

This is in agreement with the theoretical predictions in TABLE II. Taking the BES data (19.31) and Eq. (19.27) to determine C_2/C_1, we obtain

$$C_2/C_1 = 2^{+0.7}_{-1.3}. \tag{19.32}$$

This shows that C_2/C_1 is really within the estimated range (19.28).

The CLEO-c measured branching ratio is [257]

$$B\big(\psi(3770) \to J/\psi + \pi^+ + \pi^-\big) = \big(0.214 \pm 0.025 \pm 0.022\big)\%. \tag{19.33}$$

With the $\psi(3770)$ total width (19.30), the partial width is

$$\Gamma\big(\psi(3770) \to J/\psi + \pi^+ + \pi^-\big) = 50.5 \pm 16.9 \text{ keV}. \tag{19.34}$$

Considering the experimental errors, this is consistent with the BES result (19.31). We can also determine C_2/C_1 from (19.34) and (19.27), and the result is

$$C_2/C_1 = 1.52^{+0.35}_{-0.45}. \tag{19.35}$$

This is consistent with the value (19.32) determined from the BES data, but with higher precision.

Further improved measurement of the transition rate of $\psi(3770) \to J/\psi + \pi^+ + \pi^-$ at BES III to higher precision is desired for determining the fundamental parameter C_2/C_1 which also occurs in other hadronic transitions.

19.1.4 Studying the h_c State

The spin-singlet P-wave state h_c (or $\psi(1^1P_1)$) is of special interest since the difference between the mass M_{h_c} and the center-of-gravity of the χ_{cJ} states, $M_{\text{c.o.g.}}(\chi_c) = (5M_{\chi_{c2}} + 3M_{\chi_{c1}} + M_{\chi_{c0}})/9 = 3525.30 \pm 0.08$ MeV gives useful information about the spin-dependent interactions between the heavy quark and antiquark. If the spin-dependent interaction is perturbative, it is shown in Ref. [258] that M_{h_c} will be a few MeV smaller than $M_{\text{c.o.g.}}(\chi_c)$. There have been various experiments searching for the h_c state.

In $\bar{p}p$ collisions, h_c can be directly produced. The E835 experiment recently found the h_c state via the decay channel $\bar{p}p \to h_c \to \eta_c\gamma$, and the measured resonance mass is $M_{h_c} = 3525.8 \pm 0.2 \pm 0.2$ MeV with a width $\Gamma_{tot}(h_c) \lesssim 1$ MeV [259]. The measured production rate is consistent with the theoretical range given in Ref. [247] (see Ref. [259]).

At the e^+e^- colliders, the h_c state cannot be produced directly in the s-channel due to its CP quantum number. Because of the limited phase space, the best way of searching

for the h_c state at CLEO-c or BES is through the isospin violating hadronic transition [260, 247, 250]

$$\psi' \to h_c + \pi^0. \tag{19.36}$$

Recently, CLEO-c has found the h_c state via the channel $\psi' \to h_c\pi^0 \to \eta_c\gamma\gamma\gamma$ [261]. The measured resonance mass is $M_{h_c} = 3524.4 \pm 0.6 \pm 0.4$ MeV [261] which is consistent with the E835 result at the 1σ level.

Theoretical studies were given much earlier in Refs. [247, 250, 262]. The process $\psi' \to h_c + \pi^0$ is dominated by E1M1 transition. The transition amplitude is

$$\mathcal{M}_{E1M1} = i\frac{g_E g_M}{6}\frac{1}{2m_c}\sum_{KL}\frac{\langle h_c|\bar{x}_k|KL\rangle\langle KL|(s_c - s_{\bar{c}})_l|\psi'\rangle + \langle h_c|(s_c - s_{\bar{c}})_l|KL\rangle\langle KL|\bar{x}_k|\psi'\rangle}{M_{\psi'} - E_{KL}}\langle\pi^0|E_k B_l|0\rangle, \tag{19.37}$$

where $\boldsymbol{s}_c$ and $\boldsymbol{s}_{\bar{c}}$ are spins of c and $\bar{c}$, respectively. Since π^0 is a pseudoscalar, the hadronization factor $\langle\pi^0|E_k B_l|0\rangle$ is nonvanishing only when $E_k B_l = \delta_{kl}\boldsymbol{E}\cdot\boldsymbol{B}/3 = \delta_{kl}F^a_{\mu\nu}\tilde{F}^{a\mu\nu}/12$ which is related to the chiral anomaly [263]. Using the Gross-Treiman-Wilczek formula [263] without making further approximations, we obtain

$$\langle\pi^0|\alpha_s F^a_{\mu\nu}\tilde{F}^{a\mu\nu}|0\rangle = \frac{4\pi}{\sqrt{2}}\frac{m_d - m_u}{m_d + m_u}f_\pi m_\pi^2, \tag{19.38}$$

in which the factor $(m_d - m_u)/(m_d + m_u)$ reflects the violation of isospin. To predict the transition rate with these expressions, we should determine the relations between the effective coupling constants $\alpha_E = \dfrac{g_E^2}{4\pi}$, $\alpha_M = \dfrac{g_M^2}{4\pi}$ and the coupling constant α_s appearing in Eq. (19.38). With certain approximations, we can calculate the transition rates $\Gamma(\psi' \to J/\psi\,\pi\pi)$ expressed in terms of α_E [239, 247], so that α_E can be determined by taking the input data (19.16). The determined α_E is approximately $\alpha_E \approx 0.6$ which is just about the commonly estimated value of α_s at the light hadron scale. So we approximately take $\alpha_s \approx \alpha_E$. The determination of α_M is quite uncertain. Here we take a possible range [247]

$$\alpha_E \le \alpha_M \le 3\alpha_E \tag{19.39}$$

to estimate the rate. Taking account of the S-D mixing (19.25) in ψ', the transition rate (19.37) is [250]

$$\begin{aligned}\Gamma(\psi' \to h_c\pi^0) &= \frac{\pi^3}{143m_c^2}\left(\frac{\alpha_M}{\alpha_E}\right)\left|\cos\theta\left(f^{110}_{2011} + f^{001}_{2011}\right) - \sqrt{2}\sin\theta\left(f^{110}_{1211} + f^{201}_{1211}\right)\right|^2 \\ &\quad\times\frac{E_{h_c}}{M_{\psi'}}\left[\frac{m_d - m_u}{m_d + m_u}f_\pi m_\pi^2\right]^2|\boldsymbol{q}_\pi|.\end{aligned} \tag{19.40}$$

Numerical result in the CK potential model is [250]

$$\Gamma(\psi' \to h_c\pi^0) = 0.06\left(\frac{\alpha_M}{\alpha_E}\right)\text{ keV}, \qquad B(\psi' \to h_c\pi^0) = (2.2 \pm 0.2)\left(\frac{\alpha_M}{\alpha_E}\right)\times 10^{-4}. \tag{19.41}$$

Calculations show that the dependence of the transition rate on the potential model is mild [250, 247].

We know that π^0 decays 99% into two photons. Thus the signal in (19.36) is $\psi' \to h_c\gamma\gamma$ with $M_{\gamma\gamma} = m_{\pi^0}$. If the momenta of the two photons can be measured with sufficient accuracy, one can look for the monotonic $M_{\gamma\gamma}$ as the signal. From the branching ratio in (19.41), we see that, taking account of a 10% detection efficiency, hundreds of signal events can be observed for an accumulation of 10 millions of ψ'. The backgrounds are shown to be either small or can be clearly excluded [250]. Once the two photon energies ω_1 and ω_2 are measured, the h_c mass can be extracted from the relation $M_{h_c}^2 = M_{\psi'}^2 + m_{\pi^0}^2 - 2M_{\psi'}(\omega_1+\omega_2)$.

To have a clearer signal, one can further look at the decay product of h_c. It has been shown that the main decay channel of h_c is $h_c \to \eta_c\gamma$ [250]. So that the easiest signal is $\psi' \to h_c\pi^0 \to \eta_c\gamma\gamma\gamma$. The branching ratio $B(h_c \to \eta_c\gamma)$ depends on the hadronic width of h_c. In Ref. [250], the hadronic width of h_c was studied both in the conventional perturbative QCD (PQCD) and in nonrelativistic QCD (NRQCD) approaches. The predictions are [250]

$$\text{PQCD}: \qquad B(h_c \to \eta_c\gamma) = (88 \pm 2)\%, \tag{19.42}$$

$$\text{NRQCD}: \qquad B(h_c \to \eta_c\gamma) = (41 \pm 3)\%. \tag{19.43}$$

These lead to the predictions

$$\text{PQCD}: \qquad B(\psi' \to h_c\pi^0) \times B(h_c \to \eta_c\gamma) = 1.9\left(\frac{\alpha_M}{\alpha_E}\right) \times 10^{-4} = (1.9 - 5.8) \times 10^{-4}, \tag{19.44}$$

$$\text{NRQCD}: \qquad B(\psi' \to h_c\pi^0) \times B(h_c \to \eta_c\gamma) = 0.9\left(\frac{\alpha_M}{\alpha_E}\right) \times 10^{-4} = (0.9 - 2.7) \times 10^{-4}. \tag{19.45}$$

The CLEO-c measured $B(\psi' \to h_c\pi^0) \times B(h_c \to \eta_c\gamma)$ is [261]

$$\text{CLEO-c}: \qquad B(\psi' \to h_c\pi^0) \times B(h_c \to \eta_c\gamma) = (3.5 \pm 1.0 \pm 0.7) \times 10^{-4} \tag{19.46}$$

which is in good agreement with the above theoretically predicted range (19.44) in the PQCD approach. Considering the large errors in (19.46), the present CLEO-c value is also consistent with the NRQCD prediction (19.45). Future improved measurements at BES III and CLEO-c with higher precision may test these two different approaches to the hadronic decays.

Comparing the PQCD prediction (19.44) with the CLEO-c result (19.46), we can determine

$$\frac{\alpha_M}{\alpha_E} = 1.8 \pm 0.9. \tag{19.47}$$

This is really within the estimated range (19.39). Note that the 50% uncertainty in (19.47) comes from the errors in (19.46). Since α_M/α_E is a fundamental parameter in the theory of QCD multipole expansion, it is important to improve the measurement of $B(\psi' \to h_c\pi^0) \times B(h_c \to \eta_c\gamma)$ at BES III and CLEO-c to determine this fundamental parameter to a higher precision.

Since the hadronization factor (19.38) in this $\psi' \to h_c\pi^0$ process is obtained from the Gross-Treiman-Wilczek relation without taking approximations, the agreement between

(19.44) and (19.46) implies that the above theoretical approach to the heavy quark **MGE** factor in (19.37) is quite reasonable.

CLEO-c has also studied the branching ratios with some exclusive hadronic decay channels of η_c [261]. More accurate measurement of the branching ratios of these exclusive hadronic channels at BES III and CLEO-c may also be compared with the corresponding predictions in Ref. [250] to test the PQCD and NRQCD approaches.

In summary, there are many aspects which need improved experimental studies related to the h_c state at BES III and CLEO-c.

i, Because of the errors in the E835 and CLEO-c experiments, we still cannot judge whether M_{h_c} is larger or smaller than $M_{c.o.g.}(\chi_c)$. So that further improved measurements of M_{h_c}, e.g. through exclusive channel measurements as well, may make this issue clearer.

ii, For the determination of the fundamental parameter α_M/α_E and for testing the PQCD and NRQCD approaches to the hadronic decays of h_c, improved measurements of $B(\psi' \to h_c\pi^0) \times B(h_c \to \eta_c\gamma)$ to higher precisions are expected.

iii, Branching ratios for various exclusive channels have been calculated in Ref. [250] which are different in the PQCD approach and the NRQCD approach. Improved measurements of the exclusive channel branching ratios may help to test the two approaches.

iv, Some other decay modes of the h_c state have been studied in Ref. [247]. For instance, $\Gamma(h_c \to J/\psi\ \pi\pi) = 4.12 \left(\frac{\alpha_M}{\alpha_E}\right)$ keV, etc [247]. After accumulating a large enough sample of ψ', other decay modes of h_c may also be measured, so that the properties of the h_c state can be better known.

19.1.5 $\pi\pi$ Transitions of P-Wave Quarkonia

Theoretical study of the hadronic transitions $\chi_b(2^3P_{J_I}) \to \chi_b(1^3P_{J_F})\pi\pi$ have been given in Ref. [239]. Recently, CLEO measured the transition rate of $\Gamma(\chi_b(2^3P_{J_I}) \to \chi_b(1^3P_{J_F})\pi\pi)$ [264], and the results are consistent with the theoretical predictions [232].

So far, hadronic transitions of the χ_{cJ} states have not been studied yet. The observed χ_{cJ} decays are mainly hadronic decays (decaying into light hadrons), and the hadronic widths of the three χ_{cJ} states are rather different. χ_{c1} has the smallest hadronic decay rate [4], and is thus the most interesting one among the three χ_{cJ} states for studying hadronic transitions. The main hadronic transition process of χ_{c1} is $\chi_{c1} \to \eta_c\pi\pi$ which is dominated by the E1-M1 transition. Its transition rate has been studied in Ref. [265], and the obtained rate in the two-gluon approximation is

$$\Gamma(\chi_{c1} \to \eta_c\pi\pi) = \frac{4\alpha_E\alpha_M}{8505\pi m_c^2}|f_{1110}^{010} + |f_{1110}^{101}|^2\,(M_{\chi_{c1}} - M_{\eta_c})^7\,, \tag{19.48}$$

where

$$f^{LP_IP_F}_{n_Il_In_Fl_F} = \sum_K f^{LP_IP_F}_{n_Il_In_Fl_F}(K),$$
$$f^{LP_IP_F}_{n_Il_In_Fl_F}(K) \equiv \frac{\int R^*_F(r')r'^{P_F}R_{KL}(r')r'^2dr' \int R^*_{KL}(r)r^{P_I}R_I(r)r^2dr}{E_I - E_{KL}}. \quad (19.49)$$

We take the CK potential model [252] as an example to calculate the radial wave functions in (19.49). The value of α_M/α_E has been given in (19.47). To determine α_E, we take the same approximation for $\Gamma(\psi' \to J/\psi\ \pi\pi)$ which is

$$\Gamma(\psi' \to J/\psi\ \pi\pi) = \frac{8\alpha_E^2}{8505\pi}|f^{111}_{2010}|^2(M_{\psi'} - M_{J/\psi})^7, \quad (19.50)$$

and determine α_E by taking the input (19.16). This gives $\alpha_E = 0.46$. Then the predicted rate is

$$\Gamma(\chi_{c1} \to \eta_c\pi\pi) = 9.0\left(\frac{\alpha_M}{\alpha_E}\right)\text{keV} = 16.3 \pm 8.1\ \text{keV}. \quad (19.51)$$

The result in the Cornell potential model is smaller than the value in (24.2) by 14% [265], so that the model dependence of the prediction is not significant. In (24.2), the 50% uncertainty comes from the error in (19.47). The total width of χ_{c1} is $\Gamma(\chi_{c1}) = 0.89 \pm 0.05$ MeV [4]. So that the branching ratio is

$$B(\chi_{c1} \to \eta_c\pi\pi) = (1.82 \pm 1.02)\%. \quad (19.52)$$

At e^+e^- colliders, the state χ_{c1} can be produced via $\psi' \to \gamma\chi_{c1}$ at the ψ' peak. In the rest frame of ψ', the momentum of χ_{c1} is 171 MeV which is only 5% of its mass $M_{\chi_{c1}} = 3510.66$ MeV. Therefore we can neglect the motion of χ_{c1}, and simply take the branching ratio (19.52) to estimate the event numbers in the experiments.

The detection of the process

$$\psi' \to \gamma\chi_{c1} \to \gamma\eta_c\pi\pi \quad (19.53)$$

can be performed in two ways, namely the *inclusive* and the *exclusive* detections [188]. In the inclusive detection, only the photon and the two pions are detected, while η_c is regarded as a missing energy. In the exclusive detection, all the photon, the two pions, and the decay products of η_c are detected. Reconstruction of η_c and χ_{c1} from the measured final state tagging particles can suppress the backgrounds.

The inclusive detection requires measuring the momenta of the photon and the pions to certain precision. It is difficult to do this kind of analysis with the BES II data because the BES II photon detector is not efficient enough. At BES III and CLEO-c, this kind of detection is possible.

For BES III, it is not difficult to accumulate 10^8 of ψ' events. CLEO-c is now running at the ψ' peak again, and will soon accumulate 3×10^7 ψ' events. The branching ratio

of $\psi' \to \gamma\chi_{c1}$ is $B(\psi' \to \gamma\chi_{c1}) = (8.7 \pm 0.4)\%$ [4]. Taking account of a 15% detection efficiency, we obtain the number of events of (19.53) at BES III and CLEO-c

$$\text{BES III}: \quad N_{incl}(\psi' \to \gamma\chi_{c1} \to \gamma\eta_c\pi\pi) = (2.38 \pm 1.43) \times 10^4. \quad (19.54)$$

$$\text{CLEO} - \text{c}: \quad N_{incl}(\psi' \to \gamma\chi_{c1} \to \gamma\eta_c\pi\pi) = (7.15 \pm 4.27) \times 10^3. \quad (19.55)$$

These numbers are quite large that the transition (19.53) can be clearly studied.

For the exclusive detection, suitable decay modes of η_c should be taken for identifying the η_c in (19.53). Some feasible decay modes with reasonable branching ratios are [4, 261]

$$\eta_c \to \rho\rho: \quad B(\eta_c \to \rho\rho) = (2.0 \pm 0.7)\%, \quad (19.56)$$

$$\eta_c \to K^*\bar{K}^*: \quad B(\eta_c \to K^*\bar{K}^*) = (1.03 \pm 0.26)\%, \quad (19.57)$$

$$\eta_c \to \phi\phi: \quad B(\eta_c \to \phi\phi) = (0.27 \pm 0.09)\%, \quad (19.58)$$

$$\eta_c \to K^*(892)^0 K^-\pi^+: \quad B(\eta_c \to K^*(892)^0 K^-\pi^+) = (2.0 \pm 0.7)\%, \quad (19.59)$$

$$\eta_c \to K^+K^-\pi^+\pi^-: \quad B(\eta_c \to K^+K^-\pi^+\pi^-) = (1.5 \pm 0.6)\%, \quad (19.60)$$

$$\eta_c \to 2(\pi^+\pi^-): \quad B(\eta_c \to 2(\pi^+\pi^-) = (1.20 \pm 0.30)\%, \quad (19.61)$$

$$\eta_c \to \eta\pi\pi \to \gamma\gamma\pi\pi: \quad B(\eta_c \to \eta\pi\pi \to \gamma\gamma\pi\pi) = (1.9 \pm 0.7)\%, \quad (19.62)$$

$$\eta_c \to K_S K^\pm\pi^\mp: \quad B(\eta_c \to K_S K^\pm\pi^\mp) = (1.9 \pm 0.5)\%, \quad (19.63)$$

$$\eta_c \to K_L K^\pm\pi^\mp: \quad B(\eta_c \to K_L K^\pm\pi^\mp) = (1.9 \pm 0.5)\%. \quad (19.64)$$

The modes (19.63) and (19.64) have been used by CLEO-c in the search for the h_c state [261].

Table 19.3: Predictions for the numbers of events in the exclusive detection of the process (19.53) in the CK potential model using the η_c decay modes shown in (19.56)−(19.64) at BES II, BES III, and CLEO-c. The accumulated numbers of the ψ' events are taken to be 1.4×10^7 for BES II, 10^8 for BES III, and 3×10^7 for CLEO-c. The detection efficiency is taken to be 10% for BES II, and 15% for BES III and CLEO-c.

modes	BES II	BES III	CLEO-c
$\rho\rho$	44 ± 42	476 ± 454	143 ± 136
$K^*\bar{K}^*$	23 ± 20	245 ± 210	74 ± 62
$\phi\phi$	6 ± 6	64 ± 60	19 ± 18
$K^*(892)^0 K^-\pi^+$	44 ± 42	476 ± 454	143 ± 136
$K^+K^-\pi^+\pi^-$	34 ± 34	358 ± 358	107 ± 107
$2(\pi^+\pi^-)$	26 ± 23	286 ± 243	85 ± 73
$\eta\pi\pi \to \gamma\gamma\pi\pi$	42 ± 41	452 ± 439	136 ± 132
$K_S K^\pm\pi^\mp$	42 ± 36	452 ± 391	136 ± 118
$K_L K^\pm\pi^\mp$	42 ± 36	452 ± 391	136 ± 118

In the exclusive detection, the requirement of the precision of the photon momentum measurement in (19.53) is not so strict. So it is possible to do this kind of analysis with the BES II data except for those modes with photons in η_c decays. Therefore we also

calculate the event numbers at BES II. The BES II data contains 1.4×10^7 ψ' events. Considering the ability of the BES II detector, we take a detection efficiency of 10% for BES II. The Predicted numbers of events for BES II, BES III, and CLEO-c are listed in TABLE II. We see that the exclusive detection of the process (19.53) can be well studied at BES III and CLEO-c. Considering the theoretical uncertainty, the events at BES II are marginal.

As we have mentioned in the last subsection that inproved measurement of $B(\psi' \to h_c\pi^0) \times B(h_c \to \eta_c\gamma)$ to higher precision at BES III and CLEO-c will determine α_M/α_E more acurately, so that the predictions for the numbers of events of the process (19.53) will be more definite.

19.1.6 Summary

We have seen that the theory of hadronic transitions based on QCDME is quite successful (For details see Ref. [232]). Future studies may concern more hadronic transitions related to excited states close to or beyond the open-flavor threshold. Therefore developing a systematic theory of hadronic transitions including relativistic and coupled-channel effects is expected.

For the experiment, BES III will be the e^+e^- collider in the τ-charm region with the highest luminosity. So that transitions with small rates may also be detected at BES III.

19.2 Radiative transition

19.2.1 Introduction

Radiative transitions historically have played important roles in establishing new quarkonium states. Until today, these simple processes are still of considerable experimental and theoretical interests. On the theoretical side, the photon serves as a clean probe to internal structrue of quarkonium, therefore a thorough understanding of these electromagnetic processes will enrich our knowledge about the underlying dynamics [267].

Radiative transitions in heavy quarkonia are very much like electromagnetic transitions in atoms. As a result, many of the theoretical machineries developed in atomic physics can be directly borrowed to here. The crucial tactics in describing radiative transitions is *multipole expansion*, by exploiting the very soft nature of the radiated photon. In this picture, two most important types of radiative transitions are so-called electric-dipole ($E1$) and magnetic-dipole ($M1$) transitions, where the latter has a transition rate about $O(v^2/c^2)$ smaller relative to the former. The higher multipole transitions, *e.g.* $E2$, $E3$ and $M2$ transitions are further suppressed by powers of relative velocity and in general are rather difficult to be disentangled from the observed $E1$ or $M1$ transitions. For simplicity, in this Section we will mainly focus on the two lowest-order cases, keeping in mind that implementing their effects just introduces more technical, instead of conceptual, complication.

Being an old and familiar subject, radiative transitions in quarkonium have been extensively studied in various phenomenological means, notably in phenomenological potential model approach [268]. Unfortunately, it is not clear to bridge these phenomenoglocal

model with the first principle of QCD. It is certainly desirable to study them from a model-independent perspective. A study along this line, which is based on the effective-field-theory (EFT) approach, has recently become available [269] (For a review on NRQCD, see Sec. [Y. Q. Chen]; for a review on potential NRQCD, see Sec. [Brambilla et al]). To supplement, some preliminary lattice QCD measurements of electromagnetic form factor have also emerged recently [270].

Our starting point is the below interaction term in NRQCD lagrangian:

$$\mathcal{L}_{\rm int} = \frac{ee_Q}{2m}\psi^\dagger \mathbf{D}\cdot\mathbf{A}^{\rm em}\psi + \frac{c_F ee_Q}{2m}\psi^\dagger\sigma\cdot\mathbf{B}^{\rm em}\psi + (\psi\to {\rm i}\sigma^2\chi^*) + \mathcal{O}(1/m^2)\,, \quad (19.65)$$

where the first term is the leading $E1$ operator, and the second is the leading $M1$ operator. ψ stands for the Pauli spinor field annihilation the quark (χ stands for the Pauli field creating the corresponding anti-quark). e_Q and κ_Q are the electric charge and anomalous magnetic moment of the heavy quark, and $c_F = 1+\kappa_Q$ is the NRQCD matching coefficient, where κ denotes the anomalous magnetic moment of the heavy quark, obtained by integrating out the hard scale.

19.2.2 $M1$ transition

$M1$ transition flips the spin of one of heavy quarks, but without changing the orbital angular momentum. So far in charmonium sector, the only observed $M1$ transitions are $J/\psi(\psi')\to\eta_c\gamma$ [1]. In the nonrelativistic limit), M1 transition rate between two S-wave onia takes a particularly simple form:

$$\Gamma[n\,^3S_1\to n'\,^1S_0+\gamma] = \frac{4\alpha_{\rm em}e_Q^2}{3m^2}(1+\kappa_Q)^2\,k_\gamma^3\left|\int dr r^2 R_{n'0}R_{n0}\right|^2, \quad (19.66)$$

where $R_{nl}(r)$ is the radial wave functions. Since the leading magnetic dipole operator $c_F ee_Q/2m\,\sigma\cdot\mathbf{B}^{\rm em}$ only flips the spin and doesn't act on the spatial degrees of freedom, orthogonality of radial wave functions guarantees that: in the *allowed* transitions ($n=n'$), the overlap integral equals 1; in the *hindered* transitions ($n\neq n'$), the overlap integral vanishes.

It has been a long-standing problem that (19.66) overpredicts the observed $J/\psi\to\eta_c\gamma$ width by a factor of $2\sim 3$, with a normal input of m_c and κ_c from perturbative one-loop matching. This clearly indicates large relativistic corrections to (19.66), as usually expected for charmonium system. It has also been speculated that nonperturbative fluctuations may generate a large negative κ_c, so the discrepancy may be reduced.

The $\mathcal{O}(v^2)$ corrections to (19.66) has been available for a long time from potential model [267]:

$$\Gamma[n\,S\to n'\,S+\gamma] = \frac{4\alpha_{\rm em}e_Q^2}{m^2}\frac{k_\gamma^3}{2J_n+1}\left|\sum_i^5 I_i\right|^2, \quad (19.67)$$

[1] Since ψ' and η_c' are too close to the open charm threshold and they cannot be correctly described by current formulation of pNRQCD, therefore we will exclude $\psi'\to\eta_c(\eta_c')\gamma$ and $\eta_c'\to {\rm J}/\psi_{\rm c}\gamma$ in our analysis.

where $2J_n+1$ counts number of polarizations of the parent onium, and

$$\begin{aligned} I_1 &= \langle n'0 \left| (1+\kappa_Q)\left(1-k_\gamma^2 r^2/24\right)\right. \\ &+ \left. (1+2\kappa_Q)k_\gamma/4m \right| n0\rangle \ , \\ I_2 &= -\left\langle n'0 \left| (1+\kappa_Q)\frac{\mathbf{p}^2}{2m^2}+\frac{\mathbf{p}^2}{3m^2}\right| n0\right\rangle \ , \\ I_3 &= \left\langle n'0 \left| \frac{\kappa_Q}{6m} r V_0' \right| n0\right\rangle \ , \\ I_4 &= \pm\frac{4}{E_{n0}^{(0)}-E_{n'0}^{(0)}}\left\langle n'0 \left| (1+\kappa_Q)\frac{V_{\rm ss}}{m^2}\right| n0\right\rangle \ , \\ I_5 &= -\langle n'0 \left| \eta V_{\rm S}/m \right| n0\rangle \ , \end{aligned} \tag{19.68}$$

where V_0 stands for the static potential, the +/– sign in I_4 is associated with ${}^3S_1 \to {}^1S_0$ and ${}^1S_0 \to {}^3S_1$, respectively. Notice that I_4 accounts for the first-order correction to the wave function due to spin-spin potential (other higher-dimensional *local* potentials cease to contribute in S-wave transition), thus is only present in hindered transition.

I_5 is a prediction specific to popular assumption in potential models, where one usually decomposes the confining potential into a Lorentz scalar and a vector part, $V_{\rm conf} = \eta V_{\rm S} + (1-\eta)V_{\rm V}$. This term constitutes the major uncertainty in the potential model predictions, where contradictory claims often appear in the literature [268].

Presence of a hierarchy of scales in quarkonium, m, mv, mv^2, $\Lambda_{\rm QCD}$, makes the EFT approach an ideal tool to analyze this transition process. One first descends from QCD to NRQCD by integrating out hard modes ($\sim m$) [271], then descends from NRQCD to potential NRQCD (pNRQCD) by further integrating out soft modes ($\sim mv$) [272]. As a result, the inter-quark potentials appear as Wilson coefficients in pNRQCD, and the dynamical degrees of freedom of pNRQCD are ultrasoft modes ($\sim mv^2$).

A primary task of the EFT approach is to validate/invalidate (19.67). The real strength of EFT is, however, that it can further answer the following questions that are beyond the scope of potential models:

- Is it possible that a large nonperturbative correction to κ_Q arises when one descends from NRQCD to pNRQCD?
- Is it possible to reproduce I_5 in pNRQCD?
- Potential model focus exclusively on the $Q\overline{Q}$ Fock-state (with an exception of coupled-channel effects which may not be relevant as long as one excludes those states close to the open-flavor threshold). pNRQCD allows one to include ultrasoft gluons as dynamical degrees of freedom. Therefore, one naturally asks for the possibility of nonperturbative contribution arising from higher-Fock states $|Q\overline{Q}g\rangle$, which is usually referred to as *color-octet effect*.

In fact, the answers to these three questions are all `negative` [**?**], on which we will elaborate shortly. It turns out that the pNRQCD formalism is able to justify (19.67) except I_5. In the so called *weak coupling regime* (when $mv \gg \Lambda_{\rm QCD}$), this formula is complete; in the so-called *strong coupling regime* (when $mv \sim \Lambda_{\rm QCD}$), however, (19.67) is incomplete and further terms are needed.

Before going on to explanations, it is useful to first sketch the derivation of $\mathcal{O}(v^2)$ corrections in the framework of pNRQCD. One obvious source is from the contribution of higher dimensional $M1$ operators. These operators can be identified most conveniently by promoting the color gauge group of NRQCD Lagrangian to a larger gauge group $SU_c(3) \times U_{\rm em}(1)$. Explicitly, the relevant magnetic operators up to $\mathcal{O}(1/m^3)$ read [273]:

$$\begin{aligned}
\mathcal{L}_{\rm NR} &= \psi^\dagger \left(iD_0 + \frac{\mathbf{D^2}}{2m} \right) \psi + \frac{c_F e e_Q}{2m} \psi^\dagger \sigma \cdot \mathbf{B}^{\rm em} \psi + \frac{i c_S e e_Q}{8m^2} \psi^\dagger \sigma \cdot [\nabla \times, \mathbf{E}^{\rm em}] \psi \\
&+ \frac{c_{W1} e e_Q}{8m^3} \psi^\dagger \{ \nabla^2, \sigma \cdot \mathbf{B}^{\rm em} \} \psi - \frac{c_{W2} e e_Q}{4m^3} \psi^\dagger \nabla_i \sigma \cdot \mathbf{B}^{\rm em} \nabla_i \psi \\
&- \frac{c_{p'p} e e_Q}{8m^3} \left[\nabla \psi^\dagger \cdot \sigma \, \mathbf{B}^{\rm em} \cdot \nabla \psi + \nabla \psi^\dagger \cdot \mathbf{B}^{\rm em} \sigma \cdot \nabla \psi \right] + (\psi \to {\rm i}\sigma^2 \chi^*) \,, \qquad (19.69)
\end{aligned}$$

where $D_\mu \equiv \partial_\mu + igT^a A^a_\mu + iee_Q A^{\rm em}_\mu$. Various Wilson coefficients can be computed through perturbative matching at the hard scale. For example, at one loop accuracy, $\kappa_Q = C_F \alpha_s / 2\pi$, is about a few percent for charm and bottom. It is well known that some of the Wilson coefficients are related with each other because of reparameterization invariance (RPI), notably $c_S = 2c_F - 1$, $c_{W2} = c_{W_1} - 1$ and $c_{p'p} = c_F - 1$ [273]. When inherited into pNRQCD, one make replacement $\nabla \to i\mathbf{p}$ in these operators, and these RPI relations can be utilized to condense the expressions.

There are other sources of $\mathcal{O}(v^2)$ corrections, for instance, multiple expansion of photon field. One interesting contribution, first pointed out by Grotch and Sebastian [268], is the Lorentz boost effect due to the final-state recoil. Since the wave function of a moving S-wave state has a non-vanishing overlap with a P-wave, spin-flipped state at rest, the $M1$ transition can be effectively realized by a "E1" transition from the parent to this small component. Some subtlety arises in this effect, namely the recoil correction depends on which "E1" operator one uses, *i.e.*, $2ee_Q/m\, \mathbf{p} \cdot \mathbf{A}^{\rm em}$ or $ee_Q \mathbf{r} \cdot \mathbf{E}^{\rm em}$, which are connected by a redefinition of pNRQCD field. The solution to this problem is as following. The matching from NRQCD generates a new $M1$ operator induced by the *nonlocal* (depending on center-of-mass momentum) spin-orbit potential, with a coefficient proportional to $V_{LS}^{\rm CM} = -V_0'/8r$ (Gromes relation). The contribution of this operator also depends on the field redefinition. However, the sum of these two corrections is convention-independent, thus comprises a *meaningful* relativistic recoil effect.

We are now in a position in discussing general matching of $M1$ operators from NRQCD to pNRQCD. At $\mathcal{O}(1)$, those operators in (19.69) are trivially inherited to pNRQCD. In general, after integrating out soft modes, new Wilson coefficients will depend on inter-quark separation r.

Obviously the correction to c_F can be interpreted as a multiplicative $\mathcal{O}(1/m^0)$ matching coefficient of the leading $M1$ operator. Dimensional considerations require that this correction is function of $\log(r)$. We emphasize in passing that it is inappropriate to attribute this new coefficient to the magnetic moment of an individual quark, since it really arises from entangled contributions from both quarks.

The simple answer, no corrections at all, is basically nothing more than the heavy quark spin symmetry and that the $\sigma \cdot \mathbf{B}^{\rm em}$ operator behaves like a unit operator in spatial Fock space. These facts are independent of whether the matching is performed perturbatively as in weak coupling regime, or nonperturbatively, as in strong coupling regime.

In an arbitrary NRQCD diagram depicting transition, we only need to consider the case where the external ultrasoft photon is attached to one of the heavy quark lines. (photon attached on internal light quark loops can be neglected when summing over electric charges of three light flavors). Soft gluons attached on heavy quark lines must be longitudinal to avoid $1/m$ suppression. Because all the propagators and vertexes are spin-independent except the $M1$ vertex, such a diagram can factorize into the leading $M1$ operator times minus the wave function renormalization constant $\delta Z_s(r)$, which is extracted from the same diagram with the external photon removed. Therefore there is no soft contribution to this matching coefficient.

The matching at $\mathcal{O}(1/m)$ is slightly more complicated. In a NRQCD diagram with again a $M1$ insertion, a transverse gluon is allowed to end on quark line with a spin-independent $\mathbf{p}\cdot\mathbf{A}$ vertex (ending on a $\sigma\cdot\mathbf{B}$ vertex doesn't contribute). Repeating the previous argument, one doesn't obtain any new $M1$ operator from these sources. However, there are a new classes of diagrams, in which electromagnetic coupling is embedded in the covariant derivative $\mathbf{D}$, inducing an effective magnetic operator at $\mathcal{O}(1/m)$. This is just the one accompanying with the nonlocal LS-potential as mentioned before. It is important to note that there is no room for the operator of the form $V_{\rm S}/m^2\sigma\cdot\mathbf{B}^{\rm em}$. Therefore one is forced to regard I_5 in (19.67) as an artifact of potential model, which cannot bear any physical significance.

The matching at $\mathcal{O}(1/m^2)$ becomes much more cumbersome. We will not dwell on the explicit expressions for these case. However, it should be kept in mind that they may be neglected in the weak coupling regime because of suppressions by higher powers of $\alpha_s\sim v$. In the strong coupling regime, since $\alpha_s\sim 1$, these operators might be as important as other $\mathcal{O}(v^2)$ corrections. These corrections involve some nonperturbative functions such as vacuum gluonic correlators, so that predictive power is unavoidably damaged.

The color-octet effect in radiative transitions was first envisaged by Voloshin long time ago, but without a detailed study [274]. pNRQCD allows a systematic treatment of this effect. It is not surprising that the color-octet effect is nearly *absent* in $M1$ transition, because of the exactly same reason as before. Here we only give a heuristic argument based on the quantum mechanical perturbation theory. Treating chromo-E1 interaction as perturbation up to second order, one can schematically express a "true" quarkonium state as superpositions of the following Fock components (stripping off spin d.o.g.):

$$\begin{aligned}|N\rangle &= \sqrt{Z_n^{\rm us}}|Q\overline{Q}_1(n)\rangle + |Q\overline{Q}_8 g\rangle \\ &+ \sum_{m\neq n}|Q\overline{Q}_1(m)\rangle\cdots,\end{aligned}\tag{19.70}$$

where $|Q\overline{Q}_1(n)\rangle$ is the unperturbed state, and $Z_n^{\rm us}$ is the renormalization factor for state n due to ultrasoft gluons. Spin-independence of chromo-E1 interaction, plus $M1$ operator being a unit operator in coordinate space, imply that the full $M1$ transition amplitude is nothing but the inner product $\langle N'|N\rangle$. Since orthogonality condition is preserved in perturbed states, it is equal to $\langle n'|n\rangle$, the color-octet contribution thus vanishes. We emphasize that sizable color-octet effect might arise in $E1$ transition, since the $E1$ operator is no longer a unit operator in coordinate Fock space.

Finally we turn to the phenomenological implication of (19.67), with the understanding that we restrict only to the weakly-coupled system for consistency and the unphysical I_5

term has been dropped. Empirically, $\Upsilon(1S)$ and η_b are believed to lie in the weak coupling regime, whereas J/ψ, η_c fit into this regime to a less extent. One therefore expects that (19.67) provides a better prediction for $\Upsilon \to \eta_b\gamma$ than for $J/\psi \to \eta_c\gamma$. However, very narrow width of $2 \sim 3$ eV makes the former unlikely to be observed, hence we will focus on the latter, which has been observed experimentally.

For a weakly-coupled system, the dynamics is largely governed by the perturbative static potential, *i.e.*, $V_0 \approx -C_F\alpha(\mu)/r$, where the natural choice of μ is around the typical three-momentum scale. One also needs to specify the quark mass in (19.67). A naive input is to use $\hat{m}$, half of the center-of-gravity mass of ground state onia. However, this simple procedure may induce an error of order v^2, which shouldn't be neglecteId. A more consistent way is to choose the $1S$ mass m, which is defined implicitly through $\hat{m} = m - \langle 10\,|p^2/2m|\,10\rangle \approx m(1 - C_F^2\alpha_s(\mu)^2/8)$.

Many of terms in (19.67) are practically negligible. Since κ_Q remains its NRQCD value, which is small, we can simply put it to be zero in those $\mathcal{O}(v^2)$ terms (as a result, I_3 can be dropped). In fact, only I_2 in (19.67) accounts for genuine $\mathcal{O}(v^2)$ correction for allowed transition, and we end up with a simple expression

$$\Gamma[J/\psi \to \eta_c\gamma] \;\approx\; \frac{4\alpha_{\rm em}e_c^2}{3\hat{m}_c^2}\,k_\gamma^3\,\left[1 + 2\kappa_c - 2\,C_F^2\alpha_s^2(\mu)/3\right]\,. \tag{19.71}$$

This formula predicts a width of 1.5 ± 1.0 keV, where the central value is obtained by setting $\mu = 0.8$ GeV, the typical 3-momentum transfer in J/ψ. Within large error, our prediction is compatible with the measured width 1.18 ± 0.36 keV [275]. Therefore, our reasonable success may be viewed as *a posteriori* support for the weak-coupling regime assignment of J/ψ and η_c. However, rather sharp μ dependence might suggest that higher-order corrections are also important.

One can employ (19.71) to $\Upsilon \to \eta_b\gamma$ with more confidence, and finds a smaller $\mathcal{O}(v^2)$ correction with flatter scale dependence. Unfortunately, very narrow width of $2 \sim 3$ eV makes this transition unlikely to be detected.

For hindered transitions, *e.g.* $\Upsilon'(\Upsilon'') \to \eta_b\gamma$, the experimental upper bounds are already rather tight and many model predictions have been ruled out [276]. To be conservative, one would not expect (19.67) to reliably describe these transitions if excited bottomonia are indeed in the strong-coupling regime. Nevertheless, it may not be too optimistic to treat, at least Υ', as being in weak-coupling regime. Proceeding along this line, we find that the I_4 term is dominating over I_1 and I_2, and the latter two nearly cancel each other. As a result, the predicted width is about an order-of-magnitude larger than the experimental upper bound! Even though there are lots of uncertainty associated with I_4, this alarmingly large discrepancy seems to indicate that the weak-coupling assignment of Υ' is problematic and a strong-coupling analysis might be more appropriate.

We end with a brief discussion on the P-wave $M1$ transitions, which have received less attention in the past, due to lack of phenomenological impetus. Recent discovery of the h_c state [277] may arouse the interest to study these processes. Color-octet effect again vanishes because of the exactly same reason. It is straightforward to apply the pNRQCD formalism to derive the $\mathcal{O}(v^2)$ corrections. For simplicity, we just quote the weak-coupling

formula for the allowed transition:

$$\Gamma[n\,^3P_J \to n\,^1P_1 + \gamma] \;=\; \frac{4\,\alpha_{\rm em}\,e_Q^2}{3m^2}\,k_\gamma^3\,\left|1+\kappa_Q - c_J\left\langle n1\left|\frac{\mathbf{p}^2}{m^2}\right|n1\right\rangle\right|^2\,, \qquad (19.72)$$

where $c_J = 1/2, 1, 4/5$ for $J = 0, 1, 2$. For the $n\,^1P_1 \to n\,^3P_J\gamma$ transition, one simply multiplies the right side of (19.72) by a statistical factor of $(2J+1)/3$. It should be understood that this formula may be of limited use, since P-wave onia may necessarily live in the strong-coupling regime.

The fine splittings between h_c and χ_{c0}, χ_{c1} and χ_{c2} are about 110, -13, -32 MeV, respectively. It seems that only $h_c \to \chi_{c0}\gamma$ has a serious chance to be observed, with a width comparable to $\Gamma[J/\psi \to \eta_c\gamma]$. Future experimental input will enable us to infer the size of relativistic corrections, thus enriching our understanding of P-wave onia.

19.2.3 $E1$ Transition

In contrast to $M1$ transition, $E1$ transition is spin-independent but will change the orbital angular momentum of quarkonium by one unit. This type of transitions is the most dominating one and there are a variety of data available. In the nonrelativistic limit, the transition is induced by the electric operator given in (19.65), and the transition rate reads

$$\Gamma_{\rm NR}[i \to j + \gamma] \;=\; \frac{4\alpha_{\rm em}e_Q^2}{3}(2J'+1)S_{ij}^E\,k_\gamma^3\left|\int dr r^2 R_{n'0} r R_{n0}\right|^2\,, \qquad (19.73)$$

where $S_{ij}^E = S_{ji}^E$ is the statistical factor. The most phenomenologically relevant $E1$ transitions occur between P-wave and S-wave quarkonia, so we will concentrate on this case. For $^3P_J \to {}^3S_1$, $S^E = \frac{1}{9}$; for $^1P_1 \to {}^1S_0$, $S^E = \frac{1}{3}$. Because of the presence of an extra r, the overlap integral will become sensitive to the concrete profiles about radial wave functions.

One serious obstacle arises for a coherent treatment of $E1$ transition in the context of pNRQCD scheme. Notice it is impossible for both initial and final state quarkonia to reside in the same regime. For example, for the transition $\chi_{cJ} \to J/\psi + \gamma$, the initial-state χ_c lies in the strong-coupling regime, whereas the final-state J/ψ is in the weak-coupling regime. So it is difficult to cope with this process in a single pNRQCD framework, for example, it is not clear how to incorporate the color-octet effect. However, one may still use pNRQCD as a convenient mathematical device, which allows an elegant formulation of relativistic corrections.

It is important also to address the sizes of relativistic corrections. When these effects are taken into account, Eq.(19.73) becomes

$$\Gamma^{E1} \;=\; \Gamma_{\rm NR}^{E1}(1 + R_1 + R_2 + R_3)\,, \qquad (19.74)$$

where R_1 are corrections due to the modification of the nonrelativistic wave functions, R_2 originates from the relativistic modification of the transition operator, from spin-orbit c_S

term concretely, and R_3 represents the finite size corrections (arising from the multipole expansion for the emitted photon). For the $1\,^3P_J \to 1\,^3S_1\gamma$ transition, one finds

$$\begin{aligned} R_1 &= 2E_1^J + (E_1^J)^2\,, \\ R_2 &= \frac{k_\gamma \kappa_Q}{2m}\left[\frac{J(J+1)}{2} - 2\right]\,, \\ R_3 &= -\frac{1}{10}(M_i - M_f)^2\, E_2 + \frac{k_\gamma}{8m} E_3\,, \end{aligned} \tag{19.75}$$

where

$$\begin{aligned} E_1 &= \frac{1}{\varepsilon_{if}}\int dr r^3\, \left[R_{10}^{(0)}(r) R_{11}^{(1)}(r) + R_{10}^{(1)}(r) R_{11}^{(0)}(r)\right]\,, \\ E_2 &= \frac{1}{\varepsilon_{if}}\int dr r^5\, R_{10}^{(0)}(r) R_{11}^{(0)}(r)\,, \\ E_3 &= \frac{1}{\varepsilon_{if}}\int dr r^3\, \left[R_{10}^{(0)}(r)\left(2r\frac{d}{dr}R_{11}^{(1)}(r) - R_{11}^{(1)}(r)\right) - \left(2r\frac{d}{dr}R_{10}^{(0)}(r) - R_{10}^{(0)}(r)\right) R_{11}^{(0)}(r)\right]\,, \end{aligned} \tag{19.76}$$

and $R^{(1)}$ is the first order relativistic correction to the NR radial wave function, $R^{(0)}$. This confirms the early derivation by Grotch, Owen and Sebastian by using potential model approach long ago.

[The relativistic corrections are in general sizable, 25% for charmonium, as expected from velocity counting. Do we need to insert a table for the comparison of data and theory? The threshold effect not considered. **Chang-Zheng, should this part merge with what you have written about EM transition?**]

19.3 Channels for study

19.3.1 Introduction

At BESIII, since its peak luminosity is designed as 10^{33} cm^{-2}s^{-1} at the center of mass energy around ψ'' peak, the luminosity at the ψ', which is less than 100 MeV below the ψ'' peak, is about the same. As the beam energy spread of the BEPCII is around 1.4 MeV, the peak cross section of ψ' production is around 600 nb. Assuming the average luminosity is half of the peak luminosity and the effective running time each year around 10^7 s, the expected ψ' events is 3 billion in one year's running [279]. This is a huge data sample compared with the old generation experiments, and the detector performance is also much better than the old generation ones, thus makes a higher precision measurement of the ψ' decays possible, and makes the search for the modes with small decay rates possible.

The charmonium spectrum below the open charm threshold is shown in Fig. 19.2, since the mass of ψ' is higher than those of all the $n = 1$ charmonia states, all these lower mass charmonia thus can be produced by radiative and/or hadronic decays of ψ'. This has been a fruitful field in charmonium physics [308, 309] both in theoretical and in experimental aspects, however, due to the low statistics of the old generation experiments and the poor detector performance, not all of them were measured, among them, some are crucial in the development of the phenomenological models in charmonium physics.

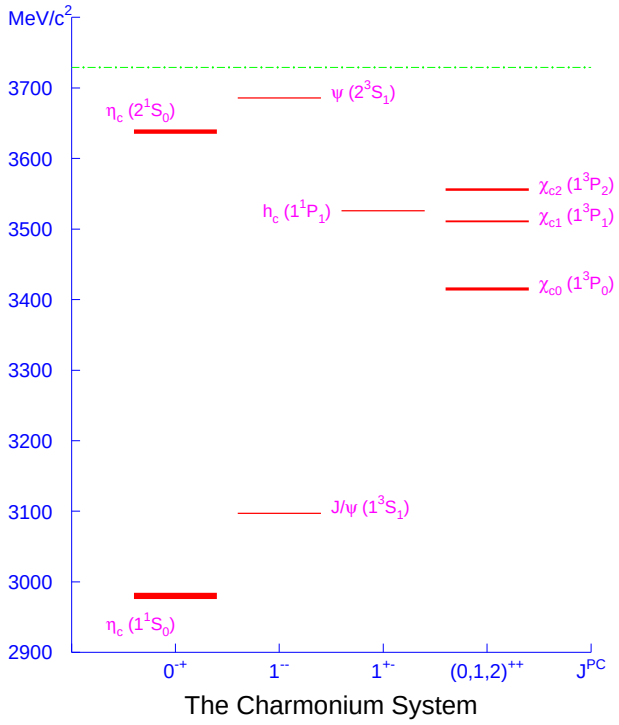

Figure 19.2: Charmonium spectroscopy below the open charm threshold.

In this note, we try to list all the allowed radiative transitions and hadronic transitions which can be studied by the large ψ' data sample which will be collected by BESIII, give an overview of the status of the study and point out some topics where theoretical efforts are called for.

19.3.2 Radiative transitions

Since there is one photon emission between the two charmonia, and the J^{PC} of photon is 1^{--}, the radiative transition only occurs between two C-parity different states. The transitions could be either electric multipole or magnetic multipole transitions depends on the spins and parities of the initial and final states. Assuming the spins of the initial and final states are S_i and S_f, respectively, the total angular momentum carried by the photon (J_γ) can be any integer between $|S_i - S_f|$ and $S_i + S_f$. If the product of the parities of the initial state (π_i) and final state (π_f) equals $(-1)^{J_\gamma}$, the transition is EJ_γ transition; otherwise, if $\pi_i \cdot \pi_f = (-1)^{J_\gamma+1}$, it is an MJ_γ transition. It is obvious that the electric multipole transitions keep the quark spins, while the magnetic multipole transitions are accompanied by quark spin-flip.

In general, when more than one multipole transitions are allowed, only the lowest one is important, however, the contributions of higher multipoles were studied both theoretically and experimentally.

The radiative transition between charmonium states has been studied extensively by many authors both theoretically and experimentally [282, 283, 284, 285, 286, 287, 288, 289]. The rates of some of the transitions were also calculated in lattice QCD [290].

ψ' decays

- $\psi' \to \gamma\chi_{cJ},\ J = 0, 1, 2$

  These are the transitions between S-wave spin triplets and the P-wave spin triplets. In $\psi' \to \gamma\chi_{c0}$, there is only $E1$ transition, while in $\psi' \to \gamma\chi_{c1}$, there are $E1$ and $M2$ transitions, and in $\psi' \to \gamma\chi_{c2}$, there could be $E1, M2$, as well as $E3$ transitions.

  In general, it is believed that $\psi' \to \gamma\chi_{cJ}$ is dominated by the $E1$ transition, but with some $M2$ (for χ_{c1} and χ_{c2}) and $E3$ (for χ_{c2}) contributions due to the relativistic correction. These contributions have been used to explain the big differences between the calculated pure $E1$ transition rates and the experimental results [283]. They will also affect the angular distribution of the radiative photon. Thus the measurement of the angular distribution may be used to determine the contributions of the higher multipoles in the transition.

  Furthermore, for $\psi' \to \gamma\chi_{c2}$, the $E3$ amplitude is directly connected with D-state mixing in ψ' which has been regarded as a possible explanation of the large leptonic annihilation rate of ψ'' [287]. Since recent studies [291, 292, 293] also suggest the S- and D-wave mixing of ψ' and ψ'' may be the key to solve the longstanding "$\rho\pi$ puzzle" and to explain ψ'' non-$D\bar{D}$ decays, the experimental information on multipole amplitudes gains renewed interest.

  Decay angular distributions were studied in $\psi' \to \gamma\chi_{c2}$ by the Crystal Ball experiment using $\psi' \to \gamma\gamma J/\psi$ [294]; the contribution of the higher multipoles were not found to be significant but the errors were large due to the limited statistics. In a recent analysis at BESII [295], $\psi' \to \gamma\chi_{c2} \to \gamma\pi^+\pi^-$ or γK^+K^- decays were used for a similar study. The analysis gives the magnetic quadrapole amplitude $a_2' = -0.051^{+0.054}_{-0.036}$ and the electric octupole amplitude $a_3' = -0.027^{+0.043}_{-0.029}$ [296]. Neither result significantly differs from zero. The results are in good agreement with what is expected for a pure $E1$ transition. As for the D-state mixing of ψ', the results do not contradict with the previous theoretical calculation within one standard deviation [297].

  The contribution of these higher multipoles are interesting theoretically, so further studies at BESIII are expected where a much higher sensitivity for probing the higher multipoles contribution would be possible.

- $\psi' \to \gamma\eta_c$

  This is a hindered $M1$ transition, as it occurs between $n = 2$ and $n = 1$ states.

- $\psi' \to \gamma\eta_c'$

  This is an $M1$ transition, in analogy to the similar transition between J/ψ and η_c, however, the transition rate is very small as the mass difference between the ψ' and η_c' is very small.

  The study of this state in ψ' decays is challenging to the experimentalists and to the detector capability.

η_c' decays

The observation of these transitions will be very helpful in understanding the η_c' properties. In experiment aspect, these final states are clean for the observation, however, the rates seem too small. It is a challenge for BESIII.

- $\eta_c' \to \gamma J/\psi$

  This is an $M1$ transition. It has long been calculated [297] to have a partial width at ??

- $\eta_c' \to \gamma h_c(^1P_1)$

  This is an $E1$ transition. It has long been calculated [286] to have a partial width at 16 keV.

χ_{cJ} decays

- $\chi_{cJ} \to \gamma J/\psi$

  These are the transitions between P-wave spin triplets and the S-wave spin triplets. In $\chi_{c0} \to \gamma J/\psi$, there is only $E1$ transition, while in $\chi_{c1} \to \gamma J/\psi$, there are $E1$ and $M2$ transitions, and in $\chi_{c2} \to \gamma J/\psi$, there could be $E1, M2$, as well as $E3$ transitions.

  Decay angular distributions were studied in $\psi' \to \gamma\chi_{c2}$ by the Crystal Ball experiment using $\psi' \to \gamma\gamma J/\psi$ [294]; the contribution of the higher multipoles were not found to be significant but the errors were large due to the limited statistics. χ_{c2} decay was also studied by E835 in $p\overline{p}$ annihilation.

- $\chi_{c2} \to \gamma h_c(^1P_1)$

  It could be $M1$, $E2$, $M3$ transitions. There was no calculation in the market.

$h_c(^1P_1)$ decays

- $h_c(^1P_1) \to \gamma\eta_c$

  $E1$ transition. This is the discovery mode of the $h_c(^1P_1)$ state at CLEO [298]. The transition branching fraction is expected to be large (more than 50% of the total $h_c(^1P_1)$ decays), this is confirmed by the CLEOc measurement. This should be measured in higher precision at BESIII.

- $h_c(^1P_1) \to \gamma\chi_{c0}$, $\gamma\chi_{c1}$

  $h_c(^1P_1) \to \gamma\chi_{c0}$ is $M1$ transition, and $h_c(^1P_1) \to \gamma\chi_{c1}$ is $M1$, $E2$ transitions. There is no calculation available.

  The measurement of these transitions as well as $\chi_{c2} \to \gamma h_c(^1P_1)$ is challenging, as the rates may be small, and the photons are very soft.

J/ψ decays

- $J/\psi \to \gamma\eta_c$

  $M1$ transition, better measurement is necessary to improve the precision, as well as to clarify the difference between measurements from J/ψ decays and from other experiments, such as $\gamma^*\gamma^*$ fusion, B decays and so on.

  This mode can be studied using either ψ' data sample, via $\psi' \to J/\psi\pi^+\pi^-$, or using the J/ψ data sample collected at the J/ψ resonance peak.

All the radiative transitions between the charmonium states listed above are summarized in Fig. 19.3.

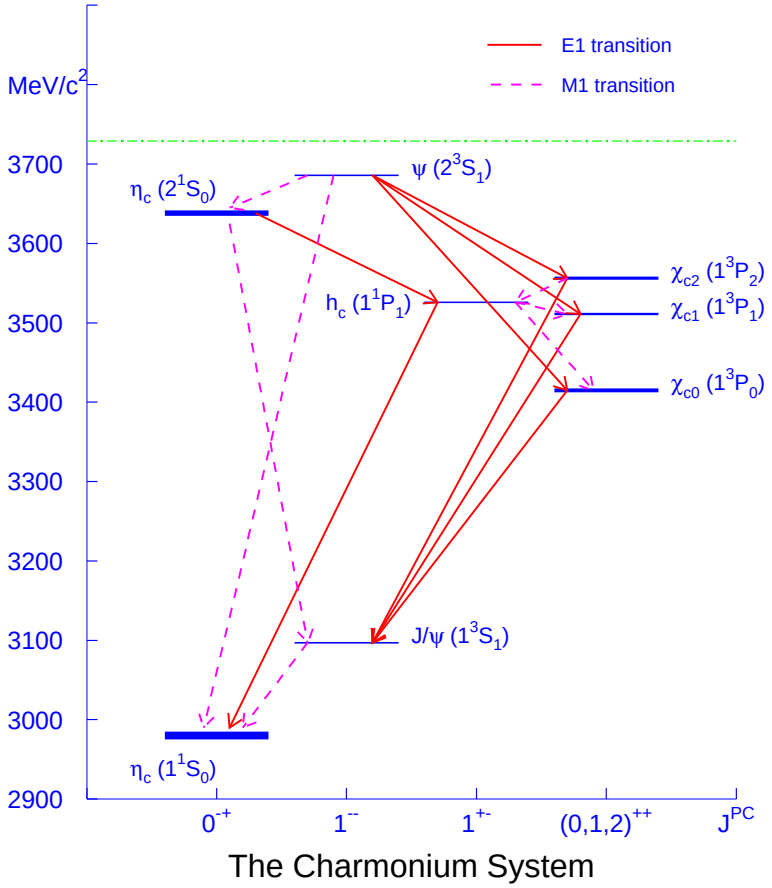

Figure 19.3: Radiative transitions between charmonium states below the open charm threshold.

19.3.3 Hadronic transitions

There are strong and electromagnetic transitions between two charmonium states if the mass difference is large enough to produce one or more π's, or η. C-parity conservation and Parity conservation may forbid some of the transitions, and they are pointed out in

this note. The study of them for a search for the rare decays and the potential signal of new physics is beyond the scope of this note.

Only the hadronic transitions of the ψ' have been studied experimentally, including $\pi^+\pi^- J/\psi$, $\pi^0\pi^0 J/\psi$, $\eta J/\psi$ and $\pi^0 J/\psi$. The theoretical calculations were also done for these transitions. The other possible transitions were only studied scarcely, we point this out below when available.

It should be noted that since the mass differences between the charmonium states are not large, the light hadrons are generally produced at very low momentum, this may supply a good laboratory for studying the physics in this energy domain.

ψ' decays

Since the mass difference between ψ' and many of the charmonium states are much larger than one π mass, thus there are many possible transitions.

All the allowed transitions are summarized in Fig. 19.4 and explained in detail below.

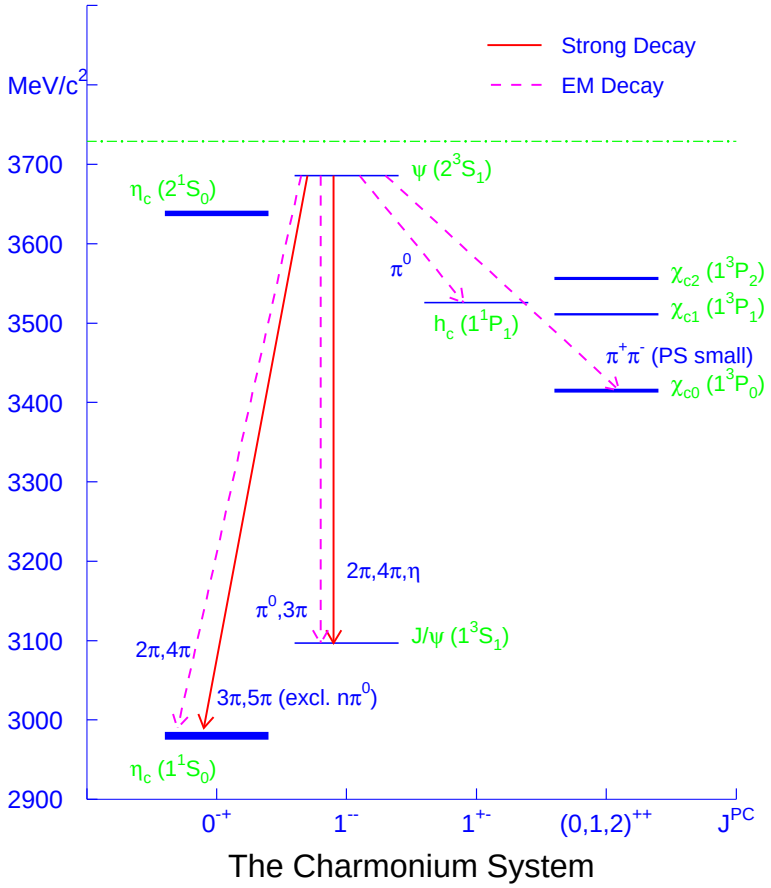

Figure 19.4: Hadronic transitions of ψ' to other charmonium states.

1. $\psi' \to \eta_c + X$

   The mass difference between ψ' and η_c is 706 MeV/c^2, greater than $5m_\pi$ and $m_\eta + m_\pi$, all the possible combinations are listed below. No measurement for the study of the channels listed here, only very few theoretical considerations.

- $\psi' \to n\pi^0\eta_c$, $n = 1, 2, 3, 4, 5$: C-violation, not allowed
- $\psi' \to \pi^+\pi^-\eta_c$: G-violation, EM decays, via ρ^*
- $\psi' \to \pi^+\pi^-\pi^0\eta_c$: strong decays, via ω^*

  It is expected that this mode should be produced at 1% level [299]. The model is developed to explain the "$\rho\pi$ puzzle" between ψ' and J/ψ hadronic decays. Using 14 M ψ' data at BESII, this decay mode is being searched for using three η_c decay modes: $p\overline{p}$, $2(\pi^+\pi^-)$, and $\pi^+\pi^-K^+K^-$. Result is expected in a few months.
- $\psi' \to 2(\pi^+\pi^-)\eta_c$: G-violation, EM decays
- $\psi' \to \pi^+\pi^-2\pi^0\eta_c$: G-violation, EM decays
- $\psi' \to 2(\pi^+\pi^-)\pi^0\eta_c$: strong decays
- $\psi' \to \pi^+\pi^-3\pi^0\eta_c$: strong decays
- $\psi' \to \eta\eta_c$: C-violation, not allowed
- $\psi' \to \eta\pi^0\eta_c$: C-violation, not allowed

2. $\psi' \to J/\psi + X$

   The mass difference between ψ' and J/ψ is 589 MeV/c^2, greater than $4m_\pi$ and m_η, all the possible combinations are listed below.

   The channels in this category were studied well both experimentally and theoretically, due to the large decay branching fractions and the clear signature of the J/ψ leptonic decays.

   - $\psi' \to \pi^0 J/\psi$: G-violation, EM decays

     Observed via $\pi^0 \to \gamma\gamma$ and $J/\psi \to \ell\ell$ by many experiments, the most recent are BESII and CLEO.

     Theoretical calculations are ...
   - $\psi' \to \pi^+\pi^- J/\psi$: strong decays

     This is one of the main transition mode of the ψ', the branching fraction is about one third. The $\pi^+\pi^-$ mass shows interesting feature (more events at high $\pi^+\pi^-$ mass) which has been the hot topic of the theoretical effort from the discover of this decay mode until now.

     $\pi\pi$ are produced mainly in S-wave, with the same quantum number as the σ, the D-wave component is found to be small from the analysis of BESI using 4 M produced ψ' events.

     The process has been analyzed in various models by many authors [375, 301, 302, 303, 304], all the models fit the data well.
   - $\psi' \to \pi^0\pi^0 J/\psi$: strong decays

     The same as $\pi^+\pi^- J/\psi$ mode. Isospin symmetry predicts its production rate is half of that of $\pi^+\pi^- J/\psi$, this is tested in high precision with the CLEO detector using 3 M produced ψ' events.

The Isospin violation effect may exist, but should be small if compare with the $\pi^0 J/\psi$ and $\eta J/\psi$ rates difference. This may be tested with more data with better precision.

- $\psi' \to \pi^+\pi^-\pi^0 J/\psi$: G-violation, EM decays
  The rate can be roughly estimated by the $\pi^0 J/\psi$ mode.
- $\psi' \to 3\pi^0 J/\psi$: G-violation, EM decays
- $\psi' \to 2(\pi^+\pi^-) J/\psi$: strong decays
  The phase space is small, the rate may not be small since it is a strong decay. The detection in experiment is hard, since the momentum of the $\pi^\pm$ is low.
- $\psi' \to \pi^+\pi^- 2\pi^0 J/\psi$: strong decays
  Similar to $\psi' \to 2(\pi^+\pi^-) J/\psi$, hard to be detected.
- $\psi' \to 4\pi^0 J/\psi$: strong decays
  Similar to $\psi' \to 2(\pi^+\pi^-) J/\psi$, detection of 8 low photons with energy around half of the $\pi 0$ mass is a challenge to the Electromagnetic Calorimeter.
- $\psi' \to \eta J/\psi$: strong decays
  Many measurements, the ratio between the rate of this mode and the isospin violation mode $\pi^0 J/\psi$ is used to measure the mass difference of the up and down quarks, and the strength of the electromagnetic decays in ψ' hadronic transition.

3. $\psi' \to \chi_{cJ} + X$

The mass difference between ψ' and χ_{c0} is 271 MeV/c^2, slightly greater than $2m_{\pi^0}$ and lower than $m_{\pi^+} + m_{\pi^-}$, considering the width of χ_{c0} is around 10 MeV/c^2, the tail of χ_{c0} can be produced in $\psi' \to \pi^+\pi^-\chi_{c0}$. The mass difference between ψ' and χ_{c1} is 176 MeV/c^2, slightly greater than m_{π^0}, and the mass difference between ψ' and χ_{c2} is 130 MeV/c^2, lower than m_{π^0}. All the possible transitions are listed below.

- $\psi' \to n\pi^0\chi_{cJ}$, $n = 1, 2$: C-violation, not allowed
- $\psi' \to \pi^+\pi^-\chi_{c0}$: G-violation, EM decays, via ρ^*, phase space very small, only low mass tail of χ_{c0} can be produced. There is no measurement and no theoretical calculation.

4. $\psi' \to h_c(^1P_1) + X$

The mass difference between ψ' and $h_c(^1P_1)$ is 160 MeV/c^2, slightly greater than m_{π^0}, the only possible transition is $\psi' \to \pi^0 h_c(^1P_1)$.

- $\psi' \to \pi^0 h_c(^1P_1)$: G-violation, EM decays
  This is the discovery mode of the $h_c(^1P_1)$ in ψ' decays by CLEO [298]. The product of the branching fraction and that of $h_c(^1P_1) \to \gamma\eta_c$ was given by the same experiment. Assuming the $E1$ transition rate of $h_c(^1P_1)$ decays, one

may estimate the $\psi' \to \pi^0 h_c(^1P_1)$ branching fraction at ?? level. Theoretical estimation of this rate ranges from ?? to ??.

More effort is needed experimentally to understand this transition, as well as study the properties of the $h_c(^1P_1)$ better.

η_c' decays

Since the mass of η_c' is only slightly smaller than that of ψ', so the mass difference between η_c' and many of the charmonium states are also much larger than one π mass, thus there are many possible transitions.

All the allowed transitions are summarized in Fig. 19.5 and explained in detail below.

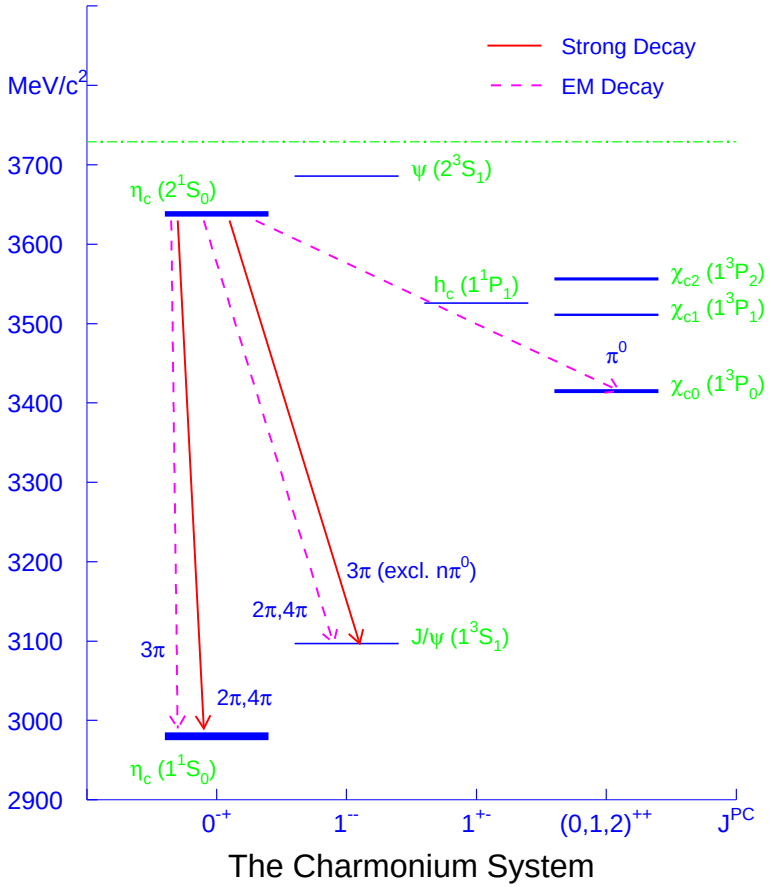

Figure 19.5: Hadronic transitions of η_c' to other charmonium states.

1. $\eta_c' \to \eta_c + X$

   The mass difference between η_c' and η_c is 658 MeV/c^2, greater than $4m_\pi$ and m_η, all the possible combinations are listed below.

   - $\eta_c' \to \pi^0 \eta_c$: P-violation, not allowed

- $\eta_c' \to \pi^+\pi^-\eta_c$: strong decays, via σ

  Voloshin [608] pointed out that this decay is related to the well studied $\psi' \to \pi^+\pi^- J/\psi$, and estimated the branching fraction in η_c' decays could be around 5-10%, together with the neutral $\pi^0\pi^0$ mode. No experiment information available yet.

  The study of this transition is very hard via the ψ' decays, since the η_c' is produced with very small branching fraction in ψ' radiative transition, and the photon energy is extremely low which is hard to be distinguished from the noises.

- $\eta_c' \to \pi^0\pi^0\eta_c$: strong decays, via σ

  Similar to $\eta_c' \to \pi^+\pi^-\eta_c$, the observation should be even harder due to multi-photons in the event.

- $\eta_c' \to \pi^+\pi^-\pi^0\eta_c$: G-violation, EM decays, high orbital angular momentum

  May not be detected at BESIII.

- $\eta_c' \to 3\pi^0\eta_c$: G-violation, EM decays, high orbital angular momentum

  May not be detected at BESIII.

- $\eta_c' \to 2(\pi^+\pi^-)\eta_c$: strong decays

  Phase space small, may not be detected at BESIII.

- $\eta_c' \to \pi^+\pi^- 2\pi^0\eta_c$: strong decays

  Phase space small, may not be detected at BESIII.

- $\eta_c' \to 4\pi^0\eta_c$: strong decays

  Phase space small, too many photons, may not be detected at BESIII.

- $\eta_c' \to \eta\eta_c$: P-violation, not allowed

2. $\eta_c' \to J/\psi + X$

   The mass difference between η_c' and J/ψ is 541 MeV/c^2, slightly greater than $4m_{\pi^0}$ and smaller than $2(m_{\pi^+} + m_{\pi^-})$. Considering the uncertainty of η_c' mass is large and the width of η_c' is at 10 MeV/c^2 level, the high mass tail of η_c' can decay into $2(\pi^+\pi^-)$. All the possible combinations are listed below.

   - $\eta_c' \to n\pi^0 J/\psi$, $n = 1, 2, 3, 4$: C-violation, not allowed
   - $\eta_c' \to \pi^+\pi^- J/\psi$: G-violation, EM decays, via ρ^*
   - $\eta_c' \to \pi^+\pi^-\pi^0 J/\psi$: strong decays, via ω^*
   - $\eta_c' \to 2(\pi^+\pi^-)J/\psi$: G-violation, EM decays, phase space very small
   - $\eta_c' \to \pi^+\pi^- 2\pi^0 J/\psi$: G-violation, EM decays, phase space very small

   The detection of these above modes maybe a bit easier than the $\eta_c' \to \eta_c$ transition, since the J/ψ tag is much simpler and it is very narrow.

   Naive estimation the rates for $\eta_c' \to J/\psi$ transition should be smaller than the $\eta_c' \to \eta_c$ transitions, since the former requires the flip of the quark spin. No serious theoretical effort on these estimations.

3. $\eta_c' \to \chi_{cJ} + X$

   The mass difference between η_c' and χ_{c0} is 223 MeV/c^2, slightly greater than m_{π^0}; the mass difference between η_c' and χ_{c1} is 128 MeV/c^2, and that between η_c' and χ_{c2} is 82 MeV/c^2, smaller than m_{π^0}. The only allowed transition is $\eta_c' \to \pi^0\chi_{c0}$.

   - $\eta_c' \to \pi^0\chi_{c0}$: G-violation, EM decays

4. $\eta_c' \to h_c(^1P_1) + X$

   The mass difference between η_c' and $h_c(^1P_1)$ is 112 MeV/c^2, smaller than m_{π^0}. No allowed transition.

$h_c(^1P_1)$ decays

The mass difference between $h_c(^1P_1)$ and many of the charmonium states are also much larger than one π mass, thus there are many possible transitions.

All the allowed transitions are summarized in Fig. 19.6 and explained in detail below.

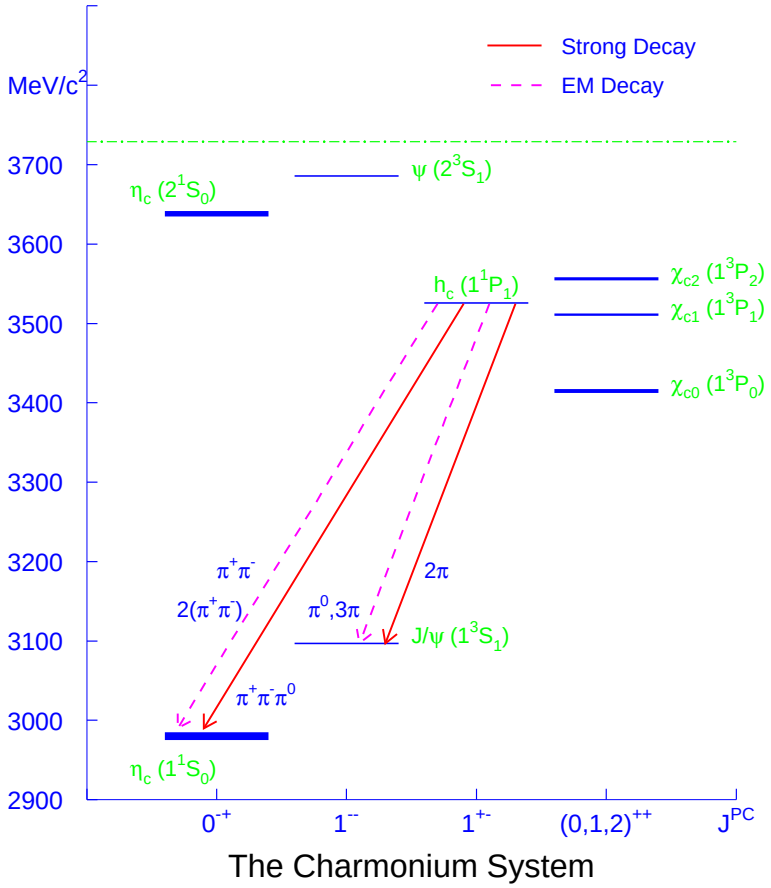

Figure 19.6: Hadronic transitions of $h_c(^1P_1)$ to other charmonium states.

1. $h_c(^1P_1) \to \eta_c + X$

The mass difference between $h_c(^1P_1)$ and η_c is 546 MeV/c^2, greater than $4m_\pi$ and about the same as m_η, all the possible combinations are listed below.

- $h_c(^1P_1) \to n\pi^0\eta_c$, $n = 1, 2, 3, 4$: C-violation, not allowed
- $h_c(^1P_1) \to \pi^+\pi^-\eta_c$: G-violation, EM decays, via ρ^*
- $h_c(^1P_1) \to \pi^+\pi^-\pi^0\eta_c$: strong decays, via ω^*
- $h_c(^1P_1) \to 2(\pi^+\pi^-)\eta_c$: G-violation, EM decays
- $h_c(^1P_1) \to \eta\eta_c$: C-violation, not allowed

$h_c(^1P_1) \to \pi^+\pi^-\eta_c$ and $h_c(^1P_1) \to \pi^+\pi^-\pi^0\eta_c$ should be looked for experimentally, $h_c(^1P_1) \to 2(\pi^+\pi^-)\eta_c$ rate may be too small to be detected at BESIII.

2. $h_c(^1P_1) \to J/\psi + X$

   The mass difference between $h_c(^1P_1)$ and J/ψ is 429 MeV/c^2, greater than $3m_{\pi^0}$. All the possible combinations are listed below.

   There is no experimental information available, neither the theoretical calculations.

   - $h_c(^1P_1) \to \pi^0 J/\psi$: G-violation, EM decays
   - $h_c(^1P_1) \to \pi^+\pi^- J/\psi$: strong decays, via σ
   - $h_c(^1P_1) \to \pi^0\pi^0 J/\psi$: strong decays, via σ
   - $h_c(^1P_1) \to \pi^+\pi^-\pi^0 J/\psi$: G-violation, EM decays
   - $h_c(^1P_1) \to 3\pi^0 J/\psi$: G-violation, EM decays

3. $h_c(^1P_1) \to \chi_{c0} + X$

   The mass difference between $h_c(^1P_1)$ and χ_{c0} is 111 MeV/c^2, smaller than m_{π^0}. No allowed transition.

χ_{c2} decays

The mass difference between χ_{c2} and many of the charmonium states are also much larger than one π mass, thus there are many possible transitions.

All the allowed transitions are summarized in Fig. 19.7 and explained in detail below.

1. $\chi_{c2} \to \eta_c + X$

   The mass difference between χ_{c2} and η_c is 576 MeV/c^2, greater than $4m_\pi$ and m_η, all the possible combinations are listed below.

   - $\chi_{c2} \to \pi^0\eta_c$: G-violation, EM decays
   - $\chi_{c2} \to \pi^+\pi^-\eta_c$: Strong decays, high orbital angular momentum
   - $\chi_{c2} \to \pi^0\pi^0\eta_c$: Strong decays, high orbital angular momentum
   - $\chi_{c2} \to \pi^+\pi^-\pi^0\eta_c$: G-violation, EM decays

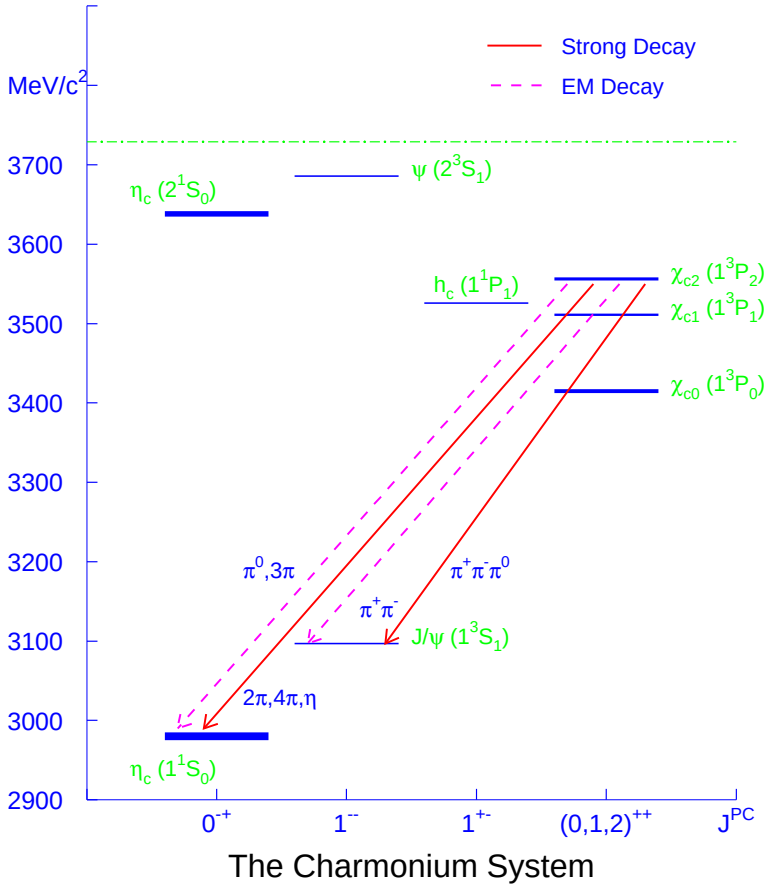

Figure 19.7: Hadronic transitions of χ_{c2} to other charmonium states.

- $\chi_{c2} \to 3\pi^0\eta_c$: G-violation, EM decays
- $\chi_{c2} \to 2(\pi^+\pi^-)\eta_c$: strong decays, phase space very small, orbital angular momentum very high
- $\chi_{c2} \to \pi^+\pi^-2\pi^0\eta_c$: strong decays, phase space very small, orbital angular momentum very high
- $\chi_{c2} \to 4\pi^0\eta_c$: strong decays, phase space very small, orbital angular momentum very high
- $\chi_{c2} \to \eta\eta_c$: strong decays, phase space small

2. $\chi_{c2} \to J/\psi + X$

   The mass difference between χ_{c2} and J/ψ is 459 MeV/c^2, slightly greater than $3m_\pi$. All the possible combinations are listed below.

   - $\chi_{c2} \to n\pi^0 J/\psi$, $n = 1, 2, 3$: C-violation, not allowed
   - $\chi_{c2} \to \pi^+\pi^- J/\psi$: G-violation, EM decays, via ρ^*
   - $\chi_{c2} \to \pi^+\pi^-\pi^0 J/\psi$: strong decays, via ω^*

3. $\chi_{c2} \to \chi_{c0} + X$, $\chi_{c1} + X$

   The mass difference between χ_{c2} and χ_{c0} is 141 MeV/c^2, slightly greater than m_{π^0}; the mass difference between χ_{c2} and χ_{c1} is 46 MeV/c^2, smaller than m_{π^0}. The only possible transition is $\chi_{c2} \to \pi^0\chi_{c0}$.

   - $\chi_{c2} \to \pi^0\chi_{c0}$: P-violation, not allowed

4. $\chi_{c2} \to h_c(^1P_1) + X$

   The mass difference between χ_{c2} and $h_c(^1P_1)$ is 30 MeV/c^2, smaller than m_{π^0}. No allowed transition.

χ_{c1} decays

The mass difference between χ_{c1} and many of the charmonium states are also much larger than one π mass, thus there are many possible transitions.

All the allowed transitions are summarized in Fig. 19.8 and explained in detail below.

1. $\chi_{c1} \to \eta_c + X$

   The mass difference between χ_{c1} and η_c is 531 MeV/c^2, greater than $3m_\pi$, all the possible combinations are listed below.

   - $\chi_{c1} \to \pi^0\eta_c$: P-violation, not allowed
   - $\chi_{c1} \to \pi^+\pi^-\eta_c$: strong decays, via σ

     A very rough measurement at BESII shows that it can not be observed using the BESII data sample.

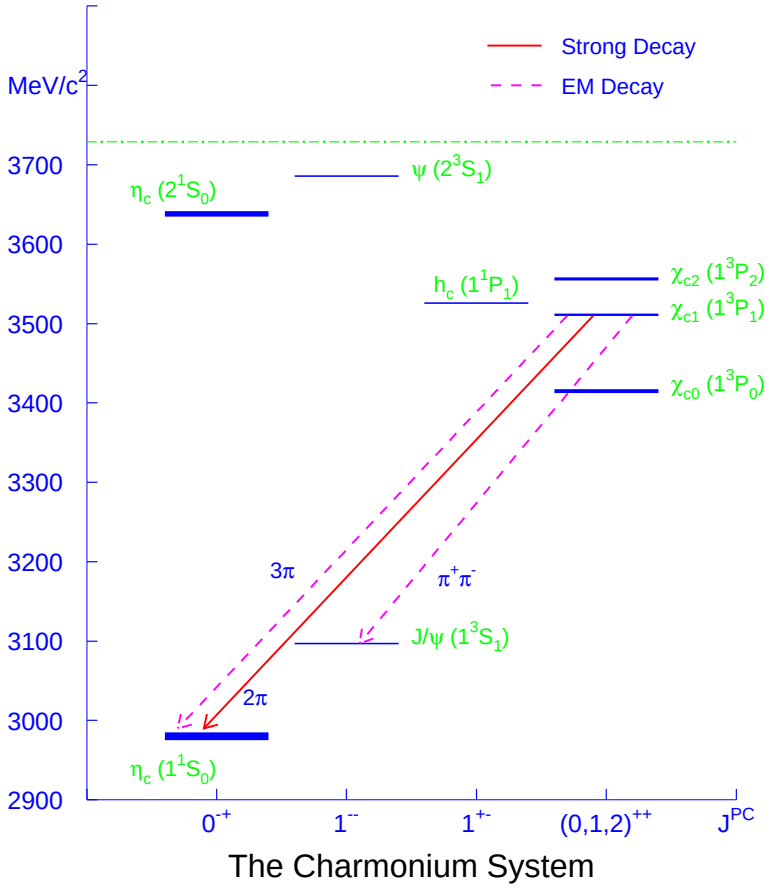

Figure 19.8: Hadronic transitions of χ_{c1} to other charmonium states.

- $\chi_{c1} \to \pi^0\pi^0\eta_c$: strong decays, via σ
- $\chi_{c1} \to \pi^+\pi^-\pi^0\eta_c$: G-violation, EM decays
- $\chi_{c1} \to 3\pi^0\eta_c$: G-violation, EM decays

2. $\chi_{c1} \to J/\psi + X$

   The mass difference between χ_{c1} and J/ψ is 413 MeV/c^2, slightly greater than $3m_{\pi^0}$ and smaller than $m_{\pi^+} + m_{\pi^-} + m_{\pi^0}$ by 2 MeV/c^2. All the possible combinations are listed below.

   - $\chi_{c1} \to n\pi^0 J/\psi$, $n = 1, 2, 3$: C-violation, not allowed
   - $\chi_{c1} \to \pi^+\pi^- J/\psi$: G-violation, EM decays, via ρ^*
   - $\chi_{c1} \to \pi^+\pi^-\pi^0 J/\psi$: no phase space

3. $\chi_{c1} \to \chi_{c0} + X$

   The mass difference between χ_{c1} and χ_{c0} is 95 MeV/c^2, smaller than m_{π^0}. No allowed transition.

χ_{c0} decays

The mass difference between χ_{c0} and many of the charmonium states are also much larger than one π mass, thus there are many possible transitions.

All the allowed transitions are summarized in Fig. 19.9 and explained in detail below.

1. $\chi_{c0} \to \eta_c + X$

   The mass difference between χ_{c0} and η_c is 435 MeV/c^2, greater than $3m_\pi$, all the possible combinations are listed below.

   - $\chi_{c0} \to \pi^0\eta_c$: G-violation, EM decays
   - $\chi_{c0} \to \pi^+\pi^-\eta_c$: P-violation, not allowed
   - $\chi_{c0} \to \pi^0\pi^0\eta_c$: P-violation, not allowed
   - $\chi_{c0} \to \pi^+\pi^-\pi^0\eta_c$: G-violation, EM decays
   - $\chi_{c0} \to 3\pi^0\eta_c$: G-violation, EM decays

2. $\chi_{c0} \to J/\psi + X$

   The mass difference between χ_{c0} and J/ψ is 318 MeV/c^2, slightly greater than $2m_\pi$. All the possible combinations are listed below.

   - $\chi_{c0} \to n\pi^0 J/\psi$, $n = 1, 2$: C-violation, not allowed
   - $\chi_{c0} \to \pi^+\pi^- J/\psi$: G-violation, EM decays, via ρ^*

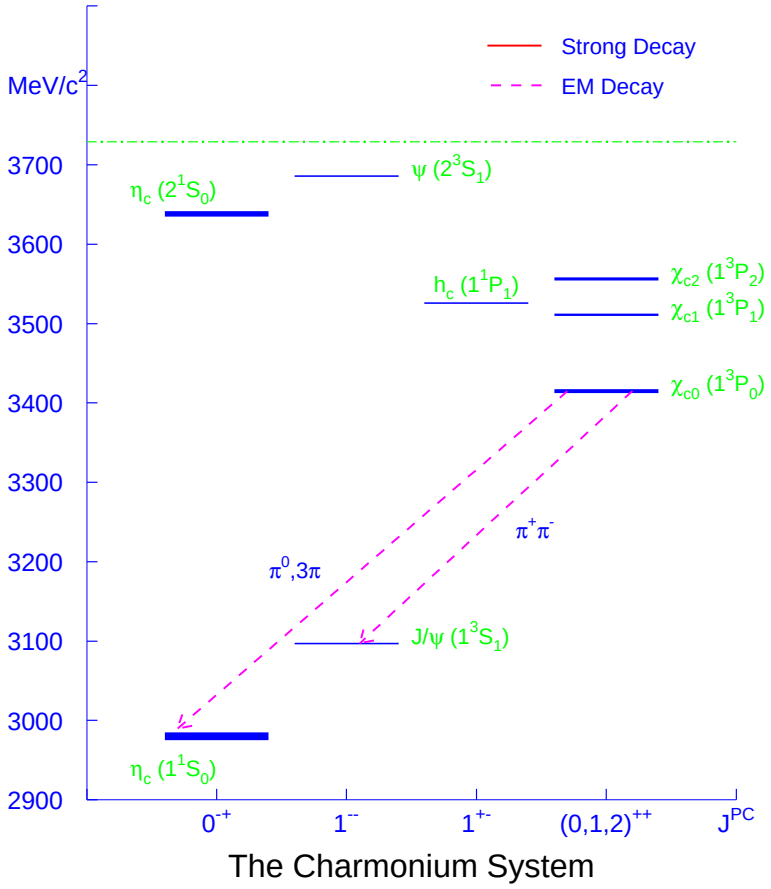

Figure 19.9: Hadronic transitions of χ_{c0} to other charmonium states.

19.3.4 Discussions and conclusions

In the above sections, we listed all the possible transitions between the known charmonium states below the charm threshold, more studies needed for a better understanding of the transitions.

It is worth to pointing out that, as the lattice QCD calculations give the lowest lying hybrid charmonium states with normal J^{PC} almost have the same mass as the charmonium states with same quantum numbers [306, 410], these states can be produced in ψ' hadronic transitions. For example, if the $J^{PC} = 1^{--}$ hybrid charmonium has mass around 3.1 GeV/c^2, the same transitions between ψ' and it are similar to that between ψ' and J/ψ. It is straightforward to list the production of the hybrids from the decays of other charmonia with the help of the channels listed in above sections.

The production rates of these hybrids should be estimated, and the experimental search for these states (new kind of hadrons) should be performed using the BESIII ψ' data sample. It is worth to have a try using the existing BESII ψ' data sample to have some feeling about the search, and simulation should be done at BESIII.

As the mass of these states are low, and the decays require the annihilation of the charm and anti-charm quark pair, the width of these states should be small, there should be no dominant decay mode(s). All these need further study.

Note added: It seems whether the $c\bar{c}g$'s calculated in the lattice QCD are the hybrid charmonium states in the quark model, or just the higher Fock states in the charmonium wave function needs to be clarified. If they are only the higher Fock states in the conventional charmonia, it will be easier to understand why their masses are the same as the charmonium states. In this case, these states will not be observed in experiment. However, the mass difference between the conventional charmonia and the hybrid charmonia for the first radial excitation states may suggest the hybrids exist experimentally. These states certainly worth to be searched for in experiment, but it can not reach at BESIII, as the maximum center of mass energy of it is only 4.2 GeV.

Chapter 20

Radiative decays

20.1 Introduction

At BESIII, there will be huge data samples of vector charmonium states, such as J/ψ, ψ', and ψ'', and possibly not small samples for $\psi(4040)$, $\psi(4160)$, $\psi(4415)$. The non-vector charmonium states, including pseudoscalars, η_c and η_c', and the P-wave states χ_{cJ}, can be produced via radiative transition of the vector states, considering the large transition rates (except $\psi' \to \gamma\eta_c'$), the data samples of these states are also large. This makes the study of the radiative decays of charmonium into light hadrons possible.

The radiative decays of the vector charmonia have been used extensively for the study of the light hadron spectroscopy, especially in J/ψ decays, this has been reviewed in the hadron spectroscopy part of this Yellow Report. The study of the other charmonium states is rather limited. In the following sections, we will review the study of the radiative decays of the states other than J/ψ, and prospect what one can achieve at BESIII.

20.2 Radiative decays of vector charmonia

The dominant radiative decays of vector charmonia is proceed via the diagram shown in Fig. 20.1. The rate of the photon radiated from the final states quarks is expected to be very small, and has been proved by the experimental observation, such as $J/\psi \to \gamma\pi^0$ [308, 309]. In the pQCD calculation, assuming emission of hard gluons, the inclusive decay rate of J/ψ is around 6%, while that for ψ' decays is around 1% [310]. There is no estimation of the other vector charmonia, such as ψ'', $\psi(4040)$, and so on, but it is expected the rates to be very small since all these states are above the open charm threshold, and thus the dominant decay mode is the OZI allowed decays.

This category of ψ' decays is expected to be about 1%, but the measurements are very limited. The only observation so far is $\psi' \to \gamma\eta'$ [311], $\gamma\pi\pi$ and $\gamma K\bar{K}$ [312], with total branching fraction about 0.05%. The final states with three pseudoscalars have been measured by BESII, without observing any significant structure in $\eta\pi^+\pi^-$ and $K\bar{K}\pi$ mass spectrum, the upper limit of the production of the pseudoscalar states $\eta(1405)$ or $\eta(1475)$ are set at 90% C.L [313].

Most recent study of the ψ' radiative decay is from BES [314], where the total and

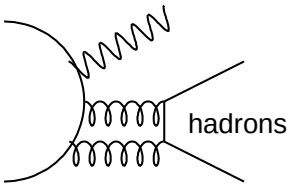

Figure 20.1: Radiative decays of vector charmonium state into light hadrons.

Table 20.1: Branching fractions of ψ' radiative decays, only modes observed are listed, for a complete list of al the measurements, refer to PDG [309].

Mode	Branching Fraction ($\times 10^{-5}$)	Experiment	Comment
$\gamma\eta'(958)$	$15.4 \pm 3.1 \pm 2.0$	BESI [311]	
	$12.4 \pm 2.7 \pm 1.5$	BESII [313]	
$\gamma\eta\pi^+\pi^-$	$36.0 \pm 14.2 \pm 18.3$	BESII [313]	
$\gamma f_2(1270)$	$21.2 \pm 1.9 \pm 3.2$	BESI [312]	
$\gamma f_0(1710) \to \gamma\pi\pi$	$3.01 \pm 0.41 \pm 1.24$	BESI [312]	
$\gamma f_0(1710) \to \gamma K\bar{K}$	$6.04 \pm 0.90 \pm 1.32$	BESI [312]	
$\gamma p\overline{p}$	$2.9 \pm 0.4 \pm 0.4$	BESII [314]	mass < 2.9 GeV/c^2
$\gamma 2(\pi^+\pi^-)$	$39.6 \pm 3.2 \pm 5.4$	BESII [314]	mass < 2.9 GeV/c^2
$\gamma K^0_S K^+\pi^- + c.c.$	$24.7 \pm 3.4 \pm 3.5$	BESII [314]	mass < 2.9 GeV/c^2
$\gamma\pi^+\pi^- K^+K^-$	$19.1 \pm 2.8 \pm 4.8$	BESII [314]	mass < 2.9 GeV/c^2
$\gamma\pi^+\pi^- p\overline{p}$	$2.8 \pm 1.2 \pm 0.4$	BESII [314]	mass < 2.9 GeV/c^2

differential branching fractions of $\psi' \to \gamma p\overline{p}$, $\gamma 2(\pi^+\pi^-)$, $\gamma K^0_S K^+\pi^- + c.c.$, $\gamma\pi^+\pi^- K^+K^-$, and $\gamma\pi^+\pi^- p\overline{p}$ are measured for the invariant mass of the charged particle system less than 2.9 GeV/c^2, the total branching fraction of all these modes is about 0.1%, which is about 10% of the total radiative decays of the ψ'. Unfortunately, due to the low statistics, the possible production of the intermediate states can not be studied. The observed modes are listed in Table 20.1, together with the branching fractions.

As the dominant decay dynamics of ψ' or J/ψ radiative decay is the $c\overline{c}$ emit a real photon and then annihilated into two gluons, it is expected that the glueball states, if exist, should be produced copiously. This has been a well spreading argument why J/ψ radiative decays should be studied carefully to search for this kind of mesons. This same argument also hold for ψ' radiative decays, in spite of the obvious disadvantage of low production rate. However, this disadvantage is not true any more at BESIII, due to the large (or huge) data sample, together with the obvious advantage that the allowed mass range for investigation is larger than in J/ψ decays.

As has been calculated in LQCD [315], except the $J^{PC} = 0^{++}$ glueball, which is at about 1.7 GeV/c^2, and $J^{PC} = 2^{++}$ glueball, which is at about 2.3 GeV/c^2, the states with other J^{PC} have rather large mass, above 2.5 GeV/c^2 for $J^{PC} = 0^{-+}$ and around 3 GeV/c^2 for $J^{PC} = 2^{-+}$, considering the widths of these states, the study of them in J/ψ decays

is a little bit cumbersome. However, it is more suitable to be searched for in ψ' decays.

As has been observed in ψ' hadronic decays, although ψ' radiative decay should have similar property as J/ψ does expected from very naive model, the ψ' and J/ψ radiative decays may turned out to be very different. For example, in the decays into $\gamma\pi\pi$, the relative strength of the resonances in $\pi\pi$ mass could be very different, thus the two decays supply different information, and may be very helpful for understanding of the meson spectroscopy. Another advantage of using the ψ' data is that the background is very different, for example, in $\gamma\pi^+\pi^-$ channels, there is almost no background from $\rho\pi$ in ψ' decays, while this is the dominant background in J/ψ decays since $J/\psi \to \rho\pi$ is the largest two-body hadronic mode in J/ψ decays.

While the $J^{PC} = 0^{++}$ and 2^{++} states can be very well studied in their decays into a pair of pseudoscalars, such as $\pi\pi$, $K\bar{K}$, $\eta\eta$, $\eta'\eta'$, or $\eta\eta'$, the $J^{PC} = 0^{-+}$ and 2^{-+} states can be studied in their decays into three pseudoscalars, such as $\eta\pi\pi$, $K\bar{K}\pi$, $\eta K\bar{K}$, $\eta'\pi\pi$ and so on. The final states like $\gamma p\overline{p}$ and $\gamma\Lambda\bar{\Lambda}$ can be used to search for the glueball with any quantum numbers, if the mass is above the baryon-antibaryon mass threshold.

The dominant decay modes of the glueballs are expected to be those multi-hadron final states, however, the spin-parity analysis of multi-hadron final states is expected to be very complicated, due to the contributions of many mesons with different spin-parity, and many different kinds of intermediate states. The technique used to study the spin-parity of the states, the partial wave analysis (PWA), in case of many parameters in the fit, may give meaningless results.

20.3 Radiative decays of pseudoscalar charmonia

So far there is no measurement on the radiative decays of η_c, let alone its excited states, $\eta_c(2S)$.

The decay rates of η_c to a γ and a vector meson (like ρ, ω and ϕ) is of great interest to probe the wave function of the η_c, which is suspected that the mixing from η and η' may exist to explain for example the decay rates of $J/\psi \to \gamma\eta$ and $\gamma\eta'$ [308]. The decays of a pure $c\overline{c}$ states into γV may be very weak, however, if the mixing from the η and η' exists, the decay rate may be enhanced to a much higher level. So far there is no theoretical estimation of the rates yet, either with or without the mixing from light quarks.

If the photon is emitted from the $c\overline{c}$ quark in η_c, the decay will be quite similar to $\eta_c \to \gamma\gamma$, with one real photon replaced by a virtual one and further coupled to a vector meson. Since $\mathcal{B}(\eta_c \to \gamma\gamma) = (2.8 \pm 0.9) \times 10^{-4}$ [309], the decay rates of $\eta_c \to \gamma V$ should not be very different from that if estimated from Vector Meson Dominance model.

20.4 Radiative decays of P-wave charmonia

There is no experimental information on the radiative decays of the P-wave charmonia, including χ_{c0}, χ_{c1}, and χ_{c2}.

A recent theoretical calculation of $\chi_{cJ} \to \gamma V$, $V = \rho$, ω, or ϕ, was given in Ref. [363] based on nonrelativistic quantum chromodynamics, the results are shown in Table 20.2.

Table 20.2: calculated branching fractions of $\chi_{cJ} \to \gamma V$ from Ref. [363], in unit of $\times 10^{-6}$.

Mode	χ_{c0}	χ_{c1}	χ_{c2}
$\gamma\rho$	1.2	14	4.4
$\gamma\omega$	0.13	1.6	0.50
$\gamma\phi$	0.46	3.6	1.1

The branching fractions are at a level which can be searched for, or be observed, using the ψ' data sample at BESIII.

20.5 Discussions and conclusions

From the above analysis, we conclude the radiative decays of the vector charmonium states, especially of J/ψ and ψ', should be studied in great care for the understanding of the light hadron spectroscopy, as well as for a better understanding of the charmonium decay dynamics. While the decays of J/ψ are much rich, the study of the ψ' is rather limited, more effort should be made to find possible new phenomena in ψ' decays.

The search for the decays into γ+Vector allows a probe for the wave functions of η_c and χ_{cJ} states, to test whether there is mixture from the light quark mesons.

Chapter 21

Hadronic decays

21.1 $\rho - \pi$ puzzle

21.1.1 Introduction

Crisply defined experimental puzzles in high-energy physics always have the prospect of leading to new discoveries. One prominent example is the θ-τ puzzle of 1956 which led to the parity revolution. Therefore puzzles in physics often draw considerable attention to theorists. The ratios of hadronic decays of the $\psi(3686)$ (shortened as ψ') to the same decays of the J/ψ is such a puzzle which has been studied substantially since 1983.

Since the OZI suppressed decays of J/ψ and ψ' to hadrons are via three gluons or a photon, in either case, the perturbative QCD (pQCD) provides a relation [479]

$$Q_h \;=\; \frac{\mathcal{B}_{\psi'\to h}}{\mathcal{B}_{J/\psi\to h}} = \frac{\mathcal{B}_{\psi'\to e^+e^-}}{\mathcal{B}_{J/\psi\to e^+e^-}} \approx 12.7\% \; . \tag{21.1}$$

This relation is referred to as the "12% rule" which is expected to be held to a reasonable good degree for both inclusive and exclusive decays. The so-called "$\rho\pi$ puzzle" is that the prediction by Eq. (21.1) is severely violated in the $\rho\pi$ and several other decay channels. The first evidence for this effect was found by Mark-II Collaboration in 1983 [318]. From then on many theoretical explanations have been put forth to decipher this puzzle.

With the recent experiment results from BESII and CLEOc about J/ψ and ψ' two-body decays, such as vector-pseudoscalar (VP), vector-tensor (VT), pseudoscalar-pseudoscalar (PP), and baryon-antibaryon ($B\overline{B}$) modes, and about multi-body decays at the J/ψ, the ψ' or event at the $\psi(3770)$ (shortened as ψ'') [319]$^-$[339], a variety of solutions proposed for the puzzle can be tested at the level of higher accuracy. In this treatise, we survey the theoretical works on the $\rho\pi$ puzzle and compare them with the available experimental data. From the theoretical point of view, since the Q-value is smaller than 12% for $\rho\pi$, it may be caused either by enhanced or suppressed J/ψ decay rate. Another possibility is by both. So we classify the relevant theoretical speculations into three categories:

1. J/ψ-enhancement hypothesis, which attributes the small Q-value to the enhanced branching fraction of J/ψ decays.

2. ψ'-suppress hypothesis, which attributes the small Q-value to the suppressed branching fraction of ψ' decays.

3. Other hypotheses, which are not included in the above two categories.

In the following content, first reviewed are the theoretical works on $\rho\pi$ puzzle, and the predictions from them are compared with the newly available experimental results; then expounded are three methods to estimate the ratio between ψ' and J/ψ decays into the same final states; after that some comments are made on the implications from the review on $\rho\pi$ puzzle; at last there is a short summary.

21.1.2 Review of theoretical works on $\rho\pi$ puzzle

J/ψ-enhancement Theory

In the earlier days of the $\rho\pi$ puzzle, it was noticed that the decay of 1^{--} charmonium into $\rho\pi$ final state violates the Hadronic Helicity Conservation (HHC) theorem (see below for expound) [340], and so such decay should be suppressed. Therefore people think there must be some mechanism which leads to the great enhancement for $J/\psi \to \rho\pi$ decays. The two schemes presented in this section were proposed following this line of reasoning.

1. J/ψ-glueball Admixture Scheme

   The idea of J/ψ decays via a glueball was proposed by Freund and Nambu [341] (FN hereafter) soon after the discovery of J/ψ particles to explain the breaking of Okubo-Zweig-Iizuka (OZI) rule [342]. In such mechanism, the breaking results from the mixing of the ω, ϕ, and J/ψ mesons with an $SU(4)$-singlet vector meson $\mathcal{O}$. They found that such an $\mathcal{O}$ meson should lie in the 1.4-1.8 GeV/c^2 mass range with the width greater than 40 MeV/c^2, and it should decay copiously into $\rho\pi$, $K^*\overline{K}$ while exhibiting severe suppression of decays into $K\overline{K}$, e^+e^- and $\mu^+\mu^-$ modes. These authors presented several quantitative predications for experimental search. Two of them are

$$R_1 = \frac{\Gamma_{J/\psi\to\rho\pi}}{\Gamma_{\phi\to\rho\pi}} = 0.0115 - 0.087 \ ,$$

$$R_2 = \frac{\Gamma_{J/\psi\to K\overline{K}}}{\Gamma_{J/\psi\to\rho\pi}} < 8\times 10^{-5} \ .$$

   With the current available data and using the three pions final state as a substitute for $\rho\pi$ in both ϕ [343] and J/ψ [319, 320] decays, we obtain the first ratio $R_1 \approx 0.003$, which is almost one order of magnitude smaller than the predication. For the second ratio, by virtue of PDG [343] value for K^+K^- and new experiment result for $K^0_SK^0_L$ [322], it is estimated that $\mathcal{B}(J/\psi \to K\overline{K}) \sim 10^{-4}$, together with the results for $\rho\pi$ [319, 320], we have $R_2 \sim 10^{-2}$ which is much larger than the predication.

   The first attempt to explain the $\rho\pi$ puzzle in terms of a glueball near J/ψ was proposed by Hou and Soni [344] (HS hereafter). They attributed the enhancement of $J/\psi \to K^*\overline{K}$ and $J/\psi \to \rho\pi$ decay modes to the mixing of the ψ with a $J^{PC} = 1^{--}$ vector gluonium, also designated by $\mathcal{O}$. The differences between FN's and HS's pictures lie in the following aspects:

- Based on the potential model applied to glueball, the mass of a low-lying three-glue state is estimated to be around 2.4 GeV/c^2 [345], rather than 1.4 to 1.8 GeV/c^2 in Ref. [341].
- The mixing of $\mathcal{O}$ with ψ' is taken into account, which has been ignored in previous work.
- Since the gauge coupling constant in QCD is momentum dependent, the mixing parameter is taken to be a function of the invariant mass q^2, which decreases rather sharply with the increase in q^2. Such propagator effect gives rise to a more suppression on the decay rates of ψ' relative to J/ψ for decays to $\rho\pi$ and $K^*\overline{K}$ channels.

By virtue of their assumption, HS suggested a search for the vector gluonium state in certain hadronic decays of the ψ', such as $\psi' \to \pi\pi + X$, $\eta + X$, $\eta' + X$, where X decays into VP final states [344].

Based on HS's idea, Brodsky, Lepage, and Tuan [346] (BLT) refined the glueball hypothesis for the $\rho\pi$ puzzle. They assumed the general validity of the pQCD theorem that the total hadron helicity is conserved in high-momentum-transfer exclusive processes, in which case the decays to $\rho\pi$ and $K^*\overline{K}$ are forbidden for both the J/ψ and ψ'. This pQCD theorem is often referred to as the rule of Hadronic Helicity Conservation (HHC) [340], which is based on the assumption of the short-range "pointlike" interactions among the constituent quarks throughout. For instance, $J/\psi(c\bar{c}) \to 3g$ has a short range $\simeq 1/m_c$ associated with the short time scale of interaction. Nevertheless, if subsequently the three gluons were to resonate forming an intermediate gluonium state $\mathcal{O}$ which has a large transverse size covering an extended time period, then HHC would become invalid. In essence the HS model takes over in this latter stage.

Final states h which proceed only through the intermediate gluonium state satisfy the ratio

$$Q_h = \frac{\mathcal{B}(\psi' \to e^+e^-)}{\mathcal{B}(J/\psi \to e^+e^-)} \frac{(M_{J/\psi} - M_{\mathcal{O}})^2 + \Gamma_{\mathcal{O}}^2/4}{(M_{\psi'} - M_{\mathcal{O}})^2 + \Gamma_{\mathcal{O}}^2/4} \ . \tag{21.2}$$

The Q_h is small if the mass of $\mathcal{O}$ is close to the mass of J/ψ. The experimental limits at that time [347, 318, 346] imply that the $\mathcal{O}$ mass is within 80 MeV/c^2 of the mass of J/ψ and its total width is less than 160 MeV/c^2. Brodsky *et al.* recommended a direct way to search for $\mathcal{O}$, that is to scan the $e^+e^- \to VP$ cross section across the J/ψ resonance.

Another related work by Chan and Hou [348] studied the mixing angle $\theta_{\mathcal{O}\psi}$ and the mixing amplitude $f_{\mathcal{O}\psi}$ of the J/ψ and vector glueball $\mathcal{O}$ based on the framework of potential models of heavy quarks and constituent gluons. They obtain $|\tan\theta_{\mathcal{O}\psi}| = 0.015$ and $f_{\mathcal{O}\psi}(m^2_{\mathcal{O}\psi}) = 0.008$ GeV^2.

On the Experimental part, BES has searched for this hypothetical particle in a $\rho\pi$ scan across the J/ψ mass region in e^+e^- annihilations as well as in the decays of $\psi' \to \pi\pi\mathcal{O}$, $\mathcal{O} \to \rho\pi$, and found no evidence for its existence [324, 349]. The data constrains the mass and width of the $\mathcal{O}$ to the range $|\ M_{\mathcal{O}} - M_{J/\psi}\ | < 80$ MeV/c^2

and $4 < \Gamma_{\mathcal{O}} < 50$ MeV/c^2 [350]. Although the absence of distortion in BES energy scan of $J/\psi \to \rho\pi$ does not rule out $M_{\mathcal{O}} \simeq M_{J/\psi}$, it puts a lower bound to $\Gamma_{\mathcal{O}}$. However, as indicated in Ref. [352], the experimentally constrained mass is several hundred MeV/c^2 lower than the mass of the lightest vector glueball calculated in lattice simulations of QCD without dynamical quarks [353].

Recently, the experimental data from BES and CLEOc turned out to be unfavorable to this glueball hypothesis. Among them is the observed large branching fractions of the isospin-violating VP mode $\psi' \to \omega\pi^0$ [325, 326, 332]. This contradicts with the assertion that the pattern of suppression depends on the spin-parity of the final state mesons. In addition, according to BLT's analysis, one obtains the relation [354]

$$\frac{\mathcal{B}(J/\psi \to \omega\pi^0)}{\mathcal{B}(J/\psi \to \rho^0\pi^0)} < 0.0037$$

which is much smaller than the PDG06 value 0.08 [343]. Another experimental result which is unfavorable to such hypothesis is the suppression of ψ' decays into vector-tensor (VT) final states [334, 335]. Since hadronic VT decays, unlike the VP decays, conserve HHC, some other mechanisms must be responsible for this suppression in the model. Furthermore, it has been argued that the $\mathcal{O}$ may also explain the decay of J/ψ into ϕf_0 (named previously S^*) but not to $\rho a_0(980)$ (named previously δ), since the $\mathcal{O}$ mixes with the ϕ and enhances a mode that would be otherwise suppressed [346]. However, the decay $\psi' \to \phi f_0$ [350] is not suppressed as found by experiments, which implies the absence of anomalous enhancement in $J/\psi \to \phi f_0$, thus contradicts with this explanation. Anselmino *et al.* extended the idea of J/ψ-$\mathcal{O}$ mixing to the case of $\eta_c \to VV$ and $p\overline{p}$ [355]. They suggested that the enhancement of these decays can be attributed to the presence of a trigluonium pseudoscalar state with a mass close to the η_c mass. So far there is no experimental evidence for such a state.

In fact, as pointed out in Ref. [356], this glueball explanation has some unanswered questions: (i) Why only the $\rho\pi$ and $K^*\overline{K}$ channels are affected but not $\mathcal{O} \to 5\pi$ etc. viz., one must assume in an *ad hoc* way that the $\mathcal{O}$ couples predominantly to $\rho\pi$ and $K^*\overline{K}$; and (ii) if such a narrow heavy 1^{--} gluonium state exists, why have the narrow 0^{++}, 2^{++} states not been found, which should be lighter and easier to search?

2. Intrinsic-charm-component Scheme

Brodsky and Karliner (BK) put forth an explanation for the puzzle based on the existence of the intrinsic charm $|q\overline{q}c\overline{c}\rangle$ Fock components of the light vector mesons [357]. They noticed the fact that quantum fluctuations in a QCD bound state wave function will inevitably produce Fock states containing heavy quark pairs. The intrinsic heavy quark pairs are multiconnected to the valence quarks of the light hadrons, and the wave functions describing these configurations will have maximal amplitude at minimal off-shellness and minimal invariant mass. In the case of the ρ meson, with the consideration of the light-cone Fock representation:

$$\rho^+ = \psi^{\rho}_{u\overline{d}}|u\overline{d}\rangle + \psi^{\rho}_{u\overline{d}c\overline{c}}|u\overline{d}c\overline{c}\rangle + \cdots \ .$$

Here we expect the wave function of the $c\bar{c}$ quarks to be in an S-wave configuration with no nodes in its radial dependence, in order to minimize the kinetic energy of the charm quarks and thus also minimize the total invariant mass.

The presence of the $|u\bar{d}c\bar{c}\rangle$ Fock state in the ρ allows the $J/\psi \to \rho\pi$ decay to proceed through rearrangement of the incoming and outgoing quark lines; in fact, the $|u\bar{d}c\bar{c}\rangle$ Fock state wave function has a good overlap with the radial and spin $|c\bar{c}\rangle$ and $|u\bar{d}\rangle$ wave functions of the J/ψ and pion. On the other hand, the overlap with the ψ' will be suppressed, since the radial wave function of the $n = 2$ quarkonium state is orthogonal to the nodeless $c\bar{c}$ in the $|u\bar{d}c\bar{c}\rangle$ state of the $\rho\pi$. Similarly, the $|u\bar{s}c\bar{c}\rangle$ Fock component of the K^* favors the $J/\psi K$ configuration, allowing the $J/\psi \to K^*\overline{K}$ decay to also proceed by quark line rearrangement, rather than $c\bar{c}$ annihilation.

These authors also suggested comparing branching fractions for the η_c and η_c' decays as clues to the importance of η_c intrinsic charm excitations in the wave functions of light hadrons.

ψ'-suppress Theory

The hypothesis of the existence of a glueball to explain the $\rho\pi$ has been questioned soon after it was proposed. In addition, it is also pointed out [358] that the helicity suppression is not a strong constraint in the charmonium energy scale. Under such case, one comes naturally to the idea that it is not $J/\psi \to \rho\pi$ which is enhanced, but rather $\psi' \to \rho\pi$ which is suppressed. Seven explanations or models collected in this section are put forth along this line.

1. Sequential-fragmentation Model

   Karl and Roberts have suggested explaining the $\rho\pi$ puzzle based on the mechanism of sequential quark pair creation [359]. The idea is that the quark-antiquark pairs are produced sequentially, as a result the amplitude to produce two mesons in their ground state is an oscillatory function of the total energy of the system. They argue that the oscillatory fragmentation probability could have a minimum near the mass of ψ', which provides an explanation for the suppressed ψ' decay. Even though their evaluations could generally accommodate the data for decays of J/ψ and ψ' to $\rho\pi$ and $K^*\overline{K}$, it runs into difficulties when it is extrapolated to Υ decays. According to their calculation, the oscillations of probability amplitude are damped out in the region of the Υ resonances, so the $\rho\pi$ channel is present in the decay of all Υ, Υ', Υ'', $\cdots$ resonances with a common rate. This leads to a prediction $\Gamma(\Upsilon \to \rho\pi) = 0.05$ keV, or equivalently $\mathcal{B}(\Upsilon \to \rho\pi) = 9.4 \times 10^{-4}$, which is above the current upper limit $\mathcal{B}(\Upsilon \to \rho\pi) < 2 \times 10^{-4}$ [343]. Moreover, their calculation seems hard to explain the large branching fraction for ϕ decays to $\rho\pi$ [343] due to the fact that their fragmentation probability tends to zero as the mass of the $\rho\pi$ decaying system approaches 1 GeV/c^2.

   In a further analysis [360], Karl and Tuan pointed out that if a suppression is observed in three-meson channels the explanation based on sequential pair creation would be undermined. Recently such a suppressed channel, viz. ϕKK, is found by CLEOc [337].

2. Exponential-form-factor Model

   Guided by suppressed ratios of ψ' to J/ψ decays to two-body hadronic modes, Chaichian and Törnqvist suggested [356] that the hadronic form factors fall exponentially as described by the overlap of wave functions within a nonrelativistic quark model. This behavior explains the drastically suppressed two-body decay rates of the ψ' compared with those of the J/ψ. Recently, the report on observation of a number of VP channels in ψ' decays [325, 326, 332] such as $\omega\eta'$, $\phi\eta'$, $\rho\eta'$ has proved that the predicted decay fractions are overestimated. Moreover, the branching fraction for $\omega\pi^0$ [343], is well below the prediction by this model which is 1.04×10^{-4}.

   Another problem of the model is that it does not single out just the VP channel, the other channels, for example VT channel, are also estimated to have small branching fractions which are not compatible with the BES measured results [335].

3. Generalized Hindered M1 Transition Model

   A so-called generalized hindered M1 transition model is proposed by Pinsky as a solution for the puzzle [361]. It is argued that because $J/\psi \to \gamma\eta$ is an allowed M1 transition while $\psi' \to \gamma\eta'$ is hindered (in the nonrelativistic limit), using the vector-dominance model to relate $\psi' \to \gamma\eta'$ to $\psi' \to \psi\eta'$ one could find the coupling $G_{\psi'\psi\eta_c}$ is much smaller than $G_{\psi\psi\eta_c}$, and then by analogy, the coupling $G_{\omega'\rho\pi}$ would be much smaller than $G_{\omega\rho\pi}$. Here $G_{\omega\rho\pi}$ can be extracted from data by virtue of the analysis using the vector-dominance model and a standard parameterization of OZI process [362]. Then assuming $\psi' \to \rho\pi$ to proceed via ψ'-ω' mixing, while $\psi \to \rho\pi$ via ψ-ω mixing, one would find that $\psi' \to \rho\pi$ is much more severely suppressed than $\psi \to \rho\pi$. The similar estimation could be preformed for $K^*\overline{K}$ and other VP final state, and one can expect a suppressed Q:

$$\frac{\mathcal{B}(\psi' \to VP)}{\mathcal{B}(\psi \to VP)} = 1.47 \frac{\Gamma_{tot}(\psi)}{\Gamma_{tot}(\psi')} \left(\frac{G_{V'VP}}{G_{VVP}}\right)^2 \frac{F_{V'}}{F_V} = 0.06\% \ , \tag{21.3}$$

   where $F_{V'}/F_V = 0.3$, $G_{\omega'\rho\pi}/G_{\omega\rho\pi} = 0.066$ according to Ref. [361]. This Q is much smaller than the present experimental results [325, 326, 332].

   Moreover, in this model, the coupling $G_{\omega'\omega f_2}$ for $\omega' \to \omega f_2$ should not be suppressed because by analogy the coupling $G_{\psi'\psi\chi_{c2}}$ is not small due to the fact that the E1 transition $\psi' \to \gamma\chi_{c2}$ is not hindered [363]. Therefore via ψ'-ω' mixing the $\psi' \to \omega' \to \omega f_2$ decay is expected to be not suppressed, which contradicts the BES result [335].

4. Higher-Fock-state Scheme

   Chen and Braaten (CB) proposed an explanation [352] for the $\rho\pi$ puzzle, arguing that the decay $J/\psi \to \rho\pi$ is dominated by a Fock state in which the $c\overline{c}$ pair is in a color-octet $^3S_1$ state which decays via $c\overline{c} \to q\overline{q}$, while the suppression of this decay mode for the ψ' is attributed to a dynamical effect due to the small energy gap between the mass of the ψ' and the $D\overline{D}$ threshold. Using the BES data on the branching fractions into $\rho\pi$ and $K^*\overline{K}$ as input, they predicted the branching

fractions for many other VP decay modes of the ψ', as listed in Table 21.1, from which we see most measured values falling in the scopes of predictions, but we also note for $\omega\pi$ mode, the deviation from the prediction is obvious. Here it should be noticed that the values adduced in Table 21.1 are calculated on the strength of the measured branching fractions from earlier experiment, the new measurements on the branching fractions for $\rho\pi$ and $K^{*0}\overline{K}^0 + c.c.$ from BES [498, 330] and CLEOc [332] may have impact on the corresponding evaluations.

Table 21.1: Predictions and measurements for Q_{VP} in unit of 1% for all VP final states. The value for $\rho\pi$ and $K^{*0}\overline{K}^0 + c.c.$ from Ref. [364] were used as input. The theoretical parameter $x = 0.64$ is due to results of Ref. [365] and the experimental results come from Refs. [325, 326, 498, 366].

VP	$x = 0.64$	Exp.
$\rho\pi$	$0 - 0.25$	0.13 ± 0.03
$K^{*0}\overline{K^0} + c.c.$	$1.2 - 3.0$	3.2 ± 0.08
$K^{*+}K^- + c.c.$	$0 - 0.36$	$0.59^{+0.27}_{-0.36}$
$\omega\eta$	$0 - 1.6$	< 2.0
$\omega\eta'$	$12 - 55$	19^{+15}_{-13}
$\phi\eta$	$0.4 - 3.0$	5.1 ± 1.9
$\phi\eta'$	$0.5 - 2.2$	9.4 ± 4.8
$\rho\eta$	$14 - 22$	$9.2^{+3.6}_{-3.3}$
$\rho\eta'$	$12 - 20$	$17.8^{+15.9}_{-11.1}$
$\omega\pi$	$11 - 17$	$4.4^{+1.9}_{-1.6}$

Besides the predictions in Table 21.1, CB's proposal also has implications for the angular distributions for two-body decay modes. In general, the angular distribution has the form $1 + \alpha\cos^2\theta$, with $-1 < \alpha < +1$. CB's conclusion implies that the parameter α for any two-body decay of the ψ' should be less than or equal to that for the corresponding J/ψ decays. But this needs further supports from analyses based on large data sample in the future.

5. Survival-chamonia-amplitude Explanation

A model put forward by Gérard and Weyers entertains the assumption that the three-gluon annihilation amplitude and the QED amplitude add incoherently in all channels in J/ψ decays into light hadrons, while in the case of ψ' decays the dominant QCD annihilation amplitude is not into three gluons, but into a specific configuration of five gluons [367]. More precisely, they suggest that the strong annihilation of the ψ' into light hadrons is a two step process: in the first step the ψ' goes into two gluons in a 0^{++} or 0^{-+} state and an off-shell $h_c(3526)$; in the second step the off-shell h_c annihilate into three gluons to produce light hadrons. Their argument implies: (a) to leading order there is no strong decay amplitude for the processes $\psi' \to \rho\pi$ and $\psi' \to K^*\overline{K}$; (b) the 12 % rule should hold for hadronic processes which take place via the QED amplitude only. As far as the second

implication is concerned, the present data give different ratios between ψ' and J/ψ decay for $\omega\pi^0$ and $\pi^+\pi^-$ final states, both of which are electromagnetic processes. Here the event form factor effect is taken into account [368], the difference between two kinds of processes is still obvious. Besides the explanation for $\rho\pi$ puzzle, this model predicts a sizable $\psi' \to (\pi^+\pi^- \text{ or } \eta)\ h_1(1170)$ branching fraction.

In a recent paper [369], Artoisenet, Gérard and Weyers (AGW) update and sharpen the above idea which lead to a somewhat unconventional point of view: all non-electromagnetic hadronic decays of the ψ' goes via a transition amplitude which contain a $c\bar{c}$ pair. AGW provide two patterns for these two-step decays, the first is

$$\psi' \to (2\mathrm{NP}g) + (3g)\ . \tag{21.4}$$

The physics picture is as follows: the excited $c\bar{c}$ pair in the ψ' does not annihilate directly. Instead, it spits out two non-perturbative gluons ($2\mathrm{NP}g$) and survives in a lower $c\bar{c}$ configuration (1^{--} or 1^{-+}) which then eventually annihilate into $3g$. The decays $\psi' \to (2\pi)J/\psi$ and $\psi' \to \eta J/\psi$ follow this pattern. The second pattern is

$$\psi' \to (3\mathrm{NP}g) + (2g)\ , \tag{21.5}$$

where the lower $c\bar{c}$ configuration (0^{-+} or 0^{++}) annihilates into $2g$. The only on-shell channel for this type of decays is $\psi' \to (3\pi)\eta_c$, whose branching fraction is estimated as $(2-2)\%$ level. Anyway, the recent measurement from CLEOc [336] provides the upper limit which is one order of magnitude below this theoretical prediction. Furthermore, the substitution of one photon for one gluon in Eqs. (21.4) and (21.5) allows

$$\psi' \to (2\mathrm{NP}g) + (2g) + \gamma\ . \tag{21.6}$$

This pattern corresponds to on-shell radiative decays such as $\psi' \to (\pi^+\pi^-)\eta_c\gamma$ and $\psi' \to \eta\eta_c\gamma$, which could be larger than the observed $\psi' \to \eta_c\gamma$ mode.

Besides the above predications, AGW also estimate

$$\mathcal{B}(\psi' \to b_1\eta) = (1.3 \pm 0.3) \times 10^{-3}\ , \tag{21.7}$$

$$\mathcal{B}(\psi' \to h_1\pi^0) = (1.9 \pm 0.4) \times 10^{-3}\ , \tag{21.8}$$

$$\mathcal{B}(J/\psi \to b_1\eta) \approx \mathcal{B}(\psi' \to b_1\eta) \approx 1\%\ . \tag{21.9}$$

All these are to be tested by experiments.

6. Nonvalence Component Explanation

Since the ψ' is a highly excited state and close to the $D\overline{D}$ threshold, it is suggested [208] that unlike the J/ψ, the ψ' may be an admixture of large nonvalence components in its wave function. The so-called nonvalence component indicates the additional gluon or the light quark-antiquark pair (or as in Ref. [208], the $c\bar{c}g$ component and a quasi-molecular $D\overline{D}$ state), which makes ψ' decays prominently distinctive from those of J/ψ. The nonvalence component of the J/ψ is expected to be less significant because it is the lowest state. In a following paper [358], Chernyak

uses this picture to explain the $\rho\pi$ puzzle. He suggested that the valence and non-valence strong contributions interfere destructively in $\rho\pi$ channel and consequently cancel to a large extent in the total $\psi' \to \rho\pi$ strong amplitude, while the role of nonvalence contributions is much less significant in $J/\psi \to \rho\pi$. From this viewpoint, there is no deep reason for the experimentally observed very strong suppression of $\psi' \to \rho\pi$, this is the result of a casual cancellation.

Chernyak also tries to use the above idea to explain qualitatively other decay modes, such as VT, AP, PP, VV and $B\overline{B}$ decay. However, such an idea remains a pure speculation, and no concrete calculations have been performed up to now.

7. S-D Wave Mixing Scheme

The ψ'' is viewed as a D-wave charmomium state. Although it is primarily $c\overline{c}(1^3D_1)$, its leptonic width indicates a contribution from mixing with S-wave states, mainly the nearby $\psi(2^3S_1)$. This leads Rosner to propose that the small $\rho\pi$ branching fraction in ψ' decay is due to the cancellation of the $2S$ and $1D$ matrix elements. By virtue of his scheme

$$\begin{aligned} \langle\rho\pi|\psi'\rangle &= \langle\rho\pi|2^3S_1\rangle\cos\theta - \langle\rho\pi|1^3D_1\rangle\sin\theta \ , \\ \langle\rho\pi|\psi''\rangle &= \langle\rho\pi|2^3S_1\rangle\sin\theta + \langle\rho\pi|1^3D_1\rangle\cos\theta \ , \end{aligned} \tag{21.10}$$

where θ is the mixing angle between pure $\psi(2^3S_1)$ and $\psi(1^3D_1)$ states [371] and is fitted from the leptonic widths of the ψ'' and the ψ' to be $(12 \pm 2)^\circ$ [372], which is consistent with the coupled channel estimates [373, 374] and with the ratio of ψ' and ψ'' partial widths to $J/\psi\pi^+\pi^-$ [375]. If the mixing and coupling of the ψ' and ψ'' lead to complete cancellation of $\psi' \to \rho\pi$ decay ($\langle\rho\pi|\psi'\rangle = 0$), the missing $\rho\pi$ decay mode of the ψ' shows up instead as decay mode of the ψ'', enhanced by the factor $1/\sin^2\theta$, the concrete estimation shows that [372]

$$\mathcal{B}_{\psi''\to\rho\pi} = (4.1 \pm 1.4) \times 10^{-4} \ . \tag{21.11}$$

To test this scenario by the data collected at the ψ'' in e^+e^- experiments, it has been pointed out [497, 377] that the continuum contribution must be considered carefully. Specifically speaking, by Rosner's estimation, the Born order cross section for $\psi'' \to \rho\pi$ is

$$\sigma^{Born}_{\psi''\to\rho\pi} = (4.8 \pm 1.9) \text{ pb} \ , \tag{21.12}$$

which is comparable in magnitude to that of the continuum cross section, viz.

$$\sigma^{Born}_{e^+e^-\to\rho\pi} = 4.4 \text{ pb} \ . \tag{21.13}$$

So what is observed is the coherent interference of the two amplitudes. Based on the analysis of experimental data, it has been suggested that there be an universal phase between strong and electromagnetic amplitudes in charmonium decays. With this assumption, the strong decay amplitude interferes with the continuum amplitude either maximum destructively, e.g. for $\rho\pi$, $\omega\eta$ and $K^{*+}K^-$ or maximum constructively, e.g. for $K^{*0}\overline{K^0}$. The destructive interference leads to the phenomena that

the measured cross section on top of the resonance could be smaller than that off the resonance. Recent experimental results [338, 329] on $\rho\pi$, $\omega\eta$ and $K^{*+}K^-$ have demonstrated such interference pattern. This provides support to the prediction of Eq.(21.11). However, to uniquely determine $\mathcal{B}_{\psi''\to\rho\pi}$, current available experimental data are insufficient, the ψ'' resonance must be scanned [378]. So the quantitative test of Rosner's scenario remains to be the task of the future experiments on τ-Charm factories.

In the consequent study [379], Wang, Yuan and Mo (WYM) extend the S-D wave-mixing scenario to PP final state, and give a constraint for $\psi'' \to K^0_S K^0_L$ decay,

$$0.12 \pm 0.07 \leq 10^5 \times \mathcal{B}(\psi'' \to K^0_S K^0_L) \leq 3.8 \pm 1.1 \ , \qquad (21.14)$$

which is compatible with both the BESII result $\mathcal{B}(\psi'' \to K^0_S K^0_L) < 2.1 \times 10^{-4}$ at 90% C.L. [328] and the CLEOc result $\mathcal{B}(\psi'' \to K^0_S K^0_L) < 1.17 \times 10^{-5}$ at 90% C.L. [339]. Extrapolating fore-study to all charmless decays [380], WYM found that this scenario could accommodate large non-$D\overline{D}$ decay of the ψ''. Although the recent experimental measurement from CLEOc favor the zero non-$D\overline{D}$ cross section at ψ'' [381], the larger error could not rule out the existence of non-$D\overline{D}$ branching fraction at 10% level.

Other Explanations

Besides the models in two previous sections, more speculations involving the $\rho\pi$ puzzle are collected in this section.

1. Final State Interaction Scheme

   Li, Bugg and Zou [382] (LBZ) pointed out that the final state interactions (FSI) in J/ψ and ψ' decays give rise to effects which are of the same order as the tree level amplitudes, they argued that $J/\psi \to \rho\pi$ is strongly enhanced by the $a_2\rho$ loop diagram, while the direct tree-production for $\rho\pi$ may be suppressed by the HHC mechanism [340]. The contribution of the $a_1\rho$ loop diagram is much smaller than that of $a_2\rho$ loop for the $J/\psi \to \rho\pi$, but they have similar strength for the $\psi' \to \rho\pi$ and may cancel each other by interfering destructively. The similar apparent suppression for $\psi' \to K^*\overline{K}$ and $f_2\omega$ may also be explained by the $K^*\overline{K}^*_{2,1}$ and $b_1\pi$ loop, respectively. Therefore, LBZ expected that FSI may provide a coherent explanation for all the observed suppressed modes of ψ' decays. However, as remarked in Ref. [383], this interference model does appear to have more assumptions that predictions. The only qualitative prediction by LBZ is to check whether the $a_1\rho$ and $K^*_1\overline{K}^*$ production rates are large for the ψ'. So far, no such measurements have been reported. Nevertheless, useful information on $a_1\rho$ and $K^*_1\overline{K}^*$ could be obtained from the BES published data as shown in Refs. [333] and [335]. The lack of evidence within the invariant mass distribution plots (see Fig.3 and Fig.5 of Ref. [333] or Ref. [335]) that the $\rho\pi$ recoiled against a ρ for events of $\psi' \to \rho^0\rho^\pm\pi^\mp$ and that $\pi^\pm K^\mp$ recoiled against a K^{*0} for events of $\psi' \to \pi^+\pi^- K^+ K^-$ suggests that they are unlikely to be the favored modes in ψ' decays.

2. Large Phase Scheme

   Suzuki gave another explanation based on FSI for J/ψ decays [354]. He performed a detailed amplitude analysis for $J/\psi \to 1^-0^-$ decay to test whether or not the short-distance FSI dominates over the long-distance FSI in the J/ψ decay. His result indicates that there is a large phase between three-gluon and one-photon amplitudes. Since the large phase cannot be produced with the perturbative QCD interaction, the source of it must be in the long-distance part of strong interaction, namely, rescattering among hadrons in their inelastic energy region. Suzuki then performed the similar analysis for $J/\psi \to 0^-0^-$ decay, and obtained the same conclusion of the large phase [384]. His analysis also shows that the exclusive decay ratio at the J/ψ is in line with that of the inclusive decay. This fact leads him to believe that the origin of the relative suppression of $\psi' \to 1^-0^-$ to $J/\psi \to 1^-0^-$ is not in the J/ψ but in the ψ'.

   As to this large phase, in Ref. [367], Gérard argued that this phase follows from the orthogonality of three-gluon and one-photon virtual processes. As a mater of fact, the conclusion of a large phase close to 90° between three-gluon and one-photon processes holds true for all two-body decays of J/ψ, such as $1^+0^-(90°)$ [385], 1^-0^- $(106 \pm 10)°$ [494, 495], 1^-1^- $(138 \pm 37)°$ [384, 495, 477], 0^-0^- $(89.6 \pm 9.9)°$ [384, 495, 477] and $N\overline{N}$ $(89 \pm 15)°$ [492, 495].

   Nevertheless, as the ψ' decays were analyzed, the experimental data at first seemed to favor a phase close to 180° [385], in contrary to the expectation that the decay of J/ψ and ψ' should not be much different. However, as pointed out by Wang *et al.* that the previous published data did not take the continuum one-photon process into account. Their reanalysis of the experimental data shows that the phase with value around $-90°$ could fit $\psi' \to 1^-0^-$ data [377] and $\pm 90°$ could fit $\psi' \to 0^-0^-$ data [390]. The latter is confirmed by more recent results by CLEO [321]. Furthermore, this large phase also shows in the OZI suppressed decay modes of the ψ''. In many decays modes of the ψ'', the strong decay amplitudes have comparable strength as the non-resonance continuum amplitude, the large phase around $-90°$ leads to destructive or constructive interference. Due to the destructive interference, the observed cross sections of some modes at the peak of the ψ'' are smaller than the cross section measured off-resonance [497]. This is demonstrated by the data from CLEOc [338].

   If the large phase between the three-gluon and one-photon virtual processes is universal not only in J/ψ decays, but also in ψ' as well as all charmonium or perhaps all quarkonium decays, then how this phase is related to the difference between the decays of J/ψ and ψ' remains to be an unanswered question.

3. Mass Reduction Explanation

   In the study [391] of radiative decays of 1^{--} quarkonium into η and η', Ma presented a QCD-factorization approach, with which he obtained theoretical predictions in consistency with CLEOc measurement. The largest possible uncertainties in analysis are from the relativistic corrections for the value of the charm quark mass. Ma argued that the effect of these uncertainties can be reduced by using quarkonium

masses instead of using quark mass. As an example of such reduction, he provided a modified relation to the original 12% rule

$$Q_{\rho\pi} = \frac{\mathcal{B}(J/\psi \to \rho\pi)}{\mathcal{B}(\psi' \to \rho\pi)} = \frac{M^8_{J/\psi}}{M^8_{\psi'}} \frac{\mathcal{B}(J/\psi \to e^+e^-)}{\mathcal{B}(\psi' \to e^+e^-)}$$

$$= (3.6 \pm 0.6)\% \ .$$

However, this value is much larger than the experimental result given in Table 21.1.

4. Vector-meson-mixing Model

Intending to give a comprehensive description of J/ψ two-body decay, Clavelli and Intemann (CI) proposed a vector-meson-mixing model in which the vector mesons ($\rho,\ \omega\ ,\phi\ , J/\psi$) are regarded as being admixture of light-quark-antiquark state and charmed-quark-antiquark state [392]. The coupling of the J/ψ to any state of light quarks is then related to the corresponding coupling of the ρ, ω, and ϕ to the same state. With few experiment inputs to determine the mixing parameters, CI calculated VP, PP, and BB decay rates for the J/ψ as a function of the pseudoscalar mixing angle. Most of the predictions agree with the experiment results at the order of magnitude level, but discrepancy is obvious for some channels, such as $K^0_S K^0_L$ final state [322]. CI also extended their model to the hadronic decays of the ψ'. Nevertheless, their evaluations for $\mathcal{B}(J/\psi \to \omega\pi^0) = 3\times10^{-5}$ and $\mathcal{B}(\psi' \to \omega\pi^0) = 3\times 10^{-3}$ contradict with the present results $(4.5\pm0.5)\times10^{-4}$ and $(2.1\pm0.6)\times10^{-4}$ [343], respectively.

Start from effective Lagrangian whereby nonet-symmetry breaking and pseudoscalar-meson mixing can be studied, Haber and Perrier parametrized the decay modes of $J/\psi \to PP$ (also for $J/\psi \to VV$ or $\eta_c \to VP$), $J/\psi \to VP$ (also for $J/\psi \to VT$ or $\eta_c \to VV$), $J/\psi \to PPP$ (also for $J/\psi \to VVP$ or $\eta_c \to PPV$), and $\eta_c \to PPP$ (also for $J/\psi \to PPV$ or $\eta_c \to VVP$) [393]. The experimental data are used to determine these phenomenological parameters. In a later work, Seiden, Sadrozinski and Haber took the doubly Okubo-Zweig-Iizuka suppression (DOZI) effect into consideration, and presented a more general parametrization of amplitudes for $J/\psi \to PP$ decays [394]. With this form, one could easily derive the relative decay strength between different final states. However, it has also been noticed that under the most general circumstances, symmetry breaking introduces too many parameters for a general analysis to be useful. In order to reduce the number of new parameters considerably and make the analysis manageable, only special cases could be considered.

A similar parametrization with mixing feature of the strong interaction mechanism was proposed by Feldmann and Kroll (FK) [395] for the hadron-helicity non-conserving J/ψ and ψ' decays, but with a different interpretation from those put forth in Refs. [352, 365, 394, 383]. FK assumed that with a small probability, the charmonium possesses Fock components built from light quarks only. Through these Fock components the charmonium state decays by a soft mechanism which is modeled by J/ψ-ω-ϕ mixing and subsequent ω (or ϕ) decays into the VP state. In

Table 21.2: Comparison of predictions [395] and measurements [343] for the branching ratios (10^{-5}) for ψ' decays. The upper limits are presented at 90% C.L.

VP	Prediction	Measurement
$\rho\pi$	1.3	3.2 ± 1.2
$K^{*0}\overline{K^0} + c.c.$	5.1	10.9 ± 2.0
$K^{*+}K^- + c.c.$	1.3	$1.7^{+0.8}_{-0.7}$
$\omega\eta$	1.2	< 1.1
$\omega\eta'$	6.3	$3.2^{+2.5}_{-2.1}$
$\phi\eta$	1.6	$2.8^{+1.0}_{-0.8}$
$\phi\eta'$	4.6	3.1 ± 1.6
$\rho\eta$	2.1	2.2 ± 0.6
$\rho\eta'$	1.2	$1.9^{+1.7}_{-1.6}$
$\omega\pi^0$	3.8	2.1 ± 0.6
$\phi\pi^0$	0.01	< 0.40

absence of the leading-twist perturbative QCD contribution, the dominant mechanism is supplemented by the electromagnetic decay contribution and DOZI violating contribution. FK argued that this mechanism can probe the charmonium wave function at all quark-antiquark separations and feels the difference between a $1S$ and a $2S$ radial wave function. The node in the latter is supposed to lead to a strong suppression of the mechanism in ψ' decays. With a few parameters adjusted to the experimental data, FK obtained a numerical description of the branching fractions for many VP decay modes of the J/ψ and ψ', which agree with the measured branching fractions at the order of magnitude level, as shown in Table 21.2. Moreover, FK has extended their mixing approach to the $\eta_c \to VV$ decays and obtained a reasonable description of the branching fractions for these decays while the $\eta_c' \to VV$ decays are expected to be strongly suppressed.

Remarks

From the brief retrospect of $\rho\pi$ puzzle history, we could notice that in the early stage, theorists concentrate on peculiar mechanism for special channels like $\rho\pi$ and $K^*\overline{K}$, such as Hou and Soni's explanation. With the development of the theory and the progress of the experiment, theorists attempt to provide a more general scheme for charmonium decays, such as the work by Feldmann and Kroll. In fact, the charmonium decay is a interconnected system as a whole, a correct explanation of $\rho\pi$ puzzle is expected to describe, quantitatively, or semi-quantitatively, the properties of all measured decay modes.

At last, a few words about Fock state component. This concept has been discussed in many works, such as by BK [357], CB [352], and FK [395]. Even from the theoretical explanation of experiments other than e^+e^- collision, the non-perturbative Fock component is also indicated to exist. For example, the analysis of charmonia photoproduction amplitude implies [396] that the $|c\overline{c}\rangle$ component is narrowly distributed in the transversal direction, while the $c\overline{c}$ pairs at larger separations may be part of higher Fock states which

contain gluons and light quarks.

21.1.3 Evaluation of ratio of J/ψ to ψ' decay

In this section, we depict three approaches to estimate the ratio of J/ψ to ψ' decay, one from theoretical analysis [479], the other two from experimental evaluation [397].

Theoretical Method

Conventionally, the measured ratios of ψ' to J/ψ branching fractions for specific exclusive hadronic decays are compared with the naive prediction of pQCD, the so-called "12% rule". In the framework of pQCD [479], the ψ particles are considered to be nonrelativistic bound states of a charm quark and its antiquark. Their decays into light hadrons are believed to be dominated by the annihilation of the $c\overline{c}$ pair into three gluons. In order to annihilate, the c and $\overline{c}$ must have a separation of order $1/m_c$, which is much smaller than the size of the charmonium state. Thus the annihilation amplitude for an S-wave state like J/ψ and ψ' must be proportional to the wave function at the origin, $\psi(\mathbf{r}=0)$ [479]. The width for decay into any specific final state h consisting of light hadrons is therefore proportional to $|\psi(0)|^2$. The width for decay into e^+e^- is also proportional to $|\psi(0)|^2$. This leads to the simple prediction that the ratio of the branching fractions between ψ' and J/ψ is given by Eq. (21.1).

However, this naive prediction suffers from several apparent approximations. Higher order corrections, which may not even be small, are not included in this calculation. For example, a first order correction to the branching fraction of $J/\psi \to e^+e^-$ could be 50% of the lowest term if $\alpha_s(m_{J/\psi}) \sim 0.2$ [398] is taken. The relativistic effect is also ignored. Since the mass difference between J/ψ and ψ' is around 20% and $< v^2/c^2 > \sim 0.24$ for J/ψ, this correction may be at the same level as the lowest order contribution [398]. The inclusion of the finite size of the decay vertex will significantly reduce the ggg decay width of the J/ψ [399]. Moreover, the effect of non-perturbative dynamics is neglected, the size of which is hard to estimate. Therefore, people may question the validity of the 12 % rule as a serious benchmark for comparing experimental data.

Experiment Estimation (I)

The first experimental estimation is based on the assumption that the decays of J/ψ and ψ' in the lowest order of QCD are classified into hadronic decays (ggg), electromagnetic decays (γ^*), radiative decays into light hadrons (γgg), and transition to lower mass charmonium states ($c\overline{c}X$) [477, 397]. Thus, using the relation $\mathcal{B}(ggg)+\mathcal{B}(\gamma gg)+\mathcal{B}(\gamma^*)+\mathcal{B}(c\overline{c}X) = 1$, one can derive $\mathcal{B}(ggg)+\mathcal{B}(\gamma gg)$ by subtracting $\mathcal{B}(\gamma^*)$ and $\mathcal{B}(c\overline{c}X)$ from unity.

The calculated values of $\mathcal{B}(\gamma^*)$ and $\mathcal{B}(c\overline{c}X)$, together with the values used to calculate them are summarized in Table 21.3. As regards to ψ', two final states $\gamma\eta(2S)$ and $h_c(1^1P_1)+X$ with faint branching fractions are neglected in our calculation. By deducting the contributions $\mathcal{B}(\gamma^*)$ and $\mathcal{B}(c\overline{c}X)$, we find that $\mathcal{B}(J/\psi \to ggg)+\mathcal{B}(J/\psi \to \gamma gg) = (73.3 \pm 0.5)\%$ and $\mathcal{B}(\psi' \to ggg)+\mathcal{B}(\psi' \to \gamma gg) = (18.9 \pm 1.3)\%$, then the ratio of them is

$$Q_g = \frac{\mathcal{B}(\psi' \to ggg+\gamma gg)}{\mathcal{B}(J/\psi \to ggg+\gamma gg)} = (25.7 \pm 1.7)\% \ . \tag{21.15}$$

Table 21.3: Experimental data on the branching fractions for J/ψ and ψ' decays through virtual photon and to lower mass charmonium states used in this analysis. Most of the data are taken from PDG [343], except for $\mathcal{B}(J/\psi, \psi' \to \gamma^* \to \text{hadrons})$, which are calculated by the product $R{\cdot}\mathcal{B}(J/\psi, \psi' \to \mu^+\mu^-)$, with $R = 2.28{\pm}0.04$ [400]. In estimating the errors of the sums, the correlations between the channels are considered [401].

Channel	$\mathcal{B}(J/\psi)$	$\mathcal{B}(\psi')$
$\gamma^* \to$ hadrons	$(13.50{\pm}0.30)\%$	$(1.66{\pm}0.18)\%$
e^+e^-	$(5.94{\pm}0.06)\%$	$(7.35{\pm}0.18){\times}10^{-3}$
$\mu^+\mu^-$	$(5.93{\pm}0.06)\%$	$(7.3\ {\pm}0.8){\times}10^{-3}$
$\tau^+\tau^-$	–	$(2.8\ {\pm}0.7){\times}10^{-3}$
$\gamma^* \to X$	$(25.37{\pm}0.35)\%$	$(3.41{\pm}0.27)\%$
$\gamma\eta_c$	$(1.3{\pm}0.4)\%$	$(2.6{\pm}0.4){\times}10^{-3}$
$\pi^+\pi^- J/\psi$		$(31.8\ {\pm}0.6)\%$
$\pi^0\pi^0 J/\psi$		$(16.46{\pm}0.35)\%$
$\eta J/\psi$		$(3.09\ {\pm}0.08)\%$
$\pi^0 J/\psi$		$(1.26{\pm}0.13){\times}10^{-3}$
$\gamma\chi_{c0}$		$(9.2{\pm}0.4)\%$
$\gamma\chi_{c1}$		$(8.7{\pm}0.4)\%$
$\gamma\chi_{c2}$		$(8.1{\pm}0.4)\%$
$c\bar{c}X$	$(1.3{\pm}0.4)\%$	$(77.7{\pm}1.2)\%$

The above estimation is consistent with the previous ones [385, 397]. The relation between the decay rates of ggg and γgg is readily calculated in pQCD to the first order as [398]

$$\frac{\Gamma(J/\psi \to \gamma gg)}{\Gamma(J/\psi \to ggg)} = \frac{16}{5}\frac{\alpha}{\alpha_s(m_c)}\left(1 - 2.9\frac{\alpha_s}{\pi}\right). \tag{21.16}$$

Using $\alpha_s(m_c) = 0.28$, one can estimate the ratio to be 0.062. A similar relation can be deduced for the ψ' decays. So we obtain $\mathcal{B}(J/\psi \to ggg) \simeq (69.0 \pm 0.5)\%$ and $\mathcal{B}(\psi' \to ggg) \simeq (17.8 \pm 1.2)\%$, while the "25.7% ratio" in Eq. (21.15) stands well for both ggg and γgg. Although Q_g is considerably enhanced relative to Q_h in Eq. (21.1), it is fairly compatible with the ratios for the K^+K^- and $K^0_S K^0_L$ decay modes between ψ' and J/ψ, which are

$$\begin{aligned} Q_{K^+K^-} &= (26.6 \pm 4.5)\%\ \text{(CLEO)}\ , \\ Q_{K^0_S K^0_L} &= (28.8 \pm 3.7)\%\ \text{(BES)}\ , \\ Q_{K^0_S K^0_L} &= (32.2 \pm 5.2)\%\ \text{(CLEO)}\ , \end{aligned}$$

according to the recent results from CLEO and BES [321, 322, 323]. The relation in Eq. (21.15) was discussed in the literature as the hadronic excess in ψ' decays [397, 385]. It implicates that while some modes are suppressed in ψ' decays, the dominant part of ψ' through ggg decays is enhanced relative to the 12% rule prediction in the light of J/ψ decays.

Experiment Estimation (II)

The second approach for estimating Q_h is to use the data on branching fractions for hadronic decays in final states containing pions, kaons, and protons that have already been measured for both the J/ψ and the ψ'. They are $\pi^+\pi^-$, K^+K^-, $p\overline{p}$, $\pi^+\pi^-\pi^0$, $p\overline{p}\pi^0$, $2(\pi^+\pi^-)$, $3(\pi^+\pi^-)$, $2(\pi^+\pi^-)\pi^0$, $3(\pi^+\pi^-)\pi^0$, $2(\pi^+\pi^-\pi^0)$, $2(K^+K^-)$, $K^+K^-\pi^+\pi^-$, $K^+K^-\pi^+\pi^-\pi^0$, $K^+K^-2(\pi^+\pi^-)$, $\pi^+\pi^-p\overline{p}$, $p\overline{p}\pi^+\pi^-\pi^0$ and so forth. Using the data compiled in Table 21.4, we have

$$\sum_{i=1}^{11} \mathcal{B}(J/\psi \to f_i) = (14.46 \pm 0.80)\%$$

and

$$\sum_{i=1}^{11} \mathcal{B}(\psi' \to f_i) = (1.70 \pm 0.23)\% \ .$$

It follows that

$$\begin{aligned} Q_s &= \sum_{i=1}^{11} \mathcal{B}(\psi' \to f_i) \Big/ \sum_{i=1}^{11} \mathcal{B}(J/\psi \to f_i) \\ &= (11.8 \pm 1.7)\% \ . \end{aligned} \tag{21.17}$$

Table 21.4: Branching fractions for ψ' and J/ψ decays, and Q_h values are also calculated. For $\psi' \to \pi^+\pi^-$, K^+K^- decays, the results are the weighted average of measurements from CLEO [321] and BES [402], while for $J/\psi \to \pi^+\pi^-\pi^0$, the result is the weighted average of measurements from BES [319] and BABAR [320]. Except for values with †, all others from PDG [343].

Final state	$\mathcal{B}_{J/\psi}(10^{-3})$	$\mathcal{B}_{\psi(2S)}(10^{-4})$	Q_h (%)
$\pi^+\pi^-$	0.147 ± 0.023	0.08 ± 0.05†	5.6 ± 3.5
K^+K^-	0.237 ± 0.031	0.63 ± 0.07†	26.5 ± 4.5
$p\overline{p}$	2.17 ± 0.08	2.65 ± 0.22	12.2 ± 1.1
$\pi^+\pi^-\pi^0$	21.2 ± 1.01†	1.68 ± 0.26	0.79 ± 0.13
$p\overline{p}\pi^0$	1.09 ± 0.09	1.33 ± 0.17	12.2 ± 1.9
$2(\pi^+\pi^-)$	3.55 ± 0.23	2.4 ± 0.6	6.8 ± 1.8
$3(\pi^+\pi^-)$	4.3 ± 0.4	3.5 ± 2.0	8.1 ± 4.7
$3(\pi^+\pi^-)\pi^0$	29 ± 6	35 ± 16	12.1 ± 6.1
$2(\pi^+\pi^-)\pi^0$	33.7 ± 2.6	26.6 ± 2.9	7.9 ± 1.1
$2(\pi^+\pi^-\pi^0)$	16.2 ± 2.1	45 ± 14	27.8 ± 9.4
$2(K^+K^-)$	0.78 ± 0.14	0.60 ± 0.14	7.7 ± 2.3
$K^+K^-\pi^+\pi^-$	7.2 ± 2.3	7.2 ± 0.5	10.0 ± 3.3
$K^+K^-\pi^+\pi^-\pi^0$	12.0 ± 3.0	12.4 ± 1.0	10.3 ± 2.7
$K^+K^-2(\pi^+\pi^-)$	4.7 ± 0.7	18 ± 9	38.3 ± 20.0
$p\overline{p}\pi^+\pi^-$	6.0 ± 0.5	6.0 ± 0.4	10.0 ± 1.1
$p\overline{p}\pi^+\pi^-\pi^0$	2.3 ± 0.9	7.3 ± 0.7	31.7 ± 12.8

Some remarks are in order here. First, we know that most of the multihadron final states in fact include sums of several two-body intermediate states, so the Q_s is not the exact ratio of ψ' to J/ψ inclusive hadronic decay rates, but the ratio on average of the exclusive decay channels as measured to date. In another word, Q_s represents a mixed effect which may deviate noticeably from the component Q-values. For example, the decay $\psi' \to \pi^+\pi^- K^+ K^-$ can proceed through intermediate state $K^*(892)^0\overline{K}_2^*(1430)^0 + c.c.$, whose $Q = 2.9 \pm 1.3$, is greatly suppressed [335] comparing with $Q = 10.0 \pm 3.3$. Second, we notice that the results obtained by two estimations vary considerably; furthermore, by virtue of Table 21.4, it is obvious that many Q-values deviate from Q_s significantly while on average, Q_s is similar to pQCD Q_h. It would be an intriguing problem that with more and more data and higher accurate measurements if Q_s and Q_g could approximate with each other and be consistent with Q_h, or if Q_s and Q_g still deviate from each other prominently.

21.1.4 Comment on the $\rho\pi$ puzzle

Theory Aspect

For all explanations involving $\rho\pi$ puzzle, there is a basic assumption that the non-relativistic potential model delineates the physics of charmonium decay to a good approximation. However, this assumption indeed requires examination in detail. First, as we have noticed in subsection 21.1.3, several corrections, should be added for the decay ratio between ψ' and J/ψ.

Second, we see the effect of non-perturbative dynamics is neglected, which is crucial for charmonium decay. Actually from various explanations of $\rho\pi$ puzzle, or more generally from the phenomenological explanation involving pQCD, we note that certain non-perturbative effect or nonlinear effect must be incorporated one way or the other in order to recount the experimental data. But this kind of effect could hardly been included in the present non-relativistic potential model.

Third, if the S-D wave mixing scenario holds as the solution of $\rho\pi$ puzzle, then the matrix element of D wave to light hadrons would be very large, which can hardly be accommodated by the potential model, or any current theory. It indicates that the current understanding of charmonium decays may not be complete.

We envisage that new development of the theory should take into account the following features involving charmonium decays

- the mass effect for different charmonium states, such as J/ψ, ψ', ψ'' and so on;
- the non-perturbative or non-linear effect on the resonance decays;
- reasonable description for the known features of charmonium spectroscopy;
- quantitative consistence (with reasonable high accuracy) with the existing experimental measurements.

Herein it is also important to distinguish the quarkonium states (theoretical states) and mass eigenstates (physical states) [367, 369]. From a fairly theoretical point of view,

if both states, say, J/ψ and ψ' did dominantly annihilate into three gluons, they would mix and could thus not be the putative quarkonium states. In a non-relativistic potential model, for example, the ψ' is simply a radial excitation of the J/ψ. This is a well defined picture in which J/ψ and ψ' are orthogonal states. If the annihilation into three gluons could be treated as a "perturbation" to the non-relativistic potential, then clearly the unperturbed states would mix and rearrange themselves into orthogonal mass eigenstates. The QCD dynamics may be such that the physical states, presumably mixtures of the theoretical $c\overline{c}$ states ($n^{2S+1}L_J$), are so built up that one of them strongly annihilates into three perturbative gluons while the other does not. Mixing of the 1^3S_1 and 2^3S_1 states via three perturbative gluons has little effect on the charmonium mass spectrum, but may be crucial for the decay pattern.

Phenomenology Aspect

One may remember that at the early stage of the discovery of a narrow state J/ψ, the $c\bar{c}$ system was hailed as the Hydrogen atom of Quantum Chromodynamics, with the implied hope that the study of the newly discovered system could shed as much light on the dynamics of quark-antiquark interactions as the study of the Hydrogen atom had on Quantum Electrodynamics. But one may also notice the historical fact, even before Bohr's theory, Balmer series had been discovered for long, and the famous Rydberg formula had also been proposed, which laid a solid foundation for further theoretical improvement. If we are conscious of the more complicatedness of charmonia system comparing with Hydrogen atom, we may prepare for more hard and meticulous works. As a first step, it is necessary to develop a reliable and extensively applicable phenomenological model (PM).

The advantage of PM lies in that a well-defined PM contains few experimentally determined parameters which have clear physical meaning; moreover, with only few parameters determined from experiment, PM could produce concrete results which can be directly confirmed or falsified by experiment and may guid experimental searches. Such a model has a good relation with elementary principle of the theory, and if correct, can be used for further theoretical refinement. This point is noteworthy for the time being, since the general QCD can hardly provide solutions for special problems; conversely, we have to establish certain effective empirical model to advance our understanding for generic QCD principle.

Here we would like to mention few ideas of PM, which have or intend to provide a general description for charmonium decay.

1. Mixing Model

   As we have noticed in subsection 4, whatever CI model or FK model, they could yield definite predictions for experimental test, and therefore provide clues for further development. In addition, according to Haber and Perrier's parametrization scheme [393], we could get the decay rate relations between different channels, and the proportions of different interaction amplitudes, all of which are useful information to understand the dynamics of charmonium decays.

The special feature of Rosner's S- and D-wave mixing scheme [372] is that it is simple, and it works both for suppressed and enhanced decay modes, and moreover, it connects the J/ψ, ψ' and ψ'' decays together, and give predictions with little uncertainty.

2. Effective FSI

   Miller once discussed the connection between the strong-coupling approximation to quantum chromodynamics and nuclear properties observed at low and medium energies and momentum transfer [403]. He suggested that the strong-coupling (corresponds to long-range interaction) version of QCD does reproduce the salient feature of the meson-baryon picture of low momentum transfer in nuclear physics. The derivation of nuclear physics indicates that quark aspects of ordinary nuclei are hidden in the hadronic degrees of freedom. Reversely, one may imagine that a quasi-meson or quasi-baryon structure could be formed in non-perturbative hadronization process. The meson-baryon picture in nuclear physics could be utilized, with some modification, as an effective FSI theory, or molecular-model theory. The recent molecular interpretations [404, 405] for the newly found state $Y(4260)$ could be treated as such an effective FSI theory.

   Furthermore, the quasi-particles could even be real particles, and then with the residual strong force between the quarks inside the quasi-particles, some multiplets can be formed as the quasi-particle and anti-quasi-particle bound states. This idea was first put forth to explain a lots of low mass baryon-antibayron enhancements newly found by CLEO, Belle and BaBar collaborations [406].

3. Glueball and Hybrid

   We have seen that the J/ψ-glueball mixing scheme is the first explanation proposed to explain the $\rho\pi$ puzzle. With the implication from lattice calculation [407], Suzuki once proposed a glueball-ψ' mixing scheme to explain the excess hadronic decays at the ψ' [408]. In fact, gluodynamics is always a tantalizing domain for theorists. Recently, some lattice evaluations suggest [409, 410] that the masses of some hybrid states could be low enough to be degenerated with charmonium states, such as J/ψ and/or χ_{cJ}. Unlike Glueball, these $c\bar{c}g$ hybrid states could be very narrow, so it may be very stimulating and noteworthy to search for and confirm these kinds of states.

Experiment Aspect

Physics is a science of experiment. Physical facts are basis for theoretical development and also criteria for checking theoretical hypotheses. It is a prominent fact that the early analyses on $\rho\pi$ puzzle based on meager experimental data often lead to unsatisfactory, sometime premature, inferences, which were washed out easily by later accurate data. In fact, the current knowledge concerning the ψ' decays from experiments is still rather limited, even summing all charmless channels presented in PDG [343], the total branching fraction is less 2%. Such situation prevents us from laying down a solid foundation for elementary dynamics exploration. However, the estimation of Q value, as discussed in

Section 21.1.3, affords us some clues concerning the exploration of charmonium decay dynamics. Since many suppressed channels have been found, especially those such as $\rho\pi$ which is greatly suppressed in ψ' decay, and if the Q_h really represents the averaged value of inclusive hadronic decay, the estimation of Q_g indicates that either lots of enhanced decays are not discovered, or some particular decays only present in ψ', or both cases exist. Therefore, systematic experimental study of ψ' decays is anxiously awaited.

Moreover, study should be carried out not only on the ratios of ψ' to J/ψ decays, but also on the other ratios such as those between η_c' and η_c [395], and those between ψ'' and J/ψ[366], and/or many other ratios between different resonances for the same channel or between different channels about the same resonance [208]. All these studies will shed light on the understanding of charmonium decays. From our point of view, the progress would be more likely obtained from the analysis of the new experimental results, rather than from the inspiration of general theoretical principle.

21.1.5 Summary

In this paper, we present a general review on the study of the $\rho\pi$ puzzle. Although there is still no satisfactory explanation for all existing experiment results, some enlightenment ideas have been put forth. In addition, we also discuss three methods of estimating the ratio of the branching fractions in J/ψ and ψ' decays. In the light of the present theoretical and experimental status, we argue that it is important to explore the potential model from a new point of view, it is necessary to search for and/or construct an effective phenomenological model, and it is especially crucial to perform systematic measurements of various charmonium decays.

As we know physics in the charm energy region is in the boundary domain between perturbative and nonperturbative QCD. Recently the observed hadronic decays of charmonium may give new challenges to the present theoretical understanding of the decay mechanisms. Many of the new charmonium states observed by Belle and BaBar which can hardly be accommodated by potential model have led to new theoretical speculations about charmonium spectroscopy and novel production mechanism [411].

Experimentally, the expected large data sample from CLEOc in the near future, and even larger sample from forthcoming detector BESIII will open for us a new era for charmonium dynamics study, even though we may not obtain a throughly revolutionary theory, we could acquire more profound understanding for the existing theory, at the same time we could expect a brand-new comprehension for the $\rho\pi$ puzzle.

21.2 $\psi(3770)$ non-$D\overline{D}$ decays

21.2.1 Introduction

Potential Models based on QCD predict the charmonium states and charmed mesons production quite well in quantity. Up to now, most of the predicted charmonium states by the models have been observed, and many decay channels and their branching fractions of the states have been observed and measured very well.

Based on the conventional charmonium potential model, the $\psi(3770)$ resonance is assigned to be a mixture of the 1^3D_1 and 2^3S_1 angular momentum eigenstate, and is expected to decay into the OZI allowed $D\bar{D}$ ($D^0\bar{D}^0$ and D^+D^-) with a branching fraction $B(\psi(3770) \to D\bar{D}) \geq 97\%$. However, there is a long-standing puzzle in the understanding of the $\psi(3770)$ production and decays. Historically published data show that there is about 38% discrepancy [412] between the observed $D\bar{D}$ production cross section $\sigma^{\rm obs}_{D\bar{D}}$ and the observed $\psi(3770)$ production cross section $\sigma^{\rm obs}_{\psi(3770)}$. In recent days, BES Collaboration measured the total branching fraction for the non$-D\bar{D}$ decay of $\psi(3770)$ to be $B(\psi(3770) \to {\rm non}-D\bar{D}) = (16.4\pm7.3\pm4.2)\%$ [413] obtained based on the measurements of the continuum light hadron cross section below $D\bar{D}$ threshold, the observed cross section for $D\bar{D}$ production and the observed cross section for inclusive hadron production at the peak of $\psi(3770)$, and $B(\psi(3770) \to {\rm non}-D\bar{D}) = (16.4 \pm 7.3 \pm 4.2)\%$ [414] obtained based on analysis of the line-shapes of the inclusive hadron and $D\bar{D}$ ($D^0\bar{D}^0$ and D^+D^-) production. These indicate that either, contrary to what was generally expected, $\psi(3770)$ could substantially decay into non$-D\bar{D}$ final states or the measured cross sections for $D\bar{D}$ and $\psi(3770)$ production still suffer from large systematic shifts even in the newest BES-II measurements; otherwise, there may exist some other effects or new phenomena which are responsible for this discrepancy.

To clarify this situation one needs to more precisely measure the $\sigma^{\rm obs}_{D\bar{D}}$, $\sigma^{\rm obs}_{\psi(3770)}$, the parameters of $\psi(3770)$ and $\psi(2S)$ resonances, directly measure the branching fractions for $\psi(3770) \to D^0\bar{D}^0, D^+D^-, D\bar{D}$, non$-D\bar{D}$, and extensively search for and study the exclusive non-$D\bar{D}$ decay modes of the $\psi(3770)$ and study the possible non$-D\bar{D}$ decay modes of $\psi(3770)$ with a large statistic data sample. These can be done with the BES-III detector at BEPC-II collider. In this paper we summarize the status of the experimental studies of non-$D\bar{D}$ decays of $\psi(3770)$ resonance and propose to extensively study the light hadron decays of the $\psi(3770)$ with the BES-III detector at the BEPC-II collider.

21.2.2 S-D mixing and mixing angle $\theta_{\rm mix}$

Charmonium model predicts the leptonic width of 1^3D_1 state of the $c\bar{c}$ system to be 70 eV [415], while earlier experiments observed the leptonic width is about 250 eV. To explain the large leptonic width, the $\psi(3770)$ is assumed to be a mixture of the 1^3D_1-wave with the 2^3S_1-wave states as well as some other 1^{--} states near by the $D\bar{D}$ thresholds, caused by some dynamic mechanism [416, 417]. The simplest mixing scheme of 1^3D_1 state with only 2^3S_1 state, which is the main component of the mixing with 1^3D_1 state, is characteristic by the mixing angle $\theta_{\rm mix}$, and the corresponding physical states $\psi(3686)$ and $\psi(3770)$ are described as,

$$|\psi(3770)>=|1^3D_1>\cos\theta_{\rm mix}+|2^3S_1>\sin\theta_{\rm mix}, \tag{21.18}$$

$$|\psi(3686)>=-|1^3D_1>\sin\theta_{\rm mix}+|2^3S_1>\cos\theta_{\rm mix}. \tag{21.19}$$

Some time this is enough to discuss some important issues in the charmonium physics experiments. From this simple model, the leptonic widths of $\psi(3770)$ and $\psi(3686)$ reso-

nances are then calculated as a function of $\theta_{\rm mix}$ by [419, 421]

$$\Gamma(\psi(3770)\to e^+e^-)=\frac{4\alpha^2e_c^2}{M^2_{\psi(3770)}}\left|\sin\theta_{\rm mix}R_{2S}(0)+\frac{5}{2\sqrt{2}m_c^2}\cos\theta_{\rm mix}R''_{1D}(0)\right|^2, \tag{21.20}$$

$$\Gamma(\psi(3686)\to e^+e^-)=\frac{4\alpha^2e_c^2}{M^2_{\psi(3686)}}\left|\cos\theta_{\rm mix}R_{2S}(0)-\frac{5}{2\sqrt{2}m_c^2}\sin\theta_{\rm mix}R''_{1D}(0)\right|^2, \tag{21.21}$$

where $e_c=2/3$, $R_{2S}(0)=\sqrt{4\pi}\Psi_{2S}(0)$ is the radial $2S$ wave function at $r=0$, and $R''_{1D}(0)$ is the second derivative of the radial $1D$ wave function at the origin. Experimentally, using the measured values of $\Gamma(\psi(3686)\to e^+e^-)$ and $\Gamma(\psi(3770)\to e^+e^-)$ one can determine the mixing angle $\theta_{\rm mix}$.

Taking the ratio of the Eq. (3) over the Eq. (4), we have the relation

$$R_{\psi(3770)/\psi(3686)}=\frac{M^2_{\psi(3773)}\Gamma(\psi(3773)\to e^+e^-)}{M^2_{\psi(3686)}\Gamma(\psi(3686)\to e^+e^-)}=\left|\frac{0.734\sin\theta_{\rm mix}+0.095\cos\theta_{\rm mix}}{0.734\cos\theta_{\rm mix}-0.095\sin\theta_{\rm mix}}\right|^2. \tag{21.22}$$

Using the recently newest parameters of $\psi(3770)$ and $\psi(3686)$ resonances measured by BES Collaboration [418], we can determine the ratio of the patial leptonic widths of the $\psi(3770)$ and the $\psi(3686)$

$$R^{BES}_{\psi(3770)/\psi(3686)}=0.105\pm0.015, \tag{21.23}$$

From the relations given in the Eqs. (5) and (6), we can extract a new precision measurement of the mixing angle, $\theta_{\rm mix}$. The relation of $R_{\psi(3770)/\psi(3686)}$ to $\theta_{\rm mix}$ is plotted as the quadrature line in Fig. 1, where the horizontal lines give the measured value of $R_{\psi(3770)/\psi(3686)}$ and the $\pm1\sigma$ interval of the value; the vertical lines give $\pm1\sigma$ intervals of the measured values of the mixing angle $\theta_{\rm mix}$. There are two solutions as shown in the figure. One is $\theta_{\rm mix}=(10.6\pm1.3)^o$ and the another is $\theta_{\rm mix}=(-25.3\pm1.3)^o$. However, only the solution $\theta_{\rm mix}=(10.6\pm1.3)^o$ is favored by comparison of the decay rates for $\psi(3770)\to J/\psi\pi^+\pi^-$ and $\psi(3686)\to J/\psi\pi^+\pi^-$. If the mixing angle is $\theta_{\rm mix}=(-25.3\pm1.3)^o$, the partial width for $\psi(3770)\to J/\psi\pi^+\pi^-$ would be larger than that for $\psi(3686)\to J/\psi\pi^+\pi^-$, which is conflict with measurements (see later).

The measurements of the $\theta_{\rm mix}$ and the rates of charmonium decays and transitions in experiments is essential for testing the theoretical predictions and in the understanding of the nature of the $\psi(3770)$.

21.2.3 Electromagnetic transitions

The predictions of $\psi(3770)$ electromagnetic transitions

A charmonium state, lying above the ground state, often significantly decays into the states with the lower mass through electromagnetic transition. For $\psi(3770)$ resonance, although it predominantly decays into $D\bar{D}$ final states, there are still electromagnetic transitions between the $\psi(3770)$ and lower mass states. According to the selection rule, the $\psi(3770)$ can decay into $\chi_{cJ(J=0,1,2)}$ through radiating a photon.

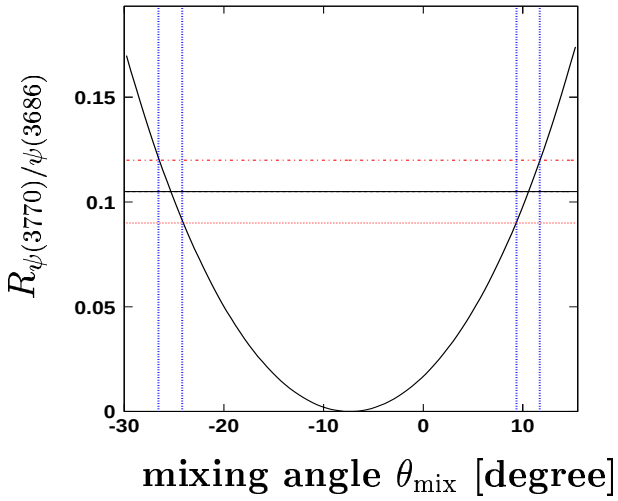

Figure 21.1: The ratio $R_{\psi(3770)/\psi(3686)}$ of the scaled leptonic widths as a function of mixing angle $\theta_{\rm mix}$, where the dashed lines show the $\pm 1\sigma$ intervals of the measured quantities.

The measurements of the rates of the E-M transition of $\psi(3770)$ to $\chi_{cJ(J=0,1,2)}$ has a special advantage. In the $1D$ to $1P$ system the radial integrals would be somehow stable due to the absence of the wave function nodes in both states. And the relativistic correction and the long distance effects might be small. So, by directly comparing the measured gamma transition rates from $\psi(3770)$ to $\chi_{cJ(J=0,1,2)}$ to the non-relativistic estimations in potential model, one can get some credible information about the transition mechanism. A non-relativistic calculation for the Electromagnetic transitions of $\psi(3770) \to \gamma\chi_{cJ(J=0,1,2)}$ gives the partial width [419, 420] as a function of θ_{mix}:

$$\Gamma(\psi(3770) \to \gamma\chi_{c0}) = 145\ \cos^2\theta_{mix}(1.73 + \tan\theta_{mix})^2\ \text{keV}, \tag{21.24}$$

$$\Gamma(\psi(3770) \to \gamma\chi_{c1}) = 176\ \cos^2\theta_{mix}(-0.87 + \tan\theta_{mix})^2\ \text{keV}, \tag{21.25}$$

$$\Gamma(\psi(3770) \to \gamma\chi_{c2}) = 167\ \cos^2\theta_{mix}(0.17 + \tan\theta_{mix})^2\ \text{keV}, \tag{21.26}$$

Inserting the mixing angle $\theta_{\rm mix} = (10.6 \pm 1.3)^o$ determined with the parameters of the $\psi(2S)$ and $\psi(3770)$ measured by BES [418] in the Eqs. (7–9) yields the partial widths

$$\Gamma(\psi(3770) \to \gamma\chi_{c0}) = 515 \pm 17 \quad \text{keV}$$

$$\Gamma(\psi(3770) \to \gamma\chi_{c1}) = 79 \pm 6 \quad \text{keV}$$

$$\Gamma(\psi(3770) \to \gamma\chi_{c2}) = 21 \pm 3 \quad \text{keV}$$

The partial widths are sensitive to the mixing schemes. Considering couple-channel effects and more general mixing scheme than the one given in the Eqs. (1) and (2) would affect these partial widths. A general mixing scheme [424], where the $\psi(3770)$ is composed of only 52% pure $c\bar{c}$ components, in which except the 2^3S_1 and 1^3D_1 states other 1^{--} chrmonium states in S and D waves are included, and the remainder of its wave function contains additional virtual or real charmed meson pairs, predicts the partial widths

$$\Gamma(\psi(3770) \to \gamma\chi_{c0}) = 225 \quad \text{or} \quad \textit{254} \quad \text{keV}$$

$$\Gamma(\psi(3770) \to \gamma\chi_{c1}) = 59 \quad \text{or} \quad \textit{183} \quad \text{keV}$$
$$\Gamma(\psi(3770) \to \gamma\chi_{c2}) = 3.9 \quad \text{or} \quad \textit{3.2} \quad \text{keV}$$

where the *values in italics* are the results if the influence of the open-charm channels is not included. However, if the $\psi(3770)$ is only a pure 1^3D_1 state, the partial widths would be

$$\Gamma(\psi(3770) \to \gamma\chi_{c0}) = 434 \quad \text{keV},$$
$$\Gamma(\psi(3770) \to \gamma\chi_{c1}) = 133 \quad \text{keV},$$
$$\Gamma(\psi(3770) \to \gamma\chi_{c2}) = 4.8 \quad \text{keV}.$$

So measurements of the partial widths for the EM transitions are important in the understanding of the nature of $\psi(3770)$ resonance and the potential model dynamics.

Measurements at BES III

Measuring these branching fractions are experimentally challenging. It needs to have a good electromagnetic calorimeter to reconstruct the low energy photon. CLEO Collaboration measured the partial width for $\psi(3770) \to \gamma\chi_{c1}$ to be $\Gamma(\psi(3770) \to \gamma\chi_{c1}) = 75 \pm 18$ keV, which agrees well with most of the theoretical predictions [419, 424, 425]. BES-III has a good electromagnetic calorimeter with expected energy resolution of $\sim 3\%$. With the coming BES-III detector, we can well measure the branching fractions for the transitions.

To study how well we can measure the transition rates with the BES-III detector, we generated the Monte Carlo events for $\psi(3770) \to \gamma\chi_{cJ(J=0,1,2)}$, where we set the $\chi_{cJ(J=0,1,2)}$ decay to $\pi^+\pi^-\pi^+\pi^-$, $K^+K^-\pi^+\pi^-$, $p\bar{p}\pi^+\pi^-$ and $\pi^+\pi^-\pi^+\pi^-\pi^+\pi^-$ final states. Figure 21.2 shows the distributions of the invariant masses of the combinations for the different charged particle final states. We find that the $\chi_{cJ(J=0,1,2)}$ states can be well reconstructed with the BES-III detector.

21.2.4 Hadronic transition

The predictions of $\psi(3770)$ hadronic transition

Comparing the large decay rates of $\psi(3686)$ hadronic transitions, the measurements of the hadronic transitions of $\psi(3770) \to J/\psi$ hadron(s) are important for consideration of non-$D\bar{D}$ decays of the $\psi(3770)$ and for check the hadronic transition mechanism in the potential model. Like the $\psi(3686)$ case the emitted light hadron(s) could also be $\pi^+\pi^-$, π^0 and η hadronized from emitted gluons. Other kind hadronic transitions with emitted different light hadron(s) are kinematic forbidden in energy for the $\psi(3770)$ too. Generally, the transition rates can be described as given in Ref. [422, 423, 426]

$$\Gamma(2S \to 1S) = |c_1|^2 G |f_{2S,1S}|^2, \tag{21.27}$$

$$\Gamma(1D \to 1S) = 4/15 |c_2|^2 H |f_{1D,1S}|^2, \tag{21.28}$$

in which G and H denote the phase space integrals of the two processes, $f_{A,B}$ represents the radial matrix element between the states A and B, and the c_1 and c_2 denote the

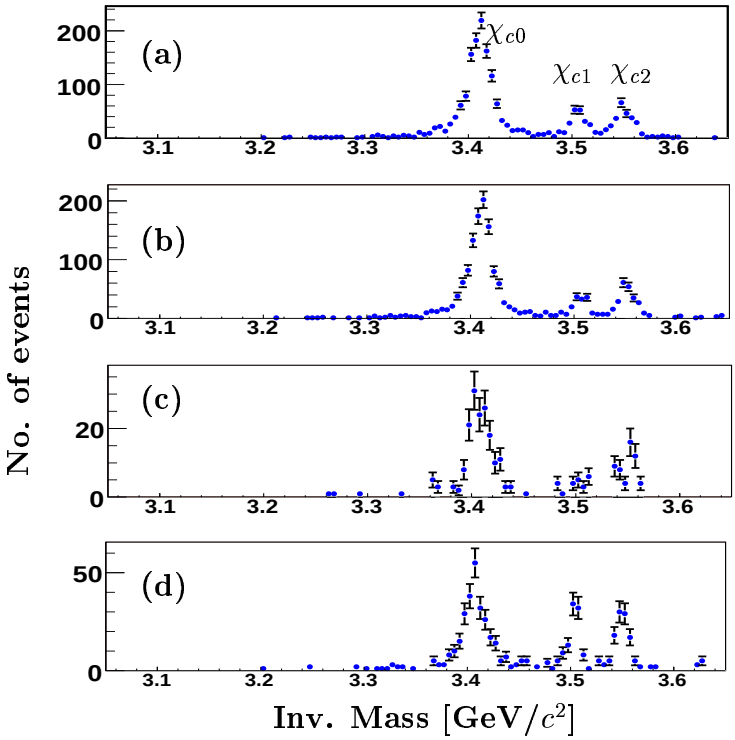

Figure 21.2: The distributions of the invariant masses of (a) $\pi^+\pi^-\pi^+\pi^-$, (b) $K^+K^-\pi^+\pi^-$, (c) $p\bar{p}\pi^+\pi^-$ and (d) $\pi^+\pi^-\pi^+\pi^-\pi^+\pi^-$ combinations, where the charged particles are coming from the $\chi_{cJ(J=0,1,2)}$ decays.

strength appear in the soft poin matrix elements of the gluon operators for S and D wave respectively. In the *S-D* mixing scheme, the partial widths for the hadronic $\pi^+\pi^-$ transitions of the two charmonium states can be obtained [426]:

$$\Gamma(\psi(3770) \to J/\psi\pi^+\pi^-) = |c_1|^2 \left[\sin^2\theta_{mix} U + \frac{4}{15}\left|\frac{c_2}{c_1}\right|^2 \cos^2\theta_{mix} V\right], \tag{21.29}$$

$$\Gamma(\psi(3686) \to J/\psi\pi^+\pi^-) = |c_1|^2 \left[\cos^2\theta_{mix} W + \frac{4}{15}\left|\frac{c_2}{c_1}\right|^2 \sin^2\theta_{mix} X\right]. \tag{21.30}$$

where $U = G_{\psi(3770)}|f_{2S,1S}(M_{\psi(3770)})|^2$, $V = H_{\psi(3770)}|f_{1D,1S}(M_{\psi(3770)})|^2$, $W = G_{\psi(3686)}|f_{2S,1S}(M_{\psi(3686)})|^2$ and $X = H_{\psi(3686)}|f_{1D,1S}(M_{\psi(3686)})|^2$. In the Eqs. (12) and (13) the values for the quantities G's, H's and $f_{A,B}$ (A=2S, 1D and B=1S), can be calculated using different models, which gave similar contribution. For example, Ref. [426] gives

$$f_{2S,1S}(M_{\psi(3686)}) = 7.018 \quad \text{GeV}^{-3}, \tag{21.31}$$

$$f_{1D,1S}(M_{\psi(3686)}) = -8.796 \quad \text{GeV}^{-3}, \tag{21.32}$$

$$f_{2S,1S}(M_{\psi(3770)}) = 8.172 \quad \text{GeV}^{-3}, \tag{21.33}$$

$$f_{1D,1S}(M_{\psi(3770)}) = 10.266 \quad \text{GeV}^{-3}, \tag{21.34}$$

$$G_{\psi(3686)} = 0.0353 \quad \text{GeV}^7, \tag{21.35}$$

$$H_{\psi(3686)} = 0.00291 \quad \text{GeV}^7, \tag{21.36}$$

$$G_{\psi(3770)} = 0.102 \quad \text{GeV}^7, \tag{21.37}$$

$$H_{\psi(3770)} = 0.00943 \quad \text{GeV}^7. \tag{21.38}$$

However, the ratios c_1/c_2 are quite different for different models [422, 423, 426]. From the decay rates of the two hadronic transitions given in Eqs. (12) and (13), we have the ratio

$$R_{\psi(3770)/\psi(3686)}(J/\psi\pi^+\pi^-) = \frac{\left[\sin^2\theta_{mix}U + \frac{4}{15}\left|\frac{c_2}{c_1}\right|^2\cos^2\theta_{mix}V\right]}{\left[\cos^2\theta_{mix}W + \frac{4}{15}\left|\frac{c_2}{c_1}\right|^2\sin^2\theta_{mix}X\right]}, \tag{21.39}$$

which can be measured in experiment. From the ratio $R_{\psi(3770)/\psi(3686)}(J/\psi\pi^+\pi^-)$ we can extract the ratio c_1/c_2.

The BES Collaboration observed the hadronic transition process $\psi(3770) \to J/\psi\pi^+\pi^-$ and measured the partial width to be $\Gamma(\psi(3770) \to J/\psi\pi^+\pi^-) = 80 \pm 33 \pm 23$ keV. Recently, CLEO confirmed the BES observation for this transition process. CLEO measured the branching fraction for $\psi(3770) \to J/\psi\pi^+\pi^-$ to be $(0.189 \pm 22^{+7}_{-4})\%$ [**?**]. Those give the weighted average partial width of $\Gamma(\psi(3770) \to J/\psi\pi^+\pi^-) = 49.0 \pm 8.4$ keV, where the error is the combined statistical and systematic errors together. The world averaged partial width for $\psi(3686) \to J/\psi\pi^+\pi^-$ process is $\Gamma(\psi(3686) \to J/\psi\pi^+\pi^-) = 89.1 \pm 6.2$ keV. These give the ratio of the partial widths

$$R_{\psi(3770)/\psi(3686)}(J/\psi\pi^+\pi^-) = 0.55 \pm 0.10. \tag{21.40}$$

Inserting θ_{mix} in Eq. (22) combining with the ratio of the partial widths yields a first measurement of the parameters of c_1 and c_2. The relation of the $R_{\psi(3770)/\psi(3686)}(J/\psi\pi^+\pi^-)$ to the ratio c_2/c_1 is plotted in Fig. 3, where the horizontal lines give the measured value of $R_{\psi(3770)/\psi(3686)}(J/\psi\pi^+\pi^-)$ and the $\pm1\sigma$ interval of the value; the vertical lines give $\pm1\sigma$ interval of the measured values of the ratio c_2/c_1. We find that the value of the ratio is

$$\frac{c_2}{c_1} = 2.08^{+0.31}_{-0.38}. \tag{21.41}$$

Inserting the solution of the ratio and the partial width $\Gamma(\psi(3770) \to J/\psi\pi^+\pi^-) = 49.0 \pm 8.4$ keV into Eq. (12), we obtain

$$c_1 = (7.25 \pm \Delta_{\text{err}}) \times 10^{-3}. \tag{21.42}$$

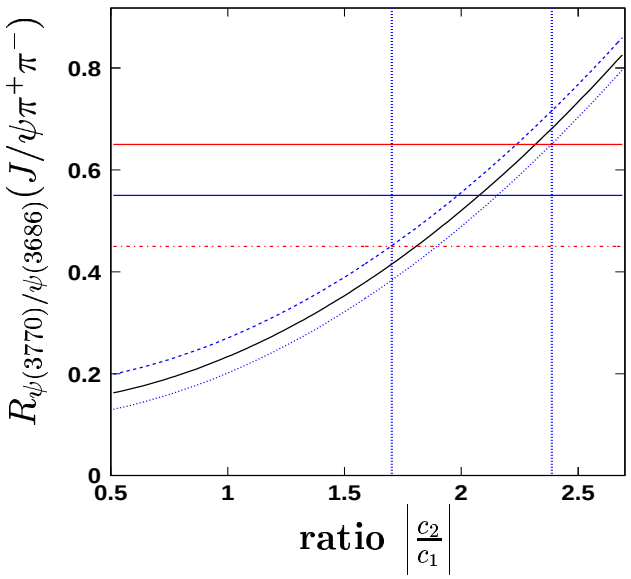

Figure 21.3: The ratio $R_{\psi(3770)/\psi(3686)}(J/\psi\pi^+\pi^-)$ of the partial widths as a function of the ratio $\left|\frac{c_2}{c_1}\right|$, where the dashed lines show the $\pm 1\sigma$ intervals of the measured quantities.

Measurements of hadronic transitions

From experimental point of view, since the mass difference between $\psi(3770)$ and J/ψ is 0.675 GeV, the typical momentum of the light hadron(s) system is low. This gives a clearly kinematics signature of the decay products with which one can easily separate the decays from most other processes. The difficult things to select these decays are how to separate the $\psi(3770)$ hadronic transitions from the same kind of $\psi(3686)$ hadronic transitions where the $\psi(3686)$ is produced due to ISR return to $\psi(3686)$ and produced at the center-of-mass energy set in the experiment. To separate the $\psi(3770)$ hadronic transitions, including $\psi(3770) \to J/\psi\pi^+\pi^-, J/\psi\pi^0\pi^0, J/\psi\eta$, one needs a precision Monte Carlo event generator to simulate these processes including the effects of ISR, and must correctly subtract the backgrounds due to the $\psi(3686)$ hadronic transitions from the candidates for the $\psi(3770)$ hadronic transitions observed in experiments. This technique of subtracting the $\psi(3686)$ background in the selected sample for $\psi(3770) \to J/\psi\pi^+\pi^-$ has been developed in analysis of BES-II data to measure the partial width for $\psi(3770) \to J/\psi\pi^+\pi^-$ [429]. The generator used in the analysis of the decay is being developed to be used in analysis of BES-III data.

21.2.5 Light hadron decays

The decay rate for $\psi(3770) \to$ light hadrons is expected small according to the theory. However, there are some models [427] to propose the origin of the non-$D\bar{D}$ decay signatures. For example, the re-annihilation amplitude of charmed meson pairs into the states containing light quarks interferes with corresponding the continuum light quark production amplitude. This re-annihilation effect may result in a significant branching fraction for the light hadron decays of $\psi(3770)$ [428]. The re-annihilation mechanisms are also

relevant for non-$K\bar{K}$ decays of the ϕ meson [428]. If this re-annihilation effect is really responsible for the non-$D\bar{D}$ decays of $\psi(3770)$, the enhanced penguin amplitudes in B decays can be explained with the similar re-annihilation effects. So experimental study of the exclusive non-$D\bar{D}$ decays of $\psi(3770)$ are important in understanding of the nature of $\psi(3770)$.

Light-hadron final states

Due to the large total width of $\psi(3770)$, the decay amplitudes of any exclusive channels can not get large amplification as those in the narrow resonance cases, the J/ψ and $\psi(3686)$. So, the corresponding amplitudes from continuum production may compete with them. In the experimental side, the most difficult things we have to consider are the possible interference between the continuum amplitude and the $\psi(3770)$ resonance decay amplitude. Due to the interference effects between the two amplitudes, it is difficult to measure the branching fractions for the exclusive light hadron decays of $\psi(3770)$ with simply considering the difference of yields observed far off $\psi(3770)$ resonance and at the peak of $\psi(3770)$. For example, the light hadron decays of $\psi(3770)$ were extensively studied by both the BES and CLEO Collaborations with the data taken at $\sqrt{s} = 3.773$ GeV and at $\sqrt{s}$ around 3.66 GeV. However, if only consider the observed cross sections for the light hadron final states at the two energies, some times one finds that, for some decay modes, the observed cross sections at $\sqrt{s} = 3.773$ GeV are less than those observed at $\sqrt{s}$ around 3.66 GeV, while, for some other decays modes, the observed cross sections at $\sqrt{s} = 3.773$ GeV are larger than those observed at $\sqrt{s}$ around 3.66 GeV. These are probably due to interference effects between the two amplitudes. Owning to these effects, one could not simply determine the branching fractions of $\psi(3770)$ light hadron decays just based on the measured cross sections at the two energy points.

To measure the branching fractions of $\psi(3770)$ light hadron decays, one should measure the cross sections for exclusive decay modes at different center-of-mass energies and fitting these cross sections to theoretical formula with taking into account the interference effects. This is probably the best method to measure the branching fractions for $\psi(3770) \to$ light hadrons, with determining the phase difference between the two amplitudes of the continuum light hadron production and the decay of $\psi(3770) \to$ light hadrons.

For some decay modes which consist of some special symmetry multiple states, say SU_3 octets, the symmetry would constrain the couplings in different ways for the different channels. Then one could fit the different couplings belong to various processes, e.g. the E-M coupling and the strong decay strength, with the observed cross sections of those channels.

The PV decays of $\psi(3770)$

The studies of the PV decay channels of $\psi(3770)$ are interesting and very important in understanding the enhancement of $\psi(3770)$ non-$D\bar{D}$ decays and the origin of the $\rho - \pi$ puzzle revealed in $\psi(3686)$ decays. The most important PV channel is the $\psi(3770) \to$ (0^{-+} octet) (1^{--} octet). CLEO has measured the production cross sections for $e^+e^- \to$ $\rho\pi$, $K^*(892)\bar{K}$, $\omega\eta$, $\omega\eta'$, $\phi\eta$, $\phi\eta'$, $\rho\eta$, $\rho\eta'$, $\omega\pi^0$ and $\phi\pi^0$ [**?**] at two center-of-mass energies

of 3.671 and 3.773 GeV. They claimed that there seem to be no evidence for which the $\psi(3770)$ decays significantly into the PV channels.

A. $\psi(3770) \to K^{*0}\bar{K}^0, K^{*\pm}K^{\mp}$, +c.c.

From the observed decay channel $\psi(3770) \to K^-\pi^+\pi^-\pi^+ +$ c.c., one can analyze two correlated modes with different charge status, i.e. $\psi(3770) \to K^{*0}\bar{K}^0 +$ c.c. with $\bar{K}^{*0} \to K^-\pi^+$ and $K^0_S \to \pi^+\pi^-$, and $\psi(3770) \to K^{*\pm}K^{\mp}$ with $K^{*\pm} \to K^0\pi^{\pm}$ and $K^0_S \to \pi^+\pi^-$ by tagging the different charge combinations of the $K^*(892)$. In this special example one can see how to determine the E-M coupling and the strong decay strength in this channel with the measurements of the two charge modes at two energy points, say at $\sqrt{s} = 3.650$ GeV which is far away from resonance and at $\sqrt{s} = 3.773$ GeV which is the peak of the $\psi(3770)$ resonance, without help from measurements of any other PV channel at all. Unlike the measurements of the most other PV channels, the observations can provide us four (not just two as others) observed numbers, which are the numbers of $K^*(892)^{\pm}K^{\mp}$ and $K^{*0}\bar{K}^0 +$ c.c. observed at the two energy points. The four observed numbers could give us four equations, and allow us to extract three unknown parameters, which are the coupling of $K^*\bar{K} +$ c.c. with γ^*, the coupling of $K^*\bar{K} +$ c.c with $\psi(3770)$ and the phase difference between them, and then finally to get the branching fraction for $\psi(3770) \to K^*(892)\overline{K} +$ c.c. and the E-M coupling for PV channel in continuum production.

With this method the BES Collaboration measured the branching fraction for the decay $\psi(3770) \to K^{*0}\bar{K}^0 +$ c.c. to be [432]

$$B(\psi(3770) \to K^{*0}\bar{K}^0 + \text{c.c.}) = (4.3^{+5.4}_{-3.4} \pm 1.3) \times 10^{-4},$$

which corresponds an upper limit on the branching fraction of

$$B(\psi(3770) \to K^{*0}\bar{K}^0 + \text{c.c.}) < 0.12\% \quad \text{at 90\% C.L.},$$

corresponding the partial width of

$$\Gamma(\psi(3770) \to K^{*0}\bar{K}^0 + \text{c.c.}) < 29 \ \text{keV} \qquad \text{at 90\% C.L.}.$$

For these two decay modes, the CLEO Collaboration observed the number of signal events at the two energy points ($\sqrt{s} = 3.671$ GeV and $\sqrt{s} = 3.773$ GeV) and measured the observed cross sections to be [**?**]

$$\mathbf{N^0_{3.773GeV} = 438} \qquad \sigma^0_{3.773\text{GeV}} = 19.1 \quad \text{pb},$$

$$\mathbf{N^0_{3.671GeV} = 38} \qquad \sigma^0_{3.671\text{GeV}} = 19.2 \quad \text{pb},$$

$$\mathbf{N^{ch}_{3.773GeV} = 4} \qquad \sigma^{ch}_{3.773\text{GeV}} = 0.09 \quad \text{pb},$$

$$\mathbf{N^{ch}_{3.671GeV} = 4} \qquad \sigma^{ch}_{3.671\text{GeV}} = 1.14 \quad \text{pb},$$

where the upper script 0 and ch mean the neutral and charged decay modes, respectively. When first looking at the numbers of the observed signal events and the values of the observed cross sections, it seems that there is no room for exist of the strong decay $\psi(3770) \to K^*(892)\bar{K} +$ c.c. due to the tiny differences between the observed cross sections at the resonance peak and off the resonance. However, the larger differences of

the cross sections observed for the two different modes at each of the two energy points may indicate that there is something behind the observations. This difference can not be explained by only the electro-magnetic coupling. What happens to this channel? One needs to consider this and gives the solution.

B. $\psi(3770) \to \rho\pi$

The partial width of this PV channel for $\psi(3770) \to \rho\pi$ decay might have a significant amount like the decay mode of $\psi(3770) \to K^*(892)\bar{K}$ mentioned above. Unfortunately BES [430] did not observe the positive signals of $\psi(3770) \to \rho\pi$ or $e^+e^- \to \rho\pi$ at the two energy points. This might be due to the lack of the data statistics. Like the mode of $K^{*\pm}K^{\mp}$, there might exist the cancellation of the two amplitudes for the E-M coupling and the strong decay in the decay of $\psi(3770) \to \rho\pi$.

C. Fit to the PV **decay of** $\psi(3770)$

Like the treatments of the PV decay channels of J/ψ and $\psi(3686)$, an important work is to measure all of the PV modes at the same time, such as $\psi(3770) \to \rho\pi$,$K^*(892)\bar{K}$, $\omega\eta$,$\omega\eta'$,$\phi\eta$,$\phi\eta'$,$\rho\eta$,$\rho\eta'$, $\omega\pi^0$ and $\phi\pi^0$, etc., and to fit all of those measured cross sections to get the information about the strong and electro-magnetic couplings, the SU_3 breaking in the decays and the mixing of $\eta - \eta'$. This kind of measurements are important in understanding of the strength of $\psi(3770)$ non-$D\bar{D}$ decays and can perhaps help in the understanding of the origin of the '$\rho\pi$' puzzle.

D. The E-M PV **decay of** $\psi(3770)$

BES has measured the production cross sections for $e^+e^- \to \omega\pi^0$, $\rho\eta$ and $\rho\eta'$ [431]. Due to isospin conservation any 1^{--} quarkonium state is only allowed to decay into $\omega\pi^0$, $\rho\eta$ and $\rho\eta'$ through its electro-magnetic coupling. However, due to the small leptonic decay width of $\psi(3770)$, the observation of the decays for $\psi(3770) \to \omega\pi^0$, $\rho\eta$ and $\rho\eta'$ is very difficult (the branching fraction is at the level of $\leq 10^{-9}$), even it is with BES-III detector at the BEPC-II collider. However, the measured cross sections for $e^+e^- \to \omega\pi^0$ ect. are meaningful, which give the form factors of those modes. These indicate the common γ^*-PV coupling of continuum hadron production in this energy region.

Monte Carlo simulation

For measurements of the branching fractions for $\psi(3770) \to$ light hadrons, we need to reconstruct the final decays of $\psi(3770)$ decays. To understand how well we can reconstruct the final states with the BES-III detector, we generated the two different kinds of the decays for $\psi(3770) \to$ light hadrons. The first kind of the decays contain only stable or long-life-time charged particles ($K^{\pm}$, $\pi^{\pm}$ and p or $\bar{p}$), and the second kind of the decays contain a sub-resonance, such as a π^0. To reconstruct the final states for the first kind of the decay, we calculate the total measured energy $E_{\rm measure}$ of the final state containing all of the charged particles. Then we calculate the ratio of the $E_{\rm measure}$ over the $E_{\rm cm}$. The most probable ratio $R = E_{\rm measure}/E_{\rm cm}$ should be around 1 for the light hadron decays of $\psi(3770)$. For the second kind of the decay modes, we simply reconstructed the π^0 from the

decay mode under study. Figure 21.4 (a), (b), (c) and (d) show the reconstructed ratio R for the final states of $\pi^+\pi^-\pi^+\pi^-$, $K^+K^-\pi^+\pi^-$, $p\bar{p}\pi^+\pi^-$ and $3(\pi^+\pi^-)$, respectively; while figure 21.4 (e), (f), (g) and (h) show the distributions of the invariant masses of the $\gamma\gamma$ combinations from the final states of $2(\pi^+\pi^-)\pi^0$, $K^+K^-\pi^+\pi^-\pi^0$, $p\bar{p}\pi^+\pi^-\pi^0$ and $3(\pi^+\pi^-)\pi^0$, respectively.

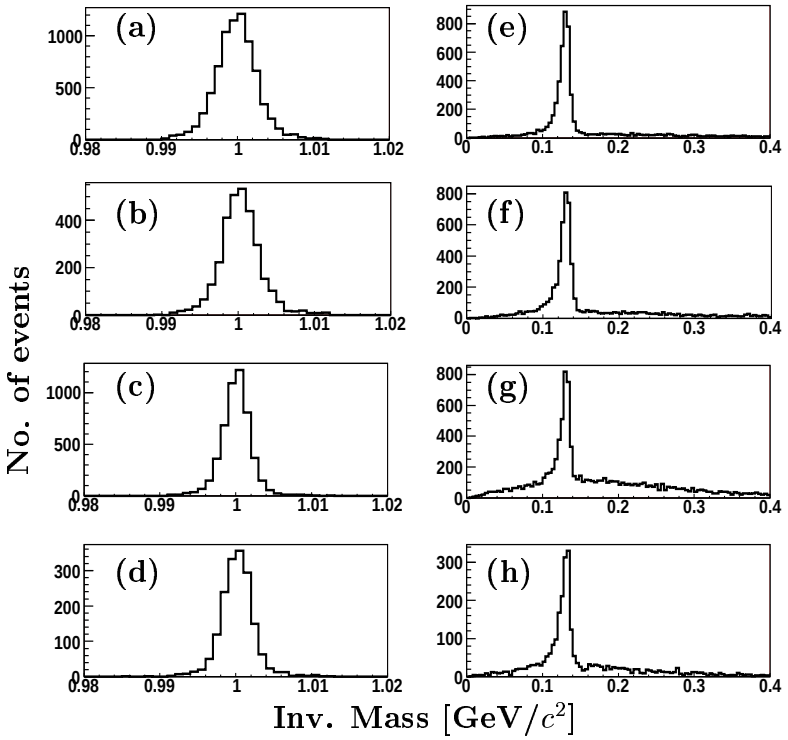

Figure 21.4: The distributions of the ratio $R = E_{\rm measure}/E_{\rm cm}$ and the invariant masses of $\gamma\gamma$ combinations, where the (a), (b), (c) and (d) show the R for the combinations of $\pi^+\pi^-\pi^+\pi^-$, $K^+K^-\pi^+\pi^-$, $p\bar{p}\pi^+\pi^-$ and $3(\pi^+\pi^-)$, respectively; while the (e), (f), (g) and (h) show the invariant masses of $\gamma\gamma$ combinations for the final states of $2(\pi^+\pi^-)\pi^0$, $K^+K^-\pi^+\pi^-\pi^0$, $p\bar{p}\pi^+\pi^-\pi^0$ and $3(\pi^+\pi^-)\pi^0$, respectively.

The Monte Carlo studies of these kind of light hadron decays and the PV decays of $\psi(3770)$ are still in progress.

21.2.6 Studies of inclusive decays

Measurement of branching fractions for $\psi(3770) \to D^0\bar{D}^0$, D^+D^-, $D\bar{D}$ and $\psi(3770) \to {\rm non}-D\bar{D}$

Recently, the BES Collaboration reported on measurements of the branching fractions for $\psi(3770) \to D^0\bar{D}^0, D^+D^-$ and the branching fraction for $\psi(3770) \to {\rm non}-D\bar{D}$. Based on analysis of two different kinds of data samples collected at $\sqrt{s} = 3.773$ GeV and at $\sqrt{s}$ around 3.66 GeV, and collected in the range from 3.65 to 3.872 GeV, BES collaboration obtained the non-$D\bar{D}$ branching fraction $B(\psi(3770) \to {\rm non}-D\bar{D}) = (16.4 \pm 7.3 \pm 4.2)\%$ [413] and $B(\psi(3770) \to {\rm non}-D\bar{D}) = (16.4 \pm 7.3 \pm 4.2)\%$ [414]. A better way to measure

Table 21.5: The input and measured branching fraction for $\psi(3770) \to \text{non} - D\bar{D}$, where the "input" means the value of the parameter set in the Monte Carlo simulation and the "measured" means the measured value of the parameters from the Monte Carlo simulation.

input/measured	$B(\psi(3770) \to D\bar{D})$ [%]	$B(\psi(3770) \to \text{non} - D\bar{D})$ [%]
input	90%	10%
measured	$88.8 \pm 2.4 \pm 2.0$	$11.2 \pm 2.4 \pm 2.0$

the branching fraction for $\psi(3770) \to \text{non} - D\bar{D}$ is to analyze the energy dependent cross sections for the inclusive hadron, $D^0\bar{D}^0$ and D^+D^- event production in the energy range covering both the $\psi(2S)$ and $\psi(3770)$ resonances, simultaneously. In this way one can also more accurately measure the parameters of the two resonances, since they are correlated to each other in the analysis of the cross section scan data.

Using the same method as that used in the measurements of the branching fractions for $\psi(3770) \to D^0\bar{D}^0$, D^+D^-, $D\bar{D}$ and non-$D\bar{D}$ [413], we study by Monte Carlo simulation how well we can measure the branching fractions with the BES-III detector at BEPC-II collider. We generated a total of 60 pb^{-1} of data at 49 energy points from 3.66 to 3.88 GeV. By analyzing these Monte Carlo events, we obtain the branching fractions for $\psi(3770) \to D\bar{D}$ and $\psi(3770) \to \text{non}-D\bar{D}$ [1]. Table 21.5 summarizes the measured branching fractions from the Monte Carlo simulation along with the branching fractions set in the Monte Carlo simulation. The errors listed in the table are the statistical and systematic, respectively. From the Monte Carlo simulation, we also obtain the measured branching fractions for the decays $\psi(3770) \to D^0\bar{D}^0$ and $\psi(3770) \to D^+D^-$ to be

$$B[\psi(3770) \to D^0\bar{D}^0] = (46.3 \pm 1.3 \pm 1.0)\%,$$

and

$$B[\psi(3770) \to D^+D^-] = (42.5 \pm 1.2 \pm 0.9)\%,$$

which correspond to the set values of the branching fractions of $B[\psi(3770) \to D^0\bar{D}^0] = 46.8\%$ and $B[\psi(3770) \to D^+D^-] = 43.2\%$ in the Monte Carlo simulation, respectively.

Figure 21.5 shows the observed cross sections for the inclusive hadron and $D\bar{D}$ production from $\psi(3770)$ decays, where the dot with errors is the observed cross section for the inclusive hadronic events from $\psi(3770)$ decays, the triangle with errors is the observed cross sections for D^+D^- from $\psi(3770)$ decays, the the triangle in change side with errors is the observed cross sections for $D^0\bar{D}^0$ from $\psi(3770)$ decays, and the square with errors is the totally observed cross sections over the neutral and the charged $D\bar{D}$ production from $\psi(3770)$ decays. The lines show the best fits to the observed cross sections.

Measurements of branching fractions for inclusive decay modes

By fitting the cross sections for the inclusive J/ψ, η, η' ... observed at different center-of-mass energies to a theoretical formula to describe the production of the inclusive final states, we can measure the branching fractions for $\psi(3770)$ decay into these final states.

[1] for detailed analysis, please read *"Measurements of 1^{--} resonance parameters and search for new 1^{--} states"* in Chapter * in Part-II.

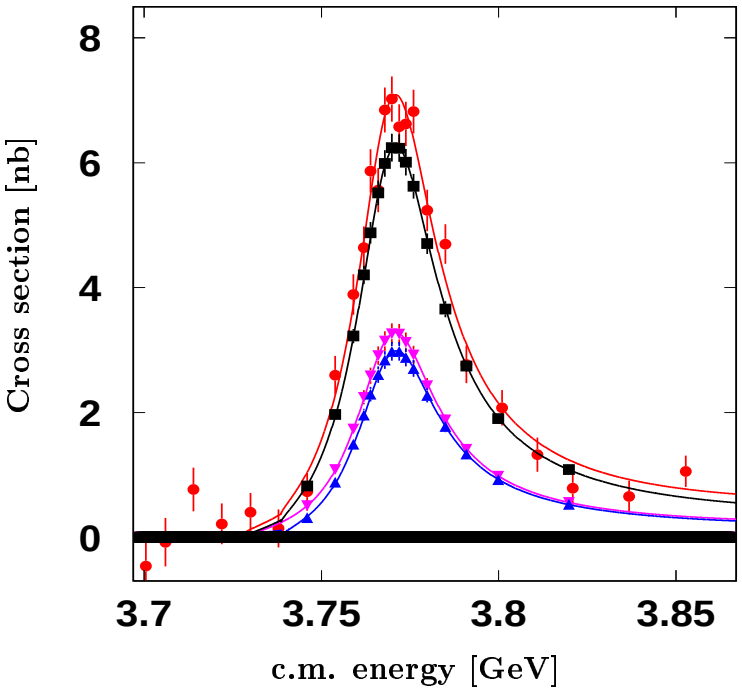

Figure 21.5: The observed cross sections versus the nominal c.m. energies.

These branching fractions are also important in the understanding of the nature of the $\psi(3770)$.

The Monte Carlo studies of these decays are still in progress.

Measurements of cross sections for $e^+e^- \to \text{hadrons}_{\text{non}-D\bar{D}}$

Another way to directly search for the non-$D\bar{D}$ decays of $\psi(3770)$ is to measure the cross section for $e^+e^- \to \text{hadrons}_{\text{non}-D\bar{D}}$, where the $\text{hadrons}_{\text{non}-D\bar{D}}$ means that the final state hadrons are not coming from the $D\bar{D}$ decays. In analysis of the cross section scan data, if we find an enhancement in the observed cross sections for the processes $e^+e^- \to \text{hadrons}_{\text{non}-D\bar{D}}$ around $\psi(3770)$ resonance, we directly observe the non-$D\bar{D}$ decays of the $\psi(3770)$ resonance. Actually, we can also examine the observed cross sections for inclusive K^0_S, K^{*0}, K^{*+} and ϕ production after removing those from $D\bar{D}$ decays. if we find an enhancement in the observed cross sections for these processes, we observe the non-$D\bar{D}$ decays of $\psi(3770)$ resonance. For these analyses, we need even more data samples taken at different center-of-mass energy.

In order to verify and calibrate the cross sections of the non-$D\bar{D}$ event production in $\psi(3770)$ resonance region, it is essentially necessary to analyze the data taken in the whole energy region covering $\psi(3686)$ resonance.

The Monte Carlo studies of these decays are still in progress.

21.2.7 Summary

In studies of the $\psi(3770)$ production in e^+e^- annihilation and its decays, there are still "puzzles" in understanding the physical $\psi(3770)$ state and its decays. What does the $\psi(3770)$ consist of and how the components of the $\psi(3770)$ affect its various non-$D\bar{D}$ decays, the γ-transition, the hadronic transition, and the different exclusive non-$D\bar{D}$ decays? It is not understood why $\psi(3770)$ decays into the non-$D\bar{D}$ final state with so large branching fraction. On the one side, the newest BES-II measurements on the branching fraction may still suffer from a large systematic shift; on the other side, if there exist some other effects or new phenomena which are responsible for the large discrepancy in the measured cross sections $\sigma^{\rm obs}_{D\bar{D}}$ and $\sigma^{\rm obs}_{\psi(3770)}$, which result in the large non-$D\bar{D}$ branching fraction. With the coming BES-III detector at BEPC-II collider, we can well measure the branching fraction for $\psi(3770) \to {\rm non}-D\bar{D}$. With about 60 pb^{-1} of data collected in the range from 3.65 to 3.88 GeV, we can measure the branching fraction at an accuracy level of 2.5%. With more data taken in $\psi(3770)$ resonance region covering $\psi(3686)$ resonance, we can extensively study the exclusive light hadron final states of $\psi(3770)$ decays and may uncover all of the "puzzles" mentioned above.

21.3 Baryonic decays

21.3.1 Introduction

The discovery of J/ψ particles [433] opens a new epoch for charmonium study. Many theoretical concepts and tools are put forth to describe the feature of charmonium decays (see the Ref. [434] for a general review). However, since the structure of baryons is more comparatively complicate than that of mesons, theoretical researches for hadronic baryon decays at present are relatively limited, moreover scattered in a variety of references. One aim of this review is at to collect the various discussions and descriptions pertinent to baryonic decays together, so that we could know what we have known about the mechanics of baryonic decays, what is unclear, what needs further exploration.

Nowadays it is believed that quantum chromodynamics (QCD) is a correct theory to describe strong interactions due to the asymptotic freedom in the high energy regime, and the theory has been successfully tested by many experiments. However, in the low energy region, perturbative methods of QCD can not be applied due to the confinement phenomenon. Since no general QCD principles could provide us with concrete prediction, and no generic suitable empirical model could be employed to calculate the decay property for a certain final state, many QCD inspired phenomenological models are put forth to explain the decay properties at charmonium region.

Recently more and more data have been collected by CLEOc and even more could be expected from further coming detector BESIII, so it provides an opportunity to test the existed predictions on baryon decays, and also provides an good opportunity to proceed extensive studies on the mechanisms of charmonium baryonic decays. So it is necessary to review the prospects both for theoretical and experimental aspects in this field. In the following sections, firstly we will briefly introduce some theoretical tools, then discuss the application of such a tool on baryonic decays.

21.3.2 Theoretical Framework

Fock expansion

Exclusive decays of J/ψ into baryon anti-baryon ($B\bar{B}$) have been investigated by many authors in the framework of perturbative QCD (pQCD) [439, 440, 441, 442], for recent review see Ref. [443]. The dominant dynamical mechanism is $c\bar{c}$ annihilation into the minimal number of gluons allowed by symmetries and subsequent creation of light quark-antiquark pairs forming the final state hadrons. The pQCD calculation is based on the factorization scheme, i.e., the non-perturbative factor of the hadronic properties is described by the wave-functions, and the hard process is described by pQCD approach as shown in Fig. 21.6. The decay amplitude is expressed as a convolution of a hard scattering amplitude and a factor that involves the charmonium wave functions for the initial state and the baryonic wave function for the final state. As shown in [444], the charmonium wave function can be organized into a hierarchy according to the scaling with the velocity of the c quark in the charmonium. The Fock expansions of the charmonium states start as:

$$\begin{aligned}
|J/\psi\rangle &= \underbrace{|c\bar{c}_1(^3S_1)\rangle}_{\mathcal{O}(1)} + \underbrace{|c\bar{c}_8(^3P_J)\, g\rangle}_{\mathcal{O}(v)} + \underbrace{|c\bar{c}_8(^3S_1)\, gg\rangle}_{\mathcal{O}(v^2)} + \ldots, \\
|\ \eta_c\ \rangle &= \underbrace{|c\bar{c}_1(^1S_0)\rangle}_{\mathcal{O}(1)} + \underbrace{|c\bar{c}_8(^1P_1)\, g\rangle}_{\mathcal{O}(v)} + \underbrace{|c\bar{c}_8(^1S_0)\, gg\rangle}_{\mathcal{O}(v^2)} + \ldots, \\
|\ \chi_{cJ}\rangle &= \underbrace{|c\bar{c}_1(^3P_J)\rangle}_{\mathcal{O}(1)} + \underbrace{|c\bar{c}_8(^3S_1)\, g\rangle}_{\mathcal{O}(v)} + \ldots,
\end{aligned} \tag{21.43}$$

where the subscripts at the $c\bar{c}$ pair specify whether it is in a color-singlet (1) or color-octet (8) state; $\mathcal{O}(1)$, $\mathcal{O}(v)$ and $\mathcal{O}(v^2)$ are the orders to which the corresponding Fock states contribute, once evaluated in a matrix element.

As shown in Ref [445], the P-wave charmonium decays into baryon anti-baryon pair are suppressed by a factor of $1/M$ relative to the S-wave charmonium decays. For the charmonium decays into $B\bar{B}$, the decay amplitude can be expressed by:

$$\mathcal{M} \sim f_c\phi_c(x) \otimes f_N\phi_N(x) \otimes f_{\bar{N}}\phi_{\bar{N}} \otimes T_H(x), \tag{21.44}$$

where T_H is the hard perturbative part, and f_i and ϕ_i are the decay constant and the hadronic wave function for charmonium and baryon/anti-baryon, respectively. It is easy to use the power counting on (21.44) to compare the S-wave charminium and P-wave charmonium, as well as the color singlet and octet contributions the decay width. For vector charmonia decays into $B\bar{B}$, the decay amplitudes are dependent on the large scale M as:

$$\begin{aligned}
\mathcal{M}_S^{(1)} &\sim M\frac{f_c^{(1)}}{M}(\frac{f_N}{M^2})^2 \sim \frac{1}{M^4}, \\
\mathcal{M}_S^{(8)} &\sim M\frac{f_c^{(8)}}{M^2}(\frac{f_N}{M^2})^2 \sim \frac{1}{M^5}.
\end{aligned} \tag{21.45}$$

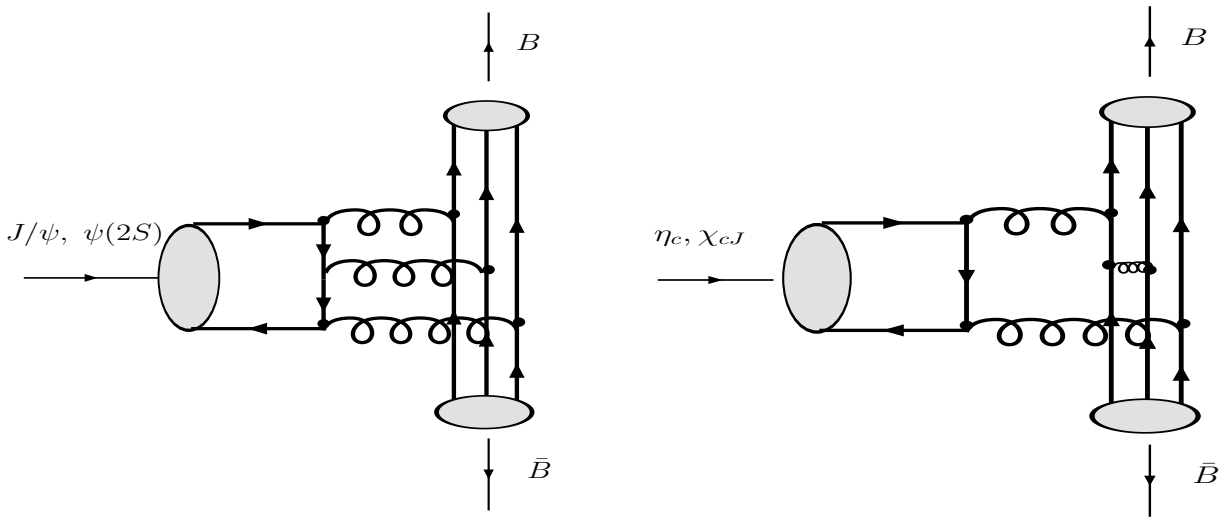

Figure 21.6: The lowest-order Feynman graphs for J/ψ or $\psi(2S)$ (left) and η_c or χ_{cJ} decays into a baryon-antibaryon pair.

For example in case of J/ψ decays into $B\bar{B}$, the color octet contribution is suppressed by energy scale $1/M$. Therefore, the color octet contribution can be neglected in the decay of a S-wave. However, for P-wave charmonium decays the color octet contribution can not be neglected. For example, the amplitudes of $\chi_{cJ} \to B\bar{B}$ are dependent on the energy scale as:

$$\mathcal{M}_P^{(1)} \sim M\frac{f_c^{(1)}}{M^2}(\frac{f_N}{M^2})^2 \sim \frac{1}{M^5},$$
$$\mathcal{M}_P^{(8)} \sim M\frac{f_c^{(8)}}{M^2}(\frac{f_N}{M^2})^2 \sim \frac{1}{M^5}. \tag{21.46}$$

For evaluation of the decay width, the hadronic information on decay constants of charmonium can be determined by the leptonic decay width. For example:

$$\Gamma(J/\psi \to e^+e^-) = \frac{4\pi}{3}\frac{e_c^2\alpha_{em}^2 f_{J/\psi}^2}{M_{J/\psi}}. \tag{21.47}$$

One gets $f_{J/\psi} = 409$ MeV,$f_{\psi(2S)} = 282$ MeV. The other soft physics information required is the leading-twist baryon distribution amplitude. In a recent analysis of the J/ψ and $\psi(2S)$ decays into baryon-antibaryon pair [446] use is made of the phenomenological proton distribution amplitude proposed in [447]

$$\Phi_{123}^p = \Phi_{AS}^B\frac{1}{2}(1+3x_1), \tag{21.48}$$

which is valid at the factorization scale $\mu_0 = 1$ GeV. This distribution amplitude goes along with the normalization parameter $f_p(\mu_0) = 6.64 \times 10^{-3}$ GeV^2. This distribution amplitude can be suitably generalized to the case of hyperons and decuplet baryon [446].

Hadronic helicity conservation

The leading-twist formation of the light hadrons in the final state has implications for their helicity configurations. As a consequence of the vector nature of QCD (and QED) time-like virtual gluons (or photons) create light, (almost) massless quarks and antiquarks in opposite helicity states, see Figure 21.7. To leading-twist accuracy such partons form the valence quarks of the light hadrons and transfer their helicities to them (see Figure 21.7). Hence, the total hadronic helicity is zero

$$\lambda_1 + \lambda_2 = 0. \tag{21.49}$$

The conservation of hadronic helicities is a dynamical consequence of QCD (and QED) which holds to leading-twist order. The violation of helicity conservation in a decay process signals the presence of higher-twist, higher Fock state and/or soft, non-factorizable contributions.

We note that hadronic helicity conservation does also not hold in η_c and χ_{c0} decays into baryon–antibaryon pairs where, in the charmonium rest frame, angular momentum conservation requires $\lambda_B = \lambda_{\overline{B}}$. A systematic investigation of higher-twist contributions to these processes is still lacking despite some attempts of estimating them, for a review see [450]. Recent progress in classifying higher-twist distribution amplitudes and understanding their properties [451, 452] now permits such analyses. The most important question to be answered is whether or not factorization holds for these decays to higher-twist order. It goes without saying that besides higher-twist effects, the leading-twist forbidden channels might be under control of other dynamical mechanisms such as higher Fock state contributions or soft power corrections.

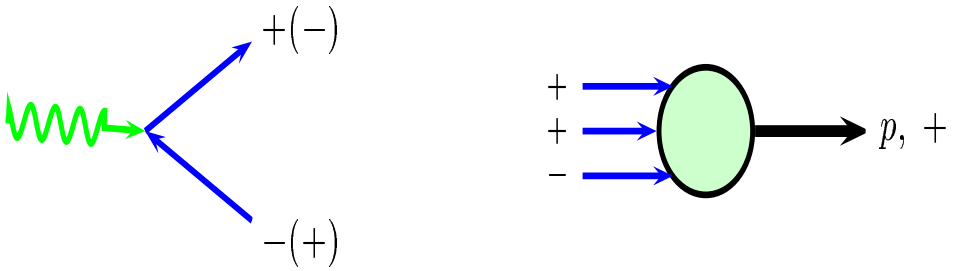

Figure 21.7: Helicity configurations in the creation of a light $q\bar{q}$ pair (left) and for a leading-twist parton–proton transition (right).

There is no reliable theoretical interpretation of these decays as yet. One proposition [464] is the use of a diquark model, a variant of the leading-twist approach in which baryons are viewed as being composed of quarks and quasi-elementary diquarks. With vector diquarks as constituents one may overcome the helicity sum rule (21.49). The diquark model in its present form, however, contends with difficulties. Large momentum transfer data on the Pauli form factor of the proton as well as a helicity correlation parameter for Compton scattering off protons are in severe conflict with predictions from the diquark model. Other phenomenological model argued that the χ_{cJ} helicity violation decays might proceed via uncommon mechanisms, such as the quark pair creation model in $\chi_{cJ} \to B\bar{B}$ decays [465] and the exchange of an intermediate state in χ_{cJ} decays [466].

Analysis based on $SU(3)$ symmetry

Under $SU(3)_{flavour}$ the baryons can be arranged in singlet, octet, and decuplet irreducible representations:

$$\mathbf{3}\otimes\mathbf{3}\otimes\mathbf{3}=\mathbf{1}_A\oplus\mathbf{8}_{M_1}\oplus\mathbf{8}_{M_2}\oplus\mathbf{10}_S\ .$$

The subscripts indicate antisymmetric, mixed-symmetric or symmetric multiplets under interchange of flavor labels of any two quarks. Each multiplet corresponds to a unique baryon number, spin, parity and its members are classified by I, I_3, and S. The lowest lying singlet, octet, and decuplet states, denoted B_1, B_8, and B_{10}, correspond to $J^P=\frac{1}{2}^-,\frac{1}{2}^+,\frac{3}{2}^+$, respectively.

In a $SU(3)$ symmetric world only the decays into final states $B_1\overline{B}_1$, $B_8\overline{B}_8$, and $B_{10}\overline{B}_{10}$ are allowed, with the same decay amplitudes for a given decay family if electromagnetic contributions are neglected. Nevertheless, the $SU(3)$ symmetry can be broken in several ways [477], so in phenomenological analysis both symmetric and symmetry-breaking terms are to be included. To simplified our discussion, we take J/ψ decays into octet-baryon pairs as an example to expound our analysis framework.

To describe $SU(3)$ octet states, it is convenient to introduce the matrix notations

$$\mathbf{B}=\begin{pmatrix}\Sigma^0/\sqrt{2}+\Lambda/\sqrt{6} & \Sigma^+ & p\\ \Sigma^- & -\Sigma^0/\sqrt{2}+\Lambda/\sqrt{6} & n\\ \Xi^- & \Xi^0 & -2\Lambda/\sqrt{6}\end{pmatrix} \tag{21.50}$$

and

$$\overline{\mathbf{B}}=\begin{pmatrix}\overline{\Sigma}^0/\sqrt{2}+\overline{\Lambda}/\sqrt{6} & \overline{\Sigma}^- & \overline{\Xi}^-\\ \overline{\Sigma}^+ & -\overline{\Sigma}^0/\sqrt{2}+\overline{\Lambda}/\sqrt{6} & \overline{\Xi}^0\\ \overline{p} & \overline{n} & -2\overline{\Lambda}/\sqrt{6}\end{pmatrix} \tag{21.51}$$

for octet baryons and antibaryons, respectively. Note the fact that, to an extremely good approximation, the J/ψ is an $SU(3)$ singlet. For the decay $J/\psi\to B\overline{B}$, to derive the consequences of $SU(3)_{flavour}$ symmetry, the $SU(3)$ multiplets containing B and $\overline{B}$ are to be combined in an $SU(3)$-invariant way. The only such an combination is

$$\mathcal{L}^0_{eff}=g\ \mathrm{Tr}(\mathbf{B}\overline{\mathbf{B}})\ , \tag{21.52}$$

where "Tr" represents the trace of matrix and the effective coupling constance g is proportional to the decay amplitude.

We now turn to the question of $SU(3)$-breaking effects. Following the recipe proposed in Ref. [520], we simulate the $SU(3)$-breaking effects by constructing an $SU(3)$-invariant amplitude involving three octets and by choosing one of the octets (called a "spurion" octet) to point in a fixed direction of $SU(3)$ space particular to the desired breaking. Two types of $SU(3)$ breaking are to be considered. First, the $SU(2)$ isospin symmetry is assumed, that is $m_u=m_d$; but $m_s\neq m_u,m_d$ and this mass difference between s and u/d quarks leads to $SU(3)$ breaking. By writing the quark mass term as

$$m_d(\overline{d}d+\overline{u}u)+m_s\overline{s}s=m_0\overline{q}q+\frac{1}{\sqrt{3}}(m_d-m_s)\overline{q}\lambda_8 q\ ,$$

where $q = (u, d, s)$; $m_0 = (2m_d + m_s)/3$ is the average quark mass; λ_8 is the 8-th Gell-Mann matrix. We see that this $SU(3)$ breaking corresponds to a spurion pointing to the 8-th direction of abstract space spanning by eight Gell-Mann matrices. Explicitly, the matrix $\mathbf{S}_m$ is introduced to describe such mass breaking effect

$$\mathbf{S}_m = \frac{g_m}{3} \begin{pmatrix} 1 & & \\ & 1 & \\ & & -2 \end{pmatrix} , \tag{21.53}$$

where g_m is effective coupling constance due to the mass difference effect.

Second, electromagnetic effects violate $SU(3)$ invariance since the photon coupling to quarks is proportional to the electric charge:

$$\frac{2}{3}\overline{u}\gamma_\mu u - \frac{1}{3}\overline{d}\gamma_\mu d - \frac{1}{3}\overline{s}\gamma_\mu s = \frac{1}{2}\overline{q}\gamma_\mu \left[\lambda_3 + \frac{\lambda_8}{\sqrt{3}}\right] q \ .$$

The above expression indicates that electromagnetic breaking can be simulated by the spurion matrix $\mathbf{S}_e$ as follows

$$\mathbf{S}_e = \frac{g_e}{3} \begin{pmatrix} 2 & & \\ & -1 & \\ & & -1 \end{pmatrix} , \tag{21.54}$$

where g_e is effective coupling constance due to the charge difference effect.

To build an $SU(3)$ invariant out of three matrices, there are two different ways of combination:

$$\mathrm{Tr}(\mathbf{B}\overline{\mathbf{B}}\mathbf{S}) \ , \quad \text{or} \quad \mathrm{Tr}(\overline{\mathbf{B}}\mathbf{B}\mathbf{S}) \ .$$

These are conventionally combined further into combinations involving the commutator and anticommutator of the two matrices and called F- and D-type[2], respectively. Therefore, the most general form of $SU(3)$ invariant effective Lagrange for three matrices is

$$\mathcal{L}_{eff} = D\ \mathrm{Tr}(\{\mathbf{B}, \overline{\mathbf{B}}\}\mathbf{S}) + F\ \mathrm{Tr}([\mathbf{B}, \overline{\mathbf{B}}]\mathbf{S}) \ , \tag{21.55}$$

Notice that $\mathbf{S}$ can either $\mathbf{S}_m$ or $\mathbf{S}_e$, together with $\mathcal{L}^0_{eff}$ for symmetric part, the synthetic Lagrange reads

$$\mathcal{L}_{eff} = g\ \mathrm{Tr}(\mathbf{B}\overline{\mathbf{B}}) + d\ \mathrm{Tr}(\{\mathbf{B}, \overline{\mathbf{B}}\}\mathbf{S}_e) + f\ \mathrm{Tr}([\mathbf{B}, \overline{\mathbf{B}}]\mathbf{S}_e) + d'\ \mathrm{Tr}(\{\mathbf{B}, \overline{\mathbf{B}}\}\mathbf{S}_m) + f'\ \mathrm{Tr}([\mathbf{B}, \overline{\mathbf{B}}]\mathbf{S}_m) \ . \tag{21.56}$$

With the expressions in Eq. (21.50), (21.51), (21.53), and (21.54) for $\mathbf{B}$, $\overline{\mathbf{B}}$, $\mathbf{S}_m$, and $\mathbf{S}_e$ respectively, the parametrization forms for octet-baryon-pair final state are worked out and presented in Table 21.6, where the coupling constants are redefined as $A = g$, $D = dg_e/3$, $F = fg_e$, $D' = dg_m/3$, and $F' = fg_m$, following the conventions in Ref. [477] and [486].

[2]The reason for the name is that the F coupling is proportional to f_{abc} while the D coupling is proportional to d_{abc}. Here d_{abc} and f_{abc} are symmetric and antisymmetric construction coefficient of Gell-mann $SU(3)$ matrixes.

Table 21.6: Amplitude parametrization forms for decays of the J/ψ into a pair of octet baryons (phase space is not included). General expressions in terms of singlet A, as well as symmetric and antisymmetric charge-breaking (D, F) and mass-breaking terms (D', F').

Final state	Amplitude parametrization form
$p\overline{p}$	$A + D + F - D' + F'$
$n\overline{n}$	$A - 2D - D' + F'$
$\Sigma^+\overline{\Sigma}^-$	$A + D + F + 2D'$
$\Sigma^0\overline{\Sigma}^0$	$A + D + 2D'$
$\Sigma^-\overline{\Sigma}^+$	$A + D - F + 2D'$
$\Xi^0\overline{\Xi}^0$	$A - 2D - D' - F'$
$\Xi^-\overline{\Xi}^+$	$A + D - F - D' - F'$
$\Lambda\overline{\Lambda}$	$A - D - 2D'$
$\Sigma^0\overline{\Lambda} + \overline{\Sigma}^0\Lambda$	$\sqrt{3}D$

Finally, we would like to add a remark concerning the treatment of charge conjugated final states. Applying the operator for charge conjugation to a baryon-antibaryon system,

$$C|B_n\overline{B}_m\rangle = |\overline{B}_nB_m\rangle \begin{cases} = |B_n\overline{B}_m\rangle & \text{for } n = m \\ \neq |B_n\overline{B}_m\rangle & \text{for } n \neq m \end{cases} , \tag{21.57}$$

generally leads to a different state. Charge conjugated states will nontheless be produced with the **same** branching ratio if **isospin** is conserved in the decay of the final state particles. We therefore adopt the convention that charge conjugated states are implicitly included in the measurement of branching ratios. In fact, the parametrization in Table 21.6 has followed such an convention.

12% rule and decay ratio

The ratio derived based on the perturbative QCD:

$$Q_h = \frac{\mathcal{B}_{\psi'\to h}}{\mathcal{B}_{J/\psi\to h}} = \frac{\mathcal{B}_{\psi'\to \ell^+\ell^-}}{\mathcal{B}_{J/\psi\to \ell^+\ell^-}} \approx (12.4 \pm 0.4)\% , \tag{21.58}$$

appears to be exist for lots of hadronic final states, but is violated severely in the $\rho\pi$ and several other decay channels. This is the so-called "$\rho\pi$ puzzle". However, the naive prediction Q_h deserves many criticism for suffering from several apparent approximations. So we will retrospect the original derivation of this Q-value to understand the assumptions underlying Eq. (21.58).

On the tree level, the decay widths of state n^3S_1 via three gluons can be calculated as [478, 479, 477]

$$\Gamma(n^3S_1 \to ggg) = \frac{40}{81} \cdot (\pi^2 - 9)\alpha_s^3(m)\frac{|\psi_n(0)|^2}{m^2} , \tag{21.59}$$

where m is constituent quark mass, and $\alpha_s^3(m)$ is the strong coupling coefficient given at energy scale m. Of course three gluons (ggg) is not a measurable final state and it materialized as light hadrons. Therefore the decay width expression used for the inclusive final state is extended to be utilized for the exclusive final state.

The detailed explanation of factor $|\psi_n(0)|$ at charmonium region can be found in Ref. [443]. A simplified explanation is as follows. Here the n^3S_1 particles are conceived as non-relativistic bound states of a charm quark and its anti-partner, whose decays into light hadrons are believed to be dominated by the annihilation of the $c\overline{c}$ pair into ggg. In order to annihilate, the c and $\overline{c}$ must have a separation of order $1/m_c$, which is much smaller than the size of the charmonium state. Thus the annihilation amplitude must be proportional to the wave function at the origin $\psi_n(\mathbf{r}=0)$.

Similarly, the leptonic decay widths for non-relativistic $c\overline{c}$ system in vector 1^{--} state to decay into $\ell^+\ell^-$ via one virtual photon can be expressed as follows [478, 479, 477]:

$$\Gamma(n^3S_1 \to \ell^+\ell^-) = \frac{64}{9}\cdot\pi\alpha^2 e_q^2 \frac{|\psi_n(0)|^2}{M_V^2} \ , \tag{21.60}$$

where M_V is the mass of vector particle in the n^3S_1 state, e_q is the charge of the relevant quark (in units of e).

For J/ψ decay, the ratio of Eq. (21.59) to (21.60) immediately gives

$$R_\Gamma^0 = \frac{\Gamma(J/\psi \to ggg)}{\Gamma(J/\psi \to \ell^+\ell^-)} = \frac{5}{72}\cdot\frac{(\pi^2-9)\alpha_s^3(m_c)}{\pi\alpha^2}\frac{M_{J/\psi}^2}{m_c^2} \ . \tag{21.61}$$

Here m_c is constituent charm quark mass. To the lowest order correction, two factors should be considered, one is for the running coupling constant α_s^3, the other for the relativistic effect. Both of them could be quantified into R_Γ^0 as:

$$R_\Gamma = R_\Gamma^0\left(1+c_\alpha\frac{\alpha_s(\mu)}{\pi}\right)\cdot\left(1+c_\beta\left\langle\frac{v^2}{c^2}\right\rangle\right) \ , \tag{21.62}$$

Notice that $\alpha_s(\mu)$ (or μ) is not equal to $\alpha_s(m_c)$ (or m_c) and the relation between two quantities can be determined under certain substraction scheme [481, 482]. Although it is reasonable to take these two factors into consideration, we will neglect their effect in the following discussion. Theoretically, there are some uncertainties not only for α_s and $\langle v^2/c^2\rangle$ but especially for c_α and c_β as well. For example, the value of α_s ranges from 0.2 to 0.3 [482] while $\langle v^2/c^2\rangle$ is around 0.23 [483]. So far as c_α and c_β are concerned, the corresponding values are estimated to be $c_\alpha = 1.6$ and $c_\beta \subset (-3.5, -2.9)$ in Ref. [482]. In Ref. [480], due to different substraction scheme $c_\alpha = 10.3$. From experiment point of view, we may argue that for J/ψ and ψ' decay, the degree of the two corrections are similar and the variation of $\alpha_s(m_c)$ (also m_c) at J/ψ and ψ' is small enough to be neglected. There is the similar expression of Eq. (21.61) for ψ', the ratio of them leads to

$$\frac{\Gamma(J/\psi \to ggg)}{\Gamma(J/\psi \to \ell^+\ell^-)}\Big/\frac{\Gamma(\psi' \to ggg)}{\Gamma(\psi' \to \ell^+\ell^-)} = \frac{M_{J/\psi}^2}{M_{\psi'}^2} \ ,$$

or

$$\frac{\mathcal{B}_{\psi'\to h}}{\mathcal{B}_{J/\psi\to h}} = \frac{\mathcal{B}_{\psi'\to \ell^+\ell^-}}{\mathcal{B}_{J/\psi\to \ell^+\ell^-}}\cdot\frac{M_{\psi'}^2}{M_{J/\psi}^2} \ .$$

Here ggg has been materialized as hadrons (h) and Γ is equivalently replaced by branching fraction. Furthermore, if the mass deference between J/ψ and ψ' is also neglected, we recover Eq. (21.58).

In the light of above narration, Q_h is really a rough ratio to depict the relation between the J/ψ and ψ' decays from theoretical point view. More detailed and quantitative analyses are needed to refine the estimation. One such a refined estimation was put forth by Chernyak [484]. Based on the investigation of asymptotic behavior of hadronic exclusive processes within the QCD framework [450], Chernyak suggest to adopt the ratio of "reduced" decay amplitudes instead of branching fractions to describe the relation between the J/ψ and ψ' decays:

$$\kappa_h \equiv \left|\frac{A'}{A}\right| = \left\{\frac{1}{f_\kappa}\cdot\frac{\mathcal{B}_{\psi'\to h}}{\mathcal{B}_{J/\psi\to h}}\right\}^{1/2} , \tag{21.63}$$

where A' and A are the "reduced" decay amplitudes of the J/ψ and $\psi' \to h$ decays; f_κ is the scaling factor:

$$f_\kappa = \frac{\mathcal{B}_{\psi'\to \ell^+\ell^-}}{\mathcal{B}_{J/\psi\to \ell^+\ell^-}}\cdot\left(\frac{M_{J/\psi}}{M_{\psi'}}\right)^{n_{eff}}\cdot\left(\frac{\xi'}{\xi}\right)^{k} . \tag{21.64}$$

Here n_{eff} is the effective index obtained by asymptotic dynamic analysis of component quarks and containing the corresponding helicity information [484]; k is kinetic index for ξ and ξ' are simply phase space factors for the J/ψ and ψ' decays. For two body decay, ξ or ξ' can be written explicitly as

$$\xi = \frac{|\mathbf{p}|}{M} = \frac{\sqrt{[M^2-(m_1+m_2)^2][M^2-(m_1-m_2)^2]}}{2M^2} ,$$

where $\mathbf{p}$ are the center-of-mass momentum of one of decay particles; M and (m_1, m_2) correspond to the masses of resonance and two decay particles, respectively. For some special decay modes, the values of n_{eff} and k are given in Ref. [484] (see Table 21.7).

Table 21.7: The values of n_{eff} and k for some kinds of the J/ψ and ψ' decay modes .

Mode	VP	VT, AP	$B\overline{B}$	PP, VV	γT	γP
n_{eff}	6	6	8	4	2	4†
k	3	1	1	2	1	3

†: the value only for $\gamma\eta$ and $\gamma\eta'$.

Although, from theoretical point of view κ_h seems more reasonable that Q_h, as commented in Ref. [485], from experimental of view the estimation of Q value affords us some clues concerning the exploration of charmonium decay dynamics. Therefore, in the following discussions Q_h and/or κ_h value will be used.

21.3.3 Two-body decays

In this section, the experiment data for baryonic decays are collected as much as possible and compared with various kinds of theoretical predictions and suggestions. For χ_{cJ}, J/ψ, and ψ', only the results on two-body decay are presented and discussed while for η_c, η_c' ψ'', and other high charmonia state, all results involving baryonic pairs are quoted since obtained measurements are rather limited.

η_c and η_c'

All experimental results up to now relevant to η_c decays into baryon-contained final state have been summarized in Table 21.8; and the results involving baryon-pair for η_c' decays are not available yet. As to the inclusive decays concerned with η_c and η_c', they will be discussed in section 21.3.5. So for η_c and η_c' decays, more work are needed both theoretically and experimentally.

Table 21.8: Experiment results of η_c decays into baryon-contained final state. The upper limits are given at 90% confidence level. $\mathcal{B}_{\eta_c\to X} = \mathcal{B}_{J/\psi,\psi'\to\gamma\eta_c,\ \eta_c\to X}/\mathcal{B}_{J/\psi,\psi'\to\gamma\eta_c}$ and the values of $\mathcal{B}_{J/\psi,\psi'\to\gamma\eta_c}$ are from PDG06 [448]; the values with $\star$ are for $\psi'\to\gamma\eta_c$ while the other for $J/\psi\to\gamma\eta_c$.

Mode	Number of events	$\mathcal{B}_{J/\psi,\psi'\to\gamma\eta_c,\ \eta_c\to X}$ $(\times10^{-4})$	$\mathcal{B}_{\eta_c\to X}$ $(\times10^{-3})$	$\mathcal{B}_{J/\psi,\psi'\to\gamma\eta_c}$ $(\times10^{-2})$	Reference
$p\overline{p}$	213 ± 33	$0.19\pm0.03\pm0.03$	1.5 ± 0.6	1.27 ± 0.36	[487]
	18 ± 6	$0.13\pm0.04\pm0.03$	$1.0\pm0.3\pm0.4$	1.27 ± 0.36	[488]
	23 ± 1	0.14 ± 0.07	1.1 ± 0.6	1.27 ± 0.36	[490]
		$0.08^{+0.08}_{-0.04}$	$2.9^{+2.9}_{-1.5}$	$0.28\pm0.06\star$	[491]
[average]			1.3 ± 0.4		[448]
$\Lambda\overline{\Lambda}$	<6	<0.25	<2	1.27 ± 0.36	[488]
			$0.87^{+0.38}_{-0.37}$		[489]
$p\overline{p}\pi^+\pi^-$		<0.05	<12	$0.28\pm0.06\star$	[491]

χ_{cJ}

The color-singlet contribution to the decays $\chi_{cJ}\to p\bar{p}$ $(J=1,2)$ has been investigated by many authors [441, 450, 453, 454]. Employing the proton distribution amplitude (Eq. 21.48) or a similar one, one again finds results that are clearly below experiment, which again signals the lack of the color-octet contributions. An analysis of the $\chi_{c1(2)}$ decays into the octet and decuplet baryons along the same lines as for the pseudoscalar meson channels [444] has been carried through by Wong [445]. The branching ratios have been evaluated from the baryon wave functions and the same color-octet χ_{cJ} wave function as in [444]. Some of the results obtained in [445] are shown and compared to experiment in Table 21.9. As can be seen from the table the results for the $p\bar{p}$ channels are in excellent agreement with experiment while the branching ratios for $\Lambda\overline{\Lambda}$ channels are much smaller

than experiment [455] although the errors are large. A peculiar fact has to be noted: the experimental $\Lambda\overline{\Lambda}$ branching ratios are larger than the proton–antiproton ones although there is agreement within two standard deviations.

Table 21.9: Comparison of theoretical and experimental branching ratios for various χ_{cJ} decays into pairs of light hadrons. The theoretical values have been computed within the modified perturbative approach, color-singlet and -octet contributions are taken into account ($B_2^\pi = B_2^\eta = B_1^K = 0$, $B_2^K = -0.1$, baryon wave functions. The branching ratios are quoted in units of 10^{-3} for the mesonic channels and 10^{-5} for the baryonic ones. Data taken from [448]. The values listed for $p\bar{p}$ branching rates do not include the most recent values $\left(27.4^{+4.2}_{-4.0} \pm 4.5\right) \cdot 10^{-5}$, $\left(5.7^{+1.7}_{-1.5} \pm 0.9\right) \cdot 10^{-5}$ and $\left(6.9^{+2.5}_{-2.2} \pm 1.1\right) \cdot 10^{-5}$ measured by BES [468] for $\chi_c 0$, χ_{c1} and χ_{c2} respectively.

process	theory	experiment
$\mathcal{B}(\chi_{c0} \to p\,\bar{p})$	–	22.4 ± 2.7
$\mathcal{B}(\chi_{c1} \to p\,\bar{p})$	6.4 [445]	7.2 ± 1.3
$\mathcal{B}(\chi_{c2} \to p\,\bar{p})$	7.7 [445]	6.8 ± 0.7
$\mathcal{B}(\chi_{c0} \to \Lambda\,\overline{\Lambda})$	–	47 ± 16
$\mathcal{B}(\chi_{c1} \to \Lambda\,\overline{\Lambda})$	3.8 [445]	26 ± 12
$\mathcal{B}(\chi_{c2} \to \Lambda\,\overline{\Lambda})$	3.5 [445]	34 ± 17

The present analyses of the χ_{cJ} decays suffer from the rough treatment of the color-octet charmonium wave function. As we mentioned before a reanalysis of the decays into the PP and $B\overline{B}$ channels as well as an extension to the VV ones is required. Our knowledge of the color-octet wave function has been improved recently due to the intense analyses of inclusive processes involving charmonia, e.g. [456]. This new information may be used to ameliorate the analysis of the $\chi_{cJ} \to PP, B\overline{B}$ decays and, perhaps, to reach a satisfactory quantitative understanding of these processes. We finally want to remark that the color-octet contribution does not only play an important role in the χ_{cJ} decays into PP and $B\overline{B}$ pairs but potentially also in their two-photon decays [457, 458, 459].

The leading-twist forbidden $\chi_{c0} \to B\overline{B}$ decays have sizeable experimental branching ratios, see Table 21.9. There is no reliable theoretical interpretation of these decays as yet. One phenomenological model argued that the quark-pair creation mechanism has a large contribution to these helicity violation decays [465]. It is assumed that the the $c\bar{c}$ quarks annihilate into two gluons, then, the two gluons are materialized into two quark-antiquark pairs. Due to the quark-gluon coupling, another quark pair is allowed to be created from QCD vacuum with the quantum number $J^{PC} = 0^{++}$, thereafter, the three (anti)quarks hadronize into the outgoing (anti)baryon. It is found that the quark pair creation mechanism, together with the $SU(3)_f$ symmetry breaking effect, the calculated branching fractions for $\chi_{cJ} \to \Lambda\bar{\Lambda}$ are comparable with the measured values.

In experimental aspects, the test of the color octet contribution needs a comparison between a reliably theoretical calculation and measurements of the decay width or other

observables, such as the information of helicity amplitudes and angular distributions and so on. More experiments on the charmonium decays into baryon anti-baryon pair are expected for determining the color octet wave function.

J/ψ and ψ'

The experimental data of two-body baryonic decays for the J/ψ and ψ' are summarized in Table 21.10. The Q_h and κ_h defined in Eq. (21.58) and (21.63) are also presented. Consulting Table 21.10, we can see for baryonic decay, Q_h is consistent with 12% rule fairly well within the corresponding error. The scaling factor defined Eq. (21.64) calculated for final states with Q_h values ranges from 3.3 to 4.6, the corresponding κ_h value is almost a constant around 2. All these indicate that the dynamics of baryonic decay is dominated by strong interaction which could be described by pQCD at the J/ψ and ψ' regions fairly well. This point will be further confirmed by the following amplitudes analysis.

As discussed in section 21.3.2, the two-body octet baryonic decay can be parametrized by five quantities, that is A (strong amplitude survives in the limit of exact $SU(3)$), D, F (the symmetric and antisymmetric charge-breaking amplitudes), D', F' (the symmetric and antisymmetric mass-breaking amplitudes), the special forms for different decay modes have been listed in Table 21.6. Anyway, these five amplitudes could principally be complex arguments, each with a magnitude together with a phase, so there are totally ten parameters which are two many for nine decay baryonic modes. Thus, we have to adopt some assumptions to make our fit practical.

1. The isospin-violating decay $J/\psi \to \Sigma^0\overline{\Lambda} + \overline{\Sigma}^0\Lambda$ is proportional to D, as indicated by the data of Table 21.10, the branching fraction for this channel is at least one order of magnitude smaller than the others. Accordingly, we set $D = 0$ which means this amplitude is negligible[3].

2. There is not relative phases between the strong-originated amplitudes such as A, D', and F'.

On the strength of above assumptions, the parametrization forms are given in Table 21.11 where A, D, F, D', and F' are real numbers now. In addition, there is another point should be noted here. The parametrization forms in Table 21.6 and 21.11 do no include the phase space effect. This effect could be eliminated by the so-called "reduced" branching fraction, which is defined as follows

$$\tilde{\mathcal{B}} = \mathcal{B}/PSF_2 \ ,$$

where PSF_2 is the phase space factor for two-body decay (the exact definition and calculation formula could be found in Appendix **??**, Eq. (**??**).). The reduced branching fractions are calculated based on the definition and data Table 21.10, the results are tabulated in Table 21.11. With the information and the corresponding parametrization forms, we do the fit and present the results in the Table 21.12.

By virtue by Table 21.12, we could notice the following points

[3]So experimentally, it is important to measurement the final state $\Sigma^0\overline{\Lambda} + \overline{\Sigma}^0\Lambda$, even the determination of an upper limit is very useful for phenomenological or theoretical analysis.

Table 21.10: Experimental data [448] of two-body baryonic decays for the J/ψ and ψ'. The Q_h and κ_h defined in Eq. (21.58) and (21.63) respectively, are also listed. The upper limits are given at 90% C.L.

Mode	$\mathcal{B}_{J/\psi\to B\overline{B}}$ (10^{-3})	$\mathcal{B}_{\psi'\to B\overline{B}}$ (10^{-4})	Q_h (%)	κ_h (%)
$p\overline{p}$	2.17 ± 0.08	2.65 ± 0.22	12.2 ± 1.1	1.91 ± 0.09
$n\overline{n}$	2.2 ± 0.4	–	–	–
$\Sigma^+\overline{\Sigma}^-$	–	2.6 ± 0.8	–	–
$\Sigma^0\overline{\Sigma}^0$	1.31 ± 0.10	2.1 ± 0.7	16.0 ± 5.5	2.09 ± 0.36
$\Sigma^-\overline{\Sigma}^+$	–	–	–	–
$\Xi^0\overline{\Xi}^0$	–	2.8 ± 0.9	–	–
$\Xi^-\overline{\Xi}^+$	0.9 ± 0.2	1.5 ± 0.7	16.7 ± 8.2	2.01 ± 0.52
$\Lambda\overline{\Lambda}$	1.54 ± 0.19	2.5 ± 0.7	16.2 ± 5.0	2.14 ± 0.33
$\Sigma^0\overline{\Lambda} + \overline{\Sigma}^0\Lambda$	< 0.15	–	–	–
$\Delta(1232)^{++}\overline{\Delta}(1232)^{--}$	1.10 ± 0.29	1.28 ± 0.35	11.6 ± 4.5	1.76 ± 0.34
$\Delta(1232)^+\overline{p}$	< 0.1	–	–	–
$\Sigma(1385)^-\overline{\Sigma}(1385)^+$ (or c.c.)	1.03 ± 0.13	1.1 ± 0.4	10.7 ± 4.2	1.53 ± 0.30
$\Sigma(1385)^-\overline{\Sigma}^+$ (or c.c.)	0.31 ± 0.05	–	–	–
$\Sigma(1385)^0\overline{\Lambda}$	< 0.2	–	–	–
$\Xi(1530)^0\overline{\Xi}(1530)^0$	–	< 0.81	–	–
$\Xi(1530)^0\overline{\Xi}^0$	0.32 ± 0.14	–	–	–
$\Xi(1530)^-\overline{\Xi}^+$	0.59 ± 0.15	–	–	–
$\Omega^-\overline{\Omega}^+$		< 0.73		

Table 21.11: The results of two-body octet baryonic final state on the reduced branching ratio $\tilde{\mathcal{B}}$ are compared with the parametrization of the squared amplitude described in the text. The numbers in the parentheses are the calculated results with fitted parameters given in Table 21.12 for $\phi = -90°$.

Final state	Parametrization	$\tilde{\mathcal{B}}_{J/\psi}$	$\tilde{\mathcal{B}}_{\psi'}(10^{-1})$
$p\overline{p}$	$\lvert A + e^{i\phi}(D+F) - D' + F'\rvert^2$	$1.29 \pm 0.05(1.30)$	$1.46 \pm 0.13(1.47)$
$n\overline{n}$	$\lvert A - e^{i\phi}(2D) - D' + F'\rvert^2$	$1.31 \pm 0.24(1.31)$	$-$ (1.11)
$\Sigma^+\overline{\Sigma}^-$	$\lvert A + e^{i\phi}(D+F) + 2D'\rvert^2$	$-$ (0.96)	$1.61 \pm 0.50(1.62)$
$\Sigma^0\overline{\Sigma}^0$	$\lvert A + e^{i\phi}(D) + 2D'\rvert^2$	$0.97 \pm 0.07(0.97)$	$1.31 \pm 0.46(1.25)$
$\Sigma^-\overline{\Sigma}^+$	$\lvert A + e^{i\phi}(D-F) + 2D'\rvert^2$	$-$ (0.99)	$-$ (1.04)
$\Xi^0\overline{\Xi}^0$	$\lvert A - e^{i\phi}(2D) - D' - F'\rvert^2$	$-$ (0.79)	$1.89 \pm 0.61(1.58)$
$\Xi^-\overline{\Xi}^+$	$\lvert A + e^{i\phi}(D-F) - D' - F'\rvert^2$	$0.82 \pm 0.18(0.81)$	$1.02 \pm 0.48(1.34)$
$\Lambda\overline{\Lambda}$	$\lvert A - e^{i\phi}(D) - 2D'\rvert^2$	$1.05 \pm 0.13(1.06)$	$1.49 \pm 0.42(1.36)$
$\Sigma^0\overline{\Lambda} + \overline{\Sigma}^0\Lambda$	$\lvert\sqrt{3}D\rvert^2$	$-$ (0.00)	$-$ (0.00)

Table 21.12: Fit results for two-body baryonic decay. The parametrization forms and data are give in Table 21.11. The $\star$ indicate the phase value is fixed in the fit.

Parameter	J/ψ decay		ψ' decay	
A	1.008 ± 0.029	1.008 ± 0.029	1.132 ± 0.096	1.143 ± 0.105
D'	-0.010 ± 0.016	-0.010 ± 0.016	-0.023 ± 0.053	-0.013 ± 0.051
F'	0.127 ± 0.110	0.127 ± 0.114	-0.167 ± 0.181	-0.103 ± 0.157
F	0.008 ± 0.107	0.020 ± 0.249	-0.221 ± 0.207	-0.290 ± 0.316
ϕ	-91.12 ± 3.675	$-90\star$	-91.11 ± 2.505	$-90\star$
χ^2	4.3×10^{-3}	4.0×10^{-3}	0.4	0.4

- The absolute values of D', F', and F are much smaller than that of A, which means the breaking effect, whatever charge-breaking (D, F) or mass-breaking (D', F'), is weak for baryonic decay at the J/ψ and ψ' regions. In addition, the antisymmetric breaking effect is about one order of magnitude stronger that that of symmetric effect.

- The phase between strong and electromagnetic amplitude is almost $-90°$ from free parameter fit for both the J/ψ and ψ' decays. This large phase result is consistent with previous analysis [492], also consists with the analyses for two-body mesonic decays, such $1^+0^-(90°)$ [493], 1^-0^- $(106 \pm 10)°$ [494, 495], 1^-1^- $(138 \pm 37)°$ [496, 495, 477], 0^-0^- $(89.6 \pm 9.9)°$ [496, 495, 477] and so on. Moreover, the fit results also support the universal phase proposed in Ref. [497].

- The electromagnetic breaking effect (due to value F) is much stronger at the ψ' region than that at the J/ψ region. This phenomenon has been noticed in analysis of $\psi' \to K^*(892)\overline{K} + c.c.$ decays [498].

Using the fit parameters, the reduced branching fractions are calculated and results are given in Table 21.11. Since enough parameters can be used to adjust, the calculated branching fractions agree with experimental values fairly well as we expect. Moreover, some branching fractions have not be measured are also calculated which provide predictions for further experimental searching.

Now we turn to another aspect of comparison between theoretical predictions and experimental measurements. As mentioned in section 21.3.2, the decay width of J/ψ (or ψ') can be calculated with information of hadronic distribution amplitude. In Ref. [446], the modified perturbative approach is adopted, where quark transverse momenta are retained and Sudakov suppressions, comprising those gluonic radiative corrections not included in the evolution of the distribution amplitude, are taken into account. The advantage of the modified perturbative approach is the strong suppression of the soft end-point regions where the pQCD can not be applied.

The evaluation of the $J/\psi \to B\bar{B}$ via the hard process $c\bar{c} \to 3g^* \to 3(q\bar{q})$ is made in [446] and listed in Table 21.13. The theoretical values are in good agreement with the measured values within errors [4]. Anyway, predictions of the absolute value of a

[4] In Ref. [446], the decay widths of $\psi' \to B\bar{B}$ are also presented, which are actually scaled results by as-

Table 21.13: Comparison between theoretical evaluation [446] and experimental data [448] (or refer to Table 21.10). Here the branching fractions are transformed into decay widths by using $\Gamma_{J/\psi} = (93.4 \pm 2.1)$ keV [448]. $\mathcal{R} \equiv \Gamma_{B\bar{B}}/\Gamma_{p\overline{p}}$.

Mode	$\Gamma_{the.}$ (eV)		$\Gamma_{exp.}$ (eV)	$\mathcal{R}_{the.}$	$\mathcal{R}_{exp.}$
	$m_s = 150$ MeV	$m_s = 350$ MeV			
$p\overline{p}$	174	174	203 ± 9	1	1
$\Sigma^0\overline{\Sigma}^0$	128	113	122 ± 10	0.649	0.604 ± 0.052
$\Lambda\overline{\Lambda}$	133	117	144 ± 19	0.672	0.710 ± 0.092
$\Xi^-\overline{\Xi}^+$	92.8	62.5	84 ± 19	0.359	0.415 ± 0.094
$\Delta^{++}\overline{\Delta}^{--}$		105	103 ± 28	0.603	0.507 ± 0.135
$\Sigma^{*-}\overline{\Sigma}^{*+}$		66.1	96 ± 13	0.380	0.475 ± 0.065

decay width are subject to many uncertainties [446] while the ratios of any two $B\bar{B}$ decay widths are robust since most of the uncertainties cancel to a large extent. So the ratios of branching fractions (normalized by $p\overline{p}$ final state) are also presented in Table 21.13. Although the good agreement can be seen for both absolute decay widths and relative ratios, there still exist 10% to 20% difference between the theoretical and experimental values. Here the results from amplitude analysis should be noted, where the electromagnetic breaking effect is at the level of 10% to 20%. Moreover, the relative phase between strong and electromagnetic interaction is around -90° is also the crucial information for improvement of calculation in Ref. [446].

Table 21.14: Angular distribution parameter α for $J/\psi \to B\bar{B}$ decays. They are assumed to be the form of $dN/d\cos\theta \propto 1 + \alpha\cos^2\theta$.

		Calculated value of α	
Decay mode	Measured value of α	Ref. [460]	Ref. [461]
$J/\psi \to p\bar{p}$	0.68 ± 0.06[435]	1	0.69
$J/\psi \to \Lambda\bar{\Lambda}$	0.65 ± 0.11[436]	1	0.51
$J/\psi \to \Sigma\overline{\Sigma}$	-0.24 ± 0.20[436]	1	0.43
$J/\psi \to \Xi^-\bar{\Xi}^+$	-0.13 ± 0.59[437]	1	0.27
$\psi' \to p\bar{p}$	0.67 ± 0.16[438]	1	0.80

Last but not least is the measurement of the angular distribution for the process $e^+e^- \to (J/\psi \text{ or } \psi') \to B_8\overline{B}_8$, which takes the form:

$$\frac{d\Gamma}{d\cos\theta} \propto 1 + \alpha\cos^2\theta, \tag{21.65}$$

where θ is the angle between the out-going baryon and the e^+e^- beam. Table 21.14 summarizes the measured angular distribution parameters and comparison with theoretical

sumption of 12% rule. In another word, the consistence between theoretical evaluations and experimental measurements for ψ' decay depends on those of J/ψ and the validity of 12% rule.

predictions. The value $\alpha = 1$ is predicted in the limit of the helicity conservation which is prominently violated for $J/\psi \to \Sigma\overline{\Sigma}$ and $\Xi^-\bar{\Xi}^+$ modes, where not only the magnitude is smaller the expected but also the sign of the value is contradict against the prediction. This violation has been modelled as a constituent quark [461, 462] and/or hadron mass effect [463], final state interactions [467], both the effects are part of the $\mathcal{O}(v^2)$ and high-twist/power corrections. Also electromagnetic effects in α have been investigated.

ψ'' and other high charmonia state

The only measurement for two-body baryonic decays of ψ' is the search for $\Lambda\bar{\Lambda}$ using 55.8 pb^{-1} data on the peak of the ψ'' and 20.70 pb^{-1} data at continuum ($\sqrt{s}$=3.67 GeV) by CLEOc [499]. With no significant signal observed, the upper limit is set as

$$\mathcal{B}(\psi'' \to \Lambda\bar{\Lambda}) < 1.2 \times 10^{-4},$$

at 90% C.L.

Since the mass of high charmonia state (the ψ-family member with mass above ψ'') is above the threshold for open charm production, the $B\bar{B}$ decay widths are likely to be every small and it is hardly conceivable that they will be measured. Therefore, up to now neither attempts have been made nor reports have been obtained for high charmonia state decay into baryon-pair-contained final state [5].

[5] The only exception is for $Y(4260)$, the upper limit at 90% C.L. is reported: $\mathcal{B}(Y \to p\bar{p})/\mathcal{B}(Y \to \pi^+\pi^- J/\psi) < 13\%$.

21.3.4 Three-body decays

Comparing with two-body decay, the theoretical analysis relevant to three-body decay becomes more difficult and only special final states have been discussed phenomenologically [506]. Anyway, the theoretical interest in baryon-contained final states are revived due to recent experimental discoveries, especially about the enhancement phenomena of baryon-anitbaryon invariant mass near their threshold. So in the next section, discussed firstly are the phenomenological explanations and their implications for experimental search about baryon-anitbaryon invariant mass enhancements, then some special analyses will be mentioned.

Baryon-antibaryon enhancement

1. Baryon-antibaryon nonet

   In charmonium decays, $p\overline{p}$ and $p\overline{\Lambda}$ enhancements are observed in $J/\psi \to \gamma p\overline{p}$ [507], $\psi' \to \pi^0 p\overline{p}$, $\eta p\overline{p}$ [508], and $J/\psi \to p\overline{\Lambda}K^- + c.c.$ [509], as well as in $\psi' \to p\overline{\Lambda}K^- + c.c.$ decays [509] by BES collaboration. In B decays, many baryon-antibayron-pair-contained final states have been measured by CLEO, Belle and BABAR collaborations, such as $B^\pm \to p\overline{p}K^\pm$ [510], $B^0 \to p\overline{\Lambda}\pi^-$ [511], $B^+ \to \Lambda\overline{\Lambda}K^+$ [512], $B^0 \to D^{*-}p\overline{n}$ [513], $\overline{B^0} \to D^{*0}p\overline{p}$, $D^0 p\overline{p}$ [514], $B^+ \to p\overline{p}\pi^+$, $p\overline{p}K^{*+}$, $B^0 \to p\overline{p}K^0$ [515], $B^0 \to \overline{D}^{*0}p\overline{p}$, $\overline{D}^0 p\overline{p}$ [516], and so on, with observed enhancements in $p\overline{p}$, $p\overline{\Lambda}$ and $\Lambda\overline{\Lambda}$ mass spectra. Except for the enhancement in $J/\psi \to \gamma p\overline{p}$, which is claimed to be very narrow and below the $p\overline{p}$ mass threshold, all other states are slightly above the baryon antibaryon mass threshold and the widths are a few ten to less than 200 MeV/c^2.

   Intend to interpret various enhancements in a unifrom framework, enlightened by the Fermi-Yang-Sakata (FYS) model [518, 519], Yuan, Mo and Wang (YMW) suggest a nonet scheme to accommodate the baryon-antibaryon enhancements observed in charmonium and B decays [517]. In the YMW scheme, the baryon and antibaryon are presumably bounded together by the residual force between the strong interaction of the quarks and gluons inside the baryon or antibaryon. On one hand, the masses of the three-quark systems (the baryon and the antibaryon) increase by a small amount due to the residual forces required to form the bound state; on the other hand, the binding energy between the two three-quark systems decreases the mass of the baryon-antibaryon system to lower than the sum of the masses of the three-quark systems, but very close to the baryon-antibaryon mass threshold. This supplies a phenomenological surmise.

   Similar to the $SU(3)$ quark-antiquark nonets, YMW postulate the existence of special octets and singlets (nonets) whose elements are baryon-antibaryon bound states, as shown in Fig. 21.8. The following study is limited to the low-mass baryons: p, n and Λ. For a baryon-antibaryon bound state, its quantum numbers are obtained in the following way:

   - Its spin (S) is 0 or 1, from the addition of the component baryons.

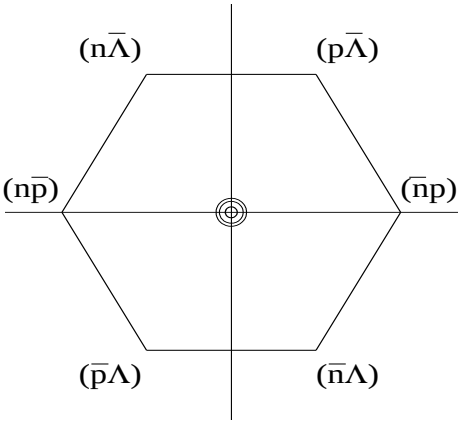

Figure 21.8: Baryon-antibaryon nonet. The J^P of this nonet is either 0^- or 1^-. The three circles in the figure indicate the following three states: $(n\overline{n} - p\overline{p})/\sqrt{2}$, $(n\overline{n}+p\overline{p}-2\Lambda\overline{\Lambda})/\sqrt{6}$, and $(n\overline{n}+p\overline{p}+\Lambda\overline{\Lambda})/\sqrt{3}$.

Table 21.15: Quantum numbers of baryon-antibaryon nonet with $J^P = 0^-$ or 1^-. I is isospin, I_3 is the third component of I, $\mathcal{S}$ is the strangeness and Q is the charge of the state. The column "symbol" gives nomenclature of the 0^- and 1^- states for easy reference in the Letter.

state	I(I_3)	$\mathcal{S}$	Q	Symbol
$(p\overline{n})$	1(+1)	0	+1	π_B^+/ρ_B^+
$(n\overline{p})$	1(−1)	0	−1	π_B^-/ρ_B^-
$\frac{(n\overline{n}-p\overline{p})}{\sqrt{2}}$	1(0)	0	0	π_B^0/ρ_B^0
$(p\overline{\Lambda})$	$\frac{1}{2}(+\frac{1}{2})$	+1	+1	K_B^+/K_B^{*+}
$(n\overline{\Lambda})$	$\frac{1}{2}(-\frac{1}{2})$	+1	0	K_B^0/K_B^{*0}
$(\overline{n}\Lambda)$	$\frac{1}{2}(+\frac{1}{2})$	−1	0	$\overline{K}_B^0/\overline{K}_B^{*0}$
$(\overline{p}\Lambda)$	$\frac{1}{2}(-\frac{1}{2})$	−1	−1	$K_B^-/\overline{K}_B^{*-}$
$\frac{(n\overline{n}+p\overline{p}-2\Lambda\overline{\Lambda})}{\sqrt{6}}$	0(0)	0	0	η_B^8/ω_B^8
$\frac{(n\overline{n}+p\overline{p}+\Lambda\overline{\Lambda})}{\sqrt{3}}$	0(0)	0	0	η_B^1/ω_B^1

- The parity is $(-1)^{L+1}$, where L is the orbital angular momentum between the baryon and the antibaryon. In case of S-wave ($L = 0$), the parity is odd ($-$), while for P-wave, the parity is even ($+$).
- For pure neutral system, such as $n\overline{n}$, $p\overline{p}$, or $\Lambda\overline{\Lambda}$, the C-parity is $(-1)^{L+S}$. For charged members, we define the generalized C-parity [520] by the neutral member of the nonet, but under C-parity transformation, the particle changes into its anti-particle.

The property of the S-wave spin-singlet states ($J^P = 0^-$) or the S-wave spin-triplet states ($J^P = 1^-$) nonet is summarized in Table 21.15, which leads to the relation of their production rates in experiments. For simplicity, we assign the particles in the nonets the same names as the meson nonets formed by quark-antiquark, but with a subscript B for distinction. For example, the 0^- isospin vector states are denoted as π_B^+, π_B^0, and π_B^-, while the 1^- strange particles are referred to as K_B^{*0}, K_B^{*+}, and their anti-particles. In general, there is mixing between the eighth component of the $SU(3)$ octet and the $SU(3)$ singlet. Since the masses of proton and neutron differ by only 1.3 MeV/c^2, but the mass of Λ is 177 MeV/c^2 greater, one is invited to assume ideal mixing between them, thus one is pure $(p\overline{p} + n\overline{n})$ and the other is pure $\Lambda\overline{\Lambda}$. This is to be verified by experiments.

Table 21.16: Decay modes containing baryon-antibaryon nonets in charmonium decays. The first J^P is for the accompanying particle while the second for the baryon-antibaryon resonance.

	decay mode	Note
$1^-\&0^-$	$\rho^0(p\overline{p})$, $\rho^+(n\overline{p})$, $\rho^-(p\overline{n})$	
	$K^{*+}(\overline{p}\Lambda)$, $K^{*-}(p\overline{\Lambda})$	$*$
	$K^{*0}(\overline{n}\Lambda)$, $\overline{K}^{*0}(n\overline{\Lambda})$	$*$
	$\omega(p\overline{p})$	
	$\phi(\Lambda\overline{\Lambda})$	$*$
$1^+\&0^-$	$b_1^0(1235)(p\overline{p})$	$*$
	$b_1^+(1235)(n\overline{p})$, $b_1^-(1235)(p\overline{n})$	$*$
	$h_1(1170)(p\overline{p})$, $h_1(1170)(\Lambda\overline{\Lambda})$	$*$
	$K_1^+(1270)(\overline{p}\Lambda)$, $K_1^-(1270)(p\overline{\Lambda})$	$*$
	$K_1^0(1270)(\overline{n}\Lambda)$, $\overline{K}_1^0(1270)(n\overline{\Lambda})$	$*$
	$K_1^+(1400)(\overline{p}\Lambda)$, $K_1^-(1400)(p\overline{\Lambda})$	$*$
	$K_1^0(1400)(\overline{n}\Lambda)$, $\overline{K}_1^0(1400)(n\overline{\Lambda})$	$*$
$0^-\&1^-$	$\pi^0(p\overline{p})$, $\pi^+(n\overline{p})$, $\pi^-(p\overline{n})$	
	$K^+(\overline{p}\Lambda)$, $K^0(\overline{n}\Lambda)$	
	$K^-(p\overline{\Lambda})$, $\overline{K}^0(n\overline{\Lambda})$	
	$\eta(p\overline{p})$, $\eta(\Lambda\overline{\Lambda})$	
	$\eta'(p\overline{p})$, $\eta'(\Lambda\overline{\Lambda})$	$*$
$0^+\&1^-$	$a_0^0(980)(p\overline{p})$	
	$a_0^+(980)(n\overline{p})$, $a_0^-(980)(p\overline{n})$	
	$a_0^0(1450)(p\overline{p})$	$*$
	$a_0^+(1450)(n\overline{p})$, $a_0^-(1450)(p\overline{n})$	$*$
	$f_0(980)(p\overline{p})$, $f_0(980)(\Lambda\overline{\Lambda})$	
	$f_0(1370)(p\overline{p})$, $f_0(1370)(\Lambda\overline{\Lambda})$	$*$
	$K_0^{*+}(1430)(\overline{p}\Lambda)$, $K_0^{*-}(1430)(p\overline{\Lambda})$	$*$
	$K_0^{*0}(1430)(\overline{n}\Lambda)$, $\overline{K_0}^{*0}(1430)(n\overline{\Lambda})$	$*$
$1^+\&1^-$	$a_1^0(1260)(p\overline{p})$	$*$
	$a_1^+(1260)(n\overline{p})$, $a_1^-(1260)(p\overline{n})$	$*$
	$f_1(1285)(p\overline{p})$, $f_1(1420)(\Lambda\overline{\Lambda})$	$*$
	$K_1^+(1270)(\overline{p}\Lambda)$, $K_1^-(1270)(p\overline{\Lambda})$	$*$
	$K_1^0(1270)(\overline{n}\Lambda)$, $\overline{K}_1^0(1270)(n\overline{\Lambda})$	$*$
	$K_1^+(1400)(\overline{p}\Lambda)$, $K_1^-(1400)(p\overline{\Lambda})$	$*$
	$K_1^0(1400)(\overline{n}\Lambda)$, $\overline{K}_1^0(1400)(n\overline{\Lambda})$	$*$
$2^+\&1^-$	$a_2^0(1320)(p\overline{p})$	$*$
	$a_2^+(1320)(n\overline{p})$, $a_2^-(1320)(p\overline{n})$	$*$
	$f_2(1270)(p\overline{p})$	$*$
	$K_2^{*+}(1430)(\overline{p}\Lambda)$, $K_2^{*-}(1430)(p\overline{\Lambda})$	$*$
	$K_2^{*0}(1430)(\overline{n}\Lambda)$, $\overline{K}_2^{*0}(1430)(n\overline{\Lambda})$	$*$

$*$: not allowed in J/ψ decays.

If the electromagnetic interaction is neglected, the production rates of these baryon-antibaryon bound states in J/ψ and ψ' decays can be simply related by $SU(3)$ symmetry except for a phase space factor [520]. For example, the production rates of baryon-antibaryon bound states with $J^P = 1^-$ accompanying by a pseudoscalar meson are related by: $\pi^0\rho_B^0 : \pi^+\rho_B^- : \pi^-\rho_B^+ : K^+\overline{K}_B^{*-} : K^0\overline{K}_B^{*0} : K^-K_B^{*+} : \overline{K^0}K_B^{*0} : \eta\omega_B : \eta\phi_B : \eta'\omega_B : \eta'\phi_B = 1:1:1:1:1:1:1:X_\eta^2 : Y_\eta^2 : X_{\eta'}^2 : Y_{\eta'}^2$. Here X_η, $X_{\eta'}$, Y_η, and $Y_{\eta'}$ are the mixing coefficients of η and η' [204, 477]:

$$\begin{aligned} |\eta\rangle &= X_\eta \frac{1}{\sqrt{2}}|u\overline{u} + d\overline{d}\rangle + Y_\eta|s\overline{s}\rangle \ , \\ |\eta'\rangle &= X_{\eta'}\frac{1}{\sqrt{2}}|u\overline{u} + d\overline{d}\rangle + Y_{\eta'}|s\overline{s}\rangle \ , \end{aligned}$$

with $X_\eta = Y_{\eta'}$, $X_{\eta'} = -Y_\eta$, and $X_\eta^2 + Y_\eta^2 = 1$. Assuming aforementioned states predominantly decay to baryon-antibaryon pair, and considering the fact that $\rho_B^0 \to n\overline{n}$ and $\omega_B \to n\overline{n}$ are hard to be detected experimentally, above relation can be reformulated in terms of the experimentally detected final states: $\pi^0(p\overline{p}) : \pi^+(n\overline{p}) : \pi^-(\overline{n}p) : K^+(\overline{p}\Lambda) : K^0(\overline{n}\Lambda) : K^-(p\overline{\Lambda}) : \overline{K^0}(n\overline{\Lambda}) : \eta(p\overline{p}) : \eta(\Lambda\overline{\Lambda}) : \eta'(p\overline{p}) : \eta'(\Lambda\overline{\Lambda}) \cong \frac{1}{2} : 1 : 1 : 1 : 1 : 1 : 1 : \frac{X_\eta^2}{2} : Y_\eta^2 : \frac{X_{\eta'}^2}{2} : Y_{\eta'}^2$. The production rates of baryon-antibaryon bound states with other quantum numbers are expressed similarly. The phase space is proportional to p^3 for the production of the $J^P = 1^-(0^-)$ baryon-antibaryon bound state with an accompanying pseudoscalar (vector) meson, where p is the momentum of the baryon-antibaryon bound state.

The $p\overline{p}$ state observed in J/ψ radiative decays is η_B or π_B^0 if it is a S-wave state due to spin-parity conservation, and the $p\overline{\Lambda}$ states in J/ψ decays is K_B^{*+} or K_B^+. In B decays, since parity is not conserved, the spin-parity of the state is to be determined by the angular distributions of the final state particles.

Because of the large phase space, B decays play important roles in the study of the baryon-antibaryon resonances. Detailed discussion could be found in Ref. [517].

Charmonium is another domain to study the baryon-antibaryon states. Unlike B decays, conservation law holds a rein on a possible decay mode herein. By virtue of the quantum numbers listed in Table 21.15, some decay modes involving the 0^- and 1^- baryon-antibaryon bound states are listed in Table 21.16. The production of the 0^- baryon-antibaryon bound states in J/ψ (or ψ') decays can be accompanied by a vector meson. For the iso-vector bound states, one may look for the $\rho N\overline{N}$ (nucleon antinucleon) final states, including $\rho^+ n\overline{p}$, $\rho^0 p\overline{p}$ and $\rho^- p\overline{n}$; for the iso-scalar bound state, one may look for the $\omega p\overline{p}$ final state; while for the strange states, one may look for the $K^{*+}\Lambda\overline{p} + c.c.$ and $K^{*0}\Lambda\overline{n} + c.c.$ final states. The neutron or anti-neutron which is not detected may be reconstructed by kinematic fit in the event selection. The $SU(3)$ singlet state can be searched for by measuring $\phi\Lambda\overline{\Lambda}$ final state. The measurement of the 0^- baryon-antibaryon bound states together with an axial-vector meson is less promising since almost all the axial-vector mesons are resonances.

The production of the 1^- baryon-antibaryon bound states can be accompanied by a pseudoscalar (π, η, η', K), scalar, tensor or axial-vector meson. The most promising

way to look for them is in the decays with a pseudoscalar meson: analyze $\pi N\overline{N}$ for the iso-vector bound states; analyze $\eta p\overline{p}$ for iso-scalar bound state; and analyze $K^+\Lambda\overline{p} + c.c.$ and $K^0\Lambda\overline{n} + c.c.$ for the strange bound states. The $SU(3)$ singlet bound state can be searched for via $\eta'\Lambda\overline{\Lambda}$.

It should be noted that the neutral non-strange 0^- baryon-antibaryon bound states can also be produced via radiative decays of J/ψ (or ψ'), while the 1^- baryon-antibaryon bound states can not be produced this way due to spin-parity conservation.

Although among charmonium decays J/ψ provides a good source of the baryon-antibaryon bound states because of the large data samples, there are disadvantages: the phase space is too small and there are many N^*'s near nucleon meson mass threshold, which affect the identification of the states [524]. The ψ' decays have larger phase space, however, the data samples are smaller, and there is a large fraction of charmonium transition. CLEOc and BESIII will surely help to improve the statistics, and the partial wave analysis is desirable to take the N^* contribution into account correctly.

2. Spectroscopy of $\mathrm{q}^3\overline{\mathrm{q}}^3$ states

More meticulous and mathematic study about baryon-antibaryon enhancement is preformed in Ref. [534], where the group technique employed in the Jaffe's studies on the $\mathrm{q}^2\overline{\mathrm{q}}^2$ system [535] is extended to the $\mathrm{q}^3\overline{\mathrm{q}}^3$ system.

The spectroscopically important interaction for the system composed of quarks and/or antiquarks is mediated by one gluon exchange. The system Hamiltonian is expressed as follows [536]

$$\mathcal{H}_{cs} = -\sum_{i>j} C_{ij}\ \vec{\sigma}_i \cdot \vec{\sigma}_j\ \vec{\lambda}_i \cdot \vec{\lambda}_j \tag{21.66}$$

where $\vec{\sigma}$ and $\vec{\lambda}$ are the Pauli matrices and Gell-Mann matrices, and the indices i and j run over all the constituent quarks and antiquarks; the coefficients C_{ij} are dependent on the quark masses of flavor i and j and the properties of the spatial wave functions of the quarks and the antiquarks in the system and parameterize the strength of the interaction. Anyway, in study of Ref. [534], the flavor $SU(3)$ breaking effect is turned off, so $C_{ij} = C$ is assumed. The interaction described by Eq. (21.66) is dominated by the spin-spin color force, which is referred to as color-magnetic hyperfine interaction. It is straightforward to express the color-magnetic interaction in terms of the quadratic Casimir operators of $SU(2)_s$ (s: spin), $SU(3)_c$ (c: color) and $SU(6)_{cs}$ (cs: colorspin) of the total system, the quarks and the antiquarks,

$$\begin{aligned} \mathcal{H}_{cs} &= C[8N + 2C_6(tot) - \tfrac{4}{3}S_{tot}(S_{tot}+1) - 2C_3(tot) \\ &+ 4C_3(Q) + \tfrac{8}{3}S_Q(S_Q+1) - 4C_6(Q) \\ &+ 4C_3(\overline{Q}) + \tfrac{8}{3}S_{\overline{Q}}(S_{\overline{Q}}+1) - 4C_6(\overline{Q})]\ , \end{aligned} \tag{21.67}$$

where C_3 and C_6 are the quadratic Casimir operator of the $\mathrm{SU}(3)_c$ and $\mathrm{SU}(6)_{cs}$, S is the spin, the labels Q, $\overline{Q}$ and tot refer to the quarks, antiquarks, and the

entire system respectively, and N is the total number of the quarks and antiquarks in the system, for the $q^3\overline{q}^3$ system $N = 6$. The Casimir operators are normalized conventionally [537]. Eigen-states of total $SU(6)_{cs}$ for $q^3\overline{q}^3$ are generally mixtures of the states with different color and spin representations of quarks and antiquarks respectively, and the color-magnetic interaction usually mixes states of different total color-spin. The wave function is expressed by

$$|D_{cs}(tot), D_c(tot), 2S(tot)+1; D_f(tot)\rangle \ ,$$

where $D_{cs}(tot)$, $D_c(tot)$, D_f denote the total system dimension of the irreducible $SU(6)_{cs}$, $SU(3)_c$, and $SU(3)_f$ representations respectively; S is the spin of the total system.

Using the tools introduced above, the spectroscopy of $q^3\overline{q}^3$ system from the common quark model is studied first in Ref. [534]. Because of the Fermi statistics, the state of three quarks must be antisymmetric in the combined wave-functions of flavor⊗color⊗spin⊗space. All the quarks in $q^3\overline{q}^3$ system is assumed to be in a relative S wave, therefore the flavor⊗color⊗spin wavefunction must be antisymmetric. The group $SU(18) \supset SU(6)_{cs} \otimes SU(3)_f \supset SU(3)_c \otimes SU(2)_s \otimes SU(3)_f$ is utilized to depict the total configuration, the eigen-states spin-**0**, -**1**, -**2**, and -**3** are scrutinized, and results are quoted in Table 21.17.

According to above Table, firstly it is noticeable that the configurations corresponding to the $p\overline{p}$, $p\overline{\Lambda}$, and $\Lambda\overline{\Lambda}$ enhancements can have rather large negative color-magnetic energies. This indicates that these states should be visible in experiments, and therefore these results are consistent with the experiments reported in Ref. [507, 508, 509, 510, 511, 512]. Secondly, it can be sees that the binding color-magnetic energy of spin-**0** and spin-**1** states are larger than those spin-**2** and spin-**3**.

Specifically, the $p\overline{p}$ enhancement can be depicted by $|\mathbf{1}, \mathbf{8}_f \otimes \mathbf{8}_f\rangle_1$, that is

$$\begin{aligned} |\mathbf{1}, \mathbf{8}_f \otimes \mathbf{8}_f\rangle_1 &= 0.394|(\mathbf{70}_{cs}, \mathbf{10}_c, \mathbf{2}; \mathbf{8}_f), (\overline{\mathbf{70}}_{cs}, \overline{\mathbf{10}}_c, \mathbf{2}; \mathbf{8}_f), \mathbf{1}_c, \mathbf{1}; \mathbf{8}_f \otimes \mathbf{8}_f\rangle \\ &+ 0.604|(\mathbf{70}_{cs}, \mathbf{8}_c, \mathbf{4}; \mathbf{8}_f), (\overline{\mathbf{70}}_{cs}, \mathbf{8}_c, \mathbf{4}; \mathbf{8}_f), \mathbf{1}_c, \mathbf{1}; \mathbf{8}_f \otimes \mathbf{8}_f\rangle \\ &- 0.576|(\mathbf{70}_{cs}, \mathbf{8}_c, \mathbf{2}; \mathbf{8}_f), (\overline{\mathbf{70}}_{cs}, \mathbf{8}_c, \mathbf{2}; \mathbf{8}_f), \mathbf{1}_c, \mathbf{1}; \mathbf{8}_f \otimes \mathbf{8}_f\rangle \\ &- 0.384|(\mathbf{70}_{cs}, \mathbf{1}_c, \mathbf{2}; \mathbf{8}_f), (\overline{\mathbf{70}}_{cs}, \mathbf{1}_c, \mathbf{2}; \mathbf{8}_f), \mathbf{1}_c, \mathbf{1}; \mathbf{8}_f \otimes \mathbf{8}_f\rangle \ , \end{aligned} \tag{21.68}$$

with the color-magnetic interaction energy $-45.547C$. Since the color-magnetic energy of the proton or antiproton is $-8C$ (refer to Table II of Ref. [534]), it easy to estimate that the mass defect of the $p\overline{p}$ enhancement is approximately $29.547C$ which is compatible with the experimental observation, that the $p\overline{p}$ enhancement is bellow the threshold [507]. Besides the states $|\mathbf{3}, \mathbf{8}_f \otimes \mathbf{8}_f\rangle_1$ with the color-magnetic energy $-29.461C$ should also be seen experimentally. Therefore authors of Ref. [534] conjecture that both the spin-**0** and spin-**1** $p\overline{p}$ enhancement may have been observed by BES[507].

Similarly, the configurations of $|\mathbf{1}, \mathbf{1}_f \otimes \mathbf{1}_f\rangle_1$ and $|\mathbf{3}, \mathbf{1}_f \otimes \mathbf{1}_f\rangle_1$ with the color-magnetic energy $-82.533C$ and $-48.331C$ respectively, correspond to the $\Lambda\overline{\Lambda}$ enhancement [512].

Table 21.17: Color-magnetic interaction energy of $q^3\overline{q}^3$ eigen-states in common quark model, and the conjugates states are not included. The subscript numbers indicate the detail configurations as explained in Ref. [534]. Here the state is denoted by symbol $|2S(tot)+1, D_f \otimes D_f\rangle$ which is the synthetic state constructed by states such as $|D_{cs}(tot), D_c(tot), 2S(tot)+1; D_f(tot)\rangle$ (refer to Ref. [534] or discussion in the text).

State	Colormagnetic Interaction Energy	State	Colormagnetic Interaction Energy
$\|\mathbf{1},\mathbf{8}_f\otimes\mathbf{8}_f\rangle_1$	$-45.547C$	$\|\mathbf{1},\mathbf{8}_f\otimes\mathbf{8}_f\rangle_2$	$16C$
$\|\mathbf{1},\mathbf{8}_f\otimes\mathbf{8}_f\rangle_3$	$-12.671C$	$\|\mathbf{1},\mathbf{8}_f\otimes\mathbf{8}_f\rangle_4$	$2.218C$
$\|\mathbf{1},\mathbf{8}_f\otimes\mathbf{1}_f\rangle$	$-24C$	$\|\mathbf{1},\mathbf{8}_f\otimes\overline{\mathbf{10}}_f\rangle$	$8C$
$\|\mathbf{1},\mathbf{1}_f\otimes\overline{\mathbf{10}}_f\rangle$	$16C$	$\|\mathbf{1},\mathbf{1}_f\otimes\mathbf{1}_f\rangle_1$	$-82.533C$
$\|\mathbf{1},\mathbf{1}_f\otimes\mathbf{1}_f\rangle_2$	$-29.467C$	$\|\mathbf{1},\mathbf{10}_f\otimes\overline{\mathbf{10}}_f\rangle_1$	$25.889C$
$\|\mathbf{1},\mathbf{10}_f\otimes\overline{\mathbf{10}}_f\rangle_2$	$-9.889C$	$\|\mathbf{3},\mathbf{8}_f\otimes\mathbf{8}_f\rangle_1$	$-29.461C$
$\|\mathbf{3},\mathbf{8}_f\otimes\mathbf{8}_f\rangle_2$	$27.631C$	$\|\mathbf{3},\mathbf{8}_f\otimes\mathbf{8}_f\rangle_3$	$-20.293C$
$\|\mathbf{3},\mathbf{8}_f\otimes\mathbf{8}_f\rangle_4$	$-10.667C$	$\|\mathbf{3},\mathbf{8}_f\otimes\mathbf{8}_f\rangle_5$	$3.456C$
$\|\mathbf{3},\mathbf{8}_f\otimes\mathbf{8}_f\rangle_6$	$-2.667C$	$\|\mathbf{3},\mathbf{8}_f\otimes\mathbf{1}_f\rangle_1$	$-45.078C$
$\|\mathbf{3},\mathbf{8}_f\otimes\mathbf{1}_f\rangle_2$	$-14.477C$	$\|\mathbf{3},\mathbf{8}_f\otimes\mathbf{1}_f\rangle_3$	$7.555C$
$\|\mathbf{3},\mathbf{8}_f\otimes\overline{\mathbf{10}}_f\rangle_1$	$24.634C$	$\|\mathbf{3},\mathbf{8}_f\otimes\overline{\mathbf{10}}_f\rangle_2$	$-12.007C$
$\|\mathbf{3},\mathbf{8}_f\otimes\overline{\mathbf{10}}_f\rangle_3$	$7.373C$	$\|\mathbf{3},\mathbf{1}_f\otimes\overline{\mathbf{10}}_f\rangle$	$-32/3C$
$\|\mathbf{3},\mathbf{1}_f\otimes\mathbf{1}_f\rangle_1$	$-48.331C$	$\|\mathbf{3},\mathbf{1}_f\otimes\mathbf{1}_f\rangle_2$	$-5.003C$
$\|\mathbf{3},\mathbf{10}_f\otimes\overline{\mathbf{10}}_f\rangle_1$	$34.397C$	$\|\mathbf{3},\mathbf{10}_f\otimes\overline{\mathbf{10}}_f\rangle_2$	$8.269C$
$\|\mathbf{5},\mathbf{8}_f\otimes\mathbf{8}_f\rangle_1$	$16C$	$\|\mathbf{5},\mathbf{8}_f\otimes\mathbf{8}_f\rangle_2$	$-12.944C$
$\|\mathbf{5},\mathbf{8}_f\otimes\mathbf{8}_f\rangle_3$	$4.944C$	$\|\mathbf{5},\mathbf{8}_f\otimes\mathbf{1}_f\rangle_1$	$16C$
$\|\mathbf{5},\mathbf{8}_f\otimes\mathbf{1}_f\rangle_2$	$-12C$	$\|\mathbf{5},\mathbf{8}_f\otimes\overline{\mathbf{10}}_f\rangle_1$	$-4C$
$\|\mathbf{5},\mathbf{8}_f\otimes\overline{\mathbf{10}}_f\rangle_2$	$16C$	$\|\mathbf{5},\mathbf{1}_f\otimes\mathbf{1}_f\rangle$	$-16C$
$\|\mathbf{5},\mathbf{10}_f\otimes\overline{\mathbf{10}}_f\rangle$	$16C$	$\|\mathbf{7},\mathbf{8}_f\otimes\mathbf{8}_f\rangle$	$16C$
$\|\mathbf{7},\mathbf{1}_f\otimes\mathbf{1}_f\rangle$	$16C$	$\|\mathbf{7},\mathbf{10}_f\otimes\overline{\mathbf{10}}_f\rangle$	$16C$

For $p\overline{\Lambda}$ enhancement [509, 511], the corresponding configurations can be both $|\mathbf{1},\mathbf{8}_f\otimes\mathbf{1}_f\rangle$ and $|\mathbf{3},\mathbf{8}_f\otimes\mathbf{1}_f\rangle_1$. However, it is noticeable that the color-magnetic energy of the latter is larger than the former, which indicates that the vector $p\overline{\Lambda}$ enhancement may be favored over the scalar one. Because the $p\overline{\Lambda}$ enhancement has been seen in the process $J/\psi \to p\overline{\Lambda}K^-$ and $\psi' \to p\overline{\Lambda}K^-$, and J/ψ and ψ' are vector mesons, K^- is a pseudoscalar meson, the relative angular momentum between K^- and the $p\overline{\Lambda}$ enhancement $l=0$ is favored, if the $p\overline{\Lambda}$ enhancement is a vector state. We also conjecture that both the spin-**0** and spin-**1** $p\overline{\Lambda}$ enhancement has been observed by BES but the main content is spin-**1** $p\overline{\Lambda}$ enhancement.

Quark correlation turns out to play important role in multiquark states [538, 539], so the effect of quark correlation in the $q^3\overline{q}^3$ system is further considered in Ref. [534]. Generally in the $q^3\overline{q}^3$ system there are many possible configurations: $(q)-(q^2\overline{q}^3)$, $(\overline{q})-(q^3\overline{q}^2)$, $(q^2)-(q\overline{q}^3)$, $(q\overline{q})-(q^2\overline{q}^2)$, $(\overline{q}^2)-(q^3\overline{q})$, $(q^3)-(\overline{q}^3)$, $(q^2\overline{q})-(q\overline{q}^2)$ and so on. Amony these configurations merely two with more symmetric feature are considered, that is $(q^3)-(\overline{q}^3)$ and $(q^2\overline{q})-(q\overline{q}^2)$, where under the changes $q \leftrightarrow \overline{q}$, the 1st-cluster and 2nd-cluster interchange each other. more symmetric than others.

Table 21.18: The allowed states of the total system in the configuration $(q^3) - (\overline{q}^3)$ and the mass splitting (Table III of Ref. [534]).

Total System States	$SU_f(3)$ Structure	Spin Structure	Mass Splitting
$\|\mathbf{70}_{cs}, \mathbf{10}_c, \mathbf{2}; \mathbf{8}_f\rangle \|\overline{\mathbf{70}}_{cs}, \overline{\mathbf{10}}_c, \mathbf{2}; \mathbf{8}_f\rangle$	$\mathbf{1}_f \oplus \mathbf{8}_f \oplus \mathbf{8}_f \oplus \mathbf{10}_f \oplus \overline{\mathbf{10}}_f \oplus \mathbf{27}_f$	$\mathbf{0}, \mathbf{1}$	8C
$\|\mathbf{70}_{cs}, \mathbf{10}_c, \mathbf{2}; \mathbf{8}_f\rangle \|\overline{\mathbf{56}}_{cs}, \overline{\mathbf{10}}_c, 4; \mathbf{1}_f\rangle$	$\mathbf{8}_f$	$\mathbf{1}, \mathbf{2}$	0
$\|\mathbf{70}_{cs}, \mathbf{8}_c, 4; \mathbf{8}_f\rangle \|\overline{\mathbf{70}}_{cs}, \mathbf{8}_c, 4; \mathbf{8}_f\rangle$	$\mathbf{1}_f \oplus \mathbf{8}_f \oplus \mathbf{8}_f \oplus \mathbf{10}_f \oplus \overline{\mathbf{10}}_f \oplus \mathbf{27}_f$	$\mathbf{0}, \mathbf{1}, \mathbf{2}, \mathbf{3}$	4C
$\|\mathbf{70}_{cs}, \mathbf{8}_c, 4; \mathbf{8}_f\rangle \|\overline{\mathbf{70}}_{cs}, \mathbf{8}_c, \mathbf{2}; \mathbf{8}_f\rangle$	$\mathbf{1}_f \oplus \mathbf{8}_f \oplus \mathbf{8}_f \oplus \mathbf{10}_f \oplus \overline{\mathbf{10}}_f \oplus \mathbf{27}_f$	$\mathbf{1}, \mathbf{2}$	0
$\|\mathbf{70}_{cs}, \mathbf{8}_c, 4; \mathbf{8}_f\rangle \|\overline{\mathbf{56}}_{cs}, \mathbf{8}_c, \mathbf{2}; \mathbf{1}_f\rangle$	$\mathbf{8}_f$	$\mathbf{1}, \mathbf{2}$	-12C
$\|\mathbf{70}_{cs}, \mathbf{8}_c, 4; \mathbf{8}_f\rangle \|\overline{\mathbf{20}}_{cs}, \mathbf{8}_c, \mathbf{2}; \overline{\mathbf{10}}_f\rangle$	$\mathbf{8}_f \oplus \overline{\mathbf{10}}_f \oplus \mathbf{27}_f \oplus \overline{\mathbf{35}}_f$	$\mathbf{1}, \mathbf{2}$	12C
$\|\mathbf{70}_{cs}, \mathbf{8}_c, \mathbf{2}; \mathbf{8}_f\rangle \|\overline{\mathbf{70}}_{cs}, \mathbf{8}_c, 4; \mathbf{8}_f\rangle$	$\mathbf{1}_f \oplus \mathbf{8}_f \oplus \mathbf{8}_f \oplus \mathbf{10}_f \oplus \overline{\mathbf{10}}_f \oplus \mathbf{27}_f$	$\mathbf{1}, \mathbf{2}$	0
$\|\mathbf{70}_{cs}, \mathbf{8}_c, \mathbf{2}; \mathbf{8}_f\rangle \|\overline{\mathbf{70}}_{cs}, \mathbf{8}_c, \mathbf{2}; \mathbf{8}_f\rangle$	$\mathbf{1}_f \oplus \mathbf{8}_f \oplus \mathbf{8}_f \oplus \mathbf{10}_f \oplus \overline{\mathbf{10}}_f \oplus \mathbf{27}_f$	$\mathbf{0}, \mathbf{1}$	-4C
$\|\mathbf{70}_{cs}, \mathbf{8}_c, \mathbf{2}; \mathbf{8}_f\rangle \|\overline{\mathbf{56}}_{cs}, \mathbf{8}_c, \mathbf{2}; \mathbf{1}_f\rangle$	$\mathbf{8}_f$	$\mathbf{0}, \mathbf{1}$	-16C
$\|\mathbf{70}_{cs}, \mathbf{8}_c, \mathbf{2}; \mathbf{8}_f\rangle \|\overline{\mathbf{20}}_{cs}, \mathbf{8}_c, \mathbf{2}; \overline{\mathbf{10}}_f\rangle$	$\mathbf{8}_f \oplus \overline{\mathbf{10}}_f \oplus \mathbf{27}_f \oplus \overline{\mathbf{35}}_f$	$\mathbf{0}, \mathbf{1}$	8C
$\|\mathbf{56}_{cs}, \mathbf{10}_c, 4; \mathbf{1}_f\rangle \|\overline{\mathbf{70}}_{cs}, \overline{\mathbf{10}}_c, \mathbf{2}; \mathbf{8}_f\rangle$	$\mathbf{8}_f$	$\mathbf{1}, \mathbf{2}$	0
$\|\mathbf{56}_{cs}, \mathbf{10}_c, 4; \mathbf{1}_f\rangle \|\overline{\mathbf{56}}_{cs}, \overline{\mathbf{10}}_c, 4; \mathbf{1}_f\rangle$	$\mathbf{1}_f$	$\mathbf{0}, \mathbf{1}, \mathbf{2}, \mathbf{3}$	-8C
$\|\mathbf{56}_{cs}, \mathbf{8}_c, \mathbf{2}; \mathbf{1}_f\rangle \|\overline{\mathbf{70}}_{cs}, \mathbf{8}_c, 4; \mathbf{8}_f\rangle$	$\mathbf{8}_f$	$\mathbf{1}, \mathbf{2}$	-12C
$\|\mathbf{56}_{cs}, \mathbf{8}_c, \mathbf{2}; \mathbf{1}_f\rangle \|\overline{\mathbf{70}}_{cs}, \mathbf{8}_c, \mathbf{2}; \mathbf{8}_f\rangle$	$\mathbf{8}_f$	$\mathbf{0}, \mathbf{1}$	-16C
$\|\mathbf{56}_{cs}, \mathbf{8}_c, \mathbf{2}; \mathbf{1}_f\rangle \|\overline{\mathbf{56}}_{cs}, \mathbf{8}_c, \mathbf{2}; \mathbf{1}_f\rangle$	$\mathbf{1}_f$	$\mathbf{0}, \mathbf{1}$	-28C
$\|\mathbf{56}_{cs}, \mathbf{8}_c, \mathbf{2}; \mathbf{1}_f\rangle \|\overline{\mathbf{20}}_{cs}, \mathbf{8}_c, \mathbf{2}; \overline{\mathbf{10}}_f\rangle$	$\overline{\mathbf{10}}_f$	$\mathbf{0}, \mathbf{1}$	-4C
$\|\mathbf{20}_{cs}, \mathbf{8}_c, \mathbf{2}; \mathbf{10}_f\rangle \|\overline{\mathbf{70}}_{cs}, \mathbf{8}_c, 4; \mathbf{8}_f\rangle$	$\mathbf{8}_f \oplus \mathbf{10}_f + \mathbf{27}_f \oplus \mathbf{35}_f$	$\mathbf{1}, \mathbf{2}$	12C
$\|\mathbf{20}_{cs}, \mathbf{8}_c, \mathbf{2}; \mathbf{10}_f\rangle \|\overline{\mathbf{70}}_{cs}, \mathbf{8}_c, \mathbf{2}; \mathbf{8}_f\rangle$	$\mathbf{8}_f \oplus \mathbf{10}_f \oplus \mathbf{27}_f \oplus \mathbf{35}_f$	$\mathbf{0}, \mathbf{1}$	8C
$\|\mathbf{20}_{cs}, \mathbf{8}_c, \mathbf{2}; \mathbf{10}_f\rangle \|\overline{\mathbf{56}}_{cs}, \mathbf{8}_c, \mathbf{2}; \mathbf{1}_f\rangle$	$\mathbf{10}_f$	$\mathbf{0}, \mathbf{1}$	-4C
$\|\mathbf{20}_{cs}, \mathbf{8}_c, \mathbf{2}; \mathbf{10}_f\rangle \|\overline{\mathbf{20}}_{cs}, \mathbf{8}_c, \mathbf{2}; \overline{\mathbf{10}}_f\rangle$	$\mathbf{1}_f \oplus \mathbf{8}_f \oplus \mathbf{27}_f \oplus \mathbf{64}_f$	$\mathbf{0}, \mathbf{1}$	20C

Table 21.19: The allowed states of the total system in the configuration $(q^2\overline{q})$-$(q\overline{q}^2)$ and the mass splitting (Table V of Ref. [534]).

States of the total system	$SU_f(3)$ structure	the Spin Structure	the Mass Splitting
$\|\mathbf{120}_{cs},\mathbf{15}_c,\mathbf{2},\mathbf{3}_f\oplus\overline{\mathbf{6}}_f\rangle\|\overline{\mathbf{120}}_{cs},\emptyset verline\mathbf{15}_c,\mathbf{2},\overline{\mathbf{3}}_f\oplus\mathbf{6}_f\rangle$	$\mathbf{1}_f(2)\oplus\mathbf{8}_f(4)\oplus\mathbf{10}_f\oplus\overline{\mathbf{10}}_f\oplus\mathbf{27}_f$	$\mathbf{0},\mathbf{1}$	$\frac{8}{3}C$
$\|\mathbf{120}_{cs},\mathbf{15}_c,\mathbf{2},\mathbf{3}_f\oplus\overline{\mathbf{6}}_f\rangle\|\overline{\mathbf{120}}_{cs},\overline{\mathbf{15}}_c,\mathbf{4},\overline{\mathbf{3}}_f\oplus\mathbf{6}_f\rangle$	$\mathbf{1}_f(2)\oplus\mathbf{8}_f(4)\oplus\mathbf{10}_f\oplus\overline{\mathbf{10}}_f\oplus\mathbf{27}_f$	$\mathbf{1},\mathbf{2}$	$\frac{-4}{3}C$
$\|\mathbf{120}_{cs},\mathbf{15}_c,\mathbf{2},\mathbf{3}_f\oplus\overline{\mathbf{6}}_f\rangle\|\mathbf{84}_{cs},\overline{\mathbf{15}}_c,\mathbf{2},\overline{\mathbf{3}}_f\oplus\overline{\mathbf{15}}_f\rangle$	$\mathbf{1}_f\oplus\mathbf{8}_f(4)\oplus\mathbf{10}_f\oplus\overline{\mathbf{10}}_f(3)\oplus\mathbf{27}_f(2)\oplus\overline{\mathbf{35}}_f$	$\mathbf{0},\mathbf{1}$	$\frac{16}{3}C$
$\|\mathbf{120}_{cs},\mathbf{15}_c,\mathbf{4},\mathbf{3}_f\oplus\overline{\mathbf{6}}_f\rangle\|\overline{\mathbf{120}}_{cs},\overline{\mathbf{15}}_c,\mathbf{2},\overline{\mathbf{3}}_f\oplus\mathbf{6}_f\rangle$	$\mathbf{1}_f(2)\oplus\mathbf{8}_f(4)\oplus\mathbf{10}_f\oplus\overline{\mathbf{10}}_f\oplus\mathbf{27}_f$	$\mathbf{1},\mathbf{2}$	$-\frac{4}{3}C$
$\|\mathbf{120}_{cs},\mathbf{15}_c,\mathbf{4},\mathbf{3}_f\oplus\overline{\mathbf{6}}_f\rangle\|\overline{\mathbf{120}}_{cs},\overline{\mathbf{15}}_c,\mathbf{4},\overline{\mathbf{3}}_f\oplus\mathbf{6}_f\rangle$	$\mathbf{1}_f(2)\oplus\mathbf{8}_f(4)\oplus\mathbf{10}_f\oplus\overline{\mathbf{10}}_f\oplus\mathbf{27}_f$	$\mathbf{0},\mathbf{1},\mathbf{2},\mathbf{3}$	$-\frac{16}{3}C$
$\|\mathbf{120}_{cs},\mathbf{15}_c,\mathbf{4},\mathbf{3}_f\oplus\overline{\mathbf{6}}_f\rangle\|\mathbf{84}_{cs},\overline{\mathbf{15}}_c,\mathbf{2},\overline{\mathbf{3}}_f\oplus\overline{\mathbf{15}}_f\rangle$	$\mathbf{1}_f\oplus\mathbf{8}_f(4)\oplus\mathbf{10}_f\oplus\overline{\mathbf{10}}_f(3)\oplus\mathbf{27}_f(2)\oplus\overline{\mathbf{35}}_f$	$\mathbf{1},\mathbf{2}$	$\frac{4}{3}C$
$\|\overline{\mathbf{84}}_{cs},\mathbf{15}_c,\mathbf{2},\mathbf{3}_f\oplus\mathbf{15}_f\rangle\|\overline{\mathbf{120}}_{cs},\overline{\mathbf{15}}_c,\mathbf{2},\overline{\mathbf{3}}_f\oplus\mathbf{6}_f\rangle$	$\mathbf{1}_f\oplus\mathbf{8}_f(4)\oplus\mathbf{10}_f(3)\oplus\overline{\mathbf{10}}_f\oplus\mathbf{27}_f(2)\oplus\mathbf{35}_f$	$\mathbf{0},\mathbf{1}$	$\frac{16}{3}C$
$\|\overline{\mathbf{84}}_{cs},\mathbf{15}_c,\mathbf{2},\mathbf{3}_f\oplus\mathbf{15}_f\rangle\|\overline{\mathbf{120}}_{cs},\overline{\mathbf{15}}_c,\mathbf{4},\overline{\mathbf{3}}_f\oplus\mathbf{6}_f\rangle$	$\mathbf{1}_f\oplus\mathbf{8}_f(4)\oplus\mathbf{10}_f(3)\oplus\overline{\mathbf{10}}_f\oplus\mathbf{27}_f(2)\oplus\mathbf{35}_f$	$\mathbf{1},\mathbf{2}$	$\frac{4}{3}C$
$\|\overline{\mathbf{84}}_{cs},\mathbf{15}_c,\mathbf{2},\mathbf{3}_f\oplus\mathbf{15}_f\rangle\|\mathbf{84}_{cs},\overline{\mathbf{15}}_c,\mathbf{2},\overline{\mathbf{3}}_f\oplus\overline{\mathbf{15}}_f\rangle$	$\mathbf{1}_f(2)\oplus\mathbf{8}_f(5)\oplus\mathbf{10}_f(2)\oplus\overline{\mathbf{10}}(2)\oplus\mathbf{27}_f(4)\oplus\mathbf{35}_f\oplus\overline{\mathbf{35}}_f\oplus\mathbf{64}_f$	$\mathbf{0},\mathbf{1}$	$8C$
$\|\mathbf{120}_{cs},\overline{\mathbf{6}}_c,\mathbf{2},\mathbf{3}_f\oplus\overline{\mathbf{6}}_f\rangle\|\overline{\mathbf{120}}_{cs},\mathbf{6}_c,\mathbf{2},\overline{\mathbf{3}}_f\oplus\mathbf{6}_f\rangle$	$\mathbf{1}_f(2)\oplus\mathbf{8}_f(4)\oplus\mathbf{10}_f\oplus\overline{\mathbf{10}}_f\oplus\mathbf{27}_f$	$\mathbf{0},\mathbf{1}$	-16C
$\|\mathbf{120}_{cs},\overline{\mathbf{6}}_c,\mathbf{2},\mathbf{3}_f\oplus\overline{\mathbf{6}}_f\rangle\|\mathbf{84}_{cs},\mathbf{6}_c,\mathbf{2},\overline{\mathbf{3}}_f\oplus\overline{\mathbf{15}}_f\rangle$	$\mathbf{1}_f\oplus\mathbf{8}_f(4)\oplus\mathbf{10}_f\oplus\overline{\mathbf{10}}_f(3)\oplus\mathbf{27}_f(2)\oplus\overline{\mathbf{35}}_f$	$\mathbf{0},\mathbf{1}$	$-\frac{8}{3}C$
$\|\mathbf{120}_{cs},\overline{\mathbf{6}}_c,\mathbf{2},\mathbf{3}_f\oplus\overline{\mathbf{6}}_f\rangle\|\mathbf{84}_{cs},\mathbf{6}_c,\mathbf{4},\overline{\mathbf{3}}_f\oplus\overline{\mathbf{15}}_f\rangle$	$\mathbf{1}_f\oplus\mathbf{8}_f(4)\oplus\mathbf{10}_f\oplus\overline{\mathbf{10}}_f(3)\oplus\mathbf{27}_f(2)\oplus\overline{\mathbf{35}}_f$	$\mathbf{1},\mathbf{2}$	$-\frac{20}{3}C$
$\|\overline{\mathbf{84}}_{cs},\overline{\mathbf{6}}_c,\mathbf{2},\mathbf{3}_f\oplus\mathbf{15}_f\rangle\|\overline{\mathbf{120}}_{cs},\mathbf{6}_c,\mathbf{2},\overline{\mathbf{3}}_f\oplus\mathbf{6}_f\rangle$	$\mathbf{1}_f\oplus\mathbf{8}_f(4)\oplus\mathbf{10}_f(3)\oplus\overline{\mathbf{10}}_f\oplus\mathbf{27}_f(2)\oplus\mathbf{35}_f$	$\mathbf{0},\mathbf{1}$	$-\frac{8}{3}C$
$\|\overline{\mathbf{84}}_{cs},\overline{\mathbf{6}}_c,\mathbf{2},\mathbf{3}_f\oplus\mathbf{15}_f\rangle\|\mathbf{84}_{cs},\mathbf{6}_c,\mathbf{2},\overline{\mathbf{3}}_f\oplus\overline{\mathbf{15}}_f\rangle$	$\mathbf{1}_f(2)\oplus\mathbf{8}_f(5)\oplus\mathbf{10}_f(2)\oplus\overline{\mathbf{10}}(2)\oplus\mathbf{27}_f(4)\oplus\mathbf{35}_f\oplus\overline{\mathbf{35}}_f\oplus\mathbf{64}_f$	$\mathbf{0},\mathbf{1}$	$\frac{32}{3}C$
$\|\overline{\mathbf{84}}_{cs},\overline{\mathbf{6}}_c,\mathbf{2},\mathbf{3}_f\oplus\mathbf{15}_f\rangle\|\mathbf{84}_{cs},\mathbf{6}_c,\mathbf{4},\overline{\mathbf{3}}_f\oplus\overline{\mathbf{15}}_f\rangle$	$\mathbf{1}_f(2)\oplus\mathbf{8}_f(5)\oplus\mathbf{10}_f(2)\oplus\overline{\mathbf{10}}(2)\oplus\mathbf{27}_f(4)\oplus\mathbf{35}_f\oplus\overline{\mathbf{35}}_f\oplus\mathbf{64}_f$	$\mathbf{1},\mathbf{2}$	$\frac{20}{3}C$
$\|\overline{\mathbf{84}}_{cs},\overline{\mathbf{6}}_c,\mathbf{4},\mathbf{3}_f\oplus\mathbf{15}_f\rangle\|\overline{\mathbf{120}}_{cs},\mathbf{6}_c,\mathbf{2},\overline{\mathbf{3}}_f\oplus\mathbf{6}_f\rangle$	$\mathbf{1}_f\oplus\mathbf{8}_f(4)\oplus\mathbf{10}_f(3)\oplus\overline{\mathbf{10}}_f\oplus\mathbf{27}_f(2)\oplus\mathbf{35}_f$	$\mathbf{1},\mathbf{2}$	$-\frac{20}{3}C$
$\|\overline{\mathbf{84}}_{cs},\overline{\mathbf{6}}_c,\mathbf{4},\mathbf{3}_f\oplus\mathbf{15}_f\rangle\|\mathbf{84}_{cs},\mathbf{6}_c,\mathbf{2},\overline{\mathbf{3}}_f\oplus\overline{\mathbf{15}}_f\rangle$	$\mathbf{1}_f(2)\oplus\mathbf{8}_f(5)\oplus\mathbf{10}_f(2)\oplus\overline{\mathbf{10}}(2)\oplus\mathbf{27}_f(4)\oplus\mathbf{35}_f\oplus\overline{\mathbf{35}}_f\oplus\mathbf{64}_f$	$\mathbf{1},\mathbf{2}$	$\frac{20}{3}C$
$\|\overline{\mathbf{84}}_{cs},\overline{\mathbf{6}}_c,\mathbf{4},\mathbf{3}_f\oplus\mathbf{15}_f\rangle\|\mathbf{84}_{cs},\mathbf{6}_c,\mathbf{4},\overline{\mathbf{3}}_f\oplus\overline{\mathbf{15}}_f\rangle$	$\mathbf{1}_f(2)\oplus\mathbf{8}_f(5)\oplus\mathbf{10}_f(2)\oplus\overline{\mathbf{10}}(2)\oplus\mathbf{27}_f(4)\oplus\mathbf{35}_f\oplus\overline{\mathbf{35}}_f\oplus\mathbf{64}_f$	$\mathbf{0},\mathbf{1},\mathbf{2},\mathbf{3}$	$\frac{8}{3}C$

It is postulated the two clusters are separated by a distance larger than the range of the colormagnetic force which is of short range and are kept together by the colorelectric force. Consequently, the colormagnetic hyperfine interaction operates only within each cluster, but is not felt between them.

Each cluster can be in a variety of $\mathrm{SU}(3)_c$ representations, and eventually two clusters together form the color singlet physical baryonium state. The group analyses are preformed and results are quoted in Table 21.18 (for $\mathrm{q}^3\overline{\mathrm{q}}^3$ configuration) and Table 21.19 (for $[\mathrm{q}^2\overline{\mathrm{q}}]$-$[\mathrm{q}\overline{\mathrm{q}}^2]$ configuration).

The lower the color-magnetic energy the more stable is the system configuration. With this rule in mind, by virtue of Table 21.18, it is readily to pick out the most stable quark configuration $|\mathbf{70}_{cs},\mathbf{8}_c,\mathbf{2};\mathbf{8}_f\rangle|\overline{\mathbf{70}}_{cs},\mathbf{8}_c,\mathbf{2};\mathbf{8}_f\rangle$ (with the color-magnetic energy $-4C$) for $p\overline{p}$ enhancement; the configuration $|\mathbf{56}_{cs},\mathbf{8}_c,\mathbf{2};\mathbf{1}_f\rangle|\overline{\mathbf{56}}_{cs},\mathbf{8}_c,\mathbf{2};\mathbf{1}_f\rangle$ (with the color-magnetic energy $-28C$) for $\Lambda_1\overline{\Lambda}_1$enhancement. For $p\overline{\Lambda}_1$ enhancement, both the states $|\mathbf{70}_{cs},\mathbf{8}_c,\mathbf{2};\mathbf{8}_f\rangle|\overline{\mathbf{56}}_{cs},\mathbf{8}_c,\mathbf{2};\mathbf{1}_f\rangle$ and $|\mathbf{56}_{cs},\mathbf{8}_c,\mathbf{2};\mathbf{1}_f\rangle|\overline{\mathbf{70}}_{cs},\mathbf{8}_c,\mathbf{2};\mathbf{8}_f\rangle$ have the same color-magnetic energy $-16C$, they are in the flavor $\mathbf{8}_f$-plet with spin $\mathbf{0}$ or $\mathbf{1}$. It should be noted that both spin-$\mathbf{0}$, spin-$\mathbf{1}$ $p\overline{p}$ enhancements and spin-$\mathbf{0}$, spin-$\mathbf{1}$ $p\overline{\Lambda}$ enhancements are predicted.

For $(\mathrm{q}^2\overline{\mathrm{q}})-(\mathrm{q}\overline{\mathrm{q}}^2)$ configuration, by virtue of Table 21.19, it can be seen the multiplet state $|\mathbf{120}_{cs},\overline{\mathbf{6}}_c,\mathbf{2},\mathbf{3}_f\oplus\overline{\mathbf{6}}_f\rangle|\overline{\mathbf{120}}_{cs},\mathbf{6}_c,\mathbf{2},\overline{\mathbf{3}}_f\oplus\mathbf{6}_f\rangle$ has the largest color-magnetic energy $-16C$, and its flavors are in $\mathbf{1}(2)_f\oplus\mathbf{8}_f(4)\oplus\mathbf{10}_f\oplus\overline{\mathbf{10}}_f\oplus\mathbf{27}_f$. The spin of these states equals $\mathbf{0}$ or $\mathbf{1}$, and with the baryon number being zero. Therefore the multiplet state $|\mathbf{120}_{cs},\overline{\mathbf{6}}_c,\mathbf{2},\mathbf{3}_f\oplus\overline{\mathbf{6}}_f\rangle|\overline{\mathbf{120}}_{cs},\mathbf{6}_c,\mathbf{2},\overline{\mathbf{3}}_f\oplus\mathbf{6}_f\rangle$ can decay to (or couple to) baryon octet plus antibaryon octet. Namely, ($\Lambda\overline{\Lambda}$, $p\overline{\Lambda}$ and $p\overline{p}$ enhancements)$\in|\mathbf{120}_{cs},\overline{\mathbf{6}}_c,\mathbf{2},\mathbf{3}_f\oplus\overline{\mathbf{6}}_f\rangle|\overline{\mathbf{120}}_{cs},\mathbf{6}_c,\mathbf{2},\overline{\mathbf{3}}_f\oplus\mathbf{6}_f\rangle$. These baryonium states may mix with the states in the $(q^3)-(\overline{q}^3)$ cluster configurations, or expressed explicitly as follows

$$|i\rangle=\alpha_i|(q^3)-(\overline{q}^3)\rangle_i+\beta_i|(q^2\overline{q})-(q\overline{q}^2)\rangle_i, \tag{21.69}$$

where $i=\{\Lambda\overline{\Lambda},\ p\overline{\Lambda},\ p\overline{p}\}$, α_i and β_i are constants, $|i\rangle$ is i^{th} physical baryonium state, $|(q^3)-(\overline{q}^3)\rangle_i$ is i^{th} baryonium state in $(q^3)-(\overline{q}^3)$ cluster configurations, and $|(q^2\overline{q})-(q\overline{q}^2)\rangle_i$ is i^{th} baryonium state in $(q^2\overline{q})-(q\overline{q}^2)$ cluster configurations. We would like to argue that the physical baryonium states may favor the cluster structure with larger mass defect over that with smaller defect. Therefore, comparing the results of Table 21.18 and 21.19, it is obtained

$$\text{to } \Lambda\overline{\Lambda} \text{ enhancement}: \quad |\alpha_{i=\Lambda\overline{\Lambda}}| \ > \ |\beta_{i=\Lambda\overline{\Lambda}}|, \tag{21.70}$$

$$\text{to } p\overline{\Lambda} \text{ enhancement}: \quad |\alpha_{i=p\overline{\Lambda}}| \ \simeq \ |\beta_{i=p\overline{\Lambda}}|, \tag{21.71}$$

$$\text{to } p\overline{p} \text{ enhancement}: \quad |\alpha_{i=p\overline{p}}| \ < \ |\beta_{i=p\overline{p}}|. \tag{21.72}$$

The Eq.(21.72) indicates that the color, spin, flavor structures of $p\overline{p}$ enhancement are mainly of $|\mathbf{120_{cs}},\overline{\mathbf{6}}_\mathbf{c},\mathbf{2},\mathbf{3_f}\oplus\overline{\mathbf{6}}_\mathbf{f}\rangle|\overline{\mathbf{120}}_\mathbf{cs},\mathbf{6_c},\mathbf{2},\overline{\mathbf{3}}_\mathbf{f}\oplus\mathbf{6_f}\rangle$ in the configuration $(\mathrm{q}^2\overline{\mathrm{q}})-(\mathrm{q}\overline{\mathrm{q}}^2)$, and mix with few $|\mathbf{70_{cs}},\mathbf{8_c},\mathbf{2},\mathbf{8_f}\rangle|\overline{\mathbf{70}}_\mathbf{cs},\mathbf{8_c},\mathbf{2},\mathbf{8_f}\rangle$ in the configuration $(\mathrm{q}^3)-(\overline{\mathrm{q}}^3)$. Similarly, the Eq.(21.70) indicates the color-spin-flavor structures of $\Lambda\overline{\Lambda}$ enhancement are mainly $|\mathbf{56}_{cs},\mathbf{8}_c,\mathbf{2};\mathbf{1}_f\rangle|\overline{\mathbf{56}}_{cs},\mathbf{8}_c,\mathbf{2};\mathbf{1}_f\rangle$ in the configuration $(\mathrm{q}^3)-(\overline{\mathrm{q}}^3)$, and

plus few mixtures of the corresponding $\Lambda\overline{\Lambda}$ enhancement state in the configuration $(q^2\overline{q}) - (q\overline{q}^2)$. Moreover, by Eq.(21.71), the $p\overline{\Lambda}$ enhancement should be half of the states in the $(q^3) - (\overline{q}^3)$ configuration plus half of that in the $(q^2\overline{q}) - (q\overline{q}^2)$ approximately.

The states $|\mathbf{120}_{cs}, \overline{\mathbf{6}}_c, \mathbf{2}, \mathbf{3}_f \oplus \overline{\mathbf{6}}_f\rangle|\mathbf{84}_{cs}, \mathbf{6}_c, \mathbf{4}, \overline{\mathbf{3}}_f \oplus \overline{\mathbf{15}}_f\rangle$ or $|\overline{\mathbf{84}}_{cs}, \overline{\mathbf{6}}_c, \mathbf{4}, \mathbf{3}_f \oplus \mathbf{15}_f\rangle$ $|\overline{\mathbf{120}}_{cs}, \mathbf{6}_c, \mathbf{2}, \overline{\mathbf{3}}_f \oplus \mathbf{6}_f\rangle$ has color-magnetic energy $-\frac{20}{3}C$ with spins **1** or **2**; they are comparatively unstable with respect to the states with **0** or **0**.

As summary, both the analysis from common quark model and from the model with quark correlation in Ref. [534] imply that the $p\overline{p}$, $p\overline{\Lambda}$, and $\Lambda\overline{\Lambda}$ enhancements are in existence, and the signal corresponding them must be visible, as have been shown experimentally by BES and Bell. Ref. [534] also predicts that spin-**1** $\Lambda\overline{\Lambda}$ enhancement will be observed in future In other words; and conjectures that BES has observed both spin-**0**, spin-**1** $p\overline{p}$ enhancement and spin-**0**, spin-**1** $p\overline{\Lambda}$ enhancement.

Experiment results

Some experimental results of three body decays involving baryon and antibaryon pairs are collected in Table 21.20. In fact, the available results of three body baryoninc decay at present are rather limited. For J/ψ decays, all quoted results are experimental measurements before 1990; for ψ' decays, the results are mainly due to BES [530, 532] and CLEOc [529]; for χ_{cJ} decays, the results are solely from CLEOc [533]. However, even with these results we could notice some interesting phenomena. One interesting fact as pointed out in Ref. [530] is that for $\pi^0 p\overline{p}$ final state, $Q_{\pi^0 p\overline{p}} = 12.2 \pm 1.9$ which agrees well with the so-called 12% rule. In contrast, for $\eta p\overline{p}$ final state, $Q_{\eta p\overline{p}} = 2.8 \pm 0.6$, which seems to be suppressed significantly. Another suppression seems also true for $\omega p\overline{p}$ final state while for $K^+\overline{p}\Lambda$ final state, there is no suppression. Here more accurate data are needed for further study.

Charmless decays of the ψ'' can shed light on S-D mixing, missing ψ' decays such as $\psi' \to \rho\pi$, the discrepancy between the total and $D\overline{D}$ cross section at the ψ'', and re-scattering effects contributing to an enhanced $b \to s$ penguin amplitude in B meson decays [500]. The phenomenological analysis [501] also indicates the possibility of large charmless branching fraction in ψ'' decays. Stimulated by theoretical suggestions and based on the data with 55.8 pb^{-1} on the peak of the ψ'' and 20.70 pb^{-1} at the continuum ($\sqrt{s}$=3.67 GeV), which is used for background subtraction, CELOc report results of searches for a wide variety of non-$D\overline{D}$ modes [499], among which the results involving baryonic pairs are reproduced in Table 21.21 (with inclusion of final states with more than three particles). However, only the upper limits are obtained which indicates that the charmless decay fraction is rather small. This seems also consistent with CLEOc's inclusive results [502].

Since the masses of high charmonium states (the ψ-family member with mass above ψ'') are above the threshold for open charm production, the $B\bar{B}$ decay widths are likely to be very small and it is hardly conceivable that they will be measured. Therefore, up to now neither attempts have been made nor reports have been obtained for high charmonium states decay into baryon-pair-contained final states.

Table 21.20: Branching ratios of three body decays involving baryons at charmonium region. Most of results from PDG06 [448], except for χ_{cJ} decays, which from CLEOc [533]. The upper limits are given at 90% C.L. and $Q_h = \mathcal{B}_{\psi'\to h}/\mathcal{B}_{J/\psi\to h}$ is also given for possible final states. The numbers in parentheses are the "reduced" branching fraction defined as $\tilde{\mathcal{B}} = \mathcal{B}/PSF_3$, where PSF_3 is the phase space factor for there-body decay (the exact definition and calculation formula of PSF_3 could be found in Appendix **??**, Eq. (**??**)). The unity of PSF_3 is 10^1 and 10^{-1} for the J/ψ and ψ' decays respectively.

Final State	J/ψ (10^{-4})	ψ' (10^{-5})	Q_h (%)	χ_{cJ} $(J=0,1,2)$ (10^{-3})
$\pi^0 p\overline{p}$	$10.9 \pm 0.9(1.84)$	$13.3 \pm 1.7(6.83)$	12.2 ± 1.9	0.59 ± 0.13
				0.12 ± 0.06
				0.44 ± 0.10
$\pi^- p\overline{n}$	$20.0 \pm 1.0(3.40)$			
$\eta p\overline{p}$	$20.9 \pm 1.0(7.23)$	$6.0 \pm 1.2(4.48)$	2.8 ± 0.6	0.39 ± 0.12
				< 0.16
				0.19 ± 0.08
$\rho^0 p\overline{p}$	< 3.7	$5.0 \pm 2.2(5.24)$	> 5.9	
$\omega p\overline{p}$	$13.0 \pm 2.5(9.91)$	$6.9 \pm 2.1(7.31)$	5.3 ± 1.9	
$\phi p\overline{p}$	$4.5 \pm 1.5(15.6)$	< 2.4	< 9.3	
$\pi^0 \Lambda\overline{\Lambda}$	$2.2 \pm 0.6(0.84)$			
$K^+ \overline{p}\Lambda$	$8.9 \pm 1.6(4.65)$	$10.0 \pm 1.4(9.18)$	11.2 ± 2.5	1.07 ± 0.21
				0.33 ± 0.10
				0.85 ± 0.18
$K^- p\overline{\Sigma}^0$	$2.9 \pm 0.8(2.05)$			
$K^- p\overline{\Sigma}(1385)^0$	$5.1 \pm 3.2(10.2)$			
$\pi^- \overline{p}\Delta^{++}(1231)$	$1.6 \pm 0.5(0.52)$			
$\eta'(958) p\overline{p}$	9 ± 4 (18.4)			

Extract two-body decay information from three-body final states

It is believed the three-body final states are saturated by the two-body intermediate states, so it is essential to get such information by a partial wave analysis to the final states observed. This has been carried out for only very limited modes in J/ψ decays, such as $\eta p\overline{p}$ [503] at BESI and $\pi^- p\overline{n} + c.c.$ [504] at BESII. At BESIII, as the statistics becomes larger, it is possible to do such an analysis for many final states.

However, while we know the PWA uses the information in the full phase space for physics study so that it is more powerful than working in one dimension (invariant mass, for example) or a bit higher dimensions, it suffers from too many free parameters and other technical problems.

First of all, the experimental data are all affected by the finite resolution in momentum, energy, or direction measurement, this was not considered in the current analyses; secondly, the parametrization of the resonance, especially the wide resonance, such as the N^* or Λ^* or Δ in the analysis with barons, still have room to improve. Finally, the effect

Table 21.21: Experiment searching for exclusive baryonic decay at ψ'' [499]. Listed are the cross section upper limit including the systematic error (90% C.L.), and the branching ratio upper limit including the systematic error (90% C.L.).

mode	σ U.L. (pb)	$\mathcal{B}$ U.L. (10^{-4})
$p\bar{p}\pi^+\pi^-$	4.5	5.8
$p\bar{p}\pi^+\pi^-\pi^0$	14.4	18.5
$\eta p\bar{p}$	4.2	5.4
$\omega p\bar{p}$	2.2	2.9
$p\bar{p}K^+K^-$	2.5	3.2
$\phi p\bar{p}$	1.1	1.3
$\Lambda\bar{\Lambda}\pi^+\pi^-$	2.0	2.5
$\Lambda\bar{p}K^+$	2.2	2.8
$\Lambda\bar{p}K^+\pi^+\pi^-$	4.9	6.3

of the imperfect simulation of the detectors is hard to be considered in a fit with a few ten or even more free parameters. These effects may not be significant when the statistics is low, however, as the statistics increases, all these effects will possibly produce significant fake signals. How to handle these, if not now, at least in the near future.

21.3.5 Multi-body and Semi-inclusive decay

Multi-body decay

By multi-body decays, we mean charmonium decays into at least four final states particles, including one pair of baryons. Since the mass of baryon pair is around 2 GeV/c^2 or larger, the allowed decay modes are not large, especially for the low lying states like η_c and J/ψ. As the mass of kaon is around 0.5 GeV/c^2, the modes with kaon is further suppressed.

So far, only the $\pi^+\pi^- p\overline{p}$ has been measured in the decays of almost all the charmonium states below open charm threshold, with observation of J/ψ, ψ', and χ_{cJ} decay; $\pi^+\pi^-\pi^0 p\overline{p}$ was observed in J/ψ and ψ' decays; while $J/\psi \to \pi^+\pi^- N\overline{N}$ was measured with 100% uncertainty.

For the final states with strangeness, $\pi^+\pi^-\Lambda\overline{\Lambda}$ was observed in ψ' decays, although it has been searched for in χ_{cJ} decays, no signal was observed; another five-body decay observed is $\psi' \to \bar{p}K^+\Lambda\pi^+\pi^-$. $K^0_S K^0_S p\overline{p}$ has been searched for in χ_{cJ} and ψ' decays, but with no signal; as a byproduct of the search for the penta-quark state candidate ($\Theta(1540)$), the upper limits of J/ψ and $\psi' \to K^0_S pK^-\bar{n}$ branching fractions have been determined.

Generally speaking, except the selection efficiency will not be high due to higher multiplicity and low track momentum, the identification of the final states with four or more final states particles with a baryon pair is quite easy and the purity is relatively high. This makes it possible to study the interaction between baryon and mesons, such as $N\pi\pi$, $N\pi\pi\pi$, NK, $NK\pi$, $N\rho$, $N\omega$, or the nucleon replaced by a Λ and so on. However, as these excited Baryon states are generally broad, and the mass difference between states is small, the successful identification of the states or the decay mode require partial wave analysis, as has been performed for $J/\psi \to p\bar{n}\pi^- + c.c.$ As one can imagine, since there are more final states particles, the PWA will be more difficult, and more model dependent, and sometimes even unreliable.

Semi-inclusive decay

1. Semi-inclusive decay of η_c and η_c'

   In earlier study of η_c and η_c' hadronic decay, Lee, Quigg, and Rosner advanced [540] a statistical model appropriate to particle decay according to which, the mean multiplicity of decay products is

   $$\begin{aligned} \langle n \rangle &= n_0 + \left(\frac{4}{\pi}\right)^{1/4} \frac{\zeta(3)}{[3\zeta(4)]^{3/4}} \left(\frac{E}{E_0}\right)^{3/4} \\ &= n_0 + 0.528(E/E_0)^{3/4} \ . \end{aligned} \tag{21.73}$$

   Here $\zeta(x) \equiv \sum_{i=1}^{\inf} 1/i^x$, is the so-called Riemann Zeta function; E is the energy available in excess of the rest mass of the lowest-multiplicity (n_0) decay channel. For the decay like $\eta_c \to N\overline{N} + (m \text{ pions})^0$, $E = (M_{\eta_c} - M_N - M_{\overline{N}})c^2$ and $n_0 = 2$. The scale E_0 is given by the hadronic radius R_0:

   $$E_0 \equiv \hbar c / R_0 \ . \tag{21.74}$$

   For a radius of 1 fm (typical of bag models of hadrons [541]), $E_0 \simeq 0.2$ GeV. As for η_c and η_c' decay calculation, the value $E_0 \simeq 0.17$ GeV is suggested in Ref. [542].

Table 21.22: Decays of η_c and η_c' into $N\overline{N}+$ pions, according to the statistical mode or the constant-matrix-element (phase-space) model. [Each allowed $N\overline{N}$ charge state occurs with half the probability tabulated under "specific charge states."] The first of each pair of entries is for η_c, the second is for η_c'.

Mean multiplicity, all modes	Decay mode	All charge states	Specific charege states No. of neutral pions 0	1	2	3	4
results for the statistical mode							
3.9, 4.8	$N\overline{N}$	15%, 6%	15%, 6%				
	$N\overline{N}\pi$	28%,17%	19%,11%	9%, 6%			
	$N\overline{N}2\pi$	27%,24%	14%,12%	9%, 8%	4%,4%		
	$N\overline{N}3\pi$	17%,22%	5%, 7%	8%,10%	3%,4%	0%,1%	
	$N\overline{N}4\pi$	8%,16%	2%, 3%	3%, 6%	3%,5%	0%,1%	...
	$N\overline{N}5\pi$	3%, 9%	0%, 1%	1%, 3%	1%,3%	1%,1%	...
	$N\overline{N}6\pi$	1%, 4%	...	0%, 1%	0%,1%	0%,1%	...
	$N\overline{N} \geq 7\pi$	0%, 2%					
results for the constant-matrix-element mode							
3.1, 4.1	$N\overline{N}$	20%, 3%	20%, 3%				
	$N\overline{N}\pi$	52%,24%	35%,16%	17%, 8%			
	$N\overline{N}2\pi$	25%,42%	12%,21%	8%,14%	4%,7%		
	$N\overline{N}3\pi$	3%,24%	1%, 7%	1%,11%	1%,5%	0%,1%	
	$N\overline{N}4\pi$	0%, 6%	0%, 1%	0%, 2%	0%,2%	0%,1%	...
	$N\overline{N}5\pi$	0%, 1%					

The Poisson distribution is assumed in the variable $(\langle n\rangle - n_0)$ with incorporating the neutral decays by means of statistical isospin weights. The calculated results for $\eta_c, \eta_c' \to N\overline{N} + (m \text{ pions })$ are listed in Table 21.22. For comparison, the results based on another model, the constant-matrix-element (phase-space) model, are also listed in Table 21.22. As to the latter model, details could be found in Ref. [542, 543]

From Table 21.22, we notice that the $p\overline{p}$ mode accounts for about 5% of all decays $\eta_c \to N\overline{N} +$ pions . In the light of the statistical model [542], the semi-inclusive rates as fractions of the total baryonic decay rate of η_c are estimated to be

$\Gamma(N\overline{N} + \text{pions})$	44%
$\Gamma(\Lambda\overline{\Lambda} + \text{pions})$	7%
$\Gamma(\Lambda\overline{\Sigma} \text{ or } \overline{\Lambda}\Sigma + \text{pions})$	24%
$\Gamma(\Sigma\overline{\Sigma} + \text{pions})$	20%
$\Gamma(\Xi\overline{\Xi} + \text{pions})$	6% .

On this basis the $p\overline{p}$ mode is approximately 2% of all the baryonic decays. For J/ψ, the $p\overline{p}$ mode makes up about 0.2% of the direct hadronic decays [448]. This suggests

that the semi-inclusive baryonic decays of η_c makes up about 10% of its hadronic width.

2. Lund model and general inclusive decay

   The first JETSET then PYTHIA are well-known Monte Carlo simulation packets to simulate the inclusive (multihadron) final states at fairly high energy region (around or above Z_0 mass). The inclusive final state simulation of JETSET or PYTHIA is based on famous Lund model [544] which adopts and synthesizes many physics models, such as massless relativistic string model, diploe cascade model, linked diploe chain model, Feynman parton model, string fragmentation model and so on. The simulated results are fairly well at high energy region.

   Recently, by virtue of the basic Lund model area law, the theoretical formalism is developed for simulation of inclusive hadronic final state at comparatively low energy region, such as the charmonium region [545]. Then the formalism is used in hadronic final state simulation for R-value measurement and the simulated results are also fairly well [546].

   We will not go into further discussion about the Lund model, area law and the details involving Monte Carlo simulation here; anyway, it worthy to notice that Lund model is a fairly successful model for the simulation of general inclusive decay. Moreover, it provides an intuitive, visualized and calculable decay model for hadronization processes and in fact provides us with many enlighten ideas for dynamics exploration. However, the study of inclusive final states is still rather limited at charmonium region due to the dearth of data and many meticulous works could be done at the forthcoming high luminosity detector BESIII.

21.3.6 Special topics

In this section we will discuss the study of $SU(3)$ flavor symmetry breaking effects, the searching for CP violation, exotic state, bound state, testing of Bell inequality and other special topics in hadronic decays of charmonium states.

SU(3) flavor symmetry breaking effects

For J/ψ baryonic decay at the level of $SU(3)$ symmetry only the decay

$$J/\psi \to B_1\bar{B}_1, B_8\bar{B}_8, B_{10}\bar{B}_{10}$$

are allowed, with the same decay amplitudes for a given decay family if electromagnetic contributions are neglected. However, MarkII collaboration first published experimental results showing a large SU(3) flavor symmetry breaking takes place in the J/ψ decays into a baryonic pair [469], especially, into octe-decplet baryon pairs, then confirmed by DM2 [470] and MarkIII [471] collaboration. Table 21.23 summarizes the DM2 results on the J/ψ SU(2) or SU(3) forbidden decays. For the $J/\psi \to \Lambda\bar{\Lambda}\pi^0$, it seems that the large contamination from $J/\psi \to \Sigma\bar{\Lambda}\pi^0$ would lead to a small branching fraction. These SU(3) flavor symmetry decays will be studied at BESII/BESIII.

Table 21.23: Summary of J/ψ SU(2) and SU(3) forbidden decay modes measured.

Decay Mode	Number of events	Branching fraction ($\times 10^{-4}$)
SU(3) forbidden decay modes		
$J/\psi \to \Sigma(1385)^-\Sigma^+$	74 ± 8	$3.0 \pm 0.3 \pm 0.8$
$J/\psi \to \Sigma(1385)^+\bar{\Sigma}^-$	77 ± 9	$3.4 \pm 0.4 \pm 0.8$
$J/\psi \to \Xi(1530)^-\bar{\Xi}^+$	80 ± 9	$5.9 \pm 0.7 \pm 1.5$
$J/\psi \to \Xi(1530)^0\bar{\Xi}^0$	24 ± 5	$3.2 \pm 0.7 \pm 1.5$
SU(2) forbidden decay modes		
$J/\psi \to \Lambda\Lambda\pi^0$	19 ± 4	$2.2 \pm 0.5 \pm 0.5$
$J/\psi \to \Sigma(1385)^0\bar{\Lambda}$	13	$< 2.0(90\%CL)$
$J/\psi \to \Sigma^0\bar{\Lambda}$	11	$< 0.9(90\%CL)$
$J/\psi \to \Delta^+\bar{p}$	50	$< 1.0(90\%CL)$

As discussed in literatures, the SU(3) flavor symmetry can be broken in several ways:

- One photon processes, i.e. $c\bar{c} \to \gamma \to B_{10}\bar{B}_8$. Because the direct product $8 \otimes \bar{10}$ contains an octet contribution, it is possible via the octet component of the photon. It is also via the processes $c\bar{c} \to gg\gamma \to B_{10}\bar{B}_8$, which represents a direct electromagnetic decay. As calculated in pQCD framework the ratio R of this decay amplitude to that of the three-gluon decay is about a few percent, $R_{QCD} = -4\alpha/(5\alpha_s)$ [472], and also in the framework of vector meson dominance, $R_{VMD} = 24\alpha/(5\alpha_s)$.

- A second SU(3) breaking mechanism arises from the mass difference of light and strange quarks. The decay chain $c\bar{c} \to (u\bar{u}+d\bar{d}+s\bar{s})_1 \to \alpha(u\bar{u}+d\bar{d})_{1\oplus 8}+\beta(s\bar{s})_{1\oplus 8} \to B_{10}\bar{B}_8$ can occur if the coupling α and β differ. The mass breaking can equivalently be described by an octet [473] or 27-plet representation to the J/ψ wave function [470].

- The third mechanism possibly arises from the intermediate states. As pointed by Genz et al. [474] that an intermediate $q\bar{q}$ state could lead to the apparent SU(3) breaking. A generalization to multi-quark intermediate states would also make the contribution of a 27-plet possible. If the decay amplitudes are decomposed into the contributions from one-photon (D), octet SU(3) breaking (D'), and 27-plet terms (D"), the ratios of branching fractions for J/ψ decays into octe-duplet baryon pairs are given by [477]

$$\begin{aligned} R_1 &= \frac{B(\Xi(1530)^0\bar{\Xi}^0)}{B(\Sigma(1385)^+\bar{\Sigma}^-)} \propto \left|\frac{2D+D'+\frac{3}{2}D"}{2D+D'-D"}\right|^2, \\ R_2 &= \frac{B(\Xi(1530)^-\bar{\Xi}^+)}{B(\Sigma(1385)^-\bar{\Sigma}^+)} \propto \left|\frac{D'+\frac{3}{2}D"}{D'-D"}\right|^2, \\ R_3 &= \frac{B(\Sigma(1385)^+\bar{\Sigma}^-)-B(\Sigma(1385)^-\bar{\Sigma}^+)}{B(\Xi(1530)^0\bar{\Xi}^0)-B(\Xi(1530)^-\bar{\Xi}^+)} \propto \frac{|2D+D'-D"|^2-|D'-D"|^2}{|2D+D'+\frac{3}{2}D"|^2-|D'+\frac{3}{2}D"|^2}. \end{aligned} \tag{21.75}$$

  If octet dominance ($D' >> D''$) would predict that $R_1 = R_2 = R_3 = 1$, in contradiction with the measurements $R_1 = 1.3\pm0.6, R_2 = 2.8\pm1.0$ and $R_3 = -0.1\pm0.3$. The more sophisticated model of Körner [476], which allows for strong mass breaking effects and final state dependent electromagnetic amplitudes but neglects a 27-plet contribution, runs into similar problems. While a model allowing electromagnetic contributions is ruled out, some electromagnetic component seems to be required, sin $B(J/\psi \to \Xi^0(1530)\bar{\Xi}^0) \neq B(J/\psi \to \Xi(1530)^-\bar{\Xi}^+)$. In the framework of the given model, the data can well be described if both electromagnetic and strong isospin breaking effects are taken into account.

CP violation

The decays of J/ψ (or $\psi(2S)$) $\to B_8B_8$ (B_8: octet baryon) can be used to search for the electric dipole momentum (EDM) of baryons. The non-zero value of EDM indicates that CP symmetry is violated. As shown in Ref. [547], for $J/\psi \to B(p_1)\bar{B}(p_2)$ the decay amplitudes can be parameterized as

$$\mathcal{M} = \epsilon^\mu \bar{u}(p_1)[\gamma_\mu(a+b\gamma_5)+(p_{1\mu}-p_{2\mu})(c+id\gamma_5)]v(p_2) \equiv \epsilon^\mu A_\mu, \tag{21.76}$$

where ϵ^μ is the polarization of J/ψ. If CP violation, $d = 0$.

From experiment point of view, the decay of $J/\psi \to \Lambda\bar{\Lambda}$ is a good laboratory to search for the EDM of Λ, since this channel has a large branching fraction ($B(J/\psi \to \Lambda\bar{\Lambda}) = (1.54 \pm 0.19) \times 10^{-3}$) and can be well reconstructed with almost no background. The polarization of Λ ($\bar{\Lambda}$) particles are measured by analyzing subsequent $\Lambda(\mathbf{s}_1) \to p(\mathbf{q}_1)\pi^-$,

$\bar{\Lambda}(\mathbf{s}_2) \to \bar{p}(\mathbf{q}_2)\pi^+$ decays with density matrices $\rho_\Lambda = 1+\alpha_+\mathbf{s}_1\cdot\mathbf{q}_1/|\mathbf{q}_1|$ and $\rho_{\bar{\Lambda}} = 1-\alpha_-\mathbf{s}_2\cdot\mathbf{q}_2/|\mathbf{q}_2|$. Experimental observable O can be constructed from $\mathbf{p}, \mathbf{q}_i$ and the electron beam direction $\mathbf{k}$. The expectation value of O is given by

$$\langle O\rangle = \frac{\sqrt{1-4m^2/M^2}}{2M\Gamma(J/\psi\to\Lambda\bar{\Lambda})8\pi}\frac{1}{(4\pi)^3}\int d\Omega_p d\Omega_{q_1} d\Omega_{q_2} OTr\{R_{ij}\rho_{ji}\rho_\Lambda\rho_{\bar{\Lambda}}\}, \tag{21.77}$$

where $R_{ij} = A_iA_j^*$ and ρ_{ij} are the density matrices for J/ψ decays into $\Lambda\bar{\Lambda}$ and J/ψ production form e^+e^-, respectively. The CP-odd observable A and CPT-even observable are constructed as:

$$\begin{aligned} A &= \theta(\hat{p}\cdot(\hat{q}_1\times\hat{q}_2)) - \theta(-\hat{p}\cdot(\hat{q}_1\times\hat{q}_2)) \\ B &= \hat{p}\cdot(\hat{q}_1\times\hat{q}_2)\ , \end{aligned} \tag{21.78}$$

where $\theta(x)$ is 1 if $x>0$ and 0 if $x<0$. The expectation values can be expressed as:

$$\begin{aligned} \langle A\rangle &= -\frac{\alpha_-^2\beta^2}{96M\Gamma(J/\psi\to\Lambda\bar{\Lambda})}M^2[2mRe(da^*)+(M^2-4m^2)Re(dc^*)] \\ \langle B\rangle &= -\frac{48}{27\pi}\langle A\rangle\ . \end{aligned} \tag{21.79}$$

The quantity $\langle A\rangle$ is equal to

$$\langle A\rangle = \frac{N^+-N^-}{N^++N^-}, \tag{21.80}$$

where $N^\pm$ indicate events with $\mathrm{sgn}[\mathbf{p}\cdot(\mathbf{q_1}\times\mathbf{q_2})] = \pm$, respectively.

The EDM d_Λ of Λ is related to the quantity $\langle A\rangle$ by the Lagrangian:

$$L_{\mathrm{dipole}} = i\frac{d_\Lambda}{2}\bar{\Lambda}\sigma_{\mu\nu}\gamma_5\Lambda F^{\mu\nu},$$

where $F^{\mu\nu}$ is the field strength of the electromagnetic field. Exchanging a photon between Λ and a c quark, the CP violating $c-\Lambda$ interaction is expressed by

$$L_{c-\Lambda} = -\frac{2}{3M^2}ed_\Lambda(p_1^\mu-p_2^\mu)\bar{c}\gamma_\mu c\bar{\Lambda}i\gamma_5\Lambda$$

From these relations one has $d = -\frac{2.5}{3M^2}ed_\Lambda$, thus

$$|\langle A\rangle| = \begin{cases} 5.6\times10^{-3}d_\Lambda/(10^{-16}e\ \mathrm{cm}), & \text{if the } a \text{ term dominates} \\ 1.25\times10^{-2}d_\Lambda/(10^{-16}e\ \mathrm{cm}), & \text{if the } c \text{ term dominates} \end{cases} \tag{21.81}$$

The experimental upper bound on d_Λ is $1.5\times10^{-16}e$ cm [448]. If d_Λ indeed has a value close to its experimental upper bound, the asymmetry $|\langle A\rangle|$ can be as large as 10^{-2}. So $\langle A\rangle$ can be used to improve the bound on d_Λ. If 10×10^9 J/ψ events can be produced, one can improve the upper bound on d_Λ by more than an order of magnitude. The same analysis can be easily applied to J/ψ to Σ, Ξ, etc.

Quantitative predictions for CP violation in hyperon decays indicating that $A = \frac{\alpha_\Lambda + \alpha_\Lambda}{\alpha_\Lambda - \alpha_\Lambda}$ should be in the range $(-2 \times 10^{-5} \sim -1 \times 10^{-4})$. Present experimental results dose not have a sufficient sensitivity to observe such a small effect, BESIII provides an opportunity to measure this quality. As shown by DM2 collaboration, the decay of $J/\psi \to \Lambda\bar{\Lambda}$ can be used to look for CP violation by test of the correlation of p and $\bar{p}$ momentum in the mother system frame [548]. The differential cross-section of the $J/\psi \to \Lambda\bar{\Lambda} \to p\pi^-\bar{p}\pi^+$ decay can be expressed as:

$$\frac{d\Gamma}{d\cos\theta d\Omega' d\Omega''} \propto 2\left|\frac{A_{++}}{A_{--}}\right| \sin^2\theta[1 - \alpha_\Lambda\alpha_{\bar{\Lambda}}(\cos\theta'\cos\theta'' - \sin\theta'\sin\theta''\cos(\phi' - \phi''))] + (1 + \cos^2\theta)(1 + \alpha_\Lambda\alpha_{\bar{\Lambda}}\cos\theta'\cos\theta'', \quad (21.82)$$

where α_Λ ($\alpha_{\bar{\Lambda}}$) is the Λ ($\bar{\Lambda}$) decay constant. $A_{\lambda_1\lambda_2}$ and θ are the helicity amplitude and polar angle of the out-going Λ for the $J/\psi \to \Lambda\bar{\Lambda}$, respectively. The angular variables of Ω' and Ω" are defined as shown in Fig. 21.9. From this equation, the quantity $\alpha_\Lambda\alpha_{\bar{\Lambda}}$ can be obtained experimentally as shown in Figure 21.10.

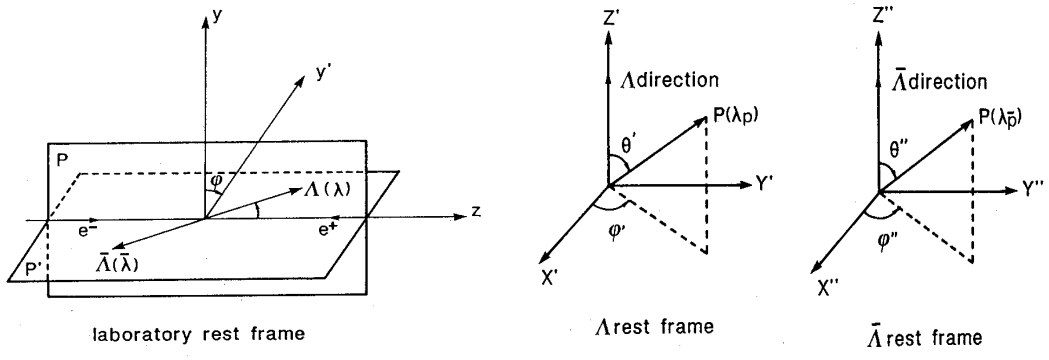

Figure 21.9: The definition of the angles for $\Lambda, \bar{\Lambda}, p, \bar{p}, \pi^+$ and π^- in helicity system.

As Tornqvist [549] demonstrated that the decay η_c, $J/\psi \to \Lambda\bar{\Lambda}$ are experimental realization of the Bell's conceptual proposition to test Quantum Mechanics versus local hidden variable theories. The initial state is well known and due to parity symmetry breaking, the Λ decay works as a spin analyzer. The proton direction plays the same part that the direction of external polarimeter in classical experiments [550]. Then the important quantity is the scalar product of p and $\bar{p}$ in the Λ and $\bar{\Lambda}$ rest frame. The differential cross-section of the $\eta_c \to \Lambda\bar{\Lambda}$ decay is directly proportional to $\vec{a}\cdot\vec{b}$. So it is the most sensitive test of Quantum Mechanics since this scalar product can be compared to Bell's inequality. The decays $\eta_c \to \Lambda\bar{\Lambda}$ was recently observed by Belle Collaboration [553] with a branching fraction of $(8.7 \pm 3.7) \times 10^{-4}$. This would result in a $\eta_c \to \Lambda\bar{\Lambda}$ sample of about 100,000 events in a 10 billion J/ψ sample, it will be a very good sample for the study. For the $J/\psi \to \Lambda\bar{\Lambda}$, Tornqvist reformulated the differential cross-section as:

$$\frac{d\Gamma}{d\cos\theta d\Omega' d\Omega"} \propto 2(1 - \frac{p_\Lambda^2}{E_\Lambda^2}\sin^2\theta)(1 - \alpha_\Lambda^2 a_n b_n) + \frac{p_\Lambda^2}{E_\Lambda^2}\sin^2\theta[1 - \alpha_\Lambda^2(\vec{a}\cdot\vec{b} - 2a_x b_x)], \quad (21.83)$$

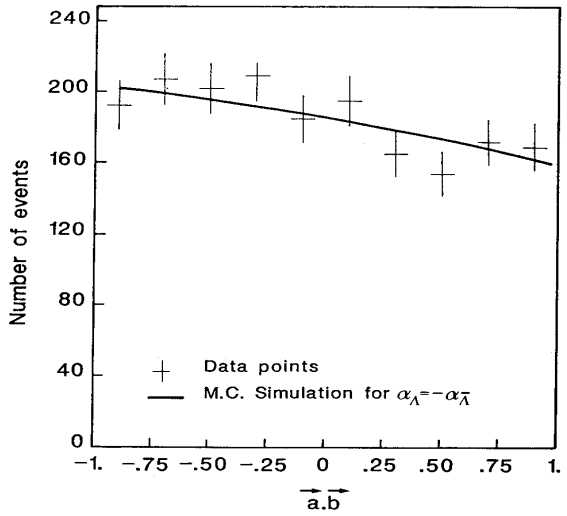

Figure 21.10: The $\vec{a}\cdot\vec{b}$ distribution, where the solid line is M.C. simulation and the crosses with error bars are data.

where $\vec{a}$ and $\vec{b}$ are the proton and antiproton momentum, respectively in the Λ ($\bar{\Lambda}$) rest frame, x is the direction orthogonal to the $\Lambda\bar{\Lambda}$ direction and to the e^+e^- beam axis and $\vec{n}$ is an axis defined to take into account the suppression of 0-spin projection in the J/ψ decays. The terms containing $a_n b_n$ or $a_x b_x$ only reduce the sensitivity of the test since they do not depend on the nature of the theory, and they play the same role as hidden parameters [549]. The contribution of the $\vec{a}\cdot\vec{b}$ term is important for the test of Quantum Mechanics. Unfortunately p_Λ^2/E_Λ^2 at J/ψ is only equal to 0.48 and α_Λ^2 to 0.412, which reduce the contribution of the $\vec{a}\cdot\vec{b}$ term in experimental measurement.

As DM2 collaboration measured, the $\vec{a}\cdot\vec{b}$ distribution is plotted in Fig. 21.9 and compared with that expected from standard physics (Quantum Mechanics and CP invariance). The agreement is very good by taking the PDG value $\alpha_\Lambda = -\alpha_{\bar\Lambda} = 0.642 \pm 0.013$. Fixing the α_Λ parameter to its standard value (0.642), the fit to the $\vec{a}\cdot\vec{b}$ distribution yields the value of $\alpha_{\bar\Lambda}$, which gives value of the asymmetry decay parameter:

$$A = \frac{\alpha_\Lambda + \alpha_{\bar\Lambda}}{\alpha_\Lambda - \alpha_{\bar\Lambda}} = 0.01 \pm 0.10$$

with observed 1077 events for the $J/\psi \to \Lambda\bar{\Lambda}$. The precision of this measurement does not permit to conclude the observation of CP violation. With 10^{10} J/ψ events, the sensitivity is expected to be 8×10^{-4}.

The measurement of the correlation between the proton and antiproton in $J/\psi \to \Lambda\bar{\Lambda}$ decay is associated with the test of Bell's inequality. For example, in the $\eta_c \to \Lambda\bar{\Lambda} \to p\bar{p}\pi^+\pi^-$ decay, the spin correction between the two nucleon predicted by Quantum Mechanics can be expressed by'[549]:

$$I(\vec{a},\vec{b}) \propto 1 + \alpha^2 \vec{a}\cdot\vec{b}, \tag{21.84}$$

while a hidden measurement of Λ polarization before the decay would reduce the slope to

$\alpha^2/3$, i.e.

$$I(\vec{a},\vec{b}) \propto 1 + \frac{\alpha^2}{3}\vec{a}\cdot\vec{b}. \tag{21.85}$$

Using invariance under rotations and reflections, one can derive special bound for Bell's inequality:

$$|E(\theta)| \leq 1 - \frac{2}{\pi}\theta,\ 0 \leq \theta \leq \pi.$$

Figure 21.11 shows the distribution in the angle θ between two pions as predicted by Quantum Mechanics and the area bounded by Bell's inequality.

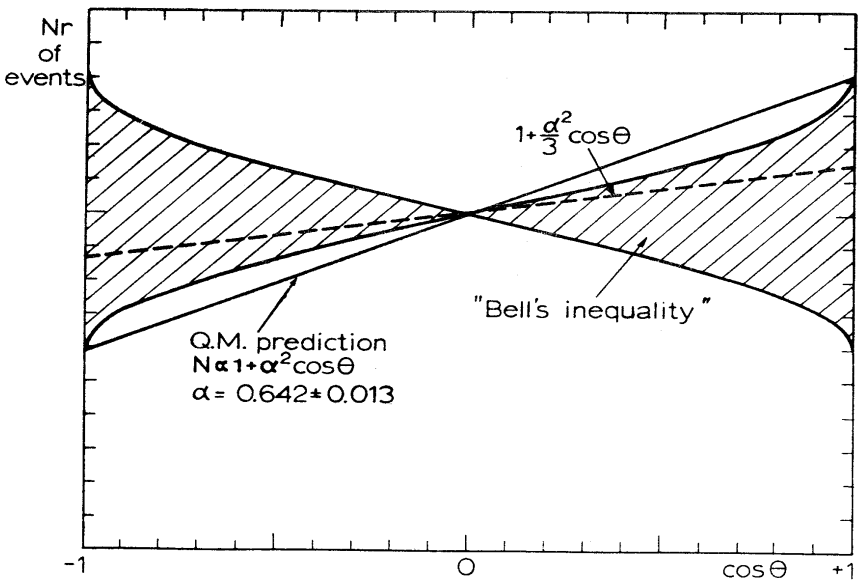

Figure 21.11: The distribution in the angle θ between the π^+ and the π^- as predicted by Quantum Mechanics (solid line), and if a "hidden" Λ polarization measurement is done before the decay (dashed line). The shaded area gives the domain where the inequality is satisfied.

Exotic states

As well known, besides conventional quark states, QCD theory also predicts the existence of multiquark states, hybrid states and other exotic states. Searching for such exotic states has been attempted for a long time, but none is established experimentally. One of the difficulty to identify exotic states is to search for their signature properties to distinguish them from the common states or get information about their mixing. So it is important for experimental experts to collaborate closely with theoretical physicist. As our knowledge about common hadronic structure, hadronic spectroscopy will continue to be a key tool to search for N^* states (see the section of "Baryon spectroscopy") and exotic states. Various models and methods have been used to predict the spectrum of hybrid mesons/baryons, such as the bag model, QCD sum rule, the flux tube model, and so on. Though each model assumes a particular description of exited glue, fortunately they

often reach similar conclusion regarding the quantum numbers and approximate masses of these states. For instance, the predictions on the light hybrid mesons are in good agreement with each other, with the so-called exotic number $J^{PC} = 1^{-+}$ and the mass about 1.5-2.0 GeV. In baryon sector, the Roper resonance $N^*(1440)$ has been suggested to be a potential candidate of hybrid baryons for a long time.

As shown in Ref. [551], BEPCI/BEPCII provides an excellent place for studying Roper resonance. Using 58×10^6 J/ψ decays, the $N^*(1440)$ is clear seen with statical significance of 11σ. For identification of Roper resonance as a hybrid state, the transitional information of amplitudes play an important role in partial wave analysis in the future. As demonstrated in Ref. [552], If the Roper resonance is assigned as a pure hybrid state, numerical results show that the ratio $\Gamma(J/\psi^{(\Lambda)} \to \bar{p}N^*)/\Gamma(J/\psi^{(\Lambda)} \to \bar{p}p) < 2\%$, and $\Gamma(J/\psi^{(\Lambda)} \to \bar{N}^*N^*)/\Gamma(J/\psi^{(\Lambda)} \to \bar{p}p) < 0.2\%$, and their angular distribution parameters are $\alpha_* = 0.42 \sim 0.57$ and $\alpha_{**} = (-0.1) - (-0.9)$, respectively. However, when the Roper resonance is assumed to be a common $2S$ state, the results are quite different, with $\Gamma(J/\psi^{(\Lambda)} \to \bar{p}N^*)/\Gamma(J/\psi^{(\Lambda)} \to \bar{p}p) = 2.0 \sim 4.5$, and $\Gamma(J/\psi^{(\Lambda)} \to \bar{N}^*N^*)/\Gamma(J/\psi^{(\Lambda)} \to \bar{p}p) = 3.2 \sim 22.0$, and with the angular distribution parameter $\alpha_* = 0.22 \sim 0.70, \alpha_{**} = 0.06 \sim 0.08$. This implies that, not only the dynamics of three gluons and created quarks , but also the structure of the final cluster state , i.e. $|qqq\rangle$ or $|qqqg\rangle$, play important roles in the evaluation of the amplitudes in these decay processes. So it is suggestive that an accurate measurement of the decay widths and angular distributions of these channels may provide us a novel tool to probe the structure of the Roper resonance. If the Roper resonance is assumed as a mixture of a pure quark state $|qqq\rangle$ with a hybrid state $|qqqg\rangle$ modelled with a mixing parameter δ, the results show that the hybrid constituent make a large contribution to the decay width of J/ψ decay into $\bar{p}N^*(1440)$ and $\bar{N}^*(1440)N^*(1440)$.

It goes without saying that the search for the pentaquark state $\Theta(1540)^+$ in J/ψ and $\psi(2S)$ decays into $p\bar{n}K_S^0K^-$ and $\bar{p}nK_S^0K^+$. With 14 million $\psi(2S)$ and 58 million J/ψ events accumulated at the BESII detector. No $\Theta(1540)$ signal is observed, and upper limits are set for $\mathcal{B}(\psi(2S) \to \Theta\bar{\Theta} \to K_S^0pK^-\bar{n} + K_S^0\bar{p}K^+n) < 0.84 \times 10^{-5}$ and $\mathcal{B}(J/\psi \to \Theta\bar{\Theta} \to K_S^0pK^-\bar{n} + K_S^0\bar{p}K^+n) < 1.1 \times 10^{-5}$ at the 90% confidence level [554]. By far there have been a number of other high statistics experiments, none of which have found any evidence for the Θ^+; and all attempts to confirm the two other claimed pentaquark states have led to negative results. As reviewed by Particle Data Group 2006, *"Pentaquarks in general, and Θ^+, in particular, do not exist, appears compelling."*

Nucleon-nucleon and meson-nucleon bound states

Searching for nucleon-nucleon and meson-nucleon bound states is an intriguing problem in study of the nuclear interaction. Recent discovery of enhancements of baryon-anitbaryon pair near threshold, as we discussed before, stimulates great interests to search for possible bound states in experiments of high energy physics. So in this section, we first introduce some studies on the bound states from point view of nuclear physics, then turn to the search for them in e^+e^- collider at charmonium energy region.

The idea of explaining the interaction between nucleons at quark level was put forth three decades ago [557]. Resorting to the quark and gluon theory, the nucleon interac-

tion at short distances which has been credited to vector-meson exchanges could then be interpreted as a manifestation of diquark-diquark and quark-quark interaction. In this line, the QCD van der Waals force was introduced to describe a special kind of bound states – charmonium-nucleon bound states [558], say η_c-N or J/ψ-N bound state. In QCD picture, the nuclear forces are identified with the residual strong color interactions due to quark interchange and multiple-gluon exchange. The peculiar feature of charmonium-nucleon bound state lies in that because of the distinct flavors of the quarks involving in the charmonium-nucleon interaction there is no quark exchange to the first order in elastic processes, and therefore no one-meson-exchange potential from which to build an usual nuclear potential. The nuclear interaction in this case is the purely gluonic and thus of a distinctive nature from the ordinary nuclear forces. The production of charmonium-nucleon bound state would be the first realization of hadronic nuclei with exotic components bound by a purely gluonic potential. In Ref. [558], the non-relativistic Yukawa-type attractive potential $V_{(Q\overline{Q})A} = -\alpha e^{-\mu r}/r$ is utilized to characterize the QCD van der Waals interaction. The estimation indicates that the QCD van der Waals interaction due to multiple-gluon exchange can provide a kind of attractive nuclear force capable of binding heavy quarkonia to nuclei.

Following the above idea, the ϕ-N bound state was studied in Ref. [559]. Similar to charmonium state, here the ϕ meson is almost a pure $s\overline{s}$ state, so one could expect that the attractive QCD van der Waals force dominates the ϕ-N interaction. Using the variational method and following Ref. [558] to assume $V_{(Q\overline{Q})N} = -\alpha e^{-\mu r}/r$, it was found [559] that a bound state of ϕ-N is possible, with the binding energy around 1.8 MeV.

Recently, the structure of ϕ-N bound state with spin-parity $J^P = 3/2^-$ and $J^P = 1/2^-$ are dynamically studied in both the chiral $SU(3)$ quark model and the extended chiral $SU(3)$ quark model [560]. In the chiral $SU(3)$ quark model, the quark-quark interaction containing confinement, one gluon exchange (OGE) and boson exchange stemming from scalar and pseudoscalar nonets, and short range quark-quark interaction is provided by OGE and quark exchange effects. Anyway, it is still a controversial problem for low-energy hadron physics whether gluon or Goldstone boson is the proper effective degree of freedom besides the constituent quark. Thus the $SU(3)$ quark model has been extended to include the coupling of the quark and vector chiral fields, and the role of OGE in the short range quark-quark interaction is then nearly replaced by the vector meson exchanges. This so-called the extended chiral SU(3) quark model can successfully reproduce many physics features as does of the chiral SU(3) quark model. Therefore, both models are adopted to study ϕ-N bound state, where N and ϕ are treated as two clusters and the corresponding resonating group method (RGM) equation are solved. The calculation results indicate the mechanisms of the quark-quark short-range interaction are quite different for two chiral models. Moreover, one result from the extended chiral SU(3) quark model indeed indicates the existence of ϕ-N bound.

Now we turn to experiment aspect of searching ϕ-N bound state in e^+e^- collider. The calculation [561] gives $M_{\phi N} \simeq 1950 \sim 1957$ MeV and $\Gamma_{\phi N} \simeq 4.4$ MeV, that is, the intrinsic width of the ϕ meson. The invariant mass of ϕ constructed from two kaons is always less than that of free ϕ due to the existence of bounding energy. Or the mass deficit can be understood as the results of the fact that the ϕ decays off its energy shell when bound to the nucleus.

As the total mass of the ϕN system and a $\bar{N}$ is close to 3.0 GeV, the production of such state in J/ψ decays will be suppressed greatly due to small phase space, however, it can be produced in ψ' decays, or from χ_{cJ} decays with much larger phase space, although with less statistics.

The decays of the ϕN bound state could be $K\bar{K}N$, with $K\bar{K}$ mass below the ϕ resonance, in experiment, one expect a shoulder in the lower mass side of the ϕ meson or another narrow peak below the ϕ resonance. In principle, there could be interference between $\phi \to K\bar{K}$ and the $K\bar{K}$ from ϕN bound state decays, this may make the identification of the bound state hard.

The annihilation of the $s\bar{s}$ quark inside the ϕ meson is not small, so another way of searching for the ϕN bound state is through its decay into $\pi^+\pi^-\pi^0 + N$, considering the large branching fraction of $\phi \to \pi^+\pi^-\pi^0$, with even smaller phase space to $K\bar{K}N$, the decay rate of the ϕN bound state to $\pi^+\pi^-\pi^0 + N$ could even be larger. However, the background may be more serious in the $\pi^+\pi^-\pi^0 + N$ mode.

21.3.7 Summary and discussion

In this review, we first collected some theoretical explorations about explaining the charmonium dynamics and some phenomenological models usually used in high energy physics.

The experiment measurements are collected as much as possible to test the theoretical predictions and provide clues for further understanding the charmonium decay dynamics.

From the review presented, we notice that on one hand most of theoretical explanations are still qualitative and on the other hand the experiment data are rather limit and with fairly large uncertainties. Anyway, with unprecedented large data sample at the forthcoming new detector BESIII, we could make a splendid systematic experiment plan for hadronic decay study, from η_c to ψ'' or even higher energy; on resonances and off resonances; for strong interaction and electromagnetic interaction; about phenomenology and dynamics; find some empirical rules, establish an considerable universal model, or come across an unexpected discovery. It seems a bright future is waiting for us.

21.4 Rare and forbidden charmonium decays[6]

At present, two general trends may be distinguished in accelerator particle physics. On one hand, the very high energy accelerators, for example LHC, will permit to explore the frontier line of high energy physics. On the other hand, smaller or low energy experiments but with very high statistics and low backgrounds (B factories and BESIII for τ-Charm) would allow to perform precise tests and accurate determinations of many parameters of the Standard Model. Moreover, the scrutiny of rare processes may enlight new physics in a complementary fashion to high-energy colliders.

With huge J/ψ and $\psi(2S)$ data samples, *BES-III* experiment will be approaching the statistics where rare ψ decays can provide important tests of the standard model and possible be able to uncover deviations.

21.4.1 Weak Decays of Charmonium

The low lying charmonium states below the open charm threshold usually decay through intermediate photons or gluons produced by the parent $c\overline{c}$ quark pair annihilation. These OZI violating but flavor conserving decays lead to narrow widths to J/ψ and $\psi(2S)$ states. In the standard model framework, the flavor changing weak decays of these states are also possible though these are expected to have rather low branching fractions. Huge J/ψ data sample at *BES-III* would afford to examine those rare decay processes, which may become detectable. The observation of any anomalous production rate of single charmed meson in J/ψ or $\psi(2S)$ decays at *BES-III* would be a hint of possible new physics either in the continuum via flavor-changing neutral currents [601] or in the decays of resonances due to unexpected effects of quark dynamics [602].

Semileptonic Decays of Charmonium

The inclusive branching fractions of J/ψ weak decays via a single quark of either c or $\overline{c}$ had been estimated to be $(2-4)\times 10^{-8}$ by ignoring any W-exchanged contribution and using the D^0 lifetime [603]. Such small branching ratios should make the observation of weak decays of J/ψ or $\psi(2S)$ extremely difficult despite the foreseen cleanness of events. However, at BEPC-II with a peak luminosity of $10^{33}cm^{-2}s^{-1}$ at $\psi(3770)$, the expected number of J/ψ is 10×10^9 per year of data taking, leading to $\cong$ 400 weak decays when combined with the predicted branching ratio. The semi-leptonic decay of vector charmonium below open charm threshold, $c\overline{c}(1^{--})$, induced by the quark level weak transition $c\to qW^*$, where W^* are virtual intermediate boson. Hence, the exclusive semi-leptonic channels are:

$$\psi(nS)\to D_q l\nu, \tag{21.86}$$

$$\psi(nS)\to D_q^* l\nu, \tag{21.87}$$

[6]By Haibo Li, Jianping Ma and Xinmin Zhang

where $n = 1, 2$, q can be down or strange quark which corresponds to $D^{\pm}$(Cabibbo-suppressed mode) or D_s (Cabibbo-allowed mode) meson. Semi-leptonic weak decays of J/ψ will offer several advantages over the purely hadronic ones both from the experimental and theoretical points of view: the prompt charged lepton $l = e, \mu$ can be used to tag the events, removing a large amount of conventional hadronic decays of $\psi(nS)$. Besides, the missing energy due to the escaping neutrino can be also employed experimentally to remove backgrounds. So the reconstructed charm meson in the final state should provide an unambiguous signature of the semi-leptonic weak decays of $\psi(nS)$. Meanwhile, radiative decays of the excited mesons D_s^* and $D^{*\pm}$ in reaction (21.87) can provide a useful extra signal, in the lab system, detectable photons are yielded in the energy interval 90 - 200 MeV for $D_s^{*\pm} \to D_s^{\pm}\gamma$, and a soft pion is produced for the reconstruction of $D^{*\pm}$ in $D^{*\pm} \to D^0\pi^{\pm}$ decay mode. Those are powerful constraint in the mass reconstruction of D_s and D^0 mesons to detect the weak decays of charmonium.

According to Heavy Quark Spin Symmetry (HQSS) [604, 605], the branching ratios for the Cabibbo-allowed modes were estimated as [603]:

$$\begin{aligned} BR(J/\psi \to D_s l\nu) &\cong 0.26 \times 10^{-8}, \\ BR(J/\psi \to D_s^* l\nu) &\cong 0.42 \times 10^{-8}, \end{aligned} \tag{21.88}$$

summing over both modes one gets $BR \cong 0.7 \times 10^{-8}$, which is about 20% of the expected total weak decay rate (4×10^{-8}) as estimated in reference [603]. Taking into account the overall theoretical uncertainty ($\cong$ 40%), the expected branching ratios are within $(0.4 - 1.0) \times 10^{-8}$. For the Cabibbo-suppressed decay modes, one can employ the following ratio:

$$\frac{BR(J/\psi \to D_s l\nu)}{BR(J/\psi \to D^{\pm} l^{\mp}\nu)} = \frac{BR(J/\psi \to D_s^* l\nu)}{BR(J/\psi \to D^{*\pm} l^{\mp}\nu)} \cong \frac{|V_{cs}|^2}{|V_{cd}|^2} \cong 20, \tag{21.89}$$

where $V_{cs} \cong 1.0$ and $V_{cd} \cong 0.22$ denote Cabibbo-Kobayashi-Mashkawa (CKM) mixing matrix elements. According to Heavy Quark Spin Symmetry (HQSS) [604, 605], the branching ratios for the Cabibbo-allowed modes were estimated as [603]:

$$\begin{aligned} BR(J/\psi \to D_s l\nu) &\cong 0.26 \times 10^{-8}, \\ BR(J/\psi \to D_s^* l\nu) &\cong 0.42 \times 10^{-8}, \end{aligned}$$

summing over both modes one gets $BR \cong 0.7 \times 10^{-8}$, which is about 20% of the expected total weak decay rate (4×10^{-8}) as estimated in reference [603]. Taking into account the overall theoretical uncertainty ($\cong$ 40%), the expected branching ratios are within $(0.4 - 1.0) \times 10^{-8}$. For the Cabibbo-suppressed decay modes, one can employ the following ratio:

$$\frac{BR(J/\psi \to D_s l\nu)}{BR(J/\psi \to D^{\pm} l^{\mp}\nu)} = \frac{BR(J/\psi \to D_s^* l\nu)}{BR(J/\psi \to D^{*\pm} l^{\mp}\nu)} \cong \frac{|V_{cs}|^2}{|V_{cd}|^2} \cong 20,$$

where $V_{cs} \cong 1.0$ and $V_{cd} \cong 0.22$ denote Cabibbo-Kobayashi-Mashkawa (CKM) mixing matrix elements.

Two-body Weak Hadronic Decays of Charmonium

For the non-leptonic weak decays of Charmonium, the two-body weak hadronic decays of J/ψ and $\psi(2S)$ in Cabibbo-allowed ($c \to s$) and Cabibbo-suppressed ($c \to d$) modes had been studied by employing the factorization scheme [606], the branching ratios for $\psi \to PP/PV$ decays (where P and V represent pseudoscalar meson and vector meson, respectively) were predicted. Using the decay rate formula (5) in Ref. [606], one computed the branching ratios of various $\psi \to PP$ decays which are listed in Table 21.24. Among the Cabibbo-allowed decays, one find that the dominated decay mode is $\psi \to D_s^+\pi^-$, having the branching ratio

$$BR(\psi \to D_s^+\pi^-) = 0.87 \times 10^{-9}, \tag{21.92}$$

and the next in order is $\psi \to D^0K^0$, whose branching ratio is

$$BR(\psi \to D^0K^0) = 0.28 \times 10^{-9}. \tag{21.93}$$

The branching ratios of $\psi \to PV$ decays in Cabibbo-allowed and Cabibbo-suppressed modes are listed in Table 21.25. For the color enhanced decay of the Cabibbo-allowed modes, one got

$$BR(\psi \to D_s^+\rho^-) = 0.36 \times 10^{-8}, \tag{21.94}$$

which is higher than the branching ratio of $\psi \to D_s^+\pi^-$. Thus, the following useful relative ratio were obtained [606]

$$\frac{BR(\psi \to D_s^+\rho^-)}{BR(\psi \to D_s^+\pi^-)} = 4.2, \tag{21.95}$$

and therefore $\psi \to D_s^+\rho^-$ may be expected to be measured at *BES-III*.

Transition Mode	Decay Modes	Branching ratio($\times 10^{-10}$)
$\Delta C = \Delta S = +1$		
	$\psi \to D_s^+\pi^-$	8.74
	$\psi \to D^0K^0$	2.80
$\Delta C = +1,\ \Delta S = 0$		
	$\psi \to D_s^+K^-$	0.55
	$\psi \to D^+\pi^-$	0.55
	$\psi \to D^0\eta$	0.016
	$\psi \to D^0\eta'$	0.003
	$\psi \to D^0\pi^0$	0.055

Table 21.24: *Branching ratios of $\psi \to PP$ decays from reference [606] in the Standard Model. The transition mode, $\Delta C = \Delta S = +1$, corresponds to Cabibbo-allowed decay modes, while $\Delta C = +1$, $\Delta S = 0$ corresponds to Cabibbo-suppressed decay modes.*

The semi-leptonic decay modes of $\psi(nS)$ can be related to the two-body hadron decay modes by applying both the spin symmetry and the non-recoil approximation to the semi-leptonic decays [603]. For $J/\psi \to D_s^+(D_s^{*+})\pi^-$ decay modes, one gets $q^2 = (p_1 - p_2)^2 =$

Transition Mode	Decay Modes	Branching ratio($\times 10^{-10}$)
$\Delta C = \Delta S = +1$		
	$\psi \to D_s^+ \rho^-$	36.30
	$\psi \to D^0 K^{*0}$	10.27
$\Delta C = +1,\ \Delta S = 0$		
	$\psi \to D_s^+ K^{*-}$	2.12
	$\psi \to D^+ \rho^-$	2.20
	$\psi \to D^0 \rho^0$	0.22
	$\psi \to D^0 \omega$	0.18
	$\psi \to D^0 \phi$	0.65

Table 21.25: *Branching ratios of $\psi \to PV$ decays from reference [606] in the Standard Model. The transition mode, $\Delta C = \Delta S = +1$, corresponds to Cabibbo-allowed decay modes, while $\Delta C = +1$, $\Delta S = 0$ corresponds to Cabibbo-suppressed decay modes.*

m_π^2 (p_1 and p_2 are the four momentum of initial and final state mesons respectively) assuming factorization, as suggested by Bjorken [607] in B decays. Keeping the non-recoil approximation in the hadronic transition amplitudes [608], from the equations (7) and (8) in reference [603], one arrives at a relative branching ratio:

$$\frac{BR(J/\psi \to D_s^{*+}\pi^-)}{BR(J/\psi \to D_s^{+}\pi^-)} \cong \left[\frac{d\Gamma(J/\psi \to D_s^{*+} l^- \nu)/dq^2}{d\Gamma(J/\psi \to D_s^{+} l^- \nu)/dq^2}\right]_{q^2=m_\pi^2} \cong 3.5, \tag{21.96}$$

if a ρ substitutes the π one gets $r \cong 1.4$. So the estimated branching ratios in Table 21.24 for $\psi(nS) \to PP$ channel can be related to $\psi(nS) \to VP$ channel if the pseudoscalar charm mesons are replaced by a vector charm mesons.

All the above estimations show an overall enhancement of final vector charm mesons with respect to the pseudoscalar ones. It suggests once more the use of D_s^* or $D^{*\pm}$ as signals to search for the weak decays of $\psi(nS)$ even in non-leptonic decays.

Searches at *BES-III*

At *BES-III*, assuming 10^{10} J/ψ sample to be collected in one year running time, the central value $BR \cong 0.7 \times 10^8$ leads to about 70 semi-leptonic decay events of the type $J/\psi \to D_s(D_s^*)l\nu$. Thus, the following event selection criteria could be applied on searching for such exclusive semi-leptonic channels :

- The prompt charged lepton can be used to tag the weak decay: in order to suppress cascade decay backgrounds from J/ψ strong decays, the tagging lepton momentum could be required in the range from 0.5 GeV to 1.0 GeV, close to the upper kinematic limit for the decay under consideration. A high quality lepton identification from the other charged pions or kaons is needed at *BES-III*.

- The missing mass of the reconstructed candidates must be consistent with zero due to the undetectable neutrino.

- The mass reconstruction of a D_s or $D^{\pm}$ meson can provide an unambiguous signature for the weak decays of $\psi(nS)$, lying below the open charm threshold. The narrow mass window of D_s with good mass resolution is useful to remove the combinatorial backgrounds.

- The soft photon with the energy interval (90- 200) MeV in D_s^* decay and soft charged pions in $D^{*\pm}$ decay can be used further to suppress the combinatorial backgrounds: the additional constraint of an intermediate D_s^* state should confirm the D_s signal again.

In general, the exclusive hadronic decays are probably too tiny to look for in a particular full reconstructed channel. Thereby, it seems that an inclusive searching for $J/\psi \to D_s^* + X$ at *BES-III* may be available. The γ from the excited meson should be useful as a kinematic constraint for the mass reconstruction of D_s meson as discussed in [603].

Finally, in the Standard model, the flavor changing neutral current (FCNC) in J/ψ decays are predicted to be unobservable [602], so they serve as a probe of new physics. The purpose of the experimental search for the FCNC processes at *BES-III* is to test whether new physics can enhance the production rate sufficiently. In reference [602], a model-independent theoretical analysis had been performed, then examine the predictions of the models, such as TopColor models, minimal supersymmetric standard model (MSSM) with R-parity violation and a general two-Higgs-doublet model [602]. They found that the branching ratio of $J/\psi \to D/\overline{D}X_u$, which is mediated by $c \to u$ transition, could be as large as $10^{-6} - 10^{-5}$ in the presence of new physics.

Experimentally with *BES-III* data, it is very hard to look for pure $c \to u$ mediated hadronic $J/\psi \to D/\overline{D}X_u$ decays. While, at *BES-III*, it is easy to search for $J/\psi \to D^0/\overline{D^0}l^+l^-$ ($l = e, \mu$) and $J/\psi \to D^0/\overline{D^0}\gamma$ decays which is dominated by FCNC processes.

21.4.2 Search for the invisible decays of Quarkonium

Invisible decays of quarkonium states such as the J/ψ and the Υ, etc., offer a window into what may lie beyond the Standard Model (SM) [609, 610]. The reason is that apart from neutrinos, the Standard Model includes no other invisible final particles that these states can decay into. It is such a window that we intend to further explore by presenting here the first experimental limits on invisible decays of the η and η', which complement the limit of 2.7 10^{-7} recently established in [611] for the invisible decays of the π°.

Theories beyond the SM generally include new physics, such as, possibly, light dark matter (LDM) particles [612]. These can have the right relic abundance to constitute the nonbaryonic dark matter of the Universe, if they are coupled to the SM through a new light gauge boson U [613], or exchanges of heavy fermions. It is also possible to consider a light neutralino with coupling to the SM mediated by a light scalar singlet in the next-to-minimal supersymmetric standard model [614].

Recently, observations of a bright 511 keV γ-ray line from the galactic bulge have been reported by the SPI spectrometer on the INTEGRAL satellite [615]. The corresponding galactic positron flux, as well as the smooth symmetric morphology of the 511 keV emission, may be interpreted as originating from the annihilation of LDM particles into e^+e^-

pairs [612] (also constrained by [616]). It is in any case very interesting to search for such light invisible particles in collider experiments. CLEO gave an upper bound on $\Upsilon(1S) \to \gamma +$ invisible, which is sensitive to dark matter candidates lighter than about 3 GeV/c^2 [617], and also provides an upper limit on the axial coupling of the new U boson to the b quark. It is crucial, in addition, to search for the invisible decays of light quarkonium ($q\overline{q}$, $q = u$,d, or s quark) states which can be used to constrain the masses of LDM particles and the couplings of the new boson to the light quarks [610].

It had been shown that the measurements on the J/ψ invisible decay widths may be sensitive to constrain the physics model [618]. It is straightforward for one to calculate the branching ratio of the invisible decays of J/ψ and its observed decays into electron-positron pairs [618]. Within the SM the invisible mode consists solely of decays into three types of neutrino-antineutrino pairs. Neglecting polarization effects and taking into account e^+e^- production through a photon only, one get [618]:

$$\frac{\Gamma(J/\psi \to \nu\overline{\nu})}{\Gamma(J/\psi \to e^+e^-)} = \frac{27G^2M_{J/\psi}^4}{256\pi^2\alpha^2}\left(1 - \frac{8}{3}sin^2(\theta_W\right)^2 = 4.54 \times 10^{-7}, \qquad (21.97)$$

with G and α being the Fermi and the fine structure constants respectively. $M_{J/\psi}$ is mass of J/ψ. The uncertainty of the above formula is about 2-3% which mainly from the correction to J/ψ wave function, e^+e- production through Z boson, electroweak radiative corrections [618].

At *BES-III*, one can then tag charmonium states which decay invisibly by looking for a particular radiative transition such as $\psi(2S) \to \pi^+\pi^- J/\psi$, $\psi(2S) \to \gamma\chi_c$ and so on, the soft $\pi^+\pi^-$ pairs or monoenergetic radiative γ can be used as tags of the invisible decays of J/ψ or χ_c states. A detail lists of these decay chains are in Table 21.26.

$\psi(2S)$ decay mode	Branching fraction (10^{-2})	Number of events in 3 billions $\psi(2S)$ sample	Invisible decay mode	Tagging topology
$\psi(2S) \to \pi^+\pi^- J/\psi$	31.7 ± 1.1	9.3×10^8	$J/\psi \to$ invisible	$\pi^+\pi^-$
$\psi(2S) \to \pi^0\pi^0 J/\psi$	18.6 ± 0.8	5.6×10^8	$J/\psi \to$ invisible	$\pi^0\pi^0$
$\psi(2S) \to \eta J/\psi$	3.08 ± 0.17	9.3×10^7	$J/\psi \to$ invisible	η
$\psi(2S) \to \pi^0 J/\psi$	0.123 ± 0.018	3.7×10^6	$J/\psi \to$ invisible	π^0
$\psi(2S) \to \gamma\chi_{c0}$	9.0 ± 0.4	2.7×10^8	$\chi_{c0} \to$ invisible	γ
$\psi(2S) \to \gamma\chi_{c1}$	8.7 ± 0.5	2.6×10^8	$\chi_{c1} \to$ invisible	γ
$\psi(2S) \to \gamma\chi_{c2}$	8.2 ± 0.3	2.5×10^8	$\chi_{c2} \to$ invisible	γ
$\psi(2S) \to \gamma\eta_c(1S)$	0.26 ± 0.04	7.8×10^6	$\eta_c(1S) \to$ invisible	γ
$J/\psi \to \gamma\eta_c(1S)$	1.3 ± 0.4	1.3×10^8	$\eta_c(1S) \to$ invisible	γ

Table 21.26: *$\psi(2S)$ and J/ψ decay modes which can be used to study the invisible decays of J/ψ, χ_{c0}, χ_{c1}, χ_{c2}, $\eta_c(1S)$ and $\eta_c(2S)$. The branching fractions are listed from PDG [619]. For each mode, a "tagging topology" is given, which is the set of visible in the detector's acceptance. In each case the tagging topology has a well-defined kinematics. The produced number of events are the expected events in 3 billions $\psi(2S)$ (10 billions J/ψ) data set, in which we did not consider the decay rate of the tagging particles.*

It is also interesting to study the invisible decays of η, η', ρ, ω and ϕ light mesons by using the two-body decay modes of J/ψ. For example, the two-body decay modes

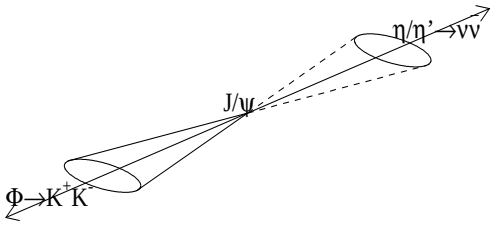

Figure 21.12: *The demonstration of $J/\psi \to \phi\eta$ or $\phi\eta'$, the ϕ, which is reconstructed in the K^+K^- decay mode, and can be used to tag the invisible decays of the missing particles.*

of $J/\psi \to \phi\eta, \phi\eta'$ can be selected in order to study the decays of η and η' to invisible final states, as shown in Fig. 21.12, in which the ϕ signals can be reconstructed easily and cleanly decaying into K^+K^-. The reconstructed ϕ particles can be used to tag the η and η' in order to allow a search for their invisible decays. Since both ϕ and η (η') have narrow widths, which are negligible compared with the detector resolution, the shape of the momentum distribution of the ϕ is approximately Gaussian. The mean value of the ϕ momentum distribution is 1.320 GeV/c for $J/\psi \to \phi\eta$ and 1.192 GeV/c for $J/\psi \to \phi\eta'$. The missing momentum, $P_{miss} = |\vec{P}_{miss}|$, is a powerful discriminating variable to separate signal events from possible backgrounds, in which the missing side is not from η (η') decay. Here, $\vec{P}_{miss} = -\vec{P}_{\phi}$. In addition, the η and η' decay regions are easy to define in the lab system due to the strong boost of the ϕ from J/ψ decay, as shown in Fig. 21.12.

Based on 58 million J/ψ data at BES-II, in $J/\psi \to \phi\eta$ and $\phi\eta'$, we had searched for the invisible decays of η and η' [620]. An unbinned extended maximum likelihood (ML) fit is used to extract the event yield for J/$\psi \to \phi\eta(\eta')$ [$\phi \to K^+K^-$ and $\eta(\eta') \to$ invisible]. In the ML fit, we use P_{miss} as the discriminating variable and require that $1.00 < P_{miss} < 1.45$ GeV/c, shown in Fig. 21.13(b), where the background shape is well understood. We construct probability density functions (PDFs) for the P_{miss} distributions for ($\mathcal{F}^{\eta}_{sig}$ and $\mathcal{F}^{\eta'}_{sig}$) signals and background ($\mathcal{F}_{bkgd}$) using detailed simulations of signal and background. The PDFs for signals are parameterized by double Gaussian distributions with common means, one relative fraction and two distinct widths, which are all fixed to the MC simulation. The PDF for background is a bifurcated Gaussian plus a first order Polynomial (P_1). All parameters related to the background shape are floated in the fit to data. The PDFs for signals and background are combined in the likelihood function $\mathcal{L}$, defined as a function of the free parameters N^{η}_{sig}, $N^{\eta'}_{sig}$, and N_{bkgd},

$$\mathcal{L}(N^{\eta}_{sig}, N^{\eta'}_{sig}, N_{bkgd}) = \frac{e^{-(N^{\eta}_{sig}+N^{\eta'}_{sig}+N_{bkgd})}}{N!} \times \prod_{i=1}^{N} [N^{\eta}_{sig}\mathcal{F}^{\eta}_{sig}(P^i_{miss}) + N^{\eta'}_{sig}\mathcal{F}^{\eta'}_{sig}(P^i_{miss}) + N_{bkgd}\mathcal{F}_{bkgd}(P^i_{miss})], \quad (21.98)$$

where N^{η}_{sig} and $N^{\eta'}_{sig}$ are the number of $J/\psi \to \phi(\to K^+K^-)\eta(\to$ invisible) and $J/\psi \to \phi(\to K^+K^-)\eta'(\to$ invisible) signal events; N_{bkgd} is the number of background events. The

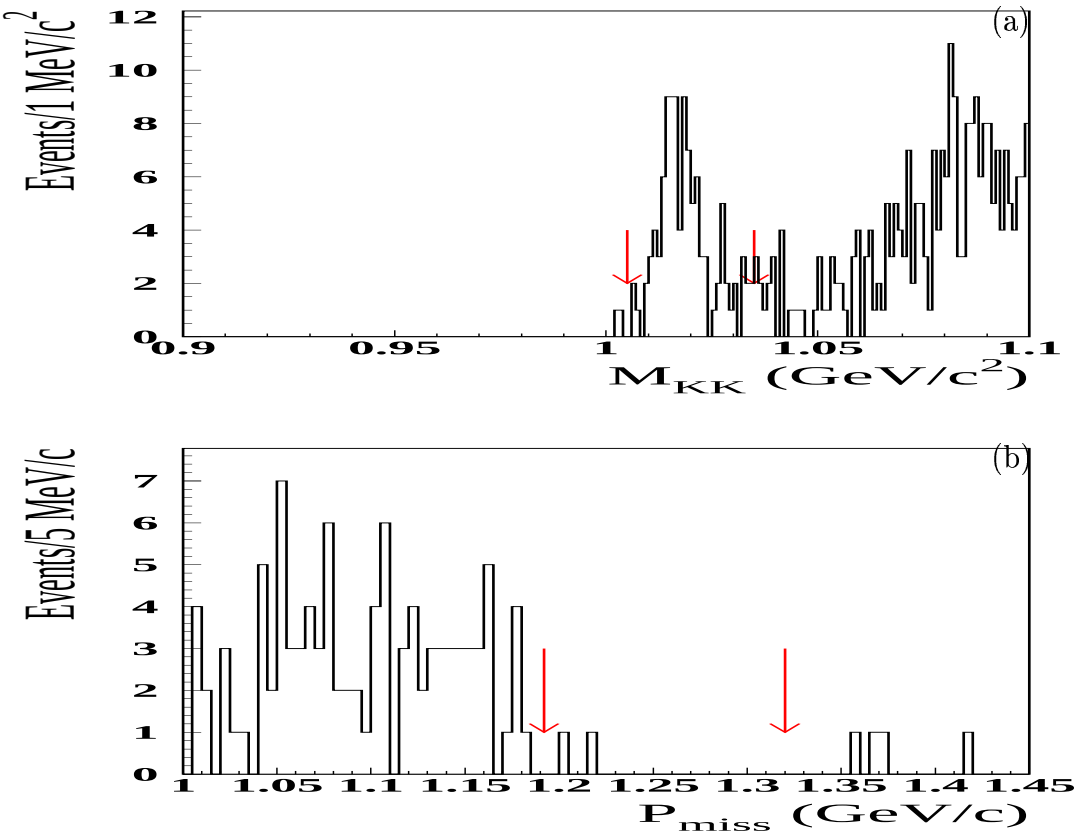

Figure 21.13: (a) The m_{KK} distribution for candidate events. The arrows on the plot indicate the signal region of ϕ candidates. (b) P_{miss} distribution for the events with $1.005 < m_{KK} < 1.035$ GeV/c^2 in (a). The means of the missing momenta for $J/\psi \to \phi\eta$ and $J/\psi \to \phi\eta'$ are located around 1.32 and 1.20 GeV/c, respectively, as indicated by the two arrows.

fixed parameter N is the total number of selected events in the fit region, and P^i_{miss} is the value of P_{miss} for the ith event. The negative log-likelihood ($-\ln\mathcal{L}$) is then minimized with respect to N^{η}_{sig}, $N^{\eta'}_{sig}$, and N_{bkgd} in the data sample. A total of 105 events are used in the fit, and the resulting fitted values of N^{η}_{sig}, $N^{\eta'}_{sig}$, and N_{bkgd} are -2.8 ± 1.4, 2.2 ± 3.4, and 106 ± 11, where the errors are statistical. Figure 21.14 shows the P_{miss} distribution and fitted result. No significant signal is observed for the invisible decay of either η or η'. We obtain upper limits by integrating the normalized likelihood distribution over the positive values of the number of signal events. The upper limits at the 90% confidence level are 3.56 events for η and 5.72 events for η', respectively.

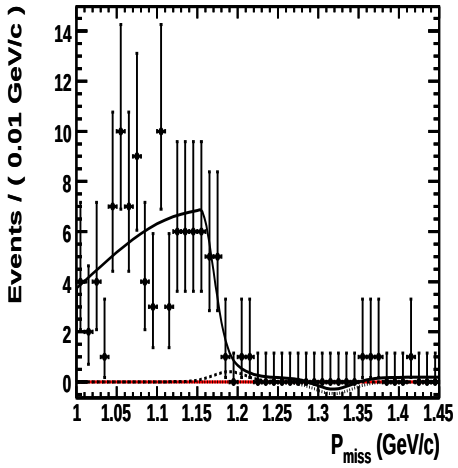

Figure 21.14: The P_{miss} distribution for candidate events. The data (black crosses) are compared to the total fit results. The dotted curve is the projection of η signal component, and the dashed curve is the projection of η' signal component, and the solid curve is the total likelihood fit result.

The branching fraction of $\eta(\eta') \to \gamma\gamma$ is also determined in $J/\psi \to \phi\eta(\eta')$ decays, in order to obtain the ratio of $\mathcal{B}(\eta(\eta') \to \text{invisible})$ to $\mathcal{B}(\eta(\eta') \to \gamma\gamma)$. The advantage of measuring $\dfrac{\mathcal{B}(\eta(\eta') \to \text{invisible})}{\mathcal{B}(\eta(\eta') \to \gamma\gamma)}$ is that the uncertainties due to the total number of J/ψ events, tracking efficiency, PID, the number of the charged tracks, the cut on m_{KK}, and residual noise in the BSC cancel.

The upper limit on the ratio of the $\mathcal{B}(\eta \to \text{invisible})$ to $\mathcal{B}(\eta \to \gamma\gamma)$ is calculated with

$$\frac{\mathcal{B}(\eta \to \text{invisible})}{\mathcal{B}(\eta \to \gamma\gamma)} < \frac{n^{\eta}_{UL}/\epsilon_{\eta}}{n^{\eta}_{\gamma\gamma}/\epsilon^{\eta}_{\gamma\gamma}} \cdot \frac{1}{(1-\sigma_{\eta})} \tag{21.99}$$

where n^{η}_{UL} is the 90% upper limit of the number of observed events for $J/\psi \to \phi\eta$, $\phi \to K^+K^-$, $\eta \to$ invisible decay, ϵ_{η} is the MC determined efficiency for the signal channel, $n^{\eta}_{\gamma\gamma}$ is the number of events for the $J/\psi \to \phi\eta$, $\phi \to K^+K^-$, $\eta \to \gamma\gamma$ decay, $\epsilon^{\eta}_{\gamma\gamma}$ is the MC determined efficiency for the decay mode, and σ_{η} is $\sqrt{(\sigma^{sys}_{\eta})^2 + (\sigma^{stat}_{\eta})^2} = 8.1\%$, where σ^{sys}_{η} and σ^{stat}_{η} are the total relative systematical error for the η case from Table 21.27 and

the relative statistical error of $n^{\eta}_{\gamma\gamma}$, respectively. For η', $\sigma_{\eta'}$ is $\sqrt{(\sigma^{sys}_{\eta'})^2+(\sigma^{stat}_{\eta'})^2}=21.6\%$. The relative statistical error of the fitted yield for $J/\psi\to\phi\eta(\eta')$, $\eta(\eta')\to\gamma\gamma$, is 2.8% (18.5%) according to the results from the fit to the invariant mass of $\gamma\gamma$. We also obtain the upper limit on the ratio of the $\mathcal{B}(\eta'\to$ invisible) to $\mathcal{B}(\eta'\to\gamma\gamma)$ by replacing η with η' in Eq. (21.99).

Table 21.27: *The numbers used in the calculations of the ratios in Eq. (21.99), where n^{η}_{UL} ($n^{\eta'}_{UL}$) is the upper limit of the signal events at the 90% confidence level, ϵ_{η} ($\epsilon_{\eta'}$) is the selection efficiency, $n^{\eta}_{\gamma\gamma}$ ($n^{\eta'}_{\gamma\gamma}$) is the number of the events of $J/\psi\to\phi\eta(\eta')$, $\phi\to K^+K^-$, $\eta(\eta')\to\gamma\gamma$, $\epsilon^{\eta}_{\gamma\gamma}$ ($\epsilon^{\eta'}_{\gamma\gamma}$) is its selection efficiency. σ^{stat}_{η} ($\sigma^{stat}_{\eta'}$) is the relative statistical error and σ^{sys}_{η} ($\sigma^{sys}_{\eta'}$) is the relative statistical error of $n^{\eta}_{\gamma\gamma}$ ($n^{\eta'}_{\gamma\gamma}$), σ_{η} ($\sigma_{\eta'}$) is the total relative error.*

quantity	value	
	η	η'
n^{η}_{UL} ($n^{\eta'}_{UL}$)	3.56	5.72
ϵ_{η} ($\epsilon_{\eta'}$)	23.5%	23.2%
$n^{\eta}_{\gamma\gamma}$ ($n^{\eta'}_{\gamma\gamma}$)	1760.2 ± 49.3	71.6 ± 13.2
$\epsilon^{\eta}_{\gamma\gamma}$ ($\epsilon^{\eta'}_{\gamma\gamma}$)	17.6%	15.2%
σ^{stat}_{η} ($\sigma^{stat}_{\eta'}$)	2.8%	18.5%
σ^{sys}_{η} ($\sigma^{sys}_{\eta'}$)	7.7	11.1
σ_{η} ($\sigma_{\eta'}$)	8.1%	21.6%

Using the numbers in Table 21.27, the upper limit on the ratio of $\mathcal{B}(\eta(\eta')\to$ invisible) and $\mathcal{B}(\eta(\eta')\to\gamma\gamma)$ is obtained at the 90% confidence level of 1.65×10^{-3} (6.69×10^{-2}).

In Table 21.28, we listed possible two-body J/ψ decay modes which can be used to study the invisible decays of η, η', ρ, ω and ϕ.

21.4.3 Search for C or P violating processes in J/ψ decays

With huge J/ψ and $\psi(2S)$ data samples, *BES-III* experiment will be approaching the statistics where rare ψ decays can provide important tests of the standard model and possible be able to uncover deviations. One of the interesting examples is C, P or CP violating processes in J/ψ decays. An example of such modes would be $\psi(nS)\to V^0V^0$, where V^0 is $J^{PC}=1^{--}$ vector mesons (ϕ, ω, ρ^0 and γ). The clearest possible signal of this class of events would be $\psi(nS)\to\phi\phi$ which would be detected in $\psi(nS)\to K^+K^-K^+K^-$. Due to C violation the $\psi(nS)\to V^0V^0$ decays can only occur via $c\bar{c}$ annihilation and W-exchanged weak decays of J/ψ as discussed in Ref. [621]. The rate of this kind of weak decay can provide a measurement of the charmonium wave function at the origin [621].

To get a rough idea, whether the weak interaction signal $\psi(nS)\to\phi\phi$ could be expected to be seen at *BES-III*. Note that an $s\bar{s}$ must be produced from the vacuum which binds with the outgoing $s\bar{s}$ from $c\bar{c}$ decays to form $\psi(nS)\to\phi\phi$ [621]. When this is done, the photon exchange piece must cancel since the final state can only occur when C (or P) violating interactions are present. In order to make a rough estimate, one can

J/ψ decay mode	Branching fraction (10^{-4})	Invisible decay mode	Tagging topology	Number of events in 10 billions J/ψ sample
$J/\psi \to \phi\eta$	6.5 ± 0.7	$\eta \to$ invisible	$\phi \to K^+K^-$	$(31.4 \pm 3.4) \times 10^5$
	6.5 ± 0.7	$\phi \to$ invisible	$\eta \to \gamma\gamma$	$(25.7 \pm 2.8) \times 10^5$
$J/\psi \to \phi\eta'$	3.3 ± 0.4	$\eta' \to$ invisible	$\phi \to K^+K^-$	$(16.2 \pm 1.9) \times 10^5$
	3.3 ± 0.4	$\phi \to$ invisible	$\eta' \to \gamma\rho^0$	$(9.6 \pm 1.2) \times 10^5$
$J/\psi \to \omega\eta$	15.8 ± 1.6	$\eta \to$ invisible	$\omega \to \pi^+\pi^-\pi^0$	$(13.9 \pm 1.4) \times 10^6$
	15.8 ± 1.6	$\omega \to$ invisible	$\eta \to \gamma\gamma$	$(6.2 \pm 0.6) \times 10^6$
$J/\psi \to \omega\eta'$	1.67 ± 0.25	$\eta' \to$ invisible	$\omega \to \pi^+\pi^-\pi^0$	$(1.5 \pm 0.2) \times 10^6$
	1.67 ± 0.25	$\omega \to$ invisible	$\eta' \to \gamma\rho^0$	$(0.7 \pm 0.1) \times 10^6$
$J/\psi \to \rho^0\eta$	1.93 ± 0.23	$\eta \to$ invisible	$\rho^0 \to \pi^+\pi^-$	$(1.9 \pm 0.2) \times 10^6$
	1.93 ± 0.23	$\rho^0 \to$ invisible	$\eta \to \gamma\gamma$	$(0.8 \pm 0.09) \times 10^6$
$J/\psi \to \rho^0\pi^0$	56 ± 7	$\rho^0 \to$ invisible	$\pi^0 \to \gamma\gamma$	$(55.3 \pm 5.8) \times 10^6$

Table 21.28: *J/ψ decay modes which can be used to study the invisible decays of η, η', ρ, ω and ϕ. The branching fractions are listed from PDG [619]. For each mode, a "tagging topology" is given, which is the set of visible in the detector's acceptance. In each case the tagging topology has a well-defined kinematics. The produced number of events are the expected events in 10 billions J/ψ data set at BES-III, in which we already considered the decay rate of the tagging particles.*

consider just the rate due to W-exchange contribution, it is straightforward to obtain [622]

$$\frac{\Gamma(J/\psi \to s\overline{s})^{weak}}{\Gamma(J/\psi \to e^+e^-)} \cong \frac{1}{2}\left(\frac{m_{J/\psi}}{m_W}\right)^4, \tag{21.100}$$

where $m_{J/\psi}$ and m_W are the masses of J/ψ and W boson, respectively. This leads to $BR(J/\psi \to s\overline{s})^{weak} \cong 10^{-7}$ for this weak contribution. It would lead one to expect $BR(\psi(nS) \to \phi\phi)$ below the level of 10^{-8} which may be even out of reach of *BES-III* experiment.

Experimentally, there are a few possible backgrounds will dilute the measurement of decay of $J/\psi \to \phi\phi$. One major background is $J/\psi \to \gamma\phi\phi$ which is mainly from $J/\psi \to \gamma\eta_c(1S)$, $\eta_c(1S) \to \phi\phi$. This kind of background can be easily removed by doing a kinematic constraint fit. A detailed calculation had been made to estimate $J/\psi \to \gamma\phi\phi$ background in Ref. [621]. Another background appears if one studies only $2(K\overline{K})$ invariant pair mass distributions. It arises from the CP-conserving reaction $J/\psi \to \phi(K\overline{K})_{S-wave}$, due to the fact that the ϕ mass is only two S-wave-widths away from the S-wave-mass, for example, $f_0(980) \to K\overline{K}$. Although it may be difficult to subtract in a small statistical sample, one can, in principle, remove this kind of background by either a spin-parity analysis for the $K\overline{K}$ pairs in a narrow window about ϕ mass, or by a subtraction normalized to an observed S-wave peak. To avoid the S-wave contribution, one can reconstruct one ϕ from K^+K^- and another ϕ from K_SK_L mode which is not allowed to form a S-wave. It will be easy to look for the missing mass of one ϕ reconstructed from K^+K^-, to see if there is any peak under the ϕ mass region by also requiring K_S and K_L information in the final states.

It is noted that there is possible continuum background produced through a two photon annihilation process. It is peaking background which can not be removed without

considering detail angular distributions with high statistic sample. So it is very hard to deal with this kind of peaking source with small sample. The only way is to off-peak data which are taken below the J/ψ mass peak. The $e^+e^- \to \gamma\gamma$ process has been investigated before [623], and it has a unique production angle (θ^*) distributions, which is defined as the angle between ϕ and e^- beam direction in the Center-mass (CM) frame. The production angle distribution for the two real photon annihilating process has the form of

$$\sigma(cos\theta^*)_{e^+e^-\to\gamma\gamma} = \frac{1+cos\theta^{*2}}{1-cos\theta^{*2}}, \tag{21.101}$$

while, in the process of two virtual photon into V^0V^0 pairs, the distribution becomes (to first order) [624]:

$$\sigma(cos\theta^*)_{e^+e^-\to\gamma^*\gamma^*\to V^0V^0} = \frac{1+cos\theta^{*2}}{k^2-cos\theta^{*2}}, \tag{21.102}$$

where factor k will be:

$$k = \frac{2m_{V^0}^2 - S}{\sqrt{S^2 - 4Sm_{V^0}^2}}, \tag{21.103}$$

where S is the square of CM energy. In principle, by using an angular analysis, one can remove the peaking background with high statistic data sample. To avoid the peaking background from continuum, $\psi(2S) \to \pi\pi J/\psi$ could be employed to study this kind of rare J/ψ decays with 3 billions $\psi(2S)$ sample, but the statistics will be lost.

21.4.4 Lepton flavor violating processes in decays of J/ψ

Lepton flavor violating (LFV) processes are strongly suppressed in the standard model by powers of small neutrino masses [625]. Therefore, such decays can be used to probe possible new physics. At present, there are many stringent bounds for μ, τ and Z boson decays, such as $BR(\mu \to 3e) \leq 10^{-12}$, $BR(\mu \to e\gamma\gamma) \leq 10^{-10}$ and somewhat weaker $O(10^{-6}$ bounds on LFV τ decays [4]. There have been a lot of studies both theoretically and experimentally on testing the lepton flavor conservation law [625, 626]. With huge J/ψ sample, *BES-III* experiment will be able to make an additional experimental searching for lepton flavor violating processes of $J/\psi \to ll'$ (l and $l' = \tau, \mu, e$, $l \neq l'$).

To estimate the branching ratio of the lepton flavor violating J/ψ decays allowed by the current experimental data, Peccei, Wang and Zhang took a model-independent approach to new physics and introduced a effective four-fermion contact interaction [625, 627, 628]:

$$\frac{4\pi}{\Lambda^2}\bar{c}\gamma^\mu c\bar{l}\gamma^\mu l', \tag{21.104}$$

where Λ is the new physics cutoff. This effective operator is forbidden in the standard model, however, it will be generated in theories where lepton flavor is not conserved, such as the MSSM with and/or without R parity, models with large extra dimension [629]. Therefore, any observed signal is a direct evidence for non-standard physics and will improve our understanding of flavor dynamics, especially in the lepton sector.

There is no direct experimental limit on Λ in equation (21.104). However, at one-loop level, attaching the neutral gauge boson Z to the charm quark loop generates an effective coupling of Z to $\bar{l}l'$. From the limits given in the particle data book on $BR(Z \to \bar{l}l'$ [4], one obtained the lower bounds on the branching ratio of the J/ψ decay into leptons [628]:

$$BR(J/\psi \to \tau^+ e^-) < 2.7 \times 10^{-5}; \tag{21.105}$$

$$BR(J/\psi \to \tau^+ \mu^-) < 4.9 \times 10^{-5}; \tag{21.106}$$

$$BR(J/\psi \to \mu^+ e^-) < 8.3 \times 10^{-6}. \tag{21.107}$$

While, recently, Nussinov, Peccei and Zhang [625] have also examined "unitarity inspired" relations between two- and three-body lepton flavor violating decays and found that the existing strong bounds on $\mu \to 3e$ and $\mu \to e\gamma\gamma$ servery constrain two-body lepton flavor violating decays of vector mesons, like J/ψ, $\Upsilon(1S)$ and ϕ into $\mu^\pm e^\mp$ final states. In reference [625], using $BR(\mu \to 3e) \leq 10^{-12}$ and data pertaining to the e^+e^- widths of the J/ψ, the bounds for the two-body LFV branching ratio of J/ψ decay is given

$$BR(J/\psi \to \mu^\pm e^\mp) < 4 \times 10^{-13}. \tag{21.108}$$

Likewise, the generic upper bounds on LPV τ decays $BR(\tau \to ll'\overline{l'}) \leq 10^{-6}$ yields

$$BR(J/\psi \to \tau^\pm l^\mp) < 6 \times 10^{-7}. \tag{21.109}$$

with $l/l' = e/\mu$. So these inferred bounds are unlikely to be improved by future experimental data on two-body decays, especially at *BES-III*. However, all these bounds derived in reference [625, 628] can be avoided if there is a kinematical suppression or as a results of some cancellations [625]. Searching for lepton flavor violating decays of J/ψ with huge sample from *BES-III* remains a worthwhile experimental challenge [628].

From 58 M J/ψ data at BESII, the following upper limits had been got [630]:

$$BR(J/\psi \to \tau^\pm e^\mp) < 8.3 \times 10^{-6}; \tag{21.110}$$

$$BR(J/\psi \to \tau^\pm \mu^\mp) < 2.0 \times 10^{-6}; \tag{21.111}$$

$$BR(J/\psi \to \mu^\pm e^\mp) < 1.1 \times 10^{-6}. \tag{21.112}$$

The sensitivity of the two-body lepton flavor violating decays of J/ψ could be $10^{-8} - 10^{-9}$ level at *BES-III* with one year luminosity at J/ψ peak. It will be a significant improvement.

Chapter 22

Miscellaneous

22.1 Bell Inequalities in High Energy Physics

In 1935, Einstein, Podolsky, and Rosen demonstrated in a work [562] that quantum mechanics could not provide a complete description for the "physical reality" of two spatially separated but quantum mechanically correlated particle system. In the paper they described the following criterion of "physical reality": *if, without in any way disturbing a system, we can predict with certainty (i.e., with probability equal to unity) the value of a physical quantity, then there exists an element of physical reality corresponding to this physical quantity.* Then they proposed the necessary condition for theories to be complete: *every element of the physical reality must have a counterpart in the physical theory.*

We adopt the illustration of EPR paradox which was proposed by Bohm [563]. He considered the two-particle spin-one-half system in spin singlet and zero angular momentum. in spin space, the wave function of this state can be expressed as

$$|\Psi\rangle = \frac{1}{\sqrt{2}}(|+\rangle_A|-\rangle_B - |-\rangle_A|+\rangle_B) \ , \tag{22.1}$$

where the single particle states $|+\rangle$ and $|-\rangle$ denote "spin up" and "spin down" in certain coordinate frame. Suppose particles are allowed to separate apart with the total spin of the system invariant, along the y direction. When they are well beyond the range of interaction, we can measure the z-component of the spin of particle A. Due to angular moment conservation at all time, we can predict that the z-component of spin B must have the opposite value. In the meantime, because the spin singlet has spacial rotation invariance, the same thing happens when we measure the x-component of spin of particle A. Since the two particles are far apart with each other, the locality condition guarantees that the particle B does not know what happens to A while the measurement performs. Therefore, it shows that the B particle spins along x and z axes should be both physical realities. In QM the spin operators along different axes do not commute and thus can not simultaneously have definite values, therefore they can not be simultaneously in physical realities. Hence, Einstein concluded that QM must be incomplete.

Bohr contested not the EPR demonstration but their premises. His point of view is that an element of reality is associated with a concretely performed act of measurement. We can not perform the measurement along different axes simultaneously on particle

A, so the spins of the particle B along different axes need not to be simultaneously physical realities. However, as Einstein questioned that these arguments make the reality of particle B depend upon the process of the measurement performed on the first particle, and he believed that *"no reasonable definition of reality could be expected to do this."*

To avoid the EPR paradox, it might be a reasonable choice to postulate some additional 'hidden variables', which presumably will restore the completeness, determinism and causality to the theory. This kind of theories are named the local hidden variable theories. Nevertheless, there are certain difference between QM and LHVT. In 1964 Bell showed [564] that in realistic LHVTs the two particle correlation functions satisfy a set of Bell inequalities (BI), whereas the corresponding QM predictions may violate these inequalities in some region of parameter space. The definition of correlation for LHVTs and QM, according to Bohm, read respectively as:

$$E(\mathbf{a},\mathbf{b}) = \int \mathrm{d}\lambda \rho(\lambda) A(\mathbf{a},\lambda) B(\mathbf{b},\lambda) \; , \tag{22.2}$$

$$E(\mathbf{a},\mathbf{b}) = \langle\psi|\sigma\cdot\mathbf{a}\otimes\sigma\cdot\mathbf{b}|\psi\rangle = -\mathbf{a}\cdot\mathbf{b} \; . \tag{22.3}$$

Here, $\rho(\lambda)$ is the distribution of hidden variable regardless of whether λ is a single variable or a set, or even a set of functions. These variables can be either discrete or continuous. $\mathbf{a}$ and $\mathbf{b}$ indicate spin directions. The original inequality obtained by Bell is

$$|E(\mathbf{a},\mathbf{b}) - E(\mathbf{a},\mathbf{c})| - E(\mathbf{b},\mathbf{c}) \leq 1 \; , \tag{22.4}$$

where $\mathbf{a},\mathbf{b},\mathbf{c}$ mean three different spin directions. In 1969, Clauser, Horne, Shimony, and Holt (CHSH) [565] generalized the inequality (22.4) to a more practical one, i.e.

$$S = |E(\mathbf{a},\mathbf{b}) - E(\mathbf{a},\mathbf{b}')| + E(\mathbf{a}',\mathbf{b}) + E(\mathbf{a}',\mathbf{b}') \leq 2 \; . \tag{22.5}$$

Here correlation function E in above inequalities can be calculated by

$$E(\mathbf{a},\mathbf{b}) = P_{++}(\mathbf{a},\mathbf{b}) - P_{+-}(\mathbf{a},\mathbf{b}) - P_{-+}(\mathbf{a},\mathbf{b}) + P_{--}(\mathbf{a},\mathbf{b}) \; , \tag{22.6}$$

where $P_{\pm\pm} = N_{\pm\pm}(\mathbf{a},\mathbf{b})/N$, N is the total number of particle pairs, and $N_{++(+-)}$ means that two particle has the same (opposite) spin directions. This leads to the possibility for an experimental test of the validity of LHVTs in comparison with QM.

Many experiments in regard of the Bell inequalities have been carried out by using the entangled photons. Of the various optical experiments, one of the important ones was carried out by Aspect *et al.* [566]. Their measurement gave $S_{exp} = 2.697 \pm 0.01$. This result is in excellent agreement with the predictions of quantum mechanics, which, for their polarizer efficiencies and lens apertures, gives $S_{QM} = 2.7 \pm 0.05$.

Some other relevant and important progresses in this direction were realized by using the parametric down-conversion (PDC) [567, 568, 569] technique in generating the entangled photon pairs. Thus far, all of these experiment results [566, 569] are substantially consistent with the prediction of standard QM.

People notice that the former experiments in testing the completeness of QM are mainly limited in the electromagnetic interaction regime, i.e., by employing the entangled photons, no matter whether the photons are generated from atomic cascade or PDC

method. Considering of the fundamental importance of the concerned question, to test the LHVT in experiment with massive quanta and with other kinds of interactions is necessary [570].

To this aim, the spin singlet state, as first advocated by Bohm and Aharonov [563] to clarify the EPR argument, is exploited in experiment at the beginning. Lamehi-Rachti and Mitting [571] performed an experiment in the low energy proton-proton scattering at Saclay tandem accelerator. Their measurement of the spin correlation of protons gave a good agreement with what the QM tells.

As early as 1960s the EPR-like features of the $K^0\bar{K}^0$ pair in the decays of $J^{PC} = 1^{--}$ vector particles were noticed by some authors [572, 573, 574, 575]. In the early attempts of testing LHVTs through the Bell inequality in high energy physics, people focused on exploiting the nature of particle spin correlations [570, 576, 577]. Typically, in Ref. [576] Törnqvist suggested to measure the BI through the following process:

$$e^+e^- \to \Lambda\bar{\Lambda} \to \pi^-\, p\, \pi^+\, \bar{p}\,. \tag{22.7}$$

Two different decay modes of $\eta_c \to \Lambda\bar{\Lambda}$ and $J/\psi \to \Lambda\bar{\Lambda}$ are considered by Törquist. In Ref. [578] the transition probability was obtain after taking the standard procedure, for η_c decay it reads:

$$R(\hat{\mathbf{a}}, \hat{\mathbf{b}}) \propto 1 + \alpha^2 \hat{\mathbf{a}} \cdot \hat{\mathbf{b}}\,, \tag{22.8}$$

where α denotes the Λ decay asymmetry parameter; $\hat{\mathbf{a}}$ and $\hat{\mathbf{b}}$ are unit vectors along the π^+ and π^- momenta in $\bar{\Lambda}$ and Λ rest frame, respectively. Törnqvist argued that apart from the constant α^2 and the sign before $\hat{\mathbf{a}}\cdot\hat{\mathbf{b}}$, (22.8) is in equivalence with Eq.(22.3) obtained in measuring the spin correlation in the Bohm's *Gedanken experiment*. Here, the directions of the pion momentum $\hat{\mathbf{a}}$ and $\hat{\mathbf{b}}$ take the place of the spin-analyzing directions of the polarimeters.

For J/ψ decays,

$$R(\hat{\mathbf{a}}, \hat{\mathbf{b}}) \propto 2(1 - \frac{k^2}{E_\Lambda^2}\sin^2\theta)(1 - \alpha^2\hat{a}_n\hat{b}_n) + \frac{k^2}{E_\Lambda^2}\sin^2\theta[1 - \alpha^2(\hat{\mathbf{a}}\cdot\hat{\mathbf{b}} - 2\hat{a}_x\hat{b}_x)]\,. \tag{22.9}$$

The DM2 Collaboration [579] observed 7.7×10^6 J/ψ events with about 10^3 being identified as from process $J/\psi \to \Lambda\bar{\Lambda} \to \pi^- p\pi^+\bar{p}$. The experimental measurement unfortunately does not give a very significant result[578] due to the insufficient statistics.

A similar process was suggested by Privitera [577], i.e.,

$$e^+e^- \to \tau^+\tau^- \to \pi^+\bar{\nu}_\tau\pi^-\nu_\tau\,. \tag{22.10}$$

In analogy with what in charmonium decays, in this case the expected correlation rate is given by

$$N(\hat{\mathbf{p}_1}, \hat{\mathbf{p}_2}) \propto 1 - \frac{1}{3}\hat{\mathbf{p}_1}\cdot\hat{\mathbf{p}_2}\,, \tag{22.11}$$

where $\hat{\mathbf{p}}_1$ and $\hat{\mathbf{p}}_2$ are unit vectors in the momentum directions of π^+ and π^-, respectively. Hereby, the strong spin correlation between two τ's reveals the nonlocal nature of the

EPR argument. The subsequent τ decay works as a spin analyzer, and the correlation is transferred to the decay products.

The above mentioned designs for experimentally measuring the violation of BI are delicate and attractive, however, people found that such proposals possess controversial assumptions [580]. They all assume that the decay matrix elements contain the nonlocal correlations, i.e., Eq.(22.8, 22.9, 22.11). However, there is no dichotomic observable which can be directly measured in real experiment. The momentum of pion is a continuous variable, and different momenta are compatible, i.e. $[(\hat{P}_{\pi^+})_i, (\hat{P}_{\pi^-})_j] = 0$ [570, 580]. Thus a LHVT can be constructed in respect of all the results from QM, and there will be no violation of Bell inequality anyway.

In testing the LHVTs in high energy physics, using the "quasi-spin" to mimic the photon polarization in the construction of entangled states is a practical way. For example, for kaon the quantum number of strangeness S, which takes either 1 or -1, can play the role of spin. Several groups suggested to study the $K^0\bar{K}^0$ system in the ϕ factory to test the LHVT (for details, see Ref. [581] and references therein). Up to now, there are two different ways in the "quasi-spin" scheme. In the first way, one fixes up the quasi-spin, but leaves the freedom in time. For example, one measures the Flavor Taste in different decaying time on each side, then the time differences plays the role of polarization angles. The second one is to leave the freedom in quasi-spin but to fix the time. In this case we measure the different eigenstates of the particles at the same time on each side, then the different eigenstates play the role of polarization angles.

A typical process produces entangled state in $K^0\bar{K}^0$ system is through $e^+e^- \to \phi \to K^0\bar{K}^0$. The wave function of the $J^{PC} = 1^{--}$ particles, like ϕ which decays into $K^0\bar{K}^0$, can be formally configured as [582]:

$$|\phi\rangle = \frac{1}{\sqrt{2}}\{|K^0\rangle|\bar{K}^0\rangle - |\bar{K}^0\rangle|K^0\rangle\} \; . \tag{22.12}$$

Similar expressiones apply to $\Upsilon(4S) \to B^0\bar{B}^0$, $\Upsilon(5S) \to B_s^0\bar{B}_s^0$, and $\psi(3770) \to D^0\bar{D}^0$ cases.

First, we consider the situation in which the meson state takes place of spin polarization discussed in preceding sections. For kaon system, there are three different kinds of eigenstates, those are: the mass, CP, and Strangeness. Define the effect of $\hat{C}\hat{P}$ operators acting on the K^0 and $\bar{K}^0$ states, like

$$\hat{C}\hat{P}|K^0\rangle = |\bar{K}^0\rangle \; , \tag{22.13}$$
$$\hat{C}\hat{P}|\bar{K}^0\rangle = |K^0\rangle \; , \tag{22.14}$$

up to an arbitrary phase. With this choice in phase the CP eigenstates can be expressed as:

$$|K_1^0\rangle = \frac{1}{\sqrt{2}}\{|K^0\rangle + |\bar{K}^0\rangle\} \; , \tag{22.15}$$
$$|K_2^0\rangle = \frac{1}{\sqrt{2}}\{|K^0\rangle - |\bar{K}^0\rangle\} \; . \tag{22.16}$$

And correspondingly the mass eigenstates are:

$$|K_S\rangle = \frac{1}{N}\{p|K^0\rangle + q|\bar{K}^0\rangle\} , \tag{22.17}$$

$$|K_L\rangle = \frac{1}{N}\{p|K^0\rangle - q|\bar{K}^0\rangle\} , \tag{22.18}$$

where $p = 1 + \varepsilon, q = 1 - \varepsilon$, and $N^2 = |p|^2 + |q|^2$. The ε is the normal CP violation parameter. With above knowledge, Eq.(22.12) can be reexpressed as:

$$|\phi\rangle = \frac{1}{\sqrt{2}}\{|K_2\rangle|K_1\rangle - |K_1\rangle|K_2\rangle\} , \tag{22.19}$$

$$|\phi\rangle = \frac{N^2}{2\sqrt{2}pq}\{|K_L\rangle|K_S\rangle - |K_S\rangle|K_L\rangle\} . \tag{22.20}$$

It is more convenient to use Wigner's inequality which can be derived from Eq. (22.4) [581], i.e.:

$$P(\mathbf{a}, \mathbf{b}) \leq P(\mathbf{a}, \mathbf{c}) + P(\mathbf{b}, \mathbf{c}) , \tag{22.21}$$

where $\mathbf{a}, \mathbf{b}, \mathbf{c}$ are the same as in Eq.(22.4). According to Ref. [583], the inequality (22.21) turns to

$$P(m_S, S = +1) \leq P(m_S, CP+) + P(CP+, S = +1) , \tag{22.22}$$

where $P(m_S, S = +1)$ means the coincident rate while on one side it is found to be K_S and on the other side is found to be K^0. The same notation applies to $P(m_S, CP+)$ and $P(CP+, S = +1)$. Substitute (22.16) and (22.18) into (22.22), the inequality becomes [583]:

$$\mathrm{Re}\{\varepsilon\} \leq |\varepsilon|^2, \tag{22.23}$$

which is obviously violated by the experimental measurements on ε [4]. As pointed out in Ref.[581], the (22.23) is taken at the beginning time, when the entangled kaon pairs are not well separated; what tested is only the contextuality rather than non-locality.

Like mentioned in above, we can also choose different time to measure the final states, the kaons, on each side. For the aim of illustration, we choose the quantum number of Strangeness as the quasi-spin in our consideration, but neglect the CP violation effect, which in some sense is a good approximation.

With the time evolution, the initial entangled state, like in (22.12), becomes:

$$\begin{aligned}|\Psi(t_l, t_r)\rangle = \frac{1}{\sqrt{2}}\{&e^{-i(m_L t_l + m_S t_r)} e^{-\frac{\Gamma_L}{2}t_l - \frac{\Gamma_S}{2}t_r}|K_L\rangle|K_S\rangle \\ &- e^{-i(m_S t_l + m_L t_r)} e^{-\frac{\Gamma_S}{2}t_l - \frac{\Gamma_L}{2}t_r}|K_S\rangle|K_L\rangle\} .\end{aligned} \tag{22.24}$$

Here in above, the small letters l and r denote left side and right side, suppose we name the two entangled particles to be left and right without lose generality. Choosing different measurement time for two sides, the correlation function is[585]:

$$E(t_l, t_r) = -\cos(\Delta m \Delta t) e^{-\frac{\Gamma_L + \Gamma_S}{2}(t_l + t_s)} . \tag{22.25}$$

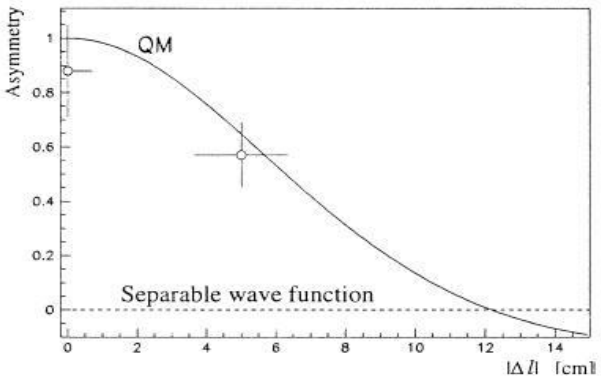

Figure 22.1: The best fit to the experimental measurement [586]. The two points with error bars correspond to time difference $\Delta t = 0$ and $\Delta t = 1.2\tau_s$. The solid line represents the QM prediction.

Inserting this correlation directly to CHSH inequality, one can immediately find that the violation of inequality depend on the ratio of $x = \Delta m/\Gamma$ [581], where the Δm characterizes of Strangeness oscillation and the Γ characterizes the weak decays. For the case of x being small, that means the oscillation is dominated by the weak decays, there will be no violation of CHSH inequalities. Among the known neutral mesons, only $B_S^0\bar{B}_S^0$ system has a big enough experimental value of x, and hence the violation of inequalities might be found there [581].

The EPR-type Strangeness correlation in the process $p\bar{p} \to K^0\bar{K}^0$ has been tested at the CPLEAR detector [586] at CERN. In the experiment the $K^0\bar{K}^0$ pairs were created in $J^{PC} = 1^{--}$ configuration. The wave function at proper time $t_l = t_r = 0$ is

$$|\Psi(0,0)\rangle = \frac{1}{\sqrt{2}}[|K^0\rangle_l|\bar{K}^0\rangle_r - |\bar{K}^0\rangle_l|K^0\rangle_r] \; . \tag{22.26}$$

In the experiment, two kinds of measurements were performed. The first one was to perform the measurements on each side of the source at the same time. Another one was to perform the measurements in different distances (so was the time) for the two sides. The strangeness was tagged via strong interaction with absorbers away from the creation point. The measured Strangeness asymmetry is

$$A(t_l, t_r) = \frac{I_{unlike}(t_l, t_r) - I_{like}(t_l, t_r)}{I_{unlike}(t_l, t_r) + I_{like}(t_l, t_r)} \; . \tag{22.27}$$

Here, $I_{(un)like}$ means the (un)like strangeness event, which are defined as

$$I_{like}(t_l, t_r) = P(K^0, t_l; K^0, t_r) + P(\bar{K}^0, t_l; \bar{K}^0, t_r) \; , \tag{22.28}$$

$$I_{unlike}(t_l, t_r) = P(K^0, t_l; \bar{K}^0, t_r) + P(\bar{K}^0, t_l; K^0, t_r) \; . \tag{22.29}$$

From Fig.22.1 one notices that the non-separability hypothesis of QM is strongly favoured by experiment.

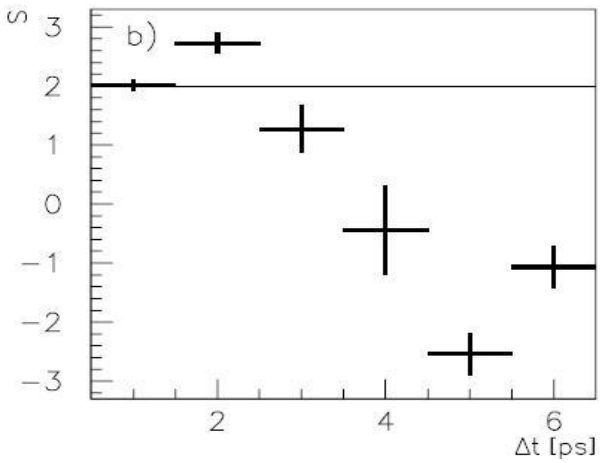

Figure 22.2: The experiment result of the violation of inequality [587]. The horizontal axis refers to Δt and the vertical axis to the S. The LHVTs limit of 2 is shown by the solid line.

The $B^0\bar{B}^0$ entangled system produced at the $\Upsilon(4S)$ resonance has also been measured in the B-factory [587]. The wave function of $\Upsilon(4S) \to B^0\bar{B}^0$ has the same formalism as the spin singlet:

$$|\Upsilon\rangle = \frac{1}{\sqrt{2}}\{|B^0\rangle_l|\bar{B}^0\rangle_r - |\bar{B}^0\rangle_l|B^0\rangle_r\} \; . \tag{22.30}$$

Here, the quantum number of flavor plays the role of spin polarization in the spin correlation system. In the first method, i.e. with fixed quasi-spin and free in time, the correlation function for $B^0\bar{B}^0$ system is

$$E(t_l, t_r) = -e^{-\frac{2t'+\Delta t}{\tau_B}} \cos(\Delta m_d \Delta t) \; , \tag{22.31}$$

where Δm_d characterizes the $B^0 - \bar{B}^0$ mixing, τ_B is the B^0 decay mean time, $t' = \min(t_l, t_r)$, and $\Delta t = |t_l - t_r|$. Normalizing the above correlation function by the undecayed B^0 pairs, one then gets the correlation function as:

$$E_R(\Delta t) = -\cos(\Delta m_d \Delta t) \; . \tag{22.32}$$

Put it into the Bell-CHSH inequality, one can get the violation parameter [587]

$$S(\Delta t) = 3E_R(\Delta t) - E_R(3\Delta t) \leq 2 \; . \tag{22.33}$$

The experiment, which based on the data sample of 80×10^6 $\Upsilon(4S) \to B\bar{B}$ decays at Belle detector at the KEKB asymmetric collider in Japan, tells $S = 2.725 \pm 0.167_{stat}$. It is obviously a result violating the Bell inequality, as shown in Fig.22.2.

However, debates on whether this quasi-spin of unstable particle can give a genuine test of LHVTs or not is still ongoing [588]. One is the unitary time evolution of an unstable quantum state, some information has to be lost into the decay products; the other is the active measurement [588]. In CPLEAR experiment the active measurement requirement is

fulfilled, because the neutral kaon meson is identified through strong interaction with the absorber. While in the B meson case, there is no way for experimenter to force B-meson to decay at a given instant t_l or $t_{l'}$ [588], at least for now. Of the unitary condition, the (22.32) is different from (22.25). The former is normalized by the undecayed $B^0\bar{B}^0$ pairs. Like in the photon case, this needs some additional assumptions to make the correlation to be comparable to what required by the Bell inequality because of the detecting efficiency.

In recently, the $B_S^0\bar{B}_S^0$ pair production is observed in experiment in $\Upsilon(5S)$ decays [589, 590]. B_S^0 meson has a suitable x value for the violation of CHSH inequality, even if considering of the interplay of weak interaction. Therefore, it should be a notable test of QM correlation if the measurement on $B_S^0\bar{B}_S^0$ system can be performed in the future.

Based on the Hardy's argument [591] on the contradiction between LHVT and QM, Bramon and Garbarino propose a new scheme [592, 593] to test the local realism by virtue of entangled neutral kaons. After neglecting the small CP-violation effect, the initial K_SK_L pair from ϕ decay, or proton-antiproton annihilation, is of the same as (22.18):

$$|\phi(T=0)\rangle = \frac{1}{\sqrt{2}}[K_SK_L - K_LK_S] \ , \tag{22.34}$$

where $K_S = (K^0 + \bar{K^0})/\sqrt{2}$ and $K_L = (K^0 - \bar{K^0})/\sqrt{2}$ are the mass eigenstates of the K mesons. One of the key points in using kaon system to test the LHVTs is to generate a nonmaximally entangled (asymmetric) state (Hardy state). That is

$$|\phi(T)\rangle = \frac{1}{\sqrt{2+|R|^2}}\left[K_SK_L - K_LK_S - re^{-i(m_L-m_S)\,T+[(\Gamma_S-\Gamma_L)/2]T}K_LK_L\right] . \tag{22.35}$$

Here, r is the regeneration parameter to be the order of magnitude 10^{-3} [593]; Γ_L and Γ_S are the K_L and K_S decay widths, respectively; T is the evolution time of kaons after their production. Technically, this asymmetric state can be achieved by placing a thin regenerator close to the ϕ decay point [592].

Four specific transition probabilities for joint measurements from QM take the following forms:

$$P_{QM}(K^0, \bar{K^0}) = \frac{|2 + \mathrm{R}e^{i\varphi}|^2}{4(2+|R|^2)} \ , \tag{22.36}$$

$$P_{QM}(K^0, K_L) = \frac{|1 + \mathrm{R}e^{i\varphi}|^2}{2(2+|R|^2)} \ , \tag{22.37}$$

$$P_{QM}(K_L, \bar{K^0}) = \frac{|1 + \mathrm{R}e^{i\varphi}|^2}{2(2+|R|^2)} \ , \tag{22.38}$$

$$P_{QM}(K_SK_S) = 0 \ , \tag{22.39}$$

where $\mathrm{R} = -|R| = -|r|e^{[(\Gamma_S-\Gamma_L)/2]T}$ and φ is the phase of R. In Ref. [593] the special case of $R = -1$ was considered, in which

$$P_{QM}(K^0, \bar{K^0}) = 1/12 \ , \tag{22.40}$$

$$P_{QM}(K^0, K_L) = 0 \ , \tag{22.41}$$

$$P_{QM}(K_L, \bar{K^0}) = 0 \ , \tag{22.42}$$

$$P_{QM}(K_S, K_S) = 0 \ . \tag{22.43}$$

In light of the arguments in Ref. [593], we can demonstrate how LHVTs conflict with QM in this case. Suppose in a typical experiment, the strangeness on both sides at a proper time T is measured. For example, a detection of K^0 on the left side and $\bar{K^0}$ on the right side is achieved. We know this may happen from Eq.(22.40), and then we can infer from (22.41) that if the decay on the right hand side is observed, the K_S exits there for certain. In this case, according to Einstein's argument the K_S on the right side corresponds to a physical reality. Similarly, if we have measured the lifetime of kaon on the left side, according to (22.42) one can confirm that it should be K_S. In all, the non-zero probability of $P_{QM}(K^0, \bar{K^0})$ leads to the non-zero probability of K_S on both sides. However, due to EPR's criterion of "physical reality" this is in contradiction with Eq.(22.43). This kind of contradiction need a null measurement of the transition probability of Eq.(22.43) that cannot be strictly performed. Bramon *et al.* derived out the following Eberhard's inequality (EI) [594]:

$$H_{LR} \equiv \frac{P_{LR}(K^0, \bar{K^0})}{P_{LR}(K^0, K_L) + P_{LR}(K_S, K_S) + P_{LR}(K_L, \bar{K^0}) + P(K^0, U_{Lif}) + P(U_{Lif}, \bar{K^0})} \leq 1 \quad (22.44)$$

where $P_{\rm LR}$ denotes the transition probability in LHVTs with the subscripts LR symbolizing the local realism. H_{LR} means the local realistic value of the fraction which must less than 1 according to LHVTs. U_{Lif} denotes the failures in lifetime detection.

For simplicity we consider an ideal case, in which the detection efficiency of the kaon decays is 100 percent. Then the EI (22.44) for the kaon system takes the following form:

$$P_{LR}(K^0, \bar{K^0}) \quad \leq \quad P_{LR}(K^0, K_L) + P_{LR}(K_S, K_S) + P_{LR}(K_L, \bar{K^0}) \ . \qquad (22.45)$$

For the case of QM, substituting equations (22.36) - (22.39) into the inequality (22.45) and assuming $\varphi = 0$, we have

$$\frac{(2+\mathrm{R})^2}{4(2+\mathrm{R}^2)} \quad \leq \quad \frac{(1+\mathrm{R})^2}{2(2+\mathrm{R}^2)} \ + \ 0 \ + \ \frac{(1+\mathrm{R})^2}{2(2+\mathrm{R}^2)} \ . \qquad (22.46)$$

The above inequality is apparently violated by QM while $\mathrm{R} = -1$. In Ref. [595] we generalized the method used in [593] to heavy quarkonium. This straightforward generalization however leads to some new observations of the nonlocal property. Upon further analyzing the R value when it gives violation of Eq.(22.46), we find out that there exist a period of time during which the violation became larger through time evolution. In quantum information theory the entanglement property of two qubits pure state are well understood, which can be characterized by the concurrence C [596]. We can also see how the degree of entanglement evolves with time. According to the definition of concurrence we have:

$$C(J/\psi) = |\langle J/\psi | \widetilde{J/\psi} \rangle| = \frac{2}{2 + |R|^2} = \frac{2}{2 + |r|^2 e^{(\Gamma_S - \Gamma_L)T}} \ , \qquad (22.47)$$

where $|\widetilde{J/\psi}\rangle = \sigma_y^1 \sigma_y^2 |(J/\psi)^*\rangle$ and $\sigma^{1,\ 2}$ are Pauli matrices. C changes between null to unit for no entanglement and full entanglement. Eq.(22.47) shows that the state become less entangled with the time evolution. So, considering of (22.46) we realize that the violation

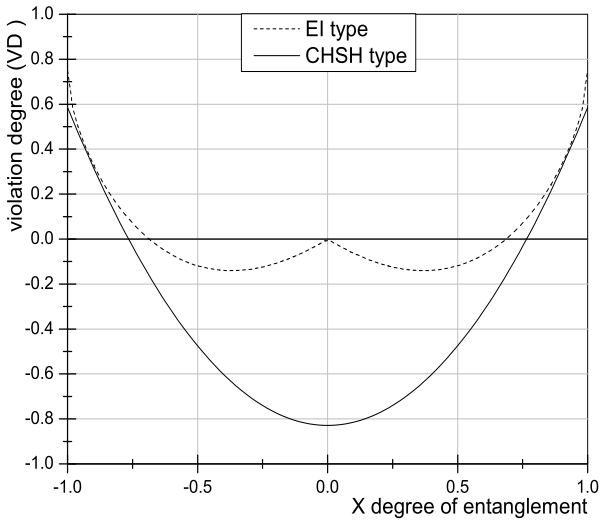

Figure 22.3: The violation degree of the Bell inequalities (the dashed line for EI type and the solid line for CHSH type) in terms of the entanglement. Here, for the sake of transparency, we make a coordinator exchange, the $C = 1 - x^2$. The magnitudes of *VD* less than zero means the broken of the BIs.

of it does not decrease monotonously with the degree of entanglement. To clarify this phenomenon we express the violation degree (*VD*) of the inequalities (left side minus the right side) in term of C and compare it with the usual CHSH inequality [565]. In Figure 22.3 different *VD* behaviors of CHSH's and Eberhard's inequalities are presented. For CHSH case, the $VD_{\rm CHSH}$ is obtained in the same condition as the maximal violation happens in the full entanglement, the $C = 1$. We have:

$$VD_{CHSH} = \sqrt{2}(1 + C) - 2 \; . \tag{22.48}$$

In fact, the above $VD_{\rm CHSH}$ can be deduced from the results given in Refs. [597, 598, 599]. For EI case,

$$VD_{EI} = \frac{-3(1 - C) + 2\sqrt{2}\sqrt{C - C^2}}{4} \; . \tag{22.49}$$

Here, in EI the counterintuitive quantum effect shows up, i.e. the less entanglement corresponding to a larger *VD* in some region (see Fig.22.3). It is worth to notice that with the time evolution, when R becomes less than $-\frac{4}{3}$, the QM and LHVTs both satisfy the inequality (22.45). Thus give a certain asymmetrically entangled state, the Hardy state, in the region of $R \in [-4/3, 0)$ the QM and LHVTs can be distinguished from the EI.

In a recent work [600], an improved measurement of branching ratio $B(J/\psi \to K^0_S K^0_L) = (1.80 \pm 0.04 \pm 0.13) \times 10^{-4}$ is reported, which is significant larger than previous ones. Entangled kaon pairs from heavy quarkonium decays can be easily space-likely separated. Thus, little evolution time T will guarantee the locality condition [595], and hence enables us to test the full range of R and so the peculiar quantum effects. It is promising

and worthwhile to implement such test in future tau-charm factories, because of both the experimental feasibility and theoretical importance.

In this article we present a brief review of EPR paradox related studies in high energy physics. To make it self-contained, we also present some basic materials on the history of EPR paradox and experimental realizations, for instance in optics. Our main concern is on the test of LHVTs in high energy physics experiments. Questions and hopes are discussed. The study of BI in high energy physics have experienced a long time. In this article it is impossible for us to cover every aspect of developments in this subject. It is almost sure that there must be some important researches are not covered and referred by us. We are sorry for those authors.

The developments of the study in Bell inequalities and quantum information theory are very important for us to further understand the elusive nature of quantum phenomena. Investigation on testing the validity of LHVTs in high energy physics is still an active and intriguing topic. The study in turn also stimulates some new experimental methods in high energy physics. Because in high energy physics the elementary particles are just the quanta, which obey the quantum theory, to test the theory in high energy physics looks unique. One can imagine there is still large capacity in high energy physics to play a more important role in the study of quantum theory.

Bibliography

[1] W. E. Caswell and G. P. Lepage, Phys. Lett. B **167**, 437 (1986).

[2] G. P. Lepage, L. Magnea, C. Nakhleh, U. Magnea and K. Hornbostel, Phys. Rev. D **46**, 4052 (1992) [arXiv:hep-lat/9205007].

[3] G. T. Bodwin, E. Braaten and G. P. Lepage, "Rigorous QCD analysis of inclusive annihilation and production of heavy Phys. Rev. D **51**, 1125 (1995) [Erratum-ibid. D **55**, 5853 (1997)] [arXiv:hep-ph/9407339].

[4] A. Pineda and J. Soto, Nucl. Phys. Proc. Suppl. **64**, 428 (1998) [arXiv:hep-ph/9707481].

[5] N. Brambilla, A. Pineda, J. Soto and A. Vairo, Nucl. Phys. B **566**, 275 (2000) [arXiv:hep-ph/9907240].

[6] N. Brambilla, A. Pineda, J. Soto and A. Vairo, Rev. Mod. Phys. **77**, 1423 (2005) [arXiv:hep-ph/0410047].

[7] M. E. Luke and A. V. Manohar, Phys. Lett. B **286**, 348 (1992) [arXiv:hep-ph/9205228].

[8] Y. Q. Chen, Phys. Lett. B **317**, 421 (1993).

[9] R. Sundrum, Phys. Rev. D **57**, 331 (1998) [arXiv:hep-ph/9704256].

[10] M. Finkemeier, H. Georgi and M. McIrvin, Phys. Rev. D **55**, 6933 (1997) [arXiv:hep-ph/9701243].

[11] Y. Q. Chen, Phys. Rev. D **69**, 096001 (2004) [arXiv:hep-ph/0207333].

[12] N. Brambilla, D. Gromes and A. Vairo, Phys. Lett. B **576**, 314 (2003) [arXiv:hep-ph/0306107].

[13] M. Gremm and A. Kapustin, Phys. Lett. B **407**, 323 (1997) [arXiv:hep-ph/9701353].

[14] E. Braaten and Y. Q. Chen, Phys. Rev. D **54**, 3216 (1996) [arXiv:hep-ph/9604237].

[15] N. Brambilla *et al.*, *Heavy quarkonium physics*, CERN-2005-005, (CERN, Geneva, 2005) [arXiv:hep-ph/0412158]; See also the talks at the last QWG meeting at BNL available at http://www.qwg.to.infn.it/.

[16] N. Brambilla, A. Pineda, J. Soto and A. Vairo, Rev. Mod. Phys. **77**, 1423 (2005) [arXiv:hep-ph/0410047].

[17] A. Pineda and J. Soto, Nucl. Phys. Proc. Suppl. **64**, 428 (1998) [arXiv:hep-ph/9707481].

[18] N. Brambilla, A. Pineda, J. Soto and A. Vairo, Nucl. Phys. B **566**, 275 (2000) [arXiv:hep-ph/9907240].

[19] W. E. Caswell and G. P. Lepage, Phys. Lett. B **167**, 437 (1986) G. T. Bodwin, E. Braaten and G. P. Lepage, Phys. Rev. D **51**, 1125 (1995) [Erratum-ibid. D **55**, 5853 (1997)] [hep-ph/9407339].

[20] M. Beneke and V. A. Smirnov, Nucl. Phys. B **522**, 321 (1998) [arXiv:hep-ph/9711391]; B. A. Kniehl and A. A. Penin, Nucl. Phys. B **563**, 200 (1999) [arXiv:hep-ph/9907489]. M. E. Luke and A. V. Manohar, Phys. Rev. D **55**, 4129 (1997) [arXiv:hep-ph/9610534].

[21] M. E. Luke, A. V. Manohar and I. Z. Rothstein, Phys. Rev. D **61**, 074025 (2000) [arXiv:hep-ph/9910209]; A. H. Hoang and I. W. Stewart, Phys. Rev. D **67**, 114020 (2003) [arXiv:hep-ph/0209340]. A. V. Manohar and I. W. Stewart, Phys. Rev. D **62**, 014033 (2000) [arXiv:hep-ph/9912226].

[22] A. Pineda, Phys. Rev. D **65**, 074007 (2002); A. Pineda and J. Soto, Phys. Lett. B **495**, 323 (2000).

[23] N. Brambilla, D. Gromes and A. Vairo, Phys. Lett. B **576**, 314 (2003); Phys. Rev. D **64**, 076010 (2001);

[24] G. S. Bali, Phys. Rept. **343**, 1 (2001) [arXiv:hep-ph/0001312].

[25] N. Brambilla and A. Vairo, arXiv:hep-ph/9904330.

[26] N. Brambilla, A. Pineda, J. Soto and A. Vairo, Phys. Rev. D **63**, 014023 (2001) [arXiv:hep-ph/0002250].

[27] A. Pineda and A. Vairo, Phys. Rev. D **63**, 054007 (2001) [Erratum-ibid. D **64**, 039902 (2001)] [arXiv:hep-ph/0009145].

[28] N. Brambilla, A. Pineda, J. Soto and A. Vairo, Phys. Rev. D **60**, 091502 (1999) [arXiv:hep-ph/9903355].

[29] A. Pineda, J. Phys. G **29**, 371 (2003) [arXiv:hep-ph/0208031].

[30] N. Brambilla, X. Garcia i Tormo, J. Soto and A. Vairo, arXiv:hep-ph/0610143.

[31] F. A. Chishtie and V. Elias, Phys. Lett. B **521**, 434 (2001) [arXiv:hep-ph/0107052].

[32] B. A. Kniehl, A. A. Penin, Y. Schroder, V. A. Smirnov and M. Steinhauser, Phys. Lett. B **607**, 96 (2005) [arXiv:hep-ph/0412083].

[33] G. S. Bali and A. Pineda, Phys. Rev. D **69**, 094001 (2004) [arXiv:hep-ph/0310130].

[34] N. Brambilla, X. Garcia i Tormo, J. Soto and A. Vairo, arXiv:hep-ph/0610143.

[35] N. Brambilla, arXiv:hep-ph/9809263; M. Baker, N. Brambilla, H. G. Dosch and A. Vairo, Phys. Rev. D **58**, 034010 (1998) [arXiv:hep-ph/9802273]. N. Brambilla and A. Vairo, Phys. Rev. D **55**, 3974 (1997) [arXiv:hep-ph/9606344]. N. Brambilla, P. Consoli and G. M. Prosperi, Phys. Rev. D **50**, 5878 (1994) [arXiv:hep-th/9401051].

[36] Y. Koma, M. Koma and H. Wittig, Phys. Rev. Lett. **97**, 122003 (2006) [arXiv:hep-lat/0607009].

[37] Y. Koma and M. Koma, arXiv:hep-lat/0609078.

[38] A. A. Penin, V. A. Smirnov and M. Steinhauser, Nucl. Phys. B **716**, 303 (2005) [arXiv:hep-ph/0501042].

[39] M. Beneke, Y. Kiyo and K. Schuller, Nucl. Phys. B **714**, 67 (2005) [arXiv:hep-ph/0501289].

[40] M. Artuso *et al.* [CLEO Collaboration], Phys. Rev. Lett. **94**, 032001 (2005) [hep-ex/0411068].

[41] N. Brambilla, Y. Jia and A. Vairo, Phys. Rev. D **73**, 054005 (2006) [arXiv:hep-ph/0512369].

[42] X. Garcia i Tormo and J. Soto, Phys. Rev. Lett. **96**, 111801 (2006) [arXiv:hep-ph/0511167].

[43] N. Brambilla and A. Vairo, Phys. Rev. D **71**, 034020 (2005) [arXiv:hep-ph/0411156].

[44] A. Ocherashvili *et al.* [SELEX Collaboration], arXiv:hep-ex/0406033; M. Mattson *et al.* [SELEX Collaboration], Phys. Rev. Lett. **89**, 112001 (2002) [arXiv:hep-ex/0208014]; M. A. Moinester *et al.* [SELEX Collaboration], Czech. J. Phys. **53**, B201 (2003) [arXiv:hep-ex/0212029]; see also the SELEX web page http://www-selex.fnal.gov/Welcome.html.

[45] N. Brambilla, A. Vairo and T. Rösch, Phys. Rev. D **72**, 034021 (2005) [arXiv:hep-ph/0506065].

[46] S. Fleming and T. Mehen, Phys. Rev. D **73**, 034502 (2006) [arXiv:hep-ph/0509313].

[47] M. J. Savage and M. B. Wise, Phys. Lett. B **248**, 177 (1990).

[48] J. M. Flynn, F. Mescia and A. S. B. Tariq [UKQCD Collaboration], JHEP **0307**, 066 (2003) [arXiv:hep-lat/0307025].

[49] R. Lewis, N. Mathur and R. M. Woloshyn, Phys. Rev. D **64**, 094509 (2001) [arXiv:hep-ph/0107037].

[50] A. Ali Khan *et al.*, Phys. Rev. D **62**, 054505 (2000) [arXiv:hep-lat/9912034].

[51] N. Mathur, R. Lewis and R. M. Woloshyn, Phys. Rev. D **66**, 014502 (2002) [arXiv:hep-ph/0203253].

[52] J. Hu and T. Mehen, Phys. Rev. D **73**, 054003 (2006) [arXiv:hep-ph/0511321].

[53] Y. Jia, arXiv:hep-ph/0607290.

[54] N. Brambilla, D. Eiras, A. Pineda, J. Soto and A. Vairo, Phys. Rev. D **67**, 034018 (2003) [arXiv:hep-ph/0208019].

[55] N. Brambilla, D. Eiras, A. Pineda, J. Soto and A. Vairo, Phys. Rev. Lett. **88**, 012003 (2002) [arXiv:hep-ph/0109130].

[56] N. Brambilla, A. Pineda, J. Soto and A. Vairo, Phys. Lett. B **580**, 60 (2004) [arXiv:hep-ph/0307159].

[57] A. Vairo, Mod. Phys. Lett. A **19**, 253 (2004) [arXiv:hep-ph/0311303].

[58] A. Vairo, Nucl. Phys. Proc. Suppl. **115**, 166 (2003) [arXiv:hep-ph/0205128].

[59] N. Brambilla, Y. Jia and A. Vairo, Phys. Rev. D **73**, 054005 (2006) [arXiv:hep-ph/0512369].

[60] A. Vairo, arXiv:hep-ph/0608327.

[61] W. M. Yao *et al.* [Particle Data Group], J. Phys. G **33**, 1 (2006).

[62] S. Fleming and A. K. Leibovich, Phys. Rev. D **67**, 074035 (2003) [arXiv:hep-ph/0212094].

[63] X. Garcia i Tormo and J. Soto, Phys. Rev. D **72**, 054014 (2005) [arXiv:hep-ph/0507107].

[64] B. Nemati *et al.* [CLEO Collaboration], Phys. Rev. D **55**, 5273 (1997) [arXiv:hep-ex/9611020].

[65] A. A. Penin, A. Pineda, V. A. Smirnov and M. Steinhauser, Nucl. Phys. B **699**, 183 (2004) [arXiv:hep-ph/0406175].

[66] A. Pineda and A. Signer, arXiv:hep-ph/0607239.

[67] H. Suganuma, T. T. Takahashi, F. Okiharu and H. Ichie, AIP Conf. Proc. **756**, 123 (2005) [arXiv:hep-lat/0412026].

[68] N. Brambilla, Y. Sumino and A. Vairo, Phys. Lett. B **513**, 381 (2001) [arXiv:hep-ph/0101305].

[69] N. Brambilla and A. Vairo, Phys. Rev. D **62**, 094019 (2000) [arXiv:hep-ph/0002075].

[70] I. F. Allison, C. T. H. Davies, A. Gray, A. S. Kronfeld, P. B. Mackenzie and J. N. Simone [HPQCD Collaboration], Phys. Rev. Lett. **94**, 172001 (2005) [arXiv:hep-lat/0411027].

[71] D. Acosta *et al.* [CDF Collaboration], Phys. Rev. Lett. **96**, 082002 (2006) [arXiv:hep-ex/0505076].

[72] N. Brambilla, X. Garcia i Tormo, J. Soto and A. Vairo "Extraction of α_s from radiative $Y(1S)$ decays" IFUM-886-FT

[73] A. X. El-Khadra and M. Luke, Ann. Rev. Nucl. Part. Sci. **52**, 201 (2002) [arXiv:hep-ph/0208114].

[74] A. Pineda, JHEP **0106**, 022 (2001) [arXiv:hep-ph/0105008].

[75] N. Brambilla, Y. Sumino and A. Vairo, Phys. Rev. D **65**, 034001 (2002) [arXiv:hep-ph/0108084].

[76] A. A. Penin and M. Steinhauser, Phys. Lett. B **538**, 335 (2002) [arXiv:hep-ph/0204290].

[77] M. Eidemüller, Phys. Rev. D **67**, 113002 (2003) [arXiv:hep-ph/0207237].

[78] T. Lee, JHEP **0310**, 044 (2003) [arXiv:hep-ph/0304185].

[79] C. Contreras, G. Cvetic and P. Gaete, Phys. Rev. D **70**, 034008 (2004) [arXiv:hep-ph/0311202].

[80] A. Pineda and A. Signer, Phys. Rev. D **73**, 111501 (2006) [arXiv:hep-ph/0601185].

[81] A. H. Hoang, A. V. Manohar, I. W. Stewart and T. Teubner, Phys. Rev. D **65**, 014014 (2002) [arXiv:hep-ph/0107144].

[82] B. A. Kniehl, A. A. Penin, A. Pineda, V. A. Smirnov and M. Steinhauser, Phys. Rev. Lett. **92**, 242001 (2004) [arXiv:hep-ph/0312086].

[83] A. A. Penin, A. Pineda, V. A. Smirnov and M. Steinhauser, Phys. Lett. B **593**, 124 (2004) [arXiv:hep-ph/0403080].

[84] K. J. Juge, J. Kuti and C. Morningstar, Phys. Rev. Lett. **90**, 161601 (2003) [arXiv:hep-lat/0207004].

[85] M. Foster and C. Michael [UKQCD Collaboration], Phys. Rev. D **59**, 094509 (1999) [arXiv:hep-lat/9811010].

[86] A. Vairo, arXiv:hep-ph/0611310.

[87] M. A. Sanchis-Lozano, arXiv:hep-ph/0503266.

[88] J. J. Aubert *et al.* [E598 Collaboration], Phys. Rev. Lett. **33**, 1404 (1974).

[89] J. E. Augustin *et al.* [SLAC-SP-017 Collaboration], Phys. Rev. Lett. **33**, 1406 (1974).

[90] T. Appelquist and H. D. Politzer, Phys. Rev. Lett. **34**, 43 (1975).

[91] A. De Rujula and S. L. Glashow, Phys. Rev. Lett. **34**, 46 (1975).

[92] T. Appelquist, A. De Rujula, H. D. Politzer and S. L. Glashow, Phys. Rev. Lett. **34**, 365 (1975).

[93] E. Eichten, K. Gottfried, T. Kinoshita, J. B. Kogut, K. D. Lane and T. M. Yan, Phys. Rev. Lett. **34**, 369 (1975) [Erratum-ibid. **36**, 1276 (1976)].

[94] W.-M. Yao *et al.* (Particle Data Group), J. Phys. G 33, 1 (2006)

[95] T. Barnes, S. Godfrey and E. S. Swanson, Phys. Rev. D **72**, 054026 (2005) [arXiv:hep-ph/0505002].

[96] S. Godfrey and N. Isgur, Phys. Rev. D32, 189 (1985).

[97] C. Quigg, arXiv:hep-ph/0403187.

[98] R. S. Galik, arXiv:hep-ph/0408190.

[99] N. Brambilla *et al.*, arXiv:hep-ph/0412158.

[100] K. K. Seth, arXiv:hep-ex/0504052.

[101] E. S. Swanson, Phys. Rept. **429**, 243 (2006) [arXiv:hep-ph/0601110].

[102] J. L. Rosner, arXiv:hep-ph/0612332.

[103] K. K. Seth, arXiv:hep-ex/0611035.

[104] M. Okamoto *et al.* [CP-PACS Collaboration], Phys. Rev. D **65**, 094508 (2002) [arXiv:hep-lat/0112020].

[105] M. di Pierro *et al.*, Nucl. Phys. Proc. Suppl. **129**, 340 (2004) [arXiv:hep-lat/0310042].

[106] T. Umeda, Prog. Theor. Phys. Suppl. **151**, 149 (2003).

[107] J. Dudek, R. Edwards, N. Mathur and D. Richards, arXiv:hep-lat/0611006.

[108] R. Van Royen and V. F. Weisskopf, Nuovo Cim. A **50**, 617 (1967) [Erratum-ibid. A **51**, 583 (1967)].

[109] R. Barbieri, R. Gatto, R. Kogerler and Z. Kunszt, Phys. Lett. B **57**, 455 (1975).

[110] J. L. Rosner, Phys. Rev. D **64**, 094002 (2001) [arXiv:hep-ph/0105327].

[111] J. L. Rosner, [arXiv:hep-ph/0405196].

[112] W. Kwong and J. L. Rosner, Phys. Rev. D **38**, 279 (1988).

[113] J. J. Dudek, R. G. Edwards and D. G. Richards, Phys. Rev. D **73**, 074507 (2006) [arXiv:hep-ph/0601137].

[114] R. A. Briere *et al.* [CLEO Collaboration], arXiv:hep-ex/0605070.

[115] Y. B. Ding, D. H. Qin and K. T. Chao, Phys. Rev. D **44**, 3562 (1991).

[116] T. Barnes, "Two photon couplings of quarkonia with arbitrary J(PC)," *Int. Workshop on Photon-Photon Collisions, La Jolla, CA, Mar 22-26, 1992.*

[117] E. S. Ackleh, T. Barnes and F. E. Close, Phys. Rev. D **46**, 2257 (1992).

[118] E. S. Ackleh and T. Barnes, Phys. Rev. D **45**, 232 (1992).

[119] D.M.Asner *et al.* (CLEO Collaboration), Phys. Rev. Lett.92, 142001 (2004) [arXiv:hep-ex/0312058].

[120] T. Barnes and S. Godfrey, Phys. Rev. D69, 054008 (2004) [arXiv:hep-ph/0311162].

[121] L. Micu, Nucl. Phys. B10, 521 (1969).

[122] A. LeYaouanc, L. Oliver, O. Pène and J.-C. Raynal, Phys. Rev. D8, (1973) 2223.

[123] R. Kokoski and N. Isgur, Phys. Rev. D35, 907 (1987).

[124] E.S.Ackleh, T.Barnes and E.S. Swanson, Phys. Rev. D54, 6811 (1996). [arXiv:hep-ph/9604355].

[125] A. Le Yaouanc, L. Oliver, O. Pène and J.-C. Raynal, Phys. Lett. B71, 397 (1977).

[126] A. Le Yaouanc, L. Oliver, O. Pène and J.-C. Raynal, Phys. Lett. B72, 57 (1977).

[127] T. Barnes, F. E. Close, P. R. Page and E. S. Swanson, Phys. Rev. D **55**, 4157 (1997) [arXiv:hep-ph/9609339].

[128] T. Barnes, N. Black and P. R. Page, Phys. Rev. D **68**, 054014 (2003) [arXiv:nucl-th/0208072].

[129] S. Capstick and N. Isgur, Phys. Rev. D **34**, 2809 (1986).

[130] S. Capstick and W. Roberts, Phys. Rev. D **49**, 4570 (1994) [arXiv:nucl-th/9310030].

[131] N.Isgur, R.Kokoski and J.Paton, Phys. Rev. Lett. 54, 869 (1985).

[132] F. E. Close and P. R. Page, Nucl. Phys. B **443**, 233 (1995) [arXiv:hep-ph/9411301].

[133] E. Eichten, K. Gottfried, T. Kinoshita, K. D. Lane and T. M. Yan, Phys. Rev. D **17**, 3090 (1978) [Erratum-ibid. D **21**, 313 (1980)].

[134] E.J.Eichten, K.Lane and C.Quigg, Phys. Rev. Lett. 89, 162002 (2002) [arXiv:hep-ph/0206018].

[135] E. J. Eichten, K. Lane and C. Quigg, Phys. Rev. D69, 094019 (2004) [arXiv:hep-ph/0401210].

[136] CLEO Collab. (T. E. Coan *et al.*), Phys. Rev. Lett. **96**, 162003 (2006) [arXiv:hep-ex/0602034].

[137] Technical Progress Report for PANDA. Strong Interaction Studies with Antiprotons. (PANDA Collaboration, Feb.2005).

[138] A. Lundborg, T. Barnes and U. Wiedner, Phys. Rev. D **73**, 096003 (2006) [arXiv:hep-ph/0507166].

[139] T. Barnes and X. Li, arXiv:hep-ph/0611340.

[140] X. H. Guo, H. W. Ke, X. Q. Li, X. Liu and S. M. Zhao, arXiv:hep-ph/0510146.

[141] M.B.Voloshin and L.B.Okun, JETP Lett. 23, 333 (1976) [Pisma Zh. Eksp. Teor. Fiz. 3, 369 (1976)].

[142] A.DeRújula, H.Georgi and S.L.Glashow, Phys. Rev. Lett. 38, 317 (1977).

[143] S.Iwao, Lett. Nuovo Cim. 28, 305 (1980).

[144] S. K. Choi *et al.* [Belle Collaboration], Phys. Rev. Lett. 91, 262001 (2003) [arXiv:hep-ex/0309032].

[145] K. Abe, arXiv:hep-ex/0505038.

[146] N. A. Tornqvist, arXiv:hep-ph/0308277.

[147] F. E. Close and P. R. Page, Phys. Lett. B578, 119 (2004) [arXiv:hep-ph/0309253].

[148] E. S. Swanson, Phys. Lett. B588, 189 (2004) [arXiv:hep-ph/0311229].

[149] N. A. Tornqvist, Phys. Lett. B **590**, 209 (2004) [arXiv:hep-ph/0402237].

[150] K. Abe, arXiv:hep-ex/0505037.

[151] C. W. Bernard *et al.* [MILC Collaboration], Phys. Rev. D **56**, 7039 (1997) [arXiv:hep-lat/9707008].

[152] Z. H. Mei and X. Q. Luo, Int. J. Mod. Phys. A **18**, 5713 (2003) [arXiv:hep-lat/0206012].

[153] X.Liao and T.Manke, [arXiv:hep-lat/0210030].

[154] G. S. Bali, Eur. Phys. J. A **19**, 1 (2004) [arXiv:hep-lat/0308015].

[155] X. Q. Luo and Y. Liu, Phys. Rev. D **74**, 034502 (2006) [Erratum-ibid. D **74**, 039902 (2006)] [arXiv:hep-lat/0512044].

[156] T. Barnes, F. E. Close and E. S. Swanson, Phys. Rev. D **52**, 5242 (1995) [arXiv:hep-ph/9501405].

[157] BABAR Collab. (B. Aubert *et al.*), Phys. Rev. Lett. **95**, 142001 (2005) [arXiv:hep-ex/0506081].

[158] B. Aubert *et al.* [BABAR Collaboration], Phys. Rev. Lett. **90**, 242001 (2003) [arXiv:hep-ex/0304021].

[159] Q. He [CLEO Collaboration], Phys. Rev. D **74**, 091104 (2006) [arXiv:hep-ex/0611021].

[160] K. Abe [Belle Collaboration], arXiv:hep-ex/0612006.

[161] B. Aubert *et al.* [BABAR Collaboration], Phys. Rev. D **73**, 011101 (2006) [arXiv:hep-ex/0507090].

[162] F. E. Close and P. R. Page, Phys. Lett. B **628**, 215 (2005) [arXiv:hep-ph/0507199].

[163] UKQCD Collab. (C. McNeile, C. Michael and P. Pennanen), Phys. Rev. D **65**, 094505 (2002) [arXiv:hep-lat/0201006].

[164] BABAR Collab. (S.Ye), presentation at the Quarkonium Working Group meeting QWG06. http:// www.qwg.to.infn.it/WS-jun06/WS4talks/Tuesday_AM/ Ye.pdf.

[165] W. E. Caswell and G. P. Lepage, Phys. Lett. B **167**, 437 (1986).

[166] G.T. Bodwin, E. Braaten, and G.P. Lepage, Phys. Rev. D 51 (1995) 1125; Erratum *ibid.* 55 (1997) 5853.

[167] A. Pineda and J. Soto, Nucl. Phys. Proc. Suppl. 64 (1998) 428.

[168] N. Brambilla, A. Pineda, J. Soto and A. Vairo, Nucl. Phys. B **566**, 275 (2000) [arXiv:hep-ph/9907240].

[169] N. Brambilla, A. Pineda, J. Soto and A. Vairo, Phys. Rev. D **63**, 014023 (2001) [arXiv:hep-ph/0002250].

[170] N. Brambilla, Y. Sumino and A. Vairo, Phys. Lett. B **513**, 381 (2001) [arXiv:hep-ph/0101305].

[171] A. Pineda, JHEP **0106**, 022 (2001) [arXiv:hep-ph/0105008].

[172] N. Brambilla, Y. Sumino and A. Vairo, Phys. Rev. D **65**, 034001 (2002) [arXiv:hep-ph/0108084].

[173] T. Lee, JHEP **0310**, 044 (2003) [arXiv:hep-ph/0304185].

[174] A. A. Penin, V. A. Smirnov and M. Steinhauser, Nucl. Phys. B **716**, 303 (2005) [arXiv:hep-ph/0501042].

[175] M. Beneke, Y. Kiyo and K. Schuller, Nucl. Phys. B **714**, 67 (2005) [arXiv:hep-ph/0501289].

[176] A. Pineda and A. Signer, Nucl. Phys. B **762**, 67 (2007) [arXiv:hep-ph/0607239].

[177] A. Pineda, Phys. Rev. D 65 (2002) 074007; Phys. Rev. D 66 (2002) 054022.

[178] B. A. Kniehl, A. A. Penin, A. Pineda, V. A. Smirnov and M. Steinhauser, Phys. Rev. Lett. **92**, 242001 (2004) [arXiv:hep-ph/0312086].

[179] A. A. Penin, A. Pineda, V. A. Smirnov and M. Steinhauser, Nucl. Phys. B **699**, 183 (2004) [arXiv:hep-ph/0406175].

[180] A. Pineda and A. Signer, Phys. Rev. D **73**, 111501 (2006) [arXiv:hep-ph/0601185].

[181] G. Källen and A. Sarby, K. Dan. Vidensk. Selsk. Mat.-Fis. Medd. 29, N17 (1955) 1.

[182] I. Harris and L.M. Brown, Phys. Rev. 105 (1957) 1656.

[183] A. Czarnecki and K. Melnikov, Phys. Rev. Lett. 80 (1998) 2531.

[184] M. Beneke, A. Signer, and V.A. Smirnov, Phys. Rev. Lett. 80 (1998) 2535.

[185] A. Czarnecki and K. Melnikov, Phys. Rev. D 65 (2002) 051501; Phys. Lett. B 519 (2001) 212.

[186] K. Melnikov and A. Yelkhovsky, Phys. Rev. **D59** 114009 (1999).

[187] A. A. Penin and A. A. Pivovarov, Nucl. Phys. B **549**, 217 (1999) [arXiv:hep-ph/9807421].

[188] A. Pineda and J. Soto, Phys. Lett. B **495**, 323 (2000) [arXiv:hep-ph/0007197].

[189] A. H. Hoang and I. W. Stewart, Phys. Rev. D **67**, 114020 (2003) [arXiv:hep-ph/0209340].

[190] E. Braaten and Y.Q. Chen, Phys. Rev. D 57 (1998) (1998) 4236; Erratum *ibid.* D 59 (1999) 079901.

[191] Y. Sumino, Phys. Rev. D 65 (2002) 054003; S. Recksiegel and Y. Sumino Phys. Rev. D 65 (2002) 054018; A. Pineda, J. Phys. G 29 (2003) 371; T. Lee, Phys. Rev. D 67 (2003) 014020.

[192] S. J. Brodsky, D. G. Coyne, T. A. DeGrand and R. R. Horgan, Phys. Lett. B **73** (1978) 203.

[193] K. Koller and T. Walsh, Nucl. Phys. B **140** (1978) 449.

[194] D. L. Scharre *et al.*, Phys. Rev. D **23** (1981) 43.

[195] B. Nemati *et al.* [CLEO Collaboration], Phys. Rev. D **55** (1997) 5273 [arXiv:hep-ex/9611020].

[196] S. Wolf, Phys. Rev. D **63** (2001) 074020 [arXiv:hep-ph/0010217].

[197] X. Garcia i Tormo and J. Soto, Phys. Rev. D **72** (2005) 054014 [arXiv:hep-ph/0507107].

[198] W. E. Caswell and G. P. Lepage, Phys. Lett. B **167** (1986) 437.

[199] G. T. Bodwin, E. Braaten and G. P. Lepage, Phys. Rev. D **51** (1995) 1125 [Erratum-ibid. D **55** (1997) 5853] [arXiv:hep-ph/9407339].

[200] A. Pineda and J. Soto, Nucl. Phys. Proc. Suppl. **64** (1998) 428 [arXiv:hep-ph/9707481].

[201] N. Brambilla, A. Pineda, J. Soto and A. Vairo, Nucl. Phys. B **566** (2000) 275 [arXiv:hep-ph/9907240].

[202] N. Brambilla, A. Pineda, J. Soto and A. Vairo, Rev. Mod. Phys. **77** (2005) 1423 [arXiv:hep-ph/0410047].

[203] I. Z. Rothstein and M. B. Wise, Phys. Lett. B **402** (1997) 346 [arXiv:hep-ph/9701404].

[204] M. Kramer, Phys. Rev. D **60** (1999) 111503 [arXiv:hep-ph/9904416].

[205] N. Brambilla, D. Eiras, A. Pineda, J. Soto and A. Vairo, Phys. Rev. D **67** (2003) 034018 [arXiv:hep-ph/0208019].

[206] M. Gremm and A. Kapustin, Phys. Lett. B **407** (1997) 323 [arXiv:hep-ph/9701353].

[207] W. Y. Keung and I. J. Muzinich, Phys. Rev. D **27** (1983) 1518.

[208] M. A. Yusuf and P. Hoodbhoy, Phys. Rev. D **54** (1996) 3345 [arXiv:hep-ph/9608244].

[209] X. Garcia i Tormo, arXiv:hep-ph/0610145.

[210] F. Maltoni and A. Petrelli, Phys. Rev. D **59** (1999) 074006 [arXiv:hep-ph/9806455].

[211] A. A. Penin and A. A. Pivovarov, Nucl. Phys. B **549** (1999) 217 [arXiv:hep-ph/9807421].

[212] K. Melnikov and A. Yelkhovsky, Phys. Rev. D **59** (1999) 114009 [arXiv:hep-ph/9805270].

[213] A. V. Manohar and P. Ruiz-Femenia, Phys. Rev. D **69** (2004) 053003 [arXiv:hep-ph/0311002].

[214] M. B. Voloshin, Mod. Phys. Lett. A **19** (2004) 181 [arXiv:hep-ph/0311204].

[215] S. Catani and F. Hautmann, Nucl. Phys. Proc. Suppl. **39BC** (1995) 359 [arXiv:hep-ph/9410394].

[216] C. W. Bauer, S. Fleming and M. E. Luke, Phys. Rev. D **63** (2001) 014006 [arXiv:hep-ph/0005275].

[217] C. W. Bauer, S. Fleming, D. Pirjol and I. W. Stewart, Phys. Rev. D **63** (2001) 114020 [arXiv:hep-ph/0011336].

[218] C. W. Bauer, C. W. Chiang, S. Fleming, A. K. Leibovich and I. Low, Phys. Rev. D **64** (2001) 114014 [arXiv:hep-ph/0106316].

[219] S. Fleming and A. K. Leibovich, Phys. Rev. D **67** (2003) 074035 [arXiv:hep-ph/0212094].

[220] S. Fleming and A. K. Leibovich, Phys. Rev. D **70** (2004) 094016 [arXiv:hep-ph/0407259].

[221] P. Aurenche, P. Chiappetta, M. Fontannaz, J. P. Guillet and E. Pilon, Nucl. Phys. B **399** (1993) 34.

[222] D. Buskulic *et al.* [ALEPH Collaboration], Z. Phys. C **69** (1996) 365.

[223] J. F. Owens, Rev. Mod. Phys. **59** (1987) 465.

[224] X. Garcia i Tormo and J. Soto, Phys. Rev. D **69** (2004) 114006 [arXiv:hep-ph/0401233].

[225] G. T. Bodwin, J. Lee and D. K. Sinclair, Phys. Rev. D **72** (2005) 014009 [arXiv:hep-lat/0503032].

[226] D. Besson *et al.* [CLEO Collaboration], Phys. Rev. D **74** (2006) 012003 [arXiv:hep-ex/0512061].

[227] R. D. Field, Phys. Lett. B **133** (1983) 248.

[228] J. H. Field, Phys. Rev. D **66** (2002) 013013 [arXiv:hep-ph/0101158].

[229] N. Brambilla, X. Garcia i Tormo, J. Soto and A. Vairo, in preparation.

[230] X. Garcia i Tormo and J. Soto, Phys. Rev. Lett. **96** (2006) 111801 [arXiv:hep-ph/0511167].

[231] H.-Y. Zhou and Y.-P. Kuang, Phys. Rev. D **44** (1991) 756.

[232] Y.-P. Kuang, Front. Phys. China **1** (2006) 19 [hep-ph/0601044]; N. Brambilla *et al.*, CERN Yellow Report, CERN-2005-005 [hep-ph/0412158].

[233] K. Gottfried, in *Proc. 1977 International Symposium on Lepton and Photon Interactions at High Energies*, edited by F. Gutbrod, DESY, Hamburg, 1977, p. 667; Phys. Rev. Lett. **40** (1978) 598.

[234] G. Bhanot, W. Fischler and S. Rudas, Nucl. Phys. **B 155** (1979) 208.

[235] M.E. Peskin, Nucl. Phys. **B 156** (1979) 365; G. Bhanot and M.E. Peskin, *ibid.* **156** (1979) 391.

[236] M.B. Voloshin, Nucl. Phys. **B 154** (1979) 365; M.B. Voloshin and V.I. Zakharov, Phys. Rev. Lett. **45** (1980) 688; V.A. Novikov and m.A. Shifman, Z. Phys. **C 8** (1981) 43.

[237] T.M. Yan, Phys. Rev. D **22** (1980) 1652.

[238] Y.-P. Kuang, Y.-P. Yi and B. Fu, Phys. Rev. D **42** (1990) 2300.

[239] Y.-P. Kuang and T.-M. Yan, Phys. Rev. D **24** (1981) 2874.

[240] S.-H. H. Tye, Phys. Rev. D **13** (1976) 3416; R.C. Giles and S.-H. H. Tye, Phys. Rev. Lett. **37** (1976) 1175; Phys. Rev. D **16** (1977) 1079; W. Buchmüller and S.-H. H. Tye, Phys. Rev. Lett. **44** (1980) 850.

[241] D.-S. Liu and Y.-P. Kuang, Z. Phys. C **37** (1987) 119; P.-Z. Bi and Y.-M. Shi, Mod. Phys. Lett. A **7** (1992) 3161.

[242] L.S. Brown and R.N. Cahn, Phys. Rev. Lett. **35** (1975) 1.

[243] W.-M. Yao *et al.* (Particle Data Group), J. Phys. G **33**, (2006) 1.

[244] E. Eichten, K. Gottfried, T. Kinoshita, K.D. Lane, and T.-M. Yan, Phys. Rev. D **17** (1978) 3090; *ibid.*, D **21** (1980) 203.

[245] W. Buchmüller, G. Grunberg, and S.-H. H. Tye, Phys. Rev. Lett. **45** (1980) 103; W. Buchmüller and S.-H. H. Tye, Phys. Rev. D **24** (1981) 132.

[246] M.B. Voloshin, Mod. Phys. Lett.A **17** (2002) 1533.

[247] Y.-P. Kuang, S.F. Tuan, and T.-M. Yan, Phys. Rev. D **37** (1998) 1210.

[248] J.Z. Bai *et al.* (BES Collaboration), Phys. Rev. D **70** (2004) 012006.

[249] Y.-P. Kuang and T.-M. Yan, Phys. Rev. D **41** (1990) 155.

[250] Y.-P. Kuang, Phys. Rev. D **65** (2002) 094024.

[251] S. Godfrey, Z. Phys. C **31** (1986) 77.

[252] Y.-Q. Chen and Y.-P. Kuang, Phys. Rev. D **46** (1992) 1165; **47** (1993) 350E.

[253] J. Adler, *et al.*, Phys. Rev. Lett. **60** (1988) 89.

[254] R.A. Partridge, Ph.D. thesis, Report No. CALT-68-1150, 1984.

[255] R.H. Schindler, Ph.D. thesis, Report No. SLAC-219, UC-34d(T/E), 1979.

[256] J.Z. Bai *et al.* (BES Collaboration), Phys. Lett. **B 605** (2005) 63.

[257] N.E. Adam *et al.* (CLEO Collaboration), Phys. Rev. Lett. **96** (2006) 082004.

[258] Y.-Q. Chen and R.J. Oakes, Phys. Rev. D **53** (1996) 5051.

[259] C. Patrignani, Nucl. Phys. Proc. Suppl., **142** (2005) 98.

[260] Crystal Ball Group, Annu. Rev. Nucl. Part. Sci. **33** (1983) 143.

[261] P. Rubin *et al* (CLEO Collaboration), Phys. Rev. D **72** (2005) 092004; J.L. Rosner *et al.* (CLEO Collabration), Phys. Rev. Lett. **95** (2005) 102003.

[262] S. Godfrey and J.L. Rosner, Phys. Rev. D **66** (2002) 014012.

[263] D.J. Gross, S.B. Treiman, and F. Wilczeck, Phys. Rev. D **19** (1979) 2188.

[264] C. Cawlfield *et al.* (CLEO Collaboration), Phys. Rev. D **73** (2006) 012003.

[265] Q. Lu and Y.-P. Kuang, hep-ph/0609091.

[266] See for example, J. Green *et al.*, Phys. Rev. Lett. **49**, 617 (1982); T. Bowcock *et al.*, *ibid.* **58**, 307 (1987).

[267] For a recent overview on radiative transitions in heavy quarkonia, see E. Eichten's review in CERN Yellow Report [N. Brambilla *et al.*, hep-ph/0412158]; also see [278].

[268] Here we give an incomplete list of references on $M1$ transition: G. Feinberg and J. Sucher, Phys. Rev. Lett. **35**, 1740 (1975); J. Sucher, Rept. Prog. Phys. **41**, 1781 (1978); J. S. Kang and J. Sucher, Phys. Rev. D **18**, 2698 (1978); R. McClary and N. Byers, *ibid.* **28**, 1692 (1983); V. Zambetakis and N. Byers, *ibid.* **28**, 2908 (1983); H. Grotch and K. J. Sebastian, *ibid.* **25**, 2944 (1982); H. Grotch, D. A. Owen and K. J. Sebastian, *ibid.* **30**, 1924 (1984); X. Zhang, K. J. Sebastian and H. Grotch, *ibid.* **44** (1991) 1606; T. A. Lahde, Nucl. Phys. A **714**, 183 (2003); D. Ebert, R. N. Faustov and V. O. Galkin, Phys. Rev. D **67**, 014027 (2003).

[269] N. Brambilla, Y. Jia and A. Vairo, Phys. Rev. D **73**, 054005 (2006) [arXiv:hep-ph/0512369].

[270] J. J. Dudek, R. G. Edwards and D. G. Richards, Phys. Rev. D **73**, 074507 (2006) [arXiv:hep-ph/0601137].

[271] G. Bodwin, E. Braaten and G. Lepage, Phys. Rev. D **51**, 1125 (1995) [E-ibid. D **55**, 5853 (1997)].

[272] A. Pineda and J. Soto, Nucl. Phys. Proc. Suppl. **64**, 428 (1998); N. Brambilla *et al*, Nucl. Phys. B **566**, 275 (2000).

[273] A. V. Manohar, Phys. Rev. D **56**, 230 (1997); T. Kinoshita and M. Nio, Phys. Rev. D **53** (1996) 4909.

[274] M. B. Voloshin, Nucl. Phys. B **154**, 365 (1979); Sov. J. Nucl. Phys. **36**, 143 (1982).

[275] S. Eidelman *et al.* [PDG Collaboration], Phys. Lett. B **592**, 1 (2004).

[276] M. Artuso *et al.* [CLEO Collaboration], Phys. Rev. Lett. **94**, 032001 (2005).

[277] J. L. Rosner *et al.* [CLEO Collaboration], Phys. Rev. Lett. **95**, 102003 (2005).

[278] E. Eichten, S. Godfrey, H. Mahlke and J. L. Rosner, arXiv:hep-ph/0701208.

[279] C. Z. Yuan, Q. Qin, and B. Y. Zhang, HEP&NP **26**, 1201 (2002).

[280] Quarkonium Working Group, yellow report.

[281] Particle Data Group, S. Eidelman *et al.*, Phys. Lett. B **592**, 1 (2004).

[282] M. A. Doncheski *et al.*, Phys. Rev. D **42**, 2293 (1990).

[283] E. Eichten *et al.*, Phys. Rev. D **21**, 203 (1980).

[284] K. J. Sebastian, Phys. Rev. D **26**, 2295 (1982).

[285] G. Hardekopf and J. Sucher, Phys. Rev. D **25**, 2938 (1982).

[286] R. McClary and N. Byers, Phys. Rev. D **28**, 1692 (1983).

[287] P. Moxhay and J. L. Rosner, Phys. Rev. D **28**, 1132 (1983).

[288] J. Z. Bai *et al.* (BES Collab.), Phys. Rev. D **70**, 012006 (2004).

[289] (CLEO Collab.), Phys. Rev. Lett. **94**, 232002 (2005).

[290] J. J. Dudek, R. G. Edwards, and D. G. Richards, hep-ph/0601137.

[291] J. L. Rosner, Phys. Rev. D **64**, 094002 (2001).

[292] P. Wang, X. H. Mo and C. Z. Yuan, Phys. Lett. B **574**, 41 (2003).

[293] P. Wang, X. H. Mo and C. Z. Yuan, Phys. Rev. D **70**, 077505 (2004).

[294] M. Oreglia *et al.*, Phys. Rev. D **25**, 2259 (1982).

[295] J. Z. Bai *et al.* (BES Collab.), Shi Xin's paper

[296] For the amplitude calculation formulas, see G. Karl, S. Meshkov and J. L. Rosner, Phys. Rev. D **13**, 1203 (1976).

[297] H. Grotch *et al.*, Phys. Rev. D **30**, 1924 (1984).

[298] (CLEO Collab.), Phys. Rev. Lett. **95**, 102003 (2005); Phys. Rev. D **72**, 092004 (2005).

[299] Gerald *et al.*, PLB.

[300] Y. P. Kuang, transition

[301] Shifman

[302] M. L. Yan

[303] Sigma in $\psi' \to J/\psi\pi^+\pi^-$

[304] F. K. Guo *et al.*

[305] M. B. Voloshin, hep-ph/0206240.

[306] T.W. Chiu and T.H. Hsieh (TWQCD Collaboration), hep-lat/0512029.

[307] X.Q. Luo and Y. Liu, hep-lat/0512044.

[308] N. Brambilla *et al.*, arXiv:hep-ph/0412158, and references therein.

[309] Particle Data Group, W. M. Yao *et al.*, J. Phys. G **33**, 1 (2006).

[310] P. Wang, C. Z. Yuan and X. H. Mo, Phys. Rev. D **70**, 114014 (2004) [arXiv:hep-ph/0410300], and references therein.

[311] J. Z. Bai *et al.* [BES Collaboration], Phys. Rev. D **58**, 097101 (1998) [arXiv:hep-ex/9806002].

[312] J. Z. Bai *et al.* [BES Collaboration], Phys. Rev. D **67**, 032004 (2003).

[313] M. Ablikim *et al.* [BES Collaboration], Phys. Rev. D **74**, 072001 (2006) [arXiv:hep-ex/0607023].

[314] M. Ablikim *et al.* [BES Collaboration], [arXiv:hep-ex/0611xxx].

[315] Y. Chen *et al.*, Phys. Rev. D **73**, 014516 (2006).

[316] Y. J. Gao, Y. J. Zhang, and K. T. Chao, Chin. Phys. Lett. **23**, 2376 (2006), hep-ph/0607278.

[317] T. Appelquist and H. D. Politzer, Phys. Rev. Lett. **34**, 43 (1975); A. De Rújula and S. L. Glashow, Phys. Rev. Lett. **34**, 46 (1975).

[318] Mark-II Collaboration, M. E. B. Franklin *et al.*, Phys. Rev. Lett. **51**, 963 (1983).

[319] BES Collaboration, J. Z. Bai, *et al.*, Phys. Rev. D **70**, 012005 (2004).

[320] Babar Collaboration, B. Aubert, *et al.*, Phys. Rev. D **70**, 072004 (2004).

[321] CLEO Collaboration, S. Dobbs *et al.*, Phys. Rev. Lett. **74**, 011150 (2006).

[322] BES Collaboration, J. Z. Bai *et al.*, Phys. Rev. D **69**, 012003 (2004).

[323] BES Collaboration, J. Z. Bai *et al.*, Phys. Rev. Lett. **91**, 052001 (2004).

[324] BES Collaboration, J. Z. Bai, *et al.*, Phys. Rev. D **54**, 1221 (1996); Erratum: ibid. **57**, 3187 (1998).

[325] BES Collaboration, M. Ablikim *et al.*, Phys. Rev. D **70**, 112003 (2004).

[326] BES Collaboration, M. Ablikim *et al.*, Phys. Rev. D **70**, 112007 (2004).

[327] BES Collaboration, M. Ablikim *et al.*, Phys. Lett. B **614**, 37 (2005).

[328] BES Collaboration, M. Ablikim *et al.*, Phys. Rev. D **70**, 077101 (2004).

[329] BES Collaboration, M. Ablikim *et al.*, Phys. Rev. D **72**, 072007 (2005).

[330] BES Collaboration, M. Ablikim *et al.*, Phys. Lett. B **619**, 247 (2005).

[331] BES Collaboration, M. Ablikim *et al.*, Phys. Rev. D **71**, 072006 (2005).

[332] CLEO Collaboration, N. E. Adam *et al.*, Phys. Rev. Lett. **94**, 012005 (2005).

[333] BES Collaboration, J. Z. Bai *et al.*, Phys. Rev. Lett. **81**, 5080 (1998).

[334] BES Collaboration, J. Z. Bai *et al.*, Phys. Rev. D **67**, 052002 (2003).

[335] BES Collaboration, J. Z. Bai *et al.*, Phys. Rev. D **69**, 072001 (2004).

[336] Z. Metreveli (for CLEO Collaboration), "Recent $\psi(2S)$ results from CLEOc", talk at Charm2006, Beijing, China, June 5-7, 2006.

[337] CLEO Collaboration, R. A. Briere *et al.*, Phys. Rev. Lett. **95**, 062001 (2005).

[338] CLEO Collaboration, G. S. Adams *et al.*, Phys. Rev. D **73**, 012002 (2006).

[339] CLEO Collaboration, D. Cronin-Hennessy *et al.*, hep-ex/0603026.

[340] S. J. Brodsky, G. P. Lepage, Phys. Rev. D **24**, 2848 (1981).

[341] P.G.O. Freund and Y. Nambu, Phys. Rev. Lett. **34**, 569 (1983).

[342] S. Okubo, Phys. Lett. **5**, 165 (1963); G. Zweig, CERN-preprint CERN-TH-401, 402, 412 (1964); Iizuka, Prog. Theor. Phys. Suppl. **37-38**, 21 (1996).

[343] Particle Data Group, W.-M. Yao *et al.*, J. Phys. **G 33** (2006) 1.

[344] W. S. Hou and A. Soni, Phys. Rev. Lett. **50**, 569 (1983).

[345] W. S. Hou and A. Soni, Phys. Rev. D **29**, 101 (1984).

[346] S. J. Brodsky, G. P. Lepage and S. F. Tuan, Phys. Rev. Lett. **59**, 621 (1987).

[347] Particle Data Group, M. Aguilar-Benitez *et al.*, Phys. Lett. B **170**, 1 (1986).

[348] C. T. Chan and W. S. Hou, Nucl. Phys. A **675**, 367c (2000).

[349] Y. H. Xie, Ph.D. thesis, IHEP, Chinese Academy of Sciences, 1998 (unpublished).

[350] F. A. Harris, hep-ex/9903036 (unpublished).

[351] W. S. Hou, Phys. Rev. D **55**, 6952 (1997).

[352] Y. Q. Chen and E. Braaten, Phys. Rev. Lett. **80**, 5060 (1998).

[353] See, for example, M. Peardon, Nucl. Phys. Proc. Suppl. **63**, 22-27, (1998).

[354] M. Suzuki,Phys. Rev. D **57**, 5171 (1998).

[355] M. Anselmino, M. Genovese, and E. Predazzi, Phys. Rev. D **44**, 1597 (1991); M. Anselmino, M. Genovese, and D. E. Kharzeev, ibid. **50**, 595 (1994).

[356] M. Chaichian and N. A. Törnqvist, Phys. Lett. B **323**, 75 (1989).

[357] S. J. Brodsky and M. Karliner, Phys. Rev. Lett. **78**, 4682 (1997).

[358] V. L. Chernyak, hep-ph/9906387.

[359] G. Karl and W. Roberts, Phys. Lett. B **144**, 263 (1984).

[360] G. Karl and S-F. Tuan, Phys. Rev. D **34**, 1692 (1986).

[361] S. S. Pinsky, Phys. Lett. B **236**, 479 (1990).

[362] S. S. Pinsky, Phys. Rev. D **31**, 1753 (1985).

[363] K.-T. Chao, Proc. 17th Intern. Symp. on Lepton-Photon Interactions at high Energies, Beijing, China, 1995, ed. Z. P. Zheng and H. S. Chen (World Scientific, Singapore, 1996) p. 106.

[364] Y. S. Zhu, in *Proceedings of the 28th International Conference on High Energy Physics*, edited by Z. Adjuk and A. K. Wroblewski (World Scientific, Singapore, 1997).

[365] A. Bramon, R. Escribano, and M. D. Scadron, Phys. Lett. B **403**, 339 (1997).

[366] C. Z. Yuan, HEP & NP **30**, 488 (2006).

[367] J. M. Gérard and J. Weyers, Phys. Lett. B **462**, 324 (1999).

[368] P. Wang, X. H. Mo and C. Z. Yuan, Phys. Lett. B **557**, 197 (2003).

[369] P. Artoisenet, J. M. Gérard and J. Weyers, Phys. Lett. B **628**, 211 (2005).

[370] V. L. Chernyak and A. R. Zhitnitsky, Phys. Rep. **112**, 173 (1984).

[371] We did not consider the possible different mixing angle extracted from the Belle results by K. Y. Liu and K. T. Chao, hep-ph/0405126.

[372] J. L. Rosner, Phys. Rev. D **64**, 094002 (2001).

[373] E. Eichten, K. Gottfried, T. Kinoshita, K. D. Lane and T. M. Yan, Phys. Rev. **D17** (1978) 3090; **D21** (1980) 313(E); **D21** (1980) 203(E).

[374] K. Heikkilä, N. A. Törnqvist and S. Ono, Phys. Rev. D **29**, 110 (1984); *ibid.* D **29**, 2136(E) (1984).

[375] Y.-P. Kuang and T. M. Yan, Phys. Rev. D **41**, 155 (1990).

[376] P. Wang, C. Z. Yuan and X. H. Mo, Phys. Lett. B **574**, 41 (2004).

[377] P. Wang, C. Z. Yuan and X. H. Mo, Phys. Rev. D **69**, 057502 (2004).

[378] P. Wang, X. H. Mo and C. Z. Yuan, Int. J. Mod. Phys. A **21**, 5163 (2006).

[379] P. Wang, X. H. Mo and C. Z. Yuan, Phys. Rev. D **70**, 077505 (2004).

[380] P. Wang, C. Z. Yuan and X. H. Mo, Phys. Rev. D **70**, 114014 (2004).

[381] CLEO Collaboration, D. Besson *et al.*, CLEO 05-27 (2005).

[382] X. Q. Li, D. V. Bugg and B. S. Zou, Phys. Rev. D **55**, 1421 (1997).

[383] S. F. Tuan, Commun. Theor. Phys. **33**, 285 (2000).

[384] M. Suzuki, Phys. Rev. D **60**, 051501 (1999).

[385] M. Suzuki, Phys. Rev. D **63**, 054021 (2001).

[386] J. Jousset *et al.*, Phys. Rev. D **41**, 138 (1990); D. Coffman *et al.*, Phys. Rev. D **38**, 2695 (1988); A. Bramon, R. Escribano and M.D. Scadron, Phys. Lett. B **403**, 339 (1997); M. Suzuki, Phys. Rev. D **58**, 111504 (1998); N.N. Achasov, Relative Phase between the Three Gluon and One Photon Amplitudes of the J/ψ Decays, in Proc. ninth International Conference on Hadron Spectroscopy (Protvino, Russia, August 2001), AIP Conf. Proc. **619** 649 (AIP, New York, 2002).

[387] G. López Castro *et al.*, Tests of Flavor Symmetry in J/ψ Decays, in: Proc. CAM-94 (ed. A. Zepeda, Cancum, Mexico, 1994), AIP Conf. Proc. **342**, 441 (AIP, New York, 1995).

[388] L. Köpke and N. Wermes, Phys. Rep. **174**, 67 (1989).

[389] R. Baldini, *et al.* Phys. Lett. B **444**, 111 (1998).

[390] C. Z. Yuan, P. Wang and X. H. Mo, Phys. Lett. B **567**, 73 (2003).

[391] J. P. Ma, Phys. Rev. D **65**, 097506 (2002).

[392] L. J. Clavelli and G. W. Intemann, Phys. Rev. D **28**, 2767 (1983).

[393] H. E. Haber and J. Perrier, Phys. Rev. D **32**, 2961 (1985).

[394] A. Seiden, H. F-W. Sadrozinski, and H. E. Haber Phys. Rev. D **38**, 824 (1988).

[395] T. Feldmann and P. Kroll, Phys. Rev. D **62**, 074006 (2000).

[396] P. Hoyer and S. Peigné, Phys. Rev. D **61**, 031501 (2000).

[397] Y. F. Gu and X. H. Li, Phys. Rev. D **63**, 114019 (2001).

[398] W. Kwong, Phys. Rev. D **37**, 3210 (1988).

[399] H. C. Chiang et al., Phys. Lett. B **324**, 482 (1994).

[400] K. K. Seth, Phys. Rev. D **69**, 097503 (2004).

[401] X. H. Mo, HEP & NP **29**, 831 (2005).

[402] S. W. Ye, "Study of some VP and PP modes of $\psi(2S)$ decays", Ph.D. thesis, University of Science and Technology of China, 1997 (in Chinese).

[403] G.A. Miller, Phys. Rev. C **39**, 1563 (1999).

[404] X. Liu, X.Q. Zeng and X. Q. Li, Phys. Rev. D **72**, 054023 (2005).

[405] P. Wang, X. H. Mo and C. Z. Yuan, hep-ph/0512329.

[406] C. Z. Yuan, X. H. Mo and P. Wang, Phys. Lett. B **626**, 95 (2005).

[407] C. J. Morningstar and M. J. Peardon, Phys. Rev. D **60**, 034509 (1999).

[408] M. Suzuki, Phys. Rev. D **65**, 097507 (2002).

[409] T-W. Chiu, hep-lat/0512029.

[410] X-Q. Luo and Y. Liu, hep-lat/0512044.

[411] E.S. Swanson, Phys. Rep. **429**, 243 (2006).

[412] G. Rong, D.H. Zhang, and J.C. Chen, hep-ex/0506051.

[413] M. Ablikim *et al.* (BES Collaboration) Phys. Rev. Lett. **97**, 121801 (2006).

[414] M. Ablikim *et al.* (BES Collaboration) Phys. Lett. B **141**, 145 (2006)

[415] E. Eichten *et al.*, Phys. Rev. D **21**,203 (1980).

[416] E. Eichten, Phys. Rev. D **22**,1819 (1980).

[417] P. Moxhay and J.L. Rosner, Phys. Rev. D**28**, 1132 (1983)

[418] BES Collaboration, M. Ablikim *et al.*, Phys. Rev. Lett., 97, 121801 (2006).

[419] J.L. Rosner, Phys. Rev. D **64**, 094002 (2001).

[420] Y. Yamamoto, A. Nishimura and Y. Yamaguchi, Prog. Theor. Phys., **58**, 347 (1977); Y. Yamamoto and A. Nishimura, Prog. Theor. Phys., **59**, 2151 (1978).

[421] Y.P. Kuang, Phys. Rev. D **65**, 094024 (2002).

[422] P. Maxhay, Phys. Rev. D **37**, 2557 (1988).

[423] A. Billoier et.al., Nucl. Phys. B **155**, 493.

[424] E.J. Eichten,K. Lane, C. Quigg, Phys. Rev. D **69**, 094019 (2004).

[425] T. Barnes, S. Godfrey, E.S. Swanson, Phys. Rev. D **72**, 054026 (2005).

[426] Yu-Ping Kuang and Tung-Mow Yan, Phys. Rev. D **41**, 155 (1990).

[427] J.L. Rosner, Anal. Phys. **319**, 1 (2005).

[428] H.J. Lipkin, Phys. Lett. B **179**, 278 (1986).

[429] BES Collaboration, J.Z. Bai *et al.*, Phys. Lett. **B 605**, 63 (2005).

[430] M. Ablikim et.al. Physi. Rev. D **72**, 072007 (2005)

[431] M. Ablikim et.al. Physi. Rev. D **70**, 112007 (2004)

[432] G. Rong, in proceedings of the 32nd International Conference on High Energy Physics, Beijing, China 16–22 August 2004, p1200.

[433] J.J. Aubert *et al.*, Phys. Rev. Lett. **33**, 1404 (1974); J.E. Augustin *et al.*, Phys. Rev. Lett. **33**, 1406 (1974).

[434] S. Bianco03 *et al.*, hep-ex/0309021.

[435] BES Collaboration, J.Z. Bai, *et al.*, Phys. Lett. B 591, 42 (2004) .

[436] BES Collaboration, M.Ablikim, *et al.*, Phys. Lett. B 632, 181 (2006) .

[437] M. W. Eaton, *et al.* Phys. Rev. D 29, 804 (1984) .

[438] Fermilab E835 Collaboration, A. Buzzo,

[439] A. Duncan and A. H. Mueller, Phys. Lett. B **93**, 119 (1980).

[440] S. J. Brodsky and G. P. Lepage, Phys. Rev. D **24**, 2848 (1981).

[441] V. L. Chernyak and A. R. Zhitnitsky, Nucl. Phys. B **201**, 492 (1982) [Erratum-ibid. B **214**, 547 (1983)].

[442] V. N. Baier and A. G. Grozin, Z. Phys. C **29**, 161 (1985).

[443] QWG group, CERN Yellow Report, CERN-2005-005, Geneva: CERN, 2005. -487. hep-ph/0412158.

[444] J. Bolz, P. Kroll and G. A. Schuler, Phys. Lett. B **392**, 198 (1997) [arXiv:hep-ph/9610265] and Eur. Phys. J. C **2**, 705 (1998) [arXiv:hep-ph/9704378].

[445] S. M. Wong, Nucl. Phys. A **674**, 185 (2000) [arXiv:hep-ph/9903221]; Eur. Phys. J. C **14**, 643 (2000) [arXiv:hep-ph/9903236].

[446] J. Bolz and P. Kroll, Eur. Phys. J. C **2**, 545 (1998) [arXiv:hep-ph/9703252].

[447] J. Bolz and P. Kroll, Z. Phys. A **356**, 327 (1996) [arXiv:hep-ph/9603289].

[448] Partical Data Group, J. Phys. G, **33**, 1 (2006).

[449] J. Z. Bai *et al.* [BES Collaboration], Phys. Lett. B **591**, 42 (2004) [arXiv:hep-ex/0402034].

[450] V. L. Chernyak and A. R. Zhitnitsky, Phys. Rept. **112**, 173 (1984).

[451] V. M. Braun and I. E. Filyanov, Z. Phys. C **48**, 239 (1990) [Sov. J. Nucl. Phys. **52**, 126 (1990 YAFIA,52,199-213.1990)]; P. Ball, V. M. Braun, Y. Koike and K. Tanaka, Nucl. Phys. B **529**, 323 (1998) [arXiv:hep-ph/9802299]; M. Beneke and T. Feldmann, Nucl. Phys. B **592**, 3 (2001) [arXiv:hep-ph/0008255].

[452] V. Braun, R. J. Fries, N. Mahnke and E. Stein, Nucl. Phys. B **589**, 381 (2000) [Erratum-ibid. B **607**, 433 (2001)] [arXiv:hep-ph/0007279].

[453] N. G. Stefanis and M. Bergmann, Phys. Rev. D **47**, 3685 (1993) [arXiv:hep-ph/9211250]; V. L. Chernyak, A. A. Ogloblin and I. R. Zhitnitsky, Z. Phys. C **42**, 583 (1989) [Yad. Fiz. **48**, 1398 (1988 SJNCA,48,889-895.1988)];

[454] A. Andrikopoulou, Z. Phys. C **22**, 63 (1984); P. H. Damgaard, K. Tsokos and E. L. Berger, Nucl. Phys. B **259**, 285 (1985).

[455] J. Z. Bai *et al.* [BES Collaboration], Phys. Rev. D **67**, 112001 (2003) [arXiv:hep-ex/0304012].

[456] E. Braaten and J. Lee, Phys. Rev. D **67**, 054007 (2003) [arXiv:hep-ph/0211085].

[457] M. L. Mangano and A. Petrelli, Phys. Lett. B **352**, 445 (1995) [arXiv:hep-ph/9503465].

[458] H. W. Huang, C. F. Qiao and K. T. Chao, Phys. Rev. D **54**, 2123 (1996) [arXiv:hep-ph/9601380].

[459] J. P. Ma and Q. Wang, Phys. Lett. B **537**, 233 (2002) [arXiv:hep-ph/0203082].

[460] S. J. Brodsky and G. P. Lepage, **24** 1981 (2848).

[461] C. Carimalo, Int. J. Mod. Phys. A2 (1987) 249.

[462] F. Murgia and M. Melis, Phys. Rev. D **51**, 3487 (1995) [arXiv:hep-ph/9412205]; R. G. Ping, H. C. Chiang and B. S. Zou, Phys. Rev. D **66**, 054020 (2002).

[463] M. Claudson, S. L. Glashow and M. B. Wise, Phys. Rev. D **25**, 1345 (1982).

[464] M. Anselmino, R. Cancelliere and F. Murgia, Phys. Rev. D **46**, 5049 (1992).

[465] R. G. Ping, B. S. Zou and H. Q. Chiang, Eur. Phys. J. A 23, 129-133 (2005).

[466] H. Q. Zhou, R. G. Ping and B. S. Zou, Physics Letters B 611 123-128 (2005).

[467] Hong Cheng, Rong-Gang Ping hep-ph/0601202.

[468] J. Z. Bai *et al.* [BES Collaboration], Phys. Rev. D **69**, 092001 (2004) [arXiv:hep-ex/0401011].

[469] M. W. Eaton et al., Phys. Rev. D **29**(1984) 804.

[470] P. Henrard et al., Nucl. Phys. B **292**(1987) 670.

[471] L. Kopke, Talk given at XXIIrd Intern Conf. on High Energy Physics (Berkeley, CA, 1986).

[472] J. -G. Korner, Z. Phys. C **33** (1987) 529.

[473] H. E. Haber and J. Perrier, Phys. Rev. D **31** (1985) 1751.

[474] H. Genz, M. Malvetti and S. Tatur, Phys. Rev. D **31** (1985) 1751.

[475] L Kopke and N. Wermes, Phys. Rep. **174** (1989) 67.

[476] J. -G. Korner, Z. Phys. C **33** (1987) 529.

[477] L. Köpke and N. Wermes, Phys. Rep. **174**, 67 (1989).

[478] E. Leader and E. Predazzi, *An introduction to gauge theory and the 'new physics'*, Cambrdge University Press (1982).

[479] T. Appelquist and H. D. Politzer, Phys. Rev. Lett. **34**, 43 (1975); A. De Rújula and S. L. Glashow, Phys. Rev. Lett. **34**, 46 (1975).

[480] W. Kwong, J.L.'Rosner, and C. Quigg, Annu. Rev. Nucl. Part. Sci. **37**, 325 (1987).

[481] S. J. Brodsky, G. P. Lepage and P. B. Mackenzie, Phys. Rev. D **28**, 228 (1983).

[482] W. Kwong, P. B. Mackenzie, R. Rosenfeld and J. L. Rosner, Phys. Rev. D **37**, 3210 (1988).

[483] W. Buchmuller and S. H. H. Tye, Phys. Rev. D **24** (1981) 132.

[484] V. Chernyak, arXiv:hep-ph/9906387.

[485] X. H. Mo, C. Z. Yuan and P. Wang, arXiv:hep-ph/0611214.

[486] H. Kowalski and T. F. Walsh, Phys. Rev. D **14**, 852 (1976).

[487] J. Z. Bai *et al.* [BES Collaboration], Phys. Lett. B **578**, 16 (2004) [arXiv:hep-ex/0308073].

[488] D. Bisello *et al.* [DM2 collaboration], Nucl. Phys. B **350**, 1 (1991).

[489] C. H. Wu *et al.*, Phys. Rev. Lett. **97**, 162003 (2006) [arXiv:hep-ex/0606022].

[490] R. M. Baltrusaitis *et al.* [Mark-III Collaboration], Phys. Rev. D **33**, 629 (1986).

[491] T. Himel *et al.*, Phys. Rev. Lett. **45**, 1146 (1980).

[492] R. Baldini, *et al.* Phys. Lett. B **444**, 111 (1998).

[493] M. Suzuki,Phys. Rev. D **63**, 054021 (2001).

[494] J. Jousset *et al.*, Phys. Rev. D **41**, 138 (1990); D. Coffman *et al.*, Phys. Rev. D **38**, 2695 (1988); A. Bramon, R. Escribano and M.D. Scadron, Phys. Lett. B **403**, 339 (1997); M. Suzuki, Phys. Rev. D **58**, 111504 (1998); N.N. Achasov, Relative Phase between the Three Gluon and One Photon Amplitudes of the J/ψ Decays, in Proc. ninth International Conference on Hadron Spectroscopy (Protvino, Russia, August 2001), AIP Conf. Proc. **619** 649 (AIP, New York, 2002).

[495] G. López Castro *et al.*, Tests of Flavor Symmetry in J/ψ Decays, in: Proc. CAM-94 (ed. A. Zepeda, Cancum, Mexico, 1994), AIP Conf. Proc. **342**, 441 (AIP, New York, 1995).

[496] M. Suzuki,Phys. Rev. D **60**, 051501 (1999).

[497] P. Wang, C. Z. Yuan and X. H. Mo, Phys. Lett. B **574**, 41 (2004).

[498] BES Collaboration, M. Ablikim *et al.*, Phys. Lett. B **614**, 37 (2005).

[499] G. S. Huang *et al.* [CLEO Collaboration], Phys. Rev. Lett. **96**, 032003 (2006) [arXiv:hep-ex/0509046].

[500] J. L. Rosner, arXiv:hep-ph/0405196.

[501] P. Wang, C. Z. Yuan and X. H. Mo, Phys. Rev. D **70**, 114014 (2004) [ArXiv:hep-ph/0410300].

[502] D. Besson *et al.* [CLEO Collaboration], Phys. Rev. Lett. **96**, 092002 (2006) [arXiv:hep-ex/0512038].

[503] J. Z. Bai *et al.* [BES Collaboration], Phys. Lett. B **510**, 75 (2001) [arXiv:hep-ex/0105011].

[504] M. Ablikim *et al.* [BES Collaboration], Phys. Rev. Lett. **97**, 062001 (2006) [arXiv:hep-ex/0405030].

[505] B. Aubert *et al.* [BABAR Collaboration], Phys. Rev. D **73**, 012005 (2006) [arXiv:hep-ex/0512023].

[506] R. Sinha and S. Okubo, Phys. Rev. D **30**, 2333 (1984).

[507] BES Collaboration, J. Z. Bai *et al.*, Phys. Rev. Lett. **91**, 022001 (2003).

[508] BES Collaboration, M. Ablikim *et al.*, Phys. Rev. D **71**, 072006 (2005).

[509] BES Collaboration, M. Ablikim *et al.*, Phys. Rev. Lett. **93**, 112002 (2004).

[510] Belle Collaboration, K. Abe *et al.*, Phys. Rev. Lett. **88**, 181803 (2002).

[511] Belle Collaboration, M.-Z. Wang *et al.*, Phys. Rev. Lett. **90**, 201802 (2003).

[512] Belle Collaboration, Y.-J. Lee *et al.*, Phys. Rev. Lett. **93**, 211801 (2004).

[513] CLEO Collaboration, S. Anderson *et al.*, Phys. Rev. Lett. **86**, 2732 (2001).

[514] Belle Collaboration, K. Abe *et al.*, Phys. Rev. Lett. **89**, 151802 (2002).

[515] Belle Collaboration, M.-Z. Wang *et al.*, Phys. Rev. Lett. **92**, 131801 (2004).

[516] BABAR Collaboration, B. Aubert *et al.*, hep-ex/0408035.

[517] C.Z. Yuan, X.H. Mo and P. Wang, Phys. Rev. Lett. **626**, 95 (2005).

[518] E. Fermi and C. N. Yang, Phys. Rep. **76**, 1739 (1949).

[519] S. Sakata, Prog. Theor. Phys. **16**, 686 (1956).

[520] H. E. Haber and J. Perrier, Phys. Rev. D **32**, 2961 (1985).

[521] A. Seiden, H. F-W. Sadrozinski, and H. E. Haber Phys. Rev. D **38**, 824 (1988).

[522] N. Morisita, I. Kitamura and T. Teshima, Phys. Rev. D **44**, 175 (1991).

[523] J. L. Rosner, Phys. Rev. D **27**, 1101 (1983).

[524] For example, compare the Dalitz plots in Ref. [508] and hep-ex/0405030.

[525] Belle Collaboration, K. Abe *et al.*, hep-ex/0409005.

[526] CLEO Collaboration, T. K. Pedlar *et al.*, hep-ex/0505057.

[527] BES Collaboration, J. Z. Bai *et al.*, Phys. Rev. D **63**, 032002 (2001).

[528] G.J. Feldman and M.L. Perl, Phys. Rep. **33**, 285 (1978).

[529] CLEO Collaboration, R. A. Briere *et al.*, Phys. Rev. Lett. **95**, 062001 (2005).

[530] BES Collaboration, M. Ablikim *et al.*, Phys. Rev. D **71**, 072006 (2005).

[531] M.E.B. Franklin *et al.*, Phys. Rev. Lett. **51**, 963 (1983).

[532] BES Collaboration, J. Z. Bai *et al.*, Phys. Rev. D **67**, 052002 (2003).

[533] CLEO Collaboration, S. B. Athar *et al.*, hep-ex/0611032.

[534] G. J. Ding, J. l. Ping and M. L. Yan, Phys. Rev. D **74**, 014029 (2006) [arXiv:hep-ph/0510013].

[535] R. Jaffe, Phys. Rev. D **72**, 074508 (2005) [arXiv:hep-ph/0507149].

[536] A. De Rujula, H. Georgi and S. L. Glashow, Phys. Rev. D **12**, 147 (1975).

[537] D. Strottman, Phys. Rev. D **20**, 748 (1979).

[538] R.L.Jaffe and F.Wilcek, Phys.Rev.Lett 91,232003(2003), hep-ph/0307341; M.Karliner and H.J.Lipkin, Phys.Lett.B575:249-255,2003, hep-ph/0402260.

[539] Gui-Jun Ding and Mu-Lin Yan,Phys.Rev.**D72**, 034014,(2005); hep-ph/0506119.

[540] B.W. Lee, C. Quigg, and J.L. Rosner, Phys. Rev. D **15**, 157 (1977).

[541] A. Chodos *et al.*, Phys. Rev. D **9**, 3471 (1974); W. Bardeen *et al.*, Phys. Rev. D **11**, 1094 (1975).

[542] C. Quigg and J.L. Rosner, Phys. Rev. D **16**, 1497 (1977).

[543] M.K. Gaillard, B.W. Lee, and J.L. Rosner, Phys. Rev. D **47**, 277 (1975).

[544] B. Andersson, *The Lund Model*, Cambridge Universaty Press, 1998.

[545] B. Andersson and H. m. Hu, arXiv:hep-ph/9910285.

[546] H. m. Hu *et al.*, HEP & NP **25** (2001) 1045-1043.

[547] Xiao-Gang He , J. P. Ma, and Bruce McKellar, Phys. Rev. D**47**(1993) 1744;
Xiao-Gang He , J. P. Ma, and Bruce McKellar, Phys. Rev. D**49**(1994) 4548;

[548] M. H. Tixier et al. DM2 Collaboration, Phys. Lett. B **212** 523.

[549] N. A. Tornqvist, Found. of Phys., 11 (1981) 171;
N. A. Tornqvist, Phys. Lett. A **117** (1986) 1.

[550] A. Aspect, Phys. Rev. Lett., **49**(1982) 91.

[551] BES Collaboration, M. Ablikim, *et al.*, Phys. Rev. Lett. **97** (2006) 62001.

[552] R.G. Ping, H.C. Chiang and B.S. Zou, Nucl. Phys. A**743** 149.

[553] Belle Collaboration, C.H. Wu *et al.*, Phys. Rev. Lett. **97**, 162003 (2006).

[554] BES Collaboration, J.G. Bian, *et al.*, Phys. Rev. D**70** (2004) 012004.

[555] J. G. Bian, et al., BES Collaboration, Phys. Rev. Lett. **91** (2003) 022001.

[556] BES Collaboration, M. Ablikim, *et al.*, Phys. Rev. Lett. **93** (2004) 112002.

[557] D.A. Liberman, Phys. Rev. D **16**, 1542 (1977);
G.W. Barry, Phys. Rev. D **16**, 2886 (1977).

[558] S.J. Brodsky, I. Schimidt, and G.F. de Téramond, Phys. Rev. Lett. **64**, 1011 (1990).

[559] H. Gao, T.-S.H. Lee, and V. Marinov, Phys. Rev. C **63**, 022201 (2001).

[560] F. Huang, Z.Y. Zhang, and Y.W. Yu, Phys. Rev. C **73**, 025207 (2006).

[561] Z.Y. Zhang's report at BES

[562] A. Einstein, B. Podolsky, and N. Rosen, Phys. Rev. **37**, 777 (1935).

[563] D. Bohm and Y. Aharonov, Phys. Rev. **108**, 1070 (1957)

[564] J.S. Bell, Physics **1**, 195 (1964).

[565] J.F. Clauser, M.A. Horne, A. Shimony, and R.A. Holt, Phys. Rev. Lett. **23**, 880 (1969).

[566] A. Aspect, P. Grangier, and G. Roger, Phys. Rev. Lett. **49**, 91 (1982),

[567] Y.H. Shih and C.O. Alley, Phys. Rev. Lett. **61**, 2921 (1988).

[568] Z.Y. Ou and L. Mandel, Phys. Rev. Lett. **61**, 50 (1988).

[569] G. Weihs *et al.*, Phys. Rev. Lett. **81**, 5039 (1998).

[570] S.A. Abel, M. Dittmar, and H. Dreiner, Phys. lett. B **280**, 304 (1992).

[571] M. Lamehi-Rachti and W. Mitting, Phys. Rev. D **14**, 2543 (1976).

[572] T.D. Lee and C.N. Yang, Lee report at ANL, May 28, 1960. (unpublished)

[573] D.R. Inglis, Rev. Mod. Phys. **33**, 1 (1961).

[574] T.B. Day, Phys. rev. **121**, 1204 (1961).

[575] H.J. Lipkin, Phys. rev. **176**, 1715 (1968).

[576] N.A. Törnqvist, Found. Phys. **11**, 171 (1981).

[577] P. Privitera, Phys. lett. B **275**, 172 (1992).

[578] N.A. Törnqvist, in: /Quantum Mechanics Versus Local Realism. (F.Selleri, ed.), Plenum Press, New York, 1988, pp.115-132.

[579] M.H. Tixier *et al.* (the DM2 Collaboration, LAL Orsay, LPC, Clermont, Padova, Frascati), Presentation at: Conference on Microphysical Reality and Quantum Formalism, Urbino, Italy (1985).

[580] A. Afriat, F. Selleri,/The Einstein Podolsky and Rosen Paradox in atomic nuclear and particle physics. (Plenum Press, New York, 1999).

[581] Reinhold A. Bertlmann, quant-ph/0410028.

[582] J. Bernabéu, N.E. Mavromatos, and J. Papavassiliou, Phys. Rev. Lett. **92**, 131601 (2004).

[583] Fumiyo Uchiyama, Phys. Lett. A **231**, 295 (1997).

[584] Review of Particle Physics, J. Phys. G: Nucl. Part. Phys. **33** 1 (2006).

[585] A. Bramon, R.Escribano, and G. Garbarino, Found. Phys. **36** 563 (2006).

[586] CPLEAR Collaboration, Phys. Lett. B **422**, 339 (1998).

[587] Apollo. Go, Journal of Modern Optics **51**, 991 (2004).

[588] R.A. Bertlmann, A. Bramon, G. Garbarino, and B.C. Hiesmayr, Phys. lett. A **332**, 355 (2004).

[589] M Artuso, *et al*, CLEO Collaboration, Phys. Rev. Lett. **95**, 261801 (2005).

[590] G. Bonvicini, *et al*, CLEO Collaboration, Phys. Rev. Lett. **96**, 022002 (2006).

[591] L. Hardy, Phys. Rev. Lett. **71**, 1665 (1993).

[592] A. Bramon and G. Garbarino, Phys. Rev. Lett. **88**, 040403 (2002).

[593] A. Bramon and G. Garbarino, Phys. Rev. Lett. **89**, 160401 (2002).

[594] A. Bramon, R. Escribano, and G. Garbarino, quant-ph/0501069.

[595] Junli Li, Cong-Feng Qiao, Phys. Rev. D **74**, 076003 (2006).

[596] William K. Wootters, Phys. Rev. Lett. **80**, 2245 (1998).

[597] N. Gisin, Phys. Lett. A **154**, 201 (1991).

[598] G.Kar, Phys. Lett. A **204**, 99 (1995).

[599] Ayman F. Abouraddy, Bahaa E.A. Saleh, Alexander V. Sergienko, and Malvin C. Teich, Phys. Rev. A **64**, 050101 (2001).

[600] BES Collaboration, Phys. Rev. D **69**, 012003 (2004).

[601] M. A. Sanchis, Phys.Lett. B **280**, 299 (1992); Phys.Lett. B **312**, 333 (1993).

[602] A. Datta, P. O'Donnell, S. Pakvasa, X. Zhang, Phys.Rev.D **60**, 014011 (1999).

[603] M. A. Sanchis-Lozano Z.Phys.C **62**, 271-280 (1994).

[604] F. Hussain, J. G. Korner and G. Thompson, Ann.Phys. **206**, 334 (1991).

[605] A. F. Falk, Nucl. Phys. **B378**, 79 (1992).

[606] K. K. Sharma and R. C. Verma, Int.J.Mod.Phys. **A14**, 937-946 (1999).

[607] J. D. Bjorken, Nucl. Phys. **B 11**, 325 (1989); D. Bortoletto and S. Stone, Phys. Rev. Lett. **65**, 2951(1990).

[608] M. B. Voloshin and M. A. Shifman, Sov. J. Nucl.Phys. **47**, 511 (1988).

[609] P. Fayet, Phys. Lett. **B 84**, 421 (1979); D. Besson *et. al.* (CLEO Collaboration), Phys. Rev. **D 30**, 1433 (1984); P. Fayet and J. Kaplan, Phys. Lee. **B 269**, 213 (1991); B. McElrath, Phys. Rev. **D 72**, 103508 (2005).

[610] P. Fayet, Phys. Rev. **D 74**, 054034 (2006).

[611] A. V. Artamonov, *et. al.* (E949 Collaboration), Phys. Rev. **D 72**, 091102 (2005).

[612] C. Boehm and P. Fayet, Nucl. Phys. **B 683**, 219(2004); C.Boehm, D. Hooper, J. Silk, M. Casse and J. Paul, Phys. Rev. Lett. **92**, 101301 (2004); P. Fayet, Phys. Rev. **D 70**, 023514 (2004).

[613] P. Fayet, Phys. Lett. **B 95**, 285 (1980); P. Fayet, Nucl. Phys. **B 187**, 184(1981).

[614] J. Ellis, J. F. Gunion, H. E. Haber, L. Roszkowski, and F. Zwirner, Phys. Rev. **D 39**, 844 (1989); J. F. Gunion, D. Hooper, and B. McElrath, Phys. Rev. **D 73**, 015011 (2006); G. Bertone, D. Hooper and J. Silk, Phys. Rept. **405**, 279 (2005) [arXiv:hep-ph/0404175].

[615] P. Jean *et al.*, Astron. Astrophys. **407**, L55 (2003).

[616] J. F. Beacom, N. F. Bell, and G. Bertone, Phys. Rev. Lett. **94**, 171301 (2005);P. Fayet D. Hooper, and G. Sigl, Phys. Rev. Lett. **96**, 211302 (2006).

[617] R. Balest, *et al.* (CLEO Collaboration), Phys. Rev. **D 51**, 2053 (1995).

[618] L. N. Chang, O. Lebedev and J. N. Ng, Phys. Lett. **B44**, 419 (1998).

[619] S. Eidelman *et al.*, Phys. Lett. **B592**, 1 (2004)

[620] A. Ablikim *et al*, BES Collaboration, hep-ex/0607006, to appear in Phys. Rev. Letts.

[621] T. Goldman, H. E. Haber, Los Alamos preprint LA-UR-83-2323, (1983).

[622] G. Goggi and G. Penso, Nucl. Phys. **B 165**, 249 (1980).

[623] Jade Collaboration, Phys.Lett. **B 92**, 806 (1980);TASSO Collaboration, Phys. Lett. **B 92**, 199 (1980); PLUTO Collaboration, Phys. Lett. **B 94**, 87 (1980).

[624] Stan Brodsky, private communication.

[625] S. Nussinov, R. D. Peccei and X. M. Zhang, Phys. Rev. **D 63**, 016003 (2000).

[626] W. Hou, C. Yue and T. Feng, Phys. Rev. **D 67**, 114001 (2003).

[627] "Probing for lepton flavor violation in decays of Charmonium and bottomonium systems", R. D. Peccei, J-X. Wang and X. Zhang, May 1998 Note (unpublished); X. Zhang, invited talk given at the national conference on high energy physics, Chengde, China, in April 1998.

[628] Xin-min Zhang, e-Print Archive: hep-ph/0010105.

[629] Z. K. Silagadze, hep-ph/9907328;T .Huang, Z. Lin and X. Zhang, hep-ph/0009353; H-M. Chan *et al.*, hep-ph/0006338;hep-ph/0007004.

[630] J. Bai *et al.*, [BES Collaboration], Phys. Lett. **B 561**, 49 (2003); M. Ablikim *et al.*, [BES Collaboration], Phys. Lett. **B 598**, 172 (2004).

Part V

Charm Physics

Conveners

Hai-Bo Li, Zhi-Zhong Xing

Contributers

D. M. Asner, I. I. Bigi, J. C. Chen, H. Y. Cheng, K. L. He, H. B. Li, H. L. Ma, Y. L. Wu, Z. Z. Xing, M. Z. Yang, Y. D. Yang, M. Zhong

Nobody doubts that the discovery of hadrons with charm of the hidden as well open variety – i.e. charmonia as well as D mesons – was instrumental for the acceptance of the SM in general and of quarks as *physical* degrees of freedom rather than objects of mere *mathematical* convenience in particular. Yet charm is all too often viewed as a quantum number with a great past, yet no truly interesting future. This is due to the SM predicting a rather dull electroweak phenomenology with known' CKM parameters, slow $D^0 - \overline{D}^0$ oscillations, tiny (at best) **CP** asymmetries and extremely rare flavor changing neutral currents with a huge background from long-distance dynamics.

Yet such a view focusses merely on the Surface'. A more profound perspective starts from the observation that charm dynamics are full of challenges as well as promises. There is actually a triple motivation for *further dedicated and comprehensive* studies:

1. Precisely since the SM weak forces are well known, charm decays provide an excellent laboratory to study the impact of QCD's nonperturbative dynamics and to validate theoretical control over them.

2. This in turn allows us to calibrate the theoretical tools available for treating B decays.

3. Charm decays provide a novel window onto New Physics in the weak sector precisely, because there is so little SM Background' in particular concerning **CP** violation.

None of the novel successes the SM has scored since the turn of the millenium in the heavy flavour sector invalidates at all the case for the SM being incomplete. Yet they strongly suggest that we can*not count* on a numerically massive impact of New Physics on heavy flavour transitions. Hence high accuracy and reliability – on the experimental as well as theoretical side – is *essential* for our (indirect) probes of New Physics in heavy flavor decays, as is the need to search in unusual places. Items (2) and (3) above can be expanded as follows:

- To saturate the discovery potential in B (and D!) decays we have to bring them under as precise theoretical control as possible. This requires much more than obtaining Engineering' input like absolute charm branching ratios or the spectrum and quantum numbers of charm hadrons: we have to map out and understand Dalitz plots of many D^0, D^+ and D_s^+ channels in a detailed way and extend such analyses to four-body final states.

- As mentioned just above the SM predicts at best small **CP** asymmetries (basically in once Cabibbo suppressed modes only) – a domain we are just now starting to probe in a quantitatively meaning way. While again we cannot count on New Physics inducing large **CP** violation in charm decays, a SM Background' is either absent or very small. In that sense the Signal-to-noise' ratio is small in **CP** studies of charm transitions. Yet large statistics are required, and complex final states have to be analyzed with good control over the systematics.

In the following these issues will be addressed in considerable detail. There are several very good reviews in the recent literature [1]. Yet we want to make this exposition as self-contained as reasonably possible.

Chapter 23

D Tag Reconstruction Efficiencies and Rates[1]

BEPCII will run at charm threshold, it provide a unprecedented physics opportunities to study the weak decay of charm mesons. Only the $D^0\overline{D^0}$ and D^+D^- are pair produced with no other particle involved at the resonance of $\psi(3770)$. This provide extremely clean and pure charm signal. The large cross section of $\psi(3770)$, large decay fractions and high tagging efficiencies allow us to reconstruction the both D's. Lots of systematic uncertainties will be canceled out while applying the double tag method. The quantum coherence of the two initial state D mesons for $\psi(3770)$ allows both simple and sophisticated methods to measure $D^0 - \overline{D^0}$ mixing parameters, strong phase, CP eigenstate branching fractions and CP violation.

The general technique used in charm physics study is referred to as tagging. Since the $D\overline{D}$ are pair produced in charm threshold, fully reconstructing a D decay from a subset of tracks in an event therefore guarantees that the remaining tracks originated from the recoiling $\overline{D}$. The reconstructed D is referred to as the tagged D or simply the tag, while everything not associated with the tag is referred to as recoil. Once a tag has been obtained, the recoil tracks can be analyzed for the decay modes of interest. Usually, Cabibbo favored hadronic decay modes, such as: $D^0 \to K^-\pi^+(\sim 4\%)$, $D^0 \to K^-\pi^+\pi^+\pi^-(\sim 8\%)$, $D^0 \to K^-\pi^+\pi^0(\sim 14\%)$, $D^+ \to K^-\pi^+\pi^+(\sim 9\%)$, $D^+ \to \overline{K^0}\pi^+(\sim 3\%)$, $D^+ \to \overline{K^0}\pi^+\pi^0(\sim 14\%)$,$D^+ \to \overline{K^0}\pi^+\pi^+\pi^-(\sim 6\%)$, $D^+ \to K^-\pi^+\pi^+\pi^0(\sim 6\%)$ and $D_s^+ \to K^-K^+\pi^+(\sim 5\%)$, $D_s^+ \to \overline{K^0}K^+(\sim 4\%)$, and some D_s^+ decays into final state with η/η's etc, with large branching ratios, are selected to be as the flavor tags.

23.1 The Tag Reconstruction

Tag reconstruction begins with the charged track selection. All charged tracks must have a good helix fit, and are required to be measured in the reliable region of drift chamber. Their parameters must be corrected for energy loss and multiple scattering according to the assigned mass hypotheses. Tracks not associated with K_S reconstruction are required to be originate from the interaction point. To reduce the combinatoric background kaons

[1]By Kang-Lin He, Sheng-Sen Sun and Da-Yong Zhang

and pions are well identified by the PID algorithm.

Neutral kaon candidates are mainly reconstructed through the decay of $K_S \to \pi^+\pi^-$. The decay vertex formed by the $\pi^+\pi^-$ pair is required to be far away from the interaction point, and the momentum vector of $\pi^+\pi^-$ pair must be aligned with the position vector of the decay vertex to the interaction point. The $\pi^+\pi^-$ invariant mass is required to be consistent with the K_S nominal mass. The track parameters and the error matrices are recalculated at the secondary vertex. The K_L tag in some double tag analysis is reconstructed by the requirements of the recoil mass of all detected particle is within the range of K_L nominal mass and the interaction in EMC or muon counter is observed in a confined region.

The neutral pions are reconstructed from $\pi^0 \to \gamma\gamma$ decays using the photons observed in the good barrel and endcap regions of EMC. At the energies of interest, a π^0 decays into two isolated photons. In the identification of neutral tracks in the EMC, one has to address a number of processes which can produce both real and spurious showers. The major source of these "fake photons" arised from hadronic interaction between π's or K's and the material before or in the crystals, the secondary particles from these interaction can "split-off" and create a shower which the pattern recognition does not associate to the main shower. Other sources of fake photon are particle decays, back splash, beam associated background and electronic noise. A shower is selected as an isolated photon by requirements of a deposit energy cut, e.g. $E_\gamma > 40$MeV and a spatial cut far away from the nearest charged tracks. In addition we also reconstruct η/η' candidates in the modes of $\eta \to \gamma\gamma$, $\eta \to \pi^+\pi^-\pi^0$, $\eta' \to \gamma\rho^0$ and $\eta' \to \eta\pi^+\pi^-$. For these modes, 3σ consistency with the $\pi^0/\eta/\eta'$ mass is required, followed by a kinematic mass constraint.

Finally for the full D reconstruction, all tracks with consistent mass hypotheses and, if appropriate, reconstructed K_S's, π^0's and η/η''s are permuted to form the candidate combinations. To be accepted as D tags, candidate combinations of final particles with the reconstructed total energy E_D, total momentum p_D must fulfill the ΔE requirements, the energy difference $\Delta E = E_D - E_{\rm beam}$ of a D candidate is consistent with zero.

23.2 Beam constrained mass

The conventional method of observing resonant signals in particle physics analyses is by selecting a set of tracks and studying the invariant mass ($M_{\rm inv}$):

$$M_{\rm inv} = \sqrt{\left(\sum_i E_i\right)^2 - \left(\sum_i \vec{p_i}\right)^2} \tag{23.1}$$

where $(E, \vec{p})_i$ are the energy and three-momentum of track i. For reconstructing D decays at the $\psi(3770)$ at BESIII, the resolution of the invariant mass is typically 6 to 8 MeV if the modes contain only charged tracks and somewhat worse, 12 MeV, if the modes contain a π^0. The resolution is mainly due to errors on the momentum and not to errors on the track angles. Improvements can be obtained by exploiting the pair production of kinematic of D mesons near threshold. Since the D's are pair produced and the laboratory frame is also the rest frame of the $D\overline{D}$ system, each D is produced with an energy equal

to that of the beam in the laboratory frame. Another mass quantity known as the beam constrained mass($\frac{\sqrt{3}}{2}M_{\rm bc}$) can therefore be constructed by replacing the energy of the D (E_D) with the energy of the beam ($E_{\rm beam}$):

$$M_{\rm bc} = \sqrt{E^2_{\rm beam} - \left(\sum_i \vec{p_i}\right)^2} = \sqrt{E^2_{\rm beam} - p^2_D} \tag{23.2}$$

This mass quantity is simply a function of the total momentum of the decay products, $p_D = \sum_i \vec{p_i}$. The resolution of $M_{\rm bc}$ can be calculated by

$$\delta M_{\rm bc} = \frac{E_{\rm beam}}{M_{\rm bc}}\delta E_{\rm beam} \oplus \frac{p_D}{M_{\rm bc}}\delta p_D \tag{23.3}$$

Because of the smaller energy spread of the beam ($\delta E_{\rm beam} \sim 0.9$ MeV) and the low value of p_D($\sim$ 270MeV/c for the D^0, $\sim$ 242 MeV/c for the D^+) and its error, $\delta p_D \sim 5$ MeV, resolution of $M_{\rm bc}$ are of the order 1.2$-$2 MeV.

Another advantage of having a second independent mass variable lies in the reduction of background from misidentification. The total energy (or the invariant mass) is sensitive to the mass hypotheses made on the decay products, while the beam constrained mass quantity requires that they have the correct momentum (the measured momentum is dependent on the mass hypotheses only to the extent that the small dE/dx correction are mass dependent). Imposing a cut to ΔE, leave the $M_{\rm bc}$ to be examined to search for a "signal"; Fitting to the plot of ΔE and $M_{\rm bc}$ simultaneously can improve the ratio of signal to background.

23.3 Multiple Counting

One event could be counted more than once as a tag candidate. The multiple counting can occur in two ways:

1) Two or more different tag channels can be reconstructed for a give event; this can occur, for example, when both D's in an event can be reconstructed.

2) Two or more possible combinations of tracks can yield a consistent tag for a given channel; tag modes with higher multiplicity like $D^+ \to \overline{K^0}\pi^+\pi^+\pi^-$ and those containing π^0's tend to be more susceptible to this problem.

To count the actual number of tagged events in an unbiased manner, the following criteria are used to select only one tag combination per event:

1) If more than one tag channel can be reconstructed, select the channel with the largest signal-to-noise ratio.

2) For all tags containing charged track only, if more than one combination of tracks form the tag, choose the combination whose lowest momentum track has the largest momentum of all the combinations.

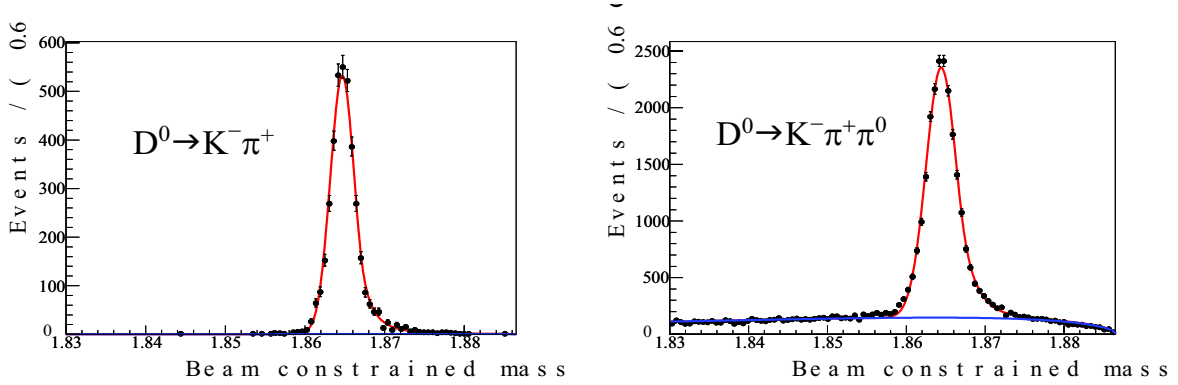

Figure 23.1: Beam constrained mass distribution for the tags of $D^0 \to K^-\pi^+$ and $D^0 \to K^-\pi^+\pi^0$. The red curves show the sum of signal and background functions. The blue curves indicate the background fits.

3) For all tags containing neutrals, if more than one combination of photon pair can reconstruct the tag, choose the combination with the lowest χ^2 from the π^0 fit, or choose the combination whose lowest energy track has the highest energy of all the combinations.

The item 2) and 3) is based on the fact that the tracking efficiency is higher for high momentum/energy track, and the measurement is more reliable.

23.3.1 Mass plots fitting

After the selection procedure described in Sec. 23.1, Sec. 23.2 and Sec. 23.3, the result mass plot of beam constrained mass are drawn in Fig. 23.1. The number of tags is determined by a extended unbinned maximum likelihood fit to a signal function on the top of background. The background shape is represented by the well known Argus function [2] which is an empirical formula to model the phase space of multi-body decays near threshold and is frequently used in B physics. The Argus function take the following form:

$$\mathcal{B}(M_{\rm bc}) = M_{\rm bc}\left[1-\left(\frac{M_{\rm bc}}{E_{\rm beam}}\right)^2\right]^p \cdot \exp\left(c\left[1-\left(\frac{M_{\rm bc}}{E_{\rm beam}}\right)^2\right]\right) \tag{23.4}$$

where p is for the power term(usually take its value as 0.5); c is a scale factor for exponential term. The shape parameters are determined by fitting $M_{\rm bc}$ distribution selected by the ΔE sidebands.

There is a tail towards the high-end of $M_{\rm bc}$ in the signal distribution, which is caused by the initial state radiation(ISR). The effect of ISR, the resonant parameters and the lineshape of $\psi(3770) \to D\overline{D}$, the beam energy spread and the detector resolution can

contribute to the signal shape, usually it takes the form of CBL[3] as:

$$\mathcal{S}(M_{\rm bc}) = \begin{cases} A \cdot \exp\left[-\frac{1}{2}\left(\frac{M_{\rm bc} - M_D}{\sigma_{M_{\rm bc}}}\right)^2\right] & \text{for } M_{\rm bc} < M_D - \alpha \cdot \sigma_{M_{\rm bc}} \\ A \cdot \frac{\left(\frac{n}{\alpha}\right)^n \exp\left(-\frac{1}{2}\alpha^2\right)}{\left(\frac{M_{\rm bc} - M_D}{\sigma_{M_{\rm bc}}} + \frac{n}{\alpha} - \alpha\right)^n} & \text{for } M_{\rm bc} > M_D - \alpha \cdot \sigma_{M_{\rm bc}} \end{cases} \tag{23.5}$$

which is similar to that used for extracting the photon signal from electromagnetic calorimeters. In Eq. 23.5, the normalized constant

$$A^{-1} = \sigma_{M_{\rm bc}} \cdot \left[\frac{n}{\alpha} \cdot \frac{1}{n-1} \exp\left(-\frac{1}{2}\alpha^2\right) + \sqrt{\frac{\pi}{2}}\left(1 + \mathrm{erf}\left(\frac{\alpha}{\sqrt{2}}\right)\right)\right], \tag{23.6}$$

where M_D is the "true" (or most likely) mass, $\sigma_{M_{\rm bc}}$ is the mass resolution, and n and α are parameters governing the shape of the high mass tail.

Chapter 24

Leptonic, semileptonic $D(D_S)$ decays and CKM matrix

24.1 Leptonic Decays

24.1.1 Theoretical Review[1]

The purely leptonic pseudoscalar charge D meson decay is the simplest and the cleanest decay mode among its decays. The hadronic dynamics is simply factorized to it's decay constant f_D, which is defined by

$$\langle 0|\bar{d}\gamma_\mu\gamma_5 c|D^+(p)\rangle = if_{D^+}p_\mu. \tag{24.1}$$

The decays $D^+ \to \ell^+\nu_l$ proceeds by the c and $\bar{d}$ quarks annihilating into a virtual W^+ with a decay width

$$\Gamma(D^+ \to \ell^+\nu) = \frac{G_F^2}{8\pi} f_{D^+}^2 m_l^2 M_{D^+}\left(1 - \frac{m_l^2}{M_{D^+}^2}\right)|V_{cd}|^2, \tag{24.2}$$

where M_{D^+} is the D^+ mass, m_l is the mass of the final lepton, V_{cd} is a CKM matrix element, respectively. Because D is a pseudoscalar, the decay is helicity suppressed, which decay rate is proportional to m_l^2. The dynamics is just the same as $\pi^- \to \mu\bar{\nu_\mu}, e\bar{\nu_e}$. Due to the helicity suppression, $D^+ \to e^+\nu$ is very small. The relative widths are $2.65 : 1 : 2.3 \times 10^{-5}$ for $\tau^+\nu, \mu^+\nu$, and $e^+\nu$ modes, respectively.

Although, $D^+ \to \mu^+\nu$ has a smaller rate than $\tau^+\nu$, it is the most favorable mode for experiment measurement since τ will decay with missing neutrino before being detected. ¿From Eq. 24.2, the measurement of $D^+ \to \mu^+\nu$ will be a measurement of the combination of $f_{D^+}|V_{cd}|$ in the Standard Model. To determine f_{D^+}, knowledge of $|V_{cd}|$ is needed.

The magnitude of $|V_{cd}|$ can be deduced from neutrino and anti-neutrino production of charm off valence d quarks in fix target experiments[5]. PDG 2004[4] average is

$$|V_{cd}| = 0.224 \pm 0.012. \tag{24.3}$$

[1]By Ya-Dong Yang

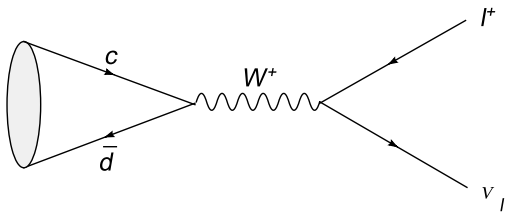

Figure 24.1: The Feynman diagram for $D^+ \to l^+\nu_\ell$

In Wolfenstein parameterizing of CKM-matrix, $V_{cd} = -V_{us}$ up to $\mathcal{O}(\lambda^4)$ with $\lambda = |V_{us}|$. Using $281pb^{-1}$ data taken on the $\Psi(3770)$ resonance with the CLEO-c detector, the most recent CLEO measurement[6] of $D^+ \to \mu^+\nu$ gives

$$\mathcal{B}(D^+ \to \mu^+\nu) = (4.40 \pm 0.66^{+0.09}_{-0.12}) \times 10^{-4}. \tag{24.4}$$

With the assumption of $|V_{cd}| = |V_{us}| = 0.2238 \pm 0.0029$, CELO-c finds[6]

$$f_{D^+} = (222.6 \pm 16.7^{+2.8}_{-3.4}) MeV. \tag{24.5}$$

In the literature, f_{D^+} has been extensively studied in various theoretical approaches[7, 8] and experimentally by MARKIII[9], BES[10] and CLEO-c [6, 11] as listed in Fig.2 ¿From Fig.2, we can see that the CLEO-c measurement is agrees with Lattice results within 1σ. The recent Lattice calculation[12] after this measurement has been performed in three flavor Lattice QCD by Fermilab Lattice, MILC and HPQCD Collaborations. They find $f_{D^+} = 201 \pm 3 \pm 17$MeV. Concerning the large error bars in both experimental measurements and theoretical predictions, the present CLEO-c result is still not yet precise enough to put theoretical predictions to stringent test.

The decay constant is a very basic hadronic parameter. It can be used to test our knowledge for hadronic dynamics. For example, f_B is hard to be determined experimentally at Belle and BABAR since pure leptonic $B^\pm$ decays is suppressed by the very small $V_{ub} = (3.6 \pm 0.7) \times 10^{-3}$. So that theoretical calculations with Lattice, QCD Sum Rules, etc., are needed. However, self-consistent calculation should include predictions for f_D. With known f_D, one can check or/fix some unknown hadronic parameters in their theoretical frameworks, then the reliable prediction for f_B which is crucial important for B physics.

The purely leptonic decay $D_s^+ \to \ell^+\nu$ is very similar to $D^+ \to \ell^+\nu$. However, it involves a large CKM element V_{cs}. So its decay rates are much larger than the corresponding $D^+ \to \ell^+\nu$ decays.

The value of $|V_{cs}|$ could be obtained from W boson charm tagged hadronic decays. In the SM, the branching ratios of W boson depend on the six CKM elements V_{ij}(i=u,c, j=d, s, b). In terms of these six CKM elements, the leptonic branching ratio $\mathcal{B}(W \to \ell\bar{\nu_{ell}})$ is given by[4]

$$\frac{1}{\mathcal{B}(W \to \ell\bar{\nu}_\ell)} = 3\left\{1 + \left[1 + \frac{\alpha_s(M_W^2)}{\pi}\right] \sum_{i,j} |V_{ij}|^2\right\}. \tag{24.6}$$

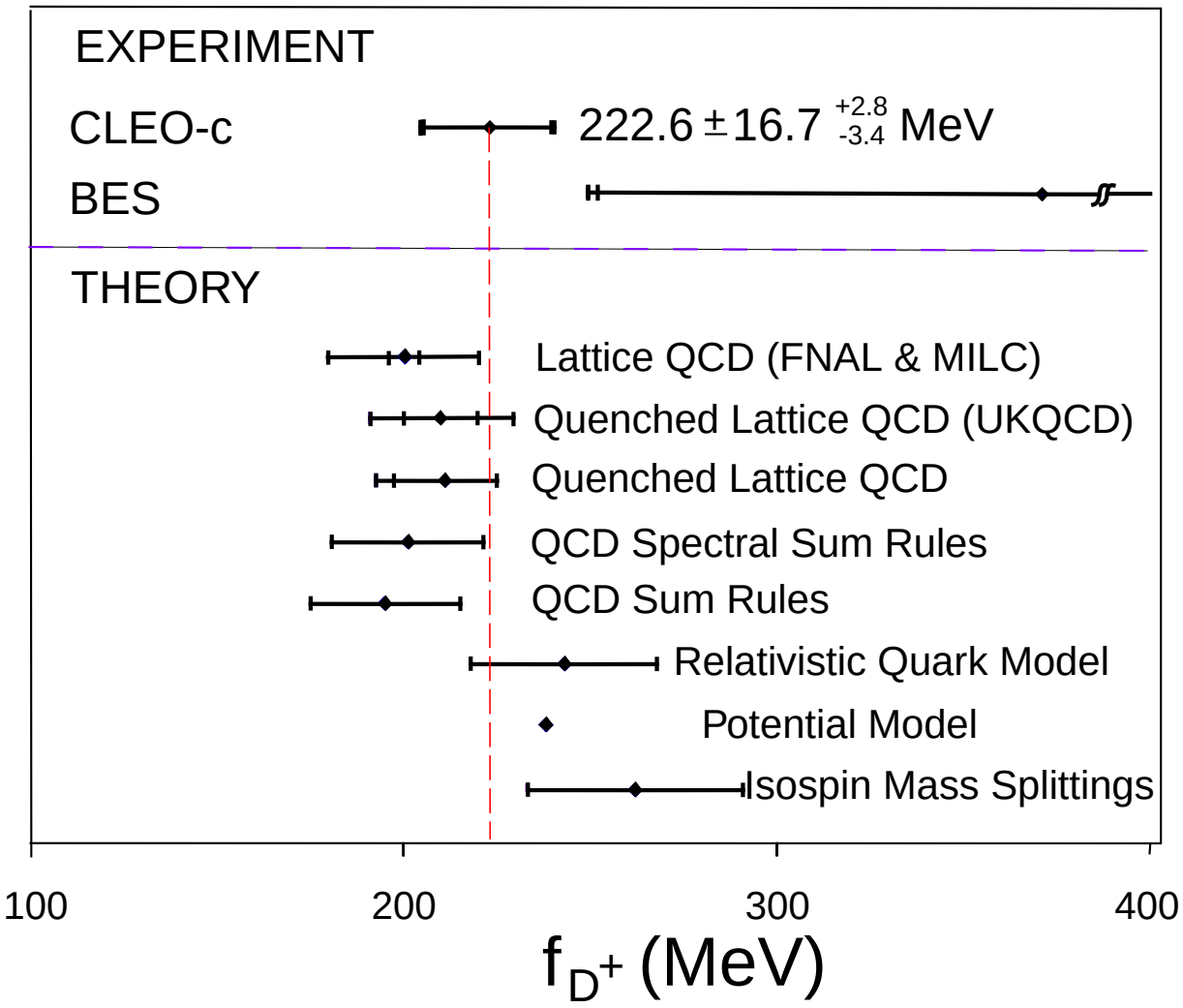

Figure 24.2: Summary of theoretical predictions and experimental data for f_{D^+}

Taking $\alpha_s(M_W^2) = 0.121 \pm 0.002$, the LEP measurement of $\mathcal{B}(W \to \ell\bar{\nu_{ell}}) = 10.69 \pm 0.06(stat.) \pm 0.07(syst.)\%$ gives

$$\sum_{i,j} |V_{ij}|^2 = 2.039 \pm 0.025 \pm 0.001. \tag{24.7}$$

Using the experimental results in PDG, one can get $|V_{ud}|^2+|V_{us}|^2+|V_{ub}|^2+|V_{cd}|^2+|V_{cb}|^2 = 1.0477 \pm 0.0074$[4]. Then the LEP result can be interpreted as a measurement of $|V_{cs}|$

$$|V_{cs}| = 0.996 \pm 0.013 \tag{24.8}$$

which is the least well determined CKM elements.

Hence, measurement of $D_s^+ \to \ell^+\nu$ decays could be a determination of f_{D_s}. At present, there are about eight published measurements of D_s^+ decaying to $\mu^+\nu_\mu$ and/or $\tau^+\nu_\tau$: WA75[13], BES[14], E653[15], L3[16], CLEO[17], BEATRICE[18], OPAL[19], and ALEPH[20]. All these experiments except BES either explicitly or implicitly measure the leptonic branching ratio relative to the nonleptonic ratio $\mathcal{B}(D^+ \to \phi\pi^+)$, or the ratios of semileptonic D_s^+ decays. PDG [4]weighted average leptonic branching ratio for all experiments except BES is

$$\mathcal{B}(D^+ \to \mu^+\nu_\mu) = 0.00547 \pm 0.00067 \pm 0.00132. \tag{24.9}$$

Since this average is 1.5σ less than the BES result of $\mathcal{B}(D^+ \to \mu^+\nu_\mu) = 0.015^{+0.013+0.003}_{-0.006-0.002}$, PDG has used the negative uncertainties of the BES measurement to calculate the weighted average for all experiments:

$$\mathcal{B}(D^+ \to \mu^+\nu_\mu) = 0.00596 \pm 0.00144. \tag{24.10}$$

Using this value and including the relatively minor uncertainties on other parameters relevant to the decay, the world average D_s^+ decay constant is extracted to be[4]

$$f_{D_s} = (267 \pm 33) MeV. \tag{24.11}$$

24.1.2 Decay Constants[2]

The ratio of f_{D^+} and $f_{D_s^+}$

The decay constant of D^0 is very important for studying $D^0 - \bar{D}^0$ mixing which is a good test ground for the SM. Due the smallness of u and d masses, the chiral symmetry holds

$$f_{D^0} = f_{D^\pm}. \tag{24.12}$$

It should be noted that $D_u^0 \to \mu^+\mu^+$ is strongly suppressed by GIM mechanism in the SM. It's branching is smaller than 10^{-12}. Any observation of the decays at present and possible future colliders will signal out new physics beyond the SM.

The ratio f_{D_s}/f_D is a very important quantity in flavor physics. At first, it characterizes $SU(3)_V$ breaking. If we take $m_s,\ m_{u,d} \to 0$, flavor $SU(3)_V$ is an exact symmetry and

[2]By Ya-Dong Yang

so $f_{D_s}/f_D = 1$. However, in nature, where $m_s \gg m_{u,d}$, this ratio will deviate from unity. To one loop order in Chiral Perturbation Theory, Grinstein *et al.*,[21] find

$$f_{D_s}/f_{D_d} = 1.2 \tag{24.13}$$

which is very near to $f_K/f_\pi = 1.25$. Secondly, it is related to f_{B_s}/f_B by the definition of the double ratio[22]

$$R_1 = \frac{f_{B_s}/f_{B_d}}{f_{D_s}/f_{D_d}}. \tag{24.14}$$

It has been shown R_1 to be very nearly unity with only very small corrections[23].

It's known that the ratio f_{B_s}/f_{B_d} is a measurement of the relative strength of $B_s - \bar{B}_s$ and $B_d - \bar{B}_d$ mixing strength. The relative strength is

$$R_2 = \frac{(\triangle M/\Gamma)_{B_s}}{(\triangle M/\Gamma)_{B_d}}. \tag{24.15}$$

In the SM many uncertain factors are cancelled out in R_2:

$$R_2 = \frac{|V_{ts}|^2}{|V_{td}|^2}\frac{f_{B_s}^2}{f_{B_d}^2}\frac{B_{B_s}}{B_{B_d}}. \tag{24.16}$$

The ratio of vacuum insertion approaching parameters B_{B_s}/B_{B_d} is unity with very small corrections. Therefore, to good approximation

$$R_2 = \frac{|V_{ts}|^2}{|V_{td}|^2}\frac{f_{D_s}^2}{f_D^2}. \tag{24.17}$$

It should be noted that leptonic decays of B_s^0, B_d^0 and $B^\pm$ are very sensitive to new physics model, e.g., MSMM, 2HDMII, etc. However, D mesons do not. Combined with measurements of $B^0 - \bar{B}^0$ and $B_s^0 - \bar{B}_s^0$ mixings, measurements of f_{D_s} and f_D will be very helpful to clarify if there are new physics activities in $B^0 - \bar{B}^0$ and $B_s^0 - \bar{B}_s^0$ mixings.

Theoretical extrapolating f_D to f_B

Heavy meson decay constants are one of the simplest quantities that can be studied with Heavy Quark Effective Theory (HQET)[24].

In HQET, one can derive

$$f_M\sqrt{m_M} = \hat{C}_{M_Q}F_{ren} + \mathcal{O}(1/m_Q), \tag{24.18}$$

where

$$\hat{C}_P(M_Q) = [\alpha_s(m_Q)]^{2/\beta_0}\left\{1 + \frac{\alpha_s(m_Q)}{\pi}(Z_{hl} + \frac{2}{3})\right\}, \tag{24.19}$$

$$\hat{C}_V(M_Q) = [\alpha_s(m_Q)]^{2/\beta_0}\left\{1 + \frac{\alpha_s(m_Q)}{\pi}Z_{hl}\right\}, \tag{24.20}$$

$$Z_{hl} = 3\frac{153 - 19n_f}{(33 - 2n_f)^2} - \frac{381 + 28\pi^2 - 30n_f}{36(33 - 2n_f)} - \frac{4}{3}. \tag{24.21}$$

It expresses the well known asymptotic scaling law that $f_M\sqrt{m_M}$ approaches to a constant as $m_M \to \infty$. HQET provides a rigorous derivation of this law. To leading order of $\mathcal{O}(1/m_Q)$, one can find that

$$r_1 = \frac{f_B}{f_D} = \sqrt{\frac{m_D}{m_B}}\left(\frac{\alpha_s(m_c)}{\alpha_s(m_b)}\right)^{6/25}\left\{1+0.894\frac{\alpha_s(m_c)-\alpha_s(m_b)}{\pi}\right\}, \quad (24.22)$$

$$r_2 = \frac{f_V}{f_P} = 1-\frac{\alpha_s(m_Q)}{3\pi}. \quad (24.23)$$

At subleading order, one must include the $1/M_Q$ and the $SU(3)_V$ corrections. To order of $1/m_Q$, on obtains

$$f_M\sqrt{m_M} = \hat{C}_{M_Q}F_{ren}\left\{1+\frac{G_1(m_Q)}{m_Q}+\frac{2d_M}{m_Q}\left[\hat{G}_2(m_Q)-\frac{\bar{\Lambda}}{12}\right]\right\}, \quad (24.24)$$

where $d_P = 3$ and $d_V = -1$. The non-trivial hadronic parameters $\hat{G}_i(m_Q)$ need to be computed by some non-perturbative techniques. In QCD sum rules, Ball[25] has estimated

$$\hat{G}_1(m_b) = -0.81 \pm 0.15GeV, \qquad \hat{G}_1(m_c) = -0.72 \pm 0.15GeV. \quad (24.25)$$

Neubert[26] has obtained

$$\hat{G}_2(m_b) = -26 \pm 4MeV, \qquad \hat{G}_2(m_c) = -0.44 \pm 7MeV. \quad (24.26)$$

The $SU(3)_V$-violating corrections to f_{B_s}/f_{f_B} is estimated to be

$$\frac{f_{B_s}}{f_B} = \sqrt{\frac{1-(\frac{7}{3}+3g^2)\frac{m_K^2}{16\pi^2f^2}\ln\frac{m_K^2}{\mu^2}}{1-\frac{2}{3}(1-3g^2)\frac{m_K^2}{16\pi^2f^2}\ln\frac{m_K^2}{\mu^2}}} \approx 1.138, \quad (24.27)$$

for $\mu = 1$GeV, $f = f_K$, $g^2 \approx 0.4$, and $f_K = 1.25f_\pi$.

24.1.3 Measurements Leptonic Decays at BESIII[3]

1. Expected Branching Fractions for Leptonic Decays of Charmed Mesons

The decay rates of $D^+ \to l+\nu_l$ and $D_s^+ \to l+\nu_l$, ignoring radiative corrections, are given by the formulas 24.28 and 24.29 [27],

$$\Gamma(D^+ \to l^+v_l) = \frac{G_F^2}{8\pi}f_{D^+}^2|V_{cd}|^2 * m_l^2 * m_{D^+}(1-\frac{m_l^2}{m_{D^+}^2}) \quad (24.28)$$

$$\Gamma(D_s^+ \to l^+v_l) = \frac{G_F^2}{8\pi}f_{D_s^+}^2|V_{cs}|^2 * m_l^2 * m_{D_s^+}(1-\frac{m_l^2}{m_{D_s^+}^2}) \quad (24.29)$$

where f_{D^+} and $f_{D_s^+}$ are the decay constant, V_{cd} and V_{cs} are CKM matrix elements, m_l is mass of the lepton, m_{D^+} and $m_{D_s^+}$ are the masses of D^+ and D_s^+, and G_F is the Fermi coupling constant. The theory calculation to estimate the branching fractions for leptonic decays of charmed mesons are listed in table 24.1 [28].

[3]By Jiang-Chuan Chen, Hai-Long Ma and Gang Rong

Table 24.1: Predicted D^+ and D_s decay rates and branching fractions assuming $f_D = f_{D_s} = 200$ MeV, $|V_{cd}| = 0.21$ and $|V_{cs}| = 0.97$.

Decay Mode	Rate(s^{-1})	Branching fraction
$D^+ \to e^+\nu_e$	7.1×10^3	7.5×10^{-9}
$D^+ \to \mu^+\nu_\mu$	3.0×10^8	3.2×10^{-4}
$D^+ \to \tau^+\nu_\tau$	6.8×10^8	7.2×10^{-4}
$D_s^+ \to e^+\nu_e$	1.6×10^5	7.5×10^{-8}
$D_s^+ \to \mu^+\nu_\mu$	6.8×10^9	3.2×10^{-3}
$D_s^+ \to \tau^+\nu_\tau$	6.1×10^{10}	2.9×10^{-2}

2. Previous Measurements of the Pure Leptonic Decays of D and D_s

(a) The measured B($D^+ \to \mu\nu_\mu$) and f_{D^+}

With the data collected in the BESI detector, BES measured a value of $f_D = (300^{+180+80}_{-150-40})$ MeV by full reconstructing $D^{*+}D^-$ at the $\sqrt{s}$=4.03 GeV. $D^- \to \mu^-\bar{\nu}_\mu$ event is searched for on the recoil side of tagged $D^{*+} \to \pi^+D^0$ with $D^0 \to K^-\pi^+$ [29]. Later, with the upgraded detector of BESII, BES measured f_D again by fully reconstructing D^+D^- close to the threshold (data taken around $\sqrt{s}$=3.773 GeV) and obtained a value of $BF(D^+ \to \mu^+\nu) = (0.122^{+0.111}_{-0.053} \pm 0.010)\%$, and the decay constant is obtained to be $f_{D^+} = (371^{+129}_{-119} \pm 25)$ MeV [30].

MARKIII determined an upper limit of $f_D \leq 290$ MeV with the data taken at 3.770 GeV on e^+e^- collider, the $D^+ \to \mu^+\nu$ events were selected with missing mass and momentum [72]. Recently, CLEOC measured the branching fraction twice for decay $D^+ \to \mu^+\nu_\mu$. Firstly, they analyzed 60 pb^{-1} data taken at Ecm=3.770 GeV and found 8 event (included 1 background). They selected the event by the measured missing mass $M^2_{miss} = (E_{beam} - E_\mu)^2 - (-p_{D^-} - p_\mu)^2$ with the total systematic error 16.4% [33]. The branching fraction was obtained to be $B(D^+ \to \mu^+\nu_\mu) = (0.035 \pm 0.014 \pm 0.006)\%$ and the f_{D^+} was determined to be $f_{D^+} = (202 \pm 41 \pm 17)MeV$. Secondly, they analyzed 281 pb^{-1} data set and found 50 $D^+ \to \mu^+\nu_\mu$ events (included $2.81 \pm 0.30 \pm 0.27$ background events) on the recoil side of 158354 ± 496 singly tagged D^-. They measured the branching fraction to be $B(D^+ \to \mu^+\nu_\mu) = (4.40 \pm 0.66^{+0.09}_{-0.12})X10^{-4}$ and determined $f_{D^+} = (222.6 \pm 16.7^{+2.8}_{-3.4})MeV$. In their last measurement they reduced the systematic error to $(^{+2.1}_{-2.5})\%$. The most improvement on the systematic error was from the background uncertainty (from 15.4% reduced to $(^{+0.6}_{-1.7})\%$ [34].

The previous measured f_D values are listed in the table 24.2

(b) The Measured B($D_s \to \mu\nu_\mu$) and f_{D_s}

BES measured a value of $B(D_s \to \mu\nu) = (1.5^{+1.3+0.3}_{-0.6-0.2})\%$ and determined $f_{D_s} = (430^{+150}_{-130} \pm 40)$ MeV by fully reconstructing $D_s^+D_s^-$ close to the threshold (taken data with BESI detector at $\sqrt{s}$=4.03 GeV). D_s are tagged with $D_s \to \phi\pi, K^{*0}K, K^0K, ...$ and searched for $D_s \to l\nu_l$ on the recoil side of D_s tags [31].

WA75 reported $f_{D_s} = (232 \pm 45 \pm 20 \pm 48)$ MeV using muon's from D_s^+ leptonic decay seen in emulsion [35]. E653 determined a value of $(194 \pm 35 \pm 20 \pm 14)$ from one prong decays into muon's seen in an emulsion [36]. BEATRICE published a value of

Table 24.2: The previous measured f_D.

Experiment	E_{cm}	Lum	Events	$B(D^+ \to \mu\nu_\mu)(\%)$	$f_D(MeV)$
BESI	4.03 GeV	$22.3pb^{-1}$	1	$0.08^{+0.16+0.05}_{-0.05-0.02}$	$300^{+180+80}_{-150-40}$
BESII	3.773 GeV	33	2.67 ± 1.74	$0.122^{+0.111}_{-0.053} \pm 0.10$	$371^{+129}_{-119} \pm 25$
MARKIII	3.773 GeV	9.3	0	$\leq 0.072(C.L.90\%)$	≤ 290 (C.L. 90%)
CLEOC	3.770 GeV	60	7.0 ± 2.8	$0.035 \pm 0.014 \pm 0.006$	$202 \pm 41 \pm 17$
CLEOC	3.770 GeV	281	$47.2 \pm 7.1^{+0.3}_{-0.8}$	$0.044 \pm 0.0066^{+0.0009}_{-0.0012}$	$222.6 \pm 16.7^{+2.8}_{-3.4}$
PDG06 [4]				0.044 ± 0.007	

Table 24.3: The previous measured f_{D_s}.

Experiment	E_{cm}	Lum	$B(D_s \to \mu\nu_\mu)(\%)$	$f_{D_s}(MeV)$
BESI	4.03 GeV	$22.3pb_{-1}$	15^{+13+3}_{-6-2}	$430^{+150+40}_{-130-40}$
WA75	350 GeV		$0.4^{+0.18+0.08}_{-0.14-0.06} \pm 1.7$	$232 \pm 45 \pm 20 \pm 48$
E653	600 GeV		$0.30 \pm 0.12 \pm 0.06 \pm 0.05$	$194 \pm 35 \pm 20 \pm 14$
BEATRICE	350 GeV		$0.83 \pm 0.23 \pm 0.06 \pm 0.18$	$323 \pm 44 \pm 12 \pm 34$
CLEO	$\Upsilon(4S)$	$2.13\ fb^{-1}$		$344 \pm 37 \pm 52 \pm 42$
CLEO	$\Upsilon(4S)$	$4.79\ fb^{-1}$		$280 \pm 19 \pm 28 \pm 34$
PDG06[4]			0.61 ± 0.19	

$B(D_s \to \mu\nu) = (0.83 \pm 0.23_{stat} \pm 0.06_{sys} \pm 0.18_{B(\phi\pi)})\%$ using interaction of π^- in copper and tungsten targets. The resulting value for the D_s decay constant was $f_{D_s} = 323 \pm 44 \pm 12 \pm 34$ MeV [37]. CLEO measured f_{D_s} twice, firstly they obtained $f_{D_s} = 344 \pm 37 \pm 52 \pm 42$ MeV by measurement of ratio $\Gamma(D_s^+ \to \mu^+\nu)/\Gamma(D_s^+ \to \phi\pi)$ with 2.13 fb^{-1} data taken at $\Upsilon(4S)$ [38]; later they presented a improved determination of f_{D_s} using 4.75 fb^{-1} data. Their new value was derived to be $f_{D_s} = 280 \pm 19 \pm 28 \pm 34$ MeV [39].

The previous measured f_{D_s} values are listed in the table 24.3

3. Study Pure Leptonic D^+/D_s^+ Decays at BESIII

BEPCII is a new collider with high luminosity (about 100 times more than than that of the BEPC). BESIII will work on the BEPCII with the much more improved properties than those of BESII. Especially the coverage solid angle of $89\% \times 4\pi$ for 9 layers RPC Muon Chmaber and the $\sigma_z = 0.6cm$ for EM calorimeter will help us on the muon identification in searching for the pure leptonic D^+/D_s^+ decays.

BESIII is planed to collect integrated luminosity of 20 fb^{-1} $\psi(3770)$ data at 3.773 GeV and some $D_s\bar{D}_s$ data set at 4.03 GeV or 4.14 GeV. By analysis of these data set, BESIII will study the pure leptonic decays of $D^+ \to \mu^+\nu$ and $D_s^+ \to \mu^+\nu$ and measure f_D and f_{D_s} with improved precision.

(a) Monte Carlo Sample for $D\bar{D}$

To measure f_D, we can take data set at peak of $\psi(3770)$ where $D\bar{D}$ produced pure pairly. The decay $D^+ \to \mu^+\nu_\mu$ can be selected on the recoil side of the singly tagged D^-, where the D^- is full reconstructed in the $D^- \to mKn\pi$ tag modes.

For study of leptonic decay $D^+ \to \mu^+\nu_\mu$, the Monte Carlo events are generated as $e^+e^- \to D\bar{D}$ at 3.773 GeV, where the D and $\bar{D}$ mesons are set to decay into all possible

final states with the branching fractions quoted from PDG [4]. The particle trajectories are simulated with the GEANT4 based Monte Carlo simulation package for the BESIII detector. The $D\bar{D}$ MC sample is generated and reconstructed with BOSS version 6.02(BESIII Offline Software System). Totally 4900000 $D\bar{D}$ Monte Carlo events are generated, which corresponded to a data sample of about $\sim$800 pb^{-1} integrated luminosity at 3.773 GeV.

(b) Monte Carlo Sample for $D_s\bar{D}_s$

According to Eichten Model (coupled-channel charm) [40], the peak of $D_s\bar{D}_s$ production cross section ($R_{D_s\bar{D}_s} \sim 0.15$) are located around $\sqrt{s} = 4.03$ GeV which is just above the $e^+e^- \to D_s^+D_s^-$ threshold, but below the threshold of $D_s^{*+}D_s^-$ production. If the data will be taken around 4.03 GeV where $D_s^+\bar{D}_s^-$ produced pure pairly, the pure leptonic $D_s^+ \to \mu^+\nu_\mu$ can be selected on the recoil side of the singly tagged D_s^-. The D_s^- tag is reconstructed via hadronic decays $D_s \to mKn\pi$, such as $KK\pi(\phi\pi)$, $\bar{K}^{*0}K(\bar{K}^{*0} \to K^-\pi^+)$, $\bar{K}^0K(K_s^0 \to \pi^+\pi^-)$, $KK\pi\pi$ etc.

For study of decay $D_s^+ \to \mu\nu_\mu$, the $D_s^+D_s^-$ Monte Carlo sample is generated and reconstructed with BOSS version 6.02 to study the pure leptonic D_s^+ decay. Totally 120000 ($D_s^+ \to X.vs.D_s^- \to \phi\pi^-$) Monte Carlo events are generated (X means any possible channel), which are corresponded to a data sample of about $\sim$10 fb^{-1} integrated luminosity at 4.03 GeV.

(c) Event Selection

All charged tracks are required to satisfy a geometry cut $|\cos\theta| < 0.93$, where θ is the polar angle of the charged track. All track must originate from the interaction region, which require that for a charged track, the distance of the closest approach be less than 1 cm in the xy plane, and less than 5 cm in the z direction.

For pions and kaons identification, a combined confidence level is calculated using the dE/dx and TOF measurements information. Pion is identified by requiring the pion hypothesis at a confidence level greater than 0.001. A kaon candidate is required to have a larger confidence level for a kaon hypothesis than that for the pion hypothesis.

The π^0 is reconstructed through the decay $\pi^0 \to \gamma\gamma$. To select good photon from the π^0 decay, the energy of a photon deposited in the SC is required to be great than 0.04 GeV, and the angle in $x-y$ plane between the photon and the nearest charged track is greater than 20°, and the angle in $r-z$ plane between the photon and the nearest charged track is greater than 20°.

The K_S^0 is reconstructed through the decay $K_S^0 \to \pi^+\pi^-$ and the mass of the $\pi^+\pi^-$ combination is required within a window of $|M_{\pi^+\pi^-} - M_{K_S^0}| < 0.025$ GeV/c^2.

(d) Singly tagged D^-

The singly tagged D^- is reconstructed in the four hadronic decay modes of $K^+\pi^-\pi^-$, $K^+K^-\pi^-$, $K^0\pi^-$ and $K^+\pi^-\pi^-\pi^0$. In order to reduce the background and improve the momentum resolution, a beam energy constraint is imposed on each $mKn\pi$ combination of the D^- tag modes. The beam-constraint masses of the $mKn\pi$ combinations are calculated by Eq. 24.30,

$$M_{tag} = \sqrt{E_{beam}^2 - p_{mKn\pi}^2} \tag{24.30}$$

where E_{beam} is the beam energy and $p_{mKn\pi}$ is the total momentum of the $mKn\pi$ combination. To suppress background from particle misidentified and fake photons, a window

within a $\pm 3\sigma_{\Delta E}$ around the E_{beam} of the event is taken as the D^- tag signal region. In which $\Delta E = E_{mKn\pi} - E_{beam}$, where $E_{mKn\pi}$ is the total energy of the $mKn\pi$ combination.

Fig. 24.3 shows the beam constraint mass distributions for the four D^- tag modes $K^+\pi^-\pi^-$, $K^+K^-\pi^-$, $K^0\pi^-$ and $K^+\pi^-\pi^-\pi^0$. The observed number of singly tagged D^- event can be obtained with a maximum likelihood fit to the mass spectrum with a Gaussian function for the D signal and a special function [41][42] to describe background shape for each tag mode. These give the total number of the singly tagged D^-, $N_{D^-} = 232803.0 \pm 801.9$.

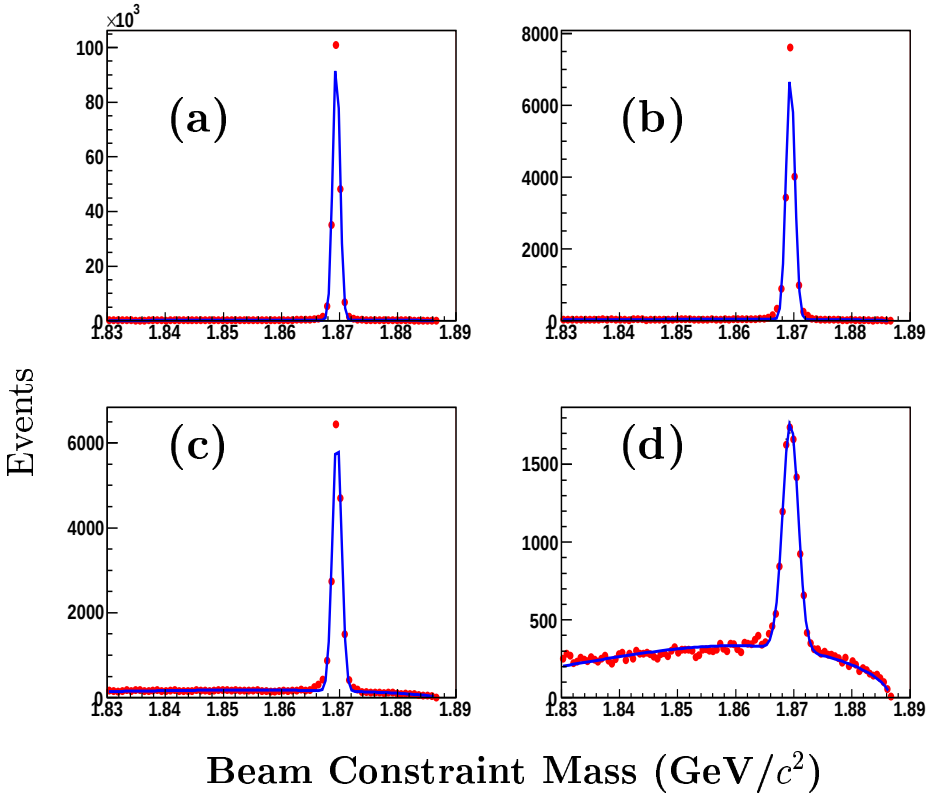

Figure 24.3: The beam constraint masses for the singly tagged $\bar{D}^-$ modes: (a) $K^+\pi^-\pi^-$, (b) $K^0\pi^-$, (c) $K^-K^+\pi^-$ and (d) $K^+\pi^-\pi^-\pi^0$.

(e) Singly tagged D_s^-

Fig. 24.4 shows the beam constraint masses distributions of the combinations for the Ds^- tag modes $\phi\pi^-$ from the Monte Carlo $D_s^+D_s^-$ sample. A maximum likelihood fit to the mass spectrum with a Gaussian function for the D_s^- signal yields the observed numbers of the singly tagged D_s^-, $N_{Ds^-} = 26793.0 \pm 318.0$.

(f) Purely leptonic event selection

Due to muon identification is not worked in the BOSS version 6.02, we do not attempt to identify the muon with the information measured by Muon Chamber.

To select the purely leptonic decay events on the recoil side of the singly tagged $D^-(D_s^-)$ sample, it is required that the events satisfied following criteria:

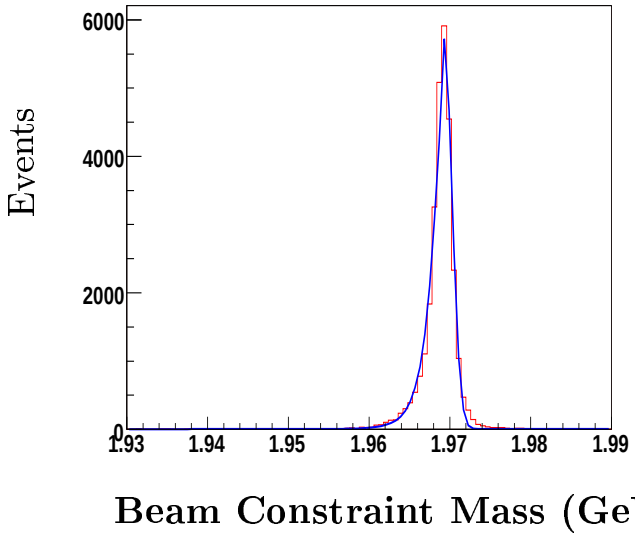

Figure 24.4: The fitted beam constraint masses for the singly tagged $\bar{D}s^-$

1. events should not contain any isolated photon which not used in the reconstruction of the single tagged $D^-(D_s^-)$ meson;

2. only one charged track to be well reconstructed in MDC on the recoil side of singly tagged D^- and with the opposite charge;

In the purely leptonic decay $D^+(D_s^+) \to \mu^+\nu_\mu$, the neutrino cannot be detected directly. One can use

$$MM^2_{miss} = E^2_{miss} - p^2_{miss}$$

to obtain the information about the missing neutrino, where $E_{miss} = E_{cm} - \sum\sqrt{\vec{p_i}^2 + m_i^2}$ and $p_{miss} = -|\sum\vec{p_i}|$ are missing energy and momentum of the event which are carried by the neutrino. In which E_{cm} is the center-mass-energy of the event, $\vec{p_i}$ and m_i are the momentum and mass of the observed particle. The MM^2_{miss} for the pure $D^+((D_s^+) \to \mu\nu_\mu$ should be around zero due to the zero mass of the ν_μ.

A further criterion requires that the momentum of muon candidate should be within the region (0.78, 1.08) GeV/c for $D^+ \to \mu^+\mu_\nu$, or (0.78, 1.22) GeV/c for $D_s^+ \to \mu^+\mu_\nu$ as shown in Fig.24.5.

Fig. 24.6 shows the distribution of the MM^2_{miss} for the $D^+ \to \mu\nu_\mu$ candidates on the recoil side of the four D^- tag modes $K^+\pi^-\pi^-$, $K^+K^-\pi^-$, $K^0_S\pi^-$ and $K^+\pi^-\pi^-\pi^0$. And Fig. 24.7 shows the distribution of the MM^2_{miss} for the $D_s^+ \to \mu\nu_\mu$ candidates on the recoil-side of the D_s^- tag modes $\phi\pi^-$. The number of the signal event can be obtained from the MM^2_{miss} distributions. A window within $3\sigma_{MM^2_{miss}}$ around zero is taken as the signal region, where σ_{MM^2} is the standard deviation of the MM^2_{miss} each for D^+ or D_s^+ decay respectively. The numbers of the $D^+ \to \mu\nu_\mu$ and $D_s^+ \to \mu\nu_\mu$ candidates can be extracted from the events in the signal regions, where the large peaks near 0.25 GeV^2 for D^+ and 0.3 GeV^2 for D_s^+ in the Fig. 24.6 and Fig. 24.7 are the main background

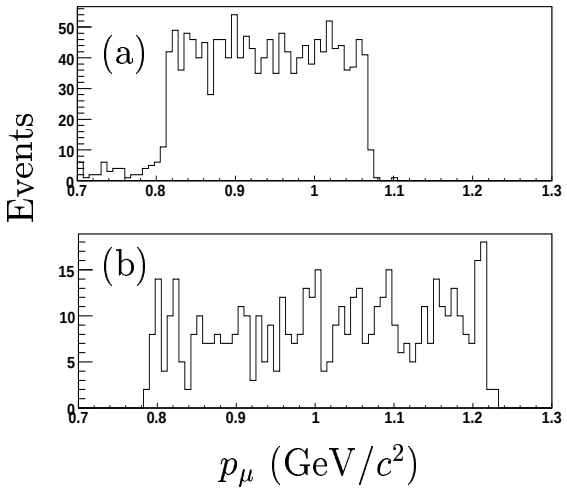

Figure 24.5: the candidate muon momentum for (a) $D^+ \to \mu^+\nu_\mu$ and (b) $D_s^+ \to \mu^+\nu_\mu$.

events $D^+ \to K_L\pi^+$ and $D_s^+ \to K_L\pi^+$. The total number of $D^+ \to \mu\nu_\mu$ and $D_s^+ \to \mu\nu_\mu$ candidates are obtained to be 91 ± 9.5 and 63 ± 7.9 respectively.

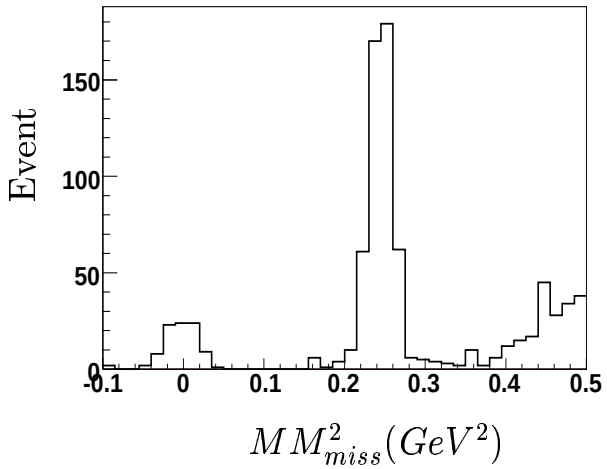

Figure 24.6: The MM^2_{miss} distribution of the muon candidates on the recoil-side of the four D^- tag modes $K^+\pi^-\pi^-$, $K^+K^-\pi^-$, $K^0_S\pi^-$ and $K^+\pi^-\pi^-\pi^0$ (about $800pb^{-1}$ sample).

(g) Branching Fractions of Pure Leptonic Decay of D^+ and D_s^+

The detection efficiency for the pure leptonic decays $D^+ \to \mu\nu_\mu$ and $D_s^+ \to \mu\nu_\mu$ can be estimated with the Monte Carlo events ($D^+ \to \mu\nu_\mu.vs.D^-_{tags}$) and ($D_s^+ \to \mu\nu_\mu.vs.D_s^-(tags)$). They are obtained to be $\epsilon_{D^+\to\mu\nu_\mu} = 53 \pm 1\%$ and $\epsilon_{Ds^+\to\mu^+\mu_\nu} = 52 \pm 1\%$ respectively.

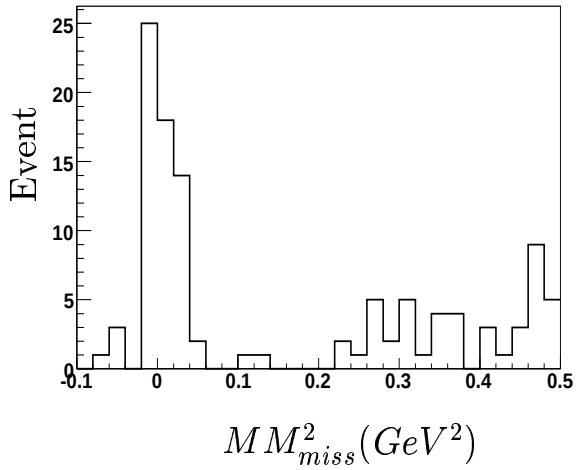

Figure 24.7: The M^2_{miss} distribution of the muon candidates on the recoil-side of the three D_s^- tag modes $\phi\pi^-$ (about 10 fb^{-1} sample).

$$BF(D^+ \to \mu\nu_\mu) = \frac{N_\mu}{N_{D^-_{tag}} \times \epsilon_{D^+\to\mu\nu_\mu}} \tag{24.31}$$

$$BF(D_s^+ \to \mu\nu_\mu) = \frac{N_\mu}{N_{D_s^-(tag)} \times \epsilon_{D_s^+\to\mu\nu_\mu}} \tag{24.32}$$

The branching fractions of $D^+ \to \mu\nu_\mu$ or $D_s^+ \to \mu\nu_\mu$ are determined by inserting the observed numbers of $D^+ \to \mu\nu_\mu$ or $D_s^+ \to \mu\nu_\mu$ events, numbers of singly tagged D^- or D_s^- and the efficiency $\epsilon_{D^+\to\mu\nu_\mu}$ or $\epsilon_{Ds^+\to\mu^+\mu_\nu}$ in Eq. 24.31 or Eq. 24.32. The branching fractions for the hadronic decays $D^+ \to \mu^+\mu_\nu$ and $Ds^+ \to \mu^+\mu_\nu$ are determined to be

$$BF(D^+ \to \mu^+\mu_\nu) = (0.074 \pm 0.008)\% \ (input \ \sim 0.08\%)$$

and

$$BF(Ds^+ \to \mu^+\mu_\nu) = (0.452 \pm 0.0057)\% \ (input \ \sim 0.40\%)$$

The statistical error for $BF(D^+ \to \mu^+\mu_\nu)$ is about 10.5% with the integrated luminosity of 800 pb^{-1} of $\psi(3770)$ sample for four tag modes. It is expected to be about (2-4)% for 20 fb^{-1} sample with six tag modes $K^+\pi^-\pi^-$, $K^+K^-\pi^-$, $K^0_S\pi^-$, $K^+\pi^-\pi^-\pi^0$, $K^0_S\pi^-\pi^0$ and $K^0_S\pi^-\pi^-\pi^+$ (PDG [4] uncertainty is about 16%). For $BF(D_s^+ \to \mu^+\mu_\nu)$, the statistical error is about 14.3% with integerated luminosity of 10 fb^{-1} of $D_s\bar{D}_s$ data set for one tag modes. It is expected to be about 6.2% for 20 fb^{-1} with five tag modes $\phi\pi^-$, $K^{*0}K^-$, $K^0_S\pi^-$, $K^0_SK^+\pi^-\pi^-$ and $f_0\pi^-$ (PDG [4] uncertainty is about 31.1%).

(h) Determination f_D and f_{D_s}

The decay constant f_D (f_{D_s}) can be obtained by inserting the measured leptonic branching fractions, the mass of the muon, the mass of the D^+ (D_s^+) meson, the CKM matrix element $|V_{cd}|$ ($|V_{cs}|$), the Fermi coupling constant G_F, the lifetime of the D^+ (D_s^+)

into the Eq. 24.28 (Eq. 24.29). The systematic error on f_{D^+} ($f_{D_s^+}$) arise from the uncertainty of D^+ (D_s^+) lifetime, uncertainty of $|V_{cd}|$ ($|V_{cs}|$), the uncertainty of measured branching fractions due to tracking finding efficiency, particle identification, photon selection, background estimation and the number of the singly tagged D^- (D_s^-). The errors of the f_{D^+} and $f_{D_s^+}$ are estimated by Eq. 24.33, where $D_q = D + (D_s^+)$, $\tau_q = \tau_{D^+}(\tau_{D_s^+})$ and $V_{cq} = V_{cd}(V_{cs})$. Table 24.4 list the expected errors of f_{D^+} and $f_{D_s^+}$ with $20fb^{-1}$ data at BESIII.

$$\frac{\delta f_{D_q}}{f_{D_q}} = \sqrt{(\frac{\Delta\tau_q}{2\tau_q})^2 + (\frac{\Delta B}{2B})^2 + (\frac{\Delta|V_{cq}|}{|V_{cq}}})^2 \tag{24.33}$$

Table 24.4: The expected errors of f_{D^+} and $f_{D_s^+}$ in the BESIII measurement with $20fb^{-1}$ data.

Decays	Decay Const.	$\frac{\delta B}{B}$	$\frac{\delta\tau}{\tau}$ [4]	$\frac{\delta\|V_{cq}\|}{\|V_{cq}}$ [43]	$\frac{\delta f_{D_q}}{f_{D_q}}$
$D^+ \to \mu^+\nu$	f_{D^+}	(2-4)%	0.6%	1.1%	1.2%
$D_s^+ \to \mu^+\nu$	$f_{D_s^+}$	(2-4)%	1.0%	0.06%	2.1%

4. Conclusion

Decay constants of f_D and f_{D_s} have been measured by many experiments but the precision of the measured values are still not satisfied up to now. BESIII is expected to measure f_{D^+} and $f_{D_s^+}$ and improve the precision obviously. From our Monte Carlo study, the statistical error for $BF(D^+ \to \mu^+\mu_\nu)$ is expected to be about (2-4)% for 20 fb^{-1} sample with six tag modes $K^+\pi^-\pi^-$, $K^+K^-\pi^-$, $K_S^0\pi^-$, $K^+\pi^-\pi^-\pi^0$, $K_S^0\pi^-\pi^0$ and $K_S^0\pi^-\pi^-\pi^+$ (PDG [4] uncertainty is about 16%); for $BF(D_s^+ \to \mu^+\mu_\nu)$, the statistical error is expected to be about 6.2% for 20 fb^{-1} with five tag modes $\phi\pi^-$, $K^{*0}K^-$, $K_S^0\pi^-$, $K_S^0K^+\pi^-\pi^-$ and $f_0\pi^-$ (PDG [4] uncertainty is about 31.1%). The systemic errors of of f_{D^+} and $f_{D_s^+}$ are expected to be about 1.2% and 2.1% respectively.

24.2 Semileptonic Decays

24.2.1 Theoretical Review[4]

Charm meson can decay into other hadrons by emitting a pair of leptons $\ell^+\nu$ through weak interaction. In quark level, this process is induced by the semileptonic decay of charm quark $c \to q\ell^+\nu$, where $q = d,\ s$. The child light quark d or s is bound with the initial light quark in the charm meson by strong interaction to form another new hadron X, which can be depicted by Feynman diagram in fig.(24.8).

Because leptons do not involve strong interaction, the lepton pair is free from the strong binding effect in the semileptonic decays. Therefore they can be factored out from

[4]By Mao-Zhi Yang

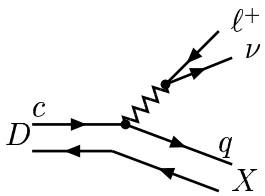

Figure 24.8: Feynman diagram of semileptonic D decay

the hadronic matrix element in the amplitude of the semileptonic decay process

$$A = \frac{G_F}{\sqrt{2}} V_{cq}^* \bar{\nu}\gamma_\mu(1-\gamma_5)l\langle X|\bar{q}\gamma^\mu(1-\gamma_5)c|D\rangle \tag{24.34}$$

All strong interactions are included in the hadronic matrix element $\langle X|\bar{q}\gamma^\mu(1-\gamma_5)c|D\rangle$. The amplitude of the semileptonic decay process depends both on the hadronic matrix element and the quark mixing parameter V_{cq}—the Cabibbo-Kobayashi-Maskawa (CKM) matrix element. So semileptonic decay of charm meson is a good laboratory for both studying the mechanism of quark mixing and testing the theoretical techniques developed for calculating the hadronic matrix element $\langle X|\bar{q}\gamma^\mu(1-\gamma_5)c|D\rangle$.

The hadronic matrix element can be decomposed into several form factors according to its Lorentz structure. The form factors are generally controlled by non-perturbative dynamics, where perturbative QCD can not be applied directly. Several methods can be used to calculate these transition form factors in theory, such as, Lattice QCD [44, 45], QCD sum rule [46, 47, 48, 49, 50], light-cone sum rule [51], quark model [53, 54, 55, 56], light-front approach [57], and large-energy and heavy-quark-effective theory [58], among which, LQCD, QCD sum rule and LCSR are based on the first principle of QCD.

Depending on the total quantum number of the child-quark system, the final hadron produced in the semileptonic decay process can be pseudoscalar meson, vector meson, or scalar meson, etc. The processes of charm meson decaying into pseudoscalar, vector, or scalar meson can be denoted as $D \to P\ell^+\nu$, $D \to V\ell^+\nu$, and $D \to S\ell^+\nu$, respectively. Here P stands for pseudoscalar, V vector, and S scalar.

(1) Transitions to pseudoscalar mesons $D \to P\ell^+\nu$

According to its Lorentz structure, the hadronic matrix element of $D \to P$ transition process can be decomposed as

$$\langle P|\bar{q}\gamma^\mu(1-\gamma_5)c|D\rangle = (p_1+p_2)_\mu F_+(q^2) + (p_1-p_2)_\mu F_-(q^2) \tag{24.35}$$

where p_1 and p_2 are the momenta of the initial D and final pseudoscalar mesons, respectively, $q = p_1 - p_2$, and $F_+(q^2)$ and $F_-(q^2)$ are the form factors. Equivalently, the decomposition can be in another form

$$\langle P|\bar{q}\gamma^\mu(1-\gamma_5)c|D\rangle = \left(p_1+p_2-\frac{m_D^2-m_P^2}{q^2}q\right)_\mu F_+(q^2) + \frac{m_D^2-m_P^2}{q^2}q_\mu F_0(q^2) \tag{24.36}$$

where $F_0(q^2)$ and $F_+(q^2)$ are respectively the longitudinal and transverse form factors.

The form factors can generally depend on all the Lorentz scalars formed by the two momenta p_1 and p_2, i.e., p_1^2, p_2^2 and $p_1 \cdot p_2$. However, p_1^2 and p_2^2 are not variables, they are on the mass shell of the initial and final particles. Therefore, the form factors can only depend on the Lorentz scalar $p_1 \cdot p_2$, which can be equivalently shifted to the variable q^2 according to the relation $q^2 = p_1^2 - 2p_1 \cdot p_2 + p_2^2$.

For the dependence of the form factors on q^2 one usually assumes the nearest pole dominance [53]

$$F_\pm(q^2) = \frac{F_\pm(0)}{1 - q^2/m_{\rm pole}^2} \tag{24.37}$$

One can choose the value of $m_{\rm pole}$ as the mass of the nearest charm resonance with the same J^P as the hadronic weak current inducing the $c \to q$ transition. This is only an assumption. For practice one can also fit the data to obtain the effective pole mass. Any deviation from the mass of the nearest charm resonance will indicate the contributions of the higher resonances. From this consideration, one can fits the data with a modified q^2 distribution [59, 60]

$$F_\pm(q^2) = \frac{F_\pm(0)}{(1 - q^2/m_{D^*_{(s)}}^2)(1 - \alpha q^2/m_{D^*_{(s)}}^2)} \tag{24.38}$$

where the parameter α describes the deviation from the single resonance contribution.

In addition to the above pole dominance ansatz, there is also another model for the q^2 dependence of the form factors in the literature [54, 55]

$$F_\pm(q^2) = F_\pm(0)e^{\alpha q^2} \tag{24.39}$$

Although the above exponential form is quite different from the pole dominance ansatz, it is difficult to test the difference in practice if the final meson is heavy because of the short range of q^2 for heavy final particle. Only for light final meson production, such as $D \to \pi$ transition, it is possible to test the different models for the q^2 dependence in experiment.

The differential decay width of $D \to P\ell^+\nu$ with lepton mass neglected is

$$\frac{d\Gamma}{dq^2}(D \to P\ell^+\nu) = \frac{G_F^2}{192\pi^3 m_D^3}|V_{cq}|^2[(m_D^2 + m_P^2 - q^2) - 4m_D^2 m_P^2]^{3/2}|F_+(q^2)|^2 \tag{24.40}$$

where only the form factor $F_+(q^2)$ contributes. The contribution of $F_-(q^2)$ is proportional to the squared lepton mass m_ℓ^2, is thus neglected. The distribution of q^2 is in the range $0 \le q^2 \le (m_D - m_P)^2$. The branching ratio of the semileptonic decay can be obtained by integrating the differential decay width over the whole physical range of q^2

$$Br(D \to P\ell^+\nu) = \tau_D \int_0^{(m_D - m_P)^2} dq^2 \frac{\Gamma}{dq^2} \tag{24.41}$$

with τ_D the mean life time of the D meson.

The semileptonic decays of $D \to \pi\ell^+\nu$ and $D \to K\ell^+\nu$ have been investigated in both theory and experiment. Theoretically the form factors of $F_+^{D\pi}$ and F_+^{DK} have been calculated in quark model, QCD sum rule, QCD light-cone sum rule (LCSR), lattice QCD

Table 24.5: Form factors of $F_+^{D\pi}(0)$ and $F_+^{DK}(0)$.

	$F_+^{D\pi}(0)$	$F_+^{DK}(0)$
LQCD1[44]	$0.57 \pm 0.06^{+0.01}_{-0.00}$	$0.66 \pm 0.04^{+0.01}_{-0.00}$
	$0.57 \pm 0.06^{+0.02}_{-0.00}$	
LQCD2[45]	$0.64 \pm 0.03 \pm 0.06$	$0.73 \pm 0.03 \pm 0.07$
QCD SR[48]	0.5 ± 0.1	$0.6^{+0.15}_{-0.10}$
LCSR[51]	0.65 ± 0.11	0.785 ± 0.11
LCSR[52]	0.67 ± 0.19	0.67 ± 0.20
Quark Model[56]	0.69	0.78
Light-Front[57]	0.67	
BES[61](Exp.)	$0.73 \pm 0.14 \pm 0.06$	$0.78 \pm 0.04 \pm 0.03$
CLEO[62](Exp.)	$\frac{\lvert F_+^{D\pi}(0)\rvert^2\lvert V_{cd}\rvert^2}{\lvert F_+^{DK}(0)\rvert^2\lvert V_{cs}\rvert^2} = 0.038^{+0.007+0.005}_{-0.007-0.003}$	
	Input $\lvert V_{cd}\rvert^2/\lvert V_{cs}\rvert^2 = 0.052 \pm 0.001$ [4]	
	$\Rightarrow \frac{\lvert F_+^{D\pi}(0)\rvert^2}{\lvert F_+^{DK}(0)\rvert^2} = 0.86 \pm 0.07^{+0.06}_{-0.04} \pm 0.01$	

(LQCD) , etc. Some numerical results are summarized in Table (24.5). The data of BES collaboration [61] is now not precise enough to challenge these theoretical prediction. The precision will be highly improved by BESIII.

For the q^2 dependence of the form factors, QCD sum rule confirms the pole dominance behavior for $F_+^{D\pi}(q^2)$ and $F_+^{DK}(q^2)$. The fitted pole masses from QCD sum rule are: $m_{\rm pole}^{D\to\pi} = (1.95 \pm 0.10)$GeV and $m_{\rm pole}^{D\to K} = (1.81 \pm 0.10)$GeV [48], which are compatible with the experimental value $m_{\rm pole}^{D\to\pi} = 1.86^{+0.10+0.07}_{-0.06-0.03}$GeV, $m_{\rm pole}^{D\to K} = 1.89 \pm 0.05^{+0.04}_{-0.03}$GeV [62]. $m_{\rm pole}^{D\to\pi}$ is consistent with the mass of D^*, while $m_{\rm pole}^{D\to K}$ is definitely different from the mass of $D_{(s)}^*$. This means that the single pole behavior of $F_+^{DK}(q^2)$ is just the mean effect of a set of resonances in cs channel.

Using the modified pole model in eq.(24.38), the value of α for both $D \to \pi$ and $D \to K$ from LCSR is consistent with zero [51], which implies the strong dominance of the $D_{(s)}^*$ pole. Experiment gives $\alpha^{D\to\pi} = 0.37^{+0.20}_{-0.31} \pm 0.15$ and $\alpha^{D\to K} = 0.36 \pm 0.10^{+0.03}_{-0.07} \pm 0.15$ [62]. The non-zero value of $\alpha^{D\to K}$ suggests the existence of contributions beyond the pure D_s^* pole to $F_+^{DK}(q^2)$.

Different theoretical techniques predict slightly different dependence behavior of the form factors on q^2. Experimental measurement of the partial decay width over different value of q^2 with high precision will check which method is the correct one to describe the non-perturbative dynamics in QCD.

The theoretical calculations of the branching ratios of $D^0 \to \pi^-\ell^+\nu$ and $D^0 \to K^-\ell^+\nu$ are compared with present experimental data in Table (24.6). Most of the theoretical predictions are consistent with experimental data under the present precision, except that the results of QCD sum rule in ref.[48] are a little lower that the experimental data.

The isospin invariance has been tested in D meson semileptonic decays [64]. The absolute branching ratios of $D^+ \to \pi^0 e^+\nu$ and $D^+ \to \bar{K}^0 e^+\nu$ are measured: $Br(D^+ \to$

Table 24.6: Branching ratios of $D^0 \to \pi^-\ell^+\nu$ and $D^0 \to K^-\ell^+\nu$.

	$Br(D^0 \to \pi^-\ell^+\nu)(\%)$	$Br(D^0 \to K^-\ell^+\nu)(\%)$
LQCD1[44]	0.23 ± 0.06	2.83 ± 0.45
	0.24 ± 0.06	2.99 ± 0.45
LQCD2[45]	$0.32 \pm 0.02 \pm 0.06 \pm 0.03$	$3.77 \pm 0.29 \pm 0.74 \pm 0.08$
QCD SR[48]	0.16 ± 0.03	2.7 ± 0.6
LCSR[51]	0.27 ± 0.10	3.6 ± 1.4
LCSR[52]	0.30 ± 0.09	3.9 ± 1.2
BES[61](Exp.)	$0.33 \pm 0.13 \pm 0.03$	$3.82 \pm 0.40 \pm 0.27$
CLEO[63](Exp.)	$0.262 \pm 0.025 \pm 0.008$	$3.44 \pm 0.10 \pm 0.10$

$\pi^0 e^+\nu) = (0.44 \pm 0.06 \pm 0.03)\%$, $Br(D^+ \to \bar{K}^0 e^+\nu) = (8.71 \pm 0.38 \pm 0.37)\%$. The ratio of the decay widthes of $D^0 \to K^- e^+\nu$ and $D^+ \to \bar{K}^0 e^+\nu$ is $\frac{\Gamma(D^0\to K^- e^+\nu)}{\Gamma(D^+\to \bar{K}^0 e^+\nu)} = 1.00 \pm 0.05 \pm 0.04$, which is consistent with unity. The ratio $\frac{\Gamma(D^0\to K^- e^+\nu)}{\Gamma(D^+\to \bar{K}^0 e^+\nu)}$ is expected to be unity under isospin invariance, therefore the experimental data confirms the isospin symmetry in $D \to K\ell^+\nu$ semileptonic decays.

The ratio of $\frac{\Gamma(D^0\to\pi^- e^+\nu)}{2\Gamma(D^+\to\pi^0 e^+\nu)}$ is measured to be $0.75^{+0.14}_{-0.11} \pm 0.04$ [64]. This ratio should also be unity due to the isospin symmetry. The result of CLEO collaboration implies that there may be large isospin breaking effect in the semileptonic decay of $D \to \pi e^+\nu$. However, the present experimental error is till too large. The precision needs to be highly improved in the future.

There are other $D_{(s)}$ to pseudoscalar semileptonic decay channels which deserve further studies. The present theoretical calculations and experimental measurements are listed in Table(24.7).

(2) Transitions to vector mesons $D \to V\ell^+\nu$

The decomposition of the transition matrix element of $D \to V$, according to its Lorentz structure, is

$$\begin{aligned}
&\langle V(\varepsilon, p_2)|\bar{q}\gamma_\mu(1-\gamma_5)c|D(p_1)\rangle = \varepsilon_{\mu\nu\alpha\beta}\varepsilon^{*\nu}p_1^\alpha p_2^\beta \frac{2V(q^2)}{m_D + m_V} \\
&-i(\varepsilon_\mu^* - \frac{\varepsilon^*\cdot q}{q^2}q_\mu)(m_D + m_V)A_1(q^2) + i[(p_1+p_2)_\mu - \frac{m_D^2 - m_V^2}{q^2}q_\mu] \\
&\times\varepsilon^*\cdot q\frac{A_2(q^2)}{m_D + m_V} - i\frac{2m_V\varepsilon^*\cdot q}{q^2}q_\mu A_0(q^2)
\end{aligned} \tag{24.42}$$

where the form factor $V(q^2)$ is contributed by the vector current $\bar{q}\gamma_\mu c$, and the form factors $A_{0,1,2}(q^2)$ by the axial-vector current $\bar{q}\gamma_\mu\gamma_5 c$.

The differential and total decay rate of $D \to V\ell^+\nu$ decay can be calculated from the above decomposition of the hadronic matrix element. There are three polarization states

Table 24.7: Branching ratios of D and D_s^+ to η, η', K transition channels.

channel	$Br(\%)$	Ref.
$D^+ \to \eta\ell^+\nu$	0.10	Ref.[58] (double pole)
	0.15	Ref.[58] (single pole)
	< 0.5	Exp.[4]
$D^+ \to \eta'\ell^+\nu$	0.016	Ref.[58] (double pole)
	0.019	Ref.[58] (single pole)
	< 1.1	Exp.[4]
$D_s^+ \to \eta\ell^+\nu$	1.7	Ref.[58] (double pole)
	2.5	Ref.[58] (single pole)
	2.3 ± 0.4	Ref.[49]
	2.5 ± 0.7	Exp.[4]
$D_s^+ \to \eta'\ell^+\nu$	0.61	Ref.[58] (double pole)
	0.74	Ref.[58] (single pole)
	1.0 ± 0.2	Ref.[49]
	0.89 ± 0.33	Exp.[4]
$D_s^+ \to K^0\ell^+\nu$	0.20	Ref.[58] (double pole)
	0.32	Ref.[58] (single pole)

for V meson: one longitudinal state, two transverse polarization states (right-handed and left-handed). The differential decay rate to longitudinally polarized V meson is

$$\frac{d\Gamma_L}{dq^2} = \frac{G_F^2|V_{cq}|^2}{192\pi^3 m_D^3}\sqrt{\lambda(m_D^2, m_V^2, q^2)}\left|\frac{1}{2m_V}\left[(m_D^2 - m_V^2 - q^2)\right.\right.$$
$$\left.\left.\times(m_D + m_V)A_1(q^2) - \frac{\lambda(m_D^2, m_V^2, q^2)}{m_D + m_V}A_2(q^2)\right]\right|^2 \tag{24.43}$$

where $\lambda(m_D^2, m_V^2, q^2) \equiv (m_D^2 + m_V^2 - q^2)^2 - 4m_D^2 m_V^2$.

The differential decay rate to transverse state is

$$\frac{d\Gamma_T^{\pm}}{dq^2} = \frac{G_F^2|V_{cq}|^2}{192\pi^3 m_D^3}q^2\lambda(m_D^2, m_V^2, q^2)^{3/2}\left|\frac{V(q^2)}{m_D + m_V} \mp \frac{(m_D + m_V)A_1(q^2)}{\sqrt{\lambda(m_D^2, m_V^2, q^2)}}\right|^2 \tag{24.44}$$

where the symbol "+" and "−" denote right and left-handed states, respectively. Finally, the combined transverse and total differential decay rates are

$$\frac{d\Gamma_T}{dq^2} = \frac{d}{dq^2}(\Gamma_T^+ + \Gamma_T^-), \qquad \frac{d\Gamma}{dq^2} = \frac{d}{dq^2}(\Gamma_L + \Gamma_T) \tag{24.45}$$

The vector meson is tagged by its decay product, for example, for $D \to K^*\ell^+\nu$, K^* is tagged according to its decay process $K^* \to K\pi$. The angular distribution for $D \to K^*\ell^+\nu$

$(K^* \to K\pi)$ is

$$\begin{aligned}\frac{d\Gamma}{dq^2 d\cos\theta_K d\cos\theta_\ell d\chi} &= \frac{3G_F^2|V_{cs}|^2}{8(4\pi)^4}\frac{p_{K^*}q^2}{m_D^2}[(1+\cos\theta_\ell)^2\sin^2\theta_K|H_+(q^2)|^2 \\ &+(1-\cos\theta_\ell)^2\sin^2\theta_K|H_-(q^2)|^2 - 4\sin^2\theta_\ell\cos^2\theta_K|H_0(q^2)|^2 \\ &+4\sin\theta_\ell(1+\cos\theta_\ell)\sin\theta_K\cos\theta_K\cos\chi H_+(q^2)H_0(q^2) \\ &-4\sin\theta_\ell(1-\cos\theta_\ell)\sin\theta_K\cos\theta_K\cos\chi H_-(q^2)H_0(q^2) \\ &-2\sin^2\theta_\ell\sin^2\theta_K\cos 2\chi H_+(q^2)H_-(q^2)] \\ &\times Br(K^* \to K\pi) \end{aligned} \tag{24.46}$$

where θ_ℓ is the polar angle of the lepton in the rest frame of the lepton pair $\ell^+\mu$, θ_K the polar angle of the kaon in the rest frame of K^*, and χ is the relative angle between the decay planes of $D \to K^*\ell^*\nu$ and $K^* \to K\pi$. The helicity functions of $H_+(q^2)$, $H_-(q^2)$ and $H_0(q^2)$ are

$$\begin{aligned} H_\pm(q^2) &= (m_D + m_{K\pi})A_1(q^2) \mp \frac{\sqrt{\lambda(m_D^2, m_{K\pi}^2, q^2)}}{m_D + m_{K\pi}} \\ H_0(q^2) &= \frac{1}{2m_{K\pi}\sqrt{q^2}}\left[(m_D^2 - m_{K\pi}^2 - q^2)(m_D + m_{K\pi})A_1(q^2)\right. \\ &\left. -\frac{\lambda(m_D^2, m_{K\pi}^2, q^2)}{m_D + m_{K\pi}}A_2(q^2)\right] \end{aligned} \tag{24.47}$$

The form factors for D to vector meson transitions can be calculated by a variety of methods, such as quark model (QM), QCD sum rule (SR), light-cone sum rule (LCSR), light-front approach (LF), etc. Some numerical results are collected in Table (24.8).

For some values, different theoretical methods give consistent results, for others, different methods give different results. These different predictions present an opportunity to test the theoretical methods. However, it is difficult to measure the absolute values of the $D \to V$ transition form factors directly, but the relative ratios of the form factors can be measure in experiment. The ratios of the $D \to V$ transition form factors are defined as

$$r_V \equiv \frac{V(0)}{A_1(0)}, \quad r_2 \equiv \frac{A_2(0)}{A_1(0)} \tag{24.48}$$

The measured values of r_V and r_2 for each decay mode can be compared with the theoretical calculations to test the theoretical techniques, see Table(24.9).

The q^2 dependence of the form factors can be calculated in theory. The result of QCD sum rule shows that the behavior of $V(q^2)$ and $A_0(q^2)$ is well compatible with the pole model [48, 50]

$$V(0) = \frac{V(0)}{1 - q^2/m_{\rm pole}^V}, \quad A_0(0) = \frac{A_0(0)}{1 - q^2/m_{\rm pole}^{A_0}} \tag{24.49}$$

The fitted pole mass $m_{\rm pole}^V$ is consistent with the low-lying charmed resonance in the $J^P = 1^-$ channel. While the q^2 dependence of $A_1(q^2)$ and $A_2(q^2)$ is very weak, this behavior implies that pole-dominance assumption for $A_1(q^2)$ and $A_2(q^2)$ is inadequate.

Table 24.8: Form factors of $D \to V$ transitions.

mode	$V(0)$	$A_0(0)$	$A_1(0)$	$A_2(0)$	Ref.
$D \to K^*$	0.82	0.47	0.57	0.75	QM [65]
	1.03		0.66	0.49	QM [56]
	1.1 ± 0.25		0.50 ± 0.15	0.60 ± 0.15	SR[48]
	0.8 ± 0.10		0.59 ± 0.10	0.55 ± 0.08	LCSR[52]
	0.99	1.12	0.62	0.31	Ref.[58]
$D \to \rho$	0.65	0.35	0.41	0.50	QM [65]
	0.90		0.59	0.49	QM [56]
	1.0 ± 0.2		0.5 ± 0.2	0.4 ± 0.1	SR[48]
	0.72 ± 0.10		0.57 ± 0.08	0.52 ± 0.07	LCSR[52]
	0.86	0.64	0.58	0.48	LF [57]
	1.05	1.32	0.61	0.31	Ref.[58]
$D \to \omega$	1.05	1.32	0.61	0.31	Ref.[58]
$D_s \to \phi$	1.10	1.02	0.61	0.32	Ref.[58]
	1.21 ± 0.33	0.42 ± 0.12	0.55 ± 0.15	0.59 ± 0.17	SR[50]
$D_s \to K^*$	1.16	1.19	0.60	0.33	Ref.[58]

Ratios of the polarized decay widthes and total branching ratios of $D \to V\ell^+\nu$ decays are been shown in Table(24.10).

The isospin symmetry can be tested in $D \to V\ell^+\nu$ decays by measuring the ratios $\frac{\Gamma(D^0\to K^{*-}\ell^+\nu)}{\Gamma(D^+\to \bar{K}^{*0}\ell^+\nu)}$ and $\frac{\Gamma(D^0\to \rho^-\ell^+\nu)}{2\Gamma(D^+\to \rho^0\ell^+\nu)}$. These ratios should be unity due to the isospin invariance. The deviation of these ratios from unity measures the degree of isospin breaking effects. The data from CLEO collaboration for these ratios are: $\frac{\Gamma(D^0\to K^{*-}e^+\nu)}{\Gamma(D^+\to \bar{K}^{*0}e^+\nu)} = 0.98 \pm 0.08 \pm 0.04$, $\frac{\Gamma(D^0\to \rho^-e^+\nu)}{2\Gamma(D^+\to \rho^0e^+\nu)} = 1.2^{+0.4}_{-0.3} \pm 0.1$ [64]. Both of the ratios are consistent with unity. The former ratio implies that the isospin symmetry in $D \to K^*$ channel is a good symmetry up to a few percentage level, while the latter one needs to be improved in precision.

(3) Transitions to scalar mesons $D \to S\ell^+\nu$

A large amount of scalar mesons have been found in experiment [4]. They include σ [or $f_0(600)$], $f_0(980)$, $f_0(1370)$, $f_0(1500)$, $f_0(1710)$, $a_0(980)$, $a_0(1450)$, κ, $K_0^*(1430)$, etc. Their structure is still not well established theoretically. Many suggestions about the components of the scalar mesons have been presented in the literture, such as $q\bar{q}$, $q\bar{q}q\bar{q}$ and meson-meson bound states. To investigate the structure of the scalar mesons, a large amount of experimental data and theoretical studies are necessary.

Semileptonic decays of D meson to scalars are important processes for studying the nature of scalar meson, because of the simpleness of semileptonic decay compared with hadronic decay. Comparing theoretical predictions with experimental data will give important information about the structure of the scalar mesons.

The Lorentz decomposition of the hadronic matrix element of $D \to S$ transition is

$$\langle S(p_2)|\bar{q}\gamma^\mu(1-\gamma_5)c|D\rangle = i[(p_1+p_2)^\mu F_+(q^2) + (p_1-p_2)^\mu F_-(q^2)] \qquad (24.50)$$

Table 24.9: Comparison of r_V and r_2 with experimental data.

mode	r_V	r_2	Ref.
$D \to K^*$	1.44	1.32	QM [65]
	2.10	1.35	QM [56]
	2.2 ± 0.2	1.2 ± 0.2	SR[48]
	1.36 ± 0.39	0.93 ± 0.29	LCSR[52]
	3.19	2.00	Ref.[58]
	1.62 ± 0.08	0.83 ± 0.05	Exp.[4]
$D \to \rho$	1.3	0.82	QM [65]
	1.84	1.20	QM [56]
	1.79	1.21	LF [57]
	3.39	1.97	Ref.[58]
	-	-	Exp.
$D \to \omega$	3.39	1.97	Ref.[58]
	-	-	Exp.
$D_s \to \phi$	3.44	1.91	Ref.[58]
	1.569	0.865	LF [57]
	2.20 ± 0.85	1.07 ± 0.43	SR[50]
	1.92 ± 0.32	1.60 ± 0.24	Exp.[4]
$D_s \to K^*$	3.52	1.82	Ref.[58]
	-	-	Exp.

The form factor $F_-(q^2)$ does not contribute to the amplitude of semileptonic decay process when neglecting the mass of the lepton. The differential decay width of $D \to S\ell^+\nu$ with the lepton-mass neglected is

$$\frac{d\Gamma}{dq^2} = \frac{G_F^2|V_{Qq}|^2}{192\pi^3 m_D^3} F_+(q^2)^2[(m_D^2 + m_S^2 - q^2)^2 - 4m_D^2 m_S^2]^{3/2}. \tag{24.51}$$

If the form factor is known, then one can predict the decay width theoretically. The form factor not only depends on the dynamics of the strong binding effects, but also depends on the components of the scalar mesons. The $D \to S$ transition form factors have been studied in QCD sum rule by treating the scalars as quark-antiquark bound states [66, 67]. Their results are listed in Table (24.11).

The q^2 dependence of $D \to S$ transition form factors calculated in QCD sum rule is well consistent with the pole-model

$$F_+(q^2) = \frac{F_+(0)}{1 - q^2/m_{\rm pole}^2} \tag{24.52}$$

Table 24.10: Ratios of the polarized decay widthes and total branching ratios of $D \to V\ell^+\nu$ decays.

mode	Γ_L/Γ_T	$Br(\%)$	Ref.
$D^0 \to K^{*-}\ell^+\nu$		4.0	QM [65]
	1.28	2.46	QM [56]
	1.15 ± 0.10	2.0 ± 0.5	LCSR[52]
	1.149	2.2	Ref.[58]
		2.15 ± 0.35	Exp.[4]
$D^+ \to K^{*0}\ell^+\nu$	0.86 ± 0.06	4.0 ± 1.6	SR[48]
	1.13	5.6	Ref.[58]
		5.73 ± 0.35	Exp.[4]
$D^0 \to \rho^-\ell^+\nu$		0.29	QM [65]
	1.16	0.17	QM [56]
	1.17 ± 0.09	0.14 ± 0.035	LCSR[52]
	1.10	0.20	Ref.[58]
	-	$0.194 \pm 0.039 \pm 0.013$	Exp.[63]
$D^+ \to \rho^0\ell^+\nu$	1.10	0.25	Ref.[58]
	-	$0.21 \pm 0.04 \pm 0.01$	Exp.[64]
$D^+ \to \omega\ell^+\nu$	1.10	0.25	Ref.[58]
	-	$0.16^{+0.07}_{-0.06} \pm 0.01$	Exp.[64]
$D_s^+ \to \phi\ell^+\nu$		2.5	QM [56]
	1.08	2.4	Ref.[58]
	0.99 ± 0.43	1.8 ± 0.5	SR[50]
	0.72 ± 0.18	2.0 ± 0.5	Exp.[4]
$D_s^+ \to K^{*0}\ell^+\nu$	1.21	0.19	QM [56]
	1.03	0.22	Ref.[58]
	-	-	Exp.

The fitted pole masses for each decay mode are [66, 67]

$$\begin{aligned} m_{\rm pole}^{D\kappa} &= 2.05 \pm 0.15 \text{ GeV}, \\ m_{\rm pole}^{DK_0^*} &= 2.9 \pm 0.3 \text{ GeV}, \\ m_{\rm pole}^{D_sK_0^*} &= 1.96 \pm 0.12 \text{ GeV}. \end{aligned} \tag{24.53}$$

The total decay widthes for each decay mode are

$$\begin{aligned} \Gamma(D \to \sigma\ell^+\nu) &= (8.0 \pm 2.5) \times 10^{-16} \text{ GeV [66]}, \\ \Gamma(D \to \kappa\ell^+\nu) &= (5.5 \pm 1.0) \times 10^{-15} \text{ GeV [66]}, \\ \Gamma(D \to K_0^*(1430)\ell^+\nu) &= (2.9^{+2.3}_{-1.6}) \times 10^{-16} \text{ GeV [67]}, \\ \Gamma(D_s^+ \to K_0^*(1430)^0\ell^+\nu) &= (3.2^{+3.0}_{-2.0}) \times 10^{-17} \text{ GeV [67]}. \end{aligned} \tag{24.54}$$

Table 24.11: Form factors of $D_{(s)} \to S\ell^+\nu$ decays.

mode	$F_+(0)$	Ref.
$D \to \sigma$	0.50 ± 0.07	SR [66]
$D \to \kappa$	0.52 ± 0.03	SR [66]
$D \to K_0^*(1430)$	0.57 ± 0.19	SR [67]
$D_s \to K_0^*(1430)$	0.51 ± 0.20	SR [67]

The corresponding branching ratios are

$$\begin{aligned} Br(D^+ \to \sigma\ell^+\nu) &= (1.26 \pm 0.40) \times 10^{-3}, \\ Br(D^0 \to \kappa^-\ell^+\nu) &= (3.43 \pm 0.62) \times 10^{-3}, \end{aligned} \tag{24.55}$$

$$\begin{aligned} Br(D^+ \to \bar{\kappa}^0\ell^+\nu) &= (8.7 \pm 1.6) \times 10^{-3}, \\ Br(D^0 \to K_0^*(1430)^-\ell^+\nu) &= (1.8^{+1.5}_{-1.0}) \times 10^{-4}, \\ Br(D^+ \to \bar{K}_0^*(1430)^0\ell^+\nu) &= (4.6^{+3.7}_{-2.6}) \times 10^{-4}, \\ Br(D_s^+ \to K_0^*(1430)^0\ell^+\nu) &= (2.4^{+2.2}_{-1.5}) \times 10^{-5}. \end{aligned} \tag{24.56}$$

The numerical results show that many of the above semileptonic decay modes are rare. Measuring them in experiment needs high statistics, but these measurements will give valuable information on the nature of the light scalar mesons. Experimental measurement of these decays are highly desired.

The other decay modes which are worthy of measuring are $D \to f_0(980)\ell^+\nu$, $D \to a_0(980)\ell^+\nu$, etc.

(4) CKM matrix elements V_{cd} and V_{cs} in semileptonic D decays

The CKM matrix elements are fundamental parameters in the standard model (SM), which describe the mixing of quark fields due to weak interaction. These parameters can not be predicted by the basic theory in the SM, they must be measured by experiment. Measuring CKM matrix element is important for understanding the dynamics of quark mixing and the source of CP violation. In the theory of more than three generations of quarks, the CKM matrix can provide a phase parameter to generate CP violation.

Semileptonic D decays involve V_{cd} and V_{cs}. Precise measurement of the branching ratios of D meson semileptonic decays can improve the precision of the quark mixing parameters of V_{cd} and V_{cs}. At present, Particle Data Group (2004) gives the magnitudes [4]

$$|V_{cd}| = 0.224 \pm 0.012, \qquad |V_{cs}| = 0.996 \pm 0.013. \tag{24.57}$$

The magnitude of $|V_{cd}|$ is deduced from neutrino and antineutrino production of charm off valence d quarks. The present error for $|V_{cd}|$ is about 5.4%. Values for $|V_{cs}|$ obtained from neutrino production of charm have errors exceeding 10% due to theoretical uncertainties. With the requirement of unitarity of the three-generation CKM matrix, the precision for $|V_{cs}|$ is greatly improved, the error of the present value given above is about 13%.

In BESIII, the absolute branching ratios of the semileptonic decay modes, $D \to \pi\ell^+\nu$, $D \to K\ell^+\nu$, $D \to \eta(\eta')\ell^+\nu$, $D \to \rho\ell^+\nu$, $D \to K^*\ell^+\nu$, $D_s \to \phi\ell^+\nu$, etc., will be measured up to the precision of 1% level. The form factor slope over q^2 distribution will be as precise as 1.5% [68]. The differential decay width is proportional to squared product of $V_{cs(s)}$ and the relevant semileptonic transition form factor $F(q^2)$

$$\frac{d\Gamma(D \to X_{d,s}\ell^+\nu)}{dq^2} \propto |V_{cd(s)}|^2 |F(q^2)|^2. \tag{24.58}$$

High precision-value of $|V_{cd(s)}|^2|F(q^2)|^2$ can be extracted from the precisely measured absolute branching ratios. This will lead to the determination of CKM matrix elements V_{cd} and V_{cs} with precision of 1% if the form factors can be calculated in theory up to the precision of 1.5% level. It is hopeful that Lattice QCD can accomplish this goal in next few years.

24.2.2 Exclusive Semileptonic Decays [5]

The effects of weak and strong interactions of the exclusive D semileptonic decay can be well separated in theory, so they are good candidates for both studying the mechanism of quark mixing and testing the theoretical techniques developed for calculating the hadronic matrix element.

On BESIII, we will collect a $\psi(3770)$ data sample of integrated luminosity of about $\mathcal{L} = 20$ fb^{-1} at the center-of-mass energy $\sqrt{s} = 3.773$ GeV as a desired goal. This make it possible to systematically study the properties of the D semileptonic decays. Based on the analyses of the data sample, the absolute branching fractions for many exclusive D semileptonic decays will be precisely measured, including $D^0 \to K^-\ell^+\nu_\ell(\ell = e,$ or $\mu)$, $D^0 \to \pi^-\ell^+\nu_\ell$, $D^0 \to K^{*-}\ell^+\nu_\ell$, $D^0 \to \rho^-\ell^+\nu_\ell$, $D^+ \to \overline{K}^0\ell^+\nu_\ell$, $D^+ \to \pi^0\ell^+\nu_\ell$, $D^+ \to \overline{K}^{*0}\ell^+\nu_\ell$, $D^+ \to \rho^0\ell^+\nu_\ell$, $D^+ \to \omega\ell^+\nu_\ell$ etc.. Using the measured branching fractions, we may extract the CKM matrix element $|V_{cs(d)}|$ with different exclusive D semileptonic decays, since their amplitudes are simply related to the CKM matrix elements. As examples of Monte Carlo simulations, we herein use the simplest pseudoscalar exclusive semileptonic decays $D^0 \to K^-e^+\nu_e$ and $D^0 \to \pi^-e^+\nu_e$, whose signal yields are the highest, backgrounds are the lowest, and theoretical contributions are the best understood.

With a Monte Carlo sample of about 800 pb^{-1} integrated luminosity at 3.773 GeV, we present Monte Carlo simulations of the measurements of the branching fractions for the semileptonic decays $D^0 \to K^-e^+\nu_e$ and $D^0 \to \pi^-e^+\nu_e$. The measurements are made based on the analyses of the singly tagged $\bar{D}^0$ sample, following the method as used by BESII [41, 42]. Using the measured branching fractions for $D^0 \to K^-e^+\nu_e$ and $D^0 \to \pi^-e^+\nu_e$, the form factor $|f_+^{K(\pi)}(0)|$, the CKM matrix element $|V_{cs(d)}|$, and the ratio $|V_{cd}|/|V_{cs}|$ are extracted, respectively. According to the simulation results, the expected precisions of these measurements for 20 fb^{-1} $\psi(3770)$ data are then estimated.

[5] By Hui-Hui Liu, Hai-Long Ma and Gang Rong

Overview of the studies of the semileptonic decays $D^0 \to K^- e^+ \nu_e$ and $D^0 \to \pi^- e^+ \nu_e$

The semileptonic decays $D^0 \to K^- e^+ \nu_e$ and $D^0 \to \pi^- e^+ \nu_e$ have been studied by many experiments [69, 70, 71, 72, 41, 73, 74, 75], since the final states only contain two easily reconstructed charged particles. The measured branching fractions for $D^0 \to K^- e^+ \nu_e$ and $D^0 \to \pi^- e^+ \nu_e$ are summarized in Table 24.12 and Table 24.13, respectively, along with the numbers of signal events. In some experiments, the branching fractions for $D^0 \to K^- e^+ \nu_e$ (or $D^0 \to \pi^- e^+ \nu_e$) are measured relative to the topologically similar mode $D^0 \to K^- \pi^+$ (or $D^0 \to K^- e^+ \nu_e$). Multiplying the measured ratio of the branching fraction by $\mathcal{B}(D^0 \to K^- \pi^+)$ or $\mathcal{B}(D^0 \to K^- e^+ \nu_e)$ [4], we obtain the absolute branching fractions for $D^0 \to K^- e^+ \nu_e$ and $D^0 \to \pi^- e^+ \nu_e$, which are also presented in Table 24.12 and Table 24.13. In the tables, the first error is statistical, the second is systematic, and the third arises from the uncertainty in $\mathcal{B}(D^0 \to K^- \pi^+)$ or $\mathcal{B}(D^0 \to K^- e^+ \nu_e)$.

Particle Data Group (2006) averages the branching fractions to be [4] $\mathcal{B}(D^0 \to K^- e^+ \nu_e) = (3.51 \pm 0.11)\%$ and $\mathcal{B}(D^0 \to \pi^- e^+ \nu_e) = (2.81 \pm 0.19) \times 10^{-3}$. These numbers give the relative errors 3.1% for $\mathcal{B}(D^0 \to K^- e^+ \nu_e)$ and 6.8% for $\mathcal{B}(D^0 \to \pi^- e^+ \nu_e)$. The most precise measurements of $\mathcal{B}(D^0 \to K^- e^+ \nu_e)$ and $\mathcal{B}(D^0 \to \pi^- e^+ \nu_e)$ are provided by the CLEO Collaboration [73]. These existing branching fractions for $D^0 \to K^- e^+ \nu_e$ and $D^0 \to \pi^- e^+ \nu_e$ suffer from larger error, which directly affect the precision in the extraction of the CKM matrix element or form factor.

Table 24.12: Summary of the measured branching fractions for $D^0 \to K^- e^+ \nu_e$ from different experiments, where 'absolute' means that the branching fraction is made absolutely.

Experiments	Number of Events	Normalizing Mode	Measured ratio of branching fraction	$\mathcal{B}(D^0 \to K^- e^+ \nu_e)$ (%)
E691[69]	250	$\frac{D^0 \to K^- e^+ \nu_e}{D^0 \to K^- \pi^+}$	$0.91 \pm 0.07 \pm 0.11$	$3.46 \pm 0.27 \pm 0.42 \pm 0.08$
CLEO[70]	584	$\frac{D^0 \to K^- e^+ \nu_e}{D^0 \to K^- \pi^+}$	$0.90 \pm 0.06 \pm 0.06$	$3.42 \pm 0.23 \pm 0.23 \pm 0.08$
CLEOII[71]	2510	$\frac{D^0 \to K^- e^+ \nu_e}{D^0 \to K^- \pi^+}$	$0.978 \pm 0.027 \pm 0.044$	$3.72 \pm 0.10 \pm 0.17 \pm 0.09$
MARKIII[72]	55	absolute		$3.4 \pm 0.5 \pm 0.4$
BESII[41]	104	absolute		$3.82 \pm 0.40 \pm 0.27$
CLEOc[73]	1311	absolute		$3.44 \pm 0.10 \pm 0.10$
PDG[4]				3.51 ± 0.11

Property of $D\bar{D}$ production around $\sqrt{s} = 3.773$ GeV

At the center-of-mass energy of 3.773 GeV, the $\psi(3770)$ resonance is produced in electron-positron (e^+e^-) annihilation. It decays to $D\bar{D}$ pairs ($D^0\bar{D}^0$ and D^+D^-) with a large branching fraction of about $(85 \pm 6)\%$ [76], and thus provides the best place to study the semileptonic decays of D^0 and D^+ mesons. This also implies that if a $\bar{D}$ meson can be fully reconstructed (this is called a singly tagged $\bar{D}$ meson) [41, 42] from the data sample, the

Table 24.13: Summary of the measured branching fractions for $D^0 \to \pi^- e^+ \nu_e$ from different experiments, where 'absolute' means that the branching fraction is made absolutely.

Experiments	Number of Events	Normalizing Mode	Measured ratio of branching fraction	$\mathcal{B}(D^0 \to \pi^- e^+ \nu_e)$ (%)
CLEO[74]	87	$\frac{D^0 \to \pi^- e^+ \nu_e}{D^0 \to K^- e^+ \nu_e}$	$0.103 \pm 0.039 \pm 0.013$	$0.37 \pm 0.14 \pm 0.05 \pm 0.02$
E687[75]	91(e and μ)	$\frac{D^0 \to \pi^- l^+ \nu_l}{D^0 \to K^- l^+ \nu_l}$	$0.101 \pm 0.020 \pm 0.003$	$0.36 \pm 0.07 \pm 0.01 \pm 0.02$
MARKIII[72]	7	absolute		$0.39^{+0.23}_{-0.11} \pm 0.04$
BESII[41]	9	absolute		$0.33 \pm 0.13 \pm 0.03$
CLEOc[73]	117	absolute		$0.262 \pm 0.025 \pm 0.008$
PDG[4]				0.281 ± 0.019

D meson must exist in the system recoiling against the singly tagged $\bar{D}$ meson. The singly tagged $\bar{D}$ meson can not only help to determine the charge and flavor of the semileptonic decays, but also help to reduce backgrounds in the selection of the semileptonic decays. Taking advantage of the nature of the $\psi(3770)$ predominately decaying into $D^0\bar{D}^0$ and D^+D^- pairs, we can do absolute measurements of the branching fractions for the D meson decays. Here, we reconstruct the singly tagged $\bar{D}^0$ mesons in the hadronic modes with larger branching fractions firstly. In the system recoiling against the singly tagged $\bar{D}^0$ mesons, we select the semileptonic decays $D^0 \to K^- e^+ \nu_e$ and $D^0 \to \pi^- e^+ \nu_e$ based on the kinematic signature of the singly tagged $\bar{D}^0$ events, and measure the branching fractions for the decays directly.

Event generation

The Monte Carlo events are generated as $e^+e^- \to D\bar{D}$ at 3.773 GeV, where the D and $\bar{D}$ mesons are set to decay into all possible final states with the branching fractions quoted from PDG [4]. The particle trajectories are simulated with the GEANT4 based Monte Carlo simulation package for the BESIII detector. The $D\bar{D}$ Monte Carlo sample is generated and reconstructed with BOSS6.02(BESIII Offline Software System). Totally 4,900,000 $D\bar{D}$ Monte Carlo events are generated, which is corresponding to a data sample of about 800 pb^{-1} integrated luminosity at 3.773 GeV. Based on the Monte Carlo sample, the semileptonic decays $D^0 \to K^- e^+ \nu_e$ and $D^0 \to \pi^- e^+ \nu_e$ are studied.

Event selection

To select good candidate events, it is required at least two charged tracks be well reconstructed in the MDC. All charged tracks are required to satisfy a geometry cut $|\cos\theta| < 0.93$, where θ is the polar angle with respect to the beam axis. Each track must originate from the interaction region, which is defined by $V_{xy} < 1.0$ cm and $|V_z| < 5.0$ cm, where V_{xy} and $|V_z|$ are the closest approach of the charged track in the xy-plane and z direction.

Pions and kaons are identified using the dE/dx and TOF measurements, with which the combined confidence levels (CL_π or CL_K) for a pion or kaon hypotheses are calculated. A pion candidate is required to have $CL_\pi > 0.001$. In order to reduce misidentification, a kaon candidate is required to satisfy $CL_K > CL_\pi$. Electrons are identified using the dE/dx, TOF and EMC measurements, with which the combined confidence level (CL_e) for the electron hypothesis is calculated. An electron candidate is required to have $CL_e > 0.001$, CL_π and CL_K.

Neutral kaons are reconstructed through the decay $K^0_S \to \pi^+\pi^-$. To select the candidates for K^0_S, it is required that the difference between the invariant mass of at least one $\pi^+\pi^-$ combination and the K^0_S nominal mass should be less than 20 MeV/c^2 in each event.

Neutral pions are reconstructed through the decay $\pi^0 \to \gamma\gamma$. To select the candidates for π^0, it is required that the difference between the invariant mass of at least one $\gamma\gamma$ combination and the π^0 nominal mass should be less than 20 MeV/c^2 in each event. A good photon candidate must satisfy the following criteria: (1) the energy deposited in the EMC is greater than 100 MeV; (2) the angle in the xy-plane between the photon and the nearest charged track is greater than 20°, and the angle in the rz-plane between the photon and the nearest charged track is greater than 20°.

Singly tagged $\bar{D}^0$ mesons

The singly tagged $\bar{D}^0$ mesons are reconstructed in four hadronic decay modes of $K^+\pi^-$, $K^+\pi^-\pi^-\pi^+$ and $K^+\pi^-\pi^0$ and $K^0\pi^+\pi^-$, which are about 30.23% of all $\bar{D}^0$ decays.

For the $Kn\pi(n = 1, 2, 3)$ combinations satisfying the above selection criteria, the beam-constraint masses of each combination is calculated by

$$M_{\rm bc} = \sqrt{E^2_{\rm beam} - \vec{p}^{\,2}_{Kn\pi}}, \tag{24.59}$$

where $E_{\rm beam}$ is the beam energy, $\vec{p}_{Kn\pi}$ is the total measured momentum of all particles in the final states. In order to suppress background due to particle misidentification and fake photons, it is required that ΔE of each combination satisfy $|\Delta E| < 3\sigma_{\Delta E}$. Here,

$$\Delta E = E_{Kn\pi} - E_{\rm beam}, \tag{24.60}$$

where $E_{Kn\pi}$ is the total energy of all particles in the final states, and $\sigma_{\Delta E}$ is the standard deviation of the ΔE distribution.

Fig.24.9 shows the resulting distributions of the beam-constraint masses of the $Kn\pi$ combinations for the singly tagged $\bar{D}^0$ modes. A maximum likelihood fit to the mass spectrum with a Gaussian function for the $\bar{D}^0$ signal and a special function [41, 42] for the background yields the number of the singly tagged $\bar{D}^0$ mesons for each mode. These give the total number $N_{\bar{D}^0_{\rm tag}}$ of the reconstructed singly tagged $\bar{D}^0$ mesons. In each mass spectra, the region within a $\pm 3\sigma_{M_{\bar{D}^0_i}}$ window around the fitted $\bar{D}^0$ mass $M_{\bar{D}^0_i}$ is defined as the singly tagged $\bar{D}^0$ signal region, where $\sigma_{M_{\bar{D}^0_i}}$ is the standard deviation of the mass spectrum for the ith tag mode. The region outside a $\pm 4\sigma_{M_{\bar{D}^0_i}}$ window around the fitted $\bar{D}^0$ mass is taken as the $\bar{D}^0$ sideband region to estimate the background in the $\bar{D}^0$ signal region.

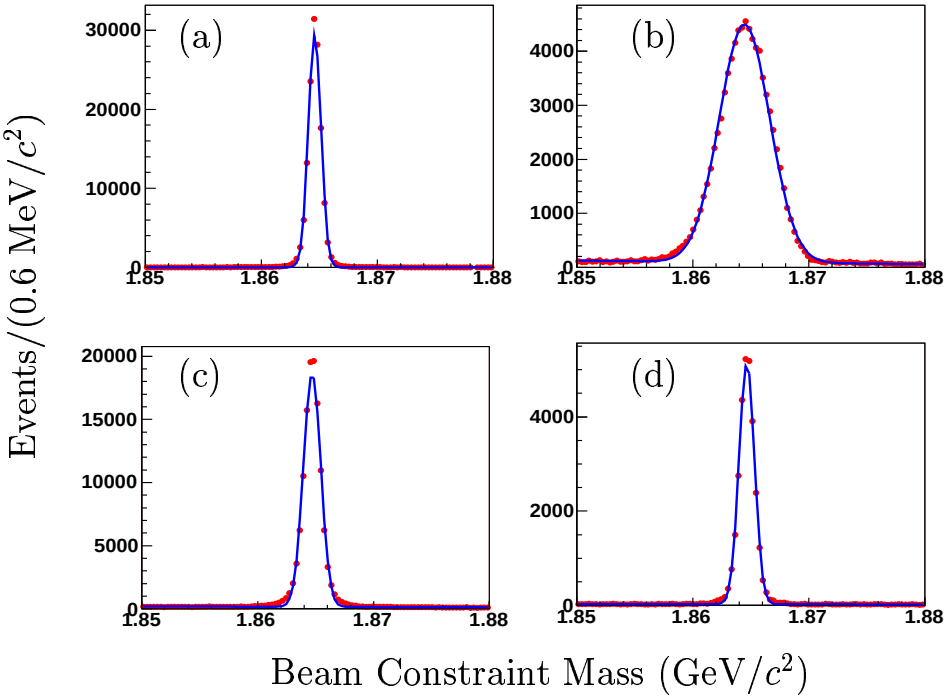

Figure 24.9: The beam constraint masses of the $Kn\pi$ combinations for the singly tagged $\bar{D}^0$ modes: (a) $K^+\pi^-$, (b) $K^+\pi^-\pi^0$, (c) $K^+\pi^-\pi^-\pi^+$ and (d) $K^0\pi^+\pi^-$.

Neutrino reconstruction

Candidates for the semileptonic decays $D^0 \to K^-e^+\nu_e$ and $D^0 \to \pi^-e^+\nu_e$ are selected from the surviving tracks in the system recoiling against the singly tagged $\bar{D}^0$ mesons. It is required that there are only two oppositely charged tracks, one of which is identified as an electron and the other as a kaon or pion. Electron should have its charge opposite to the charm of the singly tagged $\bar{D}^0$ meson, except for the mode $K^0\pi^+\pi^-$. In order to reduce the background events from the decays such as $D^0 \to K^-\pi^0e^+(\mu^+)\nu_{e(\mu)}$ and $D^0 \to K^-\pi^+\pi^0$, it is required that there should be no extra charged track or isolated photon, which has not been used in the reconstruction of the singly tagged $\bar{D}^0$ mesons. There are still possible backgrounds for each semileptonic decay due to misidentifying a pion as an electron, for example the decay $D^0 \to K^-\pi^+$ may be faked as $D^0 \to K^-e^+\nu_e$. These events can be suppressed by requiring that the invariant masses of the K^-e^+ combinations to be less than 1.8 GeV/c^2.

In the semileptonic decays, there is one massless neutrino which can not be detected on BESIII. In order to obtain information about the missing neutrinos, we use a kinematic quantity defined by

$$U_{miss} \equiv E_{miss} - p_{miss}$$

following the previous BESII works [41, 42]. Here, E_{miss} and p_{miss} are the total energy and momentum of all the missing particles. The value of U_{miss} should be close to zero if the event is correctly reconstructed. The kinematic quantity U_{miss} provides powerful

information to reject background events due to the misidentified and undetected particles.

Fig. 24.10 shows the U_{miss} distribution of the candidates for the semileptonic decays $D^0 \to K^- e^+ \nu_e$ with tags in the $\bar{D}^0$ signal regions, selected from the Monte Carlo sample. Fig. 24.11 shows the U_{miss} distribution of the selected candidates for $D^0 \to \pi^- e^+ \nu_e$, where the K^- has been allowed to be misidentified as a π^-. The signals around zero in the figures represent the production of the semileptonic decays $D^0 \to K^- e^+ \nu_e$ and $D^0 \to \pi^- e^+ \nu_e$. Fitting to each U_{miss} distribution with a Gaussian function for the signal events and a polynomial for the background, we obtain the numbers of events for the semileptonic decays $N_{D^0 \to K^- e^+ \nu_e} = 5528 \pm 75$ and $N_{D^0 \to \pi^- e^+ \nu_e} = 707 \pm 27$, respectively. However, the U_{miss} distributions of the selected events with tags in the $\bar{D}^0$ sideband regions has no peak around zero.

Monte Carlo study shows that the dominant background for $D^0 \to K^- e^+ \nu_e$ is from $D^0 \to K^- \mu^+ \nu_\mu$, and the main background for $D^0 \to \pi^- e^+ \nu_e$ is from $D^0 \to \pi^- \mu^+ \nu_\mu$, $D^0 \to K^- e^+ \nu_e$ and $D^0 \to \rho^- e^+ \nu_e$. These background events satisfy the selection criteria for the semileptonic decays in question due to misidentifying $\mu^+(K^-)$ as $e^+(\pi^-)$ and due to missing π^0. The events under the peak B in Fig. 24.11 are mainly from $D^0 \to K^- e^+ \nu_e$ because the K^- has been allowed to be misidentified as π^-. Besides $D^0 \to K^- e^+ \nu_e$, the events under the peak C are mainly from $D^0 \to K^{*-} \pi^+, K^{*-} \to K^- \pi^0$ and $D^0 \to K^- \rho^+, \rho^+ \to \pi^+ \pi^0$, which satisfy the selection criteria for $D^0 \to \pi^- e^+ \nu_e$ due to misidentifying $K^- \pi^+$ pair as $\pi^- e^+$ pair and due to missing π^0.

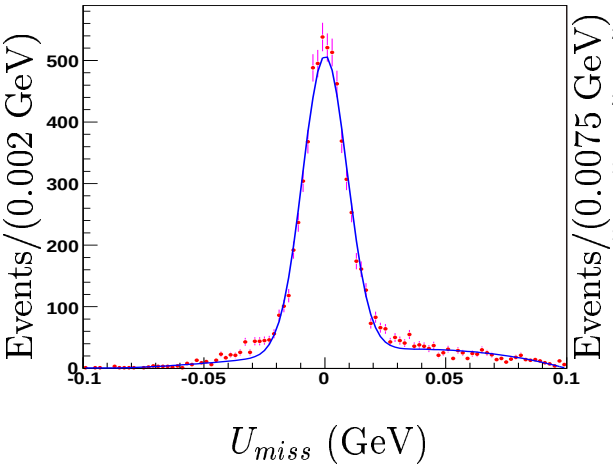

Figure 24.10: The U_{miss} distribution of the candidates for the semileptonic decay $D^0 \to K^- e^+ \nu_e$.

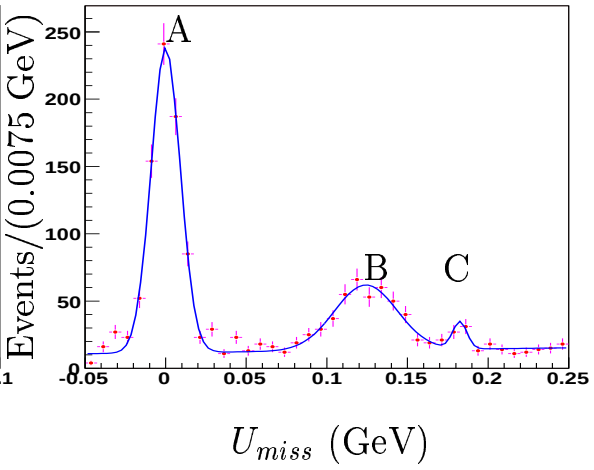

Figure 24.11: The U_{miss} distribution of the candidates for the semileptonic decay $D^0 \to \pi^- e^+ \nu_e$, where the $D^0 \to K^- e^+ \nu_e$ events have been misidentified as $D^0 \to \pi^- e^+ \nu_e$, since the K^- has been allowed to be misidentified as a π^-, see the peak B.

Branching fractions

Branching fraction for the semileptonic decay $D^0 \to K^-(\pi^-)e^+\nu_e$ is determined by

$$\mathcal{B}(D^0 \to K^-(\pi^-)e^+\nu_e) = \frac{N_{D^0\to K^-(\pi^-)e^+\nu_e}}{N_{\bar{D}^0_{\rm tag}} \times \epsilon_{D^0\to K^-(\pi^-)e^+\nu_e}}, \tag{24.61}$$

where $N_{D^0\to K^-(\pi^-)e^+\nu_e}$ is the number of the signal events for $D^0 \to K^-(\pi^-)e^+\nu_e$, $N_{\bar{D}^0_{\rm tag}}$ is the total number of the singly tagged $\bar{D}^0$ mesons, $\epsilon_{D^0\to K^-(\pi^-)e^+\nu_e}$ is the detection efficiency for $D^0 \to K^-(\pi^-)e^+\nu_e$. The detection efficiency for the semileptonic decay is estimated by analyzing the Monte Carlo events of $D^0 \to K^-(\pi^-)e^+\nu_e$ versus the singly tagged $\bar{D}^0$ mode. Detail Monte Carlo study gives the detection efficiency $\epsilon_{D^0\to K^-(\pi^-)e^+\nu_e}$ for $D^0 \to K^-(\pi^-)e^+\nu_e$.

Inserting these numbers in Eq. 24.61, we obtain the branching fractions for the semileptonic decays to be

$$\mathcal{B}(D^0 \to K^-e^+\nu_e) = (3.41 \pm 0.05 \pm 0.03)\%,$$

$$\mathcal{B}(D^0 \to \pi^-e^+\nu_e) = (0.409 \pm 0.015 \pm 0.04)\%,$$

where the first error is statistical and the second systematic. In the measurements of the branching fractions, the systematic error arises mainly from the uncertainties in tracking simulation, particle identification, photon selection, fit to the U_{miss} distribution as well as the number of the singly tagged $\bar{D}^0$ mesons. Here, it is taken to be 1.0%, which is expected to reach on BESIII.

With the simulation results, the expected relative statistical errors of $\mathcal{B}(D^0 \to K^-e^+\nu_e)$ and $\mathcal{B}(D^0 \to \pi^-e^+\nu_e)$ on BESIII are estimated, as shown in Table 24.14. The relative statistical error of the measured branching fractions $\frac{\Delta\mathcal{B}(D^0\to K^-e^+\nu_e)}{\mathcal{B}(D^0\to K^-e^+\nu_e)}_{\rm stat.} = 0.3\%$ and $\frac{\Delta\mathcal{B}(D^0\to \pi^-e^+\nu_e)}{\mathcal{B}(D^0\to \pi^-e^+\nu_e)}_{\rm stat.} = 0.7\%$ can be reachable for 20 fb^{-1} $\psi(3770)$ data.

Table 24.14: Expected relative statistical error of $\mathcal{B}(D^0 \to K^-e^+\nu_e)$ and $\mathcal{B}(D^0 \to \pi^-e^+\nu_e)$ on BESIII.

$\mathcal{L}$	4 fb^{-1}	20 fb^{-1}
$\frac{\Delta\mathcal{B}(D^0\to K^-e^+\nu_e)}{\mathcal{B}(D^0\to K^-e^+\nu_e)}_{\rm stat.}$	0.6%	0.3%
$\frac{\Delta\mathcal{B}(D^0\to \pi^-e^+\nu_e)}{\mathcal{B}(D^0\to \pi^-e^+\nu_e)}_{\rm stat.}$	1.6%	0.7%

Determinations of $|f_+^K(0)|$ and $|f_+^\pi(0)|$

The decay width of the semileptonic decay $D^0 \to K^-(\pi^-)e^+\nu_e$ relates to the form factor $|f_+^{K(\pi)}(0)|$ and the CKM matrix element $|V_{cs(d)}|$ through [77, 78, 41]

$$\Gamma(D^0 \to K^-e^+\nu_e) = \frac{\mathcal{B}(D^0 \to K^-e^+\nu_e)}{\tau_{D^0}} = 1.53|V_{cs}|^2|f_+^K(0)|^2 \times 10^{11}s^{-1} \tag{24.62}$$

$$\Gamma(D^0 \to \pi^- e^+ \nu_e) = \frac{\mathcal{B}(D^0 \to \pi^- e^+ \nu_e)}{\tau_{D^0}} = 3.01 |V_{cs}|^2 |f_+^\pi(0)|^2 \times 10^{11} s^{-1} \quad (24.63)$$

The form factors $|f_+^K(0)|$ and $|f_+^\pi(0)|$ can be extracted by using the measured branching fractions and the lifetime of the D^0 meson. Inserting the values of $|V_{cs}| = 0.996 \pm 0.013$ and $|V_{cd}| = 0.224 \pm 0.012$ [4], the lifetime $\tau_{D^0} = (410.1 \pm 1.5) \times 10^{-15}$ s and the measured branching fractions in Eqs. 24.62 and 24.63, the form factors are determined to be

$$|f_+^K(0)| = 0.74 \pm 0.01 \pm 0.01,$$

$$|f_+^\pi(0)| = 0.81 \pm 0.04 \pm 0.04,$$

where the first error is statistical and the second systematic. In the determinations of the form factors, the systematic error arises mainly from the uncertainties in the measured branching fractions, the lifetime τ_{D^0}, and the values of the CKM matrix elements $|V_{cs(d)}|$. The total systematic error in the measurement of $f_+^{K(\pi)}(0)$ can be written as

$$\frac{\Delta f_+^{K(\pi)}(0)}{f_+^{K(\pi)}(0)} = \sqrt{\left(\frac{\Delta \mathcal{B}}{2\mathcal{B}}\right)^2 + \left(\frac{\Delta \tau_{D^0}}{2\tau_{D^0}}\right)^2 + \left(\frac{\Delta V_{cs(d)}}{V_{cs(d)}}\right)^2}, \quad (24.64)$$

where the uncertainty in the measured branching fraction is taken to be $\Delta\mathcal{B}/\mathcal{B} = 1.0\%$, the uncertainty in the lifetime is $\Delta\tau_{D^0}/\tau_{D^0} = 0.4\%$, the uncertainties in the CKM matrix elements are $\Delta|V_{cs}|/|V_{cs}| = 1.3\%$ and $\Delta|V_{cs}|/|V_{cs}| = 5.4\%$. Therefore, the total systematic error in the determination of $f_+^{K(\pi)}(0)$ is estimated to be

$$\frac{\Delta f_+^K(0)}{f_+^K(0)} = 1.4\%,$$

$$\frac{\Delta f_+^\pi(0)}{f_+^\pi(0)} = 5.4\%,$$

which are dominated by the uncertainty in $|V_{cs(d)}|$, see Table 24.15.

Table 24.15: The errors of in the determination of the form factor $|f_+^{K(\pi)}(0)|$ with 20 fb^{-1} $\psi(3770)$ data on BESIII.

	$\frac{\Delta\mathcal{B}}{2\mathcal{B}}$ stat.	$\frac{\Delta\mathcal{B}}{2\mathcal{B}}$ sys.	$\frac{\Delta\tau_{D^0}}{2\tau_{D^0}}$	$\lvert V_{cs(d)}\rvert$	Total error
$\lvert f_+^K(0)\rvert$	0.15%	0.5%	0.2%	1.3%	1.4%
$\lvert f_+^\pi(0)\rvert$	0.35%	0.5%	0.2%	5.4%	5.4%

Determinations of $|V_{cs}|$ and $|V_{cd}|$

Using the measured branching fractions for $D^0 \to K^- e^+ \nu_e$ and $D^0 \to \pi^- e^+ \nu_e$, and the predicted form factors $f_+^K(0) = 0.66 \pm 0.04^{+0.01}_{-0.00}$ and $f_+^\pi(0) = 0.57 \pm 0.06^{+0.01}_{-0.00}$ [79] with the

lattice-QCD, we can extract the CKM matrix elements $|V_{cs}|$ and $|V_{cd}|$ with Eqs. 24.62 and 24.63 to be

$$|V_{cs}| = 1.12 \pm 0.06 \pm 0.02,$$
$$|V_{cd}| = 0.32 \pm 0.02 \pm 0.01,$$

where the first error is statistical and the second systematic. In the determinations of the CKM matrix elements, the systematic error can be written as

$$\frac{\Delta V_{cs(d)}}{V_{cs(d)}} = \sqrt{\left(\frac{\Delta\mathcal{B}}{2\mathcal{B}}\right)^2 + \left(\frac{\Delta\tau_{D^0}}{2\tau_{D^0}}\right)^2 + \left(\frac{\Delta f_+^{K(\pi)}(0)}{f_+^{K(\pi)}(0)}\right)^2}. \quad (24.65)$$

where the uncertainty in the measured branching fraction is taken to be $\Delta\mathcal{B}/\mathcal{B} = 1.0\%$, the uncertainty in the lifetime is $\Delta\tau_{D^0}/\tau_{D^0} = 0.4\%$. Under the assumption that the uncertainty in the theoretical prediction for the form factor $\frac{\Delta f_+^{K(\pi)}}{f_+^{K(\pi)}} = 1.5\%$ can be achievable with the lattice-QCD in the next few years, the total systematic error in the determination of the CKM matrix element is estimated to be

$$\frac{\Delta V_{cs(d)}}{V_{cs(d)}} = 1.6\%,$$

which is dominated by the uncertainty in $f_+^{K(\pi)}$, see Table 24.16.

Table 24.16: The errors of in the determination of $|V_{cs(d)}|$ with 20 fb^{-1} $\psi(3770)$ data on BESIII.

	$\frac{\Delta\mathcal{B}}{2\mathcal{B}}$ stat.	$\frac{\Delta\mathcal{B}}{2\mathcal{B}}$ sys.	$\frac{\Delta\tau_{D^0}}{2\tau_{D^0}}$	$\lvert f_+^{K(\pi)}(0)\rvert$	Total error
$\lvert V_{cs}\rvert$	0.15%	0.5%	0.2%	1.5%	1.6%
$\lvert V_{cd}\rvert$	0.35%	0.5%	0.2%	1.5%	1.6%

Determinations of the ratios $\frac{|f_+^K(0)|^2|V_{cd}|^2}{|f_+^\pi(0)|^2|V_{cs}|^2}$ and $|V_{cd}|/|V_{cs}|$

Combining Eqs. 24.62 and 24.63, the ratio of the decay widths of the semileptonic decays $D^0 \to K^- e^+ \nu_e$ and $D^0 \to \pi^- e^+ \nu_e$ relates to the form factor $|f_+^{K(\pi)}(0)|$ and the CKM matrix element $|V_{cs(d)}|$ through

$$\frac{\mathcal{B}(D^0 \to \pi^- e^+ \nu_e)}{\mathcal{B}(D^0 \to K^- e^+ \nu_e)} = \frac{\Gamma(D^0 \to \pi^- e^+ \nu_e)}{\Gamma(D^0 \to K^- e^+ \nu_e)} = 1.967 \times \frac{|f_+^K(0)|^2}{|f_+^\pi(0)|^2}\frac{|V_{cd}|^2}{|V_{cs}|^2}. \quad (24.66)$$

With the measured branching fractions for $D^0 \to K^- e^+ \nu_e$ and $D^0 \to \pi^- e^+ \nu_e$, the ratio $\frac{|f_+^K(0)|^2|V_{cd}|^2}{|f_+^\pi(0)|^2|V_{cs}|^2}$ is determined to be $0.0615 \pm 0.0031 \pm 0.0006$, where the first error is the statistical error, and the second systematic. In the determination of the ratio, some uncertainties in the measured branching fractions, such as electron tracking simulation and

particle identification, photon selection, and the number of the singly tagged $\bar{D}^0$ mesons can be canceled completely. In addition, the ratio is also independent of the lifetime τ_{D^0}. The systematic error arises mainly from those uncanceled uncertainties in the measured branching fractions, including K/π tracking simulation and particle identification, and the fit to the U_{miss} distribution. Here, the statistical error can be neglected in the case of 20 fb^{-1} $\psi(3770)$ data, while the total systematic error is taken to be 1%.

Taking the ratio of the form factors to be unity, the ratio $|V_{cd}|/|V_{cs}|$ is determined to be $|V_{cd}|/|V_{cs}| = 0.248 \pm 0.006 \pm 0.003$, where the first error is statistical, and the second systematic. The systematic error arises from the uncanceled uncertainties in the measured branching fractions as discussed above, and the uncertainty in the predicted ratio of the form factors $f_+^K(0)/f_+^\pi(0)$. If the error on the predicted ratio of the form factors can reach 1% level, the ratio $|V_{cd}|/|V_{cs}|$ can be measured with precision of 1.1% for 20 fb^{-1} $\psi(3770)$ data. We can see that directly measuring the ratio $|V_{cd}|/|V_{cs}|$ will be more precise than separately measuring each CKM element $|V_{cs(d)}|$.

BESIII will greatly improve the precisions in the measurements of the branching fractions for the exclusive D semileptonic decays and thus provide more informations which are critical to fully understand both weak physics and QCD physics. The measurements of the form factor $|f_+^{K(\pi)}(0)|$, the CKM matrix element $|V_{cs(d)}|$, and the ratio of $|V_{cd}|/|V_{cs}|$ will be several times more precise than any existing results. It is possible to measure the form factors in all pseudoscalar and vector exclusive D semileptonic decays on BESIII. These will test those theoretical predictions describing the exclusive D semileptonic decay. BESIII will also search for the scalar exclusive D semileptonic decays, which are intensely desired on experiment. Moreover, BESIII will provide more precise test the isospin invariance in the D semileptonic decays.

24.2.3 Inclusive Semileptonic Decays [6]

The study of the inclusive D semileptonic decays can serve as a check on the sum of the measured branching fractions of the exclusive D semileptonic decays. And then, one can determine whether there are still exclusive semileptonic decays which have not been observed. In addition, the lifetimes of D^0 and D^+ mesons have been accurately measured in experiments, so the measurement of the branching fraction for the inclusive semileptonic decay $D \to X\ell^+\nu_\ell(\ell = e,$ or $\mu)$ can accurately determine their corresponding decay widths, $\Gamma_{D^0}^{\rm SL}$ and $\Gamma_{D^+}^{\rm SL}$. These widths are expected to be equal if the isospin invariance holds in the inclusive D semileptonic decays. Therefore, the measurements of $\mathcal{B}(D \to X\ell^+\nu_\ell)$ will more precisely test the isospin invariance in the inclusive D semileptonic decays. Moreover, the improved knowledge of the inclusive D semileptonic decays is also helpful to the studies of the B meson decays.

With the Monte Carlo sample of about 800 pb^{-1} integrated luminosity at 3.773 GeV, we describe the analyses method for measurements of the branching fractions for the inclusive D semileptonic decays.

[6] By Hai-Long Ma, Hui-Hui Liu and Gang Rong

Overview of the studies of the inclusive D semileptonic decays

The branching fractions for the inclusive D semileptonic decays have been measured by many experiments [80, 81, 82, 83, 84, 85, 86]. The measured branching fractions for $D^0 \to Xe^+\nu_e$, $D^0 \to X\mu^+\nu_\mu$ and $D^+ \to Xe^+\nu_e$ are summarized in Table 24.17, Table 24.19 and Table 24.18, respectively, along with the numbers of signal events.

Particle Data Group (2006) averages the branching fractions to be [4] $\mathcal{B}(D^0 \to Xe^+\nu_e) = (6.87 \pm 0.28)\%$, $\mathcal{B}(D^0 \to X\mu^+\nu_\mu) = (6.5 \pm 0.8)\%$, and $\mathcal{B}(D^+ \to Xe^+\nu_e) = (17.2 \pm 1.9)\%$. These numbers give the relative errors 4.1% for $D^0 \to Xe^+\nu_e$, 12.3% for $D^0 \to X\mu^+\nu_\mu$, and 11.0% for $D^+ \to Xe^+\nu_e$. Recently, the CLEO Collaboration [85] have more precisely measured $\mathcal{B}(D \to Xe^+\nu_e)$ with about 281 pb^{-1} $\psi(3770)$ data. The precisions of the measured branching fractions have decreased to 3.3% for $D^0 \to Xe^+\nu_e$ and 2.4% for $D^+ \to Xe^+\nu_e$, including the systematic and statistical errors. On the other hand, there is always lack of the measurement of $\mathcal{B}(D \to X\mu^+\nu_\mu)$ during the past thirty years since the discoveries of the D mesons. This indicates more experimental measurements of $\mathcal{B}(D \to X\mu^+\nu_\mu)$ are drastically needed. Taking advantage of the unique capability of the μ counter on BESIII, we can measure $\mathcal{B}(D \to X\mu^+\nu_\mu)$ well.

Table 24.17: Summary of the measured branching fractions for $D^0 \to Xe^+\nu_e$ from different experiments, where ^{N} means that the measurement has not been used in average by PDG.

Experiments	Number of Events	Comment	$\mathcal{B}(D^0 \to Xe^+\nu_e)$ (%)
ARGUS [80]	1670	$e^+e^- \sim 10$ GeV	$6.9 \pm 0.3 \pm 0.5$
CLEOII[81]	4609	$e^+e^- \sim \Upsilon(4S)$	$6.64 \pm 0.18 \pm 0.29$
MARKIII[82]	137	e^+e^- 3.77 GeV	$7.5 \pm 1.1 \pm 0.4$
HYBR^N[83]		πp, pp 360, 400 GeV	15 ± 5
MARKII^N[84]	12	e^+e^- 3.771 GeV	5.5 ± 3.7
CLEOc^N[85]	2246	e^+e^- 3.773 GeV	$6.46 \pm 0.17 \pm 0.13$
PDG[4]			6.87 ± 0.28

Analysis method of the inclusive D semileptonic decays

We firstly reconstruct the singly tagged $\bar{D}$ mesons in hadronic modes. In the measurement of the branching fraction for $D^0 \to Xe^+\nu_e$, we only use the three hadronic decays $\bar{D}^0 \to K^+\pi^-$, $\bar{D}^0 \to K^+\pi^-\pi^0$ and $\bar{D}^0 \to K^+\pi^-\pi^-\pi^+$ for the reconstruction of the singly tagged $\bar{D}^0$ mesons, since the mode $\bar{D}^0 \to K^0\pi^+\pi^-$ can not determine the charm of the D^0 meson. In the measurement of the branching fraction for $D^+ \to Xe^+\nu_e$, we only use the hadronic decay $D^- \to K^+\pi^-\pi^-$ for the reconstruction of the singly tagged D^- mesons, due to the following two reasons. At first, the mode has less background. Secondly, among the hadronic modes with larger branching fractions, $D^- \to K^+\pi^-\pi^-$, $D^- \to K^+K^-\pi^-$, $D^- \to K^0\pi^-$, $D^- \to K^0\pi^-\pi^-\pi^+$, $D^- \to K^0\pi^-\pi^0$ and $D^- \to K^+\pi^-\pi^-\pi^0$, the number of the singly tagged D^- mesons reconstructed by $D^- \to K^+\pi^-\pi^-$ occupies more than 70% of that by the six modes.

Table 24.18: Summary of the measured branching fractions for $D^+ \to Xe^+\nu_e$ from different experiments, where ^{N} means that the measurement has not been used in average by PDG.

Experiments	Number of Events	Comment	$\mathcal{B}(D^+ \to Xe^+\nu_e)$ (%)
HYBR[83]		πp, pp 360, 400 GeV	20^{+9}_{-7}
MARKIII[82]	158	e^+e^- 3.77 GeV	$17.0 \pm 1.9 \pm 0.7$
MARKII [84]	23	e^+e^- 3.771 GeV	16.8 ± 6.4
DLCO^N[86]		e^+e^- 3.77 GeV	$22.0^{+4.4}_{-2.2}$
CLEOc^N[85]	8798	e^+e^- 3.773 GeV	$16.13 \pm 0.20 \pm 0.33$
PDG[4]			17.2 ± 1.9

Table 24.19: Summary of the measured branching fractions for $D^0 \to X\mu^+\nu_\mu$ from different experiments.

Experiments	Number of Events	Comment	$\mathcal{B}(D^0 \to X\mu^+\nu_\mu)$ (%)
ARGUS [80]	310	$e^+e^- \sim 10$ GeV	$6.0 \pm 0.9 \pm 1.2$
PDG[4]			6.5 ± 0.8

The resulting distributions of the beam-constraint masses of the $Kn\pi(n = 1, 2, 3)$ combinations for the singly tagged $\bar{D}$ modes are shown in Fig. 24.12. A maximum likelihood fit to the mass spectrum with a Gaussian function for the $\bar{D}$ signal and a special function [41, 42] for the background yields the number of the singly tagged $\bar{D}$ mesons for each mode. These give the total number of the reconstructed singly tagged $\bar{D}$ mesons, $N_{\bar{D}^0_{\rm tag}} = 465680 \pm 785$ and $N_{D^-_{\rm tag}} = 194780 \pm 508$.

In the system recoiling against the singly tagged $\bar{D}$, electron is selected from the surviving tracks. Kaon and pion may also pass the selection criteria for electron. Because the probability of misidentifying a pion as an electron at a given momentum is different from the probability of misidentifying a kaon to an electron, we also need know the yields of kaon and pion to subtract these background events from the electron sample. Kaons, pions (and electrons) are identified using the dE/dx, TOF (and EMC) measurements, with which the combined confidence levels CL_K, CL_π (and CL_e) for the kaon, pion (and electron) hypotheses is calculated. An electron candidate is required to have $CL_e > 0.001$, CL_π and CL_K. A kaon candidate is required to satisfy $CL_K > CL_\pi$. A pion candidate is required to have $CL_\pi > 0.001$.

We separate electrons, kaons and pions into right-sign and wrong-sign samples according to their charge correlation to the flavor tag. If the selected electron has the same charge as the kaon from the singly tagged $\bar{D}$ meson, it is defined as the right-sign electron; on the contrary, it is defined as the wrong-sign electron. Because the wrong-sign

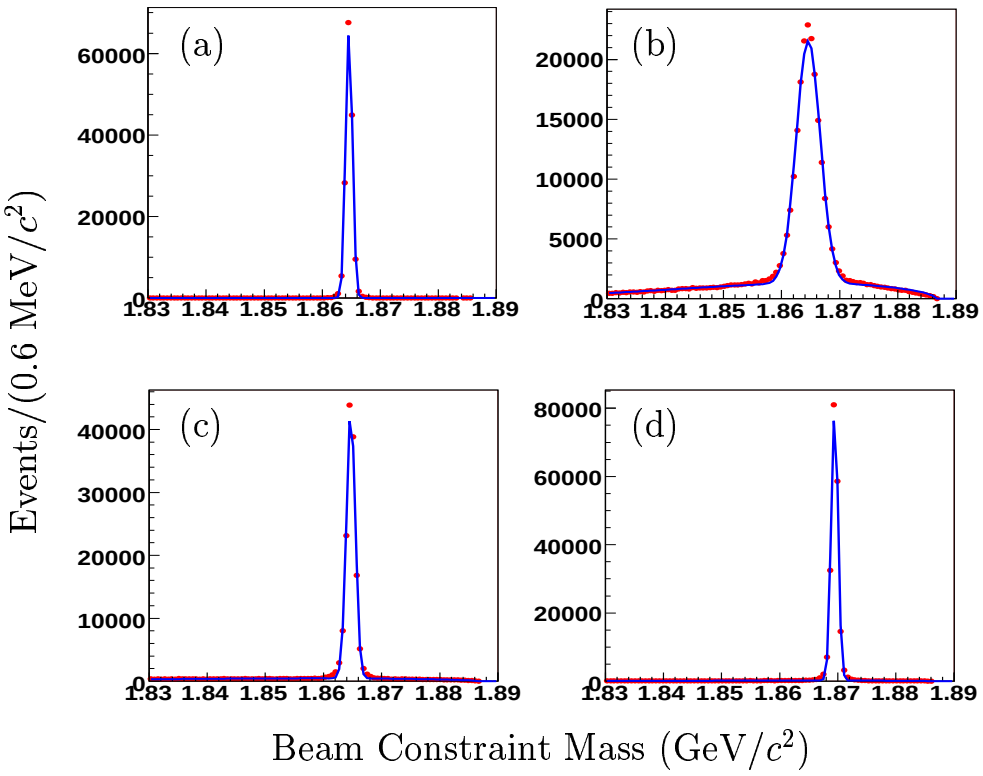

Figure 24.12: The beam constraint masses of the $Kn\pi$ combinations for the singly tagged $\bar{D}$ modes: (a) $\bar{D}^0 \to K^+\pi^-$, (b) $\bar{D}^0 \to K^+\pi^-\pi^0$, (c) $\bar{D}^0 \to K^+\pi^-\pi^-\pi^+$ and (d) $D^- \to K^+\pi^-\pi^-$.

electrons are completely from the background, these electrons can be used in the background estimation. The wrong-sign unfolded yield of electrons account for the the charge symmetric background, mostly produced by the decay $\pi^0 \to \gamma e^+ e^-$ and γ conversions. These background sources can be well represented by the wrong-sign electrons.

Fig. 24.13 show the fitted beam constraint masses for the $Kn\pi$ combinations of the events in which one right-sign or wrong-sign electron is observed in the system recoiling against the singly tagged $\bar{D}$ mesons. Because the detection efficiency for one particle and the probability of misidentifying one paricle as the other in a given momentum is different from each other, we divide momentum into n range. The yield $N_e^{\mathrm{obs},i}$ of electrons in the ith momentum range is obtained by fitting to the corresponding mass spectrum with a Gaussian function for the D^0 signal and a special function [41, 42] for the background. Similar analyses give the yields $N_K^{\mathrm{obs},i}$ and $N_\pi^{\mathrm{obs},i}$ of kaons and pions in each momentum range.

In the ith momentum range, the true number of electrons with the right-sign and wrong-sign samples are obtained through an unfolding procedure, using the matrix:

$$\begin{pmatrix} N_e^{\mathrm{obs},i} \\ N_K^{\mathrm{obs},i} \\ N_\pi^{\mathrm{obs},i} \end{pmatrix} = \begin{pmatrix} \epsilon_e^i & f_{\pi\to e}^i & f_{K\to e}^i \\ f_{e\to K}^i & \epsilon_K^i & f_{\pi\to K}^i \\ f_{e\to\pi}^i & f_{K\to\pi}^i & \epsilon_\pi^i \end{pmatrix} \begin{pmatrix} N_e^{\mathrm{real},i} \\ N_K^{\mathrm{real},i} \\ N_\pi^{\mathrm{real},i} \end{pmatrix},$$

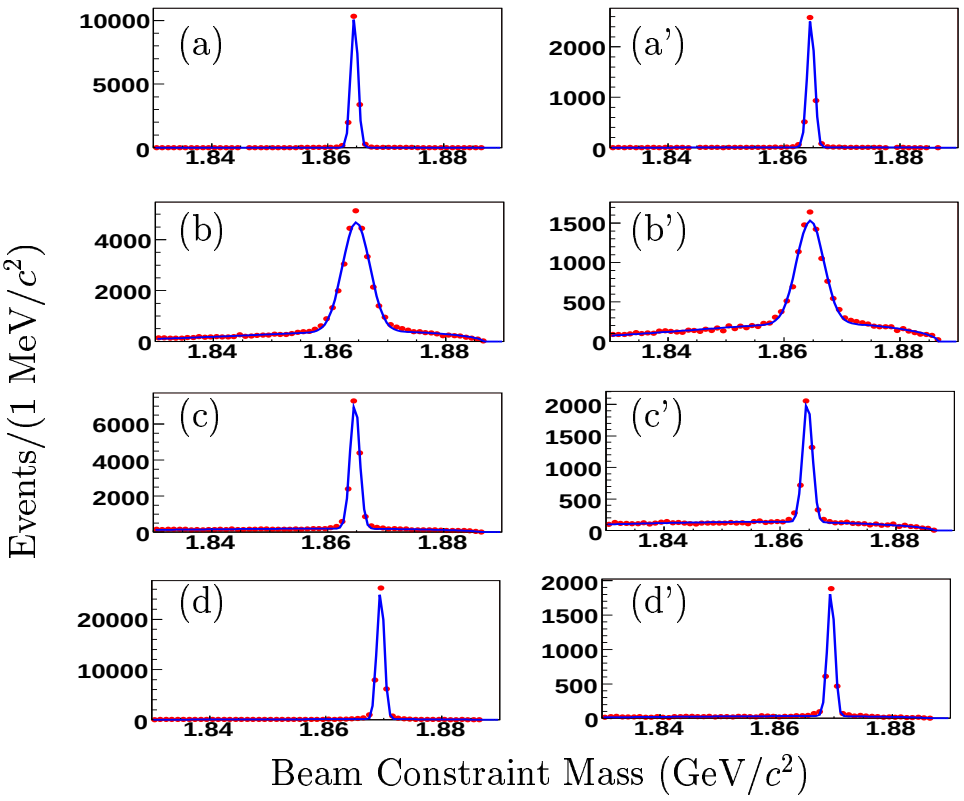

Figure 24.13: The fitted beam constraint masses for $Kn\pi$ combinations of the events in which one electron is observed in the system recoiling against the tagged $\bar{D}$: (a), (a') $\bar{D}^0 \to K^+\pi^-$; (b), (b') $\bar{D}^0 \to K^+\pi^-\pi^0$; (c), (c') $\bar{D}^0 \to K^+\pi^-\pi^-\pi^+$ and (d), (d') $D^- \to K^+\pi^-\pi^-$, where (a), (b), (c) and (d) are for the right-sign events, while (a'), (b'), (c') and (d') are for the wrong-sign events.

where $N_e^{\mathrm{obs},i}$, $N_K^{\mathrm{obs},i}$, $N_\pi^{\mathrm{obs},i}$ represent the numbers of the electrons, kaons and pions observed in the system recoiling against the singly tagged $\bar{D}$ meson; $N_e^{\mathrm{real},i}$, $N_K^{\mathrm{real},i}$, $N_\pi^{\mathrm{real},i}$ denote their corresponding true numbers; the efficiencies ϵ_e^i, ϵ_K^i, ϵ_π^i account for the losses due to track finding, track selection criteria, and particle identification; the off-diagonal element $f_{a\to b}^i$ is the probability of misidentifying the particle a as b. In the analyses for real data, the electron sample can be selected from the radiative Bhabha scattering events, the kaon and pion samples can be selected from $J/\psi \to \phi K^+K^-$ and $J/\psi \to \omega\pi^+\pi^-$ events. In the analyses for Monte Carlo simulation, the efficiencies and the misidentified probabilities can be determined by Monte Carlo simulation for each kind of track. Detail analyses of these particle samples give ϵ_e^i, ϵ_K^i, ϵ_π^i and $f_{a\to b}^i$ in each momentum range.

Subtracting the number $N_e^{\mathrm{real},i}(R)$ of right-sign electrons by the number $N_e^{\mathrm{real},i}(W)$ of wrong-sign electrons, we obtain the net number of electrons in ith momentum range,

$$N_e^{\mathrm{real},i}(net) = N_e^{\mathrm{real},i}(R) - N_e^{\mathrm{real},i}(W).$$

Adding the net number of electrons in each momentum range yields the total net number

$N^{\rm net}_{D\to X\ell^+\nu_\ell}$ of electrons,

$$N^{\rm net}_{D\to X\ell^+\nu_\ell} = \sum_i^n N_e^{{\rm real},i}(net).$$

Branching fractions

The branching fraction for the semileptonic decay $D \to X\ell^+\nu_\ell$ is determined by

$$\mathcal{B}(D \to X\ell^+\nu_\ell) = \frac{N^{\rm net}_{D\to X\ell^+\nu_\ell}}{N_{\bar{D}_{\rm tag}} \times \epsilon_{D\to X\ell^+\nu_\ell}}, \tag{24.67}$$

where $N^{\rm net}_{D\to X\ell^+\nu_\ell}$ is the net number of $D \to X\ell^+\nu_\ell$ events, $N_{\bar{D}_{\rm tag}}$ is the total number of the singly tagged D^- or $\bar{D}^0$ mesons, $\epsilon_{D\to X\ell^+\nu_\ell}$ is the detection efficiency for $D \to X\ell^+\nu_\ell$. The detection efficiency is estimated by the Monte Carlo events of $D \to X\ell^+\nu_\ell$ versus the singly tagged $\bar{D}$ mode. Here, $D \to X\ell^+\nu_\ell$ include all exclusive semileptonic decays. Similar analysis procedure as above gives the detection efficiency $\epsilon_{D\to X\ell^+\nu_\ell}$ for $D \to X\ell^+\nu_\ell$. Inserting these numbers in Eq. 24.67, we can obtain the branching fraction for the inclusive semileptonic decay.

In the measurement of the branching fraction for $D \to X\ell^+\nu_\ell$, the systematic error arises mainly from the uncertainties in electron tracking simulation and particle identification, the efficiencies and misidentified probabilities, and the number of the singly tagged $\bar{D}$ mesons. As we previously discussed, the statistical error in the measured $\mathcal{B}(D \to X\ell^+\nu_\ell)$ can be neglected in the case of 20 fb^{-1} $\psi(3770)$ data, while the systematic error is expected to reach 1.0% level.

Determination of the ratio $\frac{\Gamma^{\rm SL}_{D^+}}{\Gamma^{\rm SL}_{D^0}}$

Using the measured branching fractions for the inclusive D semileptonic decays $\mathcal{B}(D^+ \to X\ell^+\nu_\ell)$ and $\mathcal{B}(D^0 \to X\ell^+\nu_\ell)$, the well measured lifetimes of the D^+ and D^0 mesons, $\tau_{D^+} = (1040 \pm 7) \times 10^{-15}$ s and $\tau_{D^0} = (410.1 \pm 1.5) \times 10^{-15}$ s, the ratio of the two partial widths of the two inclusive semileptonic decays is determined by

$$R = \frac{\Gamma^{\rm SL}_{D^+}}{\Gamma^{\rm SL}_{D^0}} = \frac{\mathcal{B}(D^+ \to X\ell^+\nu_\ell)/\tau_{D^+}}{\mathcal{B}(D^0 \to X\ell^+\nu_\ell)\tau_{D^0}}. \tag{24.68}$$

In the determination of the ratio, the statistical error arising from the statistical error in the measured $\mathcal{B}(D \to X\ell^+\nu_\ell)$ can be neglected in the case of 20 fb^{-1} $\psi(3770)$ data. The systematic error arises from the systematic uncertainties in the measured lifetimes of D mesons, and in the uncanceled uncertainty in the measured branching fractions, where electron tracking simulation and particle identification can be canceled. It can be written as

$$\frac{\Delta R}{R} = \sqrt{\left(\frac{\Delta\tau_{D^+}}{\tau_{D^+}}\right)^2 + \left(\frac{\Delta\tau_{D^0}}{\tau_{D^0}}\right)^2 + \left(\frac{\Delta\mathcal{B}(D^+ \to X\ell^+\nu_\ell)}{\mathcal{B}(D^+ \to X\ell^+\nu_\ell)}\right)^2 + \left(\frac{\Delta\mathcal{B}(D^0 \to X\ell^+\nu_\ell)}{\mathcal{B}(D^0 \to X\ell^+\nu_\ell)}\right)^2}, \tag{24.69}$$

where the uncertainties in the lifetimes of D mesons are $\Delta\tau_{D^+}/\tau_{D^+} = 0.7\%$ and $\Delta\tau_{D^0}/\tau_{D^0} = 0.3\%$, the uncanceled uncertainty in each measured branching fraction is conservatively taken to be $\Delta\mathcal{B}(D \to X\ell^+\nu_\ell)/\mathcal{B}(D \to X\ell^+\nu_\ell) = 1.0\%$. These give the total systematic error to be 1.6%.

24.3 Combined Results and Impact on CKM Measurements

Chapter 25

Hadronic $D(D_S)$ decays[1]

25.1 Present Status and Implication for QCD

The SM's electroweak phenomenology of charm changing transitions appears dull with the CKM parameters well-known due to three-family unitarity constraints, $D^0 - \bar{D}^0$ oscillations being slow, **CP** asymmetries small at best and loop driven decays extremely rare with huge backgrounds due to long distance dynamics. Yet this very dullness can be utilized to gain new insights into nonperturbative dynamics, make progress in establishing theoretical control over them and calibrate our theoretical tools for B studies.

The issue at stake here is *not* whether QCD is the theory of the strong forces – there is no alternative – but our ability to perform calculations. Charm hadrons can act here as a bridge between the worlds of light flavours – as carried by u, d and s quarks with masses lighter or at most comparable to Λ_{QCD} and described by chiral perturbation theory – and that of the bona fide heavy b quark with $\Lambda_{QCD} \ll m_b$ treatable by heavy quark theory. Only lattice QCD (LQCD) carries the promise for a truly quantitative treatment of charm hadrons that can be improved *systematically*. Furthermore LQCD is the only framework available that allows to approach charm from lower as well as higher mass scales, which involves different aspects of nonperturbative dynamics and thus – if successful – would provide impressive validation.

At present such a program can be carried most explicitly for exclusive semileptonic decays of charm hadrons as described in detail in Sect.26.2, especially since lattice LQCD is reaching a stage where it can make rather accurate predictions for such modes. The theoretical challenges posed by nonleptonic decays are obviously more formidable. The complexities increase considerably for exclusive nonleptonic transitions, in particular due to the importance of final state interactions (FSI), which are much harder to bring under theoretical control even by using start-of-the-art LQCD.

Yet there are some strong motivations for obtaining a reliable description of exclusive nonleptonic charm decays:

- Their dynamics is largely determined by the transition region from the perturbative to the nonperturbative domain. Thus we can gain novel insights there. One should also not give up hope for a future theoretical breakthrough in LQCD (or the

[1] By Yue-Ling Wu and Ming Zhong

advent of another similarly powerful theoretical technology) allowing us to extract numerically reliable lessons.

- The most sensitive probes for New Physics are **CP** asymmetries in nonleptonic channels. The search strategies and subsequent interpretations depend on hadronic matrix elements, FSI and their phases. As already indicated we do not know how to compute them, yet one can profit here from a pragmatic exercise in 'theoretical engineering': providing a phenomenological, yet comprehensive framework for a host of charm modes allows to extract quantitative information on hadroniic matrix elements and FSI phases and evaluate their reliability through overconstraints. The huge datasets already obtained by the B factories, CLEO-c and BESII and to be further expanded including also future BESIII studies will be of essential help here.

- Analogous decays of B are being studied also as a mean to extract the complex phase of V_{ub}. One could hope that D decays might serve as a validation analysis.

- Carefully analysing branching ratios can teach us novel lessons on light-flavour hadron spectroscopy, like on characteristics of some resonances like the scalar mesons or on the η and η' mixing and a possible non-$\bar{q}q$ component in them.

25.2 Theoretical Review

25.2.1 The Effective Weak Hamiltonian

The theoretical description starts from constructing an effective $\Delta C \neq 0$ Hamiltonian through an operator product expansion (OPE) in terms of *local* operators O_i and their coefficients c_i:

$$\langle f|\mathcal{H}_{eff}|D\rangle = \frac{G_F}{\sqrt{2}} V_{CKM} \sum_i c_i(\mu)\langle f|O_i|D\rangle(\mu) \tag{25.1}$$

The *auxiliary* scale μ has been introduced – and this is a central element of the Wilsonian prescription for the OPE – to separate contributions from long and short distance dynamics: long distance $> 1/\mu >$ short distance. Degrees of freedom with typical mass scales above μ are integrated out into the coefficients c_i typically using perturbation theory, while degrees of freedom with scales below μ remain dynamical and are contained in the operators O_i. Nonperturbative dynamics enters through their hadronic expectation values.

Observables of course cannot depend on the choice μ at all. I.e., the μ dependence of the coefficients has to cancel against that of the matrix elements, when one does a complete calculation. Yet in practice one has to keep the following in mind:

- The perturbatively treated coefficients contain also the strong coupling α_S. To keep it in the perturbative domain, one needs

$$\mu \gg \Lambda_{QCD} \tag{25.2}$$

- Yet at the same time one does not want to choose too high a value for μ, since it also provides the momentum cut-off in the hadronic wave function with which the matrix element is evaluated.

These two contravening requirements can be met by $\mu \sim 1 - 1.5$GeV, which happens to be close to the charm quark mass. Thus $\mu = m_c$ provides a reasonable ansatz. In practice one has to rely on additional approximations of various kinds, which causes the computed rates to contain some sensitivity at least to μ, which can provide one gauge for the reliability of the result.

We do not know yet how to calculate these hadronic matrix elements from QCD's first principles in a numerically accurate way, although several different 'second generation' theoretical technologies have been brought to bear on them: $1/N_C$ expansions, QCD sum rules and lattice QCD. While there is reasonable hope that the latter will be validated in (semi)leptonic D decays, exclusive nonleptonic transitions provide qualitatively new challenges.

While in the SM the weak decays are driven by charged currents, the intervention of QCD affects the strength of the charged current product and induce a product of effective neutral currents in a way that depends on μ. For Cabibbo allowed transitions, one can write down the effective weak Lagragian

$$\mathcal{L}_{eff}^{\Delta C=1}(\mu = m_c) = -\frac{G_F}{\sqrt{2}} V_{ud} V_{cs}^* \cdot [c_- O_- + c_+ O_+] \ , \tag{25.3}$$

$$O_\pm = \frac{1}{2}\left[(\bar{s}_L \gamma_\nu c_L)(\bar{u}_L \gamma_\nu d_L)\right] \pm (\bar{u}_L \gamma_\nu c_L)(\bar{s}_L \gamma_\nu d_L)] \ , \tag{25.4}$$

which is conveniently rewritten as follows:

$$\mathcal{L}_{eff}^{\Delta C=1}(\mu = m_c) = -\frac{G_F}{\sqrt{2}} V_{ud} V_{cs}^* \cdot [c_1 O_1 + c_2 O_2] \ ,$$

$$O_1 = (\bar{s}_L \gamma_\nu c_L)(\bar{u}_L \gamma_\nu d_L) \ , \quad O_2 = (\bar{u}_L \gamma_\nu c_L)(\bar{s}_L \gamma_\nu d_L) \ , \tag{25.5}$$

with

$$c_1 = \frac{1}{2}(c_+ + c_-) \ , \quad c_2 = \frac{1}{2}(c_+ - c_-) \ . \tag{25.6}$$

Using different schemes one typically gets [87]:

$$c_1(m_c) = 1.25 \pm 0.03 \ , \quad c_2(m_c) = -0.48 \pm 0.05 \tag{25.7}$$

25.2.2 Factorization and First Generation Theoretical Technologies

All decay amplitudes can then be expressed as linear combinations of two terms:

$$\mathcal{A}(D \to f) \propto a_1 \langle f | J_\mu^{(ch)} J'^{(ch)\mu} | D \rangle + a_2 \langle f | J_\mu^{(neut)} J'^{(neut)\mu} | D \rangle \ , \tag{25.8}$$

with

$$a_1 = c_1 + \xi c_2 \ , \quad a_2 = c_2 + \xi c_1 \ . \tag{25.9}$$

It should be noted that the quantities c_1 and c_2 on one hand and ξ on the other are of *completely different* origin despite their common appearance in a_1 and a_2: while $c_{1,2}$ are determined by short-distance dynamics, ξ parametrizes the impact of long distance dynamics on the size of matrix elements including effects due to final state interactions (FSI). Eq.(25.9) contains two very important implicit assumptions, namely that the value of ξ is the same in the expression for a_1 and a_2 and that it does not depend on the final state.

A very convenient ansatz is to write the nonleptonic transition matrix element as a product of two simpler matrix elements [88]

$$\langle f|J_\mu J'^\mu|D\rangle \equiv \langle f_1 f_2|J_\mu J'^\mu|D\rangle \simeq \langle f_1|J_\mu|0\rangle\langle f_2|J'^\mu|D\rangle \ , \tag{25.10}$$

where f_1 and f_2 are "*effective particles*" that can contain any number of final state particles. The basic assumption here is that the colour flow mediated by gluon exchanges *between* the two 'clusters' $0 \to f_1$ and $D \to f_2$ can be ignored and all the strong interaction effects lumped into two simpler transition amplitudes. Clearly this factorization ansatz can be only an approximation rather than an identity. One should also note that Eq.(25.10) is μ dependent; i.e. changing the value of μ will transform factorized contributions into non-factorized ones and vice versa. The best chance for this ansatz to represent a decent approximation is for the separation scale μ to be around ordinary hadronic scales of about 1 GeV. This values happens to be close to m_c, yet that is a coincidence, since heavy quark masses are extraneous to QCD.

Besides these two types of diagrams which are usually referred as color favored and color suppressed diagrams, other types of considerations are the weak annihilation (WA) contributions including annihilation and exchange diagrams where the matrix element is approximately written as

$$\langle f_1 f_2|J_\mu J'^\mu|D\rangle \simeq \langle f_1 f_2|J_\mu|0\rangle\langle 0|J'^\mu|D\rangle \ . \tag{25.11}$$

Having assumed factorization we have greatly restricted the number of free parameters. The amplitudes $\langle f_1|J_{i\mu}|0\rangle$ and $\langle f_2|J_i^{\prime\mu}|D\rangle$ can be taken from data on (semi)leptonic D decays at least in principle though in practice that information is augmented by some theoretical arguments. The two quantities $a_{1,2}$ are then treated as free parameters fitted from experiment, although in practice again some theoretical judgment has to be applied concerning if and to which degree WA diagrams are included in addition to the spectator diagrams and corrections for FSI have to be applied.

Such an analysis was first carried out by Bauer, Stech and Wirbel from charmed meson two-body decays, yielding [89]

$$a_1|_{exp} \simeq 1.2 \pm 0.1 \ , \quad a_2|_{exp} \simeq -0.5 \pm 0.1 \tag{25.12}$$

to be compared with the theoretical expectations

$$a_1|_{QCD} \simeq 1.25 - 0.48\xi \ , \quad a_2|_{QCD} \simeq -0.48 + 1.25\xi \ . \tag{25.13}$$

It is remarkable that with just two fit parameters one can get a decent description of a host of nonleptonic rates. However one might say that those parameters have the wrong values: naively just counting colours one expects $\xi \simeq 1/N_C = 1/3$ and thus $a_1|_{QCD} \simeq 1.09$ and $a_2|_{QCD} \simeq -0.06$; for a_2 this is inconsistent with the experimental fit value. $\xi \simeq 0$ would reconcile Eqs.25.12 and 25.13.

25.2.3 The $1/N_C$ ansatz

The fit result $\xi \simeq 0$ leads to an intriguing speculation that these weak two-body decays can be described more rigorously through $1/N_C$ expansions [90]. They are invoked to calculate hadronic matrix elements. The procedure is the following: One employs the effective weak transition operator $\mathcal{L}_{eff}(\Delta C = 1)$ given explicitly in Eq.(25.3); since it describes short distance dynamics, one has kept $N_C = 3$ there. Then one expands the matrix element for a certain transition driven by this operators in $1/N_C$

$$\mathcal{A}(D \to f) = \langle f|\mathcal{L}_{eff}(\Delta C = 1)|D\rangle = \sqrt{N_C}\left(b_0 + \frac{b_1}{N_C} + \mathcal{O}(1/N_C^2)\right) . \qquad (25.14)$$

Using the rules for $1/N_C$ expansions, it is easy to show that the following simplifying properties hold for the contributions leading in $1/N_C$:

- one has to consider *valence* quark wave functions only;
- *factorization* holds;
- *WA* has to be ignored as have *FSI*.

To leading order in $1/N_C$ only the term b_0 is retained; then one has effectively $\xi = 0$ since $\xi \simeq 1/N_C$ represents a higher order contribution. However the next-to-leading term b_1 is in general beyond theoretical control. $1/N_C$ expansions therefore do not enable us to decrease the uncertainties *systematically*.

The $N_C \to \infty$ prescription is certainly a very compact one with transparent rules, and it provides not a bad first approximation – but not more. One can ignore neither FSI nor WA completely.

25.2.4 Treatment with QCD sum rules

A treatment of $D \to PP$ and $D \to PV$ decays based on a judicious application of QCD sum rules was developed in a series of papers [91]. The authors analyzed four-point correlation functions between the weak Lagrangian $\mathcal{L}(\Delta C = 1)$ and three currents. As usual an OPE is applied to the correlation function in the Euclidean region; nonperturbative dynamics is incorporated through condensates $\langle 0|m\bar{q}q|0\rangle$, $\langle 0|G \cdot G|0\rangle$ etc., the numerical values of which are extracted from other *light*-quark systems. They extrapolated their results to the Minkowskian domain through a (double) dispersion relation and succeed in finding a stability range for matching it with phenomenological hadronic expressions.

The analysis has some nice features:
⊕ It has a clear basis in QCD, and includes, in principle at least, nonperturbative dynamics in a well-defined way.
⊕ It incorporates different quark-level processes – external and internal W emission, WA and Pauli interference – in a natural manner.
⊕ It allows to include nonfactorizable contributions systematically.

In practice, however, it suffers from some shortcomings at the same time:
⊖ The charm scale is not sufficiently high that one could have full confidence in the various extrapolations undertaken.

$\ominus$ To make these very lengthy calculations at all manageable, some simplifying assumptions had to be made, like $m_u = m_d = m_s = 0$ and $SU(3)_{Fl}$ breaking beyond $m_K > m_\pi$ had to be ignored; in particular $\langle 0|\bar{s}s|0\rangle = \langle 0|\bar{d}d|0\rangle = \langle 0|\bar{u}u|0\rangle$ was used. Thus one cannot expect $SU(3)_{Fl}$ breaking to be reproduced correctly.
$\ominus$ *Prominent* FSI that vary rapidly with the energy scale – like effects due to narrow resonances - cannot be described in this treatment; for an extrapolation from the Euclidean to the Minkowskian domain amounts to some averaging or 'smearing' over energies.

A statement that the predictions did not provide an excellent fit to the data on about twenty-odd D^0, D^+ and D_s^+ modes – while correct on the surface, especially when $SU(3)_{Fl}$ breaking is involved – misses the main point:

- No a priori model assumption like factorization had to be made.
- The theoretical description does not contain any free parameters in principle, though in practice there is leeway in the size of some decay constants.

25.2.5 Modern Developments

As the data improved, the BSW prescription became inadequate, however most subsequent attempts to describe nonleptonic decays in the D system – except for the sum rules approach sketched above – use the assumption of naive factorization as a starting point.

Improvements and generalizations of the BSW description have been made in three areas:

1. Different parameterizations for the q^2 dependence of the form factors are used and different evaluations of their normalization are made. This is similar to what was addressed in our discussion of exclusive semileptonic decays. One appealing suggestion has been suggested to use only those expressions for form factors that asymptotically – i.e. for m_c, $m_s \to \infty$ – exhibit heavy quark symmetry.
2. Attempts have been made to incorporate FSI more reliably. Non-factorized contributions in general have been considered.
3. Contributions due to WA and Penguin operators have been included.

Two frameworks that are more firmly based on QCD than quark models have been developed to treat two-body decays of B mesons, namely 'QCD factorization' [92] and 'pQCD' [93]. While there is little reason to expect the more aggressive pQCD approach to work already for charm decays, a treatment based on QCD factorization is worth a try despite the charm mass barely exceeding ordinary hadronic scales. To illustrate the present status the branching ratios of $D \to \pi\pi$ decays as inferred from naive factorization

and QCD factorization approaches are listed here [94]:

$$BR(D^0 \to \pi^+\pi^-) = \begin{cases} 1.86 \times 10^{-3} , & (Naive\ \ Factorization) \\ 1.69 \times 10^{-3} , & (QCD\ \ Factorization) \\ (1.364 \pm 0.032) \times 10^{-3} , & (PDG06[4]) \end{cases}$$

$$BR(D^+ \to \pi^+\pi^0) = \begin{cases} 1.68 \times 10^{-3} , & (Naive\ \ Factorization) \\ 1.94 \times 10^{-3} , & (QCD\ \ Factorization) \\ (1.28 \pm 0.09) \times 10^{-3} , & (PDG06[4]) \end{cases}$$

$$BR(D^0 \to \pi^0\pi^0) = \begin{cases} 2.44 \times 10^{-5} , & (Naive\ \ Factorization) \\ 2.06 \times 10^{-5} , & (QCD\ \ Factorization) \\ (7.9 \pm 0.8) \times 10^{-4} . & (PDG06[4]) \end{cases}$$

Both the naive factorization and the QCD factorization predictions on $D^0 \to \pi^+\pi^-$ and $D^+ \to \pi^+\pi^0$ can accommodate the experimental results to the same order, while the prediction on $D^0 \to \pi^0\pi^0$ is about forty times smaller than the experimental result. For proper perspective one should note that the modes $D^0 \to \pi^+\pi^-$ and $D^+ \to \pi^+\pi^0$ are described by color *favored* tree diagram T, whereas $D^0 \to \pi^0\pi^0$ is dominated by a color *suppressed* tree diagram C. Non-factorizable corrections are found to be larger for the latter and at present are beyond theoretical control.

In summary, a theoretical description of exclusive nonleptonic decays of charmed mesons based on general principles is not yet possible. Even though the short distance contributions can be calculated and the effective weak Hamiltonian has been constructed at next-to-leading order, the evaluation of its matrix elements requires nonperturbative techniques. Some decent phenomenological descriptions have been achieved, yet realistically few frameworks can provide some openings for systematic improvements, especially when they are applied to multi-body channels.

25.2.6 Symmetry Analysis

Isospin SU(2) Symmetry

Symmetry based arguments are a powerful tool in our theoretical arsenal. Isospin invariance should hold on the $\mathcal{O}(1\%)$ level, and no evidence to the contrary has been found. Take two-body decays as an example, it leads to triangle relations among the decay amplitudes:

$$\mathcal{A}(D^0 \to \pi^+\pi^-) + \sqrt{2}\mathcal{A}(D^0 \to \pi^0\pi^0) - \sqrt{2}\mathcal{A}(D^+ \to \pi^+\pi^0) = 0 , \quad (25.15)$$

$$\mathcal{A}(D^0 \to K^-\pi^+) + \sqrt{2}\mathcal{A}(D^0 \to \bar{K}^0\pi^0) - \mathcal{A}(D^+ \to \bar{K}^0\pi^+) = 0 , \quad (25.16)$$

$$\mathcal{A}(D^0 \to \pi^+K^{*-}) + \sqrt{2}\mathcal{A}(D^0 \to \pi^0\bar{K}^{*0}) - \mathcal{A}(D^+ \to \pi^+\bar{K}^{*0}) = 0 , \quad (25.17)$$

$$\mathcal{A}(D^0 \to \rho^+K^-) + \sqrt{2}\mathcal{A}(D^0 \to \rho^0\bar{K}^0) - \mathcal{A}(D^+ \to \bar{K}^0\rho^+) = 0 . \quad (25.18)$$

The measured rates tell us that these amplitudes possess large relative phases due to strong FSI. Considering the three $D \to \pi\pi$ modes, the transition amplitudes can be

decomposed into

$$\mathcal{A}(D^0 \to \pi^+\pi^-) = \sqrt{\tfrac{2}{3}}\mathcal{A}_0 + \sqrt{\tfrac{1}{3}}\mathcal{A}_2 \ , \tag{25.19}$$

$$\mathcal{A}(D^0 \to \pi^0\pi^0) = \sqrt{\tfrac{1}{3}}\mathcal{A}_0 - \sqrt{\tfrac{2}{3}}\mathcal{A}_2 \ , \tag{25.20}$$

$$\mathcal{A}(D^+ \to \pi^+\pi^0) = \sqrt{\tfrac{3}{2}}\mathcal{A}_2 \ . \tag{25.21}$$

The subscripts 0 and 2 of the $\mathcal{A}$ describe the isospin $I = 0$ and 2 part of the $\pi\pi$ system. From the experimental data, the amplitude ratio $|A_2/A_0|$ and the relative phase $\delta = \delta_2 - \delta_0$ were extracted [95]

$$|A_2/A_0| = 0.72 \pm 0.13 \pm 0.11 \ , \quad \cos\delta = 0.14 \pm 0.13 \pm 0.09 \ . \tag{25.22}$$

Flavor SU(3) Symmetry and Its Breaking

It would seem tempting to argue that SU(3) flavor symmetry holds to within, say, 20 - 30 %. This, however, does not seem to be the case, at least not for exclusive channels, as can be read off most dramatically from the following comparison

$$\frac{\mathcal{A}(D^0 \to K^+K^-)}{\mathcal{A}(D^0 \to \pi^+\pi^-)} \simeq 1.8 \tag{25.23}$$

rather than unity. The significant SU(3) symmetry violation may come from the finite strange quark mass, FSI and resonances [96]. There are indications, however, that for inclusive rates SU(3) flavor breaking does not exceed the 20% level [97].

25.3 Two-Body Decays

Two-body modes in charmed meson nonleptonic decays have been drawn much attention since 1980s because they have the following advantages, as compared with multi-body ones, that put them to a heated place:

- The nonleptonic decays of charm mesons have been observed to proceed mainly through two-body channels, if one counts resonances as one body. A great number of precise experimental data on two-body decays, including branching ratios of about 60 decay modes, have been accumulated in the *Particle Data Group* [4].

- The phase space is trivial and the number of form factors are quite limited.

- There are less colour sources in the form of quarks and antiquarks, less different combinations for colour flux tubes to form.

- Quite a number of two-body modes allow for sizeable momentum transfers thus hopefully reducing the predominance of long-distance dynamics.

- They are one class of nonleptonic decays where one can harbor reasonable hope of some success. It is not utopian to expect lattice QCD to treat these transitions some day in full generality. Such results will however be reliable only, if obtained with incorporating fully dynamical fermions – i.e. without "quenching" and without relying on a $1/m_c$ expansion.

25.3.1 Kinematics and Topologies of Amplitudes

In the center-of-mass frame, the differential decay rate for n-body charmed meson decay is

$$d\Gamma = \frac{1}{2m_D}(\prod_{i=1}^{n}\frac{d^3p_i}{(2\pi)^3}\frac{1}{2E_i})|\mathcal{A}(m_D \to \{p_1, p_2, \cdots, p_n\})|^2(2\pi)^4\delta^4(p_D - \sum_{i=1}^{n} p_i). \quad (25.24)$$

If the number of final state particles is set to two, one can easily conduct the integral over the phase space to obtain the decay rate

$$\Gamma(D \to f_1 f_2) = \frac{p}{8\pi M_D^2}|\mathcal{A}|^2 \ , \quad (25.25)$$

where

$$p = \frac{\sqrt{(M_D^2 - (m_1 + m_2)^2)(M_D^2 - (m_1 - m_2)^2)}}{2M_D}$$

denotes the center-of-mass 3-momentum of each final particle. The branching fraction of $D \to f_1 f_2$ transition is then defined as the ratio of the decay rate to the full width of D meson

$$B(D \to f_1 f_2) = \frac{\Gamma(D \to f_1 f_2)}{\Gamma(D)} \ . \quad (25.26)$$

The amplitude $\mathcal{A}$ can be decomposed into six distinct quark-graph topologies [98]: (1) color-favored tree amplitude T, (2) color-suppressed tree amplitude C, (3) W-exchange amplitude E, (4) W-annihilation amplitude A, (5) horizontal W-loop amplitude P and (6) vertical W-loop amplitude D. The penguin diagrams P and D play little role in practice because the relation of the CKM matrix elements $V_{cs}^* V_{us} \approx -V_{cd}^* V_{ud}$ will result in cancellations among them.

25.3.2 $D \to PP$, $D \to PV$ and $D \to VV$ Decays

Among the measured experimental data on charm nonleptonic two-body decays, charmed mesons decaying to two pseudoscalar mesons ($D \to PP$), to one pseudoscalar and one vector meson ($D \to PV$) and to two vector mesons ($D \to VV$) are of dominant quality. The light pseudoscalar and vector mesons are two classes of particles that have been made clear on their basic properties like mass, lifetime, width, quark component and decay rate. The form factors of charmed mesons transiting to light pseudoscalar and vector mesons have been calculated in a variety of theoretical models. Based on the resulting form factors, most predictions on charmed meson semileptonic decays are consistent with experimental data, as shown in Section 26.2. As a result, it is an ideal place to test

the factorization assumption and understand the mysteries of FSI and unfactorizable contributions.

Provided that the definitions of form factors are adopted as in Equations (26.36) and (26.42), the four relevant amplitudes for $D \to P_1P_2$ in the formalism of factorization approach read

$$T = i\frac{G_F}{\sqrt{2}}V_{q_1q_2}V^*_{cq_3}a_1 f_{P_1}(m_D^2 - m_2^2)F_0^{D\to P_2}(m_1^2), \tag{25.27}$$

$$C = i\frac{G_F}{\sqrt{2}}V_{q_1q_2}V^*_{cq_3}a_2 f_{P_1}(m_D^2 - m_2^2)F_0^{D\to P_2}(m_1^2), \tag{25.28}$$

$$E = i\frac{G_F}{\sqrt{2}}V_{q_1q_2}V^*_{cq_3}a_2 f_D(m_1^2 - m_2^2)F_0^{P_1P_2}(m_D^2), \tag{25.29}$$

$$A = i\frac{G_F}{\sqrt{2}}V_{q_1q_2}V^*_{cq_3}a_1 f_D(m_1^2 - m_2^2)F_0^{P_1P_2}(m_D^2). \tag{25.30}$$

The amplitudes for $D \to PV$ are a little more complicated than $D \to PP$, for one should distinguish the pseudoscalar or the vector final state where the spectator quark enters. Using a subscript P or V to denote the spectator quark containing in pseudoscalar or vector final meson, one can read out the amplitudes

$$T_V = 2\frac{G_F}{\sqrt{2}}V_{q_1q_2}V^*_{cq_3}a_1 f_P m_V(\varepsilon^*\cdot p_D)A_0^{D\to V}(m_P^2), \tag{25.31}$$

$$T_P = 2\frac{G_F}{\sqrt{2}}V_{q_1q_2}V^*_{cq_3}a_1 f_V m_V(\varepsilon^*\cdot p_D)F_+^{D\to P}(m_V^2), \tag{25.32}$$

$$C_V = 2\frac{G_F}{\sqrt{2}}V_{q_1q_2}V^*_{cq_3}a_2 f_P m_V(\varepsilon^*\cdot p_D)A_0^{D\to V}(m_P^2), \tag{25.33}$$

$$C_P = 2\frac{G_F}{\sqrt{2}}V_{q_1q_2}V^*_{cq_3}a_2 f_V m_V(\varepsilon^*\cdot p_D)F_+^{D\to P}(m_V^2), \tag{25.34}$$

$$E = 2\frac{G_F}{\sqrt{2}}V_{q_1q_2}V^*_{cq_3}a_2 f_D m_V(\varepsilon^*\cdot p_D)A_0^{PV}(m_D^2), \tag{25.35}$$

$$A = 2\frac{G_F}{\sqrt{2}}V_{q_1q_2}V^*_{cq_3}a_1 f_D m_V(\varepsilon^*\cdot p_D)A_0^{PV}(m_D^2). \tag{25.36}$$

The decay modes of charm to two vector meson final states have a richer structure

than the decays with at least one pseudoscalar in the final state.

$$\begin{aligned} T(D\to V_1V_2) &= \frac{G_F}{\sqrt{2}}V_{q_1q_2}V^*_{cq_3}a_1[if_{V_1}m_1(m_D+m_2)A_1^{D\to V_2}(m_1^2)\varepsilon_1^*\cdot\varepsilon_2^* \\ &\quad -i\frac{1}{m_D+m_2}f_{V_1}m_1A_2^{D\to V_2}(m_1^2)\varepsilon_1^*\cdot(p_D+p_2)\varepsilon_2^*\cdot(p_D-p_2) \\ &\quad -\frac{2}{m_D+m_2}f_{V_1}m_1V^{D\to V_2}(m_1^2)\epsilon_{\mu\nu\alpha\beta}\varepsilon_1^{*\mu}\varepsilon_2^{*\nu}p_D^\alpha p_2^\beta]\ , \end{aligned} \tag{25.37}$$

$$\begin{aligned} C(D\to V_1V_2) &= \frac{G_F}{\sqrt{2}}V_{q_1q_2}V^*_{cq_3}a_2[if_{V_1}m_1(m_D+m_2)A_1^{D\to V_2}(m_1^2)\varepsilon_1^*\cdot\varepsilon_2^* \\ &\quad -i\frac{1}{m_D+m_2}f_{V_1}m_1A_2^{D\to V_2}(m_1^2)\varepsilon_1^*\cdot(p_D+p_2)\varepsilon_2^*\cdot(p_D-p_2) \\ &\quad -\frac{2}{m_D+m_2}f_{V_1}m_1V^{D\to V_2}(m_1^2)\epsilon_{\mu\nu\alpha\beta}\varepsilon_1^{*\mu}\varepsilon_2^{*\nu}p_D^\alpha p_2^\beta]\ . \end{aligned} \tag{25.38}$$

The terms proportional to A_1, A_2 and V represent S, longitudinal D and P waves respectively. The omitted expressions for exchange and annihilation topologies contain the vector-to-vector form factor.

Due to the historical phenomenological analysis, we can draw some general conclusions on the above factorization formalism, which serve as guides for the studies of the other charmed meson decay modes like two-body final states containing scalar (S), axial-vector (A), tensor (T) and multi-body final states.

- Nonfactorizable corrections which result from spectator interactions, FSI, resonance effects and so on are found to be significant [99]. Some phenomenological models based on one-particle-exchange method [100], resonance formation [101], the combination of heavy quark effective theory and chiral perturbation theory [102] have been developed to make some insights into them. The resonance formation via $q\bar{q}$ resonances is probably the most important one to hadronic charm decays owing to the existence of an abundant spectrum of resonances known to exist at energy close to the mass of charmed mesons. Most of the properties of resonances follow from unitarity so that the effects of resonance-induced nonfactorizable contributions can be described in a model independent manner in terms of the masses and the decay widths of the nearby resonances [103].

- The parameters a_1 and a_2 were found to be not universal but process or class dependent. For illustration purposes, we take some examples

$$a_1(\mu) = c_1(\mu) + (\frac{1}{N_c} + \chi_1(\mu))c_2(\mu)\ , \tag{25.39}$$

$$a_2(\mu) = c_2(\mu) + (\frac{1}{N_c} + \chi_2(\mu))c_1(\mu)\ , \tag{25.40}$$

with $\chi_1(\mu)$ and $\chi_2(\mu)$ partially denoting nonfactorizable effects in the case of $N_c = 3$. $\chi_2(\mu)$ was determined to be [104]

$$\begin{aligned} &\chi_2(D\to\bar{K}\pi) \simeq -0.33\ , \\ &\chi_2(D\to\bar{K}^*\pi) \simeq -(0.45\sim 0.55)\ , \\ &\chi_2(D\to\bar{K}^*\rho) \simeq -(0.6\sim 0.65)\ . \end{aligned} \tag{25.41}$$

- The light meson to light meson form factors involving in the above formula are believed to be negligibly small. Thus the factorizable formalism of the exchange and annihilation diagrams make no effect on the overall amplitudes. The main contributions of these diagrams may result from the nonfactorizable parts. Through intermediate states, they relate to the tree diagram T and color-suppressed diagram C [103, 105]. As a consequence, they have sizable magnitudes comparable to the T and C amplitudes and large strong phases relative to the T amplitude as illustrated in a SU(3) flavor symmetry analysis [106, 107]. Especially in the case of decay mode $D^0 \to K^0\overline{K}^0$ which transits thoroughly through $E-E$ diagram representation, the factorizable contribution is too trivial to be consistent with the experimental branching ratio $B = (7.1 \pm 1.9) \times 10^{-4}$. Many studies have been perform on this decay [108] and it is found that the nonfactorizable correction of E diagram can account for experimental data to the same order.

A variety of charmed meson decay processes calculated in some literatures are presented in Table 25.1 for $D \to PP$ decays and in Table 25.2 for $D \to PV$ decays. It is noted that all of these considerations have introduced more or less free parameters to describe the nonfactorizable contributions and need to be fitted out from experiments. For $D \to VV$ decays, some research articles in ten years ago can be found in [102, 111, 112, 113].

25.3.3 $D \to SP$ Decays

Scalar meson production measurements in charm decays are now available from the dedicated experiments conducted at ARGUS [114], CLEO [115], E687 [116], E691 [117], E791 [118], FOCUS [119], and BaBar [120]. Specifically, the decays $D \to f_0\pi(K)$, $D \to a_0\pi(K)$, $D \to \overline{K}_0^*\pi$ and $D^+ \to \sigma\pi^+$ have been observed through Dalitz plot analysis of three-body decays. The results of various experiments are summarized in Table 25.3 where the products of $\mathcal{B}(D \to SP_3)$ and $\mathcal{B}(S \to P_1P_2)$ are listed. In order to extract the branching ratios for $D \to f_0P$, one shall use the the result from a recent analysis [121]: $\Gamma(f_0 \to \pi\pi) = (64 \pm 8)MeV$, $\Gamma(f_0 \to K\overline{K}) = (12 \pm 1)MeV$ and $\Gamma_{f_0\ total} = (80 \pm 10)MeV$. Therefore, one has

$$\mathcal{B}(f_0(980) \to K^+K^-) = 0.08 \pm 0.01\,, \qquad \mathcal{B}(f_0(980) \to \pi^+\pi^-) = 0.53 \pm 0.09 \quad (25.42)$$

For $D \to a_0P$, one can apply the PDG average $\Gamma(a_0 \to K\overline{K})/\Gamma(a_0 \to \pi\eta) = 0.183 \pm 0.024$ [4] to obtain

$$\begin{aligned} \mathcal{B}(a_0^0(980) \to \pi^0\eta) &= 0.845 \pm 0.017 \\ \mathcal{B}(a_0^+(980) \to K^+\overline{K}^0) &= \mathcal{B}(a_0^-(980) \to K^-K^0) = 0.155 \pm 0.017\,, \\ \mathcal{B}(a_0^0(980) \to K^+K^-) &= 0.078 \pm 0.009\,. \end{aligned} \quad (25.43)$$

For $D \to K_0^*(1430)P$, $\mathcal{B}(K_0^*(1430) \to K^+\pi^-) = \frac{2}{3}(0.93 \pm 0.10)$ can be put to application [4]. It is worth noting that some of the scalar meson decays are not shown in PDG. More precise measurements of these branching ratios are of great importance for studies of charmed meson to scalar meson transitions.

Table 25.1: *Predicted branching ratios for $D \to PP$ (in 10^{-2}). Most decay modes involving a neutral K meson are given as K^0_S in PDG06 instead of $\overline{K}^0$ in PDG04 which are presented here as well.*

Decay Modes	Buccella *et al.* [109]	Du *et al.*[100]	Wu *et al.* [110]	PDG 06/04
$D^0 \to K^-\pi^+$	3.847	3.72	3.79 ; 3.80	3.80 ± 0.07
$\to \overline{K}^0\pi^0$	1.310	2.09	2.27 ; 2.24	2.28 ± 0.22 ($pdg04$)
				1.14 ± 0.12
$\to \overline{K}^0\eta$			0.80 ; 0.81	0.76 ± 0.11 ($pdg04$)
				0.38 ± 0.06
$\to \overline{K}^0\eta'$			1.85 ; 1.88	1.87 ± 0.28 ($pdg04$)
				0.91 ± 0.14
$\to \pi^+\pi^-$	0.151	0.149	0.144 ; 0.144	0.1364 ± 0.0032
$\to \pi^0\pi^0$	0.115	0.106	0.078 ; 0.097	0.079 ± 0.008
$\to K^+K^-$	0.424	0.40	0.413 ; 0.413	0.384 ± 0.010
$\to K^0\overline{K}^0$	0.130	0.0573	0.069 ; 0.062	0.071 ± 0.019 ($pdg04$)
				0.037 ± 0.007
$\to K^+\pi^-$	0.033	0.0141	0.0150 ; 0.0151	0.0143 ± 0.0004
$\to \eta\pi^0$			0.069 ; 0.068	0.056 ± 0.014
$\to \eta'\pi^0$			0.088 ; 0.091	—
$\to \eta\eta$			0.011 ; 0.016	—
$\to \eta\eta'$			0.026 ; 0.030	—
$\to K^0\pi^0$	0.008	0.0284	0.002 ; 0.005	—
$\to K^0\eta$			0.001 ; 0.002	—
$\to K^0\eta'$			0.0 ; 0.0	—
$D^+ \to \overline{K}^0\pi^+$	2.939		2.76 ; 2.76	2.77 ± 0.18 ($pdg04$)
				1.47 ± 0.06
$\to \pi^+\pi^0$	0.185	0.18	0.25 ; 0.19	0.128 ± 0.009
$\to \eta\pi^+$			0.34 ; 0.37	0.35 ± 0.032
$\to \eta'\pi^+$			0.45 ; 0.42	0.53 ± 0.11
$\to K^+\overline{K}^0$	0.764	0.64	0.62 ; 0.62	0.58 ± 0.06 ($pdg04$)
				0.296 ± 0.019
$\to K^0\pi^+$	0.053	0.0756	0.012 ; 0.026	—
$\to K^+\pi^0$	0.055	0.0296	0.021 ; 0.023	< 0.042
$\to K^+\eta$			0.011 ; 0.012	—
$\to K^+\eta'$			0.005 ; 0.006	—
$D_s^+ \to \overline{K}^0K^+$	4.623		3.06 ; 3.13	4.4 ± 0.9
$\to \pi^+\eta$	1.131		1.05 ; 1.09	2.11 ± 0.35
$\to \pi^+\eta'$			4.19 ; 4.43	4.7 ± 0.7
$\to \pi^+K^0$	0.373		0.24 ; 0.26	< 0.9
$\to \pi^0K^+$	0.146		0.047 ; 0.090	—
$\to \eta K^+$	0.300		0.055 ; 0.040	—
$\to \eta'K^+$			0.090 ; 0.102	—
$\to K^+K^0$	0.012		0.014 ; 0.010	—

Table 25.2: *Predicted branching ratios for $D \to PV$ (in 10^{-2}). Most decay modes involving a neutral K meson are given as K^0_S in PDG06 instead of $\overline{K}^0$ in PDG04 which are presented here as well.*

Decay Modes	Buccella *et al.* [109]	Du *et al.*[100]	Wu *et al.* [110]	PDG 06/04
$D^0 \to K^{*-}\pi^+$	4.656	5.22	5.93 ; 5.97	5.9 ± 0.4 ($pdg04$)
$\to K^-\rho^+$	11.201	11.1	9.99 ; 9.90	10.1 ± 0.8 ($pdg04$)
$\to \overline{K}^{*0}\pi^0$	3.208	2.72	2.72 ; 2.81	2.8 ± 0.4 ($pdg04$)
$\to \overline{K}^0\rho^0$	0.759	1.25	1.49 ; 1.25	$1.55^{+0.12}_{-0.16}$ ($pdg04$)
$\to \overline{K}^{*0}\eta$			1.50 ; 1.94	1.8 ± 0.4 ($pdg04$)
$\to \overline{K}^0\omega$	1.855		2.11 ; 1.80	2.3 ± 0.4 ($pdg04$)
				1.1 ± 0.2
$\to \overline{K}^0\phi$			0.95 ; 0.90	0.94 ± 0.11 ($pdg04$)
$\to K^+K^{*-}$	0.290		0.25 ; 0.25	0.20 ± 0.11
$\to K^-K^{*+}$	0.431		0.43 ; 0.43	0.37 ± 0.08
$\to K^0\overline{K}^{*0}$	0.052		0.08 ; 0.16	< 0.17 ($pdg04$)
				< 0.08
$\to \overline{K}^0K^{*0}$	0.062		0.08 ; 0.16	< 0.09 ($pdg04$)
				< 0.04
$\to \pi^0\phi$	0.105		0.12 ; 0.12	0.074 ± 0.005
$\to \overline{K}^{*0}\eta'$			0.004 ; 0.003	< 0.10 ($pdg04$)
$\to \eta\phi$			0.035 ; 0.034	0.014 ± 0.004
$\to \pi^+\rho^-$	0.485	0.36	0.34 ; 0.35	0.45 ± 0.04
$\to \pi^-\rho^+$	0.706	0.73	0.62 ; 0.61	1.0 ± 0.06
$\to \pi^0\rho^0$	0.216	0.11	0.19 ; 0.16	0.32 ± 0.04
$\to \pi^0\omega$	0.013		0.020 ; 0.003	< 0.026
$\to \eta\omega$			0.13 ; 0.10	
$\to \eta'\omega$			0.0007 ; 0.0003	
$\to \eta\rho^0$			0.0039 ; 0.0015	
$\to \eta'\rho^0$	0.039		0.012 ; 0.009	
$\to K^{*+}\pi^-$	0.025		0.029 ; 0.029	
$\to K^+\rho^-$	0.004		0.016 ; 0.016	
$\to K^{*0}\pi^0$	0.008		0.0052 ; 0.0064	
$\to K^0\rho^0$			0.0069 ; 0.0059	
$\to K^{*0}\eta$			0.0030 ; 0.0041	
$\to K^{*0}\eta'$			0.0 ; 0.0	
$\to K^0\omega$	0.002		0.0076 ; 0.0056	
$\to K^0\phi$			0.0 ; 0.0006	

Table 25.2: (*continued) Predicted branching ratios for $D \to PV$ (in 10^{-2}). Most decay modes involving a neutral K meson are given as K^0_S in PDG06 instead of $\overline{K}^0$ in PDG04 which are presented here as well.*

Decay Modes	Buccella *et al.* [109]	Du *et al.*[100]	Wu *et al.* [110]	PDG 06/04
$D^+ \to \overline{K}^{*0}\pi^+$	1.996	1.93	1.96 ; 1.96	1.95 ± 0.19 (*pdg*04)
$\to \pi^+\phi$	0.619		0.64 ; 0.62	0.65 ± 0.07
$\to \overline{K}^0\rho^+$	12.198	7.01	7.56 ; 8.43	6.6 ± 2.5 (*pdg*04)
$\to \pi^+\rho^0$	0.104	0.13	0.088 ; 0.088	0.107 ± 0.011
$\to K^+\overline{K}^{*0}$	0.436		0.44 ; 0.44	0.43 ± 0.06 (*pdg*04)
$\to \overline{K}^0 K^{*+}$	1.515		1.43 ; 1.25	3.1 ± 1.4 (*pdg*04)
				1.6 ± 0.7
$\to K^+\rho^0$	0.029		0.030 ; 0.025	0.025 ± 0.007
$\to K^{*0}\pi^+$	0.027		0.024 ; 0.022	0.030 ± 0.006
$\to K^+\phi$			0.0066 ; 0.0067	< 0.013 (*pdg*04)
$\to \pi^+\omega$			0.57 ; 0.58	< 0.034
$\to \eta\rho^+$			0.24 ; 0.43	< 0.7
$\to \eta'\rho^+$			0.15 ; 0.15	< 0.6
$\to \pi^0\rho^+$	0.451	0.31	0.28 ; 0.35	
$\to K^0\rho^+$	0.042		0.025 ; 0.022	
$\to \pi^0 K^{*+}$	0.057		0.037 ; 0.036	
$\to K^+\omega$			0.012 ; 0.011	
$\to K^{*+}\eta$			0.015 ; 0.015	
$\to K^{*+}\eta'$			0.00014 ; 0.00016	
$D_s^+ \to \overline{K}^{*0}K^+$	4.812		3.34 ; 3.42	3.3 ± 0.9 (*pdg*04)
$\to \overline{K}^0 K^{*+}$	2.467		4.98 ; 4.66	5.3 ± 1.3
$\to \pi^+\rho^0$			0.06 ; 0.06	< 0.07 (*pdg*04)
$\to \pi^+\phi$	4.552		3.08 ; 2.93	4.4 ± 0.6
$\to \pi^+ K^{*0}$	0.445		0.33 ; 0.35	0.65 ± 0.28 (*pdg*04)
$\to K^+\rho^0$	0.198		0.12 ; 0.12	0.26 ± 0.07
$\to K^+\phi$	0.008		0.032 ; 0.033	< 0.06
$\to K^+\omega$	0.178		0.40 ; 0.39	
$\to K^0\rho^+$	1.288		0.91 ; 0.77	
$\to \pi^0 K^{*+}$	0.076		0.13 ; 0.13	
$\to \eta K^{*+}$	0.146		0.038 ; 0.047	
$\to \eta' K^{*+}$			0.068 ; 0.059	
$\to K^{*0}K^+$	0.006		0.0015 ; 0.0015	
$\to K^{*+}K^0$	0.018		0.0076 ; 0.0085	

Table 25.3: *Experimental branching ratios of various $D \to SP$ decays measured by ARGUS, E687, E691, E791, CLEO, FOCUS and BaBar. For simplicity and convenience, The mass identification for $f_0(980)$, $a_0(980)$ and $K_0^*(1430)$ have been dropped.*

Collaboration	$\mathcal{B}(D \to SP) \times \mathcal{B}(S \to P_1P_2)$	$\mathcal{B}(D \to SP)$
PDG06	$\mathcal{B}(D^+ \to f_0\pi^+)\mathcal{B}(f_0 \to \pi^+\pi^-) = (2.1 \pm 0.5) \times 10^{-4}$	$\mathcal{B}(D^+ \to f_0\pi^+) = (4.0 \pm 1.2) \times 10^{-4}$
E791	$\mathcal{B}(D^+ \to f_0\pi^+)\mathcal{B}(f_0 \to \pi^+\pi^-) = (1.9 \pm 0.5) \times 10^{-4}$	$\mathcal{B}(D^+ \to f_0\pi^+) = (3.6 \pm 1.1) \times 10^{-4}$
FOCUS	$\mathcal{B}(D^+ \to f_0K^+)\mathcal{B}(f_0 \to K^+K^-) = (3.84 \pm 0.92) \times 10^{-5}$	$\mathcal{B}(D^+ \to f_0K^+) = (4.8 \pm 1.3) \times 10^{-4}$
PDG06	$\mathcal{B}(D^+ \to f_0K^+)\mathcal{B}(f_0 \to \pi^+\pi^-) = (5.7 \pm 3.5) \times 10^{-5}$	$\mathcal{B}(D^+ \to f_0K^+) = (1.1 \pm 0.7) \times 10^{-4}$
FOCUS	$\mathcal{B}(D^+ \to f_0K^+)\mathcal{B}(f_0 \to \pi^+\pi^-) = (6.12 \pm 3.65) \times 10^{-5}$	$\mathcal{B}(D^+ \to f_0K^+) = (1.2 \pm 0.7) \times 10^{-4}$
FOCUS	$\mathcal{B}(D^+ \to a_0^0\pi^+)\mathcal{B}(a_0^0 \to K^+K^-) = (2.38 \pm 0.47) \times 10^{-3}$	$\mathcal{B}(D^+ \to a_0^0\pi^+) = (3.1 \pm 0.7)\%$
E791	$\mathcal{B}(D^+ \to \sigma\pi^+)\mathcal{B}(\sigma \to \pi^+\pi^-) = (1.4 \pm 0.3) \times 10^{-3}$	$\mathcal{B}(D^+ \to \sigma\pi^+) = (2.1 \pm 0.5) \times 10^{-3}$
E791	$\mathcal{B}(D^+ \to \kappa\pi^+)\mathcal{B}(\kappa \to K^-\pi^+) = (4.4 \pm 1.2)\%$	$\mathcal{B}(D^+ \to \kappa\pi^+) = (6.5 \pm 1.9)\%$
E691,E687	$\mathcal{B}(D^+ \to \overline{K}_0^{*0}\pi^+)\mathcal{B}(\overline{K}_0^{*0} \to K^-\pi^+) = (2.3 \pm 0.3)\%$	$\mathcal{B}(D^+ \to \overline{K}_0^{*0}\pi^+) = (3.7 \pm 0.6)\%$
PDG06	$\mathcal{B}(D^+ \to \overline{K}_0^{*0}\pi^+)\mathcal{B}(\overline{K}_0^{*0} \to K^-\pi^+) = (2.41 \pm 0.24)\%$	$\mathcal{B}(D^+ \to \overline{K}_0^{*0}\pi^+) = (3.9 \pm 0.6)\%$
E791	$\mathcal{B}(D^+ \to \overline{K}_0^{*0}\pi^+)\mathcal{B}(\overline{K}_0^{*0} \to K^-\pi^+) = (1.14 \pm 0.16)\%$	$\mathcal{B}(D^+ \to \overline{K}_0^{*0}\pi^+) = (1.8 \pm 0.3)\%$
PDG06	$\mathcal{B}(D^+ \to \overline{K}_0^{*0}K^+)\mathcal{B}(\overline{K}_0^{*0} \to K^-\pi^+) = (3.7 \pm 0.4) \times 10^{-3}$	$\mathcal{B}(D^+ \to \overline{K}_0^{*0}K^+) = (6.0 \pm 0.9) \times 10^{-3}$
PDG06	$\mathcal{B}(D^+ \to f_0(1370)\pi^+)\mathcal{B}(f_0(1370) \to \pi^+\pi^-) = (8 \pm 6) \times 10^{-5}$	
FOCUS	$\mathcal{B}(D^+ \to f_0(1370)\pi^+)\mathcal{B}(f_0(1370) \to K^+K^-) = (6.2 \pm 1.1) \times 10^{-4}$	
PDG06	$\mathcal{B}(D^0 \to \sigma\pi^0)\mathcal{B}(f_0 \to \pi^+\pi^-) < 2.7 \times 10^{-5}$	$\mathcal{B}(D^0 \to \sigma\pi^0) < 4.1 \times 10^{-5}$
PDG06	$\mathcal{B}(D^0 \to f_0\pi^0)\mathcal{B}(f_0 \to \pi^+\pi^-) < 3.4 \times 10^{-6}$	$\mathcal{B}(D^0 \to f_0\pi^0) < 6.4 \times 10^{-6}$
PDG06	$\mathcal{B}(D^0 \to f_0K_s^0)\mathcal{B}(f_0 \to \pi^+\pi^-) = (1.36^{+0.30}_{-0.22}) \times 10^{-3}$	$\mathcal{B}(D^0 \to f_0K_s^0) = (2.6^{+0.7}_{-0.6}) \times 10^{-3}$
ARGUS,E687	$\mathcal{B}(D^0 \to f_0\overline{K}^0)\mathcal{B}(f_0 \to \pi^+\pi^-) = (3.2 \pm 0.9) \times 10^{-3}$	$\mathcal{B}(D^0 \to f_0\overline{K}^0) = (6.0 \pm 2.0) \times 10^{-3}$
CLEO	$\mathcal{B}(D^0 \to f_0\overline{K}^0)\mathcal{B}(f_0 \to \pi^+\pi^-) = (2.5^{+0.8}_{-0.5}) \times 10^{-3}$	$\mathcal{B}(D^0 \to f_0\overline{K}^0) = (4.7^{+1.7}_{-1.2}) \times 10^{-3}$
PDG06	$\mathcal{B}(D^0 \to f_0K_s^0)\mathcal{B}(f_0 \to K^+K^-) < 1.0 \times 10^{-4}$	$\mathcal{B}(D^0 \to f_0K_s^0) < 1.3 \times 10^{-3}$
BaBar	$\mathcal{B}(D^0 \to f_0\overline{K}^0)\mathcal{B}(f_0 \to K^+K^-) = (1.2 \pm 0.9) \times 10^{-3}$	$\mathcal{B}(D^0 \to f_0\overline{K}^0) = (1.5 \pm 1.1)\%$
PDG06	$\mathcal{B}(D^0 \to a_0^+K^-)\mathcal{B}(a_0^+ \to K^+K_s^0) = (6.1 \pm 1.8) \times 10^{-4}$	$\mathcal{B}(D^0 \to a_0^+K^-) = (7.9 \pm 2.5)^{-3}$
BaBar	$\mathcal{B}(D^0 \to a_0^+K^-)\mathcal{B}(a_0^+ \to K^+\overline{K}^0) = (3.3 \pm 0.8) \times 10^{-3}$	$\mathcal{B}(D^0 \to a_0^+K^-) = (2.1 \pm 0.6)\%$
PDG06	$\mathcal{B}(D^0 \to a_0^-K^+)\mathcal{B}(a_0^- \to K^-K_s^0) < 1.1 \times 10^{-4}$	$\mathcal{B}(D^0 \to a_0^-K^+) < 1.4 \times 10^{-3}$
BaBar	$\mathcal{B}(D^0 \to a_0^-K^+)\mathcal{B}(a_0^- \to K^-\overline{K}^0) = (3.1 \pm 1.9) \times 10^{-4}$	$\mathcal{B}(D^0 \to a_0^-K^+) = (2.0 \pm 1.2) \times 10^{-3}$
PDG06	$\mathcal{B}(D^0 \to a_0^0K_s^0)\mathcal{B}(a_0^0 \to K^+K^-) = (3.0 \pm 0.4) \times 10^{-3}$	$\mathcal{B}(D^0 \to a_0^0K_s^0) = (3.8 \pm 0.7)\%$
BaBar	$\mathcal{B}(D^0 \to a_0^0\overline{K}^0)\mathcal{B}(a_0^0 \to K^+K^-) = (5.9 \pm 1.3) \times 10^{-3}$	$\mathcal{B}(D^0 \to a_0^0\overline{K}^0) = (7.6 \pm 1.9)\%$
BaBar	$\mathcal{B}(D^0 \to a_0^+\pi^-)\mathcal{B}(a_0^+ \to K^+\overline{K}^0) = (5.1 \pm 4.2) \times 10^{-4}$	$\mathcal{B}(D^0 \to a_0^+\pi^-) = (3.3 \pm 2.7) \times 10^{-3}$
BaBar	$\mathcal{B}(D^0 \to a_0^-\pi^+)\mathcal{B}(a_0^- \to K^-K^0) = (1.43 \pm 1.19) \times 10^{-4}$	$\mathcal{B}(D^0 \to a_0^-\pi^+) = (9.2 \pm 7.7) \times 10^{-4}$
PDG06	$\mathcal{B}(D^0 \to K_0^{*-}\pi^+)\mathcal{B}(K_0^{*-} \to K_s^0\pi^-) = (2.8^{+0.6}_{-0.4}) \times 10^{-3}$	$\mathcal{B}(D^0 \to K_0^{*-}\pi^+) = (9.0^{+2.3}_{-1.7})^{-3}$
ARGUS,E687	$\mathcal{B}(D^0 \to K_0^{*-}\pi^+)\mathcal{B}(K_0^{*-} \to \overline{K}^0\pi^-) = (7.3 \pm 1.6) \times 10^{-3}$	$\mathcal{B}(D^0 \to K_0^{*-}\pi^+) = (1.2 \pm 0.3)\%$
CLEO	$\mathcal{B}(D^0 \to K_0^{*-}\pi^+)\mathcal{B}(K_0^{*-} \to \overline{K}^0\pi^-) = (4.3^{+1.9}_{-0.8}) \times 10^{-3}$	$\mathcal{B}(D^0 \to K_0^{*-}\pi^+) = (7.0^{+3.2}_{-1.5}) \times 10^{-3}$
PDG06	$\mathcal{B}(D^0 \to K_0^{*-}\pi^+)\mathcal{B}(K_0^{*-} \to K^-\pi^0) = (4.6 \pm 2.2) \times 10^{-3}$	$\mathcal{B}(D^0 \to K_0^{*-}\pi^+) = (1.5 \pm 0.7)\%$
CLEO	$\mathcal{B}(D^0 \to K_0^{*-}\pi^+)\mathcal{B}(K_0^{*-} \to K^-\pi^0) = (3.6 \pm 0.8) \times 10^{-3}$	$\mathcal{B}(D^0 \to K_0^{*-}\pi^+) = (1.2 \pm 0.3)\%$
PDG06	$\mathcal{B}(D^0 \to \overline{K}_0^{*0}\pi^0)\mathcal{B}(\overline{K}_0^{*0} \to K^-\pi^+) = (5.8^{+4.6}_{-1.5}) \times 10^{-3}$	$\mathcal{B}(D^0 \to \overline{K}_0^{*0}\pi^0) = (9.4^{+7.5}_{-2.6}) \times 10^{-3}$
CLEO	$\mathcal{B}(D^0 \to \overline{K}_0^{*0}\pi^0)\mathcal{B}(\overline{K}_0^{*0} \to K^-\pi^+) = (5.3^{+4.2}_{-1.4}) \times 10^{-3}$	$\mathcal{B}(D^0 \to \overline{K}_0^{*0}\pi^0) = (8.5^{+6.8}_{-2.5}) \times 10^{-3}$
PDG06	$\mathcal{B}(D^0 \to f_0(1370)K_s^0)\mathcal{B}(f_0(1370) \to \pi^+\pi^-) = (2.5 \pm 0.6) \times 10^{-3}$	
PDG06	$\mathcal{B}(D^0 \to a_0K_s^0)\mathcal{B}(a_0 \to \eta\pi^0) = (6.2 \pm 2.0) \times 10^{-3}$	
ARGUS,E687	$\mathcal{B}(D^0 \to f_0(1370)\overline{K}^0)\mathcal{B}(f_0(1370) \to \pi^+\pi^-) = (4.7 \pm 1.4) \times 10^{-3}$	
CLEO	$\mathcal{B}(D^0 \to f_0(1370)\overline{K}^0)\mathcal{B}(f_0(1370) \to \pi^+\pi^-) = (5.9^{+1.8}_{-2.7}) \times 10^{-3}$	
PDG06	$\mathcal{B}(D^0 \to f_0(1400)K_s^0)\mathcal{B}(f_0(1400) \to K^+K^-) = (1.7 \pm 1.1) \times 10^{-4}$	
PDG06	$\mathcal{B}(D_s^+ \to f_0\pi^+)\mathcal{B}(f_0 \to K^+K^-) = (5.7 \pm 2.5) \times 10^{-3}$	$\mathcal{B}(D_s^+ \to f_0\pi^+) = (7.1 \pm 3.2)\%$
E687	$\mathcal{B}(D_s^+ \to f_0\pi^+)\mathcal{B}(f_0 \to K^+K^-) = (4.9 \pm 2.3) \times 10^{-3}$	$\mathcal{B}(D_s^+ \to f_0\pi^+) = (6.1 \pm 3.0)\%$
E791	$\mathcal{B}(D_s^+ \to f_0\pi^+)\mathcal{B}(f_0 \to \pi^+\pi^-) = (5.7 \pm 1.7) \times 10^{-3}$	$\mathcal{B}(D_s^+ \to f_0\pi^+) = (1.1 \pm 0.4)\%$
FOCUS	$\mathcal{B}(D_s^+ \to f_0\pi^+)\mathcal{B}(f_0 \to \pi^+\pi^-) = (9.5 \pm 2.7) \times 10^{-3}$	$\mathcal{B}(D_s^+ \to f_0\pi^+) = (1.8 \pm 0.6)\%$
FOCUS	$\mathcal{B}(D_s^+ \to f_0\pi^+)\mathcal{B}(f_0 \to K^+K^-) = (7.0 \pm 1.9) \times 10^{-3}$	$\mathcal{B}(D_s^+ \to f_0\pi^+) = (8.8 \pm 2.6)\%$
FOCUS	$\mathcal{B}(D_s^+ \to f_0K^+)\mathcal{B}(f_0 \to K^+K^-) = (2.8 \pm 1.3) \times 10^{-4}$	$\mathcal{B}(D_s^+ \to f_0K^+) = (3.5 \pm 1.7) \times 10^{-3}$
PDG06	$\mathcal{B}(D_s^+ \to \overline{K}_0^{*0}K^+)\mathcal{B}(\overline{K}_0^{*0} \to K^-\pi^+) = (4.8 \pm 2.5) \times 10^{-3}$	$\mathcal{B}(D_s^+ \to \overline{K}_0^{*0}K^+) = (7.7 \pm 4.1) \times 10^{-3}$
E687	$\mathcal{B}(D_s^+ \to \overline{K}_0^{*0}K^+)\mathcal{B}(\overline{K}_0^{*0} \to K^-\pi^+) = (4.3 \pm 2.5) \times 10^{-3}$	$\mathcal{B}(D_s^+ \to \overline{K}_0^{*0}K^+) = (6.9 \pm 4.1) \times 10^{-3}$
FOCUS	$\mathcal{B}(D_s^+ \to K_0^{*0}\pi^+)\mathcal{B}(K_0^{*0} \to K^+\pi^-) = (1.4 \pm 0.8) \times 10^{-3}$	$\mathcal{B}(D_s^+ \to K_0^{*0}\pi^+) = (2.3 \pm 1.3) \times 10^{-3}$
E791	$\mathcal{B}(D_s^+ \to f_0(1370)\pi^+)\mathcal{B}(f_0(1370) \to \pi^+\pi^-) = (3.3 \pm 1.2) \times 10^{-3}$	

The theoretical studies of $D \to SP$ are very similar to $D \to PP$ except for the fact that the quark structure of the scalar mesons, especially $f_0(980)$ and $a_0(980)$, is still not clear (for a review, one can refer to [4] and references therein). Hence, one is facing a 'Scylla and Charybdis' dilemma at the moment when thinking to the limited theoretical control on the significant nonfactorized contributions as well. Yet it is without doubt that the study of charmed meson decays will open a new avenue to the understanding of the light scalar meson spectroscopy. One might resort to the knowledge resulting from $D \to PP$ and $D \to PV$ modes and try to make new understanding on some old puzzles related to the internal structure and parameters, e.g. the masses and widths, of light scalar mesons through the study of $D \to SP$ [123, 124, 125]. Or vice versa, one can start from the assumed structure of scalar mesons and make some predictions on the decays [126, 127, 128]. Some of the theoretical results in the literature are given in Table 25.4. In either case, the following factorization formula are useful.

$$T_S = -\frac{G_F}{\sqrt{2}} V_{q_1 q_2} V^*_{cq_3} a_1 f_P (m_D^2 - m_S^2) F_0^{D\to S}(m_P^2), \tag{25.44}$$

$$T_P = -\frac{G_F}{\sqrt{2}} V_{q_1 q_2} V^*_{cq_3} a_1 f_S (m_D^2 - m_P^2) F_0^{D\to P}(m_S^2), \tag{25.45}$$

$$C_S = -\frac{G_F}{\sqrt{2}} V_{q_1 q_2} V^*_{cq_3} a_2 f_P (m_D^2 - m_S^2) F_0^{D\to S}(m_P^2), \tag{25.46}$$

$$C_P = -\frac{G_F}{\sqrt{2}} V_{q_1 q_2} V^*_{cq_3} a_2 f_S (m_D^2 - m_P^2) F_0^{D\to P}(m_S^2). \tag{25.47}$$

25.3.4 $D \to AP$ Decays

There are two different types of axial vector mesons: ${}^3P_1$ and ${}^1P_1$, which carry the quantum numbers $J^{\rm PC} = 1^{++}$ and 1^{+-}, respectively. The isovector non-strange axial vector mesons $a_1(1260)$ and $b_1(1235)$ which correspond to ${}^3P_1$ and ${}^1P_1$, respectively, cannot have mixing because of the opposite C-parities. However, the isodoublet strange ones $K_1(1270)$ and $K_1(1400)$ are a mixture of ${}^3P_1$ and ${}^1P_1$ states due to the strange and non-strange light quark mass difference. One can usually write

$$\begin{aligned} K_1(1270) &= K_{1A} \sin\theta + K_{1B} \cos\theta \ , \\ K_1(1400) &= K_{1A} \cos\theta - K_{1B} \sin\theta \ , \end{aligned} \tag{25.48}$$

where K_{1A} and K_{1B} are the strange partners of $a_1(1260)$ and $b_1(1235)$ respectively.

Two-body hadronic $D \to AP$ decays have been studied in [129, 130, 131, 132, 133,

Table 25.4: *Branching ratios for various $D \to SP$ decays. Experimental results are taken from Table 25.3.*

Decay	*Buccella etal.*[126]	*Cheng* [125]	Experiments
$D^+ \to f_0\pi^+$	2.8×10^{-4}	3.5×10^{-4}	$(3.6 \pm 1.1) \times 10^{-4}$
$\to f_0 K^+$	2.3×10^{-5}	2.2×10^{-5}	$\sim 10^{-4}$
$\to a_0^+ \overline{K}^0$	6.4×10^{-3}	1.7×10^{-2}	
$\to a_0^0 \pi^+$	5.9×10^{-4}	1.7×10^{-3}	$(3.1 \pm 0.7)\%$
$\to \sigma\pi^+$		input	$(2.1 \pm 0.5) \times 10^{-3}$
$\to \kappa\pi^+$		input	$(6.5 \pm 1.9)\%$
$\to \overline{K}_0^{*0}\pi^+$		input	$(1.8 \pm 0.3)\%$
$\to a_0^0 \pi^+$	5.9×10^{-4}		
$\to a_0^+ \pi^0$	1.2×10^{-4}		
$\to a_0^+ \eta$	7.4×10^{-4}		
$\to a_0^0 K^+$	6.2×10^{-5}		
$\to f_0 K^+$	2.3×10^{-5}		
$D^0 \to f_0 \overline{K}^0$	7.4×10^{-4}	input	$\sim 10^{-3} - 10^{-2}$
$\to a_0^+ K^-$	7.8×10^{-4}	1.1×10^{-3}	$(2.1 \pm 0.6)\%$
$\to a_0^0 \overline{K}^0$	2.2×10^{-3}	3.6×10^{-3}	$(7.6 \pm 1.9)\%$
$\to a_0^- K^+$	4.0×10^{-5}	7.9×10^{-5}	$(2.0 \pm 1.2) \times 10^{-3}$
$\to a_0^+ \pi^-$	3.0×10^{-5}	6.5×10^{-5}	$(3.3 \pm 2.7) \times 10^{-3}$
$\to a_0^- \pi^+$	7.0×10^{-4}	1.3×10^{-3}	$(9.2 \pm 7.7) \times 10^{-4}$
$\to K_0^{*-}\pi^+$		1.1×10^{-2}	$\sim 10^{-3} - 10^{-2}$
$\to \overline{K}_0^{*0}\pi^0$		3.7×10^{-3}	$(8.5^{+6.8}_{-2.5}) \times 10^{-3}$
$\to f_0 \pi^0$	6.0×10^{-6}		
$\to f_0 \eta$	4.0×10^{-5}		
$\to a_0^0 \pi^0$	1.1×10^{-4}		
$\to a_0^0 \eta$	1.5×10^{-4}		
$D_s^+ \to f_0\pi^+$	1.1%	input	$(1.8 \pm 0.6)\%$
$\to f_0 K^+$	6.9×10^{-4}	1.2×10^{-3}	$(3.5 \pm 1.7) \times 10^{-3}$
$\to \overline{K}_0^{*0} K^+$		1.5×10^{-3}	$(6.9 \pm 4.1) \times 10^{-3}$
$\to K_0^{*0}\pi^+$		1.1×10^{-3}	$(2.3 \pm 1.3) \times 10^{-3}$
$\to a_0^+ K^0$	3.0×10^{-5}		
$\to a_0^0 K^+$	7.0×10^{-5}		
$\to a_0^+ \eta$	7.0×10^{-5}		

134, 135]. Under the factorization approximation, the decay amplitudes read

$$T_A = 2\frac{G_F}{\sqrt{2}}V_{q_1q_2}V^*_{cq_3}a_1 f_P m_A(\varepsilon^*\cdot p_D)A_0^{D\to A}(m_P^2), \quad (25.49)$$

$$T_P = 2\frac{G_F}{\sqrt{2}}V_{q_1q_2}V^*_{cq_3}a_1 f_A m_A(\varepsilon^*\cdot p_D)F_+^{D\to P}(m_A^2), \quad (25.50)$$

$$C_A = 2\frac{G_F}{\sqrt{2}}V_{q_1q_2}V^*_{cq_3}a_2 f_P m_A(\varepsilon^*\cdot p_D)A_0^{D\to A}(m_P^2), \quad (25.51)$$

$$C_P = 2\frac{G_F}{\sqrt{2}}V_{q_1q_2}V^*_{cq_3}a_2 f_A m_A(\varepsilon^*\cdot p_D)F_+^{D\to P}(m_A^2). \quad (25.52)$$

The predicted branching ratios from factorizable contributions for $D^0\to K^-a_1^+$ and $D^0\to K_1^-(1270)\pi^+$ and that for $D^0\to\overline{K}^0a_1^+$ and $D^+\to\overline{K}_1^0(1400)\pi^+$ in Refs. [129, 130, 131, 132, 133] were too small by roughly a factor of 5 and 2, respectively, when compared with experimental data. One argument is that the factorization approach may be only suitable for energetic two-body decays like $D\to PP$ and $D\to PV$; for $D\to AP$ with very little energy release, the approximation is questionable since the nonperturbative contributions grow up. A recent analysis [135] considering the sizable FSI effects showed that the predictions, which are presented in Table 25.5 and Table 25.6, are improved greatly.

Table 25.5: *Branching ratios for $D\to Ka_1(1260)$ and $D\to Kb_1(1235)$. Most decay modes involving a neutral K meson are given as K_S^0 in PDG06 instead of $\overline{K}^0$ in PDG04 which are presented here as well.*

Decay	Theory [135]		Experiment [4]
	without FSIs	with FSIs	
$D^+\to\overline{K}^0a_1^+(1260)$	12.1%	12.1%	$(3.6\pm0.6)\%$
			$(8.2\pm1.7)\%$ (*pdg*04)
$D^0\to K^-a_1^+(1260)$	3.8%	6.2%	$(7.5\pm1.1)\%$
$D^0\to\overline{K}^0a_1^0(1260)$	3.3×10^{-4}	5.6×10^{-4}	$<1.9\%$
$D^+\to\overline{K}^0b_1^+(1235)$	1.7×10^{-3}	1.7×10^{-3}	
$D^0\to K^-b_1^+(1235)$	3.7×10^{-6}	5.9×10^{-6}	
$D^0\to\overline{K}^0b_1^0(1235)$	3.9×10^{-4}	6.7×10^{-4}	

25.3.5 $D\to TP$ Decays

The observed $J^P=2^+$ tensor mesons $f_2(1270)$, $f_2'(1525)$, $a_2(1320)$ and $K_2^*(1430)$ form an SU(3) $1\,^3P_2$ nonet with quark content $q\bar{q}$. Hadronic charm decaying to a pseudoscalar meson and a tensor meson $f_2(1270)$, $a_2(1320)$ or $K_2^*(1430)$ have been found in the earlier measurements by ARGUS [114] and E687 [116], and in recent experiments from E791 [118], CLEO [115], FOCUS [119] and BaBar [120], though some of them have not yet

sufficient statistical significance. The results of various experiments are summarized in Table 25.7 where the products of $\mathcal{B}(D \to TP_3)$ and $\mathcal{B}(T \to P_1P_2)$ are shown. It is evident that most of the listed $D \to TP$ decays have branching ratios of order 10^{-3}, even though some of them are Cabibbo suppressed. In order to extract the branching ratios for $D \to TP$ decays, one must use the branching fractions of the strong decays of the tensor mesons [4]:

$$\mathcal{B}(f_2(1270) \to \pi\pi) = (84.7^{+2.5}_{-1.2})\%, \qquad \mathcal{B}(f_2(1270) \to K\overline{K}) = (4.6 \pm 0.4)\%,$$
$$\mathcal{B}(a_2(1320) \to K\overline{K}) = (4.9 \pm 0.8)\%, \qquad \mathcal{B}(K_2^*(1430) \to K\pi) = (49.9 \pm 1.2)\%. \quad (25.53)$$

Theoretical calculations based on the factorization hypothesis were conducted to understand the experimental data [136, 137, 138]. Some of the results are listed in Table 25.8 where one can find that most of the theoretical predictions are not consistent with the experimental data. At first glance, some decays like $D \to \overline{K}_2^*(1430)K$ and $D^0 \to f_2'(1525)\overline{K}^0$ *etal.*, are kinematically not allowed as the total mass of the final state particles lies outside of the phase space for the decay. Nevertheless, it is physically allowed as some tensor mesons have broad widths of order several hundred MeV [4].

25.3.6 Other Decay Modes

Measurements of other nonleptonic two-body modes, such as $D \to AV$ and so on , have been done in experiment. PDG report two fairly large branching ratios [4]: $\mathcal{B}(D^+ \to \overline{K}^{*0}a_1(1260)^+) = (9.4 \pm 1.9) \times 10^{-3}$ and $\mathcal{B}(D_s^+ \to \phi a_1(1260)^+) = (2.9 \pm 0.7)\%$, though the total masses of their final state mesons exceed their phase spaces. Given the relevant form factors, the branching fractions can be worked out by means of factorization approach. Yet one doubt that how to evaluate the reliability of factorization in these decay modes will arise since the nonfactorized corrections may be dominant due to the small momentum transfer.

25.4 Three-Body Decays

25.4.1 Kinematics and Dalitz Plot

Starting from Equation (25.24) and integrating over the solid angles, the decay rate for $D \to M_1M_2M_3$ can be obtained

$$d\Gamma = \frac{1}{(2\pi)^3}\frac{1}{32m_D^3}|\mathcal{A}|^2 dm_{12}^2 dm_{23}^2 \ , \quad (25.54)$$

where m_{ij} is the invariant mass of particles i and j. For a given value of m_{12}^2 in the range $(m_1+m_2)^2 \le m_{12}^2 \le (m_D - m_3)^2$, the upper and lower bounds of m_{23}^2 are determined

$$(m_{23}^2)_{max} = (E_2^* + E_3^*)^2 - (\sqrt{E_2^{*2} - m_2^2} - \sqrt{E_3^{*2} - m_3^2})^2 \ , \quad (25.55)$$
$$(m_{23}^2)_{max} = (E_2^* + E_3^*)^2 - (\sqrt{E_2^{*2} - m_2^2} + \sqrt{E_3^{*2} - m_3^2})^2 \ . \quad (25.56)$$

Table 25.6: *Branching ratios of $D \to K_1(1270)\pi$ and $D \to K_1(1400)\pi$ calculated for various $K_{1A} - K_{1B}$ mixing angles.*

Decay	Theory [135]				Experiment [4]
	-37°	-58°	37°	58°	
$D^+ \to \overline{K}_1^0(1270)\pi^+$	6.4×10^{-3}	7.8×10^{-3}	2.9%	4.7%	$< 7 \times 10^{-3}$
$D^+ \to \overline{K}_1^0(1400)\pi^+$	2.9%	4.0%	6.6%	6.6%	$(4.3 \pm 1.5)\%$
$D^0 \to K_1^-(1270)\pi^+$	6.3×10^{-3}	5.5×10^{-3}	4.9×10^{-4}	4.4×10^{-5}	$(1.12 \pm 0.31)\%$
$D^0 \to K_1^-(1400)\pi^+$	3.7×10^{-8}	4.2×10^{-4}	3.0×10^{-3}	3.2×10^{-3}	$< 1.2\%$
$D^0 \to \overline{K}_1^0(1270)\pi^0$	8.4×10^{-3}	8.4×10^{-3}	8.4×10^{-3}	8.4×10^{-3}	
$D^0 \to \overline{K}_1^0(1400)\pi^0$	5.7×10^{-3}	5.5×10^{-3}	5.7×10^{-3}	5.5×10^{-3}	$< 3.7\%$

Table 25.7: *Experimental branching ratios of various $D \to TP$ decays measured by BaBar, CLEO, E791, FOCUS and PDG06. For simplicity and convenience, we have dropped the mass identification for $f_2(1270)$, $a_2(1320)$ and $K_2^*(1430)$.*

Collaboration	$\mathcal{B}(D \to TP) \times \mathcal{B}(T \to P_1P_2)$	$\mathcal{B}(D \to TP)$
PDG06	$\mathcal{B}(D^+ \to f_2\pi^+)\mathcal{B}(f_2 \to \pi^+\pi^-) = (4.8 \pm 1.3) \times 10^{-4}$	$\mathcal{B}(D^+ \to f_2\pi^+) = (8.5 \pm 2.3) \times 10^{-4}$
E791	$\mathcal{B}(D^+ \to f_2\pi^+)\mathcal{B}(f_2 \to \pi^+\pi^-) = (6.0 \pm 1.1) \times 10^{-4}$	$\mathcal{B}(D^+ \to f_2\pi^+) = (1.1 \pm 0.2) \times 10^{-3}$
FOCUS	$\mathcal{B}(D^+ \to f_2\pi^+)\mathcal{B}(f_2 \to \pi^+\pi^-) = (3.8 \pm 0.8) \times 10^{-5}$	$\mathcal{B}(D^+ \to f_2\pi^+) = (6.8 \pm 1.4) \times 10^{-4}$
FOCUS	$\mathcal{B}(D^+ \to f_2\pi^+)\mathcal{B}(f_2 \to K^+K^-) = (7.0 \pm 1.9) \times 10^{-5}$	$\mathcal{B}(D^+ \to f_2\pi^+) = (3.1 \pm 0.9) \times 10^{-3}$
PDG06	$\mathcal{B}(D^+ \to K_2^{*0}\pi^+)\mathcal{B}(K_2^{*0} \to K^+\pi^-) = (5.2 \pm 3.5) \times 10^{-5}$	$\mathcal{B}(D^+ \to K_2^{*0}\pi^+) = (1.6 \pm 1.1) \times 10^{-4}$
E791	$\mathcal{B}(D^+ \to \overline{K}_2^{*0}\pi^+)\mathcal{B}(\overline{K}_2^{*0} \to K^-\pi^+) = (4.6 \pm 2.0) \times 10^{-4}$	$\mathcal{B}(D^+ \to \overline{K}_2^{*0}\pi^+) = (1.4 \pm 0.6) \times 10^{-3}$
PDG06		$\mathcal{B}(D^+ \to a_2^+ K_S^0) < 1.5 \times 10^{-3}$
PDG06	$\mathcal{B}(D^0 \to f_2 K_S^0)\mathcal{B}(f_2 \to \pi^+\pi^-) = (1.3^{+1.1}_{-0.7}) \times 10^{-4}$	$\mathcal{B}(D^0 \to f_2 K_S^0) = (2.3^{+2.0}_{-1.3}) \times 10^{-4}$
CLEO	$\mathcal{B}(D^0 \to f_2\overline{K}^0)\mathcal{B}(f_2 \to \pi^+\pi^-) = (1.6^{+2.4}_{-1.3}) \times 10^{-4}$	$\mathcal{B}(D^0 \to f_2\overline{K}^0) = (2.8^{+4.3}_{-2.3}) \times 10^{-3}$
BaBar	$\mathcal{B}(D^0 \to a_2^-\pi^+)\mathcal{B}(a_2^- \to K^0K^-) = (3.5 \pm 2.1) \times 10^{-5}$	$\mathcal{B}(D^0 \to a_2^-\pi^+) = (7.0 \pm 4.3) \times 10^{-4}$
PDG06	$\mathcal{B}(D^0 \to K_2^{*-}\pi^+)\mathcal{B}(K_2^{*-} \to K_S^0\pi^-) = (3.2^{+2.1}_{-1.1}) \times 10^{-4}$	$\mathcal{B}(D^0 \to K_2^{*-}\pi^+) = (2.0^{+1.3}_{-0.7}) \times 10^{-3}$
CLEO	$\mathcal{B}(D^0 \to K_2^{*-}\pi^+)\mathcal{B}(K_2^{*-} \to \overline{K}^0\pi^-) = (6.5^{+4.2}_{-2.2}) \times 10^{-4}$	$\mathcal{B}(D^0 \to K_2^{*-}\pi^+) = (2.0^{+1.3}_{-0.7}) \times 10^{-3}$
BaBar	$\mathcal{B}(D^0 \to K_2^{*+}K^-)\mathcal{B}(K_2^{*+} \to K^0\pi^+) = (6.8 \pm 4.2) \times 10^{-4}$	$\mathcal{B}(D^0 \to K_2^{*+}K^-) = (2.0 \pm 1.3) \times 10^{-3}$
BaBar	$\mathcal{B}(D^0 \to \overline{K}_2^{*0}K^0)\mathcal{B}(\overline{K}_2^{*0} \to K^-\pi^+) = (6.6 \pm 2.7) \times 10^{-4}$	$\mathcal{B}(D^0 \to \overline{K}_2^{*0}K^0) = (2.0 \pm 0.8) \times 10^{-3}$
PDG06		$\mathcal{B}(D^0 \to a_2^+K^-) < 2 \times 10^{-3}$
PDG06	$\mathcal{B}(D_s^+ \to f_2\pi^+)\mathcal{B}(f_2 \to \pi^+\pi^-) = (1.2 \pm 0.7) \times 10^{-3}$	$\mathcal{B}(D_s^+ \to f_2\pi^+) = (2.1 \pm 1.3) \times 10^{-3}$
E791	$\mathcal{B}(D_s^+ \to f_2\pi^+)\mathcal{B}(f_2 \to \pi^+\pi^-) = (2.0 \pm 0.7) \times 10^{-3}$	$\mathcal{B}(D_s^+ \to f_2\pi^+) = (3.5 \pm 1.2) \times 10^{-3}$
FOCUS	$\mathcal{B}(D_s^+ \to f_2\pi^+)\mathcal{B}(f_2 \to \pi^+\pi^-) = (1.0 \pm 0.3) \times 10^{-3}$	$\mathcal{B}(D_s^+ \to f_2\pi^+) = (1.8 \pm 0.5) \times 10^{-3}$
FOCUS	$\mathcal{B}(D_s^+ \to f_2K^+)\mathcal{B}(f_2 \to \pi^+\pi^-) = (2.0 \pm 1.3) \times 10^{-4}$	$\mathcal{B}(D_s^+ \to f_2K^+) = (3.5 \pm 2.3) \times 10^{-4}$

Table 25.8: *Branching ratios for various $D \to TP$ decays. Experimental results are taken from Table 25.7.*

Decay	*Katoch etal.*[136]	*Muñoz etal.*[137]	*Cheng*[138]		Experiment
			without FSIs	with FSIs	
$D^+ \to f_2(1270)\pi^+$		7.97×10^{-6}	2.9×10^{-5}	2.2×10^{-4}	$(0.9 \pm 0.1) \times 10^{-3}$
$D^0 \to f_2(1270)\pi^0$		2.47×10^{-7}			
$D^0 \to f_2(1270)\overline{K}^0$	9.0×10^{-5}		1.0×10^{-4}	2.5×10^{-4}	$(4.5 \pm 1.7) \times 10^{-3}$
$D_s^+ \to f_2(1270)\pi^+$	3.6×10^{-4}		6.6×10^{-5}	2.1×10^{-3}	$(2.1 \pm 0.5) \times 10^{-3}$
$\to f_2(1270)K^+$			5.2×10^{-6}	4.9×10^{-5}	$(3.5 \pm 2.3) \times 10^{-4}$
$D^+ \to f_2'(1525)\pi^+$		7.18×10^{-9}	1.4×10^{-6}	3.7×10^{-6}	
$D^0 \to f_2'(1525)\pi^0$		2.18×10^{-10}			
$D^0 \to f_2'(1525)\overline{K}^0$			2.5×10^{-7}	6.0×10^{-7}	
$D_s^+ \to f_2'(1525)\pi^+$	1.3×10^{-2}		1.6×10^{-4}	1.5×10^{-4}	
$\to f_2'(1525)K^+$			4.9×10^{-6}	7.5×10^{-6}	
$D^+ \to a_2^+(1320)\pi^0$		9.05×10^{-7}			
$D^+ \to a_2^0(1320)\pi^+$		5.55×10^{-6}			
$D^+ \to a_2^+(1320)\overline{K}^0$	1.1×10^{-4}		1.3×10^{-6}	1.3×10^{-6}	$< 3 \times 10^{-3}$
$D^0 \to a_2^-(1320)\pi^+$		4.21×10^{-6}	5.7×10^{-6}	6.1×10^{-6}	$(7.0 \pm 4.3) \times 10^{-4}$
$\to a_2^0(1320)\pi^0$		1.72×10^{-7}			
$\to a_2^+(1320)K^-$	0		0	8.9×10^{-8}	$< 2 \times 10^{-3}$
$\to a_2^0(1320)\overline{K}^0$	1.7×10^{-5}				
$D^+ \to \overline{K}_2^{*0}(1430)\pi^+$	9.9×10^{-3}		2.6×10^{-4}	2.6×10^{-4}	$(1.4 \pm 0.6) \times 10^{-3}$
$D^0 \to K_2^{*-}(1430)\pi^+$	4.1×10^{-3}		1.0×10^{-4}	1.1×10^{-4}	$(2.0^{+1.3}_{-0.7}) \times 10^{-3}$
$\to \overline{K}_2^{*0}(1430)\pi^0$	0		0	1.3×10^{-5}	$< 3.4 \times 10^{-3}$
$\to K_2^{*+}(1430)K^-$			0	1.3×10^{-6}	$(2.0 \pm 1.3) \times 10^{-3}$
$\to \overline{K}_2^{*0}(1430)K^0$			0	$\sim 10^{-8}$	$(2.0 \pm 0.8) \times 10^{-3}$
$D_s^+ \to \overline{K}_2^{*0}(1430)K^+$	0				
$\to \overline{K}_2^{*+}(1430)\overline{K}^0$	4.2×10^{-5}				

E_2^* and E_3^* are the energies of final state mesons M_2 and M_3 respectively in the rest frame of M_1 and M_2

$$E_2^* = \frac{m_{12}^2 - m_1^2 + m_2^2}{2m_{12}} , \tag{25.57}$$

$$E_3^* = \frac{m_D^2 - m_{12}^2 - m_2^2}{2m_{12}} . \tag{25.58}$$

The scatter plot in m_{12}^2 versus M_{23}^2 is called a Dalitz Plot. For a detailed introduction of Dalitz technique, please refer to Chapter 4 and Ref. [139]. The amplitude $|\mathcal{A}|^2$ of a nonresonant decay is parameterized as constant without variation in magnitude or phase across the Dalitz plot. Therefore, the allowed region of the plot is uniformly populated with events. A nonuniformity with bands near the mass of the resonance in the plot will reflect the appearance of resonant contribution. One can find a review of Dalitz plot application on charm decays in [140].

25.4.2 Resonant Three-Body Decays

Charmed meson three-body decays proceed dominantly via quasi-two-body decays containing an intermediate resonance state which then decays to two particles. The analysis of these resonant decays using the Dalitz plot technique enables one to study the dynamical properties of various resonances. In theoretical studies, resonant decays are often divided into product of two processes: $\mathcal{B}(D \to RM_3) \times \mathcal{B}(R \to M_1 M_2)$, just as we have shown in Section 25.3. Therefore what we confront with is in fact charmed meson two-body decays.

25.4.3 Nonresonant Three-Body Decays

The nonresonant contribution is usually a small fraction of the total 3-body decay rate. Experimentally, they are hard to be measured as the interference between nonresonant and quasi-two-body amplitudes makes it difficult to disentangle these two distinct contributions and extract the nonresonant one. Theoretically, the matrix element of D decaying to three mesons in general has two types of formalism in the factorization approximation, relying on how to distribute three final mesons into two "clusters".

For one type with a "cluster" where D transits to a light meson, one can find

$$\langle M_1 M_2 M_3 | J_{i\mu} J_i'^{\mu} | D \rangle \sim \langle M_1 M_2 | J_{i\mu} | 0 \rangle \langle M_3 | J_i'^{\mu} | D \rangle. \tag{25.59}$$

It is obvious that its contribution is negligibly small since matrix element $\langle M_1 M_2 | J_{i\mu} | 0 \rangle$ which also appears in the factorizable contributions of weak annihilation in two-body decays vanishes in the chiral limit.

For the other type with a "cluster" where D transits to two light mesons, the factorized formula reads

$$\langle M_1 M_2 M_3 | J_{i\mu} J_i'^{\mu} | D \rangle \sim \langle M_1 | J_{i\mu} | 0 \rangle \langle M_2 M_3 | J_i'^{\mu} | D \rangle. \tag{25.60}$$

Here a new matrix element $\langle M_2 M_3|J_i'^{\mu}|D\rangle$ is introduced. It has the general expression [141]

$$\begin{aligned}\langle M_2(p_2)M_3(p_3)|J_i'^{\mu}|D(p_D)\rangle &= ir(p_D-p_2-p_3)^{\mu}+i\omega_+(p_2+p_3)^{\mu}+i\omega_-(p_3-p_2)^{\mu}\\ &\quad +h\epsilon^{\mu\nu\alpha\beta}p_{D\nu}(p_2+p_3)_{\alpha}(p_3-p_2)_{\beta}\ ,\end{aligned} \tag{25.61}$$

where r, $\omega_{\pm}$ and h are form factors. In general they receive two distinct contributions: one from the point-like weak transition and the other from the pole diagrams which involve four-point strong vertices. Models based on chiral symmetry and heavy quark effective theory have been developed to make some estimates on them [141, 142, 143].

Charmed meson to three pseudoscalar nonresonant decays have been studied in the approach of effective $SU(4)_L \times SU(4)_R$ chiral Lagrangian [144, 145, 146, 147, 148], in which the predictions of the branching ratios were in general too small when compared with experiment. With the advent of heavy meson chiral perturbation theory (HMChPT) [149, 150, 151], the nonresonant D decays can be studied reliably at least in the kinematical region where the final pseudoscalar mesons are soft [152, 153, 154]. Some theoretical results are collected in Table 25.9.

25.4.4 Beyond Three-Body Decays

Some multi-body charm meson decays, even up to seven-body, have been measured in experiment [4]. Yet our available theoretical tools lose much of their power when applied to genuine multi-body transitions. The kinematics structure and strong dynamics will be more and more complicated and ultimately out of control with the number of final state particles increase.

Table 25.9: *Branching ratios (in %) for nonresonant 3-body D decays in various models. Most decay modes involving a neutral K meson are given as K^0_S in PDG06 instead of $\overline{K}^0$ in PDG04 which are presented here as well.*

Decay mode	Chau *et al.* [147]	Botella *et al.* [148]	Cheng *et al.*[154]	PDG 06/04
$D^0 \to \overline{K}^0\pi^+\pi^-$	0.13	0.19	0.03 ; 0.17	$0.026^{+0.059}_{-0.016}$
				$0.054^{+0.120}_{-0.034}$ (pdg04)
$\to K^-\pi^+\pi^0$	0.18	0.76	0.61 ; 0.28	$1.13^{+0.54}_{-0.20}$
$\to \overline{K}^0 K^+K^-$	0.02	0.006	0.16 ; 0.01	
$\to \pi^+\pi^-\pi^0$	0.04	0.11		
$\to K^+K^-\pi^0$		0.013		
$\to K^0K^-\pi^+$		0.007		0.11 ± 0.11
				0.23 ± 0.23 (pdg04)
$\to \overline{K}^0 K^+\pi^-$		0.013		$0.19^{+0.11}_{-0.08}$
				$0.38^{+0.23}_{-0.19}$ (pdg04)
$\to \overline{K}^0\pi^0\pi^0$				0.42 ± 0.11
				0.85 ± 0.22 (pdg04)
$D^+ \to \overline{K}^0\pi^+\pi^0$	0.76	1.9	1.5;0.7	0.9 ± 0.7
				1.3 ± 1.1 (pdg04)
$\to K^-\pi^+\pi^+$	1.71	0.95	6.5 ; 1.6	9.0 ± 0.7
$\to \pi^+\pi^+\pi^-$	0.15	0.19	0.50 ; 0.067	
$\to K^-K^+\pi^+$	0.02	0.016	0.48 ; 0.004	
$\to K^+\pi^+\pi^-$		0.0032		
$\to K^+K^+K^-$		1.58×10^{-5}		
$\to \pi^+\eta\eta$		0.016 ; 0.032		
$\to \pi^+\eta\eta'$		0.032		
$D^+_s \to K^-K^+\pi^+$	0.42	0.32	1.0 ; 0.69	
$\to \pi^+\pi^+\pi^-$	5×10^{-5}	4.7×10^{-4}		
$\to \pi^+\pi^0\eta$		1.1 ; 0.95		< 5
$\to \pi^+\pi^0\eta'$		0.158		< 1.8
$\to K^+\pi^+\pi^-$		0.047		0.1 ± 0.04

Chapter 26

Charm baryon production and decays[1]

26.1 Introduction

In the past years many new excited charmed baryon states have been discovered by BaBar, Belle and CLEO. In particular, B factories have provided a very rich source of charmed baryons both from B decays and from the continuum $e^+e^- \to c\bar{c}$. A new chapter for the charmed baryon spectroscopy is opened by the rich mass spectrum and the relatively narrow widths of the excited states. Experimentally and theoretically, it is important to identify the quantum numbers of these new states and understand their properties. Since the pseudoscalar mesons involved in the strong decays of charmed baryons are soft, the charmed baryon system offers an excellent ground for testing the ideas and predictions of heavy quark symmetry of the heavy quark and chiral symmetry of the light quarks.

The observation of the lifetime differences among the charmed mesons D^+, D^0 and charmed baryons is very interesting since it was realized very early that the naive parton model gives the same lifetimes for all heavy particles containing a heavy quark Q, while experimentally, the lifetimes of Ξ_c^+ and Ω_c^0 differ by a factor of six ! This implies the importance of the underlying mechanisms such as W-exchange and Pauli interference due to the identical quarks produced in the heavy quark decay and in the wavefunction of the charmed baryons. With the advent of heavy quark effective theory, it was recognized in early nineties that nonperturbative corrections to the parton picture can be systematically expanded in powers of $1/m_Q$. Within the QCD-based heavy quark expansion framework, some phenomenological assumptions can be turned into some coherent and quantitative statements and nonperturbative effects can be systematically studied.

Contrary to the significant progress made over the last 20 years or so in the studies of the heavy meson weak decay, advancement in the arena of heavy baryons is relatively slow. Nevertheless, the experimental measurements of the charmed baryon hadronic weak decays have been pushed to the Cabibbo-suppressed level. Many new data emerged can be used to test a handful of phenomenological models available in the literature. Apart from the complication due to the presence of three quarks in the baryon, a major

[1]By Hai-Yang Cheng

disparity between charmed baryon and charmed meson decays is that while the latter is usually dominated by factorizable amplitudes, the former receives sizable nonfactorizable contributions from W-exchange diagrams which are not subject to color and helicity suppression. Besides the dynamical models, there are also some considerations based on the symmetry argument and the quark diagram scheme.

The exclusive semileptonic decays of charmed baryons like $\Lambda_c^+ \to \Lambda e^+(\mu^+)\nu_e$, $\Xi_c^+ \to \Xi^0 e^+\nu_e$ and $\Xi_c^0 \to \Xi^- e^+\nu_e$ have been observed experimentally. Their rates depend on the heavy baryon to the light baryon transition form factors. Experimentally, the only information available so far is the form-factor ratio measured in the semileptonic decay $\Lambda_c \to \Lambda e\bar{\nu}$.

Although radiative decays are well measured in the charmed meson sector, e.g. $D^* \to D\gamma$ and $D_s^+ \to D_s^+\gamma$, only three of the radiative modes in the charmed baryon sector have been observed, namely, $\Xi_c^{\prime 0} \to \Xi_c^0\gamma$, $\Xi_c^{\prime +} \to \Xi_c^+\gamma$ and $\Omega_c^{*0} \to \Omega_c^0\gamma$. Charm flavor is conserved in these electromagnetic charmed baryon decays. However, it will be difficult to measure the rates of these decays because these states are too narrow to be experimentally resolvable. There are also charm-flavor-conserving weak radiative decays such as $\Xi_c \to \Lambda_c\gamma$ and $\Omega_c \to \Xi_c\gamma$. In these decays, weak radiative transitions arise from the diquark sector of the heavy baryon whereas the heavy quark behaves as a "spectator". The charm-flavor-violating weak radiative decays, e.g., $\Lambda_c^+ \to \Sigma^+\gamma$ and $\Xi_c^0 \to \Xi^0\gamma$, arise from the W-exchange diagram accompanied by a photon emission from the external quark.

Two excellent review articles on charmed baryons can be found in [155, 156].

26.2 Production of charmed baryons at BESIII

Production and decays of the charmed baryons can be studied at BESIII once its center-of-mass energy $\sqrt{s}$ is upgraded to the level above 4.6 GeV. In order to estimate the number of charmed baryon events produced at BESIII, it is necessary to know its luminosity, the cross section $\sigma(e^+e^- \to c\bar{c})$ at the energies of interest and the fragmentation function of the c quark into the charmed baryon.

26.3 Spectroscopy

Charmed baryon spectroscopy provides an ideal place for studying the dynamics of the light quarks in the environment of a heavy quark. The charmed baryon of interest contains a charmed quark and two light quarks, which we will often refer to as a diquark. Each light quark is a triplet of the flavor SU(3). Since $\mathbf{3} \times \mathbf{3} = \bar{\mathbf{3}} + \mathbf{6}$, there are two different SU(3) multiplets of charmed baryons: a symmetric sextet $\mathbf{6}$ and an antisymmetric antitriplet $\bar{\mathbf{3}}$. For the ground-state s-wave baryons in the quark model, the symmetries in the flavor and spin of the diquarks are correlated. Consequently, the diquark in the flavor-symmetric sextet has spin 1, while the diquark in the flavor-antisymmetric antitriplet has spin 0. When the diquark combines with the charmed quark, the sextet contains both spin 1/2 and spin 3/2 charmed baryons. However, the antitriplet contains only spin 1/2 ones. More specifically, the Λ_c^+, Ξ_c^+ and Ξ_c^0 form a $\bar{\mathbf{3}}$ representation and they all decay weakly. The Ω_c^0, $\Xi_c^{\prime +}$, $\Xi_c^{\prime 0}$ and $\Sigma_c^{++,+,0}$ form a $\mathbf{6}$ representation; among them, only Ω_c^0 decays weakly.

Note that we follow the Particle Data Group (PDG) [4] to use a prime to distinguish the Ξ_c in the **6** from the one in the $\bar{\mathbf{3}}$.

The lowest-lying orbital excited baryon states are the p-wave charmed baryons with their quantum numbers listed in Table 26.1. Although the separate spin angular momentum S_ℓ and orbital angular momentum L_ℓ of the light degrees of freedom are not well defined, they are included for guidance from the quark model. In the heavy quark limit, the spin of the charmed quark S_c and the total angular momentum of the two light quarks $J_\ell = S_\ell + L_\ell$ are separately conserved. It is convenient to use them to enumerate the spectrum of states. There are two types of $L_\ell = 1$ orbital excited charmed baryon states: states with the unit of orbital angular momentum between the diquark and the charmed quark, and states with the unit of orbital angular momentum between the two light quarks. The orbital wave function of the former (latter) is symmetric (antisymmetric) under the exchange of two light quarks. To see this, one can define two independent relative momenta $\mathbf{k} = \frac{1}{2}(\mathbf{p}_1 - \mathbf{p}_2)$ and $\mathbf{K} = \frac{1}{2}(\mathbf{p}_1 - \mathbf{p}_2 - 2\mathbf{p}_c)$ from the two light quark momenta $\mathbf{p}_1$, $\mathbf{p}_2$ and the heavy quark momentum $\mathbf{p}_c$. (In the heavy quark limit, $\mathbf{p}_c$ can be set to zero.) Denoting the quantum numbers L_k and L_K as the eigenvalues of $\mathbf{L}_k^2$ and $\mathbf{L}_K^2$, the k-orbital momentum L_k describes relative orbital excitations of the two light quarks, and the K-orbital momentum L_K describes orbital excitations of the center of the mass of the two light quarks relative to the heavy quark [155]. The p-wave heavy baryon can be either in the $(L_k = 0, L_K = 1)$ K-state or the $(L_k = 1, L_K = 0)$ k-state. It is obvious that the orbital K-state (k-state) is symmetric (antisymmetric) under the interchange of $\mathbf{p}_1$ and $\mathbf{p}_2$.

Table 26.1: *The p-wave charmed baryons and their quantum numbers, where S_ℓ (J_ℓ) is the total spin (angular momentum) of the two light quarks. The quantum number in the subscript labels J_ℓ. The quantum number in parentheses is referred to the spin of the baryon. In the quark model, the upper (lower) four multiplets have even (odd) orbital wave functions under the permutation of the two light quarks. That is, L_ℓ for the former is referred to the orbital angular momentum between the diquark and the charmed quark, while L_ℓ for the latter is the orbital angular momentum between the two light quarks. The explicit quark model wave functions for p-wave charmed baryons can be found in [157].*

State	SU(3)	S_ℓ	L_ℓ	$J_\ell^{P_\ell}$	State	SU(3)	S_ℓ	L_ℓ	$J_\ell^{P_\ell}$
$\Lambda_{c1}(\frac{1}{2},\frac{3}{2})$	$\bar{\mathbf{3}}$	0	1	1^-	$\Xi_{c1}(\frac{1}{2},\frac{3}{2})$	$\bar{\mathbf{3}}$	0	1	1^-
$\Sigma_{c0}(\frac{1}{2})$	**6**	1	1	0^-	$\Xi'_{c0}(\frac{1}{2})$	**6**	1	1	0^-
$\Sigma_{c1}(\frac{1}{2},\frac{3}{2})$	**6**	1	1	1^-	$\Xi'_{c1}(\frac{1}{2},\frac{3}{2})$	**6**	1	1	1^-
$\Sigma_{c2}(\frac{3}{2},\frac{5}{2})$	**6**	1	1	2^-	$\Xi'_{c2}(\frac{3}{2},\frac{5}{2})$	**6**	1	1	2^-
$\tilde{\Sigma}_{c1}(\frac{1}{2},\frac{3}{2})$	**6**	0	1	1^-	$\tilde{\Xi}'_{c1}(\frac{1}{2},\frac{3}{2})$	**6**	0	1	1^-
$\tilde{\Lambda}_{c0}(\frac{1}{2})$	$\bar{\mathbf{3}}$	1	1	0^-	$\tilde{\Xi}_{c0}(\frac{1}{2})$	$\bar{\mathbf{3}}$	1	1	0^-
$\tilde{\Lambda}_{c1}(\frac{1}{2},\frac{3}{2})$	$\bar{\mathbf{3}}$	1	1	1^-	$\tilde{\Xi}_{c1}(\frac{1}{2},\frac{3}{2})$	$\bar{\mathbf{3}}$	1	1	1^-
$\tilde{\Lambda}_{c2}(\frac{3}{2},\frac{5}{2})$	$\bar{\mathbf{3}}$	1	1	2^-	$\tilde{\Xi}_{c2}(\frac{3}{2},\frac{5}{2})$	$\bar{\mathbf{3}}$	1	1	2^-

The observed mass spectra and decay widths of charmed baryons are summarized

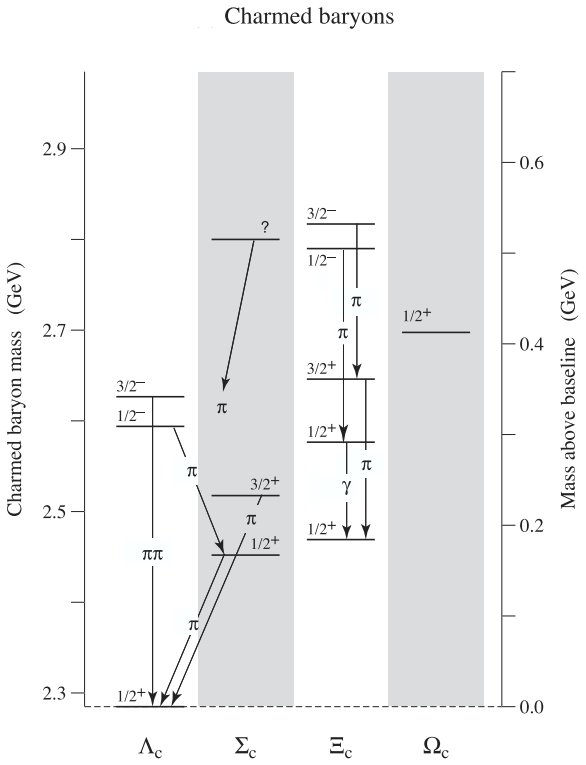

Figure 26.1: Charmed baryons and some of their orbital excitations [4].

in Table 26.2 (see also Fig. 26.1). B factories have provided a very rich source of charmed baryons both from B decays and from the continuum $e^+e^- \to c\bar{c}$. For example, several new excited charmed baryon states such as $\Lambda_c(2765)^+, \Lambda_c(2880)^+, \Lambda_c(2940)^+$, $\Xi_c(2815), \Xi_c(2980)$ and $\Xi_c(3077)$ have been measured recently and they are not still not in the list of 2006 Particle Data Group [4]. By now, the $J^P = \frac{1}{2}^+$ and $\frac{1}{2}^-$ $\bar{\mathbf{3}}$ states: $(\Lambda_c^+, \Xi_c^+, \Xi_c^0)$, $(\Lambda_c(2593)^+, \Xi_c(2790)^+, \Xi_c(2790)^0)$, and $J^P = \frac{1}{2}^+$ and $\frac{3}{2}^+$ $\mathbf{6}$ states: $(\Omega_c, \Sigma_c, \Xi_c')$, $(\Omega_c^*, \Sigma_c^*, \Xi_c'^*)$ are established. Notice that except for the parity of the lightest Λ_c^+, none of the other J^P quantum numbers given in Table 26.2 has been measured. One has to rely on the quark model to determine the J^P assignments.

In the following we discuss some of the new excited charmed baryon states:

- The highest $\Lambda_c(2940)^+$ was first discovered by BaBar in the D^0p decay mode [158] and confirmed by Belle in the decays $\Sigma_c^0\pi^+, \Sigma_c^{++}\pi^-$ which subsequently decay into $\Lambda_c^+\pi^+\pi^-$ [159, 160]. The state $\Lambda_c(2880)^+$ first observed by CLEO [161] in $\Lambda_c^+\pi^+\pi^-$ was also seen by BaBar in the D^0p spectrum [158]. It was originally conjectured that, based on its narrow width, $\Lambda_c(2880)^+$ might be a $\tilde{\Lambda}_{c0}^+(\frac{1}{2})$ state [161]. Recently, Belle has studied the experimental constraint on the J^P quantum numbers of $\Lambda_c(2880)^+$ [159]. The angular analysis of $\Lambda_c(2880)^+ \to \Sigma_c^{0,++}\pi^\pm$ indicates that $J = 5/2$ is favored over $J = 1/2$ or $3/2$, while the study of the resonant structure of $\Lambda_c(2880)^+ \to \Lambda_c^+\pi^+\pi^-$ implies the existence of the $\Sigma_c^*\pi$ intermediate states and $\Gamma(\Sigma_c^*\pi^\pm)/\Gamma(\Sigma_c\pi^\pm) = (24.1 \pm 6.4^{+1.1}_{-4.5})\%$. This value is in agreement with heavy quark

Table 26.2: Mass spectra and decay widths (in units of MeV) of charmed baryons. Experimental values are taken from the Particle Data Group [4] except $\Lambda_c(2880)$, $\Lambda_c(2940)$, $\Xi_c(2980)^{+,0}$, $\Xi_c(3077)^{+,0}$ and $\Omega_c(2768)$ for which we use the most recent available BaBar and Belle measurements.

State	quark content	J^P	Mass	Width
Λ_c^+	udc	$\frac{1}{2}^+$	2286.46 ± 0.14	
$\Lambda_c(2593)^+$	udc	$\frac{1}{2}^-$	2595.4 ± 0.6	$3.6^{+2.0}_{-1.3}$
$\Lambda_c(2625)^+$	udc	$\frac{3}{2}^-$	2628.1 ± 0.6	< 1.9
$\Lambda_c(2765)^+$	udc	$?^?$	2766.6 ± 2.4	50
$\Lambda_c(2880)^+$	udc	$\frac{5}{2}^+$	2881.5 ± 0.3	5.5 ± 0.6
$\Lambda_c(2940)^+$	udc	$?^?$	2938.8 ± 1.1	13.0 ± 5.0
$\Sigma_c(2455)^{++}$	uuc	$\frac{1}{2}^+$	2454.02 ± 0.18	2.23 ± 0.30
$\Sigma_c(2455)^+$	udc	$\frac{1}{2}^+$	2452.9 ± 0.4	< 4.6
$\Sigma_c(2455)^0$	ddc	$\frac{1}{2}^+$	2453.76 ± 0.18	2.2 ± 0.4
$\Sigma_c(2520)^{++}$	uuc	$\frac{3}{2}^+$	2518.4 ± 0.6	14.9 ± 1.9
$\Sigma_c(2520)^+$	udc	$\frac{3}{2}^+$	2517.5 ± 2.3	< 17
$\Sigma_c(2520)^0$	ddc	$\frac{3}{2}^+$	2518.0 ± 0.5	16.1 ± 2.1
$\Sigma_c(2800)^{++}$	uuc	$?^?$	2801^{+4}_{-6}	75^{+22}_{-17}
$\Sigma_c(2800)^+$	udc	$?^?$	2792^{+14}_{-5}	62^{+60}_{-40}
$\Sigma_c(2800)^0$	ddc	$?^?$	2802^{+4}_{-7}	61^{+28}_{-18}
Ξ_c^+	usc	$\frac{1}{2}^+$	2467.9 ± 0.4	
Ξ_c^0	dsc	$\frac{1}{2}^+$	2471.0 ± 0.4	
$\Xi_c'^+$	usc	$\frac{1}{2}^+$	2575.7 ± 3.1	
$\Xi_c'^0$	dsc	$\frac{1}{2}^+$	2578.0 ± 2.9	
$\Xi_c(2645)^+$	usc	$\frac{3}{2}^+$	2646.6 ± 1.4	< 3.1
$\Xi_c(2645)^0$	dsc	$\frac{3}{2}^+$	2646.1 ± 1.2	< 5.5
$\Xi_c(2790)^+$	usc	$\frac{1}{2}^-$	2789.2 ± 3.2	< 15
$\Xi_c(2790)^0$	dsc	$\frac{1}{2}^-$	2791.9 ± 3.3	< 12
$\Xi_c(2815)^+$	usc	$\frac{3}{2}^-$	2816.5 ± 1.2	< 3.5
$\Xi_c(2815)^0$	dsc	$\frac{3}{2}^-$	2818.2 ± 2.1	< 6.5
$\Xi_c(2980)^+$	usc	$?^?$	2971.1 ± 1.7	25.2 ± 3.0
$\Xi_c(2980)^0$	dsc	$?^?$	2977.1 ± 9.5	43.5
$\Xi_c(3077)^+$	usc	$?^?$	3076.5 ± 0.6	6.2 ± 1.1
$\Xi_c(3077)^0$	dsc	$?^?$	3082.8 ± 2.3	5.2 ± 3.6
Ω_c^0	ssc	$\frac{1}{2}^+$	2697.5 ± 2.6	
$\Omega_c(2768)^0$	ssc	$\frac{3}{2}^+$	2768.3 ± 3.0	

symmetry predictions [162] and favors the $5/2^+$ over the $5/2^-$ assignment.[2] Therefore, it is not a $\tilde{\Lambda}_{c2}^+(\frac{5}{2})$ state either. Since $J_\ell = 2, S_\ell = 0, L = 2$ for the diquark system of $\Lambda_c(2880)^+$, this is the first observation of a d-wave charmed baryon. It is interesting to notice that, based on the diquark idea, the assignment $J^P = 5/2^+$ has already been predicted in [164] for the state $\Lambda_c(2880)$ before the Belle experiment. As for $\Lambda_c(2980)^+$, it was recently argued that it is an exotic molecular state of D^{*0} and p [165].

- The new charmed strange baryons $\Xi_c(2980)^+$ and $\Xi_c(3077)^+$ that decay into $\Lambda_c^+ K^-\pi^+$ were first observed by Belle [166] and confirmed by BaBar [167]. In the recent BaBar measurement [167], the $\Xi_c(2980)^+$ is found to decay resonantly through the intermediate state $\Sigma_c(2455)^{++}K^-$ with $4.9\,\sigma$ significance and non-resonantly to $\Lambda_c^+ K^-\pi^+$ with $4.1\,\sigma$ significance. With $5.8\,\sigma$ significance, the $\Xi_c(3077)^+$ is found to decay resonantly through $\Sigma_c(2455)^{++}K^-$, and with $4.6\,\sigma$ significance, it is found to decay through $\Sigma_c(2520)^{++}K^-$. The significance of the signal for the non-resonant decay $\Xi_c(3077)^+ \to \Lambda_c^+ K^-\pi^+$ is $1.4\,\sigma$.

- The highest isotriplet charmed baryons $\Sigma_c(2800)^{++,+,0}$ decaying into $\Lambda_c^+\pi$ were first measured by Belle [168]. They are most likely to be the $J^P = 3/2^-$ Σ_{c2} states because the $\Sigma_{c2}(\frac{3}{2})$ baryon decays principally into the $\Lambda_c\pi$ system in a D-wave, while $\Sigma_{c1}(\frac{3}{2})$ decays mainly into the two pion system $\Lambda_c\pi\pi$. The state $\Sigma_{c0}(\frac{1}{2})$ can decay into $\Lambda_c\pi$ in an S-wave, but it is very broad with width of order 406 MeV [163]. Experimentally, it will be very difficult to observe it.

- The new $3/2^+$ $\Omega_c(2768)$ was recently observed by BaBar in the electromagnetic decay $\Omega_c(2768) \to \Omega_c\gamma$ [169]. With this new observation, the $3/2^+$ sextet is finally completed.

- Evidence of double charm states has been reported by SELEX in $\Xi_{cc}(3519)^+ \to \Lambda_c^+ K^-\pi^+$ [170]. Further observations of $\Xi_{cc}^{++} \to \Lambda_c^+ K^-\pi^+\pi^+$ and $\Xi_{cc}^+ \to pD^+K^-$ were also announced by SELEX [171]. However, none of the double charm states discovered by SELEX has been confirmed by FOCUS, BaBar [172] and Belle [160] despite the 10^6 Λ_c events produced in B factories versus 1630 Λ_c events observed at SELEX.

Charmed baryon spectroscopy has been studied extensively in various models. The interested readers are referred to [173] for further references. In heavy quark effective theory, the mass splittings between spin-$\frac{3}{2}$ and spin-$\frac{1}{2}$ sextet charmed baryon multiplets are governed by the chromomagnetic interactions so that

$$m_{\Sigma_c^*} - m_{\Sigma_c} = m_{\Xi_c'^*} - m_{\Xi_c'} = m_{\Omega_c^*} - m_{\Omega_c}, \tag{26.1}$$

up to corrections of $1/m_c$. This relation is borne out by experiment: $m_{\Sigma_c^{*+}} - m_{\Sigma_c^+} = 64.6 \pm 2.3$ MeV, $m_{\Xi_c'^{*+}} - m_{\Xi_c'^+} = 70.9 \pm 3.4$ MeV and $m_{\Omega_c^*} - m_{\Omega_c} = 70.8 \pm 1.5$ MeV.

[2] Strictly speaking, the argument in favor of the $5/2^+$ assignment is reached in [159] by considering only the F-wave contribution and neglecting the P-wave contribution to $\Lambda_c(2880)^+ \to \Sigma_c^*\pi$ (see [163] for more discussions).

26.4 Strong decays

Due to the rich mass spectrum and the relatively narrow widths of the excited states, the charmed baryon system offers an excellent ground for testing the ideas and predictions of heavy quark symmetry and light flavor SU(3) symmetry. The pseudoscalar mesons involved in the strong decays of charmed baryons such as $\Sigma_c \to \Lambda_c \pi$ are soft. Therefore, heavy quark symmetry of the heavy quark and chiral symmetry of the light quarks will have interesting implications for the low-energy dynamics of heavy baryons interacting with the Goldstone bosons.

The strong decays of charmed baryons are most conveniently described by the heavy hadron chiral Lagrangians in which heavy quark symmetry and chiral symmetry are incorporated [174, 175]. The Lagrangian involves two coupling constants g_1 and g_2 for P-wave transitions between s-wave and s-wave baryons [174], six couplings $h_2 - h_7$ for the S-wave transitions between s-wave and p-wave baryons, and eight couplings $h_8 - h_{15}$ for the D-wave transitions between s-wave and p-wave baryons [157]. The general chiral Lagrangian for heavy baryons coupling to the pseudoscalar mesons can be expressed compactly in terms of superfields. We will not write down the relevant Lagrangians here; instead the reader is referred to Eqs. (3.1) and (3.3) of [157]. Nevertheless, we list some of the partial widths derived from the Lagrangian [157]:

$$\begin{aligned}
\Gamma(\Sigma_c^* \to \Sigma_c \pi) &= \frac{g_1^2}{2\pi f_\pi^2} \frac{m_{\Sigma_c}}{m_{\Sigma_c^*}} p_\pi^3, \qquad \Gamma(\Sigma_c \to \Lambda_c \pi) = \frac{g_2^2}{2\pi f_\pi^2} \frac{m_{\Lambda_c}}{m_{\Sigma_c}} p_\pi^3, \\
\Gamma(\Lambda_{c1}(1/2) \to \Sigma_c \pi) &= \frac{h_2^2}{2\pi f_\pi^2} \frac{m_{\Sigma_c}}{m_{\Lambda_{c1}}} E_c^2 \pi_\pi, \qquad \Gamma(\Sigma_{c0}(1/2) \to \Lambda_c \pi) = \frac{h_3^2}{2\pi f_\pi^2} \frac{m_{\Lambda_c}}{m_{\Sigma_{c0}}} E_\pi^2 p_\pi, \\
\Gamma(\Sigma_{c1}(1/2) \to \Sigma_c \pi) &= \frac{h_4^2}{4\pi f_\pi^2} \frac{m_{\Sigma_c}}{m_{\Sigma_{c1}}} E_\pi^2 p_\pi, \qquad \Gamma(\tilde{\Sigma}_{c1}(1/2) \to \Sigma_c \pi) = \frac{h_5^2}{4\pi f_\pi^2} \frac{m_{\Sigma_c}}{m_{\tilde{\Sigma}_{c1}}} E_\pi^2 p_\pi, \\
\Gamma(\tilde{\Xi}_{c0}(1/2) \to \Xi_c \pi) &= \frac{h_6^2}{2\pi f_\pi^2} \frac{m_{\Xi_c}}{m_{\tilde{\Xi}_{c0}}} E_\pi^2 p_\pi, \qquad \Gamma(\tilde{\Lambda}_{c1}(1/2) \to \Sigma_c \pi) = \frac{h_7^2}{2\pi f_\pi^2} \frac{m_{\Sigma_c}}{m_{\tilde{\Lambda}_{c1}}} E_\pi^2 p_\pi,
\end{aligned} \tag{26.2}$$

where p_π is the pion's momentum and $f_\pi = 132$ MeV. Unfortunately, the decay $\Sigma_c^* \to \Sigma_c \pi$ is kinematically prohibited since the mass difference between Σ_c^* and Σ_c is only of order 65 MeV. Consequently, the coupling g_1 cannot be extracted directly from the strong decays of heavy baryons.

26.4.1 Strong decays of s-wave charmed baryons

In the framework of heavy hadron chiral pertrubation theory (HHChPT), one can use some measurements as input to fix the coupling g_2 which, in turn, can be used to predict the rates of other strong decays. We shall use $\Sigma_c \to \Lambda_c \pi$ as input [4]

$$\Gamma(\Sigma_c^{++}) = \Gamma(\Sigma_c^{++} \to \Lambda_c^+ \pi^+) \;\; = \;\; 2.23 \pm 0.30\,\text{MeV}. \tag{26.3}$$

¿From which we obtain

$$|g_2| = 0.605^{+0.039}_{-0.043}\,, \tag{26.4}$$

Table 26.3: Decay widths (in units of MeV) of s-wave charmed baryons. Theoretical predictions of [178] are taken from Table IV of [179].

Decay	HHChPT	Tawfiq et al. [178]	Ivanov et al. [179]	Huang et al. [180]	Albertus et al. [181]	Expt. [4]
$\Sigma_c^{++} \to \Lambda_c^+ \pi^+$	input	1.51 ± 0.17	2.85 ± 0.19	2.5	2.41 ± 0.07	2.23 ± 0.30
$\Sigma_c^{+} \to \Lambda_c^+ \pi^0$	2.6 ± 0.4	1.56 ± 0.17	3.63 ± 0.27	3.2	2.79 ± 0.08	< 4.6
$\Sigma_c^{0} \to \Lambda_c^+ \pi^-$	2.2 ± 0.3	1.44 ± 0.16	2.65 ± 0.19	2.4	2.37 ± 0.07	2.2 ± 0.4
$\Sigma_c(2520)^{++} \to \Lambda_c^+ \pi^+$	16.7 ± 2.3	11.77 ± 1.27	21.99 ± 0.87	8.2	17.52 ± 0.75	14.9 ± 1.9
$\Sigma_c(2520)^{+} \to \Lambda_c^+ \pi^0$	17.4 ± 2.3			8.6	17.31 ± 0.74	< 17
$\Sigma_c(2520)^{0} \to \Lambda_c^+ \pi^-$	16.6 ± 2.2	11.37 ± 1.22	21.21 ± 0.81	8.2	16.90 ± 0.72	16.1 ± 2.1
$\Xi_c(2645)^{+} \to \Xi_c^{0,+} \pi^{+,0}$	2.8 ± 0.4	1.76 ± 0.14	3.04 ± 0.37		3.18 ± 0.10	< 3.1
$\Xi_c(2645)^{0} \to \Xi_c^{+,0} \pi^{-,0}$	2.9 ± 0.4	1.83 ± 0.06	3.12 ± 0.33		3.03 ± 0.10	< 5.5

where we have neglected the tiny contributions from electromagnetic decays. Note that $|g_2|$ obtained from $\Sigma_c^0 \to \Lambda_c^+ \pi^-$ has the same central value as Eq. (26.4) except that the errors are slightly large. If $\Sigma_c^* \to \Lambda_c \pi$ decays are employed as input, we will obtain $|g_2| = 0.57 \pm 0.04$ from $\Sigma_c^{*++} \to \Lambda_c^+ \pi^+$ and 0.60 ± 0.04 from $\Sigma_c^{*0} \to \Lambda_c^+ \pi^-$. Hence, it is preferable to use the measurement of $\Sigma_c^{++} \to \Lambda_c^+ \pi^+$ to fix $|g_2|$.[3]

As pointed out in [174], within in the framework of the non-relativistic quark model, the couplings g_1 and g_2 can be related to g_A^q, the axial-vector coupling in a single quark transition of $u \to d$, via

$$g_1 = \frac{4}{3} g_A^q, \qquad g_2 = \sqrt{\frac{2}{3}} g_A^q. \tag{26.5}$$

Using $g_A^q = 0.75$ which is required to reproduce the correct value of $g_A^N = 1.25$, we obtain

$$g_1 = 1, \qquad g_2 = 0.61\,. \tag{26.6}$$

Hence, the quark model prediction is in good agreement with experiment, but deviates 2σ from the large-N_c argument: $|g_2| = g_A^N/\sqrt{2} = 0.88$ [177]. Applying (26.4) leads to (see also Table 26.3)

$$\Gamma(\Xi_c^{\prime *+}) = \Gamma(\Xi_c^{\prime *+} \to \Xi_c^+ \pi^0, \Xi_c^0 \pi^+) = \frac{g_2^2}{4\pi f_\pi^2} \left(\frac{1}{2} \frac{m_{\Xi_c^+}}{m_{\Xi_c^{\prime +}}} p_\pi^3 + \frac{m_{\Xi_c^0}}{m_{\Xi_c^{\prime +}}} p_\pi^3 \right) = (2.8 \pm 0.4)\,\text{MeV},$$

$$\Gamma(\Xi_c^{\prime *0}) = \Gamma(\Xi_c^{\prime *0} \to \Xi_c^+ \pi^-, \Xi_c^0 \pi^0) = \frac{g_2^2}{4\pi f_\pi^2} \left(\frac{m_{\Xi_c^+}}{m_{\Xi_c^{\prime 0}}} p_\pi^3 + \frac{1}{2} \frac{m_{\Xi_c^0}}{m_{\Xi_c^{\prime 0}}} p_\pi^3 \right) = (2.9 \pm 0.4)\,\text{MeV}, \tag{26.7}$$

Note that we have neglected the effect of $\Xi_c - \Xi_c'$ mixing in calculations (for recent considerations, see [182, 183]). Therefore, the predicted total width of $\Xi_c^{\prime *+}$ is in the vicinity of the current limit $\Gamma(\Xi_c^{\prime *+}) < 3.1$ MeV [184].

It is clear from Table 26.3 that the predicted widths of Σ_c^{++} and Σ_c^0 by HHChPT are in good agreement with experiment. The strong decay width of Σ_c is smaller than that

[3] For previous efforts of extracting g_2 from experiment using HHChPT, see [176, 157].

Table 26.4: Same as Table 26.3 except for p-wave charmed baryons [163].

Decay	HHChPT	Tawfiq et al. [178]	Ivanov et al. [179]	Huang et al. [180]	Zhu [185]	Expt. [4]
$\Lambda_c(2593)^+ \to (\Sigma_c^+\pi\pi)_R$	input			2.5		$2.63^{+1.56}_{-1.09}$
$\Lambda_c(2593)^+ \to \Sigma_c^{++}\pi^-$	$0.62^{+0.37}_{-0.26}$	1.47 ± 0.57	0.79 ± 0.09	$0.55^{+1.3}_{-0.55}$	0.64	$0.65^{+0.41}_{-0.30}$
$\Lambda_c(2593)^+ \to \Sigma_c^0\pi^+$	$0.67^{+0.40}_{-0.28}$	1.78 ± 0.70	0.83 ± 0.09	0.89 ± 0.86	0.86	$0.67^{+0.41}_{-0.30}$
$\Lambda_c(2593)^+ \to \Sigma_c^+\pi^0$	$1.34^{+0.79}_{-0.55}$	1.18 ± 0.46	0.98 ± 0.12	1.7 ± 0.49	1.2	
$\Lambda_c(2625)^+ \to \Sigma_c^{++}\pi^-$	≤ 0.011	0.44 ± 0.23	0.076 ± 0.009	0.013	0.011	< 0.10
$\Lambda_c(2625)^+ \to \Sigma_c^0\pi^+$	≤ 0.015	0.47 ± 0.25	0.080 ± 0.009	0.013	0.011	< 0.09
$\Lambda_c(2625)^+ \to \Sigma_c^+\pi^0$	≤ 0.011	0.42 ± 0.22	0.095 ± 0.012	0.013	0.011	
$\Lambda_c(2625)^+ \to \Lambda_c^+\pi\pi$	≤ 0.21			0.11		< 1.9
$\Sigma_c(2800)^{++} \to \Lambda_c\pi, \Sigma_c^{(*)}\pi$	input					75^{+22}_{-17}
$\Sigma_c(2800)^+ \to \Lambda_c\pi, \Sigma_c^{(*)}\pi$	input					62^{+60}_{-40}
$\Sigma_c(2800)^0 \to \Lambda_c\pi, \Sigma_c^{(*)}\pi$	input					61^{+28}_{-18}
$\Xi_c(2790)^+ \to \Xi_c^{\prime 0,+}\pi^{+,0}$	$7.7^{+4.5}_{-3.2}$					< 15
$\Xi_c(2790)^0 \to \Xi_c^{\prime +,0}\pi^{-,0}$	$8.1^{+4.8}_{-3.4}$					< 12
$\Xi_c(2815)^+ \to \Xi_c^{\prime *+,0}\pi^{0,+}$	$3.2^{+1.9}_{-1.3}$	2.35 ± 0.93	0.70 ± 0.04			< 3.5
$\Xi_c(2815)^0 \to \Xi_c^{\prime *+,0}\pi^{-,0}$	$3.5^{+2.0}_{-1.4}$					< 6.5

of Σ_c^* by a factor of ~ 7, although they will become the same in the limit of heavy quark symmetry. This is ascribed to the fact that the pion's momentum is around 90 MeV in the decay $\Sigma_c \to \Lambda_c\pi$ while it is two times bigger in $\Sigma_c^* \to \Lambda_c\pi$. Since Σ_c states are significantly narrower than their spin-3/2 counterparts, this explains why the measurement of their widths came out much later. Instead of using the data to fix the coupling constants in a model-independent manner, there exist some calculations of couplings in various models such as the relativistic light-front model [178], the relativistic three-quark model [179] and light-cone sum rules [180, 185]. The results are summarized in Table 26.3.

It is worth remarking that although the coupling g_1 cannot be determined directly from the strong decay such as $\Sigma_c^* \to \Sigma_c\pi$, some information of g_1 can be learned from the radiative decay $\Xi_c^{\prime *0} \to \Xi_c^0\gamma$, which is prohibited at tree level by SU(3) symmetry but can be induced by chiral loops. A measurement of $\Gamma(\Xi_c^{\prime *0} \to \Xi_c^0\gamma)$ will yield two possible solutions for g_1. Assuming the validity of the quark model relations among different coupling constants, the experimental value of g_2 implies $|g_1| = 0.93 \pm 0.16$ [176] (see also Sec. VIII.A).

26.4.2 Strong decays of p-wave charmed baryons

Some of the S-wave and D-wave couplings of p-wave baryons to s-wave baryons can be determined. In principle, the coupling h_2 is readily extracted from $\Lambda_c(2593)^+ \to \Sigma_c^0\pi^+$ with $\Lambda_c(2593)^+$ identified as $\Lambda_{c1}(\frac{1}{2})^+$. However, since $\Lambda_c(2593)^+ \to \Sigma_c\pi$ is kinematically barely allowed, the finite width effects of the intermediate resonant states will become important [186].

Pole contributions to the decays $\Lambda_c(2593)^+, \Lambda_c(2625)^+ \to \Lambda_c^+\pi\pi$ have been considered

in [187, 180, 157] with the finite width effects included. The intermediate states of interest are Σ_c and Σ_c^* poles. The resonant contribution arises from the Σ_c pole, while the non-resonant term receives a contribution from the Σ_c^* pole. (Since $\Lambda_c(2593)^+, \Lambda_c(2625)^+ \to \Lambda_c^*\pi$ are not kinematically allowed, the Σ_c^* pole is not a resonant contribution.) The decay rates thus depend on two coupling constants h_2 and h_8. The decay rate for the process $\Lambda_{c_1}^+(2593) \to \Lambda_c^+\pi^+\pi^-$ can be calculated in the framework of heavy hadron chiral perturbation theory to be [163]

$$\begin{aligned}\Gamma(\Lambda_c(2593) \to \Lambda_c^+\pi\pi) &= 14.48h_2^2 + 27.54h_8^2 - 3.11h_2h_8, \\ \Gamma(\Lambda_c(2625) \to \Lambda_c^+\pi\pi) &= 0.648h_2^2 + 0.143\times 10^6 h_8^2 - 28.6h_2h_8. \end{aligned} \tag{26.8}$$

It is clear that the limit on $\Gamma(\Lambda_c(2625))$ gives an upper bound on h_8 of order 10^{-3} (in units of MeV^{-1}), whereas the decay width of $\Lambda_c(2593)$ is entirely governed by the coupling h_2. This indicates that the direct non-resonant $\Lambda_c^+\pi\pi$ cannot be described by the Σ_c^* pole alone. Identifying the calculated $\Gamma(\Lambda_c(2593) \to \Lambda_c^+\pi\pi)$ with the resonant one, we find

$$|h_2| = 0.427^{+0.111}_{-0.100}\,, \qquad |h_8| \le 3.57\times 10^{-3}\,. \tag{26.9}$$

Assuming that the total decay width of $\Lambda_c(2593)$ is saturated by the resonant $\Lambda_c^+\pi\pi$ 3-body decays, Pirjol and Yan obtained $|h_2| = 0.572^{+0.322}_{-0.197}$ and $|h_8| \le (3.50 - 3.68)\times 10^{-3}\,\mathrm{MeV}^{-1}$ [157]. Using the updated hadron masses and $\Gamma(\Lambda_c(2593) \to \Lambda_c^+\pi\pi)$,[4] we find $|h_2| = 0.499^{+0.134}_{-0.100}$. Taking into account the fact that the Σ_c and Σ_c^* poles only describe the resonant contributions to the total width of $\Lambda_c(2593)$, we finally reach the h_2 value given in (26.9). Taking into account the threshold (or finite width) effect in the strong decay $\Lambda_c(2593)^+ \to \Lambda_c\pi\pi$, a slightly small coupling $h_2^2 = 0.24^{+0.23}_{-0.11}$ is obtained in [186]. For the spin-$\frac{3}{2}$ state $\Lambda_c(2625)$, its decay is dominated by the three-body channel $\Lambda_c^+\pi\pi$ as the major two-body decay $\Sigma_c\pi$ is a D-wave one.

Some information on the coupling h_{10} cane be inferred from the strong decays of $\Lambda_c(2800)$. As noticed in passing, the states $\Sigma_c(2800)^{++,+,0}$ are most likely to be $\Sigma_{c2}(\frac{3}{2})$. Assuming their widths are dominated by the two-body modes $\Lambda_c\pi$, $\Sigma_c\pi$ and $\Lambda_c^*\pi$, we have [157]

$$\begin{aligned}\Gamma\left(\Sigma_{c2}(\frac{3}{2})^{++}\right) &\approx \Gamma\left(\Sigma_{c2}(\frac{3}{2})^{++} \to \Lambda_c^+\pi^+\right) + \Gamma\left(\Sigma_{c2}(\frac{3}{2})^{++} \to \Sigma_c^+\pi^+\right) + \Gamma\left(\Sigma_{c2}(\frac{3}{2})^{++} \to \Sigma_c^{*+}\pi^+\right) \\ &= \frac{4h_{10}^2}{15\pi f_\pi^2}\frac{m_{\Lambda_c}}{m_{\Sigma_{c2}}}p_c^5 + \frac{h_{11}^2}{10\pi f_\pi^2}\frac{m_{\Sigma_c}}{m_{\Sigma_{c2}}}p_c^5 + \frac{h_{11}^2}{10\pi f_\pi^2}\frac{m_{\Sigma_c^*}}{m_{\Sigma_{c2}}}p_c^5, \end{aligned} \tag{26.10}$$

and similar expressions for $\Sigma_c(2800)^+$ and $\Sigma_c(2800)^0$. Using the quark model relation $h_{11}^2 = 2h_{10}^2$ [see also Eq. (26.13)] and the measured widths of $\Sigma_c(2800)^{++,+,0}$ (Table 26.2), we obtain

$$|h_{10}| = (0.85^{+0.11}_{-0.08})\times 10^{-3}\,\mathrm{MeV}^{-1}\,. \tag{26.11}$$

Since the state $\Lambda_{c1}(\frac{3}{2})$ is broader, even a small mixing of $\Lambda_{c2}(\frac{3}{2})$ with $\Lambda_{c1}(\frac{3}{2})$ could enhance the decay width of the former [157]. In this case, the above value for h_{10} should be regarded

[4] The CLEO result $\Gamma(\Lambda_c(2593)) = 3.9^{+2.4}_{-1.6}$ MeV [188] is used in [157] to fix h_2.

as an upper limit of $|h_{10}|$. Using the quark model relation $|h_8| = |h_{10}|$ (see Eq. (26.13) below), the calculated partial widths of $\Lambda_c(2625)^+$ are shown in Table 26.4.

The $\Xi_c(2790)$ and $\Xi_c(2815)$ baryons form a doublet $\Xi_{c1}(\frac{1}{2}, \frac{3}{2})$. $\Xi_c(2790)$ decays to $\Xi_c'\pi$, while $\Xi_c(2815)$ decays to $\Xi_c\pi\pi$, resonating through Ξ_c^*, i.e. $\Xi_c(2645)$. Using the coupling h_2 obtained (26.9) and the experimental observation that the $\Xi_c\pi\pi$ mode in $\Xi_c(2815)$ decays is consistent with being entirely via $\Xi_c(2645)\pi$, the predicted $\Xi_c(2790)$ and $\Xi_c(2815)$ widths are shown in Table 26.4 and they are consistent with the current experimental limits.

Couplings other than h_2 and h_{10} can be related to each other via the quark model. The S-wave couplings between the s-wave and the p-wave baryons are related by [157]

$$\frac{|h_3|}{|h_4|} = \frac{\sqrt{3}}{2}, \quad \frac{|h_2|}{|h_4|} = \frac{1}{2}, \quad \frac{|h_5|}{|h_6|} = \frac{2}{\sqrt{3}}, \quad \frac{|h_5|}{|h_7|} = 1\,. \tag{26.12}$$

The D-wave couplings satisfy the relations

$$|h_8| = |h_9| = |h_{10}|, \quad \frac{|h_{11}|}{|h_{10}|} = \frac{|h_{15}|}{|h_{14}|} = \sqrt{2}, \quad \frac{|h_{12}|}{|h_{13}|} = 2, \quad \frac{|h_{14}|}{|h_{13}|} = 1\,. \tag{26.13}$$

The reader is referred to [157] for further details.

26.5 Lifetimes

The lifetime differences among the charmed mesons D^+, D^0 and charmed baryons have been studied extensively both experimentally and theoretically since late 1970s. It was realized very early that the naive parton model gives the same lifetimes for all heavy particles containing a heavy quark Q and that the underlying mechanism for the decay width differences and the lifetime hierarchy of heavy hadrons comes mainly from the spectator effects like W-exchange and Pauli interference due to the identical quarks produced in the heavy quark decay and in the charmed baryons (for a review, see [189, 156, 190]). The spectator effects were expressed in 1980s in terms of local four-quark operators by relating the total widths to the imaginary part of certain forward scattering amplitudes [191, 192, 193]. (The spectator effects for charmed baryons were first studied in [194].) With the advent of heavy quark effective theory (HQET), it was recognized in early 1990s that nonperturbative corrections to the parton picture can be systematically expanded in powers of $1/m_Q$ [195, 196]. Subsequently, it was demonstrated that this $1/m_Q$ expansion is applicable not only to global quantities such as lifetimes, but also to local quantities, e.g. the lepton spectrum in the semileptonic decays of heavy hadrons [197]. Therefore, the above-mentioned phenomenological work in 1980s acquired a firm theoretical footing in 1990s, namely the heavy quark expansion (HQE), which is a generalization of the operator product expansion (OPE) in $1/m_Q$. Within this QCD-based framework, some phenomenological assumptions can be turned into some coherent and quantitative statements and nonperturbative effects can be systematically studied.

Based on the OPE approach for the analysis of inclusive weak decays, the inclusive rate of the charmed baryon is schematically represented by

$$\Gamma(\mathcal{B}_c \to f) = \frac{G_F^2 m_c^5}{192\pi^3} V_{\rm CKM} \left(A_0 + \frac{A_2}{m_c^2} + \frac{A_3}{m_c^3} + \mathcal{O}(\frac{1}{m_c^4}) \right). \tag{26.14}$$

The A_0 term comes from the c quark decay and is common to all charmed hadrons. There is no linear $1/m_Q$ corrections to the inclusive decay rate due to the lack of gauge-invariant dimension-four operators [198, 195], a consequence known as Luke's theorem [199]. Nonperturbative corrections start at order $1/m_Q^2$ and they are model independent. Spectator effects in inclusive decays due to the Pauli interference and W-exchange contributions account for $1/m_c^3$ corrections and they have two eminent features: First, the estimate of spectator effects is model dependent; the hadronic four-quark matrix elements are usually evaluated by assuming the factorization approximation for mesons and the quark model for baryons. Second, there is a two-body phase-space enhancement factor of $16\pi^2$ for spectator effects relative to the three-body phase space for heavy quark decay. This implies that spectator effects, being of order $1/m_c^3$, are comparable to and even exceed the $1/m_c^2$ terms.

The lifetimes of charmed baryons are measured to be [4]

$$\begin{aligned} &\tau(\Lambda_c^+) = (200 \pm 6) \times 10^{-15} s, \qquad &&\tau(\Xi_c^+) = (442 \pm 26) \times 10^{-15} s, \\ &\tau(\Xi_c^0) = (112^{+13}_{-10}) \times 10^{-15} s, \qquad &&\tau(\Omega_c^0) = (69 \pm 12) \times 10^{-15} s. \end{aligned} \tag{26.15}$$

As we shall see below, the lifetime hierarchy $\tau(\Xi_c^+) > \tau(\Lambda_c^+) > \tau(\Xi_c^0) > \tau(\Omega_c^0)$ is qualitatively understandable in the OPE approach but not quantitatively.

In general, the total width of the charmed baryon $\mathcal{B}_c$ receives contributions from inclusive nonleptonic and semileptonic decays: $\Gamma(\mathcal{B}_c) = \Gamma_{\rm NL}(\mathcal{B}_c) + \Gamma_{\rm SL}(\mathcal{B}_c)$. The nonleptonic contribution can be decomposed into

$$\Gamma_{\rm NL}(\mathcal{B}_c) = \Gamma^{\rm dec}(\mathcal{B}_c) + \Gamma^{\rm ann}(\mathcal{B}_c) + \Gamma_-^{\rm int}(\mathcal{B}_c) + \Gamma_+^{\rm int}(\mathcal{B}_c), \tag{26.16}$$

corresponding to the c-quark decay, the W-exchange contribution, destructive and constructive Pauli interferences. It is known that the inclusive decay rate is governed by the imaginary part of an effective nonlocal forward transition operator T. Therefore, $\Gamma^{\rm dec}$ corresponds to the imaginary part of Fig. 26.2(a) sandwiched between the same $\mathcal{B}_c$ states. At the Cabibbo-allowed level, $\Gamma^{\rm dec}$ represents the decay rate of $c \to su\bar{d}$, and $\Gamma^{\rm ann}$ denotes the contribution due to the W-exchange diagram $cd \to us$. The interference $\Gamma_-^{\rm int}$ ($\Gamma_+^{\rm int}$) arises from the destructive (constructive) interference between the u (s) quark produced in the c-quark decay and the spectator u (s) quark in the charmed baryon $\mathcal{B}_c$. Notice that the constructive Pauli interference is unique to the charmed baryon sector as it does not occur in the bottom baryon sector. From the quark content of the charmed baryons (see Table 26.2), it is clear that at the Cabibbo-allowed level, the destructive interference occurs in Λ_c^+ and Ξ_c^+ decays, while Ξ_c^+, Ξ_c^0 and Ω_c^0 can have $\Gamma_+^{\rm int}$. Since Ω_c^0 contains two s quarks, it is natural to expect that $\Gamma_+^{\rm int}(\Omega_c^0) \gg \Gamma_+^{\rm int}(\Xi_c)$. W-exchange occurs only for Ξ_c^0 and Λ_c^+ at the same Cabibbo-allowed level. In the heavy quark expansion approach, the above-mentioned spectator effects can be described in terms of the matrix elements of local four-quark operators.

Within this QCD-based heavy quark expansion approach, some phenomenological assumptions can be turned into some coherent and quantitative statements and nonperturbative effects can be systematically studied. To begin with, we write down the general expressions for the inclusive decay widths of charmed hadrons. Under the heavy

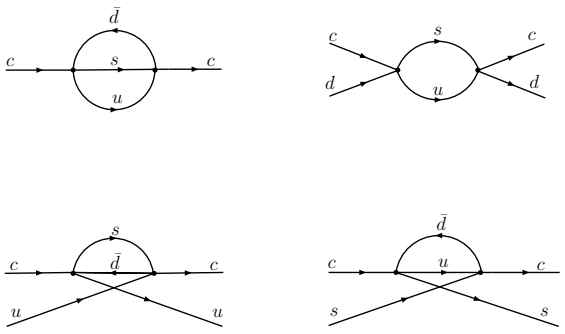

Figure 26.2: Contributions to nonleptonic decay rates of charmed baryons from four-quark operators: (a) c-quark decay, (b) W-exchange, (c) destructive Pauli interference and (d) constructive interference.

quark expansion, the inclusive nonleptonic decay rate of a charmed baryon $\mathcal{B}_c$ is given by [195, 196]

$$\begin{aligned}\Gamma_{\rm NL}(\mathcal{B}_c) &= \frac{G_F^2 m_c^5}{192\pi^3} N_c\, V_{\rm CKM}\, \frac{1}{2m_{\mathcal{B}_c}} \Bigg\{ \left(c_1^2 + c_2^2 + \frac{2c_1c_2}{N_c}\right) \Big[I_0(x,0,0) \langle \mathcal{B}_c|\bar{c}c|\mathcal{B}_c\rangle \\ &- \frac{1}{m_c^2} I_1(x,0,0) \langle \mathcal{B}_c|\bar{c}\sigma\cdot G c|\mathcal{B}_c\rangle \Big] - \frac{4}{m_c^2}\frac{2c_1c_2}{N_c} I_2(x,0,0) \langle \mathcal{B}_c|\bar{c}\sigma\cdot G c|\mathcal{B}_c\rangle \Bigg\} \\ &+ \frac{1}{2m_{\mathcal{B}_c}} \langle \mathcal{B}_c|\mathcal{L}_{\rm spec}|\mathcal{B}_c\rangle + \mathcal{O}\left(\frac{1}{m_c^4}\right), \end{aligned} \tag{26.17}$$

where $\sigma\cdot G = \sigma_{\mu\nu}G^{\mu\nu}$, $x = (m_s/m_c)^2$, N_c is the number of colors, c_1, c_2 are Wilson coefficient functions, $N_c = 3$ is the number of color and $V_{\rm CKM}$ takes care of the relevant CKM matrix elements. In the above equation, $I_{0,1,2}$ are phase-space factors

$$\begin{aligned} I_0(x,0,0) &= (1-x^2)(1-8x+x^2) - 12x^2 \ln x, \\ I_1(x,0,0) &= \frac{1}{2}(2 - x\frac{d}{dx}) I_0(x,0,0) = (1-x)^4, \\ I_2(x,0,0) &= (1-x)^3, \end{aligned} \tag{26.18}$$

for $c \to su\bar{d}$ transition.

In heavy quark effective theory, the two-body matrix element $\langle \mathcal{B}_c|\bar{c}c|\mathcal{B}_c\rangle$ in Eq. (26.17) can be recast to

$$\frac{\langle \mathcal{B}_c|\bar{c}c|\mathcal{B}_c\rangle}{2m_{\mathcal{B}_c}} = 1 - \frac{K_H}{2m_c^2} + \frac{G_H}{2m_c^2}, \tag{26.19}$$

with

$$\begin{aligned} K_H &\equiv -\frac{1}{2m_{\mathcal{B}_c}} \langle \mathcal{B}_c|\bar{c}(iD_\perp)^2 c|\mathcal{B}_c\rangle = -\lambda_1, \\ G_H &\equiv \frac{1}{2m_{\mathcal{B}_c}} \langle \mathcal{B}_c|\bar{c}\frac{1}{2}\sigma\cdot G c|\mathcal{B}_c\rangle = d_H \lambda_2, \end{aligned} \tag{26.20}$$

where $d_H = 0$ for the antitriplet baryon and $d_H = 4$ for the spin-$\frac{1}{2}$ sextet baryon. It should be stressed that the expression (26.19) is model independent and it contains nonperturbative kinetic and chromomagnetic effects which are usually absent in the quark model calculations. The nonperturbative HQET parameters λ_1 and λ_2 are independent of the heavy quark mass. Numerically, we shall use $\lambda_1^{\rm baryon} = -(0.4 \pm 0.2)\,{\rm GeV}^2$ [200] and $\lambda_2^{\rm baryon} = 0.055\,{\rm GeV}^2$ for charmed baryons [201]. Spectator effects in inclusive decays of charmed hadrons are described by the dimension-six four-quark operators $\mathcal{L}_{\rm spec}$ in Eq. (26.17) at order $1/m_c^3$. Its complete expression can be found in, for example, Eq. (2.4) of [201].

For inclusive semileptonic decays, there is an additional spectator effect in charmed-baryon semileptonic decay originating from the Pauli interference of the s quark for charmed baryons Ξ_c and Ω_c [202]. The general expression of the inclusive semileptonic widths is given by

$$\begin{aligned}\Gamma_{\rm SL}(\mathcal{B}_c) &= \frac{G_F^2 m_c^5}{192\pi^3} V_{\rm CKM}\,\frac{\eta(x,x_\ell,0)}{2m_{\mathcal{B}_c}}\Big[I_0(x,0,0)\langle\mathcal{B}_c|\bar{c}c|\mathcal{B}_c\rangle - \frac{1}{m_c^2}\,I_1(x,0,0)\langle\mathcal{B}_c|\bar{c}\sigma\cdot Gc|\mathcal{B}_c\rangle\Big] \\ &- \frac{G_F^2 m_c^2}{6\pi}|V_{cs}|^2\frac{1}{2m_{\mathcal{B}_c}}(1-x)^2\Big[(1+\frac{x}{2})(\bar{c}s)(\bar{s}c) - (1+2x)\bar{c}(1-\gamma_5)s\bar{s}(1+\gamma_5)c\Big], \qquad (26.21)\end{aligned}$$

where $\eta(x, x_\ell, 0)$ with $x_\ell = (m_\ell/m_Q)^2$ is the QCD radiative correction to the semileptonic decay rate and its general analytic expression is given in [203]. Since both nonleptonic and semileptonic decay widths scale with the fifth power of the charmed quark mass, it is very important to fix the value of m_c. It is found that the experimental values for D^+ and D^0 semileptonic widths [4] can be fitted by the quark pole mass $m_c = 1.6$ GeV. Taking $m_s = 170$ MeV, we obtain the charmed-baryon semileptonic decay rates

$$\begin{aligned}&\Gamma(\Lambda_c \to X e\bar{\nu}) = \Gamma(\Xi_c \to X e\bar{\nu}) = 1.533 \times 10^{-13}{\rm GeV}, \\ &\Gamma(\Omega_c \to X e\bar{\nu}) = 1.308 \times 10^{-13}{\rm GeV}. \qquad (26.22)\end{aligned}$$

The prediction (26.22) for the Λ_c baryon is in good agreement with experiment [4]

$$\Gamma(\Lambda_c \to X e\bar{\nu})_{\rm expt} = (1.480 \pm 0.559) \times 10^{-13}{\rm GeV}. \qquad (26.23)$$

We shall see beolw that the Pauli interference effect in the semileptonic decays of Ξ_c and Ω_c can be very significant, in particular for the latter.

The baryon matrix element of the four-quark operator $\langle\mathcal{B}_c|(\bar{c}q_1)(\bar{q}_2q_3)|\mathcal{B}_c\rangle$ with $(\bar{q}_1q_2) = \bar{q}_1\gamma_\mu(1-\gamma_5)q_2$ is customarily evaluated using the quark model. In the non-relativistic quark model (for early related studies, see [191, 192]), the matrix element is governed by the charmed baryon wave function at origin, $|\psi_{cq}^{\mathcal{B}_c}(0)|^2$, which can be related to the charmed meson wave function $|\psi_{cq}^{D}(0)|^2$. For example, the hyperfine splittings between Σ_c^* and Σ_c, and between D^* and D separately yield [204]

$$|\psi_{cq}^{\Lambda_c}(0)|^2 = |\psi_{cq}^{\Sigma_c}(0)|^2 = \frac{4}{3}\,\frac{m_{\Sigma_c^*} - m_{\Sigma_c}}{m_{D^*} - m_D}\,|\psi_{c\bar{q}}^{D}(0)|^2. \qquad (26.24)$$

This relation is supposed to be robust as $|\psi_{cq}(0)|^2$ determined in this manner does not depend on the strong coupling α_s and the light quark mass m_q directly. Defining

$$|\psi_{cq}^{\mathcal{B}_c}(0)|^2 = r_{\mathcal{B}_c}|\psi_{cq}^{D}(0)|^2, \qquad (26.25)$$

we have

$$r_{\Lambda_c} = \frac{4}{3}\frac{m_{\Sigma_c^*} - m_{\Sigma_c}}{m_{D^*} - m_D}, \quad r_{\Xi_c} = \frac{4}{3}\frac{m_{\Xi_c^*} - m_{\Xi_c'}}{m_{D^*} - m_D}, \quad r_{\Omega_c} = \frac{4}{3}\frac{m_{\Omega_c^*} - m_{\Omega_c}}{m_{D^*} - m_D}. \tag{26.26}$$

In terms of the parameter $r_{\mathcal{B}_c}|\psi^D_{cq}(0)|^2$ we have [201]

$$\begin{aligned}
\Gamma^{\rm ann}(\Lambda_c) &= \frac{G_F^2 m_c^2}{\pi} r_{\Lambda_c}(1-x)^2\Big(\eta(c_1^2+c_2^2) - 2c_1c_2\Big)|\psi^D(0)|^2,\\
\Gamma^{\rm int}_-(\Lambda_c) &= -\frac{G_F^2 m_c^2}{4\pi} r_{\Lambda_c}(1-x)^2(1+x)\Big(\eta c_1^2 - 2c_1c_2 - N_c c_2^2\Big)|\psi^D(0)|^2,\\
\Gamma^{\rm ann}(\Xi_c)/r_{\Xi_c} &= \Gamma^{\rm ann}(\Lambda_c)/r_{\Lambda_c}, \qquad \Gamma^{\rm int}_-(\Xi_c^+)/r_{\Xi_c} = \Gamma^{\rm int}_-(\Lambda_c)/r_{\Lambda_c},\\
\Gamma^{\rm int}_+(\Xi_c) &= -\frac{G_F^2 m_c^2}{4\pi} r_{\Xi_c}(1-x^2)(1+x)\Big(\eta c_2^2 - 2c_1c_2 - N_c c_1^2\Big)|\psi^D(0)|^2,\\
\Gamma^{\rm int}_+(\Omega_c) &= -\frac{G_F^2 m_c^2}{6\pi} r_{\Omega_c}(1-x^2)(5+x)\Big(\eta c_2^2 - 2c_1c_2 - N_c c_1^2\Big)|\psi^D(0)|^2,\\
\Gamma^{\rm ann}(\Omega_c) &= 6\frac{G_F^2 m_c^2}{\pi} r_{\Omega_c}(1-x^2)\Big(\eta(c_1^2+c_2^2) - 2c_1c_2\Big)|\psi^D(0)|^2,\\
\Gamma^{\rm int}(\Xi_c \to Xe\bar\nu) &= \frac{G_F^2 m_c^2}{4\pi} r_{\Xi_c}(1-x^2)(1+x)|\psi^D(0)|^2,\\
\Gamma^{\rm int}(\Omega_c \to Xe\bar\nu) &= \frac{G_F^2 m_c^2}{6\pi} r_{\Omega_c}(1-x^2)(5+x)|\psi^D(0)|^2,
\end{aligned} \tag{26.27}$$

where the parameter η is introduced via

$$\langle\mathcal{B}_c|(\bar cc)(\bar qq)|\mathcal{B}_c\rangle = -\eta\langle\mathcal{B}_c|(\bar cq)(\bar qc)|\mathcal{B}_c\rangle, \tag{26.28}$$

so that $\eta = 1$ in the valence quark approximation. In the zero light quark mass limit ($x = 0$) and in the valence quark approximation, the reader can check that results of (26.27) are in agreement with those obtained in [191, 192, 205] except the Cabibbo-suppressed W-exchange contribution to Ω_c^0, $\Gamma^{\rm ann}(\Omega_c)$. We have a coefficient of 6 arising from the matrix element $\langle\Omega_c|(\bar cs)(\bar sc)|\Omega_c\rangle = -6|\psi^{\Omega_c}_{cs}(0)|^2(2m_{\Omega_c})$ [201], while the coefficient is claimed to be $\frac{10}{3}$ in [205].

Neglecting the small difference between r_{Λ_c}, r_{Ξ_c} and r_{Ω_c} and setting $x = 0$, the inclusive nonleptonic rates of charmed baryons in the valence quark approximation have the expressions:

$$\begin{aligned}
\Gamma_{\rm NL}(\Lambda_c^+) &= \Gamma^{\rm dec}(\Lambda_c^+) + \cos^2_C\,\Gamma^{\rm ann} + \Gamma^{\rm int}_- + \sin^2_C\,\Gamma^{\rm int}_+,\\
\Gamma_{\rm NL}(\Xi_c^+) &= \Gamma^{\rm dec}(\Xi_c^+) + \sin^2_C\,\Gamma^{\rm ann} + \Gamma^{\rm int}_- + \cos^2_C\,\Gamma^{\rm int}_+,\\
\Gamma_{\rm NL}(\Xi_c^0) &= \Gamma^{\rm dec}(\Xi_c^0) + \Gamma^{\rm ann} + \Gamma^{\rm int}_- + \Gamma^{\rm int}_+,\\
\Gamma_{\rm NL}(\Omega_c^0) &= \Gamma^{\rm dec}(\Omega_c^0) + 6\sin^2_C\,\Gamma^{\rm ann} + \frac{10}{3}\cos^2_C\,\Gamma^{\rm int}_+,
\end{aligned} \tag{26.29}$$

with θ_C being the Cabibbo angle.

Assuming the D meson wavefunction at the origin squared $|\psi^D_{c\bar q}(0)|^2$ being given by $\frac{1}{12}f_D^2 m_D$, we obtain $|\psi^{\Lambda_c}(0)|^2 = 7.5\times10^{-3}{\rm GeV}^3$ for $f_D = 220$ MeV.[5] To proceed to the

[5]The recent CLEO measurement of $D^+ \to \mu^+\nu$ yields $f_{D^+} = 222.6 \pm 16.7^{+2.8}_{-3.4}$ MeV [206].

Table 26.5: Various contributions to the decay rates (in units of 10^{-12} GeV) of charmed baryons. The charmed meson wavefunction at the origin squared $|\psi^D(0)|^2$ is taken to be $\frac{1}{12} f_D^2 m_D$. Experimental values are taken from [4].

	$\Gamma^{\rm dec}$	$\Gamma^{\rm ann}$	$\Gamma^{\rm int}_-$	$\Gamma^{\rm int}_+$	$\Gamma_{\rm SL}$	$\Gamma^{\rm tot}$	$\tau(10^{-13}s)$	$\tau_{\rm expt}(10^{-13}s)$
Λ_c^+	1.006	1.342	-0.196		0.323	2.492	2.64	2.00 ± 0.06
Ξ_c^+	1.006	0.071	-0.203	0.364	0.547	1.785	3.68	4.42 ± 0.26
Ξ_c^0	1.006	1.466		0.385	0.547	3.404	1.93	$1.12^{+0.13}_{-0.10}$
Ω_c^0	1.132	0.439		1.241	1.039	3.851	1.71	0.69 ± 0.12

numerical calculations, we use the Wilson coefficients $c_1(\mu) = 1.35$ and $c_2(\mu) = -0.64$ evaluated at the scale $\mu = 1.25$ GeV. Since $\eta = 1$ in the valence-quark approximation and since the wavefunction squared ratio r is evaluated using the quark model, it is reasonable to assume that the NQM and the valence-quark approximation are most reliable when the baryon matrix elements are evaluated at a typical hadronic scale $\mu_{\rm had}$. As shown in [207], the parameters η and r renormalized at two different scales are related via the renormalization group equation, from which we obtain $\eta(\mu) \simeq 0.74\eta(\mu_{\rm had}) \simeq 0.74$ and $r(\mu) \simeq 1.36\, r(\mu_{\rm had})$ [201].

The results of calculations are summarized in Table 26.5. It is clear that the lifetime pattern

$$\tau(\Xi_c^+) > \tau(\Lambda_c^+) > \tau(\Xi_c^0) > \tau(\Omega_c^0) \tag{26.30}$$

is in accordance with experiment. This lifetime hierarchy is qualitatively understandable. The Ξ_c^+ baryon is longest-lived among charmed baryons because of the smallness of W-exchange and partial cancellation between constructive and destructive Pauli interferences, while Ω_c is shortest-lived due to the presence of two s quarks in the Ω_c that renders the contribution of $\Gamma^{\rm int}_+$ largely enhanced. From Eq. (26.27) we also see that $\Gamma^{\rm int}_+$ is always positive, $\Gamma^{\rm int}_-$ is negative and that the constructive interference is larger than the magnitude of the destructive one. This explains why $\tau(\Xi_c^+) > \tau(\Lambda_c^+)$. It is also clear from Table 26.5 that, although the qualitative feature of the lifetime pattern is comprehensive, the quantitative estimates of charmed baryon lifetimes and their ratios are still rather poor.

In [205], a much larger charmed baryon wave function at origin is employed. This is based on the argument originally advocated in [190]. The physical charmed meson decay constant f_D is related to the asymptotic static value F_D via

$$f_D = F_D \left(1 - \frac{|\mu|}{m_c} + \mathcal{O}(\frac{1}{m_c^2})\right). \tag{26.31}$$

It was argued in [190] that one should not use the physical value of f_D when relating $|\psi^{\mathcal{B}_c}(0)|^2$ to $|\psi^D(0)|^2$ for reason of consistency since the widths have been calculated through order $1/m_c^3$ only. Hence, the part of f_D which is not suppressed by $1/m_c$ should

not be taken into account. However, if we use $F_D \sim 2f_D$ for the wave function $|\psi^D(0)|^2$, we find that the predicted lifetimes of charmed baryons become too short compared to experiment except Ω_c^0. By contrast, using $|\psi^{\Lambda_c}(0)|^2 = 2.62 \times 10^{-2}\text{GeV}^3$ and the so-called hybrid renormalization, lifetimes $\tau(\Lambda_c^+) = 2.39$, $\tau(\Xi_c^+) = 2.51$, $\tau(\Xi_c^0) = 0.96$ and $\tau(\Omega_c^0) = 0.61$ in units of $10^{-13}s$ are obtained in [205]. They are in better agreement with the data except Ξ_c^+. The predicted ratio $\tau(\Xi_c^+)/\tau(\Lambda_c^+) = 1.05$ is too small compared to the experimental value of 2.21 ± 0.15. By inspecting Eq. (26.29), it seems to be very difficult to enhance the ratio by a factor of 2.

In short, when the lifetimes of charmed baryons are analyzed within the framework of the heavy quark expansion, the qualitative feature of the lifetime pattern is understandable, but a quantitative description of charmed baryon lifetimes is still lack. This may be ascribed to the following possibilities:

1. Unlike the semileptonic decays, the heavy quark expansion in inclusive nonleptonic decays cannot be justified by analytic continuation into the complex plane and local duality has to be assumed in order to apply the OPE directly in the physical region. The may suggest a significant violation of quark-hadron local duality in the charm sector.

2. Since the c quark is not heavy enough, it casts doubts on the validity of heavy quark expansion for inclusive charm decays. This point can be illustrated by the following example. It is well known that the observed lifetime difference between the D^+ and D^0 is ascribed to the destructive interference in D^+ decays and/or the constructive W-exchange contribution to D^0 decays. However, there is a serious problem with the evaluation of the destructive Pauli interference $\Gamma^{\text{int}}(D^+)$ in D^+. A direct calculation analogous to $\Gamma_-^{\text{int}}(\mathcal{B}_c)$ in the charmed baryon sector indicates that $\Gamma^{\text{int}}(D^+)$ overcomes the c quark decay rate so that the resulting nonleptonic decay width of D^+ becomes negative [190, 208]. This certainly does not make sense. This example clearly indicates that the $1/m_c$ expansion in charm decay is not well convergent and sensible, to say the least. It is not clear if the situation is improved even after higher dimension terms are included.

3. To overcome the aforementioned difficulty with $\Gamma^{\text{int}}(D^+)$, it has been conjectured in [190] that higher-dimension corrections amount to replacing m_c by m_D in the expansion parameter $f_D^2 m_D/m_c^3$, so that it becomes f_D^2/m_D^2. As a consequence, the destructive Pauli interference will be reduced by a factor of $(m_c/m_D)^3$. By the same token, the Pauli interference in charmed baryon decay may also be subject to the same effect. Another way of alleviating the problem is to realize that the usual local four-quark operators are derived in the heavy quark limit so that the effect of spectator light quarks can be neglected. Since the charmed quark is not heavy enough, it is very important, as stressed by Chernyak [208], to take into account the nonzero momentum of spectator quarks in charm decay. In the framework of heavy quark expansion, this spectator effect can be regarded as higher order $1/m_c$ corrections.

4. One of the major theoretical uncertainties comes from the evaluation of the four-quark matrix elements. One can hope that lattice QCD will provide a better handle

on those quantities.

26.6 Hadronic weak decays

Contrary to the significant progress made over the last 20 years or so in the studies of the heavy meson weak decay, advancement in the arena of heavy baryons, both theoretical and experimental, has been relatively slow. This is partly due to the smaller baryon production cross section and the shorter lifetimes of heavy baryons. From the theoretical point of view, baryons being made out of three quarks, in contrast to two quarks for mesons, bring along several essential complications. First of all, the factorization approximation that the hadronic matrix element is factorized into the product of two matrix elements of single currents and that the nonfactorizable term such as the W-exchange contribution is negligible relative to the factorizable one is known empirically to be working reasonably well for describing the nonleptonic weak decays of heavy mesons. However, this approximation is *a priori* not directly applicable to the charmed baryon case as W-exchange there, manifested as pole diagrams, is no longer subject to helicity and color suppression. This is different from the naive color suppression of internal W-emission. It is known in the heavy meson case that nonfactorizable contributions will render the color suppression of internal W-emission ineffective. However, the W-exchange in baryon decays is not subject to color suppression even in the absence of nonfactorizable terms. A simple way to see this is to consider the large-N_c limit. Although the W-exchange diagram is down by a factor of $1/N_c$ relative to the external W-emission one, it is compensated by the fact that the baryon contains N_c quarks in the limit of large N_c, thus allowing N_c different possibilities for W exchange between heavy and light quarks [209]. That is, the pole contribution can be as important as the factorizable one. The experimental measurement of the decay modes $\Lambda_c^+ \to \Sigma^0\pi^+$, $\Sigma^+\pi^0$ and $\Lambda_c^+ \to \Xi^0 K^+$, which do not receive any factorizable contributions, indicates that W-exchange indeed plays an essential role in charmed baryon decays. Second, there are more possibilities in drawing the quark daigram amplitudes as depicted in Fig. 26.3; in general there exist two distinct internal W-emissions and several different W-exchange diagrams which will be discussed in more detail shortly.

Historically, the two-body nonleptonic weak decays of charmed baryons were first studied by utilizing the same technique of current algebra as in the case of hyperon decays [210]. However, the use of the soft-meson theorem makes sense only if the emitted meson is of the pseudoscalar type and its momentum is soft enough. Obviously, the pseudoscalar-meson final state in charmed bayon decay is far from being "soft". Therefore, it is not appropriate to make the soft meson limit. It is no longer justified to apply current algebra to heavy-baryon weak decays, especially for s-wave amplitudes. Thus one has to go back to the original pole model, which is nevertheless reduced to current algebra in the soft pseudoscalar-meson limit, to deal with nonfactorizable contributions. The merit of the pole model is obvious: Its use is very general and is not limited to the soft meson limit and to the pseudoscalar-meson final state. Of course, the price we have to pay is that it requires the knowledge of the negative-parity baryon poles for the parity-violating transition. This also explains why the theoretical study of nonleptonic decays of heavy baryons is much more difficult than the hyperon and heavy meson decays.

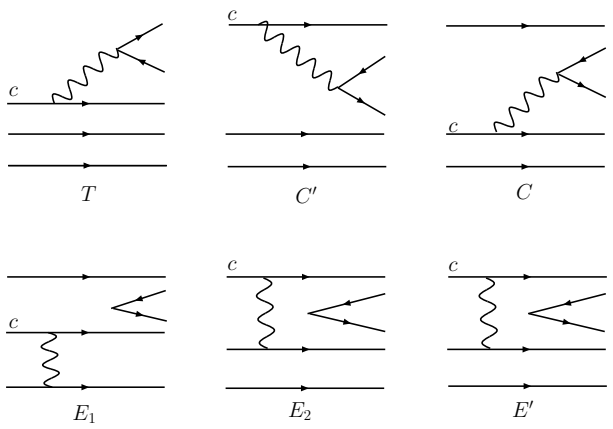

Figure 26.3: Quark diagrams for charmed baryon decays

The nonfactorizable pole contributions to hadronic weak decays of charmed baryons have been studied in the literature [211, 212, 213]. In general, nonfactorizable s- and p-wave amplitudes for $\frac{1}{2}^+ \to \frac{1}{2}^+ + P(V)$ decays (P: pseudoscalar meson, V: vector meson), for example, are dominated by $\frac{1}{2}^-$ low-lying baryon resonances and $\frac{1}{2}^+$ ground-state baryon poles, respectively. However, the estimation of pole amplitudes is a difficult and nontrivial task since it involves weak baryon matrix elements and strong coupling constants of $\frac{1}{2}^+$ and $\frac{1}{2}^-$ baryon states. This is the case in particular for s-wave terms as we know very little about the $\frac{1}{2}^-$ states. As a consequence, the evaluation of pole diagrams is far more uncertain than the factorizable terms. In short, W-exchange plays a dramatic role in the charmed baryon case and it even dominates over the spectator contribution in hadronic decays of Λ_c^+ and Ξ_c^0 [214].

Since the light quarks of the charmed baryon can undergo weak transitions, one can also have charm-flavor-conserving weak decays, e.g., $\Xi_c \to \Lambda_c \pi$ and $\Omega_c \to \Xi_c \pi$, where the charm quark behaves as a spectator. This special class of weak decays usually can be calculated more reliably than the conventional charmed baryon weak decays.

26.6.1 Quark-diagram scheme

Besides dynamical model calculations, it is useful to study the nonleptonic weak decays in a way which is as model independent as possible. The two-body nonleptonic decays of charmed baryons have been analyzed in terms of SU(3)-irreducible-representation amplitudes [215, 216]. However, the quark-diagram scheme (i.e., analyzing the decays in terms of quark-diagram amplitudes) has the advantage that it is more intuitive and easier for implementing model calculations. It has been successfully applied to the hadronic weak decays of charmed and bottom mesons [217, 218]. It has provided a framework with which we not only can do the least-model-dependent data analysis and give predictions but also make evaluations of theoretical model calculations.

A general formulation of the quark-diagram scheme for the nonleptonic weak decays of charmed baryons has been given in [219] (see also [220]). The general quark diagrams shown in Fig. 26.3 are: the external W-emission tree diagram T, internal W-emission

diagrams C and C', W-exchange diagrams E_1, E_2 and E' (see Fig. 2 of [219] for notation and for details). There are also penguin-type quark diagrams which are presumably negligible in charm decays due to GIM cancellation. The quark diagram amplitudes T, C, $C'\cdots$ etc. in each type of hadronic decays are in general not the same. For octet baryons in the final state, each of the W-exchange amplitudes has two more independent types: the symmetric and the antisymmetric, for example, E_{1A}, E_{2A}, E_{2S}, E'_A and E'_S [219]. The antiquark produced from the charmed quark decay $c \to q_1 q_2 \bar{q}_3$ in diagram C' can combine with q_1 or q_2 to form an outgoing meson. Consequently, diagram C' contains factorizable contributions but C does not. It should be stressed that all quark graphs used in this approach are topological with all the strong interactions included, i.e. gluon lines are included in all possible ways. Hence, they are *not* Feynman graphs. Moreover, final-state interactions are also classified in the same manner. A good example is the reaction $D^0 \to \bar{K}^0\phi$, which can be produced via final-state rescattering even in the absence of the W-exchange diagram. Then it was shown in [218] that this rescattering diagram belongs to the generic W-exchange topology.

Since the two spectator light quarks in the heavy baryon are antisymmetrized in the antitriplet charmed baryon $\mathcal{B}_c(\bar{\mathbf{3}})$ and the wave function of the decuplet baryon $\mathcal{B}(\mathbf{10})$ is totally symmetric, it is clear that factorizable amplitudes T and C' cannot contribute to the decays of type $\mathcal{B}_c(\bar{\mathbf{3}}) \to \mathcal{B}(\mathbf{10}) + M(\mathbf{8})$; it receives contributions only from the W-exchange and penguin-type diagrams (see Fig. 1 of [219]). Examples are $\Lambda_c^+ \to \Delta^{++}K^-, \Sigma^{*+}\rho^0, \Sigma^{*+}\eta, \Xi^{*0}K^+$ and $\Xi_c^0 \to \Sigma^{*+}\bar{K}^0$. They can only proceed via W-exchange. Hence, the experimental observation of them implies that the W-exchange mechanism plays a significant role in charmed baryon decays. The quark diagram amplitudes for all two-body decays of (Cabibbo-allowed, singly suppressed and doubly suppressed) $\Lambda_c^+, \Xi_c^{+,0}$ and Ω_c^0 are listed in [219]. In the SU(3) limit, there exist many relations among various charmed baryon decay amplitudes, see [219] for detail. For charmed baryon decays, there are only a few decay modes which proceed through factorizable external or internal W-emission diagram, namely, Cabibbo-allowed $\Omega_c^0 \to \Omega^-\pi^+(\rho^+)$, $\Xi^{*0}\bar{K}^0(\bar{K}^{*0})$ and Cabibbo-suppressed $\Lambda_c^+ \to p\phi$.

26.6.2 Dynamical model calculation

To proceed we first consider the Cabibbo-allowed decays $\mathcal{B}_c(\frac{1}{2}^+) \to \mathcal{B}(\frac{1}{2}^+) + P(V)$. The general amplitudes are

$$\begin{aligned} M[\mathcal{B}_i(1/2^+) \to \mathcal{B}_f(1/2^+) + P] &= i\bar{u}_f(p_f)(A + B\gamma_5)u_i(p_i), \\ M[\mathcal{B}_i(1/2^+) \to \mathcal{B}_f(1/2^+) + V] &= \bar{u}_f(p_f)\varepsilon^{*\mu}[A_1\gamma_\mu\gamma_5 + A_2(p_f)_\mu\gamma_5 + B_1\gamma_\mu + B_2(p_f)_\mu]u_i(p_i), \end{aligned} \tag{26.32}$$

where ε_μ is the polarization vector of the vector meson, A, (B, B_1, B_2) and A_2 are s-wave, p-wave and d-wave amplitudes, respectively, and A_1 consists of both s-wave and d-wave ones. The QCD-corrected weak Hamiltonian responsible for Cabibbo-allowed hadronic decays of charmed baryons reads

$$\mathcal{H}_W = \frac{G_F}{\sqrt{2}} V_{cs}V_{ud}^*(c_1O_1 + c_2O_2), \tag{26.33}$$

where $O_1 = (\bar{s}c)(\bar{u}d)$ and $O_2 = (\bar{s}d)(\bar{u}c)$ with $(\bar{q}_1 q_2) \equiv \bar{q}_1\gamma_\mu(1-\gamma_5)q_2$. ¿From the expression of $O_{1,2}$, it is clear that factorization occurs if the final-state meson is $\pi^+(\rho^+)$ or $\bar{K}^0(\bar{K}^{*0})$. Explicitly,

$$\begin{aligned}
A^{\rm fac}(\mathcal{B}_i \to \mathcal{B}_f + \pi^+) &= \lambda\, a_1 f_P (m_i - m_f) f_1(m_\pi^2), \\
B^{\rm fac}(\mathcal{B}_i \to \mathcal{B}_f + \pi^+) &= \lambda\, a_1 f_P (m_i + m_f) g_1(m_\pi^2), \\
A^{\rm fac}(\mathcal{B}_i \to \mathcal{B}_f + \bar{K}^0) &= \lambda\, a_2 f_P (m_i - m_f) f_1(m_K^2), \\
B^{\rm fac}(\mathcal{B}_i \to \mathcal{B}_f + \bar{K}^0) &= \lambda\, a_2 f_P (m_i + m_f) g_1(m_K^2),
\end{aligned} \tag{26.34}$$

and

$$\begin{aligned}
A_1^{\rm fac}(\mathcal{B}_i \to \mathcal{B}_f + \rho^+) &= -\lambda\, a_1 f_\rho m_\rho [g_1(m_\rho^2) + g_2(m_\rho^2)(m_i - m_f)], \\
A_2^{\rm fac}(\mathcal{B}_i \to \mathcal{B}_f + \rho^+) &= -2\lambda\, a_1 f_\rho m_\rho g_2(m_\rho^2), \\
B_1^{\rm fac}(\mathcal{B}_i \to \mathcal{B}_f + \rho^+) &= \lambda\, a_1 f_\rho m_\rho [f_1(m_\rho^2) - f_2(m_\rho^2)(m_i + m_f)], \\
B_2^{\rm fac}(\mathcal{B}_i \to \mathcal{B}_f + \rho^+) &= 2\lambda\, a_1 f_\rho m_\rho f_2(m_\rho^2),
\end{aligned}$$

and similar expressions for $\mathcal{B}_i \to \mathcal{B}_f + \bar{K}^{*0}$, where $\lambda = G_F V_{cs} V_{ud}^*/\sqrt{2}$, f_i and g_i are the form factors defined by $(q = p_i - p_f)$

$$\begin{aligned}
\langle \mathcal{B}_f(p_f)|V_\mu - A_\mu|\mathcal{B}_i(p_i)\rangle &= \bar{u}_f(p_f)[f_1(q^2)\gamma_\mu + i f_2(q^2)\sigma_{\mu\nu}q^\nu + f_3(q^2)q_\mu \\
&\quad -(g_1(q^2)\gamma_\mu + i g_2(q^2)\sigma_{\mu\nu}q^\nu + g_3(q^2)q_\mu)\gamma_5]u_i(p_i).
\end{aligned} \tag{26.35}$$

In the naive factorization approach, the coefficients a_1 for the external W-emission amplitude and a_2 for internal W-emission are given by $(c_1 + \frac{c_2}{N_c})$ and $(c_2 + \frac{c_1}{N_c})$, respectively. However, we have learned from charmed meson decays that the naive factorization approach never works for the decay rate of color-suppressed decay modes, though it usually operates for color-allowed decays. Empirically, it was learned in the 1980s that if the Fierz-transformed terms characterized by $1/N_c$ are dropped, the discrepancy between theory and experiment is greatly improved [221]. This leads to the so-called large-N_c approach for describing hadronic D decays [222]. Theoretically, explicit calculations based on the QCD sum-rule analysis [223] indicate that the Fierz terms are indeed largely compensated by the nonfactorizable corrections.

As the discrepancy between theory and experiment for charmed meson decays gets much improved in the $1/N_c$ expansion method, it is natural to ask if this scenario also works in the baryon sector? This issue can be settled down by the experimental measurement of the Cabibbo-suppressed mode $\Lambda_c^+ \to p\phi$, which receives contributions only from the factorizable diagrams. As pointed out in [211], the large-N_c predicted rate is in good agreement with the measured value. By contrast, its decay rate prdicted by the naive factorization approximation is too small by a factor of 15. Therefore, the $1/N_c$ approach also works for the factorizable amplitude of charmed baryon decays. This also implies that the inclusion of nonfactorizable contributions is inevitable and necessary. If nonfactorizable effects amount to a redefinition of the effective parameters a_1, a_2 and are universal (i.e., channel-independent) in charm decays, then we still have a new factorization scheme with the universal parameters a_1, a_2 to be determined from experiment. Throughout this paper, we will thus treat a_1 and a_2 as free effective parameters.

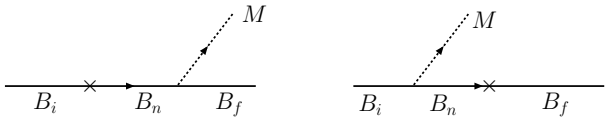

Figure 26.4: Pole diagrams for charmed baryon decay $\mathcal{B}_i \to \mathcal{B}_f + M$.

At the hadronic level, the decay amplitudes for quark diagrams T and $C'$are conventionally evaluated using the factorization approximation. How do we tackle with the remaining nonfactorizable diagrams C, E_1, E_2, E' ? One popular approach is to consider the contributions from all possible intermediate states. Among all possible pole contributions, including resonances and continuum states, one usually focuses on the most important poles such as the low-lying $\frac{1}{2}^+$, $\frac{1}{2}^-$ states, known as pole approximation. More specifically, the s-wave amplitude is dominated by the low-lying $1/2^-$ resonances and the p-wave one governed by the ground-state $1/2^+$ poles (see Fig. 26.4):

$$\begin{aligned} A^{\rm nf} &= -\sum_{\mathcal{B}_n^*(1/2^-)} \left(\frac{g_{\mathcal{B}_f \mathcal{B}_{n^*} P} b_{n^* i}}{m_i - m_{n^*}} + \frac{b_{f n^*} g_{\mathcal{B}_{n^*} \mathcal{B}_i P}}{m_f - m_{n^*}} \right) + \cdots , \\ B^{\rm nf} &= -\sum_{\mathcal{B}_n} \left(\frac{g_{\mathcal{B}_f \mathcal{B}_n P} a_{ni}}{m_i - m_n} + \frac{a_{fn} g_{\mathcal{B}_n \mathcal{B}_i P}}{m_f - m_n} \right) + \cdots , \end{aligned} \tag{26.36}$$

where $A^{\rm nf}$ and $B^{\rm nf}$ are the nonfactorizable s- and p-wave amplitudes of $\mathcal{B}_c \to \mathcal{B}P$, respectively, ellipses in Eq.(26.36) denote other pole contributions which are negligible for our purposes, and a_{ij} as well as $b_{i^* j}$ are the baryon-baryon matrix elements defined by

$$\langle \mathcal{B}_i | \mathcal{H}_{_W} | \mathcal{B}_j \rangle = \bar{u}_i (a_{ij} - b_{ij} \gamma_5) u_j, \qquad \langle \mathcal{B}_i^*(1/2^-) | \mathcal{H}_{_W}^{\rm pv} | \mathcal{B}_j \rangle = i b_{i^* j}\, \bar{u}_i u_j, \tag{26.37}$$

with $b_{j i^*} = -b_{i^* j}$. Evidently, the calculation of s-wave amplitudes is more difficult than the p-wave owing to the troublesome negative-parity baryon resonances which are not well understood in the quark model. In [211, 212], the form factors appearing in factorizable amplitudes and the strong coupling constants and baryon transition matrix elements relevant to nonfactorizable contributions are evaluated using the MIT bag model [224]. Two of the pole model calculations for branching ratios [212, 213] are displayed in Table 26.6. The study of charmed baryon hadronic decays in [225] is similar to [212, 213] except that the effect of W-exchange is parametrized in terms of the baryon wave function at origin. Sharma and Verma [225] defined a parameter $r = |\psi^{\mathcal{B}_c}(0)|^2/|\psi^{\mathcal{B}}(0)|^2$ and argued that its value is close to 1.4. A variant of the pole model has been considered in [226] in which the effects of pole-model-induced SU(4) symmetry breaking in parity-conserving and parity-violating amplitudes are studied.

Instead of decomposing the decay amplitude into products of strong couplings and two-body weak transitions, Körner and Krämer [209] have analyzed the nonleptonic weak processes using the spin-flavor structure of the effective Hamiltonian and the wave functions of baryons and mesons described by the covariant quark model. The nonfactorizable amplitudes are then obtained in terms of two wave function overlap parameters H_2 and H_3, which are in turn determined by fitting to the experimental data of $\Lambda_c^+ \to p\bar{K}^0$

Table 26.6: Branching ratios of Cabibbo-allowed $\mathcal{B}_c \to \mathcal{B} + P$ decays in various models. Results of [209, 213, 212] have been normalized using the current world averages of charmed baryon lifetimes [4]. Branching ratios cited from [225] are for $\phi_{\eta-\eta'} = -23^\circ$ and $r = 1.4$.

Decay	Körner, Krämer [209]	Xu, Kamal [213]	Cheng, Tseng [212]	Ivanov et al. [227]	Żenczykowski[226]	Sharma [225]	Expt. [4]
$\Lambda_c^+ \to \Lambda\pi^+$	input	1.62	0.88	0.79	0.54	1.12	0.90± 0.28
$\Lambda_c^+ \to \Sigma^0\pi^+$	0.32	0.34	0.72	0.88	0.41	1.34	0.99± 0.32
$\Lambda_c^+ \to \Sigma^+\pi^0$	0.32	0.34	0.72	0.88	0.41	1.34	1.00± 0.34
$\Lambda_c^+ \to \Sigma^+\eta$	0.16			0.11	0.94	0.57	0.48± 0.17
$\Lambda_c^+ \to \Sigma^+\eta'$	1.28			0.12	0.12	0.10	
$\Lambda_c^+ \to p\bar{K}^0$	input	1.20	1.26	2.06	1.79	1.64	2.3± 0.6
$\Lambda_c^+ \to \Xi^0 K^+$	0.26	0.10		0.31	0.36	0.13	0.39± 0.14
$\Xi_c^+ \to \Sigma^+\bar{K}^0$	6.45	0.44	0.84	3.08	1.56	0.04	
$\Xi_c^+ \to \Xi^0\pi^+$	3.54	3.36	3.93	4.40	1.59	0.53	0.55 ± 0.16[1]
$\Xi_c^0 \to \Lambda\bar{K}^0$	0.12	0.37	0.27	0.42	0.35	0.54	seen
$\Xi_c^0 \to \Sigma^0 K^0$	1.18	0.11	0.13	0.20	0.11	0.07	
$\Xi_c^0 \to \Sigma^+ K^-$	0.12	0.12		0.27	0.36	0.12	
$\Xi_c^0 \to \Xi^0\pi^0$	0.03	0.56	0.28	0.04	0.69	0.87	
$\Xi_c^0 \to \Xi^0\eta$	0.24			0.28	0.01	0.22	
$\Xi_c^0 \to \Xi^0\eta'$	0.85			0.31	0.09	0.06	
$\Xi_c^0 \to \Xi^-\pi^+$	1.04	1.74	1.25	1.22	0.61	2.46	seen
$\Omega_c^0 \to \Xi^0 K^0$	1.21		0.09	0.02			

Table 26.7: The predicted asymmetry parameter α for Cabibbo-allowed $\mathcal{B}_c \to \mathcal{B} + P$ decays in various models. Results cited from [225] are for $\phi_{\eta-\eta'} = -23^\circ$ and $r = 1.4$.

Decay	Körner, Krämer [209]	Xu, Kamal [213]	Cheng, Tseng [212]	Ivanov et al. [227]	Żenczykowski[226]	Sharma, [225]	Expt. [4]
$\Lambda_c^+ \to \Lambda\pi^+$	-0.70	-0.67	-0.95	-0.95	-0.99	-0.99	-0.91 ± 0.15
$\Lambda_c^+ \to \Sigma^0\pi^+$	0.70	0.92	0.78	0.43	0.39	-0.31	
$\Lambda_c^+ \to \Sigma^+\pi^0$	0.71	0.92	0.78	0.43	0.39	-0.31	-0.45 ± 0.32
$\Lambda_c^+ \to \Sigma^+\eta$	0.33			0.55	0	-0.91	
$\Lambda_c^+ \to \Sigma^+\eta'$	-0.45			-0.05	-0.91	0.78	
$\Lambda_c^+ \to pK^0$	-1.0	0.51	-0.49	-0.97	-0.66	-0.99	
$\Lambda_c^+ \to \Xi^0K^+$	0	0		0	0	0	
$\Xi_c^+ \to \Sigma^+\bar{K}^0$	-1.0	0.24	-0.09	-0.99	1.00	0.54	
$\Xi_c^+ \to \Xi^0\pi^+$	-0.78	-0.81	-0.77	-1.0	1.00	-0.27	
$\Xi_c^0 \to \Lambda\bar{K}^0$	-0.76	1.0	-0.73	-0.75	-0.29	-0.79	
$\Xi_c^0 \to \Sigma^0\bar{K}^0$	-0.96	-0.99	-0.59	-0.55	-0.50	0.48	
$\Xi_c^0 \to \Sigma^+K^-$	0	0		0	0	0	
$\Xi_c^0 \to \Xi^0\pi^0$	0.92	0.92	-0.54	0.94	0.21	-0.80	
$\Xi_c^0 \to \Xi^0\eta$	-0.92			-1.0	-0.04	0.21	
$\Xi_c^0 \to \Xi^0\eta'$	-0.38			-0.32	-1.00	0.80	
$\Xi_c^0 \to \Xi^-\pi^+$	-0.38	-0.38	-0.99	-0.84	-0.79	-0.97	-0.6 ± 0.4
$\Omega_c^0 \to \Xi^0\bar{K}^0$	0.51		-0.93	-0.81			

and $\Lambda_c^+ \to \Lambda\pi^+$, respectively. Despite the absence of first-principles calculation of the parameters H_2 and H_3, this quark model approach has fruitful predictions for not only $\mathcal{B}_c \to \mathcal{B}+P$, but also $\mathcal{B}_c \to \mathcal{B}+V$, $\mathcal{B}^*(3/2^+)+P$ and $\mathcal{B}^*(3/2^+)+V$ decays. Another advantage of this analysis is that each amplitude has one-to-one quark-diagram interpretation. While the overlap integrals are treated as phenomenological parameters to be determined from a fit to the data, Ivanov *et al.* [227] developed a microscopic approach to the overlap integrals by specifying the form of the hadron-quark transition vertex including the explicit momentum dependence of the Lorentz scalar part of this vertex.

26.6.3 Discussions

Various model predictions of the branching ratios and decay asymmetries for Cabibbo-allowed $\mathcal{B}_c \to \mathcal{B} + P(V)$ decays are summarized in Tables 26.6-26.9. In the following we shall first discuss the decay asymmetry parameter α and then turn to the decay rates.

Decay asymmetry

A very useful information is provided by the study of the polarization of the daughter baryon $\mathcal{B}'$ in the decay $\mathcal{B} \to \mathcal{B}'\pi$. Its general expression is given by

$$\mathbf{P}_{\mathcal{B}'} = \frac{(\alpha_{\mathcal{B}} + \mathbf{P}_{\mathcal{B}} \cdot \mathbf{n})\mathbf{n} + \beta_{\mathcal{B}}(\mathbf{n} \times \mathbf{P}_{\mathcal{B}}) + \gamma_{\mathcal{B}}\mathbf{n} \times (\mathbf{n} \times \mathbf{P}_{\mathcal{B}})}{1 + \alpha_{\mathcal{B}}\mathbf{P}_{\mathcal{B}} \cdot \mathbf{n}}, \tag{26.38}$$

Table 26.8: Branching ratios of Cabibbo-allowed $\mathcal{B}_c \to \mathcal{B} + V$ decays in various models. The experimental value denoted by the superscript $*$ is the branching ratio relative to $\Xi_c^+ \to \Xi^- \pi^+ \pi^+$.

Decay	Körner, Krämer [209]	Żenczykowski [226]	Cheng, Tseng [211]	Experiment [4]
$\Lambda_c^+ \to \Lambda \rho^+$	19.08	1.80	2.6	< 5
$\Lambda_c^+ \to \Sigma^0 \rho^+$	3.14	1.56	0.19	0.99± 0.32
$\Lambda_c^+ \to \Sigma^+ \rho^0$	3.12	1.56	0.19	< 1.4
$\Lambda_c^+ \to \Sigma^+ \omega$	4.02	1.10		2.7± 1.0
$\Lambda_c^+ \to \Sigma^+ \phi$	0.26	0.11		0.32± 0.10
$\Lambda_c^+ \to p K^{*0}$	3.08	5.03	3.3	1.6± 0.5
$\Lambda_c^+ \to \Xi^0 K^{*+}$	0.12	0.11		0.39± 0.14
$\Xi_c^+ \to \Sigma^+ \bar{K}^{*0}$	2.34	7.38		$0.81 \pm 0.15^*$
$\Xi_c^+ \to \Xi^0 \rho^+$	95.83	5.48		
$\Xi_c^0 \to \Lambda \bar{K}^{*0}$	1.12	1.15		
$\Xi_c^0 \to \Sigma^0 K^{*0}$	0.62	0.77		
$\Xi_c^0 \to \Sigma^+ K^{*-}$	0.39	0.37		
$\Xi_c^0 \to \Xi^0 \rho^0$	1.71	1.22		
$\Xi_c^0 \to \Xi^0 \omega$	2.33	0.15		
$\Xi_c^0 \to \Xi^0 \phi$	0.18	0.10		
$\Xi_c^0 \to \Xi^- \rho^+$	12.29	1.50		
$\Omega_c^0 \to \Xi^0 \bar{K}^{*0}$	0.59			

Table 26.9: Branching ratios and decay asymmetries (in parentheses) of Cabibbo-allowed $\mathcal{B}_c \to \mathcal{B}(3/2^+) + P(V)$ decays in various models. Experimental values denoted by the superscript $*$ are the branching ratios relative to $\Xi_c^+ \to \Xi^-\pi^+\pi^+$. The model calculations of Xu and Kamal are done in two different schemes [230].

Decay	Körner, Krämer [209]	Xu & Kamal [230]	Cheng [231]	Experiment [4]
$\Lambda_c^+ \to \Delta^{++}K^-$	2.70	1.00(0.00); 1.04(0.43)		0.86 ± 0.30
$\Lambda_c^+ \to \Delta^+ K^0$	0.90	0.34(0.00); 0.34(0.43)		0.99 ± 0.32
$\Lambda_c^+ \to \Xi^{*0}K^+$	0.50	0.08(0.00); 0.08(0.25)		0.26 ± 0.10
$\Lambda_c^+ \to \Sigma^{*+}\pi^0$	0.50	0.22(0.00); 0.24(0.40)		
$\Lambda_c^+ \to \Sigma^{*0}\pi^+$	0.50	0.22(0.00); 0.24(0.40)		
$\Lambda_c^+ \to \Sigma^{*+}\eta$	0.54			0.85 ± 0.33
$\Xi_c^+ \to \Sigma^{*+}K^0$	0	0		$1.0 \pm 0.5^*$
$\Xi_c^+ \to \Xi^{*0}\pi^+$	0	0		$< 0.1^*$
$\Xi_c^0 \to \Omega^- K^+$	0.34	0.15(0.00); 0.16(0.27)		seen
$\Xi_c^0 \to \Sigma^{*0}K^0$	0.25	0.09(0.00); 0.10(0.43)		
$\Xi_c^0 \to \Sigma^{*+}K^-$	0.49	0.18(0.00); 0.19(0.43)		
$\Xi_c^0 \to \Xi^{*0}\pi^0$	0.28	0.12(0.00); 0.13(0.40)		
$\Xi_c^0 \to \Xi^{*-}\pi^+$	0.56	0.25(0.00); 0.27(0.40)		
$\Omega_c^0 \to \Omega^-\pi^+$	$0.35a_1^2$	$1.47a_1^2(0)$; $1.44a_1^2(0)$	$0.92a_1^2(0.17)$	seen
$\Omega_c^0 \to \Xi^{*0}K^0$	$0.40a_2^2$	$0.69a_2^2(0)$; $0.61a_2^2(0)$	$1.06a_2^2(0.35)$	
$\Omega_c^0 \to \Omega^-\rho^+$	$2.02a_1^2$	$8.02a_1^2(-0.08)$; $7.82a_2^2(-0.21)$	$3.23a_1^2(0.43)$	
$\Omega_c^0 \to \Xi^{*0}K^{*0}$	$2.28a_2^2$	$3.15a_2^2(-0.09)$; $1.13a_2^2(-0.27)$	$1.60a_2^2(0.28)$	

where $\mathbf{P}_{\mathcal{B}}$ is the parent baryon polarization, $\alpha_{\mathcal{B}}$, $\beta_{\mathcal{B}}$ and $\gamma_{\mathcal{B}}$ are the parent baryon asymmetry parameters and $\mathbf{n}$ is a unit vector along the daughter baryon $\mathcal{B}'$ in the parent baryon frame. If the parent baryon is unpolarized, the above equation reduces to $\mathbf{P}_{\mathcal{B}'} = \alpha_{\mathcal{B}}\mathbf{n}$, which implies that the baryon $\mathcal{B}'$ obtained from the decay of the unpolarized baryon $\mathcal{B}$ is longitudinally polarized by the amount of $\alpha_{\mathcal{B}}$. The transverse polarization components are measured by the parameters $\beta_{\mathcal{B}}$ and $\gamma_{\mathcal{B}}$. In terms of the s- and p-wave amplitudes in Eq. (26.32), the baryon parameters have the expressions

$$\alpha = \frac{2\mathrm{Re}(S^*P)}{|S|^2+|P|^2}, \qquad \beta = \frac{2\mathrm{Im}(S^*P)}{|S|^2+|P|^2}, \qquad \gamma = \frac{|S|^2-|P|^2}{|S|^2+|P|^2}, \tag{26.39}$$

where

$$S = \sqrt{2m_{\mathcal{B}'}(E'+m_{\mathcal{B}'})}\,A, \qquad P = \sqrt{2m_{\mathcal{B}'}(E'-m_{\mathcal{B}'})}\,B. \tag{26.40}$$

When CP is conserved and final-state interactions are negligible, β vanishes. Since the sign of $\alpha_{\mathcal{B}}$ depends on the relative sign between s- and p-wave amplitudes, the measurement of α can be used to discriminate between different models.

The model predictions for the decay asymmetry α in $\Lambda_c^+ \to \Lambda\pi^+$ range from -0.67 to -0.99 (see Table 26.7). The current world average of α is -0.91 ± 0.15 [4], while the most recent measurement is $-0.78 \pm 0.16 \pm 0.19$ by FOCUS [228]. The agreement between theory and experiment implies the $V-A$ structure of the decay process $\Lambda_c^+ \to \Lambda\pi^+$.

It is evident from Table 26.7 that all the models except one model in [225] predict a positive decay asymmetry for the decay $\Lambda_c^+ \to \Sigma^+\pi^0$. Therefore, the measurement of $\alpha = -0.45 \pm 0.31 \pm 0.06$ by CLEO [229] is a big surprise. If the negative sign of α is confirmed in the future, this will imply an opposite sign between s-wave and p-wave amplitudes for this decay, contrary to the model expectation. The implication of this has been discussed in detail in [211]. Since the error of the previous CLEO measurement is very large, it is crucial to have more accurate measurements of the decay asymmetry for $\Lambda_c^+ \to \Sigma^+\pi^0$.

The decays $\Lambda_c^+ \to \Xi^0 K^+$ and $\Xi_c^0 \to \Sigma^+ K^-$ share some common features that they can proceed via W-exchange [219] and that their s-wave amplitudes are very small. As a consequence, their decay asymmetries are expected to be very tiny. Indeed, all the existing models predict vanishing s-wave amplitude and hence $\alpha = 0$ (cf. Table 26.7).

Λ_c^+ decays

Experimentally, nearly all the branching ratios of the Λ_c^+ are measured relative to the $pK^-\pi^+$ mode. Some Cabibbo-suppressed modes such as $\Lambda_c^+ \to \Lambda K^+$ and $\Lambda_c^+ \to \Sigma^0 K^+$ have been recently measured by BaBar [232]. Theoretically, only one model [233] gives predictions for the Cabibbo-suppressed decays.

The first measured Cabibbo-suppressed mode $\Lambda_c^+ \to p\phi$ is of particular interest because it receives contributions only from the factorizable diagram and is expected to be color suppressed in the naive factorization approach. An updated calculation in [234] yields

$$\mathcal{B}(\Lambda_c^+ \to p\phi) = 2.26 \times 10^{-3} a_2^2, \qquad \alpha(\Lambda_c^+ \to p\phi) = -0.10\,. \tag{26.41}$$

¿From the experimental measurement $\mathcal{B}(\Lambda_c^+ \to p\phi) = (8.2 \pm 2.7) \times 10^{-4}$ [4], it follows that

$$|a_2|_{\rm expt} = 0.60 \pm 0.10\,. \tag{26.42}$$

This is in excellent agreement with the $1/N_c$ approach where $a_2 = c_2(m_c) = -0.59$.

Ξ_c^+ decays

No absolute branching ratios have been measured. The branching ratios listed in Tables 26.6 and 26.8 are the ones relative to $\Xi_c^+ \to \Xi^-\pi^+\pi^+$. Several Cabibbo-suppressed decay modes such as $p\bar{K}^{*0}$, $\Sigma^+\phi$ and $\Xi(1690)K^+$ have been observed.

The Cabibbo-allowed decays $\Xi_c^+ \to \mathcal{B}(3/2^+) + P$ have been studied and they are believed to be forbidden as they do not receive factorizable and $1/2^\pm$ pole contributions [230, 209]. However, the $\Sigma^{*+}\bar{K}^0$ mode was seen by FOCUS before [235] and this may indicate the importance of pole contributions beyond low-lying $1/2^\pm$ intermediate states.

Ξ_c^0 decays

No absolute branching ratios have been measured so far. However, there are several measurements of ratios of branching fractions, for example [4],

$$R_1 = \frac{\Gamma(\Xi_c^0 \to \Lambda K_S^0)}{\Gamma(\Xi_c^0 \to \Xi^-\pi^+)} = 0.21 \pm 0.02 \pm 0.02, \quad R_2 = \frac{\Gamma(\Xi_c^0 \to \Omega^- K^+)}{\Gamma(\Xi_c^0 \to \Xi^-\pi^+)} = 0.297 \pm 0.022 \tag{26.43}$$

Most models predict a ratio of R_1 smaller than 0.18 except the model of Żenczykowski [226] which yields $R_1 = 0.29$ due to the small predicted rate of $\Xi_c^0 \to \Xi^-\pi^+$ (see Table 26.6). The model of Körner and Krämer [209] predicts $R_2 = 0.33$ (Table 26.9), in agreement with experiment, but its prediction $R_1 = 0.06$ is too small compared to the data.

Ω_c^0 decays

One of the unique features of the Ω_c^0 decay is that the decay $\Omega_c^0 \to \Omega^-\pi^+$ proceeds only via external W-emission, while $\Omega_c^0 \to \Xi^{*0}\bar{K}^0$ proceeds via the factorizable internal W-emission diagram C'. The general amplitudes for $\mathcal{B}_c \to B^*(\frac{3}{2}^+) + P(V)$ are:

$$\begin{aligned} M[\mathcal{B}_i \to \mathcal{B}_f^*(3/2^+) + P] &= iq_\mu \bar{u}_f^\mu(p_f)(C + D\gamma_5)u_i(p_i), \\ M[\mathcal{B}_i \to \mathcal{B}_f^*(3/2^+) + V] &= \bar{u}_f^\nu(p_f)\varepsilon^{*\mu}[g_{\nu\mu}(C_1 + D_1\gamma_5) \\ &\quad + p_{1\nu}\gamma_\mu(C_2 + D_2\gamma_5) + p_{1\nu}p_{2\mu}(C_3 + D_3\gamma_5)]u_i(p_i) \end{aligned} \tag{26.44}$$

with u^μ being the Rarita-Schwinger vector spinor for a spin-$\frac{3}{2}$ particle. Various model predictions of Cabibbo-allowed $\Omega_c^0 \to \mathcal{B}(3/2^+) + P(V)$ are displayed in Table 26.9 with the unknown parameters a_1 and a_2. From the decay $\Lambda_c^+ \to p\phi$ we learn that $|a_2| = 0.60 \pm 0.10$. Notice a sign difference of α for $\Omega_c \to \frac{3}{2}^+ + V$ in [230] and [231]. It seems to us that the sign of A_i and B_i in Eq. (58) of [230] should be flipped. A consequence of this sign change will render α positive in $\Omega_c \to \frac{3}{2}^+ + V$ decay. In the model of Xu and Kamal [230], the D-wave amplitude in Eq. (26.44) and hence the parameter α vanishes in the decay $\Omega_c \to \frac{3}{2}^+ + P$ due to the fact that the vector current is conserved at all q^2 in their scheme 1 and at $q^2 = 0$ in scheme 2.

26.6.4 Charm-flavor-conserving weak decays

There is a special class of weak decays of charmed baryons which can be studied in a reliable way, namely, heavy-flavor-conserving nonleptonic decays. Some examples are the singly Cabibbo-suppressed decays $\Xi_c \to \Lambda_c \pi$ and $\Omega_c \to \Xi_c' \pi$. The idea is simple: In these decays only the light quarks inside the heavy baryon will participate in weak interactions; that is, while the two light quarks undergo weak transitions, the heavy quark behaves as a "spectator". As the emitted light mesons are soft, the $\Delta S = 1$ weak interactions among light quarks can be handled by the well known short-distance effective Hamiltonian. The synthesis of heavy-quark and chiral symmetries provides a natural setting for investigating these reactions [236]. The weak decays $\Xi_Q \to \Lambda_Q \pi$ with $Q = c, b$ were also studied in [237].

The combined symmetries of heavy and light quarks severely restricts the weak interactions allowed. In the symmetry limit, it is found that there cannot be $\mathcal{B}_{\bar{3}} - \mathcal{B}_6$ and $\mathcal{B}_6^* - \mathcal{B}_6$ nonleptonic weak transitions. Symmetries alone permit three types of transitions: $\mathcal{B}_{\bar{3}} - \mathcal{B}_{\bar{3}}$, $\mathcal{B}_6 - \mathcal{B}_6$ and $\mathcal{B}_6^* - \mathcal{B}_6$ transitions. However, in both the MIT bag and diquark models, only $\mathcal{B}_{\bar{3}} - \mathcal{B}_{\bar{3}}$ transitions have nonzero amplitudes.

The predicted rates are [236]

$$\begin{aligned} \Gamma(\Xi_c^0 \to \Lambda_c^+ \pi^-) &= 1.7 \times 10^{-15}\,\mathrm{GeV}, \qquad \Gamma(\Xi_c^+ \to \Lambda_c^+ \pi^0) = 1.0 \times 10^{-15}\,\mathrm{GeV}, \\ &\quad \Gamma(\Omega_c^0 \to \Xi_c'^+ \pi^-) = 4.3 \times 10^{-17}\,\mathrm{GeV}, \end{aligned} \tag{26.45}$$

and the corresponding branching ratios are

$$\begin{aligned} \mathcal{B}(\Xi_c^0 \to \Lambda_c^+ \pi^-) &= 2.9 \times 10^{-4}, \qquad \mathcal{B}(\Xi_c^+ \to \Lambda_c^+ \pi^0) = 6.7 \times 10^{-4}, \\ &\quad \mathcal{B}(\Omega_c^0 \to \Xi_c'^+ \pi^-) = 4.5 \times 10^{-6}. \end{aligned} \tag{26.46}$$

As stated above, the $\mathcal{B}_6 - \mathcal{B}_6$ transition $\Omega_c^0 \to \Xi_c'^+ \pi^-$ vanishes in the chiral limit. It receives a finite factorizable contribution as a result of symmetry-breaking effect. At any rate, the predicted branching ratios for the charm-flavor-conserving decays $\Xi_c^0 \to \Lambda_c^+ \pi^-$ and $\Xi_c^+ \to \Lambda_c^+ \pi^0$ are of order $10^{-3} \sim 10^{-4}$ and should be readily accessible in the near future.

26.7 Semileptonic decays

The exclusive semileptonic decays of charmed baryons: $\Lambda_c^+ \to \Lambda e^+(\mu^+)\nu_e$, $\Xi_c^+ \to \Xi^0 e^+ \nu_e$ and $\Xi_c^0 \to \Xi^- e^+ \nu_e$ have been observed experimentally. Their rates depend on the $\mathcal{B}_c \to \mathcal{B}$ form factors $f_i(q^2)$ and $g_i(q^2)$ $(i = 1, 2, 3)$ defined in Eq. (26.35). These form factors have been evaluated in the non-relativistic quark model [238, 239, 234], the MIT bag model [238], the relativistic quark model [240], the light-front quark model [241] and QCD sum rules [242, 243]. Experimentally, the only information available so far is the form-factor ratio measured in the semileptonic decay $\Lambda_c \to \Lambda e \bar{\nu}$. In the heavy quark limit, the six $\Lambda_c \to \Lambda$ form factors are reduced to two:

$$\langle \Lambda(p)|\bar{s}\gamma_\mu(1-\gamma_5)c|\Lambda_c(v)\rangle = \bar{u}_\Lambda \left(F_1^{\Lambda_c\Lambda}(v\cdot p) + \not{p} F_2^{\Lambda_c\Lambda}(v\cdot p)\right)\gamma_\mu(1-\gamma_5)u_{\Lambda_c}. \tag{26.47}$$

Table 26.10: Predicted semileptonic decay rates (in units of $10^{10}s^{-1}$) and decay asymmetries (second entry) in various models. Dipole q^2 dependence for form factors is assumed whenever the form-factor momentum dependence is not calculated in the model. Predictions of [238] are obtained in the non-relativistic quark model and the MIT bag model (in parentheses).

Process	Pérez-Marcial et al. [238]	Singleton [239]	Cheng, Tseng [234]	Ivanov [240]	Luo [241]	Marques de Carvalho [242]	Huang, Wang [243]	Expt [4]
$\Lambda_c^+ \to \Lambda^0 e^+ \nu_e$	11.2 (7.7)	9.8	7.1	7.22 -0.812	7.0	13.2 ± 1.8 -1	10.9 ± 3.0 -0.88 ± 0.03	$10.5 \pm$ $-0.86 \pm$
$\Xi_c^0 \to \Xi^- e^+ \nu_e$	18.1 (12.5)	8.5	7.4	8.16	9.7			seen
$\Xi_c^+ \to \Xi^0 e^+ \nu_e$	18.4 (12.7)	8.5	7.4	8.16	9.7			seen

Assuming a dipole q^2 behavior for form factors, the ratio $R = \tilde{F}_2^{\Lambda_c\Lambda}/\tilde{F}_1^{\Lambda_c\Lambda}$ is measured by CLEO to be [244]

$$R = -0.31 \pm 0.05 \pm 0.04\,. \tag{26.48}$$

Various model predictions of the charmed baryon semileptonic decay rates and decay asymmetries are shown in Table 26.10. Dipole q^2 dependence for form factors is assumed whenever the form factor momentum dependence is not available in the model. The predicted rates cited from [238] include QCD corrections. However, as stressed in [155], it seems that QCD effects computed in [238] are unrealistically too large. Moreover, the calculated heavy-heavy baryon form factors in [238] at zero recoil do not satisfy the constraints imposed by heavy quark symmetry [234]. From Table 26.10 we see that the computed branching ratios of $\Lambda_c^+ \to \Lambda e^+ \nu$ lie in the range $1.4\% \sim 2.6\%$, in agreement with experiment, $(2.1 \pm 0.6)\%$ [4]. Branching ratios of $\Xi_c^0 \to \Xi^- e^+ \nu$ and $\Xi_c^+ \to \Xi^0 e^+ \nu$ are predicted to fall into the ranges $(0.8 \sim 2.0)\%$ and $(3.3 \sim 8.1)\%$, resepctively. Experimentally, only the ratios of the branching fractions are available so far [4]

$$\frac{\Gamma(\Xi_c^+ \to \Xi^0 e^+ \nu)}{\Gamma(\Xi_c^+ \to \Xi^- \pi^+ \pi^+)} = 2.3 \pm 0.6^{+0.3}_{-0.6}, \qquad \frac{\Gamma(\Xi_c^0 \to \Xi^- e^+ \nu)}{\Gamma(\Xi_c^0 \to \Xi^- \pi^+)} = 3.1 \pm 1.0^{+0.3}_{-0.5}\,. \tag{26.49}$$

26.8 Electromagnetic and Weak Radiative decays

Although radiative decays are well measured in the charmed meson sector, e.g. $D^* \to D\gamma$ and $D_s^+ \to D_s^+\gamma$, only three of the radiative modes in the charmed baryon sector have been seen, namely, $\Xi_c^{\prime 0} \to \Xi_c^0\gamma$, $\Xi_c^{\prime +} \to \Xi_c^+\gamma$ and $\Omega_c^{*0} \to \Omega_c^0\gamma$. This is understandable because $m_{\Xi_c'} - m_{\Xi_c} \approx 107$ MeV and $m_{\Omega_c^*} - m_{\Omega_c} \approx 71$ MeV. Hence, Ξ_c' and Ω_c^* are governed by the electromagnetic decays. However, it will be difficult to measure the rates of these decays because these states are too narrow to be experimentally resolvable. Nevertheless, we shall systematically study the two-body electromagnetic decays of charmed baryons and also weak radiative decays.

26.8.1 Electromagnetic decays

In the baryon sector, the following two-body electromagnetic decays are of interest:

$$\begin{aligned} B_6 \to B_{\bar{3}} + \gamma \;&:\; \Sigma_c \to \Lambda_c + \gamma, \quad \Xi_c' \to \Xi_c + \gamma, \\ B_6^* \to B_{\bar{3}} + \gamma \;&:\; \Sigma_c^* \to \Lambda_c + \gamma, \quad \Xi_c'^* \to \Xi_c + \gamma, \\ B_6^* \to B_6 + \gamma \;&:\; \Sigma_c^* \to \Sigma_c + \gamma, \quad \Xi_c'^* \to \Xi_c' + \gamma, \quad \Omega_c^* \to \Omega_c + \gamma, \end{aligned} \tag{26.50}$$

where we have denoted the spin $\frac{1}{2}$ baryons as B_6 and $B_{\bar{3}}$ for a symmetric sextet **6** and antisymmetric antitriplet $\bar{\mathbf{3}}$, respectively, and the spin $\frac{3}{2}$ baryon by B_6^*.

An ideal theoretical framework for studying the above-mentioned electromagnetic decays is provided by the formalism in which the heavy quark symmetry and the chiral symmetry of light quarks are combined [174, 175]. When supplemented by the nonrelativistic quark model, the formalism determines completely the low energy dynamics of heavy hadrons. The electromagnetic interactions of heavy hadrons consist of two distinct contributions: one from gauging electromagnetically the chirally invariant strong interaction Lagrangians for heavy mesons and baryons given in [174, 175], and the other from the anomalous magnetic moment couplings of the heavy particles. The heavy quark symmetry reduces the number of free parameters needed to describe the magnetic couplings to the photon. There are two undetermined parameters for the ground state heavy baryons. All these parameters are related simply to the magnetic moments of the light quarks in the nonrelativistic quark model. However, the charmed quark is not particularly heavy ($m_c \simeq 1.6$ GeV), and it carries a charge of $\frac{2}{3}e$. Consequently, the contribution from its magnetic moment cannot be neglected. The chiral and electromagnetic gauge-invariant Lagrangian for heavy baryons can be found in Eqs. (3.8) and (3.9) of [245].

The amplitudes of electromagnetic decays are given by [245]

$$\begin{aligned} A(B_6 \to B_{\bar{3}} + \gamma) &= i\eta_1 \bar{u}_{\bar{3}} \sigma_{\mu\nu} k^\mu \varepsilon^\nu u_6, \\ A(B_6^* \to B_{\bar{3}} + \gamma) &= i\eta_2 \epsilon_{\mu\nu\alpha\beta} \bar{u}_{\bar{3}} \gamma^\nu k^\alpha \varepsilon^\beta u^\mu, \\ A(B_6^* \to B_6 + \gamma) &= i\eta_3 \epsilon_{\mu\nu\alpha\beta} \bar{u}_6 \gamma^\nu k^\alpha \varepsilon^\beta u^\mu, \end{aligned} \tag{26.51}$$

where k_μ is the photon 4-momentum and ε_μ is the polarization 4-vector. The corresponding decay rates are [245]

$$\begin{aligned} \Gamma(B_6 \to B_{\bar{3}} + \gamma) &= \eta_1^2 \frac{k^3}{\pi}, \\ \Gamma(B_6^* \to B_{\bar{3}} + \gamma) &= \eta_2^2 \frac{k^3}{3\pi} \frac{3m_i^2 + m_f^2}{4m_i^2}, \\ \Gamma(B_6^* \to B_6 + \gamma) &= \eta_3^2 \frac{k^3}{3\pi} \frac{3m_i^2 + m_f^2}{4m_i^2}, \end{aligned} \tag{26.52}$$

where m_i (m_f) is the mass of the parent (daughter) baryon.

The coupling constants η_i can be calculated using the quark model [245]; some of them

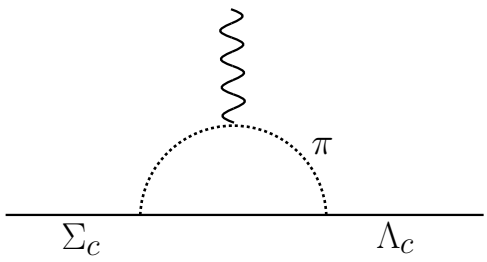

Figure 26.5: Chiral loop contribution to the E2 amplitude of $\Sigma_c^* \to \Lambda_c\gamma$.

are

$$\eta_1(\Sigma_c^+ \to \Lambda_c^+) = \frac{e}{6\sqrt{3}}\left(\frac{2}{M_u}+\frac{1}{M_d}\right), \quad \eta_2(\Sigma_c^{*+} \to \Lambda_c^+) = \frac{e}{3\sqrt{6}}\left(\frac{2}{M_u}+\frac{1}{M_d}\right),$$
$$\eta_3(\Sigma_c^{*++} \to \Sigma_c^{++}) = \frac{2\sqrt{2}e}{9}\left(\frac{1}{M_u}-\frac{1}{M_c}\right), \quad \eta_3(\Sigma_c^{*0} \to \Sigma_c^0) = \frac{2\sqrt{2}e}{9}\left(-\frac{1}{2M_d}-\frac{1}{M_c}\right),$$
$$\eta_3(\Sigma_c^{*+} \to \Sigma_c^+) = \frac{\sqrt{2}e}{9}\left(\frac{1}{M_u}-\frac{1}{2M_d}-\frac{2}{M_c}\right), \quad \eta_3(\Xi_c^{\prime *+} \to \Xi_c^+) = \frac{e}{3\sqrt{6}}\left(\frac{2}{M_u}+\frac{1}{M_s}\right),$$
$$\eta_3(\Xi_c^{\prime *0} \to \Xi_c^0) = \frac{e}{3\sqrt{6}}\left(-\frac{1}{M_d}+\frac{1}{M_s}\right), \quad \eta_3(\Omega_c^{*0} \to \Omega_c^0) = \frac{2\sqrt{2}e}{9}\left(-\frac{1}{2M_s}-\frac{1}{M_c}\right). \quad (26.53)$$

Using the constituent quark masses, $M_u = 338$ MeV, $M_d = 322$ MeV and $M_s = 510$ MeV [4], the calculated results are summarized in the second column of Table 26.11. A similar procedure is followed in [247] where the heavy quark symmetry is supplemented with light-diquark symmetries to calculate the widths of $\Sigma_c^+ \to \Lambda_c^+\gamma$ and $\Sigma_c^* \to \Sigma_c\gamma$. The authors of [240] apply the relativistic quark model to predict various electromagnetic decays of charmed baryons. Besides the magnetic dipole (M1) transition, the author of [248] also considered and estimated the electric quadrupole (E2) amplitude for $\Sigma_c^{*+} \to \Lambda_c^+\gamma$ arising from the chiral loop correction (Fig. 26.5). A detailed analysis of the E2 contributions was presented in [246]. The E2 amplitudes appear at different higher orders for the three kinds of decays: $\mathcal{O}(1/\Lambda_\chi^2)$ for $B_6^* \to B_6+\gamma$, $\mathcal{O}(1/m_Q\Lambda_\chi^2)$ for $B_6^* \to B_{\bar{3}}+\gamma$ and $\mathcal{O}(1/m_Q^3\Lambda_\chi^2)$ for $B_6 \to B_{\bar{3}}+\gamma$. Therefore, the E2 contribution to $B_6 \to B_{\bar{3}}+\gamma$ is completely negligible.

Chiral-loop corrections to the M1 electromagnetic decays and to the strong decays of heavy baryons have been computed at the one loop order in [249]. The leading chiral-loop effects we found are nonanalytic in the forms of m/Λ_χ and $(m^2/\Lambda_\chi^2)\ln(\Lambda^2/m^2)$ (or $m_q^{1/2}$ and $m_q \ln m_q$, with m_q being the light quark mass). Some results are [249]

$$\Gamma(\Sigma_c^+ \to \Lambda_c^+\gamma) = 112\,\text{keV}, \quad \Gamma(\Xi_c^{\prime +} \to \Xi_c^+\gamma) = 29\,\text{keV}, \quad \Gamma(\Xi_c^{\prime 0} \to \Xi_c^0\gamma) = 0.15\,\text{keV}, \quad (26.54)$$

which should be compared with the corresponding quark-model results: 88 keV, 16 keV and 0.3 keV (Table 26.11).

The electromagnetic decay $\Xi_c^{\prime *0} \to \Xi_c^0\gamma$ is of special interest. It has been advocated in [250] that a measurement of its branching ratio will determine one of the coupling constants in HHChPT, namely, g_1. The radiative decay $\Xi_c^{\prime *0} \to \Xi_c^0\gamma$ is forbidden at tree level in SU(3) limit [see Eq. (26.53)]. In heavy baryon chiral perturbation theory, this

Table 26.11: Electromagnetic decay rates (in units of keV) of charmed baryons.

Decay	HHChPT +QM [176, 245]	Ivanov et al. [240]	Bañuls et al. [246]	Tawfiq et al. [247]	Experiment [4]
$\Sigma_c^+ \to \Lambda_c^+\gamma$	88	60.7 ± 1.5		87	
$\Sigma_c^{**+} \to \Sigma_c^{++}\gamma$	1.4			3.04	
$\Sigma_c^{*+} \to \Sigma_c^{+}\gamma$	0.002	0.14 ± 0.004		0.19	
$\Sigma_c^{*+} \to \Lambda_c^{+}\gamma$	147	151 ± 4			
$\Sigma_c^{*0} \to \Lambda_c^{0}\gamma$	1.2			0.76	
$\Xi_c^{\prime+} \to \Xi_c^{+}\gamma$	16	12.7 ± 1.5			seen
$\Xi_c^{\prime 0} \to \Xi_c^{0}\gamma$	0.3	0.17 ± 0.02	1.2 ± 0.7		seen
$\Xi_c^{\prime *+} \to \Xi_c^{+}\gamma$	54	54 ± 3			
$\Xi_c^{\prime *0} \to \Xi_c^{0}\gamma$	1.1	0.68 ± 0.04	5.1 ± 2.7		
$\Omega_c^{*0} \to \Omega_c^{0}\gamma$	0.9				seen

radiative decay is induced via chiral loops where SU(3) symmetry is broken by the light current quark masses. By identifying the chiral loop contribution to $\Xi_c^{\prime *0} \to \Xi_c^0\gamma$ with the quark model prediction given in Eq. (26.53), it was found in [176] that one of the two possible solutions is in accord with the quark model expectation for g_1.

For the electromagnetic deacys of p-wave charmed baryons, the search of $\Lambda_c(2593)^+ \to \Lambda_c^+\gamma$ and $\Lambda_c^+(2625)^+ \to \Lambda_c^+\gamma$ has been failed so far. On the theoretical side, the interested reader is referred to [247, 240, 250, 185, 187, 251] for more details.

The electromagnetic decays considered so far do not test critically the heavy quark symmetry nor the chiral symmetry. The results follow simply from the quark model. There are examples in which both the heavy quark symmetry and the chiral symmetry enter in a crucial way. These are the radiative decays of heavy baryons involving an emitted pion. Some examples which are kinematically allowed are

$$\Sigma_c \to \Lambda_c\pi\gamma, \quad \Sigma_c^* \to \Lambda_c\pi\gamma, \quad \Sigma_c^* \to \Sigma_c\pi\gamma, \quad \Xi_c^* \to \Xi_c\pi\gamma. \tag{26.55}$$

For an analysis of the decay $\Sigma_c \to \Lambda_c\pi\gamma$, see [245].

26.8.2 Weak radiative decays

At the quark level, there are three different types of processes which can contribute to the weak radiative decays of heavy hadrons, namely, single-, two- and three-quark transitions [253]. The single-quark transition mechanism comes from the so-called electromagnetic penguin diagram. Unfortunately, the penguin process $c \to u\gamma$ is very suppressed and hence it plays no role in charmed hadron radiative decays. There are two contributions from the two-quark transitions: one from the W-exchange diagram accompanied by a photon emission from the external quark, and the other from the same W-exchange diagram but with a photon radiated from the W boson. The latter is typically suppressed by a factor of $m_q k/M_W^2$ (k being the photon energy) as compared to the former bremsstrahlung process

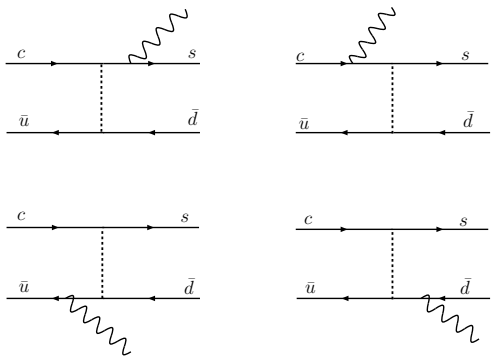

Figure 26.6: W-exchange diagrams contributing to the quark-quark bremsstrahlung process $c + \bar{u} \to s + \bar{d} + \gamma$. The W-annihilation type diagrams are not shown here.

[252]. For charmed baryons, the Cabibbo-allowed decay modes via $c\bar{u} \to s\bar{d}\gamma$ (Fig. 26.6) or $cd \to us\gamma$ are

$$\Lambda_c^+ \to \Sigma^+\gamma, \qquad \Xi_c^0 \to \Xi^0\gamma. \tag{26.56}$$

Finally, the three-quark transition involving W-exchange between two quarks and a photon emission by the third quark is quite suppressed because of very small probability of finding three quarks in adequate kinematic matching with the baryons [253, 254].

The general amplitude of the weak radiative baryon decay reads

$$A(\mathcal{B}_i \to \mathcal{B}_f\gamma) = i\bar{u}_f(a + b\gamma_5)\sigma_{\mu\nu}\varepsilon^\mu k^\nu u_i, \tag{26.57}$$

where a and b are parity-conserving and -violating amplitudes, respectively. The corresponding decay rate is

$$\Gamma(\mathcal{B}_i \to \mathcal{B}_f\gamma) = \frac{1}{8\pi}\left(\frac{m_i^2 - m_f^2}{m_i}\right)^3 (|a|^2 + |b|^2). \tag{26.58}$$

Nonpenguin weak radiative decays of charmed baryons such as those in (26.56) are characterized by emission of a hard photon and the presence of a highly virtual intermediate quark between the electromagnetic and weak vertices. It has been shown in [255] that these features should make possible to analyze these processes by perturbative QCD; that is, these processes are describable by an effective local and gauge invariant Lagrangian:

$$\mathcal{H}_{\text{eff}}(c\bar{u} \to s\bar{d}\gamma) = \frac{G_F}{2\sqrt{2}} V_{cs}V_{ud}^*(c_+O_+^F + c_-O_-^F), \tag{26.59}$$

with

$$O_\pm^F(c\bar{u} \to s\bar{d}\gamma) = \frac{e}{m_i^2 - m_f^2} \left\{ \left(e_s\frac{m_f}{m_s} + e_u\frac{m_i}{m_u}\right)\left(\tilde{F}_{\mu\nu} + iF_{\mu\nu}\right)O_\pm^{\mu\nu} \right. \tag{26.60}$$

$$\left. - \left(e_d\frac{m_f}{m_d} + e_c\frac{m_i}{m_c}\right)\left(\tilde{F}_{\mu\nu} - iF_{\mu\nu}\right)O_\mp^{\mu\nu} \right\}, \tag{26.61}$$

where $m_i = m_c + m_u$, $m_f = m_s + m_d$, $\tilde{F}_{\mu\nu} \equiv \frac{1}{2}\epsilon_{\mu\nu\alpha\beta}F^{\alpha\beta}$ and

$$O_{\pm}^{\mu\nu} = \bar{s}\gamma^{\mu}(1-\gamma_5)c\bar{u}\gamma^{\nu}(1-\gamma_5)d \pm \bar{s}\gamma^{\mu}(1-\gamma_5)d\bar{u}\gamma^{\nu}(1-\gamma_5)c. \tag{26.62}$$

For the charmed baryon radiative decays, one needs to evaluate the matrix element $\langle \mathcal{B}_f|O_{\pm}^{\mu\nu}|\mathcal{B}_i\rangle$. Since the quark-model wave functions best resemble the hadronic states in the frame where both baryons are static, the static MIT bag model [224] was thus adopted in [255] for the calculation. The predictions are

$$\begin{aligned} &\mathcal{B}(\Lambda_c^+ \to \Sigma^+\gamma) = 4.9\times 10^{-5}, \qquad \alpha(\Lambda_c^+ \to \Sigma^+\gamma) = -0.86\,, \\ &\mathcal{B}(\Xi_c^0 \to \Xi^0\gamma) = 3.6\times 10^{-5}, \qquad \alpha(\Xi_c^0 \to \Xi^0\gamma) = -0.86\,. \end{aligned} \tag{26.63}$$

A different analysis of the same decays was carried out in [256] with the results

$$\begin{aligned} &\mathcal{B}(\Lambda_c^+ \to \Sigma^+\gamma) = 2.8\times 10^{-4}, \qquad \alpha(\Lambda_c^+ \to \Sigma^+\gamma) = 0.02\,, \\ &\mathcal{B}(\Xi_c^0 \to \Xi^0\gamma) = 1.5\times 10^{-4}, \qquad \alpha(\Xi_c^0 \to \Xi^0\gamma) = -0.01\,. \end{aligned} \tag{26.64}$$

Evidently, these predictions (especially the decay asymmetry) are very different from the ones obtained in [255].

Finally, it is worth remarking that, in analog to the heavy-flavor-conserving nonleptonic weak decays as discussed in Sec. VI, there is a special class of weak radiative decays in which heavy flavor is conserved. Some examples are $\Xi_c \to \Lambda_c\gamma$ and $\Omega_c \to \Xi_c\gamma$. In these decays, weak radiative transitions arise from the diquark sector of the heavy baryon whereas the heavy quark behaves as a spectator. However, the dynamics of these radiative decays is more complicated than their counterpart in nonleptonic weak decays, e.g., $\Xi_c \to \Lambda_c\pi$. In any event, it deserves a detailed study.

Chapter 27

$D^0 - \overline{D}^0$ Mixing[1]

Meson-antimeson oscillations have been of central importance in the evolution of the Standard Model (SM) and in searches for New Physics. This is based on two seminal features [1]: (a) In such oscillations quantum mechanical effects will build up over macroscopic distances, which makes tiny mass differences measurable. (b) Oscillations and the rare decay reactions $s \to dl^+l^-$, $s \to d\nu\overline{\nu}$, $b \to s\gamma$, and $b \to sl^+l^-$ are driven by flavor changing neutral currents (FCNC), which are highly suppressed in the SM, where they are given by 1-loop processes.

Short-distance dynamics in the form of the well-known quark-box diagrams provide a good approximation for the effective $\Delta B = 2$ and the **CP** violating $\Delta S = 2$ transition operators with the superheavy top mass providing a moderate enhancement rather than the considerable GIM suppression inherent in m_c^2/M_W^2 etc.; it provides a significant contribution even for ΔM_K. The situation is fundamentally different for neutral mesons built from the *up*-type quarks (u, c, t) for a number of reasons: (i) Since top quarks decay before they can hadronize, there are no T^0 mesons, and $T^0 - \bar{T}^0$ oscillations a forteriori cannot occur. (ii) Neither can pion etc. oscillations, since pion and eta mesons are their own antimesons. (iii) Oscillations can thus proceed only for neutral D mesons, which makes charm quite unique among up-type quarks.

While $D^0 - \bar{D}^0$ oscillations do have to proceed on some level, we know on general grounds that they have to be rather slow in the SM. For while the amplitude for $D^0 \Rightarrow \bar{D}^0$ is doubly Cabibbo suppressed, its leading decay channels are not. Furthermore $D^0 - \bar{D}^0$ oscillations have to vanish already in the $SU(3)_{Fl}$ symmetry limit, which represents a considerably better approximation to the real world than the $SU(4)_{Fl}$ or $SU(6)_{Fl}$ symmetry limits constraining $K^0 - \bar{K}^0$ and $B^0 - \bar{B}^0$ oscillations, respectively. As discussed below within the SM $D^0 - \bar{D}^0$ oscillations are driven by long distance dynamics, over which our theoretical control is rather limited. It is quite difficult to make the statement that these oscillations are slow more specific. Nevertheless it is mandatory to probe $D^0 - \bar{D}^0$ oscillations as sensitively as possible; while their observation by themselves might not provide conclusive proof for the intervention of New Physics, it is an essential element in searches for CP violation, where such conclusive proof can be obtained.

[1]By David Asner and Haibo Li

27.1 Theoretical Review

27.1.1 Oscillation Formalism: the Phenomenology

It has become customary to use the terms 'oscillations' and 'mixing' in an interchangeable way. This is unfortunate. For while the two terms describe phenomena that are related, they are of a different nature with 'mixing' denoting the more general concept and 'oscillations' the more specific one.

Mixing means that classically distinct states are not necessarily so in quantum mechanics and therefore can *interfere*. For example in atomic physics wave functions are said to be *mixtures* of 'right' and 'wrong' components whose interference generates parity odd observables; it is the weak neutral current that induces such wrong parity component. Or mass eigenstates of quarks (and leptons) contain components of different flavors giving rise to a non-diagonal CKM (or PMNS) matrix described later. This is usually referred to as quark mixing. Such mixing creates a plethora of observable effects.

The most intriguing ones arise when the violation of a certain quantum number – like strangeness – leads to the stationary or mass eigenstates not being eigenstates under that quantum number. This induces *oscillations* like matter-antimatter oscillations discussed above or neutron-antineutron oscillations or neutrino oscillations. *Oscillations* thus require *mixing*, but go beyond it in the sense that they generate transitions with a very peculiar time evolution, namely an oscillatory one rather than the usual exponentially damped one.

The time evolution of the $D^0 - \overline{D}^0$ system is described by the Schrödinger-like equation as

$$i\frac{\partial}{\partial t}\begin{pmatrix} D^0(t) \\ \bar{D}^0(t) \end{pmatrix} = \left(\mathbf{M} - \frac{i}{2}\mathbf{\Gamma}\right)\begin{pmatrix} D^0(t) \\ \bar{D}^0(t) \end{pmatrix}, \tag{27.1}$$

where the $\mathbf{M}$ and $\mathbf{\Gamma}$ matrices are Hermitian, and are defined as

$$\left(\mathbf{M} - \frac{i}{2}\mathbf{\Gamma}\right) = \begin{pmatrix} M_{11} - \frac{i}{2}\Gamma_{11} & M_{12} - \frac{i}{2}\Gamma_{12} \\ M_{12}^* - \frac{i}{2}\Gamma_{12}^* & M_{22} - \frac{i}{2}\Gamma_{22} \end{pmatrix}. \tag{27.2}$$

CPT invariance imposes

$$M_{11} = M_{22} \equiv M\,,\ \Gamma_{11} = \Gamma_{22} \equiv \Gamma. \tag{27.3}$$

The off-diagonal elements of these matrices describe the dispersive and absorptive parts of $D^0 - \overline{D}^0$ mixing (for details see [257]). The two eigenstates D_1 and D_2 of the effective Hamiltonian matrix $(\mathbf{M} - \frac{i}{2}\mathbf{\Gamma})$ are given by

$$|D_1\rangle = \frac{1}{\sqrt{|p|^2 + |q|^2}}(p|D^0\rangle + q|\overline{D}^0\rangle)\,,\ |D_2\rangle = \frac{1}{\sqrt{|p|^2 + |q|^2}}(p|D^0\rangle - q|\overline{D}^0\rangle). \tag{27.4}$$

The corresponding eigenvalues are

$$\lambda_{D_1} \equiv m_1 - \frac{i}{2}\Gamma_1 = \left(M - \frac{i}{2}\Gamma\right) + \frac{q}{p}\left(M_{12} - \frac{i}{2}\Gamma_{12}\right), \tag{27.5}$$

$$\lambda_{D_2} \equiv m_2 - \frac{i}{2}\Gamma_2 = \left(M - \frac{i}{2}\Gamma\right) - \frac{q}{p}\left(M_{12} - \frac{i}{2}\Gamma_{12}\right), \tag{27.6}$$

where $m_1(m_2)$ and $\Gamma_1(\Gamma_2)$ are the mass and width of D_1 (D_2), respectively, and

$$\left|\frac{q}{p}\right|^2 = \frac{M_{12}^* - \frac{i}{2}\Gamma_{12}^*}{M_{12} - \frac{i}{2}\Gamma_{12}}. \tag{27.7}$$

From Eqs.(27.5) and (27.6), one can get the differences in mass and width:

$$\Delta m \equiv m_2 - m_1 = -2\mathrm{R}e\left[\frac{q}{p}(M_{12} - \frac{i}{2}\Gamma_{12})\right], \tag{27.8}$$

$$\Delta\Gamma \equiv \Gamma_1 - \Gamma_2 = -2\mathrm{I}m\left[\frac{q}{p}(M_{12} - \frac{i}{2}\Gamma_{12})\right]. \tag{27.9}$$

The subscripts are mere labels at this point. We have chosen the definitions of ΔM and $\Delta\Gamma$ s.t. when applied to the kaon sector with $K_S = K_1$ and $K_L = K_2$, we get both differences positive.

A pure D^0 state generated at $t = 0$ could decay to $K^+\pi^-$ state either by $D^0 - \overline{D}^0$ mixing or by DCSD, and the two amplitudes may interfere. The time evolutions of $|D_1\rangle$ and $|D_2\rangle$ are given by

$$|D_i\rangle = e_i|D_i\rangle\,,\ e_i = e^{-im_i t - \frac{1}{2}\Gamma_i t}\,,\ (i = 1, 2). \tag{27.10}$$

Under the phase convention $CP|D^0\rangle = |\overline{D}^0\rangle$, a state that is purely $|D^0\rangle$ ($|\overline{D}^0\rangle$) prepared by the strong interaction at $t = 0$ will evolve to $|D^0_{\rm phys}(t)\rangle$ ($|\overline{D}^0_{\rm phys}(t)\rangle$):

$$|D^0_{\rm phys}(t)\rangle = g_+(t)|D^0\rangle + \frac{q}{p}g_-(t)|\overline{D}^0\rangle\,, \tag{27.11}$$

$$|\overline{D}^0_{\rm phys}(t)\rangle = \frac{p}{q}g_-(t)|D^0\rangle + g_+(t)|\overline{D}^0\rangle\,, \tag{27.12}$$

where

$$g_\pm(t) = \frac{1}{2}(e_1 \pm e_2). \tag{27.13}$$

The probability to find a $\overline{D}^0$ at time t in an initially pure D^0 beam is given by

$$|\langle\overline{D}^0|D^0_{\rm phys}(t)\rangle = \frac{1}{4}\left|\frac{q}{p}\right|^2 e^{-\Gamma_2 t}\left(1 + e^{-\Delta\Gamma t} - 2e^{-\frac{1}{2}\Delta\Gamma t}\cos\Delta m t\right). \tag{27.14}$$

While the flavour of the initial meson is tagged by its production, the flavour of the final meson is inferred from its decay.

There are two dimensionless ratios describing the interplay between oscillations and decays:

$$x \equiv \frac{\Delta m}{\Gamma}\,,\ y \equiv \frac{\Delta\Gamma}{2\Gamma}, \tag{27.15}$$

where $\Gamma \equiv (\Gamma_1 + \Gamma_2)/2$ is the averaged D^0 width.

27.1.2 Standard Model Predictions for Oscillation Parameters

Oscillations arise from $\Delta C = 2$ interactions that generate off-diagonal terms in mass matrix as in Eq.(27.2) for D^0 and $\overline{D}^0$ mesons. The expansion of the off-diagonal terms in the neutral D mass matrix to second order in perturbation theory is

$$M_{12} = \langle \overline{D}^0 | \mathcal{H}_w^{\Delta C=2} | D^0 \rangle + P \sum_n \frac{\langle \overline{D}^0 | \mathcal{H}_w^{\Delta C=1} | n \rangle \langle n | \mathcal{H}_w^{\Delta C=1} | D^0 \rangle}{m_D^2 - E_n^2}\,, \tag{27.16}$$

$$\Gamma_{12} = \sum_n \rho_n \langle \overline{D}^0 | \mathcal{H}_w^{\Delta C=1} | n \rangle \langle n | \mathcal{H}_w^{\Delta C=1} | D^0 \rangle\,, \tag{27.17}$$

where the sum runs over all relevant intermediate states (virtual ones for M_{12} and real ones for Γ_{12}), P denotes the principle value, and ρ_n is the density of the states n.

The operator in the first term – $\mathcal{H}_w^{\Delta C=2}$ – is a *local* one at scale $\mu \sim m_D$, so it contributes to the M_{12} (but not to the Γ_{12}) part of the generalized mass matrix. New Physics could induce such a contribution of potentially significant size. The SM generates such a term, namely from the quark box diagram with b quarks as internal quarks, yet it is truly tiny due to its highly suppressed CKM parameters. The second term in Eq. (27.16) comes from a double insertion of $\Delta C = 1$ operators; it contributes to both M_{12} and Γ_{12}. The dominant SM contribution comes from here as described below; New Physics could make here a significant contribution to M_{12}.

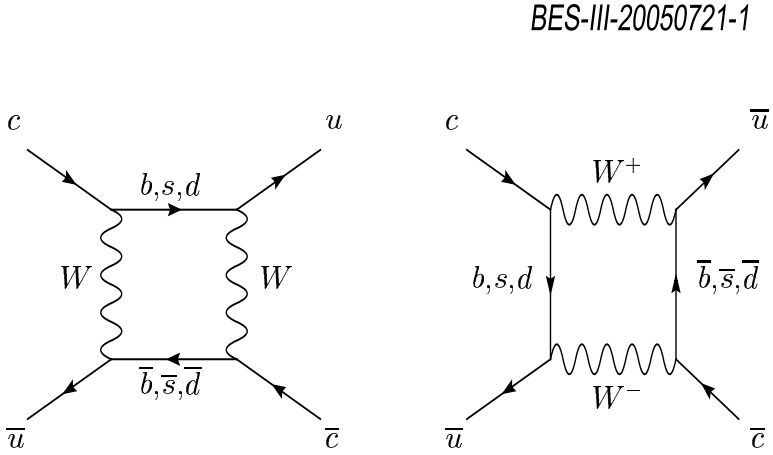

Figure 27.1: Standard Model box diagrams of flavor-changing neutral currents contributing to $D^0 - \overline{D}^0$ mixing at the quark level.

Short-Distance Contribution to x and y

In the SM there is a bona fide short-distance $\Delta C = 2$ operator, which is inferred from the quark box diagram with b quarks as the intermediate quarks, see Fig. 27.1. The effects due to intermediate b quarks are evaluated in a straightforward way since they are far

off-shell [258]:

$$\Delta m^{b\bar{b}} \simeq -\frac{G_F^2 m_b^2}{8\pi^2} |V_{cb}^* V_{ub}|^2 \frac{\langle D^0|(\overline{u}\gamma_\mu(1-\gamma_5)c)(\overline{u}\gamma_\mu(1-\gamma_5)c)|\overline{D}^0\rangle}{2M_D} ; \tag{27.18}$$

however they are highly suppressed by the tiny CKM parameters. Using factorization to estimate the matrix element one finds $x^{b\bar{b}} \sim 10^{-6}$. Loops with one b and one light quark likewise are suppressed.

For the light intermediate quarks – d, s – the momentum scale is set by the *external* mass m_c. However, it is highly GIM suppressed

$$\begin{aligned}\Delta m^{(s,d)} \quad &\simeq -\frac{G_F^2 m_c^2}{8\pi^2} |V_{cs}^* V_{us}|^2 \frac{\left(m_s^2 - m_d^2\right)^2}{m_c^4} \times \\ &\frac{\langle D^0|(\overline{u}\gamma_\mu(1-\gamma_5)c)(\overline{u}\gamma_\mu(1-\gamma_5)c) + (\overline{u}(1+\gamma_5)c)(\overline{u}(1+\gamma_5)c)|\overline{D}^0\rangle}{2M_D} .\end{aligned} \tag{27.19}$$

In contrast to $K^0 - \overline{K}^0$ and $B^0 - \overline{B}^0$ mixing, the internal quarks in the box diagrams here are down-type quarks. The b-quark contribution, which would give in principle the largest GIM violation, is suppressed by small CKM mixing factors $V_{cb}^* V_{ub}$. The leading contribution, as shown in Eq. (27.19), is given by the strange quark and therefore results in a very effective GIM suppression.

The contribution to $\Delta\Gamma$ from the bare quark box is greatly suppressed by a factor m_s^6. The GIM mass insertions yield a factor m_s^4. Contrary to the claim in Ref. [259] the additional factor of m_s^2 is *not* due to helicity suppression – the GIM factors already take care of that effect; it is of an accidental nature: it arises because the weak currents are purely $V - A$ and only in four dimensions. Including radiative QCD corrections to the box diagram yields contributions $\propto m_s^4 \alpha_S/\pi$. Numerically one finds:

$$y^{box} \ll x^{box} \simeq (10^{-6}) - (10^{-5}). \tag{27.20}$$

Long-distance Contribution to x and y

The long-distance contributions to $D^0 - \overline{D}^0$ oscillations are inherently non-perturbative, and we have not learnt yet how to calculate them from first principles. It is however extremely important to estimate their size in order to understand the origin of a possible experimental observation. These contributions come from transitions to final states $|f\rangle$ that are accessible to both $|D^0\rangle$ and $|\overline{D}^0\rangle$. For example, Figure 27.2 illustrates a contribution to mixing from transitions to two pseudoscalars. GIM cancellations are such that they become complete in the $SU(3)_{Fl}$ limit; i.e., no oscillations can occur then.

Within the SM x and y are generated only at second order in $\mathrm{SU}(3)_F$ breaking,

$$x\,,\, y \sim \sin^2\theta_C \times [SU(3)\text{ breaking}]^2\,, \tag{27.21}$$

where θ_C is the Cabibbo angle. The SM predictions for x and y thus depend crucially on estimating the size of $\mathrm{SU}(3)_F$ breaking. Although y is expected to be determined by SM processes, its value nevertheless affects significantly the sensitivity to new physics

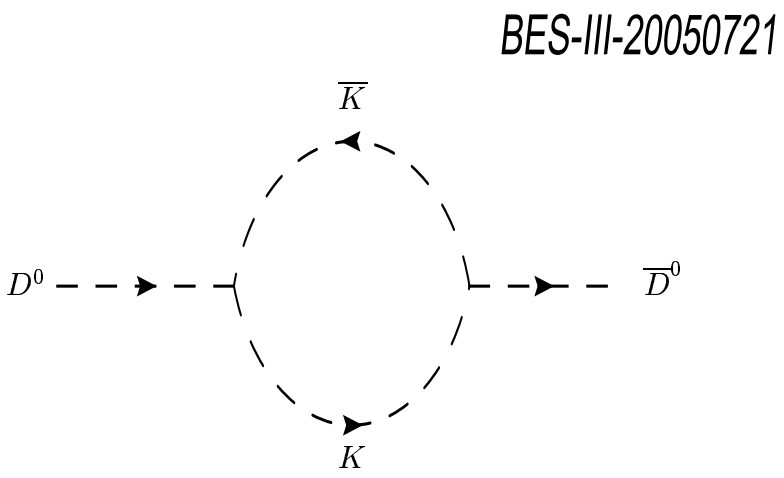

Figure 27.2: A hadron-level diagram of a long-distance physics contribution to $D^0 - \overline{D}^0$ mixing.

of experimental analyses of D mixing [261]. This circumstance would lead to the naive estimate

$$x\,,\ y \sim \sin^2\theta_C \times \left(\frac{m_s}{\Lambda_{hadron}}\right)^2 \leq O(10^{-3}), \tag{27.22}$$

with $\Lambda_{hadron} \sim O(1)$ GeV a typical hadronic scale. Beyond this simple estimate, there are two main approaches to estimating the long-distance contributions to mixing: an *inclusive* approach using an operator product expansion (OPE), and an *exclusive* approach that sums over intermediate hadronic states using experimental data. Neither approach yields accurate predictions.

The *inclusive* approach applies Heavy-Quark Expansions (HQE) to calculate contributions to D oscillations, an approach first taken by H. Georgi [262] and later extended by others [263, 264]. There are two main assumptions. The first is that the mass of the c-quark is large, $m_c \ll \Lambda_{hadr.}$. The second is that one can construct local quark-level operators that can be applied to hadron-level processes, i.e. that quark-hadron duality is applicable already at the charm scale. x and y are evaluated through the OPE as an expansion in powers of $(\Lambda_{hadr.}/m_c)$. The result of this type of approach is [264]

$$x \sim y \sim O(10^{-3}). \tag{27.23}$$

The *exclusive* approach takes all of the known hadronic states common to $|D^0\rangle$ and $|\overline{D}^0\rangle$, and groups them both according to their respective $SU(3)_F$ multiplets and to the number of particles in the final state. An example of such a set would be ($\pi^+\pi^-$, π^+K^-, K^+K^-, $K^+\pi^-$). In the limit of a perfect $SU(3)_F$ symmetry, the individual contributions within each of these groups would cancel, and there would be no mixing. If one knows the relative amplitudes and strong phases for these states, calculations of x and y can be done for each multiplet. For the example set above, this calculation gives a small contribution due to cancellations, a reasonable result since all of the states in the set are far from threshold and not affected as much by phase space considerations. Contributions to x

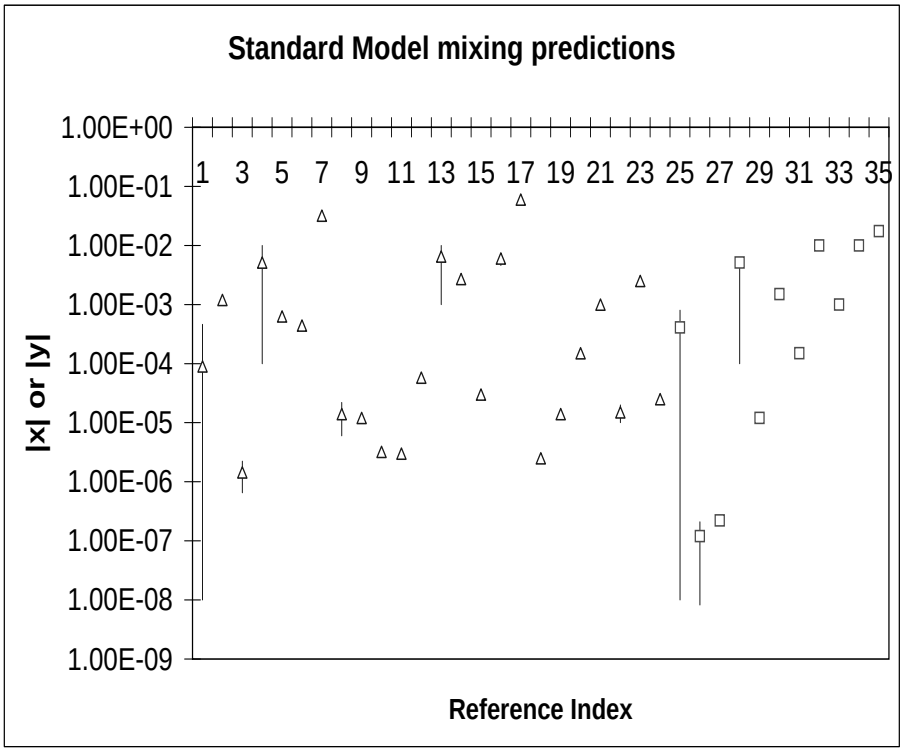

Figure 27.3: Standard Model predictions for $|x|$ (open triangles) and $|y|$ (open squares). Horizontal line references are tabulated in Table 4 in Ref. [260].

are not required to be on-shell, so in this case there is no symmetry breaking caused by limited phase space. If one assumes that all of the sets contribute incoherently in roughly the same amount, one concludes that [258]

$$x \leq O(10^{-3}). \tag{27.24}$$

By contrast, contributions to y are due to on-shell states, so phase space is a significant source of symmetry breaking. Considering phase space as the only source of symmetry breaking, one can calculate the contribution to y of each of the final state multiplets for which there is data using the measured masses of the final-particles [260]. The largest calculable contribution comes from the final-state multiplet comprising four pseudoscalars, whose elements are either near the production threshold with relatively large branching fractions, or are above threshold and entirely absent. This ansatz leads to [260]

$$y \leq O(10^{-2}). \tag{27.25}$$

The results from these two methods should not be seen as inconsistent. Rather they indicate the range of uncertainty, which can be phrased as follows: While the best a priori SM estimate yields x, $y \sim O(10^{-3})$, we cannot conclude that values as 'high' as 10^{-2} would necessarily establish the intervention of New Physics. To be more specific: while the presence of New Physics can enhance x to its present upper bound of few $\times 10^{-2}$, it should not

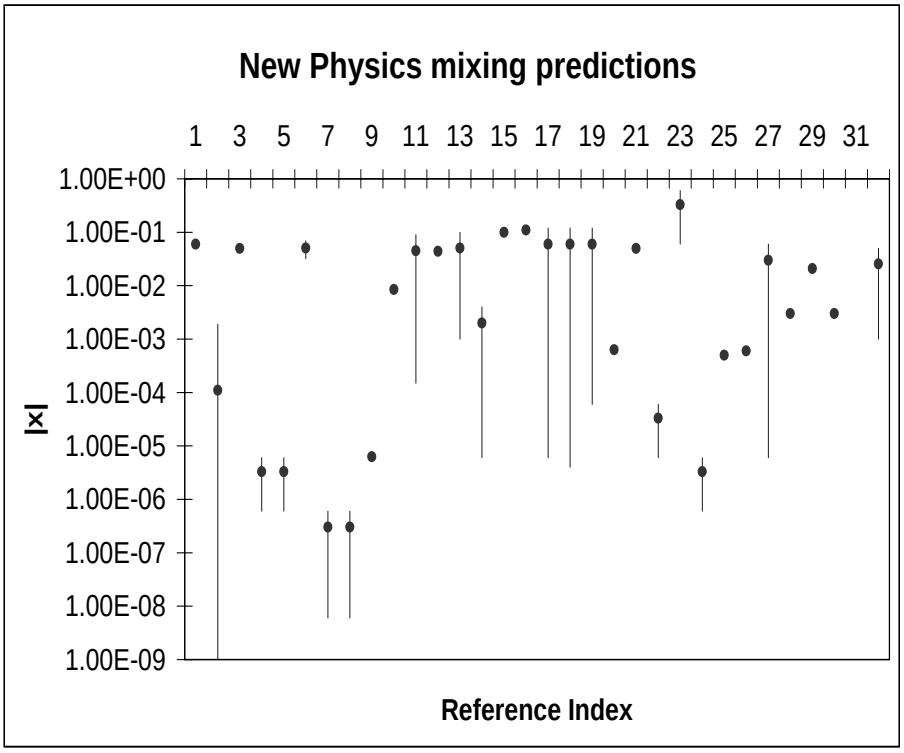

Figure 27.4: New Physics predictions for $|x|$. Horizontal line references are tabulated in Table 5 in Ref. [260].

affect y in a significant way, since $\Delta\Gamma$ is generated from *on*-shell transitions. The minimal requirement for any claim of New Physics thus is $x|_{\rm experim} \gg y|_{\rm experim}$. This appears as a rather iffy scenario at present. Nevertheless it is mandatory to probe for oscillations with as much sensitivity as possible for three main reasons: (i) With oscillations being an intriguing quantum mechanical phenomenon their observation carries intrinsic intellectual value. (ii) We might be only one breakthrough in our computational control over nonperturbative dynamics away from making precise predictions. (iii) Last and most importantly: **CP** asymmetries that involve oscillations – see Sect. 28.3 below – would conclusively establish the existence of New Physics. Having an independent measurement of those oscillations would provide a most powerful validation of such asymmetries.

27.1.3 Time-dependent Rate for Incoherent D Decays

A search for mixing attempts to identify the process $|D^0\rangle \to |\overline{D}^0\rangle$ ($|\overline{D}^0\rangle \to |D^0\rangle$) by analyzing the decay products of a particle known to be created as a $|D^0\rangle$ ($|\overline{D}^0\rangle$). In practice, this means reconstructing the state $|f\rangle$ in an attempt to observe

$$|D^0\rangle \to |\overline{D}^0\rangle \to |f\rangle \tag{27.26}$$

The difficulty comes from the fact that for hadronic systems, the decay

$$|D^0\rangle \to |f\rangle \tag{27.27}$$

can occur directly, without any mixing at all. Distinguishing process (27.26) from (27.27) is the primary goal of D mixing searches, and it relies on the fact that the decay-time distribution of the final state $|f\rangle$ is different for the two processes. The most sensitivity of mixing will be found when the amplitude for process (27.27) is as small as possible, and therefore doubly Cabibbo-suppressed (DCS) decays are chosen for this type of analysis.

Let us define $A_f \equiv \langle f|\mathcal{H}|D^0\rangle$, $\overline{A}_f \equiv \langle f||\mathcal{H}|\overline{D}^0\rangle$ with $\rho_f \equiv \frac{\overline{A}_f}{A_f}$; and $A_{\overline{f}} \equiv \langle \overline{f}|\mathcal{H}|D^0\rangle$, $\overline{A}_{\overline{f}} \equiv \langle \overline{f}||\mathcal{H}|\overline{D}^0\rangle$ with $\overline{\rho}_{\overline{f}} \equiv \frac{A_{\overline{f}}}{\overline{A}_{\overline{f}}}$. Now the time-dependent *wrong sign* decay amplitude for states of initially pure $|D^0\rangle$ ($|\overline{D}^0\rangle$) to decay to $|f\rangle$ ($|\overline{f}\rangle$) is given by (with $f = K^+\pi^-$ and $|\overline{f}\rangle \equiv CP|f\rangle$)

$$A(|D^0_{\rm phys}(t) \to f) = \frac{q}{p}\overline{A}_f \left[\lambda_f^{-1} g_+(t) + g_-(t)\right], \tag{27.28}$$

and

$$A(|\overline{D}^0_{\rm phys}(t) \to \overline{f}) = \frac{p}{q}A_{\overline{f}} \left[\lambda_{\overline{f}} g_-(t) + g_+(t)\right], \tag{27.29}$$

where

$$\lambda_f \equiv \frac{q}{p}\frac{\overline{A}_f}{A_f} \equiv \frac{q}{p}\rho_f\,,\ \lambda_{\overline{f}} \equiv \frac{q}{p}\frac{\overline{A}_{\overline{f}}}{A_{\overline{f}}} \equiv \frac{q}{p}\overline{\rho}_{\overline{f}}. \tag{27.30}$$

and

$$\frac{q}{p} = (1 + A_M)e^{i\phi}. \tag{27.31}$$

In order to describe the three types of CP violation in a convenient way, one can also parameterize λ_f ($\lambda_{\overline{f}}$) as [265, 266]

$$\lambda_f \equiv \frac{q}{p}\frac{\overline{A}_f}{A_f} = \frac{(1 + A_M)}{\sqrt{R_D}(1 + A_D)}e^{i(\delta+\phi)}, \tag{27.32}$$

$$\lambda_{\overline{f}} \equiv \frac{q}{p}\frac{\overline{A}_{\overline{f}}}{A_{\overline{f}}} = \frac{\sqrt{R_D}(1 + A_M)}{(1 + A_D)}e^{-i(\delta-\phi)}, \tag{27.33}$$

where $|q|/|p| = (1 + A_M)$ and $|\overline{A}_f|/|A_f| = \sqrt{R_D}(1 + A_D)$, and δ is the strong phase difference between $\overline{A}_f$ and A_f. Here ϕ represents the convention-independent weak phase difference between the ratio of decay amplitudes and the mixing matrix. In Chapter 28, we will use these definitions to describe the three types of CP violation in detail. In the limit of CP conservation, A_M, A_D and ϕ are all zero.

It is usual to normalize the *wrong sign* decay distributions to the integrated rate of *right sign* decays and to express time in units of the precisely measured D^0 mean lifetime, $\overline{\tau}_{D^0} = 1/\Gamma = 2/(\Gamma_1 + \Gamma_2)$. Therefore the time-dependent rates of production of the *wrong sign* final states relative to the integrated *right sign* states are:

$$r(t) = \left|\frac{q}{p}\right|^2 \left|\lambda_f^{-1} g_+(t) + g_-(t)\right|^2, \tag{27.34}$$

and

$$\overline{r}(t) = \left|\frac{p}{q}\right|^2 \left|\lambda_{\overline{f}} g_-(t) + g_+(t)\right|^2. \tag{27.35}$$

We will expand $r(t)$ and $\overline{r}(t)$ to second order in time for the modes where the ratio of the decay amplitudes $R_D = |A_f/\overline{A}_f|^2$ is very small (it is the ratio of DCSD rate and CFD rate).

27.2 Experimental Review

$D^0 - \overline{D}^0$ mixing and CP violation in charm sector have been searched for by various experimental facilities with different techniques. The principal production processes are $e^+e^- \to c\overline{c}$ at center of mass energy from threshold up to Z^0 boson peak, hadroproduction at both fixed-target experiments and the Fermilab Tevatron, photoproduction and so on. The cross sections vary from a few nb to microbarns for photoproduction, and to order of a millibarn at the Tevatron. However, the ratio of signal to background cross section are ranged from 1:1 in e^+e^- annihilation to 1:500 at the Tevatron as listed in Table 27.1. D^0

Table 27.1: *Summary of Charm experiments nowadays with different techniques, luminosity, charm production cross section and ratio of signal to noise.*

Experiment	Beam	Lumin. ($\mathrm{cm^{-2}s^{-1}}$)	Cross-Section	#events $c\overline{c}$ Per year	$\sigma(c\overline{c})/\sigma_{Total}$
BaBar	e^+e^- ($\Upsilon(4S)$)	3×10^{33}	1.3 nb	40×10^6	$\sim 1/5$
Belle	e^+e^- ($\Upsilon(4S)$)	3×10^{33}	1.3 nb	40×10^6	$\sim 1/5$
CLEO-c	e^+e^- ($\psi(3770)$)	2×10^{32}	6.4 nb	$6.4{\times}10^6$	~ 1
BES-III	e^+e^- ($\psi(3770)$)	1×10^{33}	6.4 nb	$32{\times}10^6$	~ 1
CDF	$p\overline{p}$ (1.9 TeV)		134 μb		$\sim 1/500$
LHC-b	$pp(\sqrt{s} = 14$ TeV)	2×10^{32}	1.0 mb	$1{\times}10^{11}$	$\sim 1/100$

mixing has not been observed yet, but the most stringent limits on D mixing have been set by the Belle, *BaBar* and CLEO collaborations through analyzing hadronic D decays.

The techniques, which can be used to search for mixing, can be roughly divided into four classes: mixing in semi-leptonic decays, time-dependent measurements in wrong-sign decays to hadronic non-CP eigenstates, decays to CP eigenstates and mixing measurements via Quantum Coherence at threshold.

27.2.1 Semileptonic Decays

The manifestation of D^0 mixing in semileptonic decays is relatively simple, since such transitions are flavor specific in the standard model or some of its extensions. Because of the flavor specification of $D^0 \to l^+X^-$ and $\overline{D}^0 \to l^-X^+$, it is not necessary to study the time-dependent D decay modes.

In semileptonic D decays, the wrong sign decay amplitudes $A_f = \overline{A}_{\overline{f}} = 0$. Then in the limit of weak mixing, where $|ix + y| \ll 1$, from Eq. (27.34), $r(t)$ is given by

$$r(t) = \left|\frac{q}{p}\right|^2 |g_-(t)|^2 \sim \frac{e^t}{4}(x^2 + y^2)t^2 \left|\frac{q}{p}\right|^2, \tag{27.36}$$

In the limit of CP conservation, $r(t) = \overline{r}(t)$, and integrating Eq. (27.36) over all time gives

$$R_M = \int_0^\infty r(t)dt = \left|\frac{q}{p}\right|^2 \frac{x^2+y^2}{2+x^2+y^2} \simeq \frac{x^2+y^2}{2}, \tag{27.37}$$

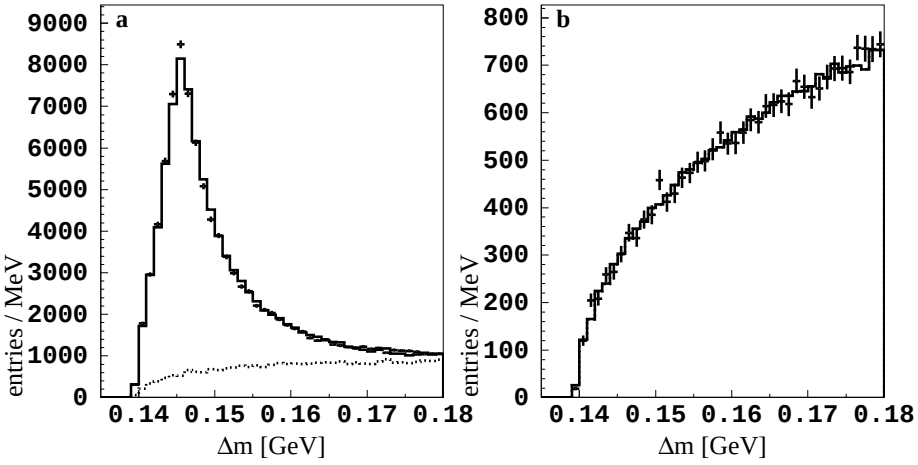

Figure 27.5: *(a)* ΔM *distribution for right-sign* $D^0 \to K^- l^+ \nu$ *candidate decays; (b) wrong-sign* $D^0 \to K^+ l^- \overline{\nu}$ *decays, from Belle using 253* fb^{-1} *of data [267]. The wrong-sign plot shows no visible signal above background.*

The semileptonic decay method usually suffers from large background (except at a τ-charm factory) due to the missing neutrino, which the final state is not fully reconstructed. The traditional method of looking for like sign $\mu^\pm\mu^\pm$ pairs is an example at fixed target experiments [268, 269, 270]. However, at an e^+e^- experiment there are enough kinematic constraints to infer the neutrino momentum. Specifically, momentum conservation prescribes $P_\nu = P_{CM} - P_{\pi_s Kl} - P_{\rm rest}$ [267], where P_{CM} is the four-momentum of the e^+e^- center-of-mass (CM) system, π_s, K, and l are daughters from decay $D^*+ \to D^0\pi_s \to \pi_s Kl\nu$, and $P_{\rm rest}$ is the four-momentum of the remaining particles in the event. In the B factory, the magnitude $|P_{\rm rest}$— is rescaled to satisfy $(P_{CM} - P_{\rm rest})^2 = m^2_{D^*}$, and after this rescaling the direction of $\overrightarrow{p_{\rm rest}}$ is adjusted to satisfy $P^2_\nu (= m^2_\nu) = 0$. One can also use information on the decay time to improve the sensitivity of the mixing [267]. The $\Delta M \equiv M_{\pi_s Kl\nu} - M_{Kl\nu}$ distribution for *right-sign* $D^0 \to K^- l^+ \nu$ and *wrong-sign* $D^0 \to K^+ l^- \nu$ samples are shown in Fig. 27.5 from Belle experiment using 253 fb^{-1} of data, which is the most stringent constraints currently. Table 27.2 is the summary of the experimental status of R_M measurements in semileptonic decays.

The best place to use the semileptonic method is probably in BES-III and CLEO-c near the charm threshold. The idea is to search for $e^+e^- \to \psi(3770) \to D^0\overline{D}^0 \to (K^- l^+\nu)(K^- l^+\nu)$ or $e^+e^- \to D^-\overline{D}^{*+} \to (K^+\pi^-\pi^-)(K^+ l^-\nu) + \pi_s$. The latter is probably the only place where the semileptonic method does not suffer from a large background. It should have a very small background, as there is only one neutrino missing in the entire event, threshold kinematic constraints should provide clean signal as shown in Fig. **??**.

Table 27.2: *Results for R_M in D^0 semileptonic decays from PDG2006.*

Year	Experiment	Final states	R_M (90% C.L.)
2005	Belle [267]	$K^{(*)+}e^-\overline{\nu}$	$< 1.0^{-3}$
2005	CLEO [271]	$K^{(*)+}e^-\overline{\nu}$	$< 7.8 \times 10^{-3}$
2004	BaBar [272]	$K^{(*)+}e^-\overline{\nu}$	$< 4.2 \times 10^{-3}$
2002	FOCUS [273]	$K^+e^-\overline{\nu}$	$< 1.01 \times 10^{-3}$
1996	E791 [274]	$K^+e^-\overline{\nu}$	$< 5.0 \times 10^{-3}$

However, it has been pointed out that one can not claim a D^0 mixing signal based on the semileptonic decay alone (unless with information on the decay time of D^0 at B factory). Bigi [275] has pointed out that an observation of a signal on $D^0 \to l^- X^+$ establishes only that a certain selection rule is violated in the processes where the charm quantum number is changed, namely, the rule $\Delta C = -\Delta Q_l$ where Q_l denotes leptonic charge. This violation can occur either through $D^0 - \overline{D}^0$ mixing (with the unique attribute of the decay time-dependence of mixing), or through new physics beyond the SM (which could be independent of time). Nevertheless, one can always use this method to set upper limit for mixing.

27.2.2 Hadronic Final States

The *wrong-sign* hadronic decay modes can occur either through $D^0 - \overline{D}^0$ mixing or through DCSD as illustrated in Eqs. (27.26) and (27.27). The major complication for this method is the need to distinguish between DCSD and mixing. In principle, there are at least three ways to distinguish between DCSD and mixing candidates experimentally: (1) use the difference in the decay time-dependence [276, 277]; (2) use the possible difference in the resonance substructure between DCSD and mixing events on the Dalitz plot in three-body $D^0 \to K^+\pi^-\pi^0$ [278], or multi-body decays, like $D^0 \to K^+\pi^-\pi^+\pi^-$, etc.; (3) use the quantum correlation of the production and decay processes at $\psi(3770)$ peak [275, 279]. Method (1) is popular at B factory since the D^0 is highly boosted, so that the decay time information can be used. Method (2) requires knowledge of the structures of the DCSD decay on the Dalitz plots, which can be done at both a B factory and a τ-charm factory. Method (3) can be done at BES-III at charm threshold region. In this subsection, we only discuss method (1), specifically.

According to Eq. (27.34), one gets:

$$r(t) = \left|\frac{q}{p}\right|^2 \left(\lambda_f^{-2} g_+^2(t) + \lambda_f^{-1} g_+(t) g_-^*(t) + (\lambda_f^{-1})^* g_+^*(t) g_-(t) + g_-^2(t)\right), \tag{27.38}$$

We can simplify Eq. (27.38) under the assumption of small mixing, $|ix + y| \ll 1$, and express

$$\begin{aligned} \lambda_f^{-2} g_+^2(t) &= |\lambda_f^{-1}|^2 \frac{e^{-t}}{2} \left[\cosh(yt) + \cos(xt)\right] \\ &\simeq |\lambda_f^{-1}|^2 e^{-t}, \end{aligned} \tag{27.39}$$

$$g_-^2(t) = \frac{e^{-t}}{2}\left[\cosh(yt) - \cos(xt)\right] \simeq e^{-t}\left(\frac{x^2+y^2}{4}\right)t^2, \quad (27.40)$$

and

$$\lambda_f^{-1} g_+(t) g_-^*(t) + (\lambda_f^{-1})^* g_+^*(t) g_-(t) = \frac{e^{-t}}{2}\left(e^{-i(\delta+\phi)}(\sinh(yt) - i\sin(xt)) + e^{i(\delta+\phi)}(\sinh(yt) + i\sin(xt))\right) \simeq |\lambda_f^{-1}| e^{-t}(y\cos(\delta+\phi) - x\sin(\delta+\phi))t. \quad (27.41)$$

If we define

$$y'_\pm \equiv y'\cos\phi \pm x'\sin\phi = y\cos(\delta \mp \phi) - x\sin(\delta \mp \phi), \quad (27.42)$$

where

$$y' \equiv y\cos\delta - x\sin\delta\,,\; x' \equiv x\cos\delta + y\sin\delta, \quad (27.43)$$

and combine Eqs. (27.32), (27.39), (27.40) and (27.41) in the limit of CP conservation ($A_D = 0$, $A_M = 0$ and $\phi = 0$), we obtain the standard form for the time-dependent decay rate, including D mixing:

$$r(t) = \overline{r}(t) = e^{-t}\left(R_D + \sqrt{R_D}y't + \frac{1}{2}R_M t^2\right) \quad (27.44)$$

The above wrong-sign decay rate includes three components: the first from the DCSD, the second from mixing, and the third from the interference between DCSD and mixing. The time-integrated wrong-sign rate relative to the integrated right-sign rate is

$$R_{WS} = \int_0^\infty r(t)dt = R_D + \sqrt{R_D}y' + \frac{1}{2}R_M \quad (27.45)$$

As shown in Eq. (27.44), D mixing is characterized in the decay rate by a small deviation from a pure exponential. In order to have the most sensitivity to (x^2+y^2), a decay channel for which R_D is relatively small is desired. The analysis technique benefits from the ability to compare the signal distribution, given by Eq. (27.44), to the CF decay distribution, which may be treated as pure exponential. In this way, systematic bias is significantly limited.

The ratio R_{WS} is the most readily accessible experimental quantity. Table 27.3 gives recent measurement of R_{WS} in $D^0 \to K^+\pi^-$ decay. The average of these results, $R_{WS} = (0.376 \pm 0.009)\%$ [4].

The interference causes the measured x and y to be rotated through an angle δ, the phase difference between the DCS and CF decay processes. By measuring the time dependence of the decay rate it is possible to sort out the mixing from the DCS decay. At B factories and CLEO experiments, wrong-sign candidate events of the types $D^0 \to K^+\pi^-$ and $\overline{D}^0 \to K^-\pi^+$ are selected by requiring the soft π_s from the D^* decay and the

Table 27.3: *Results for R_{WS} and A_D in $D^0 \to K^+\pi^-$, if one assumes that there is no mixing and CP violation in DCSD decay.*

Experiments	Techniques	Assumption	R_{WS} ($\times 10^{-3}$)	$A_D(\%)$
Belle [277]	$e^+e^- \to \Upsilon(4S)$	No mixing	$3.77 \pm 0.08 \pm 0.05$	–
FOCUS [280]	γ BeO	No mixing	$4.29 \pm 0.63 \pm 0.28$	$18.0 \pm 14.0 \pm 4.1$
BaBar [276]	$e^+e^- \to \Upsilon(4S)$	No mixing	$3.57 \pm 0.22 \pm 0.27$	$9.5 \pm 6.1 \pm 8.3$
CLEO [266]	$e^+e^- \to \Upsilon(4S)$	No mixing	$3.32^{+0.63}_{-0.65} \pm 0.40$	$2.0^{+19.0}_{-20.0} \pm 1.0$
CDF [281]	$p\overline{p} \to c\overline{c}$	No mixing	$4.05 \pm 0.21 \pm 0.11$	–

Table 27.4: *Limits on x'^2 and y', both 95% C.L. for the case where CP violation is allowed and the case where it is not allowed.*

Experiment	$x'^2(\times 10^{-3})$ (95% CL)		$y'(\times 10^{-3})$ (95% CL)	
	CPV	No CPV	CPV	No CPV
BaBar [276]	2.2	2.0	-56 $< y' <$ 39	-27$< y' <$ 22
FOCUS [280]	0.80	0.83	-120 $< y' <$ 67	-72$< y' <$ 41
CLEO [266]	0.82	0.78	-58 $< y' <$ 10	-52$< y' <$ 2
Belle [277]	0.72	0.72	-28 $< y' <$ 21	-9.9$< y' <$ 6.8

daughter K of the D^0 to have identical charge (wrong-sign tag). In order to determine the wrong-sign and right-sign yields, two powerful distinguishing variables are selected at Belle experiment, $M_{K\pi}$ and the released energy $Q \equiv M^* - M_{K\pi} - m_{\pi_s}$, where M^* is the reconstructed mass of the $K^+\pi^-\pi_s^+$ system, $M_{K\pi}$ is the reconstructed mass of $K^+\pi^-$ system, and m_{π_s} is the charged pion mass. In comparison, BaBar and CLEO experiments used mass difference $\delta m = M^* - M_{K\pi}$. Figure 27.6 shows the $M_{K\pi}$ and Q distributions superimposed with projections of the fit result. To detect a deviation from an exponential decay in wrong-sign events, a likelihood fit to the distribution of the reconstructed proper decay time t is performed for each experiment. The likelihood fit includes a signal and a background component and models each as the convolution of a decay-time distribution and a resolution function. As an example, the left plot in Fig. 27.7 shows us the wrong-sign $D^0 \to K^+\pi^-$ decay-time distribution and fit projections from Belle experiment.

Limits on x'^2 and y' from several experiments are listed in Table 27.4. The limits are somewhat more restrictive on y' when CP violation is not allowed, while those on x'^2 hardly change. While no experiment claims an effect, it is interesting that the Belle result is consistent with no mixing only at 3.9% C.L. [277]. The right plot in Fig. 27.7 shows us the 95% C.L. region in the x'^2-y' plane by using a frequentist technique based on toy Monte Carlo simulation.

The mixing has also been searched for with the wrong-sign multibody final states [282, 283, 284] $K^+\pi^-\pi^0$ and $K^+\pi^-\pi^+\pi^-$. Using 281 fb^{-1} of data, Belle collaboration has done a time-integrated analysis, and measured the time-independent ratio of wrong-sign to right-sign decays. The results are $R_{WS} = (0.229 \pm 0.015^{+0.013}_{-0.009})\%$ for the $D^0 \to K^+\pi^-\pi^0$ and $R_{WS} = (0.320 \pm 0.018^{+0.018}_{-0.013})\%$ for the $D^0 \to K^+\pi^-\pi^+\pi^-$.

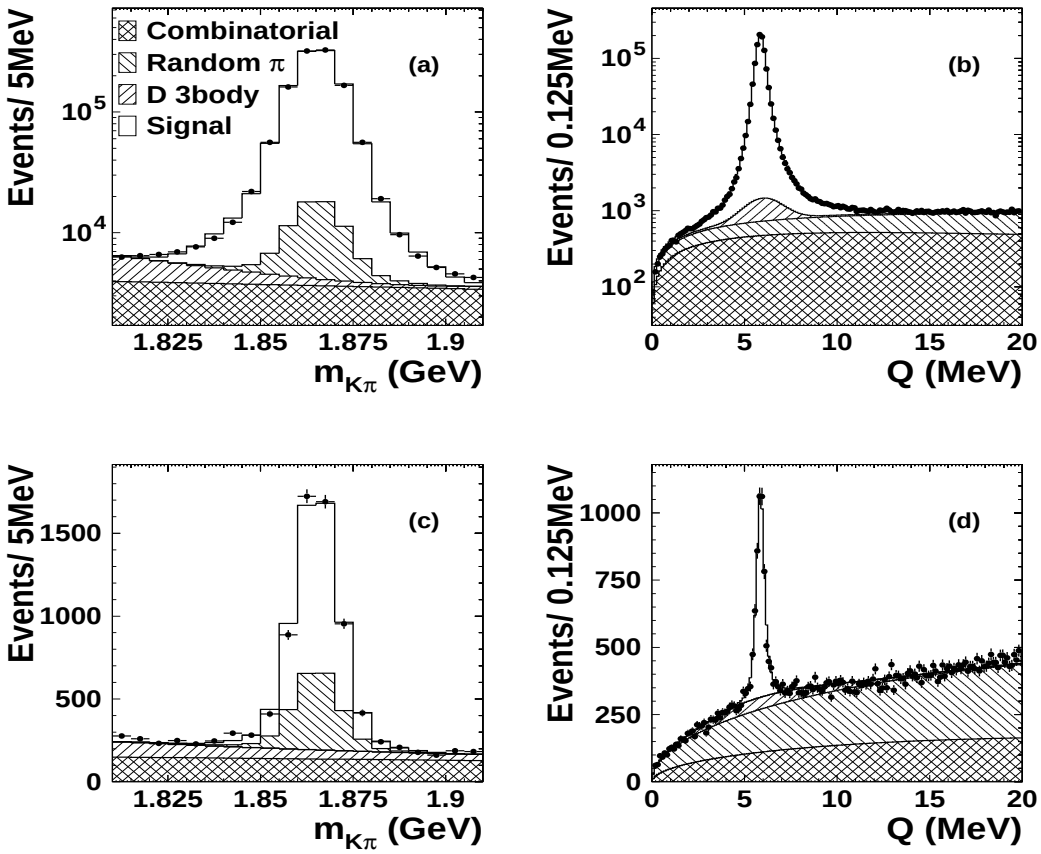

Figure 27.6: *The distribution for (a) Right-sign $M_{K\pi}$ with $0 < Q < 20$ MeV, (b) Right-sign Q with 1.81 GeV/c^2< $M_{K\pi} <$ 1.91 GeV/c^2, (c) Wrong-sign $M_{K\pi}$ with $5.3 < Q < 6.5$ MeV, and (d) Wrong-sign Q with $1.845 < m_{K\pi} < 1.885$ GeV/c^2. Note that the wrong-sign plots are shown for a 3σ signal interval in Q and $MK\pi$, respectively. Superimposed on the data (points with error bars) are projections of the $M_{K\pi} - Q$ fit. The results are from Belle experiment with 400 fb^{-1} of data.*

Recently, BaBar collaboration reported a measurement of mixing rate R_M in the decay of $D^0 \to K^+\pi^-\pi^0$ with a time-dependent analysis [278]. There are two key motivations to select $D^0 \to K^+\pi^-\pi^0$: (1) one expects the Dalitz-plot structure of DCS decay differs from that of CF decay. We note that DCS decays proceed primarily through the resonance $D^0 \to K^{*+}\pi^-$, $K^{*0}\pi^0$, while CF decays proceed primarily through the resonance $D^0 \to K^-\rho^+$. The sensitivity to R_M measurement may be increased by selecting regions of the Dalitz plot where CF decay contributes with a large amplitude relative to the corresponding DCS decay amplitude. (2) The time-integrated mixing rate $R_M = (x^2 + y^2)/2$ is independent of the decay mode and is expected to be consistent among mixing measurement. Figure 27.8 shows us the Dalitz plots for CF and DCS decay. The CF Dalitz plot is qualitatively different from the wrong-sign Dalitz plot, which is assumed to contain primarily DCS contributions. While CF decays proceed primarily through the resonance

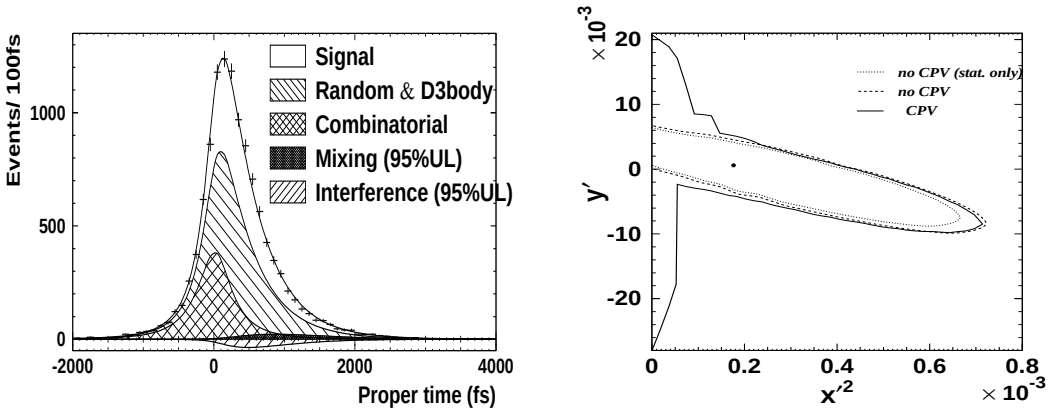

Figure 27.7: *Left: wrong-sign $D^0 \to K^+\pi^-$ decay-time distribution and fit projections. Right: 95% C.L. region for x'^2, y'. From Belle using 400 fb^{-1} of data [277].*

$D^0 \to K^-\rho^+$, DCS decays proceed primarily through the resonance $D^0 \to K^{*+}\pi^-$. So the particular regions of the phase space (i.e., the Dalitz plot) are selected by removing the K^* resonance. In the limit of CP conservation, the time-dependent ratio of wrong-sign to right-sign is expressed approximately as:

$$R_{WS} = \tilde{R}_D \quad + \quad \alpha\sqrt{\tilde{R}_D}\tilde{y}'\,t + \frac{1}{2}R_M t^2 \qquad (27.46)$$
$$0 \leq \alpha \leq 1\,,$$

where the tilde indicates quantities that have been integrated over any choice of phase space regions. Here $\tilde{R}_D$ is the integrated DCS ratio of DCS decays to CF decays; $\tilde{y}' = y\cos\tilde{\delta} - x\sin\tilde{\delta}$, $\tilde{\delta}$ is an unknown integrated strong-phase difference between the CF and the DCS decay amplitudes; α is a suppression factor that accounts for strong-phase variation over the regions. The time-integrated mixing rate R_M is independent of decay mode. By fitting the proper time distribution, they get the results $R_M = (0.023^{+0.018}_{-0.014} \pm 0.004)\%$ and $\tilde{R}_D = (0.164^{+0.026}_{-0.022} \pm 0.012)\%$ by assuming CP invariance. The upper limit is set to be $R_M < 0.054\%$ at 95% confidence level. They conclude that the observed data are consistent with no mixing at the 4.5% confidence level. By using a similar method and idea, BaBar experiment also measured the time-integrated mixing rate R_M in $D^0 \to K^+\pi^-\pi^+\pi^+$ decay mode. Assuming CP conservation, they got $R_M = (0.019^{+0.016}_{-0.015} \pm 0.002)\%$, and $R_M < 0.048\%$ at 95% C.L.. Furthermore, they combined results from both decay modes, and found that $R_M = (0.020^{+0.011}_{-0.010})\%$ and $R_M < 0.042\%$ at 95% C.L. which is the best limit with current data. The combined data sets are consistent with the no-mixing hypothesis with 2.1% confidence.

27.2.3 D^0 Decays to CP Eigenstates

D^0 mixing parameters can be measured by comparing the lifetimes extracted from the analysis of D decays into the CP-even and CP-odd final states. When the final state

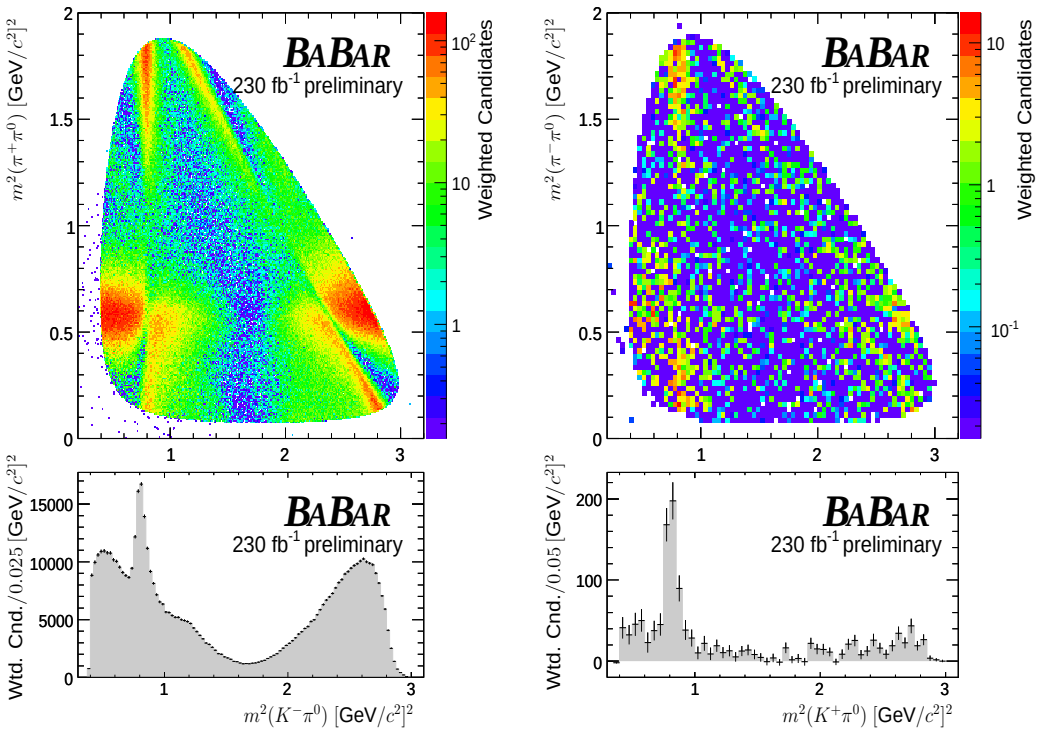

Figure 27.8: *Dalitz plot and one-dimensional projection onto $m^2_{K\pi^0}$ for CF decays (left) and DCS decays (right). The shaded histograms in the lower plots are projections of the Dalitz plots above them, with error bars superimposed. The data are from BaBar with 230 fb^{-1}.*

is CP eigenstate f (i.e., $|\overline{f}\rangle \equiv CP|f\rangle = \pm|f\rangle$), such as K^+K^-, $\pi^+\pi^-$ and $K_S\pi^0$, there is no strong phase difference between $\overline{A}_f$ and A_f. Assuming $|\overline{A}_f| = |A_f|$ (no direct CP violation), $\lambda_f = -|q|/|p|e^{i\phi}$ and $\lambda_{\bar{f}} = -|p|/|q|e^{-i\phi}$, where ϕ is the weak phase difference. Inserting these terms into Eqs. (27.34) and (27.35) gives

$$R(D^0 \to K^+K^-) \simeq |A_{K^+K^-}|^2 e^{-t} e^{-|q/p|(y\cos\phi - x\sin\phi)t}, \tag{27.47}$$

and

$$R(\overline{D}^0 \to K^+K^-) \simeq |A_{K^+K^-}|^2 e^{-t} e^{-|p/q|(y\cos\phi + x\sin\phi)t}. \tag{27.48}$$

Eqs. (27.47) and (27.48) imply that the measured D^0 and $\overline{D}^0$ inverse lifetimes are slightly different each other. We define

$$y_{CP} = \frac{\tau_{D^0\to K^-\pi^+}}{\tau_{D^0\to K^+K^-}} - 1 = \frac{q}{p}(y\cos\phi - x\sin\phi), \tag{27.49}$$

for D^0 decays, and for $\overline{D}^0$ decays, it is

$$y_{CP} = \frac{\tau_{\overline{D}^0\to K^+\pi^-}}{\tau_{\overline{D}^0\to K^+K^-}} - 1 = \frac{p}{q}(y\cos\phi + x\sin\phi). \tag{27.50}$$

For $|q/p| = 1$, i.e., no CP violation in mixing, $y_{CP} = y\cos\phi$ for equal number of D^0 and $\overline{D}^0$ decays together. If also $\phi = 0$ (no CP violation), $y_{CP} = y$.

One can also combine the two $D \to K^+K^-$ modes. To understand the consequences of such an analysis, one has to consider the relative weight of D^0 and $\overline{D}^0$ in the sample. Let us define $A_{\rm prod}$ as the production asymmetry of D^0 and $\overline{D}^0$:

$$A_{\rm prod} = \frac{N(D^0) - N(\overline{D}^0)}{N(D^0) + N(\overline{D}^0)}. \tag{27.51}$$

Then

$$\begin{aligned} y_{CP} &= \frac{\tau_{D^0\to K^-\pi^+}}{\tau_{D\to K^+K^-}} - 1 \\ &= y\cos\phi \left[\frac{1}{2}\left(\left|\frac{p}{q}\right| + \left|\frac{q}{p}\right|\right) + \frac{A_{\rm prod}}{2}\left(\left|\frac{p}{q}\right| - \left|\frac{q}{p}\right|\right)\right] \\ &\quad -x\sin\phi \left[\frac{1}{2}\left(\left|\frac{p}{q}\right| - \left|\frac{q}{p}\right|\right) + \frac{A_{\rm prod}}{2}\left(\left|\frac{p}{q}\right| + \left|\frac{q}{p}\right|\right)\right], \end{aligned} \tag{27.52}$$

Table 27.5: Summary of y_{CP}results.

Experiment	y_{CP}
FOCUS [285]	$3.4 \pm 1.4 \pm 0.7$
CLEO [286]	$-1.2 \pm 2.5 \pm 1.4$
Belle, untagged [287]	$-0.5 \pm 1.0 \pm 0.8$
Belle, tagged [288]	$1.2 \pm 0.7 \pm 0.4$
BaBar [289]	$0.8 \pm 0.4^{+0.5}_{-0.4}$

The y_{CP} is determined from the slope of the decay-time distribution in sample of $D^0 \to K^-\pi^+$, which is an equal mixture of CP-even and CP-odd final states, and $D^0 \to K^+K^-$ or $\pi^+\pi^-$, which are CP even final states. An unbinned maximum likelihood fit to the distribution of the reconstructed proper time t of the D^0 candidates is performed. To date, five experiments have measured y_{CP} as listed in Table 27.5. The most precise value is from BaBar using 91 fb^{-1} of data. To increase statistics, BaBar used both K^+K^- and $\pi^+\pi^-$ decays, and in addition, the $D^0 \to K^+K^-$ analysis used both a large inclusive D^0 sample and smaller, higher purity sample in which the D^0 is required to originate from $D^{*+} \to D^0\pi_s^+$. The respective decay time distributions are shown in Fig. 27.9. BaBar also measured $\Delta Y \equiv (\tau^+ - \tau^-)/(\tau^+ + \tau^-) \times \tau_{K^-\pi^+}/\langle\tau\rangle$, where τ^+ (τ^-) is the lifetime for $D^0 \to K^+K^-$ ($\overline{D}^0 \to K^+K^-$) and $\langle\tau\rangle = (\tau^+ + \tau^-)/2$. For $|q/p| = 1$, $\Delta Y = x\sin\phi$. The result is $\Delta Y = (-0.8 \pm 0.6 \pm 0.2)\%$, which indicates that either x or ϕ is small.

Since it needs to fit proper time distribution, this method can not be applied to the BES-III and CLEO-c experiments near the threshold of open charm.

27.2.4 Dalitz Plots

At present, the only time-dependent analysis is done by CLEO in $D^0 \to K_S\pi^+\pi^-$ decay mode. They consider a self-conjugate final state that is not CP eigenstate due to the

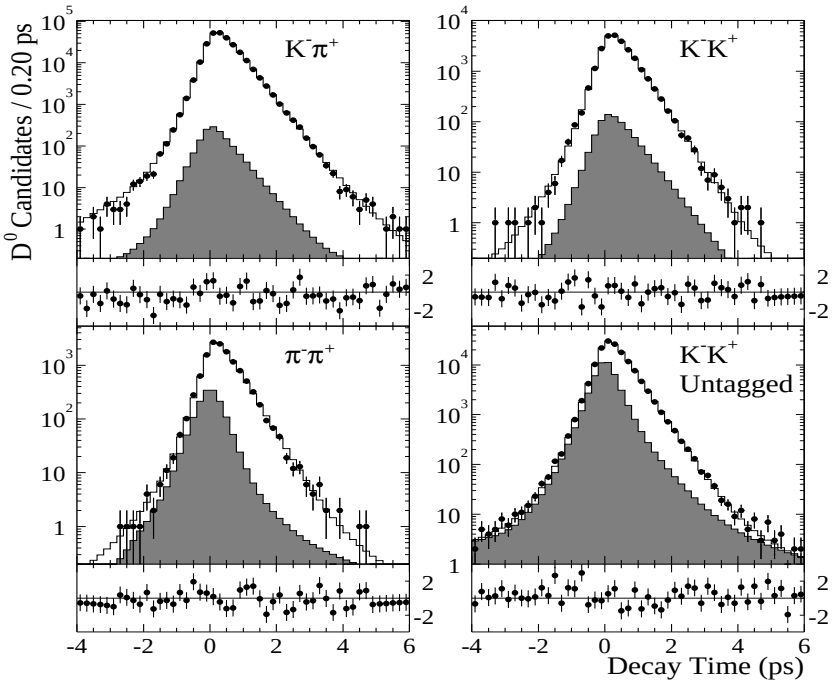

Figure 27.9: *Decay time distributions for CF $D^0 \to K^-\pi^+$ (upper left), $D^0 \to K^+K^-$ (upper right), $D^0 \to \pi^+\pi^-$ (lower left), and $D^0 \to K^+K^-$ selected without using a D^{*0} tag (lower right), from BaBar using 91 fb^{-1} of data [290]. The higtograms are fit results superimposed on the data (dotted histograms). The shaded histograms is the portion of the sample assigned by the fit to the background. The points presented below the histograms are the difference between data and dit divided by the statistical error with error bars of unit length.*

substructures with either $L = 0$ (CP-even) or $L = 1$ (CP-odd) in the three body decay. The decay rate to $K_S\pi^+\pi^-$ with ($m^2_{K_S\pi^-}$, $m^2_{\pi^+\pi^-}$) at time t of a particle tagged as $|D^0\rangle$ at $t = 0$ is

$$d\Gamma(m^2_{K\pi}, m^2_{\pi\pi}, t) = \frac{1}{256\pi^3 M^3}|\mathcal{M}|^2 dm^2_{K\pi} dm^2_{\pi\pi}, . \tag{27.53}$$

where the matrix element is defined as $\mathcal{M} = \langle f|H|D^0(t)\rangle$, and $\langle f| = \langle K_S\pi^+\pi^-(m^2_{K_S\pi^-}, m^2_{\pi^+\pi^-})|$. The $|D^0(t)\rangle$ is given in Eq. (27.11).

The decay channels can be collected into those which are CP even or CP odd (with amplitudes Amp_+ or Amp_-) and to those which are D^0 or $\overline{D}^0$ flavor eigenstates (with amplitudes $\mathrm{Amp_f}$ or $\overline{\mathrm{Amp}}_f$):

$$\langle f|\mathcal{H}|D_{+,-}\rangle = \sum a_j e^{i\delta_j}\mathcal{A}^j_{+,-} = p\mathrm{Amp}_{+,-}\,; \tag{27.54}$$

$$\langle \overline{f}|\mathcal{H}|D_{+,-}\rangle = \sum a_j e^{i\delta_j}\overline{\mathcal{A}}^j_{+,-} = q\overline{\mathrm{Amp}}_{+,-}\,; \tag{27.55}$$

$$\langle f|\mathcal{H}|D^0\rangle = \sum a_j e^{i\delta_j}\mathcal{A}^j = \mathrm{Amp}_f\,; \tag{27.56}$$

$$\langle \overline{f}|\mathcal{H}|\overline{D}^0\rangle = \sum a_j e^{i\delta_j}\overline{\mathcal{A}}^j = p\overline{\mathrm{Amp}}_{\overline{f}}; \tag{27.57}$$

where a_j and δ_j are the explicitly CP conserving amplitudes and relative strong phases (in Ref. [291], they fix $a_\rho = 1$, $\delta_\rho = 0$, all the other strong phases are relative to ρ resonance) for the jth quasi-two-body state. $\mathcal{A}^j_{+,-} = \mathcal{A}^j_{+,-}(m^2_{K_S\pi^-}, m^2_{\pi^+\pi^-})$ is the Breit-Wigner amplitude for resonance j with D decay to $CP = +$ or $CP = -$ quasi-two-body contributions. In Ref. [291], CLEO experiment considered the following ten modes: $K^{*-}\pi^+$, $K_0^*(1430)^-\pi^+$, $K_2^*(1430)^-\pi^+$, $K^*(1680)^-\pi^+$, $K_S\rho$ $K_S\omega$, $K_Sf_0(980)$, $K_Sf_2(1270)$, $K_Sf_0(1370)$, and the "wrong-sign" $K^{*+}\pi^-$ plus a small non-resonant component. Collecting terms with similar time dependence and combining Eqs. (27.11) and (27.12), one can find

$$\begin{aligned}
\mathcal{M} &= \langle f|\mathcal{H}|D^0(t)\rangle = \frac{1}{2p}(\langle f|\mathcal{H}|D_1(t)\rangle + \langle f|\mathcal{H}|D_2\rangle) \\
&= \frac{1}{2p}(\langle f|\mathcal{H}|(pD^0 + q\overline{D}^0)\rangle e_1(t) + \langle f|\mathcal{H}|(pD^0 - q\overline{D}^0)\rangle e_2(t)) \\
&= \frac{1}{2p}([p(\mathrm{Amp}_f + \mathrm{Amp}_+) + q(\overline{\mathrm{Amp}}_f + \overline{\mathrm{Amp}}_+)]e_1(t) \\
&\quad +[p(\mathrm{Amp}_f + \mathrm{Amp}_-) - q(\overline{\mathrm{Amp}}_f + \overline{\mathrm{Amp}}_-)]e_2(t)) \\
&= \frac{1}{2}([(1+\chi_f)\mathrm{Amp}_f + (1+\chi_+)\mathrm{Amp}_+]e_1(t) \\
&\quad +[(1-\chi_f)\mathrm{Amp}_f + (1-\chi_-)\mathrm{Amp}_-]e_2(t)) \\
&\equiv e_1(t)A_1 + e_2A_2\,, \qquad (27.58)
\end{aligned}$$

and

$$\begin{aligned}
\overline{\mathcal{M}} &= \langle \overline{f}|\mathcal{H}|\overline{D}^0(t)\rangle = \frac{1}{2q}(\langle \overline{f}|\mathcal{H}|D_1(t)\rangle - \langle \overline{f}|\mathcal{H}|D_2\rangle) \\
&= \frac{1}{2}([(\chi_{\overline{f}}^{-1}+1)\overline{\mathrm{Amp}}_{\overline{f}} + (\chi_+^{-1}+1)\overline{\mathrm{Amp}}_+]e_1(t) \\
&\quad -[(\chi_{\overline{f}}^{-1}-1)\overline{\mathrm{Amp}}_{\overline{f}} + (\chi_-^{-1}-1)\overline{\mathrm{Amp}}_-]e_2(t)) \\
&\equiv e_1(t)\overline{A}_1 + e_2\overline{A}_2\,, \qquad (27.59)
\end{aligned}$$

for D^0 and $\overline{D}^0$, respectively. CLEO experiment defines

$$\chi_f = \frac{q}{p}\frac{\overline{\mathrm{Amp}}_f}{\mathrm{Amp}_f} = \left|\frac{\overline{\mathrm{Amp}}_f}{\mathrm{Amp}_f}\right|(1+A_M)e^{i(\delta+\phi)} \qquad (27.60)$$

$$\chi_{\overline{f}} = \frac{q}{p}\frac{\overline{\mathrm{Amp}}_{\overline{f}}}{\mathrm{Amp}_{\overline{f}}} = \left|\frac{\overline{\mathrm{Amp}}_{\overline{f}}}{\mathrm{Amp}_{\overline{f}}}\right|(1+A_M)e^{-i(\delta-\phi)} \qquad (27.61)$$

$$\chi_\pm = \pm\frac{q}{p}\frac{\overline{\mathrm{Amp}}_\pm}{\mathrm{Amp}_\pm} = \pm\left|\frac{\overline{\mathrm{Amp}}_\pm}{\mathrm{Amp}_\pm}\right|(1+A_M)e^{\pm i\phi)}\,, \qquad (27.62)$$

where δ is the relative strong phase between D^0 and $\overline{D}^0$ to $K_S\pi^+\pi^-$, and in the limit of CP conservation, the real CP-violating parameters, A_D and ϕ, are zero. Squaring the amplitude and factoring out the time-dependent functions yield

$$|\mathcal{M}|^2 = |e_1(t)|^2|A_1|^2 + |e_2(t)|^2|A_2|^2 + 2\mathrm{Re}[e_1(t)e_2^*(t)A_1A_2^*]\,. \qquad (27.63)$$

$$|\overline{\mathcal{M}}|^2 = |e_1(t)|^2|\overline{A}_1|^2 + |e_2(t)|^2|\overline{A}_2|^2 + 2\mathrm{Re}[e_1(t)e_2^*(t)\overline{A}_1\overline{A}_2^*]\,. \tag{27.64}$$

The time-dependent terms are given explicitly by

$$|e_1(t)|^2 = e^{\Gamma_1 t} = e^{-\Gamma(1-y)t} \tag{27.65}$$

$$|e_2(t)|^2 = e^{\Gamma_2 t} = e^{-\Gamma(1+y)t} \tag{27.66}$$

$$\begin{aligned} e_1(t)e_2^*(t) &= e^{-\lambda_{D_1}t}e^{+\lambda_{D_2}t} = e^{-\Gamma(1+ix)t} \\ &= e^{\Gamma t}(\cos(\Delta m t) - i\sin(\Delta m t)) \end{aligned} \tag{27.67}$$

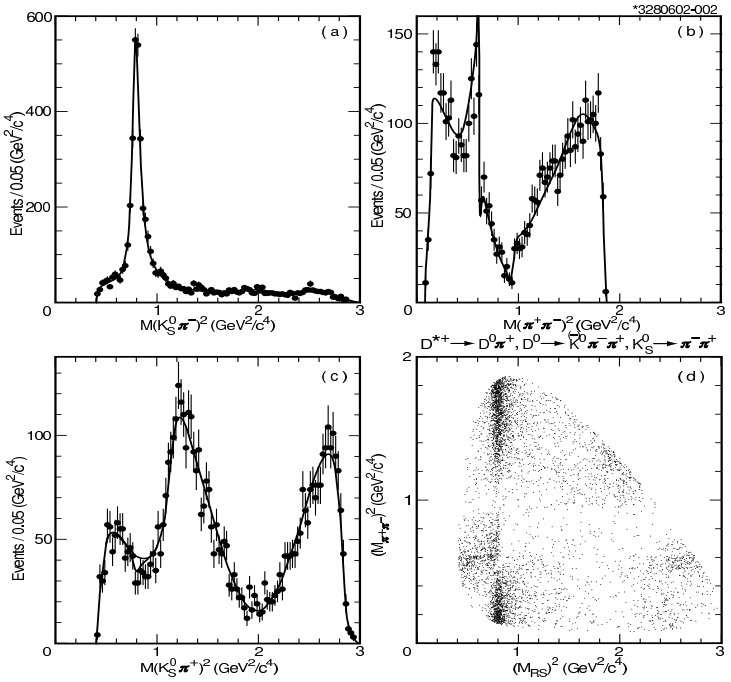

Figure 27.10: *Dalitz plot (lower right) and projections (lower left, upper plots) for* $D^0 \to K^0_S\,\pi^+\pi^-$ *decays, from CLEO using 9.0* fb^{-1} *of data.[292]*

Experimentally, y modifies the lifetime of certain contributions to the Dalitz plot while x introduces a sinusoidal rate variation. Then, $|\mathcal{M}|^2$ can be expressed as

$$\begin{aligned} |\mathcal{M}|^2 &= |A_1|^2 e^{-\Gamma(1-y)t} + |A_2|^2 e^{-\Gamma(1+y)t} \\ &\quad +2e^{\Gamma t}(\mathrm{Re}A_1A_2^*\cos(\Delta m t) + \mathrm{Im}A_1A_2^*\sin(\Delta m t)) \end{aligned} \tag{27.68}$$

Using above probability density function, CLEO does an unbinned maximum likelihood fit to the Dalitz plot and the time t distribution to determine a_j, δ_j, x and y. There is systematic uncertainty arising from the decay model, i.e., one must decide which intermediate states to include in the fit. Eq. (27.68) depends linearly on x ($x < 1$) and is therefore sensitive to the sign of x.

Table 27.6: *Limits on mixing and CP violation parameters from a t-dependent fit to the* $D^0 \to K^0_S \pi^+\pi^-$ *Dalitz plot, from CLEO using 9.0* fb^{-1}*.[291] The errors are statistical, experimental systematic, and modelling systematic, respectively.*

Fit	**Param.**	**Fit Result (%)**	**95% C.L. Inter. (%)**
No CPV	x	$1.8^{+3.4}_{-3.2} \pm 0.4 \pm 0.4$	$(-4.7, 8.6)$
	y	$-1.4^{+2.5}_{-2.4} \pm 0.8 \pm 0.4$	$(-6.3, 3.7)$
CPV Allowed	x	$2.3^{+3.5}_{-3.4} \pm 0.4 \pm 0.4$	$(-4.5, 9.3)$
	y	$-1.5^{+2.5}_{-2.4} \pm 0.8 \pm 0.4$	$(-6.4, 3.6)$
	ϵ	$1.1 \pm 0.7 \pm 0.4 \pm 0.2$	$(-0.4, 2.4)$
	ϕ	$(5.7 \pm 2.8 \pm 0.4 \pm 1.2)^\circ$	$(-0.3^\circ, 11.7^\circ)$

The time-dependent Dalitz analysis techniques are developed by CLEO [291], and their results based on 9.0 fb^{-1} of data have not yet been superseded. To minimize backgrounds, the D^0 candidate is required to originate from $D^{*+} \to D^0\pi^+$. The final Dalitz plot sample contains 5299 events with only $(2.1 \pm 1.5)\%$ background as shown in Fig. 27.10. The fit results are listed in Table 27.6; the 95% C.L. intervals corresponding to the values at which $-2ln\mathcal{l}$ rises by 3.84 units, where $\mathcal{L}$ is the likelihood function. CP violation is included in the fit

27.3 Measurements on $\psi(3770)$ peak

At BESIII, the $\psi(3770)$ decays will provide another opportunity to search for $D^0 - \overline{D}^0$ mixing and understand the source of CP violation in Charm system. The amplitude for $\psi(3770)$ decaying to $D^0\overline{D}^0$ is $\langle D^0\overline{D}^0|H|\psi(3770)\rangle$, and the $D^0\overline{D}^0$ pair system is in a state with charge parity $C = -1$, which can be defined as

$$|D^0\overline{D}^0\rangle^{C=-1} = \frac{1}{\sqrt{2}}[|D^0\rangle|\overline{D}^0\rangle - |\overline{D}^0\rangle|D^0\rangle]. \tag{27.69}$$

Although there is weak current contribution in $\psi(3770) \to D^0\overline{D}^0$ decay, which may not conserve charge parity, the $D^0\overline{D}^0$ pair can not be in a state with $C = +1$. The reason is that the relative orbital angular momentum of $D^0\overline{D}^0$ pair must be $l = 1$ because of angular momentum conservation. A boson-pair with $l = 1$ must be in an anti-symmetric state, the anti-symmetric state of particle-anti-particle pair must be in a state with $C = -1$. The $D^0\overline{D}^0$ will therefore be in an entangled state with the same quantum numbers as the parent resonance.

In general, as shown in Ref. [293], a $D^0\overline{D}^0$ pair produced through a virtual photon in the reaction $e^+e^- \to D^0\overline{D}^0 + m\gamma + n\pi^0$ is in a $C = (-1)^{m+1}$ state. Thus, as the $\psi(3770)$, where no additional fragmentation particles are produced, there is only $C = -1$, while at higher energies above $D^*\overline{D}$ threshold, we can access $C = -1$ or $C = +1$ eigenstate, such as $e^+e^- \to \psi(4140) \to \gamma(D^0\overline{D}^0)_{C=+1}$ or $\pi^0(D^0\overline{D}^0)_{C=-1}$.

We now consider decays of these correlated systems into various final states, searching in particular for interference effects depending on δ. In all cases, we integrate with respect to proper time, since vertex separation in a symmetric e^+e^- "charm factory" is likely to be problematic. Xing [294] and Gronau *et al.* [295] have considered time-integrated decays into correlated pairs of states, including some effects of a non-zero final state phase difference. In Ref. [295], Gronau *et al.* derived general expressions for time-integrated decay rates into a pair of final states f_1 and f_2, from $C = -1$ and $C = +1$ $D^0\overline{D}^0$ states:

$$\Gamma^{C=-1}(f_1, f_2) = \frac{1}{2}|a^-|^2\left[\frac{1}{1-y^2} + \frac{1}{1+x^2}\right] + \frac{1}{2}|b^-|^2\left[\frac{1}{1-y^2} - \frac{1}{1+x^2}\right], \tag{27.70}$$

$$\begin{aligned}\Gamma^{C=+1}(f_1, f_2) &= \frac{1}{2}|a^+|^2\left[\frac{1+y^2}{(1-y^2)^2} + \frac{1-x^2}{(1+x^2)^2}\right] \\ &+ \frac{1}{2}|b^-|^2\left[\frac{1+y^2}{(1-y^2)^2} - \frac{1}{(1-x^2)^2}\right] \\ &+ 2\mathcal{R}e\left\{a^{+*}b^+\left[\frac{y}{(1-y^2)^2} + \frac{ix}{(1+x^2)^2}\right]\right\},\end{aligned} \tag{27.71}$$

where

$$a^\pm = \langle f_1|D^0\rangle\langle f_2|\overline{D}^0\rangle \pm \langle f_1|\overline{D}^0\rangle\langle f_2|D^0\rangle, \tag{27.72}$$

$$b^\pm = \langle f_1|D^0\rangle\langle f_2|D^0\rangle \pm \langle f_1|D^0\rangle\langle f_2|D^0\rangle, \tag{27.73}$$

they can be easily generalized allowing for CP violation [295]:

$$a^{\pm} = \frac{p}{q} A_1 A_2 (\lambda_2 \pm \lambda_1), \tag{27.74}$$

$$b^{\pm} = \frac{p}{q} A_1 A_2 (1 \pm \lambda_1 \lambda_2), \tag{27.75}$$

where

$$A_i \equiv \langle f_i | D^0 \rangle, \quad \overline{A}_i \equiv \langle f_i | \overline{D}^0 \rangle, \quad \lambda_i \equiv \frac{q}{p} \frac{\overline{A}_i}{A_i}. \tag{27.76}$$

The definition in above equation had been discussed in detail in Section 27.1.3.

As in Refs. [295, 294, 296, 297], we consider the following categories of D^0 and $\overline{D}^0$ final states:

- Hadronic final states, f or $\overline{f}$, but not CP eigenstates, such as $K^-\pi^+$, which is produced via CF D^0 transitions or DCS $\overline{D}^0$ transitions;
- Semileptonic or pure leptonic final states, l^+ or l^-, which, in the absence of mixing, tag unambiguously the flavor of the parent D;
- CP-even (S_+) and CP-odd (S_-) eigenstates, respectively.

We will discuss different final states by assuming CP conservation. Taking into account x, $y \ll 1$, keeping terms up to order x^2, y^2 and R_D (R_D is the ratio between DCS and CF decay rate as defined in Eq. (27.33)) in the expressions, neglecting CP violation in decay and mixing, one got the following results for various cases [295]

$C = -1$ $D^0\overline{D}^0$ states:

- $(K^-\pi^+)(K^-\pi^+)$:

$$\Gamma^{C=-1}(K^-\pi^+)(K^-\pi^+) = \frac{1}{2} A^4 |1 - R_D e^{-2i\delta}|^2 (x^2 + y^2) \approx \frac{1}{2} A^4 (x^2 + y^2), \tag{27.77}$$

  where $A = |\langle K^-\pi^+ | D^0 \rangle|$ is the real-valued decay amplitudes. This process serves to measure mixing effects.

- $(K^-\pi^+)(K^+\pi^-)$:

$$\Gamma^{C=-1}(K^-\pi^+)(K^+\pi^+) = A^4 \left[1 - 2R_D \cos 2\delta - \frac{1}{2}(x^2 - y^2) \right]. \tag{27.78}$$

  The above process is not sensitive to the mixing measurements since x and y are small, and can be used as a normalization for the previous case.

- $(K^-\pi^+)(S_\chi)$:

$$\Gamma^{C=-1}(K^-\pi^+)(S_\chi) = A^2 A_{S_\chi}^2 |1 + \chi\sqrt{R_D}e^{-i\delta}|^2(1+y^2) \approx A^2 A_{S_\chi}^2(1 + 2\chi\sqrt{R_D}\cos\delta), \tag{27.79}$$

in the SU(3) limit $R_D = \tan^4\theta_C \approx 0.0025$. By comparing rate with $\chi = +1$ final states such as K^+K^- and $\chi = -1$ final states such as K_S (π^0, ω, ϕ), one can measure $\cos\delta$.

- $(K^-\pi^+)(l^-X)$: At $\psi(3770)$ peak, using a leptonic $\overline{D}^0$ flavor tag and defining $A_{l^-} = \langle l^-X|\overline{D}^0\rangle$, one finds [295, 294]

$$\Gamma^{C=-1}(K^-\pi^+)(l^-X) = A^2 A_{l^-}^2 \left[1 - \frac{1}{2}(x^2 - y^2)\right]. \tag{27.80}$$

This process is not sensitive to mixing parameters and serves as a normalization for the next.

- $(K^-\pi^+)(l^+X)$:

$$\Gamma^{C=-1}(K^-\pi^+)(l^+X) = A^2 A_{l^+}^2 \left[R_D + \frac{1}{2}(x^2 - y^2)\right]. \tag{27.81}$$

where $A_{l^+} = \langle l^+X|D^0\rangle = A_{l^-}$. This process is interesting for mixing parameters if x^2, y^2 and R_D are of comparable size but, as mentioned, it is much likely that x^2, $y^2 \ll R_D$ in which case this process can be used to measure R_D.

- $(S_\chi)(l^+X)$:

$$\Gamma^{C=-1}(S_\chi)(l^+X) = A_{S_\chi}^2 A_{l^+}^2(1+y^2). \tag{27.82}$$

The y^2 correction is one order higher than we have been keeping, since $A_{S_\chi}^2$ is already of order $\sqrt{R_D}$. This process serves as a normalization for others.

$C = +1$ $D^0\overline{D}^0$ states:

- $(K^-\pi^+)(K^-\pi^+)$.

$$\Gamma^{C=+1}(K^-\pi^+)(K^-\pi^+) = 4A^4 \left[R_D + \sqrt{R_D}y' + \frac{3}{8}(x^2 + y^2)\right]. \tag{27.83}$$

In this case, the three terms (R_D, y' and R_M) may be measurable. However, most estimates of x and y within the Standard Model are considerably less than a percent [298]. If this is so, the last term in Eq. (27.83) may be inaccessible even though there may exist evidence for the $\sqrt{R_D}y'$ term, and we need an independent determination of δ. This can be obtained in Eq. (27.79).

- $(K^-\pi^+)(K^+\pi^-)$:

$$\Gamma^{C=+1}(K^-\pi^+)(K^+\pi^+) = A^4\left[1 + 2R_D\cos2\delta + 4\sqrt{R_D}(y\cos\delta + x\sin\delta) - \frac{3}{2}(x^2 - y^2)\right]. \tag{27.84}$$

  The correction terms are probably unmeasurable, so this process serves as a normalization in comparison with previous one.

- $(K^-\pi^+)(S_\chi)$:

$$\Gamma^{C=+1}(K^-\pi^+)(S_\chi) = \approx A^2 A_{S_\chi}^2(1 - 2\chi\sqrt{R_D}\cos\delta)(1 - 2\chi y). \tag{27.85}$$

  This process thus provides information to constrain $\cos\delta$ in case R_D and y are known.

- $(K^-\pi^+)(l^-X)$:

$$\Gamma^{C=+1}(K^-\pi^+)(l^-X) = A^2 A_{l^-}^2\left[1 + 2\sqrt{R_D}(y\cos\delta + x\sin\delta) - \frac{3}{2}(x^2 - y^2)\right] \tag{27.86}$$

- $(K^-\pi^+)(l^+X)$:

$$\Gamma^{C=+1}(K^-\pi^+)(l^+X) = A^2 A_{l^+}^2\left[R_D + 2\sqrt{R_D}y' + \frac{3}{2}(x^2 + y^2)\right]. \tag{27.87}$$

27.3.1 Mixing Rate: R_M

The BESIII experiment at BEPCII searches for $D^0 - \overline{D}^0$ mixing by observing both the hadronic and semileptonic modes of D^0's coming from the decay of the $\psi(3770)$:

$$\frac{N(l^\pm l^\pm)}{N(l^\pm l^\mp)} = \frac{x^2 + y^2}{2} = R_M, \tag{27.88}$$

and in hadronic decay modes:

$$\frac{N[(K^-\pi^+)(K^-\pi^+)]}{N[(K^-\pi^+)(K^+\pi^-)]} \approx \frac{x^2 + y^2}{2} = R_M. \tag{27.89}$$

For the case where one final state is hadronic and the other semileptonic, we have

$$\frac{N[(l^+)(K^-\pi^+)]}{N[(l^+)(K^+\pi^-)]} \approx \frac{x^2 + y^2}{2} + R_D, \tag{27.90}$$

where R_D is defined in Eq. (27.33).

The measurement of R_M can be performed unambiguously with the following reactions:

$$\begin{aligned}
&(i)\ e^+e^- \to \psi(3770) \to D^0\overline{D}^0 \to (K^\pm\pi^\mp)(K^\pm\pi^\mp),\\
&(ii)\ e^+e^- \to \psi(3770) \to D^0\overline{D}^0 \to (K^-e^+\nu)(K^-e^+\nu),\\
&(iii)\ e^+e^- \to D^-D^{*+} \to (K^+\pi^-\pi^-)(\pi^+_{soft}[K^+e^-\nu]),
\end{aligned} \tag{27.91}$$

The observation of reaction (*i*) would be definite evidence for the existence of $D^0 - \overline{D}^0$ mixing since the final state $(K^{\pm}\pi^{\mp})(K^{\pm}\pi^{\mp})$ can not be produced from DCS decay due to quantum statistics [257, 275]. In particular, the initial $D^0\overline{D}^0$ pair is in an odd eigenstate of C which will preclude, in the absence of mixing between the D^0 and $\overline{D}^0$ over time, the formation of the symmetric state required by Bose statistics if the decays are to be the same final state. This final state is also very appealing experimentally, because it involves a two-body decay of both charm mesons, with energetic charged particles in the final state that form an overconstrained system. Particle identification is crucial in this measurement because if both the kaon and pion are misidentified in one of the two D-meson decays in the event, it becomes impossible to discern whether mixing has occurred. At BESIII, where the data sample is expected to be 20 fb^{-1} integrated luminosity at $\psi(3770)$ peak, the limit will be $\sqrt{R_M} = 0.4\%$, but only if the particle identification capabilities are adequate. If it were possible to obtain 500 fb^{-1} at the $\psi(3770)$, the limit would be $\sqrt{R_M} = 0.08\%$ [1].

Reactions (*ii*) and (*iii*) offer unambiguous evidence for mixing in that the mixing is searched for in the semileptonic decays for which there are no DCS decay. Of course since the time-evolution is not measured, observation of Reactions (*ii*) and (*iii*) actually would indicate the violation of the selection rule relating the change in charm to the change in leptonic charge which holds true in the standard model [275].

In Table 27.7, the sensitivity for R_M measurements in different decay modes are estimated with 4 years' run at BEPCII.

Table 27.7: *The sensitivity for R_M measurements at BESIII with different decay modes with 4 years' run at BESPCII*

$D^0\overline{D}^0$ Mixing		
Reaction	Events Right Sign	Sensitivity of R_M
$\psi(3770) \to (K^-\pi^+)(K^-\pi^+)$	87195	1×10^{-4}
$\psi(3770) \to (K^-e^+\nu)(K^-e^+\nu)$	94351	
$\psi(3770) \to (K^-e^+\nu)(K^-\mu^+\nu)$	166808	3.7×10^{-4}
$\psi(3770) \to (K^-\mu^+\nu)(K^-\mu^+\nu)$	83404	
$D^{*+}D^- \to [\pi_s^+(K^+e^-\overline{\nu})(K^+\pi^-\pi^-)]$	76000	
$D^{*+}D^- \to [\pi_s^+(K^+\mu^-\overline{\nu})(K^+\pi^-\pi^-)]$	60000	
$D^{*+}D^- \to [\pi_s^+(K^+e^-\overline{\nu})$(other D^- tag)]	60000	4.7×10^{-5}
$D^{*+}D^- \to [\pi_s^+(K^+\mu^-\overline{\nu})$(other D^- tag)]	60000	

27.3.2 Doubly Cabibbo Suppressed Rate and Strong Phase $\cos\delta_{K\pi}$

Doubly Cabibbo suppressed (DCS) decays of the D^0 mesons, and D^0 mixing, give rise to identical final states. The two processes can only be distinguished by their different time dependance, or at the $\psi(3770)$ peak, by taking advantage of effects due to quantum statistics as discussed in Section 27.3.1. In Eq. (27.45) of Section 27.2.2, the wrong-sign

decay rate relative to the right-sign rate is defined as

$$R_{WS} = R_D + \sqrt{R_D}y' + \frac{1}{2}R_M\,, \tag{27.92}$$

in absence of mixing, $R_{WS} = R_D = |A_f/\overline{A}_f|^2$. In general, the ratio of DCS decay rate relative to CF decay rate is $R_D \sim \tan^4\theta_C \sim 0.25\%$, where θ_C is the Cabibbo angle. However, as pointed out in Ref. [257], $\tan^4\theta_C$ is not the only suppression factor, the ratio may be various for different final state, such as $R_D \sim 2.1 \times \tan^4\theta_C$ for $D^0 \to K^+\pi^-$, while $R_D \sim 0.45 \times \tan^4\theta_C$ for $D^0 \to K^+\rho^-$ due to final state interaction [257].

One can also measure R_D in the multibody channels $D^0 \to K^+\pi^-\pi^0$ and $D^0 \to K^+\pi^-\pi^+\pi^+$ as discussed in Section 27.2.2.

At BESIII, at $\psi(3770)$ peak, the semileptonic decay can be used to tag hadronic decay on the other side, as the case in Eq. (27.90), by neglecting mixing effect, one got [295]

$$\frac{N[(l^+)(K^-\pi^+)]}{N[(l^+)(K^+\pi^-)]} \sim R_D, \tag{27.93}$$

since it is much more likely that x^2, $y^2 \ll R_D$, this process can be used to measure R_D directly.

We can also take advantage of the coherence of the D^0 mesons produced at the $\psi(3770)$ peak to extract the strong phase difference δ between DCS and CF decay amplitudes that appears in the time-dependent mixing measurement in Eq. (27.44). Because the CP properties of the final states produced in the decay of the $\psi(3770)$ are anti-correlated, one D^0 state decaying into a final state with definite CP properties immediately identifies or tags the CP properties of the other side. As discussed in Ref. [295], from Eq. (27.70), the process of one D^0 decaying to $K^-\pi^+$, while the other D^0 decaying to a CP eigenstate S_χ with eigenvalue $\chi = \pm 1$ can be described as

$$\Gamma(K^-\pi^+, S_\chi) = A^2 A_{S_\chi}^2 |1 + \chi\sqrt{R_D}e^{-i\delta}|^2(1+y^2) \approx A^2 A_{S_\chi}^2(1 + 2\chi\sqrt{R_D}\cos\delta), \tag{27.94}$$

where $A = |\langle K^-\pi^+|D^0\rangle|$ and $A_{S_\chi} = |\langle S_\chi|D^0\rangle|$ are the real-valued decay amplitudes. In order to estimate the total sample of events needed to perform a useful measurement of δ, we define [295] an asymmetry

$$\mathcal{A} \equiv \frac{\Gamma(S_+) - \Gamma(S_-)}{\Gamma(S_+) - \Gamma(S_-)}, \tag{27.95}$$

where $\Gamma(S_\pm)$ is a rate for the $\psi(3770) \to D^0\overline{D}^0$ configuration to decay into a flavor eigenstate and a CP-eigenstate $S_\pm$. Eq. (27.94) implies a small asymmetry, $\mathcal{A} = 2\sqrt{R_D}\cos\delta$. For a small asymmetry, a general result is that its error $\Delta\mathcal{A}$ is approximately $1/\sqrt{N}$, where N is the total number of events tagged with CP-even and CP-odd eigenstates. Thus we have

$$\Delta(\cos\delta) \approx \frac{1}{2\sqrt{R_D}\sqrt{N}}. \tag{27.96}$$

The number N of CP-tagged events decaying to $K^-\pi^+$ is related to the total number of $D^0\overline{D}^0$ pairs $N(D^0\overline{D}^0)$ through $N \approx N(D^0\overline{D}^0)\mathcal{BR}(D^0 \to K^-\pi^+) \times \mathcal{BR}(D^0 \to S_\pm) \times \epsilon_{tag} \approx$

$4.0\times10^{-4}N(D^0\overline{D}^0)$, here we assume the branching ratio-times-efficiency factor ($\mathcal{BR}(D^0\to S_\pm)\times\epsilon_{tag}$) for tagging CP eigenstates is about 1.1% (the total branching ratio into CP eigenstates is larger than about 5% [4]). With the estimation of $R_D = 1.4\times\tan^4\theta_C \approx 0.3\%$, one found [295]

$$\Delta(\cos\delta) \approx \frac{400}{\sqrt{N(D^0\overline{D}^0)}}. \tag{27.97}$$

At BESIII, about 72×10^6 $D^0\overline{D}^0$ pairs can be collected with 4 years' run. We are entitled to a factor of 2 for considering both $K^-\pi^+$ and $K^+\pi^-$ final states. We thus estimate that one may be able to reach an accuracy of about 0.05 in $\cos\delta$.

27.3.3 The Comprehensive Quantum Correlation Analysis

Chapter 28

CP and T Violation[1]

The violation of the CP symmetry, where C and P are the charge-conjugation and parity-transformation operators, respectively, is one of the fundamental and most exciting phenomena in particle physics. Although weak interactions are not invariant under P (and C) transformations, as discovered in 1957, it was believed for several years that the product CP was preserved. However, in 1964, it was discovered through the observation of $K_L \to \pi^+\pi^-$ decays that weak interactions are not invariant under CP transformations [299]. After this discovery, many observations show us that CP violation has been established in both K and B systems [300]. All these measurements are consistent with the Kobayashi-Maskawa (KM) picture of CP violation.

However, people still believe that there must be new sources of CP violation beyond the SM prediction at least for the following two reasons:

- *The baryon asymmetry of the Universe*:
  Baryogenesis is a consequence CP violating processes [301]. Therefore the present baryon number, which is accurately deduced from Big Bang Nucleosynthesis (BBN) and Cosmic Microwave Background Radiation (CMBR) constraints,

$$Y_B \equiv \frac{n_B - n_{\overline{B}}}{s} \approx 9 \times 10^{-11}, \tag{28.1}$$

  is essentially a CP violating observable. The surprising point is that the KM mechanism for CP violation fails to account for it [300].

- *Non-vanishing neutrino masses:*
  It is also interesting to note that the evidence for non-vanishing neutrino masses that we obtained over the last few years points towards on origin beyond the SM [303], raising the question of having CP violation in the neutrino sector, which could be studied, in the more distant future, at dedicated neutrino factory [304].

It is very interesting to look for CP violation in the D system, most factors favour dedicated searches for CP violation in Charm transitions:

- New physics should be somewhere in the corner, since baryogenesis implies the existence of New Physics (NP) in CP violation dynamics. It will be of interest to

[1] By Hai-Bo Li

undertake dedicated searches for CP asymmetries in Charm decays, where the SM predicts very small effects smaller than $\mathcal{O}(10^{-3})$, and they can arise only in *singly Cabibbo-suppressed* (SCS) transitions. Significant larger values would signal NP. Any asymmetry in CF and DCS decays requires the intervention of NP (except for $D^{\pm} \to K_S\pi^{\pm}$ [1], where the CP impurity in K_S induces an asymmetry of 3.3×10^{-3}).

- Secondly, the neutral D system is the only one where the external up-sector quarks are involved. Thus it probes models in which the up-sector plays a special role, such as supersymmetric models with alignment [302, 305] and, more generally, models in which CKM mixing is generated in the up sector.

- Third, SCS decays are sensitive to new physics contributions to penguin and dipole operator. As far as this point is concerned, among all hadronic D decays, the SCS decays ($c \to uq\overline{q}$) are uniquely sensitive to new contributions to the $\Delta C = 1$ QCD penguin and chromomagnetic dipole operator [306, 307]. In particular, such contributions can affect neither CF ($c \to s\overline{d}u$) nor the DCS ($c \to d\overline{s}u$) decays.

- There are rich light resonances in D mass region, and the final state interaction is large and enlarges the strong phase shift which required for the direct CP violation.

- Decays to final states of more than two pseudoscalar or one pseudoscalar and one vector meson contain more dynamical information than given by their widths. The Dalitz plot analysis can exhibit CP asymmetries that might be considerably larger than those for the width [308].

CP asymmetries in integrated partial widths depend on hadronic matrix elements and (strong) phase shifts, neither of which can be predicted accurately. However the craft of theoretical engineering can be practised with profit here. One makes an ansatz for the general form of the matrix elements and phase shifts that are included in the description of $D \to PP, PV, VV$ etc. channels, where P and V denote pseudoscalar and vector mesons, and fits them to the measured branching ratios on the Cabibbo allowed, once and twice Cabibbo forbidden levels. If one has sufficiently accurate and comprehensive data, one can use these fitted values of the hadronic parameters to predict CP asymmetries. Such analyses have been undertaken in the past [309], but the data base was not as broad and precise as one would like [308]. *CLEOc and BESIII measurements will certainly lift such studies to a new level of reliability.*

There are several ways to study CP violation in charm decays [317]. We can look for direct CP violation, even in charged decays; we can look for CP violation via mixing; T violation can be examined in 4-body D meson decays, assuming CPT conservation, by measuring triple-product correlations [318]. Finally, the quantum coherence present in correlated $D^0\overline{D}^0$ decays of the $\psi(3770)$ can be exploited [319]. In Table 28.1, we summarize the recent measurements of CP violating asymmetries, A_{CP} (or A_T) in Charm decays. BaBar compares D^+ versus D^- rates. The CLEO results are obtained using a Dalitz plot analysis. CDF uses the decay of $D^{*+} \to D^0\pi^+_{soft}$ as a flavor tag, and FOCUS uses triple product correlations to measure T violation.

Experiment	Decay Mode	$A_{CP}(\%)$	Note
BaBar [310]	$D^+ \to K^-K^+\pi^+$	$1.4 \pm 1.0 \pm 0.8$	Charge asymmetry
BaBar [310]	$D^+ \to \phi\pi^+$	$0.2 \pm 1.5 \pm 0.6$	Charge asymmetry
BaBar [310]	$D^+ \to \overline{K}^{*0}K^+$	$0.9 \pm 1.7 \pm 0.7$	Resonant Structure of $D^+ \to K^-K^+\pi^+$
Belle [311]	$D^0 \to K^+\pi^-\pi^0$	-0.6 ± 5.3	Dalitz plot analysis
Belle [311]	$D^0 \to K^+\pi^-\pi^+\pi^-$	-1.8 ± 4.4	
CLEO [312]	$D^0 \to \pi^+\pi^-\pi^0$	$1^{+9}_{-7} \pm 8$	Dalitz plot analysis
CLEO [313]	$D^0 \to K^-\pi^+\pi^0$	-3.1 ± 8.6	
CLEO [314]	$D^0 \to K_S\pi^+\pi^-$	$-0.9 \pm 2.1^{+1.0+1.3}_{-4.3-3.7}$	
CDF [315]	$D^0 \to K^+K^-$	$2.0 \pm 1.2 \pm 0.6$	Direct CPV
CDF [315]	$D^0 \to \pi^+\pi^-$	$1.0 \pm 1.3 \pm 0.6$	Direct CPV
FOCUS [316]	$D^0 \to K^+K^-\pi^+\pi^-$	$1.0 \pm 5.7 \pm 3.7$	T Violation from TPC
FOCUS [316]	$D^+ \to \overline{K}^0K^-\pi^+\pi^-$	$2.3 \pm 6.2 \pm 2.2$	T Violation from TPC
FOCUS [316]	$D_S \to \overline{K}^0K^-\pi^+$	$-3.6 \pm 6.7 \pm 2.3$	T Violation from TPC

Table 28.1: *Measurements of CP violating asymmetries, A_{CP} (or A_T) in Charm decays. BaBar compares D^+ versus D^- rates. The CLEO results are obtained using a Dalitz plot analysis. CDF uses the decay of $D^{*+} \to D^0\pi^+$ as a flavor tag, and FOCUS uses triple product correlations to measure T violation.*

In order to discuss the CP violation in neutral D system, we use the following notations as described in the previous sections:

$$\begin{aligned}
&\tau \equiv \Gamma_D t,\ \Gamma_D \equiv \frac{\Gamma_{D_H} + \Gamma_{D_L}}{2},\\
&A_f \equiv A(D^0 \to f),\ \overline{A}_f \equiv A(\overline{D}^0 \to f),\\
&A_{\overline{f}} \equiv A(D^0 \to \overline{f}),\ \overline{A}_{\overline{f}} \equiv A(\overline{D}^0 \to \overline{f}),\\
&x \equiv \frac{\Delta m_D}{\Gamma_D} \equiv \frac{m_{D_H} - m_{D_L}}{\Gamma_D},\ y \equiv \frac{\Delta\Gamma_D}{2\Gamma_D} \equiv \frac{\Gamma_{D_H} - \Gamma_{D_L}}{2\Gamma_D},\\
&\lambda_f \equiv \frac{q}{p}\frac{\overline{A}_f}{A_f},\ A_M \equiv \left|\frac{q}{p}\right| - 1,\ R_f \equiv \left|\frac{\overline{A}_f}{A_f}\right|,
\end{aligned} \tag{28.2}$$

where D_H and D_L stand for the heavy and light mass eigenstates, and q and p are defined as in Eq. (27.4). We distinguish three types of CP-violation effects in neutral D meson decays:

- CP violation in decay is defined by

$$\left|\frac{\overline{A}_{\overline{f}}}{A_f}\right| \neq 1. \tag{28.3}$$

In the charged D decays without mixing effects, it is the only possible source of CP asymmetries:

- CP violation in mixing is defined as

$$\left|\frac{q}{p}\right| \neq 1. \tag{28.4}$$

  In the charged-current semileptonic neutral D decays, $|A_{l^+X}| = |\overline{A}_{l^-X}|$ and $A_{l^-X} = \overline{A}_{l^+X} = 0$, as in the SM or most of the reasonable extensions of SM, this is the only source of CP violation, and can be measured in the asymmetry of "wrong-sign" decays induced by oscillations.

- CP-violation in the interference between a decay without mixing, $D^0 \to f$, and a decay with mixing, $D^0 \to \overline{D}^0 \to f$, and is defined by

$$\mathcal{I}m\left(\frac{q}{p}\frac{\overline{A}_f}{A_f}\right) \neq 0. \tag{28.5}$$

  This form of CP violation can be observed in the asymmetry of D^0 and $\overline{D}^0$ decays into common final states, such as CP eigenstates f_{CP}.

Example of the three types of CP violation will be given in the following sections.

28.1 CP Violation in $D^0 - \overline{D}^0$ Mixing

This kind of asymmetry can be best isolated in the semileptonic decay of the neutral D mesons, as discussed in Ref. [320], in the case of D^0 meson, it can be measured in the asymmetry of "wrong-sign" decays (A_{SL}):

$$\begin{aligned} A_{SL} &\equiv \frac{\Gamma(\overline{D}^0(t)_{\rm phys} \to l^+X) - \Gamma(D^0(t)_{\rm phys} \to l^-X)}{\Gamma(\overline{D}^0(t)_{\rm phys} \to l^+X) + \Gamma(D^0(t)_{\rm phys} \to l^-X)} \\ &= \frac{1-|q/p|^4}{1+|q/p|^4}. \end{aligned} \tag{28.6}$$

Here $\overline{D}^0(0)_{\rm phys} = \overline{D}^0$ and $D^0(0)_{\rm phys} = D^0$. Note that the final states in Eq. (28.6) contain "wrong charged" leptons and can only be reached in the presence of $D^0 - \overline{D}^0$ oscillations. This asymmetry represents effectively the difference between the rates for $\overline{D}^0 \to D^0 \to l^+X$ and $D^0 \to \overline{D}^0 \to l^-X$. As the phases in the transitions $\overline{D}^0 \to D^0$ and $D^0 \to \overline{D}^0$ differ from each other, a non-vanishing CP violation follows. This asymmetry is expected to be tiny in both the SM and many of its extensions. There are no precise predictions since the large hadronic uncertainties are involved in the calculation of the mixing rate in neutral D system.

At $\psi(3770)$ peak, this kind of CP-violating signal can manifest itself in the like-sign dilepton events of $(D^0\overline{D}^0)$ pairs:

$$A_{SL} \equiv \frac{R(l_1^+X, l_2^+X) - R(l_1^-X, l_2^-X)}{R(l_1^+X, l_2^+X) + R(l_1^-X, l_2^-X)} = \frac{1-|q/p|^4}{1+|q/p|^4}, \tag{28.7}$$

where $R(l_1^+X, l_2^+X)$ and $R(l_1^-X, l_2^-X)$ are the production rates for the like-sign dilepton on $\psi(3770)$ defined in Ref. [321]. Note that this asymmetry is not only independent of the time distributions, but also independent of the charge-conjugation parity C of the $(D^0\overline{D}^0)$ pairs, thus it can be measured by using the time-integrated dilepton events at either $\psi(3770)$ or $\psi(4170)$ resonances.

28.2 CP Violation in Decay

This type of CP violation (also called "direct CP violation") occurs when the absolute value of the decay amplitude A_f for D decaying to a final state f is different from the one of corresponding CP-conjugated amplitude, i.e. $|A_f| \neq |\overline{A}_{\overline{f}}|$. This kind of CP violation could occur in both charged and neutral D decays induced by $\Delta C = 1$ effective operators. In the charged D meson decays, where mixing effect are absent, this is the only possible source of CP asymmetries:

$$A_{f^\pm}^{CP} \equiv \frac{\Gamma(D^- \to f^-) - \Gamma(D^+ \to f^+)}{\Gamma(D^- \to f^-) - \Gamma(D^+ \to f^+)} = \frac{|\overline{A}_{f^-}/A_{f^+}|^2 - 1}{|\overline{A}_{f^-}/A_{f^+}|^2 + 1}, \tag{28.8}$$

where $\Gamma_{f^\pm}$ represents the $D^\pm \to f^\pm$ decay rate. A two-component decay amplitude with weak and strong phase differences is required for this type of CP violation. If, for example, there are two such contributions, $A_f = a_1 + a_2$, we have

$$\begin{aligned} A_f &= |a_1|e^{+i\phi_T}[1 + r_f e^{i(\Delta_f + \theta_f)}], \\ \overline{A}_{\overline{f}} &= |a_1|e^{-i\phi_T}[1 + r_f e^{i(\Delta_f - \theta_f)}], \end{aligned} \tag{28.9}$$

where Δ_f corresponds to the strong phase difference and θ_f corresponds to the weak phase difference between the CP-conserving (a_1 from tree level contribution in the SM) and CP-violating parts of the decay amplitude and r_f represents the small ratio, $r_f = |a_2|/|a_1|$, ϕ_T is the weak phase from the SM tree level contribution.

It is now straightforward to evaluate the CP asymmetry in the charged D decays as :

$$A_{f^\pm}^{CP} = -\frac{2|r_f|\sin(\Delta_f)\sin(\theta_f)}{1 + |r_f|^2 + 2|r_f|\cos(\Delta_f)\cos(\theta_f)}. \tag{28.10}$$

No reliable model-independent predictions exist for the Δ_f, it is believed that it could be quite large due to the abundance of light-quark resonances in the vicinity of the D-meson mass inducing large final-state interaction (FSI) phases. The quantity of most interest to theory is the weak phase difference θ_f. Its extraction from the asymmetry requires, however, that the amplitude ratio r_f and the strong phase difference Δ_f should be known. Both quantities are difficult to calculate due to non-perturbative hadronic parameters. In the SM, relative weak phases can only be obtained in SCS decays, for instance, via the interference between spectator and penguin amplitudes. As the most optimistic model-dependent estimates put the SM predictions for the asymmetry $A^{CP} < 0.1\%$ [322], an observation of any CP-violating signal in the current round of experiments will be a sign of new physics.

Specific model calculations [323] for $D \to K\overline{K}$, $\pi\pi$, $K^*\overline{K}$, three-body modes, etc. yield this order of magnitude for the effect. New physics could enter, for example, through large phases in penguin diagram. This could give asymmetries of the order of 1% or larger. On the other hand, CF decays do not have two amplitudes with different weak phases, and therefore the CP asymmetry is zero in the SM. Some new physics scenarios may provide extra phases and could give asymmetries as large as 1%.

28.3 CP Violation in the Interference of Decays with and without Mixing

This type of CP violation is possible for common final states to which both D^0 and $\overline{D}^0$ can decay. It is usually associated with the relative phase between mixing and decay contributions as described in Eq. (28.5). It can be studied in both time-dependent and time-integrated asymmetries.

(1) CP eigenstate

In general, for a CP even (old) eigenstate, the decay amplitudes can be written as

$$\begin{aligned} A_f &= |a_1|e^{+i\phi_T}[1 + r_f e^{i(\Delta_f+\theta_f)}], \\ \overline{A}_f &= \eta_f^{CP} \times \overline{A}_{\overline{f}} = \eta_f^{CP}|a_1|e^{-i\phi_T}[1 + r_f e^{i(\Delta_f-\theta_f)}], \end{aligned} \tag{28.11}$$

where $\eta_f^{CP} = +(-)$ for CP even (odd) state and we have used $CP|D^0\rangle = -|\overline{D}^0\rangle$. Neglecting r_f in Eq. (28.11), λ_f can be written as

$$\begin{aligned} \lambda_f &\equiv -\eta_f^{CP} R_m e^{i\phi}, \\ \overline{\lambda}_{\overline{f}} &\equiv -\eta_f^{CP} R_m^{-1} e^{-i\phi}, \end{aligned} \tag{28.12}$$

where ϕ is the relative weak phase between the mixing amplitude and the decay amplitude, and $R_m = |q/p|$. The time-integrated CP asymmetry for a final CP eigenstate f is defined as follows :

$$A_f^{CP} \equiv \frac{\Gamma(D^0 \to f) - \Gamma(\overline{D}^0 \to f)}{\Gamma(D^0 \to f) + \Gamma(\overline{D}^0 \to f)}. \tag{28.13}$$

Given experimental constraints, one can take x, y, $r_f \ll 1$ and expand to the leading order in these parameters, and get [306]:

$$A_f^{CP} = 2r_f \sin\Delta_f \sin\theta_f - \eta_f^{CP}\frac{y}{2}(R_m - R_m^{-1})\cos\phi + \eta_f^{CP}\frac{x}{2}(R_m + R_m^{-1})\sin\phi, \tag{28.14}$$

where the first term represents CP violation in the decay, the second term is related to CP violation in mixing, and the third term is for CP violation in the interference between mixing and decay amplitudes. By neglecting the CP violation in mixing and decay, one can get:

$$A_f^{CP} \approx \eta_f^{CP} x \sin\phi. \tag{28.15}$$

The above discussion is only for incoherent $D^0\overline{D}^0$ decays. In the case of $D^0\overline{D}^0$ produced coherently at BESIII, the $D^0\overline{D}^0$ pair system is in a state with charge parity $C = \eta$, which can be defined as [307, 321]

$$|D^0\overline{D}^0\rangle^{C=\eta} = \frac{1}{\sqrt{2}}\left[|D^0\rangle|\overline{D}^0\rangle + \eta|\overline{D}^0\rangle|D^0\rangle\right], \tag{28.16}$$

where η is the charge conjugation parity or orbital angular momentum of the $D^0\overline{D}^0$ pair. Thus, it is easy to see that $D^0\overline{D}^0$ occur in a P-wave (l = 1) in the reactions:

$$\begin{aligned} &e^+e^- \to \gamma^* \to D^0\overline{D}^0, \\ &e^+e^- \to \gamma^* \to D^0\overline{D}^{*0},\ D^{*0}\overline{D}^0 \to D^0\overline{D}^0\pi^0, \\ &e^+e^- \to \gamma^* \to D^{*0}\overline{D}^{*0} \to D^0\overline{D}^0\pi^0\pi^0, \end{aligned} \tag{28.17}$$

and in an S-wave (l=0) in the reactions:

$$\begin{aligned} &e^+e^- \to \gamma^* \to D^0\overline{D}^{*0},\ D^{*0}\overline{D}^0 \to D^0\overline{D}^0\gamma, \\ &e^+e^- \to \gamma^* \to D^{*0}\overline{D}^{*0} \to D^0\overline{D}^0\gamma\pi^0. \end{aligned} \tag{28.18}$$

One can use the semileptonic decay of one D meson to tag the other D decaying to a CP eigenstate f. We define the leptonic-tagging CP asymmetry $A_{fl^\pm}^{CP}$ as

$$A_{fl^\pm}^{CP} = \frac{R(l^-X,f) - R(l^+X,f)}{R(l^-X,f) + R(l^+X,f)} = \frac{N(l^-X,f) - N(l^+X,f)}{N(l^-X,f) + N(l^+X,f)}, \tag{28.19}$$

where $R(l^-X,f)$ and $R(l^+X,f)$ are the time integrated decay rates of $|D^0\overline{D}^0\rangle^{C=\eta}$ into (l^-X,f) and (l^+X,f) final states, respectively, and are defined as [307]:

$$R(l^-X,f) = \int_0^\infty dt_1 dt_2 |\langle (l^-X,f)|\mathcal{H}|D^0\overline{D}^0\rangle^{C=\eta}|^2, \tag{28.20}$$

$$R(l^+X,f) = \int_0^\infty dt_1 dt_2 |\langle (l^+X,f)|\mathcal{H}|D^0\overline{D}^0\rangle^{C=\eta}|^2, \tag{28.21}$$

and are proportional to the numbers of events, $N(l^-X,f)$ and $N(l^+X,f)$, for the semileptonic-tagged $D^0(\overline{D}^0) \to f$. After a complicated calculation, In Ref. [307], D.S. Du got:

$$A_{fl^\pm}^{CP} = (1+\eta)\eta_f^{CP}\left[-\frac{y}{2}(R_m - R_m^{-1})\cos\phi + \frac{x}{2}(R_m + R_m^{-1})\sin\phi\right]. \tag{28.22}$$

Comparing Eq. (28.22) with Eq. (28.14) and neglecting CP violation in decay (namely, the first term in Eq. (28.14) is zero), Du finds that $A_{fl^\pm}^{CP}$ is just twice as large as A_f^{CP} when charge conjugation parity or the orbital angular momentum l is even. In Table 28.2, we present an estimate of the number of all semi-leptonic tagged events of the type $K(\pi)e\nu$ and $K(\pi)\mu\nu$, where the neutrino is the only missing particle, with CP-eigenstates that can be collected in a 10^7 seconds (about 1 year) of running at $\sqrt{s} = 4.17$

GeV with luminosity of $\mathcal{L} = 10^{33}$ cm^{-2} sec^{-1}. The chain of the reactions considered is $e^+e^- \to \gamma^* \to D^0\overline{D}^{*0}$, $D^{*0}\overline{D}^0 \to D^0\overline{D}^0\gamma$ and $(D^0\overline{D}^0) \to (l^+X, f)$. The production cross-section used here is about $\sigma(e^+e^- \to D^0\overline{D}^{*0}) = 2.6$nb, and the branching ratio assumed for the decay $D^{*0} \to D^0\gamma$ is 38%. The CP-eigenstate branching ratios are taken from PDG2006. The efficiencies are estimated based on solid angle and PID criteria. All the numbers are normalized via the branching ratios and efficiencies to the estimate for the above decay chain. As the results indicated in Table 28.2, there are about 10,000 events observed in a year's running at BESIII. Consequently, the observed CP asymmetry, $A_{fl^\pm}^{CP}$, could be measured with accuracy of 1.2% in a year's time at BESIII.

Eigenstate	η_f^{CP}	Branching Ratio(%)	Efficiency	$D^0\overline{D}^0\gamma$ Events
K^+K^-	+1	(0.38 ± 0.01)	0.50	1040
$\pi^+\pi^-$	+1	(0.14 ± 0.003)	0.80	460
K_SK_S	+1	(0.037 ± 0.001)	0.26	30
$\rho^0\pi^0$	+1	(0.32 ± 0.04)	0.70	3140
$\pi^0\pi^0$	+1	(0.079 ± 0.008)	0.50	500
$K_S\pi^0$	-1	(1.14 ± 0.12)	0.26	770
$K_S\eta$	-1	(0.38 ± 0.06)	0.12	290
$K_S\rho^0$	-1	(0.75 ± 0.07)	0.42	460
$K_S\phi$	-1	(0.42 ± 0.032)	0.05	60
$K_S\omega$	-1	(1.10 ± 0.20)	0.06	320

Table 28.2: *Estimate of the number of fully reconstructed semileptonic tagged events with CP-eigenstates in one year running time at BESIII.*

(2) Non-CP eigenstate

28.4 Rate of the CP Violation in the Coherent $D^0\overline{D}^0$ Pair

Let us consider the reaction:

$$e^+e^- \to \psi(3770) \to D^0\overline{D}^0 \to f_af_b, \tag{28.23}$$

where f_a and f_b represent CP eigenstates of the same CP parity, i.e.

$$\begin{aligned} CP|f_a\rangle &= \eta_a|f_a\rangle, \\ CP|f_b\rangle &= \eta_b|f_b\rangle, \\ \eta_a\eta_b &= +. \end{aligned} \tag{28.24}$$

The process in Eq. (28.23) can proceed only in the presence of CP violation, because:

$$CP|\psi(3770)\rangle = +|\psi(3770)\rangle, \tag{28.25}$$

whereas

$$CP|f_a f_b\rangle = \eta_a \eta_b (-1)^{l=1} |f_a f_b\rangle = -|f_a f_b\rangle. \tag{28.26}$$

Thus $CP(\text{initial}) \neq CP(\text{final})$, and CP invariance is broken.

Note that all these arguments cannot be applied for D decays into vector states $D \to V_1 V_2$. For such a decay mode, in contrast to $D \to PP, PV$, is described by more than one independent amplitude. Therefore, the reaction $e^+e^- \to D^0\overline{D}^0 \to (K^*\rho)(K^*\rho)$ can occur even in the absence of mixing and CP violation since the two decays could be described by different combinations of decay amplitudes. Its analysis could actually yield some interesting information on final state interactions in these decay modes.

28.5 CP Violation on Dalitz Plots

Three-body decays typically proceed through intermediate resonant 2-body modes. The final state is the result of the interference of all the intermediate states. These intermediate resonances cause a non-uniform distribution of events in phase-space, which can be analysed with the Dalitz plot (DP) technique [324, 325]. The analysis of DP makes it possible to measure the amplitudes and the phases of the intermediate channels. From this, their relative branching fractions can be deduced and information on the resonances that contribute to the final state can be gained, along with new information on light meson spectroscopy. Most notably, it is possible to look for WS resonant submodes that proceed via mixing or DC suppression.

28.5.1 with Flavor Tag

28.5.2 with CP Tag

28.6 T Violation

There are another type of CP-violating effects which can also reveal the presence of new physics: Triple-product (TP) correlations [326]. These take the form $\vec{v}_1 \cdot (\vec{v}_2 \times \vec{v}_3)$, where each $\vec{v}_i$ is spin or momentum. Since $T(\vec{v}_i) = \vec{v}_i$, these TP's are odd under time reversal (T) and hence, by the CPT theorem, also constitute potential signals of CP violation. One can construct the non-zero TP by measuring the non-zero value of the asymmetry:

$$A_T \equiv \frac{\Gamma(\vec{v}_1 \cdot (\vec{v}_2 \times \vec{v}_3) > 0) - \Gamma(\vec{v}_1 \cdot (\vec{v}_2 \times \vec{v}_3) < 0)}{\Gamma(\vec{v}_1 \cdot (\vec{v}_2 \times \vec{v}_3) > 0) + \Gamma(\vec{v}_1 \cdot (\vec{v}_2 \times \vec{v}_3) < 0)}, \tag{28.27}$$

where Γ is the decay rate for a given process. However, a non-vanishing value for A_T is not necessarily due to the T transformation. This is because, in addition to reversing spins and momenta, the time reversal symmetry T also exchanges the initial and final states. Thus, in a given decay, a non-zero TP is not necessarily a signal of T violation. In particular, TP correlation can be due to the final state interaction, even if there is no CP violation. That is one typically finds that

$$A_T \propto \sin(\phi + \delta), \tag{28.28}$$

where ϕ is a weak, CP-violating phase and δ is a strong phase. From this we see that if $\delta \neq 0$, a TP correlation will appear, even without CP violation. To perform a stringent test of CP invariance, one has to study also the CP conjugate reaction and to construct a $\overline{A}_T$ in the CP-conjugate decay process. One get a T-violating asymmetry:

$$\mathcal{A}_T^{CP} \equiv \frac{1}{2}(A_T + \overline{A}_T). \tag{28.29}$$

This is a true T-violating signal in that it is non-zero only if $\phi \neq 0$.

In fact, TP asymmetries are similar to direct CP asymmetries in two way [327]: (i) they are both obtained by comparing a signal in a given decay with the corresponding signal in the CP-transformed process, and (ii) they both need the interference between two different decay amplitudes. However, there is one important difference between the direct CP and TP asymmetries. The direct CP asymmetry can be written

$$A_{dir}^{CP} \propto \sin\phi \sin\delta, \tag{28.30}$$

while, for the true T-violating asymmetry is given by

$$\mathcal{A}_T^{CP} \propto \sin\phi \cos\delta. \tag{28.31}$$

The key point here is that one can produce a direct CP asymmetry only if there is a non-zero strong-phase difference between the two decay amplitudes. However, TP asymmetries are maximal when the strong phase difference is zero. Thus, it may be more promising to look for TP asymmetries than direct CP asymmetries in D and B decays.

Consider the weak decay of a D meson into a pair of vector mesons, $D \to V_1(k_1, \epsilon_1)V_2(k_2, \epsilon_2)$, where k_1 and ϵ (k_2 and ϵ_2) denote the polarization and momentum of V_1 (V_2). For example, in the decay of $D^+ \to \overline{K}^{*0}(k_1, \epsilon_1)K^{*+}(k_2, \epsilon_2)$, One can then study the triple correlation

$$A_T = \frac{N(k_1 \cdot (\epsilon_1 \times \epsilon_2) > 0) - N(k_1 \cdot (\epsilon_1 \times \epsilon_2) < 0)}{N(k_1 \cdot (\epsilon_1 \times \epsilon_2) > 0) + N(k_1 \cdot (\epsilon_1 \times \epsilon_2) < 0)} \tag{28.32}$$

and the true T asymmetry, $\mathcal{A}_T^{CP} \equiv \frac{1}{2}(A_T + \overline{A}_T)$, can be studied by considering the CP conjugate decay of $D^- \to K^{*0}K^{*-}$. CP symmetry is violated if $\mathcal{A}_T^{CP} \neq 0$.

CP Violation		
Reaction	Event	Comment
$D^{*0}\overline{D^0} \to [\gamma_s(\text{semileptonic})(CP \text{ eigenstates})]$	26280	Measure mixing-dependent CP violation Asymmetry determined to 1%
$\psi(3770) \to (\text{semileptonic})(CP \text{ eigenstates})$	136000	Measure magnitude of CP violating amplitude to 0.5 %
$\psi(3770) \to (CP\pm \text{ eigenstates})(CP\pm \text{ eigenstates})$	16000	Sensitive to phase of direct CP violating amplitude (1.0%)

Table 28.3: *Summary of CP violation measurements at BES-III*

Chapter 29

Rare and Forbidden Charm Decays[1]

29.1 Introduction

The smashingly successful Standard Model of particle physics describes matter's most basic elements and the forces through which they interact. Physicists have tested its predictions to better than 1% precision. Yet despite its many successes, we know the SM is not the whole story. The questions of so-called fine-tuning, mass hierarchy and so on are remained unexplained. Testing the SM is one of the most important mission in particle physics. One most important feature of the SM is the absence of FCNC at tree level. Generally FCNC processes begin at one loop level and GIM suppressed, which have been proved to be powerful tools for probing the structure of electro-weak interactions. Examples are rare K and B decays and oscillations induced by penguin or box Feynman diagrams. Due to the large mass of top quark, the GIM suppression is mild for down-type quarks. As for charm quark FCNC processes, only down type quarks could propagate in the loop, so that the GIM suppression is very strong and the SM predictions are very tiny, which would be beyond the sensitivities of any running or planned colliders. So that such decays would be sensitive probes of New Physics beyond the SM. However, the long distance contribution could be much larger than the SM short distance effects, which are not always reliably calculable. These decays include: (i) $D \to V\gamma(V = \rho, \omega, \phi, ...)$, (ii)$D \to X\ell^+\ell^-$ $(X = \pi, K, \eta, \rho, \omega, \phi, ...)$, (iii) $D \to X\nu_\ell\bar{\nu}_\ell$ $(X = \pi, K, \eta, \dots)$, (iv) $D \to \gamma\gamma$, (v) $D \to \ell^+\ell^-$.

Theoretically, there are lots of works which have been intended to calculate both short and long distance contributions in these decays as reliably as possible in the SM and consider possible new physics scenarios with potentially large effects. In many cases, extensions of the SM could give contributions sometimes orders or magnitude larger than the SM [328]. In order to establish the existence of a clean window for observation of new physics in a given observable in rare charm decays, the SM contributions should be made clear at first. This is very important to include the long distance contributions due to the propagation of light quarks, although they are hard to be calculated with analytical methods. In what following, we will first review these decays in the SM and then in new physics models.

[1]By Hai-Bo Li and Ya-Dong Yang

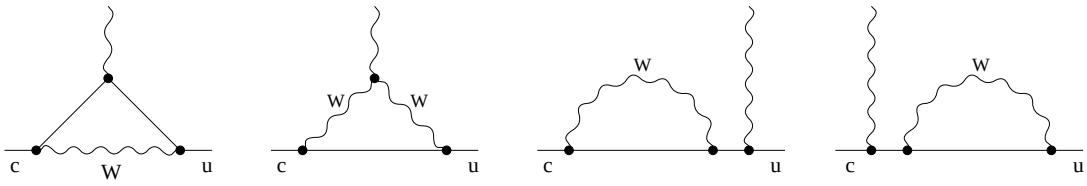

Figure 29.1: One-loop diagrams inducing the $c \to u\gamma$

29.2 The rare charm decays in the SM

In principle, the task of producing SM predictions for FCNC D meson decays is straightforward. There are two components to the analysis, short-distance (SD) and long-distance (LD), which must be separately calculated. It is known that the SD contribution can be calculated with well defined framework, but phenomenological methods have to be resorted for LD contributions.

29.2.1 Radiative charm decays

The radiative decay modes with one photon include $D \to V\gamma$, $D_s \to V\gamma$ and $D \to X_u\gamma$. The short distance effective Hamiltonian for $c \to u + \gamma$ starts from one loop diagrams as shown in Fig.1 which give

$$L_{int} = -\frac{4G_F}{\sqrt{2}} A \frac{e}{16\pi^2} m_c(\bar{u}\sigma_{\mu\nu}P_R c)F^{\mu\nu}, \tag{29.1}$$

with

$$\Delta A_{1\text{ loop}} \simeq -\frac{5}{24}\sum_{q=d,s,b} V_{cq}^* V_{uq}\left(\frac{m_q}{M_W}\right)^2. \tag{29.2}$$

The CKM factors in the above equation have very different orders of magnitude

$$|V_{cd}^* V_{ud}| \simeq |V_{cs}^* V_{us}| \simeq 0.22 \qquad \text{and} \qquad |V_{cb}^* V_{ub}| \simeq (1.3 \pm 0.4) \times 10^{-4}. \tag{29.3}$$

Consequently, $|\Delta A_{1\ loop}| \sim 2 \times 10^{-7}$. The extraordinary smallness of this number is due to the tiny factors $(m_q/M_W)^2$ for the light quarks and to the small CKM angles in the b-quark contribution.

Since the important suppression factors are independent of gauge couplings, it is possible that higher orders in perturbation theory give dominant contributions to the radiative amplitude considered because they may not suffer the same dramatic suppression and are reduced only by powers of the gauge couplings.

With RGE, one can re-sum short distance QCD corrections in the leading logarithmic approximation which results in the effective Hamiltonian

$$H_{eff}(m_b > \mu > m_c) = \frac{4G_F}{\sqrt{2}}\sum_{q=d,s} V_{cq}^* V_{uq}[C_1(\mu)O_1^q + C_2(\mu)O_2^q + \sum_{i=3}^{8} C_i(\mu)O_i], \tag{29.4}$$

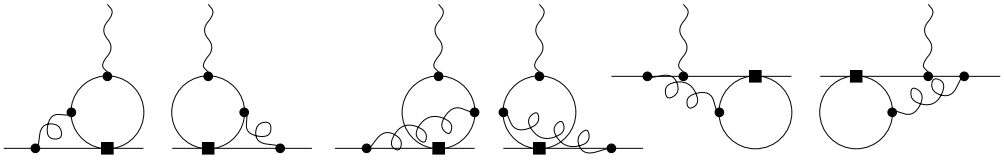

Figure 29.2: - Two-loop diagrams for the $c \to u\gamma$

where

$$O_1^q = (\bar{u}_\alpha \gamma_\mu P_L q_\beta)(\bar{q}_\alpha \gamma^\mu P_L c_\beta), \qquad q = d, s, b \tag{29.5}$$

$$O_2^q = (\bar{u}_\alpha \gamma_\mu P_L q_\alpha)(\bar{q}_\beta \gamma^\mu P_L c_\beta), \qquad q = d, s, b \tag{29.6}$$

$$O_7 = \frac{e}{16\pi^2}\, m_c (\bar{u}_\alpha \sigma_{\mu\nu} P_R c_\alpha) F^{\mu\nu}. \tag{29.7}$$

The Wilson co-efficiences C_i and remaining operators O_i are given explicitly in ref. [329].It is found that the leading logarithmic QCD correction will enhance the $c \to u\gamma$ by more than one order

$$|\Delta A_{LLA}| = [0.001 C_1(m_b) + 0.055 C_2(m_b)]\, |V_{cb}^* V_{ub}| = 0.060\, |V_{cb}^* V_{ub}| \simeq (8 \pm 3) \times 10^{-6}. \tag{29.8}$$

Moreover, including two loop contributions depicted by Fig.2, one finds the strength of $c \to u\gamma$ are further enhanced by more than two orders of magnitude

$$|A| = |V_{cs}^* V_{us}| \frac{\alpha(m_c)}{4\pi}\, (0.86 \pm 0.19) = (4.7 \pm 1.0) \times 10^{-3}. \tag{29.9}$$

After these surprising enhancements, in the SM the predicted branching ratio ($\mathcal{B}$) for $c \to u\gamma$ is found to be $\sim 10^{-8}$. However, even this is very small compared to the long distance contributions from s and u channel poles from nearby states and VMD contributions from ρ, ω, ϕ. These estimates suffer from uncertainties from several sources. The mass m_c is too large for the chiral symmetry approximation and it is too small for the HQET approximation. Hence, one has to resort to inspired guesswork [329, 330, 331]. In any case, the end results seem reasonable and agree with recent measurements. The $\mathcal{B}$ are in the range of 10^{-5} to 10^{-7}. The recent measurement of $\mathcal{B}(D^0 \to \phi^0\gamma) \sim 2.6 \times 10^{-5}$ by BELLE [332] is well within the expected range. However, it would be extremely hard to extract the small short distance contributions.

29.2.2 GIM Suppressed Decays

The short-distance component

Short-distance amplitudes are concerned with the QCD degrees of freedom (quarks, gluons) and any relevant additional fields (leptons, photons). Thus, the short distance part of the $D \to X_u \ell^+ \ell^-$ amplitude involves the quark process $c \to u\ell^+\ell^-$. It is usually most natural to employ an effective description in which the weak hamiltonian is expressed in

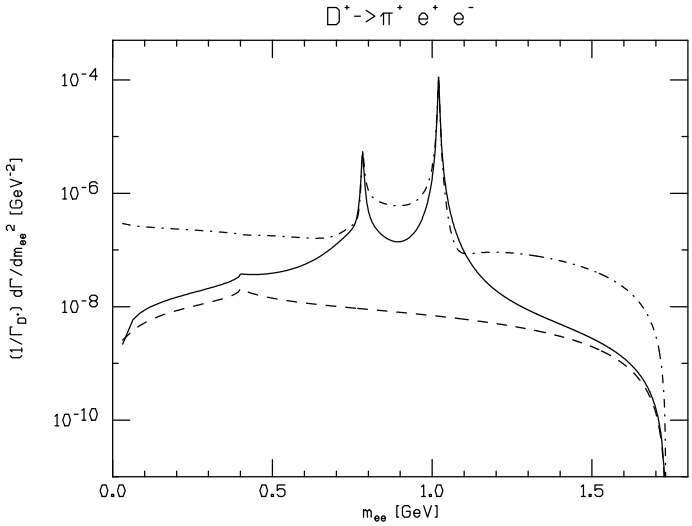

Figure 29.3: Dilepton mass distribution for $D^+ \to \pi^+ e^+ e^-$. The dashed (solid) line is the short-distance (total) SM contribution. The dot-dashed line is the R-parity violating contribution.

terms of local multiquark operators and Wilson coefficients. [333] For example, the effective hamiltonian for $c \to u\ell^+\ell^-$ with renormalization scale μ in the range $m_b \geq \mu \geq m_c$ is [2]

$$\mathcal{H}_{\rm eff}^{c\to u\ell^+\ell^-} = -\frac{4G_F}{\sqrt{2}}\left[\sum_{i=1}^{2}\left(\sum_{q=d,s} C_i^{(q)}(\mu)\mathcal{O}_i^{(q)}(\mu)\right) + \sum_{i=3}^{10} C_i'(\mu)\mathcal{O}_i'(\mu)\right] \quad . \tag{29.10}$$

In the above, $\mathcal{O}_{1,2}^{(q)}$ are four-quark current-current operators, $\mathcal{O}_{3-6}'$ are the QCD penguin operators, $\mathcal{O}_7$ ($\mathcal{O}_8$) is the electromagnetic (chromomagnetic) dipole operator and $\mathcal{O}_{9,10}$ explicitly couple quark and lepton currents. For example, we have

$$O_7' = \frac{e}{16\pi^2} m_c (\bar{u}_L \sigma_{\mu\nu} c_R) F^{\mu\nu} \ , \qquad O_9' = \frac{e^2}{16\pi^2}(\bar{u}_L \gamma_\mu c_L)(\bar{\ell}\gamma^\mu \ell) \quad . \tag{29.11}$$

The famous Inami-Lim functions [334] contribute to the Wilson coefficients C_{7-10} at scale $\mu = M_{\rm W}$.

Figure 29.3 displays the predicted dilepton mass spectrum for $D^+ \to \pi^+\ell^+\ell^-$. Several distinct kinds of contributions are included. The short-distance SM component corresponds to the dashed line, which is seen to lie beneath the other two curves. For reference, we cite the *inclusive* 'short distance' branching ratio,

$$\mathcal{B}r_{D^+\to X_u^+ e^+e^-}^{\rm (sd)} \simeq 2\times 10^{-8} \quad . \tag{29.12}$$

The long-distance component

The long-distance component to a transition amplitude is often cast in terms of hadronic entities rather than the underlying quark and gluonic degrees of freedom. For charm decays, the long-distance amplitudes are typically important but difficult to determine with

[2] Quantities with primes have had the explicit b-quark contributions integrated out

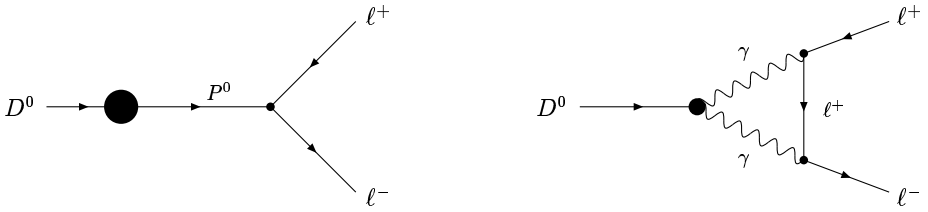

(a) (b)

Figure 29.4: Long distance contributions to $D^0 \to \ell^+\ell^-$.

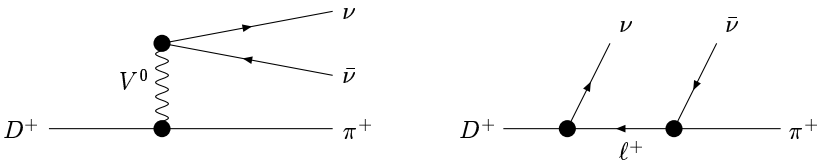

(a) (b)

Figure 29.5: Long distance contributions to $D^+ \to \pi^+\ell^+\ell^-$.

any rigor. There are generally several long-distance mechanisms for a given transition, *e.g.* as indicated for $D^0 \to \ell^+\ell^-$ in Fig.4 and for $D^+ \to \pi^+\bar{\nu}\nu$ in Fig.5.

Let us return to the case of $D^+ \to \pi^+\ell^+\ell^-$ depicted in Fig. 29.3. The solid curve represents the *total* SM signal, summed over both SD and LD contribution. In this case the LD component dominates, and from studying the dilepton mass distribution we can see what is happening. The peaks in the solid curve must correspond to intermediate resonances (ϕ, *etc*). The corresponding Feynman graph would be analogous to that in Fig.5(b) in which the final state neutrino pair is replaced by a charged lepton pair. One finds numerically that

$$\mathcal{B}r^{(\mathrm{SM})}_{D^+\to\pi^+e^+e^-} \simeq \mathcal{B}r^{(\ell\mathrm{d})}_{D^+\to\pi^+e^+e^-} \simeq 2\times 10^{-6} \quad . \tag{29.13}$$

The Standard Model Predictions

Basing the analysis in part on existing literature, [335] both SD and LD amplitudes for a number of FCNC D transitions have been calculated [328]. Results are collected in Table 29.1. As stated earlier, the current database for processes appearing in Table 29.1 consists entirely of upper bounds (or in the case of $D^0 \to \gamma\gamma$ no data entry at all). In all cases existing experimental bounds are much larger than the SM predictions, so there is no conflict between the two. For some (*e.g.* $D \to \pi\ell^+\ell^-$) the gap between SM theory and experiment is not so large and there is hope for detection in the near future. In others (*e.g.* $D^0 \to \ell^+\ell^-$) the gap is enormous, leaving ample opportunity for signals from New Physics to appear. This point is sometimes not fully appreciated and thus warrants some emphasis. It is why, for example, attempts to detect ΔM_{D} via D^0-$\bar{D}^0$ mixing experiments are so important.

Table 29.1: Standard Model predictions and current experimental limits for the branching fractions due to short and long distance contributions for various rare D meson decays.

Decay Mode	Experimental Limit	$\mathcal{B}r_{S.D.}$	$\mathcal{B}r_{L.D.}$
$D^+ \to X_u^+ e^+ e^-$		2×10^{-8}	
$D^+ \to \pi^+ e^+ e^-$	$< 4.5 \times 10^{-5}$		2×10^{-6}
$D^+ \to \pi^+ \mu^+ \mu^-$	$< 1.5 \times 10^{-5}$		1.9×10^{-6}
$D^+ \to \rho^+ e^+ e^-$	$< 1.0 \times 10^{-4}$		4.5×10^{-6}
$D^0 \to X_u^0 + e^+ e^-$		0.8×10^{-8}	
$D^0 \to \pi^0 e^+ e^-$	$< 6.6 \times 10^{-5}$		0.8×10^{-6}
$D^0 \to \rho^0 e^+ e^-$	$< 5.8 \times 10^{-4}$		1.8×10^{-6}
$D^0 \to \rho^0 \mu^+ \mu^-$	$< 2.3 \times 10^{-4}$		1.8×10^{-6}
$D^+ \to X_u^+ \nu \bar{\nu}$		1.2×10^{-15}	
$D^+ \to \pi^+ \nu \bar{\nu}$			5×10^{-16}
$D^0 \to \bar{K}^0 \nu \bar{\nu}$			2.4×10^{-16}
$D_s \to \pi^+ \nu \bar{\nu}$			8×10^{-15}
$D^0 \to \gamma\gamma$		4×10^{-10}	few $\times 10^{-8}$
$D^0 \to \mu^+ \mu^-$	$< 3.3 \times 10^{-6}$	1.3×10^{-19}	few $\times 10^{-13}$
$D^0 \to e^+ e^-$	$< 1.3 \times 10^{-5}$	$(2.3 - 4.7) \times 10^{-24}$	
$D^0 \to \mu^\pm e^\mp$	$< 8.1 \times 10^{-6}$	0	0
$D^+ \to \pi^+ \mu^\pm e^\mp$	$< 3.4 \times 10^{-5}$	0	0
$D^0 \to \rho^0 \mu^\pm e^\mp$	$< 4.9 \times 10^{-5}$	0	0

29.3 New Physics Analysis

There is a wide collection of possible New Physics models leading to FCNC D transitions. Among those considered in Ref.[328] are (i) Supersymmetry (SUSY): R-parity conserving, R-parity violating, (ii) Extra Degrees of Freedom: Higgs bosons, Gauge bosons, Fermions, Spatial dimensions, (iii) Strong Dynamics: Extended technicolor, Top-condensation.

We would restrict most of our attention to the case of supersymmetry. However, at the end a few remarks are made on the topic of large extra dimensions. The SUSY discussion divides naturally according to how the R-parity $R_{\rm P}$ is treated, where

$$R_{\rm P} \;=\; (-)^{3(B-L)+2S} \;=\; \begin{cases} +1 & \text{(particle)} \\ -1 & \text{(sparticle)} \end{cases} . \tag{29.14}$$

29.3.1 R-parity conserving SUSY

R-parity conserving SUSY will contribute to charm FCNC amplitudes via loops. To calculate R-parity conserving SUSY contributions, the so-called *mass insertion approximation* is always employed [336], which is oriented towards phenomenological studies and is also model independent. Let us first describe what is actually done and then provide a brief explanation of the underlying rationale.

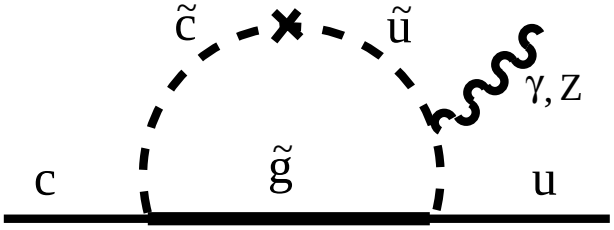

Figure 29.6: A typical contribution to $c \to u$ FCNC transitions in the MSSM. The cross denotes one mass insertion $(\delta^u_{12})_{\lambda\lambda'}$ and λ, λ' are helicity labels.

In this approach, a squark propagator becomes modified by a mass insertion (*e.g.* the '$\times$' in Fig.6 that changes the squark flavor [336, 337]. For convenience, one expands the squark propagator in powers of the dimensionless quantity $(\delta^u_{ij})_{\lambda\lambda'}$,

$$(\delta^u_{ij})_{\lambda\lambda'} = \frac{(M^u_{ij})^2_{\lambda\lambda'}}{M^2_{\tilde{q}}} \quad , \tag{29.15}$$

where $i \neq j$ are generation indices, λ, λ' denote the chirality, $(M^u_{ij})^2$ are the off-diagonal elements of the up-type squark mass matrix and $M_{\tilde{q}}$ represents the average squark mass. The exchange of squarks in loops thus leads to FCNC through diagrams such as the one in Fig.6. The role of experiment is to either detect the predicted (SUSY-induced) FCNC signal or to constrain the contributing $(\delta^u_{ij})_{\lambda\lambda'}$.

This topic is actually part of the super-CKM problem. If one works in a basis which diagonalizes the fermion mass matrices, then sfermion mass matrices (and thus sfermion propagators) will generally be nondiagonal. As a result, flavor changing processes can occur. One can use phenomenology to restrict these FCNC phenomena. The $Q = -1/3$ sector has yielded fairly strong constraints but thus far only D^0-$\bar{D}^0$ mixing has been used to limit the $Q = +2/3$ sector. In the analysis[328], charm FCNCs have been taken to be to be as large as allowed by the D-mixing upper bounds.

For the decays $D \to X_u \ell^+ \ell^-$ discussed earlier in Sect. 29.2.2, the gluino contributions will occur additively relative to those from the SM and so we can write for the Wilson coefficients,

$$C_i = C_i^{(\mathrm{SM})} + C_i^{\tilde{g}} \quad . \tag{29.16}$$

To get some feeling for dependence on the $(\delta^u_{12})_{\lambda\lambda'}$ parameters, we display the examples

$$C_7^{\tilde{g}} \;\propto\; (\delta^u_{12})_{\mathrm{LL}} \text{ and } (\delta^u_{12})_{\mathrm{LR}} \;, \qquad C_9^{\tilde{g}} \;\propto\; (\delta^u_{12})_{\mathrm{LL}} \quad , \tag{29.17}$$

whereas for quark helicities opposite [3] to those in the operators of Eq. (29.11), one finds

$$\hat{C}_7^{\tilde{g}} \;\propto\; (\delta^u_{12})_{\mathrm{RR}} \text{ and } (\delta^u_{12})_{\mathrm{LR}} \;, \qquad \hat{C}_9^{\tilde{g}} \;\propto\; (\delta^u_{12})_{\mathrm{RR}} \quad . \tag{29.18}$$

Moreover, the term in $\hat{C}_7^{\tilde{g}}$ which contains $(\delta^u_{12})_{\mathrm{LR}}$ experiences the enhancement factor $M_{\tilde{g}}/m_c$.

[3] We use the notation $\hat{C}$ for the associated Wilson coefficients.

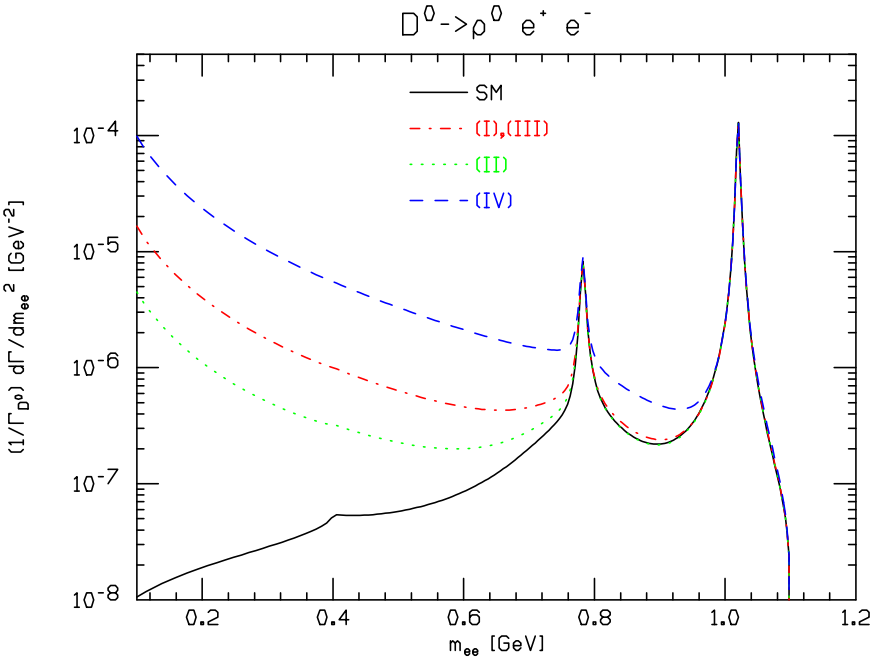

Figure 29.7: Dilepton mass distributions for $D^0 \to \rho^0 e^+ e^-$ in the mass insertion approximation of MSSM. The SM prediction (solid curve) is provided for reference and the MSSM curves refer to (i) $M_{\tilde{g}} = M_{\tilde{q}} = 250$ GeV, (ii) $M_{\tilde{g}} = 2M_{\tilde{q}} = 500$ GeV, (iii) $M_{\tilde{g}} = M_{\tilde{q}} = 1000$ GeV and (iv) $M_{\tilde{g}} = M_{\tilde{q}}/2 = 250$ GeV.

Numerically the effects in $c \to u\ell^+\ell^-$ are studied for the range of masses: (I) $M_{\tilde{g}} = M_{\tilde{q}} = 250$ GeV, (II) $M_{\tilde{g}} = 2\,M_{\tilde{q}} = 500$ GeV, (III) $M_{\tilde{g}} = M_{\tilde{q}} = 1000$ GeV and (IV) $M_{\tilde{g}} = (1/2)\,M_{\tilde{q}} = 250$ GeV. For some modes in $D \to X_u\ell^+\ell^-$, the effect of the squark-gluino contributions can be large relative to the SM component, both in the total branching ratio and for certain kinematic regions of the dilepton mass. The mode $D^0 \to \rho^0 e^+ e^-$ is given in Fig. 29.7. This figure should make clear the importance of measuring the low $m_{\ell^+\ell^-}$ part of the dilepton mass spectrum.

29.3.2 R-parity violating SUSY

The effect of assuming that R-parity can be violated is to allow additional interactions between particles and sparticles. Ignoring bilinear terms which are not relevant to our discussion of FCNC effects, we introduce the R-parity violating (RPV) super-potential of trilinear couplings,

$$\mathcal{W}_{\not R_p} = \epsilon_{ab}\left[\frac{1}{2}\lambda_{ijk}L_i^a L_j^b \bar{E}_k + \lambda'_{ijk}L_i^a Q_j^b \bar{D}_k + \frac{1}{2}\epsilon_{\alpha\beta\gamma}\lambda''_{ijk}\bar{U}_i^\alpha \bar{D}_j^\beta \bar{D}_k^\gamma\right] \quad , \tag{29.19}$$

where L, Q, $\bar{E}$, $\bar{U}$ and $\bar{D}$ are the standard chiral super-fields of the MSSM and i, j, k are generation indices. The quantities λ_{ijk}, λ'_{ijk} and λ''_{ijk} are *a priori* arbitrary couplings which total $9 + 27 + 9 = 45$ unknown parameters in the theory.

The presence of RPV means that *tree-level* amplitudes become possible in which a virtual sparticle propagates from one of the trilinear vertices in Eq. (29.19) to another.

In order to avoid significant FCNC signals (which would be in contradiction with current experimental limits), bounds must be placed on the (unknown) coupling parameters. As experimental probes become more sensitive, the bounds become ever tighter. In particular, the FCNC sector probed by charm decays involves the $\{\lambda'_{ijk}\}$. Introducing matrices $\mathcal{U}_{\rm L}$, $\mathcal{D}_{\rm R}$ to rotate left-handed up-quark fields and right-handed down-quark fields to the mass basis, we obtain for the relevant part of the superpotential

$$\mathcal{W}_{\lambda'} = \tilde{\lambda}'_{ijk}\left[-\tilde{e}^i_L \bar{d}^k_R u^j_L - \tilde{u}^j_L \bar{d}^k_R e^i_L - (\tilde{d}^k_R)^*(\bar{e^i_L})^c u^j_L + \ldots\right] \quad , \tag{29.20}$$

where neutrino interactions are not shown and we define

$$\tilde{\lambda}'_{ijk} \equiv \lambda'_{irs}\mathcal{U}^L_{rj}\mathcal{D}^{*R}_{sk} \quad . \tag{29.21}$$

Some bounds on the $\{\tilde{\lambda}'_{ijk}\}$ are already available from data on such diverse sources as charged-current universality, the ratio $\Gamma_{\pi\to e\nu_e}/\Gamma_{\pi\to\mu\nu_\mu}$, the semileptonic decay $D\to K\ell\nu_\ell$, *etc.* [339] The additional experimental implications of the preceding formalism are considered:

(i) For the decay $D^+ \to \pi^+e^+e^-$, the effect of RPV is displayed as the dot-dash line in Fig. 29.3. Here, the effect is proportional to $\tilde{\lambda}'_{11k}\cdot\tilde{\lambda}'_{12k}$ and we have employed existing limits on these couplings. Although the effect on the branching ratio is not large, but the dilepton spectrum away from resonance poles is seen to be sensitive to the RPV contributions. This case is not optimal because the current experimental limit on $\mathcal{B}r_{D^+\to\pi^+e^+e^-}$ is well above the dot-dash curve.

(ii) For $D^+ \to \pi^+\mu^+\mu^-$, the current experimental limit on $\mathcal{B}r_{D^+\to\pi^+\mu^+\mu^-}$ actually provides the new bound

$$\tilde{\lambda}'_{11k}\cdot\tilde{\lambda}'_{12k} \le 0.004 \quad . \tag{29.22}$$

(iii) Another interesting mode is $D^0\to\mu^+\mu^-$. Upon using the bound of Eq. (29.22) we obtain

$$\mathcal{B}r^{\not R_p}_{D^0\to\mu^+\mu^-} < 3.5\times10^{-6}\left(\frac{\tilde{\lambda}'_{12k}}{0.04}\right)^2\left(\frac{\tilde{\lambda}'_{11k}}{0.02}\right)^2 \quad . \tag{29.23}$$

A modest improvement in the existing limit on $\mathcal{B}r_{D^0\to\mu^+\mu^-}$ will yield a new bound on the product $\tilde{\lambda}'_{11k}\cdot\tilde{\lambda}'_{12k}$.

(iv) Lepton flavor violating processes are allowed by the RPV lagrangian. One example is the mode $D^0\to e^+\mu^-$, for which existing parameter bounds predict

$$\mathcal{B}r^{\not R_p}_{D^0\to\mu^+e^-} < 0.5\times10^{-6}\times\left[\left(\frac{\tilde{\lambda}'_{11k}}{0.02}\right)\left(\frac{\tilde{\lambda}'_{22k}}{0.21}\right)+\left(\frac{\tilde{\lambda}'_{21k}}{0.06}\right)\left(\frac{\tilde{\lambda}'_{12k}}{0.04}\right)\right] \quad . \tag{29.24}$$

An order-of-magnitude improvement in $\mathcal{B}r^{\not R_p}_{D^0\to\mu^+e^-}$ will provide a new bound on the above combination of RPV couplings.

29.3.3 Large Extra Dimensions

For several years, the study of large extra dimensions ('large' means much greater than the Planck scale) has been an area of intense study. This approach might hold the solution

of the hierarchy problem while having verifiable consequences at the TeV scale or less. Regarding the subject of rare charm decays, one's reaction might be to ask *How could extra dimensions possibly affect the decays of ordinary hadrons?*. We provide a few examples in the following.

Suppose the spacetime of our world amounts to a $3+1$ brane which together with a manifold of additional dimensions (the bulk) is part of some higher-dimensional space. A field Θ which can propagate in a large extra dimension will exhibit a Kaluza-Klein (KK) tower of states $\{\Theta_n\}$, detection of which would signal existence of the extra dimension. Given our ignorance regarding properties of the bulk or of which fields are allowed to propagate in it, one naturally considers a variety of different models.

Assume, for example, the existence of an extra dimension of scale $1/R \sim 10^{-4}$ eV such that the gravitational field (denote it simply as G) alone can propagate in the extra dimension. [340] There are then bulk-graviton KK states $\{G_n\}$ which couple to matter. In principle there will be the FCNC transitions $c \to u\ G_n$ and since the $\{G_n\}$ remain undetected, there will be apparent missing energy. However this mechanism leads to too small a rate to be observable.

Another possibility which has been studied is that the scale of the extra dimension is $1/R \sim 1$ TeV and that SM gauge fields propagate in the bulk. [341] However, precision electroweak data constrain the mass of the first gauge KK excitation to be in excess of 4 TeV [342], and hence their contributions to rare decays are small [343].

More elaborate constructions, such as allowing fermion fields to propagate in the five-dimensional bulk of the Randall-Sundrum localized-gravity model [344], are currently being actively explored. [345]. Interesting issues remain and a good deal more study deserves to be done.

29.4 Summary

The FCNC charm decays are very rare in the SM due to the strong GIM suppression. In sharp contrast to $B \to X_s\gamma, K^*\gamma$, the SD contributions in radiative charm decays are much smaller than the LD contributions in the SM, which make the extraction SD contribution from future measurements of $D \to X_u\gamma$ and $D \to V\gamma$. Although, the LD contributions still dominate the rates, just as in the radiative decays, there are decays modes such as $D \to \pi\ell^+\ell^-$ and $D \to \rho\ell^+\ell^-$ where it is possible to access the SD physics away from the resonance contributions in the low di-lepton invariant mass region. As illustrated by Fig.3 and 7, for low di-lepton mass, the sum of long and short distance effects leaves a large window where the physics beyond the SM can be observed.

In summary, the FCNC modes are most sensitive to the effects of some new physics scenarios. If the sensitivity of experiment could reach below 10^{-6}, these new physics effects could be constrained highly. Such an experimental sensitivity, of course, make many radiative D decays accessible, however, may not illuminate short distance physics.

Past searches have set upper limits for the dielectron and dimuon decay modes [4]. In Table 29.2 and Table 29.3, the current limits and expected sensitivities at BES-III are summarized for D^+ and D^0, respectively. Detailed description on rare charm decays can be found in references [350, 351]. The charm meson radiative decays are also very

important to understand final state interaction which may enhance the decay rates. In Ref. [350, 351], the decay rates of $D \to V\gamma$ (V can be ϕ, ω, ρ and K^*) had been estimated to be $10^{-5} - 10^{-6}$, which can be reached at BES-III.

Mode	Reference Experiment	Best Upper limits(10^{-6})	BES-III ($\times 10^{-6}$)
$\pi^+e^+e^-$	CLEO-c [346]	7.4	0.03
$\pi^+\mu^+\mu^-$	FOCUS [347]	8.8	0.03
$\pi^+\mu^+e^-$	E791 [348]	34	0.03
$\pi^-e^+e^+$	CLEO-c [346]	3.6	0.03
$\pi^-\mu^+\mu^+$	FOCUS [347]	4.8	0.03
$\pi^-\mu^+e^+$	E791 [348]	50	0.03
$K^+e^+e^-$	CLEO-c [346]	6.2	0.03
$K^+\mu^+\mu^-$	FOCUS [347]	9.2	0.03
$K^+\mu^+e^-$	E791 [348]	68	0.03
$K^-e^+e^+$	CLEO-c [346]	4.5	0.03
$K^-\mu^+\mu^+$	FOCUS [347]	13	0.03
$K^-\mu^+e^+$	E687 [349]	130	0.03

Table 29.2: *Current and projected 90%-CL upper limits on rare D^+ decay modes at BES-III with 20 fb^{-1} data at $\psi(3770)$ peak. We assume the selection efficiencies for all modes are 35%.*

Mode	Reference Experiment	Best Upper limits(10^{-6})	BES-III ($\times 10^{-6}$)
$\gamma\gamma$	CLEO [352]	28	0.05
$\mu^+\mu^-$	D0 [354]	2.4	0.03
μ^+e^-	E791 [348]	8.1	0.03
e^+e^-	E791 [348]	6.2	0.03
$\pi^0\mu^+\mu^-$	E653 [355]	180	0.05
$\pi^0\mu^+e^+$	CLEO [353]	86	0.05
$\pi^0e^+e^-$	CLEO [353]	45	0.05
$K_S\mu^+\mu^-$	E653 [355]	260	0.1
$K_S\mu^+e^-$	CLEO [353]	100	0.1
$K_Se^+e^-$	CLEO [353]	110	0.1
$\eta\mu^+\mu^-$	CLEO [353]	530	0.1
$\eta\mu^+e^-$	CLEO [353]	100	0.1
ηe^+e^-	CLEO [353]	110	0.1

Table 29.3: *Current and projected 90%-CL upper limits on rare D^0 decay modes at BES-III with 20 fb^{-1} data at $\psi(3770)$ peak.*

Bibliography

[1] S. Bianco, F. Fabbri, D. Benson, I.Bigi, "A Cicerone for the Physics of Charm", *La Riv.d. Nuov.Cim.* **26** (2003); G. Burdman, I. Shipsey, "$D^0 - \bar{D}^0$ Oscillations and Rare Charm Decays", *Ann.Rev.Nucl.Part.Sci.* **53** (2003).

[2] H. Albrecht *et al.* Phys. Lett. B **241**(1990)278.

[3] T. Skwarnicki, "A study of the Radiative Cascade Transitions between the Upsilon-Prime and Upsilon Resonances", DESY F31-86-02(thesis, unpublished) (1986)

[4] W.M. Yao et. al. (Particle Data Group), J. Phys. **G 33** (2006) 1.

[5] H. Abramowicz *et al.*, Z. Phys. C15, 19(1982); S. A. Rabinowitz *et al.*, Phys. Rev. Lett. **70**, 134(1993); A. O. Bazarko *et al.*, Z. Phys. **C65**, 189(1995).

[6] M. Artuso *et al.*, CLEO Collaboration, hep-ex/0508057.

[7] T. W. Chiu *et al.*, Phys.Lett. B624 (2005) 31, hep-ph/0506266;

L. Lellouch and C.J. Lin, Phys.Rev. D64, 094501(2001), hep-ph/0011086.

D. Becirevic, Phys.Rev. D60, 074501(1999). hep-lat/9811003;

[8] S. Narison, hep-ph/0202200;

A. Penin and M. Steinhauser, Phys. Rev. D65, 054006(2002), hep-ph/0108110

D. Ebert *et al.*, Mod.Phys.Lett. A17 (2002) 803, hep-ph/0204167;

Z. G. Wang, Nucl. Phys. A744, 156(2004), hep-ph/0403259;

L. Salcedo *et al.*, hep-ph/0311008, Braz. J. Phys. 34 (2004) 297;

J. Amundson, Phys. Rev. D47, 3059(1993), hep-ph/9207235.

[9] J. Adler *et al.*, MARKIII Collaboration, Phys. Rev. Lett. 60, 1375 (1988).

[10] J.Z. Bai *et al.*, Phys.Lett. B429 (1998) 188; M. Ablikim *et al.*, Phys.Lett. B610, 183(2005), hep-ex/0410050.

[11] G. Bonvicini *et al.*, CLEO Collaboration, Phys.Rev. D70, 112004(2004), hep-ex/0411050

[12] C. Aubin *et al.*, Phys. Rev. Lett. 95 (2005) 122002, hep-lat/0506030.

[13] S. Aoki *et al.*, WA75 Collaboration, Prog. Theo. Part. 89, 131(1993).

[14] J.Z. Bai *et al.*, BES Collaboration, Phys. Rev. Lett. 74, 4599(1995).

[15] K. Kodama, *et al.*, E653 Collaboration, Phys. Lett. B382, 299(1996).

[16] M. Acciarri *et al.*, L3 Collaboration, Phys. Lett. B396, 327(1997).

[17] M. Chada *et al.*, Phy. Rev. D58, 032002(1998).

[18] Y. Alexandrov *et al.*, BEATRICE Collaboration, Phys. Lett. B478, 31(2000).

[19] G. Abbiendi *et al.*, OPAL Collaboration, Phy. Lett. B516, 236(2001)

[20] A. Heister *et al.*, ALEPH Collaboration, Phys. Lett. B528, 1(2002).

[21] B. Grinstein *et al.*, Nucl. Phys. B380, 369(1992); A. Falk, Phys. Lett. B305, 268(1993).

[22] R. J. Oakes, Phys.Rev.Lett.73, 381(1994)

[23] T. Huang, Z.H. Li and C. W. Luo, Phys. Lett. B391, 451(1997); D.S. Huang and G. H. Kim, Phys. Lett. B367, 353(1996); Phys. Rev. D53, 3659(1996).

[24] For a review, M. Neubert, Phys. Rep. 245, 259(1994) and references therein. For a comprehensive book, A. Manohar and M.B. Wise, Heavy Quark Physics, CAMBRIDGE MONOGRAPHS ON PARTICLE PHYSICS, NUCLEAR PHYSICS AND COSMOLOGY, 10.

[25] P. Ball, Nucl. Phys. B421, 593(1994), hep-ph/9312325.

[26] M. Neubert, Phys. Rev. D46, 1076(1992).

[27] J.L. Rosner, Phys. Rev. **D42** (1990) 3732.

[28] J. D. Richman and P. R. Burchat, Rev. of Mod. Phys. **67** (1995) 893.

[29] J.Z. Bai *et al* Phy. Lett. **B429** (1998) 188.

[30] M. Ablikim *et al* Phy. Lett. **B610** (2005) 183.

[31] J.Z. Bai *et al* Phy. Rev. Lett. **74** (1995) 4599.

[32] J. Adler *et al* (MARKIII), Phy. Rev. Lett. **60** (1988) 1375.

[33] G. Bonvicini *et al.* (CLEOC), Phy. Rev. **D70** (2004) 112004.

[34] M. Artuso *et al* (CLEOC), Phy. Rev. Lett. **95** (2005) 251801.

[35] S. Aoki *et al* (WA75), Prog. Theo. Phys. **89** (1993) 131.

[36] K. Kodama *et al* (Fermilab E653), Phy. Lett. **B382** (1996) 299.

[37] Y. Alexandrov Phy. Lett. **B478** (2000) 31.

[38] D. Acosta *et al.* (CLEO) Phys. Rev. **D49** (1994) 5690.

[39] M. Chada *et al.* (CLEO) **58** (1998) 032002.

[40] E. Eichten *et al.* **D21** (1980) 203.

[41] M. Ablikim et al., (BES Collab.) Phys.Lett. **B597** (2004) 39, hep-ex/04060.

[42] M. Ablikim et al., (BES Collab.) Phys.Lett. **B608** (2005) 24.

[43] J. Charles et al., (CKMfitter Group) Eur. Phys. J. C **41**,(2005) 1-131

[44] A.Abada et al., Nucl Phys. B619 (2001)565.

[45] C. Aubin et al., Phys. Rev. Lett. 94 (2005) 011601.

[46] M.A. Shifman, A.I. Vainshtein and V.I. Zakharov, Nucl. Phys. B147 (1979) 385; 448.

[47] T.M. Aliev, V.L. Eletskii, and Ya. I. Kogan, Sov. J. Nucl. Phys. 40 (1984) 527; A.A. Ovchinnikov and V.A. Slobodenyyuk, Z. Phys. C44 (1989) 433; V.N. Baier and Grozin, Z. Phys. C47 (1990) 669; A.A. Ovchinnikov, Sov. J. Nucl. Phys. 50 (1989) 519.

[48] P. Ball, V.M. Braun and H.G. Dosch, Phys. Rev. D44 (1991) 3567; P. Ball, Phys. Rev. D48 (1993) 3190.

[49] P. Colangelo and F. De Fazio, Phys. Lett. B 520 (2001) 78.

[50] D.S. Du, J.W. Li and M.Z. Yang, Eur. Phys. J. C37 (2004) 173.

[51] A. Khodjamirian, R. Rückl, S. Weinzierl, C.W. Winhart, O. Yakovlev, Phys. Rev. D62 (2000) 114002.

[52] W.Y. Wang, Y.L. Wu and M. Zhong, Phys. Rev. D.67 (2003) 014024.

[53] M. Wirbel, B. Stech and M. Bauer, Z. Phys. C29 (1985) 637; M. Bauer, B. Stech and M. Wirbel, Z. Phys. C34 (1987) 103.

[54] N. Isgur, D. Scora, B. Grinstein and M.B. Wise, Phys. Rev. D39 (1989) 799.

[55] D. Scora and N. Isgur, Phys. Rev. D52 (1995) 2783.

[56] D. Melikhov and B. Stech, Phys. Rev. D62 (2000) 014006.

[57] H.Y. Cheng, C.K. Chua and C.W. Hwang, Phys. Rev. D69 (2004) 074025.

[58] S. Fajfer and J. Kamenik, Phys. Rev. D71 (2005) 014020; and Phys. Rev. D72 (2005) 034029.

[59] D. Becirevic and A. Kaidalov, Phys. Lett. B478 (2000) 417.

[60] A. Khodjamirian, R. Rückle, S. Weinzier, C.W. Winhart, and O. Yakovlev, Phys. Rev. D62 (2000) 114002

[61] M. Ablikim et al. (BES Collaboration), Phys. Lett. B597 (2004) 39.

[62] G.S. Huang et al. (CLEO Collaboration), Phys. Rev. Lett. 94 (2005) 011802.

[63] T.E. Coan et al. (CLEO Collaboration), Phys. Rev. Lett. 95 (2005) 181802.

[64] G.S. Huang et al. (CLEO Collaboration), Phys. Rev. Lett. 95 (2005) 181801.

[65] X.H. Guo and T. Huang, Phys. Rev. D43 (1991) 2931.

[66] H.G. Dosch, E.M. Ferreira, F.S. Navarra, and M. Nielsen, Phys. Rev. D 65 (2002) 114002.

[67] M.Z. Yang, Phys. ReV. D 73 (2006) 034027; Erratum-ibid, D73 (2006) 079901.

[68] Haibo Li, eprint hep-ex/0605004.

[69] E691 Collaboration, J. C. Anjos, et al., Phys. Rev. Lett. 62 (1989) 1587.

[70] CLEO Collaboration, G. Crawford, et al., Phys. Rev. **D** 44 (1991) 3394.

[71] CLEOII Collaboration, A. Bean, et al., Phys. Lett. **B** 317 (1993) 647.

[72] MARKIII Collaboration, J. Adler, et al., Phys. Rev. Lett. 62 (1989) 1821.

[73] CLEOc Collaboration, T. E. Coan, et al., Phys. Rev. Lett. 95 (2005) 181802.

[74] CLEOc Collaboration, F. Butler, et al., Phys. Rev. **D** 52 (1995) 2656.

[75] E687 Collaboration, P. L. Frabetti, et al., Phys. Lett. **B** 382 (1996) 312.

[76] BES Collaboration, M. Ablikim, *et al.*, Phys. Lett. B **641** (2006) 145; Phys. Rev. Lett. **97** (2006) 121801.

[77] R. J. Morrison, M. S. Witherell, Annu. Rev. Part. Sci. 39 (1989) 183.

[78] M. Ablikim, J. C. Chen, G. Rong, D. H. Zhang, HEP & NP 29(1) (2005) 5.

[79] A.Abada et al., Nucl Phys. **B** 619 (2001) 565.

[80] ARGUS Collaboration, H. Albrecht, et., Phys. Lett. **B** 374 (1996) 249.

[81] CLEOII Collaboration, Y. Kubota, et al., Phys. Rev. **D** 54 (1996) 2994.

[82] MARKIII Collaboration, R. M. Baltrusaitis, et al., Phys. Rev. Lett. 54 (1985) 1976.

[83] LEBC-EHS Collaboration, M. Aguilar-Benitez, et al., Z. Phys. **C** 36 (1987) 551.

[84] MARKIII Collaboration, R. H. Schindler, et al., Phys. Rev. **D**. 24 (1981) 78.

[85] CLEOc Collaboration, N. E. Adam, et al., hep-ex/0604044.

[86] DLCO Collaboration, W. Bacino et al., Phys. Rev. Lett. 45 (1980) 329.

[87] G. Buchalla, A.J. Buras and M.E. Lautenbacher, Rev. Mod. Phys.**68**, 1125 (1996).

[88] J. Schwinger, Phys. Rev. Lett. **12** (1965) 630; R. P. Feynman, in *Symmetries in Particle Physics*, ed. A. Zichichi, (Academic Press,1965), p.167; O. Haan, B. Stech, Nucl. Phys. B **22**, 448 (1970).

[89] M. Bauer, B. Stech and M. Wirbel, Z. Phys. C**34**, 103 (1987).

[90] A.J. Buras, J.M. Gerard, R. Rückl, Nucl. Phys. **B268**, 16 (1986).

[91] B. Blok, M. Shifman, *Yad.Fiz.* **45** (1987) 211, 478, 841.

[92] M. Beneke, G. Buchalla, M. Neubert and C.T. Sachrajda, Phys. Rev. Lett. **83**, 1914 (1999); M. Beneke, G. Buchalla, M. Neubert and C.T. Sachrajda, Nucl. Phys. B**591** (2000) 313.

[93] H.N. Li and H.L. Yu, Phys. Rev. Lett. **74**, 4388 (1995); Yong-Yeon Keum, Hsiang-nan Li, A.I. Sanda, Phys. Lett. B**504**, 6 (2001); Y.Y. Keum, Hsiang-Nan Li, A.I. Sanda, Phys. Rev. D**63**, 054008 (2001).

[94] X. Y. Wu, X. G. Yin, D. B. Chen, Y. Q. Guo, Y. Zeng, Mod. Phys. Lett. A**19**, 1623 (2004).

[95] CLEO Collaboration, M. Selen *et al*, Phys. Rev. Lett. **71**, 1973 (1993).

[96] L.L. Chau and H.Y. Cheng, Phys. Lett. B**333**, 514 (1994); M. Gronau and D. Pirjol, Phys. Rev. D**62**, 077301 (2000).

[97] S. Bianco, F.L. Fabbri, D. Benson, I. Bigi, Riv. Nuovo Cim. **26N7**, 1 (2003).

[98] L.L. Chau and H.Y. Cheng, Phys. Rev. Lett. **56**, 1655 (1986); Phys. Rev. D**36**, 137 (1987); Phys. Lett. B**222**, 285 (1989); Mod. Phys. Lett. A**4**, 877 (1989); L.L. Chau, Phys. Rep. **95**, 1 (1983); M. Gronau, O.F. Hernández, D. London and J.L. Rosner, Phys. Rev. D**50**, 4529 (1994); ibid. **52**, 6356, 6374 (1995).

[99] X.Q. Li and B.S. Zou, Phys. Lett. B**399**, 297 (1997); S. Fajfer and J. Zupan, Int. J. Mod. Phys. A**14**, 4161 (1999); S. Fajfer, A. Prapotnik, P. Singer and J. Zupan, Phys. Rev. D**68**, 094012 (2003).

[100] M. Ablikim, D.S. Du and M.Z. Yang, Phys. Lett. B**536**, 34 (2002); J.W. Li, M.Z. Yang and D.S. Du, hep-ph/0206154; M. Ablikim, D.S. Du and M.Z. Yang, hep-ph/0211413.

[101] F. Buccella *et al.*, Z. Phys. C **55**, 243 (1992); Phys. Lett. B **302**, 319 (1993); Phys. Rev. D**51**, 3478 (1995); Phys. Lett. B**379**, 249 (1996).

[102] B. Bajc, S. Fajfer, R.J. Oakes and S. Prelovšek, Phys. Rev. D **56**, 7207 (1997).

[103] P. Zenczykowski, Acta Phys. Polon. B**28**, 1605 (1997).

[104] H.Y. Cheng, Phys. Lett. B**335**, 428 (1994).

[105] H.Y. Cheng, Eur. Phys. J. C**26**, 551 (2003).

[106] J.L. Rosner, Phys. Rev. D**60**, 114026 (1999).

[107] C.W. Chiang, Z. Luo, and J.L. Rosner, Phys. Rev. D**67**, 014001 (2003).

[108] Y.S. Dai *et al.*, Phys. Rev. D **60**, 014014 (1999); J.M. Gerard, J. Pastieau, J. Weyers, Phys. Lett. B **436**, 363 (1998); P. Zenczykowski, Phys. Lett. B **460**, 390 (1999); K. Terasaki, Phys. Rev. D **59**, 114001 (1999); J.O. Eeg, S. Fajfer, J. Zupan, Phys. Rev. D **64**, 034010 (2001).

[109] M. Lusignoli and A. Pugliese, hep-ph/0210071.

[110] Y. L. Wu, M. Zhong and Y. F. Zhou, Eur. Phys. J. C**42**, 391 (2005).

[111] A.N. Kamal, R.C. Verma and N. Sinha, Phys. Rev. D **43**, 843 (1991).

[112] P. Bedaque, A. Das and V.S. Mathur, Phys. Rev. D **49**, 269 (1994).

[113] I. Hinchliffe and T.A. Kaeding, Phys. Rev. D **54**, 914 (1996).

[114] ARGUS Collaboration, H. Albrecht *et al.,* Phys. Lett. **B308**, 435 (1993).

[115] CLEO Collaboration, H. Muramatsu *et al.,* Phys. Rev. Lett. **89**, 251802 (2002), *ibid.* **90**, 059901(E) (2003) ; S. Kopp *et al.,* Phys. Rev. **D63**, 092001 (2001).

[116] E687 Collaboration, P.L. Frabetti *et al.,* Phys. Lett. **B351**, 591 (1995);/ibid. **B331**, 217 (1994).

[117] E691 Collaboration, J.C. Anjos *et al.,* Phys. Rev. **D48**, 56 (1993).

[118] E791 Collaboration, E.M. Aitala *et al.,* Phys. Rev. Lett. **89**, 121801 (2002);/ibid. **86**, 765 (2001);/ibid. **86**, 770 (2001).

[119] FOCUS Collaboration, J.M. Link *et al.,* Phys. Lett. **B541**, 227 (2002); talk presented by S. Erba at the DPF Meeting of the American Physical Society at Williamsburgh, Virginia, May 24-28, 2002; talk presented by S. Malvezzi at ICHEP2002, Amsterdam, July 24-31, 2002; K. Stenson, hep-ex/0111083.

[120] BaBar Collaboration, B. Aubert *et al.,* hep-ex/0207089.

[121] V.V. Anisovich, V.A. Nikonov and A.V. Sarantsev, Phys. Atom. Nucl. **65**, 1545 (2002).

[122] S. Spanier and N.A. Törnqvist, "Note on scalar mesons" in W.-M. Yao *et al.* (Particle Data Group), J. Phys. G **33**, 1 (2006).

[123] A. Deandrea, R. Gatto, G. Nardulli, A.D. Polosa and N.A. Tornqvist, Phys. Lett. B **502**, 79 (2001).

[124] F. Kleefeld, E. van Beveren, G. Rupp, M.D. Scadron, Phys. Rev. D **66**, 034007 (2002).

[125] H.Y. Cheng, Phys. Rev. D **67**, 034024 (2003).

[126] F. Buccella, M. Lusignoli, A. Pugliese, Phys. Lett. B **379**, 249 (1996).

[127] R. Gatto, G. Nardulli, A.D. Polosa, N.A. Tornqvist, Phys. Lett. B **494**, 168 (2000).

[128] I. Bediaga and M. Nielsen, Phys. Rev. D **68**, 036001 (2003).

[129] A.N. Kamal and R.C. Verma, Phys. Rev. D**45**, 982 (1992).

[130] X.Y. Pham and X.C. Vu, Phys. Rev. D**46**, 261 (1992).

[131] T.N. Pham, Phys. Rev. D**46**, 2976 (1992).

[132] A.N. Kamal, Q.P. Xu, and A. Czarnecki, Phys. Rev. D**49**, 1330 (1994).

[133] A.C. Katoch and R.C. Verma, J. Phys. G**21**, 525 (1995).

[134] H.J. Lipkin, Phys. Lett. B**515**, 81 (2001).

[135] H.Y. Cheng, Phys. Rev. D**67**, 094007 (2003).

[136] A.C. Katoch and R.C. Verma, Phys. Rev. D **49**, 1645 (1994); **55**, 7315(E) (1997).

[137] J.H. Muñoz, A.A. Rojas and G. L. Castro, Phys. Rev. D **59**, 077504 (1999).

[138] H.Y. Cheng, Phys. Rev. D **68**, 014015 (2003).

[139] D. Asner, "Dalitz Plot Analysis Formalism" in W.-M. Yao *et al.* (Particle Data Group), J. Phys. G **33**, 1 (2006).

[140] D. Asner, "Review of Charm Dalitz Plot Analyses" in W.-M. Yao *et al.* (Particle Data Group), J. Phys. G **33**, 1 (2006).

[141] C.L.Y. Lee, M. Lu, and M.B. Wise, Phys. Rev. D**46**, 5040 (1992).

[142] J. Schechter, A. Subbaraman, S. Surya, Int. J. Mod. Phys. A**9**, 3773 (1994).

[143] B. Bajc, S. Fajfer, R.J. Oakes, T.N. Pham, Phys. Rev. D**58**, 054009 (1998).

[144] P. Singer, Phys. Rev. **D16**, 2304 (1977);/Nuovo Cim. **42A**, 25 (1977).

[145] Yu. L. Kalinovsk and V.N. Pervushin,/Sov. J. Nucl. Phys. **29**, 225 (1979).

[146] H.Y. Cheng, Z. Phys. **C32**, 243 (1986).

[147] L.L. Chau and H.Y. Cheng, Phys. Rev. **D41**, 1510 (1990).

[148] F.J. Botella, S. Noguera, and J. Portolés, Phys. Lett. **B360**, 101 (1995).

[149] T.M. Yan, H.Y. Cheng, C.Y. Cheung, G.L. Lin, Y.C. Lin, and H.L. Yu, Phys. Rev. **D46**, 1148 (1992); **55**, 5851(E) (1997).

[150] M.B. Wise, Phys. Rev. **D45**, 2118 (1992).

[151] G. Burdman and J.F. Donoghue, Phys. Lett. **B280**, 287 (1992).

[152] D.X. Zhang, Phys. Lett. **B382**, 421 (1996).

[153] A.N. Ivanov and N.I. Troitskaya,/Nuovo Cim. **A111**, 85 (1998).

[154] H. Y. Cheng and K. C. Yang, Phys. Rev. **D66**, 054015 (2002).

[155] J.G. Körner, M. Krämer, and D. Pirjol, Prog. Part. Nucl. Phys. **33**, 787 (1994) [hep-ph/9406359].

[156] S. Bianco, F.L. Fabbri, D. Benson, and I.I. Bigi, Riv. Nuovo Cim. **26**, #7-8 (2003) [hep-ex/0309021].

[157] D. Pirjol and T.M. Yan, Phys. Rev. D **56**, 5483 (1997).

[158] BaBar Collaboration, B. Aubert *et al.,* hep-ex/0603052.

[159] Belle Collaboration, K. Abe *et al.,* hep-ex/0608043.

[160] R. Mizuk, talk presented at the XXXIIIth International Conference on High Energy Physics, July 26-August 2, 2006, Moscow, Russia.

[161] CLEO collaboration, M. Artuso *et al.,* Phys. Rev. Lett. **86**, 4479 (2001).

[162] N. Isgur and M.B. Wise, Phys. Rev. Lett. **66**, 1130 (1991).

[163] H.Y. Cheng and C.K. Chua, in preparation.

[164] A. Selem, *A Diquark Interpretation of the Structure and Energies of Hadrons*, Senior thesis, M.I.T. (2005); A. Selem and F. Wilczek, hep-ph/0602128.

[165] X.G. He, X.Q. Li, X. Liu, and X.Q. Zeng, hep-ph/0606015.

[166] Belle Collaboration, R. Chistov *et al.,* hep-ex/0606051.

[167] BaBar Collaboration, B. Aubert *et al.,* hep-ex/0607042

[168] Belle Collaboration, R. Mizuk *et al.,* Phys. Rev. Lett. **94**, 122002 (2005).

[169] BaBar Collaboration, B. Aubert *et al.,* hep-ex/0608055.

[170] SELEX Collaboration, M. Mattson *et al.,* Phys. Rev. Lett. **89**, 112001 (2002).

[171] SELEX Collaboration, A. Ocherashvili *et al.,* Phys. Lett. B **628**, 18 (2005).

[172] BaBar Collaboration, B. Aubert *et al.,* hep-ex/0605075.

[173] S. Migura, D. Merten, B. Metsch, and H.R. Petry, Eur. Phys. J. A **28**, 41 (2006); D. Ebert, R.N. Faustov, and V.O. Galkin, Phys. Rev. D **66**, 014502 (2005); D.W. Wang and M.Q. Huang, Phys. Rev. D **68**, 034019 (2003); E. Jenkins, Phys. Rev. D **54**, 4515 (1996); ibid. **55**, 10 (1997); S. Capstick and N. Isgur, Phys. Rev. D **34**, 2809 (1986); L.A. Copley, N. Isgur, and G. Karl, Phys. Rev. D **20**, 768 (1979).

[174] T.M. Yan, H.Y. Cheng, C.Y. Cheung, G.L. Lin, Y.C. Lin, and H.L. Yu, Phys. Rev. D **46**, 1148 (1992); Phys. Rev. D **55**, 5851(E) (1997).

[175] M.B. Wise, Phys. Rev. D **45**, 2188 (1992); G. Burdman and J. Donoghue, Phys. Lett. B **280**, 287 (1992).

[176] H.Y. Cheng, Phys. Lett. B **399**, 281 (1997).

[177] Z. Guralnik, M. Luke, and A.V. Manohar, Nucl. Phys. **B390**, 474 (1993); E. Jenkins, Phys. Lett. B **315**, 431 (1993).

[178] S. Tawfiq, P.J. O'Donnell, and J.G. Körner, Phys. Rev. D **58**, 054010 (1998).

[179] M.A. Ivanov, J.G. Körner, V.E. Lyuboviyskij, and A.G. Rusetsky, Phys. Rev. D **60**, 094002 (1999).

[180] M.Q. Huang, Y.B. Dai, and C.S. Huang, Phys. Rev. D **52**, 3986 (1995); Phys. Rev. D **55**, 7317(E) (1997).

[181] C. Albertus, Hernández, J. Nieves, and J.M. Verde-Velasco, Phys. Rev. D **72**, 094022 (2005).

[182] C.G. Boyd, M. Lu, and M.J. Savage, Phys. Rev. D **55**, 5474 (1997).

[183] T. Ito and Y. Matsui, Prog. Theor. Phys. **96**, 659 (1996).

[184] CLEO Collaboration, P. Avery *et al.,* Phys. Rev. Lett. **75**, 4364 (1995); L. Gibbons *et al.,* Phys. Rev. Lett. **77**, 810 (1996).

[185] S.L. Zhu, Phys. Rev. D **61**, 114019 (2000).

[186] A.E. Blechman, A.F. Falk, D. Pirjol, and J.M. Yelton, Phys. Rev. D **67**, 074033 (2003).

[187] P. Cho, Phys. Rev. D **50**, 3295 (1994).

[188] CLEO Collaboration, K.W. Edwards *et al.,* Phys. Rev. Lett. **74**, 3331 (1995).

[189] I.I. Bigi, hep-ph/9508408, hep-ph/9612293; G. Bellini, I.I. Bigi, and P.J. Dornan, Phys. Rep. **289**, 1 (1997).

[190] B. Blok and M. Shifman, in *Proceedings of the Third Workshop on the Physics at a Tau-Charm Factory*, Marbella, Spain, June 1993, eds. J. Kirkby and R. Kirkby (Editions Frontieres, 1994) [hep-ph/9311331].

[191] N. Bilić, B. Guberina, and J. Trampetić, Nucl. Phys. B **248**, 261 (1984).

[192] B. Guberina, R. Rückl, and J. Trampetić, Z. Phys. C **33**, 297 (1986).

[193] M.A. Shifman and M.B. Voloshin, Sov. J. Nucl. Phys. **41**, 120 (1985); Sov. Phys. JETP **64**, 698 (1986).

[194] R. Rückl, Phys. Lett. B **120**, 449 (1983).

[195] I.I. Bigi, N.G. Uraltsev, and A.I. Vainshtein, Phys. Lett. B **293**, 430 (1992); B **297**, 477(E) (1992).

[196] B. Blok and M. Shifman, Nucl. Phys. B **399**, 441 (1993); B **399**, 459 (1993).

[197] I.I. Bigi, M. Shifman, N.G. Uraltsev, and A. Vainshtein, Phys. Rev. Lett. **71**, 496 (1993); A. Manohar and M.B. Wise, Phys. Rev. D **49**, 1310 (1994); B. Blok, L. Koyrakh, M. Shifman, and A. Vainshtein, Phys. Rev. D **49**, 3356 (1994).

[198] J. Chay, H. Georgi, and B. Grinstein, Phys. Lett. B **247**, 399 (1990); J. Chay and S.J. Rey, Z. Phys. C **68**, 431 (1995).

[199] M.E. Luke, Phys. Lett. B **252**, 447 (1990).

[200] For a review of the nonperturbative HQET parameters, see M. Neubert, Int. J. Mod. Phys. A **11**, 4173 (1996).

[201] H.Y. Cheng, Phys. Rev. D **56**, 2783 (1997).

[202] M.B. Voloshin, Phys. Lett. B **385**, 369 (1996).

[203] Q. Hokim and X.Y. Pham, Phys. Lett. B **122**, 297 (1983).

[204] J.L. Rosner, Phys. Lett. B **379**, 267 (1996).

[205] B. Guberina and B. Melić, Eur. Phys. J. C **2**, 697 (1998).

[206] CLEO Collaboration, M. Artuso *et al.,* Phys. Rev. Lett. **95**, 251801 (2005).

[207] M. Neubert and C.T. Sachrajda, Nucl. Phys. B **483**, 339 (1997).

[208] V. Chernyak, Nucl. Phys. **B457**, 96 (1995).

[209] J.G. Körner and M. Krämer, Z. Phys. C **55**, 659 (1992).

[210] J.G. Körner, G. Kramer, and J. Willrodt, Phys. Lett. B **78**, 492 (1978); Z. Phys. C **2**, 117 (1979); B. Guberina, D. Tadić, and J. Trampetić, Z. Phys. C **13**, 251 (1982); F. Hussain and M.D. Scadron, Nuovo Cimento, A **79**, 248 (1984); F. Hussain and K. Khan, ibid. A **88**, 213 (1985); R.E. Karlsen and M.D. Scadron, Europhys. Lett. **14**, 319 (1991); D. Ebert and W. Kallies, Phys. Lett. B **131**, 183 (1983); B **148**, 502(E) (1984); Yad. Fiz. **40**, 1250 (1984); Z. Phys. C **29**, 643 (1985); H.Y. Cheng, Z. Phys. C **29**, 453 (1985); Yu.L. Kalinovsky, V.N. Pervushin, G.G. Takhtamyshev, and N.A. Sarikov, Sov. J. Part. Nucl. **19**, 47 (1988); S. Pakvasa, S.F. Tuan, and S.P. Rosen, Phys. Rev. D **42**, 3746 (1990); G. Kaur and M.P. Khanna, Phys. Rev. D **44**, 182 (1991); ibid. D **45**, 3024 (1992); G. Turan and J.O. Eeg, Z. Phys. C **51**, 599 (1991).

[211] H.Y. Cheng and B. Tseng, Phys. Rev. D **46**, 1042 (1992); D **55**, 1697(E) (1997).

[212] H.Y. Cheng and B. Tseng, Phys. Rev. D **48**, 4188 (1993).

[213] Q.P. Xu and A.N. Kamal, Phys. Rev. D **46**, 270 (1992).

[214] H.Y. Cheng, Phys. Lett. B **289**, 455 (1992).

[215] M.J. Savage and R.P. Springer, Phys. Rev. D **42**, 1527 (1990).

[216] S.M. Sheikholeslami, M.P. Khanna, and R.C. Verma, Phys. Rev. D **43**, 170 (1991); M.P. Khanna and R.C. Verma, Phys. Rev. D **53**, 3723 (1996).

[217] L.L. Chau, in *Proceedings of the VPI Workshop on Weak Interactions*, AIP Conf. Proc. No. 72, Particles and Fields, Subseries No. 23, eds. G.B. Collins, L.N. Chang, J.R. Ficence, Blacksburg, Virginia, December 3–6, 1980; Phys. Rep. **95**, 1 (1983).

[218] L.L. Chau and H.Y. Cheng, Phys. Rev. Lett. **56**, 1655 (1986); Phys. Rev. D **36**, 137 (1987); ibid. D **39**, 2788 (1989); Phys. Lett. B **222**, 285 (1987); Mod. Phys. Lett. A **4**, 877 (1989).

[219] L.L. Chau, H.Y. Cheng, and B. Tseng, Phys. Rev. D **54**, 2132 (1996).

[220] Y. Kohara, Phys. Rev. D **44**, 2799 (1991).

[221] M. Fukugita, T. Inami, N. Sakai, and S. Yazaki, Phys. Lett. B **72**, 237 (1977); D. Tadić and J. Trampetić, ibid. B**114**, 179 (1982); M. Bauer and B. Stech, ibid. B **152**, 380 (1985).

[222] A.J. Buras, J.-M. Gérard, and R. Rückl, Nucl. Phys. **B268**, 16 (1986).

[223] B. Blok and M. Shifman, Sov. J. Nucl. Phys. **45**, 35, 301, 522 (1987).

[224] A. Chodos, R.L. Jaffe, K. Johnson, and C.B. Thorn, Phys. Rev. D **10**, 2599 (1974); T. DeGrand, R.L. Jaffe, K. Johnson, and J. Kiskis, Phys. Rev. D **12**, 2060 (1975).

[225] K.K. Sharma and R.C. Verma, Eur. Phys. J. C **7**, 217 (1999).

[226] P. Żenczykowski, Phys. Rev. D **50**, 5787, 3285, 402 (1994).

[227] M.A. Ivanov, J.G. Körner, V.E. Lyubovitskij, and A.G. Tusetsky, Phys. Rev. D **57**, 1 (1998).

[228] FOCUS Collaboration, J.M. Link *et al.,* Phys. Lett. B **634**, 165 (2006).

[229] CLEO Collaboration, M. Bishai *et al.,* Phys. Lett. B **350**, 256 (1995).

[230] Q.P. Xu and A.N. Kamal, Phys. Rev. D **46**, 3836 (1992).

[231] H.Y. Cheng, Phys. Rev. D **56**, 2799 (1997).

[232] BaBar Collaboration, B. Aubert *et al.,* hep-ex/0601017.

[233] T. Uppal, R.C. Verma, and M.P. Khana, Phys. Rev. D **49**, 3417 (1994).

[234] H.Y. Cheng and B. Tseng, Phys. Rev. D **53**, 1457 (1996); Phys. Rev. D **55**, 1697(E) (1997).

[235] FOCUS Collaboration, J.M. Link *et al.,* Phys. Lett. B **571**, 139 (2003).

[236] H.Y. Cheng, C.Y. Cheung, G.L. Lin, Y.C. Lin, T.M. Yan, and H.L. Yu Phys. Rev. D **46**, 5060 (1992).

[237] M.B. Voloshin, Phys. Lett. B **476**, 297 (2000).

[238] R. Pérez-Marcial, R. Huerta, A. Garcia, and M. Avila-Aoki, Phys. Rev. D **40**, 2955 (1989); ibid. D **44**, 2203(E) (1991).

[239] R. Singleton, Phys. Rev. D **43**, 2939 (1991).

[240] M.A. Ivanov, V.E. Lyubovitskij, J.G. Körner, and P. Kroll, Phys. Rev. D **56**, 348 (1998).

[241] C.W. Luo, Eur. Phys. J. C **1**, 235 (1998).

[242] R.S. Marques de Carvalho *et al.,* Phys. Rev. D **60**, 034009 (1999).

[243] M.Q. Huang and D.W. Wang, hep-ph/0608170.

[244] CLEO Collaboration, J.W. Hinson *et al.,* Phys. Rev. Lett. **94**, 191801 (2005).

[245] H.Y. Cheng, C.Y. Cheung, G.L. Lin, Y.C. Lin, T.M. Yan, and H.L. Yu Phys. Rev. D **47**, 1030 (1993).

[246] M.C. Baũls, A. Pich, and I. Scimemi, Phys. Rev. D **61**, 094009 (2000).

[247] S. Tawfiq, J.G. Körner, and P.J. O'Donnell, Phys. Rev. D **63**, 034005 (2001).

[248] M.J. Savage, Phys. Lett. B **345**, 61 (1995).

[249] H.Y. Cheng, C.Y. Cheung, G.L. Lin, Y.C. Lin, T.M. Yan, and H.L. Yu Phys. Rev. D **49**, 5857 (1994).

[250] M. Lu, M.J. Savage, and J. Walden, Phys. Lett. B **369**, 337 (1996).

[251] Z.A. Baccouche, C.K. Chow, T.D. Cohen, and B.A. Gelman, Nucl. Phys. A **696**, 638 (2001).

[252] A.N. Kamal and Riazuddin, Phys. Rev. D **28**, 2317 (1983).

[253] A.N. Kamal and R.C. Verma, Phys. Rev. D **26**, 190 (1982).

[254] L.C. Hua, Phys. Rev. D **26**, 199 (1982).

[255] H.Y. Cheng, C.Y. Cheung, G.L. Lin, Y.C. Lin, T.M. Yan, and H.L. Yu Phys. Rev. D **51**, 1199 (1995).

[256] T. Uppal and R.C. Verma, Phys. Rev. D **47**, 2858 (1993).

[257] I. I. Bigi and A. I. Sanda, Phys. Lett. B **171**, 320 (1986).

[258] S. Bianco, F. Fabbri, D. Benson, I. Bigi, *la Riv. Nuov. Cim.* **26** # 7& 8 (2003).

[259] A. F. Falk *et al.*, Phys. Rev. **D65**, 054034 (2002).

[260] A. A. Petrov, hep-ph/0311371; for the most updated version, see http://www.physics.wayne.edu/ apetrov/mixing/.

[261] S. Bergmann, *et al.*, Phys. Lett. **B 486**, 418(2000).

[262] Phys. Lett. **B 297**, 353 (1992).

[263] T. Ohl *et al.*, Nucl. Phys. **B 403**, 605 (1993).

[264] I. I. Bigi and N. Uraltsev, Nucl. Phys. **B 592**, (92 (2001).

[265] Y. Nir, Lectures given at 27th SLAC Summer Institute on Particle Physics: *CP* violation in and beyond the Standard Model (SSI 99), Stanford, California, 7-16 Jul. 1999. Published in Trieste 1999, *Particle Physics*, pp. 165-243.

[266] CLEO Collaboration, R. Godang, *et al.*, Phys. Rev. Lett. bf 84, 5038 (2000).

[267] Belle Collaboration, U. Bitenc, *et al.*, Phys. Rev. **D 72**, 071101() (2005).

[268] J. J. Aubert, *et al.*, Phys. Lett. **B 106**, 419 (1981).

[269] A. Benvenuti, *et al.*, Phys. Lett. **B 158**, 531 (1985).

[270] W. C. Louis *et al.*, Phys. Rev. Lett. **56**, 1027 (1986).

[271] CLEO Collaboration, C. Cawlfield, *et al.*, Phys. Rev. **D 71**, 077101 (2005).

[272] BaBar Collaboration, B. Aubert, *et al.*, Phys. Rev. **D 70**, 091102(R) (2004).

[273] K. Stenson, Presented at the April Meeting of the American Physical Society (APS03), Philadelphia, Pennsylvania, April 5-8, 2003; M. Hosack, (FOCUS Collaboration), Fermilab-Thesis-2002-25.

[274] E791, E. M. Aitala *et al.*, Phys. Rev. Lett. **77**, 2384 (1996).

[275] I. I. Bigi, in: *Proceed. of the Tau-Charm Workshop*, L.V. Beers (ed.), SLAC-Report-343, 1989, p. 169.

[276] BaBar Collaboration, B. Aubert, *et al.*, Phys. Rev. Lett. **91**, 171801 (2003).

[277] Belle Collaboration, L. Zhang *et al.*, Phys. Rev. Lett. **96**, 151801 (2006); Belle Collaboration, J. Li *et al.*, Phys. Rev. Lett. **94**, 071801 (2005).

[278] M. G. Wilson, hep-ex/0605046; BaBar Collaboration, B. Aubert, *et al.*, hep-ex/0607090.

[279] D. Asner, W. M. Sun, *Phys. Rev.* **D73** (2006) 034024.

[280] FOCUS, J. M. Link, *et al.*, Phys. Lett. **B 618**, 23 (2005).

[281] CDF Collaboration, A. Abulencia, *et al.*, hep-ex/0605027.

[282] FNAL-E791, E. M. Aitala *et al.*, Phys. Rev. **D57**, 13 (1998).

[283] CLEO Collaboration, G. Brandenburg *et al.*, Phys. Rev. Lett. **87**, 071802 (2001); CLEO, S. A. Dytman *et al.*, Phys. Rev. **D 64**, 111101 (2001).

[284] Belle Collaboration, X. C. Tian *et al.*, Phys. Rev. Lett. **95**, 231801 (2005).

[285] J. Link *et al.*, (FOCUS), Phys. Lett. B**485**, 62(2000).

[286] S. E. Csorna, *et al.*, (CLEO), Phys. Rev. D **65**, 092001 (2002).

[287] K. Abe, *et al.* (Belle), Phys. Rev. Lett. **88**, 162001 (2002).

[288] K. Abe, *et al.*, (Belle), "Measurement of the $D^0 - \overline{D}^0$ Lifetime Difference Using $D^0 \to K\pi/KK$ Decays", submitted to Lepton-Photon Conference [Belle-CONF-347] (2003).

[289] B. Aubert, *et al.*, (BaBar), Phys. Rev. Lett. **71**, 077101 (2005).

[290] B. Aubert, *et al.*, (BaBar), Phys. Rev. Lett. **91**, 121801 (2003).

[291] D. M. Asner, *et al.*, (CLEO), Phys. Rev. D **72**, 012001 (2005).

[292] H. Muramatsu *et al.*, (CLEO), Phys. Rev. Lett. **89**, 251802(2002).

[293] M. Goldhaber and J. L. Rosner, Phys. Rev. **D 15**, 1254 (1977).

[294] Z. Z. Xing, Phys. Rev. **D 53**, 204 (1996); Z. Z. Xing, Phys. Lett. **B 372**, 317 (1996); Z. Z. Xing, Phys. Lett. **B 379**, 257 (1996); Z. Z. Xing, Phys. Rev. **D 55**, 196 (1997); Z. Z. Xing, Phys. Lett. **B 463**, 323 (1999).

[295] M. Gronau, Y. Grossman, and J. Rosner, Phys. Lett. **B 508**, 37 (2001).

[296] D. Atwood and A. A. Petrov, Phys. Rev. **D 71**, 054032 (2005).

[297] D. M. Asner and W. M. Sun, Phys. Rev. **D 73**, 034024 (2006).

[298] H. Nelson, Talk given at the 19th International Symposium on Lepton and Photon Interations at High-Energies, Stanford, CA, 9-14 Auguest, 1999, UCSB-HEP-99-08, hep-ex/9908021.

[299] J. H. Christenson, J. W. Croin, V. L. Fitch and R. Turlay, Phys. Rev. Lett. **13**, 138 (1964).

[300] Y. Nir, hep-ph/0510413.

[301] A. D. Sakharov, Pisma Zh. Eksp. Teor. Fiz. 5, 32 (1967) [JETP Lett. **5**, 24 (1967)].

[302] Y. Nir and N. Seiberg, Phys. Lett. **B309**, 337 (1993).

[303] G. Altarelli and F. Feruglio, hep-ph/0306265.

[304] A. De Rujula, M. B. Gavela and P. Hernandez, Nucl. Phys. **B547**, 21 (1999); K. Dick, M. Freund, M. Lindner and A. Romanino, Nucl. Phys. **B562**, 29 (1999); P. Huber, M. Lindner, M. Rolinec, T. Schwetz and W. Winter, hep-ph/0403068.

[305] M. Leurer, Y. Nir and N. Seiberg, Nucl. Phys. **B420**, 468 (1994).

[306] Y. Grossman, A. L. Kagan and Y. Nir, hep-ph/0609178.

[307] D. S. Du, hep-ph/0608313;

[308] I. I. Bigi, Talk at the first International Workshop on τ-Charm Physics (Charm2006), 6-7 June 2006, Beijing, hep-ph/0608073.

[309] F. Buccella *et al.*, hep-ph/9411286.

[310] B. Aubert *et al.*, (BaBar Collaboration), Phys. Rev. **D71**, 091101 (2005).

[311] X. C. Tian, *et al.* (Belle Collaboration), Phys. Rev. Lett. **95**, 231801 (2005).

[312] D. Cronin-Hennessy, *et al.* (CLEO Collaboration), Phys. Rev. **D72**, 031102 (2005).

[313] S. Kopp, *et al.* (CLEO Collaboration), Phys. Rev. **D63**, 092001 (2001).

[314] D. M. Asner *et al.* (CLEO Collaboration), Phys. Rev. **D70**, 091101 (2004).

[315] D. Acosta *et al.* (CDF Collaboration), Phys. Rev. Lett. **94**, 122001(2005).

[316] J. M. Link *et al.* (FOCUS Collaboration), Phys. Lett. **B622**, 239 (2005).

[317] A. A. Petrov, Nucl. Phys. Proc. Suppl. **142**, 333 (2005) [hep-ph/0409130].

[318] I. I. Bigi, Talk in KAON2001: International Conference on CP violation, (2001) [hep-ph/0107102].

[319] D. Cinabro, "*Interference Effects in D Meson Decays*" Presented at Flavor Physics and CP Violation, April 9-12, 2006, Vancouver, BC, Canada.

[320] A. J. Buras, hep-ph/0505175.

[321] H. B. Li and M. Z. Yang, hep-ph/0610073, to appear in Phys. Rev. D.

[322] F. Buccella, M. Lusignoli, and A. Pugliese, Phys. Lett. **B379**, 249 (1996).

[323] F. Buccella, *et al.* Phys. Lett. **B302**, 319 (1993).

[324] R. H. Dalitz, Phil. Mag. 44, 1068 (1953).

[325] J. D. Jackson, Nuovo Cim. 34, 1644 (1964).

[326] B. Kayser, Nucl. Phys. B (Proc. Suppl.) **13**, 487 (1990); G. Valencia, Phys. Rev. **D 39**, 3339 (1989).

[327] A. Datta and A. London, Int. J. of Mod. Phys. **A 19**, 2505 (2004).

[328] G. Burdman, E. Golowich, J. Hewett and S. Pakvasa, Phys. Rev. **D66**, 014009(2002). And references therein.

[329] G. Burdman, E. Golowich, J. Hewett and S. Pakvasa, Phys. Rev. **D52**, 6383 (1995).

[330] C. Greub, T. Hurth, M. Misiak, and D. Wyler, Phys. Lett. B382, 415 (1996).

[331] C. Bajc, S. Fajfer and R. Oakes, Phys. Rev. D54, 5883 (1996); S. Fajfer, S. Prevlosek and P. Singer, Eur. Phys. J. C6, 471 (1999).

[332] O. Tajima et. al. (the Belle Collaboration), Phys. Rev. Lett. 92, 101803 (2004).

[333] G. Buchalla, A. J. Buras and M. E. Lautenbacher, Rev. Mod. Phys. **68**, 1125 (1996).

[334] T. Inami and C.S. Lim, Prog. Theor. Phys. **65**, 1772 (1981).

[335] Such references include C. Greub *et al.*, Phys. Lett. **B382**, 415 (1996); C-H. V. Chang, G-L. Lin and Y-P. Yao, Phys. Lett. **B415**, 395 (1997); L. Reina, G. Ricciardi and A. Soni, Phys. Rev. **D56**, 5805 (1997); D. Choudhury and J. Ellis, Phys. Lett. **B433**, 102 (1998); S. Fajfer, P. Singer and J. Zupan, Phys. Rev. **D64**, 074008 (2001); C. S. Lim, T. Morozumi and A. I. Sanda, Phys. Lett. **B218**, 343 (1989); N.G. Deshpande, J. Trampetic, and K. Panrose, Phys. Rev. **D39**, 1461 (1989); P. Singer and D.-X. Zhang, Phys. Rev. **D55**, R1127 (1997).

[336] L.J. Hall, V.A. Kostelecky, and S. Raby, Nucl. Phys. **B267**, 415 (1986).

[337] For a comprehensive study of FCNC effects in supersymmetry see, S. Bertolini, F. Borzumati, A. Masiero, and G. Ridolfi, Nucl. Phys. **B193**, 591 (1991); F. Gabbiani, E. Gabrielli, A. Masiero and L. Silvestrini, Nucl. Phys. **B477**, 321 (1996); J.L. Hewett and J.D. Wells, Phys. Rev. **D55**, 5549 (1997); P. Cho, M. Misiak, and D. Wyler, Phys. Rev. **D54**, 3329 (1996). For a review see M. Misiak, S. Pokorski and J. Rosiek, in "*Heavy Flavors II*", eds. A.J. Buras and M. Lindner, Adv. Ser. Direct. High Energy Phys. **15**, 795 (1998).

[338] *E.g.*, see J. Ellis and D.V. Nanopoulos, Phys. Lett. **110B**, 44 (1982).

[339] For a recent review, see, B. C. Allanach, A. Dedes and H. K. Dreiner, Phys. Rev. **D60**, 075014 (1999).

[340] N. Arkani-Hamed, S. Dimopoulos, and G. Dvali, Phys. Lett. **B429**, 263 (1998), and Phys. Rev. **D59**, 086004 (1999); I. Antoniadis, N. Arkani-Hamed, S. Dimopoulos, and G. Dvali, Phys. Lett. **B436**, 257 (1998).

[341] I. Antoniadis, Phys. Lett. **B246**, 377 (1990); J. Lykken, Phys. Rev. **D54**, 3693 (1996); E. Witten, Nucl. Phys. **B471**, 135 (1996); P. Horava and E. Witten, Nucl. Phys. **B460**, 506 (1996), *ibid.*, **B475**, 94 (1996).

[342] T.G. Rizzo and J.D. Wells, Phys. Rev. **D61**, 016007 (2000); P. Nath and M. Yamaguchi, Phys. Rev. **D60**, 116006 (1999); M. Masip and A. Pomarol, Phys. Rev. **D60**, 096005 (1999); W.J. Marciano, Phys. Rev. **D60**, 093006 (1999).

[343] See, for example, K. Agashe, N.G. Deshpande, G.H. Wu, Phys. Lett. **B514**, 309 (2001).

[344] L. Randall and R. Sundrum, Phys. Rev. Lett. **83**, 3370 1999 , and *ibid.*, 4690, (1999).

[345] J.L. Hewett, F.J. Petriello, and T.G. Rizzo, SLAC-PUB-9146; arXiv:hep-ph/0203091.

[346] Q. He *et al.*, Phys. Rev. Lett. **95** (2005) 221802.

[347] J. M. Link *et al.*, Phys. Lett. **B572** (2003) 21.

[348] E. M. Aitala *et al.*, Phys. Lett. **B462** (1999) 401.

[349] P. L. Frabetti *et al.*, Phys. Lett.**B398** (1997) 239.

[350] G. Burdman *et al.*, Phys. Rev. **D52** (1995) 6383; Phys. Rev. **D66** (2002) 014009.

[351] G. Burdman and I.Shipsey, Ann. Rev. Nucl. Part. Sci. **53** (2003) 431; S. Bianco, F. L. Fabbri, D. Benson and I. Bigi, Riv. Nuovo Cim. **26N7** (2003) 1.

[352] T. E. Coan *et al.*, Phys. Rev. Lett. **90** (2003) 101801.

[353] A. Freyberger *et al.*, Phys. Rev. Lett. **76** (1996) 3065; erratum, Phys. Rev. Lett. **77** (1996) 2147.

[354] A. Korn *et al.*, hep-ex/0305054.

[355] K. Kodama *et al.*, Phys. Lett. **B345** (1995) 85.

Part VI

τ Physics

Toni Pich, Changzheng Yuan.
Authors: A. A, B. B,....

Chapter 30

τ mass near threshold

Chapter 31

Leptonic τ decays

Chapter 32

Hadronic τ decays

Chapter 33

Search for CP Violation in τ decays[1]

The origin and source of CP violation in fundamental fermion interactions are topics of great interest. CP violation was first seen in the kaon system about 40 years ago and was observed in B decays some 6 years ago [1]. Indication for the existence of neutrino masses and their mixing opens the possibility of CP violation in the neutrino sector [2]. It would be odd if the mixing effects are limited only to the quarks and neutrinos and do not appear in the charged lepton sector. Such mixing may lead CP violation. With in SM, the CKM theory says that CP violation should not occur in the lepton sector. These basic assumptions of CMK must be tested [3].

All CP-violating effects come about due to the interference of at least two amplitudes with a relative weak phase. In the SM all τ decays involve only a virtual W boson, all CP violation in τ decays should vanish. That is, the observation of CP violation in τ decays would be a smoking-gun signal of the New Physics. (Note that there can be a SM CP asymmetry in $\tau \to \pi K_S \nu_\tau$ due to the several amplitudes in K_S. The CP asymmetry is predicted to be $O(10^{-3})$, see Ref. [3]).

Thus if we see CP or T violation in τ hadronic decays, we can infer immediately the existence of another charged boson mediating the weak interaction [4]. In general, the τ decay process described by two amplitudes illustrated in Fig. **??** may have CP-even and $-$odd phases δ and ϕ relative each other. The probability density for such a process is given by [5]:

$$\begin{aligned} |\mathcal{A}|^2 &= (A_1 + A_2 e^{i\phi} e^{i\delta})(A_1 + A_2 e^{-i\phi} e^{-i\delta}) \\ &= A_1^2 + A_2^2 + 2A_1 A_2 \cos(\phi)\cos(\delta) - 2A_1 A_2 \sin(\phi)\sin(\delta). \end{aligned} \tag{33.1}$$

The last term is CP odd since the phase ϕ changes sign under CP conjugation. In this example the CP-odd term is not equal to zero if A_1, A_2, $\sin(\phi)$ and $\sin(\delta)$ are not equal to zero. A_1 and A_2 denote the amplitudes and for physical processes they must be different from zero. Thus the CP-odd term is not equal to zero if the factor $e^{i\phi}$ and $e^{i\delta}$ differ from zero and are complex.

In a theoretical physics model, the possible charged boson is the charged Higgs boson of Lee and Weinberg [6]. The most striking feature of its prediction is that the heavier the particle the larger the CP violation. This should be tested experimentally. However,

[1] By Hai-Bo Li

we should note that the charged boson is not limited only to the charged Higgs boson in Lee-Weinberg model.

Chapter 34

Study of the Lorentz structure in the τ Lepton Decays[1]

34.1 Michel parameters

The Lorentz structure of leptonic decays of the charged leptons is usually described using a set of the coupling constants of the leptons. For the tau lepton decays $\tau \to \ell \nu_\tau \overline{\nu_\ell}$ the matrix element can be written in the form

$$\mathcal{M} = \frac{4G_F}{\sqrt{2}} \sum_{\gamma=S,V,T} \sum_{i,j=L,R} g_{ij}^{\gamma} \langle \overline{\ell}_i | \Gamma^{\gamma} | \nu_\ell \rangle \langle \overline{\nu}_\tau | \Gamma_\gamma | \tau_j \rangle, \tag{34.1}$$

where G_F is the Fermi constant, Γ^γ represents the different types of the charged current - scalar, vector or tensor ($\gamma = S, V \mathrm{or} T$), and i, j are the chiralities of the tau lepton and the daughter lepton.

The g_{ij}^{γ} are the twelve complex coupling constants, of which two, g_{LL}^{T} and g_{RR}^{T} are exactly zero. In the Standard model $g_{LL}^{V} = 1$ and all the other couplings are zero. Therefore the precision measurement of the constants g_{ij}^{γ} provides an important test of the Standard Model.

The coupling constants can be experimentally accessed via the energy spectra of the daughter leptons from the tau decays. The polarisation of the daughter leptons usually can not be measured; however the polarisation of the tau lepton P_τ in principle can be measured through its decay spectra. Under these assumptions the spectrum of the tau decays predicted by (34.1) can be parametrized at Born level by the following sum of polynomials h:

$$\frac{1}{\Gamma}\frac{d\Gamma}{dx_\ell} = h_0(x_\ell) + \eta h_\eta(x_\ell) + \rho h_\rho(x_\ell) - P_\tau \left[\xi h_\xi(x_\ell) + \xi\delta h_{\xi\delta}(x_\ell)\right], \tag{34.2}$$

where P_τ is the average tau polarization and $x_\ell = E_\ell / E_{max}$ is the "reduced energy" of the daughter lepton, or the ratio of its energy to the maximum possible energy. Examples of the polynomials h are illustrated in Fig.34.1.

[1] By Igor R. Boyko. and Dedovich Dima

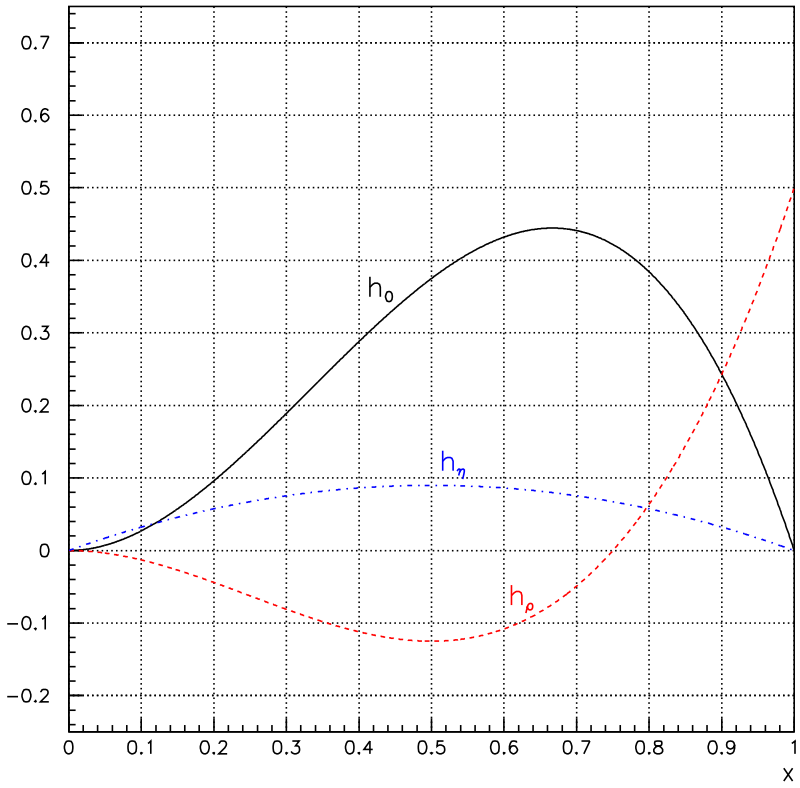

Figure 34.1: The shapes of polynomial functions h for the Michel parametrisation of tau decays.

The coefficients η, ρ, ξ, $\xi\delta$ known as Michel parameters [7] are bilinear combinations of the coupling constants from (34.1). The set of the four Michel parameters carries the full information on the coupling constants that can be extracted from the decay spectra of the tau leptons (without the measurement of the polarisation of the final state leptons).

In the Standard Model the following values of the Michel parameters are predicted: $\rho = 0.75$; $\eta = 0$; $\xi = 1$; $\xi\delta = 0.75$. An observation of different values of the Michel parameters would indicate a violation of the standard Model.

34.2 Anomalous tenzor coupling

The parametrization presented in Eq.34.1 is based on certain assumptions; namely it assumes the lepton number conserving, derivative-free, local, Lorentz invariant, 4-fermion point interaction. While most of these assumptions are quite natural, there is no fundamental reason to assume that the interaction Lagrangian does not include derivatives.

Such anomaluos interaction involving the derivatives (which can only be a tenzor interaction) can be represented in the following form [8]:

$$\mathcal{L} = \frac{g}{\sqrt{2}}\, W^{\alpha} \left\{ \overline{\tau}\gamma_{\alpha}\frac{1-\gamma^5}{2}\nu + \frac{\kappa_{\tau}^{W}}{2m_{\tau}}\partial_{\beta}\left(\overline{\tau}\sigma_{\alpha\beta}\frac{1-\gamma^5}{2}\nu\right)\right\} + \text{h.}c., \tag{34.3}$$

where κ_{τ}^{W} is the strength of the anomalous coupling. Such anomaluos interaction can be studied through the possible distortions of the energy spectra of tau decays. Since the Lagrangian (34.3) explicitly contains derivatives, the distortions of the energy spectra can not be described in terms of the known Michel parameters.

The matrix element for the purely leptonic tau decays takes the form:

$$\mathcal{M} = \frac{4G}{\sqrt{2}}\langle\overline{v}_{l}\mid\gamma_{\alpha}\mid v_{\overline{\nu}_{l}}\rangle\left(\langle\overline{v}_{\nu_{\tau}}\mid\gamma_{\alpha}\mid u_{\tau_{L}}\rangle - i\frac{\kappa_{\tau}^{W}}{2m_{\tau}}q_{\beta}\langle\overline{v}_{\nu_{\tau}}\mid\sigma_{\alpha\beta}\mid u_{\tau_{R}}\rangle\right), \tag{34.4}$$

where q is the momentum of W. The first summand in (34.4) is the Standard model prediction, while the second one is the contribution of the anomalous coupling (in the framework of the Standard model $\kappa_{\tau}^{W} = 0$). In principle, both the anomalous coupling κ_{τ}^{W} and the "standard" couplings g_{ij}^{γ} can take non-Standard model values simultaneously. In this case the first summand in (34.4) has to be replaced by the full parametrisation (34.1).

Like the case of Michel parameters, the contribution of the anomalous tenzor coupling can be also parametrized in terms of the polynomials. The approximate shape of the energy spectrum is

$$\frac{1}{\Gamma}\frac{d\Gamma}{dx_{\ell}} \sim x_{\ell}^{2}\cdot\left(-2x_{\ell}+3+2\cdot\kappa_{\tau}^{W}\cdot x_{\ell}\right) \tag{34.5}$$

Fig.34.2 compares the deviations of the decay spectrum from the Standard Model prediction for the non-Standard Model values of κ_{τ}^{W} and of the Michel parameter ρ. One can see that the change of shape is significantly different for the two cases, which makes it makes it possible to measure the two parameters simultaneously.

34.3 Measurement of Michel parameters and search for the anomaluos tenzor coupling

The Michel parameters have been extensively measured in tau lepton decays by many experiments. The current experimental uncertainty is typically one or few percent. For example, the uncertainty on the parameter ρ is about 0.008 and for η the uncertainty is 0.07 . The anomalous tenzor coupling so far has been studied only by DELPHI experiment. The coupling constant κ_{τ}^{W} was measured with a precision of 0.04 and was found to be consistent with zero.

The BES-III experiment will be an abundant source of tau lepton decays with accurately measured energy spectrum. This provides an excellent possibility to improve significantly the current knowledge on the Lorentz structure in tau decays. This section presents a Monte-Carlo estimate of the possible reach of BES-III in measuring the Michel parameters and in the search for the anomaluos tenzor coupling. For simplicity only two Michel parameters ρ and η were considered.

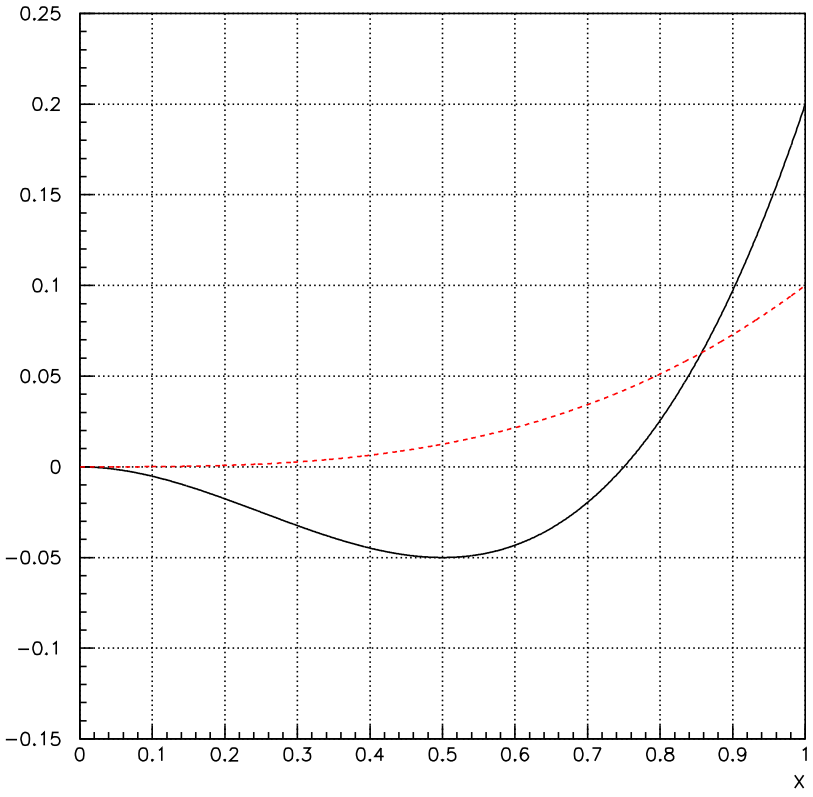

Figure 34.2: The deviation of the spectrum of leptons from tau decays from the Standard model prediction. Dashed line: for the non-zero value of the anomaluos tenzor coupling. Solid line: for $\rho \neq 0.75$.

The simulation was based on the version 5.1 of BESIII software release. The events were generated at the CMS energy 3.69 GeV, where the background from hadronic events is minimal. The following statistics has been simulated: 100K Bhabha scattering events $ee \to ee$; 20K dymuon events $ee \to \mu\mu$; 100K hadronic events $ee \to qq$. The total number of simulated tau pair events was 100K. The simulated signal was limited to the decay channel $ee \to \tau\tau \to e\mu(+neutrinos)$. This channel represents only about 3% of the total tau pairs, but it is rather easy for the events selection. A possible inclusion of the hadronic tau decays can increase the available statistics very significantly, therefore the results presented in this section can be considered as a conservative estimate of the possible BES-III reach.

The analysis was restricted to the angular region $|\cos\theta| < 0.83$. The event selection was based on the particle identification. Exactly two charged particles had to be reconstructed in the event. One of them was required to be identified as an electron, another had to be a muon. The main criterion for particle identification was based on the dE/dx pull variable, i.e. the deviation of the measured dE/dx value from the expected

one, expressed in units of dE/dx uncertainty. Fig. 34.3 shows the pulls of muon and electron hypotheses for the electron and muon candidates respectively. One can see that the dymuon and Bhabha events are rejected very efficiently.

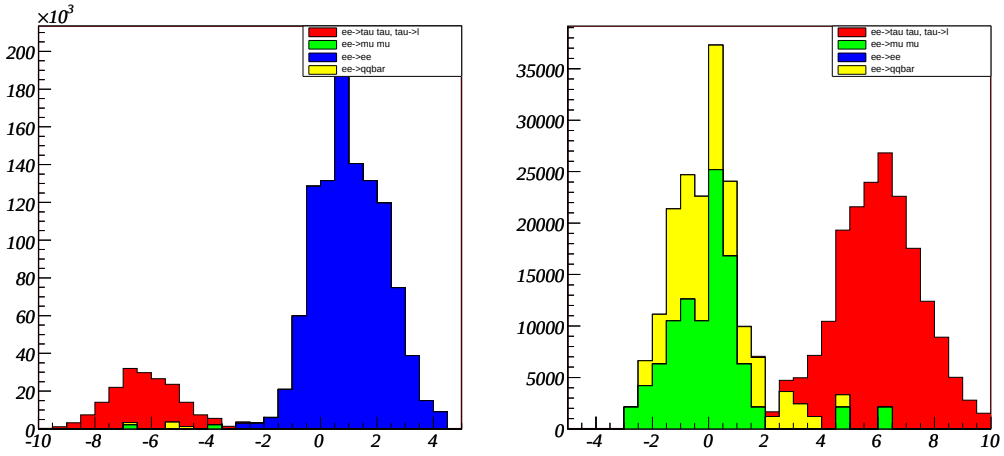

Figure 34.3: Left: the muon hypothesis pull for the electron candidate. Right: the electron hypothesis pull for the muon candidate. The selection cuts were +3 for the electron candidate and -3 for the muon candidate.

Several additional cuts were applied for the further background suppression. The electron and muon candidates had to be identified by EMC and muon chambers respectively. Fig.34.4 illustrates the selection criteria. In addition, TOF identification was used to reject protons and kaons from hadronic events in the momentum regions where dE/dx of these particles is close to that of electrons.

The signal selection efficiency was found to be about 30% (with respect to the full solid angle). For the 5 fb^{-1} integrated luminosity such efficiency corresponds to 180K selected signal events. The residual background was 6%, about half of which were the hadronic events $ee \to qq$. The momentum spectra of the selected electron and muon candidates are presented in Fig.34.5

The spectra of reconstructed momenta of electrons and muons from tau decays were fitted by the expectations for the different values of the Michel parameter ρ and the anomalous coupling constant κ_τ^W. The statistical uncertainties of the fit parameters were the following:

$$\sigma(\rho) = 0.003$$

$$\sigma(\eta) = 0.02$$

$$\sigma(\kappa_\tau^W) = 0.002$$

The statistical errors correspond to the 5 fb^{-1} collected at the CMS energy 3.69 GeV.

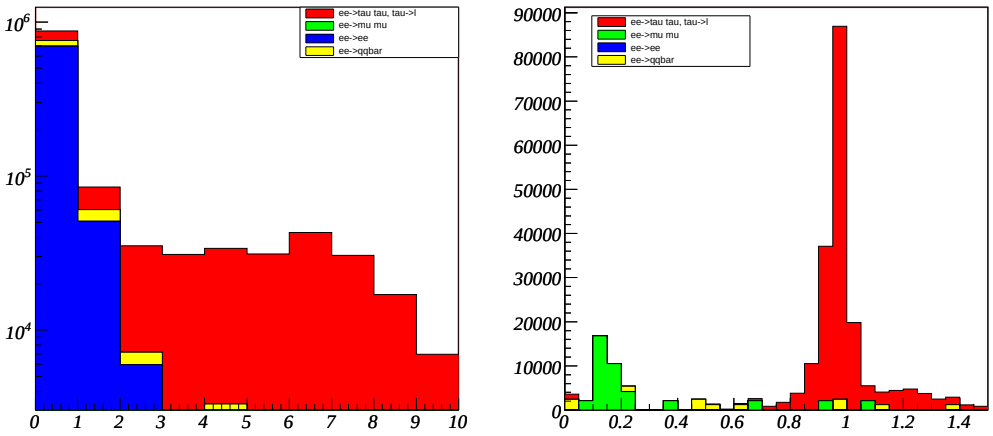

Figure 34.4: Left: the number of hits in muon chambers associated with the muon candidates. Right: the relative electromagnetic energy deposition E/P in the EMC for the electron candidates. The selection cuts were: $N_{HIT} \geq 3$ for muons and $E/P > 0.8$ for electrons.

34.4 Summary

The BES-III experiment will provide an excellent possibility to study the Lorentz structure in tau decays, including the measurements of the Michel parameters and a search for the anomalous tenzor coupling. The conservative estimates based on Monte-Carlo simulation suggest that the current precision on the Michel parameters can be improved by factors of 2-4, and the limits on the anomalous coupling constant κ_τ^W can be improved by at least a factor of 10. Inclusion of the hadronic tau decays into analysis can significantly improve the precision.

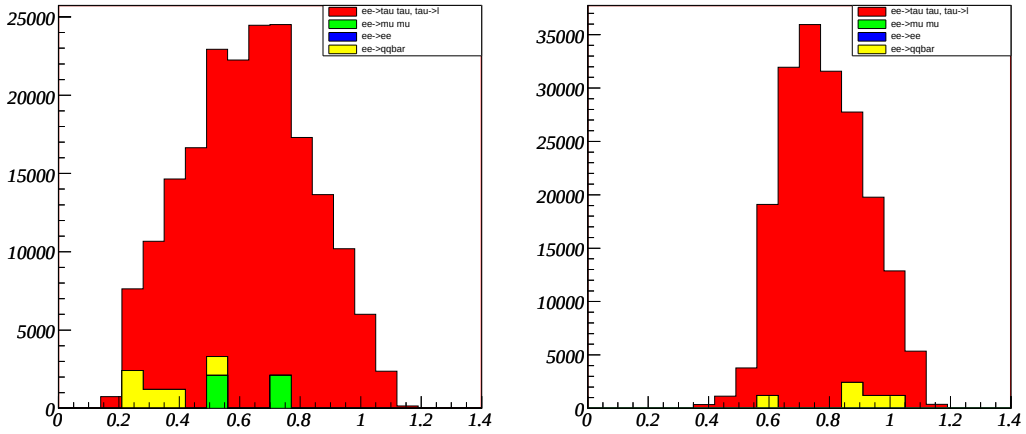

Figure 34.5: The momentum spectra of the selected muon (left) and electron (right) candidates. The statistics corresponds to 5 fb^{-1}.

Bibliography

[1] W.M. Yao et. al. (Particle Data Group), J. Phys. **G 33** (2006) 1.

[2] W. J. Marciano, hep-ph/0108181.

[3] I. I. Bigi and A. I. Sanda, Phys. Lett. B **625**, 47 (2005).

[4] Y. S. Tsai, Nucl. Phys. B (Proc. Suppl.) bf 55C, 293 (1997);J. H. Kuhn and E. Mirkes, Phys. Lett. **B 398**, 407 (1997).

[5] CLEO Collaboration, P.Avery *et al.*, Phys. Rev. **D 64**, 092005 (2001).

[6] T. D. Lee, Phys. Rev. **D 8**, 1226 (1973); S. Weinberg, Phys. Rev. Lett. **37**, 657 (1976).

[7] L. Michel, Proc. Phys. Soc. **A63** (1950) 514;
C. Bouchiat and L. Michel, Phys. Rev. **106** (1957) 170.

[8] M.Chizhov, hep-ph/9612399

Part VII

Comparison with other facilities and future prospects

Cai-Dian Lu, Shan Jin.
Authers: A. A, B. B, ...

Chapter 35

τ-Charm physics at B factories

Chapter 36

Opportunities of τ-Charm physics at Super-B factories

Chapter 37

Do we need a Super-Charm factories

In order to establish the need for Super-Charm factories we need to first assess the charm physics reach of existing and potential future facilities including BESIII, the B-factories BABAR and Belle, and a Super B-factory. We compare the physics reach in the following tables

1. Hadronic D, D^+, D_s^+ Decays
2. Exclusive Semileptonic Decays
3. Inclusive Semileptonic Decays
4. Leptonic Decacys
5. Rare Decays
6. Charm Mixing
7. CPV
8. Λ_c

Also we should consider the impact of these measurements on the CKM matrix.

Luminosity assumptions are

1. CLEO-c 0.75 pb^{-1} at $\psi(3770)$ and 0.75 pb^{-1} at 4170 MeV obtained by 2008
2. BESIII 20 pb^{-1} at $\psi(3770)$ and 12 pb^{-1} at 4170 MeV - 8 years of running
3. BaBar + Belle 2 ab^{-1} in 2009
4. 1 year at Super-B 15 ab^{-1}
5. 5 years at Super-B 75 ab^{-1}

Table 37.1: Hadronic D, D^+, D_s^+ Decays

Process	CLEO-c	BESIII	B-factory	Super-B (1)	Super-B (5)
Normalization Modes					
$D^0 \to K\pi$	1.25%		2.1%		
$D^+ \to K\pi\pi$	1.4%				
$D_s^+ \to KK\pi$	4%				
Cabibbo Favored BF					
D^0[1]	0.35%/track,1.1%/K_S^0,2.0%/π^0				
D^+[1]	0.35%/track,1.1%/K_S^0,2.0%/π^0				
D_s^+[1]	0.35%/track,1.1%/K_S^0,2.0%/π^0				
CF Dalitz Plots					
$D \to K^-\pi^+\pi^0$					
$D^+ \to K^-\pi^+\pi^+$					
$D_s^+ \to K^-K^+\pi^+$					
SCS Dalitz Plots					
$D^0 \to \pi\pi\pi^0$					
DCS Dalitz Plots					
$D \to K^+\pi^-\pi^0$					
Inclusive BF					
K (D^0, D^+, D_s^+)					
η (D^0, D^+, D_s^+)	4.0%(sys.)[3]				
η' (D^0, D^+, D_s^+)	4.7%(sys.)[3]				
ϕ (D^0, D^+, D_s^+)	3.4%(sys.)[3]				
Dalitz Plots -impact					
D^0 (CKM angle γ[4])	6^o(sys.)	$< 2^o$(sys.)	7°	$< 3^o$	$\sim 1^o$
D^0 (D had BF)	okay[5]	okay[5]			
D^+ (D had BF)	okay[5]	okay[5]			
D_s^+ (D had BF)	okay[5]	okay[5]			
SCS BF					
$D^0 \to \pi\pi$	3%[6]				
$D^0 \to \pi\pi\pi^0$	3%[6]				
$D^0 \to \pi\pi\pi^0\pi^0$[6]	6%				
$D^+ \to \pi\pi^0$	5%[6]				
$D^+ \to \pi\pi^0\pi^0$	6%[6]				
DCS BF					
$D^0 \to K^0\pi^0$					
$D^+ \to K^0\pi^+$					

Table 37.2: Exclusive Semileptonic Decays

Process	CLEO-c	BESIII	B-factory	Super-B (1)	Super-B (5)	Comment
$D^0 \to K\ell\nu$ (BF)	1%	0.2%[7]	0.75%			$\|Vcs\|$
$D^+ \to K\ell\nu$ (BF)		0.3%[7]				$\|Vcs\|$
$\frac{\Gamma(D^0\to K^- e^+\nu)}{\Gamma(D^+\to \bar{K}^0 e^+\nu)}$						
$\frac{\Gamma(D^0\to K^{*-} e^+\nu)}{\Gamma(D^+\to \bar{K}^{*0} e^+\nu)}$						
$\frac{\Gamma(D^0\to \pi^- e^+\nu)}{\Gamma(D^+\to \pi^0 e^+\nu)}$						
$\frac{\Gamma(D^0\to \rho^- e^+\nu)}{\Gamma(D^+\to \rho^0 e^+\nu)}$						
$D \to K\ell\nu$ (α_{pole})						$\|Vcs\|$
$D \to K\ell\nu$ (m_{pole})						$\|Vcs\|$
$D \to (K^*, K\pi)\ell\nu$ (BF)						$\|Vcs\|$
$D \to (K^*, K\pi)\ell\nu$ (α_{pole})						$\|Vcs\|$
$D \to (K^*, K\pi)\ell\nu$ (m_{pole})						$\|Vcs\|$
$D^0 \to \pi\ell\nu$ (BF)	2.3%	0.4%[7]	2.8%			$\|Vcd\|$, $\|Vub\|$
$D^+ \to \pi\ell\nu$ (BF)		0.8%[7]				$\|Vcd\|$, $\|Vub\|$
$D \to \pi\ell\nu$ (α_{pole})						$\|Vcd\|$, $\|Vub\|$
$D \to \pi\ell\nu$ (m_{pole})						$\|Vcd\|$, $\|Vub\|$
$D \to (\eta, \rho, \omega, \pi\pi)\ell\nu$ (BF)						$\|Vcd\|$, $\|Vub\|$
$D \to (\eta, \rho, \omega, \pi\pi)\ell\nu$ (α_{pole})						$\|Vcd\|$, $\|Vub\|$
$D \to (\eta, \rho, \omega, \pi\pi)\ell\nu$ (m_{pole})						$\|Vcd\|$, $\|Vub\|$
$D_s \to \phi\ell\nu$ (BF)		1.2%[7]				
$D_s \to \eta\ell\nu$ (BF)						
$D_s \to (\eta, \phi)\ell\nu$ (α_{pole})						
$D_s \to (\eta, \phi)\ell\nu$ (m_{pole})						
$D_s \to (K, K^*, K\pi)\ell\nu$ (BF)						
$D_s \to (K, K^*, K\pi)\ell\nu$ (α_{pole})						
$D_s \to (K, K^*, K\pi)\ell\nu$ (m_{pole})						

Table 37.3: Inclusive Semileptonic Decays

Process	CLEO-c	BESIII	B-factory	Super-B (1)	Super-B (5)	Comment
$D^0 \to \ell X$ (BF)	2%					
$D^+ \to \ell X$ (BF)	2%					
$D \to \ell X$ (e, μ spectra)						
$D \to \nu X$ (BF)						
$D \to \nu X$ (ν spectrum)						
$D_s \to \ell X$ (BF)						
$D_s \to \ell X$ (e, μ spectra)						

Table 37.4: Leptonic Decays

Process	CLEO-c	BESIII[7]	B-factory	Super-B (1)	Super-B (5)	Comment
$D \to \mu\nu$	9%[9]	2%				f_D, f_B
$D \to e\nu$	1e-3[9]	(e-5,e-6)				NP
$D_s \to \mu\nu$	9%[9]	2%				f_{D_s}, f_{B_s}
$D_s \to \tau\nu$		1.5%				f_{D_s}, f_{B_s}, NP
$D_s \to e\nu$						NP
$D \to ee$	3e-6[8]	3e-8				
$D \to \mu\mu$	3e-6[8]	3e-8				
$D \to e\mu$	3e-6[8]	3e-8				

Table 37.5: Rare Decays

Process	CLEO-c[8]	BESIII[7]	B-factory	Super-B (1)	Super-B (5)	Comment
Radiative						
$D \to \rho\gamma$	4e-6	(e-5,e-6)				
$D \to \omega\gamma$	2e-5	(e-5,e-6)				
$D \to \phi\gamma$	1e-5	(e-5,e-6)				
$D \to K^*\gamma$	3e-5	(e-5,e-6)				
$D \to \gamma\gamma$	3e-6	5e-8				
Leptonic						
$D \to ee$	3e-6	3e-8				
$D \to \mu\mu$	3e-6	3e-8				
$D \to e\nu$	1.5e-5[9]					
$D_s \to e\nu$						
GIM suppressed						
$D^0 \to \pi^0 ee$	1e-5	5e-8				
$D^0 \to \pi^0\mu\mu$		5e-8				
$D^0 \to \eta ee$	2.5e-5	1e-7				
$D^0 \to \eta\mu\mu$		1e-7				
$D^0 \to K^0_S ee$	1.8e-5	1e-7				
$D^0 \to K^0_S\mu\mu$		1e-7				
$D^+ \to hee$	4e-6[10]	3e-8				
$D^+ \to h\mu\mu$		3e-8				
LFV						
$D \to e\mu$	3e-6	3e-8				
$D^0 \to \pi^0 e\mu$		5e-8				
$D^0 \to \eta e\mu$		1e-7				
$D^0 \to K^0_S e\mu$		1e-7				
$D^+ \to he\mu$		3e-8				
LNV						
$D^+ \to he^+e^+$	2.4e-6[10]	3e-8				
$D^+ \to h\mu^+\mu^+$		3e-8				
$D^+ \to he^+\mu^+$		3e-8				
$D^+_s \to K^-e^+e^+$						
$D^+_s \to K^-\mu^+\mu^+$						
$D^+_s \to K^-e^+\mu^+$						

Table 37.6: Charm Mixing

Process	CLEO-c	BESIII	B-factory[11]	Super-B (1)	Super-B (5)	Comment
Time Dependent						
hadronic (95% C.L.)						
$x'^2/2$	-	-	$< 0.016\%$			
y'	-	-	$< 1\%$			
$\delta_{K\pi}$	-	-	-			
CP eigenstate (1σ)						
y	-	-	2e-3			
A_Γ	-	-	2e-3			
Semileptonic (95% C.L.)						
R_M	-	-	4e-4			
Dalitz Plots (95% C.L.)						
x			0.5%			
y			0.3%			
Quantum Correlation[12]						
x	2.5%		-	-	-	-
y	1.2%		-	-	-	-
$\cos\delta_{K\pi}$	0.13		-	-	-	-

Table 37.7: CP and T Violation

Process	CLEO-c	BESIII	B-factory	Super-B (1)	Super-B (5)	Comment
Cabibbo Favoured						
SCS						
DCS						
Mixing						
Dalitz-plots						
T-odd Correlations						

Table 37.8: Λ_c

Process	CLEO-c	BESIII	B-factory	Super-B (1)	Super-B (5)	Comment
$\Lambda_c \to pK\pi$	-	-				
$\Lambda_c \to \Lambda\ell\nu$	-	-				
$\Lambda_c \to \ell X$	-	-				

Table 37.9: CKM Impact

Process	CLEO-c	BESIII	B-factory	Super-B (1)	Super-B (5)	Comment
$\|V_{cd}\|$ $\|V_{cs}\|$ $\|V_{cb}\|$ $\|V_{ts}\|$ $\|V_{td}\|$ $\|V_{ub}\|$	2%					
CKM angle α $\pi\pi\pi^0$ Dalitz plot $\rho\pi$ $\rho\rho$						
CKM angle β tree penguin						
CKM angle γ ADS GLW Dalitz 4-Body						

Bibliography

[1] update of Ref.[2] with 281 pb^{-1} to be presented at ICHEP06.

[2] Q. He *et al.* [CLEO Collaboration], Phys. Rev. Lett. **95**, 121801 (2005) [arXiv:hep-ex/0504003].

[3] Private Communication with Sheldon Stone.

[4] A. Bondar and A. Poluektov, arXiv:hep-ph/0510246.

[5] For D^0, D^+, and D_s^+ from produced at threshold the amplitude analysis for multibody modes should always result in a systematic uncertaintly less the statistical error.

[6] Extrapolated from P. Rubin *et al.* [CLEO Collaboration], Phys. Rev. Lett. **96**, 081802 (2006) [arXiv:hep-ex/0512063].

[7] H. Li, arXiv:hep-ex/0605004.

[8] R. A. Briere *et al.* [CLEO Collaboration], CLNS 01-1742, (2001).

[9] Extrapolated from M. Artuso *et al.* [CLEO Collaboration], Phys. Rev. Lett. **95**, 251801 (2005) [arXiv:hep-ex/0508057].

[10] Extrapolated from Q. He *et al.* [CLEO Collaboration], Phys. Rev. Lett. **95**, 221802 (2005) [arXiv:hep-ex/0508031].

[11] Extrapolated from D. Asner, "$D^0! - \overline{D}^0$ Mixing", to appear in the Review of Particle Physics, 2006.

[12] D. M. Asner and W. M. Sun, Phys. Rev. D **73**, 034024 (2006) [arXiv:hep-ph/0507238].

Acknowledgements

The authors would like to thank .....

Appendix A

Statistics in HEP data analysis[1]

This Appendix introduces an overview of two aspects of statistical methods used in High Energy Physics (HEP)- parameter estimation and hypothesis testing. For the detail, it is recommended to refer to the relevant textbooks [1, 2, 3] and literatures [4], and references quoted in this Appendix. In an experiment of HEP, an observable x usually is a random variable, its *pdf* is expressed as $f(x,\theta)$ with parameter θ, what the experiment obtained is an sample of x:$\overrightarrow{x} = (x_1, ..., x_n)^T$. The task of the statistical inference is based on the sample of data to determine the value and error, or a confidence interval at given confidence level for the parameter θ, or infer observable's *pdf* $f(x,\theta)$.

A.1 Parameter estimation

Parameter θ is estimated with a function of sample of observed data: $\hat{\vartheta}(x_1, ..., x_n)$, which is called an estimator of θ. The sample of observed data $\overrightarrow{x} = (x_1, ..., x_n)^T$ is also a random variable, the value of the estimator to a specific measurement of $(x_1, ..., x_n)^T$ is called an estimate. Throughout this Appendix, we will use same donation to denote estimate and estimator. An good estimator should have properties of consistency, unbiasedness and high efficiency.

The consistency means when the size of the data sample $(x_1, ..., x_n)$ goes to infinity, the estimator $\hat{\theta}$ converges to the true value of parameter θ.

The bias of an estimator is defined as the difference of the expectation of the estimator and the true value θ: $E(\hat{\theta}) = \theta + b(\theta)$. The unbiasedness is a property of an estimator in finite sample, namely, it is required $E(\hat{\theta}) = \theta$. If it has to be estimated with a biased estimator, then the bias b of the estimator should be known or can be obtained by some way.

The efficiency is a measure of the variance of an estimator. Under the regularity conditions, namely, if the range of $\vec{x}$ is independent of θ and the first and second derivatives of the sample's joint *pdf* - Likelihood function $L(\vec{x}|\theta) = \prod_{i=1}^{n} f(x_i,\theta)$ - with respect to θ exist, there exists a lower bound on the variance of the estimates derived from an estimator, which is called the minimum variance bound MVB, given by Cramer-Rao

[1] By Yong-Sheng Zhu

inequality:

$$MVB = \frac{(1 + \frac{\partial b}{\partial \theta})}{I(\theta)}, \tag{A.1}$$

where $I(\theta)$ is the Fisher information:

$$I(\theta) = E[(\frac{\partial lnL}{\partial \theta})^2] = \int (\frac{\partial lnL}{\partial \theta})^2 \cdot Ld\vec{x} = E[-\frac{\partial^2 lnL}{\partial \theta^2}] = \int (-\frac{\partial^2 lnL}{\partial \theta^2}) \cdot Ld\vec{x}. \tag{A.2}$$

The efficiency of an estimator $\hat{\theta}$ is defined as $e(\hat{\theta}) = MVB/V(\hat{\theta})$. Apparently, we hope the efficiency of the used estimator is close or equal to 1.

The mean-square error (MSE) of an estimator is a convenient quantity which combine the uncertainties in an estimator due to bias and variance:

$$MSE = E[(\hat{\theta} - \theta)^2] = V(\hat{\theta}) + b^2. \tag{A.3}$$

A.1.1 Estimators for mean and variance

Suppose we are interested in the expectation μ of an observable x (random variable) and its variance, σ^2. We have a set of n independent measurements x_i, which have same unknown expectation μ and common unknown variance σ^2. This corresponds to, for instance, a set of n measurements for an observable x in an experiment. Then their consistent and unbiased estimate are the sample mean $\bar{x}$ and sample variance S^2, respectively:

$$\hat{\mu} = \bar{x} = \frac{1}{n}\sum_{i=1}^{n} x_i, \tag{A.4}$$

$$\hat{\sigma^2} = S^2 = \frac{1}{n-1}\sum_{i=1}^{n}(x_i - \bar{x})^2. \tag{A.5}$$

The variance of $\hat{\mu}$ is σ^2/n, while the variance of $\hat{\sigma^2}$ is

$$V(\hat{\sigma^2}) = \frac{1}{n}(m_4 - \frac{n-3}{n-1}\sigma^4), \tag{A.6}$$

where m_4 is the 4th central moment of x.

For the known μ, the consistent, unbiased estimator of variance is

$$\hat{\sigma^2} = \frac{1}{n}\sum_{i=1}^{n}(x_i - \mu)^2, \tag{A.7}$$

which gives a somewhat better estimator of σ^2 compared with Eq. A.5 for unknown μ case. For the binomial, Poisson and Gaussian variables x_i, which are often used in data analysis, the sample mean is an efficient estimator for μ; For the normal variables, Eq. A.7 is an efficient estimator of σ^2 in the case of known μ, and sample variance S^2 is an asymptotic efficient estimator for σ^2.

For the Gaussian distributed x_i, Eq. A.6 becomes $V(\hat{\sigma^2}) = 2\sigma^4/(n-1)$ for any $n \geq 2$, and for large n the standard deviation of $\hat{\sigma}$ (the "error of the error") is $\sigma/\sqrt{2n}$.

If the x_i have different, known variance σ_i^2, which corresponds to the situation that different experiments measure the same quantity with different uncertainties. Assume x_i can be considered as a measurement of the Gaussian distributed variable $N(\mu, \sigma_i^2)$, then the unbiased estimator of the physics quantity μ is a weighted average

$$\hat{\mu} = \frac{1}{\omega} \sum_{i=1}^{n} \omega_i x_i, \tag{A.8}$$

where $\omega_i = 1/\sigma_i^2$, $\omega = \sum_i \omega_i$, and the standard deviation of $\hat{\mu}$ is $1/\sqrt{\omega}$.

A.1.2 The method of maximum likelihood(ML)

From the statistical point of view, the method of maximum likelihood (ML) is the most important general method of estimation, as the ML estimator of parameter has many good properties.

The ML estimators for parameter and its error

Suppose $x_i, i = 1, ..., n$ are the n independent measurements of a random variable x with the *pdf* $f(x, \vec{\theta})$, where $\vec{\theta} = (\theta_1, ..., \theta_k)^T$ are k parameters to be determined, then the ML estimators $\hat{\vec{\theta}}(x_1, ..., x_n)$ are the values of $\vec{\theta}$ that maximize the likelihood function

$$L(\vec{x}|\hat{\vec{\theta}}) = \prod_{i=1}^{n} f(x_i; \vec{\theta}). \tag{A.9}$$

Since both lnL and L are maximized for the same parameters values $\vec{\theta}$ and it is usually easier to work with lnL, therefore, the ML estimators can be found by solving the likelihood equations

$$\frac{\partial lnL}{\partial \theta_i} = 0, \qquad i = 1, ..., k. \tag{A.10}$$

The ML estimator is invariant under change of parameter, namely, under an one-to-one change of parameters from $\vec{\theta}$ to $\vec{\eta}$, the ML estimators $\hat{\vec{\theta}}$ transform to $\vec{\eta}(\vec{\theta}) : \hat{\vec{\eta}}(\vec{\theta}) = \vec{\eta}(\hat{\vec{\theta}})$. Moreover, the ML estimators are asymptotic unbiased. When the likelihood function satisfies the regularity conditions, the ML estimators are consistent estimators. If there exist the efficient estimators for parameters or their functions, then the efficient estimators must be the ML estimators, and the likelihood equations give the unique solutions; while if the efficient estimators do not exist, the ML estimators give possibly minimum variance for $\vec{\theta}$. For large size n and the likelihood function satisfies the regularity conditions, $\hat{\vec{\theta}}$ asymptotically distributed as a normal variable with the mean being the true values $\vec{\theta}$ and the variances reach the MVB.

The ML estimators give only the values of the parameters. To know the errors of the parameters, one has to know the variances of parameters. The expression of the covariance between parameters $\hat{\theta}_i$ and $\hat{\theta}_j$ for any size of sample n is

$$V_{ij}(\hat{\vec{\theta}}) = \int (\hat{\theta}_i - \theta_i)(\hat{\theta}_j - \theta_j) L(\vec{x}|\vec{\theta}) d\vec{x}, \qquad i, j = 1, ..., k. \tag{A.11}$$

The calculation of this integral is sometimes troublesome, however, in general, it can be calculated with numerical method in any case.

For the case that $\hat{\theta}$ is an efficient estimator of single parameter, following equation is applicable for any size of sample n:

$$V(\hat{\theta}) = \frac{(1+\frac{\partial b}{\partial \theta})^2}{(-\frac{\partial^2 lnL}{\partial \theta^2})_{\theta=\hat{\theta}}}; \tag{A.12}$$

In particular, if $\hat{\theta}$ is an unbiased efficient estimator

$$V(\hat{\theta}) = \frac{1}{(-\frac{\partial^2 lnL}{\partial \theta^2})_{\theta=\hat{\theta}}}. \tag{A.13}$$

For multi-parameters and large n, if there exists a set of k jointly sufficient statistics $t_1, ..., t_k$ for the k parameters $\theta_1, ..., \theta_k$, the inverse of the covariance matrix $V_{ij} = cov(\hat{\theta}_i, \hat{\theta}_j)$ for a set of ML estimators can be calculated by

$$V_{ij}^{-1}(\hat{\vec{\theta}}) = (-\frac{\partial^2 lnL}{\partial \theta_i \partial \theta_j})_{\vec{\theta}=\hat{\vec{\theta}}}\ , \qquad i,j = 1, ..., k. \tag{A.14}$$

Besides, for large n and the likelihood function satisfying the regularity conditions, the ML estimators $\hat{\vec{\theta}}$ asymptotically distributed as a multi-dimensional normal variable, then one has

$$V_{ij}^{-1}(\hat{\vec{\theta}}) = E(-\frac{\partial^2 lnL(\vec{x}|\vec{\theta})}{\partial \theta_i \partial \theta_j})_{\vec{\theta}=\hat{\vec{\theta}}} = \int (-\frac{\partial^2 lnL(\vec{x}|\vec{\theta})}{\partial \theta_i \partial \theta_j})_{\vec{\theta}=\hat{\vec{\theta}}} \cdot L d\vec{x}, \qquad i,j = 1, ..., k; \tag{A.15}$$

or, one can use the *pdf* of the random variable x to calculate the covariance matrix:

$$V_{ij}^{-1}(\hat{\vec{\theta}}) = n \int \frac{1}{f}(\frac{\partial f}{\partial \theta_i})(\frac{\partial f}{\partial \theta_j}) dx, \qquad i,j = 1, ..., k. \tag{A.16}$$

Wherein, the last equation uses only the *pdf* of the random variable x and does not need the measured data sample, which is particularly useful in the design stage of an experiment.

If the observable x is a normal random variable, or the size of sample n is sufficiently large, then the likelihood function is an asymptotically normal distribution and lnL is a parabolic function, a numerically equivalent way of determining s-standard-deviation errors is from the contour given by the $\vec{\theta}'$ such that

$$lnL(\vec{\theta}') = lnL_{max} - \frac{s^2}{2}, \tag{A.17}$$

where L_{max} is the value of lnL at the solution point. The extreme limits of this contour on the θ_i axis give an s-standard-deviation likelihood interval for θ_i. In the case lnL is not a parabolic function, the approximate 1-standard-deviation likelihood interval can also be estimated by this equation, and it will give an asymmetric positive and negative errors for each parameter, namely, $\sigma^+(\theta_i) \neq \sigma^-(\theta_i), i = 1, ..., k$.

The ML method for binned data

In the case that the size n of data sample $\vec{x} = (x_1, ..., x_n)^T$ is sufficiently large, the measurements often are expressed as a histogram binned data. For constant n, the likelihood function (joint *pdf*) of $n_i (i = 1, ..., m)$ measurement values appearing in i-th bin is expressed as a multinomial distribution

$$L(n_1, ..., n_m|\vec{\theta}) = n! \prod_{i=1}^{m} \frac{1}{n_i!} p_i^{n_i}. \tag{A.18}$$

The probability of one measurement value appearing in i-th bin is calculated with *pdf* $f(x|\vec{\theta})$

$$p_i = p_i(\vec{\theta}) = \int_{\triangle x_i} f(x|\vec{\theta}) dx. \tag{A.19}$$

Then the likelihood equation becomes

$$(\frac{\partial lnL}{\partial \theta_i})_{\vec{\theta}=\hat{\vec{\theta}}} = \frac{\partial}{\partial \theta_i} [\sum_{i=1}^{m} n_i ln p_i(\vec{\theta})]_{\vec{\theta}=\hat{\vec{\theta}}} = 0, \qquad i = 1, ..., m, \tag{A.20}$$

Solving this set of equations gives the ML estimators $\hat{\vec{\theta}}$.

The extended ML method

If the size n of data sample is not a constant but a Poisson random variable with the expectation ν, then the likelihood function is the product of usual likelihood function and the Poisson probability of observing n events

$$L(\nu, \vec{\theta}) = \frac{\nu^n}{n!} e^{-\nu} \prod_{i=1}^{n} f(x_i, \vec{\theta}), \tag{A.21}$$

which is called the extended likelihood function [5]. Then the solutions of the likelihood equations

$$\frac{\partial lnL(\nu, \vec{\theta})}{\partial \theta_j} = 0, \qquad j = 1, ..., k, \tag{A.22}$$

$$\frac{\partial lnL(\nu, \vec{\theta})}{\partial \nu} = 0 \tag{A.23}$$

give the ML estimators $\hat{\vec{\theta}}$.

In the case that ν is irrelevant to $\vec{\theta}$, $\frac{\partial lnL(\nu,\vec{\theta})}{\partial \nu} = 0$ gives $\hat{\nu} = n$, the solutions of Eq. A.22 give the same $\hat{\vec{\theta}}$ as those from Eqs. A.9, A.10. If ν is a function of $\vec{\theta}$, the likelihood function becomes (dropping terms irrelevant to $\vec{\theta}$)

$$lnL(\vec{\theta}) = -\nu(\vec{\theta}) + \sum_{i=1}^{n} ln[\nu(\vec{\theta}) \cdot f(x_i, \vec{\theta})]. \tag{A.24}$$

The variances of the ML estimators $\hat{\vec{\theta}}$ derived from the extended likelihood function are usually smaller than those from usual likelihood function because the former uses the information from both n and $\vec{x}$.

For the binned data, the extended likelihood function is

$$L(n_1, ..., n_m|\vec{\theta}) = \prod_{i=1}^{m} \frac{1}{n_i!} \nu_i^{n_i} e^{-\nu_i}, \tag{A.25}$$

where the expectation of n_i, ν_i, is

$$\nu_i = \nu \int_{\triangle x_i} f(x|\vec{\theta}) dx, \qquad \nu = \sum_{i=1}^{m} \nu_i. \tag{A.26}$$

In the case that ν is irrelevant to $\vec{\theta}$, the likelihood equations become

$$\frac{\partial ln L}{\partial \theta_j}|_{\vec{\theta}=\hat{\vec{\theta}}} = \frac{\partial}{\partial \theta_j}[\sum_{i=1}^{m} n_i ln \nu_i]_{\vec{\theta}=\hat{\vec{\theta}}} = 0, \qquad j = 1, ..., m, \tag{A.27}$$

which has the same form of Eq. A.20 with $p_i(\vec{\theta})$ replaced by $\nu_i(\vec{\theta})$, and $\hat{\nu} = n$. If ν is a function of $\vec{\theta}$, then the likelihood equations are

$$\frac{\partial ln L}{\partial \theta_j}|_{\vec{\theta}=\hat{\vec{\theta}}} = \frac{\partial}{\partial \theta_j}[\sum_{i=1}^{m} n_i ln \nu_i - \nu]_{\vec{\theta}=\hat{\vec{\theta}}} = 0, \qquad j = 1, ..., m. \tag{A.28}$$

The variances of the ML estimators $\hat{\vec{\theta}}$ derived from these equations are usually smaller than those from usual likelihood function because the random property of n has been taken into account here.

Combining measurements with ML method

Suppose the observations in two independent experiments are $\vec{x} = (x_1, ..., x_l)^T$ and $\vec{y} = (y_1, ..., y_m)^T$, and their *pdf* $f_x(x, \vec{\theta})$ and $f_y(y, \vec{\theta})$, depend on same parameters $\vec{\theta}$, which are the quantities to be measured in the experiments. The joint likelihood function of these two experiments are

$$L(\vec{x}, \vec{y}; \vec{\theta}) = L(\vec{x}; \vec{\theta}) \cdot L(\vec{y}; \vec{\theta}) = \prod_{i=1}^{l} f_x(x_i, \vec{\theta}) \prod_{j=1}^{m} f_y(y_i, \vec{\theta}). \tag{A.29}$$

Solving the likelihood equations of this likelihood function with respect to parameters $\vec{\theta}$ and obtaining the ML estimator $\hat{\vec{\theta}}$ gives the combined measurement of these two experiments for parameters $\vec{\theta}$.

In the case $f_x(x, \theta)$ and $f_y(y, \theta)$ are Gaussians and the parameter θ is the mean of Gaussians, the combined estimator of the parameter and its variance have simple forms:

$$\hat{\theta} = (\frac{\theta_x}{\sigma_x^2} + \frac{\theta_y}{\sigma_y^2})/(\frac{1}{\sigma_x^2} + \frac{1}{\sigma_y^2}), \tag{A.30}$$

$$V(\hat{\theta}) = 1/(\frac{1}{\sigma_x^2} + \frac{1}{\sigma_y^2}), \tag{A.31}$$

where θ_x and σ_x are the measured value of parameter θ and its error from experiment x, respectively. Above expressions can be directly extended to the situation of multi-experiments.

If the likelihood function is unknown, and only the results of parameter θ and its errors, $\theta_i, \sigma_i^+, \sigma_i^-$, are reported in each experiment, the combined results for parameter θ and its errors of multi-experiments can be deduced with the method suggested by R.Barlow [6]. The essence of the method is using the measured values $\theta_i, \sigma_i^+, \sigma_i^-$ to construct an approximate parametric likelihood function for each experiment. The *variable width Gaussians* are concluded as the best approximation for our purpose. The likelihood function can be approximated as

$$lnL(\theta_i|\theta) = -\frac{(\theta-\theta_i)^2}{2V_i(\theta)}, \tag{A.32}$$

where the true value of parameter is θ, and the measured value is θ_i in i-th experiment. For the *linear σ parametrization*, we have

$$V_i(\theta) = [\sigma_i(\theta)]^2, \qquad \sigma_i(\theta) = \sigma_i + \sigma_i'(\theta-\theta_i), \tag{A.33}$$

$$\sigma_i = \frac{2\sigma_i^+\sigma_i^-}{\sigma_i^+ + \sigma_i^-}, \qquad \sigma_i' = \frac{\sigma_i^+ - \sigma_i^-}{\sigma_i^+ + \sigma_i^-}, \tag{A.34}$$

where σ_i^+, σ_i^- are the measured positive and negative errors of θ_i in i-th experiment. For the *linear V parametrization*,

$$V_i(\theta) = V_i + V_i'(\theta-\theta_i), \tag{A.35}$$

$$V_i = \sigma_i^+\sigma_i^-, \qquad V_i' = \sigma_i^+ - \sigma_i^-. \tag{A.36}$$

Thus, the joint likelihood function of multi-experiments for parameter θ is approximately

$$lnL(\theta) = -\frac{1}{2}\sum_i \frac{(\theta-\theta_i)^2}{V_i(\theta)}. \tag{A.37}$$

The best estimate of θ, $\hat{\theta}$, is determined by the maximum of above likelihood function. For the linear σ form, the solution is

$$\hat{\theta} = \Sigma_i\omega_i\theta_i/\Sigma_i\omega_i, \tag{A.38}$$

$$\omega_i = \frac{\sigma_i}{[\sigma_i + \sigma_i'(\hat{\theta}-\theta_i)]^3}. \tag{A.39}$$

For the linear V form, the solution is

$$\hat{\theta} = \Sigma_i\omega_i[\theta_i - \frac{V_i'}{2V_i}(\hat{\theta}-\theta_i)^2]/\Sigma_i\omega_i, \tag{A.40}$$

$$\omega_i = \frac{V_i}{[V_i + V_i'(\hat{\theta}-\theta_i)]^2}. \tag{A.41}$$

Two sets of equations shown above are non-linear for $\hat{\theta}$ and the solution must be found by iteration. The $\triangle lnL$=0.5 points of the likelihood function in Eq. A.37 are used to determine the positive and negative errors for $\hat{\theta}$, which also need to be determined numerically. The program of combining results from multi-experiments using parametrization likelihood function has been coded, and obtainable under http://www.slac.stanford.edu/ barlow/statistics.html.

A.1.3 The method of least squares(LS)

The LS estimator for parameter and its error

Suppose n observations $\vec{y} = (y_1, ..., y_n)^T$ are measured at n points $\vec{x} = (x_1, ..., x_n)^T$, the covariance matrix of observations $\vec{y}$ is expressed as $V_{ij} = cov(y_i, y_j)$, and the true values of $\vec{y}$, $\vec{\eta}$, are described by model $\eta_i = f(x_i, \vec{\theta})$,$i = 1, ..., n$, where $\vec{\theta} = (\theta_1, ..., \theta_k)^T$ are the parameters to be determined. The least squares (LS) estimators of $\vec{\theta}$, $\hat{\vec{\theta}}$, can be found by minimizing the LS function $Q^2(\vec{\theta})$ with respect to $\vec{\theta}$:

$$Q^2(\vec{\theta}) = (\vec{y} - \vec{\eta}(\vec{\theta}))^T V^{-1} (\vec{y} - \vec{\eta}(\vec{\theta})) = \Sigma_{i=1}^n \Sigma_{j=1}^n (y_i - \eta_i) V_{ij}^{-1} (y_j - \eta_j). \tag{A.42}$$

In the case of $y_i, i = 1, ..., n$ being n independent measurements, the LS function has simple form

$$Q^2(\vec{\theta}) = \Sigma_{i=1}^n \frac{(y_i - \eta_i)^2}{\sigma_i^2}, \tag{A.43}$$

where σ_i is the error of y_i. An usual case is y_i is a Poisson variable, then σ_i^2 can be approximated by y_i or its predicted value η_i. If $y_i, i = 1, ..., n$ are n independent Gaussians, $y_i \sim N(\eta_i, \sigma_i^2)$, the likelihood function of $\vec{y}$ is $L(\vec{\theta}) \propto exp[-\frac{1}{2} \sum_{i=1}^n (\frac{y_i - \eta_i}{\sigma_i})^2]$. In this case maximizing $L(\vec{\theta})$ with respect to parameters $\vec{\theta}$ is equivalent to minimizing the LS function $Q^2(\vec{\theta}) = \Sigma_{i=1}^n \frac{(y_i - \eta_i)^2}{\sigma_i^2}$, namely, the estimators of ML and LS methods for $\vec{\theta}$ are identical.

For the linear LS model, *i.e.* $f(x_i, \vec{\theta})$ is the linear function of $\vec{\theta}$:

$$f(x_i, \vec{\theta}) = \Sigma_{j=1}^k a_{ij} \theta_j, \qquad i = 1, ..., n, \quad k < n, \tag{A.44}$$

where a_{ij} equals x_i^{j-1} or is the $(j-1)$-th Legendre polynomial of x_i, minimizing the LS function $Q^2(\vec{\theta})$ simplified to solve a set of k linear equations. Define a_{ij} being the elements of a $n \times k$ matrix A, minimizing the LS function $Q^2(\vec{\theta})$ gives the LS estimator of parameters $\vec{\theta}$:

$$\hat{\vec{\theta}} = (A^T V^{-1} A)^{-1} A^T V^{-1} \vec{y}, \tag{A.45}$$

the covariance matrix of $\hat{\vec{\theta}}$ is

$$V(\hat{\vec{\theta}}) = (A^T V^{-1} A)^{-1}, \tag{A.46}$$

or equivalently

$$(V^{-1}(\hat{\vec{\theta}}))_{ij} = \frac{1}{2} \frac{\partial^2 Q^2}{\partial \theta_i \partial \theta_j} |_{\vec{\theta} = \hat{\vec{\theta}}} = \Sigma_{l,m=1}^n a_{li} a_{mj} (V^{-1})_{lm}, \qquad i, j = 1, ..., k. \tag{A.47}$$

If $y_i, i = 1, ..., n$ are independent each other, the non-diagonal elements equal to zeros, then the above equation is simplified to

$$(V^{-1}(\hat{\vec{\theta}}))_{ij} = \Sigma_{m=1}^n a_{mi} a_{mj} / \sigma_m^2, \qquad i, j = 1, ..., k. \tag{A.48}$$

The linear LS estimators provide the exact solutions for parameters $\vec{\theta}$, and they are unique and unbiased, and have minimum variances.

Expanding $Q^2(\vec{\theta})$ about $\hat{\vec{\theta}}$, one finds that the contour in parameter space defined by

$$Q^2(\vec{\theta}) = Q^2(\hat{\vec{\theta}}) + s^2 = Q^2_{min} + s^2 \tag{A.49}$$

has tangent planes located at plus or minus s- standard deviation from the LS estimates $\hat{\vec{\theta}}$.

For the linear LS model, if the observations $\vec{y}$ are multi-normal variables, the minimum of the LS function $Q^2(\vec{\theta})$

$$Q^2_{min}(\vec{\theta}) = \Sigma_{i=1}^n \Sigma_{j=1}^n (y_i - \hat{\eta}_i) V_{ij}^{-1} (y_j - \hat{\eta}_j) \tag{A.50}$$

is a χ^2 variable with degree of freedom of $n - k$. This means the Q^2_{min} obtained by LS method is a quantitative measure of the consistency between the measured values $\vec{y}$ and their fitted value $\hat{\vec{\eta}}$, *i.e.*, the Q^2_{min} represents the goodness of fit (see section A.3.1., goodness of fit tests).

For the non-linear LS model, *i.e.* $f(x_i, \vec{\theta})$ is the non-linear function of $\vec{\theta}$, usually the minimizing of the LS function $Q^2(\vec{\theta})$ is implemented via iteration procedure to obtain an approximate solution of $\hat{\vec{\theta}}$. The non-linear LS estimator is a biased estimator, its variance does not reach MVB, and the exact distribution of Q^2_{min} is unknown. However, if n is sufficiently large, the LS estimator is asymptotically unbiased, and its Q^2_{min} is approximately a χ^2 variable.

The LS method for binned data

For sufficiently large size n of data sample $\vec{x} = (x_1, ..., x_n)^T$ and the measurements expressed as a histogram binned data, assuming the observed number of measurements in i-th bin is $n_i, i = 1, ..., m$, and its corresponding expectation from assumed model is

$$f_i(\vec{\theta}) = np_i, \qquad p_i(\vec{\theta}) = \int_{\triangle x_i} g(x|\vec{\theta}) dx, \tag{A.51}$$

where $g(x|\vec{\theta})$ is the *pdf* of observable x and $\vec{\theta}$ are the parameters to be determined. The normalization $\Sigma_{i=1}^m p_i = 1$ requires

$$\Sigma_{i=1}^m n_i = \Sigma_{i=1}^m f_i(\vec{\theta}) = n. \tag{A.52}$$

It can be proved for a given n, the LS function $Q^2(\vec{\theta})$ is of the form

$$Q^2(\vec{\theta}) = \Sigma_{i=1}^m \frac{(n_i - np_i)^2}{np_i} = \Sigma_{i=1}^m \frac{(n_i - f_i)^2}{f_i}. \tag{A.53}$$

The f_i in the denominator can be approximated by n_i. Minimizing this LS function leads to the LS estimates for parameters $\vec{\theta}$, which usually needs to be implemented by numerical iteration procedure. The n_i is a Poisson variable with the expectation np_i, if n is sufficiently large, n_i can be approximated by a Gaussian, then $(n_i - f_i)/\sqrt{f_i}$ or $(n_i - f_i)/\sqrt{n_i}$ is approximately a standard normal variable, therefore, the $Q^2_{min}(\vec{\theta})$ distributed approximately as a $\chi^2(m-1)$ variable, where the degree of freedom of $m - 1$ is due to the existence of a constraint equation A.52.

General LS estimation with constraints

Often in the estimation problem there exist a set of constraint equations between the true values of observations $\eta_i, i = 1, ..., n$. The typical example is in the kinematic analysis of a particle reaction or decay, the momentum and energy conservation laws constitute a set of restrictions relating the various momenta and angles for the particle combination defining the kinematic hypothesis. Some of the quantities have been measured to a certain accuracy (say, the momenta and angles of curved tracks), and some are completely unknown (the variables for an unseen particle). The purpose of the LS estimation is to investigate the kinematic hypothesis: for a successful minimization the constraint equations will supply estimates for the unmeasured variables as well as "improved measurements" for the measured quantities.

Assume $\vec{y} = (y_1, ..., y_n)^T$ are the measured values with covariant matrix $V(\vec{y})$, let the true values of $\vec{y}$ be $\vec{\eta}$. In addition, we have a set of J unmeasurable variables $\vec{\xi} = (\xi_1, ..., \xi_J)^T$. The n measurable and J unmeasurable variables are related and have to satisfy a set of K constraint equations

$$f_k(\vec{\eta}, \vec{\xi}) = 0, \qquad k = 1, ..., K.$$

According to the LS principle, we should adopt as the best estimates of the unknown $\vec{\eta}$ and $\vec{\xi}$ those values for which

$$Q^2(\vec{\eta}) = (\vec{y} - \vec{\eta})^T V^{-1}(\vec{y})(\vec{y} - \vec{\eta}) = minimum, \tag{A.54}$$

$$f(\vec{\eta}, \vec{\xi}) = \vec{0}. \tag{A.55}$$

Usually the method of the Lagrangian multipliers are used to solve above equations. We introduce K additional unknowns $\vec{\lambda} = (\lambda_1, ..., \lambda_K)^T$ and rephrase the problem by requiring

$$Q^2(\vec{\eta}, \vec{\xi}, \vec{\lambda}) = (\vec{y} - \vec{\eta})^T V^{-1}(\vec{y})(\vec{y} - \vec{\eta}) + 2\vec{\lambda}^T \vec{f}(\vec{\eta}, \vec{\xi}) = minimum. \tag{A.56}$$

We have now a total of $n + J + K$ unknowns. When the derivatives of Q^2 with respect to all unknowns are put equal to zero we get following set of equations

$$V^{-1}(\vec{y})(\vec{\eta} - \vec{y}) + F_\eta^T \vec{\lambda} = \vec{0}, \tag{A.57}$$

$$F_\xi^T \vec{\lambda} = \vec{0}, \tag{A.58}$$

$$\vec{f}(\vec{\eta}, \vec{\xi}) = \vec{0}, \tag{A.59}$$

where the matrices F_η (of dimension $K \times N$) and F_ξ (of dimension $K \times J$) are defined by

$$(F_\eta)_{ki} \equiv \frac{\partial f_k}{\partial \eta_i}, \qquad (F_\xi)_{kj} \equiv \frac{\partial f_k}{\partial \xi_j}. \tag{A.60}$$

The solution of this set of equations for the $n + J + K$ unknowns and their errors must in general case be found by iterations, producing successively better approximations.

In the linear LS estimation problem for the n measurable and J unmeasurable variables which are related and have to satisfy a set of K constraint equations, if the measured values $\vec{y} = (y_1, ..., y_n)^T$ is a multi-normal variable, the Q^2_{min} is a χ^2 variable with the degree of

freedom $(K - J)$. For the non-linear LS estimation problem of non-linear constraint equations, and/or $\vec{y}$ is not a multi-normal variable, the Q^2_{min} may be approximated by $\chi^2(K - J)$.

The momentum-energy conservation laws constitute a set of 4 constraint equations. If all the particle's parameters in a reaction or a decay process have been measured (no unmeasurable variables) and the momentum-energy conservation laws are applied to obtain better values of particles parameters (4C kinematic fit), the Q^2_{min} of the LS estimator is then an approximate $\chi^2(4)$ variable. If there exist J unmeasurable variables and r intermediate resonances which promptly decayed to observed final state particles, and the invariant masses of daughter particles of these resonances are constrained to their mother particles' masses, then the Q^2_{min} is approximately a $\chi^2(4 + r - J)$ variable.

A.2 Interval estimation, confidence interval and upper limit

The task of the interval estimation is to locate a region which contains the true value of the parameter θ to be studied with a probability γ. This region is called the confidence interval with coverage probability γ. When the goal of an experiment is to determine a parameter θ, the result is usually expressed by quoting, in addition to the point estimate, some sort of confidence interval which reflects the statistical precision of the measurement. In the simplest case this can be given by the parameter's estimated value $\hat{\theta}$ plus/minus an estimate of the standard deviation of $\hat{\theta}$, $\sigma_{\hat{\theta}}$. If the parameter θ has boundary (without losing generality, we assume it is lower boundary with the value zero throughout this Appendix), and the estimate of θ in an experiment is close to this boundary, then the determination of the interval estimation is difficult and needs to be treated in special way.

A.2.1 Frequentist confidence interval

Neyman method for confidence interval

Confidence interval refers to frequentist interval obtained with a procedure due to Neyman [7]. Consider a *pdf* $f(x;\theta)$ where x represents the measurement of the experiment and θ the unknown parameter for which we want to construct a confidence interval. The variable x could (and often does) represent an estimator of θ. Using $f(x;\theta)$ we can find for a pre-specified probability $\gamma = 1 - \alpha$ and for every value of θ a set of values $x_1(\theta,\alpha)$ and $x_2(\theta,\alpha)$ such that

$$P(x_1 < x < x_2;\theta) = 1 - \alpha \equiv \gamma = \int_{x_1}^{x_2} f(x;\theta)dx. \tag{A.61}$$

This is illustrated in Fig. A.1: a horizontal line segment $[x_1(\theta,\alpha), x_2(\theta,\alpha)]$ is drawn for representative values of θ. The union of such intervals for all values of θ, designated in the figure as $D(\alpha)$, is known as the confidence belt. Typically the curves $x_1(\theta,\alpha)$ and $x_2(\theta,\alpha)$ are monotonic functions of θ, which we assume for this discussion.

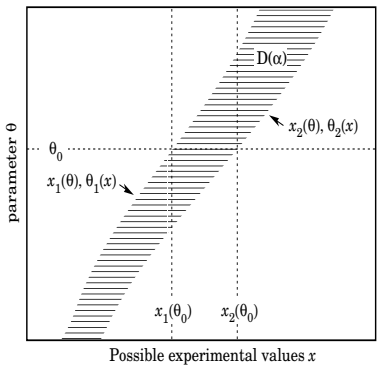

Figure A.1: Construction of the confidence belt

Upon performing an experiment to measure x and obtaining a value x_0, one draws a vertical line through x_0. The confidence interval for θ is the set of all values of θ for which the corresponding line segment $[x_1(\theta,\alpha), x_2(\theta,\alpha)]$ is intercepted by this vertical line. Such confidence intervals are said to have a confidence level (CL) equal to $\gamma = 1-\alpha$.

Now suppose that the true value of θ is θ_0, indicated in the figure.We see from the figure that θ_0 lies between $\theta_1(x)$ and $\theta_2(x)$ if and only if x lies between $x_1(\theta_0)$ and $x_2(\theta_0)$. The two events thus have the same probability, and since this is true for any value θ_0, we can drop the subscript 0 and obtain

$$\gamma = 1-\alpha = P(x_1(\theta) < x < x_2(\theta)) = P(\theta_2(x) < \theta < \theta_1(x)). \tag{A.62}$$

In this probability statement $\theta_1(x)$ and $\theta_2(x)$, *i.e.*, the endpoints of the interval, are the random variables and θ is an unknown constant. If the experiment were to be repeated a large number of times, the interval $[\theta_1, \theta_2]$ would vary, covering the fixed value θ in a fraction $\gamma = 1-\alpha$ of the experiments.

The condition of coverage probability does not determine x_1 and x_2 uniquely and additional criteria are needed. The most common criterion is to choose central intervals such that the probabilities below x_1 and above x_2 are each $\alpha/2$. In other cases one may want to report only an upper or lower limit, then the probability excluded below x_1 or above x_2 can be set to zero.

When the observed random variable x is continuous, the coverage probability obtained with the Neyman construction is $\gamma = 1-\alpha$, regardless of the true value of the parameter. If x is discrete, however, it is not possible to find segments $[x_1(\theta,\alpha), x_2(\theta,\alpha)]$ that satisfy Eq. A.62 exactly for all values of θ. By convention one constructs the confidence belt requiring the probability $P(x_1 < x < x_2)$ to be greater than or equal to $\gamma = 1-\alpha$. This gives confidence intervals that include the true parameter with a probability greater than or equal to $\gamma = 1-\alpha$.

Gaussian distributed measurements

An important example of constructing a confidence interval is when the data consist of a single random variable x that follow a Gaussian distribution; this is often the case when x represents an estimator for a parameter and one has a sufficiently large data sample.

If there is more than one parameter being estimated, the multivariate Gaussian is used. For the univariate case with known σ,

$$\gamma = 1 - \alpha = \frac{1}{\sqrt{2\pi}\sigma} \int_{\mu-\delta}^{\mu+\delta} e^{-(x-\mu)^2/2\sigma^2} dx = erf(\frac{\delta}{\sqrt{2}\sigma}) \tag{A.63}$$

is the probability that the measured value x will fall within $\pm\delta$ of the true value μ. From the symmetry of the Gaussian with respect to x and μ, this is also the probability for the interval $x \pm \delta$ to include μ. The choice $\delta = \sigma$ gives an interval called the standard error which has $\gamma = 1 - \alpha = 68.27\%$ if σ is known. Values of α for other frequently used choices of δ are given in Table A.1. The relation of α and δ can be also represented by the cumulated distribution function for the χ^2 distribution for $\chi^2 = (\delta/\sigma)^2$ and $n = 1$ degree of freedom:

$$\gamma = 1 - \alpha = F(\chi^2; n = 1). \tag{A.64}$$

For multivariate measurements of, say, n parameter estimates $\hat{\vec{\theta}} = (\hat{\theta}_1, ..., \hat{\theta}_n)^T$, one

Table A.1: Area of the tails α outside $\pm\delta$ from the mean of a Gaussian distribution.

α	δ	α	δ
0.3173	1σ	0.2	1.28σ
0.0455	2σ	0.1	1.64σ
0.0027	3σ	0.05	1.96σ
6.3×10^{-5}	4σ	0.01	2.58σ
5.7×10^{-7}	5σ	0.001	3.29σ
2.0×10^{-9}	6σ	0.0001	3.89σ

requires the full covariance matrix $V_{ij} = cov(\hat{\theta}_i, \hat{\theta}_j)$, which can be estimated by ML or LS method.

If the parameters $\vec{\theta}$ are estimated with the ML method, for sufficient large n and the likelihood function satisfies the regularity conditions, the likelihood function distributed asymptotically as a multi-Gaussian, then we have

$$lnL(\vec{\theta}) = lnL_{max} - Q(\vec{\theta})/2, \tag{A.65}$$

where $Q(\vec{\theta}) = (\vec{\theta} - \hat{\vec{\theta}})^T V^{-1}(\vec{\theta})(\vec{\theta} - \hat{\vec{\theta}})$ is asymptotically a $\chi^2(k)$ variable, and k is the dimension of $\vec{\theta}$. The intersection contour of super-plane $lnL = lnL_{max} - Q_\gamma/2$ and super-surface $lnL(\vec{\theta})$ forms the boundary of the confidence region of $\vec{\theta}$ with coverage probability of $\gamma = 1 - \alpha$, which is calculated by the cumulated χ^2 function

$$\gamma = 1 - \alpha = P(Q \le Q_\gamma) = \int_0^{Q_\gamma} \chi^2(Q; \nu = k) dQ = F_\alpha(Q_\gamma; \nu = k). \tag{A.66}$$

In the case that the parameters $\vec{\theta}$ are estimated with LS method, for linear LS estimator and multi-Gaussian measurements, we have

$$Q^2(\vec{\theta}) = Q^2_{min} + Q^2_{LS}, \tag{A.67}$$

where $Q^2_{LS}(\vec{\theta}) = (\vec{\theta} - \hat{\vec{\theta}})^T V^{-1}(\vec{\theta})(\vec{\theta} - \hat{\vec{\theta}})$ is a $\chi^2(k)$ variable and k is the dimension of $\vec{\theta}$ for non-constraint LS estimation, and the dimension of $\vec{\theta}$ minus the number of independent linear constraint equations for constraint LS case. The intersection contour of super-plane $Q^2(\vec{\theta}) = Q^2_{min} + Q_\gamma$ and super-surface $Q^2(\vec{\theta})$ forms the boundary of the confidence region of $\vec{\theta}$ with coverage probability of $\gamma \equiv 1 - \alpha$, which is also calculated by Eq. A.66. Values of Q_γ for $k = 1, 2, 3$ are given in Table A.2 for several values of the coverage probability $\gamma = 1 - \alpha$.

Table A.2: Q_γ for $k = 1, 2, 3$ corresponding to a coverage probability $\gamma = 1 - \alpha$ in the large data sample limit.

$\gamma(\%)$	k=1	k=2	k=3
68.27	1.00	2.30	3.53
90.	2.71	4.61	6.25
95.	3.84	5.99	7.82
95.45	4.00	6.18	8.03
99.	6.63	9.21	11.34
99.73	9.00	11.83	14.16

If the mentioned conditions are not fully satisfied, the confidence region determined by Eqs. A.65 and A.67 are not exact but an approximate one.

The ML method has an advantage that is easier to calculate the confidence region for combining several independent measurements of same parameters. Assume N independent measurements give likelihood functions $lnL_i(\vec{\theta}), i = 1, ..., N$, then the combined likelihood function is simply

$$lnL(\vec{\theta}) = \sum_i^N lnL_i(\vec{\theta}). \tag{A.68}$$

Then using this likelihood functions in Eq. A.65 can give the confidence region with coverage probability γ for combined estimate $\hat{\vec{\theta}}$.

Poisson distributed measurements

If n represents the number of events produced in a reaction with cross section σ, say in a fixed integrated luminosity L, then it follows a Poisson distribution with mean $s = \sigma L$ in the case there is no background. Therefore, to determine the cross section of a reaction or the branching ratio of a decay process in terms of the number of observed events, the interval estimation of Poisson distributed data must be met. The probability of observing n events of the Poisson distribution with the mean s is

$$P(n, s) = \frac{s^n e^{-s}}{n!}. \tag{A.69}$$

The upper and lower (one sided) limits on the mean s can be found from the Neyman procedure to be

$$s_{lo} = \frac{1}{2} F^{-1}_{\chi^2}(\alpha_{lo}; 2n), \tag{A.70}$$

$$s_{up} = \frac{1}{2} F^{-1}_{\chi^2}(1-\alpha_{up}); 2(n+1)), \tag{A.71}$$

where the upper and lower limits are at confidence levels of $1-\alpha_{lo}$ and $1-\alpha_{up}$, respectively, and $F^{-1}_{\chi^2}$ is the quantile of the χ^2 distribution (inverse of the cumulative distribution). The quantiles $F^{-1}_{\chi^2}$ can be obtained from standard tables or from the CERNLIB routine CHISIN. For central confidence intervals at CL $1-\alpha$, set $\alpha_{lo} = \alpha_{up} = \alpha/2$. Values for confidence levels of 90% and 95% are shown in Table A.3.

Table A.3: Lower and upper (one-sided) limits for the mean s of a Poisson variable given n observed events in the absence of background, for CL of 90% and 95%

.

	$1-\alpha = 90\%$		$1-\alpha = 95\%$	
n	s_{lo}	s_{up}	s_{lo}	s_{up}
0		2.30		3.00
1	0.105	3.89	0.051	4.74
2	0.532	5.32	0.355	6.30
3	1.10	6.68	0.818	7.75
4	1.74	7.99	1.37	9.15
5	2.43	9.27	1.97	10.51
6	3.15	10.53	2.61	11.84
7	3.89	11.77	3.29	13.15
8	4.66	12.99	3.98	14.43
9	5.43	14.21	4.70	15.71
10	6.22	15.41	5.43	16.96

If the number of observed events n contains both signal and background events, which are Poisson variables with mean s and b, respectively, then we have

$$P(n,s) = \frac{(s+b)^n e^{-(s+b)}}{n!}. \tag{A.72}$$

For a specific value of s, the upper and lower limit of the central confidence region, $[n_l, n_u]$, and the lower limit of the upper confidence belt, n_{l_0}, at given confidence level $\gamma = 1-\alpha$ can be determined by

$$\sum_{n=0}^{n_l} P(n,s) \leq \frac{\alpha}{2}, \qquad \sum_{n=n_u+1}^{\infty} P(n,s) \leq \frac{\alpha}{2}, \tag{A.73}$$

$$\sum_{n=0}^{n_{lo}} P(n,s) \leq \alpha, \tag{A.74}$$

respectively. For all s values, such calculations give the confidence belts for central region and upper confidence belt. The inequality sign is to ensure the actual coverage greater or equal to the given coverage in the discrete variable case.

Confidence interval near the physics boundary

A number of issues arise in the construction and interpretation of confidence intervals when the parameter can only take on values in a restricted range. An important sample is where the mean of a Gaussian variable is constrained on physical grounds to be non-negative. This arises, for example, when the square of the neutrino mass is estimated from $\hat{m}^2 = \hat{E}^2 - \hat{p}^2$, where $\hat{E}$ and $\hat{p}$ are independent, Gaussian distributed estimates of the energy and momentum. Although the true m^2 is constrained to be positive, random errors in $\hat{E}$ and $\hat{p}$ can easily lead to negative values for the estimate $\hat{m}^2$.

If one uses the prescription given above for Gaussian distributed measurements, which says to construct the interval by taking the estimate plus/minus one standard deviation, then this can give intervals that are partially or entirely in the unphysical region. In fact, by following strictly the Neyman construction for the central confidence interval, one finds that the interval is truncated below zero; nevertheless an extremely small or even a zero-length interval can result.

An additional important example is where the experiment consists of counting a certain number of events, n, which is assumed to be Poisson distributed. Suppose the expectation value $E(n) = \mu$ is equal to $s + b$, where s and b are the means for signal and background processes, and assume further that b is a known constant. Then $\hat{s} = n - b$ is an unbiased estimator for s. Depending on true magnitudes of s and b, the estimate $\hat{s}$ can easily fall in the negative region. Similar to the Gaussian case with the positive mean, the central confidence interval or even the upper limit for s may be of zero length.

An additional difficulty arises when a parameter estimate is not significantly far away from the boundary, in which case it is natural to report a one-sided confidence interval (often an upper limit). It is straightforward to force the Neyman prescription to produce only an upper limit by setting $x_2 = \infty$ in Eq. A.61 . Then x_1 is uniquely determined and the upper limit can be obtained. If, however, the data come out such that the parameter estimate is not so close to the boundary, one might wish to report a central (*i.e.*, two-sided) confidence interval. As pointed out by Feldman and Cousins [8], however, if the decision to report an upper limit or two-sided interval is made by looking at the data ("flip-flopping"), then the resulting intervals will not in general cover the parameter with the probability $1 - \alpha$.

With the confidence intervals suggested by Feldman and Cousins [8], the prescription determines whether the interval is one- or two-sided in a way which preserves the coverage probability. Intervals with this property are said to be unified. Furthermore, this prescription is such that null intervals do not occur. For a given choice of $1 - \alpha$, if the parameter estimate is sufficiently close to the boundary, then the method gives an one-sided limit. In the case of a Poisson variable in the presence of background, for example, this would occur if the number of observed events is compatible with the expected background. For parameter estimates increasingly far away from the boundary, *i.e.*, for increasing signal significance, the interval makes a smooth transition from one- to two-sided, and far away from the boundary one obtains a central interval. The intervals according to this method for the mean of Poisson variable in the absence of background are given in Table A.4.

The intervals constructed according to the unified procedure in Ref. [8] for a Poisson variable n consisting of signal and background have the property that for $n = 0$ observed

Table A.4: Unified confidence interval $[s_1, s_2]$ for a mean s of a Poisson variable given n observed events in the absence of background, for CL of 90% and 95%

.

	$1-\alpha = 90\%$		$1-\alpha = 95\%$	
n	s_1	s_2	s_1	s_2
0	0.00	2.44	0.00	3.09
1	0.11	4.36	0.05	5.14
2	0.53	5.91	0.36	6.72
3	1.10	7.42	0.82	8.25
4	1.47	8.60	1.37	9.76
5	1.84	9.99	1.84	11.26
6	2.21	11.47	2.21	12.75
7	3.56	12.53	2.58	13.81
8	3.96	13.90	2.94	15.29
9	4.36	15.30	4.36	16.77
10	5.50	16.50	4.75	17.82

events, the upper limit decreases for increasing expected background. This is counter-intuitive, since it is known that if $n = 0$ for the experiment in question, then no background was observed, and therefore one may argue that the expected background should not be relevant. Roe and Woodroofe [9] proposed a solution to this problem by using such a fact that, given an observation n, the background b can not be larger than n in any case. Therefore, the usual Poisson *pdf* should be replaced by a conditional *pdf*, and then this conditional *pdf* is used to construct the confidence intervals following Feldman and Cousins' procedure.

Confidence interval incorporating systematic uncertainties

A modification of the Neyman method incorporating systematic uncertainty of the signal detection efficiency has been proposed by Highland and Cousins [10], in which a "semi-Bayesian" approach is adopted, where an average over the probability of the detection efficiency is performed. This method is of limited accuracy in the limit of high relative systematic uncertainties. On the other hand, an entirely frequentist approach has been proposed for the uncertainty in the background rate prediction [11]. This approach is based on a two-dimensional confidence belt construction and likelihood ratio hypothesis testing and treats the uncertainty in the background as a statistical uncertainty rather than as a systematic one. Recently, Conrad *etal* extend the method of confidence belt construction proposed in [12] to include systematic uncertainties in both the signal and background efficiencies as well as systematic uncertainty of background expectation prediction. It takes into account the systematic uncertainties by assuming a *pdf* which parameterizes our knowledge on the uncertainties and integrating over this *pdf*. This method, combining classical and Bayesian elements, is referred to as semi-Bayesian approach. A FORTRAN program, POLE, has been coded to calculate the confidence intervals for a maximum of observed events of 100 and a maximum signal expectation of 50 [13].

A.2.2 Bayesian confidence interval

In Bayesian approach one has to assume a prior *pdf* of an unknown parameter and then perform an experiment to update the prior distribution. The prior *pdf* reflects the experimenter's subjective degree of belief about unknown parameter before the measurement was carried out. The updated prior, called posterior *pdf*, is used to draw inference on unknown parameter. This updating is done with the use of Bayes theorem [14]. Assuming that n represents the number of observed events, s is the expectation of the number of signal events which is unknown and to be inferred, $p(s|n)$ is the conditional *pdf* of observing n events with given signal s, $\pi(s)$ is the prior *pdf*, the Bayes theorem gives the posterior *pdf*:

$$h(s|n) = \frac{p(s|n)\pi(s)}{\int_0^\infty p(s|n)\pi(s)ds}. \tag{A.75}$$

Here the lower limit of the integral is zero, which is the possible minimum of the signal expectation. Using this posterior *pdf*, one can calculate a Bayesian confidence interval for the signal expectation s at given confidence level $CL = 1 - \alpha$:

$$1 - \alpha = \int_{s_L}^{s_U} h(s|n)ds. \tag{A.76}$$

However, such intervals are not uniquely determined. Often, the highest posterior density (HPD) confidence interval I is chosen, which is determined in following way:

$$1 - \alpha = \int_I h(s|n)ds, \quad h(s_1|n) \geq h(s_2|n) \quad for\ any\ s_1 \in I\ and\ s_2 \notin I. \tag{A.77}$$

The upper limit of the signal expectation s at given confidence level $CL = 1 - \alpha$, s_{UP}, is naturally given by:

$$1 - \alpha = \int_0^{s_{UP}} h(s|n)ds. \tag{A.78}$$

The nice feature of the Bayesian approach is that the zero value of an upper limit s_{UP} always corresponds to the zero value of confidence level $CL = 1 - \alpha$, which is not necessarily true for the classical approach. The most important issue is to determine a prior *pdf* of the parameter. This is an issue which brings most of controversies into Bayesian methods. An important question is that if one should use an $informative$ prior, *i.e.*, a prior which incorporates results of previous experiments, or a $non - informative$ prior, *i.e.*, a prior which claims total ignorance. The major objection against informative prior is based on such argument: if we assume a prior which incorporates results of previous experiments, then our measurement will not be independent, hence, we will not be able to combine our results with previous results by taking a weighted average.

Thus, we only discuss the Bayesian inference that assumes a non-informative prior *pdf* for the non-negative parameter of a Poisson distribution. For the case that in the "signal region" where the signal events resides, the number of signal events is a Poisson variable with unknown expectation s , and the number of background events is a Poisson variable with expectation b, the conditional *pdf* of observing total events n, $p(s|n)$, can be represented by

$$P(s|n) = \frac{(s+b)^n e^{-(s+b)}}{n!}. \tag{A.79}$$

To deduce the posterior *pdf*, one has to assume a prior *pdf*. Bayes stated that, the non-informative prior for any parameter must be flat [14]. This statement does not based on any strict mathematical argument, but merely his intuition. The obvious weakness of Bayes prior *pdf* is that if one can assume a flat distribution of an unknown parameter, then one can also assume a flat distribution for any function of this parameter, and these two prior functions are apparently not identical. Jeffreys [15] resolves this problem by introducing an invariate non-informative prior *pdf*, which can be deduced from Fisher information. For the *pdf* shown by Eq. A.79, the Jeffreys prior *pdf* is proportional to $1/\sqrt{s+b}$. In general, we can use a prior *pdf* of

$$\pi(s) \propto \frac{1}{(s+b)^m}, \qquad s \geq 0, \quad 0 \leq m \leq 1. \tag{A.80}$$

$m = 0$ corresponds to Bayes prior, and $m = 0.5$ to Jeffreys prior. One can choose m value as he/she thinks appropriate, however, it should always be kept in mind that different m value will give different answer for the confidence interval or upper limit. Substituting $p(n|s)$ of Eq. A.79 and $\pi(s)$ of Eq. A.80 into Eq. A.75, the posterior *pdf* is then given by

$$h(s|n) = \frac{(s+b)^{n-m}e^{-(s+b)}}{\Gamma(n-m+1,b)}, \tag{A.81}$$

where

$$\Gamma(x,b) = \int_0^\infty s^{x-1}e^{-x}ds, \qquad x > 0, b > 0 \tag{A.82}$$

is an incomplete gamma function.

In the case that the systematic uncertainties of the signal efficiency and background expectation can be neglected, the signal expectation s is an unknown constant and the background expectation b is a known value. Substituting the posterior *pdf* of Eq. A.81 into Eq. A.78, we obtain

$$\alpha = \frac{\Gamma(n-m+1, s_{UP}+b)}{\Gamma(n-m+1,b)}. \tag{A.83}$$

If the flat prior$m = 0$is used, Eq. A.83 turns into

$$\alpha = e^{-s_{UP}} \cdot \frac{\sum_{k=0}^{n} \frac{(s_{UP}+b)^k}{k!}}{\sum_{k=0}^{n} \frac{b^k}{k!}}. \tag{A.84}$$

The upper limit s_{UP} at given confidence level $1-\alpha$ can be acquired by solving Eq. A.83 or Eq. A.84 numerically from measured values of n and b. Eq. A.84 has been recommended by PDG [4], therefore, widely used in particle physics experiments. However, from statistics point of view, the Jeffreys prior seems to be a more appropriate non-informative prior as mentioned above, therefore, using Eq. A.83 with $m = 0.5$ to determine s_{UP} seems a reasonable choice.

Now we turn to the question of inclusion of systematic uncertainties. First we consider only the uncertainty of background expectation is present, and the distribution of the background expectation is represented by a pdf $f_{b'}(b, \sigma_b)$ with the mean b and standard deviation σ_b . The conditional pdf expressed by Eq. A.79 now is modified to

$$q(n|s)_b = \int_0^\infty p(n|s)_{b'} \cdot f_{b'}(b, \sigma_b)db', \tag{A.85}$$

where $p(n|s)_{b'}$ has the same expression in Eq. A.79 with b replaced by b'.

Next we take into account the uncertainties of the signal efficiency and background expectation simultaneously, and consider they are independent each other. The distribution of the signal relative efficiency ε (with respect to the nominal signal detection efficiency) is described by a *pdf* $f_\varepsilon(1, \sigma_\varepsilon)$ with the mean 1 and standard deviation σ_ε. The conditional *pdf* described by Eq. A.79 is then further modified to

$$q(n|s)_b = \int_0^\infty \int_0^\infty p(n|s\varepsilon)_{b'} f_{b'}(b, \sigma_b) f_\varepsilon(1, \sigma_\varepsilon) db' d\varepsilon, \tag{A.86}$$

where $p(n|s\varepsilon)_{b'}$ represents that in Eq. A.79 b is replaced by b' , and s by $s\varepsilon$. One notices that the lower limits of integrals in Eqs. A.85, A.86 are all zeros, which are the possible minimum value of any efficiencies and number of background events.

Using $q(s|n)_b$ in Eqs. A.85, A.86 to construct posterior *pdf*

$$h(s|n) = \frac{q(n|s)_b \pi(s)}{\int_0^\infty q(n|s)_b \pi(s) ds}, \tag{A.87}$$

one can calculate the confidence interval or upper limit s_{UP} on s at any given confidence level with inclusion of systematic uncertainties in terms of Eq. A.76 or A.78.

An algorithm for calculating the upper limit at given confidence level with or without inclusion of systematic uncertainties in pure Bayesian approach has been coded. It has been implemented as a FORTRAN program, BPULE (Bayesian Poissonian Upper Limit Estimator) [16], where an iterative procedure is carried out by minimizing the difference between the given confidence level and the calculated value in terms of Eq. A.78 until a convergence is reached.

A.3 Tests of hypotheses

In addition to estimating parameters, one often wants to assess the validity of certain statements concerning the data's underlying distribution. Hypothesis tests provide a rule for accepting or rejecting hypotheses depending on the outcome of a measurement. We restrict ourselves here to discuss the Goodness-of-fit tests - one of the non-parametric tests, which deals with questions of the functional form for the distribution of the data and gives the probability to obtain a level of incompatibility with a certain hypothesis that is greater than or equal to the level observed with the actual data. Two methods will be stated: Pearson's χ^2 test and Kolmogorov-Smirnov test, which is applicable for the large and small size of the measured data sample, respectively. Finally, we have a section to discuss an important concept in particle physics experiment-the statistical significance of signal.

A.3.1 Goodness-of-fit test

Pearson's χ^2 test

We assume that n observations on the variable x belong to N mutually exclusive classes, such as successive intervals in a histogram, non-overlapping regions in two-dimentional

plot, etc. The number of events $n_1, n_2, ..., n_N$ in the different classes will then be multinomially distributed, with probabilities p_i for the individual classes as determined by the underlying distribution $f(x)$ for continuous variable x:

$$p_i = \int_{\triangle x_i} f(x)dx, \qquad i = 1, 2, ..., N,$$

or $q_j = P(x = x_j), j = 1, 2, \cdots$ for discrete variable x:

$$p_i = \sum_{j, x_j \in \triangle x_i} q_j, \qquad i = 1, 2, ..., N,$$

where $\triangle x_i$ represents the i-th interval. The hypothesis we wish to test specifies the class probabilities according to a certain prescription,

$$H_0 : p_i = p_{0i}, \qquad i = 1, 2, ..., N, \tag{A.88}$$

where

$$\sum_{i=1}^{N} p_{0i} = 1, \tag{A.89}$$

is the overall normalization and

$$p_{0i} = \int_{\triangle x_i} f_0(x)dx, \quad or \quad p_{0i} = \sum_{j, x_j \in \triangle x_i} q_{0j}.$$

Therefore, what we wish to test is if the distribution of the observation $f(x)$ or q_j is consistent with the assigned distribution $f_0(x)$ or q_{0j}, or equivalently, if the hypothesis H_0 is accepted by the observed data, given that the total number in all classes is n? To test whether the set of predicted numbers np_{0i} is compatible with the set of observed numbers n_i we take as our test statistic the quantity

$$X^2 = \sum_{i=1}^{N} \frac{(n_i - np_{0i})^2}{np_{0i}} = \frac{1}{n} \sum_{i=1}^{N} \frac{n_i^2}{p_{0i}} - n. \tag{A.90}$$

When H_0 is true this statistic is approximately $\chi^2(N-1)$ distributed. This is called the Pearson theorem.

If H_0 is true and the experiment is repeated many times under the same conditions with n observations, the actual values obtained for X^2, X^2_{obs}, will therefore be distributed nearly like $\chi^2(N-1)$; in particular, the mean value for X^2_{obs} will be $\simeq N-1$ and the variance $\simeq 2(N-1)$. If, on the other hand, H_0 is not true, the expectation for each n_i is not np_{0i}, and the sum of terms $(n_i - np_{0i})^2/np_{0i}$ will tend to become on the average larger than if H_0 were true. Hence it seems reasonable to reject H_0 if X^2_{obs} becomes too large. The criteria to reject H_0 at *significance level* α is

$$X^2_{obs} > \chi^2_\alpha(N-1), \tag{A.91}$$

where $\chi^2_\alpha(N-1)$ is determined by the $\chi^2(N-1)$ *pdf* $f(y;N-1)$ such that

$$\alpha = \int_{\chi^2_\alpha(N-1)}^{\infty} f(y;N-1)dy.$$

Often, the model which to describe the distribution of the measured data includes L unknown parameters. For a Least-Square estimation we know that the comparison between data and fitted model is made using the χ^2 distribution with a number of degrees of freedom equal to the number of independent observations minus the number of independent parameters estimated. This procedure is exact only in the limit of infinitely many observations and with a linear parameter dependence; otherwise it is an approximation. Thus, if there are L parameters in H_0 which are estimated by the LS method and N classes subject to an overall normalization condition, Pearson's χ^2 test for goodness-of-fit consists in comparing the fitted (minimum) value X^2_{min} to the χ^2 distribution with $(N-1-L)$ degrees of freedom.

Kolmogorov-Smirnov test

The Kolmogorov-Smirnov (KS) test avoids the binning of individual observations and may be more sensitive to the data, and is superior to the χ^2 test in particular for small samples and has many nice properties when applied to problems in which no parameters are estimated.

Given n independent observations on the variable x we form an *ordered sample* by arranging the observations in ascending order of magnitude, $x_1, x_2, \cdots, x_n$. The cumulative distribution for this sample of size n is now defined by

$$S_n(x) = \begin{cases} 0, & x < x_i, \\ \frac{i}{n}, & x_i \le x \le x_{i+1}, \\ 1, & x \ge x_n. \end{cases} \tag{A.92}$$

Thus $S_n(x)$ is an increasing step function with a step of height $1/n$ at each of the observational points $x_1, x_2, \cdots, x_n$.

The KS test involves a comparison between the observed cumulative distribution function $S_n(x)$ for the data sample and the cumulative distribution function $F_0(x)$ which is determined by some theoretical model. We state the null hypothesis as

$$H_0: \quad S_n(x) = F_0(x). \tag{A.93}$$

For H_0 true one expects that the difference between $S_n(x)$ and $F_0(x)$ at any point should be reasonably small. The KS test looks at the difference $S_n(x) - F_0(x)$ at all observed points and takes the maximum of the absolute value of this quantity, D_n, as a test statistic

$$D_n = max|S_n(x) - F_0(x)|. \tag{A.94}$$

It can be shown that provided no parameter in $F_0(x)$ has been determined from the data, and assuming H_0 true, the variable D_n has a distribution which is independent of $F_0(x)$, *i.e.* D_n is *distribution free*. This holds irrespective of the sample size.

For continuous variable x and finite n, the D_n has the distribution of [17]

$$P(D_n < z + \frac{1}{2n}) = \begin{cases} 0, & z \le 0, \\ \int_{\frac{1}{2n}-z}^{\frac{1}{2n}+z} \int_{\frac{3}{2n}-z}^{\frac{3}{2n}+z} \cdots \int_{\frac{2n-1}{2n}-z}^{\frac{2n-1}{2n}+z} f(y_1, \cdots, y_n) dy_1 \cdots dy_n, & 0 < z < 1 - \frac{1}{2n} \\ 1, & z \ge 1 - \frac{1}{2n}, \end{cases} \tag{A.95}$$

where

$$f(y_1, \cdots, y_n) = \begin{cases} n!, & when\ 0 < y_1 < \cdots < y_n < 1, \\ 0, & others. \end{cases} \tag{A.96}$$

For large n the D_n has the cumulative distribution of

$$\lim_{n\to\infty} P(D_n \le \frac{z}{\sqrt{n}}) = 1 - 2\sum_{r=1}^{\infty} (-1)^{r-1} e^{-2r^2 z^2}, \qquad (z > 0). \tag{A.97}$$

This relation is approximately valid at $n \simeq 80$.

If H_0 is true, the D_n tends to be small, while if H_0 is not true, the D_n tends to be larger than if H_0 were true. Hence it seems reasonable to reject H_0 if D_n becomes too large. The criteria to reject H_0 at significance level α is

$$P(D_n > D_{n,\alpha}). \tag{A.98}$$

A table in the Appendix of the book [2] or [3] gives the critical values $D_{n,\alpha}$ at 5 different significance level α for $n \le 100$, and the approximate expression for $n > 100$.

A.3.2 Statistical significance of signal

The statistical significance of a signal in an experiment of particle physics is to quantify the degree of confidence that the observation in the experiment either confirm or disprove a null hypothesis H_0, in favor of an alternative hypothesis H_1. Usually the H_0 stands for known or background processes, while the alternative hypothesis H_1 stands for a new or a signal process plus background processes with respective production cross section. This concept is very useful for usual measurements that one can have an intuitive estimation, to what extent one can believe the observed phenomena are due to backgrounds or a signal. It becomes crucial for measurements which claim a new discovery or a new signal. As a convention in particle physics experiment, the "5σ" standard, namely the statistical significance $S \ge 5$ is required to define the sensitivity for discovery; while in the cases $S \ge 3$ ($S \ge 2$), one may claim that the observed signal has strong (weak) evidence.

However, as pointed out in Ref. [18], the concept of the statistical significance has not been employed consistently in the most important discoveries made over the last quarter century. Also, the definitions of the statistical significance in different measurements differ from each other. Listed below are various definitions for the statistical significance in counting experiment (see, for example, refs. [19] [20] [21]):

$$S_1 = (n - b)/\sqrt{b}, \tag{A.99}$$

$$S_2 = (n - b)/\sqrt{n}, \tag{A.100}$$

$$S_{12} = \sqrt{n}/\sqrt{b}, \tag{A.101}$$

$$S_{B1} = S_1 - k(\alpha)\sqrt{n/b}, \tag{A.102}$$

$$S_{B12} = 2S_{12} - k(\alpha), \tag{A.103}$$

$$\int_{-\infty}^{S_N} N(0,1)dx = \sum_{i=0}^{n-1} e^{-b}\frac{b^i}{i!}, \tag{A.104}$$

where n is the total number of the observed events, which is the Poisson variable with the expectation $s+b$, s is the expected number of signal events to be searched, while b is the known expected number of Poisson distributed background events. All numbers are counted in the "signal region" where the searched signal events are supposed to appear. In equations A.102 and A.103 the $k(\alpha)$ is a factor related to the α that the corresponding statistical significance assumes $1-\alpha$ acceptance for positive decision about signal observation, and $k(0.5) = 0, k(0.25) = 0.66, k(0.1) = 1.28, k(0.05) = 1.64$, etc [20]. In equation A.104, $N(0,1)$ is a notation for the standard normal function. On the other hand, the measurements in particle physics often examine statistical variables that are continuous in nature. Actually, to identify a sample of events enriched in the signal process, it is often important to take into account the entire distribution of a given variable for a set of events , rather than just to count the events within a given signal region of values. In this situation, I. Narsky [21] gives a definition of the statistical significance via likelihood function

$$S_L = \sqrt{-2\ln L(b)/L(s+b)} \tag{A.105}$$

under the assumption that $-2\ln L(b)/L(s+b)$ distributes as χ^2 function with degree of freedom of 1.

Upon above situation, it is clear that we desire to have a self-consistent definition for statistical significance, which can avoid the ambiguity that the same S value in different measurements may imply virtually different statistical significance, and can be suitable for both counting experiment and continuous test statistics.

Definition of the statistical significance

In the PDG [4], the $p-$value is defined to quantify the level of agreement between the experimental data and a hypothesis. Assume an experiment makes a measurement for test statistic t being equal to t_{obs}, and t has a probability density function $g(t|H_0)$ if a null hypothesis H_0 is true. We further assume that large t values correspond to poor agreement between the null hypothesis H_0 and data, then the $p-$value of an experiment would be

$$p(t_{obs}) = P(t > t_{obs}|H_0) = \int_{t_{obs}}^{\infty} g(t|H_0)dt. \tag{A.106}$$

A very small $p-$value tends to reject the null hypothesis H_0.

Since the $p-$value of an experiment provides a measure of the consistency between the H_0 hypothesis and the measurement, Zhu [22] define the statistical significance S in terms of the $p-$value in the following form

$$\int_{-S}^{S} N(0,1)dx = 1 - p(t_{obs}) \tag{A.107}$$

under the assumption that the null hypothesis H_0 represents that the observed events can be described merely by background processes. Because a small $p-$value means a small probability of H_0 being true, corresponds to a large probability of H_1 being true, one would get a large signal significance S by this expression. The left side of equation A.107 represents the integral probability of the normal distribution in the region within S standard deviation ($S\sigma$). In such a definition, some correlated S and $p-$values are listed in Table A.5.

Table A.5: *Statistical Significance S and correlated $p-$value.*

S	$p-$value
1	0.3173
2	0.0455
3	0.0027
4	6.3×10^{-5}
5	5.7×10^{-7}
6	2.0×10^{-9}

Statistical significance in counting experiment

A group of particle physics experiment involves the search for new phenomena or signal by observing a unique class of events that can not be described by background processes. One can address this problem to that of a "counting experiment", where one identifies a class of events using well-defined criteria, counts up the number of observed events, and estimates the average rate of events contributed by various backgrounds in the signal region, where the signal events (if exist) will be clustered. Assume in an experiment, the number of signal events in the signal region is a Poisson variable with the expectation s, while the number of events from backgrounds is a Poisson variable with a known expectation b, then the observed number of events distributes as the Poisson variable with the expectation $s + b$. If the experiment observed n_{obs} events in the signal region, then the $p-$value is

$$\begin{aligned} p(n_{obs}) &= P(n > n_{obs}|H_0) = \sum_{n=n_{obs}}^{\infty} \frac{b^n}{n!} e^{-b} \\ &= 1 - \sum_{n=0}^{n_{obs}-1} \frac{b^n}{n!} e^{-b}. \end{aligned} \tag{A.108}$$

Substituting this relation to equation A.107, one immediately has

$$\int_{-S}^{S} N(0,1)dx = \sum_{n=0}^{n_{obs}-1} \frac{b^n}{n!} e^{-b} \tag{A.109}$$

Then, the signal significance S can be easily determined. Comparing this equation with equation A.104 given by Ref. [21], we found the lower limit of the integral is different.

Statistical significance in continuous test statistics

The general problem in this situation can be addressed as follows. Suppose we identify a class of events using well-defined criteria, which are characterized by a set of n observations $x_1, \cdots, x_n$ for a random variable x. In addition, one wish to test a hypothesis which predicts the probability density function of x, say $f(x|\vec{\theta})$, where $\vec{\theta} = (\theta_1, \theta_2, ..., \theta_k)$ is a set of parameters which need to be estimated from the data. Then the problem is to define a statistic that gives a measure of the consistency of the distribution of data with the distribution given by the hypothesis.

To be concrete, we consider the random variable x is, say, an invariant mass, and the n observations $x_1, \cdots, x_n$ give an experimental distribution of x. Assuming parameters $\vec{\theta} = (\theta_1, \cdots, \theta_k) \equiv (\vec{\theta_s}; \vec{\theta_b})$, where $\vec{\theta_s}$ and $\vec{\theta_b}$ represent the parameters belong to signal (say, a resonance) and backgrounds contribution, respectively. We assume the null hypothesis H_0 stands for that the experimental distribution of x can be described merely by the background processes, namely, the null hypothesis H_0 specifies fixed values for a subset of parameters $\vec{\theta_s}$. Therefore, the parameters $\vec{\theta}$ are restricted to lie in a subspace ω of its total space Ω. On the basis of a data sample of size n from $f(x|\vec{\theta})$ we want to test the hypothesis $H_0 : \vec{\theta}$ belongs to ω. Given the observations $x_1, \cdots, x_n$, the likelihood function is $L = \prod_{i=1}^{n} f(x_i|\vec{\theta})$. The maximum of this function over the total space Ω is denoted by $L(\hat{\Omega})$; while within the subspace ω the maximum of the likelihood function is denoted by $L(\hat{\omega})$, then we define the likelihood-ratio $\lambda \equiv L(\hat{\omega})/L(\hat{\Omega})$. It can be shown that for H_0 true, the statistic

$$t \equiv -2 \ln \lambda \equiv 2(\ln L_{max}(s+b) - \ln L_{max}(b)) \tag{A.110}$$

is distributed as $\chi^2(r)$ (r is the number of parameters specified by H_0) when the sample size n is large [1]. In equation A.110 we use $\ln L_{max}(s+b)$ and $\ln L_{max}(b)$ denoting $L(\hat{\Omega})$ and $L(\hat{\omega})$, respectively. If λ turns out to be in the neighborhood of 1, the null hypothesis H_0 is such that it renders $L(\hat{\omega})$ close to the maximum $L(\hat{\Omega})$, and hence H_0 will have a large probability of being true. On the other hand, a small value of λ will indicates that H_0 is unlikely. Therefore, the critical region of λ is in the neighborhood of 0, corresponding to large value of statistic t. If the measured value of t in an experiment is t_{obs}, from equation A.106 we have $p-$value

$$p(t_{obs}) = \int_{t_{obs}}^{\infty} \chi^2(t; r) dt. \tag{A.111}$$

Therefore, in terms of equation A.107, one can calculate the signal significance according to following expression:

$$\int_{-S}^{S} N(0,1) dx = 1 - p(t_{obs}) = \int_{0}^{t_{obs}} \chi^2(t; r) dt. \tag{A.112}$$

For the case of $r = 1$, we have

$$\begin{aligned} \int_{-S}^{S} N(0,1) dx &= \int_{0}^{t_{obs}} \chi^2(t; 1) dt \\ &= 2 \int_{0}^{\sqrt{t_{obs}}} N(0,1) dx. \end{aligned} \tag{A.113}$$

and immediately obtain

$$\begin{aligned} S &= \sqrt{t_{obs}} \\ &= [2(\ln L_{max}(s+b) - \ln L_{max}(b))]^{1/2}, \end{aligned} \tag{A.114}$$

which is identical to the equation A.105 given by Ref. [21].

Bibliography

[1] W.T. Eadie *et al*, Statistical methods in experimental physics, North-Holland publishing Co., Amsterdam, 1971.

[2] A. Frodesen *et al*, Probability and Statistics in particle physics, Universitetsforlaget, Bergen-Oslo-Tromsø, 1979.

[3] Yongsheng Zhu, Probability and statistics in experimental physics, 2nd edition, Academic Press, Beijing, 2006.

[4] Particle Data Group, W.-M. Yao *et al*, Journal of Physics G, **33**, 1 (2006).

[5] G. Cowan, Statistical data analysis, Oxford Univ. Press Inc., New York, 1998.

[6] R. Barlow, arXiv Physics/0406120, 2004.

[7] J. Neyman, Phil. Trans. Royal Soc. London, Series A, **236**, 333 (1937)

[8] G. Feldman and R.D. Cousins, Phys. Rev. **D57**, 3873 (1998).

[9] B.P. Roe and M.B. Woodroofe, Phys. Rev. **D63**, 013009 (2001).

[10] R.D. Cousins and V.L. Highland, Nucl. Instr. Meth. in Phys. Res. **A320**, 331 (1992).

[11] W.A. Rolke and A.M. Lopez, Nucl. Instr. Meth. in Phys. Res. **A458**, 745 (2001).

[12] J. Conrad *et al*, Phys. Rev. **D67**, 012002 (2003).

[13] http://www3.tsl.uu.se/~conrad/pole.html.

[14] T. Bayes, Phil. Trans. Roy. Soc., **53**,370(1763).

[15] H. Jeffreys, Theory of probability, 3rd edition, Clarendon, Oxford, 1961.

[16] http://psip.ihep.ac.cn/~dusx/zhuys/Bayes/

[17] V. Rohatgi, An introduction to probability theory and mathematical statistics, John Wiley & Sons, New York, 1976.

[18] P.K. Sinervo, Proc of Conf. "Advanced statistical techniques in particle physics", Durham, UK, 18-22 March, 2002, p64.

[19] S.I. Bityukov *et al*, Nucl.Intr.Meth. **A452**, 518 (2000)

[20] S.I. Bityukov *et al*, Proc of Conf. "Advanced statistical techniques in particle physics", Durham, UK, 18-22 March, 2002, p77.

[21] I. Narsky, Nucl.Intr.Meth. **A450**, 444 (2000)

[22] Yongsheng Zhu, HEP&NP, **30**, 331 (2006)